

*The Third International Conference*  
**NONLINEAR DYNAMICS**

*Dedicated to the 125<sup>th</sup> Anniversary  
of the National Technical University  
“Kharkov Polytechnic Institute”*

September, 21-24, 2010

**PROCEEDINGS**

**Ministry of Science and Education of Ukraine  
National Technical University “Kharkov Polytechnic Institute”  
(Kharkov, UKRAINE)**

**National Committee of Ukraine on Theoretical and Applied Mechanics  
S. Timoshenko Institute of Mechanics NAS of Ukraine (Kiev, UKRAINE)**

**McGill University (Montreal, CANADA)**

**Aberdeen University (Aberdeen, UK)**

**Glasgow University (Glasgow, UK)**

*The Third International Conference*  
**“Nonlinear Dynamics – 2010”**

*Dedicated to the 125<sup>th</sup> Anniversary  
of the National Technical University  
“Kharkov Polytechnic Institute”*



**Proceedings**

September, 21-24, 2010

УДК: 531; 534; 621.

Нелинейная динамика

// Тезисы докладов 3-й Международной конференции (21-24 сент., 2010г.).

– Харьков: НТУ «Харьковский политехнический институт», 2010. – 519 с.

В сборник включены расширенные тезисы докладов 3-й Международной конференции по нелинейной динамике, посвященной 125-й годовщине со дня основания Национального технического университета «Харьковский политехнический институт».

The book of Proceedings includes extended abstracts of presentations on the Third International conference on nonlinear dynamics dedicated to the 125-th anniversary of the National Technical University “Kharkov Polytechnic Institute” foundation.

***Dear Colleagues and Guests,***

*It is my honor and pleasure to invite you to participate at the Third International Conference "Nonlinear Dynamic-2010" to be held on September, 21-24, 2010 in Kharkov, Ukraine.*

*During the past decades, the Nonlinear Dynamics has been evolving in a revolutionary way, resulting in a range of well developed theory, with the essential contribution to performance, effectiveness, reliability and safety of technical systems as well as offering new more effective systems, technologies and designs. The importance of the Nonlinear Dynamics is also confirmed by numerous conferences, which are held in different countries.*

*One of them is the Third International Conference on Nonlinear Dynamics, which takes place in our University and gathers leading scientists actively working in this field from around the world. I am pleased that the scientists of our university actively continue and develop traditions and teachings of known scientists Mechanics and Mathematics such as V.L.Kirpichov, A.M.Lyapunov, V.A.Steklov, L.D.Landau, I.M.Babakov, A.S.Voljmir, A.P.Filippov, V.L.Rvachov and many others, that have created the glory of our university, as one of the leading universities of Ukraine.*

*Our University was founded in 1885 as Kharkov Practical Technological Institute. Excellent scientist and organizer Vladimir L. Kirpichov was the first rector of this Institute. In 2010 the National Technical University "Kharkov Polytechnic Institute" celebrates 125-th anniversary of the foundation. Our University is one of the best Universities of Ukraine.*

*At present NTU "KhPI" includes 23 faculties, 91 departments, scientific institutes. Teaching staff of the university consists of 1,700 teachers, 160 of which are doctors sci. and professors, more than 800 employees are PhD and senior lecturers, 17 honored workers of science and technology, and highly respected workers in higher education of Ukraine, 8 State Prize laureates, 3 academicians and corresponding members of the National Academy of Sciences of Ukraine, 26 academicians of the Academy of Sciences of Ukraine's industry. Over 22 thousand students and 320 graduate students, among them about 1000- foreigners from 31 countries are studied at NTU "KhPI)" The University has over 250,000 post-graduates, which formed and will form the technical policy of Ukraine.*

*We thank to co-sponsors of this conference, Prof. Christophe Pierre from McGill University and Prof. Marian Wiercigroch from the Aberdeen University for their financial support which is very useful for the conference organization. We also thank members of the scientific and the organizing committees and other people for their efforts in organization of the conference. We try in friendly atmosphere for work and discussions, for establishment of new contacts and for exchange of ideas.*

*I wish the conference participants to get acquainted with the history of sights of the city of Kharkov, which was the first capital of Ukraine, as well as the NTU "KhPI", which is one of the oldest Universities in our city.*

*Rector of National Technical University "Kharkov Polytechnic Institute"  
Chairman of Organizing Committee, Professor L.L. Tovazhnyansky*

### **Scope of the conference**

The objective of the Conference is to bring together scientists and engineers to present and discuss recent developments on the different problems of nonlinear dynamics.

### **Scientific Committee**

Prof. Altenbach H. (Halle, Germany)  
Prof. Amabili M. (Montreal, Canada)  
Prof. Andrianov I. V. (Aachen, Germany)  
Prof. Avramov K. V. (Kharkov, Ukraine)  
Prof. Awrejcewicz J. (Lodz, Poland)  
Prof. Balthazar J. M. (Sao Paulo, Brasil)  
Prof. Breslavsky D.V. (Kharkov, Ukraine)  
Prof. van Campen D.H. (Eindhoven, Netherlands)  
Prof. Cartmell M. (Glasgow, UK) – co-Chairman  
Prof. Epureanu B. (Ann Arbor, USA)  
Dr. Gendelman O. (Haifa, Israel)  
Prof. Gulyayev V.I. (Kiev, Ukraine)  
Prof. Hedrih Katica R. (Stevanović) (Belgrade, Serbia)  
Corresponding member of the NAS of Ukraine, Prof. Kovalev A.M. (Donetsk, Ukraine)  
Prof. Kapitaniak T. (Lodz, Poland)  
Prof. Kreuzer E. (Hamburg, Germany)  
Academician of the NAS of Ukraine, Prof. Kubenko V.D. (Kiev, Ukraine) – co-Chairman  
Prof. Kurpa L.V. (Kharkov, Ukraine)  
Prof. Lamarque C.-H. (Lyon, France)  
Prof. Manevitch L.I. (Moscow, Russia)  
Academician of the NAS of Ukraine, Prof. Martynyuk A.A. (Kiev, Ukraine)  
Prof. Mikhlin Yu.V. (Kharkov, Ukraine) – co-Chairman  
Prof. Morachkovsky O.K. (Kharkov, Ukraine)  
Prof. Paidoussis M. (Montreal, Canada)  
Prof. Pellicano F. (Modena, Italy)  
Prof. Pierre C. (Montreal, Canada) – co-Chairman  
Prof. Pilipchuk V.N. (Detroit, USA)  
Prof. Potapov A.I. (Nyzhny Novgorod, Russia)  
Prof. Rega G. (Roma, Italy)  
Prof. Ribeiro P.L. (Porto, Portugal)  
Prof. Shaw S. W. (Lansing, USA)  
Prof. Ueda Y. (Waseda, Japan)  
Prof. Vakakis A. (Urbana, USA; Athens, Greece)  
Prof. Vorobiev Yu. S. (Kharkov, Ukraine)  
Prof. Warminski J. (Lublin, Poland)  
Prof. Wiercigroch M. (Aberdeen, UK) - co-Chairman  
Academician of the RAS, Prof. Zhuravlev V. Ph. (Moscow, Russia)

### **Scientific Committee of the mini-symposium**

#### **«Creep and plasticity at cyclic loading»**

Prof. Altenbach H. (Halle, Germany) Co-chairman  
Prof. Borodiy M. (Kiev, Ukraine)  
Prof. Breslavsky D. (Kharkov, Ukraine) Co-chairman  
Prof. Kowalewski Z. (Warsaw, Poland)  
Prof. Kruch S. (ONERA, France)  
Prof. Morachkovsky O. (Kharkov, Ukraine) Co-chairman  
Dr. hab. K. Naumenko (Halle, Germany)  
Prof. Shukayev S. (Kiev, Ukraine)  
Prof. Spiliopoulos K. (Athens, Greece)  
Prof. Yasniy P. (Ternopil, Ukraine)

### **Organizing Committee**

Prof. Tovazhnyansky, L.L., rector of the NTU “KhPI” - Chairman  
Prof. Breslavsky D.V. - vice-Chairman  
Prof. Kurpa L.V. - vice-Chairman  
Prof. Kravets V.A. - vice-Chairman  
Prof. Mikhlin Yu.V. - vice-Chairman  
Dr. Larin A.A. - Secretary  
Prof. Marchenko A.P.  
Prof. Morachkovsky O.K.  
Dr. Rudnyeva G.V.

## CONTENT

### NONLINEAR DYNAMICS OF DISCRETE SYSTEMS

1. **L. Akulenko, D. Leshchenko, Y. Zinkevich, A. Rachinskaya.** Response-optimal deceleration of the rotation of a symmetric free rigid body in a resistive medium. **9**
2. **I.V. Andrianov, V.I. Olevs'kyy.** Critical re-examination of Adomian's decomposition and homotopy perturbation methods in nonlinear mechanics. **15**
3. **K.V. Avramov, O.V. Borysiuk.** Bifurcations of elastic rotors in journal bearings. **21**
4. **J. Awrejcewicz, L.P. Dzyubak.** Chaos caused by hysteresis in 2-DOF rotor vibrations. **27**
5. **A.B. Batkhin.** Families of periodic solutions of Hill's problem. **33**
6. **I.I. Blekhman, N.P. Yaroshevich.** Transient regimes in systems with inertial excitation of oscillations. **39**
7. **I. Bula.** On some chaotic mappings in symbol space. **45**
8. **A. Bychkov.** Investigation of stability with respect to part of variables in hybrid automata. **50**
9. **G. Chechin, G. Bezuglova, P. Goncharov.** Existence and stability of discrete breathers with different symmetries in 2D square lattices. **56**
10. **T.N. Dragunov, R.E. Kondrashov, A.D. Morozov.** On visualization of resonance structures in dynamical systems with two degrees of freedom. **62**
11. **A.G. Grechnev, A.S. Kovalev, M.L. Pankratova.** Hysteresis phenomenon in ferro/antiferro layered system. **67**
12. **E.Zh. Harutyunyan.** Investigation of the nonlinear oscillation of the passenger car suspension. **73**
13. **K.R. (Stevanović) Hedrih, L. Veljović.** The kinetic pressures of the gyro-rotor eigen shaft bearings and rotators. **78**
14. **K.R. (Stevanović) Hedrih, V. Raičević, S. Jović.** The phase portrait of the vibro-impact dynamics of two mass particle motions along rough circle. **84**
15. **I. Ivanov.** Stability for a class of systems with uncertain structure. **90**
16. **W. Jarzyna, M. Augustyniak, J. Warمیński, M. Bocheński.** Model based identification of active beam composite structure - application MRAS algorithm. **96**
17. **A.A. Kireenkov.** Coupled dry friction model for the heavy disk slid with spinning on the rough plane. **102**
18. **Yu. Kivshar.** Nonlinear physics and energy localization in periodic systems. **108**
19. **Yu.A. Kosevich, L.I. Manevitch.** Irreversible transfer of vibration energy in linear and nonlinear coupled parametric systems. **109**
20. **P.V. Krot.** Dynamics and diagnostics of the rolling mills drivelines with non-smooth stiffness characteristics. **115**
21. **V.V. Kulyabko.** Nonlinear structural dynamics in XXI century: specified models, vibro-comfort buildings, nonlinear dampening devices. **121**
22. **O.G. Kyselova, I.A. Nastenکو.** Estimation of heart rate complexity of behavior using different methods of nonlinear dynamics. **125**
23. **V.A. Lykah, E.S. Syrkin.** Nonlinear rotational modes in molecular chains. **129**
24. **G. Martynenko.** Method of detuning from resonance modes for rotors in active magnetic bearings with nonlinear force characteristics. **135**
25. **M. Merkurjev.** Constructing an optimal Lyapunov function for investigation of stability of linear fuzzy hybrid automaton. **141**
26. **Yu.V. Mikhlin, A.A. Klimenko.** Nonlinear normal modes in pendulum systems. **146**

27.	<b>Yu.V. Mikhlin, G.V. Rudnyeva.</b> Construction of transient in mechanical systems.	152
28.	<b>I. Mukherjee.</b> Stability analysis of periodic solutions for a class of fractionally damped system of engineering interest.	158
29.	<b>E.D. Pechuk, T.S. Krasnopolskaya.</b> Reconstruction of the third order dynamical systems from signals.	164
30.	<b>N.V. Perepelkin, Yu.V. Mikhlin.</b> Nonlinear normal modes of forced vibrations in rotor systems.	170
31.	<b>V.N. Pilipchuk.</b> On algebraic structures induced by U-turns and non-invertible time substitutions.	176
32.	<b>S.N. Polukoshko, S.V. Sokolova, V.Y. Jevstignejev.</b> Impact vibration absorber of pendulum type.	177
33.	<b>A.Yu. Shvets, V.A. Pechernyi.</b> New aspects of chaotic dynamics of pendulum systems with a limited power-supply.	183
34.	<b>A.Yu. Shvets, V.A. Sirenko.</b> Chaos and hyperchaos in deterministic nonideal hydrodynamic systems.	189
35.	<b>V.V. Sidorenko.</b> Some remarks about quasi-steady dynamics.	195
36.	<b>V.V. Smirnov, L.I. Manevitch.</b> Limiting phase trajectories and dynamical transitions in the nonlinear periodic systems.	200
37.	<b>M.M. Tkachuk, A.V. Grabovsky, M.A. Tkachuk.</b> An approach to identification of impact interaction model for a vibroimpact system.	207
38.	<b>Y. Ueda.</b> At the very instant when the author came across an inexperienced behavior.	213
39.	<b>V.G. Verbitskii, V.G. Khrebet, N.O. Velmagina.</b> The bifurcation set for a two-axes vehicle model with the non-linear dependence of slipping forces.	219
40.	<b>M. Wiercigroch.</b> Grazing induced bifurcations in impacting systems.	225
41.	<b>A. Zotov.</b> Oscillation of systems which have force-displacement characteristics with rectangular loops of hysteresis.	226

## NONLINEAR DYNAMICS OF DISTRIBUTED SYSTEMS

1.	<b>H. Altenbach, V.A. Eremeyev.</b> On the oscillations of nonlinear magnetoelastic solids.	230
2.	<b>H. Altenbach, V.A. Eremeyev, M.M. Ievdokymov.</b> On the impact on a plate made of hyperelastic foam.	236
3.	<b>M. Amabili, Y. Kurylov, R. Garziera.</b> Polynomial versus trigonometric expansions for nonlinear vibrations of shells with different boundary conditions.	242
4.	<b>K.V. Avramov.</b> Nonlinear dynamics of traveling waves of circular plates with cutouts.	248
5.	<b>K.V. Avramov, H. Strel'nikova, I. Breslavsky.</b> Nonlinear dynamics of plates and shallow shells interacting with moving fluid.	250
6.	<b>J. Awrejcewicz, L. Kurpa, O. Mazur.</b> Investigation of the parametric vibration of the orthotropic plates subjected to periodic in plane forces by multi-modal approximation and R-functions method.	256
7.	<b>M. Bochenski, J. Warminski, W. Jarzyna, P. Filipek, M. Augustyniak.</b> PPF versus saturation control for a strongly nonlinear beam structure.	262
8.	<b>I.D. Breslavsky, K.V. Avramov.</b> Nonlinear oscillations of turbomachinery blades.	266
9.	<b>D.V. Breslavsky, O.K. Morachkovsky, N.V. Shyriaieva.</b> Nonlinear vibrations and long-term strength of turbine blades.	272
10.	<b>D.V. Breslavsky, I. Naumov, A. Onyshchenko.</b> Numerical and experimental investigations of fracture in thin-walled structures at impact loading.	278

11.	<b>V. Burlayenko, T. Sadowski.</b> Numerical modal analysis of sandwich plates partially damaged due to impacts.	284
12.	<b>V.Z. Gristchak, V.V. Lysenko.</b> A hybrid asymptotic WKB-Galerkin method with application to the correlation analysis of stochastic behavior of non-linear systems with time-depended parameters.	290
13.	<b>V.I. Gulyayev, O.V. Glushakova.</b> The Poincare – Andronov – Hopf bifurcations in the torsion wave models of superdeep drill columns.	296
14.	<b>K.R. (Stevanović) Hedrih.</b> Stochastic stability of the deformable forms and vibration modes of a parametrically excited sandwich double hereditary beam system.	302
15.	<b>K.R. (Stevanović) Hedrih, J. Simonović.</b> Resonant jumps in multi-frequency regimes of mylti-circular plate system non-linear dynamics.	314
16.	<b>S.N. Hudolij, E.I. Borshch.</b> Stability of whirl vibrations of drill string bottom assembly.	320
17.	<b>R.E. Kochurov, K.V. Avramov.</b> Nonlinear parametric vibrations of cylindrical shells.	326
18.	<b>T.S. Krasnopolskaya, V.N. Il'chenko, V.V. Meleshko.</b> Transport and mixing across Gulf Stream.	332
19.	<b>L.V. Kurpa.</b> Geometrically non-linear vibration and meshless discretization of the composite laminated shallow shells with complex shape.	338
20.	<b>L.V. Kurpa, N.A. Budnikov.</b> Multi-modal geometrical non-linear free vibrations of composite laminated plates with the complex shape.	344
21.	<b>O.O. Larin, O.S. Stepchenko.</b> Investigation of forced vibrations of turbine blades in consideration of rolling contact in the detachable shroud.	349
22.	<b>M. Legrand, C. Pierre.</b> Wear of abradable coatings. Towards multi-physics analyses for the design of turbomachines.	352
23.	<b>A. Manevich.</b> Dynamics of a Timoshenko beam on an elastic foundation.	358
24.	<b>M.V. Marchuk, V.S. Pakosh.</b> Geometrically nonlinear transversal vibrations of pliable to shear and compression plates.	364
25.	<b>O. Mazur, A. Linnik, V. Tkachenko.</b> Nonlinear analyses of the laminated plates of the symmetric structure subjected to static in the plane forces.	369
26.	<b>Sh.A. Nazirov, N.G. Eshkaraeva.</b> Mathematical modeling of deformation processes of the flexible viscoelastic plates with complex form.	375
27.	<b>A.A. Osetrov.</b> Application of the R-functions theory and spline-approximation to finding eigen functions as basic ones for meshless discretization of the laminated shallow shells.	377
28.	<b>A.N. Pasechnik, V.A. Pasechnik, N.N. Novotna.</b> Research of natural oscillations of a plate with mixed conditions of contour fastening.	378
29.	<b>F. Pellicano.</b> Dynamic instabilities of a seismically excited shell with shaker-shell interaction modeling.	384
30.	<b>E. Petrov.</b> Analysis of resonance nonlinear vibrations for high-fidelity models of structures with contact interfaces.	390
31.	<b>Yu.V. Romashov.</b> Equation of motion with implicit functions of phase coordinates velocities and its applications for engineering constructions rupture life evaluation.	392
32.	<b>S.Yu. Sayenko, O.K. Morachkovsky, D.V. Lavinsky, V.N. Sobol, Yu.M. Andreev.</b> Modeling of impact deformation processes of the ceramic container for radioactive waste storage.	398
33.	<b>T.V. Shmatko.</b> Investigation of dynamical instability of vibration modes for laminated plates and shallow shells.	403
34.	<b>V.M. Spector, T.S. Krasnopolskaya.</b> Surface waves in a fluid annulus with a vibrating inner cylinder.	409

35.	<b>M.J. Temis, A.M. Egorov.</b> Influence of gas turbine parameters changes to nonlinear vibrations of rotor-bearings system.	415
36.	<b>J.M. Temis, A.V. Selivanov.</b> Aeroelastic self-oscillations of plane channel wall.	421
37.	<b>G.N. Timchenko, I.O. Morachkovska, N.A. Budnikov.</b> Research of the nonlinear free vibration of the fully clamped composite laminated plates of an arbitrary planform.	427
38.	<b>Yu. Turbal.</b> The trajectories of self-reinforcing solitary wave in the gas disc of galaxies.	431
39.	<b>K.A. Volosov, S.O. Sinitsyn, A.K. Volosova, E.K. Vdovina.</b> Stochastic systems under periodic and white noise external excitations, and the alternative classification for the PDE solutions.	437
40.	<b>A.V. Yelagin.</b> Analysis of nonlinear anharmonic perturbations for axisymmetric longitudinal-shear waves in a cylindrical waveguide.	443

### MINI-SYMPOSIUM

#### «CREEP AND PLASTICITY AT CYCLIC LOADING»

1.	<b>H. Altenbach, S. Kozhar, K. Naumenko.</b> Modeling creep ratcheting of an aluminum-silicon eutectic alloy.	449
2.	<b>M.V. Borodii, M.P. Adamchuk.</b> Ratcheting simulation of structural steel under low-cycle asymmetric loading.	455
3.	<b>D.V. Breslavsky, A. Chuprynin, O. Tatarinova.</b> Creep-damage behaviour of thin shells subjected to cyclic loading.	461
4.	<b>D.V. Breslavsky, Yu. Korytko, O.K. Morachkovsky.</b> High temperature creep and damage accumulation in cyclically loaded axisymmetrical bodies of revolution.	467
5.	<b>Yu.A. Chernyakov, A.S. Polishchuk.</b> On accounting for deformation by twinning in the theory of microstrains.	473
6.	<b>S. Gladkov, B. Svendsen.</b> Towards coupled finite element modeling of grain growth with plasticity.	478
7.	<b>Z.L. Kowalewski, S. Mackiewicz, J. Szelażek, T. Szymczak, B. Augustyniak.</b> An influence of long-term exploitation on material behaviour under constant and monotonically increasing loading.	481
8.	<b>O.K. Morachkovsky, V.N. Sobol.</b> Problem statement of dynamic creep for isotropic and orthotropic bodies.	487
9.	<b>K.V. Spiliopoulos, K.D. Panagiotou.</b> A direct method for the cyclic elastoplastic analysis of simple structures.	492
10.	<b>A. Tkachuk.</b> A contact-stabilized Newmark method for coupled dynamical thermo-elastic problem.	497
11.	<b>M. Wolff, M. Böhm.</b> Two-mechanism models and modelling of creep.	503
12.	<b>P. Yasniy, V. Hlado, S. Fedak, I. Shulhan.</b> Numerical simulation of crack tip opening at static and dynamic creep.	509

	<b>ALPHABETICAL INDEX</b>	<b>516</b>
--	---------------------------	------------

## RESPONSE-OPTIMAL DECELERATION OF THE ROTATION OF A SYMMETRIC FREE RIGID BODY IN A RESISTIVE MEDIUM

**Akulenko Leonid**

A. Ishlinsky Institute for  
 Problems in Mechanics  
 Russian Academy of  
 Sciences  
 Moscow, Russia

**Leshchenko Dmytro,  
 Zinkevich Yanina<sup>1</sup>**

Odessa State Academy of  
 Civil Engineering and  
 Architecture  
 Odessa, Ukraine

**Rachinskaya Alla**

Odessa National  
 Mechnikov University  
 Odessa, Ukraine

---

### ABSTRACT

---

The problem of time-optimal deceleration of rotation of a free rigid body is studied. It is assumed that the body contains a moving mass connected to the body by an elastic coupling with square-law friction. Low deceleration torque of viscous friction forces also acts on the rigid body. It is assumed that the body is dynamically symmetric. The optimal control law for deceleration of rotation of the rigid body in the form of synthesis, the operation time, and the phase trajectories are determined.

### INTRODUCTION

Analysis of passive motion of a rigid body with a cavity filled with viscous liquid, motion of a rigid body with a moving mass connected to the body by an elastic coupling with viscous or square-law friction and motion in a resistive medium is fulfilled in [1-8]. The problem of control of rotation of “quasi-rigid” bodies via concentrated torques of forces important for application was insufficiently studied. A class of systems resulting in smooth control actions and allowing one to apply methods of singular perturbations without accumulation of “boundary-layer”-type errors was separated [2, 9-13].

The problem of time-optimal deceleration of rotation of a dynamically symmetric body connected at a point on the axes of symmetry with a mass concerning the small linear sizes by an elastic coupling with square-law friction dissipation is studied. Furthermore, low decelerating torque of a resisting medium acts on the rigid body. Rotation is controlled by the torque of forces with the bounded absolute value. The considered model continues those studied performed earlier in [2, 9-13].

### 1. STATEMENT OF THE PROBLEM

Based on approach [3, 13] the equations of controlled rotations in projections onto the axes of the coordinate system attached to the fixed rigid body (Euler equations) can be represented in the form [3, 5, 6, 11, 13]

$$\begin{aligned}
 A\dot{p} + (C - A)qr &= M_p + FG^2qr + Spr^6\omega_{\perp} - \chi Ap \\
 A\dot{q} + (A - C)pr &= M_q - FG^2pr + Sqr^6\omega_{\perp} - \chi Aq \\
 C\dot{r} &= M_r - AC^{-1}Sr^5\omega_{\perp}^3 - \chi Cr
 \end{aligned} \tag{1}$$

---

<sup>1</sup> Corresponding author. Email yaninaz@mail.ru

Here  $p, q, r$  are the projections of the vector of absolute angular velocity  $\boldsymbol{\omega}$  onto the attached axes,  $\mathbf{J} = \text{diag}(A, A, C)$  is the tensor of inertia of the unperturbed body,  $M_{p,q,r}$  are the projections of the vector of control torque of forces  $\mathbf{M}$ ; and  $\mathbf{G} = \mathbf{J}\boldsymbol{\omega}$  is the angular momentum of the body; its absolute value is

$$G = |\mathbf{G}| = [A^2\omega_{\perp}^2 + C^2r^2]^{1/2}, \quad \omega_{\perp}^2 = p^2 + q^2$$

For simplification of the problem the structural constraint is introduced in system (1). It is assumed that the diagonal tensor of the torque of viscous resistance forces is proportional to the tensor of moment of inertia forces; i.e., the torque of dissipation forces is proportional to the angular momentum.

$$\mathbf{M}^r = -\chi\mathbf{J}\boldsymbol{\omega} \quad (2)$$

where  $\chi$  is some constant coefficient of proportionality depending on the properties of the medium and the shape of the body. The resistance acting on the body is represented by a pair of applied forces. In this case the projections of the torque of this pair of forces on the principal axes of inertia of the body are  $\chi Ap, \chi Aq, \chi Cr$  [4, 5]. Such assumption is not conflicting.

It is additionally assumed that the admissible values of the torque of control forces  $\mathbf{M}$  are bounded by the sphere [13]

$$\mathbf{M}^u = b\mathbf{u}, \quad |\mathbf{u}| \leq 1, \quad b = b(t, \mathbf{G}), \quad 0 < b_* \leq b < b^* < \infty \quad (3)$$

where  $b$  is the scalar function bounded in the considered region of variation of the arguments  $t, \mathbf{G}$ , according to the conditions (3). This domain is determined a priori or can be estimated via the initial data for  $\mathbf{G}$ ,  $\mathbf{G}(t_0) = \mathbf{G}^0$ .

The notations of  $F, S$ , introduced in (1), are expressed in terms of the system parameters as

$$F = m\rho^2\Omega^{-2}CA^{-3}, \quad S = m\rho^3\lambda\Omega^{-3}d|d|C^4A^{-4}, \quad d = 1 - CA^{-1} \quad (4)$$

The coefficients  $F, S$  characterize the torque of forces due to a presence of elastic element. Here  $m$  is the mass of the moving point,  $\rho$  is the radius-vector of the fixing point  $O_1$  of the moving mass on the axis of symmetry. The constants,  $\Omega^2 = c/m$ ,  $\lambda = \mu/m = \Lambda\Omega^3$  determine oscillation frequency and velocity of their damping respectively;  $c$  is the stiffness of the elastic coupling;  $\mu$  is the coefficient of square-law friction.

However, if we assume that the coupling coefficients  $\lambda$  and  $\Omega$  are such that “free” motion of the point  $m$  resulting from the initial deviations attenuates much more rapidly than the rigid body makes one revolution, then in this case the motion of the rigid body is similar to the Euler – Poinot motion, and the relative oscillations of the point by this motion will be small. It is supposed that

$$\Omega \ll \omega \quad (5)$$

In equation (5) provides introducing a small parameter into (4) and assumed stated perturbed torques to be small with purpose to apply asymptotic averaging methods. Note also that the mass  $m$  can be large, comparable with the mass of the body.

The time-optimal deceleration of rotation is formulated

$$\boldsymbol{\omega}(T) = 0, \quad T \rightarrow \min_{\mathbf{u}}, \quad |\mathbf{u}| \leq 1 \quad (6)$$

It is necessary to find the optimal control law in the form of the synthesis  $u = u(t, \boldsymbol{\omega})$ , the corresponding trajectory  $\boldsymbol{\omega}(t, t_0, \boldsymbol{\omega}^0)$  and the operation time  $T = T(t_0, \boldsymbol{\omega}^0)$ , as well as the Bellman function of the problem  $W = T(t, \boldsymbol{\omega}) - t$ .

## 2. SOLUTION OF THE OPTIMAL DECELERATION PROBLEM

Note that the torque of forces due to motion of a rigid body with a moving mass connected to the body by an elastic coupling with square-law friction is internal for the fictitious body, and the torque of viscous friction forces is external.

Based on dynamic programming, the synthesis of time-optimal control has the form [13]

$$M_p = -b \frac{Ap}{G}, M_q = -b \frac{Aq}{G}, M_r = -b \frac{Cr}{G}, b = b(t, G) \quad (7)$$

Here, the following can be assumed for further simplification:  $b = b(t, G)$ ,  $0 < b_1 \leq b < b_2 < \infty$ .

Let us multiply the first equation of (1) by  $Ap$ , the second equation by  $Aq$ , and the third equation by  $Cr$  and sum them up. We obtain the equation of the form

$$\dot{G} = -b(t, G) - \chi G, G(t_0) = G^0, G(T, t_0, G^0) = 0, T = T(t_0, G^0), W(t, G) = T(t, G) - t$$

In the assumption that  $b = b(t)$ , we obtain the solution and a condition for  $T$  determination,

$$G(t) = G^0 e^{-\chi(t-t_0)} - \int_{t_0}^t b(\tau) e^{-\chi(t-\tau)} d\tau, G^0 = e^{-\chi t_0} \int_{t_0}^T b(\tau) e^{\chi\tau} d\tau, T = T(t_0, G^0) \quad (8)$$

Here,  $t$  is the current deceleration time and  $T$  is operation time.

For  $b = \text{const}$  the solution to equation and boundary value problem (8) is written as

$$G(t) = \frac{1}{\chi} [(G^0 \chi + b) \exp(-\chi t) - b], T = \frac{1}{\chi} \ln \left( G^0 \frac{\chi}{b} + 1 \right), t_0 = 0 \quad (9)$$

Below, case (9) is analyzed in details.

## 3. ANALYSIS OF AXIAL ROTATION FOR CONTROLLED BODY MOTION

Substituting known expression for  $G$  into the third equation of (1) results in a nonlinear equation with respect to  $r$

$$\dot{r} = -r \left[ bG^{-1} + A^{-2} C^{-2} S r^4 (G^2 - C^2 r^2)^{3/2} + \chi \right] \quad (10)$$

Replacing the axial component of the vector of angular velocity,  $r = GR$ , where  $R$  is the unknown function, equation (10) is reduced to the form admitting separation of variables and trivial integration,

$$\dot{R} = -A^{-2} C^{-2} S G^4 R^5 [G^2 (1 - C^2 R^2)]^{3/2} \quad (11)$$

The vector of the angular momentum  $\mathbf{G}$  upon projection onto principal central axes of inertia of the body results in the expression is  $Cr = G \cos \theta$ , where  $\theta$  is the nutation angle. As a result, the following relation is obtained for the unknown  $R$ :  $CR = \cos \theta$ . Equation (11) after transition to the unknown  $\theta$  can be written in the form

$$\dot{\theta} = A^{-2}C^{-6}S \sin \theta |\sin \theta| \cos^5 \theta \chi^{-7} \left| (G^0 \chi + b) \exp(-\chi t) - b \right|^7, \quad \theta(0) = \theta^0 \quad (12)$$

The solution to this equation is written as

$$2 \sec^4 \theta \cos ec \theta + 5(\sec^2 \theta - 3) \cos ec \theta - 2 \sec^4 \theta^0 \cos ec \theta^0 - \\ - 5(\sec^2 \theta^0 - 3) \cos ec \theta^0 + 15 \ln \left| \operatorname{tg} \left( \frac{\pi}{4} + \frac{\theta}{2} \right) \operatorname{tg}^{-1} \left( \frac{\pi}{4} + \frac{\theta^0}{2} \right) \right| = K(t), \quad (13)$$

where

$$K(t) = \pm 8A^{-2}C^{-6}S\chi^{-7} \left[ -(7\chi)^{-1} (G^0 \chi + b)^7 (\exp(-7\chi t) - 1) + \right. \\ + 7b(6\chi)^{-1} (G^0 \chi + b)^6 (\exp(-6\chi t) - 1) - 21b^2(5\chi)^{-1} (G^0 \chi + b)^5 (\exp(-5\chi t) - 1) + \\ + 35b^3(4\chi)^{-1} (G^0 \chi + b)^4 (\exp(-4\chi t) - 1) - 35b^4(3\chi)^{-1} (G^0 \chi + b)^3 (\exp(-3\chi t) - 1) + \\ \left. + 21b^5(2\chi)^{-1} (G^0 \chi + b)^2 (\exp(-2\chi t) - 1) - 7b^6 \chi^{-1} (G^0 \chi + b) (\exp(-\chi t) - 1) - b^7 t \right]$$

It can be assumed without losing generality that the value of  $\theta^0$  (and  $\theta$ ) lies in the first quarter ( $0 \leq \theta^0 \leq \pi/2$ ). If  $\theta^0$  takes values in this interval, then the nutation angle also does not go beyond these limits in the course of evolution of rotation, since  $\theta^* = 0$  and  $\theta^* = \pi/2$  are the stationary points of equation (12).

For  $A \approx C$ , and  $\theta^0$  the perturbation methods can be applied in the neighborhood of stationary points; in this case these methods result in elementary expressions. For example, after the first iteration we have the following expression for  $\theta$

$$\theta(t) = \theta^0 + \frac{1}{8} \sin^2 \theta^0 \cos^5 \theta^0 K(t) \quad (14)$$

Formula (14) provides the temporal analysis of the nutation angle for different values of the system parameters and initial data.

#### 4. NUMERICAL ANALYSIS AND CONCLUSIONS

Let us consider the problem of determination of the nutation angle  $\theta(t)$  in the particular case  $b = \text{const}$  according to (12). Let us transform this equation to the dimensionless form. We introduce the notation

$$\tau = \chi t, \quad k^* = \frac{kS^{1/7}}{A^{2/7}C^{6/7}\chi^{1/7}}, \quad G_0^* = \frac{G_0S^{1/7}}{A^{2/7}C^{6/7}\chi^{1/7}}, \quad k = b\chi^{-1} \quad (15)$$

As a result of these transformations, we obtain the equations for the nutation angle  $\theta$ ,

$$\frac{d\theta}{d\tau} = \operatorname{sign}(d) \left| (G_0^* + k^*) \exp(-\tau) - k^* \right|^7 \sin \theta |\sin \theta| \cos^5 \theta \quad (16)$$

Equations (16) was numerically integrated for arbitrary values of  $G_0^*$ ,  $k^*$  and initial angle  $\theta^0 = \pi/2$  rad. The plots of variation of the nutation angle  $\theta$  are shown in Figs. 1-2. Figure 1 corresponds to the dynamically prolate body, and Fig. 2 to the oblate body.

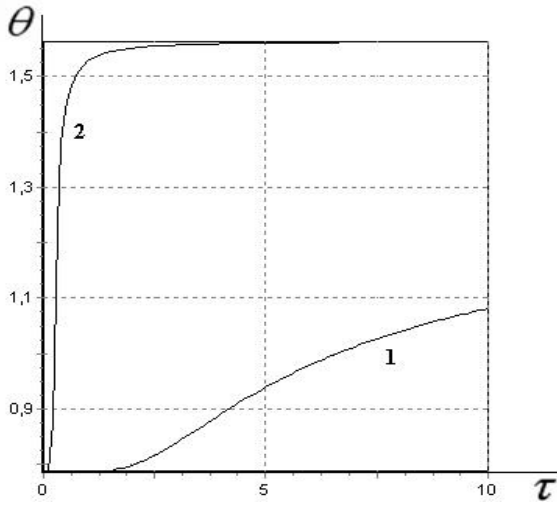


Fig. 1

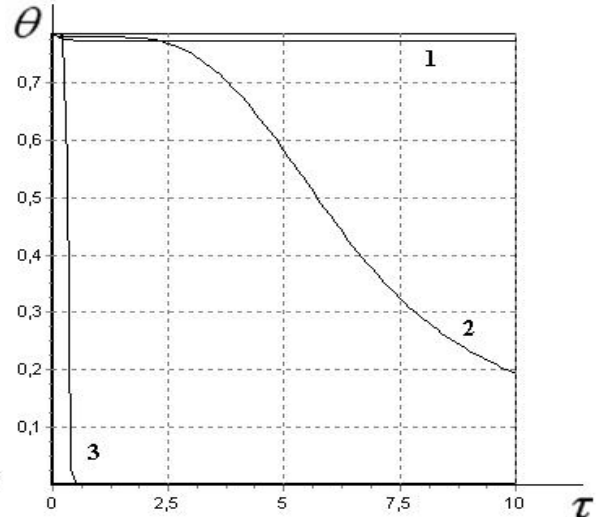


Fig.2

Fig. 1 corresponds to the dimensionless initial value of the angular momentum  $G_0^* = 1$ . Curves 1, 2 and 3 were calculated for arbitrary values of  $k^* = 0.1, 1, 10$  respectively. According to the calculation for dynamically prolate body ( $A > C$ ) the nutation angle tends to a limiting value  $\pi/2$  rad. Numerical interval of the dimensionless time  $\tau \leq 10$  is shown in Fig. 1. According to Fig. 2 it can be seen that under the essential action of the dimensionless coefficient of control torque of forces ( $k^* = 10$ ) the nutation angle reaches the limiting value fast. In addition the body has time to brake since the operation time is the current deceleration time order over. The more smaller the value  $k^*$ , the more slowly the axis of symmetry of the body tends to the limiting position, though the body has a time to brake in the calculated time interval in all cases.

The variation of the nutation angle for dynamically oblate body was numerically studied ( $A < C$ ). The graphs of variation of the function  $\theta(t)$  for value  $G_0^* = 1$  are shown in Fig. 2. Curve 1 corresponds to value  $k^* = 0.1$ , curve 2 corresponds to value  $k^* = 1$ , and curve 3 corresponds to value  $k^* = 10$ . According to curves 2 and 3 dynamically oblate body tends to its stable limiting position of the rotation axis corresponded to  $\theta \rightarrow 0$  rad. It can be seen that the character of the tendency depends on the value of the dimensionless coefficient of the control torque of forces. The more larger this coefficient, the more faster the axis of the body tends to limiting position. In addition the operation time decreases essentially.

The numerical computation shows that the character of behavior of the function  $\theta(t)$  in given problem coincides with the character of behavior of the function of the nutation angle variation for the rigid body with the moving internal masses [2].

Therefore the direction of the angular momentum vector  $\mathbf{G}$  in the coordinate system fixed to the body approached a steady state along the axis corresponding to the largest moment of inertia.

## CONCLUSIONS

The problem of the synthesis of time-optimal deceleration of rotation of the dynamically symmetric rigid body with a moving mass connected to the body by an elastic coupling with square-law friction in the resistive medium, is studied analytically and numerically. In the framework of the asymptotic approach, the control, the operation time (Bellman function), and the nutation angle are determined. The qualitative properties of optimal motion are established.

## REFERENCES

- [1] F.L. Chernousko, Motion of a rigid body with cavities filled with viscous liquid for small Reynolds number, *Zh. Vychisl. Mat. Mat. Fiz [Comput. Math. Math. Phys]*, Vol. 5, № 6,

- pp. 1049-1070, 1965.
- [2] F.L. Chernousko, Motion of a rigid body with moving internal masses, *Izv. Akad. Nauk SSSR. Mekh.Tverd.Tela [Mechanics of Solids]*, № 4, pp. 33-44, 1973.
  - [3] L.D. Akulenko and D.D.Leshchenko, Some problems on the motion of a rigid body with moving mass, *Izv. Akad. Nauk SSSR. Mekh.Tverd.Tela [Mechanics of Solids]*, № 5, pp. 29-34, 1978.
  - [4] D.D.Leshchenko and S.N. Sallam, Some problems on the motion of a rigid body with internal degrees of freedom, *Prikl.Mekh.*, Vol. 28, № 8, pp. 58-63, 1992.
  - [5] E.J. Raus, *Dynamics of a system of rigid bodies*, Vol. II, Nauka, Moscow, 1983.
  - [6] V.N. Koshlyakov, *Problems in the dynamics of solid body and applied gyroscope theory: Analytical methods*, Nauka, Moscow, 1985.
  - [7] L.D. Akulenko, D.D. Leshchenko, and F.L. Chernousko, Fast motion of a heavy rigid body about a fixed point in a resistive medium, *Izv. Akad. Nauk SSSR. Mekh.Tverd.Tela [Mechanics of Solids]*, № 3, pp. 5-13, 1982.
  - [8] L.D. Akulenko, D.D. Leshchenko and A.L. Rachinskaya, Evolution of satellite fast rotation due to the gravitational torque in a dragging medium, *Izv. Ros. Akad. Nauk. Mekh.Tverd.Tela [Mechanics of Solids]*, № 2, pp. 13-26, 2008.
  - [9] L.D. Akulenko and D.D.Leshchenko, Some problems of stabilization of the bodies with internal degrees of freedom, *Mechanics of gyroscopic systems*, № 2, pp. 90-97, 1983.
  - [10] L.D. Akulenko and D.D. Leshchenko, Optimal deceleration of rotation of a rigid body with internal degrees of freedom, *Izv. Ros. Akad. Nauk. Teor.Sist.Upr[Comp.Syst.Sci]*, № 2, pp. 115-122, 1995.
  - [11] D.D.Leshchenko, Response-optimal braking of rotation of a rigid body with internal degrees of freedom, *Izv. Ros. Akad. Nauk. Teor.Sist.Upr[Comp.Syst.Sci]*, № 1, pp. 80-85, 1996.
  - [12] L.D. Akulenko, D.D. Leshchenko and A.L. Rachinskaya, Optimal deceleration of rotation of a dynamically symmetric body with a cavity filled with viscous liquid in a resistive medium, *Izv. Ros. Akad. Nauk. Teor.Sist.Upr[Comp.Syst.Sci]*, № 2, pp. 56-60, 2010.
  - [13] L.D. Akulenko, *Asymptotic methods of optimal control*, Nauka, Moscow, 1987.

## CRITICAL RE-EXAMINATION OF ADOMIAN'S DECOMPOSITION AND HOMOTOPY PERTURBATION METHODS IN NONLINEAR MECHANICS

**Igor V. Andrianov**

Institute of General  
Mechanics RWTH Aachen  
University  
Aachen, Germany

**Victor I. Olevs'kyi**<sup>1</sup>

TH – Dnipropetrovsk  
welding materials plant  
Dnepropetrovsk, Ukraine

---

ABSTRACT

---

This paper provides a systematic account of Adomian's decomposition method and the homotopy perturbation method from the standpoint of the theory of expansion in parameter for an approximate analytical integration of systems of equations in nonlinear dynamics. It was shown that approximations which have got by using those methods represent the expansions of the exact solution in the form of the Taylor series for the independent variable. A modified method of the continuation parameter is proposed, which combines both approaches. The method allows simplifying the calculations, both at the model building phase, and for its further use. Two-dimensional approximation was used of Padé type, which has shown its effectiveness for acceleration of approximations convergence and their analytic continuation. On the basis of the proposed method it was calculated solution for Riccati equation of special type, which is widely used in theory of solitons.

---

### INTRODUCTION

Adomian's decomposition method (ADM) [2,3,5] and homotopy perturbation method (HPM) [8] are widely used for an approximate analytical integration of equations in nonlinear dynamics. Recently, they have a significant impact on development of the theory of analytical solution of nonlinear equations with strong nonlinearity.

Convergence of the ADM is examined by a number of authors in different ways [2,5]. This problem for HPM is studied in Ref. [12] for the case of algebraic equations only. At the same time, the authors of the HPM and their followers do not analyze in the above cited papers the type of homotopy mapping and the properties of the obtained approximations (the existence, the area of applicability, stability, rate of convergence, etc.).

For ODEs with polynomial terms the ADM and HPM give a solution in the form of a polynomial (a series) in powers of the integration variable. Terms in the other type of ODEs can be approximated by Taylor series in powers of independent variable, desired function and its derivatives. This version of ADM is called the modified ADM (MADM) [10].

It is worth mentioning that ADM and HPM can be satisfactorily applied only with an effective method of summation. The most natural analytical continuation method is Padé approximants (PAs) [4,5]. PAs effectively solves the problem of analytical continuation of power series, and this is a basis of their successful application in the study of applied problems. Currently, the method of PAs is one of the most promising non-linear methods of summation of power series, and the localization of its singular points. PAs have turned into quite a separate section in the approximation theory, and they found a variety of applications in the study of differential equations depending on a parameter. Recently, the method of PAs for single-variable functions (1-D PAs) has been successfully extended to the approximation of two variable functions (2-D PAs) [13].

In some cases, solutions of both ADM and HPM methods coincide, but this is not always the case. A natural question arises about the correlation of ADM and HPM. Note that for non-linear

---

<sup>1</sup> Corresponding author. Email [volevnew@gmail.com](mailto:volevnew@gmail.com)

algebraic equations, this question was recently resolved in Ref. [9] and a coincidence of approximations due to certain selection of parameters was shown. In the case of ODEs, both methods can be combined on the basis of a new synthetic approach, the development of which this work is devoted to.

## 1. A SYSTEMATIC ACCOUNT AND COMPARISON OF METHODS

Let us introduce a formal definition of ADM and HPM for systems of ODEs using the terminology of the perturbation method. It is known that in vicinity of regular point any ODE or system of ODEs may be represented by a normal system of ODEs of the first order in respect to the unknown functions  $\{u_i = u_i(\xi)\}_{i=1}^n$  on the interval  $\Omega: \xi \in ]0,1[$  with the BC on the bounds  $\partial\Omega: \xi = 0 \cup 1$

$$Lu_i + R_i(\xi, u_1, \dots, u_n) + N_i(\xi, u_1, \dots, u_n) = g_i(\xi), G_i(u_1, \dots, u_n)|_{\partial\Omega} = 0, L = \frac{d}{d\xi}, i = \overline{1, n} \quad (1)$$

Here  $L$  and  $R_i$  are the linear operators,  $N_i$  and  $G_j$  are the non-linear operators. We assume also that the point  $\xi_0 = 0$  belongs to closure  $\Omega$ , and  $R_i$ ,  $N_i$  and  $G_j$  are the holomorphic functions for  $\{u_i\}_{i=1}^n$ . According to ADM, the solution represents in the form

$$Lu_{ij}^A = A_{ij}, u_i = \sum_{j=0}^{\infty} u_{ij}^A, i = \overline{1, n}, j = \overline{0, \infty} \quad (2)$$

where  $A_{ij}$  are the Adomian's polynomials [3], defined by the formulas

$$A_{i0} = g_i, A_{ij} = -\frac{1}{j!} \frac{\partial^j}{\partial \lambda^j} \left( N_i \left( \sum_{m=0}^j u_{im}^A \lambda^m \right) + R_i \left( \sum_{m=0}^j u_{im}^A \lambda^m \right) \right) \Big|_{\lambda=0}, i = \overline{1, n}, j = \overline{1, \infty} \quad (3)$$

As it was shown in Ref. [5], ADM is equivalent to the perturbation of the governing equation and its solution in respect of parameter  $\lambda$  which is introduced as follows

$$u_i = \sum_{j=0}^{\infty} u_{ij}^A \lambda^j, Lu_i + \lambda (R_i(u_1, \dots, u_n) + N_i(u_1, \dots, u_n)) = g_i, i = \overline{1, n}$$

According to the HPM governing BVP has to be written in the following form

$$Lu_i - Lu_i|_{\partial\Omega} + R_i(\{u_k\}_{k=1}^n) + N_i(\{u_k\}_{k=1}^n) + F(Lu_1, \{u_k\}_{k=1}^n) \delta_i^1 - g_i = 0 \\ G_i(\{u_k|_{\partial\Omega}\}_{k=1}^n) \Big|_{\partial\Omega} = 0, i = \overline{1, n} \quad (4)$$

where  $F$  is the non-linear differential operator,  $\delta_i^1$  is the Kronecker's delta,  $u_i|_{\partial\Omega}$  are the so-called «trial» functions that satisfy the BCs [8]. We have to introduce a parameter  $\varepsilon$  as follows to obtain the sequence of BVPs for the HPM

$$Lu_i + \varepsilon (Lu_i|_{\partial\Omega} + R_i + N_i + F \delta_i^1 - g_i) = 0, G_i(\{u_k|_{\partial\Omega}\}_{k=1}^n) \Big|_{\partial\Omega} = 0, u_i = \sum_{j=0}^{\infty} u_{ij}^H \varepsilon^j, i = \overline{1, n} \quad (5)$$

Consider  $\{u_i = u_i(\xi)\}_{i=1}^n$  and their derivatives as independent arguments, we introduce operators  $R_i$ ,  $N_i$ ,  $F$  and  $G_j$  as multidimensional Taylor series

$$\begin{aligned}
R_i + N_i &= \sum_{j=1}^n \left( N_{ij} u_j + \frac{1}{2} \sum_{p=1}^n N_{ijp} u_j u_p + \dots \right), F = \left( F_0 L u_1 + \frac{1}{2!} \sum_{p=1}^n F_{0p} u_p L u_1 + \dots \right) + \sum_{j=1}^n \left( F_j u_j + \frac{1}{2} \times \right. \\
&\times \left. \sum_{p=1}^n F_{jp} u_j u_p + \dots \right), G_i = \sum_{q=1}^n \left( G_{iq} (u_q - u_q|_{\partial\Omega}) + \frac{1}{2} \sum_{p=1}^n G_{iqp} (u_q - u_q|_{\partial\Omega}) (u_p - u_p|_{\partial\Omega}) + \dots \right), i = \overline{1, n} \\
N_{ij} &= \sum_{r=0}^{\infty} N_{ij}^r \xi^r, N_{ijp} = \sum_{r=0}^{\infty} N_{ijp}^r \xi^r, \dots, F_i = \sum_{r=0}^{\infty} F_i^r \xi^r, F_{ij} = \sum_{r=0}^{\infty} F_{ij}^r \xi^r, \dots, g_i = \sum_{j=0}^{\infty} g_{ij} \xi^j, i, j = \overline{1, n}
\end{aligned} \tag{6}$$

Let's substitute series (6) into Eqs. (3)

$$A_{ij} = -\frac{1}{j!} \frac{\partial^j}{\partial \lambda^j} \left( \sum_{r=1}^n \left( N_{ir} u_r + \frac{1}{2!} \sum_{p=1}^n N_{irp} u_r u_p + \dots \right) \right) \Big|_{\lambda=0} = -\sum_{r=1}^n (N_{ir} u_{rj}^A + \sum_{p=1}^n N_{irp} \sum_{k=0}^j u_{rk}^A u_{p(j-k)}^A + \dots) \tag{8}$$

We obtain successive approximations for the ADM:

$$\begin{aligned}
u_i &= \xi^0 \left( [u_i|_{\partial\Omega}] + [0] + [0] + \dots \right) + \\
&+ \xi^1 \left( [g_{i0}] + \left[ - \left( \sum_{j=1}^n \left( N_{ij}^0 + \frac{1}{2!} \sum_{p=1}^n N_{ijp}^0 u_j|_{\partial\Omega} u_p|_{\partial\Omega} \right) + \dots \right) \right] + [0] + \dots \right) + \dots, i = \overline{1, n}
\end{aligned} \tag{9}$$

For the HPM one obtains:

$$\begin{aligned}
u_1 &= \xi^0 \left( [u_1|_{\partial\Omega}] + [0] + [0] + \dots \right) + \xi^1 \left( [0] + [g_{10} - \sum_{r=1}^n ((N_{1r}^0 + F_r^0) u_r|_{\partial\Omega} + \right. \\
&\left. \frac{1}{2!} \sum_{p=1}^n (N_{1rp}^0 + F_{rp}^0) u_r|_{\partial\Omega} u_p|_{\partial\Omega} + \dots) \right] + \left[ - \left( F_0^0 + F_{00}^0 \sum_{p=1}^{\infty} u_p|_{\partial\Omega} \right) \left( g_{10} - \sum_{r=1}^n ((N_{1r}^0 + F_r^0) u_r|_{\partial\Omega} + \right. \right. \\
&\left. \left. + \frac{1}{2!} \sum_{p=1}^n (N_{1rp}^0 + F_{rp}^0) u_r|_{\partial\Omega} u_p|_{\partial\Omega} + \dots) \right) \right] + \dots \right) + \dots, u_i = \xi^0 \left( [u_i|_{\partial\Omega}] + [0] + [0] + \dots \right) + \\
&+ \xi^1 \left( [0] + \left[ g_{i0} - \sum_{r=1}^n \left( N_{ir}^0 u_r|_{\partial\Omega} + \frac{1}{2!} \sum_{p=1}^n N_{irp}^0 u_r|_{\partial\Omega} u_p|_{\partial\Omega} + \dots \right) \right] + [0] + \dots \right) + \dots, i = \overline{2, n}
\end{aligned} \tag{10}$$

The brackets contain the expression corresponding to the successive approximations in powers of the parameter.

Comparison of the ADM and HPM are based on the comparison of the nonlinear operators in ODEs in normal and general forms. If one takes into account terms up to the second order in the Eqs. (6), the normal form of Eqs. (4) can be written as follows

$$\begin{aligned}
L u_1 + \sum_{j=1}^n \left( \frac{N_{1j} + F_j}{1 + F_0} u_j + \frac{1}{2} \sum_{p=1}^n \frac{(N_{1jp} + F_{jp})(1 + F_0) - F_{0p}(N_{1j} + F_j) - F_{0j}(N_{1p} + F_p)}{2(1 + F_0)^2} u_j u_p \right) &= \\
= \frac{g_1}{1 + F_0}, L u_i + R_i(u_1, \dots, u_n) + N_i(u_1, \dots, u_n) &= g_i, i = \overline{2, n}
\end{aligned} \tag{11}$$

In other words, in this case ADM applied to Eqs. (11) is equivalent to the HPM applied to Eqs. (4).

There are several special cases that are interesting to consider from a practical point of view. Thus, for singular perturbed nonlinear equations for  $F_j \equiv F_{jp} \equiv 0$ ,  $j, p = \overline{1, n}$  from the Eqs. (9) - (10) we obtain

$$Lu_1 + \sum_{j=1}^n \left( \frac{N_{1j}}{\varepsilon} u_j + \frac{1}{2} \sum_{p=1}^n \frac{N_{1jp}}{2\varepsilon} u_j u_p \right) = \frac{g_1}{\varepsilon}, u_1 = \xi^0 u_1|_{\partial\Omega} + \xi^1 \left( (g_{10} - \sum_{r=1}^n (N_{1r}^0 u_r|_{\partial\Omega} + \frac{1}{2!} \sum_{p=1}^n N_{1rp}^0 u_r|_{\partial\Omega} u_p|_{\partial\Omega} + \dots) - (\varepsilon - 1) \left( g_{10} - \sum_{r=1}^n (N_{1r}^0 u_r|_{\partial\Omega} + \frac{1}{2!} \sum_{p=1}^n N_{1rp}^0 u_r|_{\partial\Omega} u_p|_{\partial\Omega} + \dots) \right) + \dots \right) + \dots$$

In other words, the coefficients in the power of the independent variable in the HPM solution represent expansion of coefficients of ADM on the natural small parameter in the vicinity of  $x = 1$ .

## 2. USING THE PAS

From Eqs. (10) and (11) we see that, if the equation is solved in respect to the highest derivative, the coefficients with the same degree of variable solutions ADM and HPM converges each to other as far as order of approximation increases. It was shown in Ref. [5] that the solution of the ADM converges to the decomposition of exact solution in Taylor series in the area of its holomorphy in the vicinity of  $x = 0$ . That is the reason that the same properties will have a solution of HPM in the case when equation is in normal form. This allows the use meromorphic continuation in the form of PAs [5].

For ADM such a continuation procedure was proposed in Ref. [5]. Later, this approach has been developed by a number of authors [1, 7], and was named the modified Adomian's decomposition method and PAs (MADM-Padé). Thus, it is possible to use PAs to HPM with modifications, by decomposition of nonlinear terms in the series as for the independent variable, so for the desired function (MHPM-Padé).

2-D PAs in the form of V. Vavilov [13] has a great promise for use as an analytic continuation. This technique allows us to choose the coefficients of 2-D Taylor series for construction of an unambiguous 2-D PA with a given structure of the numerator and denominator, as well as ensures optimal PAs features in the sense of Theorem Montessus de Ballore-type. That is means the homogenous convergence of PA to approximated function with increasing of the degree of the numerator and the denominator in all points of its meromorphy area. It should be noted that direct application of 2-D PAs does not leads to the anticipated merging of 1-D approximations. This is due to the initial requirements to the 2-D approximation to ensure its transition to 1-D in the case when the second variable equal to zero [13]. At the same time as for the method of parameter continuation it is necessary to ensure such a transition when parameter is equal to one. This can be achieved by combining of this method with 2-D PAs from a converted parameter, which maps the unit to zero.

## 3. MODIFIED METHOD OF THE PARAMETER CONTINUATION

The modified method of the parameter continuation (MMPC) proposed in this paper consists of perturbation technique of special form and the analytic continuation of obtained approximations by PAs. It coincides with the HPM for  $F \equiv 0$ , and with the ADM - when  $g \equiv 0$ , and thus generalizes them. The method does not imply the introduction of «trial» functions that satisfy the BC, they will be satisfied in successive approximations, and this gives us an opportunity to solve the BVP with complicated BCs [5]. To implement the MMPC, we introduce a parameter  $\varepsilon$  as follows

$$Lu_i = \varepsilon \left( g_i - R_i(\{u_k\}_{k=1}^n) - N_i(\{u_k\}_{k=1}^n) \right), G_i(\{u_k|_{\partial\Omega}\}_{k=1}^n)|_{\partial\Omega} = 0, u_i = \sum_{j=0}^{\infty} u_{ij}^M \varepsilon^j, i = \overline{1, n} \quad (13)$$

Substitute the power series into Eqs. in (13) and split it with respect to the powers of  $\varepsilon$ , after summation of the coefficients with the same degrees of  $\xi$  for  $\varepsilon = 1$ , we get

$$u_i = \xi^0 \left( [u_i|_{\partial\Omega}] + [0] + [0] + \dots \right) + \xi^1 \left( [0] + \left[ g_{i0} - \sum_{r=1}^n \left( N_{ir}^0 u_r|_{\partial\Omega} + \frac{1}{2!} \sum_{p=1}^n N_{irp}^0 u_r|_{\partial\Omega} u_p|_{\partial\Omega} + \dots \right) \right] + [0] + \dots \right) + \dots, i = \overline{1, n} \quad (14)$$

Approximation thus obtained is converted to 1-D PA in respect to  $\xi$  or 2-D PA.. MMPC approximation is simpler than ADM and HPM. Analysis of the obtained approximation suggests that, in contrast to the ADM and HPM, it gives the exact value of the coefficients in the power of the independent variable to the extent equal to the order of approximation (taking into account the expansion in power series of expressions in the equation). This guarantees the stability of computation with a limit-order approximation of the independent variable.

One of the possible fields for application of the proposed approach is the nonlinear problems of plates and shells dynamics theory [12]. The equations of dynamics of geometrically nonlinear thin-walled structures can be reduced to the resolving equations which contain the products and squares of the desired functions and their derivatives. In this case the solution of Eqs. (14) can be written without three dots.

#### 4. NUMERICAL RESULTS

Let us consider the computational aspects of the proposed approach on following BVPs

$$\alpha z' + z = 1, z(0) = 0, x \geq 0, \alpha = 0,1 \quad (15)$$

$$\alpha z' = -z^2 + x - 1, z(0) = 1, x \geq 0, \alpha = 0,2 \quad (16)$$

We consider three types of PAs - on the independent variable  $z_{(x)}$ , on the specified parameters  $z_{(\varepsilon)}$ , and 2-D -  $z_{(2)}$ . Typical behavior of approximations for the BVP (15) shown in Fig. 1a. ADM approximation describes the exact solution well only for a distance which is comparable with the value of the natural small parameter  $\alpha$ . Despite the fact that the error of solutions HPM is substantially less than the ADM, HPM is not accurately reflect the nature of solutions, namely the phenomenon of boundary layer in vicinity to zero. At the same time, PAs for the ADM approximations for independent variable and PAs for the MMPC (1-D and 2-D) give satisfactory qualitative and quantitative results.

A more complex picture arises when considering the significantly non-linear inhomogeneous ODE, for example, the type of special Riccati equation (16). For the Riccati equation, which is not solved in quadrature, cites a number of problems of optimal control theory, in some cases nonlinear differential equations of Painlevé are reduced to it, which are successfully used now in the theory of solitons. Fig. 1b shows graphs of approximations for BVP (16).

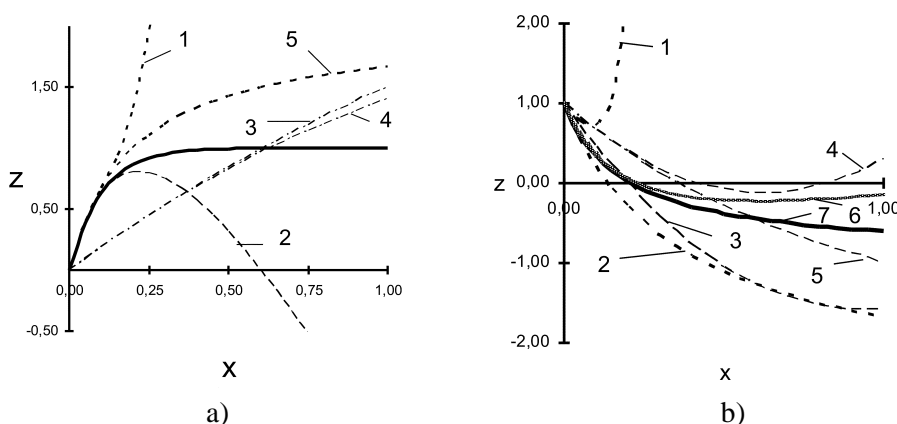


Fig. 1 Solutions of BVPs by different methods.

a – for BVP (15): solid line - the exact solution, 1 – three terms ADM, 2 –  $z_{(\varepsilon)}$  for ADM, 3 – three terms HPM, 4 –  $z_{(x)}$  for HPM, 5 – 2-D Padé  $z_{(2)}$  for MMPC, ADM and HPM; .b - for BVP (16): 1 – three terms ADM, 2 –  $z_{(\varepsilon)}$  for ADM, 3 –  $z_{(\varepsilon)}$  for ADM, , 4 – three terms HPM, 5 –  $z_{(x)}$  for HPM, 6 –  $z_{(\varepsilon)}$  for HPM and MMPC, 7 –  $z_{(x)}$  and 2-D Padé  $z_{(2)}$  for MMPC

The graphs show that the solution is described well by HPM approximation and MHPM-Padé «in average», and badly - in the boundary layer. ADM approximation and MADM-Padé, on the contrary, is in good agreement with the behavior of solution in vicinity of zero and in the bad one - on

the stationary part. At the same time, 1-D and 2-D PAs, based on approximations of the MMPC, is well described the solution on the whole interval.

## CONCLUSIONS

This paper gives a systematic description of Adomian's decomposition method and homotopy perturbation method. Here were obtained analytical expressions for calculating the coefficients of approximation for these methods. We conducted a comparison between the approximations and identified the conditions when they coincide.

We propose a modified method of the parameter continuation (MMPC) that combines both approaches. This method allows to simplifying the calculations both at the stage of constructing the model, and also within its continuation use due to the precise values of the Taylor coefficients for the solution of the degree which is not exceeding the number of approximation. We present the expression to calculate approximations by the MMPC in the general case and with the nonlinearity type of products and squares of the desired functions.

We analyzed using of fractional-rational transformation for the polynomial approximation in the form of the 1-D and 2-D PAs which is used to increase degree of convergence and for analytic continuation of the approximation in the region of its meromorphy. It was concluded that such a transformation is justified if it is applied to polynomials which depend on the variable of integration. We used 2-D PAs for the independent variable and for the artificial parameter using the scheme of V.°Vavilov. In this paper we have shown that this transformation provides a satisfactory quality for the approximation behavior and minimize its error, in spite of the fact that usage of 2-D PAs requires further theoretical justification.

We conducted a study of numerical results by applying the methods for model examples which were perturbed with natural small parameter. It is shown that the application of PAs provides them a sufficient accuracy in the studied area. In this paper it is shown the advantage of the approximations which were obtained on the basis of the MMPC.

## REFERENCES

- [1] T.A. Abassy , M.A. El-Tawil, and H.K. Saleh, The solution of Burgers' and good Boussinesq equations using ADM– Padé technique, *Chaos, Solitons and Fractals*, 32, pp. 1008-1026, 2007.
- [2] K. Abbaoui and Y. Cherruault, Convergence of Adomian's method applied to differential equations, *Comp. Math. Appl.*, 28, pp. 103-109, 1994.
- [3] G. Adomian, A review of the decomposition method and some recent results for nonlinear equations, *Comp. Math. Appl.*, 21, pp. 101-127, 1989.
- [4] I. Andrianov, J. Awrejcewicz, and A. Ivankov, Artificial small parameter method – solving of mixed boundary value problems, *Mathematical Problems in Engineering (Open Access Journal)*, 3, pp. 325-340, 2005.
- [5] I.V. Andrianov, V.I. Olevskij, and S. Tokarzhevskij, A modified Adomian's decomposition method, *J. Appl. Math. Mech.*, 62 (2), pp. 309-314, 1998 (in Russian); English cover-to-cover translation from *Prikl. Mat. Mekh.*, 62 (2), pp. 334-339, 1998.
- [6] J. Awrejcewicz, I. V. Andrianov, and L. I. Manevitch, *Asymptotic Approaches in Nonlinear Dynamics: New Trends and Applications*, Springer Series in Synergetics, Springer, Berlin, 1998.
- [7] M. Chrysos, F. Sanchez, and Y. Cherruault, Improvement of convergence of Adomian's method using Pade' approximants, *Kybernetes*, 31 (6), pp. 884-895, 2002.
- [8] J.H. He, Recent developments of the homotopy perturbation method, *Top. Meth. Nonlin. Anal.*, 31, pp. 205-209, 2008.
- [9] Jian-Lin Li, Adomian's decomposition method and homotopy perturbation method in solving nonlinear equations, *J. Comp. Appl. Math.*, 228 (1), pp. 168-173, 2009.
- [10] Jung-Chang Hsu, Hsin-Yi Lai, and C.K. Chen, Free vibration of non-uniform Euler–Bernoulli beams with general elastically end constraints using Adomian modified decomposition method, *Journal of Sound and Vibration*, 318, pp. 965-981, 2008.
- [11] S. J. Liao, *Beyond Perturbation - Introduction to the Homotopy Analysis Method*, Chapman & Hall/CRC, Boca Raton, 2003.
- [12] A. H. Nayfeh and B. Balachandran, *Applied Nonlinear Dynamics*, Wiley Interscience, New York, 1995.
- [13] V. V. Vavilov, M. K. Tchobanou, and P. M. Tchobanou, Design of multidimensional recursive systems through Padé type rational approximation, *Nonlinear Analysis: Modelling and Control*, 7 (1), pp. 105-125, 2002.

## BIFURCATIONS OF ELASTIC ROTORS IN JOURNAL BEARINGS

**Konstantin V. Avramov**<sup>1</sup>

A.N. Podgorny Institute for  
Mechanical Engineering  
Problems  
Kharkov, Ukraine

**Oleksii V. Borysiuk**

NTU KhPI  
Kharkov, Ukraine

### ABSTRACT

The model of nonlinear vibrations of one disk rotor supported by two journal bearing is obtained. The fluid film of journal bearing is described by the Reynolds' equation. Shaw-Pierre nonlinear modes, harmonic balance method and continuation technique are used to study the rotor dynamics. Self-sustained vibrations of the rotor take place at rotor angular velocity much lower than the angular velocity of Hopf bifurcation. These self vibrations occur due to saddle-node bifurcations.

### INTRODUCTION

Self-sustained vibrations of rotors take place due to influence of carrier fluid film on the rotor motions. Self-sustained vibrations lead up to failure of several turbines [1]. Now the modern methods of nonlinear dynamics are used to analyze the self-sustained vibrations of rotors [2]. Akers [3] analyzed the pressure of a fluid film of the journal bearing. Poznjak [4] analytically describe the pressure of fluid film as a function of general coordinates, velocities and acceleration. Olimpiev [5] obtained the asymptotic solution of the Reynolds' equation using the variational approach. Karintsev, Shul'genko [6] obtained the model of pressure in fluid film of short journal bearings. The vibrations of symmetric rotor supported by short journal bearings are treated in [7]. Ovcharova, Goloskokov [8] analyzed the rotor forced vibrations accounting short journal bearings. They described the shaft dynamics by three discrete masses. Muszynska [9, 10] considers the symmetric rotor with one journal bearing. The mathematical model of rotor dynamics based on experimental data is treated.

In this paper one disk rotor supported by two journal bearings are considered. Shaw-Pierre nonlinear modes are used to study self-sustained vibrations of rotor.

### 1. PROBLEM FORMULATION AND MAIN EQUATIONS

It is assumed that the disk is rigid and the shaft is elastic (Fig.1). The shaft is supported by two short journal bearings.

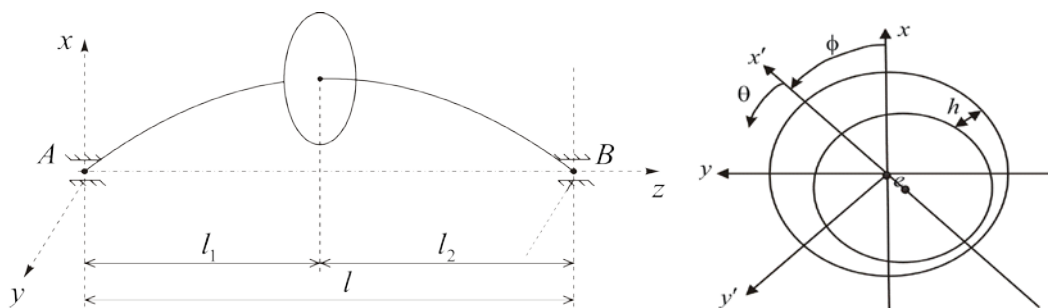


Fig. 1 Sketch of one disk rotor

During disk vibrations, the parts of the shaft in journal bearings A and B are vibrated too. The vibrations of the journals A and B (Fig.1) is described by the general coordinates  $(x_1, y_1)$  and

<sup>1</sup>Corresponding author. Email [kavramov@kharkov.ua](mailto:kavramov@kharkov.ua).

$(x_2, y_2)$ , respectively. Two journal bearings are identical. Forces of carrier fluid film occur due to journal motions. The projections of these forces on the axes  $x$  and  $y$  are denoted by  $F_x(x_i; y_i)$ ;  $F_y(x_i; y_i)$ ;  $i = \overline{1,2}$ . The rotor is rotated with constant angular velocity  $\Omega$  about  $z$  axes; the angular velocity of the disk has the following form:

$$\begin{aligned}\vec{\omega} &= \omega_1 \vec{e}_1 + \omega_2 \vec{e}_2 + \omega_3 \vec{e}_3 \\ \omega_1 &= \dot{\theta}_1 \cos \theta_2 \cos \theta_3 + \dot{\theta}_2 \sin \theta_3 \\ \omega_2 &= \dot{\theta}_2 \cos \theta_3 - \dot{\theta}_1 \cos \theta_2 \sin \theta_3 \\ \omega_3 &= \dot{\theta}_3 + \dot{\theta}_1 \sin \theta_2\end{aligned}\quad (1)$$

Then angular velocity of the rotor has following form:  $\Omega = \dot{\theta}_3 + \dot{\theta}_1 \sin \theta_2$ . The kinetic energy of the disk are the following form:

$$T = \frac{I_e}{2} (\dot{\theta}_2^2 + \dot{\theta}_1^2 \cos^2 \theta_2) + \frac{I_p}{2} (\dot{\theta}_3 + \dot{\theta}_1 \sin \theta_2)^2 + \frac{m}{2} (\dot{x}^2 + \dot{y}^2) \quad (2)$$

where  $x, y$  are displacements of the point, when the axis of the shaft and the disk are intersected;  $I_e, I_p$  are diametrical and polar moment of inertia of the rotor, respectively. The shaft potential energy has the following form:

$$\begin{aligned}\Pi &= \frac{1}{2} c_{11} \left[ (x - \varsigma_1 x_2 - \varsigma_2 x_1)^2 + (y - \varsigma_2 y_1 - \varsigma_1 y_2)^2 \right] + \\ &+ \frac{1}{2} c_{22} \left[ \left( \theta_2 - \frac{x_2 - x_1}{l} \right)^2 + \left( \theta_1 + \frac{y_2 - y_1}{l} \right)^2 \right] + \\ &+ c_{12} \left[ (x - \varsigma_1 x_2 - \varsigma_2 x_1) \left( \theta_2 - \frac{x_2 - x_1}{l} \right) - (y - \varsigma_2 y_1 - \varsigma_1 y_2) \left( \theta_1 + \frac{y_2 - y_1}{l} \right) \right]\end{aligned}\quad (3)$$

where  $c_{11}, c_{22}, c_{12}$  are elements of stiffness matrix,  $\varsigma_1 = \frac{l_1}{l}$ ;  $\varsigma_2 = \frac{l_2}{l}$ .

The equations of system motions with respect to the general coordinates  $(x, y, \theta_1, \theta_2, x_1, y_1, x_2, y_2)$  have the following form:

$$\begin{aligned}m\ddot{x} + c_{11}(x - \varsigma_1 x_2 - \varsigma_2 x_1) + c_{12} \left( \theta_2 - \frac{x_2 - x_1}{l} \right) &= -mg \\ m\ddot{y} + c_{11}(y - \varsigma_1 y_2 - \varsigma_2 y_1) - c_{12} \left( \theta_1 + \frac{y_2 - y_1}{l} \right) &= 0 \\ I_e \ddot{\theta}_1 \cos^2 \theta_2 - I_e \dot{\theta}_1 \dot{\theta}_2 \sin 2\theta_2 + I_p \ddot{\theta}_3 \sin \theta_2 + I_p \Omega \dot{\theta}_2 \cos \theta_2 - \frac{I_p}{2} \dot{\theta}_1 \dot{\theta}_2 \sin 2\theta_2 + \\ + I_p \ddot{\theta}_1 \sin^2 \theta_2 + I_p \dot{\theta}_1 \dot{\theta}_2 \sin 2\theta_2 + c_{22} \left( \theta_1 + \frac{y_2 - y_1}{l} \right) - c_{12} (y - \varsigma_2 y_1 - \varsigma_1 y_2) &= 0 \\ I_e \ddot{\theta}_2 + \frac{I_e}{2} \dot{\theta}_1^2 \sin(2\theta_2) - I_p \Omega \dot{\theta}_1 \cos \theta_2 + c_{22} \left( \theta_2 - \frac{x_2 - x_1}{l} \right) + c_{12} (x - \varsigma_1 x_2 - \varsigma_2 x_1) &= 0 \\ \left( \frac{c_{12}}{l} - \varsigma_2 c_{11} \right) (x - \varsigma_1 x_2 - \varsigma_2 x_1) + \left( \frac{c_{22}}{l} - \varsigma_2 c_{12} \right) \left( \theta_2 - \frac{x_2 - x_1}{l} \right) &= F_x(x_1, y_1)\end{aligned}\quad (4)$$

$$\begin{aligned}
& \left( \frac{c_{12}}{l} - \zeta_2 c_{11} \right) \left( y - \zeta_1 y_2 - \zeta_2 y_1 \right) + \left( \zeta_2 c_{12} - \frac{c_{22}}{l} \right) \left( \theta_1 + \frac{y_2 - y_1}{l} \right) = F_y(x_1, y_1) \\
& \left( \zeta_1 c_{11} + \frac{c_{12}}{l} \right) \left( x - \zeta_1 x_2 - \zeta_2 x_1 \right) + \left( \frac{c_{22}}{l} + \zeta_1 c_{12} \right) \left( \theta_2 - \frac{x_2 - x_1}{l} \right) = -F_x(x_2, y_2) \\
& \left( \frac{c_{22}}{l} + \zeta_1 c_{12} \right) \left( \theta_1 + \frac{y_2 - y_1}{l} \right) - \left( \zeta_1 c_{11} + \frac{c_{12}}{l} \right) \left( y - \zeta_2 y_1 - \zeta_1 y_2 \right) = F_y(x_2, y_2)
\end{aligned}$$

Under the action of the gravity, the rotor takes up some equilibrium positions, which defines by the following values of the general coordinates:  $(\bar{x}, \bar{y}, \bar{\theta}_1, \bar{\theta}_2, \bar{x}_1, \bar{y}_1, \bar{x}_2, \bar{y}_2)$ . The rotor vibrations with respect to this equilibrium position are analyzed. Then the following change of the variables is used:

$$\begin{aligned}
& (x, y, \theta_1, \theta_2, x_1, y_1, x_2, y_2) \rightarrow \\
& \rightarrow (\bar{x} + x, \bar{y} + y, \bar{\theta}_1 + \theta_1, \bar{\theta}_2 + \theta_2, \bar{x}_1 + x_1, \bar{y}_1 + y_1, \bar{x}_2 + x_2, \bar{y}_2 + y_2)
\end{aligned} \tag{5}$$

As a result the following dynamical system is derived:

$$\begin{aligned}
m \ddot{x} &= R_X^{(1)} & I_e \ddot{\theta}_2 - I_p \Omega \dot{\theta}_1 + R_X^{(2)} &= 0 \\
m \ddot{y} &= R_Y^{(1)} & I_e \ddot{\theta}_1 + I_p \Omega \dot{\theta}_2 - R_Y^{(2)} &= 0
\end{aligned} \tag{6}$$

where  $R_Y^{(1)} = \tilde{F}_Y(x_1, y_1) + \tilde{F}_Y(x_2, y_2)$ ;  $R_X^{(1)} = \tilde{F}_X(x_2, y_2) + \tilde{F}_X(x_1, y_1)$ ;

$R_Y^{(2)} = l_1 \tilde{F}_Y(x_1, y_1) - l_2 \tilde{F}_Y(x_2, y_2)$ ;  $R_X^{(2)} = l_1 \tilde{F}_X(x_1, y_1) - l_2 \tilde{F}_X(x_2, y_2)$ .

The forces of carrier fluid film of short journal bearing are obtained as:

$$F_x = - \int_0^{L_b} \int_0^\pi (\cos(\theta + \phi) p(\theta, z) R) d\theta dz; \quad F_y = - \int_0^{L_b} \int_0^\pi (\sin(\theta + \phi) p(\theta, z) R) d\theta dz \tag{7}$$

where  $L_B$  is a length of short journal bearing;  $\phi$  is an angle of center lines. It is assumed, that the fluid film is disposed in the region  $\theta \in [0; \pi]$ . The pressure of the fluid film  $p(z_1, \theta)$  is determined from the solution of Reynolds' equation [2]. This solution for the short journal bearing has the following form:

$$p = \frac{3\mu}{h^3} \left[ \Omega \frac{\partial h}{\partial \theta} + 2 \frac{\partial h}{\partial t} \right] z_1 (z_1 - L_b) \tag{8}$$

where  $\mu$  is a fluid viscosity;  $z_1$  is local longitudinal coordinate of a journal bearing. The value  $h$  is determined as:  $h = c + e \cos \theta = c - x \cos(\theta + \phi) - y \sin(\theta + \phi)$ , where  $c$  is the nominal clearance between the shaft and the bearing.

Future analysis of fluid film forces will be carried out for the journal bearing A. The obtained results are true for the journal bearing B, if the general coordinates  $(x_1, y_1)$  are changed on  $(x_2, y_2)$ .

The following dimensionless variables and parameters are used in the future analysis:

$$\tilde{x}_j = \frac{x_j}{c}; \quad \tilde{y}_j = \frac{y_j}{c}; \quad H = \frac{h}{c}; \quad \tau = \Omega t \tag{9}$$

Then the forces of the fluid film can be presented as:

$$\begin{aligned}
F_x &= \frac{L_B^3 \mu R \Omega}{2c^2} \int_0^\pi H^{-3} \cos(\theta + \phi) \{ \tilde{x}_1 \sin(\theta + \phi) - \tilde{y}_1 \cos(\theta + \phi) - 2\tilde{x}_1' \cos(\theta + \phi) - 2\tilde{y}_1' \sin(\theta + \phi) \} d\theta \\
F_y &= \frac{L_B^3 \mu R \Omega}{2c^2} \int_0^\pi H^{-3} \sin(\theta + \phi) \{ \tilde{x}_1 \sin(\theta + \phi) - \tilde{y}_1 \cos(\theta + \phi) - 2\tilde{x}_1' \cos(\theta + \phi) - 2\tilde{y}_1' \sin(\theta + \phi) \} d\theta
\end{aligned} \tag{10}$$

where  $H = 1 - \tilde{x}_1 \cos(\theta + \phi) - \tilde{y}_1 \sin(\theta + \phi)$ ;  $(\ )' = \frac{d(\ )}{d\tau}$ .

The equilibrium position of the rotor under the action of gravity is determined. Then equilibrium of the journal A can be presented as:

$$\tilde{x}_{1,0} = -\varepsilon_1 \cos \phi_{e1}; \quad \tilde{y}_{1,0} = -\varepsilon_1 \sin \phi_{e1}; \quad tg \phi_{e1} = \pi \sqrt{1 - \varepsilon_1^2} / (4\varepsilon_1) \quad (11)$$

The dynamics of the rotor with respect to the equilibriums positions is analyzed. Then the change of the variables (5) is rewritten with respect to dimensionless variables:  $\tilde{x}_i \rightarrow \tilde{x}_i + \tilde{x}_{i,0}$ ;  $\tilde{y}_i \rightarrow \tilde{y}_i + \tilde{y}_{i,0}$ ;  $i = 1, 2$ . Then the nonlinear forces (10) are presented as power series with respect to  $\tilde{x}_1, \tilde{y}_1, \tilde{x}'_1, \tilde{y}'_1$ :

$$\begin{aligned} F_X &= F_{X,0} + F_{X,1}(\tilde{x}_1, \tilde{y}_1, \tilde{x}'_1, \tilde{y}'_1) + F_{X,2}(\tilde{x}_1, \tilde{y}_1, \tilde{x}'_1, \tilde{y}'_1) + F_{X,3}(\tilde{x}_1, \tilde{y}_1, \tilde{x}'_1, \tilde{y}'_1) + \dots \\ F_Y &= F_{Y,0} + F_{Y,1}(\tilde{x}_1, \tilde{y}_1, \tilde{x}'_1, \tilde{y}'_1) + F_{Y,2}(\tilde{x}_1, \tilde{y}_1, \tilde{x}'_1, \tilde{y}'_1) + F_{Y,3}(\tilde{x}_1, \tilde{y}_1, \tilde{x}'_1, \tilde{y}'_1) + \dots \end{aligned} \quad (12)$$

where  $F_{X,0}; F_{Y,0}$  are constant parts of fluid film forces;  $F_{X,1}; F_{Y,1}$  are linear parts of forces with respect to  $\tilde{x}_1, \tilde{y}_1, \tilde{x}'_1, \tilde{y}'_1$ ;  $F_{X,2}; F_{Y,2}; F_{X,3}; F_{Y,3}$  are nonlinear parts of the forces of the second and the third orders with respect to the general coordinates and velocities. The nonlinear forces (12) are substituted into (6). As the result, the equations of rotor motions have the following matrix form:

$$[M]\ddot{q} + [G]\dot{q} = [K_1]q + [D_1]q' + W(q_1, q'_1) \quad (13)$$

where  $q = [x, \theta, y, \theta_2]^T$ ;  $q_1 = [\tilde{x}_1, \tilde{y}_1, \tilde{x}_2, \tilde{y}_2]^T$ ;  $W(q_1, q'_1)$  are vector of nonlinear parts of forces (12). Nonlinear terms within the cubic summands of  $q$  and  $\dot{q}$  are included in the model of self-sustained vibrations of rotor.

## 2. THE METHOD OF DYNAMICS ANALYSIS

Now the nonlinear modes for self-sustained vibrations analysis are considered. The motions of the system (13) close to the Hopf bifurcation are analyzed. Then the linear part of the system (13) can be presented as:

$$\dot{z} = \begin{bmatrix} 0 & E \\ -Q & -F \end{bmatrix} z = [\Gamma] z \quad (14)$$

where  $z = [z_1, \dots, z_8] = [q \ \dot{q}]^T = [q \ v]^T$ ;  $E$  is an identity matrix. As follows from the results of the numerical simulations, all eigenvalues of the matrix  $[\Gamma]$  are complex conjugate; the solution of the system (14) has the following form:

$$z(t) = \sum_{j=1}^4 [C_{2j} W_{2j} \exp(\lambda_{2j} t) + C_{2j-1} W_{2j-1} \exp(\lambda_{2j-1} t)] \quad (15)$$

where  $\lambda_{2j} = \bar{\lambda}_{2j-1}$ ;  $W_{2j} = \bar{W}_{2j-1}$ ;  $C_{2j} = \bar{C}_{2j-1}$ ;  $(\bar{\ })$  is denoted the complex conjugation.

If the equilibrium position loses stability, then in this bifurcation point two characteristics exponents have the following values:  $\lambda_{1,2} = \pm i \chi_1$ . The rotor loss of stability describes by the following particular solution of the system (15):  $z(t) = C_2 W_2 \exp(\lambda_2 t) + C_1 W_1 \exp(\lambda_1 t)$ , where  $W_1 = \gamma_1 - i\delta_1$ ;  $C_1 = K_1^{(1)} - iK_1^{(2)}$ ;  $\lambda_1 = \alpha_1 - i\chi_1$ ;  $K_1^{(1)}, K_1^{(2)}$  are constants of integration;  $\gamma_1 = \{\gamma_1^{(1)}, \dots, \gamma_1^{(8)}\}$ ;  $\delta_1 = \{\delta_1^{(1)}, \dots, \delta_1^{(8)}\}$ . This solution can be presented as

$$z_\nu(t) = \gamma_1^{(\nu)} \eta_1(t) + \delta_1^{(\nu)} \eta_2(t); \quad \nu = \bar{1}, 8 \quad (16)$$

where

$$\begin{aligned}\eta_1(t) &= 2 \exp(\alpha_1 t) \left[ K_1^{(1)} \cos(\chi_1 t) - K_1^{(2)} \sin(\chi_1 t) \right]; \\ \eta_2(t) &= -2 \exp(\alpha_1 t) \left[ K_1^{(1)} \sin(\chi_1 t) + K_1^{(2)} \cos(\chi_1 t) \right].\end{aligned}$$

The following equation is true:

$$x = \gamma_1^{(1)} \eta_1(t) + \delta_1^{(1)} \eta_2(t); \quad \dot{x} = \gamma_1^{(5)} \eta_1(t) + \delta_1^{(5)} \eta_2(t)$$

These two equations can be rewritten as

$$\eta_1(t) = \frac{x \delta_1^{(5)} - \dot{x} \delta_1^{(1)}}{\gamma_1^{(1)} \delta_1^{(5)} - \gamma_1^{(5)} \delta_1^{(1)}}; \quad \eta_2(t) = \frac{\dot{x} \gamma_1^{(1)} - x \gamma_1^{(5)}}{\gamma_1^{(1)} \delta_1^{(5)} - \gamma_1^{(5)} \delta_1^{(1)}} \quad (17)$$

Combining (16) and (17), the linear part of the nonlinear mode is obtained as

$$\begin{bmatrix} \theta_1 \\ y \\ \theta_2 \\ \dot{\theta}_1 \\ \dot{y} \\ \dot{\theta}_2 \end{bmatrix} = \begin{bmatrix} a_{21} & a_{22} \\ a_{31} & a_{32} \\ a_{41} & a_{42} \\ a_{61} & a_{52} \\ a_{71} & a_{62} \\ a_{81} & a_{72} \end{bmatrix} \begin{bmatrix} x \\ \dot{x} \end{bmatrix} \quad (18)$$

where  $a_{\nu 1} = \frac{\gamma_1^{(\nu)} \delta_1^{(5)} - \delta_1^{(\nu)} \gamma_1^{(5)}}{\gamma_1^{(1)} \delta_1^{(5)} - \gamma_1^{(5)} \delta_1^{(1)}}; a_{\nu 2} = \frac{\delta_1^{(\nu)} \gamma_1^{(1)} - \gamma_1^{(\nu)} \delta_1^{(1)}}{\gamma_1^{(1)} \delta_1^{(5)} - \gamma_1^{(5)} \delta_1^{(1)}}; \nu = 2, \dots, 8; \nu \neq 5$ .

The nonlinear terms are added into the equation (18) to study nonlinear modes of the self-sustained vibrations. Then the nonlinear mode can be presented as

$$\begin{aligned}q_j &= Q_j(x, v) = a_{j1} x + a_{j2} v + a_{j3} x^2 + a_{j4} v^2 + a_{j5} xv + \dots \\ \dot{q}_j &= Q_{j+4}(x, v) = a_{4+j,1} x + a_{4+j,2} v + a_{4+j,3} x^2 + a_{4+j,4} v^2 + a_{4+j,5} xv + \dots; j = \overline{2, 4}\end{aligned} \quad (19)$$

In order to obtain coefficients of the nonlinear part (19) classical Shaw-Pierre nonlinear modes are used [11].

In order to obtain the motions, which are not nonlinear modes, harmonic balance method is used. Then the motions can be presented in the following form:

$$\begin{aligned}x &= A_0 + A_1 \cos(\omega t) & \theta_1 &= B_0 + B_1 \cos(\omega t) + B_2 \sin(\omega t) \\ y &= C_0 + C_1 \cos(\omega t) + C_2 \sin(\omega t) & \theta_2 &= D_0 + D_1 \cos(\omega t) + D_2 \sin(\omega t)\end{aligned} \quad (20)$$

The solutions (20) are substituted in (13); the system of nonlinear algebraic equations with respect to amplitudes and frequency  $A_0, A_1, \dots, D_2, \omega$  is derived. This system is solved numerically in order to obtain the frequency response.

### 3. NUMERICAL ANALYSIS

Numerical solution of the nonlinear algebraic system is used to study amplitudes of self-sustained vibrations. Fig. 2 shows the frequency response of the rotor. The eigenvalues of linear system is calculated to obtain the point of the Hopf bifurcation. At  $\Omega = 1710 \text{ rad/s}$  the equilibrium loses stability and Hopf bifurcation take place. As the result, the unstable self vibrations occur. These unstable limit cycles undergo saddle-node bifurcation at the point  $A_1$ . The alternative branch of self vibration was found. This branch marked as  $(C_2 A_2 B_2)$ . The curve  $(C_2 A_2)$  of this branch describes the stable limit cycles, which become unstable at point  $A_2$ , where saddle-node bifurcation occur.

Direct numerical integration take place to verify the semi-analytical solutions. The Runge-Kutta method is used. Initial conditions for the direct numerical integration were chosen from the results of harmonic balance method. The calculation results are shown on Fig.2 as points. The solutions obtained by harmonic balance method are in good agreement with numerical simulation of the system.

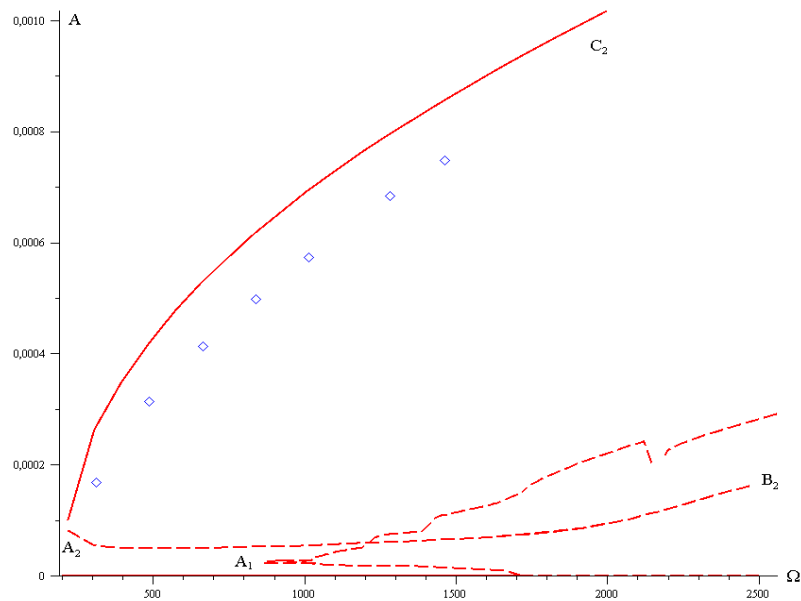


Fig. 2 The frequency response

## CONCLUSIONS

Bistability of self vibrations of one disk rotor is investigated. Two types of stable motions are observed at  $\Omega \in [300; 1700] \text{ rad/s}$ . The first type reflects the uniform rotation of rotor. Self-sustained vibrations occur due to saddle-node bifurcation  $A_2$ .

## REFERENCES

- [1] Zhang X. Y. On site testing and analysis of the oil whirl phenomena in national made 200MW stream turbine generator systems *Power Industry*, Vol. 12 (5), pp. 32-37, 1992.
- [2] Legrand M., Jiang D., Pierre C., Shaw S.W. Nonlinear normal modes of a rotating shaft based on the Invariant Manifold Method *International Journal of Rotating Machinery*, Vol. 10(4), pp. 319-335, 2004.
- [3] Akers Pressure due inertia in a journal bearing *The Journal of Mechanical Engineering Science*, February 1969.
- [4] Pozniak E.L. Dynamical properties of journal bearing oil film *Izd. Akad. Nauk SSSR, Mechanics and Mechanical Engineering*, pp. 22-29, 1961 (in Russian).
- [5] Olimpiev V.I. Eigenfrequencies of rotor-bearing system *Izd. Akad. Nauk SSSR, Mechanics and Mechanical Engineering*, Vol. 3, pp. 24-29, 1960 (in Russian).
- [6] Karintsev I.B., Shul'genko N.G. Static and dynamic properties of short journal bearing oil film *Dinamica i Prochnost' Mashin*, Vol. 16, pp. 109-114, 1974 (in Russian).
- [7] Filippov A.P., Shul'genko N.G. Stability of vibrations of loaded rotors in short journal bearing *Mashinovedenie*, Vol. 4, pp. 21-28, 1973.
- [8] Ovcharova D.K., Goloskokov E.G. Forced vibrations of rotors in journal bearings *Soviet Applied Mechanics*, Vol. 11(3), 1976.
- [9] Muszynska A. Whirl and whip-rotor bearing stability problems *Journal of Sound and Vibration*, Vol. 110(3), pp. 443-462, 1986.
- [10] Muszynska A. Stability of whirl and whip in rotor bearing systems *Journal of Sound and Vibration*, Vol. 127(1), pp. 49-64, 1988.
- [11] Shaw, S.W., Pierre, C. Normal modes for nonlinear vibratory systems *Journal of Sound and Vibration*, Vol. 164, pp. 58-124, 1993.

## CHAOS CAUSED BY HYSTERESIS IN 2-DOF ROTOR VIBRATIONS

**Jan Awrejcewicz**

Department of Automatics  
and Biomechanics,  
Technical University of  
Łódź, Poland

**Larisa P. Dzyubak**<sup>1</sup>

Department of Applied  
Mathematics, National  
Technical University  
"KhPI", Kharkov, Ukraine

---

### ABSTRACT

---

2-dof non-linear dynamics of the rotor suspended in a magneto-hydrodynamic field in the case of rigid magnetic materials is studied. Hysteresis is considered using the Bouc-Wen hysteretic model. It was shown that hysteresis may generate chaotic vibrations of the rotor under certain conditions. Influence of hysteretic dissipation on chaos occurring is investigated using an approach based on the analysis of wandering trajectories. The regions of chaotic behavior of the rotor are obtained in various control parameter planes: amplitude of external excitation versus dynamic oil film action characteristics, amplitude of external excitation versus magnetic control parameters, versus hysteretic dissipation as well as versus frequency of external excitation. The amplitude level contours of the horizontal and vertical vibrations of the rotor are obtained.

---

### INTRODUCTION

In [1] 2-dof nonlinear dynamics of the rotor supported by the magneto-hydrodynamic bearing was studied. In the case of soft magnetic materials the analytical solutions were obtained by means of the method of multiple scales. In the non-resonant case the system exhibits linear properties. The perturbation solutions are in good agreement with the numerical solutions. The cases of primary resonances with and without internal resonance were investigated. The frequency-response curves were obtained. The saturation phenomenon was demonstrated. When the amplitude of the external excitation increases, after some critical value the energy pumping between various submotions of the rotor occurs. A comparison of the analytical and numerical solutions based on the approximate harmonic analysis was made. The amplitude level contours of the horizontal and vertical vibrations of the rotor were obtained. When hysteretic dissipation is increased the amplitude level of the rotor vibrations is decreased and resonance peaks correspond to the regions with lower frequencies of external excitation.

The next step is studying of conditions for chaotic vibrations of the rotor in various control parameter planes. As it was demonstrated in [2], systems with hysteresis may reveal an unexpected behaviour. On the one hand, hysteresis as any dissipation promotes to stabilization of motion and may restrain the occurrence of chaos. On the other hand, it may be a cause of chaotic vibrations in the system. 1-dof Bouc-Wen oscillator is linear in absence of hysteresis (when  $\delta=1$ ). Adding hysteretic dissipation leads to chaotic responses occurring in this system. Fig. 1 represents the region where chaotic behaviour of the 1-dof Bouc-Wen oscillator is possible in the amplitude of external harmonic excitation versus hysteretic dissipation plane –  $(F, \delta)$  plane. Chaotic responses are not observed until  $\delta=\delta_{cr}$ , when the influence of the nonlinear terms becomes critical. This demonstrates the *generating effect* of the hysteretic dissipation on chaos occurring in the hysteretic system. Some information about chaotic responses of the 1-dof Bouc-Wen hysteretic oscillator is contained also in [3].

The present work has confirmed the ability of hysteresis to generate chaotic vibrations of the rotor.

---

<sup>1</sup> Corresponding author. Email [ldzyubak@kpi.kharkov.ua](mailto:ldzyubak@kpi.kharkov.ua)

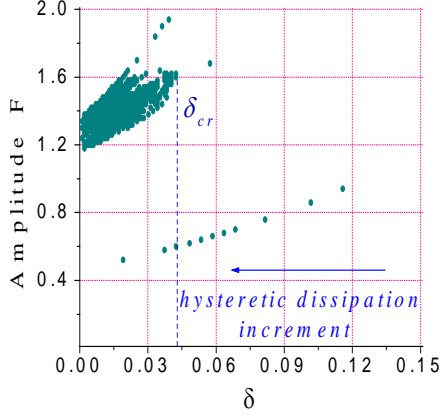


Fig. 1 The influence of hysteretic dissipation on chaos occurring in the case of 1-dof Bouc-Wen hysteretic model

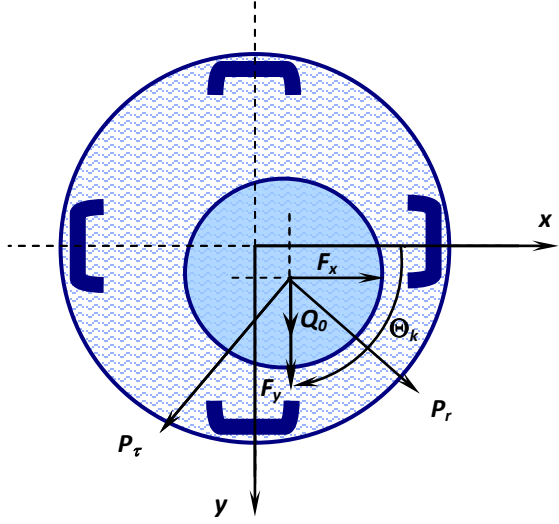


Fig. 2 The cross-section diagram of a rotor symmetrically supported on the magneto-hydrodynamic bearing

## 1. MATHEMATICAL MODEL

Consider a uniform symmetric rigid rotor (Fig. 2) which is supported by a magneto-hydrodynamic bearing (MHDB) system. The four-pole legs are symmetrically placed in the stator.  $F_k$  is the electromagnetic force produced by the  $k$ th opposed pair of electromagnet coils. This force, controlled by electric currents  $i_k = i_0 \pm \Delta i_k$ , can be expressed in the form

$$F_k = -\frac{2\mu_0 AN^2 i_0}{(2\delta + l/\mu^*)^2} \Delta i_k,$$

where  $i_0$  denotes bias current in the actuators electric circuits,  $\mu_0$  is the magnetic permeability of vacuum,  $A$  is the core cross-section area,  $N$  is the number of windings of the electromagnet,  $\delta$  is the air gap in the central position of the rotor with reference to the bearing sleeve,  $l$  is the total length of the magnetic path, the constant value  $\mu^* = B_s/(\mu_0 H_s)$  denotes the magnetic permeability of the core material; the values of the magnetic induction  $B_s$  and magnetizing force  $H_s$  define the magnetic saturation level.  $\theta_k$  is the angle between axis  $x$  and the  $k$ th magnetic actuator.  $Q_0$  is the vertical rotor load identified with its weight,  $(P_r, P_\tau)$  are the radial and tangential components of the dynamic oil-film action. Equations of motion of the rotor are represented in the dimensionless form [1, 4]

$$\begin{aligned} \ddot{x} &= P_r(\rho, \dot{\rho}, \dot{\phi}) \cos \phi - P_\tau(\rho, \dot{\rho}, \dot{\phi}) \sin \phi + F_x, \\ \ddot{y} &= P_r(\rho, \dot{\rho}, \dot{\phi}) \sin \phi + P_\tau(\rho, \dot{\rho}, \dot{\phi}) \cos \phi + F_y + Q_0 + Q \sin \Omega t, \\ P_r(\rho, \dot{\rho}, \dot{\phi}) &= -2C \left\{ \frac{\rho^2(1-2\dot{\phi})}{p(\rho)q(\rho)} + \frac{\rho\dot{\rho}}{p(\rho)} + \frac{2\dot{\rho}}{\sqrt{p(\rho)}} \arctg \frac{\sqrt{1+\rho}}{\sqrt{1-\rho}} \right\}, \quad P_\tau(\rho, \dot{\phi}) = \pi C \frac{\rho(1-2\dot{\phi})}{q(\rho)\sqrt{p(\rho)}}. \end{aligned}$$

Here

$$x = \rho \cos \phi, \quad y = \rho \sin \phi, \quad \dot{\phi} = \frac{\dot{y}x - x\dot{y}}{\rho^2}, \quad \dot{\rho} = \frac{x\dot{x} + y\dot{y}}{\rho}, \quad \rho = \sqrt{x^2 + y^2}, \quad \cos \phi = \frac{x}{\sqrt{x^2 + y^2}}, \quad \sin \phi = \frac{y}{\sqrt{x^2 + y^2}};$$

the magnetic control forces are expressed as follows  $F_x = -\gamma\dot{x} - \lambda(x - x_0)$ ,  $F_y = -\gamma\dot{y} - \lambda(y - y_0)$ , where  $(x_0, y_0)$  are the coordinates of the rotor static equilibrium,  $\gamma$  and  $\lambda$  are the control parameters.

In the case of rigid magnetic materials the hysteretic properties of system described can be considered using the Bouc-Wen hysteretic model. It was shown [2] that this modeling mechanism for energy dissipation was sufficiently accurate to model loops of various shapes in accordance with a real experiment, reflecting the behavior of hysteretic systems from very different fields. The hysteretic model of the rotor-MHDB system is as follows

$$\begin{aligned}
\ddot{x} &= P_r(\rho, \dot{\rho}, \dot{\phi}) \cos \phi - P_\tau(\rho, \dot{\phi}) \sin \phi - \gamma_m \dot{x} - \lambda_m [\delta(x - x_0) + (1 - \delta)z_1], \\
\ddot{y} &= P_r(\rho, \dot{\rho}, \dot{\phi}) \sin \phi + P_\tau(\rho, \dot{\phi}) \cos \phi - \gamma_m \dot{y} - \lambda_m [\delta(y - y_0) + (1 - \delta)z_2] + Q_0 + Q \sin \Omega t, \\
\dot{z}_1 &= [k_z - (\gamma + \beta \operatorname{sgn}(\dot{x}) \operatorname{sgn}(z_1)) |z_1|^n] \dot{x}, \\
\dot{z}_2 &= [k_z - (\gamma + \beta \operatorname{sgn}(\dot{y}) \operatorname{sgn}(z_2)) |z_2|^n] \dot{y}.
\end{aligned} \quad (1)$$

Here  $z_1$  and  $z_2$  are the hysteretic forces. The case  $\delta=0$  corresponds to maximal hysteretic dissipation and  $\delta=1$  corresponds to the absence of hysteretic forces in the system, parameters  $(k_z, \beta, n) \in \mathbb{R}^+$  and  $\gamma \in \mathbb{R}$  govern the shape of the hysteresis loops.

## 2. CONDITIONS FOR CHAOTIC VIBRATIONS OF THE ROTOR

Conditions for chaotic vibrations of the rotor have been found using the approach based on the analysis of the wandering trajectories. The description of the approach, its advantages over standard procedures and a comparison with other approaches can be found, for example, in [2, 5, 6].

Figure 3 displays the regions of rotor chaotic vibrations in  $(\delta, Q)$  plane. In Fig. 4 chaotic regions for the horizontal and vertical vibrations of the rotor are depicted in the  $(\Omega, Q)$  parametric plane.

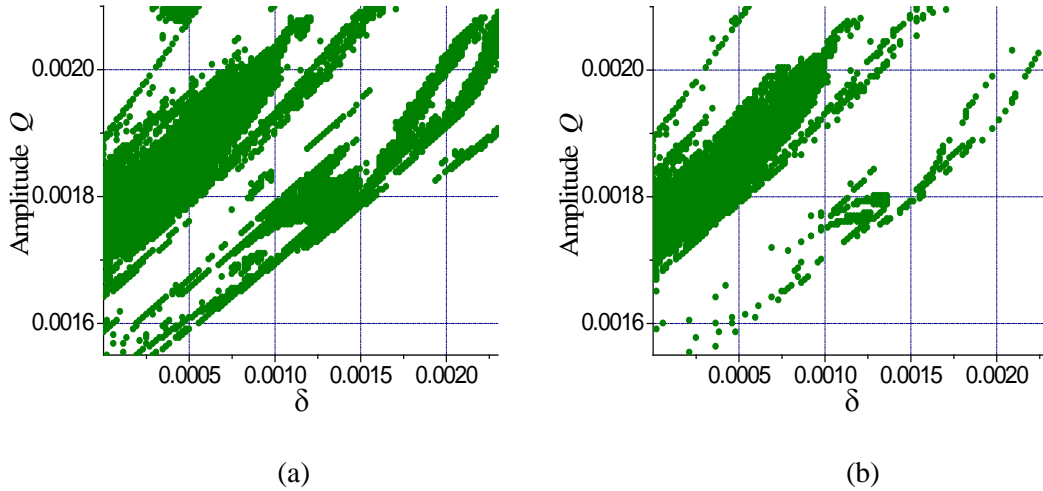


Fig. 3 The influence of hysteretic dissipation  $\delta$  on chaos occurring in horizontal (a) and vertical (b) vibrations of the rotor (1):  $C=0.2$ ,  $\gamma_m=0$ ,  $\lambda_m=500$ ,  $k_z=0.000055$ ,  $\gamma=15$ ,  $\beta=0.25$ ,  $n=1.0$ ,  $\Omega=0.87$ ,  $Q_0=0$ ,  $x_0=0$ ,  $y_0=0$ ,  $x(0)=y(0)=10^{-8}$ ,  $\dot{x}(0)=\dot{y}(0)=0$ ,  $z_1(0)=z_2(0)=0$

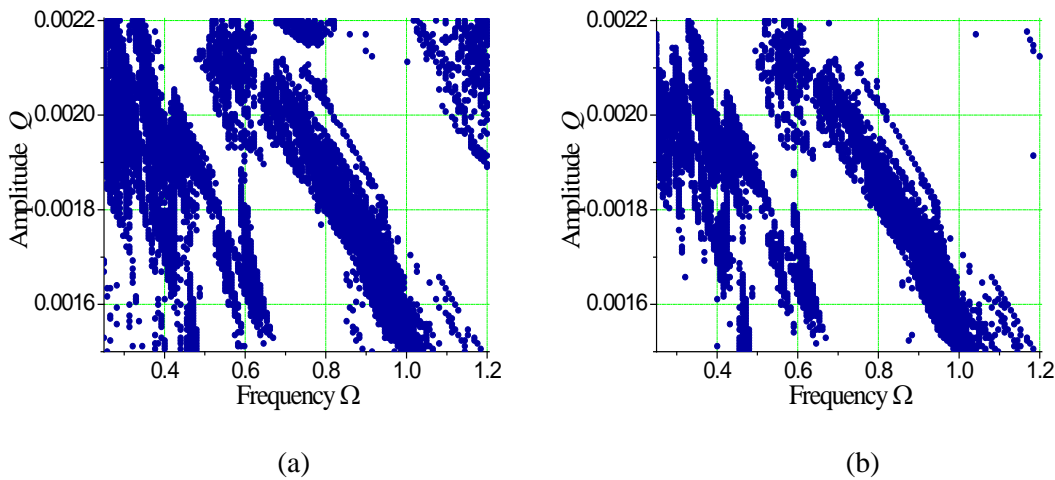


Fig. 4 Chaotic regions for the horizontal (a) and vertical (b) vibrations of the rotor (1) in the  $(\Omega, Q)$  parametric plane at  $\delta=0.0001$ ,  $C=0.2$ ,  $\gamma_m=0$ ,  $\lambda_m=500$ ,  $k_z=0.000055$ ,  $\gamma=15$ ,  $\beta=0.25$ ,  $n=1.0$ ,  $Q_0=0$ ,  $x_0=0$ ,  $y_0=0$ ,  $x(0)=y(0)=10^{-8}$ ,  $\dot{x}(0)=\dot{y}(0)=0$ ,  $z_1(0)=z_2(0)=0$

All domains have complex structure. There are a number of scattered points, streaks and islets here. Such structure is characteristic of domains where chaotic vibrations are possible. For each

aggregate of control parameters there is some critical value of the hysteretic dissipation ( $1-\delta_{cr}$ ) that, if  $(1-\delta) < (1-\delta_{cr})$ , chaos is not observed in the system considered. Figure 5 shows the phase portrait and hysteretic loop of chaotic motion of the rotor. Parameters of motion correspond to the parameters of chaotic regions depicted in Fig. 3 and Fig. 4. The phase portrait and hysteretic loop of the periodic rotor motion that also agree well with the regions of regular/irregular behaviour of the rotor (Fig. 4) are shown in Fig. 6.

The influence of the dynamic oil-film action characteristics on chaos occurring in the rotor motion can be observed in Fig. 7. The restraining of chaotic regions with decreasing of hysteretic dissipation ( $1-\delta$ ) occurs.

The influence of the magnetic control parameters  $\gamma_m, \lambda_m$  on chaotic vibrations of the rotor can be observed in Figs. 8, 9.

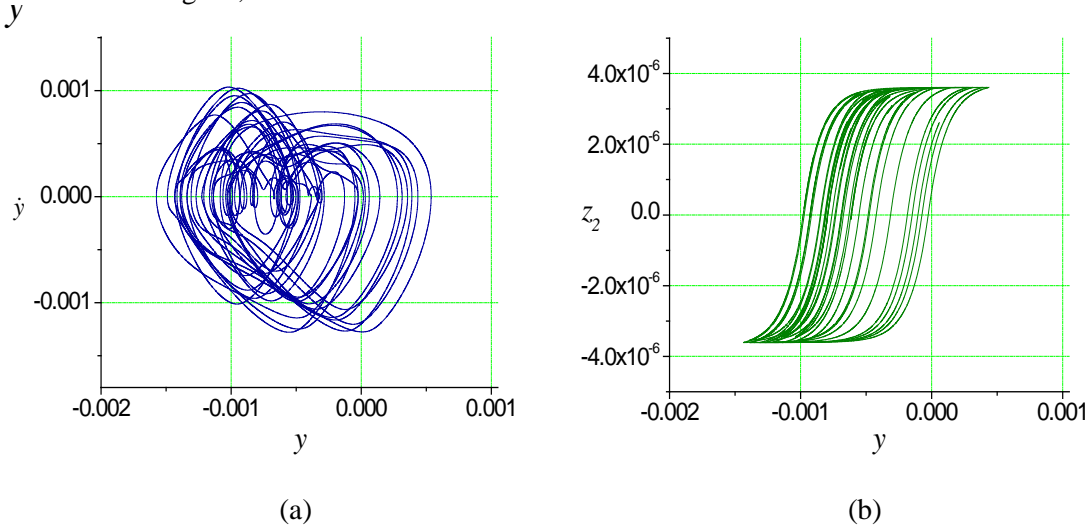


*Fig. 5 Phase portrait (a) and hysteresis loop (b) of the rotor motion that agree with the chaotic regions in Figs. 3, 4. The parameters  $\Omega=0.87, Q=0.00177, \delta=0.0001, C=0.2, \gamma_m=0, \lambda_m=500, k_z=0.000055, \gamma=15, \beta=0.25, n=1.0, Q_0=0, x_0=0, y_0=0, x(0)=y(0)=10^{-8}, \dot{x}(0)=\dot{y}(0)=0, z_1(0)=z_2(0)=0$  are fixed*

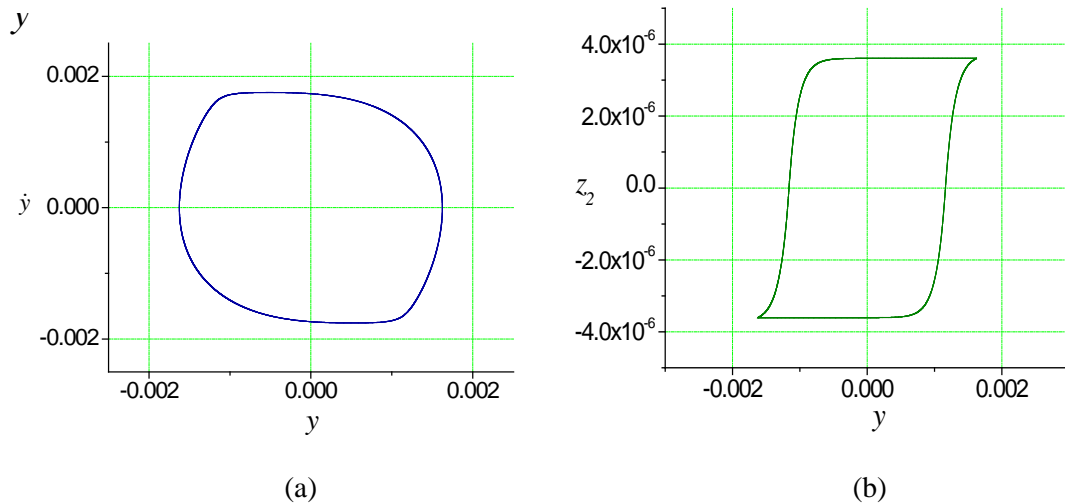
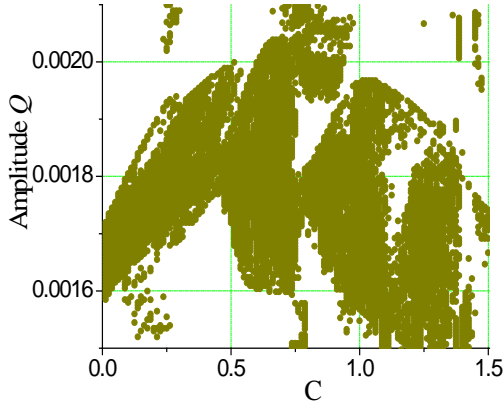
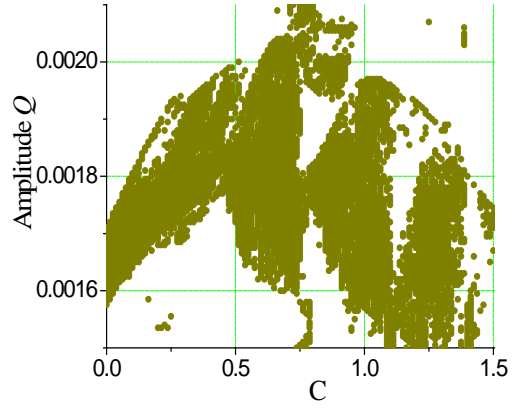


*Fig. 6 Phase portrait (a) and hysteresis loop (b) of the periodic rotor motion that agree with the regions of regular motion in Fig. 4. The parameters  $\Omega=1.2, Q=0.0017, \delta=0.0001, C=0.2, \gamma_m=0, \lambda_m=500, k_z=0.000055, \gamma=15, \beta=0.25, n=1.0, Q_0=0, x_0=0, y_0=0, x(0)=y(0)=10^{-8}, \dot{x}(0)=\dot{y}(0)=0, z_1(0)=z_2(0)=0$  are fixed*

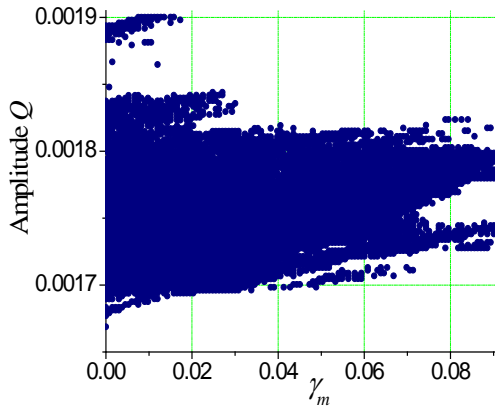


(a)

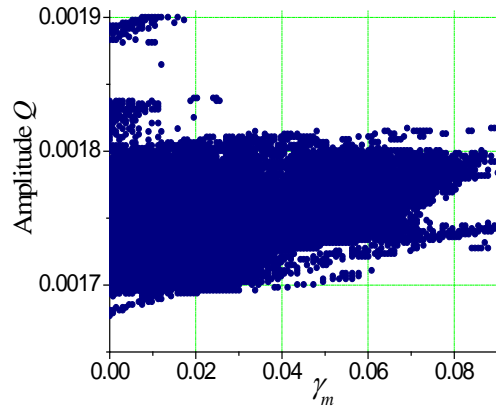


(b)

Fig. 7 The influence of the dynamic oil-film action characteristics on chaos occurring in horizontal (a) and vertical (b) vibrations of the rotor (1):  $\delta=0.000001$ ,  $\gamma_m=0$ ,  $\lambda_m=500$ ,  $k_z=0.000055$ ,  $\gamma=15$ ,  $\beta=0.25$ ,  $n=1.0$ ,  $\Omega=0.87$ ,  $Q_0=0$ ,  $x_0=0$ ,  $y_0=0$ ,  $x(0)=y(0)=10^{-8}$ ,  $\dot{x}(0)=\dot{y}(0)=0$ ,  $z_1(0)=z_2(0)=0$

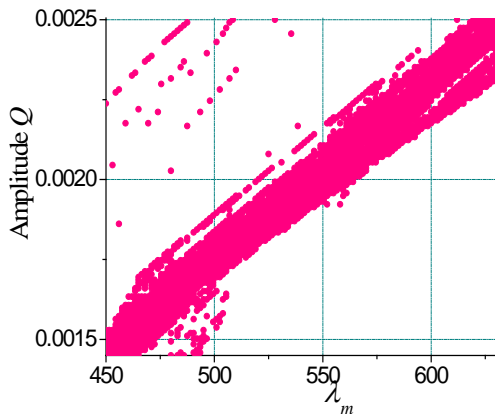


(a)

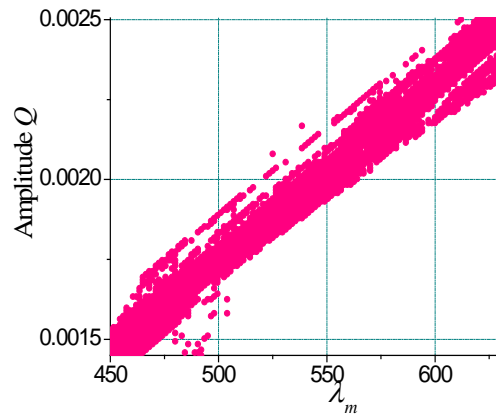


(b)

Fig. 8 The influence of magnetic control parameter  $\gamma_m$  on chaos occurring in horizontal (a) and vertical (b) vibrations of the rotor (1):  $\delta=0.000001$ ,  $C=0.2$ ,  $\lambda_m=500$ ,  $k_z=0.000055$ ,  $\gamma=15$ ,  $\beta=0.25$ ,  $n=1.0$ ,  $\Omega=0.87$ ,  $Q_0=0$ ,  $x_0=0$ ,  $y_0=0$ ,  $x(0)=y(0)=10^{-8}$ ,  $\dot{x}(0)=\dot{y}(0)=0$ ,  $z_1(0)=z_2(0)=0$



(a)



(b)

Fig. 9 The influence of magnetic control parameter  $\lambda_m$  on chaos occurring in horizontal (a) and vertical (b) vibrations of the rotor (1):  $\delta=0.000001$ ,  $C=0.2$ ,  $\gamma_m=0$ ,  $k_z=0.000055$ ,  $\gamma=15$ ,  $\beta=0.25$ ,  $n=1.0$ ,  $\Omega=0.87$ ,  $Q_0=0$ ,  $x_0=0$ ,  $y_0=0$ ,  $x(0)=y(0)=10^{-8}$ ,  $\dot{x}(0)=\dot{y}(0)=0$ ,  $z_1(0)=z_2(0)=0$

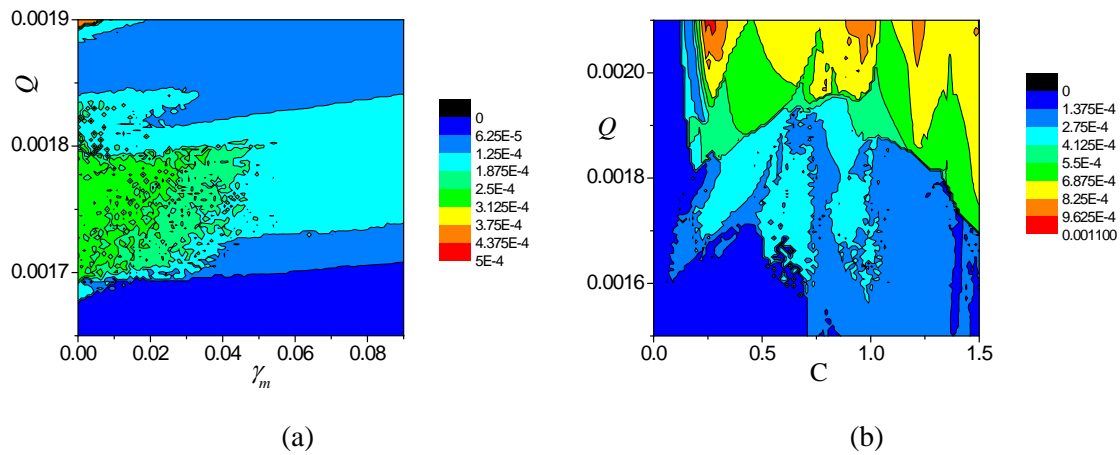


Fig. 10 The amplitude level contours of the rotor vibrations (a) in  $(\gamma_m, Q)$  parametric plane that correspond to Fig. 8; (b) in  $(C, Q)$  parametric plane that correspond to Fig. 7

In order to see if the rotor chaotic motion is accompanied by increasing of the amplitude of vibrations, the amplitude level contours of the horizontal and vertical vibrations of the rotor have been obtained. In Fig 10 (a) the amplitude level contours are presented in  $(\gamma_m, Q)$  parametric plane with the same parameters as in Fig. 8. Some “consonance” between the chaotic vibrations regions and the amplitude level contours is observed. The amplitudes of chaotic rotor vibrations are greater in comparison with the periodic vibrations. In Fig 10 (b) the amplitude level contours are presented in  $(C, Q)$  parametric plane with the same parameters as in Fig. 7. Although some “consonance” between the chaotic vibrations regions and the amplitude level contours is observed, in this case it can not be concluded that chaos leads to essential increasing of the rotor vibrations amplitude.

## CONCLUSIONS

2-dof non-linear dynamics of the rotor suspended in a magneto-hydrodynamic field is studied. In the case of rigid magnetic materials, hysteresis was considered using the Bouc-Wen hysteretic model. It was shown, that hysteresis may be a cause of chaotic vibrations of the rotor. Using the approach based on the analysis of the wandering trajectories the regions of chaotic vibrations of the rotor were found in various control parameter planes: amplitude of external harmonic excitation versus hysteretic dissipation, versus frequency of external harmonic excitation, dynamic oil-film action characteristics as well as versus the magnetic control parameters. The amplitude level contours of the horizontal and vertical vibrations of the rotor were obtained. Phase portraits and hysteretic loops are in good agreement with the chaotic regions obtained.

## ACKNOWLEDGEMENT

This paper has been financially supported by the grant 0040/B/T02/2010/38 of the Ministry for Science and Higher Education of Poland for years 2010-2012.

## REFERENCES

- [1] J. Awrejcewicz and L.P. Dzyubak, 2-dof nonlinear dynamics of a rotor suspended in the magneto-hydrodynamic field in the case of soft and rigid magnetic materials, *Int. J. of Non-Linear Mechanics*, (2010) Pages 1–12, doi:10.1016/j.ijnonlinmec.2010.01.006.
- [2] J. Awrejcewicz, L.P.Dzyubak, Hysteresis modelling and chaos prediction in one- and two-dof hysteretic models, *Archive of Applied Mechanics*. vol. 77, pp. 261-279, 2007.
- [3] J. Awrejcewicz, L. Dzyubak, Hysteresis simulation and investigation of the control parameter planes, *Int. Conference on Nonlinear Dynamics, Kharkov, Ukraine, 2004*, Proc., pp.25-29.
- [4] J. Awrejcewicz, L. Dzyubak, Nonlinear dynamics of a rotor active magnetic bearings system, *The Second International Conference on Nonlinear Dynamics dedicated to the 150<sup>th</sup> Anniversary of A.M.Lyapunov, Kharkov, Ukraine, 2007*, Book of extended abstracts, pp. 28-33.
- [5] J. Awrejcewicz, L. Dzyubak, C. Grebogi, A direct numerical method for quantifying regular and chaotic orbits, *Chaos, Solitons and Fractals* 19, pp. 503-507, 2004.
- [6] J. Awrejcewicz, R. Mosdorf, *Numerical Analysis of Some Problems of Chaotic Dynamics*. WNT, Warsaw, 2003.

## FAMILIES OF PERIODIC SOLUTIONS OF HILL'S PROBLEM

Alexander B. Batkhin<sup>1</sup>

ABSTRACT

Keldysh Institute of  
Applied Mathematics  
Moscow, Russia

Generating periodic solutions of Kepler problem in case of Hill's perturbation are investigated. Existence of two kinds of generated solutions by means of normal forms is proved.

### INTRODUCTION

An efficient method of periodic orbits search is the method of generating solutions which was independently developed by A.D. Bruno [1] and M. Henon [2]. This method suggests to consider a nonintegrable problem as a perturbation of integrable one, therefore it makes possible to isolate such periodic solutions of unperturbed problem that may be continued into the periodic solution of nonintegrable one.

We study generating solutions of Kepler problem in synodical coordinates which is perturbed with polynomial. This perturbation allows investigating families of period solutions of Hill's problem by periodic orbits of Kepler problem. The majority of known families of periodic solutions of Hill's problem were studied as continuation of generating solutions of a linear Hamiltonian system perturbed with singular function [3]. We propose to study families of periodic solutions of Hill's problem using the continuation of generating solutions of Kepler problem. These generating solutions are obtained with the help of approach described in [1, Chapter VII].

### 1. HILL'S PROBLEM EQUATIONS AND THEIR PROPERTIES

Hill's problem is a limiting case of the well-known restricted three-body problem (RTBP). It describes the dynamics of a massless body (satellite) in the vicinity of the minor primary (Earth). Hill's problem equations may be obtained in several ways but usually RTBP equations are transformed with so called Hill's transformation. Hill's transformation consists of two linear transformations. The first is a shift of coordinate origin at the position of the minor primary and the second is a special coordinate scaling. In the planar case Hill's transformation is written in form

$$\begin{aligned}x_1 &= \mu - 1 + \mu^{1/3}X_1, & y_1 &= \mu^{1/3}Y_1, \\x_2 &= \mu^{1/3}X_2, & y_2 &= \mu - 1 + \mu^{1/3}Y_2\end{aligned}\quad (1)$$

The easier way to obtain Hill's problem equations of motion is to apply Hill's transformation (1) to Hamiltonian of RTBP with generating function [4] or using Power Geometry technique [5].

Hamiltonian of the planar circular Hill's problem is

$$H = \frac{1}{2}(y_1^2 + y_2^2) + x_2y_1 - x_1y_2 - \frac{1}{r} - x_1^2 + \frac{1}{2}x_2^2, \text{ where } r = \sqrt{x_1^2 + x_2^2}, \quad (2)$$

here  $x$  – vector of canonic coordinates,  $y$  – vector of canonically conjugate momenta. Canonical equations of motion are invariant under finite group of transformations of order 4

<sup>1</sup> Corresponding author. Email [batkhin@gmail.com](mailto:batkhin@gmail.com)

$$\begin{aligned}\Sigma_1: (t, x_1, x_2, y_1, y_2) &\rightarrow (-t, x_1, -x_2, -y_1, y_2) \\ \Sigma_2: (t, x_1, x_2, y_1, y_2) &\rightarrow (-t, -x_1, x_2, y_1, -y_2)\end{aligned}\quad (3)$$

and their composition  $\Sigma_1 \circ \Sigma_2$ . In the configuration space these transformations act as axial symmetries relative to abscissa axis, ordinate axis and the coordinate origin correspondingly. The presence of these symmetries leads to the fact that all the families of periodic solutions form four classes.

Nonsymmetrical orbits. Three more orbits correspond to each such orbit with the same period and initial conditions which are obtained with mentioned above transformations.

$\Sigma_1$ -symmetric orbits. One more orbit corresponds to each such orbit which is symmetrical with respect to the ordinate axis.

$\Sigma_2$ -symmetric orbits. One more orbit corresponds to each such orbit which is symmetrical with respect to the abscissa axis.

Double symmetric orbits. These orbits are symmetrical with respect to coordinate axes to themselves.

Hill's problem equations of motion possess the single first integral of motion which called Jacobi integral:

$$C = 3x_1^2 + 2/r - \dot{x}_1^2 + \dot{x}_2^2 = -2H \quad (4)$$

and therefore it is nonintegrable problem [2].

Hill's problem has complex set of one-parameter families of periodic solutions which can be continued into the periodic solutions of the RTBP. There are a lot of various applications of Hill's problem [4].

## 2. HILL'S PROBLEM AS A SINGULARLY PERTURBED LINEAR HAMILTONIAN SYSTEM

Canonical change of variables  $x = \sqrt{|C|}X$ ,  $y = \sqrt{|C|}Y$  allows to write Hamiltonian (2) of Hill's problem as a perturbation of linear Hamiltonian system  $H_0$  called *Henon's intermediate problem* with singular function  $R$ :  $H = H_0 + \varepsilon R$ , where

$$H_0 = \frac{1}{2}(Y_1^2 + Y_2^2) + X_2Y_1 - X_1Y_2 - X_1^2 + \frac{1}{2}X_2^2 = \frac{1}{2}, \quad R = -\frac{1}{r}, \quad \varepsilon = \frac{1}{|C|^{3/2}}. \quad (5)$$

Normal form  $H_0 = (Q_1^2 + P_1^2)/2 - 3/2P_2^2$  of Hamiltonian  $H_0$  is obtained with the help of generating function  $S_2(X, P) = X_1(P_2 - X_2) + P_2(X_2 - 2P_1)$ , which produces canonical variable change  $X_1 = Q_1 + 2P_2, X_2 = Q_2 + 2P_1, Y_1 = -P_1 - Q_2, Y_2 = -P_2 - Q_1$ .

Canonical equations of motions defined by Hamiltonian  $H_0$  has one-parameter family of periodic orbits with period  $T_0 = 2\pi$  in form of ellipses with semi-axes 1 and 2 and with the center at point  $(0, Q_2^0)$ . One more canonical variable change  $Q_1 = \sqrt{2L}\cos \varphi$ ,  $P_1 = \sqrt{2L}\sin \varphi$  of the first pair of conjugated coordinates together with time inversion  $t = -\tau$  allow to write Hamiltonian  $H_0$  in the form  $H_0 = -L + 3/2P_2^2$ . So one-parameter family of periodic solutions is defined by following values

$$\varphi = -\tau, \quad L = 1/2, \quad Q_2 = Q_2^0, \quad P_2 = 0 \quad (6)$$

The generating solutions of unperturbed problem satisfy condition  $\partial[R]/\partial Q_2^0 = 0$ , where square brackets mean averaging along solution (6) (see Chapter VII, §1 [1]):

$$[R](Q_2^0) = \frac{1}{2\pi} \int_0^{2\pi} R(Q_2^0, \tau) d\tau = \frac{1}{2\pi} \int_0^{2\pi} \frac{d\tau}{\sqrt{Q_2^0(Q_2^0 - 4\sin \tau) + 3\sin^2 \tau + 1}} \quad (7)$$

Function (7) has the only extremum at the point  $Q_2^0 = 0$ , therefore the only regular generating solution of Henon's intermediate problem is an ellipse (6) with center at the origin. This solution is easily identified with retrograde single-turn orbits of family  $f$  originally computed by J. Jackson (1913) and T. Matukuma (1932) (see [3]). The first order correction to the period of generating solution is computed by formula  $T = T_0 + \varepsilon T_0 \partial[R]/\partial L + O(\varepsilon^2)$ , where averaging is calculated along the generating solution (6). Finally, the asymptotic of the period of family  $f$  is of form

$$T = 2\pi - 2K(\sqrt{3}/2)/|C|^{3/2} + O(|C|^{-3}), \quad (9)$$

here  $K$  is complete elliptic integral of the first kind. It is necessary to notice that the first order corrections to the period and initial conditions of the family  $f$  were calculated in [6] but formulas mentioned in the pages 345-346 are wrong.

### 3. HILL'S PROBLEM AS A REGULARLY PERTURBED KEPLER PROBLEM

Hill's problem may be presented in a form of perturbed Kepler problem in synodical coordinates:  $\tilde{H} = H_K + \varepsilon R$ , where

$$H_K = \frac{1}{2}(y_1^2 + y_2^2) + x_2y_1 - x_1y_2 - \frac{1}{r}, R = \frac{1}{2}x_2^2 - x_1^2 \quad (10)$$

One can obtain Hamiltonian of Kepler problem in synodical coordinates for  $\varepsilon = 0$  and Hamiltonian of Hill's problem for  $\varepsilon = 1$ . Let's consider three main types of periodic solutions of Kepler problem: stationary points, circular orbits and elliptic orbits. It should be noticed that periodic solutions of Kepler problem in inertial (sidereal) coordinates are preserved in synodical coordinates in two cases: either sidereal orbit is circular or period of siderial orbit is commensurable with  $2\pi$ . We investigate only last case in this paper.

#### 3.1 Perturbation of the stationary points

Stationary points of canonical equations of motion of Kepler problem form the unit circle  $r = 1$  on the plane  $XOY$ , but perturbation  $R$  from (10) destroys it and leaves two pairs of stationary points. First pair of stationary points with coordinates  $(\pm(1 + 2\varepsilon)^{-1/3}, 0)$  lays on X-axis and corresponds to the well known collinear Lagrange libration points. Second pair of stationary points with coordinates  $(0, \pm(1 - \varepsilon)^{-1/3})$  lays on Y-axis and tends to infinity while  $\varepsilon \rightarrow 1$ . It is possible to expect that periodic orbits situated outside the unit circle of stationary points will be destroyed at Hill's perturbation (10).

#### 3.2 Perturbation of elliptic orbits

Let's write Hamiltonian of generating problem in modified Delaunay coordinates [7, Chapter 7] which provide the normal form of Hamiltonian  $H_K$  at vicinity of integral manifold of direct and retrograde elliptic orbits  $\mathcal{D}d_N$  and  $\mathcal{D}r_N$  [1, Chapter 7, §2]. The first approximation of normal form of Hamiltonian  $\tilde{H}$  is obtained by averaging of perturbation  $R$  (see Chapter 3 [8]). So Delaunay variables  $(l, g, L, G)$  provide the following form of the functions (10)

$$H_K = -G - \frac{1}{L^2}, R = \frac{1}{2}r^2 - \frac{3}{2}r^2 \cos^2 h \quad (11)$$

here  $r$  and  $h$  are polar coordinates. Elliptic orbites are defined by the following values of Delaunay variables in case  $\varepsilon = 0$ :

$$L = \sqrt{a}, G = \varepsilon' \sqrt{a(1 - e^2)}, l = Nt, g = \theta - t \quad (12)$$

here  $a$  is a semimajor axis of the orbit,  $e$  is its eccentricity,  $N = a^{-3/2}$  is mean motion,  $\theta$  is pericentre angle and  $\varepsilon' = \pm 1$  specifies the direction of the motion. The value  $\varepsilon' l$  is mean anomaly which defines the position of the point on the elliptic orbit at specified moment of time, and the value  $g$  defines the motion of the orbit pericentre, which uniformly rotate anticlockwise in synodical coordinates. Finally,  $L$  is defined by energy integral and  $G$  is area integral of Kepler problem.

Let's consider an integral manifold  $\mathcal{M} \in \mathcal{D}d_N \cup \mathcal{D}r_N$  which consists of periodic orbits with rational mean motion  $N = 1 + q/p$  and with period  $T_0 = 2\pi p$ . Hamiltonian  $\tilde{H}$  be a function of angle variable  $\theta$  and generalized momentum  $G$  along manifold  $\mathcal{M}$ . Generating orbits are specified by condition

$$\partial[R(\theta, G)]/\partial\theta = 0 \quad (13)$$

according to formula (1.15) [1, Chapter 7], where square brackets means averaging along the elliptic orbit (12). The averaging of function  $R$  is carried out over mean anomaly  $l$ , so

$[R] = \frac{1}{2\pi} \int_0^{2\pi(p+q)} R(l)N^{-1}dl$ . Function  $R$  may be written in form  $R = R_1 + R_2$ , where  $R_1 = -r^2/4$  and  $R_2 = -(3/2)r^2 \cos 2h$ . Since function  $R_1$  does not depend on  $\theta$  so condition (13) becomes trivial for its averaging. Function  $R_2$  may be written in the form of Fourier series over mean anomaly with coefficients depending on Bessel functions of the first kind [9].

The following statement is proved:

$$[R_2] = \begin{cases} -\frac{3\sqrt[3]{p}}{2e} \cos 2\theta S_{2p}(\varepsilon', e) & \text{if } p + q = 1, \\ -\frac{3\sqrt[3]{p}}{\sqrt[3]{4}e} \cos 2\theta S_p(\varepsilon', e) & \text{if } p + q = 2, \\ 0 & \text{if } p + q > 2, \end{cases}$$

where  $S_p(\varepsilon', e) = (1 - e^2) J_p'(pe) - \frac{2-e^2}{pe} J_p(pe) + \varepsilon' e \sqrt{1 - e^2} J_p''(pe)$  and  $J_p$  is Bessel function of the first kind. Function  $S_p(\varepsilon', e)$  was numerically investigated for  $p \leq 1000$  and it has following properties:

1.  $S_p(\varepsilon', e)$  is analytical in the interval  $0 \leq e < 1$ ,
2.  $S_p(\varepsilon', 1) = -J_p(p)/p < 0$ ,
3. Equation  $S_p(\varepsilon', e) = 0$  has the unique root  $e_p^*$  in the interval  $0 < e < 1$  if  $\varepsilon' = 1$  and  $p > 1$ .

Thus there are two main families of generating solutions satisfying condition (13).

Case 1. Symmetric orbits with  $\theta = k\pi/2$ ,  $k = 0, 1, 2, 3$  and  $0 < e < 1$ .

If  $p + q = 1$  then evenness of integers  $p$  and  $q$  is different and there are two families of  $\Sigma_1$ -symmetric orbits corresponding  $\theta = 0, \pi$  and two families of  $\Sigma_2$ -symmetric orbits corresponding  $\theta = \pi/2, 3\pi/2$ . Some orbits for this case are shown on fig. 1.

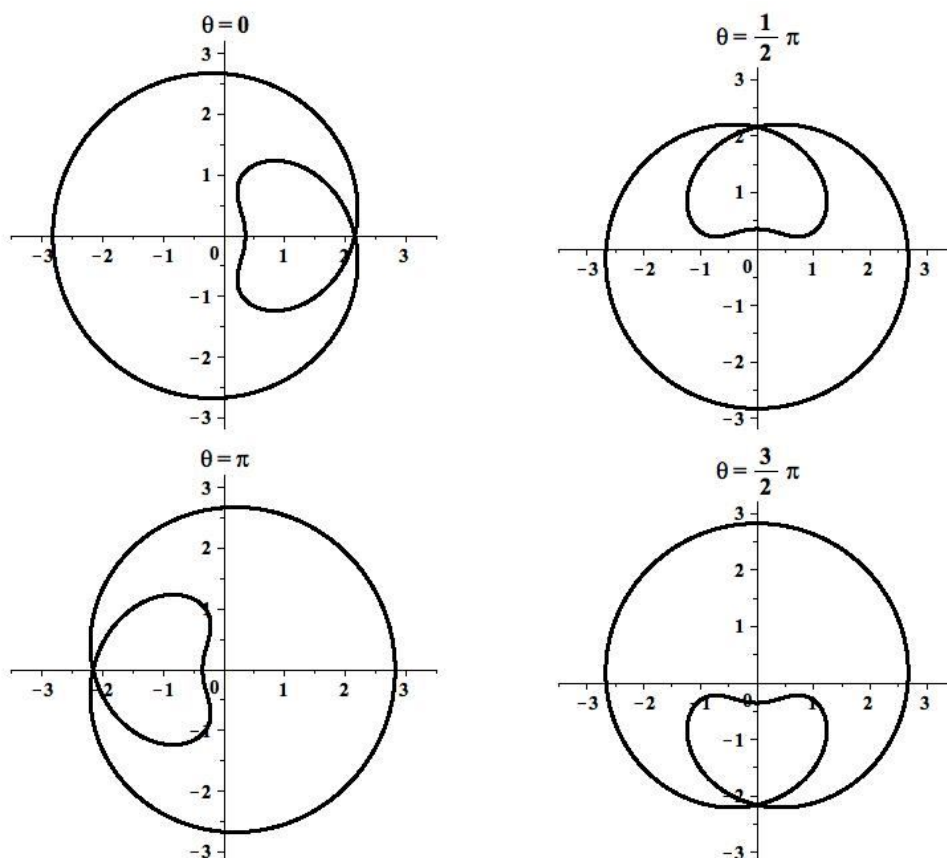


Fig. 1 Single symmetric generating orbits for  $p = 2, q = -1, e = 7/9, \varepsilon' = 1$ .

If  $p + q = 2$  then both  $p$  and  $q$  are odd and there are two families of double symmetric orbits with  $\theta = 0, \pi/2$ , respectively. Some orbits for this case are shown on the fig. 2.

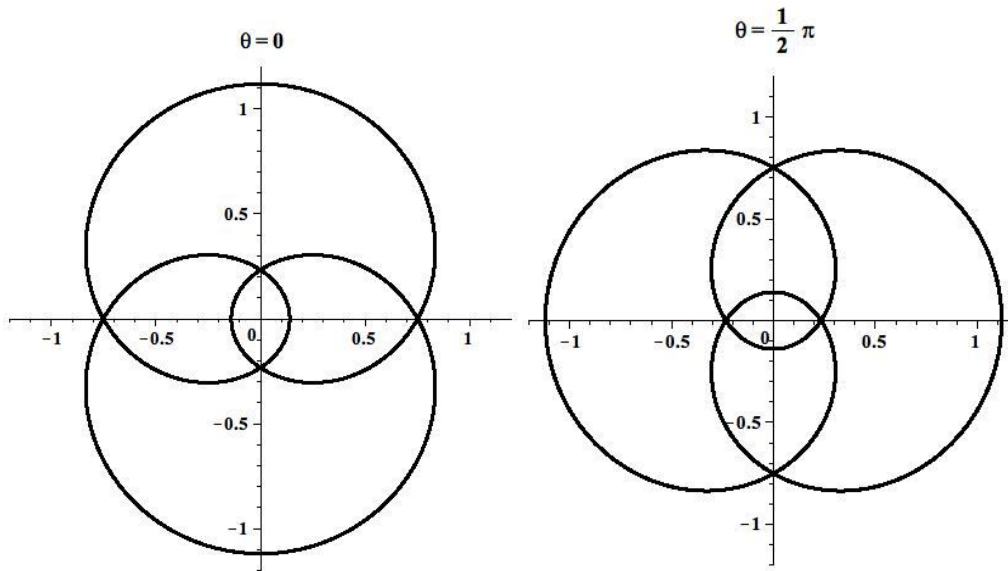


Fig. 2 Double symmetric generating orbits for  $p = 1, q = 1, e = 7/9, \varepsilon' = -1$ .

Case 2. Asymmetric orbits with  $\theta \neq k\pi/2, k = 0, 1, 2, 3, p > 1, \varepsilon' = 1$  and  $e = e_p^*$ . Approximate values of eccentricity  $e$  corresponding to asymmetric generating orbits for  $p = 2, \dots, 10$  are listed in table 1.

Table 1 Critical value of eccentricity for asymmetric generating orbits

N	$p$	$e_p^*$
1	2	0.75822858044480
2	3	0.85254323545950
3	4	0.89215536030911
4	5	0.91403781912693
5	6	0.92797039943780
6	7	0.93765362124966
7	8	0.94479628596787
8	9	0.95029677982004
9	10	0.95467290426209

Asymmetric generating orbits are shown in fig. 3. Left picture corresponds the case  $p = 2, q = -1$  and right picture corresponds the case  $p = 3, q = -1$ .

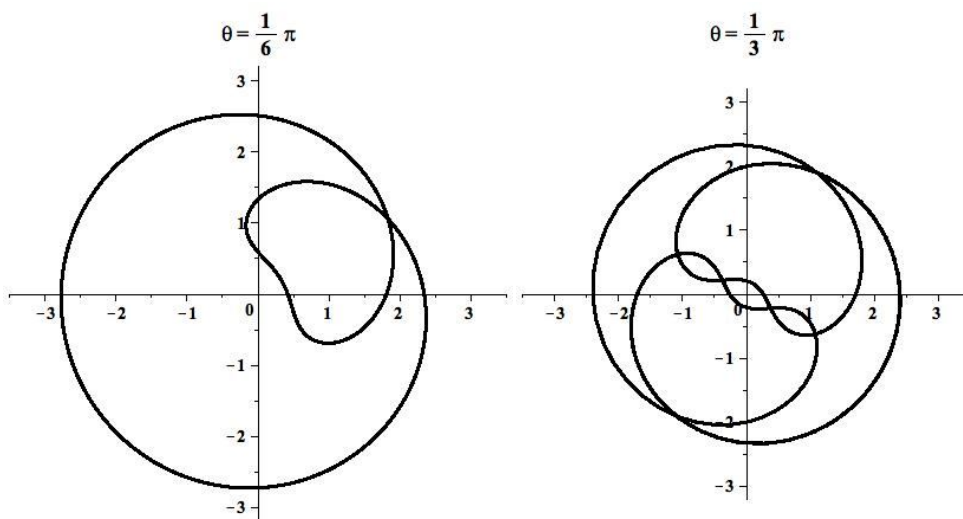


Fig. 1 Asymmetric generating orbits with  $p = 2, q = -1$  (left) and  $p = 3, q = -1$  (right).

## CONCLUSIONS

Hill's problem may be investigated as perturbation of two different integrable limiting cases: as singular perturbation of linear Hamiltonian system call Henon's intermediate problem or as regular perturbation of Kepler problem in synodical coordinates. In first case the correct approximation of period of orbits of family  $\mathbf{f}$  is obtained. In second case two kind of families of generating orbits were found: symmetric and asymmetric.

## REFERENCES

- [1] Bruno A.D. *The Restricted 3-Body Problem: Plane Periodic Orbits*. De Gruyter Exposition in Math, 1994.
- [2] Henon M. *Generating Families in the Restricted Three-Body Problem*. Springer, 1997.
- [3] Henon M. Numerical exploration of the restricted problem. V. Hill's case: Periodic orbits and their stability, *Astron. & Astrophys.*, Vol. 1, pp. 223-238, 1969.
- [4] Batkhin A.B., Batkhina N.V. *Hill's problem*. Volgograd: Volgograd Scientific Publisher, 2009 (Russian).
- [5] Bruno A.D. On periodic flybus of the Moon, *Celestial Mechanics*, Vol. 24, pp. 255-268, 1981.
- [6] Perko L. Families of symmetric periodic solutions of Hill's problem I: First species periodic solutions for  $C \ll 1$ , *Amer. J. Math.*, Vol. 104, no. 2, pp. 321-352, 1981.
- [7] Szebehely V. *Theory of Orbits*. Academic Press, New York and London, 1967.
- [8] Bruno A.D. *Local Methods in Nonlinear Differential Equations*. Springer-Verlag: Berlin-Heidelberg-New York-London-Paris-Tokyo, 1989.
- [9] Subbotin M.F. *Introduction into Theoretical Astronomy*. Nauka, Moscow, 1968 (Russian).

## TRANSIENT REGIMES IN SYSTEMS WITH INERTIAL EXCITATION OF OSCILLATIONS

**I.I.Blekhman**

Institute for Problems in  
Mechanical Engineering  
RAS, Mekhanobr-tekhnika  
Corp.,  
St. Petersburg, Russia

**N.P.Yaroshevich**<sup>1</sup>

Lutsk National Technical  
University,  
Lutsk, Ukraine

ABSTRACT

A problem of passing the resonance frequency zone at start and run-out of vibrational machine with inertial exciter of oscillations is considered with application of method of direct separation of motions in conjunction with method of sequential approximation. Expression for retarding moment and equation of semi slow oscillations of so called "internal" pendulum has been obtained.

### INTRODUCTION

The problem of passing through resonance frequencies zone arises in start and run-out periods of vibration machines operation. In particular, sticking of rotor rotating frequency close by one of its own frequencies may occur at starting, that is, Zommerfield's effect may develop. Passing through resonance zone in these cases involves considerable oscillations in the system and, correspondingly, dynamic loads on the construction elements. Besides, up rated engine power is needed.

Zommerfield's effect is considered with the application of various methods in a number of works (books [1-6], paper [7], see also works [8-11]). Rigorous investigation of Zommerfield's effect by Poincare's method was carried out in work [1]. Book [4] shows that theoretical explanation and numerical description of the known appropriateness of Zommerfield's effect may be easily obtained by means of the method of direct separation of motions. In [7] the problem for the case of oscillating system with one degree of freedom is solved by the method of successive approximation coupled with the method of direct separation of motions. It is shown that such approach, rougher than in known works, allows to comparatively easier describe the system behavior in both pre- and post- resonance zones of rotor rotation frequencies. Such approach is used in the offered work for systems whose oscillating part is a rigid body with plane-parallel motion.

### 1. SCHEME OF THE SYSTEM AND MOTION EQUATIONS

Carrying body (vibrating member of machine) is considered to be a rigid body capable to execute small plane-parallel oscillations, that is, it has, in general case, three degrees of freedom (Fig. 1). It is linked with stationary base by the system of elastic and damping elements. An unbalanced rotor, set to rotation by asynchronous electric motor or by d.c. current motor, is mounted on the carrying body.

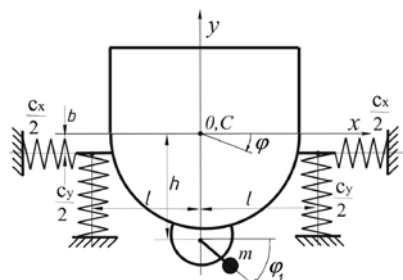


Fig. 1 Scheme of oscillatory system

<sup>1</sup> Corresponding author. Email [m\\_yaroshevich@mail.ru](mailto:m_yaroshevich@mail.ru)

Let  $x$  and  $y$  be masses C centre coordinates in the rest system  $xOy$  and  $\varphi, \varphi_1$  be correspondingly angles of rotation of carrying body and rotor exciter. Differential equations of motion of the system under consideration are presented as

$$I\ddot{\varphi}_1 = L(\dot{\varphi}_1) - R(\dot{\varphi}_1) + m\varepsilon(\ddot{x} \sin \varphi_1 + \ddot{y} \cos \varphi_1 - \ddot{\varphi} h \sin \varphi_1), \quad (1)$$

$$M\ddot{x} + \beta_x \dot{x} + c_x x = m\varepsilon(\ddot{\varphi}_1 \sin \varphi_1 + \dot{\varphi}_1^2 \cos \varphi_1), \quad M\ddot{y} + \beta_y \dot{y} + c_y y = \varepsilon(\ddot{\varphi}_1 \cos \varphi_1 - \dot{\varphi}_1^2 \sin \varphi_1),$$

$$J\ddot{\varphi} + \beta_\varphi \dot{\varphi} + h_\varphi \varphi = -\varepsilon(\ddot{\varphi}_1 \sin \varphi_1 + \dot{\varphi}_1^2 \cos \varphi_1), \quad (2)$$

where  $M$  is total mass of the system;  $J$  is a moment of inertia in respect to the axes passing through the masses centre;  $I$  is a total moment of vibro exciter rotor inertia in respect to its axis of rotation;  $m, \varepsilon$  are, correspondingly, vibro exciter mass and its eccentricity;  $\beta_x, \beta_y, \beta_\varphi$  are coefficients of viscous resistance,  $c_x, c_y$  are longitudinal rigidities of vertical and horizontal springs;  $c_\varphi = c_y l^2 + c_x b^2$ ;  $l, b$  are parameters determining attaching point of the upper spring ends in respect to the masses centre of carrying body;  $h$  is the distance from centre the masses of carrying body to exciter rotor axis;  $L(\dot{\varphi}_1), R(\dot{\varphi}_1)$  are correspondingly, motor torque and a moment of forces resistant to rotation.

## 2. THE FIRST APPROXIMATION, PECULIARITIES OF ZOMMERFIELD'S EFFECT MANIFESTATION IN THE SYSTEM

To study motion of unbalanced excites rotor at passing through the resonance zone the method of direct separation of motions is used [4], according to the main precondition of the method let us assume that motions under consideration may be presented in the form:  $\varphi_1 = \omega t + \psi(t, \omega t)$ ,  $x = x(t, \omega t)$ ,  $y = y(t, \omega t)$ ,  $\varphi = \varphi(t, \omega t)$  where  $\omega = \omega(t)$  is slow and  $\psi$  and  $x, y, \varphi$  are fast time functions, they are  $2\pi$ -periodical at  $\tau = \omega t$  and they value average equals zero; it is also assumed that  $\dot{\psi} \ll \omega$ .

Such presentation of equations (1), (2) at studying the vibroexciter rotor passing through resonance zone, when Zommerfield's effect is taking place and, correspondingly, the frequency of rotor rotation  $\dot{\varphi}_1$  changes slowly enough seems to be rightful.

In the capacity of the first approximation let us assume  $\psi = \psi^{(1)} = 0$ ,  $\varphi_1 = \varphi_1^{(1)} = \omega t$ . Then we come to the equation of slow motions of rotor exciter at passing through resonance zone in the form

$$I\dot{\omega} = L(\omega) - R(\omega) + V(\omega). \quad (3)$$

$$\text{Here } V(\omega) = -(m\varepsilon\omega)^2 \left[ \frac{n_x}{MB_x^2} + \frac{n_y}{MB_y^2} + \frac{h}{J} \frac{n_\varphi}{B_\varphi^2} \right] \quad (4)$$

is so called vibrational moment,

$$B_x = \sqrt{(1 - \lambda_x^2)^2 + 4n_x^2}, \quad \lambda_x = \frac{p_x}{\omega}, \quad p_x = \sqrt{\frac{c_x}{M}}, \quad n_x = \frac{\beta_x}{2M\omega}, \quad B_y = \sqrt{(1 - \lambda_y^2)^2 + 4n_y^2}, \quad \lambda_y = \frac{p_y}{\omega},$$

$$p_y = \sqrt{\frac{c_y}{M}}, \quad n_y = \frac{\beta_y}{2M\omega}, \quad B_\varphi = \sqrt{(1 - \lambda_\varphi^2)^2 + 4n_\varphi^2}, \quad \lambda_\varphi = \frac{p_\varphi}{\omega}, \quad p_\varphi = \sqrt{\frac{c_\varphi}{J}}, \quad n_\varphi = \frac{\beta_\varphi}{2J\omega}.$$

At obtaining this system linearization of expressions  $L(\dot{\varphi}_1), R(\dot{\varphi}_1)$ , as in [1], close by value

$$\dot{\varphi}_1 = \omega \text{ (where } \omega \text{ is frequency of rotor "sticking")} \text{ is performed, } k = - \left. \frac{d(L-R)}{d\dot{\varphi}_1} \right|_{\dot{\varphi}_1 = \omega} > 0 \text{ being a}$$

total damping coefficient.

All components in formula (4) are negative. Thus, as it is for the system with one oscillatory degree of freedom, vibrational moment is always retarding, i.e., it is an additional load upon the

engine rotor, its dependency on frequency is of resonance character, and, therefore, its retarding effect manifests itself in comparatively narrow frequency range.

Rotor rotational speed in stationary regimes is determined from equation  $L(\omega) = R(\omega) - V(\omega)$ . Solutions of this equation are in conformity with cross-points of plots  $L(\omega)$  and  $M_s = R(\omega) - V(\omega)$ , where curves  $L$  correspond to static characteristics of the motor (Fig. 2). According to the figure, the presence of several resonance peaks of the vibrational moment curve may lead to the emergence of additional cross-points of curves  $M_s$  and  $L$  in comparison with the system with rectilinear oscillations of the working head. Thus, several regimes of motion, close to uniform rotation of the rotor and having different average angular velocities are possible in the system. Solution  $\omega_1 < p_1$  under conditions of the picture is pre resonance  $\omega_2, \omega_3$  ( $p_1 < \omega_2, \omega_3 < p_3$ ) is inter resonance,  $\omega_4 > p_3$  is post resonance and  $\omega_5 \gg p_3$  is a post resonance. Inequality  $R'(\omega_*) - V'(\omega_*) > L'(\omega_*)$  is a condition of stability of the regime under consideration [4]. Thus, solution  $\omega_1, \omega_3, \omega_5$  and  $\omega_5^{(1)}$  are stable and  $\omega_2, \omega_4$ , corresponding to descending branches of the curve  $M_s$  are unstable. Characteristic  $L$  corresponds to “sticking” of the system with motor of deficient power close to resonance at frequencies  $\omega_1$  or  $\omega_3$  (motor, on coming to this regime in the process of acceleration would not be able to overcome the resonance peak and reach nominal angular velocity  $\omega_5$ ) and characteristic  $L_1$  of more powerful motor corresponds to coming to post resonance regime of motion with velocity  $\omega_5^{(1)}$ . Hence, as it is in the system with one oscillatory degree of freedom, only two basically different regimes of motion take place: “sticking” of the system in resonance zone and a post resonance regime, or if motor power is sufficient for acceleration, the system, as a rule, after some retardation, rapidly (“by a leap”) comes to the second stationary regime, corresponding to angular velocity  $\omega_5$ .

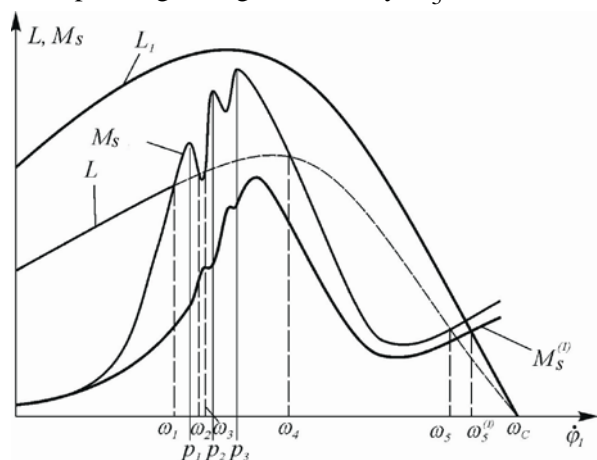


Fig. 2 Stationary regimes of rotor of oscillations rotation

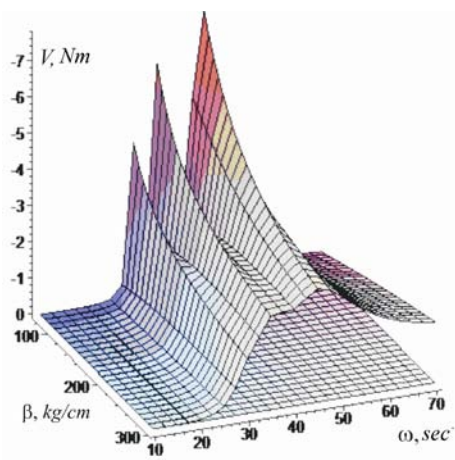


Fig. 3 Dependency of vibrational moment on frequency and resistance coefficient  $\beta$

Expression (4) for vibrational moment may be considered as the sum  $V(\omega) = \sum_{q=x,y,\varphi} v_q$ , summands of which  $v_q = -(m\varepsilon\omega)^2 \frac{n_q}{M_q B_q^2}$ , are “particular” vibrational moments characterizing the affect of oscillations exciter upon rotor rotation, corresponding to  $q$  generalized coordinate. (Here  $q = x$ , if  $q = y$ , to  $M_q = M$ ; if  $q = \varphi$ , to  $M_q = M \frac{\rho^2}{h^2}$ ).

If should, be noted that expression for “particular” vibrational moment may be presented in the form  $v_q = \frac{1}{2} F a_q \sin \gamma_q$ , where  $F = m \varepsilon \omega^2$  is an amplitude of driving force developed by exciter

rotor at stationary carrying body,  $a_q = \frac{m\varepsilon}{M_q \sqrt{(1 - \lambda_q^2)^2 + 4n_q^2}}$  is an amplitude of platform oscillations, corresponding to  $q$  oscillatory coordinate.

Both particular and general vibrational moments characterize vibrational link between carrying body oscillatory motions and rotating motions of vibro exciter rotor.

According to formula (4) the retarding effect of vibration at starting is the less, the stronger the resistance of the system in coordinates  $x$ ,  $y$ ,  $\varphi$ . Fig.3 shows the dependency of vibrational moment on viscous resistance coefficient  $\beta$  ( $\beta = \beta_x = \beta_y / 1, 1 = \beta_\varphi / 0,05$ ) at passing through the resonance zone.

It should be emphasized that the value of maximal retarding vibrational moment sufficiently depends, according to (4), on the frequencies of natural oscillations of the system; decreasing natural frequency we may decrease the retarding moment and, in consequence, decrease resonance amplitudes of oscillations as well as the power of the engine necessary for passing through the resonance zone. Taking into account dependency of vibrational moment on natural frequencies we may assume that the most significant retarding effect is exerted by a particular vibrational moment  $v_\varphi$ , whose frequency is  $p_\varphi$ , as a rule, the highest for the range of machines under consideration. Thus, for instance, in the case of damper application for decreasing the level of oscillations at passing through the resonance the mounting of only one damper of rotational oscillations will be enough.

A particular case of the system when the axle of unbalanced rotor passes through the centre of the carrying body masses has been considered. The exciter axle and attaching chamber spring points are in the same plane ( $b \approx 0$ ). Thus, carrying body performs only transitional motion in plane  $xOy$ .

### 3. SECOND APPROXIMATION. SEMISLOW OSCILLATIONS OF EXCITER ROTOR

For further analysis of rotor motion at passing through the resonance zone we shall use methods offered for investigation of the simplest system in work [7]. We assume  $\varphi_1 = \varphi_1^{(2)} = \omega t + \psi$ ,  $x = x^{(1)} + x^{(2)}$ ,  $y = y^{(1)} + y^{(2)}$ ,  $\varphi = \varphi^{(1)} + \varphi^{(2)}$ . Then we come to the following system of equations for  $\psi$  and  $x^{(2)}$ ,  $y^{(2)}$ ,  $\varphi^{(2)}$ :

$$\begin{aligned}
 I\ddot{\psi} + k\dot{\psi} &= -m\varepsilon\{[\ddot{x}^{(1)} + \ddot{x}^{(2)} - (\ddot{\varphi}^{(1)} + \ddot{\varphi}^{(2)})h]\sin(\omega t + \psi) + (\ddot{y}^{(1)} + \ddot{y}^{(2)})\cos(\omega t + \psi)\} - \\
 &\quad - \frac{m\varepsilon\omega}{2\pi} \int_0^{2\pi} [(\ddot{x}^{(1)} - \ddot{\varphi}^{(1)}h)\sin \omega t + \ddot{y}^{(1)}\cos \omega t] d\tau, \\
 M\ddot{x}^{(2)} + \beta_x \dot{x}^{(2)} + c_x x^{(2)} &= m\varepsilon[(\dot{\omega} + \dot{\psi})\sin(\omega t + \psi) + (\omega + \dot{\psi})^2 \cos(\omega t + \psi) - \omega^2 \cos \omega t], \\
 M\ddot{y}^{(2)} + \beta_y \dot{y}^{(2)} + c_y y^{(2)} &= m\varepsilon[(\dot{\omega} + \dot{\psi})\cos(\omega t + \psi) + (\omega + \dot{\psi})^2 \sin(\omega t + \psi) + \omega^2 \sin \omega t], \\
 J\ddot{\varphi}^{(2)} + \beta_\varphi \dot{\varphi}^{(2)} + c_\varphi \varphi^{(2)} &= m\varepsilon h[(\dot{\omega} + \dot{\psi})\sin(\omega t + \psi) + (\omega + \dot{\psi})^2 \cos(\omega t + \psi) - \omega^2 \cos \omega t]. \quad (5)
 \end{aligned}$$

For the solution of system (5) we shall again use the method of direct separation of motions assuming that  $\psi = \Psi + \gamma$ ,  $x^{(2)} = X + \delta_x$ ,  $y^{(2)} = Y + \delta_y$ ,  $\varphi^{(2)} = \Phi + \delta_\varphi$ , where  $\Psi$ ,  $X$ ,  $Y$ ,  $\Phi$  are slow and  $\gamma$ ,  $\delta_x$ ,  $\delta_y$ ,  $\delta_\varphi$  -fast  $2\pi$ -periodic in fast time  $\tau$  components with average zero values.

In the long run we come to the equations of semi slow (or semi fast) oscillations of exciter rotor angular velocity with respect to uniform rotation (equation of "internal pendulum" oscillations) in the form obtained in [7] for the system with rectilinear oscillations of carrying body

$$\ddot{\Psi} + 2n_1 \dot{\Psi} + B \sin \Psi - P \sin^2 \frac{\Psi}{2} = 0, \quad (6)$$

here  $2n_1 = k/I$ ,  $B = b_x + b_y + b_\varphi$ ,  $P^2 = \rho_x^2 + \rho_y^2 + \rho_\varphi^2$ ,

$$\begin{aligned}
b_x &= \frac{(m\varepsilon\omega^2)^2}{2MI} \frac{p_x^2 - \omega^2}{(p_x^2 - \omega^2)^2 + 4n_x^2\omega^4}, & \rho_x^2 &= \frac{(m\varepsilon\omega^2)^2}{MI} \frac{2n_x\omega^2}{(p_x^2 - \omega^2)^2 + 4n_x^2\omega^4}, \\
b_y &= \frac{(m\varepsilon\omega^2)^2}{2MI} \frac{p_y^2 - \omega^2}{(p_y^2 - \omega^2)^2 + 4n_y^2\omega^4}, & \rho_y^2 &= \frac{(m\varepsilon\omega^2)^2}{MI} \frac{2n_y\omega^2}{(p_y^2 - \omega^2)^2 + 4n_y^2\omega^4}, \\
b_\varphi &= \frac{(m\varepsilon\omega^2)^2 h^2}{2JI} \frac{p_\varphi^2 - \omega^2}{(p_\varphi^2 - \omega^2)^2 + 4n_\varphi^2\omega^4}, & \rho_\varphi^2 &= \frac{(m\varepsilon\omega^2)^2 h^2}{JI} \frac{2n_\varphi\omega^2}{(p_\varphi^2 - \omega^2)^2 + 4n_\varphi^2\omega^4}.
\end{aligned} \quad (7)$$

In the case of consideration of small oscillations, having linearized equation (6) we may present it in classical form  $\ddot{\Psi} + 2n_1\dot{\Psi} + \beta\Psi = 0$ .

At satisfaction of condition  $\omega \ll \omega^2$  frequency of rotor rotational speed  $\omega$  changes slowly and value  $q = \sqrt{|B|}$  is frequency of small free oscillations of the linearized model of internal pendulum (without account of the force of resistance).

Conclusions, made in work [7], about the validity of equation (6) for the system with one oscillatory degree of freedom apply to the cases with two or three degrees of freedom as well.

It follows from the analysis of equation (6) that at  $B > 0$  the solution  $\Psi = \Psi_1 = 0$ , corresponding to “lower” position of internal pendulum, is stable and at  $B < 0$  the solution  $\Psi = \Psi_2 = \pi$  corresponding to “upper” position is stable. Therefore, solution  $\Psi_1 = 0$  is stable in pre resonance zone of variations of frequency  $\omega < p_{\min}$ , where  $p_{\min}$ -is the smallest of values  $p_x, p_y, p_\varphi$  - and in post resonance zone solution  $\Psi_2 = 0$  is stable. So, as in the case of oscillatory system with one degree of freedom, we may say that the internal pendulum turns over in the post resonance zone of frequencies  $\omega > p_{\max}$ . The fact that in intermediate zone  $p_{\min} < \omega < p_{\max}$  pendulum may have time to turn over several times is a sufficient distinction of the system under consideration. In other words, complicated behavior of the system may be expected in the mentioned zone. It is natural, that such effect may take place in the system with any number of oscillatory degrees of freedom.

The obtained results are corroborated by numerical experiment. Fig.3 shows “sticking” of the system I pre-and inter resonance zones with motor of deficient power. Fig.4 shows the effect of emergence of semi slow oscillations of exciter rotor angular velocity close to the resonance zone in the case of rotor “sticking” for the system with one and two degrees of oscillatory freedom.

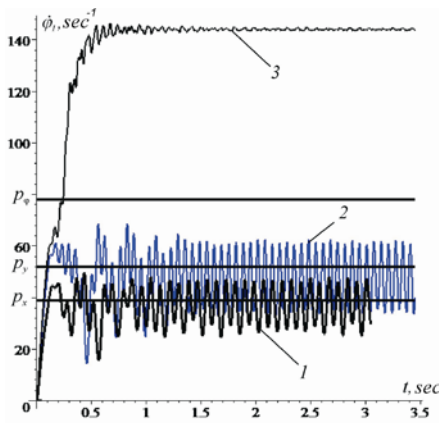


Fig. 4

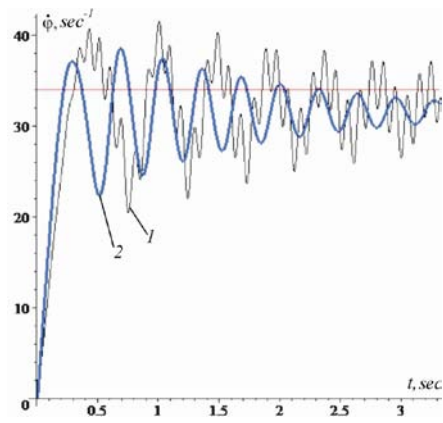


Fig. 5

Fig. 4. Dependency of the vibro exciter rotor rotation frequency time: 1- rotor “sticking” in pre resonance zone, 2- rotor “sticking” in inter resonance zone, 3- acceleration with coming to post resonance regime

Fig. 5. Change of vibroexciter rotor rotation frequency in case of “sticking” in the resonance zone: 1- system with one; 2- system with two oscillatory degrees of freedom.

It should be noted that simulation was performed with account of dynamic response of asynchronous motor. According to the presented plots the ratio of frequencies of semi slow free oscillations of exciter rotor velocity for such oscillatory systems makes up 1.4, as it should be according to the formula  $q = \sqrt{(B)}$ .

## CONCLUSIONS

The work deals with the problem of passing the resonance frequency zone at start and run-out of vibrational machine with inertial exciter of oscillations. The case have been studied when oscillatory part of the system is linear and is a plane-parallelly oscillating rigid body. As in the simplest case of the system with one oscillatory degree of freedom, the problem is comparatively simply solved by application of the method of direct separation of motions coupled with the method of successive approximations.

Expression for the retarding vibrational moment which must be overcome by the motor at passing through the resonance zone consists in the considered case with three components, corresponding to each of three frequencies of free oscillations of the body. These components are of pronouncedly manifested resonance character. Accordingly, the obtained expression for the square of the frequency of semi slow oscillations of the internal pendulum (rotor “swinging”) also consists of three components. As in the simplest system, this pendulum as if turns over at passing through resonance frequency: its “lower” position is stable in pre resonance zone and its “upper” position is stable in post resonance zone. Stable positions may alternate in the interval between the smallest and the greatest resonance frequencies. A complicated behavior of the system may be expected in this interval. Absence of fast oscillations of rotor with doubled frequency of rotation in the case of symmetry of the oscillatory part of the system is a peculiar feature of the considered system.

## REFERENCES

- [1] Blekhman I.I. *Synchronization of dynamic system*. Nauka, Moscow, 896 p., 1971 (in Russian)
- [2] *Oscillations of nonlinear mechanical systems. Vibration in technology: Handbook in 6 volumes*, Vol.2, Mashinostroyeniye, Moscow, 551p., 1978 (in Russian).
- [3] Alifof F.F, Frolov K.V. *Interaction of nonlinear oscillatory system with sources of power*. Nauka, Moscow, 328 p., 1985 (in Russian).
- [4] Blekhman I.I. *Vibrational mechanics*, Fizmatlit, Moscow – 400 (in Russian). English translation : *Vibrational mechanics*. World Scientific, Singapore, 509 p., 2000.
- [5] Fildin A. *Nonlinear Oscillations in Mechanical Engineering*. Springer-Verlag, Berlin, Heidelberg. 358 p., 2006.
- [6] Krasnopolskaya T.Z., Shvets A. Yu. *Regular and random dynamics of the system with limited excitation*. Chaotic&Regular Dynamics, Moscow – Izhevsk, 280 p., 2008.
- [7] Blekhman I.I., Indieytshev D.A., Fradkov A.I. Slow motions in systems with inertial excitation of Oscillations. *Problems of machine building and reliability of machines*. №1, pp.25-31, 2008.
- [8] Rand R.H., Kinsey R.J., Mingori D.L. Dynamics of spin-up through resonance. *Int. J. of Nonlinear Mechanics*, Vol. 27, № 3, pp. 489-502, 1992.
- [9] Balthazar J.M., Mook D.T., Weber H.I. et al. An overview on non-ideal vibrations. *Meccanica* 38 (6), pp. 613-621, 2003.
- [10] Zniber A., Quinn D.D. Resonance capture in a damped three-degree-of-freedom system: Experimental and analytical comparison. *Int. J. of Nonlinear Mechanics*, 41 (10), pp. 1128-1142, 2006.
- [11] Perepelkin N.V., Mikhlin Y.V. Nonlinear dynamics of the system with limited excitation. Proc. of the National Technical University “Kharkiv Polytechnic Institute”. Dynamics and strength of machines, №36, pp. 153-163, 2008.

## ON SOME CHAOTIC MAPPINGS IN SYMBOL SPACE

Inese Bula<sup>1</sup>

University of Latvia and  
Institute of Mathematics  
and Computer Science of  
University of Latvia,  
Riga, Latvia

---

### ABSTRACT

---

A chaotic dynamical system consists of a compact metric space together with a chaotic continuous mapping. A well known chaotic mapping in symbol space is a shift mapping. However, other chaotic mappings in symbol space exist too. We consider the increasing mapping as a generalization of the shift mapping and the  $k$ -switch mapping too, and combination of both mappings. All these mappings are chaotic. Models with chaotic mappings are not predictable in long-term.

---

### INTRODUCTION

Chaotic dynamical systems have received a great deal of attention in the past. Chaotic systems are nonlinear dynamical systems with certain distinct characteristics. In this paper we consider chaotic mappings in symbol space.

The technique of characterizing the orbit structure of a dynamical system via infinite sequences of symbols is known as symbolic dynamics. If the process is a discrete process such as the iteration of a function  $f$ , then the theory hopes to understand the eventual behavior of the points (the orbit of  $x$  by  $f$ )  $x, f(x), f^2(x), \dots, f^n(x), \dots$  as  $n$  becomes large. That is, dynamical systems ask to somewhat nonmathematical sounding question: where do points go and what do they do when they get there?

A well known chaotic mapping in symbol space is a shift mapping ([8], [9], [10], [14]). However, other chaotic mappings in symbol space exist too. The basic change is to consider the process (physical or social phenomenon) not only at a set of times which are equally spaced, say at unit time apart (a shift mapping), but at a set of times which are not equally spaced, say if we cannot fixed unit time (an increasing mapping). There is a philosophy of modeling in which we study idealized systems that have properties that can be closely approximated by physical systems. The experimentalist takes the view that only quantities that can be measured have meaning. This is a mathematical reality that underlies what the experimentalist can see.

The paper is structured as follows. It starts with preliminaries concerning notations and terminology that is used in the paper followed by a definition of the chaotic mapping. The increasing mapping and the  $k$ -switch mapping is considered in Section 2. The combination of both listed mappings is considered in Section 3. Finally we give some conclusions.

### 1. PRELIMINARIES

The section presents the notation and terminology used in this paper. Terminology comes from combinatorics on words (for example, [12] or [13]).

We give some notations at first:  $\bar{k}, n = \{k, k+1, \dots, n\}$ ,  $k \leq n$  and  $k, n \in \{0, 1, 2, \dots\}$ ,

$Z$  is the set of integers,  $Z_+ = \{x | x \in Z \ \& \ x > 0\}$ ,  $N = Z_+ \cup \{0\}$ .

From now on  $A$  will denote a finite *alphabet*, i.e., a finite nonempty set  $\{a_0, a_1, a_2, \dots, a_n\}$  and the elements are called *letters*. We assume that  $A$  contains at least two symbols. By  $A^*$  we will denote the set of all finite sequences of letters, or finite *words*, this set contains empty word (or sequence)  $\lambda$  too.  $A^+ = A^* \setminus \{\lambda\}$ . A word  $\omega \in A^+$  can be written uniquely as a sequence of letters

---

<sup>1</sup> Corresponding author. Email [ibula@lanet.lv](mailto:ibula@lanet.lv)

as  $\omega = \omega_1\omega_2\dots\omega_l$ , with  $\omega_i \in A$ ,  $1 \leq i \leq l$ . The integer  $l$  is called the *length* of  $\omega$  and denoted  $|\omega|$ . The length of  $\lambda$  is 0. An extension of the concept of finite word is obtained by considering infinite sequences of symbols over a finite set. *One-sided* (from left to right) infinite sequence or word, or simply *infinite word*, over  $A$  is any total map  $\omega: \mathbb{N} \rightarrow A$ . The set  $A^\omega$  contains all infinite words.  $A^\infty = A^* \cup A^\omega$ . If the word  $u = u_0u_1u_2\dots \in A^\infty$ , where  $u_0, u_1, u_2, \dots \in A$ , then finite word  $u_0u_1u_2\dots u_n$  is called the *prefix* of  $u$  of length  $n+1$ . The empty word  $\lambda$  is assumed to be the prefix of  $u$  of length 0.  $\text{Pref}(u) = \{\lambda, u_0, u_0u_1, u_0u_1u_2, \dots, u_0u_1u_2\dots u_n, \dots\}$  is the set of all prefixes of word  $u$ .

Secondly we introduce in  $A^\infty$  a metric  $d$  as follows.

**Definition 1.1** ([13]). Let  $u, v \in A^\infty$ . The mapping  $d: A^\infty \times A^\infty \rightarrow \mathbb{R}$  is called a *metric (prefix metric)* in the set  $A^\infty$  if  $d(u, v) = \begin{cases} 2^{-m}, & u \neq v, \\ 0, & u = v, \end{cases}$  where  $m = \max\{|\omega| \mid \omega \in \text{Pref}(u) \cap \text{Pref}(v)\}$ .

The metric space  $(A^\omega, d)$  is compact metric space ([15]).

The term ‘‘chaos’’ in reference to functions was first used in Li and Yorke’s paper ‘‘Period three implies chaos’’ ([11], 1975). Although there is no universally accepted mathematical definition of chaos, Devaney’s definition [6] of chaos is one of the most popular. In order to introduce the definition of chaos in the sense of Devaney, we first present several preliminary concepts.

Let  $(X, \rho)$  be metric space and  $A \subset X$  and  $F \subset A$ .

We say that the set  $F$  is *dense* in  $A$  ([6], [8], [14]) if for each point  $x$  in  $A$  and each  $\varepsilon > 0$ , there exists  $y$  in  $F$  such that  $\rho(x, y) < \varepsilon$ .

We say that the function  $f$  is *topologically transitive* on  $A$  ([6], [8], [14]) if for any two points  $x$  and  $y$  in  $A$  and any  $\varepsilon > 0$ , there is  $z \in A$  such that  $\rho(z, x) < \varepsilon$  and  $\rho(f^n(z), y) < \varepsilon$  for some  $n$ .

We say that the function  $f: A \rightarrow A$  exhibits *sensitive dependence on initial conditions* ([6], [8], [14]) if there exists a  $\delta > 0$  such that for any  $x$  in  $A$  and any  $\varepsilon > 0$ , there is a  $y$  in  $A$  and natural number  $n$  such that  $\rho(x, y) < \varepsilon$  and  $\rho(f^n(x), f^n(y)) > \delta$ .

**Definition 1.2** ([6]). The function  $f: A \rightarrow A$  is *chaotic* if

- a) the set of periodic points of  $f$  are dense in  $X$ ,
- b)  $f$  is topologically transitive and
- c)  $f$  exhibits sensitive dependence on initial conditions.

Devaney’s definition is not the unique classification of a chaotic map. For example, another definition can be found in [14]. Also mappings with only one property - sensitive dependence on initial conditions - frequently are considered as chaotic (see [7]). Banks, Brooks, Cairns, Davis and Stacey [1] have demonstrated that for continuous functions, the defining characteristics of chaos are topological transitivity and the density of the set of periodic points. But if the set of periodic points of function  $f$  is dense in  $A$  and there is a point whose orbit under iterations of  $f$  is dense in the set  $A$ , then  $f$  is topologically transitive on  $A$  ([8]). Therefore in this case if  $f$  is invariant in the set  $A$  and continuous, then it is chaotic mapping.

## 2. INCREASING MAPPING AND $k$ -SWITCH MAPPING

We have introduced the notion of increasing mapping in [3].

Let  $f_\omega(x) = x_{g(0)}x_{g(1)}x_{g(2)}\dots x_{g(i)}\dots, i \in \mathbb{N}, x \in A^\omega$ . In this case the function  $g$  is called the *generator function* of mapping  $f_\omega$ .

**Definition 2.1** ([3]). A function  $g: \mathbb{N} \rightarrow \mathbb{N}$  is called *positively increasing function* if  $0 < g(0)$  and  $\forall i \forall j [i < j \Rightarrow g(i) < g(j)]$ . The mapping  $f_\omega: A^\omega \rightarrow A^\omega$  is called *increasing mapping* if its generator function  $g: \mathbb{N} \rightarrow \mathbb{N}$  is positively increasing.

The well known shift map is increasing mapping in one-sided infinite symbol space  $A^\omega$ , in this case the generator function is a positively increasing function  $g: \mathbb{N} \rightarrow \mathbb{N}$ , where  $g(x) = x + 1$ .

**Theorem 2.1** ([3]). *The increasing mapping  $f_\omega : A^\omega \rightarrow A^\omega$  is continuous in the set  $A^\omega$ . For increasing mapping  $f_\omega : A^\omega \rightarrow A^\omega$  exists a dense orbit in the set  $A^\omega$ . The set of periodic points set of increasing mapping  $f_\omega : A^\omega \rightarrow A^\omega$  is dense in the set  $A^\omega$ .*

**Theorem 2.2** ([3]). *The increasing mapping  $f_\omega : A^\omega \rightarrow A^\omega$  is chaotic in the set  $A^\omega$ .*

Now we can give two **conclusions** about mappings in symbol space which are not chaotic:

1) If the generator function  $g : N \rightarrow N$  of mapping  $f_\omega : A^\omega \rightarrow A^\omega$  is such that  $g(0) = 0$ , then the generated mapping  $f_\omega$  is not chaotic in the set  $A^\omega$ ;

2) If the generator function  $g : N \rightarrow N$  of mapping  $f_\omega : A^\omega \rightarrow A^\omega$  is not one-to-one function, then the generated mapping  $f_\omega$  is not chaotic in the set  $A^\omega$ .

We have introduced the notion of  $k$ -switch mapping in [4].

**Definition 2.2.** The mapping  $f_{\overline{1k}} : A^\omega \rightarrow A^\omega$  is called  $k$ -switch ( $k \in N$ ) mapping if for every

$$s = s_0 s_1 s_2 s_3 \dots s_k s_{k+1} \dots \in A^\omega : f_{\overline{1k}}(s) = \overline{s_1 s_2 s_3 \dots s_k s_{k+1} s_{k+2} \dots},$$

where  $\overline{s_i}, i = \overline{1, k}$ , there is the same symbol (letter) as  $s_i$  or  $\exists a \in A : \overline{s_i} = a$ . In other words, at first, this mapping is shift and, secondly, this mapping switches some symbols (not more as  $k$  symbols).

For example, let  $A = \{0,1\}$  and  $f_{\overline{1,3}}(s_0 s_1 s_2 s_3 s_4 \dots) = \overline{s_1 s_2 s_3 s_4 s_5 \dots}$  is 3-switch mapping that switch first and third symbol. Indices by mapping  $f$  show which symbols switches to another by defined rule. For example, if  $s = 1111111\dots$ , then  $f_{\overline{1,3}}(s) = 0101111\dots$ . If we consider situation with  $A$  that contains at least three symbols  $A = \{a_0, a_1, a_2, \dots, a_n\}$ , then we define rule which  $a_i$  switches to  $a_j$  and for every  $a_j \in A$  only one  $a_i \in A$  exists with this rule.

More formally: we set a bijection  $\overline{\phantom{x}} : A \rightarrow A$ , we fix indices  $1 \leq i_1 < i_2 < \dots < i_n = k$ . Then

$$f_{\overline{1k}}(s_0 s_1 s_2 \dots) = \overline{t_0 t_1 t_2 \dots},$$

$$\text{where } t_j = \begin{cases} \overline{s_{j+1}}, & \text{if } \exists \eta \ i_\eta = j+1, \\ s_{j+1}, & \text{otherwise.} \end{cases}$$

**Theorem 2.3** ([4]). *The  $k$ -switch mapping  $f_{\overline{1k}} : A^\omega \rightarrow A^\omega$  is continuous in the set  $A^\omega$ . The  $k$ -switch mapping  $f_{\overline{1k}} : A^\omega \rightarrow A^\omega$  is topologically transitive in the set  $A^\omega$ . The set of periodic points of  $k$ -switch mapping  $f_{\overline{1k}} : A^\omega \rightarrow A^\omega$  is dense in the set  $A^\omega$ .*

**Theorem 2.4** ([4]). *The  $k$ -switch mapping  $f_{\overline{1k}} : A^\omega \rightarrow A^\omega$  is chaotic in the set  $A^\omega$ .*

We have demonstrated two different classes of chaotic mappings. It is possible for increasing mapping (from two symbols 0 and 1 space) to construct corresponding mapping in the unit segment that is chaotic ([2], [5]). Similarly we can obtain the chaotic map in the interval  $[0, 1]$  from every chaotic mapping of two symbols 0 and 1 space.

### 3. COMBINATION OF INCREASING MAPPING AND $k$ -SWITCH MAPPING

Now we consider the new class of mappings.

**Definition 3.1.** The mapping  $f_{\alpha|\beta} : A^\omega \rightarrow A^\omega$  is called *increasing-switch mapping* if for every  $s = s_0 s_1 s_2 s_3 \dots s_k s_{k+1} \dots \in A^\omega$ , firstly, some symbols are “forgets” – these indices of symbols

are designated in  $\alpha$  part, secondly, some symbols are switched to another's - these indices of symbols are designated in  $\beta$  part and thirdly,  $\alpha \cap \beta$  is an empty set.

For example, let  $A = \{0,1\}$  and

$$f_{0,2,4|1,5}(s_0 s_1 s_2 s_3 s_4 s_5 \dots) = \overline{s_1 s_3 s_5 s_6 s_7 \dots}$$

This mapping “forgets” symbols  $s_0, s_2, s_4$  and switch symbols  $s_1, s_5$ . Exactly, if we consider the infinite sequence  $s = 0110010111000\dots \in A^\omega$ , then

$$f_{0,2,4|1,5}(s) = 0000111000\dots$$

If we consider situation with  $A$  that contains more than two symbols  $A = \{a_0, a_1, a_2, \dots, a_n\}$ , then we define the rule which  $a_i$  switches to  $a_j$  and for every  $a_j \in A$  exist only one  $a_i \in A$  with this rule (analogical as case of  $k$ -switch mapping).

We note that the increasing-switch mapping is not a function composition of increasing mapping and  $k$ -switch mapping in general case since  $f_\omega(f_{1/k}^- (s))$  and  $f_{1/k}^- (f_\omega (s))$  “forgets” two first symbols of the sequence  $s$ . But, on the other hand, every composition of increasing mapping and  $k$ -switch mapping ( $f_\omega(f_{1/k}^- (s))$  or  $f_{1/k}^- (f_\omega (s))$ ) is increasing-switch mapping.

It is possible to show that every mapping that changes the finite number of symbols (“forgets”, switch with or without bijection rule, or another changes) is continuous mapping in metric space  $(A^\omega, d)$ . But every continuous mapping in this space is not chaotic (see conclusions below Theorem 2.2).

**Theorem 3.1.** *The increasing-switch mapping  $f_{\alpha|\beta} : A^\omega \rightarrow A^\omega$  is continuous in the set  $A^\omega$ . The increasing-switch mapping  $f_{\alpha|\beta} : A^\omega \rightarrow A^\omega$  is topologically transitive in the set  $A^\omega$ . The set of periodic points of increasing-switch mapping  $f_{\alpha|\beta} : A^\omega \rightarrow A^\omega$  is dense in the set  $A^\omega$ .*

**Theorem 3.2.** *The increasing-switch mapping  $f_{\alpha|\beta} : A^\omega \rightarrow A^\omega$  is chaotic in the set  $A^\omega$ .*

By Lind and Marcus [10] terminology: a dynamical system  $(X, f)$  consists of a compact metric space  $X$  together with a continuous map  $f : X \rightarrow X$ . We have found three dynamical systems  $(A^\omega, f_\omega)$ ,  $(A^\omega, f_{1/k}^-)$  and  $(A^\omega, f_{\alpha|\beta})$  which all are chaotic.

## CONCLUSIONS

Let

$$x(t_0), x(t_1), \dots, x(t_n), \dots$$

be the flow of discrete signals. Suppose that we have the experimentally observed subsequence

$$x(T_0), x(T_1), \dots, x(T_n), \dots$$

If

$$T_0 = t_1, T_1 = t_2, \dots, T_n = t_{n+1}, \dots,$$

then we have the shift map. Notice if we have the infinite word

$$x = x_0 x_1 \dots x_n \dots$$

instead of flow of discrete signals, then we have respectively the infinite word

$$y = y_0 y_1 \dots y_n \dots$$

instead of the experimentally observed subsequence. Here  $\forall t \quad y_t = x_{t-1}$ . Hence, we obtain the shift map  $g(t) = t + 1$ , namely,

$$y = f_\omega(x) = x_{g(0)} x_{g(1)} x_{g(2)} \dots x_{g(n)} \dots$$

We do not claim that the function  $g(t) = t + 1$  is chaotic on the real line  $\mathbf{R}$  but we had proved that this function as a generator creates the chaotic map  $f_\omega$  in the symbol space  $A^\omega$ . We had proved

something more, namely, every positively increasing function  $g$  as a generator creates the chaotic map  $f_\omega$  in the symbol space  $A^\omega$ . In other words, if we had detected in our experiment only subsequence

$$x(t_1), x(t_3), \dots, x(t_{2n-1}), \dots$$

even then we can reveal chaotic behavior.

Now we have proved that every  $k$ -switch mapping  $f_{\frac{-}{1k}} : A^\omega \rightarrow A^\omega$  and every increasing-switch mapping  $f_{\alpha|\beta} : A^\omega \rightarrow A^\omega$  are chaotic in the symbol space  $A^\omega$ . In other words, if we had detected in our experiment only subsequence  $x(t_1), x(t_2), \dots, x(t_n), \dots$  with some kind of regular distortion, even then we can reveal chaotic behavior.

## REFERENCES

- [1] Banks J., Brooks J., Cairns G., Davis G., Stacey P. On Devaney's definition of chaos, *Amer. Math. Monthly*, V.99, pp.29-39, 1992.
- [2] Bula I., Topological semi-conjugacy and chaotic mappings, *Proc. of 6th EUROMECH Nonlinear Dynamics Conference (ENOC 2008)*, 2008, <http://lib.physcon.ru/?item=1603>
- [3] Bula I., Bula J., Rumbeniec I. *Why can we detect the chaos?* Journal of Vibroengineering, Vol.10, pp.468-474, 2008.
- [4] Bula I., Bula J., Rumbeniec I. On chaotic mappings in symbol space, *Proc. of the 10<sup>th</sup> conf. on Dynamical Systems – Theory and Applications*, Vol.2, Lodz, Poland, pp.955-962, 2009.
- [5] Bula I., Rumbeniec I. Construction of chaotic dynamical system, *Mathematical Modelling and Analysis*, Vol.15 (1), pp.1-8, 2010.
- [6] Devaney R. *An introduction to chaotic dynamical systems*. Benjamin Cummings: Menlo Park, CA, 1986.
- [7] Gulick D. *Encounters with chaos*. McGraw-Hill, Inc., 1992.
- [8] Holmgren R.A. *A first course in discrete dynamical systems*. Universitext, sec. ed., Springer-Verlag, 1996.
- [9] Kitchens B.P. *Symbolic Dynamics. One-sided, two-sided and countable state Markov shifts*. Springer-Verlag, 1998.
- [10] Lind D., Marcus B. *An introduction to symbolic dynamics and coding*. Cambridge University Press, Cambridge, 1995.
- [11] Li T.Y., Yorke J. A. Period three implies chaos. *Amer. Math. Monthly*, V.82(12), P.985-992, 1975.
- [12] Lothaire M. Combinatorics on Words. *Encyclopedia of Mathematics and its Applications*, V.17, Addison-Wesley, Reading, MA, 1983.
- [13] de Luca A., Varricchio S. *Finiteness and regularity in semigroups and formal languages*. Monographs in Theoretical Computer Science, Springer-Verlag, 1999.
- [14] Robinson C. *Dynamical systems. Stability, symbolic dynamics, and chaos*. CRS Press, Boca Raton, Florida, 1995.
- [15] Wiggins S. *Global Bifurcations and Chaos. Analytical Methods*. Springer-Verlag, New York, 1988.

## INVESTIGATION OF STABILITY WITH RESPECT TO PART OF VARIABLES IN HYBRID AUTOMATA

**Alexei Bychkov**

National Taras  
 Shevchenko University of  
 Kyjv, Ukraine

ABSTRACT

In the article new constructive conditions for stability of trivial equilibrium point of hybrid automaton with respect to part of variables are proposed. Conditions are based on construction of a sequence of values of Lyapunov functions at state switching points. Proposed conditions principally differ from existing conditions in that they do not depend on the values of hybrid automaton's solutions at moments of switching.

### INTRODUCTION

Hybrid automaton is a tuple  $H = (Q, X, F, Init, Inv, Jump, \tau)$ , where

- $\tau$  is a hybrid time,
- $X = \{x_1, \dots, x_n\}$ ,  $n \geq 0$ ,  $x_i \in R$  is a phase space;
- $F = \{f_i : Q \times R^n \rightarrow R^n, i = \overline{1, N}\}$  are right hand sides of differential equations which describe dynamics in local states;
- $Init : Init \subset Q \times R^n$  is a set of initial states;
- $Inv : Inv \subset Q \times R^n$  is an invariant set of each local state;
- $Jump : Q \times R^n \rightarrow \beta(Q \times R^n)$  is a map which describes automaton's transitions.

We describe now the usage of Lyapunov's second method for investigation of stability of equilibrium point of hybrid automata.

One refer to existing methods of investigation of stability of hybrid automata.

Suppose that dynamics in  $i$ -th local state is described by systems of differential equations  $\dot{x}(t) = f_i(t, x(t))$ ,  $i = 1, \dots, N$ . Most of methods require a set of Lyapunov functions  $\{V_i, i = 1, \dots, N\}$  to be defined.

Existing approaches require non-increasing of Lyapunov functions at switching points on values of hybrid automaton's trajectories:

- 1) R. DeCarlo, D. Liberzon, A. Morse [1,2]:

$$V_j(x(t_{j+1})) - V_i(x(t_{i+1})) \leq -\gamma \|x(t_{i+1})\|^2, \gamma > 0,$$

where  $t_i < t_j, i < j$  are switching moment (asymptotic stability).

- 2) M. Branicky [3]:

$$V_i(x(t_{i,k})) \leq V_i(x(t_{i,k-1})),$$

where  $t_{i,k}$  is a  $k$ -th moment of switching to the vector field  $f_i$ .

- 3) H. Ye, A. Michel [4] use the "weak Lyapunov function":

$$V_i(x(t)) \leq h(V_i(x(t_j))), t \in (t_j, t_{j+1}),$$

where  $h : R^+ \rightarrow R^+$  is a continuous function which satisfies initial condition  $h(0) = 0$ ,  $t_j$  is an arbitrary switching moment.

As noted earlier, proposed conditions depend on values of trajectory at switching moments.

# 1. HYBRID AUTOMATA STABILITY CONDITIONS

Let the space  $R^2$  and two local states be given. The first local state is defined by subset of phase space,

$$\Omega_1 = \{x \in R^2 : x_2 - kx_1 < 0\},$$

the second one is defined as,

$$\Omega_2 = \{x \in R^2 : x_2 - kx_1 > 0\}.$$

Thereby transition from the state  $I$  to the state  $II$  occurs when a trajectory reaches the line  $x_2 = kx_1$ . Suppose that in local states dynamics is described by systems of linear differential equations.

Assume that for each system there exists a positive-definite Lyapunov function such that

$$\left. \frac{dV_i(x)}{dt} \right|_{(i)} < 0, \text{ if } x \in \Omega_i, i = 1, 2. \tag{1}$$

Thus we require (1) only on the set which defines current local state.

Choose an arbitrary point  $x^0$  on the switching line. Let  $I$  be an initial state. Let us build a level set of the function  $V_1(x)$  which starts at  $x^0$  (fig. 1).

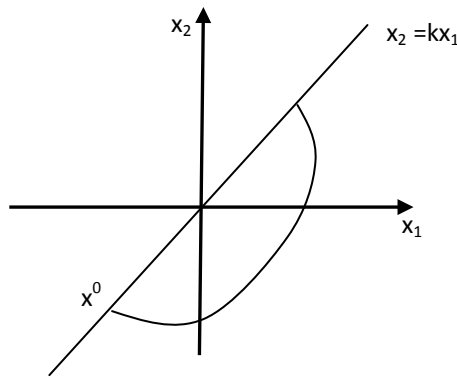


Fig. 1. The first Lyapunov's function level-line

Denote  $c^0 = V_1(x^0)$ . Let us find an intersection point of a level set  $C_1 = \{x \in R^2 : V_1(x) = c^0, x \in \Omega_1\}$  with the line  $x_2 = kx_1$ . Denote it by  $x^1$  (fig. 1).

At the point  $x^1$  the switching occurs from the state  $I$  to the state  $II$ . Therefore let  $c^1 = V_2(x^1)$ . Let us build a level set of the Lyapunov function  $V_2(x)$ , which starts at  $x^1$  in the second local state  $C_1 = \{x \in R^2 : V_1(x) = c_0, x \in \Omega_1\}$  (fig. 2).

Let us find an intersection point of the level set  $C_1 = \{x \in R^2 : V_1(x) = c_0, x \in \Omega_1\}$  with the line  $x_2 = kx_1$ . Denote it by  $x^2$  (fig. 2).

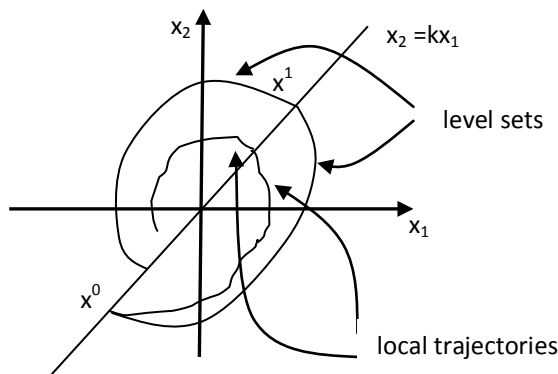


Fig. 2. The  $R^2$  Lyapunov's function level-line and trajectories

From the inequality  $\left. \frac{dV_1(x)}{dt} \right|_{(1)} < 0$  in the first local state it follows that a trajectory, which starts at  $x^0$  can not leave a domain bounded by the level set  $C_1 = \{x \in R^2 : V_1(x) = c^0, x \in \Omega_1\}$ . Analogously, trajectory of the second local state, which starts at  $x^1$  can not leave a domain bounded by the level set  $C_1 = \{x \in R^2 : V_1(x) = c_0, x \in \Omega_1\}$  (fig. 2).

Therefore it can be assumed that if

$$|x^2| < |x^0|, \quad (2)$$

then the trivial equilibrium point of the hybrid automaton is asymptotically stable.

It should be noted that condition (2) can not be applied in cases when transition occurs on non-straight lines. For example, suppose that transition occurs on the curve shown on the fig. 3.

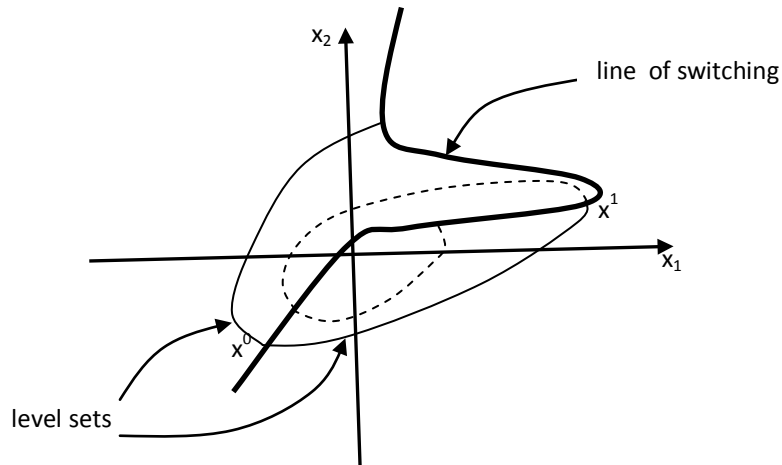


Fig. 3. The  $R^2$  Lyapunov's function level-line and trajectories with non-straight line of switching

It is obvious that condition (2) is not satisfied but trivial equilibrium can be stable. Therefore it is reasonable to use the following condition instead of (2)

$$|c_2| < |c_0|$$

Condition (2) can be generalized to the cases when phase space is  $R^n$  and switching surfaces are arbitrary (fig. 4).

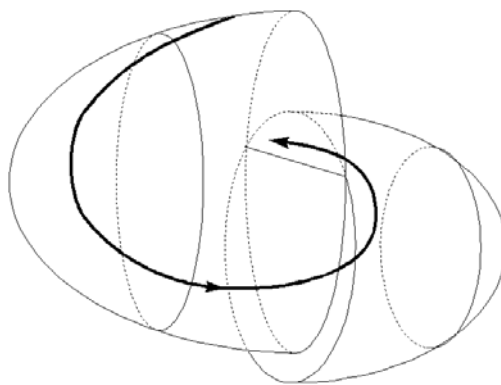


Fig. 4. The  $R^3$  Lyapunov's function level-line and trajectories

Suppose that trajectory of hybrid automaton starts in the first state. We use the notation  $x|_{i \rightarrow i+1}$  to indicate that hybrid automaton switches from state  $i$  to state  $i+1$  at the point  $x$ .

To obtain constructive stability conditions let us build the following sequence (s-condition):

$$c^0 \in (0, C), \quad c^1 = \max_{\substack{x^1|_{1 \rightarrow 2} \\ V^1(x^1) \leq c_0}} V^2(x^1), \quad c^2 = \max_{\substack{x^2|_{2 \rightarrow 3} \\ V^2(x^2) \leq c_1}} V^3(x^2), \dots, \quad c^N = \max_{\substack{x^N|_{N \rightarrow 1} \\ V^N(x^N) \leq c_{N-1}}} V^1(x^N) \quad (3)$$

Here we take into account the case when a level set intersects with a switching surface before (in time), a trajectory reaches switching surface.

In the condition (3) the second restriction allows to take into account a value of Lyapunov function at the switching point and to use it for construction of the next level set.

## 2. STABILITY WITH RESPECT TO PART OF VARIABLES IN HYBRID AUTOMATA

Let us build the following sequence  $\{c^i\}$ ,  $i = \overline{0, N}$ :

$$c^0 \in (0, C), \quad c_k(h) = \sup\{V_{k+1}(x) \mid x \in J_k, V_k(x) \leq h\} \quad (4)$$

It can be built starting from arbitrary initial state (not only from the first state). We introduce the following notation:  $B_r = \{x \in R^n : |x| \leq r\}$ ,  $S_r = \{x \in R^n : |x| = r\}$ .

We define a hybrid time  $\tau$  either as a finite sequence  $\tau_H = \{\tau_i\}_1^N$ , where:  $\tau_i = (Pre\_jump_i, [t_{i-1}^*, t_i^*], Post\_jump_i), i = 1..N; t_0 = 0; [t_{i-1}^*, t_i^*]$  are closed segments, and the last element is a semi-open interval  $\tau_N = [t_N, \infty)$ , or as an (infinite) sequence  $\tau_H = \{\tau_i\}_1^\infty$  of closed segments  $[t_{i-1}^*, t_i^*]$ . Denote  $T$  is the set of all possible  $\tau$ .

**Definition 1.** A phase orbit of hybrid automaton  $H$  is a set  $\chi = \{(\tau, i, x)\}$ , where  $\tau \in T$ ,  $i$  – a number of a local state and  $x : \tau \rightarrow R^n$  is a function such that  $(i(\tau_0), x(\tau_0)) \in Init$ , for all  $u$  such that  $\tau_i < \tau'_i$ . Here  $(i(t), x(t)) \in Inv$  defines continuous dynamics in  $i$ -th local state and  $(i(\tau_{i+1}), x(\tau_{i+1})) \in Jump(i(\tau'_i), x(\tau'_i))$  defines discrete dynamics.

**Definition 2.** Continuous state  $x = 0$  is called a trivial equilibrium point of hybrid automaton if (i) there exists a non-empty set  $\overline{Q} \subset Q$ , such that for all  $i \in \overline{Q}$  condition  $(i', z') \in Jump(i, 0)$  implies that  $z' = 0$  and  $i' \in \overline{Q}$ ; (ii)  $f(i, 0) = 0$  for all  $i \in \overline{Q}$ .

**Definition 3.** Trivial equilibrium of hybrid automaton  $H$  is called stable (in sense of Lyapunov), if for each  $\varepsilon > 0$  there exists  $\delta > 0$  such that for every trajectory the condition  $|x(t_0)| < \delta$  implies that  $|x(t)| < \varepsilon$  for all  $t \in \tau$ . Here  $|\cdot|$  denotes Euclidean norm.

Let us denote  $\Omega_i$  the set which describes  $i$ -th local state.

Assume that there exist Lyapunov functions defined on the sets  $\Omega_i$ .

**Definition 4.** An indexed family  $V(i, x) = \{V^i(x)\}$ ,  $i = \overline{1, N}$  is called a hybrid  $s$ -function, if each  $V^i(x)$  is positive definite and for every sequence  $\{c^i\}$ ,  $i = \overline{0, N}$  defined as in (4) the inequality  $c^N \leq c^0$  holds.

We will use hybrid  $s$ -function for investigation of stability of trivial equilibrium point of hybrid automata.

**Definition 5.** The following expression is called a derivative of hybrid  $s$ -function with respect to hybrid automaton:

$$\dot{V}(i, x) = \left\{ \frac{dV^i(x)}{dx} f_i(x(t)), i = \overline{1, N} \right\}.$$

**Theorem 1.** [5] Suppose that hybrid automaton  $H$  has a trivial equilibrium point,  $|Q| < \infty$ ,  $i = \overline{1, N-1}$ ,  $Jump(N, x) = (1, x)$ . Also suppose that a neighborhood of the coordinate origin  $D \subset X$  is given. If there exists a positive-definite hybrid  $s$ -function  $V(i, x) : Q \times D \rightarrow R$  for hybrid automaton  $H$ , such that  $\frac{dV^i(x)}{dx} f_i(x(t)) \leq 0$  for all  $x \in D \cap \Omega_i$  and  $i = \overline{1, N}$ , then  $x = 0$  is stable trivial equilibrium point of hybrid automaton  $H$ .

It should be noted that checking of the proposed condition does not require investigation of reachability of switching surface by hybrid automaton's trajectories. It is connected with the fact that if switching surface is not reachable and  $s$ -condition is satisfied, then stability of equilibrium follows from classical Lyapunov theorem, because in this case we can simply consider system on the whole phase space.

Also a principal value has the fact that proposed theorem does not require computation of hybrid automaton's solution.

Let us construct stability conditions from impulsive hybrid automata.

Suppose that hybrid automaton's trajectory starts in the first state. We use the notation  $x^{i-} \rightarrow x^{i+} |_{i \rightarrow i+1}$  to indicate that hybrid automaton switches from the state  $i$  to  $i+1$  and the value  $x^{i-}$  is taken from the set which determines jump condition, while  $x^{i+}$  is the value of phase coordinate after jump, i.e.  $x^{i+} = q(x^{i-})$ .

Theorem 2. Suppose that hybrid automaton  $H$  has the trivial equilibrium point  $x=0$ ,  $|Q| < \infty$ ,  $Jump(i, x) = \{(i+1, q_i(x))\}$ , for  $i = \overline{1, N-1}$ ,  $Jump(N, x) = (1, q_N(x))$ . Also suppose that a neighborhood of the origin  $D \subset X$  is given. If for each local state  $\Omega_i$  there exist positive-definite functions  $V(i, x): Q \times D \rightarrow R$  such that

1.  $\frac{dV^i(x)}{dx} f_i(x(t)) \leq 0$  for all  $x \in D \cap \Omega_i$ ,  $i = \overline{1, N}$ ;

2. for every sequence  $c^i$  which starts in arbitrary state the condition  $c^N \leq c^0$  is satisfied;

3. there exists a continuous monotone increasing function  $\psi(\cdot): R^+ \rightarrow R^+$ , such that  $\psi(0) = 0$  and  $\|q_i(z)\| < \psi(\|z\|)$ ,  $\forall i \in Q$ . Then  $x=0$  is stable trivial equilibrium point of impulsive hybrid automaton  $H$ .

Also corresponding theorems about instability and exponential stability have been proved.

Now let us turn to the problem of stability with respect to part of variables. Consider a hybrid automaton described by the equations of the following kind in it's local states:

$$\dot{y} = f_q(y), \quad y \in Inv_q, \quad y = \begin{pmatrix} y_1 \\ y_2 \end{pmatrix}, \quad y(t_0) = 0, \quad (5)$$

where  $y_1 \in R^{n_1}$ ,  $y_2 \in R^{n_2}$ . We call a variable  $y_1$  as observable,  $y_2$  as hidden. We assume that transitions between states  $q \in Q$  are continuous ( $Jump(q, y) = \emptyset \vee \{(r, y)\}$ ).

A problem: determine stability of hybrid automaton (5) with respect to vector of observable coordinates  $y_1$ . We assume that  $y_1 = 0$  is a trivial equilibrium point of hybrid automaton for each values of hidden vector  $y_2$ .

Denote  $n = n_1 + n_2$ ,  $|x|$  as Euclidean norm in  $0_1$ ,  $|x|_1$  and  $|x|_2$  as Euclidean norms in  $R^{n_1}$  and  $R^{n_2}$  correspondingly. Similarly,  $0_1$  denotes null-vector in  $R^{n_1}$ ,  $0$  is a null-vector in  $R^n$ .

Definition 5. A trajectory  $y(\bar{y}^0, t)$  of dynamical system  $y(y^0, t)$  is called stable with respect to variables  $y_1$ , if for every  $\varepsilon > 0$  there exists  $\delta > 0$  such that inequality  $\|y^0 - \bar{y}^0\| < \delta$  implies  $\|y_1(\bar{y}^0, t) - y_1(y^0, t)\| < \varepsilon$ .

Partial case 1. Suppose that switching in automaton (5) occurs only with respect to hidden coordinates  $y_2$ . If for the system (1) in some neighborhood  $y_1 \in B_r(0_1)$  there exists a Lyapunov's function  $V(y_1)$  such that  $\dot{V}|_{f_q} \leq 0$ , then solution is stable.

Partial case 2. Suppose that for automaton (5) there exists a set of  $y_1$ -positive definite Lyapunov functions such that  $\dot{V}^q|_{f_q} \leq 0$ , and on switching  $y|_{q \rightarrow r}$  the inequality  $V^r(y) \leq V^q(y)$  holds. Then trivial equilibrium point of hybrid automaton is stable.

Let us mention a theorem about stability in general case.

Definition 6. A function  $V(y): B_r(0_1) \times R^{n_2} \rightarrow R$  is called  $y_1$ -uniform-positive-definite if there exist two positive definite functions  $W(y_1), U(y_1): B_r(0_1) \rightarrow R$  such that for each  $y = (y_1, y_2) \in B_r(0_1) \times R^{n_2}$  the inequality  $W(y_1) \leq V(y_1, y_2) \leq U(y_1)$  holds.

Theorem 3. Suppose that hybrid automaton has cyclic continuous switching. If for a cylinder  $D \times R^{n_2}$ , where  $D \subseteq R^{n_1}$ , there exists a set of  $y_1$ -uniform-positive-definite Lyapunov functions  $V^q: D \times R^{n_2} \rightarrow R$  such that  $\dot{V}^q|_{f_q} \leq 0$  for all  $y \in D \times Inv_q$  and  $c^N \leq c^0$ , then  $x=0$  is a stable trivial equilibrium point.

## CONCLUSIONS

In the paper the constructive conditions for stability of trivial equilibrium point of hybrid automaton are proposed. Conditions are based on existence of hybrid  $s$ -functions and they do not depend on solutions as in classical Lyapunov theory. Obtained conditions are extended to impulsive hybrid automata. For investigation stability with respect to part of variables of hybrid automata a notion of  $y_1$ -uniform-positive-definite function is introduced, where  $y_1$  is a phase subspace vector analyzed for stability.

## REFERENCES

- [1] Peleties P. and DeCarlo R. Asymptotic stability of m-switched systems using Lyapunov-like functions. *Proc. American Control Conf.*, pp. 1679–1684, Boston, 1991.
- [2] Liberzon D. and Morse A.S. Basic problems in stability and design of switched systems. *IEEE Control Systems Magazine*, 19(5):59–70, 1999.
- [3] Branicky M.S. Stability of switched and hybrid systems. *Proc. IEEE Conf. on Decision and Control*, pp. 3498–3503, Lake Buena Vista, FL., 1994.
- [4] Ye H., Michel A., and Wang K. Stability theory for hybrid dynamical systems. *Proc. IEEE Conf. Decision and Control*, New Orleans, 1995.
- [5] Bychkov O.S. Application of Lyapunov second method to investigation of stability of hybrid systems. *Bulletin of Kyiv University, Series Phys.-Math. Sciences*, Vol. 1, pp.121-127, 2005.

## EXISTENCE AND STABILITY OF DISCRETE BREATHERS WITH DIFFERENT SYMMETRIES IN 2D SQUARE LATTICES

George Chechin<sup>1</sup>,  
Galina Bezuglova,  
Petr Goncharov  
Southern Federal  
University, Department of  
Physic, Rostov-on-Don,  
Russia

---

ABSTRACT

---

Symmetry-related invariant manifolds admitting existence of localized vibrations in square lattice are found. Discrete breathers on these manifolds and their stability are analyzed for a case of homogeneous potentials of different degrees.

---

### INTRODUCTION

Discrete breathers (DBs) represent spatially localized and time-periodic excitations in nonlinear Hamiltonian lattices [1, 2]. During two last decades these dynamical objects were studied by different analytical, numerical and experimental methods in a great number of papers. However, the majority of papers treat discrete breathers in one-dimensional chains and only few articles discuss these dynamical objects in 2D and 3D periodic structures [3 – 7].

In the present paper, we consider discrete breathers in 2D square lattice with one degree of freedom per lattice site (we refer to it as scalar model of square lattice). Different physical interpretation can be given to this mathematical model. For example, it have been used for describing transversal mechanical vibrations of the plane lattice in [3], charge vibrations in an electrical network of nonlinear capacitors coupled to each other with linear inductors [5], etc.

DBs in the above mentioned scalar model of square lattice for the case of homogeneous potentials of different degrees were found with high precision in [3]. However, the problem of stability of the obtained breathers was not considered in this paper.

We add on-site potential to the model [3] and treat the problem of the breather stability with respect to the relative strength of on-site and inter-site parts of the potential energy  $U$  of the considered system. Moreover, we develop a group-theoretical approach for finding symmetry-related invariant manifolds which can simplify essentially the studying of DBs in 2D and 3D periodic structures independently of the type of the interparticle interaction potential.

### 1. INVARIANT MANIFOLDS

Different vibrational regimes of any nonlinear physical system can be classified by subgroups of the “parent” symmetry group consisting of all transformations which do not change the system dynamical equations. This idea was used for constructing *bushes* of *extended* nonlinear normal modes in physical systems with discrete symmetry (see [8, 9, 10]). Obviously, the same idea can also be used for classification of *localized* nonlinear modes in 2D and 3D periodic structures.

We discuss existence and stability of DBs in two-dimensional square lattice whose equilibrium state symmetry is described by space (plane) group  $G_0=C_{4v}^1$ .

We consider a scalar dynamical model associated with this lattice admitting that only one dynamical variable  $q_{ij}(t)$  corresponds to  $(i,j)$  site of the lattice ( $i=1..N, j=1..M$ ). In general case, dynamical equations of our model can be written as follows

$$\ddot{Q}_{NxM} = F(Q_{NxM}) \quad (1)$$

Here matrix

---

<sup>1</sup> Corresponding author. Email: gchechin@gmail.com

$$Q_{N \times M} = \begin{pmatrix} q_{11} & q_{12} & \dots & q_{1N} \\ q_{21} & q_{22} & \dots & q_{2N} \\ \dots & \dots & \dots & \dots \\ q_{M1} & q_{M2} & \dots & q_{MN} \end{pmatrix} \quad (2)$$

determines the set of all variables  $q_{ij}(t)$  corresponding to the  $N \times M$  fragment of the considered lattice.

It can be shown that dynamical equations (1) are invariant under all transformations generated by symmetry elements of the parent group  $C_{4v}^1$ . Moreover, for an even potential energy  $U$ , there is an additional symmetry transformation  $P$  which changes the signs of all the particles without their transposition. Since DBs represent localized dynamical objects, they can be classified by *point* subgroups of the parent group  $G_0 = C_{4v}^1 \times (E, P)$ , where  $E$  is identical element. To find such classification, we first look for symmetry-related *invariant manifolds* of the dynamical equations with the aid of the methods which were previously developed in the framework of the theory of phase transitions in crystals [11].

We will investigate *strongly localized* discrete breathers and, therefore, it is sufficient to deal with *small* lattice fragments (2). We choose concrete values of  $N$  and  $M$  from the condition that amplitudes of  $q_{ij}(t)$  for peripheral sites must be much smaller than those for the breather core.

If a given fragment  $Q_{N \times M}(t)$ , possesses the symmetry group  $G \subset G_0$ , then it is *invariant* under the action of all symmetry elements  $g_i \in G$ :

$$\hat{g}_i Q_{N \times M}(t) = Q_{N \times M}(t), \quad \forall g_i \in G.$$

Here  $\hat{g}_i$  is operator acting in  $N \times M$  functional space which is induced by the symmetry element  $g_i$  of the group  $G$ . It acts on an arbitrary function  $f(\vec{r})$  in line with the conventional definition [12]:

$$\hat{g}_i f(\vec{r}) = f(g_i^{-1} \vec{r}).$$

In practice, as a rule, the subgroups  $G_i$  of the parent group  $G_0$  ( $G_i \subset G_0$ ) are unknown, as well as the invariant manifolds corresponding to them.

In [11], we described an algorithm which allows one to single out invariant subspaces corresponding to all possible subgroups of a given parent group. To this end, we first find invariant subspaces of all the individual matrices of the natural representation of the group  $G_0$ . Then we find subsequently all possible *intersections* of these subspaces, because each *intersection* corresponds to a subgroup which is a *union* of those subgroups who correspond to these subspaces.

This way (see [11] for details) provides us with all the *nonequivalent* subspaces of the configuration space simultaneously with the complete list of corresponding subgroups of the given parent group  $G_0$ .

Each of the above invariant subspaces represents an invariant manifold relative to time evolution of our dynamical model described by Eqs. (1). However, not all of these manifolds can be used for constructing discrete breathers, since the *structure* of some of them does not permit existence of *localized* vibrations. Indeed, the manifold

$$\begin{pmatrix} c & b & c \\ b & a & b \\ c & b & c \end{pmatrix}$$

allows localized mode when  $|a| \gg |b| \gg |c|$ , while the manifold

$$\begin{pmatrix} b & a & c \\ b & a & c \\ b & a & c \end{pmatrix}$$

does not admit localization, because variables  $q_{ij}$ , expressed via  $a, b, c$  have no tendency to decrease by amplitude from its center to periphery.

We have revealed only *five* symmetry-related invariant manifolds for our model (see Fig. 1), which admit existence of localized vibrations (in general, these vibrations can be quasiperiodic). In Fig. 1, we depict the corresponding symmetry group  $G$  below the fragment of each manifold. Such information can be useful when it is necessary to enlarge this fragment because of weak decreasing of dynamical variables from the center of the manifold to its periphery.

$$\begin{array}{ccc}
Q_{3 \times 3}^{(1)} = \begin{bmatrix} c & b & c \\ b & a & b \\ c & b & c \end{bmatrix} & Q_{3 \times 3}^{(2)} = \begin{bmatrix} d & b & d \\ c & a & c \\ d & b & d \end{bmatrix} & Q_{3 \times 3}^{(3)} = \begin{bmatrix} e & b & d \\ b & a & c \\ d & c & f \end{bmatrix} \\
\{C_4, \sigma_x\} & \{\sigma_x, \sigma_y\} & \{\sigma_{xy}\} \\
Q_{3 \times 3}^{(4)} = \begin{bmatrix} e & b & f \\ c & a & d \\ e & b & f \end{bmatrix} & Q_{3 \times 4}^{(5)} = \begin{bmatrix} c & b & -b & -c \\ b & a & -a & -b \\ c & b & -b & -c \end{bmatrix} & \\
\{\sigma_y\} & \{\sigma_x P, \sigma_y\} & 
\end{array}$$

Fig. 1. Symmetry-related invariant manifolds

## 2. CONSTRUCTING DISCRETE BREATHERS FOR HOMOGENEOUS POTENTIALS

Each invariant manifold depends on a number of arbitrary parameters (a, b, c, ...). To construct discrete breather we must find such values of these parameters which lead to a *time-periodic* vibration when they are used as initial values for integrating dynamical equations of the considered model.

In the present paper, we use a model which differ from that of [3] by the presence of the on-site potential. Dynamical equations of the model for homogeneous potential of  $m$  degree read

$$\ddot{q}_{i,j} + \gamma q_{i,j}^{m-1} = (q_{i,j+1} - q_{i,j})^{m-1} - (q_{i,j} - q_{i,j-1})^{m-1} + (q_{i+1,j} - q_{i,j})^{m-1} - (q_{i,j} - q_{i-1,j})^{m-1} \quad (3)$$

$i = 1..N, j = 1..M.$

The periodic boundary conditions are supposed to be hold.

The specific structure of Eqs. (3) admits the space-time separation and, as a consequence, we can treat DBs for the case of homogeneous potential in terms of localized nonlinear normal modes by Rosenberg [13]. To this end, we assume that

$$q_{i,j}(t) = k_{ij} \cdot f(t), \quad (4)$$

where  $i=1..N, j=1..M$ , while  $k_{ij}$  are constant coefficients.

Substituting the ansatz (4) into differential equations (3), we reduce them to a number of nonlinear algebraic equations, which determine the spatial profile of DB, and one (“governing”) differential equation, which determines time-dependence of all the dynamical variables  $q_{ij}(t)$ . This time-dependence is described by the single function  $f(t)$ .

If we now take into account particular structures of the invariant manifolds depicted in Fig. 1, the number of unknown coefficients  $k_{ij}$  will be equal to the number of the manifold arbitrary parameters a, b, c, ... minus one, since one of these parameters can be assumed equal to 1. For the invariant manifold  $Q_{3 \times 3}^{(1)}$  we can write the following algebraic equations (here we assume  $a=1$ )

$$\begin{aligned}
b[-\gamma + 4(b-1)^{m-1}] &= -\gamma b^{m-1} + 2(c-b)^{m-1} + (1-b)^{m-1}, \\
c[-\gamma + 4(b-1)^{m-1}] &= -\gamma c^{m-1} + 2(b-c)^{m-1}
\end{aligned} \quad (5)$$

while the governing equation takes the form

$$\ddot{f}(t) + [\gamma - 4(b-1)^{m-1}]f(t)^{m-1} = 0. \quad (6)$$

Demanding  $|a| > |b| > |c|$ , we restrict ourselves by localized breather profile.

For the homogeneous potential of  $m=4$  degree, we have obtained the following breather spatial profile on the invariant manifold  $Q_{3 \times 3}^{(1)}$  for  $\gamma=0$ :  $a=1, b=0.25439, c=0.00439$ .

The time-dependence of the corresponding breather solution is determined by the governing equation

$$\ddot{f}(t) + p^2 \cdot f(t)^3 = 0, \quad p^2 = -4(b-1)^3 \quad (7)$$

with analytical solution of the form

$$f(t) = cn(\omega t, \frac{1}{\sqrt{2}}), \quad \omega = p \cdot f(0). \quad (8)$$

Proceeding in such manner, we can construct discrete breathers for the analyzed invariant manifold  $Q_{3 \times 3}^{(1)}$  for *different* values of  $\gamma$  which determines relative strength of the on-site and inter-site parts of the potential energy of the considered dynamical system. We plot the functions  $b=b(\gamma)$  and  $c=c(\gamma)$  in Fig. 2A (note that  $a=1$  is not depicted in this figure).

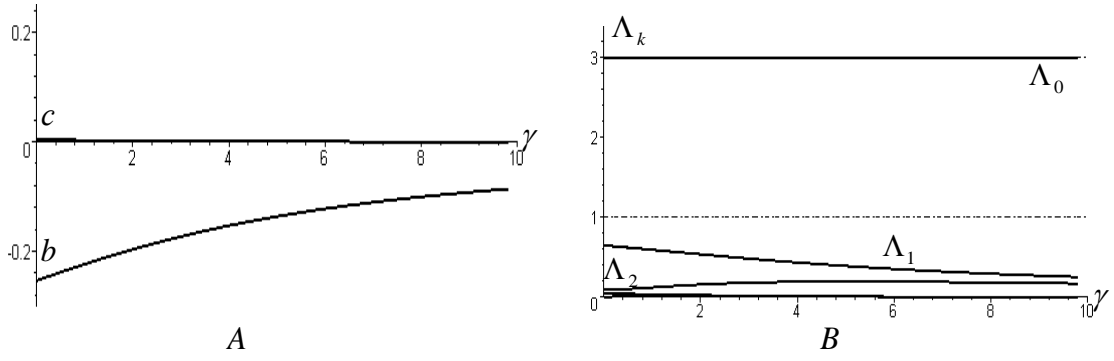


Fig. 2. DBs for invariant manifold  $Q_{3 \times 3}^{(1)}$ : A) profiles; B) stability indicators.

### 3. STABILITY OF DISCRETE BREATHERS FOR HOMOGENEOUS POTENTIALS

DBs represent time-periodic dynamical regimes and, therefore, standard Floquet method can be used for analyzing their stability. However, for the models with homogeneous potentials, more simple method was developed in [14, 15]. In this case, equations, linearized near the exact breather solution, can be written as follows:

$$\ddot{\delta} = g(t)A \cdot \delta \quad (9)$$

Here  $\delta(t)$  is a vector perturbation of the exact breather solution,  $g(t) = -(m-1)f^{m-2}(t)$  is a time-periodic function determined by  $f(t)$  from Eq. (6), while  $A$  is a certain time-independent matrix.

Because of the above structure of the variational equations (9), one can reduce the matrix  $A$  to a diagonal form with an appropriate orthogonal transformation in  $\delta$ -space. As a result, the coupled equations (9) turn out to be split into independent scalar equations of one and the same form. For example, for the homogeneous potential of  $m=4$  degree, we obtain from Eq. (3)  $N \times M$  independent Lamé's equations

$$\ddot{z}_{i,j} + \Lambda_k f^2(t) \cdot z_{i,j} = 0, \quad (10)$$

Coefficients  $\Lambda_k = \frac{3\lambda_k}{p^2}$ , which we call *stability indicators*, depend on eigenvalues  $\lambda_k$  of the matrix  $A$ .

On the other hand, the boundaries of the regions of stable and unstable motion for the Lamé equation in the form (10) turn out to be integer numbers  $\frac{n(n-1)}{2}$  where  $n=1, 2, 3, \dots$ . Moreover, the stable regions of zero solution of Eqs. (10) satisfy the condition  $\Lambda_k \in [0;1], [3;6], [10;15], \dots$ . Therefore, the breather solution will be stable if *all*  $\Lambda_k$  fall in the above stability intervals.

In Fig. 2B, we plot the functions  $\Lambda_k(\gamma)$  for all eigenvalues of the matrix  $A$  (note that some of them are equal to each other and some are too small to be visible in this figure). From Fig. 2B, we see that DBs constructed on the invariant manifold  $Q_{3 \times 3}^{(1)}$  for  $m=4$  are stable for *all values* of  $\gamma$ .

Note that  $\Lambda_0 = 3$  lies exactly on the lower boundary of the *second* stability region for all the values of the parameter  $\gamma$ . Since the corresponding eigenvector of the matrix  $A$  coincides with the breather's profile, the indicator  $\Lambda_0$  does not affect the breather stability. Below, we don't depict such marginal stability indicators in all figures similar to Fig. 2B.

Slightly another situation takes place for the breather stability analysis in cases with homogeneous potential of higher than 4 degrees ( $m > 4$ ). Indeed, the coupled variational equations (9) can also be split into independent equations:

$$\ddot{z}_{i,j} + \Lambda_k f^{m-2}(t) \cdot z_{i,j} = 0. \quad (11)$$

Unlike the Lamé-case, we do not know any analytical results for detecting stability-instability regions for Eq. (11). However, our numerical experiments lead to very interesting result. It turns out that for homogeneous potential of  $m$  degree the first stability regions for zero solution of Eq. (11) are

$$\Lambda_k \in [0;1], [m-1; m+2], [3m-2; 3m+3], \dots \quad (12)$$

The regions of instability lie between the above listed stable regions. We believe that these numerical finding can be proved rigorously by some analytical method, but we have not such a proof at the present time.

In any case, we can detect stability of DBs in the lattices with homogeneous potentials of degree  $m$  using the condition that all the indicators  $\Lambda_k$  in Eq. (11) lie in the stability regions (12).

We plot  $\Lambda_k$  as functions of  $\gamma$  for DBs constructed on invariant manifold  $Q_{3 \times 3}^{(1)}$  for  $m=6$  and  $m=8$  in Fig. 3. As one can see from this figure for  $m=8$ , the discrete breather, being stable for  $\gamma > \gamma_c$ , becomes unstable for  $0 \leq \gamma < \gamma_c$ , where  $\gamma_c = 5.8848$ .

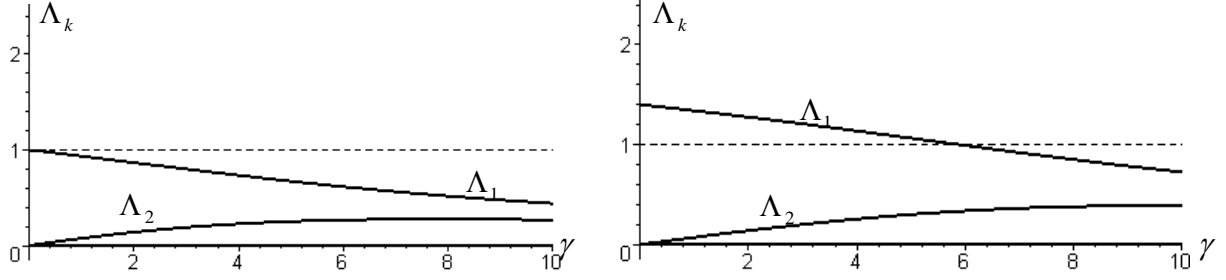


Fig. 3. Stability indicators  $\Lambda_k$  for DBs associated with invariant manifold  $Q_{3 \times 3}^{(1)}$  for  $m=6$  (left) and  $m=8$  (right).

Note that for  $m=6$  discrete breather possesses a tendency to lose its stability with decreasing  $\gamma$ , because  $\Lambda_1 \rightarrow 1$  for  $\gamma \rightarrow 0$ .

#### 4. RESULTS AND DISCUSSION

Above we have discussed DBs constructed on the invariant manifold  $Q_{3 \times 3}^{(1)}$  which depends on three arbitrary parameters  $a, b, c$  (see Fig. 1). If we enlarge  $3 \times 3$  lattice fragment, corresponding to this manifold, with the aid of the symmetry group  $\{C_4, \sigma_x\} = C_{4v}$ , new arbitrary parameters appear. However, the numerical values of these additional parameters which are obtained as a result of constructing DBs on the considered manifold turn out to be very small because of the breather's strong localization and, therefore, they can be neglected. Because of this reason, we don't indicate below the size of lattice fragments near the manifolds depicted in Fig. 1 and refer to them as  $Q^{(j)}$  ( $j=1..5$ ).

We have already considered DBs on the  $Q^{(1)}$ . Let us discuss these dynamical objects associated with other invariant manifolds.

1. The manifolds  $Q^{(2)}$  and  $Q^{(3)}$  with symmetry groups  $\{\sigma_x, \sigma_y\} = C_{2v}$  and  $\{\sigma_{xy}\} = C_s$ , respectively.

- $m=4$ .

We did not obtain any DBs with such symmetries. For example, for the manifold  $Q^{(2)}$ , we found only Rosenberg mode with  $a=b$  which corresponds to the more symmetric manifold  $Q^{(1)}$  with the point group  $C_{4v}$ .

- $m=6$ .

DBs exist only for  $\gamma \in [0; \gamma_c = 0.0476]$ . For  $\gamma > \gamma_c$  these breathers transform into DBs associated with the manifold  $Q^{(1)}$ . Moreover, these breathers turn out to be *unstable*.

- $m=8$ .

DBs exist only for  $\gamma \in [0; \gamma_c = 5.8848]$  and they are *unstable*.

2. Invariant manifold  $Q^{(4)}$  with symmetry group  $\{\sigma_y\} = C_s$ .

- $m=4$ .

There are no DBs associated with this manifold.

- $m=6$ .

DBs exist only in two intervals  $\gamma \in [0; 0.0476]$  and  $\gamma \in [0.0484; 3.8716]$ . These DBs are *unstable*.

- $m=8$ .

DBs exist only in two intervals  $\gamma \in [0; 5.8848]$  and  $\gamma \in [5.8862; 17.9037]$ . These DBs are *unstable*.

3. Invariant manifold  $Q^{(3)}$  with symmetry group  $\{\sigma_x P, \sigma_y\}$ .

Note that only this manifold is associated with symmetry group whose some elements contain the operator  $P$  changing signs of all the displacements without their transposition. As a consequence, arbitrary parameters  $a, b, c$  enter this manifold with different signs.

- $m=4$ .

DBs exist for *all values*  $\gamma$ , but they are *unstable*.

- $m=6$  and  $m=8$ .

DBs exist for *all values*  $\gamma$ . They are stable only for  $\gamma \in [0; 3.9535]$  and  $\gamma \in [0; 18.0117]$ , respectively.

Up to this point, we have associated DBs in systems with homogeneous potential with localized nonlinear normal modes by Rosenberg. However, for more general potentials, such type of modes, as a rule, *don't* exist, while DBs can exist. In this case, DBs represent localized vibrations for which, unlike the Rosenberg modes, displacements of different particles are described by *different time-dependent functions*, although their vibrational periods are equal or commensurate [15].

In conclusion, let us emphasize that symmetry-related invariant manifolds, which are found in the present paper, can be used for constructing DBs in square lattice with *arbitrary* potentials even those who prevent existence of the Rosenberg modes. Certainly, in this case, we must apply more general methods for search breather solution described in [16] or the method of pair synchronization [15].

## REFERENCES

- [1] Aubry S. Breathers in nonlinear lattices: existence, linear stability and quantization *Physica D*, Vol. 103. pp. 201-250, 1997.
- [2] Flach S. and Willis C. R. Discrete Breathers *Physics Reports*, Vol. 295. pp. 181 – 264, 1998.
- [3] Fischer F., Self-localized single-anharmonic vibrational modes in two-dimensional lattices. *Annalen der Physik*, Vol. 2, pp. 296 – 307, 1993.
- [12] Feng B. F. and Kawahara T. Discrete breathers in two-dimensional nonlinear lattices. *Wave Motiom*, Vol. 45, pp. 68 – 82, 2007.
- [5] Butt I. A. and Wattis J. A. D. Discrete breathers in a two-dimensional Fermi-Pasta-Ulam lattice *J Phys A: Math Theor*, Vol. 39, pp. 4955, 2006.
- [6] Kiselev S. A. and Sievers A. J. Generation of intrinsic vibrational gap modes in three-dimensional ionic crystals *Phys. Rev. B*, Vol. 55, pp. 5755 – 5758, 1997.
- [7] Manley M. E., Sievers A. J., Lynn J. W., Kiselev S. A., Agladze N. I., Chen Y., Llobet A., and Alatas A. Intrinsic localized modes observed in the high-temperature vibrational spectrum of NaI *Phys. Rev. B*, Vol. 79, pp. 134304, 2009.
- [8] Sakhnenko, V. P. and Chechin, G. M. Symmetrical selection rules in nonlinear dynamics of atomic systems *Dokl. Akad. Nauk*, Vol. 330. pp. 308, 1993 [*Phys. Dokl.*, Vol. 38, pp. 219, 1993].
- [9] Chechin G. M. and Sakhnenko V. P. Interactions between normal modes in nonlinear dynamical systems with discrete symmetry. Exact results *Physica D*, Vol. 117, pp. 43 – 76, 1998.
- [10] Chechin G. M., Ryabov D.S., Sakhnenko V.P. Bushes of Normal Modes as Exact Excitations in Nonlinear Dynamical Systems with Discrete Symmetry *Nonlinear Phenomena Research Perspectives* / Ed. by C. W. Wang. Nova Science Publishers, NY, pp. 225 – 327, 2007.;
- [11] Chechin, G. M. Computers and group-theoretical methods for studying structural phase transition *Comput. Math. Applic.*, Vol. 17, pp. 255—278, 1989.
- [12] Elliott, J. P. and Dawber, P. J. *Symmetry in Physics. Vol. 1. Principles and Simple Applications* Macmillan Press Ltd., London, 1979.
- [13] Rosenberg, R. M. The normal modes of nonlinear n-degree-of-freedom systems *J. Appl. Mech.*, Vol. 29, pp. 7 – 14, 1962.
- [14] Chechin G. M., Dzhelauhova G. S. and Mehonoshina E. A. Quasibreathers as a generalization of the concept of discrete breathers *Physical Review E*, Vol. 74, 036608-15, 2006.
- [15] Chechin G. M. and Dzhelauhova G. S. Discrete breathers and nonlinear normal modes in monoatomic chains *Journal of Sound and Vibration*, Vol. 322, pp. 490 – 512, 2009.
- [16] Flach S. Computational studies of discrete breathers in "Energy Localization and Transfer", Eds. T. Dauxois, A. Litvak-Hinenzon, R. MacKay and A. Spanoudaki, World Scientific, pp.1-71 (2004).

ON VISUALIZATION OF RESONANCE STRUCTURES IN DYNAMICAL SYSTEMS  
WITH TWO DEGREES OF FREEDOM

T.N. Dragunov<sup>1</sup>,  
R.E. Kondrashov,  
A.D. Morozov  
University of Nizhniy  
Novgorod  
Nizhniy Novgorod, Russia

---

ABSTRACT

---

Resonance zones in a system of two weakly connected Duffing - van der Pol nonlinear oscillators are analyzed by calculation of three-dimensional averaged system. Numerical visualization is suggested by using a two-dimensional Poincare map which is similar to the Poincare map for a system with 3/2 degrees of freedom. Visualization of resonance zones is performed using a computer program WInSet developed by authors.

---

INTRODUCTION

General essentially nonlinear systems close to integrable ones were considered in a book [1]. But papers concerning particular systems of two connected nonlinear oscillators and containing analysis of resonance structures have been presented only recently [2]. This may be connected with complexity of finding solution of unperturbed oscillator equation. In simplest cases the solution can be expressed in elliptic functions which significantly complicate an analysis of averaged systems. On the other hand, frequency of unperturbed oscillator depends on value of the energy integral and this fact leads to existence of dense set of its resonant values.

1. RESONANCE ZONES

A system of two weakly connected oscillators may be conveniently rewritten in variables of action  $I$  and angle  $\mathcal{G}$ :  $I = (I_1, I_2)$ ,  $\mathcal{G} = (\mathcal{G}_1, \mathcal{G}_2)$ .

$$\begin{aligned}\dot{I} &= \varepsilon F(I, \mathcal{G}) \\ \dot{\mathcal{G}} &= \omega(I) + \varepsilon G(I, \mathcal{G})\end{aligned}\tag{1}$$

where  $\omega = (\omega_1, \omega_2)$  and  $\omega_k = \omega_k(I_k)$ ,  $k = 1, 2$ ,  $\varepsilon$  is a small positive parameter, functions  $F = (F_1, F_2)$ ,  $G = (G_1, G_2)$  are sufficiently smooth in the domain  $D(I_1, I_2) \times T^2(\mathcal{G}_1, \mathcal{G}_2)$ , where  $T^2$  is a two-dimensional torus and  $D \subset \mathbf{R}^2$ .

It is said that there is a resonance in the system (1) if

$$\omega_1(I_1) = \frac{q}{p} \omega_2(I_2),\tag{2}$$

where  $p, q$  are relatively prime integers. Relation (2) defines resonance curves on the plane  $(I_1, I_2)$ . Let us fix certain point  $(I_{1pq}, I_{2pq})$  on a resonance curve. Inside the  $\sqrt{\varepsilon}$ -neighborhood of this point the system (1) can be reduced as in [1] by averaging and neglecting the terms  $O(\varepsilon^{3/2})$  to the form

---

<sup>1</sup> Corresponding author. Email [dtm@mm.unn.ru](mailto:dtm@mm.unn.ru)

$$\begin{aligned} u_k' &= A_k(v; I_{1pq}, I_{2pq}) + \mu[P_{k1}u_1 + P_{k2}u_2] \\ v' &= b_{10}u_1 + b_{20}u_2 + \mu[b_{11}u_1^2 + b_{21}u_2^2 + G_0(v; I_{1pq}, I_{2pq})] \end{aligned} \quad (3)$$

where  $\mu = \sqrt{\varepsilon}$ , the prime denotes a derivation by the “slow” time  $\tau = \mu t$ ,

$$\begin{aligned} A_k &= \frac{1}{2\pi p} \int_0^{2\pi p} F_k(I_{1pq}, I_{2pq}, v - q\varphi/p, \varphi) d\varphi \\ P_{k1} &= \frac{1}{2\pi p} \int_0^{2\pi p} \frac{\partial F_k(\cdot)}{\partial I_1} d\varphi, \quad P_{k2} = \frac{1}{2\pi p} \int_0^{2\pi p} \frac{\partial F_k(\cdot)}{\partial I_2} d\varphi \\ G_0 &= \frac{1}{2\pi p} \int_0^{2\pi p} [G_1(I_{1pq}, I_{2pq}, v - q\varphi/p, \varphi) + qG_2(I_{1pq}, I_{2pq}, v - q\varphi/p, \varphi)/p] d\varphi \\ b_{1,j-1} &= \frac{d\omega_1(I_{1pq})}{jdI_1^j}, \quad b_{2,j-1} = \frac{q}{p} \frac{d\omega_2(I_{2pq})}{jdI_2^j}, \quad j = 1, 2. \end{aligned}$$

Functions  $A_k$  are periodic by  $v$ . Concluding the averaged system (3) we neglected terms  $O(\mu^3)$  which depend on all variables  $u_1, u_2$ , and  $\varphi$ . Using the change of variables

$$\begin{aligned} u_2 &= (w - b_{10}u_1 - \mu Q_0(v, I_{1pq}, I_{2pq}))/b_{20} \\ u_1 &= u, \end{aligned}$$

we can transform the equations (3) to a more convenient form for analysis

$$\begin{aligned} v' &= w + \mu[a_{20}u^2 + a_{02}w^2 + a_{11}uw] \\ w' &= A(v; I_{1pq}, I_{2pq}) + \mu[C_1(v; I_{1pq}, I_{2pq})u + C_2(v; I_{1pq}, I_{2pq})w], \\ u' &= A_1(v; I_{1pq}, I_{2pq}) + \mu[C_3(v; I_{1pq}, I_{2pq})u + C_4(v; I_{1pq}, I_{2pq})w] \end{aligned} \quad (4)$$

where

$$\begin{aligned} A &= b_{10}A_1 + b_{20}A_2 \\ a_{20} &= b_{11} + b_{21}b_{10}^2/b_{20}^2, \quad a_{02} = b_{21}/b_{20}, \quad a_{11} = -2b_{21}b_{10}/b_{20}^2 \\ C_1 &= b_{10}P_{11} - (b_{10}^2/b_{20})P_{12} + b_{20}P_{21} - b_{10}P_{22} \\ C_2 &= (b_{10}/b_{20})P_{12} + P_{22} + Q_0' \\ C_3 &= P_{11} - (b_{10}/b_{20})P_{12} \\ C_4 &= P_{11}/b_{20} \end{aligned}$$

## 2. MODEL SYSTEM

One considers a particular system of two connected Duffing-van der Pol equations

$$\begin{aligned} \ddot{x} + \alpha x + \beta x^3 &= \varepsilon[(p_1 - x^2)\dot{x} + p_2 y] \\ \ddot{y} + \gamma y + \delta y^3 &= \varepsilon[(p_3 - y^2)\dot{y} + p_4 x] \end{aligned} \quad (5)$$

where  $\alpha, \beta, \gamma, \delta, p_1, p_2, p_3, p_4$  are parameters and  $\alpha, \beta, \gamma, \delta = \pm 1$ . Let us illustrate recent features of program WInSet [3] to provide visualization of resonance structures. The averaged system (3) is three-dimensional and phase space of original system (5) is four-dimensional. First, let us use the following simplification. It is known that for systems with 3/2 degrees of freedom a two-dimensional Poincare map describes the behavior of original system solutions. Therefore in the first approximation we can reduce our task to a system with 3/2 degrees of freedom. According to the small parameter method, a solution of system (5) can be found in the form of power series, namely

$$y(t) = y_0(t) + \varepsilon y_1(t) + \dots \quad (6)$$

where  $y_0(t)$  is a solution of unperturbed equation. Substituting (6) in the first equation in (5) we obtain

$$\ddot{x} + \alpha x + \beta x^3 = \varepsilon[(p_1 - x^2)\dot{x} + p_2 y_0(t)] + O(\varepsilon^2) \quad (7)$$

Neglecting the terms  $O(\varepsilon^2)$  in (7) we get a system with 3/2 degrees of freedom which can be analyzed numerically using the Poincare map. Particularly, we can visualize structure of resonance zones.

### 3. NUMERICAL VISUALIZATION

We have recently updated a program WInSet [3] and added features of numerical plotting of the Poincare map for systems similar to (5) and (7) without  $O(\varepsilon^2)$  terms. The program first calculates the period of oscillation of second oscillator and then using numerical computation of Cauchy problem for the entire system (5) the program performs plotting of Poincare map on plane  $(x, \dot{x})$  for the obtained value of period. Dependency  $y_0(t)$  for system (5) with  $\gamma = 1, \delta = 1$  is expressed in terms of elliptic cosine ( $cn$ ). With  $\gamma = 1, \delta = -1$  this dependency is expressed in terms of elliptic sine ( $sn$ ). When  $\gamma = -1, \delta = 1$  then inside separatrix loops this dependency is expressed in terms of delta amplitudinis ( $dn$ ). So with the new version of program WInSet we can effectively analyze perturbations given by Jacobi elliptic functions.

#### 3.1 Poincare map

To demonstrate plotting of the Poincare map for equation like (7) consider conservative case, i.e. exclude the first term of perturbation in (7).

$$\ddot{x} + \alpha x + \beta x^3 = \varepsilon p_2 y_0(t) \quad (8)$$

When  $\alpha = \beta = \gamma = \delta = 1, \varepsilon = 0.1$  if we select initial conditions for the second oscillator as  $(y = 0, \dot{y} = 12)$  then we will obtain picture of invariant curves shown on Fig. 1. The plotted image allow us make a conclusion on global behaviour of solutions of the original system. At this picture we observe two resonance zones  $I_{1pq}$ : one zone with  $p = 1$  and other zone with  $p = 3$ .

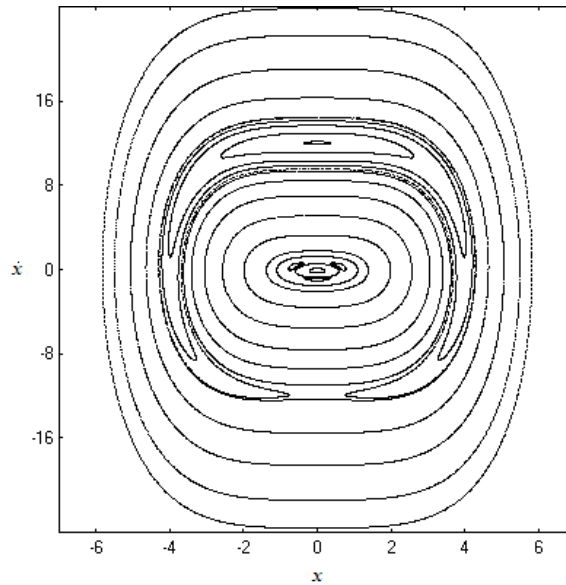


Fig. 1 Poincare map for eq. (8),  $\alpha = \beta = \gamma = \delta = 1, \varepsilon = 0.1$ ;  $y(0) = 0, \dot{y}(0) = 12$ .

#### 3.2 Visualization of averaged system

To perform detailed local analysis of solutions of equation (7) in a neighborhood of a resonance  $(I_{1pq}, I_{2pq})$  it is necessary to explicitly calculate and investigate the averaged system (4). Below we demonstrate phase portraits of three-dimensional system (4) and their projections on  $(v, w)$  plane for the case with  $\alpha = 1, \beta = 1, \gamma = 1, \delta = 1$ .

Phase curves of system (4) for system (7) with  $p_1 = 0.2, p_2 = 0.2, p_3 = 0.3, p_4 = 3, \varepsilon = 0.1$  are shown on Fig. 2. In this case there is a stable equilibrium and a limit cycle in the upper half plane,  $(v, w)$ .

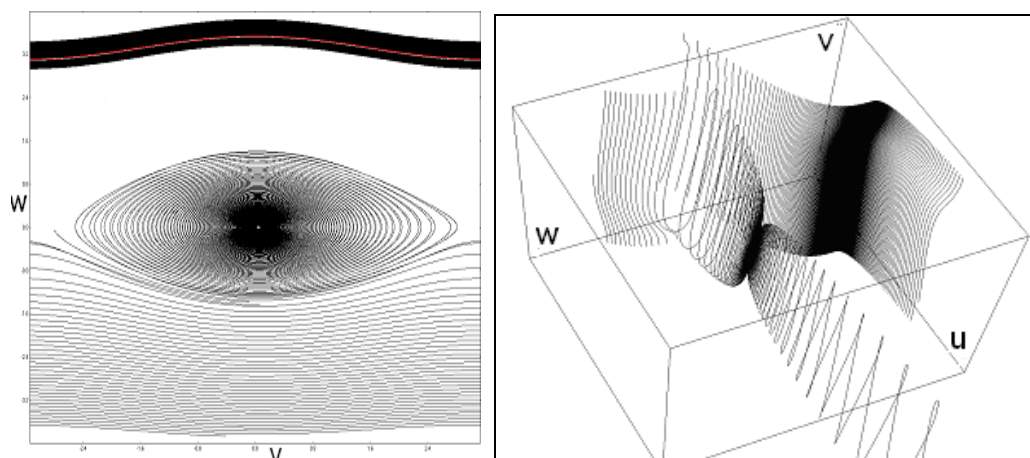


Fig. 2 Phase curves of system (4) with  $\alpha = 1, \beta = 1, \gamma = 1, \delta = 1,$   
 $p_1 = 0.2, p_2 = 0.2, p_3 = 0.3, p_4 = 3, \varepsilon = 0.1$

On Fig. 3 we show phase curves of system (4) with  $p_1 = 0.3$  and the same values of other parameters. In this case the system has only a stable equilibrium.

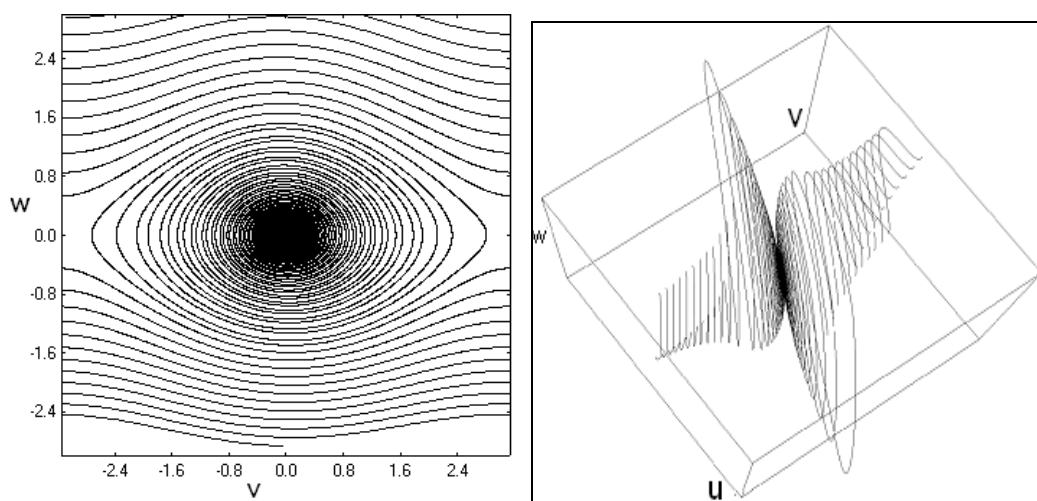


Fig. 3 Phase curves of system (4) with  $\alpha = 1, \beta = 1, \gamma = 1, \delta = 1,$   
 $p_1 = 0.3, p_2 = 0.2, p_3 = 0.3, p_4 = 3, \varepsilon = 0.1$

If we increase the value of parameter  $p_1$  then we get another case: a stable equilibrium and a limit cycle in the lower half plane  $(v, w)$ . This case is shown on Fig. 4.

This work is supported by RFBR grant 09-01-00356 and Federal Agency for Education grant NK-13P-13.

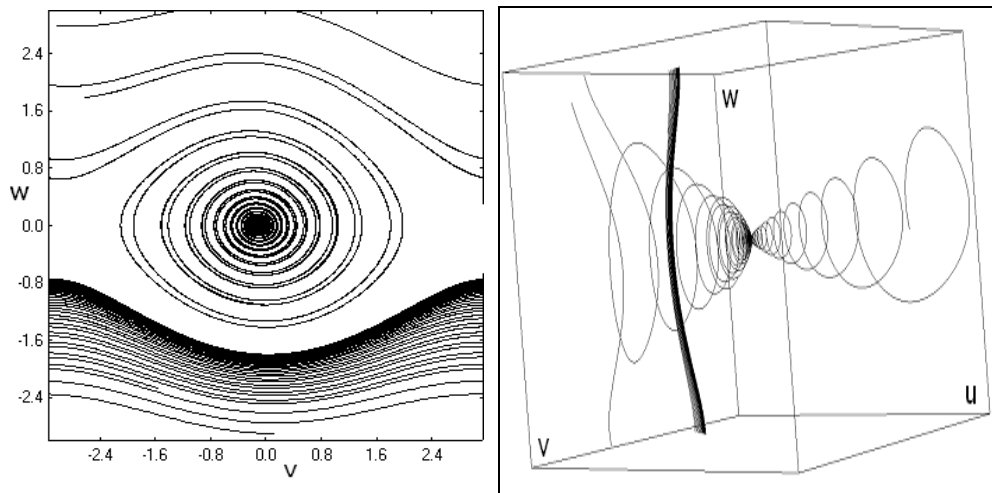


Fig. 4 Phase curves of system (4) with  $\alpha = 1, \beta = 1, \gamma = 1, \delta = 1,$   
 $p_1 = 0.6, p_2 = 0.2, p_3 = 0.3, p_4 = 3, \varepsilon = 0.1$

#### REFERENCES

- [1] A.D. Morozov *Resonances, Cycles and Chaos in Quasi-conservative Systems*, Regular and Chaotic Dynamics, Moscow-Izhevsk, 2005.
- [2] A.D. Morozov, R.E. Kondrashov On Resonances in Systems of Two Weakly Coupled Oscillators *Int. J. Regular and Chaotic Dynamics*, Vol. 14, No 2, pp. 237-247, 2009.
- [3] A.D. Morozov, T.N. Dragunov *Visualization and Analysis of Invariant Sets of Dynamical Systems*, Institute for Computer Studies, Moscow-Izhevsk, 2003.

## HYSTERESIS PHENOMENON IN FERRO/ANTIFERRO LAYERED SYSTEM

**A.G. Grechnev**

**A.S. Kovalev**

**M.L. Pankratova**

B. Verkin Institute for Low  
Temperature Physics and  
Engineering,  
Kharkov, Ukraine

ABSTRACT

A simple model for description of certain unusual properties of exchange bias phenomenon is proposed. In our model a half-space of AFM with fixed magnetic configuration contacts with a FM film, which consists of only two magnetic layers. While the magnetic anisotropy is taken into account and anisotropy constants  $\beta_i$  are larger than certain critical value, the hysteresis loops are observed. The obtained analytical results describe some features which are observed in experiments

### INTRODUCTION

At present, due to their technological importance for data recording, investigation of complex layered magnetic systems and, first of all, the ones including contacting layers of ferromagnetic (FM) and antiferromagnetic (AFM), draw an increasing experimental attention. In 1956, an interesting phenomenon called **exchange bias** was found in such FM/AFM systems. In contrast to the bulk FM, where the hysteresis loop of the magnetization  $\vec{M} = \vec{M}(\vec{H})$  is symmetric with respect to the point  $H = 0$ , for the exchange biased systems it is shifted along the field:  $\vec{M}(\vec{H}) \neq -\vec{M}(-\vec{H})$ . In the case of a layered AFM with a non-compensated magnetic interface ( $\vec{M}|_s \neq 0$ ), the simplest explanation is the following. The boundary layer of AFM creates an effective field which acts through the interface on the FM-subsystem and breaks the symmetry of the problem. However, the last experimental works show that the phenomenon of exchange bias may be more complicated [3, 4]. In these experiments the inclined parts of the  $\vec{M} = \vec{M}(\vec{H})$  curves are observed. Their slopes are not caused by the kinetics of the magnetization reversal (by the finite field change velocity in the experiment) and can be associated with non-homogeneous states of the magnetic subsystems. Secondly, the shelves (horizontal plateaus with non-saturated magnetization) in the  $\vec{M} = \vec{M}(\vec{H})$  curves are observed, where the magnetization does not change with the change of the field in a certain domain of  $H$  values. Finally, the hysteresis loop is not symmetric with regard to the exchange bias field. Earlier there were suggestions that these features could correspond to the bulk non-homogeneous states similar to incomplete domain walls. Supporting this idea, in the previous works [5, 6] we studied this phenomenon in the framework of two simple models: (1) the “2-spin model”, where the FM-subsystem consists of only two magnetic layers (the simplest model which admits magnetic states inhomogeneous in the direction perpendicular to the interface) and (2) the “continuous model” of a FM-film with a finite number of layers treated in the continuous approximation. For both models the strong easy plane anisotropy of a magneto-dipole origin was considered, and the anisotropy in the easy plane was neglected. Furthermore, several observed phenomena, i.e., the appearance of the shelves, inclined parts of the magnetization curve and asymmetry of these curves in the exchange bias field were qualitatively explained. However, the presence of the hysteresis was beyond the scope of these papers, as one needs to consider the easy-axis anisotropy to obtain the hysteresis behavior.

## 1. MODEL

Consider a FM/AFM system consisting of a magnetic hard AFM subsystem, in which all magnetic moments are fixed and do not rotate in the external field, and a FM subsystem consisting of two magnetic layers with the strong easy plane anisotropy. For the case of the FM-film with a finite thickness it is determined by the magneto - dipole interaction. The magnetic state is determined by the rotation angles of the magnetization vectors in the easy plane. In addition, a weak anisotropy in this plane is taken into account. It is also assumed that the external magnetic field is directed along the “easy” axis in the plane. The system state is assumed to be homogeneous along the interface of the media. The complete magnetic energy of the system includes the exchange interactions between the FM layers and with the first uncompensated AFM layer (across the interface), the energy of magnetic anisotropy in the easy plane as well as Zeeman energy:

$$E = -J_0 \cos \varphi_1 - J \cos(\varphi_1 - \varphi_2) - \frac{\beta_1}{2} \cos^2 \varphi_1 - \frac{\beta_2}{2} \cos^2 \varphi_2 - H(\cos \varphi_1 + \cos \varphi_2), \quad (1)$$

where the indices 1,2 correspond to the layer adjacent to the interface and the other FM layer (on the free boundary of the FM) respectively. The exchange interaction across the interface with constant  $J_0$  is assumed to be ferromagnetic while the anisotropy values in the ferromagnetic subsystem and on the interface ( $\beta_2$  and  $\beta_1$ ) may general be different. The possible equilibrium states are given by the following equations:

$$(H + J_0) \sin \varphi_1 + J \sin(\varphi_1 - \varphi_2) + \beta_1 \sin \varphi_1 \cos \varphi_1 = 0 \quad (2)$$

$$H \sin \varphi_2 + J \sin(\varphi_2 - \varphi_1) + \beta_2 \sin \varphi_2 \cos \varphi_2 = 0. \quad (3)$$

We start the study of this system for the simple model with  $\beta_1 = \beta_2$ . Even in this case in the presence of anisotropy the dependencies  $\varphi_i = \varphi_i(H)$  for the “canted” phase (with  $\varphi_i \neq 0, \pi$ ) cannot be found analytically. But a general picture of the magnetic structure of the FM-layer and the corresponding field dependences for different values of the parameters  $J$ ,  $J_0$  and  $\beta$  can be easily found. Firstly, we note that the system admits collinear structures with vectors  $\vec{M}_i$  parallel to each other and parallel (or antiparallel) to the direction of the magnetic field (which coincides with the easy axis of anisotropy and the vector of antiferromagnetism of the AFM-subsystem). Besides, the states with antiparallel directions of the vectors  $\vec{M}_i$  (that remain collinear with the field direction) are also possible. As it is shown in our previous works, the hysteresis loop for this case  $\beta_1 = \beta_2$  is antisymmetric with respect to the exchange bias field  $H = -J_0/2$ . Therefore, it is sufficient to consider the transformation of the parallel ( $\uparrow\uparrow$ ) and antiparallel ( $\uparrow\downarrow$ ) phases into the canted one.

## 2. THE TRANSFORMATION OF COLLINEAR STATE INTO THE CANTED PHASE.

In order to analyze the transformation of the collinear phase ( $\uparrow\uparrow$ ) with  $\varphi_1 = \varphi_2 = 0$  into the canted one, we must find the corresponding bifurcation point with respect to the field. In this limit we linearize Eqs. (1,2) with respect to the angles  $\varphi_1, \varphi_2 \ll 1$  and put the corresponding determinant to zero to obtain the nonzero solutions of the system of linear equations. This gives the bifurcation field

$$H_{\uparrow\uparrow} = \left( \sqrt{J_0^2 + 4J^2} - (J_0 + 2J) \right) / 2 - \beta. \quad (4)$$

It is marked in Fig.1 by the point (a).

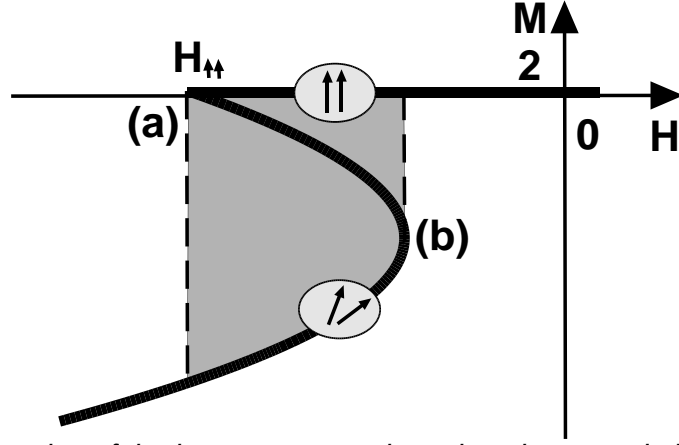


Fig.1. The transformation of the homogeneous phase into the canted phase: (a)- bifurcation point, (b) – the point with  $\frac{dM}{dH} = \infty$ . The hysteresis loop is hatched.

The stability of the collinear structure is determined by the Hessian of the potential energy surface  $E = E(\varphi_1, \varphi_2)$ , i.e.

$$K = \frac{\partial^2 E}{\partial \varphi_1^2} \frac{\partial^2 E}{\partial \varphi_2^2} - \left( \frac{\partial^2 E}{\partial \varphi_1 \partial \varphi_2} \right)^2 \quad (5)$$

A structure is stable for  $K > 0$ , which corresponds to the minimum of the potential energy. In the saddle point of the potential energy surface ( $K = 0$ ) the structure loses stability. For the collinear phase

$$K = (H + \beta)(H + J_0 + \beta) + J(2H + J_0 + 2\beta), \quad (6)$$

and, comparing this with (4,6) we obtain that it loses stability in the bifurcation point.

### 3. THE BOUNDARIES OF THE HYSTERESIS LOOP.

Relation (4) also determines one of the boundaries of the hysteresis loop (or, in general, region of the magnetization reversal) in the  $H$  axis. As it will be shown below, for small enough anisotropy there is no hysteresis and the magnetization switches via the uniform magnetization reversal process through a region of the canted phase. To determine the critical values of the parameters for which the hysteresis appears, we find the slope of the  $M(H)$  curve in the canted phase near the bifurcation point. To do this, we expand the equations (2,3) into the series with respect to the variables  $\varphi_i$  up to the cubic terms:

$$(H + J_0 + J + \beta)\varphi_1 - J\varphi_2 - \frac{1}{6}(H + J_0 + 4\beta)\varphi_1^3 - \frac{J}{6}(\varphi_1 - \varphi_2)^3 = 0, \quad (7)$$

$$(H + J + \beta)\varphi_2 - J\varphi_1 - \frac{1}{6}(H + 4\beta)\varphi_2^3 + \frac{J}{6}(\varphi_1 - \varphi_2)^3 = 0, \quad (8)$$

and look for the solutions in the form of power series with respect to the small deviations of the magnetic field from its bifurcation value  $\varepsilon = \sqrt{H - H_{\uparrow\uparrow}}$ :  $\varphi_i \approx \varphi_i^{(0)}\varepsilon + \varphi_i^{(1)}\varepsilon^3 + \dots$ . In the first order in  $\varepsilon$  we obtain the bifurcation field and the relation between the amplitudes of the angles:

$$\varphi_2 \approx \varphi_1 \left( J_0 + \sqrt{J_0^2 + 4J^2} \right) / 2J, \quad (9)$$

In the third order in  $\varepsilon$  we obtain the values of the angle displacements  $\varphi_{1,2}$ :

$$\varphi_{1,2}^2 \approx \frac{\varepsilon^2 \sqrt{J_0^2 + 4J^2} \left( \sqrt{J_0^2 + 4J^2} \mp J_0 \right)}{\beta(J_0^2 + 2J^2) - J^2 \left( \sqrt{J_0^2 + 4J^2} - 2J \right)}. \quad (10)$$

The dependence of the magnetization of the system on the magnetic field near the bifurcation point is given by the formulae

$$M(H) \approx 2 - (H - H_{\uparrow\uparrow}) \frac{(J_0^2 + 4J^2)}{\beta(J_0^2 + 2J^2) - J^2 \left( \sqrt{J_0^2 + 4J^2} - 2J \right)}. \quad (11)$$

For the given values of the parameters  $J$  and  $J_0$  the hysteresis near the homogeneous state ( $\uparrow\uparrow$ ) appears for the critical value of the anisotropy parameter:

$$\beta_c = J^2 \frac{\sqrt{J_0^2 + 4J^2} - 2J}{J_0^2 + 2J^2}. \quad (12)$$

Relation (12) shows that the hysteresis picture is different for different values of  $\beta$ . For  $\beta > \beta_* \approx 0.08J_0$  the relation (12), considered as an equation for  $J$ , has no solution. This means that the hysteresis takes place for any exchange interaction value. For  $\beta < \beta_*$  the equation (12) has two roots  $J_c$  and  $J_{c'}$  which correspond to the points ( $c$ ) and ( $c'$ ) in Fig 2.b. There is no hysteresis in the interval  $J_c < J < J_{c'}$ .

In the domain of existence of the hysteresis the bifurcation point (4) determines the lower boundary of the field dependence of the hysteresis loop. The upper boundary corresponds to the field value for which the derivative  $dM/dH$  becomes infinite (point (b) in Fig.1). Moreover, the derivative  $d\varphi_2/dH$  also becomes infinite. Using this fact in equations (2,3), it is easy to find the dependence of the corresponding field on the exchange constants and the anisotropy:

$$J_2 = -H(H + J_0) \frac{\beta + \sqrt{J_0(2H + J_0)}}{J_0(2H + J_0)}. \quad (13)$$

This dependence is depicted in the Fig. 2 as the curve  $A_2$ . The curve  $A_1$  stands for the dependence (4)  $J = J(H_{\uparrow\uparrow})$  for the bifurcation point of the appearance of the canted phase from the homogeneous state ( $\uparrow\uparrow$ );

$$J_1 = -\frac{(H + \beta)(H + J_0 + \beta)}{(2H + J_0 + 2\beta)}. \quad (14)$$

For  $\beta < \beta_*$  the two curves given by Eqs. (13) and (14) intersect (see Fig.2a). The crossing points correspond to the solutions of equation (12) for  $J$  with the fixed parameter  $\beta$ . For the values of  $J$  between the crossing points there is no hysteresis. For  $\beta > \beta_*$  the curves  $A_1$  and  $A_2$  in Fig.2b do not intersect and the hysteresis takes place for all values of the parameters.

The analysis of the stability of the homogeneous state ( $\downarrow\downarrow$ ) with  $\varphi_{1,2} = \pi$  and the study of the hysteresis of the field dependences near this state can be done in a similar way. The corresponding dependencies are presented in Fig.2 as the curves  $A_3$  and  $A_4$ . It is easy to see that the picture is symmetric with respect to the point ( $M = 0$ ,  $H = -J_0/2$ ). Notice that this symmetry follows directly from equations (2,3).

Finally, let us consider the antiparallel phase ( $\uparrow\downarrow$ ) which corresponds to the ‘shelf’ (y) domain with  $M = \text{const}$ ) in the field dependence of magnetization with  $\varphi_1 = 0$  and  $\varphi_2 = \pi$ . Linearizing equations (2,3) near this state, we find the bifurcation point which corresponds to the transition from the antiparallel structure of the ferromagnetic subsystem into the canted phase. The corresponding relation between the parameters reads:

$$J_5 = -\frac{(H - \beta)(H + J_0 + \beta)}{(J_0 + 2\beta)}. \quad (15)$$

It is given by the curve  $A_5$  in Fig.2. The curves  $A_i$  in these figure determine the domains of existence of the different structures of the FM system and the hysteresis (marked out).

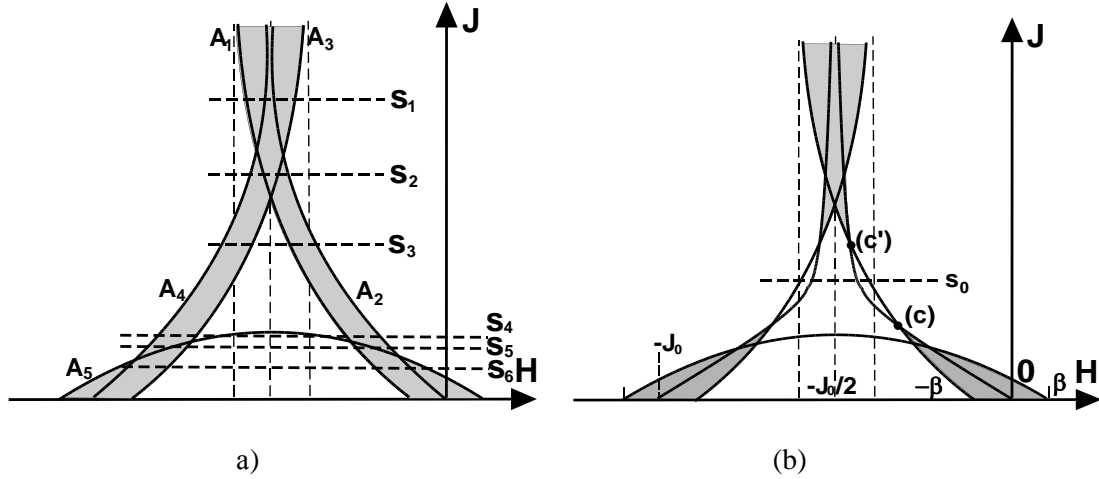


Fig.2. Domains of the hysteresis (hatched) in the plane of the parameters  $(J, H)$  for the fixed values of the anisotropy  $\beta$ :  $\beta > \beta_*$  (a) u  $\beta < \beta_*$  (b).

In Fig.2 the domain of the stability of the parallel phase ( $\uparrow\uparrow$ ) is situated to the right of the curve  $A_1$ , which starts at the point  $H = -\beta$  in the limit  $J \rightarrow 0$  and asymptotically tends to the infinity as  $H \rightarrow -J_0/2 - \beta$ . The domain of the stability of the parallel phase ( $\downarrow\downarrow$ ) is located on the left of the curve  $A_3$ , which starts at the point  $H = -J_0 + \beta$  and asymptotically tends to the infinity as  $H \rightarrow -J_0/2 + \beta$ . The domain under the curve  $A_5$  (with lies between the points  $H = -J_0 - \beta$  and  $H = \beta$ ) corresponds to the antiparallel phase ( $\uparrow\downarrow$ ). Finally, a triangular domain between the curves  $A_1, A_3, A_5$  corresponds to the canted phase. For the fixed anisotropy parameter, the shape of the hysteresis loop changes with the change of parameter  $J$ . The field dependences corresponding to some characteristic values of exchange interaction are depicted in Fig.3 as the lines  $S_i$ . The simplest form of the hysteresis is observed for the large values of exchange interaction (or for the small values of the magnetic anisotropy) for  $J > \tilde{J} \sim 0.1 J_0^2 / \beta$ . This corresponds to the line  $S_1$  in Fig.2. The hysteresis loop is shifted along the field to the value  $-J_0/2$  and has the width  $\Delta = 2\beta - \left(\sqrt{4J^2 + J_0^2} - 2J\right)$  (Fig.3,  $S_1$ ). For lower values of  $J$  (but for  $J > (J_0^2 - 4\beta^2)/8\beta$ ), there appears the domain of the canted phase and the hysteresis loop has the form given in Fig.3 ( $S_2$ ).

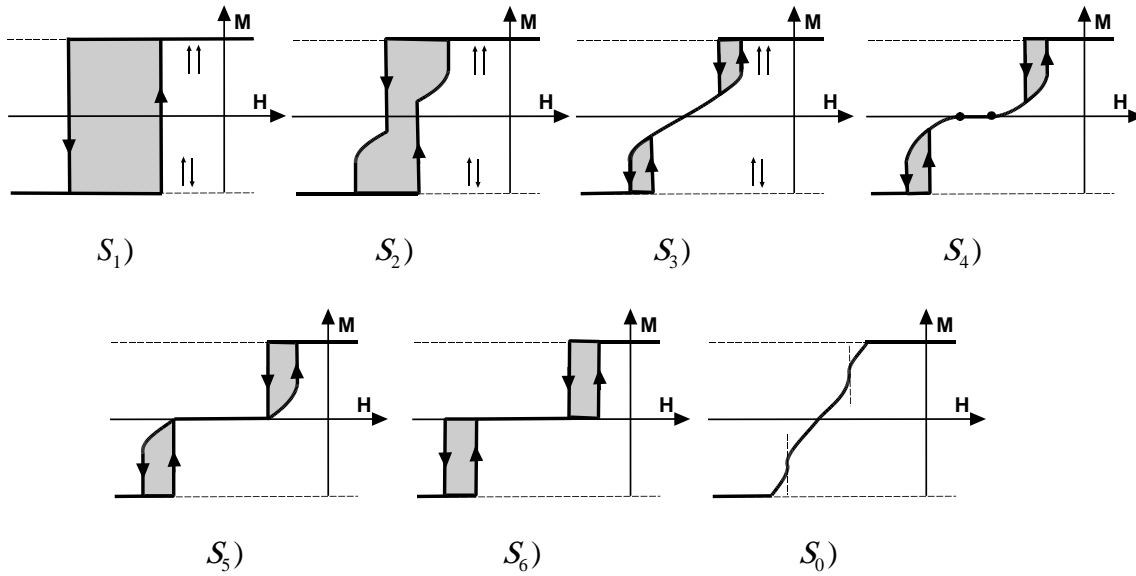


Fig.3. Different shapes of the  $M(H)$  hysteresis loop for different values of the magnetic anisotropy  $\beta$  and the FM exchange parameter  $J$ .

For the domain  $S_3$  (see Fig.2) the hysteresis loop splits into two loops (Fig. 3,  $S_3$ ). For the line  $S_4$  (with  $J < J_0 + 2\beta$ ) we observe the “shelf” of the antiparallel phase ( $\uparrow\downarrow$ ) in the  $M(H)$  dependence (Fig. 3,  $S_4$ ). Upon further decreasing of the exchange interaction, the shelf occupies all the domain of the fields between the hysteresis loops ( $S_5$ ), but the canted phase still remains in the two hysteresis loops. Finally, for the smaller values of  $J$  ( $S_6$ ), the hysteresis loops corresponds to the transitions between parallel and antiparallel phases, and the canted phase disappears. If the magnetic anisotropy is small enough (Fig. 2b), there exists a domain of parameter  $J$  for which there is no hysteresis (in contrast to the FM-systems without exchange bias).

## CONCLUSION

In the present paper, we analytically studied the exchange bias phenomenon in the framework of a simple model of ferromagnetic subsystem with two layers in contact with a hard antiferromagnet. The different shapes of  $M(H)$  hysteresis loops were founded for different values of the parameters of the system (anisotropy and exchange interaction) of the ferromagnetic layers. The results can be used to explain the experimentally observed features of the exchange bias phenomenon.

## REFERENCES

- [1]. Maklejohn W.H., Bean C.P., New Magnetic Anisotropy, *Phys. Rev.*, Vol. N.102, p. 1413, 1956.
- [2] Kiwi M., Exchange bias theory, *J. Magn.Mag. Mater.*, Vol. N. 234, p. 584, 2001.
- [3] Gnatchenko S.L., Merenkov D.N., Baran M., Szymchak R., Novoszd V.A., Exchange anisotropy of polycrystalline FeNi/FeMn films with hysteresis loop asymmetric, *Low Temp Phys*, 33, p. 957 , 2007.
- [4] Gnatchenko S.L., Merenkov D.N., Bludov A.N., Pishko V.V., Shakhaeva Yu.A., Baran M., Szymchak R., Novoszd V.A., Asymmetrically shaped hysteresis loop in exchange-biased FeNi/FeMn film, *J. Magn. Mater.*, Vol. N. 307, p. 263 , 2006.
- [5] Grechnev A.G., Kovalev A.C., Pankratova M.L. Magnetization field dependences and “exchange bias” in ferro/antiferromagnetic systems. I. Two-layers ferromagnet model, *Low Temp. Phys.*, 35, 526, 2009.
- [6] Grechnev A.G., Kovalev A.C., Pankratova M.L. Field dependence of magnetization and “exchange bias” in ferro/antiferromagnetic systems. II. Continual model of ferromagnetic layer, *Low Temp. Phys.*, 35, 476, 2009.

## INVESTIGATION OF THE NONLINEAR OSCILLATION OF THE PASSENGER CAR SUSPENSION

**Edgar Zh. Harutyunyan<sup>1</sup>**  
National Academy of Sciences of Armenia  
Yerevan, Armenia

---

### ABSTRACT

---

The model of oscillations in vertical plane of passenger automobile suspension with the nonlinear characteristic is developed by finite elements method. The oscillation process of suspension is investigated. As the result the gain-frequency characteristic of the passenger automobile suspension is obtained.

---

Here the oscillation of the passenger car body is examined, when the ratio of the stiffness of the springing medium and damper ratio of the shock absorber can be changing in time. It means that the calculations are nonlinear.

The oscillation process is described by the following equation [1].

$$[M]\{u''\} + [C]\{u'\} + [K]\{u\} = \{F(t)\} \quad (1)$$

where  $[M]$ ,  $[C]$  and  $[K]$  are the matrices of finite elements mass, damper and stiffness, correspondingly. Here  $\{u''\}$  is a vector of the nodal accelerations,  $\{u'\}$  is a vector of the nodal velocities,  $\{u\}$  is a vector of the nodal displacements,  $\{F\}$  is a vector of the external loads and  $(t)$  is time.

The process of the suspension oscillation is nonlinear. Here  $[C]$  and  $[K]$  are not constant in time. During the calculation the iteration procedure based on the Newton–Raphson method is taking place. At each iteration step the convergence of the system should be checked. As a result of finite element reducing of the oscillation system and using the nodal equilibrium equations the following algebraic equation system is obtained [2]:

$$[K]\{u\} = \{F^a\} \quad (2)$$

where  $[K]$  is a coefficient matrix,  $\{u\}$  is a vector of the unknown degrees of freedom,  $\{F^a\}$  is a vector of applied loads.

The iteration procedure is done in the following succession.

1. Assume  $\{u_0\}$ .  $\{u_0\}$  is usually the converged solution from the previous time step. On the first time step,  $\{u_0\} = \{0\}$ .
2. Compute the updated tangent matrix  $[K_i^T]$  and the restoring load  $[F_i^{nr}]$  from configuration  $\{u_i\}$ .
3. Calculate  $\{\Delta u_i\}$ .
4. To obtain next approximation  $\{u_{i+1}\}$  the vectors  $\{\Delta u_i\}$  and  $\{u_i\}$  are augmented.
5. Steps from the second to the fourth points are repeated until the system reached convergence.

If the analysis includes path-dependent nonlinearities, then the solving process requires that some intermediate steps be in equilibrium in order to correctly follow the load path. This is reached

---

<sup>1</sup> Corresponding author. Email [edgar.harutyunyan@gmail.com](mailto:edgar.harutyunyan@gmail.com)

effectively by specifying a step-by-step incremental analysis. It means that the final loading vector is obtained by increasing current vector at each step and implementing Newton-Raphson iterations. Graphically the mentioned procedure has the view shown in Fig. 1.

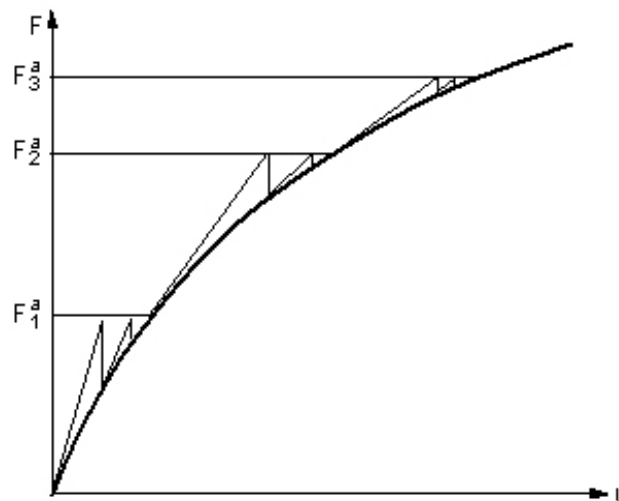


Fig. 1 Approximation of Newton – Raphson procedure

Except the Finite Element MASS21, which is used for automobile's cushioned and unsprung masses modeling the Finite Element with library name COMBIN39 is used, which is appropriate for nonlinear calculations. In the current article mentioned Finite Element is used for modeling of the automobile's suspension.

**COMBIN39** is unidirectional Finite Element with generalized force-deflection capability. The element has longitudinal and torsional one, two and three-dimensional applications [2-5].

The element has large displacement capability for which there can be two or three degrees of freedom at each node. The geometry of the Finite Element is shown in the Fig. 2.

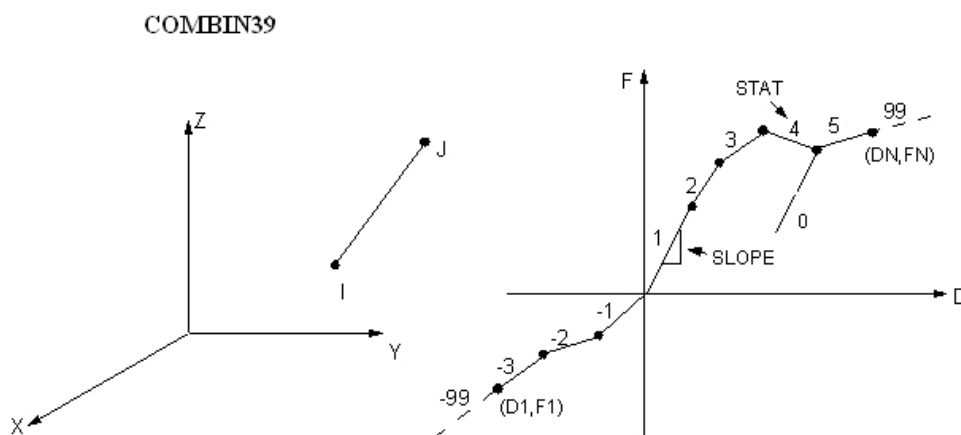
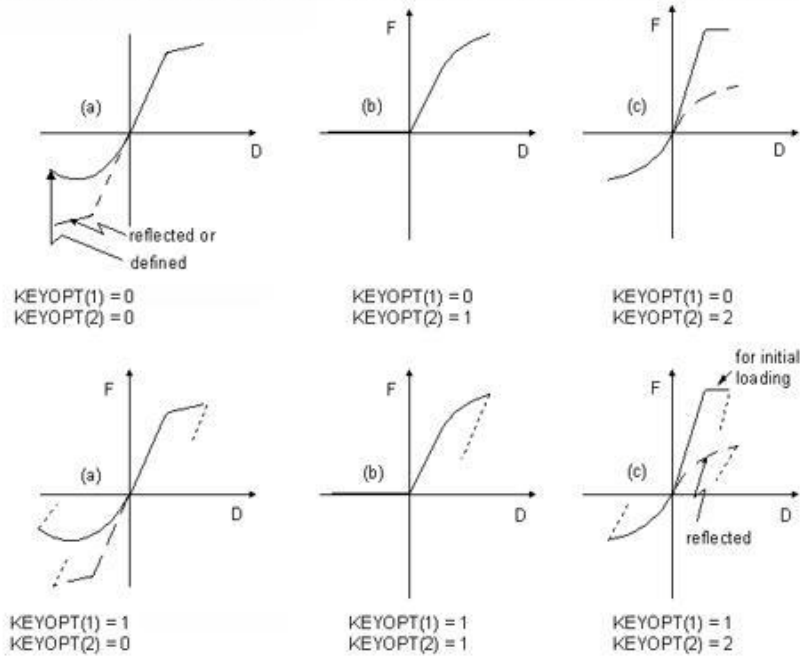


Fig 2 Mode of COMBIN39

The element is defined by two node points and by a generalized force-deflection curve. The special case of mentioned curve is shown on Fig. 2.

The force deflection curve, in connection with the input options of the element, can vary. The possible cases are shown in the Fig. 3.

**force-deflection curve modes for options KEYOPT (1) and KEYOPT (2)**



*Fig. 3 Possible modes of force-deflection curve*

The bicycle model of the passenger car is examined. As an example the Volkswagen Passat passenger car was taken to develop the computational model. In modelling almost all parameters were inputted by variables, which gives an opportunity to investigate any passenger car body of this class by changing them ( $m_1, m_2, m_3, m_4, k_1, k_2, k_3, k_4, c_1, c_2, c_3, c_4$  etc.).

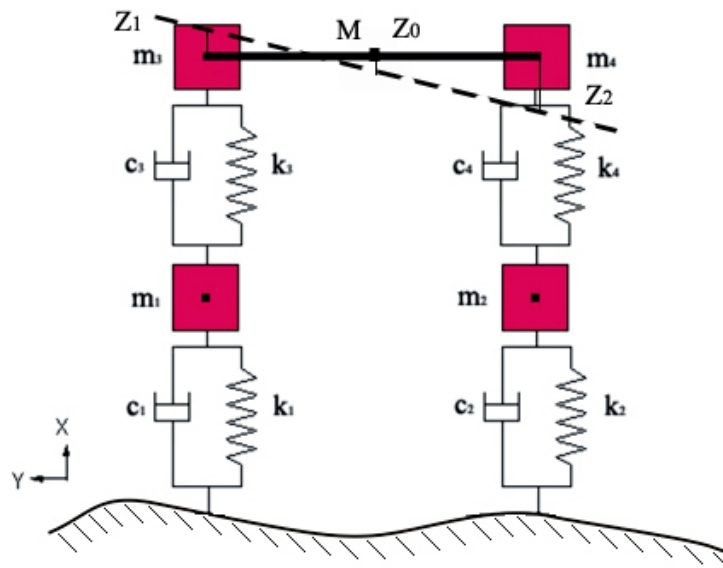


*Fig. 4 The oscillation model*

During the nonlinear calculations, as it was mentioned above, the convergence of the system at each step of iteration is checked. Here as a criterion of convergence of finite elements their deformation is used. The value of deformation would not exceed the input number during all process.

Used program packet gives an opportunity to obtain the displacement at the current moment of the time during the loading. On figure below the input criterion and displacement at each step of iteration are shown.

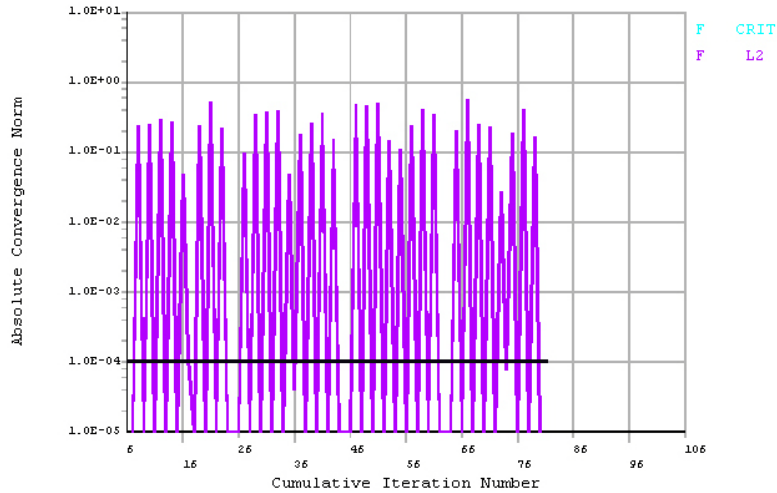


Fig. 5 Convergence check during the calculation

Investigation of the passenger car suspension by the Finite Element Method is done. The oscillation process of passenger car in vertical plane is examined, when the road irregularities are sinusoidal.

In order to obtain the gain-frequency characteristics of an automobile, it is assumed that

$$\varepsilon_y = 1 \tag{3}$$

It means that the oscillation of the front axle of an automobile does not influence on the oscillation of the rear axle. This means that the association of the wheelbase of the car and length of the irregularity wave (that is phase of sinusoid) are not taken into account. Using mentioned assumption, the oscillation of the one axle of the bicycle model is examined.

In this case the gain-frequency characteristic has the form shown on the Fig. 6.

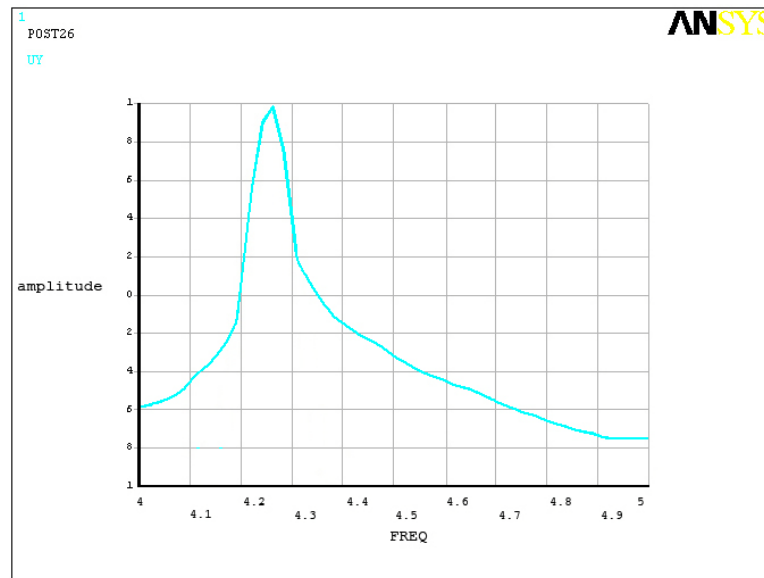


Fig. 6 Gain-frequency characteristic of nonlinear oscillation

So the development of the calculation model of an automobile’s suspension by method of Finite Elements and investigation of its oscillation when stiffness is not constant are implemented. Above described method gives an opportunity to implement the investigation with higher accuracy, to apply loads with maximum approximation and to obtain more accurate results.

## REFERENCES

- [1] Rotenberg I.S. *Automobile's suspension and its oscillation*, MashLit., Moscow, 1960.
- [2] Musayelyan G.V. *Utilization of Method of Finite Elements in Transporting Systems*, SEUA, Yerevan, 2003.
- [3] Zenkevitsch O. *The Finite Element Method in technics*, Mir, Moscow, 1975.
- [4] Pippert H. *Karosserietechnik*, Vogel Verlag, 1998.
- [5] Müller G. *FEM für Praktiker*, Expert Verlag, 1997.
- [6] Litvinov A.S., Pharobin Y.E. *Automobile: Theory of exploitation characteristics*, Mashinostroenie, Moscow, 1989.

## THE KINETIC PRESSURES OF THE GYRO-ROTOR EIGEN SHAFT BEARINGS AND ROTATORS

**Katica R. (Stevanović)  
Hedrih<sup>1</sup>**

Mathematical Institute  
SANU,  
Belgrade, Serbia,

**Ljiljana Veljović**

University of Kragujevac,  
Kragujevac, Serbia

---

### ABSTRACT

---

In our previous published paper the gyro-rotor was analyzed as a shaft-disc system with coupled rotations. The disc is eccentric and shaft is supported on both sides, at first side with a hinged fixed bearing and at other side with cylindrical sliding bearing on the support. The axes of a shaft self rotation and shaft support was with a cross section. In this paper, we presented special case when the support shaft is vertical and the gyro-rotor shaft of self rotation is horizontal, but they are without intersection. A system of non-linear differential equation is determined for such gyro-rotor dynamics. When the angular velocity of support shaft axis is constant, the motion of gyro-rotor was presented by means of phase trajectories and that is done for different cases of disk eccentricity and angle of skew disk inclination. Some numerical analysis of obtained analytical expressions is performed through Math Cad and corresponding graphs visualization of the non-linear kinetic parameters. From obtained analytical expressions for kinetic pressures to the gyro-rotor shaft bearings four vector components are separated. A pure kinematical vector rotator which depends on angular velocity and angular acceleration of the gyro-rotor shaft self rotation is defined and its properties are analyzed.

---

### INTRODUCTION

Numerous engineering systems and machines include many elements which rotate around axes. Such elements we usually call as rotors. Some rotors rotate around fixed axes but some rotate around moveable axes. The rotors are the basic working parts and sub-systems in many machines so that the problem of rotor vibrations has existed for a long time. The Vertical Gyro is a two-degree of freedom attitude gyro. It provides electrical outputs of the vehicle's pitch and roll angles, which are supplied to various systems including artificial horizons, autopilots, antenna stabilizers, and weapon delivery systems. Pickoff sensors such as potentiometers, resolvers or synchros are mounted on the gimbals and provide instantaneous pitch and roll output signals as the vehicle maneuvers.

The dynamic of such element motion is very old engineering problem beside that it is actually nowadays. Numerous applications of the gyro-rotor system dynamics are reason for numerous investigations of the non-linear dynamics of gyro- rotors as well non-linear phenomena appeared in this dynamics.

There are many research results and discoveries of new non-linear phenomena and of stationary and no stationary vibration regimes with different kinetic parameters of the dynamical system. But, many researches pay attention to this problem again. There are new numerical and experimental methods that help us to discover the properties of non-linear dynamics

Elementary model of the gyro-rotor was presented as a theoretical example in the Reference [1] by Andronov, Vitt and Haykin. This example is mass particle motion along rotate circle around vertical axis through center of circle and along circle vertical diameter. Monograph [2] by Gerard I. and Daniel J. contain basic of the elementary stability and bifurcation theory necessary for investigation non-linear dynamics and its kinetic parameter properties. Also, the monograph [3] by Guckenheimer and Holmes related to non-linear oscillations, dynamical systems and bifurcations of

---

<sup>1</sup> Corresponding author. E-mail [khedrih@eunet.rs](mailto:khedrih@eunet.rs)

fields contain numerous fundamental theorems useful for application for investigation gyro-rotor dynamics.

University books [13] and [14] by Rašković give us a basic knowledge necessary for use in the descriptions of the gyro-rotor models and possible comparison by simplest models of the gyro-rotor dynamics and corresponding system of the forces with active of reactive sources, or gyroscopic effects. It is necessary to point out a Reference [15] by Stoker which contains an example with nonlinear dynamics mass particle in the turbulent damping very useful for applications in the investigation of the gyro-rotor dynamics.

Series published References [4-11] by Hedrih (Stevanović) present new results concerning non-linear dynamics of a heavy material particle along circle which rotates and optimal control in such system dynamics. In the Reference [5] series of the theorems of trigger of coupled singularities are defined with corresponding proofs. The optimal control in non-linear mechanical systems with trigger of the coupled singularities is contained in References [6] and [7]. Monograph [8] is related to the vector method of the heavy rotor kinetic parameter analysis and nonlinear dynamics and present series of the elementary examples with gyro-rotors non-linear phenomena presented by phase trajectory portraits with trigger of coupled singularities and homoclinic orbits in the form of number eight.

References [10] and [11] are related to the influence of the no ideal rough line with Coulomb's type friction and introduced non-linearity with alternation of the friction force directions.

Previous published paper [12] by authors of this paper is related to nonlinear dynamics of the heavy gyro-rotor with two skew rotating axes, and this paper present our new results in some area – investigation of the non-linear dynamics and kinetic parameter properties of the gyro-rotors.

## 1. THE MODEL OF THE GYRO-ROTOR SYSTEM AND BASIC EQUATIONS

In this paper we presented eccentric disc (eccentricity is  $e$ ), with mass  $m$  and radius  $r$ , which is inclined to the axes of its own rotation by the angle  $\beta$  (see Figure 1.). The shaft is supported on both sides, on the first side with a hinged rigid bearing and at other side by cylindrical sliding bearing. In special case when the support shaft is vertical and the gyro-rotor shaft is horizontal, but they are without intersection between corresponding their axes. The normal distance between axes is  $a$ . The angle of own rotation around moveable horizontal axis oriented by the unit vector  $\vec{n}_1$  is  $\varphi_1$  and the angular velocity is  $\omega_1$ . The angle of rotation around the vertical shaft support axis oriented by the unit vector  $\vec{n}_2$  is  $\varphi_2$  and the angular velocity is  $\omega_2$ . The angular velocity of rotor is  $\vec{\omega}_1 = \omega_1 \vec{n}_1 + \omega_2 \vec{n}_2 = \dot{\varphi}_1 \vec{n}_1 + \dot{\varphi}_2 \vec{n}_2$ . The angles  $\varphi_1$  and  $\varphi_2$  are generalized coordinates in case when, we investigate system with two degrees of freedom. In this case  $\varphi_1$  is independent generalized coordinate, and coordinate  $\varphi_2$  is rheonomic coordinate with kinematical excitation, programmed by forced support rotation by constant or changeable angular velocity. When the angular velocity of shaft support axis is constant, that is  $\varphi_2 = \omega_2 t + \varphi_{20}$ ,  $\dot{\varphi}_2 = \omega_2 = const$ ,  $\dot{\omega}_2 = 0$  (in this case the angle  $\varphi_2$  is a rheonomic coordinate defined by previous time dependent function), and system is with two degree of mobility, but with one degree of freedom. For that case the differential equation of the gyro-rotor system rotation can be written in a following form (see Ref. [12]):

$$\dot{\omega}_1 + \Omega^2 (\lambda - \cos \varphi_1) \sin \varphi_1 - \Omega^2 \Psi \cos \varphi_1 = 0 \quad (1)$$

where we use the following notation:

$$\Omega^2 = \frac{\varepsilon \sin^2 \beta - 1}{\varepsilon \sin^2 \beta + 1} \omega_2^2 \quad \lambda = \frac{g(\varepsilon - 1) \sin \beta}{(\varepsilon \sin^2 \beta - 1) e \omega_2^2} \quad (2)$$

$$\Psi = \frac{8ea}{(\varepsilon \sin^2 \beta - 1)r^2} \sin \beta \quad \varepsilon = 1 + 4 \left( \frac{e}{r} \right)^2 \quad (3)$$

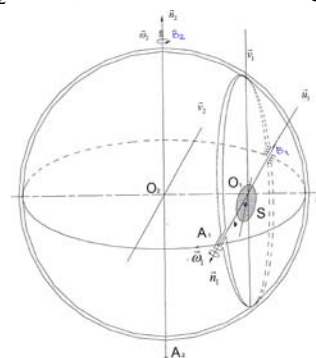


Fig. 1. Gyro-rotor

The motion of gyro-rotor was presented by means of phase trajectories and that is done for different cases of disk eccentricity and angle of skew. For that reason it is necessary to find first integral of the differential equation (1). After integration of the differential equation (10 the non-linear equation of the phase trajectories of the gyro rotor dynamics with the initial conditions  $t_0 = 0$ ,  $\varphi_1(t_0) = \varphi_{10}$ ,  $\dot{\varphi}_1(t_0) = \dot{\varphi}_{10}$  is obtained in a form:

$$\dot{\varphi}_1^2 = \dot{\varphi}_{10}^2 + 2\Omega^2 \left[ \lambda(\cos \varphi_1 - \cos \varphi_{10}) + \frac{1}{2}(\cos^2 \varphi_{10} - \cos^2 \varphi_1) + \Psi(\sin \varphi_1 - \sin \varphi_{10}) \right] \quad (4)$$

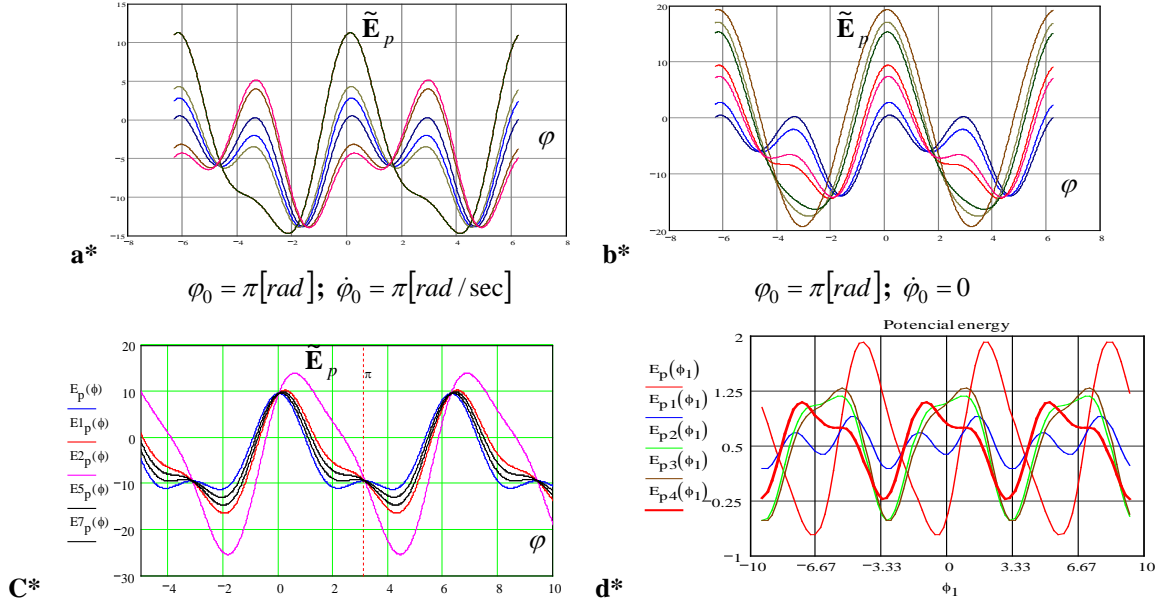


Fig. 2. The transformation of the graphical presentation of the potential energy analog of the heavy gyro rotor with rotating axis that are without intersection for different values ( $d^*$ ) of the eccentricity  $e$  and ( $a^*$ ,  $b^*$  and  $c^*$ ) of the angle  $\beta$  of disk inclination to the proper shaft axis rotation.

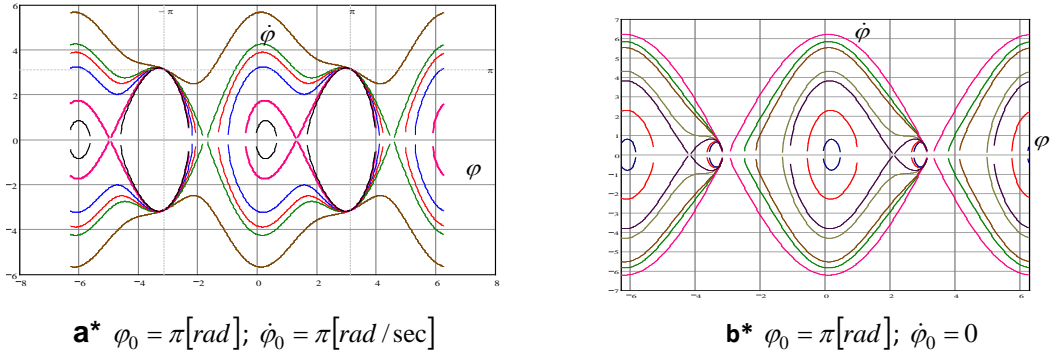


Fig. 3. Transformation of a phase trajectory of the heavy gyro rotor with rotating axis that are without intersection for different values of disk inclination angle  $\beta$  to the axis of self rotation and for two different initial conditions:

$$(a^*) \varphi_0 = \pi \text{ [rad]}; \dot{\varphi}_0 = \pi \text{ [rad/sec]} \quad \text{and} \quad (b^*) \varphi_0 = \pi \text{ [rad]}; \dot{\varphi}_0 = 0$$

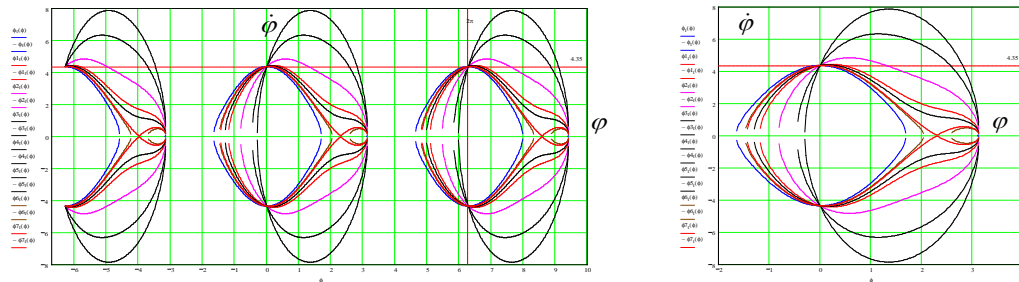


Fig. 4. Transformation of a phase trajectory presentation of the heavy gyro-rotor with rotating axis that are without intersection for different values of normal distance between axes and for a corresponding initial condition.

As the analyzed system is conservative it is the energy integral. For that case we can separate part of expressions in the equation (4) in the following form:

$$\tilde{E}_p = \Omega^2(\beta, \varepsilon, \omega_2) \left[ \lambda(\beta, \varepsilon, e, \omega_2)(\cos \varphi_1 - \cos \varphi_{10}) + \frac{1}{2}(\cos^2 \varphi_{10} - \cos^2 \varphi_1) + \Psi(\beta, e, a, r)(\sin \varphi_1 - \sin \varphi_{10}) \right] \quad (5)$$

as a analog to the potential energy in this rheonomic system. The analog to the potential energy exchange curves for different values of the system parameters (the eccentricity  $e$  and the angle  $\beta$  of the disk inclination) are given on Fig.2.

In Figure 3 a transformation of a phase trajectory of the heavy gyro-rotor with rotating axis that are without intersection for different values of disk inclination angle  $\beta$  to the axis of self rotation and for two different initial conditions: (**a\***)  $\varphi_0 = \pi[\text{rad}]$ ;  $\dot{\varphi}_0 = \pi[\text{rad}/\text{sec}]$  and (**b\***)  $\varphi_0 = \pi[\text{rad}]$ ,  $\dot{\varphi}_0 = 0$  is presented. In Figure 4 a transformation of a phase trajectory presentation of the heavy gyro-rotor with rotating axis that are without intersection for different values of normal distance between axes and for a corresponding initial condition is presented.

## 2. THE KINETIC PRESURES ON SHAFT BEARINGS OF THE GYRO-ROTOR

The shafts and axis are supported by bears so they are subjected to static and kinematics forces. Bearing force analysis of mechanisms is an important field in which mechanical engineers study a motion in order to design mechanisms to perform useful tasks. The forces whose nature is static have constant intensity but those with kinetics nature are changeable. So, the kinetic pressures on bearings can be very changeable in intensity and could involve some damages. The task is minimizing kinetic components.

An analytical formulation of forces in a form of four components is obtained by using two theorems: the theorem of linear momentum derivative and the theorem of angular momentum. By application of the two theorems we can write:

$$\frac{d\vec{K}}{dt} = \sum_i \vec{F}_i \quad \text{and} \quad \frac{d\vec{L}_o}{dt} = \vec{M}_o(\vec{F}_i) + m\vec{\rho}_c \times (\vec{v}_o \times \vec{\omega} - \vec{a}_o) \quad (6)$$

By solving these vector equations, we get of bearing forces in a form of four components. We separate some new unit vectors, also, as orientation of the kinetic pressure components applied to bearings in the following forms;:

$$F_{B1}^{kin} = \frac{1}{2\ell}(J_{vn}\omega_2 \cos \varphi_1 - J_n\dot{\varphi}_1)\omega_2 \quad F_{A1}^{kin} = \frac{1}{2\ell}(J_{vn}\omega_2 \cos \varphi_1 + J_n\dot{\varphi}_1)\omega_2 \quad (7)$$

$$F_{B2}^{kin} = \frac{1}{2\ell}(J_u - J_v)\omega_2\dot{\varphi}_1 \quad F_{A2}^{kin} = -\frac{1}{2\ell}(J_u - J_v)\omega_2\dot{\varphi}_1 \quad (8)$$

$$F_{B3}^{kin} = \frac{1}{2}m\omega_2^2(a + e \sin \beta \cos \varphi_1 + 2e\frac{a}{\ell} \cos \beta) \quad F_{A3}^{kin} = \frac{1}{2}m\omega_2^2(a + e \sin \beta \cos \varphi_1 - 2e\frac{a}{\ell} \cos \beta) \quad (9)$$

$$F_{B4}^{kin} = \frac{1}{2}\left(me \sin \beta - \frac{1}{\ell}J_{vn}\right)\sqrt{\dot{\varphi}_1^2 + \dot{\varphi}^4} \quad F_{A4}^{kin} = \frac{1}{2}\left(me \sin \beta + \frac{1}{2\ell}J_{vn}\right)\sqrt{\dot{\varphi}_1^2 + \dot{\varphi}^4} \quad (10)$$

The first components (7) are directed in line with unit vector  $\vec{w}_1 = \vec{u}_1 \sin \varphi_1 + \vec{v}_1 \cos \varphi_1$ , the second components (8) are directed in line with unit vector  $\vec{w}_2 = \vec{u}_1 \sin \varphi_1 - \vec{v}_1 \cos \varphi_1$ . These components are depending on angular velocity  $\omega_2$  and angular velocity  $\omega_1$ , the body disk mass distribution, the body mass axial inertia moment for the rotating axis,  $J_n$ , the body mass axial inertia moment for the axes normal on rotating axis,  $J_u$  and  $J_v$ , and the deviational moment of the body mass for a couple of normal axis oriented by the unit vectors  $\vec{n}_1$  and  $\vec{v}_1$ ,  $J_{nv}$ . These are periodical components with period of  $2\pi$  and with extreme values, too.

The third components (9) are depending on the body mass, the disk eccentricity,  $\varepsilon$ , distance between two axes,  $a$ , the angle of disk inclination,  $\beta$ , and they are proportional to square angular velocity  $\omega_2$ . These components are directed in line with unit vector  $\vec{w}_3 = -\vec{u}_1 \cos \varphi_1 + \vec{v}_1 \sin \varphi_1$ .

The fourth components (10) are directed in line with vector named rotator. The intensity of these components depends on the deviational moment of the body gyro-rotor (disk) mass for a couple of normal axis oriented by the unit vectors  $\vec{n}_1$  and  $\vec{v}_1$ ,  $J_{nv}$  the body gyro-rotor mass  $m$ , eccentricity  $e$  and the angle of disk inclination,  $\beta$ .

## 3. THE ROTATOR

In the expressions of the kinetic pressure components (10) to bearings of shaft self rotation, there are intensity as multiplication by the member with constant intensity (this means that its intensity depends only on mass and geometrical characteristics of rotor) and multiplied by a member depending only of kinematical parameters, angular velocity and angular acceleration of self rotation

of gyro-rotor. That kinetic pressure component is directed is in line with the vector which is named rotator [8]. The rotator is pure kinematics vector and it rotates and increases by angular velocity and angular acceleration of the gyro-rotor rotation around self shaft of self rotation. Its intensity dependences on angular velocity and angular acceleration, that is,

$$\mathfrak{R} = \left| \vec{\mathfrak{R}}(\varphi_1) \right| = \sqrt{\ddot{\varphi}^2 + \dot{\varphi}^4} \quad (11)$$

Figures 5.a\* show the dependence on the vector rotator intensity in the function of the elongation and for different values of the initial parameters h of the energy. The rotator is different from zero so the dynamic pressures on the bearings are different from zero, too. The smallest values of the rotator are corresponding to the position of the unstable static equilibrium position, while the greatest values of the rotator are corresponding to the position of the stable static equilibrium position.

Figures 5.b\* show the rotator trajectories. There are some shapes of trajectories and their shapes depend on parameters of the system. The parametric equations of rotator trajectories are:

$$\begin{aligned} u_{\mathfrak{R}}(\varphi_1) &= \Omega^2 \left[ -(\lambda - \cos \varphi_1) \sin \varphi_1 + \psi \cos \varphi_1 \right] \\ v_{\mathfrak{R}}(\varphi_1) &= 2\Omega^2 \left( \lambda \cos \varphi_1 - \frac{1}{2} \cos^2 \varphi_1 + \psi \sin \varphi_1 \right) + h \end{aligned} \quad (12)$$

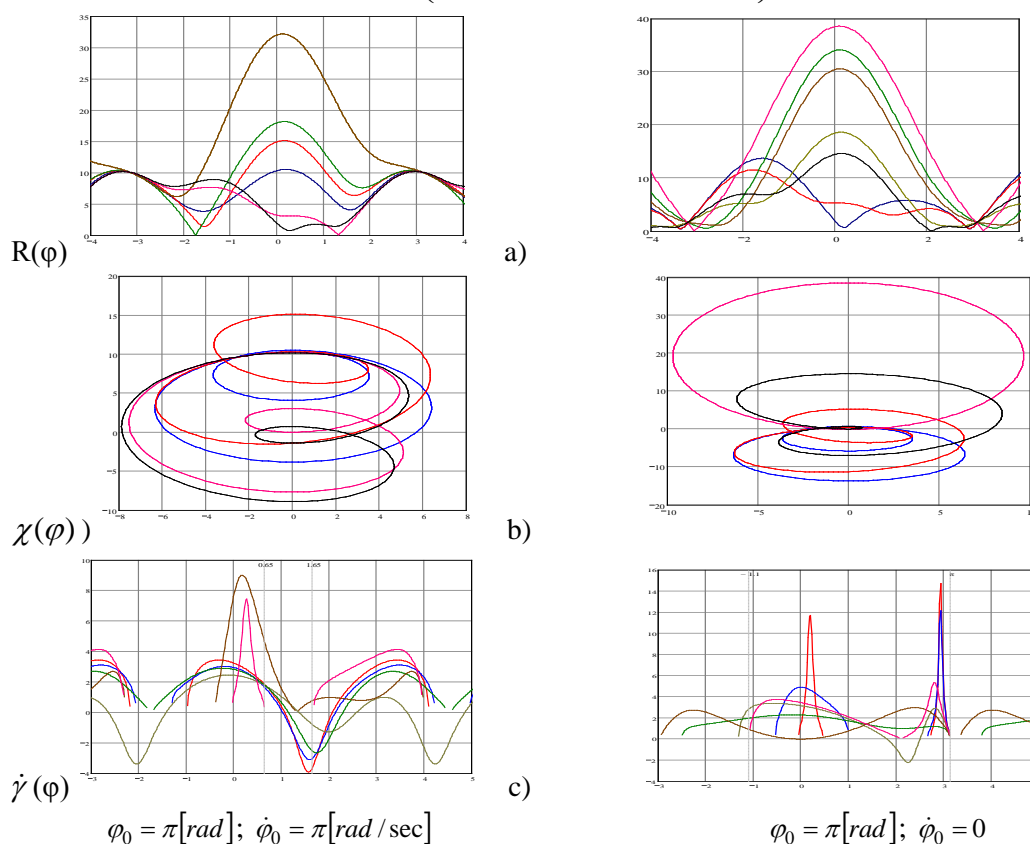


Fig. 5. Vector rotator of the heavy gyro rotor: a) the intensity portrait; b) the hodograph; c) the angular velocity for different values of angle  $\beta$  and for different initial conditions

The angle that rotator form with axis  $\vec{u}_1$  is determined by express:  $\text{tg} \gamma = \frac{\dot{\varphi}^2}{\ddot{\varphi}}$ . The derivative by time is:

$$\dot{\gamma} = \frac{\dot{\varphi}(2\ddot{\varphi}^2 - \ddot{\varphi})}{\ddot{\varphi}^2 + \dot{\varphi}^4} = \frac{\dot{\varphi}(2\ddot{\varphi}^2 - \ddot{\varphi})}{\mathfrak{R}^2} \quad (13)$$

and its graphical presentation is shown on Figure 5.c\*.

## CONCLUSIONS

By use analytical expressions of the kinetic components of the kinetic pressures to the gyro-rotor shaft bearings through MathCad program numerous visualizations are presented through characteristic graphs and qualitatively analyzed. Special attentions are focused to the vector rotators, as well as to the absolute and relative angular velocities of the rotation of the kinetic components of the kinetic pressures to the gyro-rotor self rotation shaft bearings.

From obtained analytical expressions for kinetic pressures to the gyro-rotor shaft bearings four vector components are separated. One component of the kinetic pressures to the gyro-rotor shaft bearings of self rotation is caused by deviation properties of the gyro-rotor mass distribution around self rotation shaft axis and is expressed as product between deviation mass inertia moment according shaft axis of self rotation and pure kinematical vector rotator which depends on angular velocity and angular acceleration of the gyro-rotor shaft self rotation. Three other components of the kinetic pressures to the gyro-rotor shaft bearings are functions of the both angular coordinates and angular velocities of the gyro-rotor system dynamics as well as of the gyro-rotor mass distributions and deviational properties.

**Acknowledgment.** *Parts of this research were supported by the Ministry of Sciences and Environmental Protection of Republic of Serbia through Mathematical Institute SANU Belgrade Grant ON144002 and Faculty of Mechanical Engineering University of Nis.*

## REFERENCES

- [1] Andronov A.A., Vitt A.A., Haykin S.E. *Teoriya kolebaniy*, Nauka, Moscow., 568 p., 1981 (in Russian).
- [2] Gerard I. and Daniel J. *Elementary Stability and Bifurcation Theory*, Springer Verlag, 1980.
- [3] Guckenheimer, J. and Holmes, Ph. *Nonlinear Oscillations, Dynamical Systems, and Bifurcations of Fields*, Springer-Verlag, 461 p., 1983.
- [4] Hedrih (Stevanović) K. Nonlinear Dynamics of a Heavy Material Particle Along Circle which Rotates and Optimal Control, in the book: *Chaotic Dynamics and Control of Systems and Processes in Mechanics* (Eds: G. Rega, and F. Vestroni), IUTAM Book, in Series *Solid Mechanics and Its Applications*, Edited by G.M.L. Gladwell, Springer, XXVI, pp. 37-45, 2005.
- [5] Hedrih (Stevanović) K. A Trigger of Coupled Singularities, *MECCANICA*, Vol.39, No. 3, pp. 295-314, 2004.
- [6] Hedrih (Stevanović) K., The optimal control in nonlinear mechanical systems with trigger of the coupled singularities, in the book: *Advances in Mechanics: Dynamics and Control. Proceedings of the 14th International Workshop on Dynamics and Control* (ed. by F.L. Chernousko, G.V. Kostin, V.V. Saurin). A.Yu. Ishlinsky Institute for Problems in Mechanics RAS. – Moscow : Nauka, pp. 174-182, 2008.
- [7] Katica (Stevanović) Hedrih, Optimal Control of Dissipative Nonlinear Dynamical Systems with Triggers of Coupled Singularities, *Journal of Physics: Conference Series*, 96, 2008. 012220doi:10.1088/1742-6596/96/1/012220, IOP Publishing <http://www.iop.org/EJ/main/-list=current/>
- [8] Hedrih (Stevanović) K. *The Vector Method of the Heavy Rotor Kinetic Parameter Analysis and Nonlinear Dynamics*, University of Niš, pp. 252 p., 2001.
- [9] Hedrih (Stevanović) K. Dynamics of coupled systems, *Nonlinear Analysis: Hybrid Systems*, Vol. 2, Issue 2, pp. 310-334, 2008.
- [10] H Hedrih (Stevanović) K. Vibrations of a Heavy Mass Particle Moving along a Rough Line with Friction of Coulomb Type, *Int. Journal of Nonlinear Sciences & Numerical Simulation*, 10(11), pp.1705-1712, 2009.
- [11] Katica (Stevanović) Hedrih. Free and forced vibration of the heavy material particle along line with friction: Direct and inverse task of the theory of vibrorheology, in the book: *7<sup>th</sup> EUROMECH Solid Mechanics Conference*, (J. Ambrósio et.al. eds.), Lisbon, Portugal, September 7-11, 2009, CD –MS-24, Paper 348, pp. 1-20, 2009.
- [12] Katica (Stevanović) Hedrih and Ljiljana Veljović. Nonlinear dynamics of the heavy gyro-rotor with two skew rotating axes, *Journal of Physics: Conference Series*, 96, 2008. 012221doi:10.1088/1742-6596/96/1/012221, IOP Publishing <http://www.iop.org/EJ/main/-list=current/>
- [13] Rašković D. *Mehanika - Dinamika (Dynamics)*, Naučna knjiga, 1972.
- [14] Rašković D. *Teorija oscilacija (Theory of oscillations)*, Naučna knjiga, 1952.
- [15] Stoker J. J. *Nonlinear Vibrations*, Interscience Publish, 1950.

THE PHASE PORTRAIT OF THE VIBRO-IMPACT DYNAMICS OF  
TWO MASS PARTICLE MOTIONS ALONG ROUGH CIRCLE

**Katica R. (Stevanović)  
Hedrih<sup>1</sup>**

Mathematical Institute  
SANU  
Belgrade, Serbia,

**Vladimir Raičević,  
Srdjan Jović**

University of Priština,  
Kosovska Mitrovica,  
Serbia

ABSTRACT

The paper presents combinations of analytical and numerical results and some visualizations of some kinetic parameters of the non-linear dynamics of a vibro-impact system with two degree of freedom and one side impact limiter of system elongations.

System of two heavy mass particles free oscillations along a rough circle in vertical plane, with Coulomb's type friction and with impacts between mass particles and also, with one side, impact limiter of the angle elongations of one mass particle, is object of the analytical and numerical research. The corresponding system of two ordinary non-linear differential double equations of non-linear dynamic equilibrium states of two mass particles is derived accompanying with corresponding initial conditions and impact conditions, as well as conditions of the direction alternation of the friction forces of the Coulomb's type as reactions to the two mass particles motions. Analytical expressions of the phase trajectory branches of both mass particles in the intervals between two kind impacts are derived with corresponding integral constants depending of initial representative phase point coordinates for each phase trajectory branch. In considered vibro-impact system dynamics two kind of impacts appear: one kind of impacts are impacts between two mass particles, and second kind of impacts are impacts of the one of mass particles into one left side right impact limiter of its angle elongations. Then it is necessary to calculate the moments of time of each kind of impacts as well as time intervals between two successive impacts and velocities of the mass particles, before and after each of impacts and angular coordinate of the place of each impact. Description of the methodology of problem investigation is possible express by analytical approach, but for each particular case it is necessary to use numerical methods for solutions step by step. MathCAD is applied by us in this vibro-impact system dynamics investigation. Analytical results in combinations with numerical experiment gives to us a set of numerical data for visualizations of the non-linear phenomena of this vibro-impact system with two degree of freedom.

For all of considered cases of the heavy two mass particles motions along rough line we can identify a member in the both differential double equations proportional to the square of the corresponding generalized coordinate derivation with respect to time by which both non-linear differential double equations of the mass particle motions are expressed. This corresponds to the known case of turbulent damping.

Changes of the friction forces directions, as an alternation of the directions of the both mass particle motions, are strong discontinuities and non-linearities followed to the double alternate equilibrium position as a bifurcation of positions of the equilibrium depending of the direction of the mass particles motions.

## INTRODUCTION

Non-linear phenomena in dynamics of vibro-impact systems are special types of non-linearity caused by series of impacts, followed by discontinuities of kinetic parameter properties and alternations of the motion and velocity direction, as strong non-linearity. In the case, that the basic system dynamics is pure linear, series of vibro-impacts are source of strong non-linearity

<sup>1</sup> Corresponding author. Email [khedrih@eunet.rs](mailto:khedrih@eunet.rs)

appearance in the system dynamics. In the case, that the basic system dynamics is non-linear, series of vibro-impacts are source of interaction between two types of non-linearity and in the system appear very complex non-linear vibration regimes.

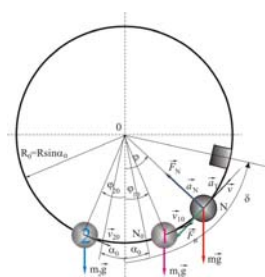
Also, no ideal constraints with Coulomb's type friction forces are source of the strong non-linearity caused by alternations of the friction force directions. Theoretical knowledge and analytical results concerning vibro-impact system dynamics are very valuable in the trends that large numbers of researchers focused to the computation investigations. Also, knowledge of vibro-impact phenomena and vibro-dynamics with impacts is very important for engineering applications, taking into account that working processes of many new engineering system are based on the vibro-impact processes. Series of monographs [3] and [4] by Babickii and Kolovskii, and [2] by Babickii and papers [17], [18] and [19] by Peterka and [5] by Bapat and Popplewell and other contain important scientific and advances to the topic properties of vibro-impact dynamics with corresponding particular methodology applied to the particular classes of the vibro-impact system dynamics.

Some classical problems of mechanical system motion with no ideal constraints and friction as well as an oscillator with Coulomb's type friction are presented in the university books on the level of monographs [20] and [21] written by Rašković contain basic analytical results in this topic. Expellant paper [16] written by Matrosov and Finogenko contain the theory of right solutions of equations for mechanical systems dynamics with sliding friction in one-degree-of-freedom kinematics pairs, which has been developed by the authors. Also, some difficulties bound up with "non-uniqueness" of motion in course of description of such systems, which are known as P. Painlevé's paradoxes are discussed.

New series of published papers by Hedrih (Stevanović) K., present new research results regarding heavy mass particle motions along circles which rotate, as well as hybrid dynamics in the form of the coupled rotations (see References [6-12]). Analysis of the mathematical pendulum dynamics in the field with turbulent damping (see Ref. [22] by Stoker) and papers written by Hedrih (Stevanović) K. [6-12] related to the heavy mass particle dynamics along rotate circle as well as to the heavy mass particle dynamics along rough curvilinear line with Admonton-Coulomb's type frictions are basic inspiration of the series of research results of vibro-impact nonlinear dynamics co-authored by Hedrih (Stevanović) K., Raičević V. and Jović S. and presented in the published co-author papers [13], [14], and [15] in period 2009 and 2010 and listed in the reference list of this paper, as well as in the magistar of science thesis defended by Jović S. in 2009.

## 1. BASIC SYSTEMS OF THE DOUBLE EQUATIONS OF TWO HEAVY MASS PARTICLES DYNAMICS ALONG ROYGH CIRCLE WITH COULOMB'S TYPE FRICTION

Let consider free vibro-impact dynamics of the two heavy mass particle motions, in vertical plane, along rough circle with Coulomb's type friction and one, one side impact limiter of the angular elongations of the right hand side heavy mass particle. System is shown in Figure 1. The system of two ordinary non-linear differential double equations of non-linear dynamic equilibrium kinetic states of two mass particles is in the following form:



$$\ddot{\varphi}_1 \pm \dot{\varphi}_1^2 \operatorname{tg} \alpha_0 + \frac{g}{R \cos \alpha_0} \sin(\varphi_1 \pm \alpha_0) = 0 \begin{cases} za \dot{\varphi}_1 > 0 \\ za \dot{\varphi}_1 < 0 \end{cases} \quad (1)$$

$$\ddot{\varphi}_2 \pm \dot{\varphi}_2^2 \operatorname{tg} \alpha_0 + \frac{g}{R \cos \alpha_0} \sin(\varphi_2 \pm \alpha_0) = 0 \begin{cases} za \dot{\varphi}_2 > 0 \\ za \dot{\varphi}_2 < 0 \end{cases} \quad (2)$$

where  $\varphi_1, \varphi_2$  are independent generalized angular coordinate of the system;  $\mu = \operatorname{tg} \alpha_0$  is coefficient of Coulomb's type friction.

Fig. 1. The two mass particle vibro-impact system dynamics along rough circle

Let consider case that initial conditions satisfy the following relations:  $\varphi_{10} > \varphi_{20}$ ;  $\dot{\varphi}_{10} > \dot{\varphi}_{20}$ . For full determination of the heavy mass particles it is necessary to add to the each of differential double equations (1) and (2) the following initial conditions:  $a^*$  for first mass particle and differential double equation (1):  $\varphi_{1(0)} = \varphi_{10}$  and  $\dot{\varphi}_{1(0)} = \dot{\varphi}_{10}$ ;  $b^*$  for second mass particle and differential double equation (2):  $\varphi_{2(0)} = \varphi_{20}$  and  $\dot{\varphi}_{2(0)} = \dot{\varphi}_{20}$  and we accept that is  $(\dot{\varphi}_1 > 0, \dot{\varphi}_2 > 0)$ .

For describing and determining vibro-impact dynamics of the presented research task it is necessary to the system of differential double equations (1) – (2) with initial conditions to join conditions of the impact limitations of the angular elongations of the second mass particle:  $\varphi_{1ul_i} = \delta$ ,

$\dot{\varphi}_{odl_i} = -k\dot{\varphi}_{ul_i}$ ,  $i=1,2,3,\dots,n$ , where  $k$  is coefficient of the restitution of the second mass particle impacts to the impact limiter of the angular elongations which take values:  $k=0$  for ideally plastic impacts and  $k=1$  for ideally elastic impacts.

Also, for full describing and full determining vibro-impact dynamics of the presented research task it is necessary to the system of differential double equations (1) – (2) with initial conditions and conditions of the impact limitations of the angular elongations of the second mass particle to join conditions of the impacts between mass particles, which not determined at initial moment. For each of impacts between mass particles it is necessary to take into account initial positions of the mass particles, as well as initial velocities with corresponding directions of the each of mass particle motions along rough circle and calculate moment of the impact, as well as position of each of the impacts as well as velocities of each mass particle before and after each of the impacts. These values of the kinetic parameters of the mass particles after each of impacts are initial conditions of the next phase trajectory branch with corresponding one of the two signs in the differential double equation (1) for first mass particle and (2) for second mass particle with corresponding sign depending of direction of the first and second mass particle.

Equations of the phase trajectories of the non-linear free dynamics of two mass particles motions along rough circle in analytical forms by integrations of the differential double equations (1) and (2) for the case that right hand side are equal to zeros are obtained and presented in the References [11] and [12] written by Hedrih (Stevanović) K.(2009,2010). In these References an analysis of the bifurcation of the zero equilibrium position into two one side (half) stable equilibrium positions is pointed out. These information about basic system non-linear dynamics and forms of the phase trajectories and integral form of phase portrait as well as of the constant mechanical energy of the basic linearized system in intervals between friction force alternation of direction are important for investigation of the forms of phase trajectory branches for vibro-impact dynamics of the two mass particle motions along rough circle.

Then, by use cited references [11] and [12], the system of two non-linear double equations of the phase trajectories of non-linear dynamic equilibrium kinetic states of two mass particles are in the following form: 1\* for first mass particle:

$$\dot{\varphi}_1(\varphi_1)^2 = \frac{2g}{(1+4tg^2\alpha_0)R\cos\alpha_0} [\cos(\varphi_1 \pm \alpha_0) - 2tg\alpha_0 \sin(\varphi_1 \pm \alpha_0)] + C_1 e^{\mp 2\varphi_1 tg\alpha_0} \begin{cases} za \dot{\varphi}_1 > 0; \\ za \dot{\varphi}_1 < 0 \end{cases}; \quad (3)$$

2\* for second mass particle:

$$\dot{\varphi}_2(\varphi_2)^2 = \frac{2g}{(1+4tg^2\alpha_0)R\cos\alpha_0} [\cos(\varphi_2 \pm \alpha_0) - 2tg\alpha_0 \sin(\varphi_2 \pm \alpha_0)] + C_2 e^{\mp 2\varphi_2 tg\alpha_0} \begin{cases} za \dot{\varphi}_2 > 0 \\ za \dot{\varphi}_2 < 0 \end{cases} \quad (4)$$

where  $C_1$  and  $C_2$  are integral constant depending of initial conditions of each phase trajectory branche.

Next analysis of two heavy mass particles vibro-impact dynamics along rough circle is realized by use a example with numerical data and through series of intervals of motions between two impacts or between impact and alternations of the Coulomb's type friction force. For corresponding interval phase trajectory branchess of the corresponding mass particle motion are obtained by use previous system of the double equations (3)-(4) and in combinations of the analytical and numerical approach and by calculations of the same time and equal positions of both mass particles. Corresponding velocities before impacts of the mass particles are obtained numerically by use MatchCad program for graphical presentation of the next phase trajectory branches of the mass particles and for to read comon position of the impact between themnad the corresponding time and velocities. By use theory of impacts velocitis of the both masses after impacts are obtained.

## 2. PHASE TRAJECTORY BRANCHES AND KINETC PARAMETERS OF IMPACTS BETWEEN MASS PARTICLES

Conditions of the first impact of the first mass particle are:  $t=t_{ul_1-}$ ,  $\varphi_1(t_{ul_1-})=\delta$ ,  $\dot{\varphi}_1(t_{ul_1-})=\dot{\varphi}_{1ul_1-}$ . Angular velocity ( $\dot{\varphi}_{1ul_1-}$ ) of the first impact of first mass particle into impact limiter of angular elongations we read from phase trajectory branch obtained by double equation (3) defined with upper sign and passing through initial kinetica state by which integral constant is determined in the form

$$C_{11}(\varphi_{10}, \dot{\varphi}_{10}) = e^{+2\varphi_{10} tg\alpha_0} \left\{ \dot{\varphi}_{10}^2 - \frac{2g}{(1+4tg^2\alpha_0)R\cos\alpha_0} [\cos(\varphi_{10} + \alpha_0) - 2tg\alpha_0 \sin(\varphi_{10} + \alpha_0)] \right\} \quad (5)$$

and graphically presented in Figure 2. a\* by use MathCad program, on the coordinate  $\varphi_1(t_{ul1-}) = \delta$ . Angular velocity of the first impact of first mass particle into angular elongation limiter is:

$$\dot{\varphi}_{1ul1} = \sqrt{\frac{2g}{(1+4tg^2\alpha_0)R\cos\alpha_0} [\cos(\delta + \alpha_0) - 2tg\alpha_0 \sin(\delta + \alpha_0)] + C_{11}(\varphi_{10}, \dot{\varphi}_{10})e^{-2\delta g\alpha_0}} \quad (6)$$

Time ( $t_{1ul1}$ ) of the first impact of the first mass particle to the to the impact limiter, we calculate by

$$t_{1ul1} = \int_{\varphi_{10}}^{\delta} \frac{d\varphi_1}{\sqrt{\frac{2g}{(1+4tg^2\alpha_0)R\cos\alpha_0} [\cos(\varphi_1 + \alpha_0) - 2tg\alpha_0 \sin(\varphi_1 + \alpha_0)] + C_{11}(\varphi_{10}, \dot{\varphi}_{10})e^{-2\varphi_1 g\alpha_0}}} \quad (7)$$

and take at angular coordinate  $\varphi_1(t_{ul1-}) = \delta$ . Next, it is necessary to find angular coordinate of the second mass particle position at the moment of the first mass particle impact into angular elongation impact limiter. By use phase trajectory double equation (4) of the second mass particle motion passing through their initial kinetic state with upper sign, and with integral constant

$$C_{21}(\varphi_{20}, \dot{\varphi}_{20}) = e^{+2\varphi_{20} g\alpha_0} \left\{ \dot{\varphi}_{20}^2 - \frac{2g}{(1+4tg^2\alpha_0)R\cos\alpha_0} [\cos(\varphi_{20} + \alpha_0) - 2tg\alpha_0 \sin(\varphi_{20} + \alpha_0)] \right\} \quad (8)$$

a first phase trajectory branch is presented at Figure 1 b\* in the MathCad program. At the end of the time interval  $t_{1ul1}$  of the motion, corresponding angular coordinate of the second mass particle position  $\varphi_2(t_{1ul1})$  is obtained numerically by the following expression:

$$t_{21} = \int_{\varphi_{20}}^{\varphi_2} \frac{d\varphi_2}{\sqrt{\frac{2g}{(1+4tg^2\alpha_0)R\cos\alpha_0} [\cos(\varphi_2 + \alpha_0) - 2tg\alpha_0 \sin(\varphi_2 + \alpha_0)] + C_{21}(\varphi_{20}, \dot{\varphi}_{20})e^{-2\varphi_2 g\alpha_0}}} \quad (9)$$

and using MathCad program for graphical presentation relation (9).

Second impact in the system vibro-impact dynamics is first impact between mass particles which appear in the second interval of the first mass particle motion and in the first interval of the motion of the second mass particle for considered case of the initial conditions. For different cases of the chosen initial conditions and relation between system parameters are possible different cases.

Second phase trajectory branch and interval of the first mass particle motion, after first impact into angular elongation limiter, is defined by double equation (3) with lower sign and starting through kinetic state after first impact,  $t_1 = t_{1ul1+}$ ,  $\varphi_1(t_{1ul1+}) = \delta$ ,  $\dot{\varphi}_1(t_{1ul1+}) = \dot{\varphi}_{1odl1} = -\dot{\varphi}_{1ul1-}$ , determining integral constant in the form:

$$C_{12} = \frac{1}{e^{2\delta g\alpha_0}} \left\{ (-\dot{\varphi}_{1ul1})^2 - \frac{2g}{(1+4tg^2\alpha_0)R\cos\alpha_0} [\cos(\delta - \alpha_0) - 2tg\alpha_0 \sin(\delta - \alpha_0)] \right\} \quad (10)$$

Next step is to find time of the impact between mass particles and common positions of the mass particles in this interval of motions in which first impact between mass particles appear and corresponding velocities before and after impacts (arrival velocity and leaving velocity of the impact). This task can be realized numerically by use the following expressions with two unknown, time  $t_{sud1}$  of first impacts between mass particles and common position  $\varphi_{sud1}$  of this their first impact:

$$t_{sud1} = \int_{\delta}^{\varphi_{sud1}} \frac{d\varphi_1}{\sqrt{\frac{2g}{(1+4tg^2\alpha_0)R\cos\alpha_0} [\cos(\varphi_1 - \alpha_0) - 2tg\alpha_0 \sin(\varphi_1 - \alpha_0)] + C_{12}(\delta, \dot{\varphi}_{1odl1})e^{2\varphi_1 g\alpha_0}}} \quad (11)$$

$$t_{sud1} = \int_{\varphi_{2ud1}}^{\varphi_{sud1}} \frac{d\varphi_2}{\sqrt{\frac{2g}{(1+4tg^2\alpha_0)R\cos\alpha_0} [\cos(\varphi_2 + \alpha_0) - 2tg\alpha_0 \sin(\varphi_2 + \alpha_0)] + C_{21}(\varphi_{2ud1}, \dot{\varphi}_{2ud1})e^{-2\varphi_2 g\alpha_0}}} \quad (12)$$

After using MathCad program, and obtained time  $t_{sud1}$  and position  $\varphi_{sud1}$  of the first impact between mass particles it is easy to obtain arrival velocities unreachable before their first impact,  $\dot{\varphi}_{1sud1,ul}$  and  $\dot{\varphi}_{2sud1,ul}$  using expressions (3) with lower sign with corresponding integral constant  $C_{12}(\delta, \dot{\varphi}_{1odl1})$  and (4) with upper sign and corresponding integral constant  $C_{21}(\varphi_{2ud1}, \dot{\varphi}_{2ud1})$ . Then, expression for the leaving velocities  $\dot{\varphi}_{2sud1,odl}$  and  $\dot{\varphi}_{1sud1,odl}$  of the mass particles after first impact between mass particles are in the following form:

$$\dot{\varphi}_{2sud1,odl} = \frac{m_1(1+k)}{m_1+m_2} \dot{\varphi}_{1sud1,ul} - \frac{m_2-km_1}{m_1+m_2} \dot{\varphi}_{2sud1,ul}, \quad \dot{\varphi}_{1sud1,odl} = \frac{km_2-m_1}{m_1+m_2} \dot{\varphi}_{1sud1,ul} + \frac{m_2(k+1)}{m_1+m_2} \dot{\varphi}_{2sud1,ul} \quad (14)$$

Coordinate of position  $\varphi_{sud1}$  of the first impact between mass particles and leaving velocities  $\dot{\varphi}_{2sud1,odl}$  and  $\dot{\varphi}_{1sud1,odl}$  of the mass particles after first impact between mass particles are starting (initial) coordinates and velocities of the next phase trajectory branches of mass particles for next interval of the their motions. Methodology to build next phase trajectory branches in the next intervals of the mass particle motions between impacts and friction force alternation of direction is clear visible from previous explanations and taking into account limitation of this paper pages no possible to present all details of this used methodology. From previous presented methodology is not difficult to applied to the next intervals of the mass particle motion and numerically determine kinetic parameters of the next impacts up to the rest of the mass particles.

### 3. NUMERICAL ANALYSIS OF THE VIBRO-IMPACT DYNAMICS –AN EXAMPLE

For numerical investigation we use a vibro-impact dynamics of two heavy mass particle motions along rough circle with following kinetic and geometrical data:  $m_1 = 0,2[kg]$ ,  $m_2 = 0,2[kg]$ ,  $R = 0,5[m]$ ,  $\alpha_0 = 0.05$ ,  $g = 9,81\left[\frac{m}{s^2}\right]$ ,  $\delta = \frac{\pi}{4}[rad]$ ,  $\varphi_{10} = \frac{\pi}{12}[rad]$ ,  $\dot{\varphi}_{10} = 7\left[\frac{rad}{s}\right]$ ,  $\varphi_{20} = -\frac{\pi}{12}[rad]$ ,  $\dot{\varphi}_{20} = 5\left[\frac{rad}{s}\right]$ .

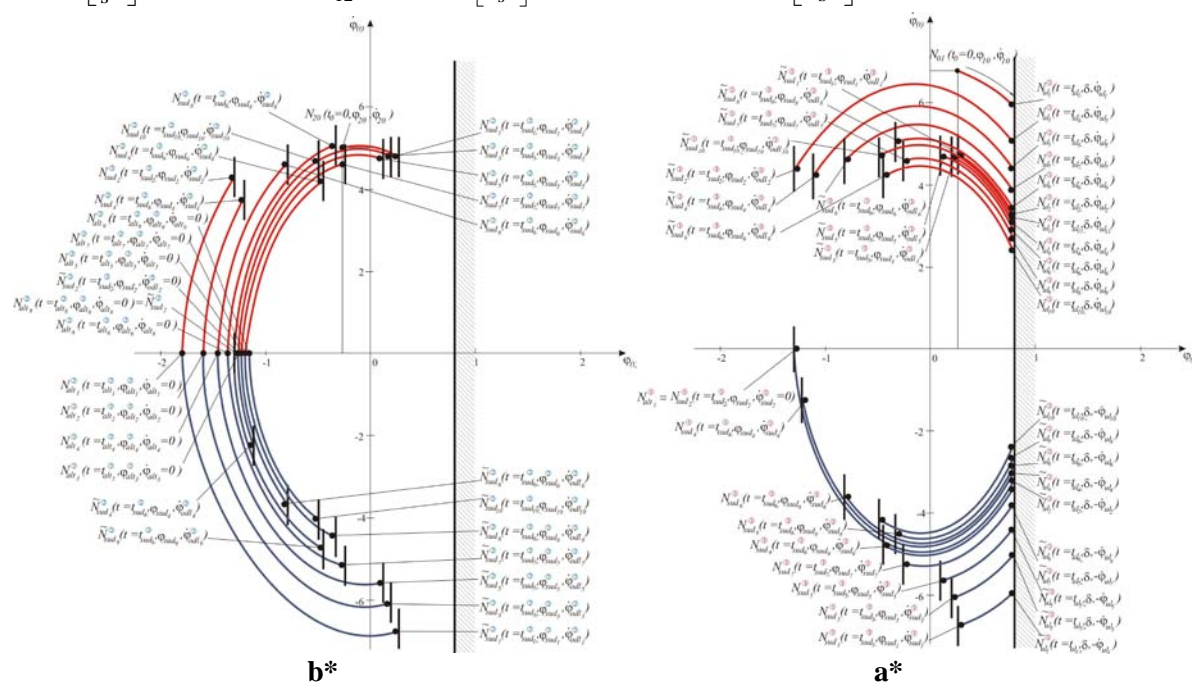


Fig. 2. Phase portrait  $(\varphi, \dot{\varphi})$  of the two mass particle vibro-impact system dynamics along rough circle with Coulomb's type friction and one side right impact limiter of the angular elongations of the second mass particle. (a\*) Phase trajectory branches of the first mass particle and (b\*) phase trajectory branches of the second mass particle, each between two successive impacts .

Graphical visualizations of the numerical experiment of the two mass particle vibro-impact dynamics, by use, in previous part described methodology for obtaining phase trajectory branches and for the defined system data, are presented in Figure 2 a\* and b\*. In Fig.1.a\* for first mass particle vibro-impact dynamics, phase trajectory branches are presented. In Figure 6, for second mass particle vibro-impact dynamics, phase trajectory branches are presented.

### CONCLUSIONS

Non-linear properties in the considered vibro-impact two mass particles motions along rough circle are caused by three type of the nonlinearities, which are:

a\* first is the basic system non-linearity of the curvilinear mass particle path in circle form induced non-linear dependence of the proper weigh components of both heavy mass particles, as a primary non-linearity;

b\* second is the strong non-linearity induced in the system by no ideal circle line and Coulomb's type friction force with alternations of the friction force directions in the form of the discontinuity and also a member in the differential double equations expressed by members containing square of the mass particles velocities,  $\dot{\varphi}_1^2, \dot{\varphi}_2^2$ ;

c\* third is the strong non-linearity induced in the system by impacts first mass particle into impact limiter of the angular elongations and by impacts between mass particles caused discontinuities of the mass particles velocities before and after impacts.

**Acknowledgment.** Parts of this research were supported by the Ministry of Sciences and Environmental Protection of Republic of Serbia through Mathematical Institute SANU Belgrade Grant ON144002 and Faculty of Mechanical Engineering University of Niš as well as Faculty of Technical Sciences Kosovska Mitrovica University of Priština.

## REFERENCES

- [1] Andronov A.A., Vitt A.A., Haykin S.E. *Teoriya kolebaniy*, Nauka, Moscow, 568 p., 1981 (in Russian).
- [2] Babickii V. I. *Theory of vibro-impact systems*, Nauka, Moscow, 1978 (in Russian).
- [3] Babickii V. I., Kolovskii M.Z. Vibrations of linear system with limiters, and excited by random excitation, *Mehanika tverdogo tela*, No 3, 1967 (in Russian).
- [4] Babickii V. I., Kolovskii M.Z. Investigation of the vibro-impact systems by resonant regimes, *Mehanika tverdogo tela*, No 4, 1976 (in Russian).
- [5] Bapat C. N., Popplewell N. Several Similar Vibroimpact Systems, *Journal of Sound and Vibration*, 113 (1), pp. 17-28, 1987.
- [6] Hedrih (Stevanović) K. Nonlinear Dynamics of a Heavy Material Particle Along Circle which Rotates and Optimal Control, in the book: *Chaotic Dynamics and Control of Systems and Processes in Mechanics* (Eds: G. Rega, and F. Vestroni), *IUTAM Book, in Series Solid Mechanics and Its Applications*, Edited by G.M.L. Gladwell, Springer, XXVI, pp. 37-45, 2005.
- [7] Hedrih (Stevanović) K. A trigger of coupled singularities, *Meccanica*, Vol. 39, No. 3, pp. 295-314, 2004.
- [8] Hedrih (Stevanović) K. *The optimal control in nonlinear mechanical systems with trigger of the coupled singularities*, in the book: *Advances in Mechanics : Dynamics and Control : Proceedings of the 14th International Workshop on Dynamics and Control* (ed. by F.L. Chernousko, G.V. Kostin, V.V. Saurin). A.Yu. Ishlinsky Institute for Problems in Mechanics RAS. Nauka, Moscow, pp. 174-182, 2008.
- [9] Hedrih (Stevanović) K. *The Vector Method of the Heavy Rotor Kinetic Parameter Analysis and Nonlinear Dynamics*, University of Niš, 2001, pp. 252., 2001.
- [10] Hedrih (Stevanović) K. Dynamics of coupled systems, *Nonlinear Analysis: Hybrid Systems*, Vol. 2, Issue 2, pp. 310-334, 2008.
- [11] Hedrih (Stevanović) K., Vibrations of a Heavy Mass Particle Moving along a Rough Line with Friction of Coulomb Type, *Int. J. of Nonlinear Sciences & Numerical Simulation*, Vol. 11, No.3, pp. 203-210, 2010.
- [12] Katica (Stevanović) Hedrih, Free and forced vibration of the heavy material particle along line with friction: Direct and inverse task of the theory of vibrorheology, In the book: *7<sup>th</sup> EUROMECH Solid Mechanics Conference*, J. Ambrósio et.al. (eds.), Lisbon, Portugal, September 7-11, 2009, CD –MS-24, Paper 348, pp. 1-20, 2009.
- [13] Hedrih (Stevanović) K. Raičević V. Jović S. Vibro-impact of a Heavy Mass Particle Moving along a Rough Circle with Two Impact Limiters, *Int. Journal of Nonlinear Sciences & Numerical Simulation* Vol. 11, No.3, pp. 211-223, 2010.  
[http://www.freundpublishing.com/International\\_Journal\\_Nonlinear\\_Sciences\\_Numerical%20Simulation/MathPrev.htm](http://www.freundpublishing.com/International_Journal_Nonlinear_Sciences_Numerical%20Simulation/MathPrev.htm)
- [14] Hedrih (Stevanović) K., Jović S. Models of Technological Processes on the Basis of Vibro-impact Dynamics, *Scientific Technical Review*, Vol. LIX, No.2, pp.51-72, 2009.
- [15] Hedrih (Stevanović) Katica and Srdjan Jović. Vibroimpact System Dynamics: Heavy Material Particle Oscillations along Rough Circle with One Side Impact Limit, In the book: *10<sup>th</sup> Conference on Dynamical Systems – Theory and Applications, Proceedings, DSTA Lody 2009*, Edited by J.A. Awrejcewicz, M. Kazmierczak, P. Olejnik, J. Mrozowski, Lodz, December 7-10, 2009, Poland, Vol. I, pp. 213-220, 2009.
- [16] Matrosov V. M. and Finogenko O.A. The theory of differential equations which arise in the dynamics of a system of rigid bodies with Coulomb friction, Vol. 2, pp. 18-108, 2008.
- [17] Peterka F. Laws of Impact Motion of Mechanical Systems with one Degree of Freedom: Part I - Theoretical Analysis of n- Multiple (1/n) - Impact Motions, *Acta Technica CSAV*, No 4, pp 462-473, 1974.
- [18] Peterka F., Laws of Impact Motion of Mechanical Systems with one Degree of Freedom: Part II - Results of Analogue Computer Modelling of the Motion, *Acta Technica CSAV*, No 5, pp 569-580, 1974.
- [19] Peterka F. Bifurcations and transition phenomena in an impact oscillator, *Chaos, Solitons and Fractals*, Vol. 7, No 10, pp. 1635-1647, 1996.
- [20] Rašković D. *Mehanika - Dinamika (Dynamics)*, Naučna knjiga, 1972.
- [21] Rašković D. *Teorija oscilacija (Theory of oscillations)*, Naučna knjiga, 1952.
- [22] Stoker J. J. *Nonlinear Vibrations*, Interscience Publish, 1950.

**STABILITY FOR A CLASS OF  
SYSTEMS WITH UNCERTAIN STRUCTURE**

**Ievgen Ivanov<sup>1</sup>**

Taras Shevchenko  
National University of Kyiv  
Kyiv, Ukraine

---

ABSTRACT

---

In the article a class of continuous-discrete dynamical systems with switching at uncertain moments of time is constructed on the basis of possibility theory. A notion of stability with given necessity level is introduced and stability properties of systems of constructed class are investigated.

---

**INTRODUCTION**

Recent years have witnessed growing interest in hybrid systems, e.g. dynamical systems which combine continuous dynamics and switching between several different discrete states. Well known formal models of such systems include switched systems [1], hybrid automata [2], etc. In many practical applications exact circumstances or moments of switching in these systems are unknown and therefore at any moment of time, active set of laws which govern continuous dynamics ("structure" of the system) can not be determined. In such cases it is reasonable to model switching as a random or likewise "uncertain" process. One promising approach of this kind is the use of systems with random structure [3], in which switching is modeled as (continuous time) jump Markov process. However stochastic models are difficult to apply in cases when statistical information about switching process is absent, because the distribution of a random process can not be estimated. In this situation models based on non-probabilistic uncertainty theories can be more adequate.

One promising theory of such kind is the possibility theory [4, 5, 6, 7], which allows one to estimate a level of credibility of some event with respect to other events. In this theory each event is characterized by two numeric values – levels of possibility and necessity. Furthermore only relative comparison of levels (more, less, equal) is meaningful. For chosen basic events these levels are usually determined on the basis of expert opinions (instead of statistics). For non-basic events levels can be determined with a help of possibility and necessity composition rules, or more generally, possibility and necessity measure extension theorems [5, 8, 9].

In this paper we present a formal model – a system with fuzzy structure (note that the term *fuzzy* is used in this paper in sense of possibility theory rather than L. Zadeh fuzzy set theory), analogous to systems with random structure, but constructed on the basis of possibility theory. Despite its formal similarity to stochastic models, its properties and associated methods of investigation are quite different. But there is a reason to believe that it can be useful in the case of absence of statistical information. Systems with fuzzy structure require introduction of special notions of stability. We will define a notion of stability with given necessity level and provide sufficient conditions for stability of trivial equilibrium point of systems with fuzzy structure.

The paper is organized as follows: in section 1 we give necessary preliminaries on fuzzy Markov processes and possibility theory, in section 2 we introduce systems with fuzzy structure, in section 3 we introduce the notion of stability with given necessity level and investigate stability of trivial equilibrium points of systems with fuzzy structure with a help of a variant of Lyapunov comparison principle [10].

**1. FUZZY MARKOV PROCESSES**

Much like in probability theory, in possibility theory uncertain quantities (possibilistic variables) are formalized as (measurable) functions defined on a space of (atomic) events. But instead of probability measure, possibility and necessity measures are used. Fuzzy processes can be viewed as

---

<sup>1</sup> Corresponding author. Email [ivanov.eugen@gmail.com](mailto:ivanov.eugen@gmail.com)

time-varying possibilistic variables. A notion of independence of possibilistic variables [4, 6] allows to define class fuzzy Markov processes [11] analogously to the class of stochastic Markov processes.

Let  $X$  be a space of atomic events. Let  $P:2^X \rightarrow [0,1]$  be a possibility measure, i.e.  $P(\bigcup_k A_k) = \sup_k P(A_k)$  for any family  $\{A_k\}_k$  of subsets of  $X$  (non-atomic events), and  $N:2^X \rightarrow [0,1]$  be a necessity measure, i.e.  $N(\bigcap_k A_k) = \inf_k N(A_k)$  for any family  $\{A_k\}_k$ . Note that assumption of totality of measures is not restrictive because possibility measure extension theorem [5, 9] guarantees that possibility (and necessity) measure on algebra of sets can be extended to power set. We assume that measures are normed and coherent, i.e. equalities  $N(A) = 1 - P(\neg A)$  for all  $A \subseteq X$  (here  $\neg A$  denotes complement of a set),  $P(X) = 1$  and  $N(X) = 1$  hold.

Now we briefly recall some notions of possibility theory. Denote by  $X_0$  the set of atomic events of non-zero possibility,  $T$  – the timeline  $[0, +\infty)$ ,  $Y$  – a set. For total of measures, possibilistic variable is an arbitrary partial function  $X \rightarrow Y$ , defined on a superset of  $X_0$ . Similarly, a (continuous-time) fuzzy process in possibility theory is a partial function  $T \times X \rightarrow Y$ , defined on a superset of  $T \times X_0$ .

A (possibility) distribution of possibilistic variable  $\xi: X \rightarrow Y$  is a mapping  $y \mapsto P\{x \in X_0 \mid \xi(x) = y\}$ . A distribution of a fuzzy process  $p: T \times X \rightarrow Y$  is a functional  $F_p: 2^{T \times Y} \rightarrow L$ , defined by equality  $F_p(q) = P\{x \in X \mid \forall t p(t, x) = q(t)\}$ , where  $q: T \rightarrow Y$ , i.e.  $F_p$  gives a possibility of  $q$  to be a trajectory of  $p$ . An  $\alpha$ -trajectory of  $p$  (where  $\alpha \in [0,1)$ ) is a mapping  $q: T \rightarrow Y$ , such that  $F_p(q) > \alpha$ , i.e.  $q$  is a trajectory of  $p$  with possibility greater then  $\alpha$ .

Like in theory of stochastic processes, an important role in fuzzy processes play fuzzy Markov processes. Let  $q_1, q_2$  be trajectories of a fuzzy process  $p$ , which intersect at some moment  $t^* \in T$ , i.e.  $q_1(t^*) = q_2(t^*)$ . Then cross trajectories of  $q_1$  and  $q_2$  at  $t^*$  are defined as functions  $\bar{q}_1, \bar{q}_2$ , such that  $\bar{q}_1(t) = q_1(t)$  if  $t \leq t^*$ ,  $\bar{q}_1(t) = q_2(t)$  if  $t \geq t^*$  and  $\bar{q}_2(t) = q_2(t)$  if  $t \leq t^*$ ,  $\bar{q}_2(t) = q_1(t)$  if  $t \geq t^*$ . Informally,  $\bar{q}_1$  and  $\bar{q}_2$  are obtained by gluing together parts of  $q_1$  and  $q_2$  before and after  $t^*$ .

Definition 1.1 [11]. A fuzzy process  $p$  has Markov property if for every  $\alpha$ -trajectories  $q_1, q_2$  of  $p$ , such that  $q_1(t^*) = q_2(t^*)$  for some  $t^*$ , cross trajectories of  $q_1$  and  $q_2$  at  $t^*$  are itself  $\alpha$ -trajectories of  $p$ .

This definition can be viewed as a formalization of a property of independence of future and past in the case of fixed present.

In this paper we consider fuzzy Markov processes with piecewise-constant trajectories.

Definition 1.2 [11]. A fuzzy Markov process  $p$  is called a fuzzy jump Markov process if for each trajectory  $q$  of  $p$  (which have non-zero possibility) the following conditions are satisfied:

- 1)  $q$  is piecewise constant and right-continuous;
- 2)  $P\{x \mid \forall t p(t, x) = q(t)\} = \lim_{t^* \rightarrow +\infty} P\{x \mid \forall t \leq t^* p(t, x) = q(t)\}$  (continuity of possibility).

Distribution of a fuzzy jump Markov process  $p: T \times X \rightarrow I$  (where  $I$  is a state space) is uniquely determined by its transition (possibility) distribution – an indexed family  $(\varphi_{i,j})_{i,j \in I}$  of functions, defined as  $\varphi_{i,j}(t) = P\{x \mid p(t, x) = i, \lim_{\tau \rightarrow t+} p(\tau, x) = j\}$ ,  $t \in T$ , i.e.  $\varphi_{i,j}(t)$  is a possibility of transition from  $i$  to  $j$  at moment  $t$ . The following lemma allows to compute distribution of  $p$ :

Lemma 1.1 [11].  $F_p(q) = P\{x \mid \forall t p(t, x) = q(t)\} = \inf_{t \in T} \varphi_{q(t), q(t+)}(t)$  for every piecewise constant right-continuous function  $q: T \rightarrow Y$  (where  $q(t+)$  denotes right limit).

Not every family of functions  $(\varphi_{i,j})_{i,j \in I}$  can be a transition distribution of some fuzzy jump Markov process. Unlike situation in probability theory, conditions for a family of functions to be a transition possibility distribution are not simple.

Lemma 1.2 [11]. A family  $(\varphi_{i,j})_{i,j \in I}$  is a transition distribution of some fuzzy jump Markov process if and only if the following conditions are satisfied:

- 1)  $\sup_{i,j \in I} \varphi_{i,j}(t) = 1$  for all  $t \in T$ ;

2)  $\varphi_{i,j}(t_0) = \sup \left\{ \inf_{t \in T} \varphi_{q(t), q(t+)}(t) \mid \text{a function } q: T \rightarrow I \text{ is piecewise constant, right-continuous and } q(t_0) = i, q(t_0+) = j \right\}$ , for all  $i, j \in I, t_0 \in T$ .

It is hard to expect that transitions possibility levels derived from expert opinions will satisfy the second condition of this lemma. It is better to derive upper bounds for possibility levels of transitions (or alternatively, lower bounds for necessity levels) from expert opinions, and then find a transition distribution which (optimally) fits these bounds.

Formally, a family of functions  $(\psi_{i,j})_{i,j \in I}$  (where  $\psi_{i,j}: T \rightarrow [0,1]$ ) is called an upper transition distribution, if there exists a transition distribution  $(\varphi_{i,j})_{i,j \in I}$ , such that  $\varphi_{i,j}(t) \leq \psi_{i,j}(t)$  for all  $i, j \in I, t \in T$ . A transition distribution, (optimally) generated by upper transition distribution  $(\psi_{i,j})_{i,j \in I}$  is defined as a transition distribution  $(\varphi_{i,j})_{i,j \in I}$ , such  $\varphi_{i,j}(t) \leq \psi_{i,j}(t), i, j \in I, t \in T$  and  $\varphi'_{i,j}(t) \leq \varphi_{i,j}(t), i, j \in I, t \in T$  for each transition distribution  $(\varphi'_{i,j})_{i,j \in I}$ , such that  $\varphi'_{i,j}(t) \leq \psi_{i,j}(t), i, j \in I, t \in T$ . Existence of generated distributions is guaranteed by the following lemma.

Lemma 1.3. Each upper transition distribution generates (unique) transition distribution.

Still not every family of functions  $(\psi_{i,j})_{i,j \in I}$  is an upper transition distribution. However it is expected that expert opinions can be used to form upper transition distribution [11].

Lemma 1.4. A family  $(\varphi_{i,j})_{i,j \in I}$  is an upper transition distribution if and only if  $\sup \left\{ \inf_{t \in T} \varphi_{q(t), q(t+)}(t) \mid q: T \rightarrow I \text{ is piecewise constant and right-continuous} \right\} = 1$ .

In this paper we do not consider problems of checking of condition of lemma 1.4 and finding generated transition distribution. We only note that for certain classes of functions  $(\psi_{i,j})_{i,j \in I}$ , generated upper transition distribution can be effectively computed by iterative numerical methods. The following definition describes one important example of such class.

Definition 1.3. A transition distribution  $(\varphi_{i,j})_{i,j \in I}$  is called piecewise-monotone if for every  $t_0 \in T$  there exists a relatively open (in  $T$ ) neighborhood  $O(t_0)$  of  $t_0$ , such that every function  $\varphi_{i,j}, i, j \in I$  is monotone on sets  $O \cap [0, t_0)$  and  $O \cap (t_0, +\infty)$  (if they are non-empty).

Note that the character of monotonicity (increasing or decreasing) of functions on these sets can be different for the same or different  $i, j \in I$ .

## 2. SYSTEMS WITH FUZZY STRUCTURE

Let  $I$  be a non-empty finite set of states,  $T = [0, +\infty)$ ,  $p: T \times X \rightarrow I$  – a fuzzy jump Markov process,  $f_i: T \times \mathbf{R}^d \rightarrow \mathbf{R}^d, i \in I$  – a family of functions.

Definition 2.1. A system with fuzzy structure (SFS) is an equation of the form

$$\dot{y}(t, x) = f_{p(t,x)}(t, y(t, x)) \quad (1)$$

Definition 2.2. A fuzzy process  $y: T \times X \rightarrow \mathbf{R}^d$  is called a solution of SFS (1) if for any (fixed)  $x \in X_0$ , a trajectory  $t \mapsto y(t, x)$  satisfies equation in sense of Caratheodory (i.e. is absolutely continuous on every compact segment in  $T$  and satisfies (1) almost everywhere with respect to Lebegue measure).

Definition 2.3. Let  $\alpha \in [0,1]$ . A total function  $\bar{y}: T \rightarrow \mathbf{R}^d$  is called a (complete)  $\alpha$ -trajectory of SFS (1) if  $\bar{y}$  is an  $\alpha$ -trajectory of some solution of (1).

Consider initial condition

$$y(0, x) = y_0 \text{ for every } x \in X_0 \quad (2)$$

We say that a problem (1), (2) has unique solution (up to trajectories of possibility zero) if every two solutions of (1) satisfying (2) coincide on  $T \times X_0$ .

The following theorem is an adaptation of Caratheodory existence theorem to SFS.

Theorem 2.1 [11]. Suppose that the following conditions are satisfied:

1) for each  $i \in I$  and  $t \in T$ , a function  $y \mapsto f_i(t, y)$  is defined and continuous on  $\mathbf{R}^d$ , and for each  $y \in \mathbf{R}^d$ , a function  $t \mapsto f_i(t, y)$  is measurable;  $t \in T$

2) for every  $i \in I$  there exists a function  $h_i : T \rightarrow \mathbf{R}_+$ , bounded on every bounded segment in  $\mathbf{R}$ , such that  $\|f_i(t, y)\| \leq h_i(t)(1 + \|y\|)$  for all  $t \in T$ ,  $y \in \mathbf{R}^d$  (here  $\mathbf{R}_+ = [0, +\infty)$ ,  $\|\cdot\|$  denotes Euclidean norm);

3) for every  $i \in I$  there exists a function  $L_i : T \rightarrow \mathbf{R}_+$  (Lipschitz constant), bounded on every bounded segment in  $\mathbf{R}$ , such that  $\|f_i(t, y_1) - f_i(t, y_2)\| \leq L_i(t)\|y_1 - y_2\|$  for all  $y_1, y_2 \in \mathbf{R}^d$ .

Then for every  $y_0 \in \mathbf{R}^d$  the problem (1), (2) has a unique solution.

Denote by  $(\varphi_{i,j})_{i,j \in I}$  a transition distribution of the process  $p$ . The following theorem is a consequence of the lemma 1.1.

**Theorem 2.2.** Suppose that conditions of the theorem 2.1 are satisfied. Then a function  $\bar{y} : T \rightarrow \mathbf{R}^d$  is an  $\alpha$ -trajectory of (1) if and only if there exists a piecewise constant and right-continuous function  $q : T \rightarrow I$  such that  $\inf_{t \in T} \varphi_{q(t), q(t+)}(t) > \alpha$ , and  $\bar{y}$  satisfies equation  $\dot{y}(t) = f_{q(t)}(t, y(t))$  on  $T$  in sense of Caratheodory.

### 3. STABILITY OF EQUILIBRIUM POINTS OF SYSTEMS WITH FUZZY STRUCTURE

In this section we assume that conditions of theorem 2.1 are satisfied and hence the problem (1), (2) has unique solution for every initial value. Also we assume that transition distribution of fuzzy jump Markov process  $p$  in piecewise-monotone.

Denote by  $\mathbf{0}$  a fuzzy process  $T \times X \rightarrow \mathbf{R}^d$  which is identically equal to null vector. We say that SFS (1) has trivial equilibrium point if  $\mathbf{0}$  is a solution of (1).

Suppose that (1) has trivial equilibrium point.

**Definition 3.1.** Let  $\alpha \in [0, 1)$ . Trivial equilibrium point of SFS (1) is called stable with necessity  $1 - \alpha$  if there exist an open neighborhood of the origin  $O \subseteq \mathbf{R}^d$  and a function  $h : \mathbf{R}_+ \rightarrow \mathbf{R}_+$  of class  $K$  (i.e. continuous, strictly increasing and  $h(0) = 0$ ) such that

$$N\{x \mid \|y(t, x; y_0)\| \leq h(\|y_0\|) \text{ for all } y_0 \in O \text{ and } t \in T\} > 1 - \alpha.$$

This definition means that  $\|y(t, x; y_0)\| \leq h(\|y_0\|)$  holds for all atomic events  $x$  which have possibility greater then  $\alpha$ . Note that the property of stability with given necessity level is possibilistic, i.e. it depends on distribution of the process  $p$ .

Let us introduce the following notation:  $y(t, x; y_0)$  is a value of trajectory of solution of (1) which satisfies  $y(0, x) = y_0$  for all  $x \in X_0$ . It follows from conditions of theorem 2.1 and Caratheodory existence theorem that initial value problem  $\dot{y}(t) = f_i(t, y(t))$ ,  $y(t_0) = y_0$  has a unique solution on  $[t_0, +\infty)$  for every  $t_0, y_0$ . Denote by  $y_i(t; t_0; y_0)$  a value of this solution at time moment  $t$ .

Now we are going to investigate stability with necessity  $1 - \alpha$  of trivial equilibrium point of SFS. The first step is to characterize points reachable by  $\alpha$ -trajectories of SFS (1).

For any set  $Y_0 \subseteq \mathbf{R}^d$  and  $\bar{t} \in T$  let us define a closure of  $\alpha$ -reach set:

$cReach^\alpha(Y_0, \bar{t}) = cl(\{\bar{y}(\bar{t}) \mid \bar{y} : T \rightarrow \mathbf{R}^d \text{ is an } \alpha\text{-trajectory of SFS (1) and } y(0) \in Y_0\})$ , where  $cl(\cdot)$  denotes closure of a subset of  $\mathbf{R}^d$ , i.e.  $cReach^\alpha(Y_0, \bar{t})$  is a closure of the set of points reachable by  $\alpha$ -trajectories of SFS (1) from  $Y_0$  at moment of time  $\bar{t}$ .

We will use the following lemma to describe  $cReach^\alpha(Y_0, \bar{t})$ :

**Lemma 3.1.** Let  $I$  be a finite set,  $(\varphi_{i,j})_{i,j \in I}$  be a piecewise-monotone transition distribution and  $\alpha \in [0, 1)$ . Then there exists a sequence of moments of time  $\tau_0, \tau_1, \tau_2, \dots \in T$  such that for every  $k = 0, 1, 2, \dots$  and  $i, j \in I$  a function  $\varphi_{i,j}$  is monotonous on  $(\tau_k, \tau_{k+1})$  and either  $\varphi_{i,j}(t) > \alpha$  for all  $t \in (\tau_k, \tau_{k+1})$  or  $\varphi_{i,j}(t) \leq \alpha$  for all  $t \in (\tau_k, \tau_{k+1})$ .

In this paper we do not discuss computation of the sequence  $\tau_0, \tau_1, \tau_2, \dots$  from given transition distribution. However we note that if functions  $\varphi_{i,j}$  are defined symbolically by suitable lattice terms, then a general expression for members of sequence  $\tau_0, \tau_1, \tau_2, \dots$  can also be computed symbolically.

Suppose that  $\alpha \in [0, 1)$  is fixed and a sequence  $\tau_0, \tau_1, \tau_2, \dots$  described in lemma 3.1 is given. For all  $i, j \in I$  and  $t_0, t_1 \in T$ , such that  $t_0 < t_1$ , denote:

$LS_{i,j}^\alpha(t_0, t_1) = \{i_1 i_2 \dots i_n \in I^+ \mid n \geq 1, \varphi_{i_1}^\alpha(t_0) > \alpha, \varphi_{i_n}^\alpha(t_1^-) > \alpha, i_n = j, (i_l, i_{l+1}) \in H^\alpha(t_0, t_1) \text{ for all } l = \overline{1, n-1}\}$ , where  $H^\alpha(t_0, t_1) = \{(i, j) \in I^2 \mid \forall t \in (t_0, t_1) \varphi_{i,j}^\alpha(t) > \alpha\}$ .

Note that  $LS_{i,j}^\alpha(t_0, t_1)$  is a regular language in alphabet  $I$ .

For any formal language  $L \subseteq \mathbf{R}^d$ , moments  $t_0 < t_1$  and set  $Y_0 \subseteq \mathbf{R}^d$  let us define:  $reach(L, t_0, Y_0, t_1) = \{\bar{y}(t_1) \mid \bar{y}: [t_0, t_1] \rightarrow \mathbf{R}^d \text{ is a function such that } \bar{y}(t_0) \in Y_0 \text{ and there exists a piecewise-constant function } q: [t_0, t_1] \rightarrow I \text{ and time moments } \bar{t}_0, \dots, \bar{t}_n \in T \text{ such that } t_0 = \tau_0 < \tau_1 < \dots < \tau_{n-1} < \tau_n = t_1, q(t) = i_{k+1} \text{ for all } t \in (\tau_k, \tau_{k+1}), k = \overline{0, n-1}, \text{ and } \bar{y} \text{ satisfies equation } \dot{y}(t) = f_{q(t)}(t, y(t)) \text{ in sense of Caratheodory}\}$ , i.e. a set of points reachable from  $Y_0$  by means of switching sequences described by words in  $L$ .

Also let us define an indexed family of sets:

$$Y_{i,j}^0 = Y_0 \text{ if } i = j, \text{ and } Y_{i,j}^0 = \emptyset \text{ if } i \neq j;$$

$$Y_{i,j}^k = \bigcup_{l \in I} reach(LS_{l,j}^\alpha(\tau_{k-1}, \tau_k), \tau_{k-1}, Y_{i,l}^{k-1}, \tau_k), \text{ } i, j \in I, k \geq 1.$$

The following theorem describes  $cReach^*$ .

Theorem 3.1. Let  $\bar{t} \in [\tau_n, \tau_{n+1})$  for some  $n$ . Denote  $J_0(\bar{t}) = \{j \in I \mid \max_{j \in I} \varphi_{j,j}^\alpha(\bar{t}) > \alpha\}$ .

1) If  $\bar{t} = \tau_n$ , then  $cReach^\alpha(Y_0, \bar{t}) = \bigcup_{i \in I, j \in J_0(\bar{t})} cl(Y_{i,j}^n)$ ;

2) If  $\bar{t} \in (\tau_n, \tau_{n+1})$ , then  $cReach^\alpha(Y_0, \bar{t}) = \bigcup_{i, l \in I, j \in J_0(\bar{t})} cl(reach(LS_{l,j}^\alpha(\tau_n, \bar{t}), \tau_n, Y_{i,l}^n, \bar{t}))$ .

This theorem characterized reachable points of phase space. But we also need to characterize reachable (discrete) states.

To compute reachable states let us denote  $next_k(I_0) = \{j \in I \mid LS_{i,j}^\alpha(\tau_k, \tau_{k+1}) \neq \emptyset\}$  for any  $I_0 \subseteq I$ ,  $k \geq 0$  and build the following sequence of state sets:  $I_0 = J_0(0)$  and  $I_{k+1} = next_k(I_k)$ ,  $k \geq 0$ . Note that this sequence becomes periodic after some  $k$  due to finiteness of  $I$ . Then the sequence of sets states reachable at some time moment in  $[\tau_k, \tau_{k+1})$  can be computed as follows:

$$I_k^\alpha = \{i \in I \mid w_1 w_2 \in LS_{i',j'}^\alpha(\tau_k, \tau_{k+1}), i' \in I_k, j' \in I_{k+1}, w_1 \in I^*, w_2 \in I^+\}, k \geq 0.$$

Now we can formulate a theorem which gives sufficient condition for stability of SFS.

Let  $O \subseteq \mathbf{R}^d$  be some open neighborhood of the origin and  $V: \mathbf{R}^d \rightarrow \mathbf{R}_+$  be a continuously differentiable positive-definite (Lyapunov-like) function. Let  $g_k: \mathbf{R}_+ \times \mathbf{R} \rightarrow \mathbf{R}$ ,  $k \geq 0$  be a sequence of functions such that  $\max_{i \in I_k} \frac{dV(y)}{dy} f_i(t, y) \leq g_k(t, V(y))$  for all  $t \in T$ ,  $y \in \mathbf{R}^d$ ,  $k \geq 0$  and initial value problem  $\dot{z}(t) = g_k(t, z(t))$ ,  $z(t_0) = z_0$  has unique solution in sense of Caratheodory on  $[t_0, +\infty)$  for all  $t_0 \in T$ ,  $z_0 \in \mathbf{R}_+$ ,  $k \geq 0$ . Denote by  $z_k(t; t_0; z_0)$  the value of this solution at moment  $t$ .

Theorem 3.2. Let  $\alpha \in [0, 1)$ . Suppose that there exists an indexed family of monotonically non-decreasing functions  $r_k^\alpha: \mathbf{R}_+ \rightarrow \mathbf{R}_+$ ,  $k \geq 0$  such that  $r_k^\alpha(0) = 0$  for all  $k \geq 0$ ,  $\max_{t \in [\tau_k, \tau_{k+1})} z_k(t; \tau_k; v) \leq r_k^\alpha(v)$  for all  $v \in \mathbf{R}_+$ , and 0 is a Lyapunov-stable equilibrium point of recurrence relation  $v_{k+1} = r_k^\alpha(v_k)$ ,  $k \geq 0$ . Then the trivial equilibrium point of SFS (1) is stable with necessity  $1 - \alpha$ .

Proof. From conditions of the theorem it follows that there exists  $\varepsilon > 0$  and a function  $h: \mathbf{R}_+ \rightarrow \mathbf{R}_+$  of class K such that  $v_k \leq h(v_0)$  for all  $k \geq 0$  if  $v_0 \in [0, \varepsilon)$ . The function  $V$  is positive definite and continuous, therefore there exists an open neighborhood of the origin  $O_1 \subseteq \mathbf{R}^d$ , and a function  $h_1: \mathbf{R}_+ \rightarrow \mathbf{R}_+$  of class K such that  $\|y\| \leq h_1(\|y_0\|)$  if  $y_0 \in O_1$  and  $V(y) \leq h(V(y_0))$  (we can define  $h_1$  to be a function of class K such that  $h_1(v) \geq \max\{\|y\| \mid y \text{ belongs to a connected component of the set } \{y \in O_1 \mid V(y) \leq h(\max_{\|y_0\| \leq v} V(y_0))\}\}$ , which contains null vector).

Let  $\bar{y}: T \rightarrow \mathbf{R}^d$  be some  $\alpha$ -trajectory of SFS (1). Then there exists an  $\alpha$ -trajectory  $q: T \rightarrow \mathbf{R}^d$  of the process  $p$  such that  $\bar{y}$  satisfies equation  $\dot{y}(t) = f_{q(t)}(t, y(t))$  in sense of Caratheodory. For any  $k \geq 0$  an inclusion  $\{q(t) \mid t \in [\tau_k, \tau_{k+1})\} \subseteq I_k^\alpha$  holds. Therefore

$\frac{dV(\bar{y}(t))}{dy} f_{q(t)}(t, \bar{y}(t)) \leq g_k(t, V(\bar{y}(t)))$  for all  $t \in [\tau_k, \tau_{k+1})$ . The function  $V$  is continuously differentiable and  $\bar{y}$  is absolutely continuous on every bounded segment. From this it follows that that the function  $t \mapsto V(\bar{y}(t))$  is also absolutely continuous on every bounded segment. Also the function  $t \mapsto V(\bar{y}(t))$  satisfies  $\frac{dV(\bar{y}(t))}{dt} = \frac{dV(\bar{y}(t))}{dy} f_{q(t)}(t, \bar{y}(t))$  almost everywhere. From the comparison theorem [12] for Caratheodory differential inequality  $\frac{dV(\bar{y}(t))}{dt} \leq g_k(t, V(\bar{y}(t)))$  and differential equation  $\dot{z}(t) = g_k(t, z(t))$  we conclude that  $V(\bar{y}(t)) \leq z_k(t; \tau_k; V(\bar{y}(\tau_k))) \leq r_k^\alpha(V(\bar{y}(\tau_k)))$  for all  $k \geq 0$  and  $t \in [\tau_k, \tau_{k+1}]$ . In particular case an inequality  $V(\bar{y}(\tau_{k+1})) \leq r_k^\alpha(V(\bar{y}(\tau_k)))$  holds. Suppose that  $v_0 = V(\bar{y}(\tau_0)) = V(\bar{y}(0)) < \varepsilon$ . Then from monotonicity of  $r_k^\alpha$  we conclude that  $V(\bar{y}(\tau_k)) \leq v_k \leq h(v_0) = h(V(\bar{y}(0)))$  for all  $k \geq 0$ , and therefore  $V(\bar{y}(t)) \leq h(V(\bar{y}(0)))$  for all  $t \in T$ . Hence  $\|\bar{y}(t)\| \leq h_1(\|\bar{y}(0)\|)$  if  $\bar{y}(0) \in O_1$ . Note that  $O_1$  and  $h_1$  does not depend on chosen  $\alpha$ -trajectory  $\bar{y}$ . Therefore trivial equilibrium point of SFS (1) is stable with necessity  $1 - \alpha$ . Theorem is proved.

This theorem reduces the problem of determining stability of trivial equilibrium point of SFS to a known problem of determining Lyapunov stability of equilibrium point of a recurrence relation.

## CONCLUSIONS

On the basis of possibility theory we have constructed a class of continuous-discrete dynamical systems with switching at uncertain moments of time – a class of systems with fuzzy structure. We have introduced a notion of stability with given necessity level and have studied stability properties of systems with fuzzy structure. Obtained results can be useful for modeling of dynamical systems with uncertainty in cases when application of probabilistic models is hard or impossible due to lack of statistical information.

## REFERENCES

- [1] Liberzon D. *Switching in systems and control*, Birkhauser, Boston, 2003.
- [2] Henzinger T.A. The theory of hybrid automata *Proceedings of the 11th Annual Symposium on Logic in Computer Science*, pp. 278-292, 1996.
- [3] Kats I.Y., Martynyuk A.A. *Stability and stabilization of nonlinear systems with random structure*, Taylor and Francis, London, 2002.
- [4] Pyt'ev Yu.P. *Possibility as an alternative of probability*, Fizmatlit, Moscow, 2007.
- [5] Cooman G. Possibility theory I: the measure- and integral-theoretic groundwork *Int. J. of General Systems*, Vol. 25, pp. 291-323, 1997.
- [6] Belov Yu.A., Bychkov O.S., Merkurjev M.G., Chulichkov A.I. About an approach to modeling of fuzzy dynamics *Reports of the National Academy of Sciences of Ukraine*, Vol. 10, pp. 14-19, 2006 (in Ukrainian).
- [7] Zadeh L.A. Fuzzy sets as a basis for a theory of possibility *Fuzzy Sets and Systems*, Vol. 1, pp. 3-28, 1978.
- [8] Bychkov A.S., Ivanov Ie.V. On convergence of sequences of fuzzy perceptive elements defined on different possibility spaces *Cybernetics and systems analysis*, Vol. 2, pp.142-151, 2010 (in Russian).
- [9] Bychkov O.S., Ivanov Ie.V. Existence of coherent k-additive extension of measures in possibility theory *Control systems and computers*, Vol. 6, pp. 35-41, 2009 (in Ukrainian).
- [10] Matrosov V. M.; Malikov A. I. The development of the ideas of A. M. Lyapunov over one hundred years: 1892-1992. *Izv. Vyssh. Uchebn. Zaved. Mat.*, Vol. 4, pp. 3-47, 1993 (in Russian).
- [11] Ivanov Ie.V. Modeling of systems of fuzzy structure *Proceedings of the International Scientific Conference "Simulation-2010"*, Kyiv, pp. 78-85, 2010 (in Russian).
- [12] Lakshmikantham V., Leela S. *Differential and integral inequalities*, Vol. 1, Academic Press, New York, 1969.

## MODEL BASED IDENTIFICATION OF ACTIVE BEAM COMPOSITE STRUCTURE - APPLICATION MRAS ALGORITHM

**Wojciech Jarzyna<sup>1</sup>**  
**Michał Augustyniak**  
**Jerzy Warmiński**  
**Marcin Bocheński**  
Lublin University of  
Technology  
Lublin, Poland

---

### ABSTRACT

---

Parameter identification of the electromechanical system allows to match the knowledge about the state of the system and its properties. Execution of identification procedure during normal operation of the system without its stopping is a major problem of the carried out investigation. Implementation of such research requires measurement instrumentation saving transient data and processing them. Such system is expensive therefore some of measurement equipment we replace by software Model Based Identification methods. In the presented paper we characterize the possibility of applying these methods to identify active composite beam with embedded piezoelectric structure. Simulation results we present for Model Reference Adaptive System (MRAS). Applied adaptive algorithms satisfy Lyapunov stability. The selection of these algorithms take into account the condition of a short execution time compared to other methods. This condition is particularly important in future implementation in systems based on microprocessor Digital Signal Processor architecture (DSP).

---

### THE AIM OF THE PARAMETER IDENTIFICATION OF ACTIVE COMPOSITE BEAM WITH EMBEDDED PIEZOELECTRIC STRUCTURE

Active composite structures are materials, whose internal design is the result of research actuators of high performance, lightweight, direct control and high-speed response. These are mainly: piezoelectric composites, nanoconductive particles, shape memory alloys and magneto-rheological elastomers structures [4]. Composite technology is getting popular in advanced constructions, especially in space and aircraft systems, biomedical actuators as well as high precision and responsible for safety reason systems. Special embedded structures practically do not influence on mechanical, thermal and geometrical properties and above all do not alter fundamental functionalities. Moreover, due to possibilities of electric, magnetic or thermal control, they may satisfy active functions of actuators or measuring segments, improving dynamic and static characteristics.

Planned application in aviation of the tested composite actuators impose specific requirements on these structures. Their application in skin plates of aerodynamic aircraft components demands of flat design, large deformation and work in closed loop system control. These requirements meet piezoelectric systems.

Unfortunately, piezoelectric composites are nonlinear systems. As confirmed in laboratory tests, piezoelectric elements are have unstable of parameters [6]. The internal parameters as e.g. resistance and capacity of the studied actuators varied depending on the level of voltage and frequency of power supply. These changes also concern mechanical parameters as e.g. stiffness and damping coefficients. Composite with embedded piezoelectric MFC structure changes their stiffness parameter determining the own frequency of the tested beam. Moreover, operation with significant deformations, may cause shift of the own frequency and nonlinear component in the motion equation (3).

---

<sup>1</sup> Corresponding author. Email [w.jarzyna@pollub.pl](mailto:w.jarzyna@pollub.pl)

For these reasons application linear PID controllers or dumping filters to stabilize the work with predetermined stable parameters, however, has limited application. Due to the mentioned parameter changes of the mathematical model, nominal settings of filters and regulators give poor results, and sometimes even cause the generation of unexpected oscillations. For this reason, current identification of relevant parameters of the model or the use adaptive or nonlinear controllers are required.

Determination of parameters of the models typically are carried out during the specialized laboratory tests, when the bench can be equipped with a large number of measuring equipment. During normal operation of a craft, the possibility of measurements in transient states are usually very limited, and obtained measured data are insufficient to identify an object in real time. Therefore, implementation of real time identification methods, usually require application of Model Based Identification methods. These methods include mainly observer models, self-tuning systems and Model Reference Adaptive Systems.

## 1. OVERVIEW OF MODEL BASED IDENTIFICATION METHODS

Application of mathematical modeling to solve problems of nonlinear identification and control allows to limit the number of sensors. General scheme of parameter determination is based on a comparison of the measured variable with calculated variable, or comparison of two calculated variables provided, that they have been appointed on the basis of two different sets of equations [4]. Then, the result of his comparison is the input to certain adaptation block. This principle is presented in Fig.1.

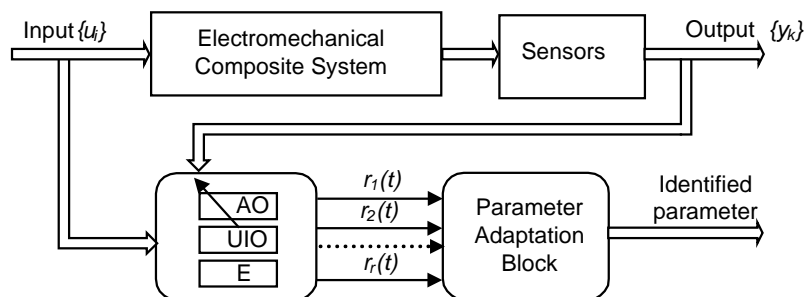


Fig.1 The overall structure of identification system, were: AO - is adaptive observer, UIO – unknown input observer, E – estimator or simulator of unknown input

Of the above methods, good results can be obtained using a computational observer structure introducing the unknown parameters  $\Delta A$  to the mathematical description of the state equation system (1), Fig.2.

$$\begin{cases} \dot{\mathbf{x}} = \mathbf{Ax} + \mathbf{Bu} + \Delta\mathbf{Ax} \\ \mathbf{y} = \mathbf{Cx} \end{cases} \quad (1)$$

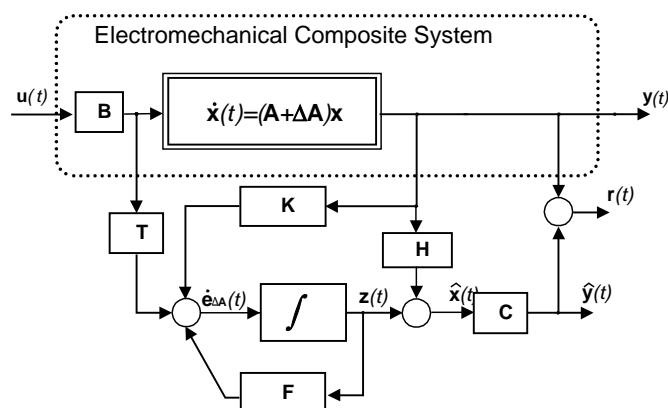


Fig.2 Electromechanical system with Decoupling Observer, where  $\mathbf{F}$  – state observer matrix,  $\mathbf{T}$ ,  $\mathbf{H}$  – transposition matrices of input and output,  $\mathbf{K}$  feedback matrix,  $\mathbf{C}$  – output matrix,  $\mathbf{z}(t)$ ,  $\hat{\mathbf{x}}(t)$  and  $\hat{\mathbf{y}}(t)$  – estimated variables.

Properly selected transposition matrices of inputs and outputs, together with the state matrix  $\mathbf{F}$  of the observer and feedback matrix  $\mathbf{K}$ , allow to decouple estimated value of  $\hat{\mathbf{y}}(t)$  from the change in the system are identified. This feature makes the UIO convenient tool for determining the unknown

values of  $\Delta\mathbf{A}$  in complex computational structures [5]. The condition, which should meet the observer matrices presents formula (2).

$$\dot{\mathbf{e}}_{\Delta\mathbf{A}}(t) = \mathbf{F} \mathbf{e}_{\Delta\mathbf{A}}(t) + \mathbf{T} \Delta\mathbf{A} \mathbf{x}(t) + (\mathbf{F} \mathbf{H} - \mathbf{K}) \mathbf{y}(t) \quad (2)$$

An alternative solution is application a Self-Tuning Method (STM) or Model Reference Adaptive System (MRAS). Both methods have gained wide application in control systems and identification of parameters. Their main advantage, is simple structure resulting in less time-consuming calculations. Among the several varieties of this method, cited example of flowcharts (Fig.3) is beneficial especially for parameter identification.

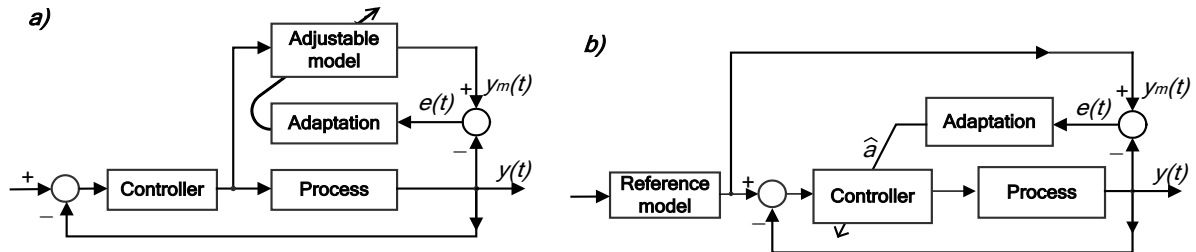


Fig.3 Model Reference Adaptive System. a) with adjustable model for parameter identification, b) with SetPoint generator

In the alternative solutions (Fig.3), MRAS adaptive models are used directly to control adaptation parameters and are rarely used as SetPoint generators with adaptive controllers [1]. In systems designed to identify the parameters, adaptation algorithm adjust parameters of reference model due to the  $e(t)$  output error. Received estimated parameters  $\hat{\mathbf{a}}$  may be applied in diagnostic systems as well as in control systems.

## 2. REFERENCE MODEL AND THE CHOICE OF IDENTIFICATION METHODS

The composite beam with embedded Macro Fiber Composite (MFC) inside its structure has been tested at laboratory stand. During the tests, this actuator was used for vibration damping and positional adjustment.

During operation, especially at large deformations, the mathematical model of the beam must take into account the nonlinear units. A simple one-dimension model, the equation can be represented as formula (3).

$$\ddot{y} + 2\mu\omega\dot{y} + \omega^2 y + \beta y^3 - \delta(y\dot{y}^2 + y^2\ddot{y}) = f \cos(\Omega t) \quad (3)$$

where:  $y$  – beam deflection,  
 $\omega$  – own frequency,  
 $\mu$  – damping coefficient,  
 $\beta, \delta$  – factors determining the intensity of the nonlinearity,  
 $f$  – forcing amplitude,  
 $\Omega$  – frequency of the external force.

The existence of nonlinear units by factors  $\beta$  and  $\delta$ , causes a shift of the natural frequency or the total value of the damping force. These changes have adverse impact on the effectiveness of the work the piezoelectric actuator, causing the upset the control system. Therefore, there is a need for continuous monitoring, especially monitoring of natural frequencies of the beam.

In the considered system assumed, that the strain gauge signal is available. Resistive nature of this sensor can determine the level of strain and rate of change with any significant delay effect. The reference model for system control as well as for parameter adjustment does not take into account  $\beta$  and  $\delta$  factors of non-linear components. These nonlinearities we take account adding new variables  $\Delta\omega$  and  $\Delta\mu$ . These addition update parameters (3a) are trending to the meet with current values. This interpretation allows to obtain higher processing speed, by eliminating time-consuming procedures of multiplication and exponentiation.

$$\begin{bmatrix} \dot{y} \\ \ddot{y} \end{bmatrix} = \begin{bmatrix} 0 & 1 \\ -(\omega + \Delta\omega)^2 & -2(\mu + \Delta\mu) \cdot (\omega + \Delta\omega) \end{bmatrix} \begin{bmatrix} y \\ \dot{y} \end{bmatrix} + \begin{bmatrix} 0 \\ f \cos(\Omega t) \end{bmatrix} \quad (3a)$$

Verifying conditions of the decoupling observer Fig.2, and regarding the changes of parameters  $\Delta\omega$  and  $\Delta\mu$ , it is easy to see that the required matrix transposition  $\mathbf{T}$  (Fig. 2) does not exist [5]. For that reason canceled the identification of parameters with decoupled observers. The attention has been drawn to the identification based on the Model Reference Adaptive Systems (MRAS) shown in Fig. 3.

Real time identification requires the use of high-speed data processing algorithms that can be implemented in a microprocessor system. Considered two methods, first using an algorithm of Model Identification Techniques (MIT) and second adjusting algorithm satisfying Lyapunov stability condition.

The MIT rule has historically been the first adjustment mechanism used in model reference adaptive systems [2]. Its application give good results during adjusting nonlinear system parameters. The main idea is based upon the reduction of the loss function  $J(\theta, t)$  (4).

$$\begin{aligned} J(\theta, t) &= \frac{1}{2} e^2(\theta, t) \\ e(\theta, t) &= y(t) - y_m(\theta, t) \end{aligned} \quad (4)$$

where  $\theta$  determines the differences of model parameters against the reference model and  $e(\theta, t)$  is a difference in real output  $y$  and the reference model  $y_m$ . Identification method is based on the search for extremum of the loss function with respect to variable  $\theta$ , according to formula (5).

$$\dot{\theta} = -\gamma \nabla J(\theta) = -\gamma e(\theta) \nabla e(\theta) \quad (5)$$

where

$$\nabla e(\theta) = \left[ \frac{\partial e}{\partial \theta_1} \quad \frac{\partial e}{\partial \theta_2} \quad \dots \quad \frac{\partial e}{\partial \theta_r} \right]^T$$

Considering that the real model  $y(t)$  does not depend on  $\theta$ , we can rewrite MIT rule in the following form

$$\dot{\theta} = -\gamma e(\theta) \nabla y_m(\theta) \quad (6)$$

An alternative method of adaptation is the choice of the controller according to the Lyapunov criterion, searching for asymptotic stability conditions [2]. The used formula defining the criterion is created by equations (7, 8)

$$V(x) = \int_0^e u(y) dy + \frac{e^2}{2} \quad (7)$$

where  $V(y)$  is interpreted as a Lyapunov function of the energy, corresponding output of the test. This function should be positively determined, and its derivative with respect to time should be less than zero.

$$\dot{V}(e) = \frac{\partial V}{\partial t} + \frac{\partial V}{\partial e} \dot{e} \leq 0 \quad \text{and} \quad \dot{e} = f(y, t, u) \quad (8)$$

Using the set of rules, derived the stability of adaptive MRAS system. Comparing the number of necessary operations, for further study data processing satisfying the Lyapunov condition has been selected, as more faster method in microprocessor DSP system. Chosen method should ensure compliance with stringent requirements in time.

### 3. SIMULATION AND LABORATORY TESTS

Simulation studies were conducted as pre-testing phase of research to prepare and verify numerical procedures for DSP laboratory stand. Therefore, one of the selection criteria was obtaining a high-speed processing. For this reason, a reference model has been written in the form of linear second order differential equation. Actual model, which was the equivalent of the process presented in Fig.3, was written in the form of nonlinear differential equations (3).

The aim of the executed tests was to examine the level to which it is possible to determine the change in frequency of the working beam.

Among the many results, as the representative to submit in the article, selected cases where the own frequency of the reference model differs significantly from the frequency of real process model (Fig.4) and when this difference is small (Fig.5). In addition, studies were carried out for different degrees of non-linearity of the process, when the coefficients  $\delta$  and  $\beta$  in equation (3) are close to zero (Fig.4 a, b) or are equal to unity (Fig.4 c, d and Fig.5)

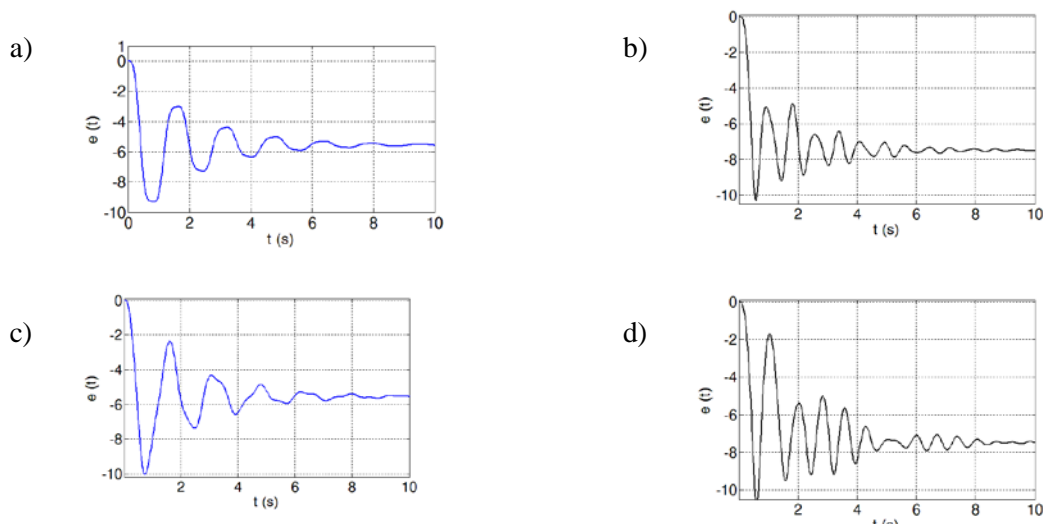


Fig. 4 The errors  $e(t)$  were obtained for significantly different own frequencies of the reference model and the process model. The a) and b) results received for the linear model, c) and d) for non-linear. In addition, the plots a) and c) correspond to open-loop adaptation, while the plots b) and d) correspond to the structure of the closed-loop adaptation with proportional controller.

The results indicate the good convergence of the simulation. Unfortunately, there is no linear relationship between the corresponding output and the difference in own frequencies of its reference model and process. These relationship also depend on the current value of the frequency of its own process. It could be therefore formulated as a three-dimensional function .

For the closed-loop system with the adaptive loop and proportional controller, the fixed off-set error is still different from zero. The increase of amplifier's coefficient of the controller results in accelerating the  $e(t)$  transition state and error's amplitude. Replacement P controller by PI changes the qualitative results. The proper choice of integration and amplifier constants, accelerate operation of the adaptive system and minimize the off-set error.

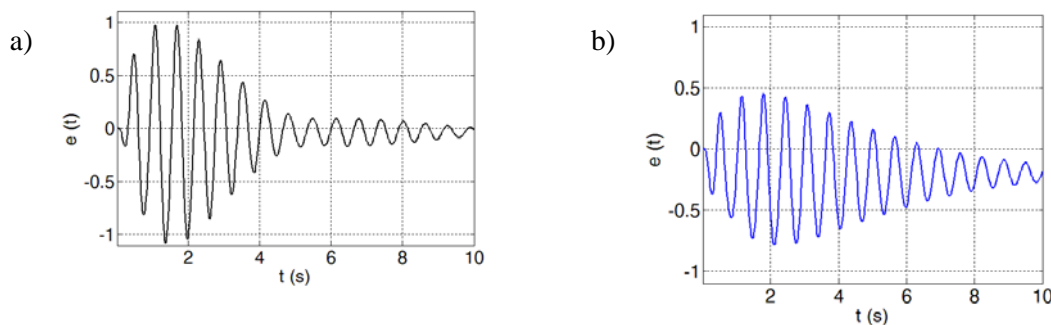


Fig. 5. The error from the close-loop adaptation system, when the frequency difference of the process and its reference model differs by the value a)  $(\omega_p - \omega_r) / \omega_p = 2\%$ , b)  $(\omega_p - \omega_r) / \omega_p = 10\%$

An interesting situation occurs in a transient states, if the process frequency and frequency of the reference model is not too far away. This phenomenon may cause beat vibrations occurrence which may generate an initial increase in amplitude of the transient signal (Fig.5, b).

Besides, simulations of step response tests were carried out also for harmonic inputs. Their interpretation requires a slightly different presentation of results. Due to the convergence of  $e(t)$  output error to zero, regardless of differences in the own frequencies, direct estimation of the frequency difference  $\omega_p - \omega_r$  (process frequency, and reference model frequency) is relevant. Simulated models, however, require further optimization of the time, which will be verified at laboratory tests.

#### 4. RESULTS AND CONCLUSIONS

Obtained results indicate the identification possibility of the own frequency of the beam during normal operation. For step inputs, the convergence and control time depend on the parameters of adaptation algorithm. Ill-defined controls cause increasing vibrations of the observed variable. To ensure zero error in steady state, simple and effective solution gives proportional corrector or properly selected proportional integral corrector.

The presented stage of the research is preliminary in nature, preparing procedures for the laboratory tests. The measurement data from the real process will certainly differ from the applied at the simulation process model. These differences, however, will not affect the performance of the adaptation algorithm.

Sharp temporary requirements decided about the selection of a linear dynamic model as the reference model. This form of the model should provide adequately fast response of microprocessor system. The obtained in results give promising effects both for the purposes of identification and regulation.

#### ACKNOWLEDGEMENTS

Financial support of Structural Funds in the Operational Programme - Innovative Economy (IE OP) financed from the European Regional Development Fund - Project "Modern material technologies in aerospace industry", No. POIG.01.01.02-00-015/08-00 is gratefully acknowledged.

#### REFERENCES

- [1] Amerongen, J. van, A MRAS-based Learning Feed-forward Controller, *MECHATRONICS 2006 - 4th IFAC-Symposium on Mechatronic Systems*, Heidelberg, Germany, September 12th-14th, 2006, pp. 6, 2006.
- [2] K. J. Astrom. *Adaptive Control*. Prentice Hall 1994
- [3] M. Bocheński, J. Warmiński, W. Jarzyna, P. Filipek, M. Augustyniak. Active Suppression of nonlinear composite beam vibrations by various control algorithms application. *10-th Conference on DYNAMICAL SYSTEMS THEORY AND APPLICATIONS December 7-10, 2009*. Lodz, Poland
- [4] Chen Jie, Patton R.J.: Robust model-based fault diagnosis for dynamic systems. *Kluwer Academic Publishers, 1999*
- [5] W. Jarzyna, M. Charlak, *Power Electronics and Electrical Drives*, chapter *Modeling and Diagnosis of Wind Turbine of a Power Station*. Power Electronics and Electrical Drives. Polish Academy of Sciences, Electrical Engineering Committee, pp.463-474. Wroclaw 2007, Poland
- [6] W. Jarzyna, M. Augustyniak, J. Warmiński, M. Bocheński. Characteristics and implementation of the piezoelectric structures in active composite systems, *Electrical Review*, 7/2010.

**COUPLED DRY FRICTION MODEL FOR THE HEAVY DISK  
SLIDED WITH SPINNING ON THE ROUGH PLANE.**

**Alexey Albertovich  
Kireenkov**

Institute for Problems in  
Mechanics of the Russian  
Academy of Sciences  
Moscow, Russia

ABSTRACT

It is presented a dynamically coupled dry friction model describing the sliding of the heavy rotating disk along the rough plane. The procedure of the models constructing is based on the well known results from the theory of elasticity that tangent stresses lead to shift in the symmetric diagram of the normal contact stresses in the direction of the instantaneous sliding velocity. To use the theory of elasticity results in the dynamics problems, a simple linear approximation of symmetric distribution of normal contact stresses is proposed. The subsequent integration on the spot contact of the net vector and torque differentials yields the exact couple integral model of the sliding and spinning friction. To escape the double integrals calculation in the motion equations, the exact integral expressions are replaced by appropriate Pade expansions. It is shown that the distortion of the symmetry in the distribution of normal contact stresses in the case of circular contact sites results in the appearance of the friction force component directed along the normal to the trajectory of the mass center of the rubbed solids and, consequently, the disk mass center trajectory is declined from the straight line..

**INTRODUCTION**

The sliding of the heavy rotating disk along the incline plane in the presence of dry friction is one of the classical models in theoretical mechanics. It has been thoroughly studied by numerous authors. In a majority of publications, the authors have used the Coulomb dry friction model, where the force at the point of contact is assumed to be directed opposite to the relative sliding velocity and be independent of its modulus. But there are numerous experimental data testifying that these assumptions do not agree with the real situation in which the interacting bodies simultaneously participate in translation and rotation.

One of the first models describing the relation between the sliding friction and the whirling friction in the case of non-point contact between the moving bodies was proposed by in [1]. A principally new development of the theory was given by in [2], where exact analytic expressions for the resultant vector and the frictional moment for circular contact sites were obtained under the assumption that the distribution of contact stresses in the contact spot obeys the Hertz law. In [2], to apply the obtained dependencies to problems of dynamics, the linear-fractional Pade approximations of these dependencies were constructed. The developed in [2] theory was used in [3] to study the dynamics of a homogeneous circular disk sliding with rotation on a plane. Under the assumption that the distribution of contact stresses obeys the Galin law, exact analytic expressions for the resultant vector and the frictional moment were obtained and their linear-fractional Pade' approximations were constructed.

The convenience in the use of the Pade' approximations, which permit describing the effects of combined dry frictions for the entire range of angular and linear velocities, allowed one to construct principally new the two-dimensional coupled models of the sliding and whirling friction the basis of these approximations [4]. All these models were constructed in the assumption that, in the case of circular contact sites, the distributions of normal contact stresses depend only on the position vector with origin at the contact spot center. But, it is known [5] that

<sup>1</sup> Corresponding author. Email [kireenk@ipmnet.ru](mailto:kireenk@ipmnet.ru)

in the case of the rigid solids sliding it is appears tangent stresses that leads to shifting in the symmetric diagram of the normal contact stresses in the direction of the instantaneous sliding velocity. Proposed below models permit to use the theory of elasticity results in the dynamics problems.

### 1. BASIC RELATIONSHIPS

All described in introduction models were constructed in the assumption that, in the case of circular contact sites, the distributions of normal contact stresses depend only on the position vector with origin at the contact spot center. But, it is known [5] that in the case of the rigid solids sliding it is appears a tangent stress that leads to shifting in the symmetric diagram of the normal contact stresses in the direction of the instantaneous sliding velocity  $v$  (Fig. 1).

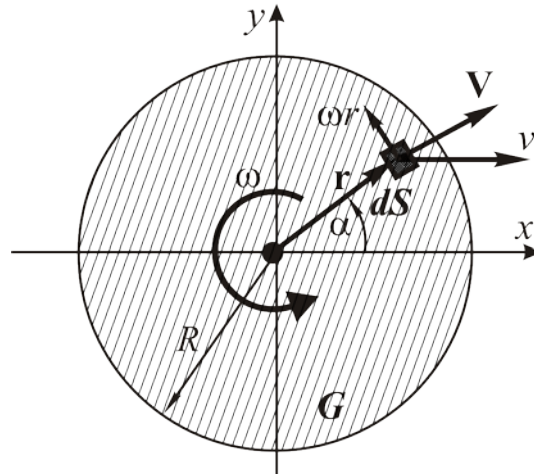


Fig. 1 Kinematics inside the contact spot letters

To use the theory of elasticity results in the dynamics problems, a simple linear approximation of the normal contact stresses distribution is proposed:

$$\sigma(x, y) = \sigma_0(x, y)(1 + kx/R). \quad (1)$$

Typical behavior of the function (1) (red line) is presented on the Fig. 2 in the supposition that symmetric distribution  $\sigma_0(x, y)$  (blue line) of the normal contact stresses in the absence of sliding is describing by Galin law:

$$\sigma_0(x, y) = N \left( 2\pi R^2 \sqrt{1 - x^2/R^2 - y^2/R^2} \right)^{-1} \quad (2)$$

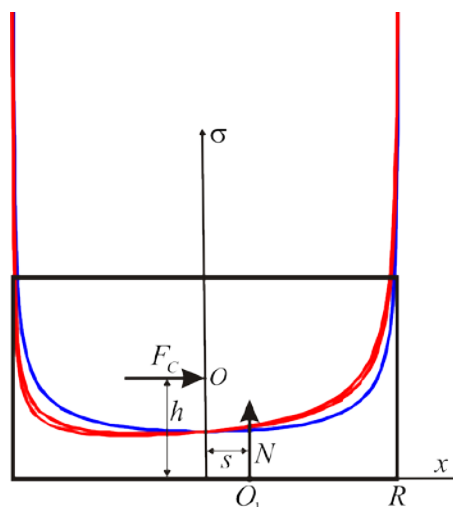


Fig. 2 Distribution of the normal contact stresses

where  $N$  - normal reaction,  $R$  - disk radius.

To calculate coefficient  $k$  in the formula (1) it is used the condition of equality of the external force  $F$  torque to the normal reaction force  $N$  torque which is appears from the shifting of the center of gravity of the contact spot in the direction of sliding on the value  $s$  (Fig.2):

$$Fh = Ns, \quad N = mg \quad (3)$$

where  $m$  - mass of disk and  $h$  - distance from disk center mass to the plane of sliding (Fig. 2). On the other hand the shifting  $s$  of the disk gravity center relatively of the contact spot center can be defined by the following formula:

$$s = \frac{\iint_G x\sigma(x, y)dxdy}{\iint_G \sigma(x, y)dxdy} \quad (4)$$

Substitution of the functions (1) and (2) to the (4) yields:  $s = kR/3$ . Equalization values  $s$  calculated from the formulas (3) and (4) gives

$$k = 3hF/(NR) \quad (5)$$

## 2. COUPLED MODELS OF THE SLIDING AND SPINNING FRICTION

The combined model of sliding and rolling friction is constructed for circular contact sites under the assumption that the Coulomb law in differential form holds for the small surface element  $dS$  in the interior of the contact spot, according to which the differentials of the resultant vector  $d\mathbf{F}$  and the moment of friction  $dM_c$  with respect to the disk center are determined by the formulas:

$$d\mathbf{F} = -f\sigma \frac{\mathbf{V}}{|\mathbf{V}|} (1 + \mu_1 |\mathbf{V}|^3 - \mu_2 |\mathbf{V}|) dS, \quad dM_c = -f\sigma \frac{\mathbf{r} \times \mathbf{V}}{|\mathbf{V}|} (1 + \mu_1 |\mathbf{V}|^3 - \mu_2 |\mathbf{V}|) dS, \quad (6)$$

$$\mathbf{V} = (v - \omega y, \omega x), \quad \mathbf{r} = (x, y)$$

where  $f$  is the coefficient of friction,  $\mathbf{r} = (x, y)$  is the position vector of an elemental area in the interior of the contact spot with respect to its center (Fig. 1),  $\omega$  is the angular velocity of rotation of the contact spot center, but  $\mu_1$  and  $\mu_2$  are the coefficients which can be defined in practice from experiments.

To obtain the resultant vector and the moment of friction, it is necessary to integrate the expressions (6) over the contact spot. The obtained dependencies, where  $F_{\parallel}$  and  $F_{\perp}$  denote the respective components of the resultant vector directed along the tangent and the normal to the trajectory of motion, present an exact combined integral model of sliding and spinning friction

$$F_{\parallel}(u, v) = -f \iint_G \frac{(v - \omega y)\sigma_0(x, y)}{\sqrt{\omega^2(x^2 + y^2) + v^2 - 2\omega y}} dxdy -$$

$$-f \left( (\mu_1 v^3 - \mu_2 v) \iint_G \sigma_0(x, y) dxdy + 2\mu_1 v \omega^2 \iint_G (x^2 + y^2)\sigma_0(x, y) dxdy \right)$$

$$F_{\perp}(u, v) = -\frac{kf}{R} \iint_G \frac{\omega x^2 \sigma_0(x, y)}{\sqrt{\omega^2(x^2 + y^2) + v^2 - 2\omega y}} dxdy \quad (7)$$

$$M_c(u, v) = -f \iint_G \frac{(\omega(x^2 + y^2) - vy)\sigma_0(x, y)}{\sqrt{\omega^2(x^2 + y^2) + v^2 - 2\omega y}} dxdy -$$

$$-f \left( (2\mu_1 v^2 - \mu_2)\omega \iint_G (x^2 + y^2)\sigma_0(x, y) dxdy + \mu_1 \omega^3 \iint_G (x^2 + y^2)^2 \sigma_0(x, y) dxdy \right)$$

$$u \equiv \omega R, \quad G = \{(x, y) : x^2 + y^2 \leq R^2\}$$

After introducing dimensionless variables:  $x = \hat{x}R$ ,  $y = \hat{y}R$  and  $\sigma(\hat{x}, \hat{y}) = \hat{\sigma}(\hat{x}, \hat{y})N/R^2$  and under the assumption that the distribution of normal contact stresses without spinning has the central symmetry  $\sigma_0(x, y) = \sigma(r)$ , it is convenient to calculate the modulus of integrals (8) in the

polar coordinates:  $x = r \cos \varphi$ ,  $y = r \sin \varphi$ ,  $r \in [0, 1]$ ,  $\varphi \in [0, 2\pi]$  (Fig. 1) in which the functions (7) take the form

$$\begin{aligned} F_{\parallel} &= fN \int_0^{2\pi} \int_0^1 \frac{(v - ur \sin \varphi)r\sigma(r)}{\sqrt{u^2 r^2 + v^2 - 2uvr \sin \varphi}} dr d\varphi + 2\pi f \left( (\mu_1 v^3 - \mu_2 v) \int_0^R r\sigma(r) dr + 2\mu_1 v \omega^2 \int_0^R r^3 \sigma(r) dr \right) \\ F_{\perp} &= kfN \int_0^{2\pi} \int_0^1 \frac{ur^3 \sigma(r) \cos^2 \varphi}{\sqrt{u^2 r^2 + v^2 - 2uvr \sin \varphi}} dr d\varphi \\ M_C &= fRN \int_0^{2\pi} \int_0^1 \frac{(ur^2 - vr \sin \varphi)r\sigma(r)}{\sqrt{u^2 r^2 + v^2 - 2uvr \sin \varphi}} dr d\varphi + 2\pi f \left( (2\mu_1 v^2 - \mu_2) \omega \int_0^R r^3 \sigma(r) dr + \mu_1 \omega^3 \int_0^R r^5 \sigma(r) dr \right) \end{aligned} \quad (8)$$

where the ‘‘hat’’ symbol is omitted for brevity, but  $\sigma(r) = 1 / (2\pi\sqrt{1-r^2})$ .

If  $k = 0$ , then model (8) fully is agree to the model, investigated in [3] and can be considered as the first approximation, but presented in this investigation as the second approximation. Thus, we have substantial approximation to the real situation in dependence on the general properties of the normal contact stresses distribution. The coefficient  $k$  in formula (1), (5), (8) is defined by the friction force component  $F_{\parallel}$  from the first expressions in the relations (7-8) and, consequently, the coupled integral friction model which is defined the dynamics of heavy disk on the rough plane under conditions of combined kinematics is

$$\begin{aligned} F_{\parallel} &= fN \int_0^{2\pi} \int_0^1 \frac{(v - ur \sin \varphi)r\sigma(r)}{\sqrt{u^2 r^2 + v^2 - 2uvr \sin \varphi}} dr d\varphi + 2\pi f \left( (\mu_1 v^3 - \mu_2 v) \int_0^R r\sigma(r) dr + 2\mu_1 v \omega^2 \int_0^R r^3 \sigma(r) dr \right) \\ F_{\perp} &= kfN \int_0^{2\pi} \int_0^1 \frac{ur^3 \sigma(r) \cos^2 \varphi}{\sqrt{u^2 r^2 + v^2 - 2uvr \sin \varphi}} dr d\varphi, \quad k = \frac{3hf}{R} \int_0^{2\pi} \int_0^1 \frac{(v - ur \sin \varphi)r\sigma(r)}{\sqrt{u^2 r^2 + v^2 - 2uvr \sin \varphi}} dr d\varphi \\ M_C &= fRN \int_0^{2\pi} \int_0^1 \frac{(ur^2 - vr \sin \varphi)r\sigma(r)}{\sqrt{u^2 r^2 + v^2 - 2uvr \sin \varphi}} dr d\varphi + 2\pi f \left( (2\mu_1 v^2 - \mu_2) \omega \int_0^R r^3 \sigma(r) dr + \mu_1 \omega^3 \int_0^R r^5 \sigma(r) dr \right) \end{aligned} \quad (9)$$

Plot of tangent friction force component  $F_{\parallel}/F_0$  as function of velocity of sliding  $v$  at the constant velocity of whirling  $u=1$  (left figure) and plot of the normal friction force component  $F_{\perp}/(\mu F_0)$  as function of  $k = v/u$  (right figure) are presented on the fig. 3.: As concerned friction torque then, qualitatively, its behavior is the same as case of using classical form Coulomb law: there are only small quantitative distinctions.

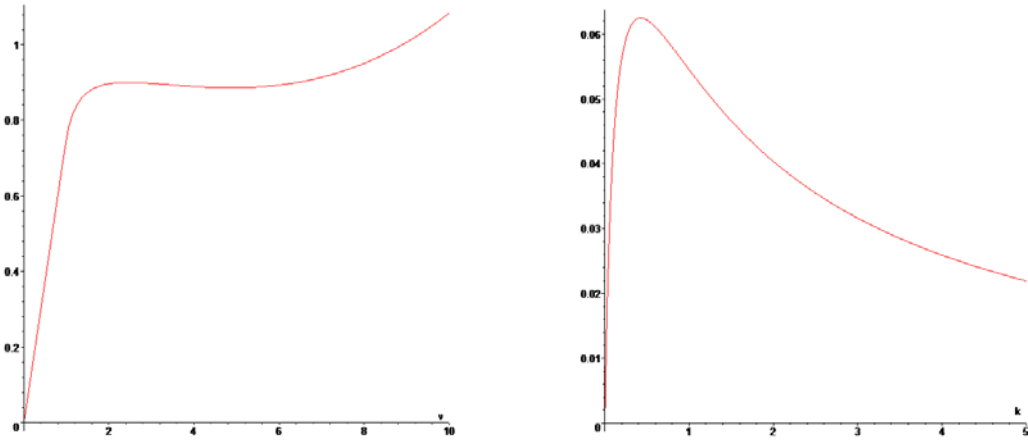


Fig. 2 Tangent and normal friction force components

The expressions for the components of the resultant vector and the moment of friction in relations (9) have several important properties as functions of  $u$  and  $v$ .

*Property 1.* The distortion in symmetric diagram of the normal contact stresses distribution results in the appearance of the resultant vector component  $F_{\perp}$  directed along the normal to the trajectory of motion. The resultant vector is not directed opposite to the velocity of sliding.

*Property 2.* The distortion in the symmetric diagram of distribution of normal stresses does not affect to the moment  $M_C$  and the resultant vector component  $F_{\parallel}$  directed along the tangent to the trajectory.

*Property 3.* The tangent  $F_{\parallel}$  and normal  $F_{\perp}$  components of the friction force, just as the moment  $M_C$ , are homogeneous functions of the variables  $u$  and  $v$  of zero order of homogeneity and hence are invariant under the similarity group:

*Property 4.* The expressions (9), for the moment and both components of the friction force as functions of  $u$  and  $v$  have a singularity at the point  $(u, v) = (0, 0)$ , because they do not have any limit at this point with respect to both of the variables  $u$  and  $v$ .

*Property 5.* In the case of pure sliding  $u=0$  or spinning  $v=0$ , the moment  $M_C$  and the tangential component  $F_{\parallel}$  are homogeneous models corresponding to the usual Coulomb law:

$$F_{\parallel}(0, v) = F_0 \equiv fN, \quad M_C(u, 0) = M_0, \quad M_0 = \pi fNR / 4$$

*Property 6.* In the case of pure sliding, the normal component vanishes:  $F_{\perp}(0, v) = 0$ , and hence the friction force is directed opposite to the velocity vector; in the case of pure spinning, it is equal to  $F_{\perp}(u, 0) = \mu F_0$ ,  $\mu = 3\pi hf / (4R)$ .

*Property 7.* The moment  $M_C$  and both components of the friction force  $F_{\parallel}$  and  $F_{\perp}$  have only one nonzero first partial derivative (the others are zero):

$$\left. \frac{\partial M_C}{\partial u} \right|_{u=0} = \frac{M_0}{3v}, \quad \left. \frac{\partial F_{\parallel}}{\partial v} \right|_{v=0} = \frac{\pi F_0}{4u}, \quad \left. \frac{\partial F_{\perp}}{\partial u} \right|_{u=0} = \frac{4\mu F_0}{9\pi v}$$

The integral models (9) give a good description of the combined sliding and spinning friction, but are inconvenient to be used in problems of dynamics, because it is required to calculate multiple integrals in the right-hand sides of the equations of motion. This difficult procedure can be eliminated by replacing the exact integral expressions by the corresponding Pade approximations. The simplest of them is the linear-fractional approximation preserving the value at zero and at infinity of both for the torque  $M_C$  and for the tangent force component  $F_{\parallel}$ . But, for the normal friction force component, corresponded Pade approximation, naturally, became of the second order.

$$\begin{aligned} M_C &= M_0 \left( \frac{u}{u + mv} + 2\pi \left( (2\mu_1 v^2 - \mu_2) u I_3 + \mu_1 u^3 I_5 \right) \right), \quad \frac{1}{m} = \frac{v}{M_0} \left. \frac{\partial M_C}{\partial u} \right|_{u=0} \equiv \frac{1}{3} \\ F_{\parallel} &= F_0 \left( \frac{v}{v + au} + 2\pi \left( (\mu_1 v^3 - \mu_2 v) I_1 + 2\mu_1 v u^2 I_3 \right) \right), \quad \frac{1}{a} = \frac{u}{F_0} \left. \frac{\partial F_{\parallel}}{\partial v} \right|_{v=0} \equiv \frac{\pi}{4} \\ F_{\perp} &= \frac{\mu F_0 uv}{(u + bv)(v + au)}, \quad \frac{1}{b} = \frac{v}{\mu F_0} \left. \frac{\partial F_{\perp}}{\partial u} \right|_{u=0} \equiv \frac{4}{9\pi} \end{aligned} \quad (10)$$

The linear-fractional Pade' approximations (10) preserve the values of the functions  $F_{\parallel}(u, v)$  and  $M_C(u, v)$  at zero, as well as their behavior and the behavior of their first derivatives at infinity. But model of this type cannot completely preserve the values of all first partial derivatives of these functions at zero. To obtain a correct description of the behavior of the first derivatives at zero, it is required to use the second-order Pade' approximations, and then the coupled model of sliding and spinning friction takes the form

$$\begin{aligned}
M_c &= M_0 \left( \frac{u^2 + muv}{v^2 + muv + u^2} + 2\pi \left( (2\mu_1 v^2 - \mu_2) u I_3 + \mu_1 u^3 I_5 \right) \right), \quad m = \frac{v}{M_0} \frac{\partial M_c}{\partial u} \Big|_{u=0} \equiv \frac{1}{3} \\
F_{\parallel} &= F_0 \left( \frac{v^2 + auv}{v^2 + auv + u^2} + 2\pi \left( (\mu_1 v^3 - \mu_2 v) I_1 + 2\mu_1 v u^2 I_3 \right) \right), \quad a = \frac{u}{F_0} \frac{\partial F_{\parallel}}{\partial v} \Big|_{v=0} \equiv \frac{\pi}{4} \\
F_{\perp} &= \frac{\mu F_0 uv}{(u + bu)(v + u/a)}, \quad \frac{1}{b} = \frac{v}{\mu F_0} \frac{\partial F_{\perp}}{\partial u} \Big|_{u=0} \equiv \frac{4}{9\pi}
\end{aligned} \tag{11}$$

The second-order model (11) completely satisfies all properties 1–7 of the exact integral models (9). But, for the majority of the problems of dynamics, it is sufficient to use the order model (10). The second-order model (11) is required for a more precise qualitative analysis, for example, for determining the boundaries of the stagnant region and the motion stopping time.

The approximations (10) and (11) hold for positive values of  $u$  and  $v$ . They can be easily generalized to the case of arbitrary (in sign) velocities  $u$  and  $v$  by a formal change by absolute values in the denominators of the corresponding expressions.

The use of the friction models based on the Pade' expansions allows one to avoid calculations of multiple integrals over the contact spot, which significantly simplifies their use in problems of dynamics. Moreover, the models (10) and (11) can be considered as the phenomenological models. To obtain a correct description of the combined sliding and spinning dry friction in the complete statement based on the models (10) and (11), it is necessary to know at most six coefficients, which can be determined experimentally in solving the real practical problems.

## CONCLUSIONS

It is developed a dynamically coupled integral dry friction model describing the sliding of the heavy rotating disk along the rough plane. To escape the double integrals calculation in the motion equations, the exact integral expressions are replaced by appropriate Pade expansions.

It is shown that the distortion of the symmetry in the distribution of normal contact stresses in the case of circular contact sites results in the appearance of the friction force component directed along the normal to the trajectory of the mass center of the rubbed solids and, consequently, the disk mass center trajectory is declined from the straight line.

## REFERENCES

- [1] Contensou P. Couplage Entre Frottement de Glissement et Frottement de Pivotelement Dans la Th'eorie de la Toupie, in *Kreiselpromble Gyrodynamics: IUTAM Symp. Celerina, 1962* (Springer, Berlin etc., 1963; Mir, Moscow, 1967), pp. 201–216 (60–77)
- [2] Zhuravlev V.Ph. The Model of Dry Friction in the Problem of the Rolling of Rigid Bodies, *Prikl. Mat. Mekh.* Vol. 62. No. 5. pp. 762–767, 1998.
- [3] Kireenkov A.A. On the Motion of a Homogeneous Rotating Disk along a Plane in the Case of Combined Friction, *Izv. Akad. Nauk. Mekh. Tverd. Tela*, No. 1, pp. 60–67, 2002.
- [4] Zhuravlev V.Ph., Kireenkov A.A. Pade Expansions in the Two-Dimensional Model of Coulomb Friction, *Izv. Akad. Nauk. Mekh. Tverd. Tela*, No. 2, pp. 3–14, 2005.
- [5] Goryacheva I.G., *Mechanics of friction interaction*, NAUKA, Moscow, 2001.

## NONLINEAR PHYSICS AND ENERGY LOCALIZATION IN PERIODIC SYSTEMS

---

Yuri Kivshar<sup>1</sup>

Nonlinear Physics Center,  
Research School of  
Physics and Engineering,  
Australian National  
University, Canberra,  
Australia

ABSTRACT

---

The recent progress in the study of the energy localization and solitons in a variety of nonlinear systems where the effects of *discreteness* and *periodicity* become important, is overviewed.

---

The recent progress in the study of the energy localization and solitons in a variety of nonlinear systems where the effects of *discreteness* and *periodicity* become important, is overviewed. This panoramic presentation will cover (i) generation and control of optical gap solitons in waveguide arrays and photonic lattices, including the most recent observation of polychromatic gap solitons and dynamics localization of light generated by a supercontinuum source, (ii) localized matter waves of Bose-Einstein condensates in two- and three-dimensional optical lattices, (iii) discrete localized modes in composite metamaterials and nanophotonic structures, and (iv) energy localization in carbon nanotubes and graphene nanoribbons.

First of all, the most important recent advances in nonlinear photonics where many of novel theoretical findings have been verified in experiment, is emphasized. This includes the observation of surface solitons in one- and two-dimensional photonic lattices, the observation of polychromatic "rainbow" gap solitons in photonic lattices generated by a supercontinuum source [1], the generation of topologically stable spatially localized multivortex solitons, etc.

One of the recent concepts in the theory of nonlinear waves is associated with a novel type of broad nonlinear states which appear in the gaps of the bandgap spectra of periodic systems such as light waves in periodic photonic lattices and Bose-Einstein condensates in optical lattices. These localized states cannot be treated by familiar multi-scale asymptotic expansion techniques, and they can be better understood as truncated nonlinear Bloch waves [2]. I demonstrate that these self-trapped localized nonlinear modes can be found in one-, two-, and three-dimensional periodic potentials, and they have been readily observed in experiments on nonlinear self-trapping of matter waves in one-dimensional optical lattices.

Finally, the energy localization in graphene structures and demonstrate the existence of spatially localized nonlinear modes in the form of discrete breathers in carbon nanotubes and nanoribbons [3], is discussed. In nanotubes with the chirality index  $(m,0)$  there exist three types of discrete breathers associated with longitudinal, radial, and torsion anharmonic vibrations, however only *twisting breathers* survive in a curved geometry remaining long-lived modes even in the presence of thermal fluctuations.

## REFERENCES

- [1.] A. Szameit, I.L. Garanovich, M. Heinrich, A.A. Sukhorukov, F. Dreisow, T. Pertsch, S. Nolte, A. Tunnermann, and Yu.S. Kivshar, *Nature Physics*, 5, 271, 2009.
- [2.] T.J. Alexander, E.A. Ostrovskaya, and Yu.S. Kivshar, *Phys. Rev. Lett.*, 96, 040401, 2006.
- [3] A.V. Savin and Yu.S. Kivshar, *Phys. Rev. B*, 81, 165418, 2010.

---

<sup>1</sup> Corresponding author. Email: [yks124@rsphysse.anu.edu.au](mailto:yks124@rsphysse.anu.edu.au)

## IRREVERSIBLE TRANSFER OF VIBRATION ENERGY IN LINEAR AND NONLINEAR COUPLED PARAMETRIC SYSTEMS

Yu. A. Kosevich <sup>1</sup>

**L. I. Manevitch**  
Semenov Institute of  
Chemical Physics,  
Russian Academy of  
Sciences,  
Moscow, Russia

ABSTRACT

We present a novel principle of vibration energy trapping based on vibration analogue of nonadiabatic Landau-Zener tunneling. We demonstrate analytically and numerically that in a system of two weakly coupled pendulums or oscillators, linear or nonlinear, an efficient irreversible transfer of vibration energy from one subsystem to another occurs when the coupled subsystems pass through the internal resonance. The internal resonance takes place due to parametric drive when the length, mass or spring stiffness of at least one of the pendulums or oscillators varies in the course of vibrations. Nonlinear effects result in a separatrix mode of vibration energy transfer, in the vicinity of which the irreversible character of the energy transfer is substantially enhanced.

### INTRODUCTION

Tunneling is one of the most striking manifestations of quantum behavior and has been the subject of extensive research both in fundamental and applied physics. A well-known generic example of tunneling phenomenon is Landau-Zener tunneling (LZT), in which a quantum system subject to an external force tunnels across an energy gap between anti-crossing energy levels [1,2]. Quantum LZT was observed in semiconductor superlattices for electrons, as well as in optical lattices for ultracold atoms and Bose-Einstein condensates. In the case of electrons in semiconductor superlattice, the external force responsible for nonadiabatic energy-level crossing and LZT is exerted by an external electric field. LZT of optical waves was observed in optical lattices [3] and optical waveguide arrays [4]. Recently, LZT of bulk and surface acoustic waves in ultrasonic superlattices was predicted and observed [5,6]. Effective external forces in optical or acoustic LZT are produced by the perturbation of the corresponding optical or ultrasonic lattice.

The common feature of the aforementioned examples of nonadiabatic LZT is the irreversible (and almost unidirectional) exchange of energy between two states caused by external forces or perturbations. The possibility of this type of exchange would also be desirable in vibrating mechanical systems, e.g., in towers or in an airplane's wings. Here the impact excitation threatening the structural integrity of the system must be irreversibly transferred to a sacrificial subsystem. It turns out that a system governed by equations similar to that of a quantum system can in fact be designed. We noticed earlier a profound analogy between adiabatic quantum tunneling and energy exchange between weakly coupled oscillators, both linear and nonlinear [7]. In this work we present a vibration analogue of nonadiabatic quantum Landau-Zener tunneling that reveals a new type of energy trapping. We demonstrate analytically and numerically that a Landau-Zener-like transition can take place in a system of two weakly coupled oscillators. This can occur when the length, mass or spring stiffness of at least one of the oscillators varies during vibration. In result, an efficient irreversible transfer of vibration energy from one oscillator to another takes place when the coupled subsystems pass through the internal resonance. Such mechanical oscillatory systems represent new types of energy traps. These can be easily generalized for the dynamic protection of more complex systems from vibro-impact actions, with numerous potential applications in nano-, micro-, and macromechanics. Nonlinear effects can enhance the irreversible character of the vibration energy transfer.

<sup>1</sup> Corresponding author. Email [yukosevich@gmail.com](mailto:yukosevich@gmail.com)

# 1. IRREVERSIBLE TRANSFER OF VIBRATION ENERGY IN LINEAR COUPLED PARAMETRIC SYSTEMS

We consider a system of two plane pendulums with lengths  $l_1$  and  $l_2$ , and masses  $m_1$  and  $m_2$ , weakly coupled by a spring (with a comparable with  $l_1$  equilibrium length). The Lagrange function of the system is written as follows:

$$L = \frac{1}{2} \left( m_1 l_1^2 \left( \frac{d\varphi_1}{dt} \right)^2 + m_2 l_2^2 \left( \frac{d\varphi_2}{dt} \right)^2 \right) - g \left[ m_1 l_1 (1 - \cos \varphi_1) + m_2 l_2 (1 - \cos \varphi_2) \right] - \frac{1}{2} k_{12} (l_1 \sin \varphi_1 - l_2 \sin \varphi_2)^2 \quad (1)$$

where  $\varphi_1$  and  $\varphi_2$  are the deflection angles, and  $k_{12}$  is the spring constant. Let  $l_1$  be a constant and  $l_2$  be a function of time. Then the corresponding equations of motion are:

$$m_1 l_1^2 \frac{d^2 \varphi_1}{dt^2} + m_1 g l_1 \sin \varphi_1 + k_{12} l_1 \cos \varphi_1 (l_1 \sin \varphi_1 - l_2 \sin \varphi_2) = 0$$

$$m_2 l_2^2 \frac{d^2 \varphi_2}{dt^2} + 2m_2 l_2 \frac{dl_2}{dt} \left( \frac{d\varphi_2}{dt} \right) + m_2 g l_2 \sin \varphi_2 + k_{12} l_2 \cos \varphi_2 (l_2 \sin \varphi_2 - l_1 \sin \varphi_1) = 0 \quad (2)$$

We assume that

$$l_2(t) = l_1 (1 + \Delta_2(t)) \quad (3)$$

where  $\Delta_2(t)$  describes a (relatively small) change in time of  $l_2$ . In order to avoid a superfluous decrease in  $l_2$ , in the following we assume that

$$\Delta_2(t) = \delta_2 - f_2 T_2 \tanh(t/T_2) \quad (4)$$

where  $\delta_2$  and  $f_2/\omega_1$  are independent small parameters of the same sign,  $\omega_1 = \sqrt{g/l_1}$ .

Since the LZT is basically linear phenomenon, we start with the analysis of linearized Eqs. (2) for the case of  $\varphi_1 \ll 1$  and  $\varphi_2 \ll 1$ . There are several ways to proceed from two real equations of the second order (2) to four complex equations of the first order. Following the approach used in [8], we introduce two *complex envelopes*  $a_1$  and  $a_2$  of the real deflection angles  $\varphi_1$  and  $\varphi_2$ :

$$\varphi_{1,2} = \frac{1}{2} [a_{1,2} e^{-i\omega_1 t} + a_{1,2}^* e^{i\omega_1 t}] \quad (5)$$

where we assume that  $d a_i / dt \ll \omega_1 a_{i,2}$ . As follows from Eq. (5), the real part of the variable  $a_i$  determines the envelope of  $\varphi_i$ , while its imaginary part determines the envelope of the dimensionless time derivative  $d\varphi_i/dt/\omega_1$ ,  $i=1,2$ . These properties of complex envelopes allow us to easily relate the envelope modulus  $|a_i|$  with the vibration energy of the linearized  $i$ -th pendulum:  $E_i = 0.5 g l_i |a_i|^2$ .

Substituting Eqs. (3) and (5) in linearized Eqs. (2), we get the following two evolution equations for the complex envelopes  $a_1$  and  $a_2$  in the main approximation with respect to small parameters  $\delta_2$ ,  $f_2/\omega_1$ , and  $k_{12}/\mu\omega_1^2$  ( $\mu = 1/(1/m_1 + 1/m_2)$  is a reduced mass of  $m_1$  and  $m_2$ ):

$$i \frac{da_1}{dt} = \frac{k_{12}}{2m_1\omega_1} (a_1 - a_2)$$

$$i \frac{da_2}{dt} = \frac{k_{12}}{2m_2\omega_1} (a_2 - a_1) - \frac{1}{2} \omega_1 \Delta_2(t) a_2 \quad (6)$$

We also obtain two corresponding equations for the complex-conjugated envelopes  $a_1^*$  and  $a_2^*$ . The total vibration energy of the coupled pendulums is given by  $0.5gl_1(m_1|a_1|^2 + m_2|a_2|^2)$ , which is the integral of motion. For  $t < T_2$  and  $\Delta_2(t)$  given by Eq. (4), Eqs. (6) coincide with the modified description of the quantum Landau-Zener-like transition [3]. The multiple scale expansion procedure, presented, e.g., in [9], leads to similar complex evolution equations.

The same Eqs. (6) describe the dynamics of the complex envelopes of the displacements  $u_1$  and  $u_2$  of two oscillators with masses  $m_1$  and  $m_2$  and springs with equal coefficient of stiffness  $\kappa_1$  or two oscillators with equal masses  $m_1$  and springs with coefficients of stiffness  $\kappa_1$  and  $\kappa_2$ , weakly coupled by a spring with coefficient of stiffness  $k_{12} \ll \kappa_1$ , when either  $m_2$  or  $1/\kappa_2$  changes in time according to Eq. (3) ( $l_{1,2}$  should be replaced by  $m_{1,2}$  or  $1/\kappa_{1,2}$ ). Introducing two complex envelopes  $a_1$  and  $a_2$  of the real displacements  $u_1$  and  $u_2$  according to Eq. (5), under the same assumption  $d a_{1,2} / d t \ll \omega_1 a_{1,2}$  we obtain LZT-like Eqs. (6) for the complex envelopes  $a_1$  and  $a_2$ . Here now  $\omega_1 = \sqrt{\kappa_1 / m_1}$  and parameter  $m_2$  equals  $m_1$  in the evolution equation for  $a_2$ .

The asymptotic analytical solution of Eqs. (6) for large positive  $t$  with  $\Delta_2(t)$  given by Eq. (4) and the initial conditions  $|a_1(-\infty)|^2 = 1, a_2(-\infty) = 0$  can be written as:

$$|a_1(\infty)|^2 = \exp(-R), \quad R = \pi k_{12}^2 / (m_1 m_2 |f_2| \omega_1^3) \quad (7)$$

This equation describes the part of the initial vibration energy that is retained asymptotically in pendulum 1.

To check the efficiency of the system of pendulums in the capacity of an energy trap, we calculated the time evolution of vibration energies of the coupled pendulums from the solution of linearized Eqs. (2) for the deflection angles  $\varphi_1$  and  $\varphi_2$  and compare it with the numerical solution of LZT-like Eqs. (6) for the complex envelopes  $a_1$  and  $a_2$ . Since the damping of low-frequency vibrations of pendulums is very small, the effect of damping on the energy exchange between pendulums can be neglected in the main approximation.

In Fig. 1 we plot the vibration energies  $E_1$  and  $E_2$  of pendulums 1 and 2 with  $m_1 = m_2$  and their total energy  $E_T$  versus time from the solution of linearized Eqs. (2) (lines 1, 2 and 3) alongside with a solution of LZT-like Eqs. (6) (lines 4 and 5) and with the LZT-like prediction, given by Eq. (7), for the part of initial vibration energy which is retained asymptotically in pendulum 1, line 6. The initial conditions correspond to the impact excitation of pendulum 1. The following realistic parameters and initial conditions were taken:  $l_1 = 0.305$  m,  $m_1 = 0.244$  kg,  $k_{12} = 0.784$  N/m,  $\delta_2 = 0.22$ ,  $f_2 = 0.062$  s<sup>-1</sup> and  $T_2 = 15.6$  s, and

$$\begin{aligned} \varphi_1(0) = 0, \varphi_2(0) = 0, \dot{\varphi}_2(0) = 0, \dot{\varphi}_1(0) = 0.61 \text{ rad/s} \\ ia_1(0) = \dot{\varphi}_1(0) / \omega_1, a_2(0) = 0 \end{aligned} \quad (8)$$

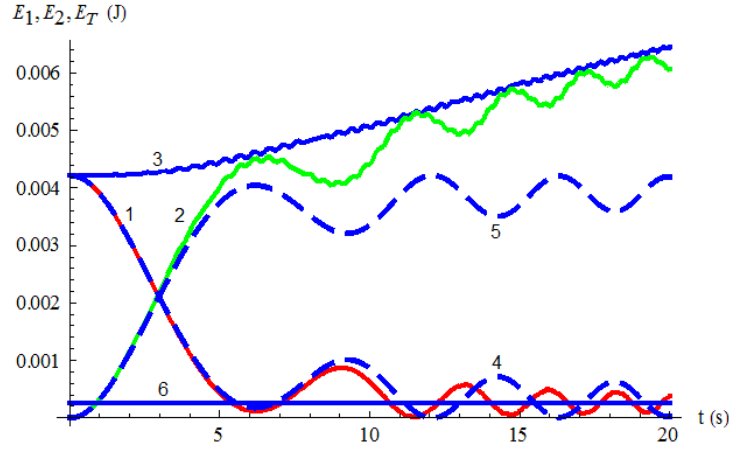


Fig. 1. Solid lines 1, 2 and 3: Vibration energies  $E_1$  and  $E_2$  of pendulums 1 and 2 and their total energy  $E_T$  versus time as solutions of linearized Eqs. (2). Dashed lines 4 and 5: Vibration energies of pendulums 1 and 2 as solutions of LZT-like envelope Eqs. (6). Solid line 6: Part of initial vibration energy which is retained asymptotically in pendulum 1, given by Eq. (7). Parameters used in the calculations are given by Eqs. (3), (4) and (8) in the case of equal pendulum masses.

As one can see, the irreversible and intensive energy flow from the pendulum 1 to the pendulum 2 occurs. One can also conclude from Fig. 1 that the LZT-like envelope equations (6) correctly reflect the regularities of the process during its initial stage, when the most intensive resonance energy transfer occurs. The LZT-like prediction for the part of initial vibration energy, which is retained asymptotically in pendulum 1, is also impressively confirmed in our simulations, although the factor  $R$  in Eq. (7) is not small ( $R = 2.85$ ). According to our simulations, this value of  $R$  gives an approximate upper limit of the applicability of Eq. (7) for the considered classical systems. Large enough saturation time  $T_2$  influences only the transient dynamics without affecting the asymptotic energy of pendulum 1.

From the physical point of view, the irreversible energy exchange revealed above can be considered as the targeted energy transfer (TET) [7,10]. The exact internal resonance is fulfilled when  $l_2 = l_1$  (or  $m_2 = m_1$ ,  $\kappa_2 = \kappa_1$ ) and the eigenfrequencies of the coupled oscillators become equal (which occurs at  $t = \delta_2 / f_2$ ). As the system moves out of resonance (for  $t > \delta_2 / f_2$ ), there is no considerable reverse energy flow from pendulum 2 to pendulum 1. This phenomenon makes the second oscillator a vibration energy trap.

Our calculations also show that the use of the lower or larger mass of pendulum 2 does not essentially suppress the irreversible TET. By corresponding change of the parameters  $\delta_2$  and  $k_{12}$  together with the ratio between  $m_2$  and  $m_1$ , we can obtain a good agreement with the LZT-like prediction given by Eq. (7) both for  $m_2 < m_1$  (e.g., for  $m_2 = 0.5m_1$ ) and  $m_2 > m_1$  (e.g., for  $m_2 = 2m_1$ ). Importantly in all the considered cases, the most interesting for possible applications time evolution and average asymptotic value of vibration energy of pendulum 1 are correctly described by conservative LZT-like equations (6), although the original classical system is a non-conservative one.

## 2. IRREVERSIBLE TRANSFER OF VIBRATION ENERGY IN NONLINEAR COUPLED PARAMETRIC SYSTEMS

Now we describe briefly the effect of nonlinear properties (anharmonicity) of the coupled pendulums or oscillators on the irreversible vibration energy exchange between them. The effect of nonlinearities on the energy transfer in the considered coupled parametric system, described by Eqs.

(2), increases with the increase of initial pulse given to pendulum 1, which is proportional to  $\dot{\varphi}_1(0)$ . In Fig. 2(a) we present numerical solution of nonlinear Eqs. (2) for the time dependence of energies of the coupled pendulums in the case of relatively high initial pulse given to pendulum 1,  $\dot{\varphi}_1(0) = 7.93$  rad/s for  $m_1 = m_2$ , when the rest of parameters is the same as in Fig. 1. Due to energy transfer from pendulum 1 and parametric drive, at  $t \approx 15$  s pendulum 2 finds itself in the whirling mode, in which

the reverse energy flow to pendulum 1 is suppressed. Such transition to the whirling mode of pendulum 2 is clearly seen in Fig. 2(b), which shows time dependence of pendulums deflection angles. Thus figure 2(a) demonstrates that nonlinear effects, together with optimized initial conditions and other parameters of the system, can make the energy transfer very effective: almost 100% energy of pendulum 1 is irreversibly transferred to pendulum 2 in 10 seconds.

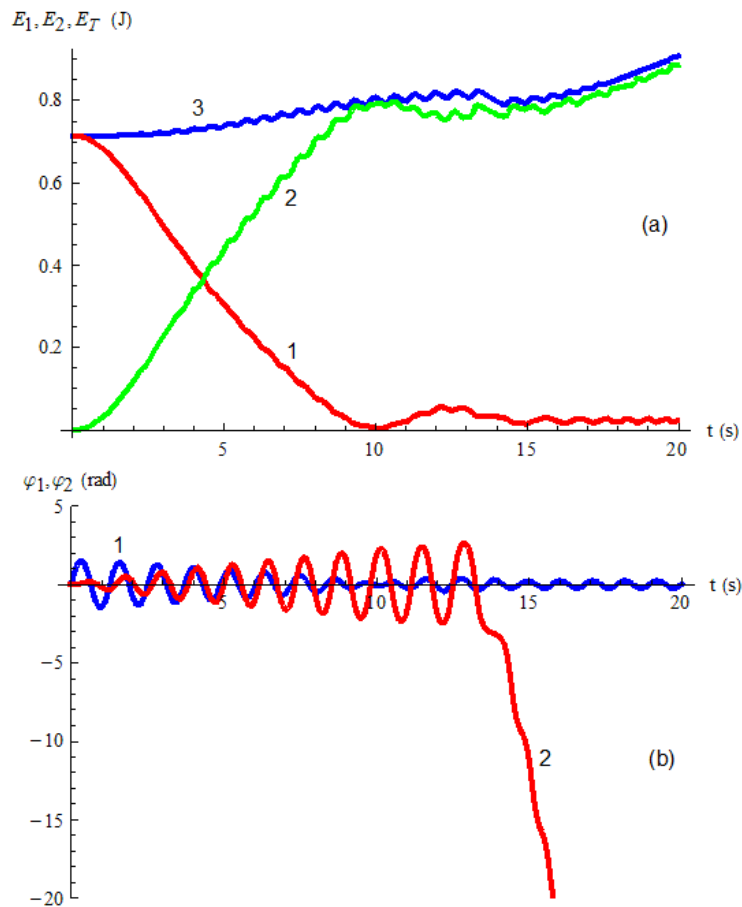


Fig. 2 (a) Vibration energies  $E_1$  and  $E_2$  of pendulums 1 and 2 and their total energy  $E_T$  versus time as solutions of nonlinear Eqs. (2), lines 1, 2 and 3, respectively. (b) Deflection angles  $\varphi_1$  and  $\varphi_2$  versus time as solutions of nonlinear Eqs. (2), lines 1 and 2, respectively. Parameters used in the calculations are given by Eqs. (3), (4) and (8) in the case of  $\dot{\varphi}_1(0) = 7.93$  rad/s and equal pendulum masses.

For the high enough initial pulse given to pendulum 1, it will immediately be excited to the whirling mode, in which further energy transfer to pendulum 2 is strongly suppressed. This means that the considered parametric system is characterized by an effective *TET separatrix*, which detaches two modes with almost complete and strongly suppressed incomplete energy exchange. TET separatrix is known for the energy transfer in *passive* nonlinear systems, in which the nonlinearity substantially changes the rate and completeness of the TET through the self-trapping of energy in one of the coupled subsystems [7,10]. Our results demonstrate that nonlinearities of the coupled elements can substantially affect TET in the *active* (parametric) systems also.

## CONCLUSIONS

We present a novel principle of trapping of the vibration energy. This principle is based on the profound analogy that we have found between the irreversible transfer of the vibration energy in a classical parametric system and quantum nonadiabatic Landau-Zener tunneling. We demonstrate analytically and numerically that in a system of two weakly coupled pendulums or oscillators an efficient irreversible transfer of vibration energy from one subsystem to another occurs when the coupled subsystems pass through the internal resonance. Nonlinear effects can substantially enhance the irreversible character of the transfer of the vibration energy. The revealed phenomena open up the possibility of designing the fundamentally new types of energy traps for the dynamic protection of various nano-, micro-, and macromechanical systems.

## REFERENCES

- [1] L.D. Landau, *Phys. Z. Sowjetunion* **2**, 46, 1932.
- [2] C. Zener, *Proc. R. Soc. London, Ser. A* **137**, 696, 1932.
- [3] M. Ghulinyan *et al.*, *Phys. Rev. Lett.* **94**, 127401, 2005.
- [4] H. Trompeter *et al.*, *Phys. Rev. Lett.* **96**, 023901, 2006.
- [5] H. Sanchis-Alepuz, Yu. A. Kosevich and J. Sanchez-Dehesa, *Phys. Rev. Lett.* **98**, 134301, 2007.
- [6] M. M. de Lima, Jr., Yu. A. Kosevich, P. V. Santos and A. Cantarero, *Phys. Rev. Lett.* **104**, 165502, 2010.
- [7] Yu. A. Kosevich, L. I. Manevitch and A.V. Savin, *Phys. Rev. E* **77**, 046603, 2008.
- [8] Yu. A. Kosevich and S. Lepri, *Phys. Rev. B* **61**, 299, 2000.
- [9] A. I. Manevich and L. I. Manevitch, *The Mechanics of Nonlinear Systems with Internal Resonances*, Imperial College Press, London, 2005.
- [10] A.F. Vakakis, O.V. Gendelman, L.A. Bergman, D.M. McFarland, G. Kerschen, and Y.S. Lee, *Nonlinear Targeted Energy Transfer in Mechanical and Structural Systems*, Springer, Berlin, 2009.

## DYNAMICS AND DIAGNOSTICS OF THE ROLLING MILLS DRIVELINES WITH NON-SMOOTH STIFFNESS CHARACTERISTICS

**Pavel V. Krot**<sup>1</sup>  
 Iron and Steel Institute  
 Dnepropetrovsk, Ukraine

### ABSTRACT

The rolling mills drivelines are under investigation. Their dynamics is characterized by the extremely high torque amplification factors. The main problem is to identify non-smooth piece-wise linear stiffness characteristics in the multi-body system produced by the angular and radial backlashes. Different smoothing functions are analyzed. Frequency domain is used to determine amplitudes and phases of natural frequencies and harmonics due to angular and radial backlashes appearance. It was shown that interrelations between the static torsional loads and dynamic responses can be utilized for diagnostics.

### INTRODUCTION

The rolling mills drivelines are operated under the extremely high loads and simultaneously are characterized by the increased wear. Backlashes and step-like impulse loads during the hot metal rolling cause the most frequent failures in the drivelines. Standard methods of vibration diagnostics based on envelope curve spectrum analysis require stationary drive speed and load for signal averaging. It is quite difficult to provide constant load in the rolling mills because of metal temperature and friction forces variation in the work rolls gap. Therefore the new approach is proposed for wear diagnostics based on torque and vibration transient processes analysis. It allows avoiding inconveniences of standard diagnostics methods.

Different kinds of backlashes in the rolling mills equipment are given in the Fig.1, where following notation are used:  $F$  – force (torque),  $\delta$  – generalized coordinate. Function like in the Fig.1a describes clearance with a dead zone in the driveline couplings caused by wear or assembly errors (both positive and negative  $\delta$ ). In general, transient process calculation supposes that the opened part of gap  $b$  may not be equal to a closed part  $a$  (the whole gap is  $a+b$ ). The Fig.1b describes “softening” stiffness function for bearings, housing and bolting (positive  $\delta$ ). The fracture point means stiffness decreasing when gap is opening between gearbox housing and bearing cover under the action of severe shock torsional vibrations. A “hardening” function in Fig.1c shows the 4-high stand rolls stack vertical stiffness for low and high rolling loads (positive  $\delta$ ).

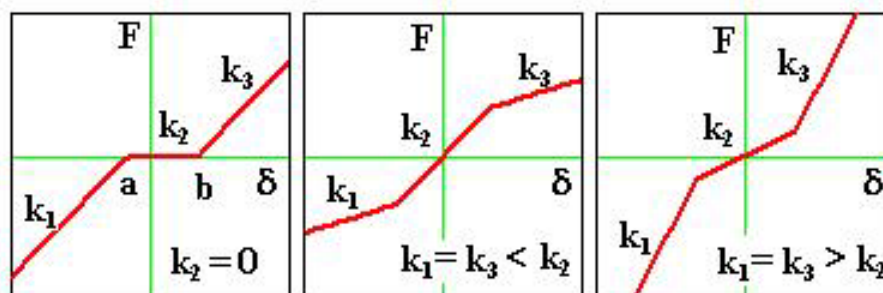


Fig. 1 Piecewise linear non-smooth stiffness characteristics in the rolling mills

<sup>1</sup> Corresponding author. Email paul\_krot@mail.ru

Angular wear increases torque amplification factor (TAF) in all driveline elements and, if overload occurs, it consequently leads to sudden failures. Therefore, backlashes should be considered as the main parameters of the rolling mills drive trains technical condition. The prognostic maintenance based on gaps diagnostics is complicated because of short period of transient process when the work torque is appearing and the backlashes are closing. Under the full load it is difficult to determine the backlashes exactly by the modulation characteristics of the vibration signal.

## 1. DRIVELINES DYNAMICS

An analysis of clearance non-linearity and vibration impacts in torsional systems was conducted in [1] and in many other works. Unfortunately, there are a few works on rolling mills drivelines having certain particularities.

The hot rolling mills spring-mass model (see Fig.2) has the following elements: direct current or synchronous electric motor (Q1), intermediate gear couplings (C12, C34), gearbox (Q2, C23, Q3), pinion stand (Q4, C45, Q5), two spindles (C46, C57) and the rolling stand itself with two pairs of upper (Q7) and lower (Q6) work rolls (WR) and backup rolls (BUR). System has a branched structure due to spindles.

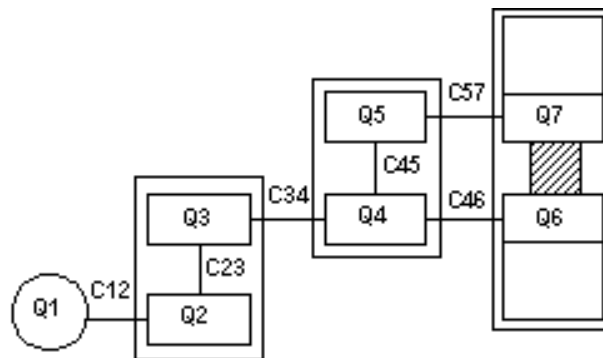


Fig. 2 The multi-body calculation scheme of the hot rolling mill (one stand)

The WR's coupling via the rolled strip is not considered during transient process simulation. The every coupling has an uncertain part of gap opened before transient. First of all, it concerns spindles, which are, usually, under- or over-weighted because of imperfect spring type balancing units. Even  $\pm 5\%$  error of spindles weight (0.2-2 KN) tuning will cause their periodical (twice per rotation) vertical motion and gaps opening. Beside it, steel strip higher velocity than the WR linear velocity will also produce gaps in the spindle couplings and pinion stand.

The analytical research of nonlinear multi-body systems, usually, assumes reducing the initial system to less DOF. That is possible, but inefficient, if the every coupling diagnostics is required. Then, those coupling is necessarily even, if its contribution to overall dynamics is not significant.

A well known earlier fact that backlashes, when are opening, cause high frequency vibrations, was also confirmed by this research. But it was cleared up what the frequencies exactly appear in the signals of torque and bearings vibration and the how they could be used for backlashes diagnostics. It has been shown that higher natural frequencies associated, but not equal, with partial frequencies of the torsional system will appear in torque spectrum. Also, as it is known, the higher harmonics of the main frequency will be produced by nonlinearities. Such regularities have been taken into consideration for wear diagnostics methods. The main idea is to compare linear system as reference with a response of a nonlinear real driveline in the range of natural frequencies.

### 1.1 Static load influence on dynamic response

Torque amplification factor (TAF) is the main parameter, usually, used for system dynamics estimation. However, for nonlinear systems, dynamic response depends on static load (rolling torque). It was shown (see Fig. 3) that with less torque  $T_{static}$  we obtain bigger TAF for different angular wear (0.000...0.012 rad). Such nonlinearity is almost invisible for  $T_{max}$  curves and, usually, is not taken into account for the durability calculations in the rolling mills.

The field torque measurements were fulfilled in the industrial hot rolling mill in the corresponding motor shaft. The newly designed in the Iron and Steel Institute 8-channel telemetry system was utilized. Vibration was measured with the 4-channel signal conditioner (PCB Piezotronics model 48A22) and IMI Sensors accelerometers (model 603C01). The special software was used for

signals recording and FFT transform in conjunction with low-pass filtering and other signal processing procedures. Results of torque measurements are represented in Fig. 4 where we can see the same nonlinear relation between static load  $M_{st}$  and dynamic response  $M_{max}$  and TAF.

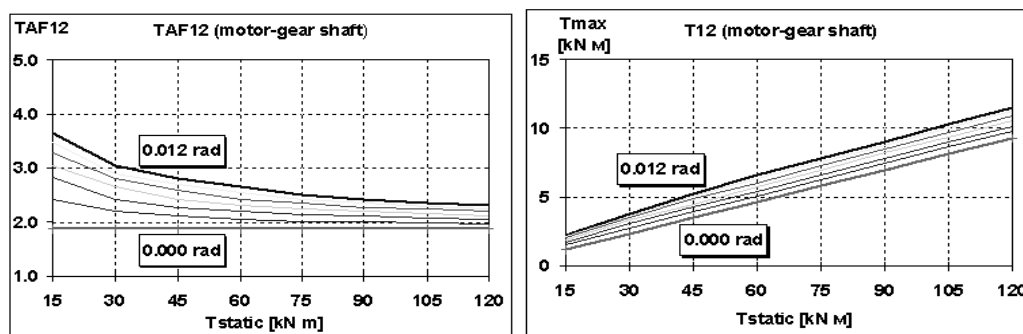


Fig. 3 Static torque influence on TAF and peak torque  $T_{max}$  in motor shaft (C12) (Simulation)

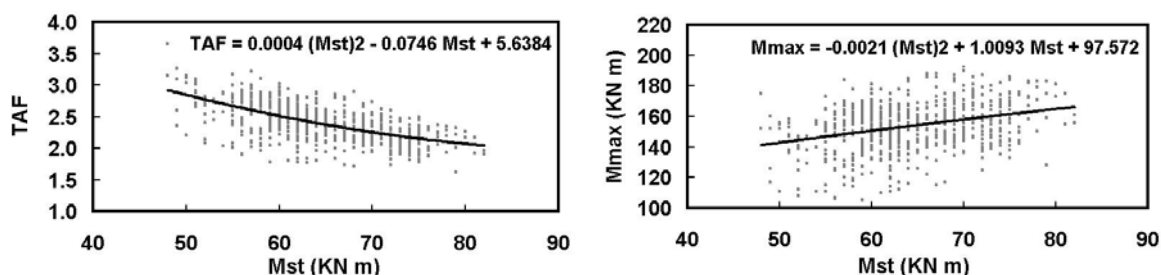


Fig. 4 Static torque influence on TAF and peak torque  $M_{max}$  in motor shaft (C12) (Telemetry measurements with the strain gauges)

## 1.2 Smoothing functions

Because of backlashes are described by a non-analytical and non-differential discontinuous function of logical type (see below), it worsens model numerical simulations. Therefore, some smoothing functions were analyzed and issues of their implementation were discussed. They are as following (see Fig.5):

1. Logical type: 
$$g_1(\delta) = \begin{cases} k_3(\delta - b) + k_2b \Rightarrow b < \delta \\ k_2\delta \Rightarrow -a \leq \delta \leq b \\ k_1(\delta + a) - k_2a \Rightarrow \delta < -a \end{cases}$$
2. Polynomial type: 
$$g_2(\delta) = a_1 \cdot \delta + a_2 \cdot \delta^2 + a_3 \cdot \delta^3$$
3. Arc-tangent type: 
$$g_3(\delta) = \delta \cdot a_0 \cdot \arctan(\sigma \cdot |\delta|)$$
4. Hyperbolic-tangent type: 
$$g_4(\delta) = \delta \cdot a_0 \cdot \tanh(\sigma \cdot |\delta|)$$

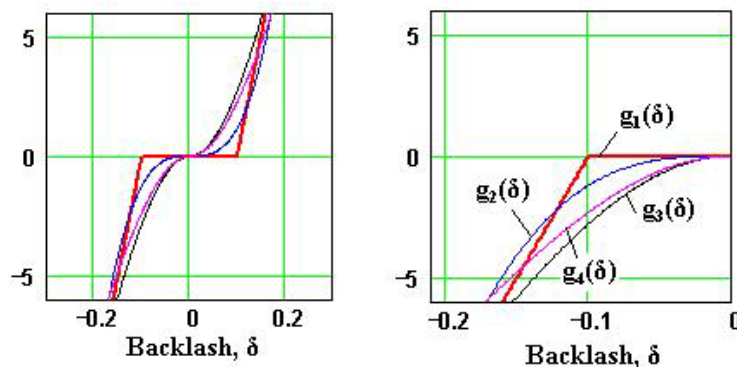


Fig. 5 Non-smooth stiffness characteristic approximation with continuous functions

Adjusting of the approximation functions  $g_1(\delta)$ - $g_4(\delta)$  is carrying out by the following parameters  $a_0, a_1, a_2, a_3, \sigma$ . Although a flexibility of such functions, there are certain restrictions for their implementation. Only small dimensionless values of gaps (0.01-0.1) and stiffness (10-100) combinations are available for accurate approximation. Otherwise, scaling factors for transition to model parameters should be introduced to get acceptable accuracy. A linear component ( $a_1$ ) in  $g_1(\delta)$  is responsible for gap size, while the cubic component ( $a_3$ ) for stiffness approximation. The values  $a_1 < 0.01$  do not affect curvature near the zero point. A square component ( $a_2$ ) gives possibility to simulate with a polynomial  $g_2(\delta)$  function the asymmetry in gap opening conditions (it corresponds to  $a \neq b$  in  $g_1(\delta)$ ). Coupling preloading conditions are also available due to square component ( $a_2$ ) in  $g_2(\delta)$  when symmetry point is shifted beyond the initial point of coordinates. However, when  $a_2 > \sqrt{3 \cdot a_1 a_3}$  or  $a_1 < 0$ , two points - maximum and minimum - appear in the  $g_2(\delta)$  graph instead of one saddle point. That has to be taken into account during parameters tuning.

The every coupling in the driveline with its unique gap and stiffness values requires special function for approximation. Right function choice depends not only on gap and stiffness values, but is also related to actual torque amplitudes. For example, polynomial type function  $g_2(\delta)$  is more accurate near the fraction points of stiffness curve (within the  $\pm 2(a+b)$  range), then, it crosses the original function  $g_1(\delta)$  and begins to deviate significantly from it. On the other hand, the arc-tangent  $g_3(\delta)$  and hyperbolic  $g_4(\delta)$  functions (the are similar in behavior) are more accurate for large amplitudes far from fracture points (beyond the  $\pm 2(a+b)$  range). So, there are no general recommendations for any cases.

The interaction of  $a_0$  and  $\sigma$  is not fully understood and actual limits have not yet been determined definitely. For sure, a smaller  $\sigma$  value corresponds to smaller stiffness, but smaller  $a_0$  fits larger gap. The larger the  $\sigma$  value, the closer is the approximated  $g_3(\delta), g_4(\delta)$  curve to the original piecewise linear function  $g_1(\delta)$ .

### 1.3 Frequency domain analysis of smoothening functions

Effect of smoothening functions on the frequency response of an oscillator with clearance non-linearity was investigated in [2]. The Nonlinear Identification through Feedback Outputs (NIFO) technique was also used in [3] to estimate the nominal linear FRFs for SDOF system using three different generating functions to describe the modulation in frequency response:  $\Delta y^{p+(n/m)}$ , where  $\Delta y$  is the relative motion across the nonlinear element and  $n$  and  $m$  are integers such that  $m > n$ . In order to estimate here the influence of different approximation functions ( $g_1 - g_4$ ) on frequency response functions (FRF), some calculations were carried out on a SDOF system (see Fig.6).

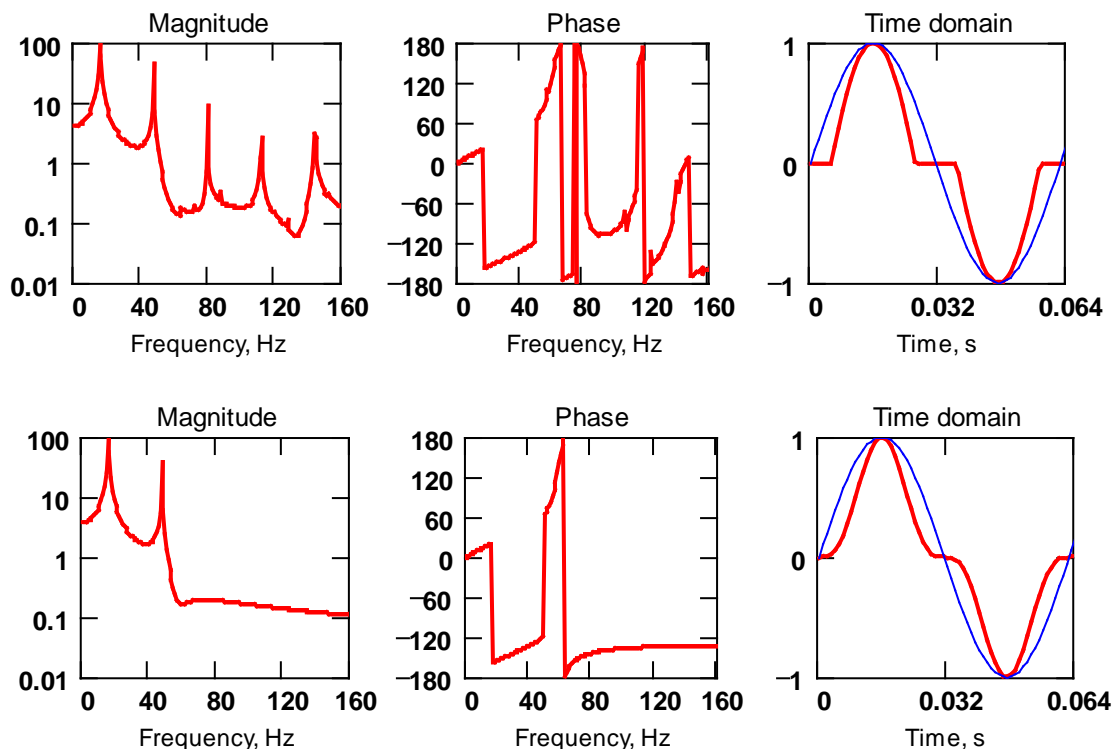


Fig. 6 FRF and time domain signal for  $g_1$  (logical) and  $g_2$  (polynomial) functions

We can see that piecewise function generates more harmonics and irregular phase spectrum. The same output exhibit  $g_3$  and  $g_4$  functions (not shown). Polynomial function gives only two harmonics in FRF and clearer phase portrait. Again, it depends on actual amplitudes of torque and gap value. Than the more trajectory beyond the stiffness fracture points (larger amplitudes), the less influence of nonlinearities. That coincides with experimental results.

## 2. BACKLASHES DIAGNOSTICS.

The torsional natural frequencies, calculated on investigated rolling stand driveline, were as following: 12, 15, 20, 34, 45 and 81 Hz. As it was expected, measured torque signal had peaks at the lower frequencies and the vibration had them in the higher range. Spectrum peaks amplitudes (A12...A81 Hz) and according phases at the natural frequencies (see Fig. 7) were taken for different gearbox and spindles wear (angular backlashes) by the torque signals.

### 2.1 Angular gap diagnostics

Diagnostics algorithms are based on combination the amplitudes and phases at the different natural frequencies. In this case, variable A20 Hz and its phase are most sensitive to wear in torque signal. After the 2.5 mm wear in spindles A45 Hz amplitude becomes less than A20 Hz. In such manner other variables may be analyzed to build diagnostics algorithms which differ for other points of torque measurement.

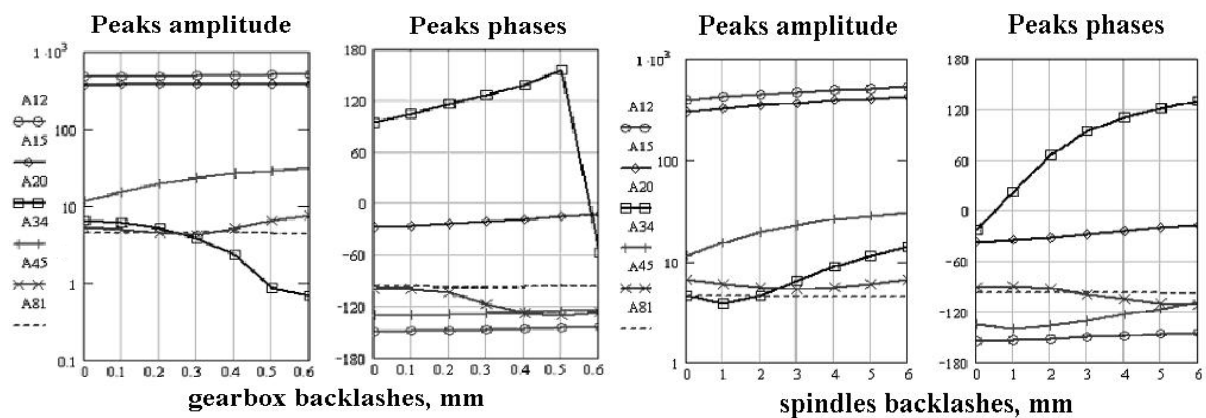


Fig. 7 Variation of the torsional natural frequencies and phases due to backlashes in the gearbox and spindles

Calculation of FRFs is not a problem for analytical linear models. On the other hand, experimental time-domain data converting into the frequency domain and corresponding FRFs, depending on the types of external excitation, may not be perfect over the whole frequency range. For example, for the transient impacts, signal-to-noise ratios tend to be poor, but this will mostly affect the FRFs at non-resonant frequencies. Another difficulty in FRF comparison is that FRFs are very sensitive to sensors and excitors placement. That restriction is avoided due to a naturally constant strip impact in the WRs and, more importantly, stable position of torque sensor on the shaft.

### 2.2 Bearings diagnostics

Radial wear and backlashes are the most important maintenance parameters because they cause transient shaft motion within gaps and significant strains appear on the marginal parts of teeth. Beside it, bearing's housing bolts have plastic deformation due to shock vibration. The screwing up is the standard maintenance operation for the rolling mills gearboxes and pinion stands. Therefore it is important to diagnose the bearings radial backlashes and the housing gap opening.

The calculation scheme of shaft, bearings and housing nonlinear system is represented in Fig.8a. Bearing backlash is the first stage of wear. The next stage is the housing gap opening, which may lead to teeth fraction. During the bearing wear its natural frequency is decreasing slowly. Then, bolting plastic deformation begins and the main frequency amplitude falls down. Also, higher harmonics appear. During the housing gap opening phases of all harmonics change significantly.

Beside the frequency domain it is useful for diagnostics purposes to obtain time domain trajectory of shaft center during the transient process (see Fig.8b). The initial position of shaft was in the bottom. The places where trajectory is out of geometrical circle correspond to bearing deformation and possible damages, if it exceeds the elastic limit of material. It gives a possibility to determine a

relation of radial dynamical loads in the bearing and housing by the wear. For example, a certain limit of load (about 1000 kN) will be overrun at the 1.8 mm wear of bearing (see Fig.8c). It allows predicting a maintenance period for the rolling mills gearboxes and pinioning stands.

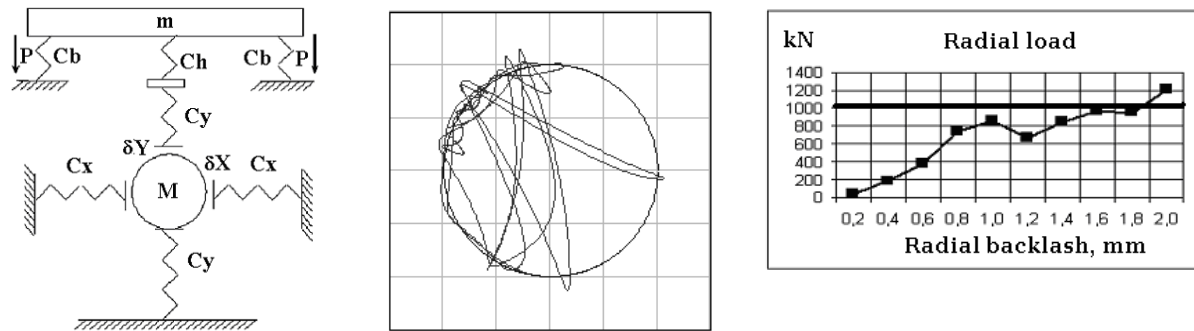


Fig. 8 Calculation scheme of shaft-bearing-housing nonlinear system, shaft motion trajectory and maximal radial loads on bearing

It was shown by the calculations that radial backlashes have the same influence on torsional nonlinear vibration as the angular ones. The biggest transient dynamic loads appear when the shaft weight force and teeth coupling reaction force have the opposite directions.

## CONCLUSIONS

Angular and radial backlashes are the most important parameters of the rolling mills drivelines technical condition and maintenance. Transient torsional nonlinear vibration initiated by the step-like rolling load may be used for wear diagnostics as in time domain, so in frequency domain. The main idea of backlashes diagnostics is to compare dynamic response of real system with the signals simulated by the linear model. Some features of nonlinear torsional vibration, such as static load and dynamic torque relation, may be used for backlashes diagnostics. Natural frequencies and their higher harmonics amplitudes and phases are used in algorithms for driveline, gearboxes bearings and bolting diagnostics. The smoothing functions, in general, affect those frequency response regimes that are influenced by the stiffness curves fractions. However, the peak values and TAF during transient appear to be insensitive to the choice of smoothing function.

## REFERENCES

- [1] T.C. Kim. *Analysis of Clearance Non-Linearities and Vibro-Impacts in Torsional Systems*, PhD. Thesis, Ohio State University, 2003.
- [2] T. C. Kim, T. E. Rook and R. Singh. Effect of Smoothing Functions on the Frequency Response of an Oscillator with Clearance Non-Linearity *Journal of Sound and Vibration*, 2003.
- [3] D. E. Adams and R. J. Allemang. Polynomial, Non-Polynomial, and Orthogonal Polynomial Generating Functions for Nonlinear System Identification, *ISMA2000*, Belgium, 2000.

**NONLINEAR STRUCTURAL DYNAMICS IN XXI CENTURY: SPECIFIED MODELS, VIBRO-COMFORT BUILDINGS, NONLINEAR DAMPENING DEVICES**

**Vladimir V. Kulyabko<sup>1</sup>**

Prydneprovsk State  
Academy of Civil  
Engineering and  
Architecture  
Dnepropetrovsk, Ukraine

---

ABSTRACT

---

In this paper methods of nonlinear structural dynamics, which were reported by the author on the ND-KhPI-2004, 2007, are applied to dynamics of modern buildings and structures. Schemes and models of new dampers are created. Three types of nonlinearities can be detected in operating period of these devices: geometric, physical and structural ones. The complexity of calculation of structure dynamics with such nonlinearities is explained by the fact that the systems have variable structure. It is presented five variants of ways to reduce the level of bending vibrations of structures (declarative patents of Ukraine are obtained).

---

On previous conference ND-KhPI 2007 (Kharkov, Ukraine) several works were devoted to the vortex-induced vibration of constructions in the flow (see, for example, the work [1]) and to the different variants of the analysis and reduction of linear and nonlinear vibrations (see, for example, works by Avramov and Mikhlin). The author of this article developed [2-8] certain approaches in analysis not less than three of types of different non-linearity, in correct design of devices to reduce amplitudes of vibrations in buildings and structures.

Therefore, the aim of this work is to show some ways of "useful" application of nonlinear devices and characteristics. This is an example of design of the new damping devices to reduce the level of bending vibrations of structures and their elements.

One of the main places here is the development of non-linear calculated models to make the correct choice of damping, parameters and shapes of steel and composite structures. Such subject was also presented by the author on the conference "Steel & composite structures" in Manchester-2007.

In this work we consider an theoretical and some practical issues, based on theories of nonlinear dynamics of building objects. Modern building industry has reached literally enormous heights (the height of the building Burj Dubai, had been raised in eve 2010, is 818 m) and stairwells (bridge in Messina strait with stairwell more than 3 km). So, the achievements for this field of nonlinear dynamics are exceedingly important.

It's very interesting to watch the stages, taking into account the dynamics, the "race" of competitive process of the scientific and engineering elaboration of unique industrial and civil engineering structures:

- a schematic design of a new object. Approximate calculations of the main carrying constructions on simplified linear dynamic model can be produced on this stage;

- a creation of Special Technical Conditions (STC) for design, construction and operational monitoring of structures technical state. In this and subsequent stages of the building's exploitation, scientific organizations are usually involved to prepare corresponding documents and guarantee the "scientific support" on the object. For example, in Moscow the STC has been made for buildings having height of 60-75m or more (the requirements for the calculations: the model, modal analysis, the interaction of the object with a base, etc., are given);

---

<sup>1</sup> Corresponding author. Email [kulyabko-vv@mail.ru](mailto:kulyabko-vv@mail.ru)

• on the stage of final detailed design the "shuttle" method of designing and nonlinear dynamic calculations is made. The very important aspect is the purpose of the form of the nonlinear dynamic model and all its parameters. In complicated cases we determine the dissipative properties and other parameters of the model, the dynamic testing of separate subsystems and elements of buildings are entered into the shuttle scheme.

In such a "race" we can see, that some technical problems of building non-linear dynamics are similar to the problems of mechanical engineering and machine building. For example, builders can learn from machine builders to design and to test the dumping devices, which use the dry friction force (in dynamics of suspension of vehicles, etc.). But modern unique building objects have enormous sizes. So, it is very difficult not only to determine dynamical loadings for them, but to compose the space model, which could take into account peculiarities of all subsystems and elements of these objects. Unfortunately, modern domestic computer construction systems are too carried away with the quantitative aspect of calculations, using for many problems the finite element method (FEM), but losing, as a result, many qualitative effects of real non-linear structural dynamics.

Modern software (PC) is correct if, in particular, it can take into account in dynamical estimate of the new model multi-story building, a damping of vibrations by means of small relative shifts and displacements of elements in nodes of the construction. So-called "semi-rigid" nodes are becoming the innovation in the large-scale building structures, created at the end of XX and the beginning of XXI centuries. Their work and efficiency depend on the level of amplitudes of forced oscillations. At the low level nodes with dry friction are blocked and "do not breathe", the relative displacements do not occur, and at higher levels, nodes work as a friction dampers; their elements are mutually displaced. In other words, the construction works like a "system with variable structures".

In such "complex nonlinear" systems the term "modal analysis" is not clear yet, because it is not only non-linear, but also "instantly changing", that is depending on the method of excitation and research of free oscillations.

Let's consider the following variants:

- I. Theoretical and experimental researches of natural vibrations of the nonlinear system can be carried out in the time domain if the chosen initial displacements correspond to ones of the considered nonlinear natural mode. In this case the initial velocities must be chosen equal to zero.
- II. Researches can be "active" using the force-machine (in particular, using the resonant method).
- III. Research can be organized "passively", that is from some effects of varying the oscillating object, making records of arbitrary moments, processing these records, spectral analysis, etc.

Naturally, it is impossible to obtain single-valued results for a system with variable structure. Frequencies and modes of free (not their own ones, typical for conservative systems) oscillations in the nonlinear systems are unstable, in some cases are chaotic (see, for example, Hayashi's research) and depend on the level of disturbances of the structure, the input spectrum, the initial conditions, etc.

For small oscillations of the whole structure the free oscillations modes in some cases can be converted into linear ones. Increased disturbance will add relative vibration displacements alternately in one or more nodes.

Such analysis show the complicity both for a description and functioning of the separate subsystems, and for the whole buildings, bridges, towers if they contain non-linear damping devices. Probably, only such efficient devices (absorbing external energy of the dynamic loads) allow design and use reliable and safe objects as vibro-defensive, winds-stability, seismo-steadfast and terror-protected ones.

The following main particularities of the design and usages (and analysis of the nonlinear vibrations) of the buildings and structures in XXI age are discussed in this report:

1. The new dynamic loads and influences which appeared recently, connected with new large sizes of buildings and power of machine technology, climate changes and unexpected social events (in the form, for example, of terrorist acts) etc.
2. The unbeneficial combinations of the loads become more complicated. In nonlinear characteristics of systems and models the use of the superposition principle is impossible.
3. Requirements for the "vibro-ecology" quality of life and work in building and structures are increased. In particular, the admissible range of vibration frequencies of the pedestrian and other town bridges is limited. The monitoring of velocity and acceleration is introduced. A limitation of the "doze of vibration", obtained by people, that is the integral level of obtained vibration energy for the limit interval of time, is very important at present.

4. New materials and nodes (with poorly known properties), often very different in the same building, which does not allow to conduct the study of their vibrations on former linear models with similar (in type and value) dissipation, springy and inertia parameter "general on object" have been used.
5. Possibilities of mathematical and computer modeling are changed, alternative methods and approaches to solve the nonlinear dynamics problems, are appeared. But there is a small number of works on comparison of such methods and approaches. Works on more precise definition of these approaches limitation in nonlinear dynamics are desirable, in particular, of the analytical and numerical methods (including FEM), researches in the time domain etc.

In given report it is expected a consideration of the ways of creation and testing nonlinear models by using multiple examples of dynamics of the buildings and structures. We will demonstrate examples of accurate models in dynamic calculation of the buildings, structures and their element with different non-linearity:

- a) "geometric" one (cable, threads);
  - b) "constructional" one (the systems with clearance, slippage and others);
  - c) " physical" one:
- nonlinear-springy (see the theory of Duffing`s equations and Prandtl`s diagrams for bodies which are springy-plastic, plastic and springy; see the under-changing rubber in shock absorber, air-cushion and others);
  - nonlinear-dissipative (with dry friction).

As a result of the works [2-7] we have successfully patented five inventions in 2009. Methods of the nonlinear dynamics calculation and tests, together with PGASA and DonNASA, was created and tested in natural conditions.

These inventions (see their schemes and corresponding patents in *Table 1*) are directed only on one of the type of vibrations of the large structures, namely, they reduce the vibration bending of the buildings and their elements. These principles allow to provide protection of the object from different forces and vibrations, to reduce the level not only bending, but also longitudinal and other types of the vibrations in building constructions (high-altitude buildings, overlapping, tower, masts, bridges).

Detailed description of the work for each device is given, drawing up of the dynamic models, nonlinear differential equations of the vibrations of the objects with devices and vibrograms, proving efficient device.

In conclusion it needs to indicate a necessity of the further development of the alternative methods of the nonlinear devices calculation. Otherwise the correct design of the modern buildings and structures, working at dynamic loads, is impossible.

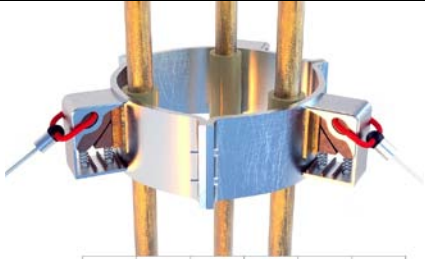
## REFERENCES

- [1] Keber M., Wiercigroch M., Sanches C., Mazzilli C.. Modelling of vortex-induced vibration of vertical offshore risers, *Proc. of the Int. Conference "Nonlinear Dynamics"*, Kharkov, KhPI, p.44, 2007.
- [2] Kulyabko V.V., Maslovskiy A.V., Banakh A.V. Research of nonlinear dynamics of complex constructions and mediums (in time history, without application FEM, *Proc. of the Second Int. Conference "Nonlinear Dynamics"*, Kharkov, KhPI, p.56, 2007.
- [3] Kulyabko V.V., Maslovskiy A.V., Banakh A.V. Simulation of nonlinear oscillations and protection of modern unique buildings and structures, *Advanced Problems in Mechanics*, IPME RAN, Saint-Petersburg, pp.73-74, 2007.
- [4] Kulyabko V., Maslovskiy A., Miheev A. About the theoretical and experimental researches of variants of the nonlinear damping of vibrations and seismic-certification of structures, *Constructions, iss. 69. Construction in seismic regions of Ukraine*. NDIBK, Kiev, pp. 289-297, 2008.
- [5] Vladimir Kulyabko, Anton Maslovskiy, Denis Sartakov. Development in principal new device for damping oscillations of constructions on base calculation nonlinear oscillations of the structures, *Theoretical Foundations in Civil Engineering, Polish-Ukrainian-Lithuanian Transactions*, №17, Warsaw, pp. 185-192, 2009.
- [6] Kulyabko V.V., Banakh V.A. Nonlinear simplified models of bearing constructions of the structures with damping devices for the analysis of "problems of the dynamic interaction" in the time-history. *Actual problems of research on the theory of structures*, V.3, TsNIISK, Moscow, pp.1-4. 2009.

[7] Gorokhov Ye.V., Mushchanov V.F., Kulyabko V.V., Denisov E.V., Maslovsky A.V., Ways of antihunting rigid conductors structures of outdoor switchgears of the power supply network construction, *Modern Building Materials, Structures and Techniques*, Vilnius Gediminas Technical University, Publishing House "Technika", pp. 619–627, 2010.

[8] Kulyabko V.V. Nonlinear interaction of bridges, roads, infrastructures - with the base and the inertia of a discrete moving loads of general form: calculations, testing, vibration damping, *Bulletin of DIIT*, Vol. 33, DIIT, Dnepropetrovsk, pp. 146-149, 2010.

*Table 1. Patents of Ukraine on useful models device, which reduce the bending vibrations of the constructions*

<p>1 № 4 0 4 3 1</p>		<p>4 № 4 0 4 3 4</p>	
<p>2 № 4 0 0 9 9</p>		<p>5 № 4 0 4 3 4</p>	
<p>3 № 4 0 0 9 4</p>		<p>6 № 4 0 4 3 5</p>	

**ESTIMATION OF HEART RATE COMPLEXITY OF BEHAVIOR  
USING DIFFERENT METHODS OF NONLINEAR DYNAMICS**

**Olga G. Kyselova**<sup>1</sup>  
National Technical  
University of Ukraine 'KPI'  
Kyiv, Ukraine

**Ievgen A. Nastenko**  
National M. Amosov  
Institute of Cardio-  
Vascular Surgery  
Kyiv, Ukraine

---

ABSTRACT

---

The main goal of the research is a development of system for analysis of heart rate behavior complexity by methods of nonlinear dynamics. For this task main algorithms for qualitative and quantified estimation of 24-hours heart rate regularity were explored. Also, the software utilizing the Kolmogorov's algorithm, Poincare equation, approximate entropy, flicker noise, distribution bar chart as well the Lorenz diagram, is developed. The results of calculation can be used to define the diagnostic signs of human health state on the basis of daily heart rate regularity estimation.

---

**INTRODUCTION**

Formation of a new interdisciplinary field – Synergetics, opens new opportunities for assessment and analysis of complex biomedical systems, in particular of the cardiovascular system.

Heart rate is an integrative indicator that reflects integral properties of the circulatory system and whole body. Creation of the new systems analysis of the heart rate based on the nonlinear dynamic parameters gives an opportunity to evaluate a wide range of regulatory, the state regulatory body reserves and to diagnose the reduction of adaptive properties and approximation regulatory limits to the range at a new level. It is important for diagnostics of pathological processes, dysadaptation states of practical healthy persons, sportsmen's "overtraining", elimination of overload regimes emergencies etc.

Main methods of heart rate variability (HRV) analysis, which found the most application of modern diagnostic systems, can be divided into statistical, geometric and temporal frequency. But the chaotic process of HRV requires the use of mathematical apparatus to refine results of diagnostic and predictable assessments obtained by standard methods. This instrument is the mathematical theory of nonlinear dynamics.

The goal of the research is synthesis of diagnostic system based on the combined estimates of nonlinear dynamics to refine methods of predicted dysadaptive states and to bring an organism to limits of the regulatory range.

**1. METHODS OF NONLINEAR DYNAMICS FOR ESTIMATION OF HEART RATE VARIABILITY**

A literature review showed that to describe the nonlinear properties of heart rate variability the Poincare equation, cluster spectral analysis, Lorentz graphics, singular expansion, Lyapunov's exponent, Kolmogorov entropy and others are used.

**1.1. Algorithmic compression method by Kolmogorov**

A great interest is the definition of algorithmic methods (in opposition to physical and chemical methods), or computing of complexity, the concept was introduced by Kolmogorov. Using this approach, a numerical sequence is processed using linear algorithms of archiving, as it is made in

---

<sup>1</sup> Corresponding author. Email [olga.mmif@gmail.com](mailto:olga.mmif@gmail.com)

computer systems. The length of minimized, archived, packed sequence is compared with the original length. It enables to determine quantitatively the ratio of organized and random components of numerical series.

HRV assessment method based on Kolmogorov's algorithmic approach is to determine the level of algorithmic complexity of heart rate variations. The essence of the method is to use linear archiver and to compare the original and compressed sequences of cardiac intervals. Additionally, this method along with an approximating entropy index can be used to assess the frequency of fragments of heart rhythm. By output plot of heart rhythm and/or sequence of differences is built regularity dictionary. It is estimated as the frequency of repetition and length of the analyzed regularities and their temporary location (time of day when they meet).

Selection of regularities in time sequence allows archiving. Thus, the compression coefficient (the ratio of length of archived sequences to the length of output sequences) is a quantitative characteristic of HRV.

To identify repetitive areas of heart rate Lempel-Ziv-Welch (LZW) compression algorithm is used.

To register cardiointervals's sequences, found in the SR, the dictionary is used. Dictionary is a table that contains the code sequence, the sequence itself and its number of occurrences in the output. Based on this dictionary the conclusions about the variability of heart patients can be drawn.

## 1.2. The method of fractal dimension

In the theory of fractals the method of fractal dimension is used. It is the most known method of return map, or that the same thing, the box counting method. With it quantitatively determined by self-similarity, repeatability fragments ( $x_i, x_{i+1}$ ) of numeric sequence depending on changes of the scale  $Dx$ .

## 1.3. The method of approximating entropy

Approximating entropy is a quantitative assessment of the frequency of fragments of dynamic series of cardio intervals regardless of frequency range. A sharp drop of index approximating entropy, especially in combination with a lower variability of interval's plot is quite formidable feature reducing regulatory redundancy organism and can be viewed as a sign of increasing the likelihood of occurrence of sudden cardiac death. Such situations are often observed in patients of cardioreanimation offices in particularly serious condition (e.g., acute myocardial infarction (MI), several transferred MI in anamnesis, etc.). The advantage of this estimation is its applicability for processing sequences cardio intervals relatively small length. For example, one minute, ten minutes.

Method of calculating approximation entropy was established as a conventional quantitative assessment of the availability of regular structures, i.e. structures, repetitive sequences in temporal parameters. Such as may be monitoring records of physiological indicators.

## 1.4. Flicker-noise method

Universal theory of flicker-noise, proposed in 1987 by P. Bak and entered intensive development in subsequent years, is called the theory of self-organized criticality (SOC).

To the characteristics of the variety of behavior, at least in part, be attributed and  $\beta$  flicker-noise characteristics used in the theory of self organized criticality (SOC). According to the latter, much of the complex processes of nature, represented as time sequences, has a reverse dependence of spectral power on frequency  $E = 1/f^\beta$ . This dependence corresponds to the so-called flicker noise or flickering noise - low-rate fluctuations in the frequency range ( $4,0 \cdot 10^{-3} \dots 4,0 \cdot 10^{-2}$  Hz), which is compared, or even exceeds the observation time system.

It is known that the flicker-noise observed in fluctuations of many indicators of living systems: heart rate, blood pressure, brain electrical activity and others.

## 2. PROGRAM REALIZATION METHODS OF NONLINEAR DYNAMICS FOR EVALUATION HEART RATE VARIABILITY

Methods for estimation of heart rate variability was developed using special software:

- graphical programming environment NI LabVIEW;
- mathematical modeling system MatLab 6.0;
- Visual Studio.NET.

The main availability of the developed software:

- 1) analysis of heart rate variability in time domain;
- 2) analysis of heart rate variability in the frequency domain (calculation of spectral indices of heart rate, construction diagrams balance of power frequency ranges HF / LF / VLF);
- 3) analysis of heart rate variability using methods of fractal dimension (Lorentz plot and Poincare points);
- 4) analysis of heart rate variability by flicker-noise method;
- 5) analysis of heart rate variability using algorithmic compression method by Kolmogorov;
- 6) generation of the report of the calculation for each selected time interval.

Interfaces of some functional modules are shown in Fig. 1 and 2.

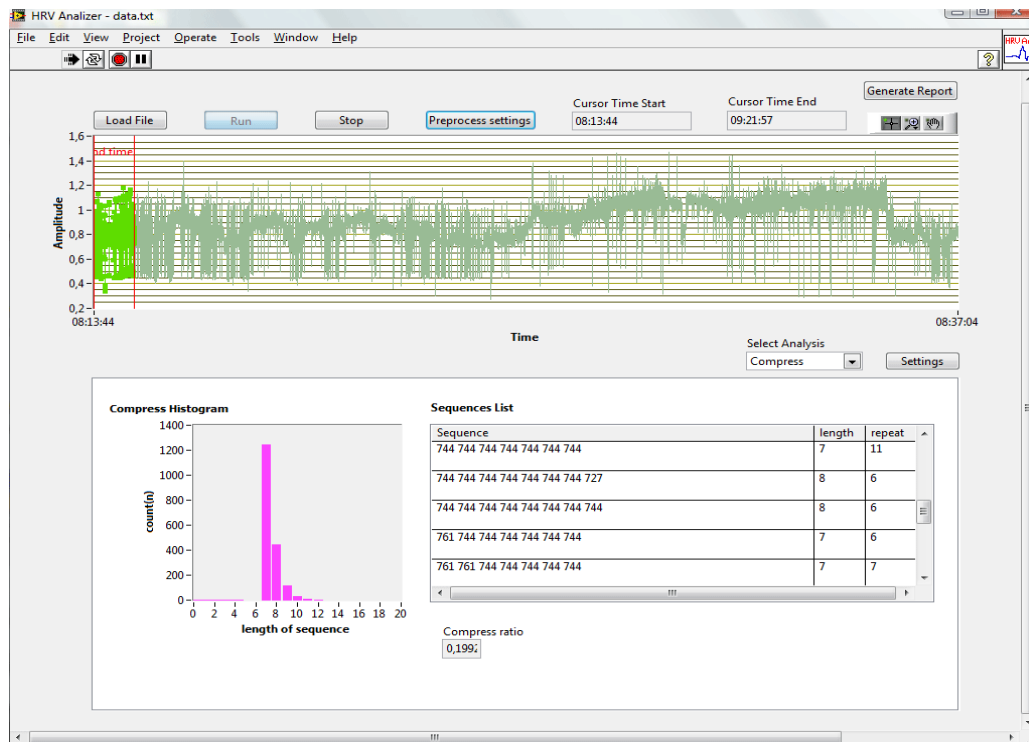


Fig. 1 The interface of software (algorithmic compression method by Kolmogorov)

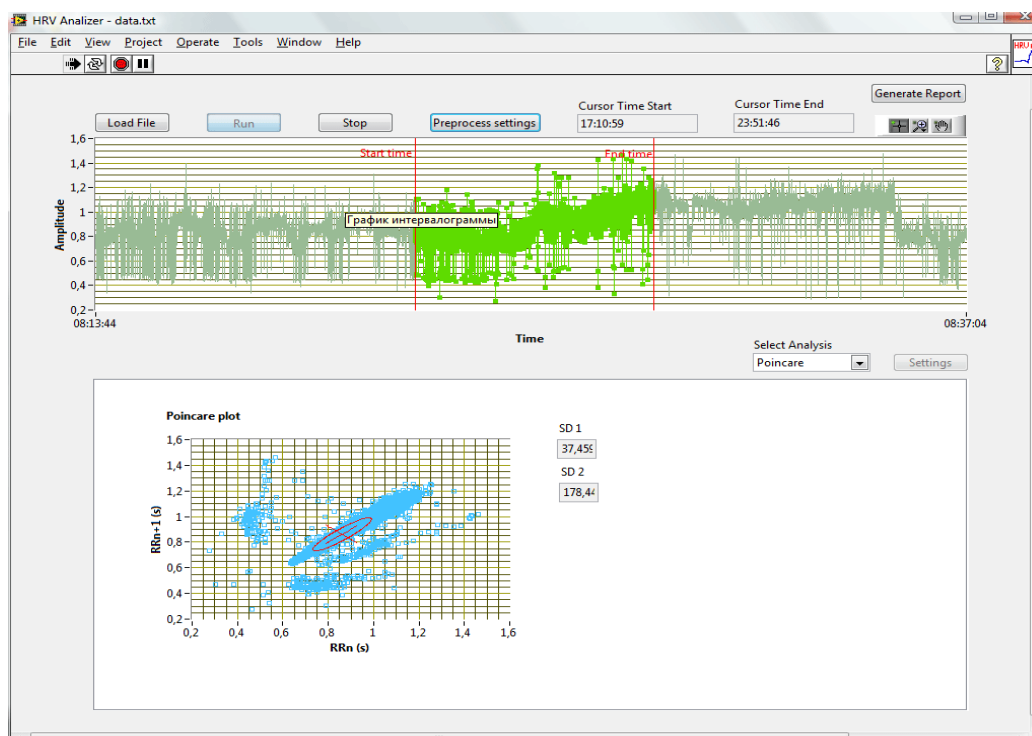


Fig. 1 The interface of software (analysis of heart rate variability using methods of Lorentz plot)

## CONCLUSIONS

The above estimates describe various aspects of complex behavior of the cardiovascular system. Therefore, they represent of interest investigation of their values and comparing and mutual correlation, to find the most convenient method of estimation of complexity of behavior of the cardiovascular system. The successful solution of this problem will provide a quantitative assessment of the regulatory provisions of the human body.

The software developed in this work can be used to automate the calculation method of nonlinear analysis as well as to found the basis for the development of expert system evaluation of the functional state of the human body.

The implementation and, in a perspective, the methodic implementation is provided for groups of people with a risk of sudden death, and also for the overload regimes estimation in a group of practically healthy people. The method does not require load tests, and the observation of the state of human cardiovascular systems is realized in the mode of natural functioning. The main perspectives of implementation are: 'health medicine', sports medicine, control of organism response on high psycho-emotional and/or physical load, sudden cardiac death risk estimation.

## REFERENCES

1. Prigogine I., Nicolis G. *Self-Organization in Nonequilibrium Systems*. N.Y.: Wiley-Interscience, 1977.
2. Nicolis G., Prigogine I. *Exploring Complexity*. N.Y.: W.H. Freeman, 1989.
3. Usupov R., Polonnikov R. *Telemedicine – new information technology in XXI century*. Sankt-Peterburg. 1998.
4. Cohen M.E., Hudson D.Z., Anderson M.F. The effects of drugs on chaotic blood flow analysis in an animal model. *Proc. Annu. Inf. Conf IEEE Eng. Med and Biol. Soc.*, Orlando, Fl.-New York, Vol. 13, Pt 5/5, pp. 2200-2201, 1991.
5. Goldberger A.L., Rigney D.R. *Sudden death is not chaos. Dynamic Patterns in Complex Systems*. Singapore: World Scientific, pp. 119-124, 1988.
6. Goldberger A.J., Rigney D.R., West B.J. Chaos and fractal in physiology. *Scientific Amer.*, N2, pp. 35-41, 1990.
7. Pincus S.M. Approximate entropy as a measure of system complexity. *Proc. Natl. Acad. Sci. USA*, 88, pp. 2297-2301, 1991.
8. Pincus S.M., Goldberger A.L. Physiological time-series analysis: What does regularity quantify? *Am J Physiol.*, 266 (Heart Circ Physiol), pp. H1643-H1656, 1994.
9. Ryan S.M., Goldberger A.L., Pincus S.M., Mietus J., Lipsitz L.A. Gender and age-related differences in heart rate dynamics: Are women more complex than men? *J Am Coll Cardiol.*, 24, pp. 1700-1707, 1994.
10. Ho KKL, Moody G.B., Peng C.K., Mietus J., Larson M.G., Levy D., Goldberger A.L. Predicting survival in heart case and control subjects by use of fully automated methods for deriving nonlinear and conventional indices of heart rate dynamics. *Circulation.*, 96 (3), pp. 842-848, 1997 (August).
11. Beckers F., Remaekers D., Aubert A.E. Approximate entropy of heart rate variability: validation of methods and application in heart failure. *Cardiovascular Engineering*, V.1, #4, pp. 177-182, 2001.

## NONLINEAR ROTATIONAL MODES IN MOLECULAR CHAINS

**Victor A. Lykah**<sup>1</sup>

National Technical  
 University "Kharkov  
 Polytechnic Institute",  
 Kharkov, Ukraine

**Eugene S. Syrkin**

Institute for Low  
 Temperature Physics and  
 Engineering, National  
 Academy of Sciences of  
 Ukraine, Kharkov, Ukraine

ABSTRACT

The continual nonlinear wave equations are derived for the rotational excitations of the molecules in wide energy interval: from equilibrium through rotational melting point to rotational disordered phase. Dispersion is considered to be small. Nonlinear oscillations are described by the coordinate along the "valleys" of the effective potential. Local normal coordinates are introduced. Linear equation describes waves of the stiffer normal mode. Nonlinear Sin-Gordon type equation is derived for waves of the softer mode in wide energy interval. The nonlinear wave solutions are analyzed.

### INTRODUCTION

An analytical description of the molecular rotor chain dynamics and thermodynamics is developed for low and high energy intervals [1]. The problem is to create theoretical description in the middle range of energies, especially in the vicinity of the point of orientational melting.

Adsorbates [2] or crystals with low-dimensional motives are real 1D and 2D structures. Chain models are necessary stage of investigation of dynamics and thermodynamics of crystals [3], nonlinear lattices [4]. Complexity of models even for 1D linear molecular chain requires some approximations: a model potential and 1D rotation and very hard translational potential, so translation vibrations are frozen and they can be neglected [2,5]. The potential energy of the molecular chain with realistic quadrupolar potential [5] can be written as [6-9]:

$$U_{ch} = \Gamma \left\{ a_0 N + \sum_{i=1}^N [a(\cos 2\phi_i + \cos 2\phi_{i+1}) + b \cos 2(\phi_i - \phi_{i+1}) + c \cos 2(\phi_i + \phi_{i+1})] \right\} \quad (1)$$

$$\Gamma = 3Q^2 / 4R^5; a_0 = 3/4; a = 5/4; b = 3/8; c = 35/8$$

Here  $Q$  is a quadrupolar moment of a molecule,  $R$  is a distance between molecules,  $\phi_m$  is an angle between the principal axis of a molecule and the chain axis. The chain energy (1) has minimum [6,7] for the molecules' alternating ordering (two sublattices) at the angles:

$$\phi_{2n} = \frac{\pi}{2} + \pi j; \phi_{2n+1} = \pi j; \quad \text{or} \quad \phi_{2n} = \pi j; \phi_{2n+1} = \frac{\pi}{2} + \pi j \quad (2)$$

where  $j, m, n = 0, \pm 1, \pm 2, \dots$ , index  $m = 2n$  ( $m = 2n + 1$ ) defines even (odd) site.

Lagrangian of the system is  $L = K - U$ . Here  $U$  and  $K = \frac{1}{2} \sum_{m=1}^N J_i \dot{\phi}_i^2$  are potential and kinetic energies

of the chain, a molecule has a moment of inertia  $J_i$  and an angle velocity  $\dot{\phi}_i$ . Then the Lagrangian variation yields system of equations for chain motion:

<sup>1</sup> Corresponding author. Email [lykah@ilt.kharkov.ua](mailto:lykah@ilt.kharkov.ua)

$$J_i \ddot{\phi}_i - 2\Gamma \{ 2a \sin \phi_i + b [\sin 2(\phi_i - \phi_{i-1}) + \sin 2(\phi_i - \phi_{i+1})] + c [\sin 2(\phi_i + \phi_{i-1}) + \sin 2(\phi_i + \phi_{i+1})] \} = 0 \quad (3)$$

Let us rewrite these equations for two sublattices that have different equilibrium state (2) in the long-wave limit [8] and introduce new variables for even ( $\phi$ ) and odd ( $\psi$ ) sites. More convenient for further analysis is following form of the equations and variables

$$\ddot{p} - 8\{a \sin p \cos m + c \sin 2p\} = 0 \quad (4)$$

$$\ddot{m} - 8\{a \sin m \cos p + b \sin 2m\} = 0$$

$$m = \phi - \psi; \quad p = \phi + \psi \quad (5)$$

Here dimensionless time and characteristic frequency are introduced:  $t \rightarrow \tau = t\omega_0$ ,  $\omega_0^2 = \Gamma / J_0$ ,  $J_i = J_0$ . Integral of the rotational motion for the molecular chain can be found [8] for the system (4):  $W_{ef} = W_k + W_p$ . The integral includes "kinetic"  $W_k$  and "potential"  $W_p$  contributions:

$$W_k = \frac{1}{2}(\dot{p}^2 + \dot{m}^2); \quad W_p = 4[2a \cos p \cos m + b \cos 2m + c \cos 2p] \quad (6)$$

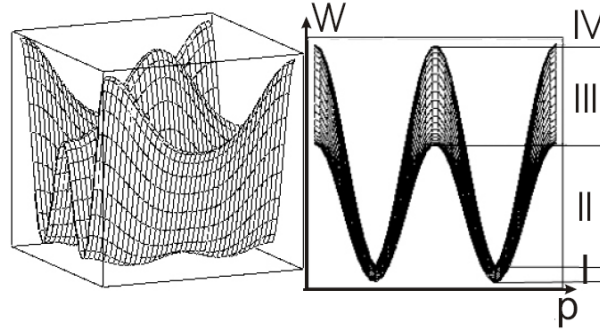


Fig. 1. The potential relief  $W_p$  in a quadrupolar molecular chain. (left) 3D image. (right) View along a valley. (I) Ordered phase. (II) Phase of correlated movements when  $p$  is finite,  $m$  is infinite. (III) Phase of correlated movements when both  $p$  and  $m$  are infinite. (IV) Completely disordered phase.

The rotational excitations demonstrate strong anisotropy in the angle space, easy directions ("valleys" on the potential) exist [8] (see fig. 1). Excitations that spread along "valleys" do not destroy correlation between molecules but a structural data can show rotational disorder (melting). We used the strong anisotropy ('valleys') and the normal modes to split equations for linear and nonlinear (softer mode) molecular chain oscillations [9]. Nonlinear Schrodinger equation was derived for the softer mode, its wave solutions were obtained.

In the present work, the continual nonlinear wave equations are derived for the rotational excitations of the molecules with quadrupolar interaction in wide energy interval: from equilibrium through rotational melting point to disordered phase. Nonlinear oscillations are described by the coordinate along the "valleys". Local normal coordinates are introduced. Linear equation describes waves of the stiffer normal mode. Sin-Gordon equation is derived for the softer mode in wide energy interval, their wave solutions are analyzed.

## 1. DERIVATION OF THE CONTINUAL EQUATIONS FOR AN INHOMOGENEOUS CHAIN.

The system of equations (3) is a strongly nonlinear and differential-difference. Let us rewrite these equations for two sublattices which have different equilibrium state (2), and introduce new variables for even ( $\phi_{2m}$ ) and odd ( $\phi_{2m+1}$ ) sites:

$$\begin{aligned}
& \ddot{\varphi}_i - 2\{2a \sin \varphi_i + b[\sin 2(\varphi_i - \psi_{i-1}) + \sin 2(\varphi_i - \psi_{i+1})] + \\
& + c[\sin 2(\varphi_i + \psi_{i-1}) + \sin 2(\varphi_i + \psi_{i+1})]\} = 0 \\
& \ddot{\psi}_{i+1} - 2\{2a \sin \psi_{i+1} + b[\sin 2(\psi_{i+1} - \varphi_i) + \sin 2(\psi_{i+1} - \varphi_{i+2})] + \\
& + c[\sin 2(\psi_{i+1} + \varphi_i) + \sin 2(\psi_{i+1} + \varphi_{i+2})]\} = 0
\end{aligned} \tag{7}$$

Here the new variables for even ( $\varphi_{2m}$ ) and odd ( $\varphi_{2m+1}$ ) sites are introduced. Orientation difference in the same sublattice is distinguished by account of a site number.

Let us introduce more convenient variables instead of (5) to account the sites difference:

$$m_i = \phi_i - \psi_{i+1}; p_i = \phi_i + \psi_{i+1} \tag{8}$$

With purpose to organize these variations let us find sum (for  $p$ ) and difference (for  $m$ ) of equations (7), then write expansion for variables  $\phi$  and  $\psi$  around values which form  $p_i$  and  $m_i$ . After grouping we obtain the continual variables  $p \equiv p_i$  and  $m \equiv m_i$ . Then we hold the lowest derivations (no more than the second derivation or multiplication of the first ones). As a result the system of dynamical nonlinear continual differential equations can be yielded:

$$\begin{cases} \ddot{p} = 2\{4a \sin p \cos m - 4b[(m' + p'') \cos 2m - 2m' p' \sin 2m] + \\ \quad 4c[(m' + p'') \cos 2p + (1 - m'^2 - p'^2) \sin 2p]\} \\ \ddot{m} = 2\{4a \sin m \cos p + 4b[(p' + m'') \cos 2m + (1 - m'^2 - p'^2) \sin 2m] - \\ \quad 4c[(p' + m'') \cos 2p - 2m' p' \sin 2p]\} \end{cases} \tag{9}$$

Here we introduce dimensionless coordinate:  $\xi = x/R_0$ . Derivations are  $p' = \partial p / \partial \xi$  and  $p'' = \partial^2 p / \partial \xi^2$ , and the same formulae for  $m, m'$ . We suppose that derivations are relatively small:  $p'' \ll p' \ll p$ ;  $m'' \ll m' \ll m$ ;  $p \ll m$ . The attractive feature of the system (9) is symmetry on the coordinates  $p, m$  and the interaction parameters over pair exchange:

$$p, c \longleftrightarrow m, b \tag{10}$$

Let us discuss general properties of the yielded system of equations (9). It was obtained in continuum approximation and describes any nonlinear time-dependent processes in the molecular chain. The system has too complicated construction as over the generalized angle coordinates  $p$  and  $m$  as their derivations. In comparison with Landau-Lifshits nonlinear equations that describe ferromagnets [10] the space derivations are distributed by especially complicated way: dispersion and nonlinear terms are entangled. Integral of the system (9) is.

$$\frac{1}{2}(\dot{p}^2 + \dot{m}^2) + 4[2a \cos p \cos m + b(1 + p'^2 - m'^2) \cos 2m + c(1 - p'^2 + m'^2) \cos 2p] = C \tag{11}$$

This integral has the same symmetry (10) as the original system of the equations. The integral includes only the first derivations in the second powers. This integral can be applied to investigation of any nonlinear processes in the molecular chains with alternating ordering.

## 2. LOCAL NORMAL COORDINATES AND VARIABLES SPLITTING.

The integral (11) is not enough for integration of the considered two-dimensional system in stationary case. We need two integrals of motion and a set of boundary conditions [11]. Nevertheless there is another way to reach integrability. It is the way of the probe orbits [12] when two variables are connected by some kind of dependence and energy minimum is reached under some parameters' value. Generally, integration in spaces with dimension more than 1 requires excluding of extra coordinates. Choice of an orbit is many variant procedure even for power potential [12]. Here we have more complicated case when potential consist of trigonometric functions of the variables. Therefore

we have to elect some path in the p-m plane that seems to provide minimum of the inhomogeneous behavior of the interacting molecular system. This way is not better or worse in comparison with construction of a domain wall in ferromagnetic materials [10] in the cases of Bloch (magnetic moment rotates in the DW plane) or Neel (magnetic moment rotates at right angle to the DW plane).

According to topological analysis in long-wave case [8] the potential relief of 1D chain has very low narrow valleys. We propose the orbit which coincides with the valley bottom, see Fig.2. General equation for the 'valley's' bottom can be obtained from (4):

$$\cos p = -\beta \cos m; \beta = \frac{a}{2c} = \frac{1}{7} \quad (12)$$

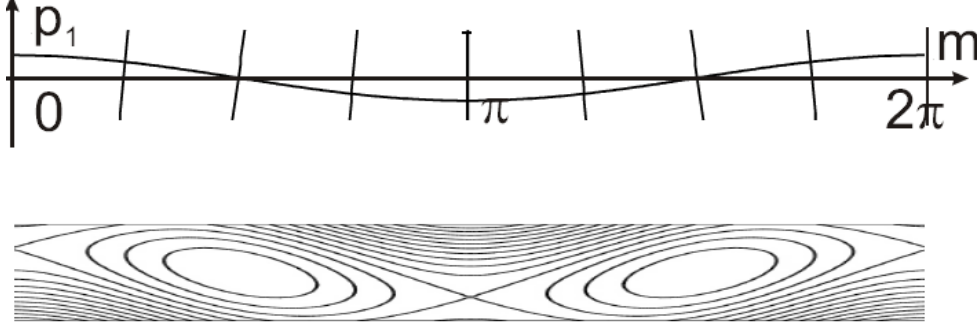


Fig.2. Local normal coordinates (curve close to a sinusoid and rectilinear) and relief of a bottom of a valley. The scales on axis are identical.

Accounting values of  $a$  and  $c$  we have  $|\cos p| \leq \beta \ll 1$ . So condition  $p = \pi/2 + \pi j = const$  is satisfied at any 'valley's' bottom. For  $b$  and  $c$  evaluation gives  $b/c = 3/35 \ll 1$ . Other small terms contain  $\alpha = a^2/4c^2 \ll 1$ . Relation (12) allows rewrite terms containing variable  $p$  through  $m$ . So the final form of the system (9) of differential equations can be written as:

$$\begin{aligned} 8cm'' - \ddot{m} + 8(b - 4\alpha c)\sin 2m &= 0 \\ \ddot{p}_1 + 16cp_1 + 8cp_1'' &= 8\{\pm a \cos m - m'(c + b \cos 2m)\} \end{aligned} \quad (13)$$

After the variable transformation we obtain dimension form of equation ( $c_0$  and  $\lambda_0$  are characteristic velocity and length) which coincides with canonical sin-Gordon equation [13]:

$$\begin{aligned} \frac{\partial \varphi^2}{\partial x^2} - \frac{1}{c_0^2} \frac{\partial \varphi^2}{\partial t^2} &= \frac{1}{\lambda_0^2} \sin \varphi; \quad \varphi = 2m - \pi \\ \lambda_0^2 &= \frac{cR_0^2}{2(b - 4\alpha c)}; c_0^2 = 8c\omega_0^2 R_0^2 \end{aligned} \quad (14)$$

### 3. THE CHAIN DYNAMICS IN THE MIDDLE ENERGY INTERVAL.

Equation (14) has two big classes of stationary solutions  $\varphi(\theta)$ ,  $\theta = x - x_0 - Vt$  which move with velocity  $V$  [13]. 1) spacelike  $1 - V^2/c_0^2 > 0$ ; 2) timelike  $1 - V^2/c_0^2 < 0$ . They are related to the magnetic (spacelike) or electric (timelike) states in a Josephson contact (or the spacelike or timelike intervals in the relativity theory).

For the spacelike solutions the equation (14) has integral of motion  $E$ ; and for the timelike solutions these equations have another integral of motion  $B$ :

$$\left(1 - \frac{V^2}{c_0^2}\right)(\varphi')^2 = \frac{2}{\lambda_0^2}(E - \cos \varphi); \quad E \geq -1 \quad (15)$$

$$\left(\frac{V^2}{c_0^2} - 1\right)(\varphi')^2 = \frac{2}{\lambda_0^2}(B + \cos \varphi); \quad B \geq -1 \quad (16)$$

The integral  $B$  in (16) has meaning of mechanical energy of a reversible pendulum with length  $l=1$ ,  $\varphi$  has meaning of angle of vertical deflection of a pendulum rod. At  $-1 < B < 1$  the pendulum oscillates near equilibrium position  $\varphi = 0$ . At  $B > 1$  the pendulum rotates around the suspending point, the rotation direction is topological invariant  $\sigma = \pm 1$ . The same is true for the integral of motion  $E$ . The only difference is equilibrium position  $E = -1$  at  $\varphi = \pi$ . At  $-1 < E < 1$  the pendulum executes an oscillating movement near equilibrium position.

### 3.1 The spacelike solutions ( $V < c_0$ )

At  $|E| < 1$  stationary solution of (14) describes space oscillations near equilibrium position:

$$m(\theta) = \frac{\pi}{2} + \sin^{-1} [dn(\xi_v, k)]; \quad \xi_v = \frac{\theta}{\lambda_0 \sqrt{1 - V^2 / c_0^2}}; \quad \theta = x - Vt \quad (17)$$

Here  $dn(\xi_v, k)$  is Jacobi elliptic function with elliptic module  $k$  which is defined by relation  $k^2 = (E + 1) / 2$ ;  $0 \leq k \leq 1$ . In the limit case  $k \rightarrow 0$  the periodic function transforms into small oscillations. In the limit case  $k \rightarrow 1$  the periodic function transforms into solitary peak.

At  $E=1$  stationary solution (14) describes domain wall between two domains (2):

$$m(\theta) = \frac{\pi}{2} + 2 \arctan[\sigma \exp \xi_v] \quad (18)$$

### 3.2 The timelike solutions ( $V > c_0$ )

At  $|B| < 1$  continual equation of motion (14) due integral (16) has periodic stationary solution which corresponds to time oscillations near equilibrium position:

$$m(\theta) = \frac{\pi}{2} + \cos^{-1}[dn(\xi_v, k)]; \quad \xi_v = \frac{\theta}{\lambda_0 \sqrt{V^2 / c_0^2 - 1}} \quad (19)$$

Here elliptic module  $k$  is defined by relation  $k^2 = (B + 1) / 2$ ;  $0 \leq k \leq 1$ . In the limit  $k \rightarrow 0$  one has small oscillations. In the limit  $k \rightarrow 1$  one has periodic peaks.

At  $B=1$  stationary solution describes domain wall between time domains:

$$m(\theta) = 2 \arctan[\exp \sigma \xi_v] \quad (20)$$

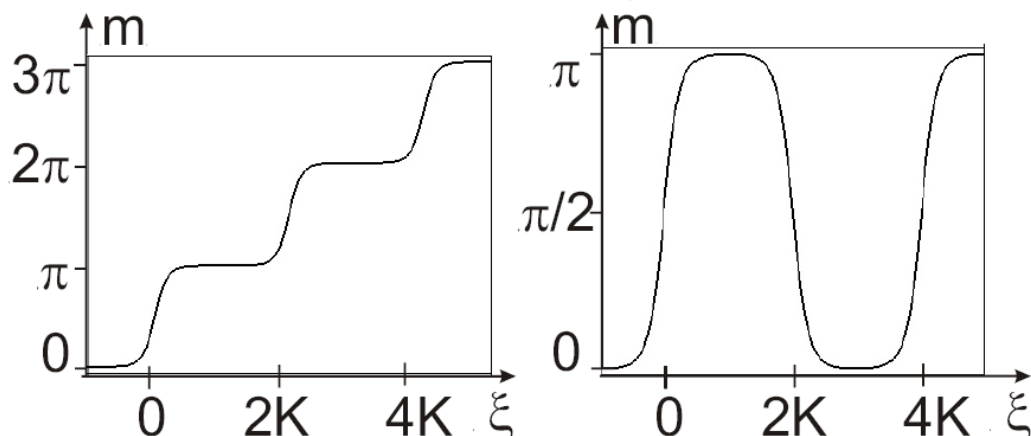


Fig.3. Angles of the molecules orientation in the chain for the timelike solutions (right) according (19) at  $|B| < 1$  (oscillations) and (left) according (20) at  $B > 1$  (rotation,  $\sigma = +1$ ). Periodic structures at  $k=0.99$  i.e.  $B=0.996$  and  $B=1.004$ .

In dependence on topological charge  $\sigma = \pm 1$  this solution give kink ( $\sigma = +1$ ,  $m(-\infty) = 0$ ,  $m(+\infty) = \pi$ ) or antikink ( $\sigma = -1$ ,  $m(-\infty) = \pi$ ,  $m(+\infty) = 0$ ) shown in Fig.3.

At  $B > 1$  continual equation of motion also has periodic stationary solution (time rotation). The solution can be written in following forms:

$$m(x) = \frac{\pi}{2} + \sin^{-1}[\sigma \operatorname{sn}(\xi_v, k)]; \quad \xi_v = \frac{\theta}{k\lambda_0\sqrt{V^2/c_0^2 - 1}} \quad (21)$$

Here  $\operatorname{sn}(\xi_v, k)$  is Jakobi elliptic function with elliptic module  $k$  defined by relation  $k^2 = 2/(B+1)$ ;  $0 \leq k \leq 1$ . In the limit  $k \rightarrow 0$  one has homogeneous rotation of the molecules in the chain. In the limit  $k \rightarrow 1$  the periodic set of kinks (20) arises as in Fig.3.

## CONCLUSIONS

The nonlinear excitations of the molecular chain with quadrupolar interaction are considered in the energy range covering the point of the orientational melt. We derive the dynamic continuum equations for the two-sublattice chain with arbitrary nonlinearity and small dispersion. The symmetry of the system of the equations and its integral are found. We used previously found a strong anisotropy of molecular rotation on the angles plane, the 'valley' of the effective potential. To integrate the equations on the plane the trial trajectory (orbit) was introduced, it coincides with the bottom of the valley. Construction of the normal curvilinear coordinates on the plane makes it possible to uncouple the equations for linear and nonlinear vibrations. Linear oscillations are perpendicular to the valley and meet more rigid subsystem. Nonlinear oscillations are along the valley and correspond to a soft subsystem, so unstable state is easily achieved. For the nonlinear subsystem the sine-Gordon equation is derived, one allows to describe the vibration modes around the equilibrium position in the ordered phase and the transition states. Scope of applicability of the description extends from the point of equilibrium to the vicinity of the upper saddle point, i.e. within the valley effective potential (phases I and II in Figure 1). This range of energies in the order of magnitude larger than the region of existence of orientationally ordered phase. To date, dynamical models of molecular chains described only states with small or large energies [1].

## REFERENCES

- [1] S. Lepri, R. Livi and A. Politi. *Phys. Rep.* 377, 2003.
- [2] D.Marx, H.Wiechert. Ordering and phase transitions in adsorbed monolayers of diatomic molecules. I.Prigogine and Stuart A.Rice eds. *Adv. Chem. Phys., XCV, John Wiley & Sons, USA 1996*, pp. 213-394.
- [3] M. Born, Kun Huang. *Dynamical Theory of Crystal Lattices*. Claridon Press, Oxford, 1954
- [4] M. Toda, *Theory of Nonlinear Lattices*. Springer-Verlag, Berlin, 1981.
- [5] Yu. A. Freiman, V.G.Manzhelii. *Cryocrystals*. Woodbury, NY, 1996.
- [6] V. A. Lykah, E. S. Syrkin, Rotational oscillations of molecular chain with quadrupolar interaction. *Physica Status Solidi (C)*, **1**, pp. 3052-3056, 2004.
- [7] V. A. Lykah, E. S. Syrkin, Small rotational oscillations of molecular chain with quadrupolar interaction. *Phys.~Low-dimension~Structures*. 7/8, pp. 103-116, 2004.
- [8] V. A. Lykah, E. S. Syrkin, Phase transitions in the adsorbed molecular chains. *Central European Physics Journals. CEPJ*, **3**, N1, pp. 61-68, 2005.
- [9] V. A. Lykah, E. S. Syrkin. Nonlinear rotational waves in a molecular chain. *J. Phys.:Condens.Matter*, **20**, 224022, 2008; V. A. Lykah, E. S. Syrkin. Rotational normal modes and nonlinear waves in molecular chain. Proc. of the Second Int. Conference «Nonlinear dynamics», Kharkov, September, pp.192-197, 2007.
- [10]A. Hubert, R. Schafer. *Magnetic domains*. Springer, Berlin, 1998.
- [11]E. Kamke. *Handbook of Ordinary Differential Equations*. Nauka, Moscow, 1971 (in Russian).
- [12]R. Rajaraman. *Solitons and Instantons*. North-Holland, New-York, Oxford, 1982.
- [13]A. S. Davydov, *Solitons in molecular systems*. Naukova dumka, Kiev, 1984.

**METHOD OF DETUNING FROM RESONANCE MODES FOR ROTORS IN ACTIVE  
 MAGNETIC BEARINGS WITH NONLINEAR FORCE CHARACTERISTICS**

**G. Martynenko**<sup>1</sup>  
 National Technical  
 University "Kharkiv  
 Polytechnic Institute",  
 Kharkiv, Ukraine

ABSTRACT

In the report, the investigator offers a method of reducing the amplitude of vibrations of turbo machinery rotors with passive and active magnetic bearings (AMB) in resonances and resonance zones corresponding to one of the critical speeds from zero to working rotational speeds. The method is based on the ability to vary the nonlinear force characteristic and the damping properties of AMB by changing the electric parameters of the electromagnet circuits.

**INTRODUCTION**

One of the methods of reducing vibrations in rotor machines in different applications is to use the self-centering rotor effect, which is manifested during supercritical operation [1]. The model in Fig. 1 illustrates the physical essence of this phenomenon. It implies that, when a unbalanced rotor reaches the critical rotational speed  $\omega$ , the direction of deflection  $y$  and eccentricity  $e$  become opposite, the centre of mass  $C$  is displaced and occupies a position between the geometric centre  $O$  and axis of rotation  $O^*z$  (Fig. 1a). Further rotational speed increasing makes the absolute value of shaft deflection approach eccentricity  $e$  (Fig. 1b), i.e. the centre of mass approaches the axis of rotation. For rotors in rigid supports, the value of the first critical velocity is comparatively big. In this case, the zone of working rotational speeds can be located at an insufficient distance from the critical speed one to reduce rotor vibration amplitudes (Fig. 1b).

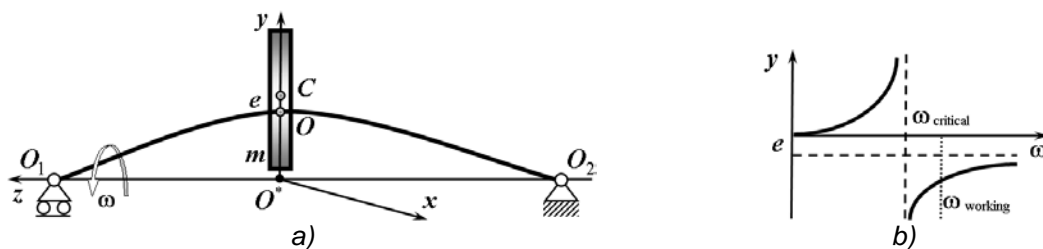


Fig. 1 Rotor model (a) and shaft deflection vs. rotational frequency (b)

In practice, one of two methods is used to offset the rotor machine from resonance modes. The first method implies displacement of increased vibration zones in the increasing direction so that the entire range of working rotational speeds is located before the first critical speed (rigid rotor). The second method implies machine operation in supercritical areas (a flexible rotor). In this case, it is necessary to reduce the values of the first critical rotational speed, i.e. the increased vibration zone threshold, and at the same time ensure safe transition through critical speeds in the range up to maximal working rotational speeds [1]. This is achieved by reducing the stiffness of the "rotor-support" dynamical system. To do this, the rotors are mounted in flexible supports (FS) with specified stiffness [1]. The vibration amplitudes can be reduced with the help of elastic-dampening supports (EDS) by introducing artificial dampeners into their design. This will decrease the amplitudes of resonance vibrations; however, machine efficiency will drop.

Fig. 2 shows rotor vibration modes in different supports corresponding to the first three critical

<sup>1</sup> Corresponding author. Email [gmartynenko@kpi.kharkov.ua](mailto:gmartynenko@kpi.kharkov.ua)

rotational speeds. For extremely yielding supports, the rotor passes the first two critical speeds with formation of cylindrical and conical precession (Fig. 2a). A curved vibration mode corresponds to the third critical speed.

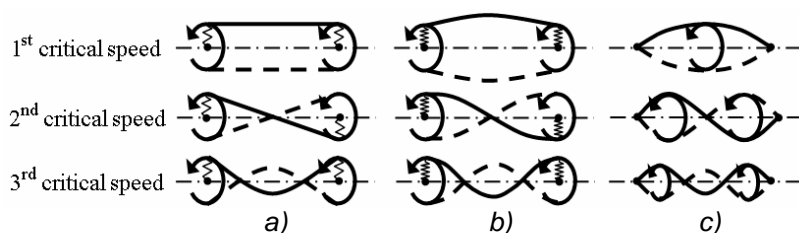


Fig. 2 Lateral vibration modes of rotors in different supports:  
a) extremely yielding, b) yielding, c) rigid

The most common vibrations of rotors are those caused by static and moment imbalance. The amplitudes of such vibrations can be reduced dramatically by utilising the properties of a stiff rotor in an ES [1]. However, there are also other kinds of hazardous vibrations directly related to using mechanical ES. They are autovibrations caused by the properties of the oil film in sleeve bearings; different kinds of nonlinear vibrations related to nonlinearity of the force characteristics of roller bearings as preloaded systems, and others.

When a rotor is mounted in an ES, troubles can occur during rotor acceleration and its passing through critical speeds when the rotor vibrates as a rigid body [1]. The paper offers a method of passing such increased vibration zones by a short-time change of ES stiffness during rotor acceleration or its rundown, i.e. stiffness control as a function of rotational speed. Then the ES force characteristics will be adaptive, allowing for offsetting the “rotor in ES” system from critical speeds over the entire range from zero to working rotational speeds of the rotor machine. Active magnetic bearings (AMB) are suggested to be used as an ES with variable stiffness. In these bearings, rotor position stability is ensured by a control system (CS) with negative feedback [2]. The force characteristics of these bearings, in contrast to those of mechanical ES, can change by varying the electric parameters (voltages or control currents) [3]. By changing the values of active resistances in AMB circuits, one can control damping by increasing it only in the resonance zones. In this case, AMB will be an EDS with variable parameters.

Yet another feature of AMBs to be mentioned is the nonlinear dependence of their force characteristics on displacement of rotor support sections (i.e. on the gap between the journal and stator poles) as well as on the currents in the pole coil windings. They change as a function of rotor position defined by the control system according to a preset law.

## 1. DESCRIPTION OF THE METHOD OF OFFSETTING A ROTOR IN AN AMB FROM CRITICAL ROTATIONAL SPEEDS DURING ACCELERATION AND RUNDOWN

The suggested method of offsetting the rotor from critical speeds (passing the resonances) during acceleration or rundown implies that the control system (CS) changes rapidly the stiffness and/or damping parameters of magnetic bearings. Besides having position sensors, the CS also has an angular speed sensor [3]. Fig. 3 is the structural diagram of a system version for a radial AMB. The stiffness properties of the AMB can be varied within a certain range of angular speeds by changing the values of control voltages  $u_{c1}, \dots, u_{c4}$ . This results in a change of average currents  $i_{c1}, \dots, i_{c4}$  (bias currents) in the windings of electromagnets and allows changing the force characteristics of the support [4]. The AMB damping properties can be increased for a short time by increasing the active resistances  $r_{c1}, \dots, r_{c4}$  in the circuits of the electromagnets in the zone of rotor critical rotational speeds. This will reduce the amplitudes of resonance vibrations [4].

The algorithm of operation of the control system suggested assumes prior selection of two (or more) operating conditions. In the first condition (the design one), the AMB force characteristics should ensure required motion stability of the supercritical rotor in a certain range of angular velocities spanning the working rotational speeds. The second operating condition assumes operation with greater (lesser) support stiffness as compared to the first case. The stiffness should be such that the first critical speeds of the rotor be higher (lower) as compared to the system operating in the first (design) condition. Rotor acceleration is initiated in the first operating condition. Then, as the rotor approaches the critical zones, the operating condition is switched to the second one, and when the resonance areas of the first operating condition have been passed, the operating condition is switched back to the first (design) one. If there are several resonances prior to onset of working rotational speeds, successive switching from the first operating condition to the second one and vice versa will

exclude completely vibrations with increased amplitudes. During rotor rundown, the process of resonance passing is similar. In general, there can be several such operating conditions. In this case, switching between them should take place according to a predefined program.

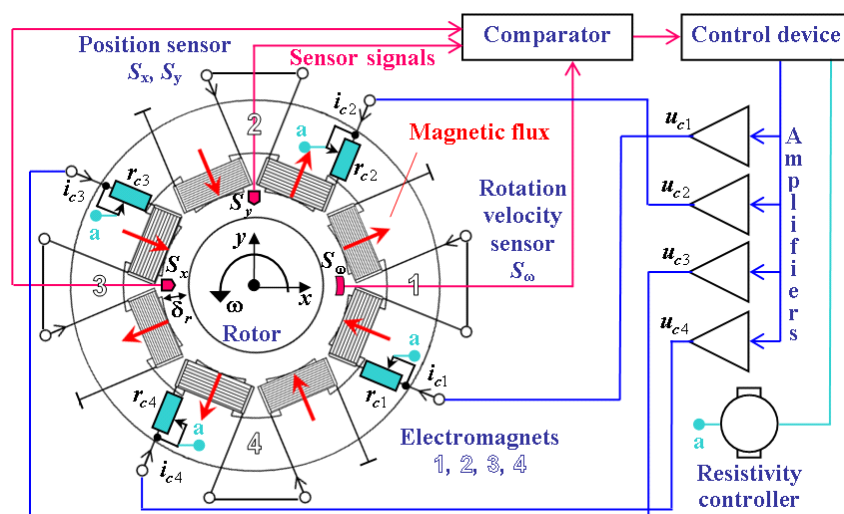


Fig. 3 Structural diagram of a CS for controlling rotor motion in a radial AMB with controlled stiffness and damping parameters

Fig. 4 is a schematic presentation of how the supercritical rotor reaches working rotational speeds and passes through the first resonance (critical speed). The diagram shows the dependence of the amplitude of the first forced vibrations harmonic ( $A_1$ ) on the frequency ( $\omega$ ) of the harmonic driving force for a stiff AMB force characteristic.  $A_1'$  and  $A_1''$  designate the resonance curves for different stiffness values, which are ensured by different values of average currents or bias currents. The resonance curve  $A_1''$  corresponds to bigger stiffness values, and curve  $A_1'$  is the amplitude-frequency response (AFR) of the design operating condition. The dashed lines in Fig. 4 are skeleton curves  $\omega_0'$  and  $\omega_0''$  corresponding to different stiffness values. Solid lines designate the resulting system AFR obtained when using the method proposed. It is implemented by passing from one resonance curve  $A_1'$  to another one  $A_1''$  by changing the stiffness of magnetic bearings in a preset range  $[\omega_{1min}, \omega_{1max}]$ . In this case, the maximum values of vibration amplitudes  $A_{1max}$  are significantly smaller than the maximums  $A_{1max}'$  and  $A_{1max}''$  of both resonance curves  $A_1'$  and  $A_1''$ .

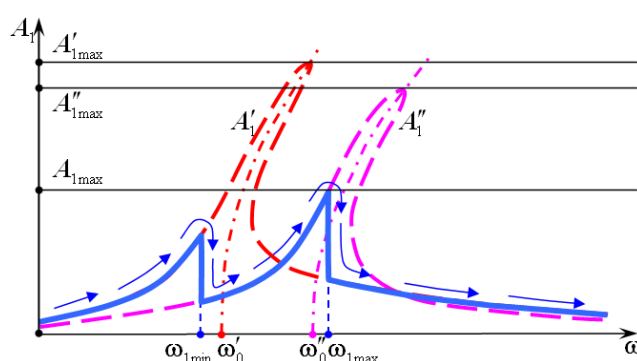


Fig. 4 Schematic presentation of the AFR of a rotor in an AMB with controlled stiffness

The vibration amplitude near the resonance can also be reduced by increasing the damping in the system. This is achieved by increasing the active resistances in the circuits of the coils of the AMB electromagnets (Fig. 4, curve  $A_1''$ ) [4]; however, this extends the resonance zone and results in additional energy consumption.

## 2. METHOD VALIDATION WITH NUMERICAL SIMULATION

To validate the functionality of the method suggested, a series of numerical experiments for a model of a magnetic suspension of a small-size high-speed rotor were conducted. Such a rotor suspension scheme can be suggested for application, for example, in rotors of expansion-compression units.

## 2.1 Mathematical model of the dynamics of a rigid rotor in magnetic bearings

Fig. 5 visualises the design model of a combined magnetic suspension, where  $O^*xyz$  are fixed right-hand Cartesian coordinates;  $O_1(x_1, y_1, z_1), O_2(x_2, y_2, z_2)$  are centres of support sections of the rotor in radial magnetic bearings in permanent ring magnets (MBPRM) located at distances  $l_1, l_2$  from the centre of mass  $C$ ;  $O_3(x_3, y_2, z_3)$  is the centre of the rotor support section in the axial AMB (disk centre of mass);  $u_{c1}, u_{c2}$  are control voltages applied across the windings of the axial AMB;  $i_{c1}, i_{c2}$  are currents in the windings of the axial AMB;  $e, \gamma$  are linear and angular eccentricities; and  $\omega$  is rotor angular speed.

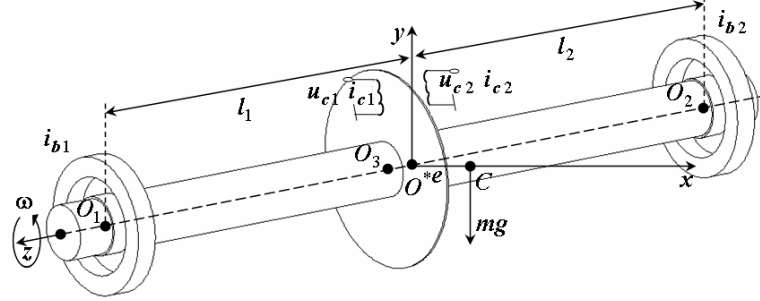


Fig. 5 Design model of a rotor in AMB with controlled stiffness

This combined magnetic suspension uses magnetic bearings shown in Fig. 6. The radial supports here are self-aligning MBPRM mounted in opposition to compensate for the axial force introduced by them. Their additional bias winding serves for implementing stiffness control. The axial support is a double-side action AMB. Fig. 6a shows the radial magnetic forces in MBPRM vs. rotor radial displacement at different values of parameters:  $F_{M0}$  at  $i_{b1,2}=0$ ,  $F_{M1}$  at  $i_{b1,2}=\pm 10$  A ( $w=150$ ),  $F_{M2}$  at  $i_{b1,2}=\pm 3.5$  A ( $w=500$ ) and  $F_{M3}$  at  $i_{b1,2}=\pm 1.3$  A ( $w=1,500$ ), where  $w$  is number of turns in windings [3]. Fig. 6b shows the axial magnetic forces vs. axial rotor displacement at different maximum voltage values  $U_0$  applied across AMB windings according to the preset control algorithm  $u_{c1}(z_3), u_{c2}(z_3)$  [3].

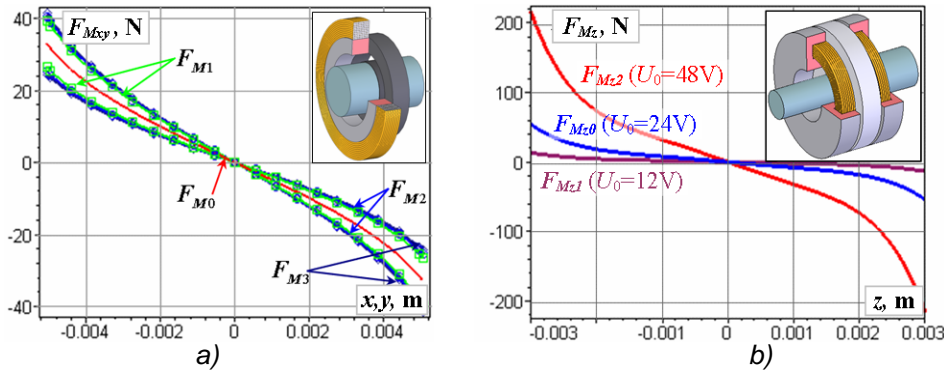


Fig. 6 Forces vs. displacements of rotor support sections in an experimental model: a) radial MBPRM with permanent magnets and an additional bias winding, b) double-sided action AMB

The dynamics of a rigid rotor in a combined magnetic suspension is described mathematically by a system of five differential equations, nonlinear with respect to generalised coordinates  $x_1, x_2, y_1, y_2, z_3$  and their time derivatives [5]:

$$\begin{cases} m_{11}\ddot{x}_1 + m_{12}\ddot{x}_2 + m_{13}\omega(\dot{y}_1 - \dot{y}_2) + b_{x1}\dot{x}_1 + f_{x1}(x_1, \dots, \ddot{z}_3) = F_{M_x}(x_1, y_1) + Q_{x1} + H_{x1}(t), \\ m_{22}\ddot{x}_2 + m_{12}\ddot{x}_1 - m_{13}\omega(\dot{y}_1 - \dot{y}_2) + b_{x2}\dot{x}_2 + f_{x2}(x_1, \dots, \ddot{z}_3) = F_{M_y}(x_1, y_1) + Q_{x2} + H_{x2}(t), \\ m_{11}\ddot{y}_1 + m_{12}\ddot{y}_2 - m_{13}\omega(\dot{x}_1 - \dot{x}_2) + b_{y1}\dot{y}_1 + f_{y1}(x_1, \dots, \ddot{z}_3) = F_{M_x}(x_2, y_2) + Q_{y1} + H_{y1}(t), \\ m_{22}\ddot{y}_2 + m_{12}\ddot{y}_1 + m_{13}\omega(\dot{x}_1 - \dot{x}_2) + b_{y2}\dot{y}_2 + f_{y2}(x_1, \dots, \ddot{z}_3) = F_{M_y}(x_2, y_2) + Q_{y2} + H_{y2}(t), \\ m\ddot{z}_3 + b_{z3}\dot{z}_3 + f_{z3}(x_1, \dots, \ddot{z}_3) = F_{M_z}(z_3) + Q_{z3} + H_{z3}(t); \end{cases} \quad (1)$$

where  $m_{ij}$  are inertia and gyroscopic coefficients including rotor mass  $m$  and moments of inertia (equatorial  $J_1$  and polar  $J_3$  ones);  $b_{x1, \dots, z3}$  are viscosity coefficients;  $f_{x1, \dots, z3}$  are nonlinear terms of

inertia and potential field forces whose order with regard to generalised coordinates and their derivatives is comparable with that of magnetic forces dependencies (Fig. 6)  $F_{M_y}(x, y)$ ,  $F_{M_x}(x, y)$ ,  $F_{M_z}(x, y, z)$ ;  $Q_{x_1, \dots, z_3}$  are other generalised forces, in particular, force of gravity;  $H_{x_1, \dots, z_3}(t)$  are external time-dependent disturbing forces caused, in particular, by nonequilibrium.

## 2.2 Vibrograms of rotor vibrations for different rotational speeds

Computational studies were conducted for a laboratory model of a combined magnetic suspension of a rotor with the following parameters [5]:  $m = 2.5 \text{ kg}$ ,  $l_1 = 106.75 \text{ mm}$ ,  $l_2 = 176.75 \text{ mm}$ ,  $J_1 = 0.0107386 \text{ kg}\cdot\text{m}^2$ ,  $J_3 = 0.003377 \text{ kg}\cdot\text{m}^2$ ,  $\delta_r = 5.5 \text{ mm}$ ,  $\delta_a = 3 \text{ mm}$ ,  $b_{x_1 \dots y_2} = 2.325 \text{ kg}\cdot\text{s}$ ,  $e = 0.06 \text{ mm}$ ,  $\gamma = 0.003 \text{ rad}$ , and dependencies of forces  $F_{M_0}$  and  $F_{M_{z_0}}$ . The Runge-Kutta fifth-order method was used for numerically solving the system of motion equations (1) for angular speed values in the range of  $0-40\pi$  with a step of  $\pi/2 \text{ rad/s}$ . For each angular speed value, the stationary solution was analysed spectrally using the Fast Fourier Transform (FFT). Fig. 7 visualises the results of such order analysis in the form of spectrograms of generalised coordinates, where  $f$  is spectrum frequency,  $\omega$  is angular speed (rotational speed), and  $A$  is amplitude of the respective generalised coordinate.

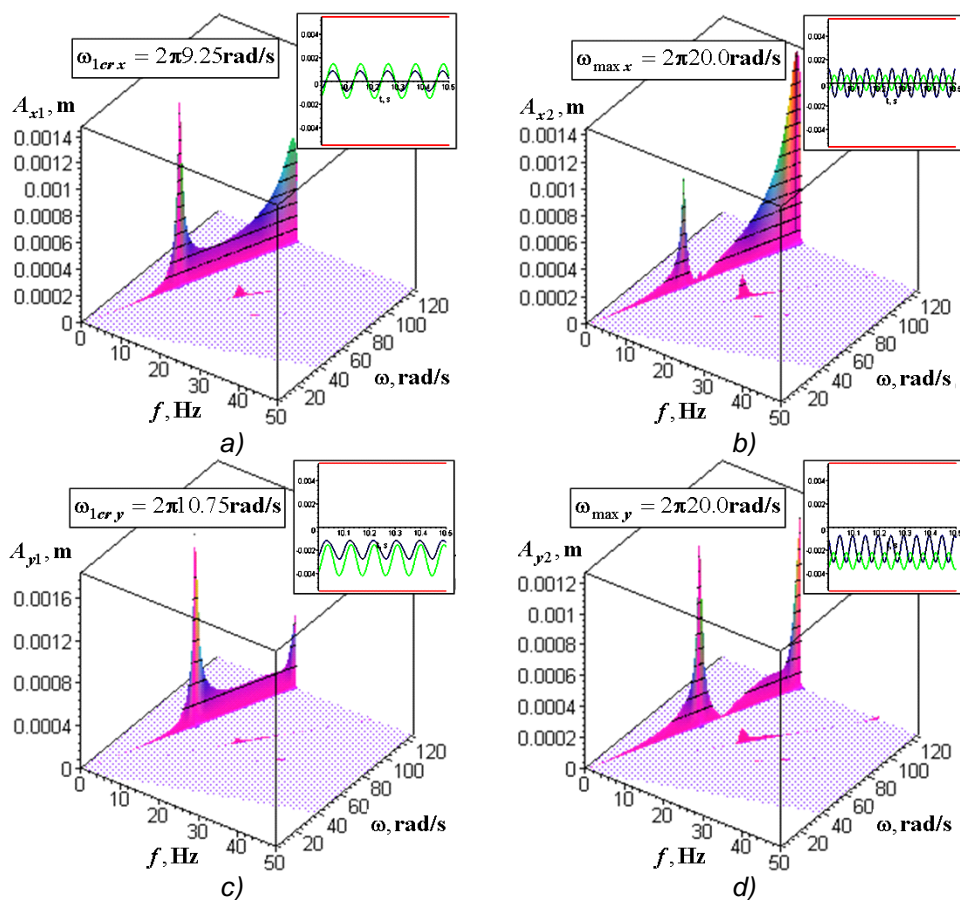


Fig. 7 Results of order analysis of rotor motion vibrograms with FFT expansion into harmonics in the direction of generalised coordinates: a)  $x_1$ , b)  $x_2$ , c)  $y_1$ , d)  $y_2$

Besides visualising the results of order analysis, the graphs show vibrograms corresponding to the first resonance mode and the end of the calculation range. It was found that the rotor motion in the first critical speed zone is of the direct cylindrical precession type (Fig. 2a). Here, the resonances during vibration in the  $x$  and  $y$  directions are displaced as per angular speed by  $9.5 \text{ rad/s}$ . Besides, these vibrations differ by the presence of superharmonics (Fig. 7). At the end of the angular speed calculation range, there is a transition to the second resonance with occurrence of subharmonics, and the rotor motion corresponds to direct conical precession (Fig. 2a). All these phenomena are in agreement with experimental studies [5]. This confirms the adequacy of the mathematical model and the validity of numerical analysis results.

## 2.3 System amplitude-frequency responses

Fig. 8 shows the first harmonic amplitudes  $A_1$  vs. field frequency dependence for generalised

coordinates  $y_1$  (light dotted line) and  $y_2$  (dark solid line) under different CS operating conditions resulting from using the force characteristics of MBPRM and AMB: operating condition I,  $F_{M0}$  and  $F_{Mz0}$ , operating condition II,  $F_{M2}$  (at  $i_{b1,2} = +3.5A$ ) and  $F_{Mz1}$ , operating condition III,  $F_{M2}$  (at  $i_{b1,2} = -3.5A$ ) and  $F_{Mz2}$ . The amplitude frequency responses corresponding to these three operating conditions are shown, respectively, in Figs. 8a, 8b and 8c. The horizontal lines show the geometrically possible deflections with account of the static equilibrium position for each coordinate. The graphs also show the motion trajectories of the rotor radial support sections in the gap for three frequency values, viz. the  $x$  resonance, the  $y$  resonance and the range end.

The AF responses shown demonstrate the possibility of passing the first critical speed when the CS is operating in design condition I without significant amplitude growth by smooth shock-free switching from one operating condition to another one according to a predesigned program, e.g., I-III-II-I (Fig. 8d).

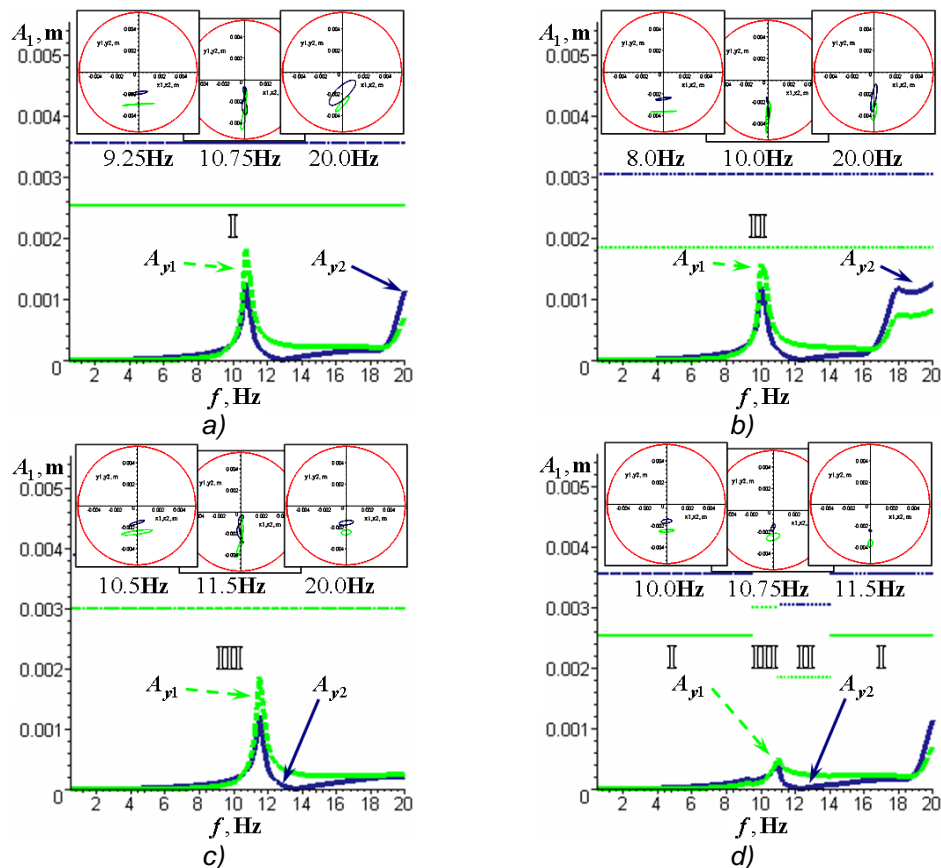


Fig. 8 Amplitude-frequency responses for first harmonic at different CS operating conditions: a) operating condition I, b) operating condition II, c) operating condition III, d) operating conditions I-III-II-I

## CONCLUSIONS

The paper shows that, by selecting the parameters of the CS of the AMB or MBPRM with a bias winding, one can ensure such force characteristics of magnetic bearings, which will prevent rotor operation in a resonance mode and in the resonance zone of any critical speed within zero to working rotational speeds. The described method of offsetting supercritical rotors from resonances and decreasing the amplitudes of resonance vibrations due to a short-time damping increase makes AMB a more preferable type of EDS as compared to other (mechanical) ones.

## REFERENCES

- [1] Kel'zon A.S. *Rotor dynamics in elastic supports*, Nauka, Moscow, 1982 (in Russian).
- [2] Schweitzer G., Bleuler H. and Traxler A. *Active magnetic bearings*, ETH, Zurich, 1994.
- [3] Martynenko G.Y. Magnetic bearings as the elastic-damping support rotors with controlled stiffness *Visnyk NTU «KhPI»*, Vol. 47, pp. 111–124, 2008 (in Russian).
- [4] G. Martynenko Modelling the dynamics of a rigid rotor in active magnetic bearings *Proceedings 6<sup>th</sup> EUROMECH Nonlinear Dynamics Conference (ENOC 2008)*, St. Petersburg, 2008.
- [5] Martynenko G. Authentication of the mathematical model of a rigid rotor on the passively-active magnetic suspension on the basis of experimental data *Mashynoznavstvo*, Vol. 12 Lviv, 2009. (in Ukrainian).

## CONSTRUCTING AN OPTIMAL LYAPUNOV FUNCTION FOR INVESTIGATION OF STABILITY OF LINEAR FUZZY HYBRID AUTOMATON

**M. Merkuryev**<sup>1</sup>

Taras Shevchenko  
National University of Kiev

ABSTRACT

In this paper the condition of  $\alpha$ -level stability of linear fuzzy hybrid automaton is converted to a numerical algorithm. A computational procedure that is a hybrid of the Lagrange method and the method of projection of generalized anti-gradient is proposed.

### INTRODUCTION

The most common method for investigation of stability of hybrid automata is the method of the Lyapunov functions. General theory of stability of hybrid automata is rather complicated, since the Lyapunov functions needed for investigation of stability should satisfy some complex conditions. For hybrid automata that contain only linear subsystems two approaches are frequently used.

The first of them is based on construction of the Lyapunov quadratic form common for all subsystems. For hybrid automata that have more than two local states there is a theorem: a sufficient condition of existence of the common Lyapunov function is an existence of stable convex combination of matrices  $A_i$ , i.e. there are positive  $\alpha_i$ , where  $\sum_i \alpha_i = 1$ , such that matrix  $A = \sum_{i=0}^N \alpha_i A_i$  is stable [1].

When  $N = 2$ , this condition is also necessary. But the determination of the convex combination of matrices  $A_i$  satisfying this condition is a combinatorial problem with non-linear polynomial complexity. Moreover, there is a large class of systems that don't satisfy this condition, but a stabilizing sequence of switchings exists, and hybrid automaton is stable.

It's shown in [2] that if positive-definite matrices  $R_i$  exist,  $i = 1..N$  such as  $\sum_i (A_i^T R_i + R_i A_i) > 0$ , the common quadratic Lyapunov function doesn't exist.

Another approach is a construction of own Lyapunov function for each local state of automaton [3]. This approach assumes a finding of  $N$  positive-definite matrices  $H_i$ , each of them satisfies its own Lyapunov equation, one symmetric matrix and  $2N$  matrices with non-negative elements. These matrices should satisfy a complex system of matrix equations.

In this paper we suggest a constructive approach to check the conditions of stability of linear hybrid automaton. For this we use methods of operational research.

### 1. OBTAINING AN OPTIMIZATION PROBLEM

We investigate stability of a fuzzy linear hybrid automaton

$$HA = (Q, y, A, B, Init, Inv, Jump), \quad (1)$$

where

$Q = \{1..N\}$  is a set of local states (discrete variable),

$y \in R^n$  is a continuous variable, changing according to law

<sup>1</sup> Corresponding author. Email [mercury13@ukr.net](mailto:mercury13@ukr.net)

$$y(t) = y(t_i) + \int_{t_i}^t Ay(s)ds + \int_{t_i}^t By(s)dw(s, x)$$

where  $w(s, x)$ ,  $x \in X$  is a process of fuzzy roaming with distribution  $\mu(u) = \varphi(\sigma u^2)$  [4],  $(X, 2^X, P, N)$  is a PN space [5]

$$Init = Inv \subseteq \{(q, y) : G_q y \geq 0\},$$

a state of switching (*Jump*) is cyclic  $(1 \rightarrow 2 \rightarrow \dots \rightarrow N \rightarrow 1)$ , continuous ( $y(t_i + 0, x) = y(t_i - 0, x)$ ) and is implemented on hyperplane  $y = U_q z$ ,  $z \in R^{n-1}$ .

**Definition 1.** Funnel  $y(\bar{y}_0, t, x)$  of fuzzy dynamical system  $y(y_0, t, x)$  (not necessarily hybrid automaton) is called  $\alpha$ -level stable, if for all  $x_0 \in X$  for which  $P(\{x_0\}) > \alpha$  for every  $\varepsilon > 0$  exists  $\delta(\varepsilon)$  such that  $|y_0 - \bar{y}_0| < \delta$  implies  $|y(y_0, t, x_0) - y(\bar{y}_0, t, x_0)| < \varepsilon$ .

**Theorem 1** (about the piecewise-quadratic  $s$ -function). A linear hybrid automaton (1) is given. If positive-definite matrices  $H_k$  (sized  $n \times n$ ) exist such that

$$a_q = \max_{\substack{G_q x \geq 0 \\ x^T x = 1}} x^T (A_q^T H_q + H_q A_q) x + \left| B_q^T H_q + H_q B_q \right| \sqrt{\varphi^{-1}(\alpha) \sigma} < 0$$

and for every switching  $q \rightarrow (k \bmod N) + 1 = r$  matrix  $U_q^T (H_r - H_q) U_q$  is negative-semidefinite, then  $x = 0$  is an asymptotically  $\alpha$ -level stable stationary point.

So, to check these conditions, we should create an algorithm to obtain matrices  $H_q$  that maximally satisfy the theorem. In other words, we should build such matrices  $H_q$  that minimize values of  $a_q$ . If this minimal value is less than zero, the conditions of the theorem are not fulfilled and we cannot investigate stability of the automaton using the method of the Lyapunov functions. If that value is less than zero, the trivial stationary point is asymptotically stable.

To check stability, we should solve the optimization problem

$$\Phi_1(H) = \max_{\substack{G_q y \geq 0, G_q z \geq 0 \\ y^T y = 1, z^T z = 1 \\ q \in Q}} \left( y^T (A_q^T H_q + H_q A_q) y + z^T (B_q^T H_q + H_q B_q) z \sqrt{\varphi^{-1}(\alpha) \sigma} \right) \rightarrow \min_{H_q} \quad (2)$$

with conditions: matrices  $H_q$  are positive-definite, for all switchings  $q \rightarrow r$  matrices  $U_q^T (H_r - H_q) U_q$  are seminegative-definite, and elements of matrices  $H = \{H_q, q \in Q\}$  are located in some compact domain  $D$  that envelops 0. For simplicity of denotes

$$\Psi(q, H, y, z) = y^T (A_q^T H_q + H_q A_q) y + z^T (B_q^T H_q + H_q B_q) z \sqrt{\varphi^{-1}(\alpha) \sigma}$$

$$L_1 = D \cap \left\{ H : \lambda_{\min}(H_q) \geq 0; \lambda_{\max}(U_q^T (H_r - H_q) U_q) \leq 0 \right\}$$

**Lemma 1.** If function  $\psi(H, y) : R^{N_1} \times R^{N_2} \rightarrow R$  is continuous and  $K$  is a compact on  $R^{N_2}$ , then function  $\Phi(H) = \min_{y \in K} \psi(H, y)$  is continuous.

**Corollary.** Minimum and maximum eigenvalues are continuously dependent on coefficients of  $H$ .

**Theorem 2.** Set  $L_0 = \left\{ H : \lambda_{\min}(H_q) \geq 0; \lambda_{\max}(U_q^T (H_r - H_q) U_q) \leq 0 \right\}$  is a convex closed cone.

**Corollary.**  $L_1$  is compact.

**Theorem 3.** Optimization problem (1) has a solution.

**Proof.** For this we should prove three facts.

1. Function  $\Phi_1(H)$  is continuous;
2. There is at least one point  $H \in L_1$ ;
3. Domain  $L_1$  is compact.

*Continuity.*

$$\Phi_1(H) = \max_{q \in Q} \max_{\substack{G_q y \geq 0, G_q z \geq 0 \\ y^T y = 1, z^T z = 1}} \left( y^T (A_q^T H_q + H_q A_q) y + z^T (B_q^T H_q + H_q B_q) z \sqrt{\varphi^{-1}(\alpha) \sigma} \right)$$

Function  $\max_{\substack{G_q, y \geq 0, G_q, z \geq 0 \\ y^T y = 1, z^T z = 1}} \left( y^T (A_q^T H_q + H_q A_q) y + z^T (B_q^T H_q + H_q B_q) z \sqrt{\varphi^{-1}(\alpha)} \sigma \right)$  is continuous

according to Lemma 1. That's why  $\Phi_1(H)$ , that is a minimum of finite number of continuous functions, is continuous.

*Existence.* For sufficiently small  $\gamma$ , point  $H = \{H_q = \gamma E_n = \{h_{ij}^q = \delta_{ij}\}\}$  is located inside  $L_1$ . Indeed, for this  $H$  limitations  $H \in D$ ,  $\lambda_{\max}(H_r - H_q) = 0$  and  $\lambda_{\min}(H_q) \geq 0$ .

*Compactness.* Proved above.

These three conditions, according to the Weierstrass theorem, imply existence of solution of the optimization problem.

**Theorem 4.** Function  $\Phi_1(H)$  is convex.

**Proof.** For this, it's enough to prove convexity of function

$$\Phi_1^q(H) = \max_{\substack{G_q, y \geq 0, G_q, z \geq 0 \\ y^T y = 1, z^T z = 1}} \left( y^T (A_q^T H_q + H_q A_q) y + z^T (B_q^T H_q + H_q B_q) z \sqrt{\varphi^{-1}(\alpha)} \sigma \right)$$

So, given  $H'$  and  $H''$ , denote  $H = \gamma H' + (1 - \gamma) H''$ .

$\Phi_1^q(H)$  is essentially  $\max_{y, z} L(H, y, z)$ , where  $L$  is a linear functional of  $H$ . Then

$\Phi_1^q(\alpha H_1 + \beta H_2) \leq \Phi_1^q(\alpha H_1) + \Phi_1^q(\beta H_2) = \alpha \Phi_1^q(H_1) + \beta \Phi_1^q(H_2)$ , when  $\alpha, \beta \geq 0$ . So,  $\Phi_1^q(H)$  is convex.

## 2. METHOD OF NUMERICAL SOLUTION

As it was said above, there are three limitations for the coefficients  $h_{ij}^q : H \in D$ ,  $\lambda_{\min}(H_q) \geq 0$ ,  $\lambda_{\max}(U_q^T (H_r - H_q) U_q) \leq 0$ . For implementation of the first condition we can use projection of gradient, if we pick specially-shaped  $D$ . For the second – the gradient is projected as  $H'_q = H_q + \lambda_{\min}(E_n)$ . And for the third one it's impossible to project the gradient. So, we use a hybrid of Lagrange method and gradient projection method. We construct next Lagrange function:

$$\Phi(H) = \Phi_1(H) + \sum_{\substack{q \rightarrow r \\ q, r \in Q}} \theta^{qr} \Phi^{qr}(H)$$

where  $\Phi^{qr}(H) = \lambda_{\max}(U_q^T (H_r - H_q) U_q)$ . Let us assume  $D = \{h_{ij}^q \mid \leq 1\}$ .

**Definition 2.** Generalized gradient of function  $\Phi(x)$  is a vector  $\nabla^*(x)$  such that  $\Phi(z) - \Phi(x) \geq (\nabla^*(x), z - x)$ .

**Theorem 5.** The following equation is a generalized gradient of  $\Phi_1(H)$ :

$$\nabla_{\Phi_1}^*(H) = \{h_{ij}^q = y_0^T (A^T \Delta_{ij} + \Delta_{ij} A) y_0 + z_0^T (A^T \Delta_{ij} + \Delta_{ij} A) z_0\}$$

where  $y_0$  and  $z_0$  are  $n$ -dimensional vectors that realize maximum of function  $\Psi$ ;  $\Delta_{ij}$  is a matrix  $n \times n$  that has one unit element on intersection of  $i$  and  $j$ .

The only remaining thing is finding the generalized gradient of the function  $\Phi^{kl}(H) = \lambda_{\max}(U_k^T (H_\ell - H_k) U_k)$ .

**Theorem 6.** Equation  $\nabla_{\Phi^{kl}}^*(H) = \{h_{ij}^q\}$ , where  $h_{ij}^q = \begin{cases} 0; & q \neq k, \ell \\ -u_0^T U_k^T \Delta_{ij} U_k u_0; & q = k; u_0 \text{ is a vector of} \\ u_0^T U_k^T \Delta_{ij} U_k u_0; & q = \ell \end{cases}$

dimension  $n-1$  and norm 1 that realizes maximum of  $\|u^T U_k^T (H_\ell - H_k) U_k u\|$ , is a generalized gradient of function  $\Phi^{kl}(H)$ .

**Proof.**

$$\Phi^{kl}(H_1) - \Phi^{kl}(H_0) = \lambda_{\max}(U_k^T (H_1^\ell - H_1^k) U_k) - \lambda_{\max}(U_k^T (H_0^\ell - H_0^k) U_k)$$

The matrix  $U_k^T (H_1^\ell - H_1^k) U_k$  is positive-definite, so one has

$$\lambda_{\max}(U_k^T (H_1^\ell - H_1^k) U_k) = \max_{\|u\|=1} u^T U_k^T (H_\ell - H_k) U_k u$$

Thus, the following holds

$$\Phi^{k\ell}(H_1) - \Phi^{k\ell}(H_0) = u_1^T U_k^T (H_1^\ell - H_1^k) U_k u_1 - u_0^T U_k^T (H_0^\ell - H_0^k) U_k u_0$$

where  $u_0 = \arg \max_{\|u\|=1} u^T U_k^T (H_0^\ell - H_0^k) U_k u$ ,  $u_1$  is the same for matrix  $H_1$ .

This equation may be rewritten as

$$\begin{aligned} \Phi^{k\ell}(H_1) - \Phi^{k\ell}(H_0) &= u_1^T U_k^T (H_1^\ell - H_1^k) U_k u_1 - u_0^T U_k^T (H_1^\ell - H_1^k) U_k u_0 \\ &+ u_0^T U_k^T [(H_1^\ell - H_1^k) - (H_0^\ell - H_0^k)] U_k u_0. \end{aligned}$$

Because maximum for matrix  $H_1$  holds for vector  $u_1$ ,

$$u_1^T U_k^T (H_1^\ell - H_1^k) U_k u_1 - u_0^T U_k^T (H_1^\ell - H_1^k) U_k u_0 \geq 0$$

Then

$$\Phi^{k\ell}(H_1) - \Phi^{k\ell}(H_0) \geq u_0^T U_k^T [(H_1^\ell - H_1^k) - (H_0^\ell - H_0^k)] U_k u_0$$

We get a definition of generalized gradient:

$$\Phi^{k\ell}(H_1) - \Phi^{k\ell}(H_0) \geq \langle \nabla_{\Phi^{k\ell}}^*(H_0), H_1 - H_0 \rangle$$

## 2.1 Movement down the “canyon”

Sometimes a situation happens when on some step a maximum of function  $\Psi$  holds simultaneously for two different  $q$ :  $q = q_0$  and  $q = q_1$ . We can call this situation a “canyon”. Target function in the “canyon” is continuous, but it has a discontinuous derivative, so in general case the generalized gradient may not exist. For simplicity let us rewrite our problem as

$$\Phi(H) = \max_{y,q} \Psi(H, y, q) \rightarrow \min$$

One denotes:  $\Phi(H, q) = \max_y \Psi(H, y, q)$ .

Calculating a generalized gradient of the function  $\Phi(H)$ , in reality we calculate a generalized gradient of all  $\Phi(H, q)$ . By definition of a generalized gradient, it defines a semi-space  $\Omega$ , for which for every  $H_1 \in \Omega$  (close enough to  $H$ ) holds  $\Phi(H_1, q) < \Phi(H, q)$ . If we intersect the subspaces that correspond to  $q = q_0$  and  $q = q_1$ , we obtain an infinite pyramid that corresponds to all possible movements from current point  $H$ .

Number of “blocking”  $q$  is always less than number of free variables in  $H$ . That’s why the set of possible direction is non-empty. We can find at least one element of intersection of mentioned semi-spaces from the system  $\langle \nabla_i^*, H_1 \rangle \leq 0, i \in \{0,1\}$ .

The target function is uniform ( $\Phi(kH) = k\Phi(H)$ ). That’s why we treat the solution as optimal, when on the next step we are on the boundary of  $D$ , and because of “canyon” limitation we cannot move without moving beyond  $|h_{ij}^q| \leq 1$ .

## 2.2 Computational procedure

First treat all variables of matrix  $H$  as “unlocked”. Repeat the procedure:

1. Compute  $\nabla_{\Phi}^*(H, \theta)$ . If the maximum holds for several  $q \in Q$ , compute generalized gradient for all such  $q$  and find a vector that is in the intersection of subspaces.

2. For all “locked” variables: if the corresponding coordinate of generalized anti-gradient  $\nabla$  leads inside cube  $|h_{ij}^q| \leq 1$ , “unlock” the variable. If not, replace the coordinate of anti-gradient with zero. If after these limitations the anti-gradient turns to zero, STOP: no solution found.

3. Find  $\rho$ , for which  $H - \rho\nabla$  doesn’t move beyond  $|h_{ij}^q| \leq 1$ . If  $\Phi(H - \rho\nabla) < \Phi(H)$ , set  $H := H - \rho\nabla$  and “lock” the coordinate that became a limitation.

4. If  $\Phi(H - \rho\nabla) \geq \Phi(H)$ , find optimal  $\rho$  according to rules of gradient method. Assign:  $H := H - \rho\nabla$ .

5. If for some  $q$   $\lambda_{\min}(H_q) < 0$  holds, for all  $q$  assign:  $H_q := H_q + \min_q \lambda_{\min}(H_q) E_n$ . If because of this limitation rule  $|h_{ij}^q| \leq 1$  is broken, norm the matrices ( $H_q := \frac{H_q}{\max_{i,j,q} |h_{ij}^q|}$ ) and update the lock list.

6. If  $\Phi(H) < 0$ , STOP: solution is found.

In general, this method doesn't guarantee convergence. But if we use  $\varepsilon$ -subdifferential every step (picking from it an element of the least norm), theorem about  $\varepsilon$ -subgradient [6] guarantees that the sequence of matrices  $H$  converges to optimal value with error not exceeding  $\varepsilon$ .

## CONCLUSION

Using the optimization problem, we managed to coin a constructive algorithm of checking  $\alpha$ -level stability of linear fuzzy hybrid automaton, based on modified method of generalized gradient. Criterion of optimality and the generalized gradient are proposed, together with a computation procedure.

## REFERENCES

- [1] M. Wicks, P. Peleties, R. DeCarlo. Switched controller synthesis for the quadratic stabilization of a pair of unstable linear systems. *Eur. J. Contr.*, Vol. 4, 1998.
- [2] S. Pettersson, B. Lennartson. Stability and robustness for hybrid systems. *Control Engineering Laboratory, Chalmers Univ. of Technology, Tech. Rep. I-96/003*, 1996.
- [3] M. Johansson, A. Rantzer Computation of piecewise quadratic Lyapunov functions for hybrid systems. *IEEE Trans. Automat. Contr.*, Vol. 43, No. 4, 1998.
- [4] A. Bychkov, M. Merkurjev Existence and uniqueness of solutions of fuzzy differential equation. *Bulletin of the Kiev University, Phys.-Math. Sciences*. No.3, pp.131–135, 2006 (in Ukrainian).
- [5] A. Bychkov. On one approach to description of fuzzy events. *Bulletin of Kiev University, Phys.-Math. Sciences*. 2006, No.3, pp.138–142 (in Ukrainian).
- [6] I. Beyko, B. Bublik, P. Zinko. *Methods and algorithms of solving optimization problems*, High School, Kiev, 1983 (in Russian)

**NONLINEAR NORMAL MODES IN PENDULUM SYSTEMS.**

**Yu. V. Mikhlin<sup>1</sup>,**  
**A.A.Klimenko**  
 National Technical  
 University "Kharkov  
 Polytechnic Institute",  
 Kharkov, Ukraine

ABSTRACT

Nonlinear normal modes in some pendulum systems and a stability of these modes are analyzed. Namely, dynamics of the spring pendulum and of the 2-DOF system, containing a linear oscillator and the attached pendulum, is considered. Nonlinear normal modes are obtained as by the multiple scales method, as well by construction of trajectories in configuration space. Stability of nonlinear normal modes is investigated by using the Mathieu and Hill equations, and by the algebraization of the equations in variations. Numerical simulation confirms an exactness of obtained analytical results.

**INTRODUCTION**

Pendulum systems are classical models in mechanics and theory of nonlinear vibrations. Their analysis permits to select important nonlinear dynamical effects [1,2]. Besides, such systems are used in engineering, in particular, in the absorption problems [3,4], and to describe some physical processes [5,6]. In spite of numerous investigations of the pendulum dynamics, as in the past [7], as well at present [8,9], analytical results are obtained only for vibrations having not large amplitudes. In this work new asymptotical methods and numerical simulations are used to construct nonlinear normal modes and analyze their stability. Dynamics of the spring pendulum and of the 2-DOF system, containing a linear oscillator and the attached pendulum, is considered as for small, as well for large vibration amplitudes. Stability of the nonlinear normal modes is investigated too.

**1. PENDULUM SYSTEMS UNDER CONSIDERATION**

A model of the spring pendulum is shown in the Fig.1. Free vibrations of the system is described by two generalized coordinates,  $\rho$  and  $\varphi$ . Dissipation forces are not taken into account.

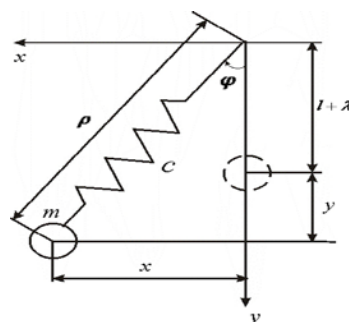


Fig. 1. The spring pendulum

Equations of motion are the following:

$$\begin{cases} \ddot{\rho} - \rho\dot{\varphi}^2 = -\frac{c}{m}(\rho - l) + g \cos \varphi; \\ \rho^2\ddot{\varphi} + 2\rho\dot{\rho}\dot{\varphi} = -g \rho \sin \varphi. \end{cases} \quad (1)$$

<sup>1</sup> Corresponding author. Email [muv@kpi.kharkov.ua](mailto:muv@kpi.kharkov.ua)

Terms of the power more than three by  $\varphi$  in Taylor expansions of the functions  $\cos \varphi$  and  $\sin \varphi$ , are discarded. One has the next transformation for a case of small values of the angle and spring dilation:  $\varphi \rightarrow \mu\varphi$ ,  $\rho - \rho_0 \rightarrow \mu z$ , where  $\mu$  is a small parameter. Then the equations of motion can be rewritten as

$$\begin{aligned} \ddot{z} + z &= \mu(\rho_0 \dot{\varphi}^2 + 0.5g\varphi^2) + \mu^2 \dot{\varphi}^2 z; \\ \rho_0^2 \ddot{\varphi} + g\rho_0\varphi &= \mu(-2\rho_0\ddot{\varphi} - 2\rho_0\dot{\varphi}\dot{z} - gz\varphi) + \mu^2(-z^2\ddot{\varphi} - 2z\dot{z}\dot{\varphi} + g\rho_0\varphi^3/6) + \mu^3gz\varphi^3/6 \end{aligned} \quad (2)$$

where  $\rho_0 = l - \frac{gm}{c}$  is the spring extension in the system equilibrium position.

It is possible to select two next vibration modes in the system: a) longitudinal vibrations, when the rotation is absent,  $\varphi = 0$ ,  $z = z(t)$ ; b) coupled vibrations,  $\varphi = \varphi(t)$ ,  $z = z(t)$ .

The other two-DOF system is shown in the Fig. 2. A pendulum in the system can be considered as absorber of linear vibrations of the main linear oscillator. Vibrations of the system is described by two generalized coordinates,  $x$  and  $\theta$ .

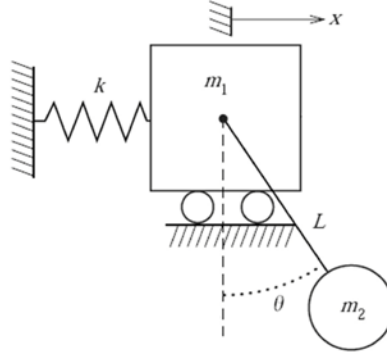


Fig. 2. The two-DOF system containing the pendulum as absorber.

Equations of motion are here the following:

$$\begin{cases} (m_1 + m_2)\ddot{x} + m_2l\ddot{\theta}\cos\theta - m_2l\dot{\theta}^2\sin\theta + kx = 0; \\ \ddot{x}\cos\theta + l\ddot{\theta} + g\sin\theta = 0. \end{cases} \quad (3)$$

Using the Taylor expansions for functions  $\cos \varphi$  and  $\sin \varphi$ , we save only terms of the power not more than three by  $\varphi$ . One assumes that the mass of the pendulum is essentially smaller than one of the linear subsystem. Using the next transformation,  $m_2 \rightarrow \varepsilon m_2$ , where  $\varepsilon$  is a formal small parameter, it is possible to obtain equations of motion of the form:

$$\begin{cases} (m_1 + \varepsilon m_2)\ddot{x} + \varepsilon m_2 l \ddot{\theta} \left(1 - \frac{\theta^2}{2}\right) - \varepsilon m_2 l \dot{\theta}^2 \left(\theta - \frac{\theta^3}{6}\right) + kx = 0; \\ \ddot{x} \left(1 - \frac{\theta^2}{2}\right) + l \ddot{\theta} + g \left(\theta - \frac{\theta^3}{6}\right) = 0. \end{cases} \quad (4)$$

Two vibration modes exist in the system, namely: a) coupled vibrations,  $x = x(t)$ ,  $\theta = \theta(t)$ ; b) localized vibration mode, when values of vibration amplitude of the pendulum are essentially large than ones of the linear subsystems of the mass  $m_1$ .

## 2. NONLINEAR NORMAL MODES IN PENDULUM SYSTEMS

### 2.1. Construction of nonlinear normal modes for small amplitudes

To construct the mode of coupled vibrations for the system (2) the multiple scales method is used. Namely, series by the small parameter:  $z = z_0 + \mu z_1 + \mu^2 z_2 + \dots$ ,  $\varphi = \varphi_0 + \mu \varphi_1 + \mu^2 \varphi_2 + \dots$ , and the presentations  $z(t, \mu) = z(T_0, T_1, T_2, \dots; \mu)$ ; where  $T_0 = t$ ,  $T_1 = \mu t$ ,  $T_2 = \mu^2 t, \dots$ , are used. The next

$$\varphi(t, \mu) = \varphi(T_0, T_1, T_2, \dots; \mu),$$

transformations to construct the periodic solution are not presented here. As a result, one has the periodic solution of the system (2):

$$\begin{aligned}
z_1 &= A_1 \cos \omega_1 T_0 + B_1 \sin \omega_1 T_0 + \frac{g}{4}(C_0^2 + D_0^2) + \\
&+ \frac{g}{1-4\omega_2^2} \left( -\frac{3}{2} C_0 D_0 \sin 2\omega_2 T_0 + \frac{3}{4} (D_0^2 - C_0^2) \cos 2\omega_2 T_0 \right); \\
\varphi_1 &= C_1 \cos \omega_2 T_0 + D_1 \sin \omega_2 T_0 + \\
&+ \frac{\omega_2 \left( \omega_1 + \frac{\omega_2}{2} \right)}{g - \rho_0 \left( \omega_1 + \omega_2 \right)^2} \left( (A_0 C_0 - B_0 D_0) \cos \left( \omega_1 + \omega_2 \right) T_0 + (B_0 C_0 + A_0 D_0) \sin \left( \omega_1 + \omega_2 \right) T_0 \right) + \\
&\frac{\omega_2 \left( \omega_1 - \frac{\omega_2}{2} \right)}{g - \rho_0 \left( \omega_1 - \omega_2 \right)^2} \left( (B_0 D_0 - A_0 C_0) \cos \left( \omega_1 - \omega_2 \right) T_0 + (A_0 D_0 - B_0 C_0) \sin \left( \omega_1 - \omega_2 \right) T_0 \right). \tag{5}
\end{aligned}$$

where  $\omega_1 = \sqrt{c/m}$ ,  $\omega_2 = \sqrt{g/m}$ , expressions of the functions  $A_0 = A_0(T_2, T_3, \dots)$ ,  $B_0 = B_0(T_2, T_3, \dots)$ ,  $C_0 = C_0(T_2, T_3, \dots)$ ,  $D_0 = D_0(T_2, T_3, \dots)$  are not presented here. One has the very good coincidence of the analytical results and numerical simulation by the Runge-Kutta method for nor large vibration amplitudes.

In the Fig.3 it is presented a comparison of the analytical results and numerical simulation by the Runge-Kutta method for nor large vibration amplitudes. In the Fig.3,a it is shown a change in time of the variation  $z$ , and in the Fig. 3,b it is shown a change of the variation  $\varphi$ .

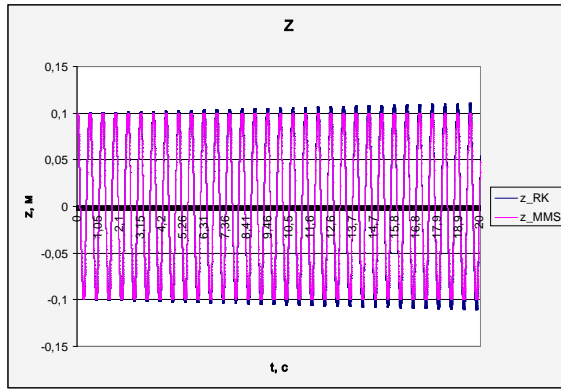


Fig. 3,a

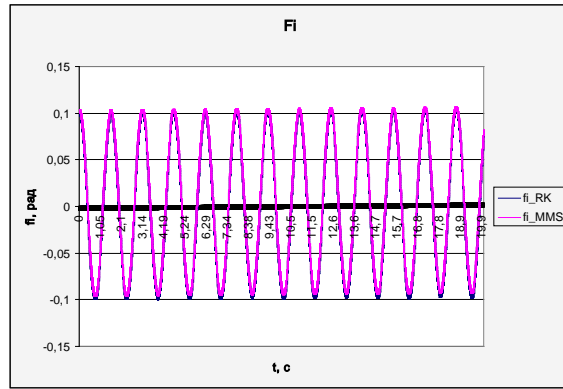


Fig. 3,b

Fig.3. Mode of the coupled vibrations obtained by the method of multiple scales and by the numerical simulation.

The same approach is used to construct vibrations of the system (3). A good correspondence of the analytical and numerical results is obtained.

## 2.2. Construction of nonlinear normal modes for large amplitudes

To construct coupled vibrations with large amplitudes theory of nonlinear normal modes (NNMs) is used [10-12]. Equation for trajectories of motions  $z = z(\varphi)$  for the system (2) may be obtained of the form:

$$\begin{aligned}
&(h - V)m((\mu z + \rho_0)(z'' - (z + \rho_0)) - 2\mu z'^2) + \\
&+ \tilde{K} \left( (\mu z + \rho_0) \left( c(z + \rho_0 - l) - mg \left( 1 - \frac{\varphi^2}{2} \right) \right) - m z' g \varphi \right) = 0 \tag{6}
\end{aligned}$$

where prime means a derivation by  $\varphi$ ;  $V$  and  $\tilde{K}$  are respectively the system potential energy and the system kinetic energy. Equation (6) has singular points on the maximal equipotential surface,  $h - V = 0$ . Additional boundary conditions guarantee an analytical continuation of the NNM trajectory to this surface [10-12]:

$$-m z' g \varphi \tilde{K} + c \tilde{K} (z + \rho_0 - l) (\mu z + \rho_0) - mg \tilde{K} (\mu z + \rho_0) (1 - \varphi^2 / 2) = 0, \tag{7}$$

where  $\varphi = \varphi_0$ , and  $\dot{\varphi} = 0$ . Solution of the boundary problem (6) and (7) can be obtained in power series by  $\varphi$ . Amplitudes values  $\varphi = \varphi_0$  depending on the energy value  $h = h_0$  are obtained too.

Numerical simulation shows a very good exactness of the analytical solution for large vibration amplitudes (Fig.4).

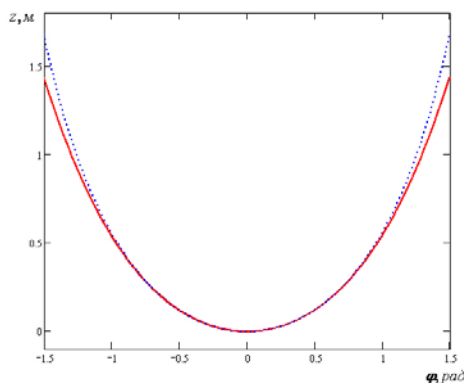


Fig.4. Trajectory of mode of coupled vibrations in configuration space. Entire line represents the analytical solution; point line represents the checking numerical calculation.

Construction of the mode of coupled vibrations in the power series by  $\cos \varphi$ ,

$$z(\varphi) = z_0 + \mu z_1 = \alpha_0 + \alpha_1 \cos \varphi + \alpha_2 \cos^2 \varphi + \mu(\beta_0 + \beta_1 \cos \varphi + \beta_2 \cos^2 \varphi) + \dots, \quad (8)$$

is very effective for large vibrations too.

Nonlinear normal modes of the system (3) are determined by construction of their trajectories in a configuration space too. Equations and boundary conditions similar to ones (6), (7), are used. The power series are used for the NNMs construction. In Fig. 5 trajectories of the NNMs are presented. The non-localized mode of coupled vibrations, obtained in the form  $x = x(\theta)$  is shown in Fig 5.a, and the localized mode, determined in the form  $\theta = \theta(x)$ , is shown in the Fig. 5b.

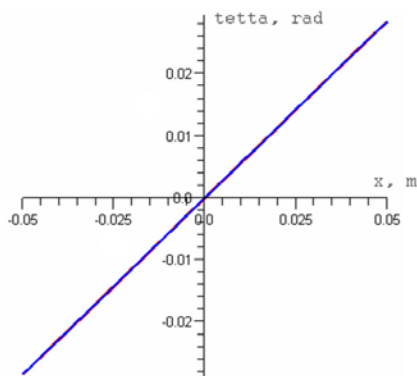


Fig.5a.

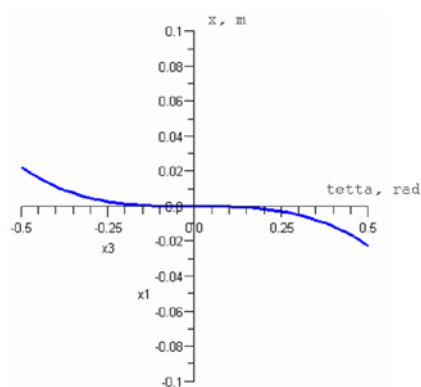


Fig 5.b.

Fig.5. Trajectories of mode of coupled vibrations in the system (3) configuration space. Fig.5a. Trajectory of the mode of coupled vibrations; Fig.5b. Trajectory of localized mode.

### 3. STABILITY OF NONLINEAR NORMAL MODES IN PENDULUM SYSTEMS

Stability of longitudinal motions investigated in details by many authors. The equation in variations, which are orthogonal to the rectilinear trajectory of the longitudinal vibration mode, is considered. The stability analysis may be made by reduction of the equation in variations to the Mathieu equation, or by the method of Hill determinants. In the last variant results are very close to ones obtained by the checking numerical simulation.

Stability of mode of the coupled vibrations are investigated by approach which is connected with the well known classical definition of stability by Lyapunov [13,14]. In this case the values of variables are compared with their initial values. Necessary condition of stability of motion is the following:

$$\sqrt{(\Delta z(t))^2 + (\Delta \varphi(t))^2} \leq \xi \sqrt{(\Delta z(0))^2 + (\Delta \varphi(0))^2}, \quad (9)$$

where  $\Delta z(t) = z(t) - z_0$ ,  $\Delta \varphi(t) = \varphi(t) - \varphi_0$ ,  $\Delta z(0) = z_0 / k$ ,  $\Delta \varphi(0) = \varphi_0 / k$ . Here  $z_0$  и  $\varphi_0$

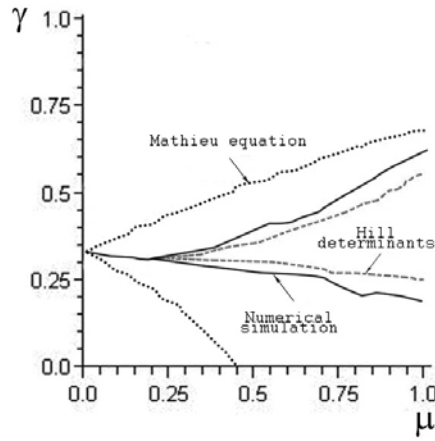


Fig.6. Boundaries of the stability/instability regions of the longitudinal vibrations.

are initial values of the corresponding variables. It exists some arbitrariness in choosing of the constants  $\xi, k$ . It is used that  $\xi = 10, k = 100$ . Violation of the condition (9) shows to instability of the solution. Numerical calculation is made in points of some mesh on a plane of the system parameters until boundaries of the stability/instability regions on this plane will be stabilized. These boundaries are shown in Fig.7 on the plane of parameters  $\omega^2 = c\rho_0/mg$  and  $A$  which is the angle vibrations amplitude. The instability region is inside of the lines.

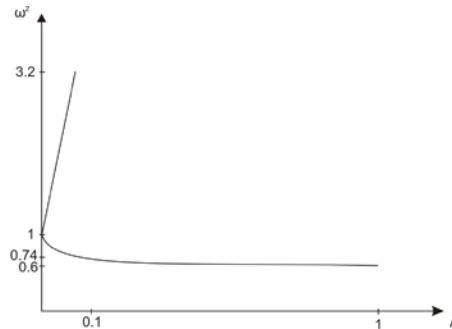


Fig.7. Boundaries of the stability/instability regions for mode of coupled vibrations.

The pairs of solutions fork from the mode of coupled vibrations in bifurcation points which correspond to the stability/instability boundaries. Examples of trajectories of these forking solutions are shown in Fig. 7 for different values of the angle amplitude.

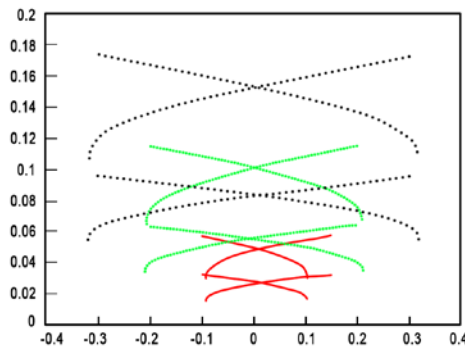


Fig.8. Trajectories of forking solutions in the pendulum configuration space.

In the Fig.9 it is presented boundaries of the stability/instability regions for the mode of coupled vibrations for the system (3), obtained by using the reduction to the Mathieu equation (exterior lines), and by using the more exact method of the Hill determinants (interior lines). Unstable vibrations are observed inside the lines. The forking solutions are shown for some values of the system parameters in the Fig. 10.

Stability of the localized vibration mode is investigated by the Hill determinants for the equation in variations. It is obtained that regions of the mode instability are very narrow.

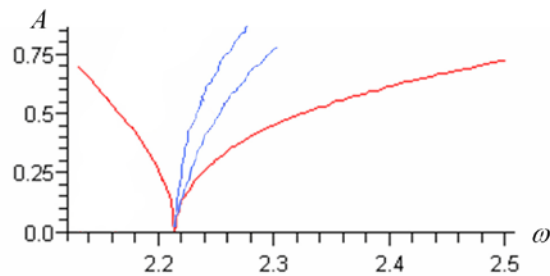


Fig.9. Boundaries of the stability/instability regions of the non-localized mode of the system (3)

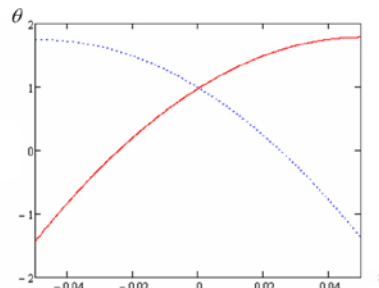


Fig.10. Trajectories of the forking solutions for the non-localized vibration mode.

## CONCLUSIONS

The nonlinear normal modes in pendulum systems and their stability are investigated both for small, and for large vibration amplitudes. Numerical simulation shows a good exactness of the obtained analytical results.

## REFERENCES

- [1] I.G.Malkin. *Some Problems of the Theory of Nonlinear Oscillations*, Gostechteorizdat, Moscow, 1956 (in Russian).
- [2] A.H.Nayfeh, D. Mook. *Nonlinear Oscillations*, John Wiley, New York, 1984.
- [3] *Vibrations in engineering* (K.V.Frolov, editor), Mashinostroenie, Moscow, 1995 (in Russian).
- [4] O.Cuvalci, A.Ertas. Pendulum as vibration absorber for flexible structures: experiments and theory, *Trans. of the ASME. Journal of Vibrations and Acoustics*, Vol. 118, pp. 558-566, 1996.
- [5] G.S.Gorelik, A.A.Witt. Swing of an elastic pendulum as an example of two parametrically bound linear vibration systems, *J. of Tech. Physics (USSR)*, Vol. 3, № 2—3, pp. 294-307, 1933 (in Russian).
- [6] A.C.Scott. *Active and Nonlinear Wave Propagation in Electronics*, Wiley-Interscience, New York, 1970.
- [7] V.M.Starzhinskii. *Applied Methods in Nonlinear Vibrations*, Nauka, Moscow, 1977 (in Russian).
- [8] F.Wang, A.Bajaj, K.Kamiya. Nonlinear normal modes and their bifurcations for an inertially coupled nonlinear conservative system, *Nonlinear Dynamics*, 42 (3), 2005, pp. 233-265.
- [9] J.Warminski, K.Kecik. Regular and chaotic motions of an autoparametric real pendulum system with the use of a MR damper. In: *Modeling, simulation and control of nonlinear engineering dynamical systems* ( J. Awrejcewicz, editor). Springer, 2009.
- [10] L.I.Manevitch, Yu.V.Mikhlin, V.N.Pilipchuk. *The Method of Normal Vibrations for Essentially Nonlinear Systems*, Nauka, Moscow, 1989 (in Russian).
- [11] Yu.Mikhlin. Normal vibrations of a general class of conservative oscillators, *Nonlinear Dynamics*, V. 11, pp. 1–16, 1996.
- [12] A.F.Vakakis, L.I.Manevitch, Yu.V.Mikhlin, V.N.Pilipchuk, A.A.Zevin. *Normal Modes and Localization in Nonlinear Systems*, Wiley Interscience, New York, 1996.
- [13] Yu.V.Mikhlin, T.V.Shamatko, G.V.Manucharyan. Lyapunov definition and stability of regular or chaotic vibration modes in systems with several equilibrium positions, *Computers and Structures*, V.82, pp. 2733-2742, 2004.
- [14] Yu.V.Mikhlin, G.V.Manucharyan. Determination of the chaos onset in mechanical systems with several equilibrium positions, *Meccanica*, Vol. 41, pp. 253-267, 2006.

## CONSTRUCTION OF TRANSIENT IN MECHANICAL SYSTEMS

**Yu. V. Mikhlin<sup>1</sup>,**  
**G.V.Rudnyeva**  
National Technical  
University "Kharkov  
Polytechnic Institute",  
Kharkov, Ukraine

---

### ABSTRACT

---

The transient in a system containing a linear oscillator, linearly coupled to an essentially nonlinear attachment with a comparatively small mass, is considered. A damping is taken into account. A transfer of energy from the initially perturbed linear subsystem to the nonlinear absorber is observed. The modified multiple scales method is used to construct a process of transient in the system under consideration. Numerical simulation confirms an efficiency of the analytical construction. A similar construction is made to describe the transient in a system which contains a linear oscillator and a vibro-impact attachment with a comparatively small mass. A transient in such system under the external periodical excitation is considered too.

---

### INTRODUCTION

An investigation of transient is important in engineering, in particular, in problem of absorption. Over the past years different new devices have been used for the vibration absorption and for the reduction of the transient response of structures [1-5 et al.]. It seems useful to study nonlinear passive absorbers for this reduction.

In presented paper the transient in a system containing a linear oscillator, linearly coupled to an essentially nonlinear attachment with a comparatively small mass, is considered. A damping is taken into account. It is assumed that some initial excitation implies vibrations of the linear oscillator. The multiple scales method [6] is used to construct a process of transient in some nonlinear systems. A transfer of energy from the initially perturbed linear subsystem to the nonlinear attachment is observed. A similar construction is made to describe the transient in a system which contains the main linear subsystem and a vibro-impact absorber with a comparatively small mass. Both an exact integration with regards to conditions of impact, and the multiple scales method are used for this construction. The transient in such system under the external periodical excitation is considered too. Numerical simulation confirms an efficiency of the analytical construction in all considered systems.

### 1. TRANSIENT IN A SYSTEM CONTAINING AN ESSENTIALLY NONLINEAR ATTACHMENT

Let us consider a system with two connected oscillators, namely, one linear and one nonlinear with a comparatively small mass, which can be considered as absorber of the linear oscillator vibrations (Fig.1). Here  $M$  is a mass of the main linear subsystem,  $m$  is a mass of the nonlinear attachment,  $\omega^2$ ,  $\gamma$  and  $C$  characterize elastic springs,  $\delta$  characterizes the linear dissipation force. To emphasis a smallness of some inertial and elastic characteristics of the attachment, as well a smallness of the dissipation force, the next transformations will be used:  $m \rightarrow \varepsilon m$ ,  $C \rightarrow \varepsilon C$ ,  $\gamma \rightarrow \varepsilon \gamma$ ,  $\delta \rightarrow \varepsilon^2 \delta$ , where  $\varepsilon$  is the small parameter ( $\varepsilon \ll 1$ ). So, the system under consideration is described by the following differential equations:

---

<sup>1</sup> Corresponding author. Email [muv@kpi.kharkov.ua](mailto:muv@kpi.kharkov.ua)

$$\begin{cases} \varepsilon m \ddot{x} + \varepsilon c x^3 + \varepsilon^2 \delta \dot{x} + \varepsilon \gamma (x - y) = 0, \\ M \ddot{y} + \omega^2 y + \varepsilon^2 \delta \dot{y} + \varepsilon \gamma (y - x) = 0, \end{cases} \quad (1)$$

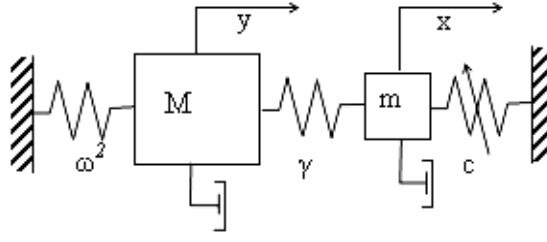


Fig. 1. The system  $m$  with two connected oscillators

The solution of the system (1) will be found by the multiple-scale method. One has

$$\begin{aligned} x &= x_0(t_0, t_1, t_2, \dots) + \varepsilon x_1(t_0, t_1, t_2, \dots) + \varepsilon^2 x_2(t_0, t_1, t_2, \dots) + \dots \\ y &= y_0(t_0, t_1, t_2, \dots) + \varepsilon y_1(t_0, t_1, t_2, \dots) + \varepsilon^2 y_2(t_0, t_1, t_2, \dots) + \dots, \end{aligned} \quad (2)$$

where

$$\begin{aligned} t_0 = t, t_1 = \varepsilon t, t_2 = \varepsilon^2 t, \dots, t_n = \varepsilon^n t, \dots, \quad \frac{d}{dt} = \frac{\partial}{\partial t_0} \frac{dt_0}{dt} + \frac{\partial}{\partial t_1} \frac{dt_1}{dt} + \frac{\partial}{\partial t_2} \frac{dt_2}{dt} + \dots = \\ = \frac{\partial}{\partial t_0} + \varepsilon \frac{\partial}{\partial t_1} + \varepsilon^2 \frac{\partial}{\partial t_2} + \varepsilon^3 \frac{\partial}{\partial t_3} + \dots = D_0 + \varepsilon D_1 + \varepsilon^2 D_2 + \varepsilon^3 D_3 + \dots \end{aligned}$$

One obtains in zero approximation by the small parameter the next equation:

$$\varepsilon^0 : MD_0^2 y_0 + \omega^2 y_0 = 0.$$

The solution of this equation is the following:

$$y_0 = A_1(t_1, t_2, \dots) \cos \psi_0, \quad \text{where } \psi_0 = \Omega t_0 + \varphi_0(t_1, t_2, \dots), \quad \Omega^2 = \frac{\omega^2}{M}.$$

One has in the next approximation by the small parameter the following ODE system:

$$\varepsilon^1 : \begin{cases} mD_0^2 x_0 + c x_0^3 + \gamma(x_0 - y_0) = 0, \\ MD_0^2 y_1 + 2MD_0 D_1 y_0 + \omega^2 y_1 + \gamma(y_0 - x_0) = 0. \end{cases} \quad (3)$$

The presentation of the  $x_0$  in the essentially nonlinear system of the zero approximation is chosen of the form

$$x_0 = B_1(t_1, t_2, \dots) \cos \psi_0 + B_2(t_1, t_2, \dots) \cos \psi_1$$

where  $\psi_1 = \bar{\Omega}(t_1, t_2, \dots)t_0 + \varphi_1(t_1, t_2, \dots)$ .

Equating cosine coefficients in the first equation and eliminating secular terms in the second one, we get nonlinear functional equations of the form:

$$\begin{cases} -mB_1 \Omega^2 + c \left( \frac{3}{4} B_1^3 + \frac{3}{2} B_1 B_2^2 \right) + \gamma B_1 = \gamma A_1 \\ \gamma - m \bar{\Omega}^2 + \frac{3}{4} c B_2^2 + \frac{3}{2} c B_1^2 = 0 \end{cases}, \quad \begin{cases} 2MA_1 \Omega \frac{\partial \varphi_0}{\partial t_1} + \gamma B_1 - \gamma A_1 = 0 \\ \frac{\partial A_1}{\partial t_1} = 0 \end{cases} \quad (4)$$

Thus  $A_1 = A_1(t_2, t_3, \dots)$ ,  $\frac{\partial \varphi_0}{\partial t_1} = \frac{\gamma(A_1 - B_1)}{2MA_1\Omega}$ .

Escaping calculations of the next approximations in the multiple scale method we give expressions for the amplitudes, frequencies and phases of zero-approximation  $x_0, y_0$  of (2), namely:

$$B_2 = \bar{c}(t_2, t_3, \dots)e^{-\frac{\delta}{2m}t_1}, \quad B_1 = c_0(t_2, t_3, \dots) + c_2(t_2, t_3, \dots)e^{-\frac{\delta}{m}t_1},$$

$$A_1 = \frac{\gamma - m\Omega^2}{\gamma}c_0 + \frac{3}{4\gamma}cc_0^3, \quad \bar{\Omega}^2 = (\gamma + (3/4)cB_2^2 + (3/2)cB_1^2)/m.$$

After time-averaging one has the following:  $\bar{\Omega}^2 \cong (\gamma + (3/2)cc_0^2)/m$ ,

$$\varphi_0 = \frac{\gamma}{2M\Omega}t_1 - \frac{\gamma}{2M\Omega A_1} \left( c_0 t_1 - c_2 \frac{m}{\delta} e^{-\frac{\delta}{m}t_1} \right) + c_2^*, \quad \text{where } c_2 = \frac{\frac{3}{2}c\bar{c}^2 c_0}{m\Omega^2 - \gamma - \frac{9}{4}cc_0^2}.$$

In such a way we have got the zero-approximation of sought solution containing four constants with respect to the variable  $t_0$ , namely,

$$c_1^* = c_1^*(t_3, t_4, \dots), c_2^* = c_2^*(t_2, t_3, \dots), c_3^* = c_3^*(t_2, t_3, \dots), \bar{c} = \bar{c}(t_2, t_3, \dots)$$

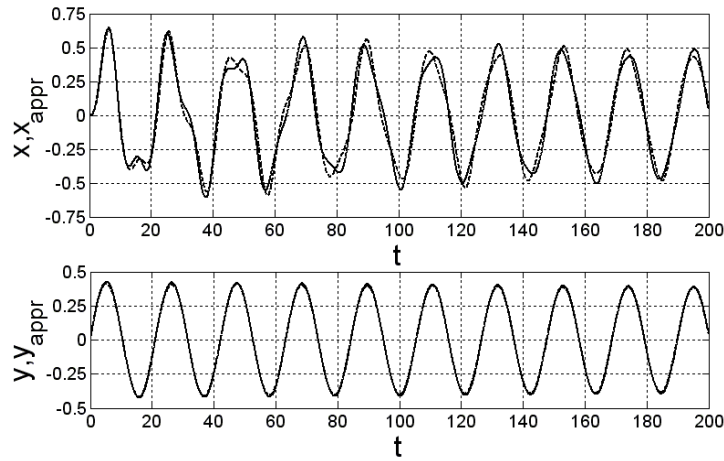


Fig. 2a.

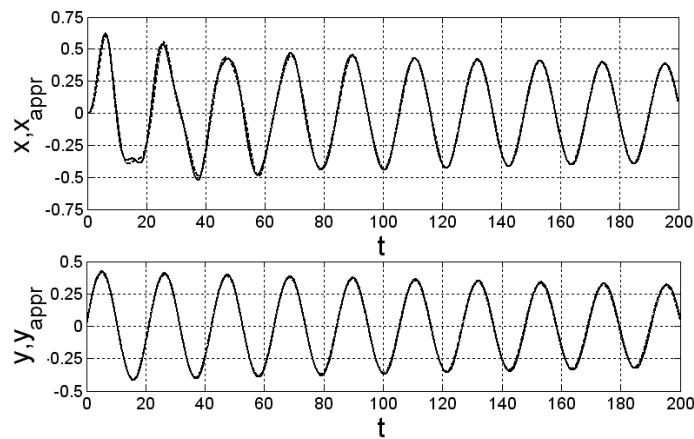


Fig. 2.b

Fig. 2. Comparison of results of analytical approximation (solid line) and ones obtained by Runge-Kutta procedure (dash line)

They were found numerically by Newton method from initial conditions:

$$x(0) = \dot{x}(0) = 0, \quad y(0) = 0, \dot{y}(0) = V,$$

which describe the impact initial excitation of vibrations in the linear subsystem.

In the Figure 2 results of comparing of the analytical solution with the numerical simulation obtained by using the Runge-Kutta procedure for different initial values are shown.

## 2. TRANSIENT IN THE VIBRO-IMPACT SYSTEM

One considers the 2-DOF vibro-impact system with the one-sided catch (Fig.3). This system contains the linear oscillator and the attachment with a comparatively small mass. It is presupposed to obtain analytical description of transient, both for free and forced oscillations, by using the multiple-scale method.

Equations of motion for the system under consideration in a case of the free vibrations are the following:

$$\begin{cases} \varepsilon m \ddot{x} + \varepsilon \gamma (x - y) + \varepsilon^2 \delta \dot{x} = 0; \\ M \ddot{y} + c^2 y + \varepsilon \gamma (y - x) + \varepsilon^2 \delta \dot{y} = 0, \end{cases} \quad (5)$$

where all notations and transformations of parameters are the same as in the Section 2. The small parameter ( $\varepsilon \ll 1$ ) is introduced to select a smallness of the attachment mass, the connection between oscillators and the dissipation force.

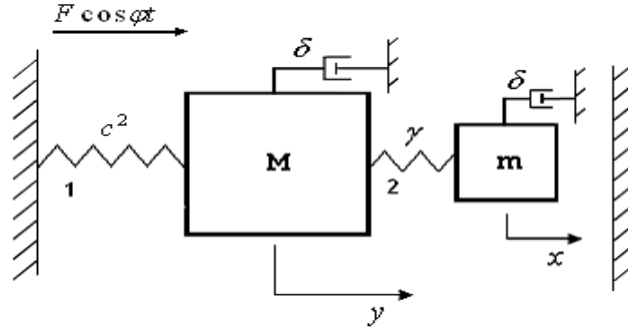


Fig. 3. The vibro-impact system under consideration

It is presupposed that an impact here is instantaneous. The restoration coefficient ( $0 \leq e \leq 1$ ) characterizes a lost of velocity in the instant of impact. One has the following conditions of the impact:  $x(t_k^+) = x(t_k^-) = x_{\max}$ ,  $\dot{x}(t_k^+) = -e\dot{x}(t_k^-)$ ,  $y(t_k^+) = y(t_k^-)$ ,  $\dot{y}(t_k^+) = \dot{y}(t_k^-)$ .

Here:  $t_k$  is the impact instant, where  $k$  is a number of the impact;  $t_k^-$  is an instant before impact,  $t_k^+$  is one after impact,  $x_{\max}$  is a distance between the equilibrium state and the catch.

### 2.1 Free oscillations in vibro-impact systems

To construct an analytical solution by using the multiple scale method, the expansions (2) are used. In zero approximation by small parameter the next solution can be obtained:

$$y_0 = A_0(t_1, t_2, t_3, \dots) \cos \Omega t_0 + B_0(t_1, t_2, t_3, \dots) \sin \Omega t_0,$$

$$\text{where } \Omega_0^2 = c^2/M; \quad \begin{cases} x_0 = \beta(A_0(t_1, \dots) \cos \Omega t_0 + B_0(t_1, \dots) \sin \Omega t_0) + \\ + A_1(t_1, \dots) \cos \sqrt{\gamma/m} t_0 + B_1(t_1, \dots) \sin \sqrt{\gamma/m} t_0, \end{cases} \quad \beta = \frac{\gamma}{m(\gamma/m - \Omega_0^2)}.$$

Conditions of secular terms elimination in the next approximation by the small parameter give us the following expressions for amplitudes of the zero approximation:

$$A_0 = -C_1 \sin \Omega_1 t_1 + C_2 \cos \Omega_1 t_1, \quad B_0 = C_1 \cos \Omega_1 t_1 + C_2 \sin \Omega_1 t_1,$$

$$\text{where } \Omega_1 = \frac{\gamma(\beta - 1)}{2M\Omega_0}.$$

Taking onto account the next approximation, one has the approximate solution of the form:

$$\begin{aligned}
x &= \beta(\cos \Omega_2 t \cdot (-R_1 C_1 + R_2 C_2) + \sin \Omega_2 t \cdot (R_2 C_1 + R_1 C_2)) + e^{\alpha t} \{C_3 \sin \beta_3 t + C_4 \cos \beta_3 t\}, \\
y &= C_1 \sin \Omega_2 t + C_2 \cos \Omega_2 t + \varepsilon \beta_1 e^{\alpha t} \{C_3 \sin \beta_3 t + C_4 \cos \beta_3 t\}, \\
R_1 &= \frac{\varepsilon \delta \Omega}{m \left( \frac{\gamma}{m} - \Omega^2 \right)}, \quad R_2 = 1 - \frac{2 \varepsilon \Omega \Omega_1}{\frac{\gamma}{m} - \Omega^2}, \quad \beta_3 = \sqrt{\frac{\gamma}{m}} - \beta_2 \varepsilon, \quad \Omega_2 = \Omega - \varepsilon \Omega_1.
\end{aligned} \tag{6}$$

Impact conditions (4) give the next relations connecting coefficients  $C_i$  before ( $C_i^k$ ) and after impact ( $C_i^{k+1}$ ):

$$\begin{aligned}
&\beta(\cos \Omega_2 t \cdot (-R_1 C_1^{k+1} + R_2 C_2^{k+1}) + \sin \Omega_2 t \cdot (R_2 C_1^{k+1} + R_1 C_2^{k+1})) + \\
&+ e^{\alpha t} \{C_3^{k+1} \sin \beta_3 t + C_4^{k+1} \cos \beta_3 t\} = \beta(\cos \Omega_2 t \cdot (-R_1 C_1^k + R_2 C_2^k) + \\
&+ \sin \Omega_2 t \cdot (R_2 C_1^k + R_1 C_2^k)) + e^{\alpha t} \{C_3^k \sin \beta_3 t + C_4^k \cos \beta_3 t\}. \\
&\Omega_2 \beta (-\sin \Omega_2 t \cdot (-R_1 C_1^{k+1} + R_2 C_2^{k+1}) + \cos \Omega_2 t \cdot (R_2 C_1^{k+1} + R_1 C_2^{k+1})) + \\
&+ e^{\alpha t} (\alpha \varepsilon \{C_3^{k+1} \sin \beta_3 t + C_4^{k+1} \cos \beta_3 t\} + \beta_3 \{C_3^{k+1} \cos \beta_3 t - C_4^{k+1} \sin \beta_3 t\}) = \\
&= -\varepsilon \Omega_2 \beta (-\sin \Omega_2 t \cdot (-R_1 C_1^k + R_2 C_2^k) + \cos \Omega_2 t \cdot (R_2 C_1^k + R_1 C_2^k)) + \\
&+ e^{\alpha t} (\alpha \varepsilon \{C_3^k \sin \beta_3 t + C_4^k \cos \beta_3 t\} + \beta_3 \{C_3^k \cos \beta_3 t - C_4^k \sin \beta_3 t\}) \\
&C_1^{k+1} \sin \Omega_2 t + C_2^{k+1} \cos \Omega_2 t + \varepsilon \beta_1 e^{\alpha t} \{C_3^{k+1} \sin \beta_3 t + C_4^{k+1} \cos \beta_3 t\} = \\
&= C_1^k \sin \Omega_2 t + C_2^k \cos \Omega_2 t + \varepsilon \beta_1 e^{\alpha t} \{C_3^k \sin \beta_3 t + C_4^k \cos \beta_3 t\} \\
&\Omega_2 (C_1^{k+1} \cos \Omega_2 t - C_2^{k+1} \sin \Omega_2 t) + \varepsilon \beta_1 e^{\alpha t} \{ \alpha \varepsilon (C_3^{k+1} \sin \beta_3 t + C_4^{k+1} \cos \beta_3 t) + \\
&+ \beta_3 (C_3^{k+1} \cos \beta_3 t - C_4^{k+1} \sin \beta_3 t) \} = \\
&= \Omega_2 (C_1^k \cos \Omega_2 t - C_2^k \sin \Omega_2 t) + \varepsilon \beta_1 e^{\alpha t} \{ \alpha \varepsilon (C_3^k \sin \beta_3 t + C_4^k \cos \beta_3 t) + \\
&+ \beta_3 (C_3^k \cos \beta_3 t - C_4^k \sin \beta_3 t) \}.
\end{aligned} \tag{7}$$

The numeric simulation is realized for the next values of parameters:  $M=1$ ,  $m=1$ ,  $\varepsilon=0.01$ ,  $\delta=10$ ,  $e=0.9$ ,  $x_{\max}=1.4$ ,  $\gamma=1.5$ ,  $c=1$ . Initial values simulate the instant impact to the linear subsystem:  $x(0)=0$ ,  $\dot{x}(0)=0$ ,  $y(0)=0$ ,  $\dot{y}(0)=\dot{V}_0=1$ . Comparison of the analytical solution and numerical simulation shows a good exactness of the analytical approximation (Fig.4).

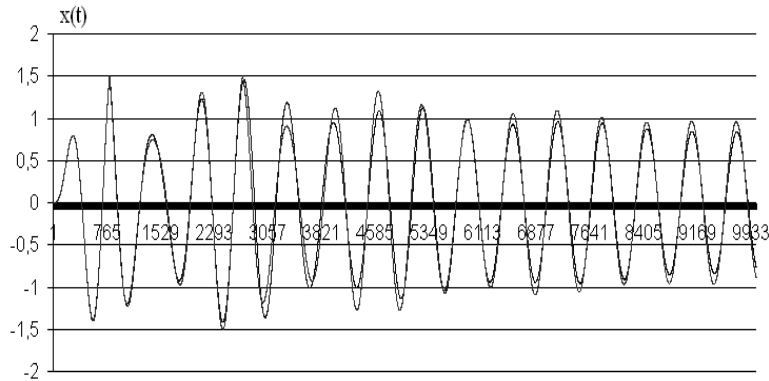


Fig. 4. Transient in a case of free oscillations in the vibro-impact system

## 2.2 Transient in a case of forced oscillations

One considers the same 2-DOF vibro-impact system in a case when an external periodic force acts to linear subsystem. The multiple scales method can be successfully used in this case too. In contrast with the solution, obtained in the sub-section 3.1, the part corresponding to the external excitation, has to be added. One writes the solution of the form:

$$\begin{aligned}
x &= \beta(\cos \Omega_2 t \cdot (-R_1 C_1 + R_2 C_2) + \sin \Omega_2 t \cdot (R_2 C_1 + R_1 C_2)) + \\
&+ e^{\alpha \varepsilon t} \{C_3 \sin \beta_3 t + C_4 \cos \beta_3 t\} + (F_2 + \varepsilon F_5) \cos \varphi t + \varepsilon F_6 \sin \varphi t, \\
y &= C_1 \sin \Omega_2 t + C_2 \cos \Omega_2 t + \varepsilon \beta_1 e^{\alpha \varepsilon t} \{C_3 \sin \beta_3 t + C_4 \cos \beta_3 t\} + \\
&+ (F_1 + \varepsilon F_3) \cos \varphi t + \varepsilon F_4 \sin \varphi t,
\end{aligned} \tag{8}$$

$$\text{where } F_1 = \frac{F}{(\Omega^2 - \varphi^2)}, \quad F_2 = \frac{\gamma F_1}{m(\gamma/m - \varphi^2)}, \quad F_3 = \frac{-\gamma(F_1 - F_2)}{M(\Omega^2 - \varphi^2)}, \quad F_4 = \frac{2\varphi F_1}{\Omega^2 - \varphi^2},$$

$$F_5 = \frac{\gamma F_3}{m(\gamma/m - \varphi^2)}, \quad F_6 = \frac{\frac{\gamma}{m} F_4 + \left(2 + \frac{\delta}{m}\right) F_2 \varphi}{\gamma/m - \varphi^2}.$$

Impact conditions (4) give some relations connecting coefficients  $C_i$  before ( $C_i^k$ ) and after impact ( $C_i^{k+1}$ ). These relations are not presented here.

Numerical simulation was made for the same parameters and initial values, as in the preceding sub-section. Comparison of the analytical solution and numerical simulation (Fig.5) shows a good exactness of the obtained analytical approximation. Vibrations of the linear subsystem with big mass are presented in the Fig. 5.

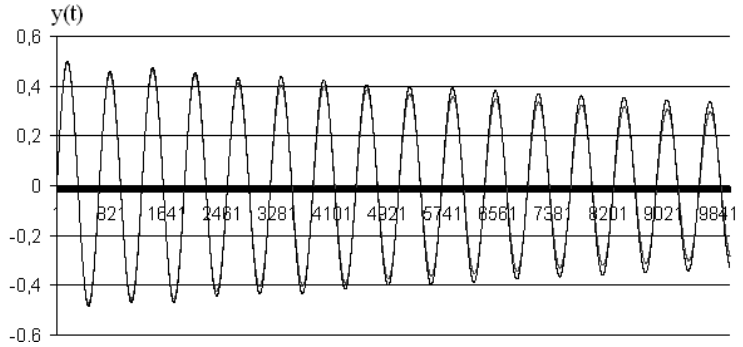


Fig. 5. Transient in a case of forced vibrations in the vibro-impact system.

## CONCLUSIONS

It is shown an efficiency of the multiple-scales method to describe a transient in essentially nonlinear finite-DOF systems.

## REFERENCES

- [1] *Vibrations in engineering* (K.V.Frolov, editor), Mashinostroenie, Moscow, 1995 (in Russian).
- [2] J. Shaw, S.Shaw, A.J.Haddow. On the response of the non-linear vibration absorber, *Int. Journal of Nonlinear Mechanics*, Vol. 24, pp. 281-293, 1989.
- [3] M.P. Karyeacis, T.K. Caughey. Stability of a Semi-active Impact Damper, *Trans. of the ASME. Journal of Applied Mechanics*, Vol. 56, pp. 926-940, 1989.
- [4] K. Avarmov, Yu. Mikhlin. Snap-through truss as a vibration absorber, *Journal of Vibration and Control*, Vol. 10, N 2, pp. 291-308, 2004.
- [5] Yu. Mikhlin, S. Reshetnikova. Dynamical interaction of an elastic system and essentially nonlinear absorber, *Journal of Sound and Vibration*, Vol. 283, pp. 91-120, 2005.
- [6] A.H. Nayfeh, D. Mook. *Nonlinear Oscillations*, John Wiley, New York, 1984.

**STABILITY ANALYSIS OF PERIODIC SOLUTIONS FOR A CLASS OF  
FRACTIONALLY DAMPED SYSTEM OF ENGINEERING INTEREST**

**Indrajit Mukherjee<sup>1</sup>**  
Indian Institute of Science,  
Bangalore, India

---

ABSTRACT

---

In this paper, a novel method is outlined to investigate the stability of periodic solutions for a class of dynamical systems with fractional derivative based damping. The present method essentially replaces the given fractional derivative based system by an equivalent partial differential equation, which is further approximated by a set of ordinary differential equations obtained by Galerkin projection based technique. The stability analysis is then carried on with the set of ordinary differential equations which is well established and well understood.

---

**INTRODUCTION AND BASIC THEORY**

The use of passive vibration elements to mitigate excessive level of vibration in structures and machines is a well established and accepted technique. These damping elements generally are polymeric in nature, for example elastomeric rubber. Viscous damping models, though being widely used in literature and practice doesn't turn out to be accurate enough to capture structural damping behaviors of these materials. Polymers have a strong dependency of their parameters on the frequency of vibrations and it is seen that the use of fractional derivative based damping model can circumvent these modeling difficulties. This has spurred the interest of researchers for fractional derivative based models, which are now being considered as one of the most effective techniques to model materials having memory or hereditary characteristics. Earlier works on Fractional Derivative based damping were done by Bagley and Torvik [1-3] who showed that half-order fractional derivative model describe the frequency dependence of polymer based damping material very well. Koeller [4] considered a fractional calculus model to describe creep and relaxation for viscoelastic materials. Some notable contributions on the developments of analytical techniques and numerical methods on fractional order systems can be found in [5-8]. There exist different ways of defining fractional derivative. We adopt, for our problem, the Riemann-Liouville definition, as stated below

$$D_a^\alpha [x(t)] \equiv \frac{d^\alpha x(t)}{d(t-a)^\alpha} \equiv \frac{1}{\Gamma(n-\alpha)} \frac{d^n}{dt^n} \int_a^t \frac{x(\tau)}{(t-\tau)^{\alpha-n+1}} d\tau, \quad (1)$$

where  $n$  is the smallest integer greater than or equal to  $\alpha$  and  $\Gamma$  represents the gamma function. Structural damping is best represented when coefficient  $\alpha$  lies in the range  $0 < \alpha < 1$ . For systems starting from rest i.e.  $a = 0$ , like the one which would be discussed here, where  $x(t) \equiv 0$  for  $t < 0$ , we have  $D^\alpha(-\infty) = D^\alpha(0)$ . We will drop the  $a$ -subscript and all fractional derivative will be based on  $a = 0$ . The above expression of fractional derivative now becomes

---

<sup>1</sup> Corresponding author. Email [mukherjee.indra@gmail.com](mailto:mukherjee.indra@gmail.com), [inder@aero.iisc.ernet.in](mailto:inder@aero.iisc.ernet.in)

$$D^\alpha [x(t)] \equiv \frac{d^\alpha}{dt^\alpha} x(t) \equiv \frac{1}{\Gamma(1-\alpha)} \frac{d}{dt} \int_0^t \frac{x(\tau)}{(t-\tau)^\alpha} d\tau. \quad (2)$$

In the present treatise we would choose half order derivative, i.e. when  $\alpha = \frac{1}{2}$ , as this best captures the damping characteristics of rubber like material. The expression of fractional derivative in that case reduces to

$$D^{\frac{1}{2}} [x(t)] \equiv \frac{d^{\frac{1}{2}}}{dt^{\frac{1}{2}}} x(t) \equiv \frac{1}{\Gamma(\frac{1}{2})} \frac{d}{dt} \int_0^t \frac{x(\tau)}{(t-\tau)^{\frac{1}{2}}} d\tau. \quad (3)$$

So the governing equation of motion of a single degree of freedom system having half order fractional derivative based damping and linear stiffness element driven by a harmonic load can be stated as

$$mD^2 [x(t)] + c_{df} D^{\frac{1}{2}} [x(t)] + kx(t) = F_0 \cos(\omega t), \quad (4)$$

where  $m, c_{df}, k, F_0, \omega$  are respectively mass, damping coefficient, spring stiffness, amplitude of impressed harmonic forcing and forcing frequency. Operator  $D^2$  denotes second derivative wrt. time  $t$ . However the price we pay in using fractional derivative based law for accurately modeling structural damping is by increasing the complexity of the systems. The governing equations of an oscillator with fractional law based damping no longer remains an ordinary differential equation (ODE). It becomes a FDE (Fractional differential equation) which actually is an integro-differential equation (IDE) or can also be labeled as a delay differential equation (with distributed delay) resulting in significant reduction in analytical tractability. Studies otherwise straightforward for a viscously-damped oscillator become fairly non-trivial for its fractionally damped counterpart. For example stability analysis for a viscous damped oscillator having time varying coefficients can easily be obtained by invoking the celebrated Floquet theory, a detailed account of which can be obtained in [9,10]. However the stability analysis for fractionally damped system having time varying coefficients still continues to remain an area not well addressed and to the best of author's knowledge very little or almost no work has been done having an engineering flavor. However we often arrive at situations where carrying out such analysis becomes a mandatory check for qualitative treatment of such systems like while analyzing the stability behavior of periodic solutions of fractionally damped nonlinear system. In this article a method is discussed which enables us to obtain a qualitative treatment of stability behavior of a fractionally damped nonlinear oscillator. The method can also be applied for stability analysis of parametric fractional order differential equation. Before embarking on the problem of interest it seems logical to have a quick perfunctory glance at the formulation of stability analysis of periodic solutions for linear and nonlinear systems with time varying coefficients describable by ordinary differential equation.

## 1. STABILITY ANALYSIS OF STEADY STATE SOLUTION

The stability of the periodic solutions obtained by using Galerkin projection based methods can be investigated by perturbing the state variables about the steady state solutions. Consider the governing equation of a general nonlinear system, whose stability characteristics of steady state response needs to be evaluated, given by

$$\mathbf{M}\ddot{\mathbf{q}} + \mathbf{C}\dot{\mathbf{q}} + \mathbf{K}\mathbf{q} + \mathbf{F}(\mathbf{q}, \dot{\mathbf{q}}) = \mathbf{P}(t), \quad (5)$$

where  $\mathbf{M}, \mathbf{C}$  and  $\mathbf{K}$  are respectively mass, stiffness and damping matrices of size  $n \times n$ ,  $\mathbf{F}$  and  $\mathbf{P}$  are vectors of size  $n \times 1$  containing nonlinear terms and impressed forcing. Let  $\mathbf{q}_0$  be the steady state solution of the system, such that  $\mathbf{q}_0(t+T) = \mathbf{q}_0(t)$ . Perturbing the obtained steady state solution  $\mathbf{q}_0$  by  $\Delta\mathbf{q}$  we get the incremental equation of the following form

$$\mathbf{M}\Delta\ddot{\mathbf{q}} + \bar{\mathbf{C}}\Delta\dot{\mathbf{q}} + \bar{\mathbf{K}}\Delta\mathbf{q} = \mathbf{0}, \quad (6)$$

where

$$\bar{\mathbf{K}} = \mathbf{K} + \left(\frac{\partial \mathbf{F}}{\partial \mathbf{q}}\right)_{(\mathbf{q}_0, \dot{\mathbf{q}}_0)}, \quad \bar{\mathbf{C}} = \mathbf{C} + \left(\frac{\partial \mathbf{F}}{\partial \dot{\mathbf{q}}}\right)_{(\mathbf{q}_0, \dot{\mathbf{q}}_0)}.$$

The stability of the steady state solutions corresponds to the stability of the incremental equation (6), which is a linear ordinary differential equation with periodic coefficients in  $\bar{\mathbf{K}}$  and  $\bar{\mathbf{C}}$ . Equation (6) can be re written as

$$\dot{\mathbf{X}} = \mathbf{Q}(t)\mathbf{X}, \quad (7)$$

where

$$\mathbf{Q}(t) = \begin{bmatrix} \mathbf{0} & \mathbf{I} \\ -\bar{\mathbf{K}}\mathbf{M}^{-1} & -\bar{\mathbf{C}}\mathbf{M}^{-1} \end{bmatrix}, \quad \mathbf{0} \text{ and } \mathbf{I} \text{ are identity matrices of}$$

order  $n \times n$ . Since each component of  $\mathbf{q}_0$  is a periodic solution of  $t$  with period  $T$ .

Each element of  $\mathbf{Q}$  is also a periodic function with the same period. For equation (7) there exists a fundamental set of solutions

$$\mathbf{y}_k = [y_{1k}, y_{2k}, \dots, y_{Nk}], \quad k = 1, 2, \dots, N, \quad (8)$$

where  $N = 2n$ ,  $n$  being the degrees of freedom of the system. This fundamental set can be expressed in a matrix called fundamental solution matrix  $\mathbf{Y}$ ,

$$\mathbf{Y} = \begin{bmatrix} y_{11} & y_{12} & \cdots & y_{1N} \\ y_{21} & y_{22} & \cdots & y_{2N} \\ \vdots & \vdots & \vdots & \vdots \\ y_{N1} & y_{N2} & \cdots & y_{NN} \end{bmatrix}.$$

It can easily be verified that  $\mathbf{Y}$  satisfies matrix equation

$$\dot{\mathbf{Y}} = \mathbf{Q}(t)\mathbf{Y}. \quad (9)$$

Since  $\mathbf{Q}(t+T) = \mathbf{Q}(t)$ , therefore the following relation also holds

$$\mathbf{Y}(t+T) = \mathbf{P}\mathbf{Y}(t), \quad (10)$$

where  $\mathbf{P}$  is a non-singular constant matrix called the transition matrix. Floquet theory states that stability of the periodic solution of the system given by equation (5) is governed by the eigenvalues of the matrix  $\mathbf{P}$ . If all the moduli of the eigenvalues of  $\mathbf{P}$  are less than unity, the motion is bounded and the solution is stable. The transition matrix  $\mathbf{P}$  can be numerically evaluated by using initial condition  $\mathbf{Y}(0) = \mathbf{I}$ . Then we get  $\mathbf{P} = \mathbf{Y}(T)$ , whose eigenvalues dictates the stability of the system.

## 2. PROBLEM FORMULATION

The method adopted for stability analysis in this article hinges mainly on the formulation given in [11], wherein Singh et al. used it for their numerical scheme for fractional order system. It has already been stated that fractionally damped system are in fact infinite dimensional system. The present scheme essentially replaces this original infinite dimensional system with an equivalent infinite dimensional system which in this case is a partial differential equation (PDE). We then take recourse to the Galerkin projection technique. The Galerkin projection method using suitably chosen shape functions ideally reduces a PDE to an infinite system of ordinary differential equations (ODEs). However for a practicable analysis we introduce an approximation at this stage by reducing the PDE to a finite numbers of ODEs which, is adequate to capture the essential dynamics of the original system. Once this set of ODEs is obtained it then becomes a routine exercise to carry out the stability analysis which is already illustrated in the previous section. The method can be described in details as follows. Consider the PDE in  $t$  with a free parameter  $\xi$ , which could also be viewed as an ODE.

$$\frac{\partial}{\partial t} u(\xi, t) + \xi^{\frac{1}{\alpha}} u(\xi, t) = \delta(t), \quad u(\xi, 0^-) \equiv 0, \quad (11)$$

where  $\alpha > 0$  and  $\delta(t)$  is the Dirac delta function. The solution is

$$u(\xi, t) = h(\xi, t) = e^{\xi^{-\frac{1}{\alpha}} t}, \quad (12)$$

where the notation  $h(\xi, t)$  is used to denote impulse response function. On integrating the function  $h$  with respect to  $\xi$  between 0 and  $\infty$  we get a function only of  $t$ , given by

$$g(t) = \int_0^{\infty} h(\xi, t) d\xi = \frac{\Gamma(1+\alpha)}{t^\alpha}. \quad (13)$$

Now if we replace the forcing  $\delta(t)$  in equation (11) with some sufficiently well-behaved function  $\dot{x}(t)$ , then the corresponding impulse response  $r(t)$  of the same system, again starting from rest at  $t = 0$ , is (the last two expressions are equivalent)

$$r(t) = \int_0^t g(t-\tau)\dot{x}(t)d\tau = \Gamma(1+\alpha) \int_0^t \frac{\dot{x}(t)}{(t-\tau)^\alpha} d\tau = \Gamma(1+\alpha) \int_0^t \frac{\dot{x}(t-\tau)}{t^\alpha} d\tau. \quad (14)$$

On comparison with equation (2) we find that  $r(t) = \Gamma(1-\alpha)\Gamma(1+\alpha)D^\alpha[x(t)]$ . In this way an  $\alpha$  order derivative has been replaced by operations which involve solving the PDE in  $u(\xi, t)$ ,

$$\frac{\partial}{\partial t} u(\xi, t) + \xi^{\frac{1}{\alpha}} u(\xi, t) = \dot{x}(t), \quad u(\xi, 0^-) \equiv 0 \quad (15)$$

By integrating it is possible to find

$$D^\alpha[x(t)] = \frac{1}{\Gamma(1-\alpha)\Gamma(1+\alpha)} \int_0^{\infty} u(\xi, t) d\xi, \quad (16)$$

which is the expression to be evaluated. The system chosen above was first prompted by Chatterjee [12] which later was used in [11]. Equation (15) represents an infinite dimensional system, and so we have replaced one infinite dimensional system (fractional derivative) with another. The advantage gained is that we can use a Galerkin projection to reduce equation (15) to a finite dimensional system

of ODEs. We, next assume  $u(t) = \sum_{i=1}^n a_i(t)\Phi_i(\xi)$  to be an approximate solution to the equation (15),

where  $n$  is finite, the shape functions  $\Phi_i(\xi)$  are user defined and the  $a_i$  are the unknowns to be solved for. We substitute approximate expression for  $u(\xi, t)$  in the equation (15) and define

$$R(\xi, t) = \sum_{i=1}^n \left\{ a_i(t)\Phi_i(\xi) + \xi^{\frac{1}{\alpha}} a_i(t)\Phi_i(\xi) \right\} - \dot{x}(t), \quad (17)$$

where  $R(\xi, t)$ , is the residual. The residual is made orthogonal to the shape functions, yielding  $n$  equations

$$\int_0^{\infty} R(\xi, t)\Phi_m(\xi)d\xi = 0, \quad m = 1, 2, \dots, n. \quad (18)$$

Equations (18) constitute  $n$  ODEs, which can be written in the form

$$\mathbf{A}\dot{\mathbf{a}} + \mathbf{B}\mathbf{a} = \mathbf{c}\dot{x}(t), \quad (19)$$

where  $\mathbf{A}$  and  $\mathbf{B}$  are  $n \times n$  matrices  $\mathbf{a}$  is  $n \times 1$  vector containing  $a_i$ s and  $\mathbf{c}$  is also a  $n \times 1$ . The entries of  $\mathbf{A}$ ,  $\mathbf{B}$  and  $\mathbf{c}$  can be expressed in terms of indicial notations as

$$A_{mi} = \int_0^{\infty} \Phi_m(\xi)\Phi_i(\xi)d\xi = 0, \quad B_{mi} = \int_0^{\infty} \xi^{\frac{1}{\alpha}}\Phi_m(\xi)\Phi_i(\xi)d\xi, \quad c_m = \int_0^{\infty} \Phi_m d\xi.$$

So given a system, linear or nonlinear with half order fractional derivative based damping shown as

$$\ddot{x} + f(x, \dot{x}, D^{\frac{1}{2}}x, t) = 0. \quad (20)$$

We can replace it after approximating the terms containing fractional derivative by the following expression

$$D^{\frac{1}{2}}[x(t)] = \frac{1}{\Gamma(1/2)\Gamma(3/2)} \int_0^{\infty} u(\xi, t) d\xi \approx \frac{1}{\Gamma(1/2)\Gamma(3/2)} \mathbf{c}^T \mathbf{a}, \quad (21)$$

and then augmenting the equation with equation (19). This is shown in equation (22),

$$\begin{cases} \ddot{x} + f_1(x, \dot{x}, \mathbf{c}, \mathbf{a}, t) = 0 \\ \mathbf{A}\dot{\mathbf{a}} + \mathbf{B}\mathbf{a} = \mathbf{c}\dot{x}(t), \end{cases} \quad (22)$$

The size of vectors  $\mathbf{a}$  and  $\mathbf{c}$  depend on the numbers of shape functions chosen to approximate the expression containing fractional derivative. With a little effort equation (22) can be expressed in the state space form as

$$\dot{\bar{x}} + \bar{f}_1(\bar{x}, t) = 0, \quad (23)$$

where  $\bar{\mathbf{x}} = [\mathbf{x}, \mathbf{a}]^T$  is the vector of extended state variable and  $\bar{f}_1 = [f_1, \mathbf{A}^{-1}\mathbf{c}\dot{x}(t) - \mathbf{A}^{-1}\mathbf{B}\mathbf{a}]^T$  is the augmented function vector. With the above formulation at hand it now becomes a routine exercise to carry out the stability analysis in a manner as laid out in section 1.

## 2.1 Example.

Consider the equation as shown below

$$m\ddot{x} + c_{df} D^{\frac{1}{2}}x + (\delta + \varepsilon \cos(t))x = 0, \quad (24)$$

This can be treated as a fractionally damped non-autonomous equation or it could be the incremental equation obtained after linearizing some equation about its steady state solution in the same way as we arrive at equation (6). It should be noted that for the second case it suffices to have the incremental equation as this only dictates the stability behavior. So the parent equation is not mentioned here. We first arrive at the state space form as shown in equation (23) by choosing 12 shape functions to approximate the fractional order term, wherein  $\mathbf{A}$  and  $\mathbf{B}$  matrices are of size  $12 \times 12$  and  $\mathbf{c}$  is a  $12 \times 1$  vector. Due to space constraint  $\mathbf{A}$ ,  $\mathbf{B}$  and  $\mathbf{c}$  are not reproduced here. The following case studies are done to establish the proposed technique.

### 2.1.1 Case (a) : Stable

The following values for the parameters of the system are considered for the case study.  $m = 1, c_{df} = 0.4, \delta = 0.25, \varepsilon = 0.5$ . The eigenvalues of the transition matrix (refer section 1) are obtained as  $\mu = [-0.42, -0.24, 0.57, 0.04, 0.92, 0.98, 0.99, 0.99, 0, 0, 0, 0, 0, 0]^T$ . The analysis based on the present method states the system is stable as moduli of all the eigenvalues are less than unity. A numerical solution of the systems response confirms this result (refer Fig. 1)

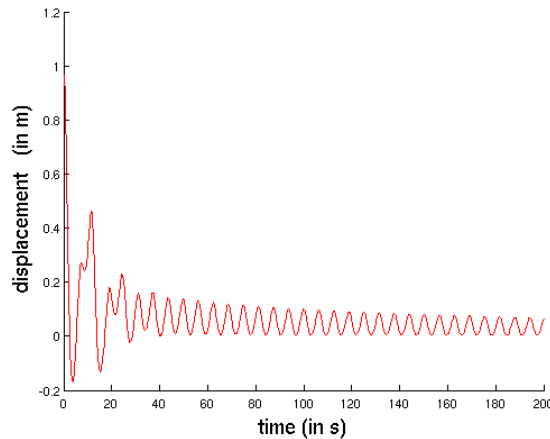


Fig. 1 The displacement time plot showing bounded system response

### 2.1.2 Case (b) : Unstable

For the second example we choose  $m = 1, c_{df} = 0.4, \delta = 0.25, \varepsilon = 1$ . The eigenvalues of the transition matrices (having size  $12 \times 12$ ) is shown below :

$\mu = [-1.917, 0.54, 0.92, 0.98, 0.999, 0.998, -0.0643, 0.041, 0, 0, 0, 0, 0]^T$ . Our analysis predicts that the steady state solution is unstable as the modulus of first eigenvalue is greater than unity. We confirm this result by numerically obtaining the displacement vs. time plot which depicts its unbounded nature. (refer the Fig. 2)

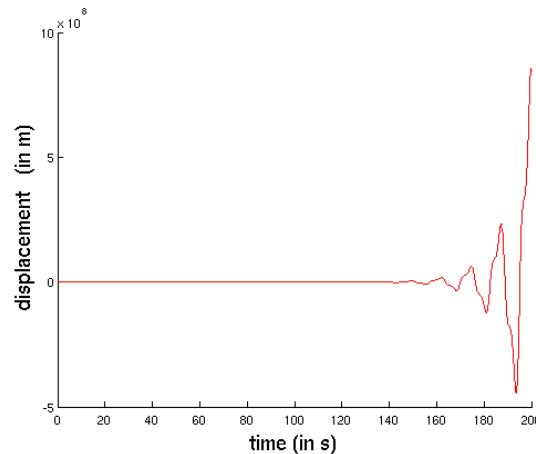


Fig. 2 The displacement time plot showing unbounded system response

## CONCLUSIONS

A method for obtaining stability of fractionally damped system with periodic coefficients is obtained. The benchmark problems carried out establishes the method to be effective and easy to implement.

## REFERENCES

- [1] Bagley R. L. and Torvik P. J. Fractional calculus: A different approach to the analysis of viscoelastically damped structures, *AIAA Journal*, 21(5), pp. 741-748, 1983.
- [2] Bagley R. L. and Torvik P. J. A theoretical basis for the application of fractional calculus to viscoelasticity, *Journal of Rheology*, 27(3), pp. 201-210, 1983.
- [3] Bagley R. L. and Torvik P. J. Fractional calculus in the transient analysis of viscoelastically damped structures, *AIAA Journal*, 23(6), pp. 918-925, 1985.
- [4] Koeller R. C. Application of fractional calculus to the theory of viscoelasticity, *ASME, Journal of Applied Mechanics*, 51, pp. 299-307, 1984.
- [5] Rossikhin Y. A. and Shitikova M. V. Application of fractional calculus for analysis of nonlinear damped vibrations of suspension bridges, *ASCE, Journal of Engineering Mechanics*, 27, pp. 1029-1036, 1998.
- [6] Wahi P. and Chatterjee A. Averaging oscillations with small fractional damping and delayed terms, *Nonlinear Dynamics*, 38, pp. 3-22, 2004.
- [7] Padovan J. Computational algorithms for finite element formulation involving fractional operators, *Computational Mechanics*, 2, pp. 271-287, 1987.
- [8] Yuan L. and Agrawal O. A numerical scheme for dynamic systems containing fractional derivatives, *Transaction of ASME, J. Vibration and Acoustics*, 124, pp. 321-324, 2002.
- [9] Richard H. Rand. *Lecture Notes on Nonlinear Vibration*, available online at <http://www.tam.cornell.edu/randdocs/>.
- [10] Ferdinand Verhulst. *Nonlinear Differential Equations and Dynamical Systems*, Springer, Berlin, 1996.
- [11] Singh S. J. and Chatterjee A. Galerkin projections and finite elements for fractional order derivatives, *Nonlinear Dynamics*, 45, pp. 183-216, 2006.
- [12] Chatterjee A. Statistical origins of fractional derivatives in viscoelasticity, *Journal of Sound and Vibration*, 284, pp. 1239-1245, 2005.

## RECONSTRUCTION OF THE THIRD ORDER DYNAMICAL SYSTEMS FROM SIGNALS

**Evgeniy D. Pechuk<sup>1</sup>**

Institute of  
Hydromechanics NASU  
Kyiv, Ukraine

**Tatyana S. Krasnopol'skaya**

Institute of  
Hydromechanics NASU  
Kyiv, Ukraine

---

### ABSTRACT

---

The problem of reconstruction of the deterministic dynamical system from output signals is very important. Two reconstruction methods have been used and compared. First one is the method of successive differentiation and the second is based on delay coordinates. It was firstly suggested to choose time delay parameter from the stable region of a divergence of the reconstructed system. Results show that both methods can capture regular and chaotic signals from reconstructed systems of the third order with nonlinear terms up to sixth order. Types of signals were examined with spectral methods, construction of phase portraits and Lyapunov exponents. The first method gives the solution which the power spectrum for the regular signals coincides with the output signal spectrum up to 96% for the first three peaks. The second method gives a mistake around 2 % and determines the maximum Lyapunov exponent more precisely for chaotic regimes (with a precision to  $O(10^{-3})$ ) than the first method.

---

### INTRODUCTION

The problem of reconstruction of deterministic dynamical system from output signals is of great importance in studying of properties of experimental signals such as acoustic signals, ECG, EEG and so on. Reconstructed dynamical system may add a significant qualitative information to chaotic data analysis. Stability conditions, bifurcation curves, all types of steady – state regimes could be studied for solutions of a reconstructed system.

Two reconstruction methods have been developed by Crutchfield and McNamara [1] and used for variety of signals later [2-4].

The first method is based on suggestion that the signal can be presented by a function that has at least three derivatives, so this is method of successive differentiation. Applying this method the dynamical system has a following form [1-4]:

$$\begin{cases} \frac{dx_1}{dt} = x_2 \\ \frac{dx_2}{dt} = x_3 \\ \frac{dx_3}{dt} = F_3(x_1, x_2, x_3) \end{cases} \quad (1)$$

where  $F_3(x_1, x_2, x_3)$  is a nonlinear function.

The second method of reconstruction is based on delay coordinates. We need to reconstruct the dynamical system from the time series of some state variable  $x(t)$  with the fixed sampling step  $dt$ . We have series of  $s_k = x(kdt)$ ,  $k=0,1,2,\dots,N$ , using value of time delay  $\tau = ndt$  (which is chosen to yield optimal reconstruction [1]) we construct the dynamical system in the form [1-4]:

---

<sup>1</sup> Corresponding author. Email [uzuzun@i.ua](mailto:uzuzun@i.ua)

$$\begin{cases} \frac{dx_1}{dt} = F_1(x_1, x_2, x_3) \\ \frac{dx_2}{dt} = F_2(x_1, x_2, x_3) \\ \frac{dx_3}{dt} = F_3(x_1, x_2, x_3) \end{cases} \quad (2)$$

where  $x_1(t) = x(t)$ ;  $x_2(t) = x(t + \tau)$ ;  $x_3(t) = x(t + 2\tau)$ ,  $F_i(x_1, x_2, x_3)$  are nonlinear functions.

## 1. RECONSTRUCTION OF DYNAMICAL SYSTEMS FOR OUTPUT SIGNALS OF PENDULUM SYSTEM

Reconstruction methods are applied to the signals of a deterministic dynamical system (3) of pendulum oscillations which may have regular and chaotic regimes [5]:

$$\begin{cases} \frac{dy_1}{dt} = -0.1y_1 - y_2y_3 - \frac{1}{8}(y_1^2y_2 + y_2^3) \\ \frac{dy_2}{dt} = -0.1y_2 + y_1y_3 - \frac{1}{8}(y_2^2y_1 + y_1^3) + 1 \\ \frac{dy_3}{dt} = -0.5y_2 - 0.61y_3 + F \end{cases} \quad (3)$$

Nonlinear functions  $F_i(x_1, x_2, x_3)$  in the systems (1) and (2) have the following form

$$F(x_1, x_2, x_3) = a + \sum_{i=1}^3 a_i x_i + \sum_{i,j=1}^3 a_{ji} x_j x_i + \dots + \sum_{o,m,n,k,j,i=1}^3 a_{omnkji} x_o x_m x_n x_k x_j x_i \quad (4)$$

with nonlinear terms up to third order for the regular signals and up to the six order for the chaotic.

The traditional way to obtain time delay parameter  $\tau = ndt$  for the second method of reconstruction is to use time interval when the autocorrelation function is equal to zero [2-4]. For such chosen  $\tau$  the divergence of a reconstructed system may not be negative. So that we introduce other way to choose  $\tau$ . Real system is nonconservative and, the divergence of systems should be negative too. For example, for the original system (3)  $div$  is equal to -0.81. In Fig. 1 the dependence of reconstructed systems divergence on  $n$  in the steady – state regimes is shown. We choose  $n$  for time delay  $\tau$  from the stable region of  $div$ .

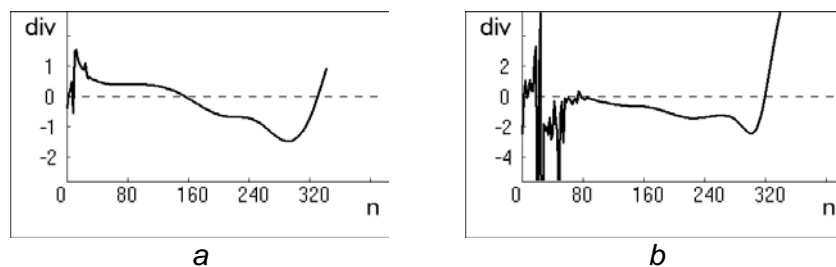


Fig. 1 The dependence of reconstructed systems divergence on  $n$  for regular initial signal ( $F = 0.257$ ) (a) and chaotic ( $F = 0.114$ ) (b).

For every value of the bifurcation parameter  $F$  from the interval  $0.1 \leq F \leq 0.3$  the reconstructed systems were built and the output signals were determined. And then the largest Lyapunov exponents [6] were calculated. For that purpose we use the fifth – order Runge – Kuttas method with the precision of  $O(10^{-7})$ . Initial conditions were selected in the vicinity of the original signal, and for the steady – state regime signals we choose  $N = 2^{18}$ ,  $dt = 0.004$ .

The dependence of the largest Lyapunov exponent of the system (3) on values of the bifurcation parameter  $F$  is shown in Fig. 2 (a). The dependences of the largest Lyapunov exponent on  $F$  for reconstructed dynamical systems (1) and (2) are shown in Fig. 2 (b) – (c) correspondingly.

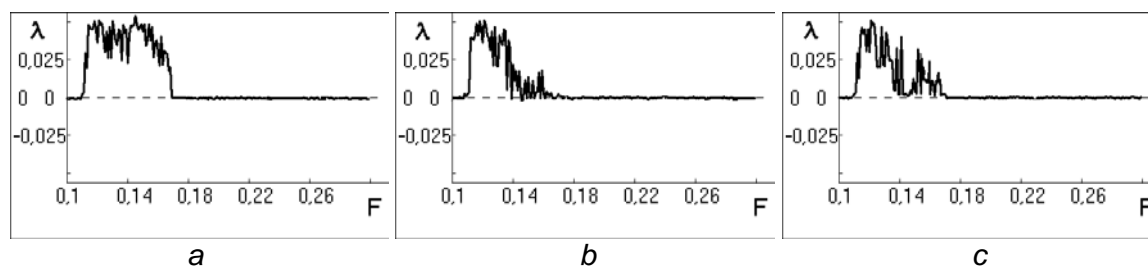


Fig. 2. The largest Lyapunov exponent of the system (3) (a), of the reconstructed systems (b) – (c).

We may see similarity of both graphs to the dependence for the original system in Fig. 2 (a) with the exception of the region  $0.15 \leq F \leq 0.18$  where the transition to chaos occurs.

## 2. RECONSTRUCTED SYSTEMS FOR REGULAR OUTPUT SIGNALS

As was shown in the book [5] the solution of the pendulum system would be regular if bifurcation parameter is  $F = 0.257$ . We used this value and solved the system (3) in order to get the output signal. Then we reconstruct the system using the two methods. As a result the first method gives the system [7,8]

$$\left\{ \begin{array}{l} \frac{dx_1}{dt} = x_2 \\ \frac{dx_2}{dt} = x_3 \\ \frac{dx_3}{dt} = -1.146 - 0.8x_1 - 2.211x_2 - 1.736x_3 - 0.466x_1^2 - 1.234x_1x_2 + \\ -0.507x_1x_3 - 0.119x_2^2 + 0.034x_2x_3 - 0.144x_3^2 + \\ -0.134x_1^3 - 0.08x_1^2x_2 + 0.004x_1^2x_3 - 0.041x_1x_2^2 - 0.05x_1x_2x_3 + \\ + 0.006x_1x_3^2 - 0.041x_2^3 + 0.003x_2^2x_3 - 0.01x_2x_3^2 + 0x_3^3 \end{array} \right. \quad (5)$$

For the second method we reconstruct the system using small initial value for the delay parameter and build the dependence of the divergence on value  $n$  and choose  $n$  from the stable interval of the delay parameter ( Fig. 1 (a),  $n = 240$ ). As the result the system gets the form (6), if we take into account nonlinear terms only to the third order of nonlinearity.

Projections of the limit cycle with two loops on the plane are shown in Fig. 3 (a) – (c) for the solution of the original system (3) (Fig. 3 (a)) and the reconstructed dynamical systems (5) – (6) (Fig. 3 (b) – (c)). Since for reconstruction we use only the first variable signal phase portrait projections on the plane with the second variable only qualitatively are look like the original limit cycle with two loops. Time realizations of the first variable and their power spectrums are presented in Fig. 3 (d) – (i). Fig. 3 (d) and Fig. 3 (g) describe the solution of the original system (3), and Fig. 3 (e) – (f) and Fig. 3 (h) – (i) give the information about solutions of the dynamical systems (5) –(6).

Since power spectrum indicates the power contained at each frequency, the peak heights corresponds to the squared wave amplitudes (i.e. the wave energy) at the corresponding frequencies. The first method of reconstruction gives the solution which the power spectrum for the regular signals coincides with the output signal power spectrum up to 96% for the first three peaks. The second method gives the precision up to 98%. Also the second method determines the maximum Lyapunov exponent more precisely for chaotic regimes (with a precision to  $O(10^{-3})$ ) than the first method.

$$\begin{cases}
\frac{dx_1}{dt} = -0.266 - 2.135x_1 + 3.545x_2 - 1.574x_3 - 0.131x_1^2 + 0.685x_1x_2 + \\
- 0.352x_1x_3 - 0.393x_2^2 + 0.298x_2x_3 - 0.176x_3^2 + \\
+ 0.011x_1^3 + 0.017x_1^2x_2 - 0.042x_1^2x_3 - 0.037x_1x_2^2 + 0.093x_1x_2x_3 + \\
- 0.018x_1x_3^2 - 0.008x_2^3 - 0.035x_2^2x_3 + 0.006x_2x_3^2 - 0.007x_3^3 \\
\frac{dx_2}{dt} = 0.042 - 0.505x_1 - 0.427x_2 + 0.944x_3 + 0.072x_1^2 - 0.171x_1x_2 + \\
+ 0.048x_1x_3 - 0.013x_2^2 - 0.096x_2x_3 - 0.006x_3^2 + \\
- 0.005x_1^3 + 0.002x_1^2x_2 + 0.013x_1^2x_3 - 0.003x_1x_2^2 + 0.003x_1x_2x_3 + \\
- 0.015x_1x_3^2 + 0.002x_2^3 + 0.006x_2^2x_3 + 0.009x_2x_3^2 - 0.001x_3^3 \\
\frac{dx_3}{dt} = -0.06 + 0.31x_1 - 1.576x_2 + 1.224x_3 - 0.081x_1^2 + 0.125x_1x_2 + \\
- 0.021x_1x_3 + 0.048x_2^2 - 0.107x_2x_3 - 0.046x_3^2 + \\
+ 0.005x_1^3 - 0.009x_1^2x_2 + 0.006x_1^2x_3 - 0.006x_1x_2^2 - 0.056x_1x_2x_3 + \\
+ 0.056x_1x_3^2 + 0.008x_2^3 - 0.007x_2^2x_3 - 0.028x_2x_3^2 + 0x_3^3
\end{cases} \quad (6)$$

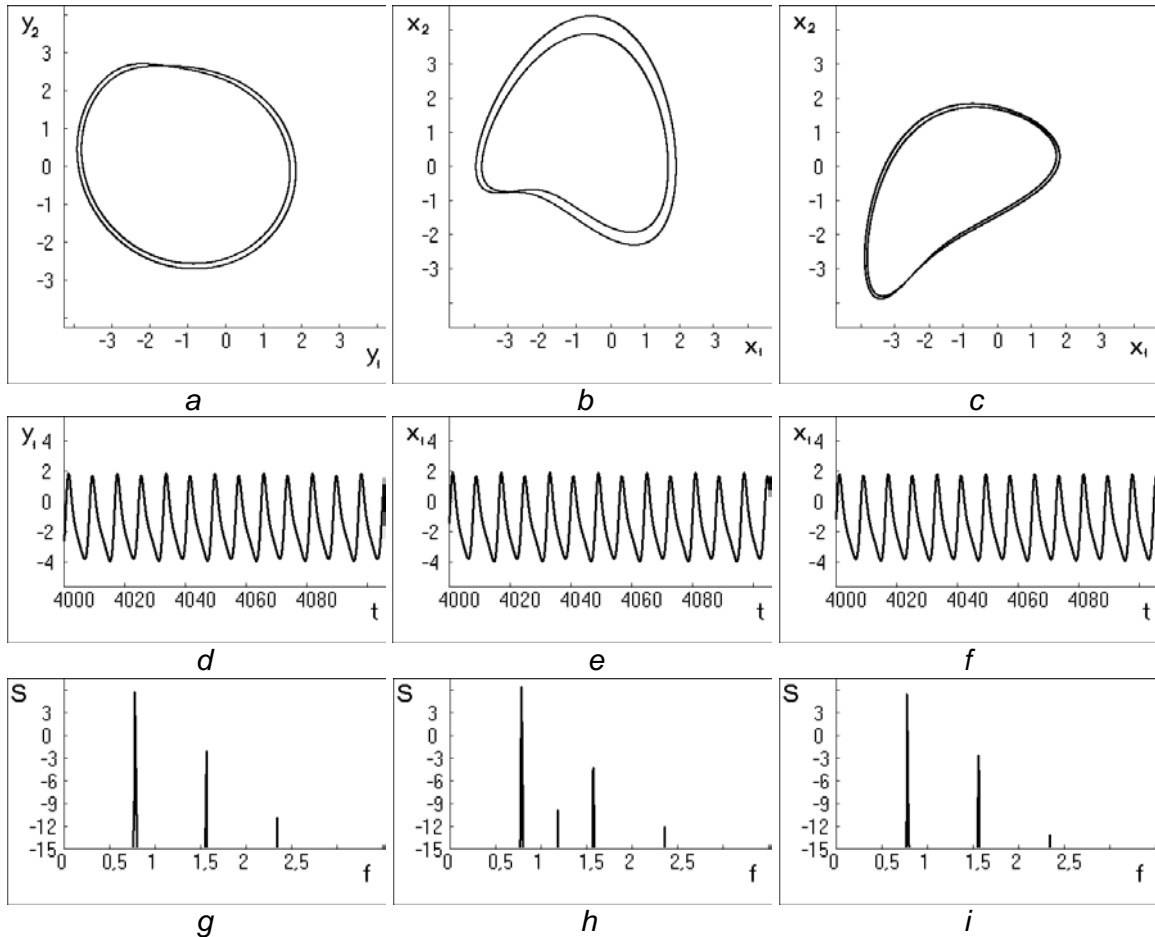


Fig. 3 The portrait of initial system (a) ( $F = 0.257$ ), the portraits of the systems (5) – (6) (b)–(c), their time realizations (d)–(f) and power spectrums (g)–(i).

### 3. RECONSTRUCTED SYSTEMS FOR CHAOTIC OUTPUT SIGNALS

Now we use such parameter  $F$  for the pendulum original system when this system has the chaotic solution, namely  $F = 0.114$ . Then we reconstruct the system using the two methods of reconstruction with nonlinear function  $F_i(x_1, x_2, x_3)$  with nonlinear terms up to the sixth order. For the second method we reconstruct the system using small initial value for the delay parameter and build the dependence of the divergence on value  $n$  and choose  $n$  from the stable interval of the delay parameter ( Fig. 1 (b),  $n = 120$ ).

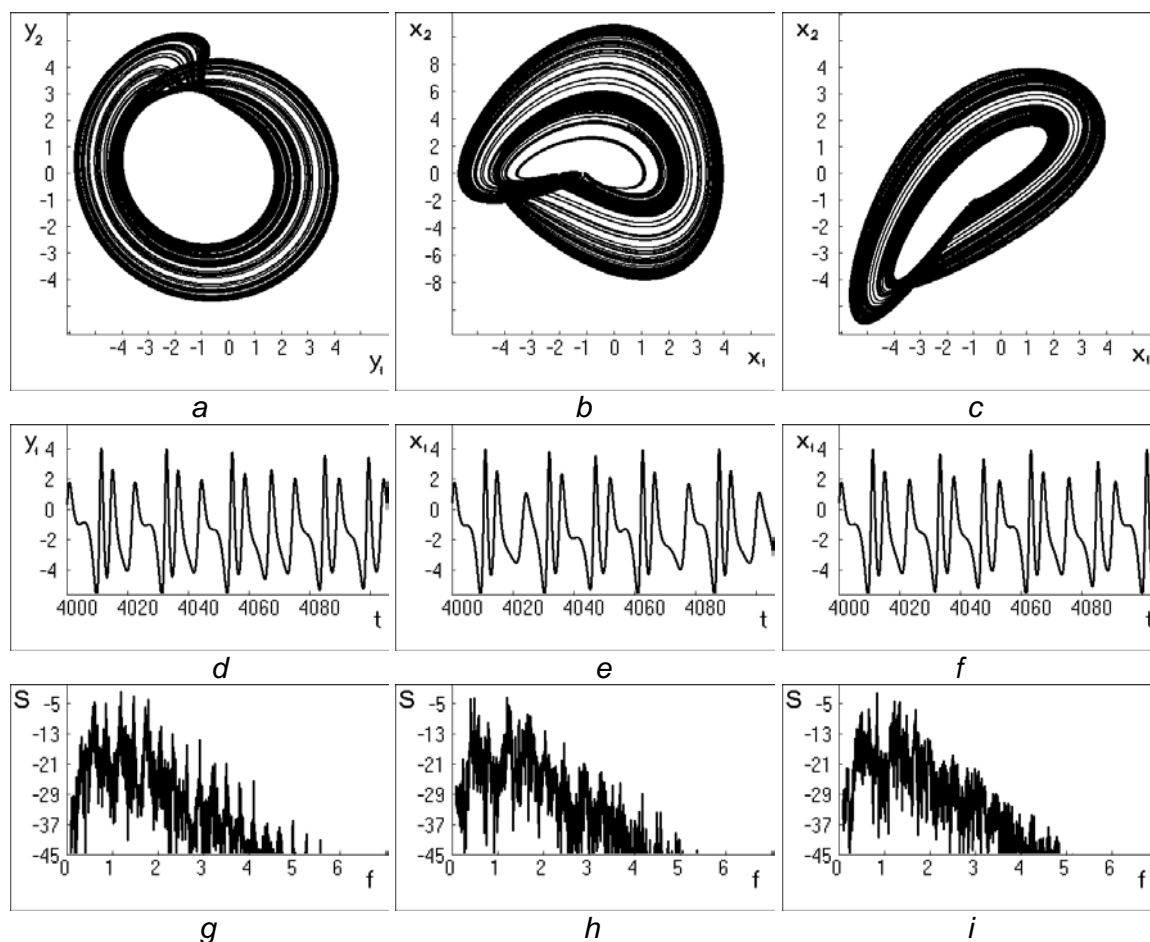


Fig. 4 The portrait of initial system (a) ( $F = 0.114$ ), the portraits of the reconstructed systems (b) –(c), their time realizations (d) –(f) and power spectrums (g) –(i).

Projections of the chaotic attractor of the system (3) and of the reconstructed systems are shown in Fig. 4 (a) – (c). As could be seen from Fig. 4 the both methods qualitatively good approximate chaotic attractor of the original system (3).

Time realizations of the chaotic attractors after finished transient regimes are also similar and given in Fig. 4 (d) – (f). Power spectrums for the original signal and for the signals from the reconstructed systems are shown in Fig. 4(g) – (i) and may be approximated by the same decay function  $S = -6.75 - 8.5f$ .

Lyapunov exponents could be calculated directly from signals without using the dynamical systems. So that, we calculated the largest Lyapunov exponents both from original signal (Fig. 5 (a)) and from solutions of the reconstructed systems (Fig. 5 (b), (c)). Comparison those Lyapunov exponents with the given ones in Fig. 2 shows that the regions of values  $F$ , where chaotic regimes are realized, are almost the same, but Lyapunov exponents for the reconstructed signals have inside of chaotic regions more windows of regularity than the largest Lyapunov exponent for the reconstructed systems. Moreover more precisely the region of chaotic signals gives the second method of reconstruction. For example, for  $F = 0.114$  the largest Lyapunov exponent for original signal is  $\lambda = 0.04238$ , and for signals from reconstructed systems by the first method it is equal  $\lambda = 0.03368$  and by the second method is  $\lambda = 0.04046$ .

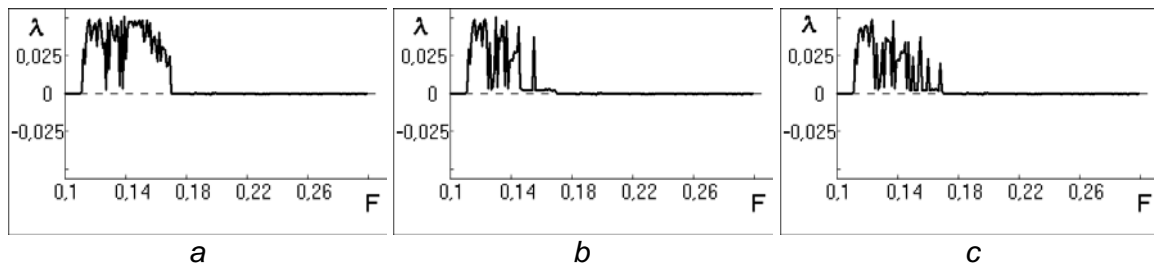


Fig. 5. The largest Lyapunov exponent of the initial signals (a), of the solutions of reconstructed systems (b) – (c).

## CONCLUSIONS

Results show that both methods can capture regular and chaotic signals from reconstructed systems of the third order with nonlinear terms up to sixth order. Types of signals were examined with spectral methods, construction of phase portraits and Lyapunov exponents. The first method gives the solution which the power spectrum for the regular signals coincides with the output signal spectrum up to 96 % for the first three peaks. The second method gives a mistake around 2 %. And the second method determines the maximum Lyapunov exponent more precisely for chaotic regimes (with a precision to  $O(10^{-3})$ ) than the first method.

Real systems are nonconservative and, a divergence of systems should be negative. It was suggested for the first time that the delay parameter for the second reconstruction method must be chosen from the stable region of the divergence behaviour of the reconstructed system.

The both methods qualitatively good approximate the phase portrait of chaotic attractor of the original system. Moreover, time realizations of the chaotic attractors after finished transient regimes are quiet similar. And what is more important, power spectrums for the original signal and for the signals from the reconstructed systems may be approximated by the same decay function  $S = -6.75 - 8.5f$ . Calculations also show that more precisely the value of bifurcation parameter for chaotic regimes gives the second method of reconstruction.

The Lyapunov exponents were calculated directly from signals without using the dynamical systems. Comparison the largest Lyapunov exponent for the signals with the largest Lyapunov exponent of the systems shows that the regions of values  $F$ , where chaotic regimes are realized, are almost the same, but Lyapunov exponents from reconstructed signals have inside of the chaotic region more windows of regularity.

## REFERENCES

- [1] Crutchfield, J.P., McNamara, B.S. Equations of Motion from a Data Series *Complex Systems*, Vol.1, pp. 417-452, 1987.
- [2] Janson, N.B., Pavlov, A.N., Kapitaniak, T., Anishenko V.S. Reconstruction of the dynamical systems from the short signals *Letters into JTP*. Vol. 25, N. 11. pp. 7-13, 1999.
- [3] Anishenko, V. S. *Acquaintance with nonlinear dynamics*. Institute of Computer Science, Moscow-Izhevsk, 2002.
- [4] Kouznetsov, S.P. *Dynamic chaos*. Physmatlit, Moscow, 2001.
- [5] Krasnopolskaya, T.S., Shvets, A.Yu. *Regular and chaotic dynamics of the systems with limited excitation*. Institute of Computer Science, Moscow-Izhevsk, 2008.
- [6] Benettin, G., Galgani, L., Strelcyn, J.M. Kolmogorov entropy and numerical experiments *Phys. Rev.*, Vol. 14, pp. 2338-2345, 1976.
- [7] Kennel, M.B., Brown, R. and Abarbanel, H. D. I. Determining embedding dimension for phase-space reconstruction using a geometrical construction *Phys. Rev. A.*, Vol. 45 N. 6, p. 3403, 1992.
- [8] Anishchenko, V.S., Pavlov, A.P. Global reconstruction in application to multichannel communication *Phys. Rev. E.*, Vol. 57 N. 2, pp. 2455-2458, 1998.

## NONLINEAR NORMAL MODES OF FORCED VIBRATIONS IN ROTOR SYSTEMS

**N.V. Perepelkin,**  
**Yu.V.Mikhlin<sup>1</sup>**  
National Technical  
University "Kharkov  
Polytechnic Institute",  
Kharkov, Ukraine

---

### ABSTRACT

---

Forced vibrations of the disk elastic rotor on nonlinear flexural base for a case of internal resonance are considered. The gyroscopic moments are taken into account. The Shaw-Pierre conception of nonlinear normal vibration modes and the modified Rausher method are used to construct resonance forced vibrations.

---

### INTRODUCTION

Rotor systems are important elements of machines and mechanisms. Different nonlinear effect must be taken into account in analysis of dynamical behavior of such systems. Moreover, internal resonances in the rotor systems dynamics must be taken into account too. One selects some principal publications on the rotor nonlinear dynamics. V.A. Grobov [1] suggested apply asymptotic methods to analyze the rotating shafts dynamics. A.P. Filippov [2] analyzed non-stationary vibrations of one disc rotor with nonlinear flexible base assuming that one support is nonlinear. V.V. Bolotin [3] took into account nonlinear inertia in the model of one disk rotor. Different models of rotor vibrations and analysis of motions stability are treated in the book [4]. Non-stationary vibrations of rotor interacting with limited power supply are considered in [5]. In [6,7] it is investigated the periodic and chaotic vibrations in the model of the Laval-Jeffcott rotor with two degree-of-freedoms with the internal resonance phenomena, using asymptotic method. Note that in many publications mostly the simplest model of the Laval-Jeffcott rotor is considered, when for the centrally mounted disk, the system is symmetric and the first two fundamental translational and rotational motions are decoupled and can be considered separately.

The Shaw-Pierre nonlinear modes of rotors accounting gyroscopic terms are considered in the paper [8]. In the present paper nonlinear forced vibrations of rotor taking into account gyroscopic effects and nonlinear flexible base are considered. An asymmetrical disposition of the disk in the shaft is considered. The Shaw-Pierre nonlinear normal modes (NNMs) together with the modified Rausher method are used to construct resonance vibrations. In contrast to results presented in [8], here it is constructed NNMs is a system having the internal resonance. This situation is always realized in the rotor system with the isotropic-elastic shaft and the isotropic-elastic supports.

### 1. THE SHAW-PIERRE NONLINEAR NORMAL VIBRATION MODES

Nonlinear normal vibrations modes (NNMs) are a generalization of the normal vibrations of linear systems. In the normal mode, a finite-dimensional system behaves like a conservative one having a single degree of freedom [9,10]. A generalization of the NNMs conception to non-autonomous systems is possible too. In [11,12] the authors reformulated the concept of NNMs for a general class of nonlinear discrete oscillators. The analysis is based on the computation of invariant manifolds of motion on which the NNMs take place.

To use this approach the original ODE system must be presented of the next standard form,

$$\frac{dx}{dt} = y, \frac{dy}{dt} = f(x, y) \quad (1)$$

---

<sup>1</sup> Corresponding author. Email [muv@kpi.kharkov.ua](mailto:muv@kpi.kharkov.ua)

where  $\mathbf{x} = \{x_1 \dots x_N\}^T$  is a vector of the generalized coordinates,  $\mathbf{y} = \{y_1 \dots y_N\}^T$  is a vector of the generalized velocities, and  $\mathbf{f} = \{f_1 \dots f_N\}^T$  is a vector of the forces. One chooses a couple of new independent phase variables  $(u, v)$ , so-called *master coordinates*, where  $u$  is some *dominant generalized coordinate*, and  $v$  is *the corresponding generalized velocity*. By the Shaw-Pierre approach, the nonlinear normal mode is such regime when all generalized coordinates and velocities are univalent functions of the selected couple of variables, named master coordinates. Denoting these master coordinates as the coordinate and velocity with the index 1, one writes the nonlinear normal mode of the form:

$$x_1 = u, y_1 = v, x_i = X_i(u, v), y_i = Y_i(u, v) \quad (i \neq 1) \quad (2)$$

Computing derivatives of all variables in the system (1), and taking into account that  $u = u(t)$  and  $v = v(t)$ , then substituting the obtained expressions to the system (2), one has the following system of partial derivation equations:

$$\begin{aligned} \frac{\partial X_i}{\partial u} v + \frac{\partial X_i}{\partial v} f_1(x, y) &= Y_i(u, v), \\ \frac{\partial Y_i}{\partial u} v + \frac{\partial Y_i}{\partial v} f_1(x, y) &= f_i(x, y), \\ i &= \overline{1..N}. \end{aligned} \quad (3)$$

One presents the system solution in the form of the power series by new independent variables  $u$  and  $v$ :

$$\begin{aligned} x_i = X_i(u, v) &= a_{1i}u + a_{2i}v + a_{3i}u^2 + a_{4i}uv + a_{5i}v^2 + \dots, \\ y_i = Y_i(u, v) &= b_{1i}u + b_{2i}v + b_{3i}u^2 + b_{4i}uv + b_{5i}v^2 + \dots \end{aligned} \quad (4)$$

The series (4) are introduced to equations (3), then coefficients in terms of the same degree by independent variables, are equated. So, a system of recurrent algebraic equations can be written. Coefficients of the series (4) can be determined from these equations, and, as a result, the corresponding nonlinear normal mode is obtained.

In a case of internal resonance it can observe an interaction of two NNMs. So, four phase coordinates are active, and they must be chosen as master coordinates. In this important case all other phase coordinates are presented as univalent functions of the selected four coordinates. Namely this situation occurs in the problem of the rotor dynamics which will be considered later.

## 2. USE OF THE MODIFIED RAUSHER METHOD TO CONSTRUCT FORCED VIBRATION MODES

One considers the nonlinear dynamical system under an external periodical excitation, which is written in principal (normal) coordinates of the following standard form:

$$\begin{cases} \dot{q}_1 = s_1 \\ \dot{s}_1 = -\nu_1^2 q_1 - f_1(\bar{q}, \bar{s}) + F_1 \cos(\Omega t) \\ \dot{q}_2 = s_2 \\ \dot{s}_2 = -\nu_2^2 q_2 - f_2(\bar{q}, \bar{s}) + F_2 \cos(\Omega t) \\ \dots \\ \dot{q}_N = s_N \\ \dot{s}_N = -\nu_N^2 q_N - f_N(\bar{q}, \bar{s}) + F_N \cos(\Omega t) \end{cases} \quad (5)$$

where  $\bar{q} = \{q_1, q_2, \dots, q_N\}^T$ ,  $\bar{s} = \{s_1, s_2, \dots, s_N\}^T$ . It is assumed that the frequencies  $\nu_1$  and  $\nu_2$  are close, and they are close to the external frequency,  $\Omega$ . In this case two active coordinates,  $q_{1,2}$ , and two corresponding velocities,  $s_{1,2}$ , may be taken as independent master coordinates to construct expansions which are analogous to the series (4).

One assumes that there is a representation of the master coordinates in the form of the following Fourier series:

$$\begin{aligned}
q_1 &= A_1 \cos(\Omega t) + B_1 \sin(\Omega t) + A_2 \cos(2\Omega t) + \\
&\quad + B_2 \sin(2\Omega t) + A_3 \cos(3\Omega t) + B_3 \sin(3\Omega t) + \dots \\
s_1 &= B_1 \Omega \cos(\Omega t) - A_1 \Omega \sin(\Omega t) + 2B_2 \Omega \cos(2\Omega t) - \\
&\quad - 2A_2 \Omega \sin(2\Omega t) + 3B_3 \Omega \cos(3\Omega t) - 3A_3 \Omega \sin(3\Omega t) + \dots \\
q_2 &= \dots \\
s_2 &= \dots
\end{aligned} \tag{6}$$

When slave coordinates are essentially smaller than the master coordinates, we can obtain such trigonometric expansions from the next ODE system:

$$\begin{cases} \dot{q}_1 = s_1 \\ \dot{s}_1 = -\nu_1^2 q_1 - f_1(\bar{q}, \bar{s}) + F_1 \cos(\Omega t) \\ \dot{q}_2 = s_2 \\ \dot{s}_2 = -\nu_2^2 q_2 - f_2(\bar{q}, \bar{s}) + F_2 \cos(\Omega t) \\ q_i = 0 \\ s_i = 0 \end{cases}, i = \overline{3, N} \tag{7}$$

One has from here, using some trigonometric transformations that

$$\cos(\Omega t) = \alpha_1 q_1 + \alpha_2 s_1 + \alpha_2 q_2 + \alpha_3 s_2 + \alpha_5 q_1^2 + \alpha_6 s_1^2 + \dots \tag{8}$$

This relation is substituted to right parts of the equations (5); it corresponds to the principal idea of the Rausher method. As a result, the autonomous system is obtained:

$$\begin{cases} \dot{q}_1 = s_1 \\ \dot{s}_1 = -\nu_1^2 q_1 - f_1(\bar{q}, \bar{s}) + F_1 (\alpha_1 q_1 + \alpha_2 s_1 + \alpha_2 q_2 + \alpha_3 s_2 + \alpha_5 q_1^2 + \dots) \\ \dots \\ \dot{q}_N = s_N \\ \dot{s}_N = -\nu_N^2 q_N - f_N(\bar{q}, \bar{s}) + F_N (\alpha_1 q_1 + \alpha_2 s_1 + \alpha_2 q_2 + \alpha_3 s_2 + \alpha_5 q_1^2 + \dots) \end{cases} \tag{9}$$

In the system (9) the NNMs by Shaw-Pierre can be constructed from the equations similar to (3). But in a case of the internal resonances the four independent coordinates are used, and the corresponding equation in partial derivatives must be used. These equations are not presented here. Solution of these equations is obtained in form of the Taylor series:

$$\begin{cases} q_n = a_{1,0,0,0}^{(n)} q_1 + a_{0,1,0,0}^{(n)} s_1 + a_{0,0,1,0}^{(n)} q_2 + a_{0,0,0,1}^{(n)} s_2 + a_{2,0,0,0}^{(n)} q_1^2 + \dots \\ s_n = b_{1,0,0,0}^{(n)} q_1 + b_{0,1,0,0}^{(n)} s_1 + b_{0,0,1,0}^{(n)} q_2 + b_{0,0,0,1}^{(n)} s_2 + b_{2,0,0,0}^{(n)} q_1^2 + \dots \end{cases}, n = \overline{3, N} \tag{10}$$

Then the expansions (10) are substituted to the system (5). It permits to reduce the n-DOF system to the two-DOF one. Two master coordinates are obtained from this system. So, the solution (6) is made more precise.

The pointed out series of operations can be repeated some times to reach a necessary exactness.

As some simple example, a system of three oscillators, connected by elastic springs, one of them is nonlinear, is considered. Equations of motion are the following:

$$\begin{cases} m_1 \ddot{x}_1 + \beta \dot{x}_1 + c_1 x_1 + c_2 (x_1 - x_2) + \gamma x_1^3 = 0 \\ m_2 \ddot{x}_2 + \beta \dot{x}_2 + c_2 (x_2 - x_1) + c_3 (x_2 - x_3) + c_5 x_2 = 0 \\ m_3 \ddot{x}_3 + \beta \dot{x}_3 + c_3 (x_3 - x_2) + c_4 x_3 = f \cos(\Omega t) \end{cases} \tag{11}$$

It is assumed that two vibration modes of the linearized system (11) have close frequencies. Use of the proposed approach permits to construct NNMs of the non-autonomous system (11). A transformation to principal coordinates  $q_1, q_2, q_3$  is made, where two first coordinates correspond to

modes with close frequencies. The frequency response of the system is obtained. In the Fig.1 the frequency response for the first harmonic of the principal coordinate  $q_3$  is shown. The entire line is obtained by the NNMs approach, and the dashed line is obtained by the harmonic balance method. Numerical simulation confirms a good exactness of the proposed approach too.

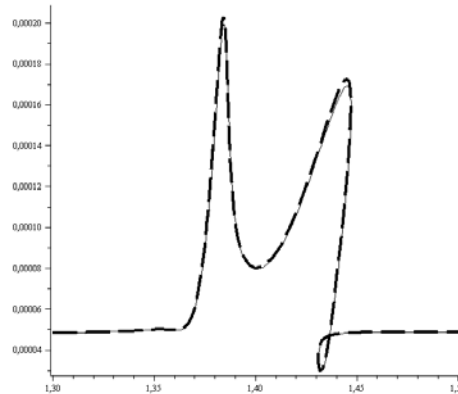


Fig. 1. Frequency response for the first harmonic of the generalized coordinate  $q_3$  of the system (11).

### 3. PRINCIPAL MODEL OF THE ROTOR NONLINEAR DYNAMICS.

A model of the rotor dynamics with an asymmetrical disposition of the disk in the shaft is considered. Gyroscopic effects and nonlinear flexible base are taken into account. The fixed and moving coordinate systems and positional angles are shown in the Fig. 2.

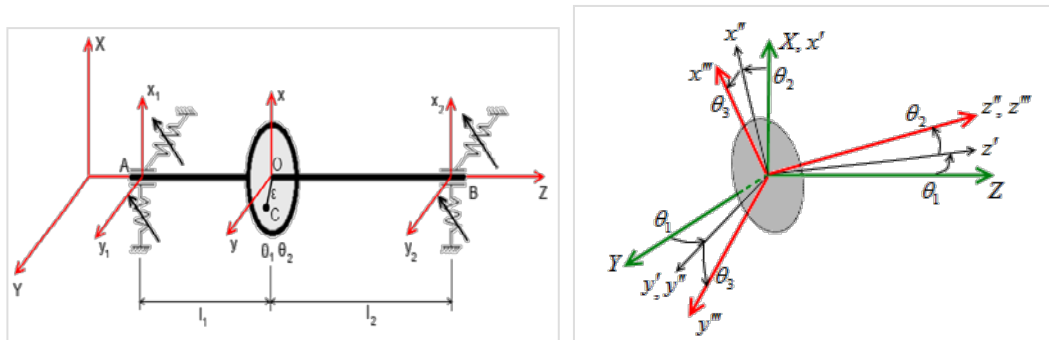


Fig.2. Principal model of the rotor dynamics. Fixed and moving coordinate systems.

Equations of the rotor motion can be written of the following form:

$$\begin{aligned}
 m\ddot{x} + \rho_1\dot{x} + c_{11}(x - h_1x_2 - h_2x_1) + m\left(\theta_2 - \frac{x_2 - x_1}{l}\right) &= \varepsilon\Omega^2 \cos \Omega t \\
 m\ddot{y} + \rho_1\dot{y} + c_{11}(y - h_2y_1 - h_1y_2) - c_{12}\left(\theta_1 + \frac{y_2 - y_1}{l}\right) &= \varepsilon\Omega^2 m \sin \Omega t \\
 I_e\ddot{\theta}_1 + \rho_2\dot{\theta}_1 + I_p\Omega\dot{\theta}_2 + c_{22}\left(\theta_1 + \frac{y_2 - y_1}{l}\right) - c_{12}(y - h_2y_1 - h_1y_2) &= 0 \\
 I_e\ddot{\theta}_2 + \rho_2\dot{\theta}_2 - I_p\Omega\dot{\theta}_1 + c_{22}\left(\theta_2 - \frac{x_2 - x_1}{l}\right) + c_{12}(x - h_1x_2 - h_2x_1) &= 0 \\
 \beta\dot{x}_1 + \left(\frac{c_{12}}{l} - h_2c_{11}\right)(x - h_1x_2 - h_2x_1) + \left(\frac{c_{22}}{l} - h_2c_{12}\right)\left(\theta_2 - \frac{x_2 - x_1}{l}\right) + c_x^{(1)}x_1 + c_x^{(2)}x_1^3 &= 0 \\
 \beta\dot{y}_1 + \left(\frac{c_{12}}{l} - h_2c_{11}\right)(y - h_2y_1 - h_1y_2) + \left(h_2c_{12} - \frac{c_{22}}{l}\right)\left(\theta_1 + \frac{y_2 - y_1}{l}\right) + c_y^{(1)}y_1 + c_y^{(2)}y_1^3 &= 0
 \end{aligned} \tag{12}$$

$$\beta \dot{x}_2 + \left( -\frac{c_{12}}{l} - c_{11}h_1 \right) (x - h_1x_2 - h_2x_1) + \left( -\frac{c_{22}}{l} - h_1c_{12} \right) \left( \theta_2 - \frac{x_2 - x_1}{l} \right) + k_x^{(1)}x_2 + k_x^{(2)}x_2^3 = 0$$

$$\beta \dot{y}_2 + \left( -\frac{c_{12}}{l} - h_2c_{11} \right) (y - h_2y_1 - h_1y_2) + \left( \frac{c_{22}}{l} + h_1c_{12} \right) \left( \theta_1 + \frac{y_2 - y_1}{l} \right) + k_y^{(1)}y_2 + k_y^{(2)}y_2^3 = 0$$

where  $c_{11}, c_{12}, c_{22}$  are static coefficients of shaft stiffness;  $l$  is the shaft length;  $l_1, l_2$  are distances of the disk up to left and right supports, correspondently;  $h_1 = l_1/l; h_2 = l/l_2$ ;  $c_x^{(1)}, c_y^{(1)}$  are coefficients which characterize linear terms in the left support restoring force;  $k_x^{(1)}, k_y^{(1)}$  are similar coefficients for the right support;  $c_x^{(2)}, c_y^{(2)}$  are coefficients which characterize cubic terms in the left support restoring force;  $k_x^{(1)}, k_y^{(1)}$  are similar coefficients for the right support;  $\beta$  is a coefficient of damping in supports;  $\rho_1, \rho_2$  are coefficients of damping during the disk motion;  $m$  is the mass of the disk;  $\varepsilon$  is an eccentricity of the disk mass center.

#### 4. FORCED VIBRATIONS IN ROTOR DYNAMICS.

The procedure, which was described in the Section 2, is used. As a result, nonlinear normal modes of the non-autonomous rotor system are obtained.

Numerical simulation of the rotor forced dynamics is made for the following values of the system parameters :  $m=15.3$  kg,  $I_e=0.22$  kg·m<sup>2</sup>,  $I_p=0.441$  kg·m<sup>2</sup>,  $l=1$  m,  $h_1=1/3$ ,  $h_2=2/3$ ,  $c_x^{(1)}=c_y^{(1)}=k_x^{(1)}=k_y^{(1)}=9.8 \cdot 10^5$  N/m,  $c_x^{(2)}=c_y^{(2)}=k_x^{(2)}=k_y^{(2)}=1.96 \cdot 10^{12}$  N/m<sup>3</sup>,  $\varepsilon=10^{-4}$  m,  $\beta=3000$  N·s/m,  $\rho_1=1.5$  N·s/m,  $\rho_2=1.5$  N·s. Elastic shaft is described by following parameters: the Young's modulus  $E=2.1 \cdot 10^{11}$  Pa, the cross-section radius  $r=0.015$  m, the shaft is considered to be massless.

The phase trajectory of the obtained NNM for  $\omega = 0.9922$ , where  $\omega$  is a ratio of the frequency of external excitation and the first frequency of the linearized system, is presented in the Fig. 3. Here the analytical solution is shown by points, and the numerical simulation is shown by the entire line.

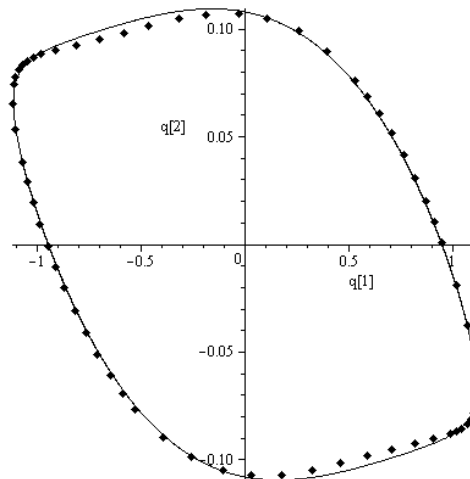


Fig. 3. The NNM phase trajectory. Analytical solution (points) and numerical simulation (entire line).

A comparison of the analytical and numerical forced NNM in time for the same ratio of the external frequency and the first linear frequency is presented in Fig. 4, where points correspond to the analytical results, and the entire line corresponds to the numerical simulation.

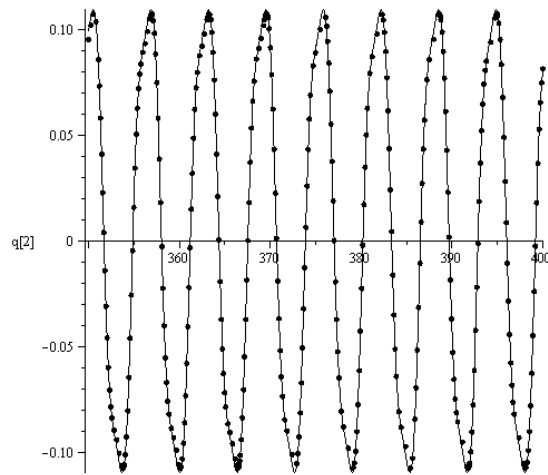


Fig. 4. Presentation of the NNM in time for the non-autonomous rotor system. Points correspond to the analytical solution; entire line corresponds to numerical simulation.

## CONCLUSIONS

The forced vibrations of the non-autonomous rotor system for a case of the internal resonance is obtained by use of the nonlinear normal modes conception and the generalized Rausher method. Numerical simulation confirms an efficiency of the proposed analytical procedure.

## ACKNOWLEDGMENTS

This work was supported in part by a grant M9403 ДР 0109U002426 from the Ministry of Science and Education of Ukraine and by a grant Ф28/257 from the National Academy of Science of Ukraine and Russian Foundation for Basic Research.

## REFERENCES

- [1] Grobov V.A. *Asymptotic Methods for Calculations of Bending Vibrations of Turbo- Machines Shafts*. Published by the USSR Academy of Sci., Moscow, 1961 (in Russian).
- [2] Filippov A.P. *Vibrations of Elastic Systems*, Mashinostroenie, Moscow, 1970 (in Russian).
- [3] Bolotin V.V. *Nonconservative Problems of the Theory of Elastic Stability*. Pergamon Press, New York, 1963.
- [4] Tondl A. *Some Problems of Rotor Dynamics*, Chapman and Hall, London, 1965.
- [5] Iwatsubo J., Kanki H., Kawai R. Vibration of asymmetric rotor through critical speed with limited power supply. *J. of Mechanical Engineering Science*, 14, pp.184-194, 1972.
- [6] Ishida Y., Inoue T. Internal resonance phenomena of the Jeffcott rotor with nonlinear spring characteristics. *ASME J. of Vibration and Acoustics*, 126, pp. 476-484, 2004.
- [7] Inoue T., Ishida Y. Chaotic vibrations and internal resonance phenomena in rotor systems. *ASME J. of Vibration and Acoustics*, 128, pp.156-169, 2006.
- [8] Serra Villa C.V., Sinou J.-J., Thouverez F. The invariant manifold approach applied to nonlinear dynamics of a rotor-bearing system. *European J. of Mechanics A/ Solids*, 24, pp.676-689, 2005.
- [9] Mikhlin Yu. Normal vibrations of a general class of conservative oscillators, *Nonlinear Dynamics*, 11, pp.1–16, 1996
- [10] Vakakis A., Manevitch L., Mikhlin Yu., Pilipchuk V. and Zevin A. *Normal Modes and Localization in Nonlinear Systems*. Wiley, New-York, 1996.
- [11] S. Shaw and C. Pierre. Nonlinear normal modes and invariant manifolds. *J. of Sound and Vibration*, 150, pp.170–173, 1991.
- [12] S. Shaw and C. Pierre. Normal modes for nonlinear vibratory systems. *J. of Sound and Vibration*, 164, pp.85–124, 1993.

**ON ALGEBRAIC STRUCTURES INDUCED BY U-TURNS  
AND NON-INVERTIBLE TIME SUBSTITUTIONS**

**Valery N. Pilipchuk**<sup>1</sup>  
Wayne State University  
Detroit, USA

---

ABSTRACT

---

In this work, we discuss such time substitutions that capture the basic temporal symmetries of dynamic processes in advance to facilitate any further use of the methods of dynamic analyses. For instance, if a particle makes a U-turn, then the corresponding substitution reverses the time direction exactly when the velocity changes its sign regardless other properties of the dynamics, namely – classes of smoothness, levels of unharmonicity, etc. From such a viewpoint, an oscillating process represents just a sequence of U-turns. In this case, the oscillating time substitutions fold time into bounded or half-bounded domains that promises quite essential advantages for both analytical and numerical approaches. Interestingly enough, transforming the temporal variable, brings the spatial coordinates into the specific set of complex elements – hyperbolic numbers – whose “imaginary number” squared is plus one. Such algebraic structures appeared to be known in mathematical literature in a very abstract way, regardless any dynamic problems or non-smooth functions, and often regarded to as a simple example of so-called Clifford’s algebras; see [1] and references therein for introduction. Nevertheless, some geometrical interpretations from this theory hint on useful manipulations with dynamical systems when implementing non-smooth temporal substitutions [2]. In this work a series of illustrations and solutions is presented.

---

**REFERENCES**

- [1] Antonuccio F. Hyperbolic numbers and the Dirac spinor, <http://arxiv.org/abs/hep-th/9812036v1>, 1998  
[2] Pilipchuk V.N. *Nonlinear Dynamics: Between Linear and Impact Limits*, Springer – Verlag Berlin Heidelberg (in production), <http://www.springer.com/engineering/book/978-3-642-12798-4>, 2010.

---

<sup>1</sup> Valery N. Pilipchuk, Email: [pilipchuk@wayne.edu](mailto:pilipchuk@wayne.edu)

## IMPACT VIBRATION ABSORBER OF PENDULUM TYPE

**Polukoshko, S.N.**<sup>1</sup>

Ventspils University  
 College "VSRC"  
 Ventspils, Latvia

**Sokolova, S.V.,  
 Jevstignejev, V.Y.**

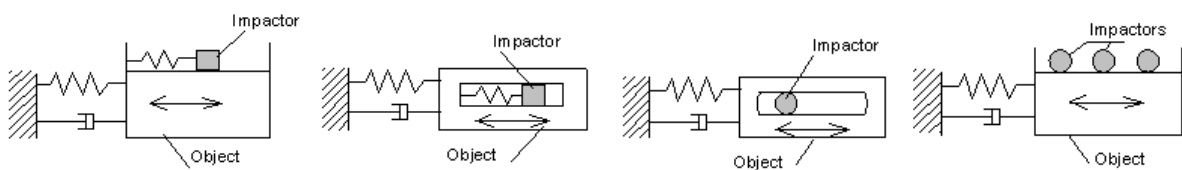
Riga Technical University  
 Riga, Latvia

### ABSTRACT

In this work the impact vibration absorber of pendulum type is examined. It consists of pendulum with motion limiting stops attached to the vibrating system. Pendulum vibration absorbers are widely used in practice. The influence of pendulum parameters on the possibility of suppression of vibrations of the basic system under harmonic excitation are discussed in this study.

### INTRODUCTION

Vibration is a repetitive, periodic or oscillatory response of mechanical system. Since most of machines and structures undergo some degree of vibrations, engineers have to consider the results of vibrations in the designing process [4], [8]. It is usually required to control the vibrations because it causes fatigue and failure of the vibrating elements and discomfort for the people. One of the most effective passive control methods is adding an impact vibration absorber to the system under excitation [1],[2],[5]. Impact vibration absorbers (IVA) consist of an impact mass which is placed on basic vibrating mass so, that periodically collides with it. The transfer of momentum to the mass from the main mass and dissipation of energy in every impact provides reduction in amplitude response of the main mass. IVA are fulfilled with one, two and more degrees of freedom; noncontrollable and regulated; with unilateral or with bilateral constraints. In accordance with structural type impact vibration absorbers may be spring (Fig.1), floating (Fig.2) and pendular (Fig.3).



*a) outer                      b) inner*  
 Fig.1.a-b. Spring impact absorbers.

*a) single-unit              b) multi-unit*  
 Fig.2.a-b. Floating impact absorbers.

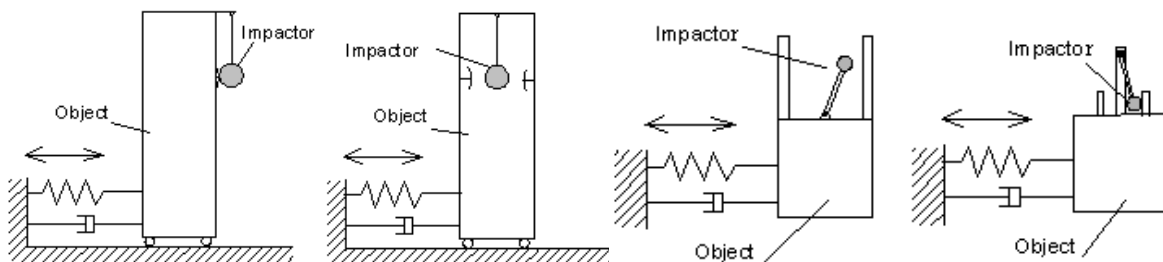


Fig.3. Pendulum impact absorber

<sup>1</sup>Corresponding author. E-mail: pol.svet@inbox.lv

In this work the impact absorber of pendulum type is examined. It consists of pendulum with motion limiting stops attached to the vibrating system. Pendulum vibration absorbers are used in practice for decreasing of vibration level of different engineering structures: flue pipes, television towers, bridges, high-rise buildings, aerial masts, for shaft autobalancing and others [3], [6], [8]. The purpose of this research is to study the influence of parameters of the pendulum on possibility of vibration suppression of the basic system under harmonic excitation, and the effect of the system parameters on system dynamics. This involved determination the effect of mass ratio, excitation amplitude, and clearance between impact stop walls. A pendulum with one and two impacts during the period is considered. Dependence of suppression ability of absorber on pendulum length, coefficient of restitution at impact, mass ratio of the basic system and pendulum, and gap size are found.

## 1. ANALITICAL MODEL OF ABSORBER

### 1.1 Mathematical model

The analytical models of single and double impact pendulum absorbers are presented in Fig.4.

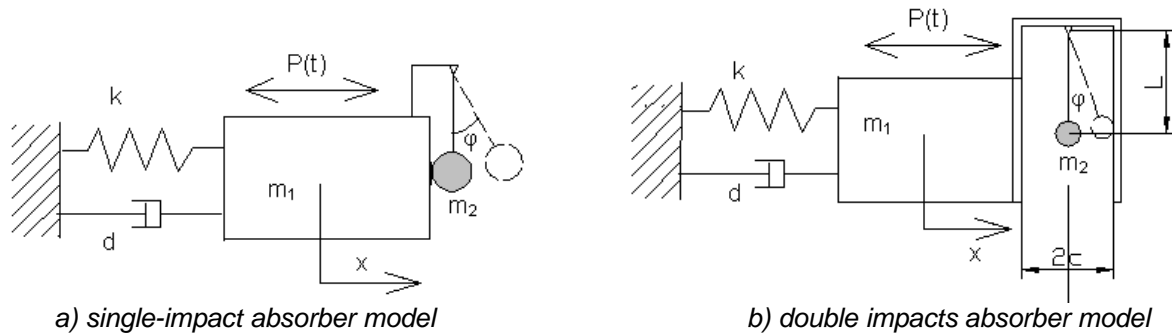


Fig.4. Model of the pendulum impact absorber.

Parameters of system:

$m_1$  – mass of the main body;  $m_2$  – mass of the damper;  $\mu = m_2/m_1$  - mass ratio;

$d$  – inherent damping coefficient of the main system;  $k$  – stiffness coefficient of main system;

$\lambda$  – natural frequency of the main system;  $\omega$  – the frequency of pendulum;  $l$  – length of pendulum;

$c$  – size of gap;  $\alpha$  – max angle for two-impacts absorber,  $\tan \alpha = c/l$ ;

$r$  – coefficient of restitution of the velocity after impact;

The system is considered under harmonic excitation:  $P(t) = P_0 \sin \Omega t$ , where  $P_0$  – amplitude of excitation force;  $\Omega$  – frequency of excitation.

### 1.2 The equations of motion of the system

The Lagrange's equations of motion of the examined system are derived:

$$\begin{cases} m_1 \ddot{x} + m_2 l \ddot{\varphi} \cos \varphi = -kx - d\dot{x} + m_2 l \dot{\varphi}^2 \sin \varphi + P_0 \sin \Omega t - S \sum_{R=0}^{\infty} \delta(t - RT) \\ m_2 l^2 \ddot{\varphi} + m_2 \ddot{x} l \cos \varphi = -m_2 g l \sin \varphi + S \sum_{R=0}^{\infty} \delta(t - RT) \end{cases} \quad (1)$$

where  $S$  is an impact impulse,  $\delta(t - RT)$  is a delta function,  $T$  is a period of collisions.

The stereomechanical theory of impact without friction is used for impact impulse definition [7]:

$$S = (1 + r) \frac{m_1 m_2}{m_1 + m_2} (v_{01} - v_{02}), \quad (2)$$

where  $v_{01}$  and  $v_{02}$  are velocity of main body and velocity of impactor just before impact.

The velocity of impactor consists of translational velocity and relative velocity:

$$v_{01} - v_{02} = v_{01} - (v_{01} + v_{2r}) = -l \dot{\varphi}_{01}, \quad (3)$$

here the angular velocity is pendulum velocity just before impact,

$$\dot{\varphi}_{01} = \dot{\varphi}(T).$$

Taking into account (3) impact impulse may be represented as:

$$S = (1+r) \frac{m_2}{1+\mu} (-l\dot{\varphi}(T)). \quad (4)$$

Taking into account (4) the equations of system (4) after rearrangement of may be written:

$$\begin{cases} \ddot{x} + b\dot{x} + \lambda^2 x = \mu\dot{\varphi}^2 l \sin \varphi - \mu\ddot{\varphi} \cdot l \cos \varphi + p_0 \sin \Omega t + \frac{(1+r)\mu}{(1+\mu)} l\dot{\varphi}(T) \sum_{R=0}^{\infty} \delta(t-RT) \\ \ddot{\varphi} + \omega^2 \sin \varphi = -\frac{\ddot{x}}{l} \cos \varphi - \frac{1+r}{1+\mu} \frac{\dot{\varphi}(T)}{l} \sum_{R=0}^{\infty} \delta(t-RT) \end{cases} \quad (5)$$

where  $\lambda = \sqrt{\frac{k}{m_1}}$ ,  $b = \frac{d}{m_1}$ ,  $p_0 = \frac{P_0}{m_1}$ ,  $\omega = \sqrt{\frac{g}{l}}$ .

### 1.3 Numerical solution of equations of motion

In this work the numerical solution of system (5) was obtained with help of Euler method using the kinematics conditions – pre-impact and post-impact velocities of moving bodies if coefficient of restitution is known. The velocity of the main body  $v_1$  and velocity of impactor  $v_2$  just after impact are:

$$v_1 = v_{01} + l\dot{\varphi}_{01} \frac{\mu(1+r)}{1+\mu}, \quad v_2 = v_{01} + l\dot{\varphi}_{01} \frac{\mu-r}{1+\mu}. \quad (6)$$

Algorithm of Euler's method for the single-impact damper, taking into account (8),(9):

$$\begin{aligned} t_{n+1} &= t_n + \Delta t \\ x_{n+1} &= x_n + \dot{x}_n \Delta t \\ \varphi_{n+1} &= (\varphi_n + \dot{\varphi}_n \Delta t) \text{if } (\varphi_n \geq 0, 0, 1) \\ \dot{x}_{n+1} &= \dot{x}_n + \ddot{x}_n \Delta t + l\dot{\varphi}_n \frac{\mu(1+r)}{1+\mu} \text{if } (\varphi_n \leq 0, 1, 0) \\ \dot{\varphi}_{n+1} &= \dot{\varphi}_n + \ddot{\varphi}_n \Delta t + \dot{\varphi}_n \frac{\mu-r}{1+\mu} \text{if } (\varphi_n \leq 0, 1, 0) \\ \ddot{x}_{n+1} &= -b\dot{x}_n - \lambda^2 x_n + p_0 \sin \Omega t_n + \mu\dot{\varphi}_n^2 l \sin \varphi_n - \mu\ddot{\varphi}_n l \cos \varphi_n + \frac{(1+r)\mu}{1+\mu} l\dot{\varphi}_n \text{if } (\varphi_n \leq 0, 1, 0) \\ \ddot{\varphi}_{n+1} &= -\omega^2 \sin \varphi_n - \frac{\dot{x}_n}{l} \cos \varphi_n - \frac{1+r}{1+\mu} \frac{\dot{\varphi}_n}{l} \text{if } (\varphi_n \leq 0, 1, 0) \end{aligned} \quad (7)$$

Here *if* is special logic function in Mathcad program.

Euler method gives good results if time interval  $\Delta t$  is small. The equations of motion are solved numerically with help of Matcad program. The received results enable to analyze all parameters of motion of the system. Examples of the solution of motion are presented below for single and two-impact absorbers.

## 2. NUMERICAL EXAMPLE

For the numeral solution next value of system parameters are accepted:  $\lambda=1.5$ ,  $b = 0.1$ ,  $p_0 = 0.5$ . Parameters values are chosen for civil engineering conditions. The structure is modeled as single-degree of freedom system, after adding the pendulum absorber it becomes two freedom degrees, the exiting force is harmonic. Parameters of motion of single-impact absorber are shown in Fig. 5 a-e, two-impact absorbers - in Fig. 6 a-e.

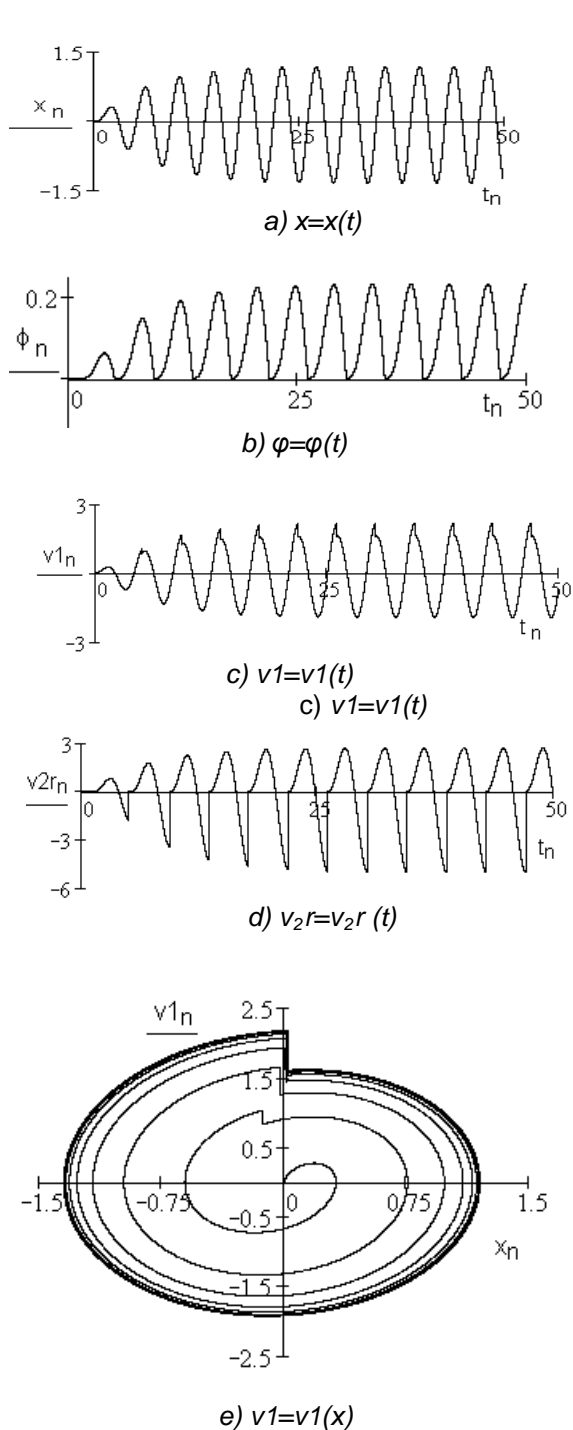


Fig. 5. Plots of dependence of the motion parameters on time and phase map for single-impact absorber in case of:  $\Omega=1.5$ ,  $\lambda=1.5$ ,  $\omega=0.75$ ,  $\mu=0.04$ ,  $r=0.6$ .

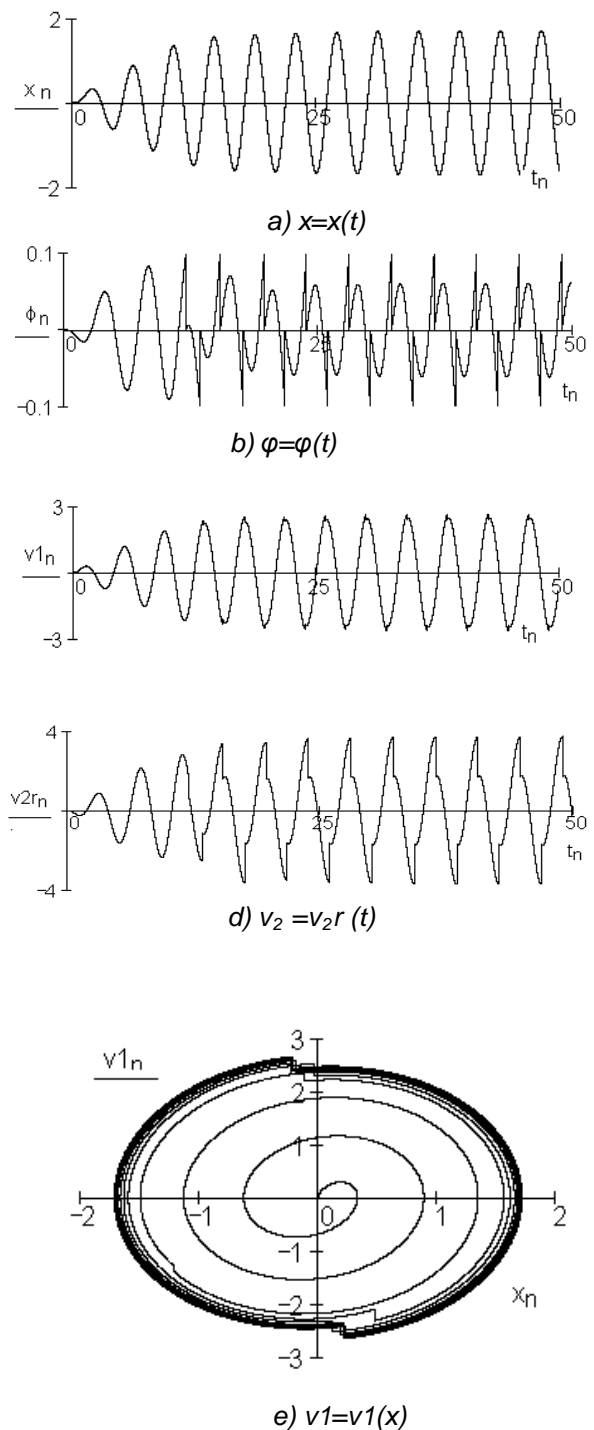


Fig. 6. Plots of dependence of the motion parameters on time and phase map for double-impact absorber in case of:  $\Omega=1.5$ ,  $\lambda=1.5$ ,  $\omega=0.75$ ,  $\alpha=0.1$ ,  $\mu=0.04$ ,  $r=0.6$ .

Plots in Fig.5-6 represent: a)  $x=x(t)$  - displacement of mass  $m_1$ , b)  $\varphi=\varphi(t)$  - rotation angle of pendulum, c)  $v_2r=v_2r(t)$  - relative velocity of mass  $m_2$ , d)  $v=v(t)$  - velocity of mass  $m_1$ , as functions of time  $t$ , e)  $v=v(x)$  - velocity of mass  $m_1$  as function of mass displacement  $x$ .

Plots of maximal amplitude  $A_{\max}$  of main body in relation to exciting force frequency  $\Omega$  for different pendulum frequencies  $\omega$  are presented in Fig.7, plots of  $A_{\max}$  depending on mass ratio  $\mu$  are in Fig.8, depending on the coefficient of restitution are in Fig.9, depending on angle  $\alpha$  are in Fig.10.

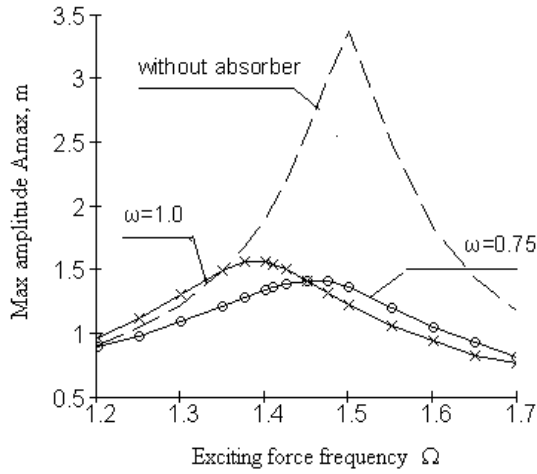


Fig.7. Maximal amplitude  $A_{max}$  in relation to exciting force frequencies  $\Omega$  for single impact pendulum absorber ( $\mu=0.04$ ,  $r=0.6$ ).

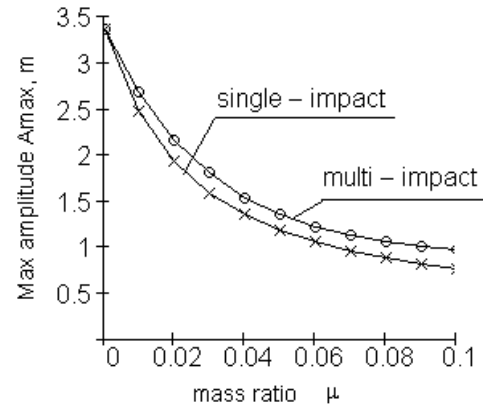


Fig.8. Maximal amplitude depending on  $\mu$ -ratio for single-impact absorber ( $\omega=0.75$ ,  $r=0.6$ ) and multi-impact absorber ( $\omega=0.75$ ,  $r=0.6$ ,  $\alpha=0.05$ ) and  $\Omega=1.5$  for both case.

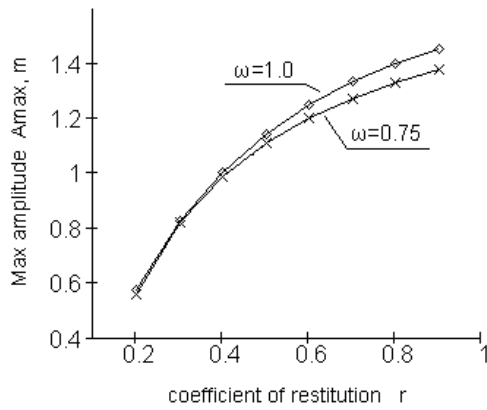


Fig.9. Maximal amplitude  $A_{max}$  in relation to coefficient of restitution  $r$  for single impact pendulum absorber ( $\mu=0.04$ ,  $r=0.6$ ).

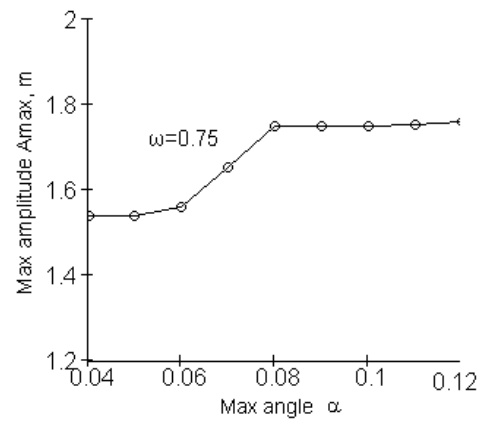


Fig.10. Maximal amplitude  $A_{max}$  depending on pendulum clearance angle  $\alpha$  ( $\mu=0.04$ ,  $r=0.6$ ) for multi-impact absorber shown in Fig.4b.

### 3. COMPARISON WITH CLASSICAL IMPACT ABSORBER

The analytical models of classical impact absorbers are presented in Fig.11.

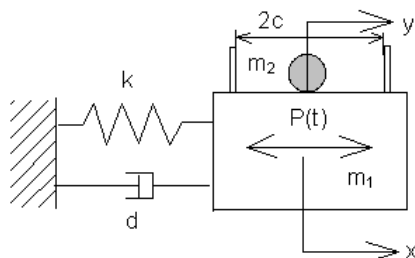


Fig.11. Model of classical impact absorber.

The differential equations of the system motion:

$$\begin{cases} m_1 \ddot{x} = -kx - d\dot{x} + P_0 \sin \Omega t - S \sum_{R=0}^{\infty} \delta(t - RT) \\ m_2 \ddot{y} = -m_2 \ddot{x} + S \sum_{R=0}^{\infty} \delta(t - RT) \end{cases} \quad (8)$$

Impact impulse  $S$  and post-impact velocities of the main body  $v_1$  and velocity of impactor  $v_2$  are:

$$S = (1+r) \frac{m_2}{1+\mu} (-\dot{y}(T)), \quad v_1 = \dot{x}(T) + \dot{y}_0(T) \frac{\mu(1+r)}{1+\mu}, \quad v_2 = \dot{x}(T) + \dot{y}(T) \frac{\mu-r}{1+\mu}. \quad (9)$$

Further the system with the same characteristics as for pendulum absorber is considered:  $\lambda=1.5$ ,  $b=0.1$ ,  $p_0=0.5$ ,  $\Omega=1.5$ . In Fig.12 the parameters of motion in dependence on time are presented. The

absorber with parameters  $c=1$ ,  $m_c=1$ ,  $\mu=0.04$ ,  $r=0.6$  admits multi-impacts; it shows four impacts during a period.

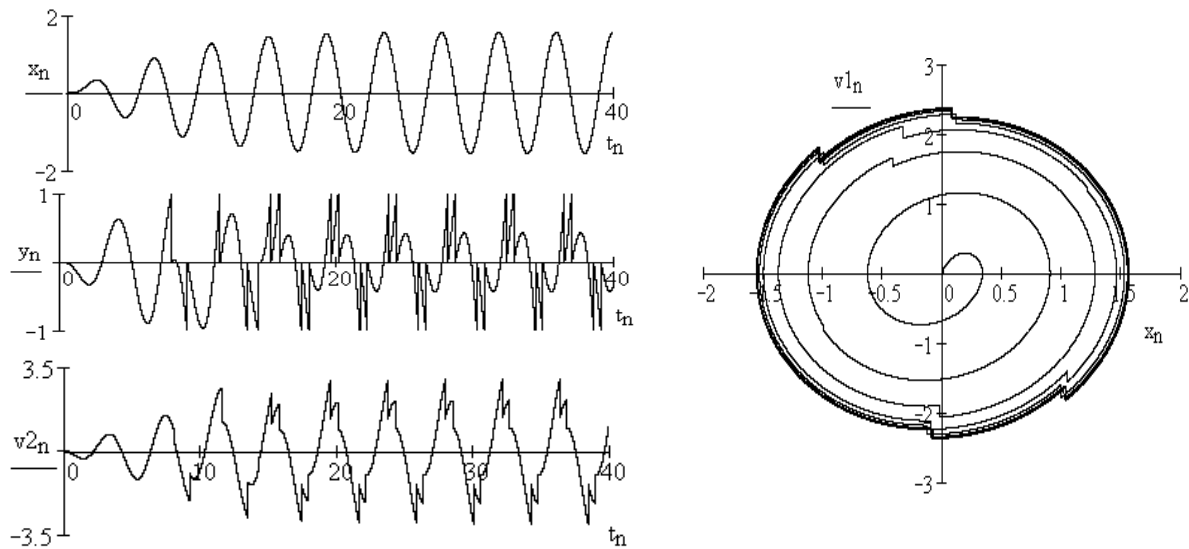


Fig. 12. Plots of dependence of motion parameters on time:  $x=x(t)$ ,  $y=y(t)$ ,  $v_2r=v_2r(t)$  and phase map for classical impact absorber in case of:  $\Omega=1.5$ ,  $\lambda=1.5$ ,  $c=1$ ,  $\mu=0.04$ ,  $r=0.6$ .

## CONCLUSIONS

The differential equations of motion of the vibrating system are derived on the basis of Lagrange's equation of the second type. The impacts in the system are described as impacts of perfectly rigid bodies taking into account the coefficient of restitution. The equations of motion are solved numerically with help of Matcad program, using Euler's method. Numerical solution allows calculating not only the parameters of motion in the steady-state mode, but also in a transitional process. All parameters of transient motion and steady-state motion were defined, results were analyzed. Dependences of amplitude of vibrations are shown graphically on correlation of the masses, maximal of pendulum amplitude in the graphs is shown maximal, instead of amplitude of the set motion. For a one-impact absorber, adjusted on resonance frequency, attenuation ability is greater, but velocity of collisions is great, that can result in the damage of material. In the future it is necessary to take into account resilient properties of impact contacts using the dynamics conditions – to add the contact forces in impact contact point. Taking into account that in real structures the velocity of impact or maximum amplitude of the main system may be limited due to the danger of damage, choice of the damper parameters is made accordingly.

## REFERENCES

- [1] Cheng Jianlian, Hui Xu. Inner mass impact damper for attenuating structure vibration. *International Journal of Solids and Structures*. Vol. 43, Issue 17, pp. 5355-5369, 2006.
- [2] Cheng C.C., Wang J.Y. Free vibration analysis of a resilient impact damper. *International Journal of Mechanical Sciences*, Vol. 45, pp. 589– 604, 2003.
- [3] Chua Sy G., Pacheco B.M., Fujino Y. and Ito M. Classical impact damper and pendulum impact damper for potential civil engineering application. *Structural Eng./Earthquake Eng.*, Vol.7, No1, pp. 110-112, 1990.
- [4] Clarence W. de Silva. *Vibration. Fundamental and Practice*. CRC Press LLC, New-York, 2000.
- [5] Ema S., Marui E. A fundamental study on impact dampers, *International Journal of Machine Tools and Manufacturers*, Vol. 36, pp. 93–306, 1996.
- [6] Korenev B.G., Reznikov L.M. *Dynamic vibration absorber*. Nauka, Moscow, 1988. (in Russian)
- [7] Viba J. *Optimisation and syntesis of vibro-impact mashines*. Zinatne, Riga 1988. (in Russian)
- [8] *Vibrations in engineering: V.6. Protection from vibrations and impacts*. Frolov, K.F., editor, Mashinostroenie, Moscow, 1995. (in Russian)

## NEW ASPECTS OF CHAOTIC DYNAMICS OF PENDULUM SYSTEMS WITH A LIMITED POWER-SUPPLY

**A. Yu. Shvets<sup>1</sup>**  
 NTUU "KPI"  
 Kyiv, Ukraine

**V. A. Pechernyi**  
 NTUU "KPI"  
 Kyiv, Ukraine

---

### ABSTRACT

---

In represented paper some new aspects of chaotic behavior of spherical pendulum with limited (non-ideal) excitation are considered. Chaotic regimes in such system arise due to feedback influence of pendulum oscillations on a mechanism of its excitation. For considered system chaotic attractors and scenarios of its origin were investigated in details. New peculiarities of scenario of transition to chaos through cascade of bifurcations of period doubling were identified. In research map of dynamic regimes, phase portraits, Poincare's sections, distributions of spectral density of regular and chaotic attractors of the system were constructed.

---

### INTRODUCTION

Pendulum systems throughout centuries constantly draw to themselves attention of researchers in various areas of mathematics, mechanics and physics. Recently pendulum models have started to be applied widely at research of dynamic behavior of oscillating systems of the diversified nature in biology, medicine, economy, sociology etc. Problems of global power savings have made especially actual researches of pendulum systems with limited excitations. In such systems it is in essence supposed that the power of source of excitation of oscillations comparable with power consumed by oscillating system. This case is non-ideal for Sommerfeld and Kononenko [1]. It was established later that feedback influence of pendulum oscillations on a mechanism of its excitation leads to chaotic regimes in coupled system [2-4].

In present work we continue previous researches of pendulum system with a limited power-supply [2- 4]. Our main purpose is to investigate new aspects of its chaotic dynamics.

### 1. DESCRIPTION OF THE SYSTEM AND ITS MATHEMATICAL MODEL

We consider the two-degree-of-freedom pendulum when the point of support is vibrated by an electromotor with a limited power-supply (fig. 1). The mathematical model which takes into account non-ideal of excitation is built in [3, 4]. The mathematical model can be written as

$$\begin{aligned}
 \dot{y}_1 &= Cy_1 - \left[ y_3 + \frac{1}{8}(y_1^2 + y_2^2 + y_4^2 + y_5^2) \right] y_2 - \frac{3}{4}(y_1 y_5 - y_2 y_4) y_4 + 2y_2 \\
 \dot{y}_2 &= Cy_2 + \left[ y_3 + \frac{1}{8}(y_1^2 + y_2^2 + y_4^2 + y_5^2) \right] y_1 - \frac{3}{4}(y_1 y_5 - y_2 y_4) y_5 + 2y_1 \\
 \dot{y}_3 &= D(y_1 y_2 + y_4 y_5) + Ey_3 + F \\
 \dot{y}_4 &= Cy_4 - \left[ y_3 + \frac{1}{8}(y_1^2 + y_2^2 + y_4^2 + y_5^2) \right] y_5 + \frac{3}{4}(y_1 y_5 - y_2 y_4) y_1 + 2y_5 \\
 \dot{y}_5 &= Cy_5 + \left[ y_3 + \frac{1}{8}(y_1^2 + y_2^2 + y_4^2 + y_5^2) \right] y_4 + \frac{3}{4}(y_1 y_5 - y_2 y_4) y_2 + 2y_4
 \end{aligned} \tag{1}$$

---

<sup>1</sup> Corresponding author. Email [alex.shvets@bigmir.net](mailto:alex.shvets@bigmir.net)

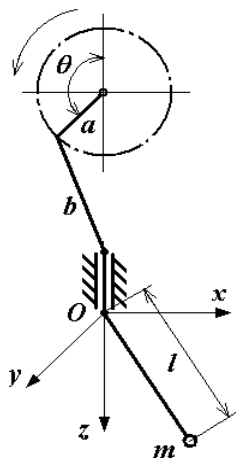


Fig. 1 System "pendulum – electromotor"

It is assumed that conditions of basic parametric resonance are realized, when the speed of the engine shaft is close to double own frequency of the pendulum. There variables  $y_1, y_2$  and  $y_4, y_5$  determine angles of pendulum deviation from coordinate plane  $XZ$  and  $YZ$  (fig. 1), variable  $y_3$  determine rotation speed of electromotor shaft.

The system of equations (1) obviously has four control parameters:  $C, D, E$  and  $F$  that determined through electrical and mechanical characteristics of the investigated system. Parameter  $E$  directly determined angle of motor static characteristics, the parameter  $C$  is proportional to the resistance of environment.  $D$  and  $F$  are multi-parameters of dynamical system (1). They depend on the length and mass of pendulum, its own frequency and coefficient of damping, linear dimensions of connecting rod mechanism and the moment of inertia of the rotor and also on the parameters of the static characteristics of an electromotor. Such mathematical model allows specifying the existence of deterministic chaos in investigated system and the main effects of nonlinear interaction between pendulum and electromotor [3, 4].

Since the mathematical model (1) of the system "spherical pendulum–electromotor" is nonlinear with the dimension of phase space equal to five, so complex of numerical methods is used in the research of regular and chaotic regimes. For computer implementation of these methods was developed a specialized package of software modules. In this complex there are such methods as Runge-Kutta methods, algorithm of Benettin, Galgani and others, Henon's methods and so on. General methodology for research of nonlinear dynamics of oscillations systems defined in [4].

## 2. RESEARCH OF DYNAMICS REGIMES

To observe for the nontrivial evolution of attractors and accordingly regular and chaotic regimes of the system at variation of parameters map of dynamic regimes was constructed (fig. 2). Algorithm of map constructing is based on practical criteria for the existence of deterministic chaos. It consists in diagnostic of regimes of interaction established between the pendulum and electromotor on a set of values of bifurcation parameters [4].

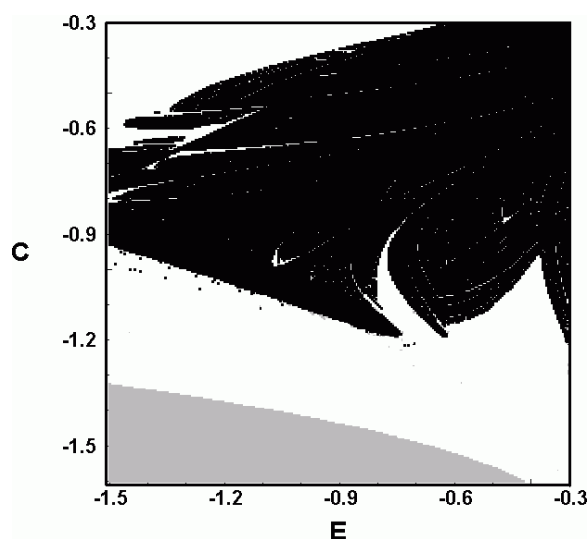


Fig. 2 Map of dynamic regimes

Shown in fig. 2 map of dynamic regimes is obtained due to analysis and data processing of computer experiments. It is built relative to the parameters  $C$  and  $E$ . Correspondingly the parameters  $D$  and  $F$  are assumed equal to  $-1$  and  $0.5$ . Initial conditions are varied in the neighborhood of origin of coordinates of phase space. There are areas of three different types of dynamic regimes in the fig. 2. In gray marked regions of parameters values equilibrium positions arise in the system. Signature of the spectrum of Lyapunov's characteristic exponents (LCE) in this case will look like  $\langle -, -, -, -, - \rangle$ . In white marked regions the system "spherical pendulum – electromotor" has limit cycles with signature of spectrum LCE  $\langle 0, -, -, -, - \rangle$ . In black marked regions of parameters values chaotic attractors arise in the phase space of the system. Signature LCE in this case will look like  $\langle +, 0, -, -, - \rangle$ . As seen from the fig. 2, the black areas of the map have white inclusion, so-called windows of periodicity.

In previous researches of the system “spherical pendulum – electromotor” realization of two main types of scenarios of transition from regular to chaotic regimes were established. These are transition to chaos through intermittency of Pomeau-Manneville [5] and through cascade of bifurcation of period-doubling or Feigenbaum’s scenario [6]. For second scenario new specificities of its realization were revealed. Thus, let’s analyze the characteristics for last mentioned scenario.

For this purpose let’s make a cross-section of the map (fig. 2) at  $E = -0.5$  and consider the bifurcations occurring in the system at the change of the parameter  $C$ . In fig. 3(a) the dependence on the maximal distinct from zero characteristic exponent of the parameter  $C$  are shown. As is known, the main practical criterion for the existence of deterministic chaos in the system is the presence in the spectrum of LCE at least one positive exponent [4]. In fig. 3(a) is shown that there is wide region of chaotic regimes where maximum characteristic exponent have positive value. These regions correspond to black areas of the map (fig. 2).

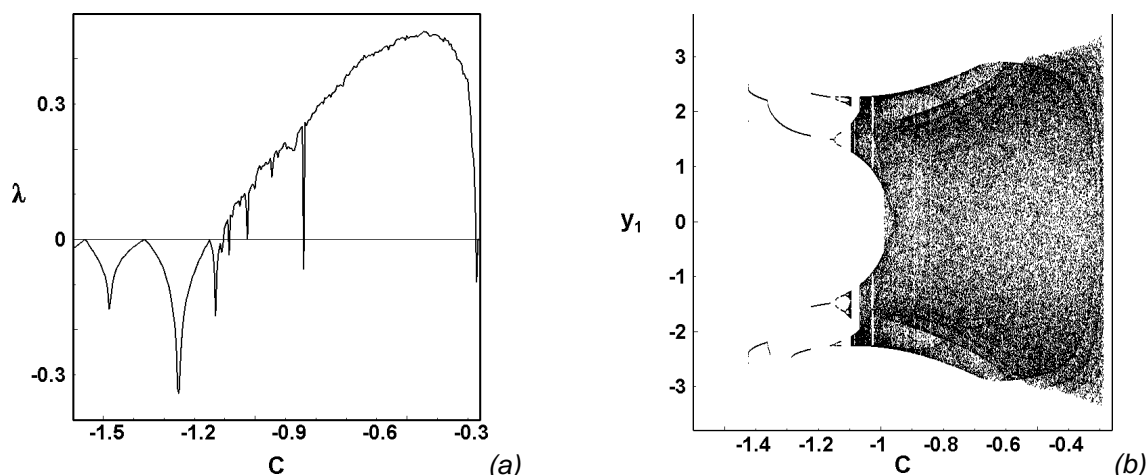


Fig. 3 The dependence on the maximum distinct from zero characteristic exponents of the parameter  $C$  (a); Bifurcation tree at  $E = -0.5$  (b)

In fig. 3(b) the bifurcation tree of the system is shown. Close study of fig. 3(b) allows determining areas of existence of regular and chaotic regimes. The light sites of “crown” of this tree correspond to periodic regimes of the steady state oscillations of the system, and densely blacked out – to chaotic. Points of a bifurcation, at which transition from regular periodic regime to the non-regular chaotic one occurs, are precisely visible. So, as can be seen from the fig. 3(b) there is cascade of bifurcation of period-doubling in the interval  $C \in (-1.3, -1.1)$ . In this interval current tree has specificity structure. After each bifurcation tree branches break off and appear in another area. Let’s analyze the system dynamics in this case.

At  $C = -1.21$  there is stable limit cycle in the system. Its phase portrait is shown in fig. 4(a). The signature of spectrum LCE of this cycle looks like  $(0, -, -, -, -)$ . In the system “spherical pendulum – electromotor” regular regime of interaction is fixed in which the pendulum has periodic oscillations.

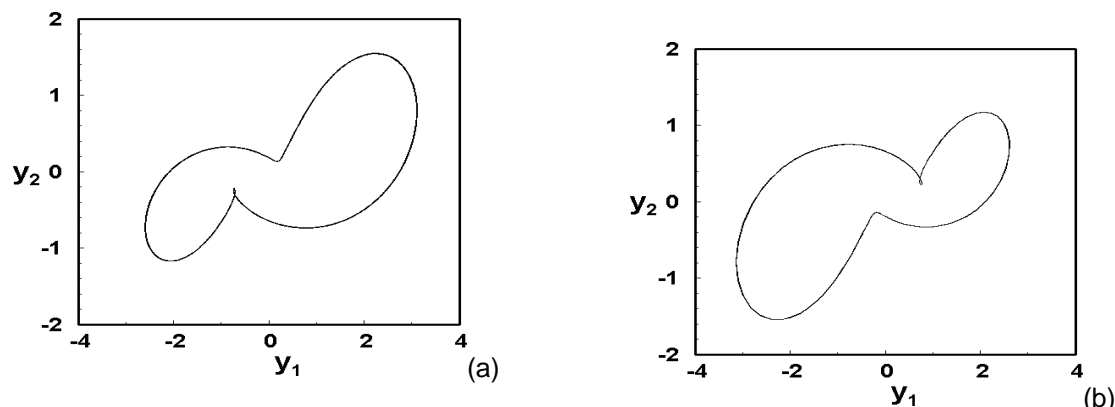


Fig. 4 Projections of phase portrait of limit cycles at  $C = -1.21$  (a), at  $C = -1.2$  (b)

At reducing the absolute value for the parameter  $C$  another stable limit cycle appears in the system. Arisen cycle is symmetrical for previous one and has the same period. The projection of phase portrait of such cycle at  $C = -1.2$  is built in fig. 4(b).

In this case we should consider the system oscillations by the temporary realization, for example  $y_2$ . In fig. 5 temporary realizations of the system at  $C = -1.21$  and  $C = -1.2$  combined by phase are shown. These realizations are built after transition process of the system is passed. Limit cycle at  $C = -1.21$  (fig. 4(a)) corresponds to black dot line in fig. 5. Another limit cycle of the system at  $C = -1.2$  corresponds to gray line in fig. 5. As can be seen from fig. 5 the inverse of oscillations occurs in the system at such changes of dynamic regimes. Thus, arisen at  $C = -1.2$  limit cycle we will call inverted cycle relative to previous limit cycle. And such property of rotation of a phase portrait of a cycle we will name inversion.

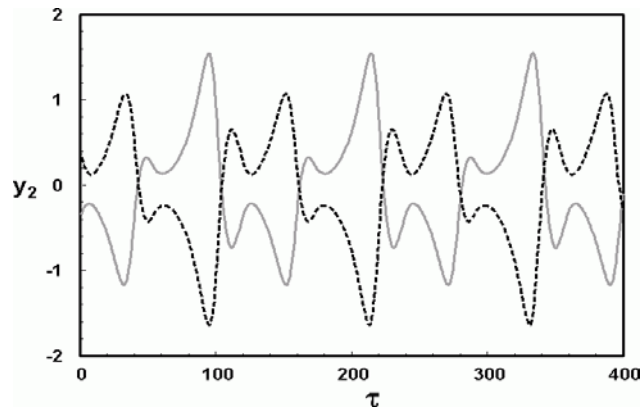


Fig. 5. Temporary realizations of the system at  $C = -1.21$  and  $C = -1.2$

As a result of the period doubling bifurcation of inverted cycle a new limit cycle arises in the system at  $C = -1.125$ . Projection of its phase portrait is built in fig. 6(a). At reducing the absolute value for the parameter  $C$  the inversion of limit cycles is taken place again. The inverted limit cycle of the same period arises in the system (fig. 6(b)). At the further increase of value  $C$  the next bifurcation of period doubling is taken place. After this bifurcation the limit cycle presented in fig. 6(c) arises in the system. Then at the further increase of value  $C$  after second bifurcation new inversion of limit cycle is taken place. The inverted limit cycle (fig. 6(d)) arises.

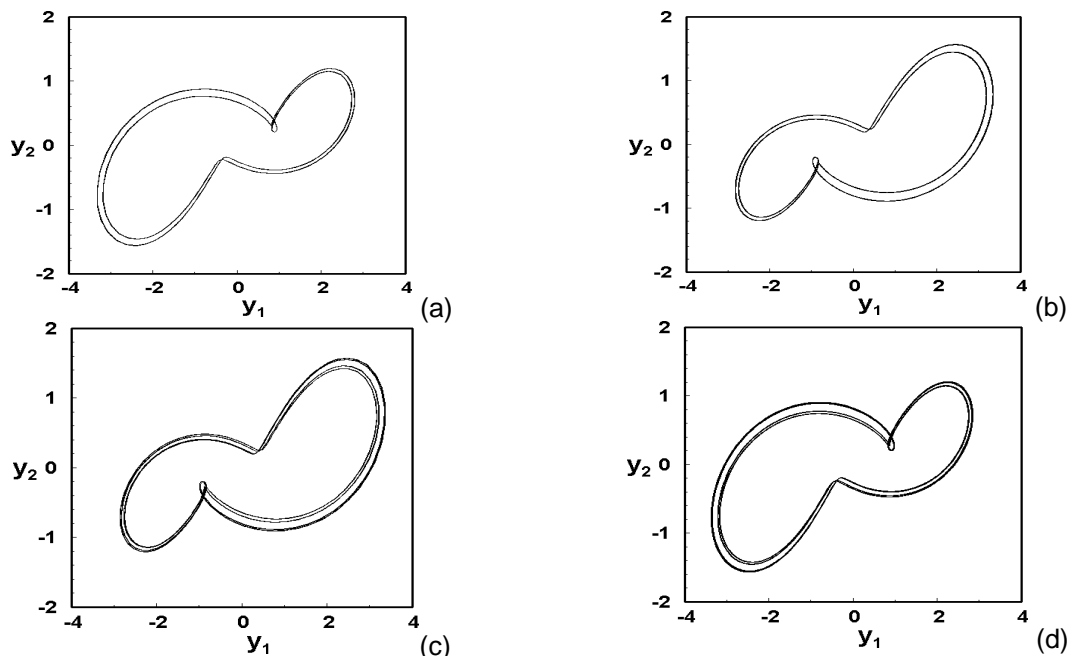


Fig. 6 Projections of phase portrait of limit cycles at  $C = -1.125$  (a), at  $C = -1.115$  (b), at  $C = -1.110$  (c), at  $C = -1.108$  (d)

The cascade of bifurcations of period doubling with inversion repeats infinite number of times. An end result of such process is origin in system of a chaotic attractor at  $C \approx -1.1$ . The projection of phase portrait of arisen chaotic attractor is built in fig. 7(a). In this case signature of spectrum LCE will look like  $(+, 0, -, -, -)$ . An important feature of this cascade is preservation of attractor inversions

in chaotic region. Really, arisen at  $C = -1.08$  chaotic attractor (fig. 7(b)) is inverted relative to chaotic attractor presented in fig. 7(a).

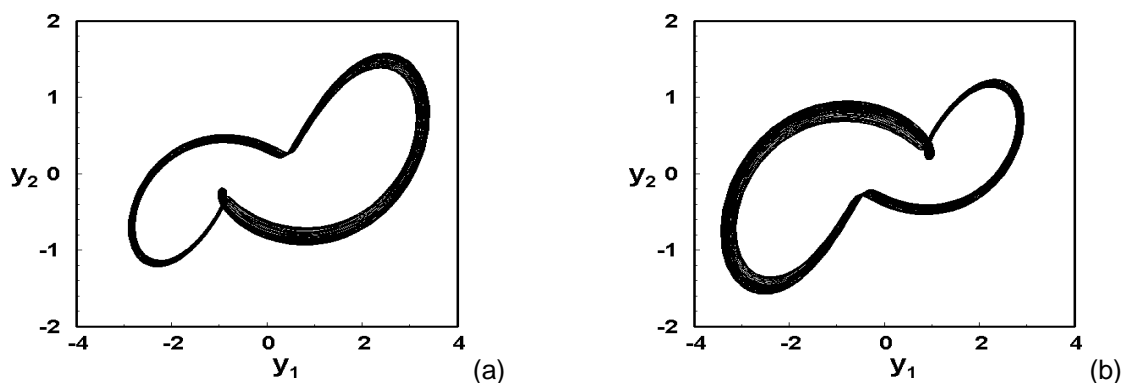


Fig. 7 Projections of phase portraits of chaotic attractors at  $C = -1.09$  (a) and at  $C = -1.08$  (b)

After each period-doubling bifurcation in the Fourier-spectrum appears sub-harmonic component exactly midway between the main harmonics of previous period (fig. 8). In the critical point a reverse process of destruction of sub-harmonic components is beginning and intervals of continuous spectrum are occurring.

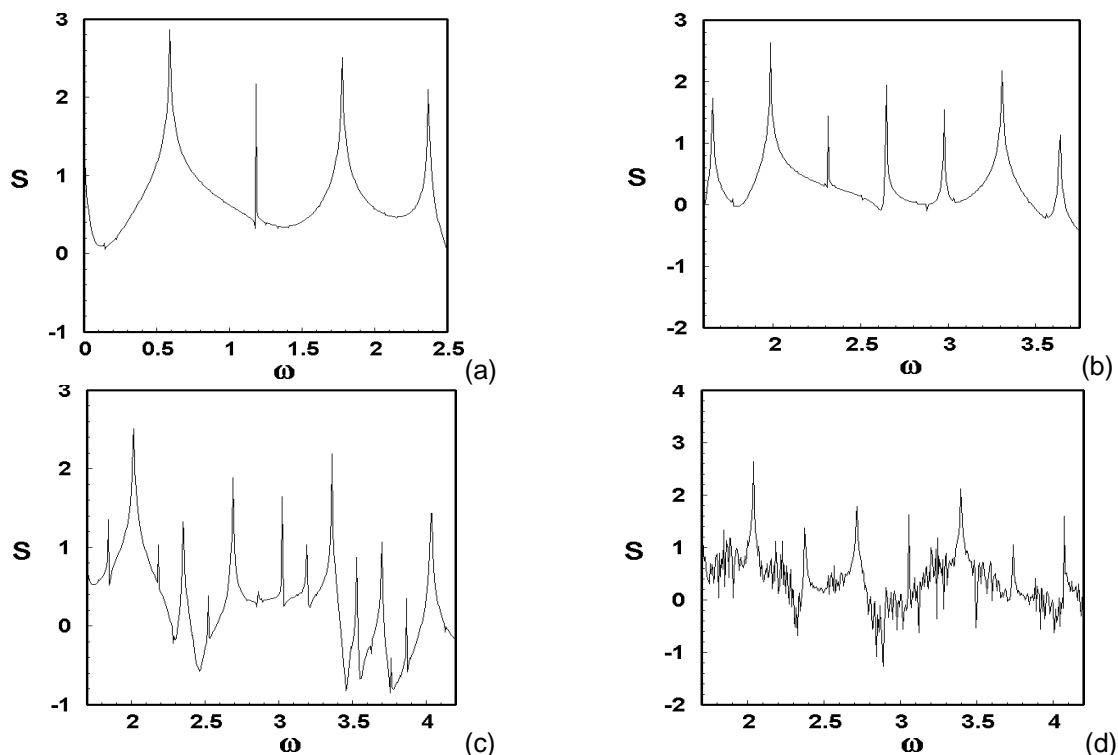


Fig. 8 Distributions of spectral densities of limit cycles at  $C = -1.125$  (a), at  $C = -1.115$  (b), at  $C = -1.110$  (c), at  $C = -1.108$  (d)

Let's consider Poincare sections of arisen chaotic attractors. Projection of Poincare section of chaotic attractor at  $C = -1.09$  by the plane  $y_3 = -2$  is built in fig. 9(a). This section represents some chaotic set which number of points increases with increasing time of numeric integration of system. As arisen chaotic attractor at  $C = -1.08$  rotates with another inverted chaotic attractor, the same its Poincare section rotates with inverted section at  $C = -1.08$  (fig. 9(b)).

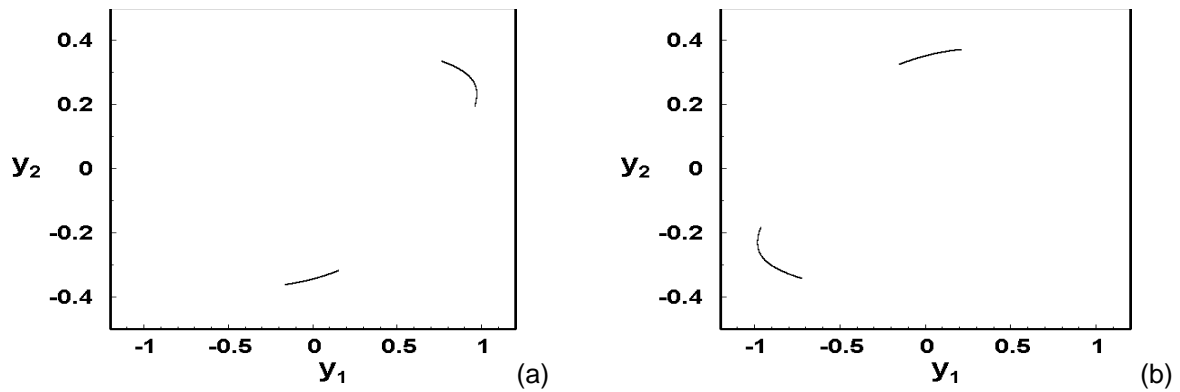


Fig. 9 Projections of Poincaré section of chaotic attractors at  $C = -1.09$  (a) and at  $C = -1.08$  (b)

## CONCLUSIONS

In current paper we obtain new aspects of chaotic dynamics of the system “spherical pendulum – electromotor”. Constructed map of dynamic regimes shows existence of regular and chaotic attractors in the system. Herewith, chaotic regimes are not unusual. They occupy largest area of system parameters in such map.

New peculiarity of scenario of transition to chaos through cascade of bifurcations of period doubling was identified. This peculiarity consists in the rotation of limit cycles with inverted to them after each bifurcation of period doubling. Also such process is preserved after origin of chaotic regimes in the system when arisen chaotic attractor rotates with inverted one. This peculiarity is traced in bifurcation tree, phase portraits, temporary realizations and Poincaré section of regular and chaotic attractors.

Thus, received in work results extend previous researches and in aggregate with results of works [3, 4] expose a great variety of chaotic behavior of the system “spherical pendulum – electromotor”.

## REFERENCES

- [1] Kononenko V.O. Vibrating system with a limited power-supply, London, Iliffe, 1969.
- [2] T.S. Krasnopolskaya, A.Yu. Shvets. Chaos in vibrating systems with limited power-supply. *Chaos*, 3, 3:387-395, 1993.
- [3] A. Yu. Shvets. Deterministic chaos of a spherical pendulum under limited excitation. *Ukrainian Mathematical Journal*, 59(4): 602-616, 2007.
- [4] Krasnopolskaya T. S., Shvets A. Yu. *Regular and chaotic dynamics of systems with limited excitation*, Moskow-Izhevsk, RCD, 2008 (in Russian).
- [5] Y. Pomeau, P. Manneville. Intermittent transition to turbulence in dissipative dynamical systems. *Comm. Math. Phys.*, 74(2):189-197, 1980.
- [6] M.J. Feigenbaum. Quantative universality for a class of nonlinear transformations. *J.Stat. Phys.*, 19(1):25-52, 1978.

## CHAOS AND HYPERCHAOS IN DETERMINISTIC NONIDEAL HYDRODYNAMIC SYSTEMS

**A. Yu. Shvets<sup>1</sup>**  
**V. A. Sirenko**  
National Technical  
University of Ukraine  
"KPI"  
Kyiv, Ukraine

---

### ABSTRACT

---

The steady-state dynamics regimes of deterministic nonideal systems «tank with a liquid - electric motor» are considered. The atlas of maps of dynamic regimes of the given system is constructed. For the first time existence of quasiperiodic and hyperchaotic attractors is revealed.

---

### INTRODUCTION

The study of oscillations of free surface of liquid in rigid tanks was carrying out of many works, which detailed bibliography are in monographies [1-3]. Excepting the big research interest, the given problems have wide practical application in many areas of modern technics, so long as modern machinery, mechanisms and vehicles as constructive elements, which contain varied in form tanks with liquids.

In overwhelming majority of works the oscillation of liquid in tanks are considered in, so-called, "ideal" statement of problem. At such statement of problem it is supposed that the source of excitation of oscillations of a liquid has an unlimited power. In consequence of that, probably to neglect feedback influence of oscillating system, in this case tank with liquid, on source of excitation of oscillations. The problems of global power savings demands the maximum minimisation of power of applied sources of excitation of oscillations. It leads to that the power of source of excitation becomes comparable to power consumed by oscillating system. Such situation more often takes place in real machines and mechanisms. In such cases application of "ideal" mathematical models can lead to gross errors in exposition of dynamics of systems «source of excitation of oscillations - oscillating subsystem». Thus there can be completely lost information about the deterministic chaos really existing in system [4, 5]. Because nonlinear interaction between oscillating subsystem and device of excitation of oscillations is one of reasons of origin of deterministic chaos.

The major aim of given work is a construction of atlas of maps of dynamic regimes of deterministic dynamic system «tank with a liquid - electric motor». On the basis of the constructed maps the careful study of types of steady-state regimes and detection of scenarios of transition between various types of regimes of system can be carrying out. The researches conducted in this work is prolongation and development the researches begun in [4-6].

### 1. MATHEMATICAL MODEL AND TECHNIQUE OF CARRYING OUT NUMERICAL CALCULATIONS

Let's consider rigid cylindrical tank partially filled with a liquid. We will assume that the electric motor of limited power excite horizontal oscillations of platform of tank. The given hydrodynamic system is typical nonideal, in sense of Kononenko [7], deterministic dynamic system. As shown in [4-6] mathematical model of system «tank with a liquid - electric motor» is described by following system of differential equations:

---

<sup>1</sup> Corresponding author. Email [alex.shvets@bigmir.net](mailto:alex.shvets@bigmir.net)

$$\begin{aligned}
\frac{dp_1}{d\tau} &= \alpha_1 p_1 - \left[ \beta + \frac{A}{2} (p_1^2 + q_1^2 + p_2^2 + q_2^2) \right] q_1 + B(p_1 q_2 - p_2 q_1) p_2 \\
\frac{dq_1}{d\tau} &= \alpha_1 q_1 + \left[ \beta + \frac{A}{2} (p_1^2 + q_1^2 + p_2^2 + q_2^2) \right] p_1 + B(p_1 q_2 - p_2 q_1) q_2 + 1 \\
\frac{d\beta}{d\tau} &= N_3 + N_1 \beta - \mu_1 q_1 \\
\frac{dp_2}{d\tau} &= \alpha_1 p_2 - \left[ \beta + \frac{A}{2} (p_1^2 + q_1^2 + p_2^2 + q_2^2) \right] q_2 - B(p_1 q_2 - p_2 q_1) p_1 \\
\frac{dq_2}{d\tau} &= \alpha_1 q_2 + \left[ \beta + \frac{A}{2} (p_1^2 + q_1^2 + p_2^2 + q_2^2) \right] p_2 - B(p_1 q_2 - p_2 q_1) q_1
\end{aligned} \tag{1}$$

The system (1) is a nonlinear system of differential equations of fifth order. Phase variables  $p_1, q_1$  and  $p_2, q_2$ , accordingly amplitudes of dominant modes of oscillations of free surface of liquid. The phase variable  $\beta$  is proportional to velocity of rotation of shaft of the electric motor. There are six parameters  $A, B, \alpha, N_1, N_3, \mu_1$  of system (1), which are defined through physical and geometrical characteristics of tank with a liquid and electric motor. The detailed expositions of these parameters are presented in works [4-6].

In works [4-6] existence of the deterministic chaos in system (1) has been proved, some types of chaotic attractors are classified and shown that chaotic attractors are typical attractors of the given system. We will notice that the detailed and all-round study of chaotic dynamics of system (1) is possible only by means of a series of numerical methods and algorithms. The technique of carrying out of such researches is described in works [4-5].

The particular interest calls construction of maps of dynamic regimes of system (1). Maps of dynamic regimes represent diagrammes on plane on which axes values of arbitrary parameters of system which are called as bifurcation are put aside. Various colours on maps plot areas corresponding to various types of the steady-state dynamical regimes. The basic classification of this or that type of dynamic regimes is the analysis of its spectrum of Lyapunov's characteristic exponents (LCE) [4, 8]. The boundaries between areas of dynamic regimes of different types are especially carefully analyzed. In these cases for correct classification of type of dynamic regimes its phase portraits, Poincare sections and maps, distributions of spectral densities and invariant measures are taken in consideration.

## 2. CONSTRUCTION OF THE ATLAS OF MAPS OF THE STEADY-STATE DYNAMIC REGIMES

First, we shall consider parameters  $N_3$  and  $\alpha$  as a bifurcation ones. Let's assume that,  $A=1.12$ ;  $B=-1.531$ ;  $\mu_1=0.5$ ;  $N_1=-1$ . In fig. 1 the sheet of atlas of maps of dynamic regimes of systems «tank with a liquid – electric motor» is shown. This map is obtained as a result of the analysis and data processing of computer experiments according to earlier stated technique.

In fig. 1 areas of existence of three various types of attractors of system (1) are plotted. By white colour plots areas of values of parameters and  $N_3$  at  $\alpha$  which equilibrium positions will be attractors of a system. The signature of their spectrum LCE looks like  $\langle -, -, -, -, - \rangle$ . The areas of grey colour correspond to limit cycles (periodic regimes) of system(1) with the signature of spectrum LCE  $\langle 0, -, -, -, - \rangle$ . Black colour plots areas of the deterministic chaos with the signature of spectrum LCE  $\langle +, 0, -, -, - \rangle$ . As from fig. 1 in some parts of a map black areas of chaotic attractors "incise" into areas of periodic regimes, in other parts, on the contrary, light gleams in chaotic areas which are called as "periodicity windows" are looked through.

Let's consider examples of regular and chaotic attractors corresponding to various areas of a map. So, at values and  $N_3 = -1.5$   $\alpha = -0.4$  the corresponding point in map locates in area of white colour. Position of the equilibrium which coordinates have values:  $p_1 = 0.699$ ,  $q_1(0) = 0.214$ ,  $\beta(0) = -1.607$ ,  $p_2 = q_2 = 0$  will be a system attractor. At  $N_3 = -1$ ,  $\alpha = -0.48$  and at  $N_3 = -0.72$ ,  $\alpha = -0.3$  corresponding points in the map locate in area of grey colour. Limit cycles will be system attractors in this case. Projections of phase portraits of the given cycles are shown in fig. 2a and 2b. Both cycles represent closed lines in a phase space, however the second of these cycles has more complicated, multistage structure. At last at  $N_3 = -0.4$ ,  $\alpha = -0.3$  the corresponding point locates in

black area of a map of dynamic regimes. In this case the system (1) has a chaotic attractor. Projection of a phase portrait of given chaotic attractor are shown in fig. 2c.

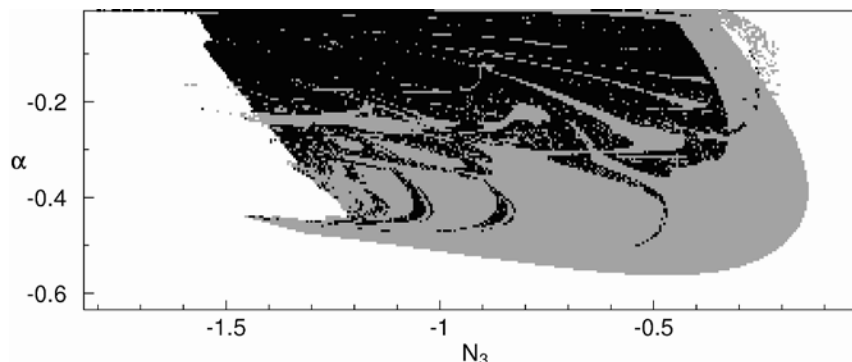


Fig. 1. Sheet of maps of dynamic regimes at changing of parametres  $N_3$  and  $\alpha$ .

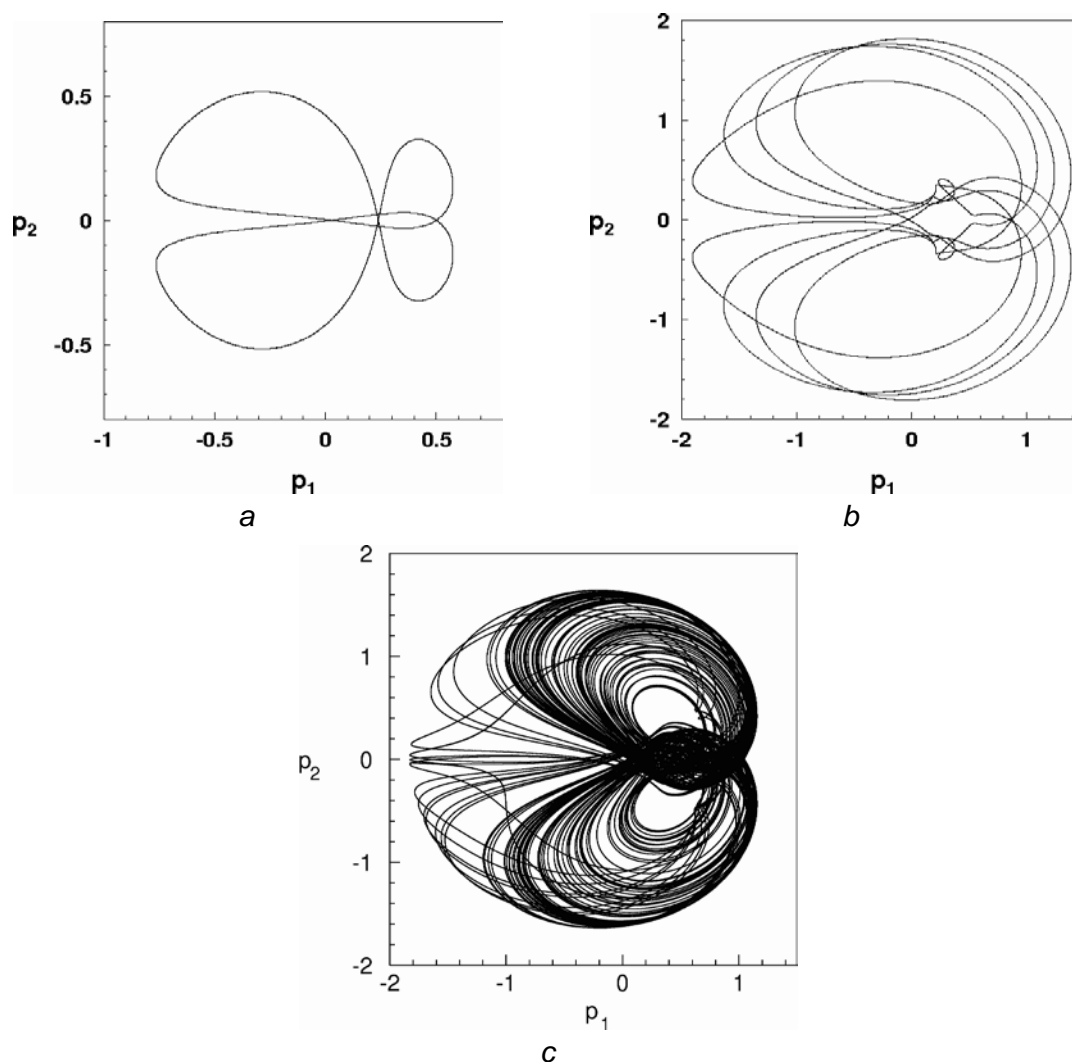


Fig. 2. Projections of limit cycles phase portraits at  $N_3 = -1$ ,  $\alpha = -0.48$ (a); and at  $N_3 = -0.72$ ,  $\alpha = -0.3$ (b); of chaotic attractor at  $N_3 = -0.4$ ,  $\alpha = -0.3$ (c).

Further we will assume that  $N_3 = -0.1$ . Parameters  $N_1$  and  $\alpha$  we will choose as bifurcation parameters. The values  $A$ ,  $B$  and  $\mu_1$  it is considered by the invariable. In fig. 3a the new sheet of the atlas of maps of dynamic regimes in which areas of four types of dynamic regimes are plotted. By white colour denote areas in space of parameters in which in system exist the equilibrium positions. The areas of light grey colour correspond to limit cycles of system (1). Dark grey colour areas corresponds to areas of chaotic attractors. And, at last, areas of black colour correspond to areas of quasiperiodic regimes with the signature of spectrum  $LCE < 0, 0, -, -, - >$ . In fig. 3b the increased fragment of the constructed map is shown. On this increased fragment the black area of quasiperiodic

attractors, which places near to boundary of areas of existence of regular and chaotic attractors, is clear visible. We will notice that areas in space of parameters of system (1) in which attractors of system are limit toruses have not been discovered in the previous researches of system (1). Thus quasiperiodic attractors are new type of attractors for the given systems.

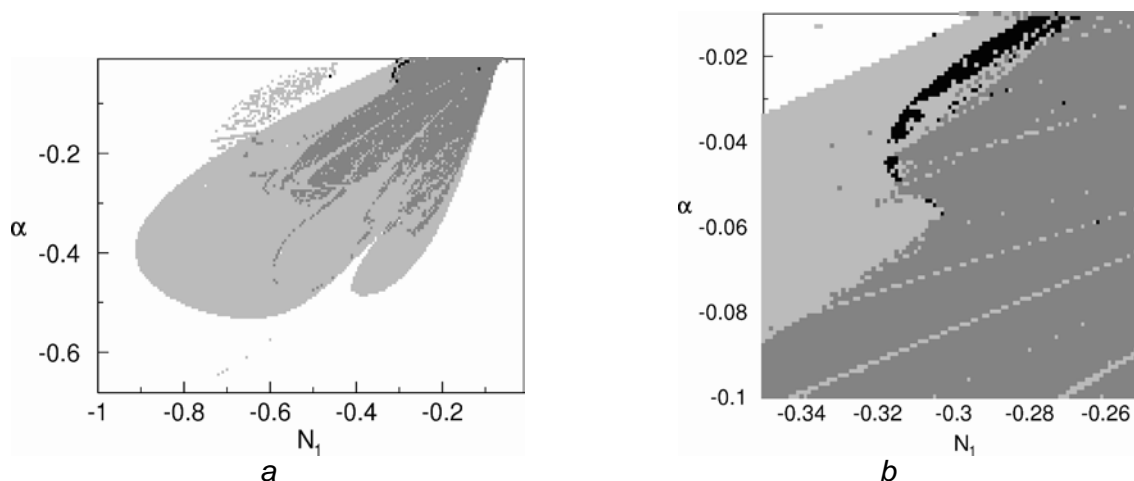


Fig. 3. Sheet of maps of dynamic regimes at changing of parametres  $N_1$  and  $\alpha$ .

Let's consider examples of attractors of system (1) which exist in various areas of a map from fig. 3. So in fig. 4a the projection of phase portrait of quasiperiodic attractor (limit torus), constructed at values  $N_1 = -0.32, \alpha = -0.045$  is shown. In fig. 4b the limit cycle projection (resonance cycle in torus), constructed at values  $N_1 = -0.314, \alpha = -0.045$  is shown. At last in fig. 4c the projection of one of chaotic attractors of system (1), constructed at values  $N_1 = -0.3131, \alpha = -0.045$  is shown. In this case transition to chaos through destruction of a quasiperiodic attractor is realised.

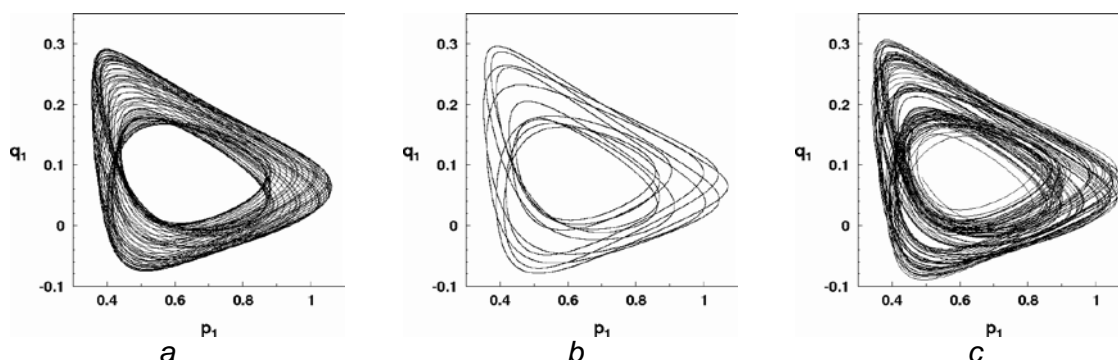
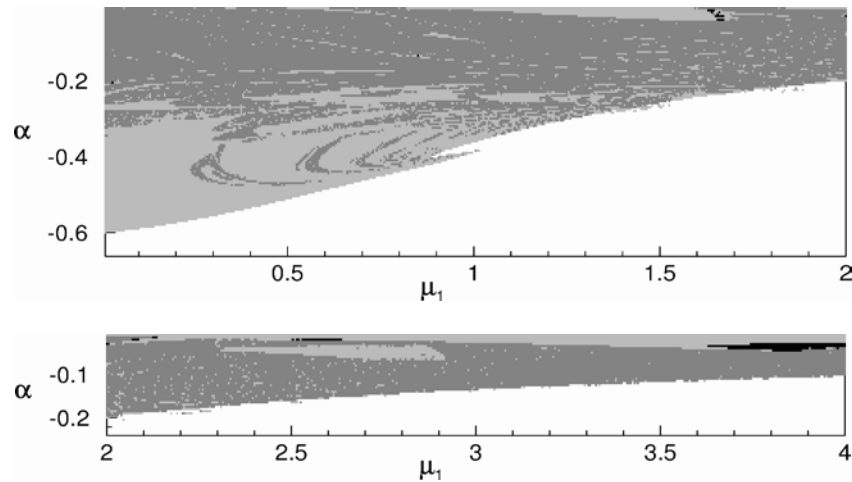


Fig. 4. Projections of phase portraits of quasiperiodic attractor at  $N_1 = -0.32, \alpha = -0.045$  (a); limit cycle at  $N_1 = -0.314, \alpha = -0.045$  (b); chaotic attractor at  $N_3 = -0.3131, \alpha = -0.045$  (c).

Now we will assume that  $N_3 = N_1 = -1$ . Parameters  $\mu_1$  and  $\alpha$  we will choose as bifurcation parameters. The values  $A, B$  it is considered by the invariable. In fig. 5 (a-b) a few fragments of new sheet of the atlas of maps of dynamic regimes are plotted. The areas of dynamic regimes of five types be present in given maps. By white colour areas of existence of positions of equilibrium are plotted. The areas of light grey colour correspond to periodic regimes of system. By grey colour notes areas of existence of chaotic attractors. Areas of quasiperiodic regimes are designated by black colour. And at last, areas of existence of hyperchaotic attractors are plotted by dark grey colour. The signature of spectrum LCE of hyperchaotic attractors looks like  $\langle +, +, 0, -, - \rangle$ . So two positive exponents are at spectrum of hyperchaotic attractors. We will notice that hyperchaotic attractors not discovered at earlier researches of system (1).

Let's consider some of hyperchaotic attractors existing in system (1). So in fig. 6a the projection of phase portrait of hyperchaotic attractor constructed at values  $\mu_1 = 4.125, \alpha = -0.04$  is shown. In fig. 6b the projection hyperchaotic attractor, constructed at values  $\mu_1 = 4.125, \alpha = -0.0403$  is shown. Phase portraits of these attractors noticeably differ one from another. First of all the hyperchaotic attractor presented in fig. 6b differs from a hyperchaotic attractor presented in fig. 6a appreciable increasing of volume of its area of localisation in a phase space. In fig. 6c the increased fragment of a central part of

an attractor from fig. 6b. Apparently from fig. 6c in this fragment contours of a hyperchaotic attractor presented in fig. 6a are accurately looked through. Such qualitative similarity of a fragment of one attractor to other attractor has allowed to make clear existing in system the transition of type of «hyperchaos - hyperchaos». It was possible to prove that this transition is realised under the scenario of intermittency generalising the known scenario of Pomeau and Manneville. And if in works [4, 5] it was possible to generalise the scenario of Pomeau and Manneville for type of transition of «chaos - chaos», now it succeed to be generalised and on type of transition of «hyperchaos - hyperchaos».



*Fig. 5a Fragments of sheet of the atlas of maps of dynamic regimes at changing of parametres  $\mu_1$  and  $\alpha$  .*

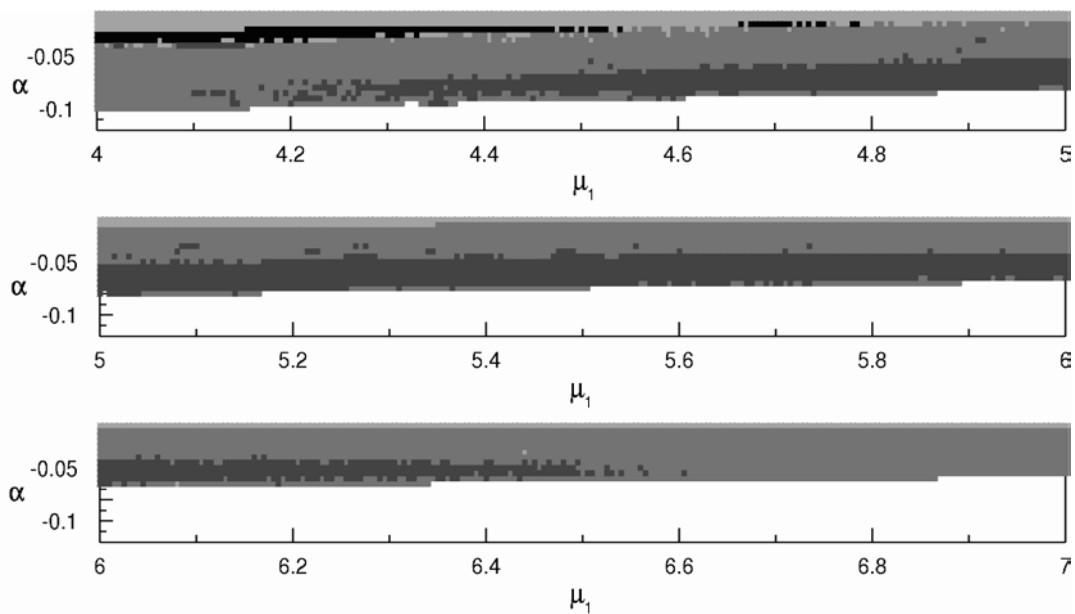


*Fig. 5b. Fragments of sheet of the atlas of maps of dynamic regimes at changing of parametres  $\mu_1$  and  $\alpha$  .*

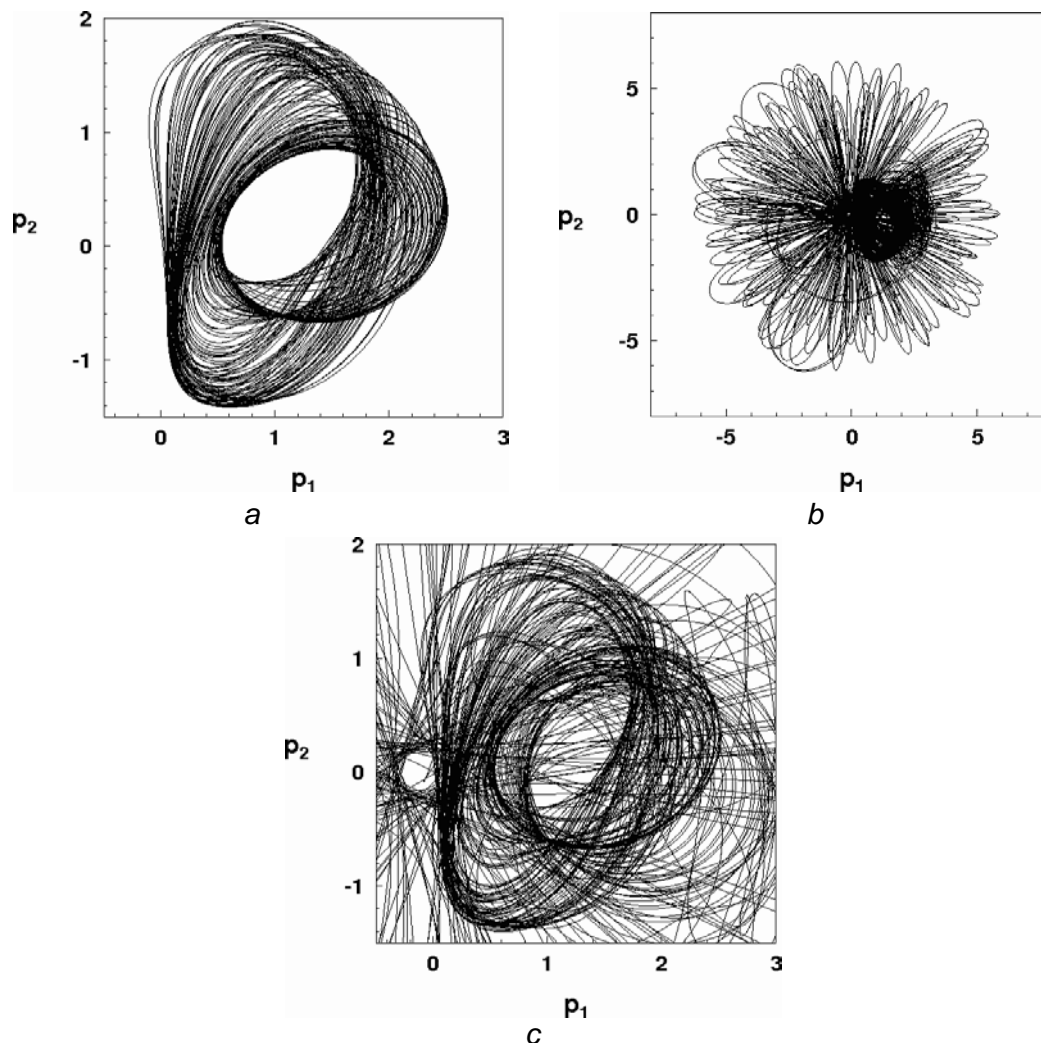


Fig 6 Projections of hyperchaotic attractors phase portraits at  $\mu_1 = 4.125$ ,  $\alpha = -0.04$  (a) and at  $\mu_1 = 4.125$ ,  $\alpha = -0.0403$  (b-c).

## CONCLUSIONS

Thus, in this work maps of dynamic regimes of nonideal deterministic system "tank with a liquid-electric motor" for the first time are constructed. The constructed maps are of great importance for detailed research of regular and chaotic attractors of the given system. The knowledge of such maps allows essentially abridge duration of time of carrying out of natural experimental researches of dynamic systems of this kind. Also in space of parameters of system for the first time the discovered areas of existence of hyperchaotic and quasiperiodic attractors.

## REFERENCES

- [1] Rabinovich B.I. *Introduction in Dynamics of Carrier Rockets of Space Apparatus*, Moscow: Mechanical Engineering, 1983 (in Russian).
- [2] Lukovsky I.A. *Introduction in Nonlinear Dynamics of Rigid body with Concavities Containing Liquid*, Kiev: Naukova Dumka, 1990 (in Russian).
- [3] Ibrahim R.A. *Liquid Sloshing Dynamics: Theory and Applications*, Cambridge University Press, 2005.
- [4] Krasnopolskaya T. S., Shvets A. Yu. *Regular and chaotic dynamics of systems with limited excitation*, Moskow-Izhevsk, RCD, 2008 (in Russian).
- [5] Krasnopolskaya T. S., Shvets A. Yu. Dynamical chaos for a limited power supply oscillations in cylindrical tanks, *Journal of Sound and Vibration*, volume 322, 2009, P. 532—553.
- [6] Krasnopolskaya T.S., Shvets A.Yu. Chaotic surface waves in limited power-supply cylindrical tank vibrations, *Journal of Fluids AND Structures*, 1994, Vol. 8, № 1, P. 1—18.
- [7] Kononenko V.O. *Vibrating Systems With a Limited Power-Supply*, London, Iliffe, 1969.
- [8] Kuznetsov S. P. *Dynamical Chaos*, Moskow, Physmatlit, 2006 (in Russian).

## SOME REMARKS ABOUT QUASI-STEADY DYNAMICS

**V.V. Sidorenko**<sup>1</sup>  
 Keldysh Institute of  
 Applied Mathematics  
 Moscow, RUSSIA

ABSTRACT

A mechanical system consisting of two interacting subsystems is considered. When the interaction is removed, one subsystem is Hamiltonian and the other one is a dissipative linear oscillatory system. Integral manifolds theory is used to study the motions that are established after the high-frequency normal oscillations of the dissipative subsystem are damped. Evolution equations are constructed to describe a behavior of the Hamiltonian subsystem over long time interval.

### 1. SYSTEM DESCRIPTION. BASIC ASSUMPTIONS

We consider a dynamical system consisting of two interacting subsystems,  $S_H$  and  $S_D$ . When the interaction is removed, the subsystem  $S_H$  becomes the Hamiltonian system with  $n$  degrees of freedom and the subsystem  $S_D$  becomes a dissipative linear oscillatory system with  $m$  degrees of freedom. The characteristic period of oscillations in subsystem  $S_D$  and the characteristic damping time of these oscillations are comparable in magnitude and much smaller than the characteristic time of motions in  $S_H$ . Below we will call  $S_H$  the damped system and  $S_D$  the damper one.

The equations of motion of the system  $S_H + S_D$  can be written in Routhian form:

$$\mathbf{P}^{\bullet} = -\nabla_{\mathbf{Q}}R, \quad \mathbf{Q}^{\bullet} = \nabla_{\mathbf{P}}R, \quad (\nabla_{\mathbf{v}}R)^{\bullet} - \nabla_{\mathbf{q}}R = -\nabla_{\mathbf{v}}\Phi \quad (1)$$

Here  $\mathbf{P} = (P_1, \dots, P_n)^T$  and  $\mathbf{Q} = (Q_1, \dots, Q_n)^T$  are canonical variables used to describe the motion in  $S_H$ ,  $\mathbf{q} = (q_1, \dots, q_m)^T$  is the generalized coordinate vector of the damper with  $\mathbf{v} = \mathbf{q}^{\bullet}$ . Dots denote derivatives with respect to time  $t$ .

The Routhian function  $R$  in (1) is a combination of the Hamiltonian  $H$  of subsystem  $S_H$ , the Lagrangian  $L$  of subsystem  $S_D$ , and a function  $K$  characterizing the interaction of the subsystems:

$$R = H + K - L$$

Given these assumptions the Lagrangian  $L$  and the dissipative function  $\Phi$  of the damper can be written in the form

$$L(\mathbf{v}, \mathbf{q}, \varepsilon) = \frac{1}{2} [(\mathbf{v}, M\mathbf{v}) - \varepsilon^{-2}(\mathbf{q}, \Lambda\mathbf{q})], \quad \Phi(\mathbf{v}, \varepsilon) = \frac{1}{2\varepsilon} (\mathbf{v}, D\mathbf{v}) \quad (2)$$

$$\varepsilon = T_D / T_H \ll 1$$

Here  $M$ ,  $\Lambda$  and  $D$  are positive-definite symmetric matrices with constant coefficients,  $T_D$  and  $T_H$  are characteristic times of processes in  $S_D$  and  $S_H$  respectively.

We take

<sup>1</sup> Corresponding author. Email [sidorenk@keldysh.ru](mailto:sidorenk@keldysh.ru)

$$K(\mathbf{P}, \mathbf{Q}, \mathbf{v}, \mathbf{q}) = (\mathbf{u}, \mathbf{q}) + \frac{1}{2}(\mathbf{v}, \Gamma \mathbf{q}) + K_2(\mathbf{P}, \mathbf{Q}, \mathbf{q})$$

to be the interaction function with  $\mathbf{u} = (u_1(\mathbf{P}, \mathbf{Q}), \dots, u_m(\mathbf{P}, \mathbf{Q}))^T = \nabla_{\mathbf{q}} K(\mathbf{P}, \mathbf{Q}, 0, 0)$ ,  $\Gamma$  is an antisymmetric matrix whose elements are functions of  $\mathbf{P}$ ,  $\mathbf{Q}$  and the function  $K_2(\mathbf{P}, \mathbf{Q}, \mathbf{q}) = O(q^2)$ ,  $q = |\mathbf{q}| = (q_1^2 + \dots + q_m^2)^{1/2}$ .

With this choice of  $K$  the system  $S_H + S_D$  is a finite-dimensional model of systems encountered in studies of the motion of a deformable solid about its centre of mass (Section 5).

## 2. MAIN THEOREM

When studying the dynamics of  $S_H + S_D$  over time intervals comparable to or substantially greater than  $T_H$ , it is desirable to consider the motion of the damper to be forced and to describe it by the relations of the form

$$\mathbf{v} = \mathbf{v}_*(\mathbf{P}, \mathbf{Q}, \varepsilon), \quad \mathbf{q} = \mathbf{q}_*(\mathbf{P}, \mathbf{Q}, \varepsilon) \quad (3)$$

Substituting (3) into the equations for  $\mathbf{P}^*$ ,  $\mathbf{Q}^*$  in (1) we obtain a closed system of equations describing the behavior of subsystem  $S_H$  after the normal oscillations of the damper have decayed away.

Various modifications of these equations for the quasi-steady motions of specific systems were constructed in [1-3]. There have been attempts [4,5] to give a justification for using such equations to describe the regular components of the motion by boundary function theory methods [6].

Relations (3) define a hypersurface  $\Sigma$ ,  $\dim \Sigma = 2m$  in the phase space of the system  $S_H + S_D$ . If this hypersurface is invariant with respect to the phase flow of the system, it is called an integral manifold (IM) [7,8].

**Theorem.** *For sufficiently small values of the parameter  $\varepsilon$  system (1) possesses an IM  $\Sigma$  described by the relations of the form (3). On the manifold  $\Sigma$  system (1) is equivalent to the system*

$$\begin{aligned} \mathbf{P}^* &= -\nabla_{\mathbf{Q}} H - \nabla_{\mathbf{Q}} K(\mathbf{P}, \mathbf{Q}, \mathbf{v}_*(\mathbf{v}, \mathbf{q}, \varepsilon), \mathbf{q}_*(\mathbf{v}, \mathbf{q}, \varepsilon)) \\ \mathbf{Q}^* &= \nabla_{\mathbf{P}} H + \nabla_{\mathbf{P}} K(\mathbf{P}, \mathbf{Q}, \mathbf{v}_*(\mathbf{v}, \mathbf{q}, \varepsilon), \mathbf{q}_*(\mathbf{v}, \mathbf{q}, \varepsilon)) \end{aligned} \quad (4)$$

The functions  $\mathbf{v}_*(\mathbf{P}, \mathbf{Q}, \varepsilon)$ ,  $\mathbf{q}_*(\mathbf{P}, \mathbf{Q}, \varepsilon)$  satisfy the inequalities

$$|\mathbf{v}_*(\mathbf{P}, \mathbf{Q}, \varepsilon)| \leq \varepsilon^2 C_1, \quad |\mathbf{q}_*(\mathbf{P}, \mathbf{Q}, \varepsilon)| \leq \varepsilon^2 C_1, \quad C_1 = \text{const} > 0$$

The proof of this theorem consists of constructing a special contraction mapping  $\mathfrak{S}$  on the set of functions specifying hypersurfaces in phase space [9].

## 3. APPROXIMATE EQUATIONS FOR QUASI-STEADY MOTION

It is not difficult to find that in quasi-steady motion

$$\mathbf{v} = -\varepsilon^2 \Lambda^{-1} \{\mathbf{u}, H\} \quad (5)$$

with an error of  $O(\varepsilon^3)$ , and

$$\mathbf{q} = -\varepsilon^2 \Lambda^{-1} \mathbf{u} + \varepsilon^3 \Lambda^{-1} D \Lambda^{-1} \{\mathbf{u}, H\} \quad (6)$$

with an error of  $O(\varepsilon^3)$ . Here  $\{\cdot, \cdot\}$  are Poisson brackets for the subsystem  $S_H$ .

Substituting expressions (5),(6) into (4) we obtain a system of approximate equations for the quasi-steady motion

$$\begin{aligned}\mathbf{P}^\bullet &= -\nabla_{\mathbf{Q}}\hat{H} - \varepsilon^3 U_{\mathbf{Q}} \Lambda^{-1} D \Lambda^{-1} \{\mathbf{u}, H\} \\ \mathbf{Q}^\bullet &= \nabla_{\mathbf{P}}\hat{H} + \varepsilon^3 U_{\mathbf{P}} \Lambda^{-1} D \Lambda^{-1} \{\mathbf{u}, H\}\end{aligned}\quad (7)$$

where

$$\begin{aligned}\hat{H}(\mathbf{P}, \mathbf{Q}, \varepsilon) &= H(\mathbf{P}, \mathbf{Q}) + \varepsilon^2 H_2(\mathbf{P}, \mathbf{Q}), \quad H_2(\mathbf{P}, \mathbf{Q}) = -\frac{1}{2}(\mathbf{u}, \Lambda^{-1} \mathbf{u}) \\ U_{\mathbf{P}} &= \begin{pmatrix} \frac{\partial u_1}{\partial P_1} & \dots & \frac{\partial u_m}{\partial P_1} \\ \dots & \dots & \dots \\ \frac{\partial u_1}{\partial P_n} & \dots & \frac{\partial u_m}{\partial P_n} \end{pmatrix}, \quad U_{\mathbf{Q}} = \begin{pmatrix} \frac{\partial u_1}{\partial Q_1} & \dots & \frac{\partial u_m}{\partial Q_1} \\ \dots & \dots & \dots \\ \frac{\partial u_1}{\partial Q_n} & \dots & \frac{\partial u_m}{\partial Q_n} \end{pmatrix}\end{aligned}$$

The nearly-Hamiltonian system of equations (7) describes the influence of the interaction with the damper on the dynamics of subsystem  $S_H$  to an accuracy of  $O(\varepsilon)$  over a time interval  $\varepsilon^{-3}$ .

#### 4. EVOLUTION OF QUASI-STEADY MOTION IN AN INTEGRABLE SUBSYSTEM $S_H$

Suppose that  $\mathbf{I} = (I_1, \dots, I_n)^T$ ,  $\varphi = (\varphi_1, \dots, \varphi_n)^T$  are ‘‘action-angle’’ variables in  $S_H$ . In  $\mathbf{I}, \varphi$  variables the equations of quasi-steady motion have the form

$$\begin{aligned}\mathbf{I}^\bullet &= -\varepsilon^2 \nabla_{\varphi} H_2 - \varepsilon^3 U_{\varphi} \Lambda^{-1} D \Lambda^{-1} U_{\varphi}^T \omega \\ \varphi^\bullet &= \omega(\mathbf{I}) + \varepsilon^2 \nabla_{\mathbf{I}} H_2 + \varepsilon^3 U_{\mathbf{I}} \Lambda^{-1} D \Lambda^{-1} U_{\varphi}^T \omega\end{aligned}\quad (8)$$

Here  $\omega(\mathbf{I}) = \nabla_{\mathbf{I}} H(\mathbf{I})$  is the frequency vector of the subsystem  $S_H$ .

The variables of (8) separate: the  $\mathbf{I}$  variables are slow ( $\mathbf{I}^\bullet = O(\varepsilon^2)$ ) and the  $\varphi$  variables are fast ( $\varphi^\bullet = O(1)$ ).

We shall study the behavior of the slow variables using an averaging method [10]. For simplicity we restrict ourselves to the case when the Fourier series of the function  $\mathbf{u}(\mathbf{I}, \varphi)$  with respect to  $\varphi$  contains a finite number of terms

$$\mathbf{u}(\mathbf{I}, \varphi) = \sum_{\mathbf{k} \in \mathbb{Z}^n, |\mathbf{k}| \leq N} \mathbf{u}_{\mathbf{k}}(\mathbf{I}) e^{i\langle \mathbf{k}, \varphi \rangle}, \quad \langle \mathbf{k}, \varphi \rangle = k_1 \varphi_1 + \dots + k_n \varphi_n$$

In system (8) we perform two consecutive averaging changes of variables

$$(\mathbf{I}, \varphi) \xrightarrow{1} (\tilde{\mathbf{I}}, \tilde{\varphi}) \xrightarrow{2} (\tilde{\tilde{\mathbf{I}}}, \tilde{\tilde{\varphi}})$$

The first change of variables removes the second-order terms in  $\varepsilon$  in the slow variable equations and is a canonical transformation with generating function

$$S(\tilde{\mathbf{I}}, \varphi) = \langle \tilde{\mathbf{I}}, \varphi \rangle - i\varepsilon^2 \sum_{\mathbf{k} \in \mathbb{Z}^n \setminus \{0\}, |\mathbf{k}| \leq 2N} \frac{H_{2\mathbf{k}}(\tilde{\mathbf{I}})}{\langle \mathbf{k}, \varphi \rangle} e^{i\langle \mathbf{k}, \varphi \rangle}$$

where

$$H_{2\mathbf{k}}(\mathbf{I}) = -\frac{1}{2} \sum_{\mathbf{k}' \in \mathbb{Z}^n, |\mathbf{k}'| \leq N, |\mathbf{k} - \mathbf{k}'| \leq N} (\mathbf{u}_{\mathbf{k}'}(\mathbf{I}), \Lambda^{-1} \mathbf{u}_{\mathbf{k} - \mathbf{k}'}(\mathbf{I}))$$

The second change of variables removes terms of the third order in  $\varepsilon$  depending on  $\varphi$  from the slow variable equations. In asymptotically small neighborhoods of the resonance surfaces

$$\langle \omega(\mathbf{I}), \mathbf{k} \rangle = 0 \quad (\mathbf{k} \in \mathbb{Z}^n, |\mathbf{k}| \leq 2N)$$

the introduced changes of variables become meaningless. The properties of the solutions of system (8) at resonance must be investigated by the methods described in [11, Chapter III].

Far from the resonance surfaces the behavior of the slow variables with accuracy  $O(\varepsilon)$  in the time interval  $\varepsilon^{-3}$  is described by the following evolution equations (we use the original notation for the averaged variables)

$$\mathbf{I}^* = -\nabla_{\omega} \Phi_{eff}(\omega(\mathbf{I}), \mathbf{I}) \quad (9)$$

where

$$\begin{aligned} \Phi_{eff}(\omega, \mathbf{I}) &= \frac{\varepsilon^3}{2} \langle \omega, D_{eff} \omega \rangle \\ D_{eff} &= \langle\langle U_{\varphi} \Lambda^{-1} D \Lambda^{-1} U_{\varphi}^T \rangle\rangle = \sum_{\mathbf{k} \in \mathbb{Z}^n, |\mathbf{k}| \leq N} (\mathbf{u}_{\mathbf{k}}, \Lambda^{-1} D \Lambda^{-1} \mathbf{u}_{-\mathbf{k}}) \mathbf{k}^T \mathbf{k} \\ \langle\langle \cdot \rangle\rangle &= \frac{1}{(2\pi)^n} \int_0^{2\pi} \dots \int_0^{2\pi} (\cdot) d\varphi_1 \dots d\varphi_n \end{aligned}$$

The quadratic form  $\Phi_{eff}(\omega, \mathbf{I})$  in (9) is an analogue of the function  $\Phi(\mathbf{v}, \varepsilon)$  in (1) and describes the dissipation of energy in quasi-steady motion

$$\langle\langle \Phi(\mathbf{v}_*(\mathbf{I}, \varphi, \varepsilon), \varepsilon) \rangle\rangle = \Phi_{eff}(\omega(\mathbf{I}), \mathbf{I}) + O(\varepsilon^4)$$

## 5. THE $S_H + S_D$ SYSTEM AS A MODEL OF A DEFORMABLE SOLID PERFORMING TRANSLATIONAL-ROTATIONAL MOTION

In many investigations, for example, when studying the dynamics of large space structures or the tidal evolution of planetary rotation [3,12,13], the question arises of the translational-rotational motion of a deformable body in a potential field.

The motion of a deformable body with respect to its centre of mass consists of the rotation of the body as a whole and the elastic displacements  $\mathbf{s}$  of its individual elements. The dissipation of mechanical energy during relative displacements leads to the damping of high-frequency normal oscillations and influences the motion of the body as a whole.

As a rule, the decay time of the natural oscillations is considerably less than the characteristic time of the motion of the body as a whole. Hence quasi-steady motion is fundamental for a deformable body.

We say that the system  $S_H + S_D$  is an  $N$ th order model if the subsystem  $S_H$  describes the motion of the body as a whole taking no account of deformation, while the subsystem  $S_D$  describes the deformation of the body on the basis of a finite-dimensional approximation of the deformation field, using forms of free oscillation corresponding to the  $N$  lowest frequencies of the body.

As  $N \rightarrow \infty$  the right-hand sides of equations for quasi-steady motion for models of corresponding order form a rapidly converging functional series. This enables us to consider low-order models for a qualitative analysis of the influence of deformations on the motion of specific objects.

## REFERENCES

- [1] Chernous'ko F.L. On the motion of a solid body with elastic and dissipative elements, *Prikl. Mat. Mekh.* 42, pp 34-42, 1978.
- [2] Chernous'ko F.L. On the motion of a visco-elastic body about its centre of mass, *Izv. Akad. Nauk SSSR. MTT.* V. 1, pp 22-26, 1980.

- [3] Vil'ke V.G. *Analytic and Qualitative Methods in the Mechanics of Systems with an Infinite Number of Degrees of Freedom*, Izd. Moscow Gos. University, Moscow, 1986.
- [4] Chernous'ko F.L., Shamayev A.S. Asymptotic form of singular perturbations in the dynamics of a body with elastic and dissipative elements, *Izv. Akad. Nauk SSSR. MTT*. V. 3, pp 33-42, 1983.
- [5] Sinitsyn Ye.V. Asymptotic form of singular perturbations in the investigation of the translational-rotational motion of a visco-elastic body, *Izv. Akad. Nauk SSSR. MTT*. V. 1, pp 104-110, 1991.
- [6] Vasil'yeva A.B., Butuzov V.F. *Asymptotic Expansions of Solutions of Singularly Perturbed Equations*. Nauka, Moscow, 1973.
- [7] Mitropol'skii Yu.A., Lykova O.B. *Integral Manifolds in Non-linear Mechanics*, Nauka, Moscow, 1973.
- [8] Strygin V.V., Sobolev V.A. *Separation of Motions by Integral Manifold Methods*, Nauka, Moscow, 1988.
- [9] Sidorenko V.V. The dynamic evolution of a mechanical system with a very rigid linear damper, *Prikl. Mat. Mekh.* 59, pp 562-568, 1995.
- [10] Bogolyubov N.N., Mitropol'skii Yu.A., *Asymptotic Methods in the Theory of Non-linear Oscillations*, Fizmatgiz, Moscow, 1963.
- [11] Arnol'd V.I., Kozlov V.V., Neishtadt A. I. Mathematical aspects of classical and celestial mechanics, *In Results of Science and Technology. Modern Problems in Mathematics. Basic Trends*, V. 3, VINITI, Moscow, 1985.
- [12] Markeyev A.P. The effect of longitudinal elastic oscillations of a body on its rapid rotation in a gravitation field, *Izv. Akad. Nauk SSSR. MTT*. V. 6, pp 38-45, 1989.
- [13] Kholostova O.V. On the rapid rotations of an elastic spherical shell in a gravitation field, *Izv. Akad. Nauk SSSR. MTT*. V. 2, 129-139, 1991.

## LIMITING PHASE TRAJECTORIES AND DYNAMICAL TRANSITIONS IN THE NONLINEAR PERIODIC SYSTEMS

Valeri V. Smirnov<sup>1</sup>,  
Leonid I. Manevitch

N.N. Semenov  
Institute of Chemical  
Physics RAS,  
Moscow, Russia

---

### ABSTRACT

---

The efficient energy exchange in the nonlinear periodic Frenkel-Kontorova and Klein-Gordon lattices has been studied in the framework of the concept of Limiting Phase Trajectories proposed earlier. Two dynamical transitions occur while the nonlinearity of interaction grows. The first of them is connected with the lowest frequency normal mode bifurcation that leads to its instability and appearance of two new nonlinear normal modes. In the principal asymptotic approximation corresponding stationary points at the phase plane are circled by separatrix. However, a complete energy exchange between different parts of the system remains yet possible. The second dynamical transition corresponds with coalescence of separatrix and LPT that leads to prohibition of the energy transfer from one part of the system to another one. As the result, the energy input in some part of the system is confined in it. The results of analytical study are in accordance with computer simulation data

---

### INTRODUCTION

Nonlinear dynamics of many-particle systems is a one of the key directions of the contemporary science [1]. The researches in this area give numerous surprising results. The one of the most wonderful and widely studied phenomena is the existence of localized excitations in the spatially uniform systems in which a uniform energy distribution should be expected *a priori*. Such self-organized localized states which are not induced by any intrinsic inhomogeneity or any external impact play an essential role in many dynamical processes relating to solid state physics and chemistry. Particularly, the most of qualitative transitions associated with chemical processes or structural transformations in the large molecules and crystals happen via the energy localization.

On the other side in the linear limit the systems under consideration demonstrate the dynamical behavior which is well described with using the Linear Normal Modes (LNMs). Their specific property is the absence of any intermodal interactions. In such limit the system turns out to be completely integrable that allows the exact description of its evolution. The concept of normal modes can be extended to nonlinear systems, and then they can be denoted as Nonlinear Normal Modes (NNMs) [2-7]. The exact determination of NNMs is an enough complicate problem; therefore their approximate representation may be useful, in particular in connection with the problem of energy localization in the reciprocal space of the system [8, 9].

However, one can see that both LNMs and NNMs are non-appropriate for the description of the process in which the intensive energy exchange or transfer along the chain occurs because the normal modes preserve the energy put into them. The processes of the energy transfer require the formation of wave packet which contains several NNMs and the number of NNMs in the packet increases if the localization becomes more distinct. To avoid the dispersive packet spreading the intermodal interaction associated with the nonlinear part of the potential energy is necessary. However the origin of the energy localization in oscillatory chains has not been still clarified.

In this paper we show that the analysis of a minimal wave packet containing the zone-boundary mode and nearest one in the discrete model of the sin-Gordon or Klein-Gordon chains leads

---

<sup>1</sup> Corresponding author. Email [vs@polymer.chph.ras.ru](mailto:vs@polymer.chph.ras.ru)

to correct description of the energy localization in terms of “effective oscillators”. Then the “beating” phenomenon observed in the small-amplitude limit is associated with the energy transfer from one half of the chain to another one. This phenomenon is described as the motion along the phase trajectory which bounds the attraction area of the zone-boundary normal mode (we call this trajectory as the Limiting Phase Trajectory – LPT; it was earlier introduced for weakly coupled oscillators [10-11] and for Fermi-Pasta-Ulam chain [12-14]). When the excitation level increases the topology of the phase space of the system is changed. We show that the first dynamical transition occurs when the zone-boundary mode turns out to be unstable, but the full energy exchange is possible yet. This transition is accompanied by the creation of two new stationary points (nonlinear normal modes which have not any analog in the linear spectrum of the system) which correspond to the partially localized states. The second dynamical transition changes the phase space of the system drastically: the LPT becomes discontinued and no trajectories associated with complete energy exchange between two parts of the chain occur. After this transformation of the phase space of the system the energy input in some part of the system is confined in it.

## THE MODEL

Let us consider the nonlinear chain containing the  $N$  particles with the periodic boundary conditions. The respective Hamiltonian can be written as follows:

$$H = \sum_{j=1}^N \frac{p_j^2}{2} + \frac{c^2}{2} (q_{j+1} - q_j)^2 + V(q_j) \quad (1)$$

where the potential function

$$V(q) = \omega_0^2 (1 - \cos(\frac{2\pi}{d} q)) \quad (2)$$

corresponds to the Frenkel-Kontorova model and

$$V(q) = \frac{\omega_0^2}{2} q^2 + \frac{\beta}{4} q^4 \quad (3)$$

corresponds to the Klein-Gordon chain.

The linearized spectrum of eigenvalues is described as

$$\omega_k^2 = \omega_0^2 + 4c^2 \sin^2 \frac{\pi k}{N} \quad (4)$$

Introducing the normal modes

$$q_j = \sum_{k=0}^{N-1} \sigma_{j,k} \xi_k$$

with

$$\sigma_{j,k} = \frac{1}{\sqrt{N}} \left( \sin \frac{2\pi k j}{N} + \cos \frac{2\pi k j}{N} \right),$$

one can see that the lowest-frequency normal mode ( $\omega = \omega_0$ ) corresponds to the uniform energy distribution the  $\xi_k$  being the amplitude of the  $k$ -th NM. As it was mentioned above we would like to analyse the minimal wave packet containing the low-frequency zone-boundary mode ( $k=0$ ) and the mode belonging to nearest integral manifold ( $k=1$ ). It is easy to show that such a combination leads to the energy distribution profile in which the main part of the energy is concentrated in the one half of the chain. Taking to account the mentioned NNMs only, we can write the potential energy up to four order as follows:

$$U[\xi_0, \xi_1] = \frac{1}{2} (\omega_0^2 \xi_0^2 + \omega_1^2 \xi_1^2) + \frac{\beta}{2N} \left( \frac{1}{2} \xi_0^4 + 3 \xi_0^2 \xi_1^2 + \frac{3}{4} \xi_1^4 \right) \quad (5)$$

(The Frenkel-Kontorova model is associated with the negative (soft) nonlinearity  $\beta < 0$  and the Klein-Gordon chain – with positive (hard) one  $\beta > 0$ .)

One should note that the frequency difference

$$\omega_1 - \omega_0 = \sqrt{\omega_0^2 + 2c^2 \sin^2 \frac{\pi}{N}} - \omega_0 \approx \frac{2c^2 \pi^2}{\omega_0 N^2} \ll 1 \quad (6)$$

at  $N \sim 10$ .

Now we can introduce the complex variables corresponding to normal modes [15]:

$$\Psi_k = \frac{1}{\sqrt{2}} \left( \frac{d\xi_k}{dt} + i\omega_k \xi_k \right), \quad \Psi_k^* = \frac{1}{\sqrt{2}} \left( \frac{d\xi_k}{dt} - i\omega_k \xi_k \right)$$

and use the multiple scale expansion:

$$\begin{aligned} \Psi_k &= \Phi_k e^{i\omega_k t} = \sqrt{\varepsilon} (\chi_k + \varepsilon \chi_{k,1} + \varepsilon^2 \chi_{k,2} + \dots) e^{i\omega_k t} \\ \tau_0 &= t, \tau_1 = \varepsilon \tau_0, \tau_2 = \varepsilon^2 \tau_0, \dots \end{aligned} \quad (7)$$

After some algebra we get the following equations describing the main order amplitudes dynamics by small parameter [13-14]:

$$\begin{aligned} i \frac{\partial \chi_0}{\partial \tau_2} + \frac{3\beta}{4\omega_0^3} [|\chi_0|^2 \chi_0 + 2|\chi_1|^2 \chi_0 + \chi_0^* \chi_1^2] &= 0 \\ i \frac{\partial \chi_1}{\partial \tau_2} + \nu \chi_1 + \frac{3\beta}{8\omega_0^3} [3|\chi_1|^2 \chi_1 + 4|\chi_0|^2 \chi_1 + 2\chi_1^* \chi_0^2] &= 0 \end{aligned} \quad (8)$$

Eqs (8) correspond to the Hamiltonian

$$H_\chi = \nu |\chi_1|^2 + \frac{3}{16} \frac{\beta}{\omega_0^3} [2|\chi_0|^4 + 3|\chi_1|^4 + 8|\chi_0|^2 |\chi_1|^2 + 2(\chi_0^2 \chi_1^{*2} + \chi_0^{*2} \chi_1^2)] \quad (9)$$

and allow the additional integral of motion named ‘‘occupation number’’:

$$X = |\chi_0|^2 + |\chi_1|^2 \quad (10)$$

As it was mentioned above the  $\chi$ -variables are not convenient ones for the description of energy transfer. Therefore one should introduce the new variables which correspond to the ‘‘effective oscillators’’ as each of new variables describes the energy distribution concentrated at one half of the chain [14]:

$$\begin{aligned} \varphi_0 &= \frac{1}{\sqrt{2}} (\chi_0 + \chi_1), \quad \varphi_1 = \frac{1}{\sqrt{2}} (\chi_0 - \chi_1) \\ |\varphi_0|^2 + |\varphi_1|^2 &= X \end{aligned} \quad (11)$$

Because the value  $X$  is the integral of motion it is convenient to rewrite the  $\varphi$ -functions as follows:

$$\varphi_0 = \sqrt{X} \cos \theta e^{i\delta_0}, \quad \varphi_1 = \sqrt{X} \sin \theta e^{i\delta_1} \quad (12)$$

where the angular variables allow us to study the phase plane of the system [16]. Then the equations of motion can be written in the form:

$$\begin{aligned} \sin 2\theta \frac{\partial \Delta}{\partial \tau_2} - \frac{\cos 2\theta}{16\omega_0^3} [(3\beta X + 16\nu\omega_0^3) \cos \Delta - 3\beta X \cos^2 \Delta \sin 2\theta + 27\beta X \sin 2\theta] &= 0 \\ \sin 2\theta \left[ \frac{\partial \theta}{\partial \tau_2} - \frac{1}{32\omega_0^3} (3\beta X + 16\nu\omega_0^3 - 3\beta X \cos \Delta \sin 2\theta) \sin \Delta \right] &= 0 \\ \Delta &= \delta_1 - \delta_0 \end{aligned} \quad (13)$$

There are two stationary points at the small level of occupation number  $X$  (fig.1). The first of them ( $\Delta=0$ ,  $\theta=\pi/4$ ) corresponds to the zone-boundary mode ( $k=0$ ) and the second one ( $\Delta=\pi$ ,  $\theta=\pi/4$ ) describes the nearest mode ( $k=1$ ). The LPT is the trajectory which consists of two branches surrounding the attraction areas of both modes. It is easy to show that the  $\varphi_0$  and  $\varphi_1$  correspond to the parts of LPT which pass through the states  $\theta=\pi/2$  and  $\theta=0$ , respectively. So the motion along the LPT is accompanied with the transfer energy from one half of the chain to another. This process looks like

the beating in the system of two weakly coupled oscillators. One should note that this phenomenon has to manifest itself beginning from the linear limit.

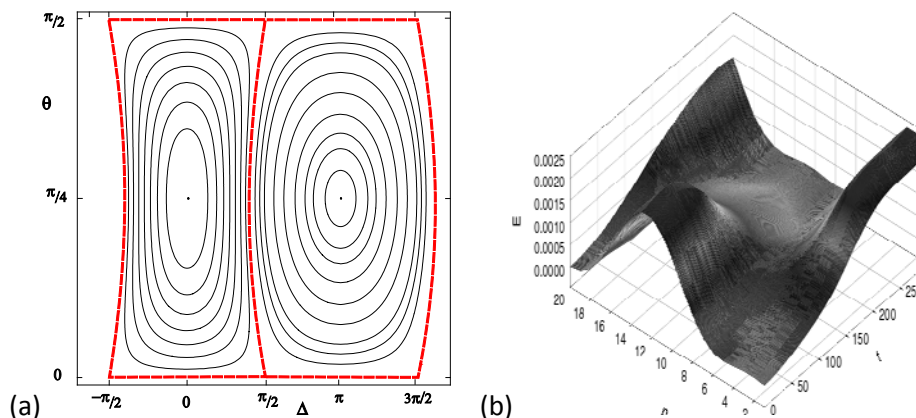


Fig.1 The phase plane portrait (a) and the 3D plot of the energy (b) of the FK-chain with 20 particles with two excited modes in the terms of angular variables.

While the excitation level grows the topology of the phase plane is changed. Two new stationary points

$$\begin{aligned}
 (a) \quad & \begin{cases} \sin 2\theta = -\frac{3\beta X + 16v\omega_0^3}{24\beta X} \\ \cos \Delta = 1 \end{cases} \quad (FK - chain) \\
 (b) \quad & \begin{cases} \sin 2\theta = \frac{3\beta X + 16v\omega_0^3}{24\beta X} \\ \cos \Delta = -1 \end{cases} \quad (KG - chain)
 \end{aligned} \tag{15}$$

arise in the phase plane because the zone-boundary mode turns out to be unstable at the excitation level corresponding to critical values

$$\begin{aligned}
 (a) \quad X_{cr} &= -\frac{64\pi^2 c^2 \omega_0^2}{27\beta} \quad (\beta < 0) \\
 (b) \quad X_{cr} &= \frac{64\pi^2 c^2 \omega_0^2}{15\beta} \quad (\beta > 0)
 \end{aligned} \tag{16}$$

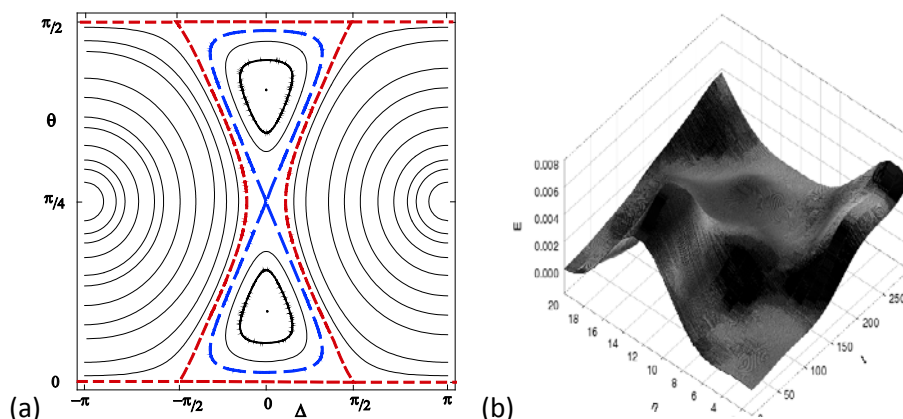


Fig.2 The phase plane portrait (a) and the 3D plot of the energy (b) of the FK-chain with 20 particles above the first excitation threshold  $X_{cr}$ .

These new stationary points correspond to new nonlinear elementary excitations which describe the partially localized states when only some part of the energy of the system is concentrated in the one half of the chain the rest of the energy being distributed uniformly along the chain. The

separatrix that surrounds the attraction area of the new stationary point separates the phase plane into the domains where the complete energy exchange is forbidden (inside the separatrix) and where it is possible yet (out of the separatrix). The further growth of the excitation is accompanied with decreasing of domain corresponding to complete energy exchange and this domain becomes degenerate when the energies of LPT and unstable stationary point ( $\theta=\pi/4$ ) turn out to be equal:

$$E(\theta = \pi / 4, \Delta = 0) = E(\theta = 0, \Delta = 0)$$

where the energy is defined by the Hamiltonian in the angular variables:

$$H = \frac{X}{256\omega_0^3} [159\beta X + 128v\omega_0^3 + 45\beta X \cos 4\theta - 8(3\beta X + 16v\omega_0^3) \cos \Delta \sin 2\theta + 6\beta X \cos 2\Delta \sin^2 2\theta]$$

The respective values of occupation number X are equal to:

$$\begin{aligned} (a) \quad X_t &= -\frac{64\pi^2 c^2 \omega_0^2}{27\beta} \quad (FK - chain) \\ (b) \quad X_t &= \frac{64\pi^2 c^2 \omega_0^2}{15\beta} \quad (KG - chain) \end{aligned} \quad (17)$$

The Fig.3.a shows that the topology of phase plane is change drastically: no trajectory started near the amplitude value  $\theta=0$  ( $\theta=\pi/2$ ) can not approach to the value  $\theta=\pi/4$  that means the absence of complete energy exchange between two parts of the chain. Moreover, the maximal localization turns out to be possible when the main part of the energy is confined in the one part of the chain. This phenomenon is clearly seen in the fig. 3b. The periodic variation of the energy distribution (so called “breathing” mode) is correlated with the traveling along the phase trajectory surrounding the stationary points (17.a) or (17.b).

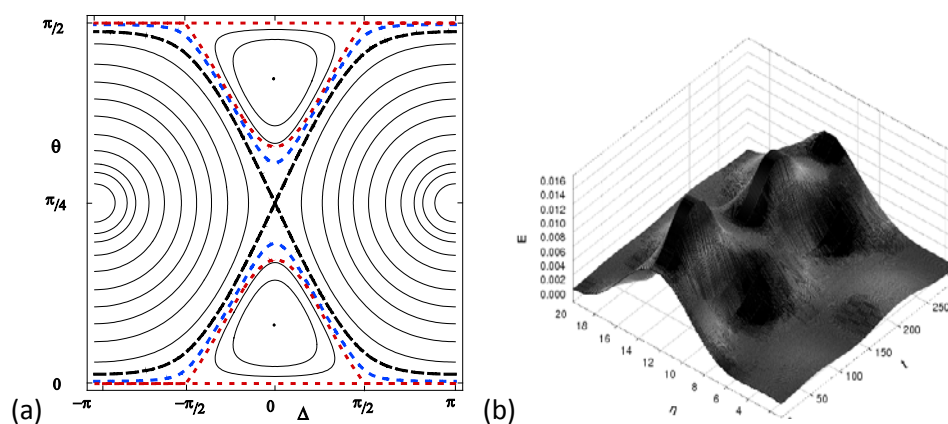
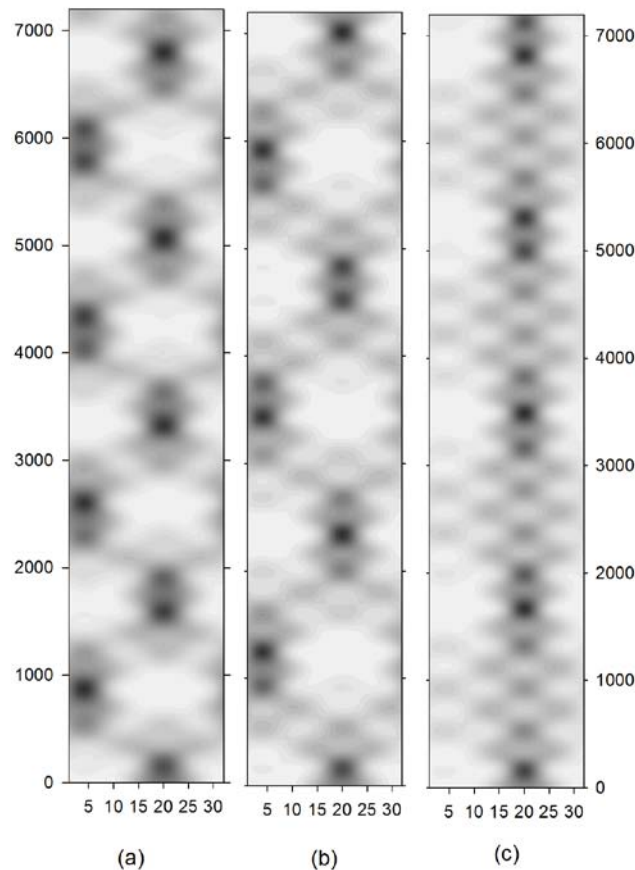


Fig.3 The phase plane portrait (a) and the 3D plot (b) of energy for the FK-chain with 20 particles above the threshold of localization  $X_t$ .

One should point the essential difference between FK and KG chains that becomes apparent at the threshold of the localization. The localization occurs in the FK chain if the excitation level exceeds the value  $X_t$ , while the dynamics of KG-chain demonstrates the partial localization only. This difference results from the fact that the unstable mode in the FK-chain is the zone-boundary one while the nearest to zone-boundary mode turns out to be unstable in the KG-chain. The figures 4(a-c) illustrate the results described above.

It is clearly seen that high energy area jumps from  $n=20$  to  $n=5$  (beating phenomenon) if the occupation number X is smaller than the localization threshold  $X_t$  and it is confined at  $n=20$  if X has overcome the threshold of localization. The lighter regions dividing the nearest dark ones are

associated with passing of representation point near the  $\theta=\pi/4$  in the reduced phase plane (see figs 1-3). Thus one can explain the origin of “breathing” mode of the localized vibrations (breathers).



*Fig.4. Energy contour map for the FK-chain with 32 particles at various values of occupation number  $X$ : (a)  $X < X_{cr}$ , (b)  $X_{cr} < X < X_t$ , (c)  $X_t < X$ . The horizontal and vertical axes correspond to the particle's number and the time measured in the oscillation period of low-frequency zone-boundary mode, respectively. Darker regions correspond to oscillators with more energy, lighter regions to oscillators with less energy.*

## CONCLUSION

The analysis made above has shown that the origin of the energy localization in the nonlinear chains is the resonant interaction of the NNMs corresponding to the edge of the linear spectrum. At that, the loss of stability of the zone-boundary mode is the necessary but not sufficient condition for complete energy localization. This instability leads to arising two new stationary points corresponding to the states with only partial energy localization while the complete localization turns out to be possible after the second dynamical transition (when the domain of the phase trajectories associated with the full energy exchange becomes degenerate and the LPT is discontinued. The last results in forbidding the complete energy exchange between different parts of the chain (the energy put in the some part of the chain is confined in it). One should note that this simplified description taking into account two boundary modes only reflects the principal peculiarities of the process. As the computer simulation data show, the presence of other modes leads to some narrowing of the profile of the energy distribution, but does not change the main features of the process. It can be shown that an similar scenario of energy localization is valid for the high-frequency edge of the spectrum, but at that the KG chain trends to the energy localization while the FK chain does not do it. One should note that the critical density of the energy is inversely to the square of the particle number and it converges to zero when the number of particles go to infinity.

In conclusion we would like to make one more remark concerning the LPT and the notice of “effective oscillator”. As it was mentioned in the Introduction, the description of energy localization in the terms of the NNMs is not adequate one because they turn out to interact strongly near the localization threshold. Therefore, the introduction of the new objects which can be defined well and the interaction between which is weak is the adequate procedure to describe the process under consideration. In the case considered the “effective oscillators” are two halves of the chain. Therefore,

the LPT is the phase trajectory which describes the energy exchange between two “effective oscillators”.

## ACKNOWLEDGEMENTS

This work was supported by the RBRF (grant 08-03-00420a) and the Department of Chemistry and Material Science of RAS (the Program no 2).

## REFERENCES

- [1] Scott A., *Nonlinear science: emergence and dynamics of coherent structures*, Oxford Univ. Press, 2003
- [2] Rosenberg R.M. *Adv. Appl. Mech.*, N.-Y.: Academic Press, v.9, pp. 156-243, 1966.
- [3] Manevitch L.I., Mikhlin Yu.V., Pilipchuk V.N.: *The normal vibrations method for essentially nonlinear systems*, Nauka Publ., Moscow, 1989 (in Russian).
- [4] Vakakis A.F., Manevitch L.I., Mikhlin Yu.V., Pilipchuk V.N., Zevin A.A.: *Normal Modes and Localization in Nonlinear Systems*, Wiley, New York, 1996.
- [5] Poggi P., Ruffo S., *Physica D* 103, p.251, 1997.
- [6] Rink B., *Commun. Math. Phys.* 218, p.665, 2001.
- [7] Henrici A., Kappeler T., *Commun. Math. Phys.* 278, p.145, 2008.
- [8] Flach S., Ivanchenko M.V. and Kanakov O.I. *Phys. Rev. Lett.*, 95:064102-1-4, 2005.
- [9] Manevich A.I., Manevitch L.I., *The mechanics of nonlinear systems with internal resonances*, Imperial College Press, London, 2005.
- [10] Manevitch L.I.. *8th Conference on Dynamical Systems-Theory and Applications, Proceedings. Lodz*, December 12-15, 2005, Poland, V.1, pp. 119-136, 2005.
- [11] Manevitch L.I.. *Arch. Appl. Mech.* v.77 (5), 301-312, 2007.
- [12] Manevitch L.I., Smirnov V.V., *Advanced Problem in Mechanics, APM-2007*, Ed. by D.A.Indeitsev, 289, St.Petersburg (Repino), Russia, June 20-28, 2007.
- [13] Manevitch L.I., Smirnov V.V., *9th Conference on Dynamical Systems Theory and Applications*, J.Awrejcewicz and P. Olejnik and J. Mrozowski (Eds),301, DSTA-2007, Łódź, Poland December 17-20, 2007.
- [14] Manevitch L.I., Smirnov V.V. in: *Advanced Nonlinear Strategies for Vibration Mitigation and System Identification*, ed. A.F.Vakakis, Springer, Wien, New York, pp.207-258, 2010.
- [15] Manevitch L.I.. *Nonlinear Dynamics*, 25, pp. 95-109, 2001.
- [16] Kosevitch A.M., Kovalev A.C., *Introduction to Nonlinear Physical Mechanics*, Naukova Dumka, Kiev, 1989 (in Russian)

## AN APPROACH TO IDENTIFICATION OF IMPACT INTERACTION MODEL FOR A VIBROIMPACT SYSTEM

**Tkachuk M.M.**  
**Grabovsky A.V.**  
**Tkachuk M.A.**<sup>1</sup>

National Technical  
University 'KhPi', Kharkov,  
Ukraine

---

### ABSTRACT

---

In this work a new approach to the modelling of vibroimpact systems was proposed. Verification criteria estimating the quality of the identified model of contact interaction were offered. The applicability of the approach was shown for numerical and experimental studies of a real shake-out machine.

---

### INTRODUCTION

Dynamics of vibroimpact machines is quite a peculiar area of mechanical engineering. On the one hand oscillations with impact have very complex nature. On the other hand this dynamical process has to be modelled with high precision as soon as it concerns the robust design of such machines. Particularly, a good estimate of the value of the altering forces acting on their elements is really essential for the durability of the design. This motivates the development of a new model for the dynamics of vibroimpact systems proposed in this work. This model is elaborated here with a strong reference to the highly loaded shake-out machines. Such machines are used to separate the casting from its mould. For the dynamics of these machines the two specific factors are of a major significance. The first factor is the impact of the moulding upon shake-out grid. That takes place when a heavy moulding comes into contact with the oscillating grid and is characterized by high impact velocities and high impact loads. The other factor considered is the damage of the mould. At each collision some amount of sand lumps breaks off from the moulding. This separation dissipates some part of the kinetic energy.

In the developed model there's a strong emphasis on the two phenomena. We propose a new approach to their treatment. The key feature of this approach is that it enables to overcome the uncertainty that is characteristic for the considered class of mechanical systems. Generally most of the constructive elements of a shake-out machine have clearly and easily determined mechanical properties. The design parameters such as the mass of the grid frame, the stiffness of the elastic supports, the properties of the dampers are well known and are controlled by the designer. The uncertainty comes from the two factors mentioned above that govern the impact interaction of the moulding and the shake-out grid. The impact force is the key quantity that describes this interaction. It is influenced by many different factors some of which are random to a great extend. The existing models found in the literature [1 - 6] postulate only some simplistic laws expressing this dependency. Such an empirical approach can not capture in detail the important characteristics of the impact process, namely the duration of the impact, the amplitude and the time distribution of the impact force and the amount of energy dissipated during the collision at all the possible conditions.

### APPROACH DESCRIPTION

The approach is described here for two-body vibroimpact system depicted on the Fig. 1. It represents in general the shake-out machine as soon as only vertical motion of its elements is considered. Such representation captures all the peculiar features this work is focused on. The first body  $m_1$  can be viewed as the grid frame. It rests on elastic supports of total stiffness  $C_1$  and dampers of viscosity  $H_1$ . It oscillates under action of a cyclic force  $A \sin \omega t$ . In the real shake-out machine this force is produced by debalance drive. The second body  $m_2$  represents the moulding. It periodically falls onto the first body and pops back into the air. Hence there's a non-linear one-sided constraint between these two bodies that is only active when they are in contact.

---

<sup>1</sup> Corresponding author. Email [tma@kpi.kharkiv.ua](mailto:tma@kpi.kharkiv.ua)

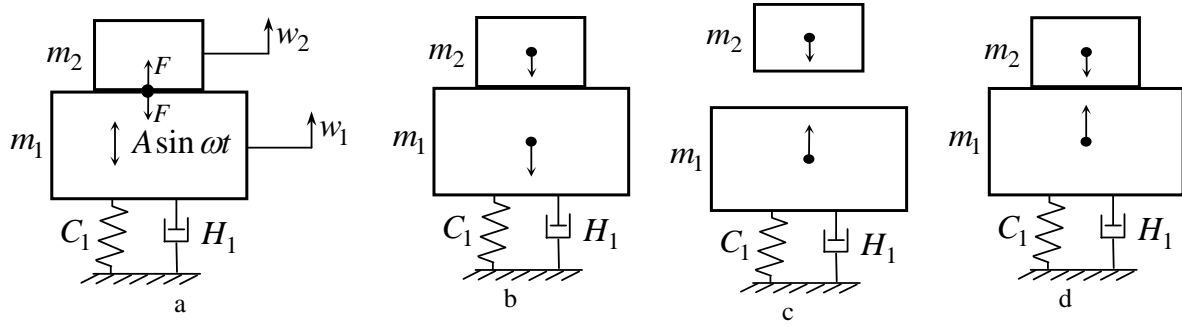


Fig. 1 Two-body vibroimpact system

According to the proposed approach the form of this impact interaction is not postulated and is initially unknown. The model for the impact force is established by an identification procedure based on the specially designed verification criteria.

### BASIC MODEL

This procedure starts with the basic model that is set up in the beginning and does not change during the verification. First of all, it describes the known part of the examined object. For the considered vibroimpact system the equation of motion are well established and can be written as

$$\begin{cases} m_1 \ddot{w}_1 + C_1 \dot{w}_1 + H_1 w_1 + A \sin \omega t + m_1 g + F = 0 \\ m_2 \ddot{w}_2 + m_2 g - F = 0. \end{cases} \quad (1)$$

Secondly, the initial setting postulates some properties the identified part of the developed model is either known or assumed to possess. In the considered case this concerns the unknown impact force  $F$  only. The main assumption about this force is that it depends on the interpenetration  $\zeta = w_1 - w_2$  of the two bodies and the penetration velocity  $\dot{\zeta} = \dot{w}_1 - \dot{w}_2$

$$F = F(\zeta, \dot{\zeta}). \quad (2)$$

As if it were produced by a viscoelastic interface layer as depicted on Fig. 2. This layer effectively represents the elastic deformations of the moulding and its dissipative damage. Based on the representation (2) of the unknown impact response some further conditions can be formulated. Thus naturally the following two conditions must hold

$$F = 0, \quad \zeta < 0, \quad (3)$$

$$F \geq 0. \quad (4)$$

The first one expresses the fact that the contact force vanishes when there's no interpenetration (no contact) of the bodies. The second follows from a natural assumption that the force between the moulding and the grid is non-adhesive. Another property of  $F$  we determine in the initial setting concerns the influence of the penetration velocity. The dependency of  $F$  on  $\dot{\zeta}$  is introduced in order to represent the dissipative damage of the moulding that we link to the viscoelastic layer. We postulate that damage and separation of sand lumps from the moulding takes only place when penetration velocity is positive. That means that the negative values of  $\dot{\zeta}$  have no effect on the impact force:

$$F(\zeta, \dot{\zeta}) = F(\zeta, 0), \quad \dot{\zeta} < 0. \quad (5)$$

We also guarantee the dissipativeness of the impact response by introducing another condition related to the penetration velocity:

$$F(\zeta, \dot{\zeta}) > F(\zeta, 0), \quad \dot{\zeta} > 0. \quad (6)$$

The effect of these conditions on the character of impact interaction is illustrated on Fig.2. Consider a single collision depicted on the penetration-force diagram on Fig.2. Point 1 on this diagram corresponds to the moment of time  $t_1$  when the bodies come into contact ( $\zeta(t_1) = 0$ ) with some positive impact velocity  $\dot{\zeta}(t_1) > 0$ . At this moment one will observe a jump of the force  $F$  from 0 value before contact to a positive finite value  $F(\zeta(t_1), \dot{\zeta}(t_1)) = F(0, \dot{\zeta}(t_1)) > F(0, 0) = 0$  after the impact. The penetration grows until the repulsive contact force stops the motion of the two bodies towards each other at time  $t_2$ , corresponding to the point 2 on the diagram. At this moment the relative velocity changes its sign from the positive to the negative, hence  $\dot{\zeta}(t_2) = 0$ . The subsequent unloading is elastic and according to (5) follows the curve  $F(\zeta, 0)$  to the point 3 at which the two bodies disengage and the contact force vanishes again. It should be noted that the viscoelastic loading branch 1-2 is always above the elastic unloading branch 2-3 in case if contact interaction law (2) satisfies the condition (6). This fact guarantees the positiveness of the hysteresis of the impact force and a priori dissipativeness of the identified model. The Fig. 2 illustrates the above discussed effect of the constraints (3-6) in the two-dimensional phase space for a single phase trajectory of a typical collision.

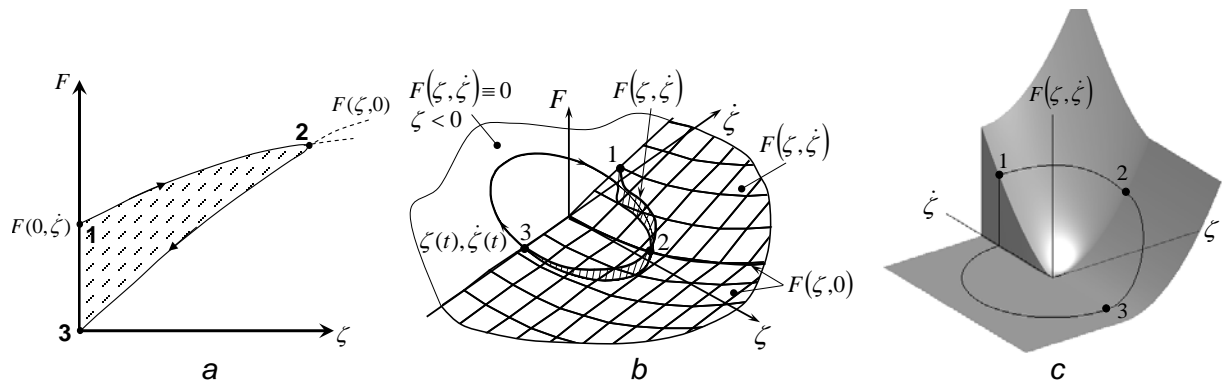


Fig. 2 The loading curve for a single collision (a) and the general form of the viscoelastic force (2) satisfying the conditions (3-6) (b, c)

## PARAMETRIC APPROXIMATION

With the initial setting at hand one can begin the identification of the unknown part, which in the considered case is the unknown impact force  $F$ . One needs to establish it as a function of the penetration  $\zeta$  and the penetration velocity  $\dot{\zeta}$  which would satisfy the conditions (3-6). In this approach this function is sought for in the form of a series expansion in the domain  $\zeta > 0, \dot{\zeta} > 0$  (for the other values of  $\zeta$  and  $\dot{\zeta}$  the impact force is determined then according to the identities (3) and (5)). Particularly, one can think of a polynomial representation

$$\begin{cases} F^\wedge(\zeta, \dot{\zeta}) = \alpha_1 \zeta + \alpha_2 \dot{\zeta} + \alpha_3 \zeta \dot{\zeta} + \dots, & \zeta, \dot{\zeta} > 0 \\ F^\wedge(\zeta, \dot{\zeta}) = F^\wedge(\zeta, 0), & \dot{\zeta} < 0 \\ F^\wedge(\zeta, \dot{\zeta}) = 0, & \zeta < 0 \end{cases}, \quad (7)$$

parameterized by unknown positive coefficients  $\alpha_i$  that need to be established.

The approximate law of the dependency of the impact force on the penetration and its velocity given by (7) has to be verified. This is done by comparison of the numerical simulation results obtained for the approximate model of the impact interaction.

## VERIFICATION CRITERIA

In order to validate the approximation (7) some definite verification criteria have to be chosen. One can think of different quantities measures that would estimate the discrepancy between the prediction provided by approximate model and the real behaviour observed in the experiment. One can take different dynamic parameters of the examined vibroimpact system for this comparison. In the proposed approach the time distribution of the identified impact force is verified towards its experimental values. Particularly we focus on the on the steady-state oscillations regime since that is

most essential for the performance of the shake-out machine. Consider two time distributions of the impact force for the steady oscillations with frequency  $\nu = 2\pi\omega$  and period  $T = 1/\nu$  plotted on the Fig. 3. One curve  $F_E$  is experimentally derived at the considered regime. The other  $F_N$  is obtained from a numerical simulation with all the known parameters set to be identical to the experiment and some approximate model for the impact interaction parameterized by coefficients  $\alpha_i$ . We put both distributions on a common time axis setting the beginning of the impact both in the experiment and the simulation to a same time point  $t^*$ . The difference between the non-negative values  $F_E(t)$  and  $F_N(t)$  as well as the durations of the impulse  $\tau_E$  and  $\tau_N$  derived from the experiment and the simulation is essential for the verification.

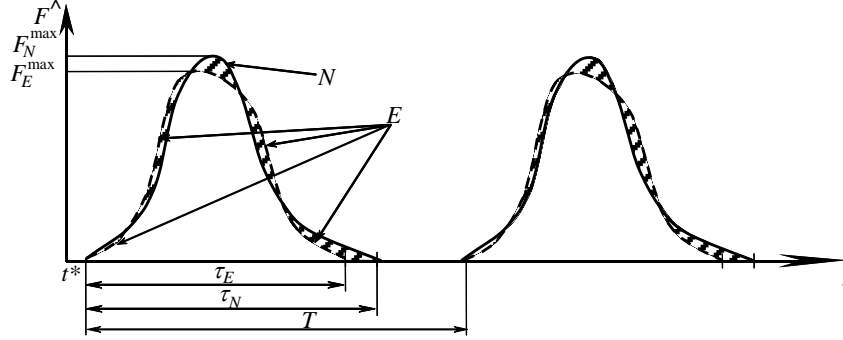


Fig. 3 Numerically predicted time distribution of the impact impulse at the steady-state regime compared to the experimental observation

In order to measure this discrepancy we introduce several functionals of the time distributions  $F_E(t)$  and  $F_N(t)$ :

$$I_1 = \frac{\max |F_N^{\hat{}} - F_E^{\hat{}}|}{\max |F_E^{\hat{}}|}; \quad I_2 = \frac{\int |F_N^{\hat{}} - F_E^{\hat{}}| dt}{\int |F_E^{\hat{}}| dt}; \quad (8)$$

$$I_3 = \sqrt{\frac{\int (F_N^{\hat{}} - F_E^{\hat{}})^2 dt}{\int (F_E^{\hat{}})^2 dt}}; \quad I_4 = \frac{\int |\text{sign}(F_N^{\hat{}}) - \text{sign}(F_E^{\hat{}})| dt}{\int \text{sign} F_E^{\hat{}} dt} = \frac{\tau_N - \tau_E}{\tau_E}.$$

This functionals have the properties of a norm

$$I_k \geq 0 \quad \forall \quad F_N^{\hat{}}, F_E^{\hat{}}, k; \quad (9)$$

$$I_k = 0 \Rightarrow F_N^{\hat{}} \equiv F_E^{\hat{}}, k = 2, 3. \quad (10)$$

The lesser is their value the closer is the simulation results to the experimental observation, and hence the better is the approximation (7) for some definite set of the parameters  $\alpha_i$  to the true impact interaction law.

## VERIFICATION

We identify the parameters  $\alpha_i$  of the approximate model by minimizing the value of one of the norms in (8). The choice of the functional turns out to be really essential. In order to illustrate this consider a model verification problem.

Assume that the impact force is really expressed by

$$F = \bar{\alpha}_1 \zeta + \bar{\alpha}_2 \dot{\zeta}, \quad (\zeta, \dot{\zeta}) > 0, \quad (11)$$

with the known  $\bar{\alpha}_1 = 2.06 \cdot 10^8 \text{ N/m}$ ,  $\bar{\alpha}_2 = 1.28 \cdot 10^7 \text{ N} \cdot \text{s/m}$ . In this artificial situation the approximation (7) with only two members of the series reproduces this “real” impact interaction law for  $\alpha_1 = \bar{\alpha}_1$  and  $\alpha_2 = \bar{\alpha}_2$ . Consider then the sensitivity of the functionals  $I_k$  to the identified parameters. It is known that  $I_k(\bar{\alpha}_1, \bar{\alpha}_2) = 0$ , since for these values of expansion coefficients  $F(\zeta, \dot{\zeta})$

coincides with  $F^{\wedge}(\zeta, \dot{\zeta})$  and hence  $F_E(t) = F_N(t)$  (the experimental curve  $F_E(t)$  is attained from the virtual numerical experiment just repeats the simulation). On the Fig. 4 one can see the values of  $I_k(\alpha_1, \alpha_2)$  in the domain  $\alpha_1 \in [1.03 \cdot 10^8, 3.09 \cdot 10^8] \times \alpha_2 \in [0.64 \cdot 10^7, 1.92 \cdot 10^7]$ . One can observe that the functionals  $I_2$  and  $I_3$  have a distinctive minimum at  $\alpha_1 = \bar{\alpha}_1, \alpha_2 = \bar{\alpha}_2$ . To the contrary the functionals  $I_1$  and  $I_4$  display bad sensitivity towards the identified parameters, which will definitely hinder the minimization procedure. The situation can be improved by introducing an alternative functional  $I_0 = (I_1 + I_4)/2$  that is their combination and has better shape as can be seen on the Fig. 5.

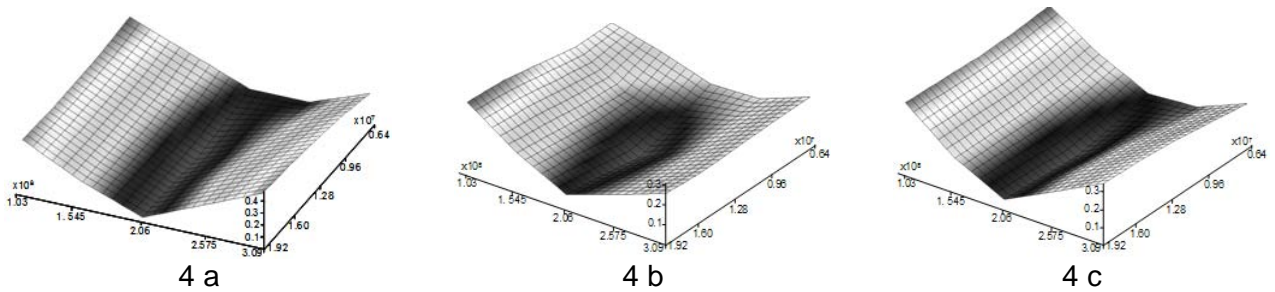


Fig. 4 Variation of verification norms with  $I_1$  (a),  $I_2$  (b),  $I_3$  (c),  $I_4$  (d)

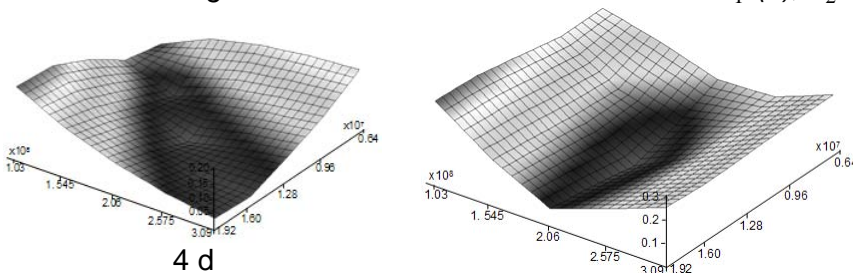


Fig. 5 Enhanced functional  $I_0 = (I_1 + I_4)/2$

With a good choice of the functional norm one obtains stable convergence of the identification process. The minimization can be performed by an accelerated coordinated descent method. Particularly the choice of  $I_2$

functional lead to the following results. The consequent iterations are shown on the Fig. 6. The curves on the Fig. 7 show the convergence of the impact force distribution  $F_N(t)$  to its “exact” value.

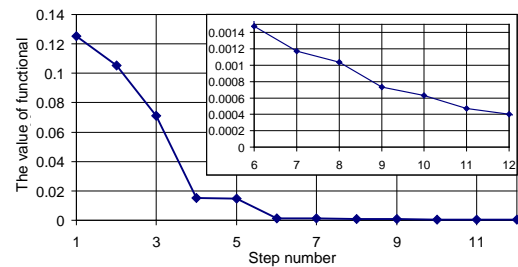
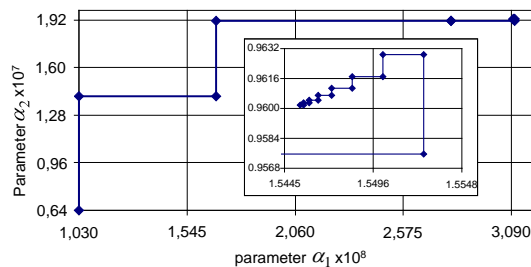


Fig. 6 Iterative minimization process for  $I_2$

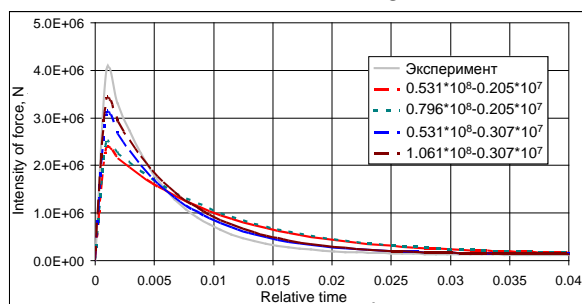


Fig. 7 Proximity of the impact force for the consequent iterations to its exact distribution

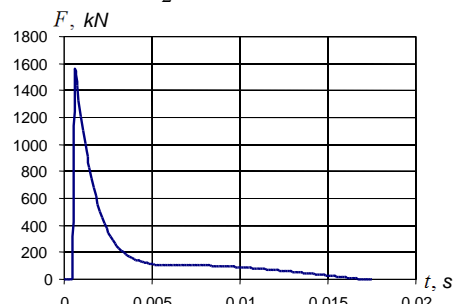


Fig. 8 The predicted character of the time distribution of the impact force by the approximate model

The verification procedure displays for this model problem the performance similar to the illustrated above for the two other functionals  $I_3$  and  $I_0$ . Thus minimization of  $I_2, I_3$  or  $I_0$  can be advised as the verification criteria for the general case.

## APPROACH PERFORMANCE

The proposed approach was employed for the identification of the model for the impact force between the grid frame and the moulding for the shake-out machine produced by Azovmash. A 4-member polynomial expansion was taken for the verification.

The proposed approximation captures most of the key characteristic features of the real impact interaction, which was proposed by the sensitivity analysis [7]. Particularly the non-linear members allow to introduce a shift of the maximum of the impact force from the beginning of the collision closer to its middle part (Fig.8).

Ultimately a good agreement of the experimental data with the simulation with the identified model was achieved. Fig.9 shows the discrepancy between the experimental and numerical values of the stresses in the shake-out grid frame controlled during the verification [7]. The result model provides a very good prediction of the parameters of the dynamics of the examined vibro-impact system such as duration of the impact impulse, accelerations and force amplitude in the shake-out machine with a precision of 11-18% [7].

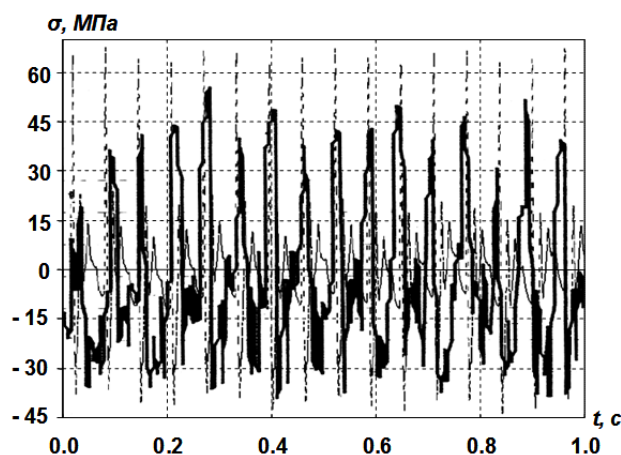


Fig. 9 Comparison of numerically predicted and experimental values of controlled stress in the shake-out grid frame character of the time distribution of the impact force by the approximate model

## CONCLUSIONS

In this work a new approach to the modelling of vibroimpact systems was proposed.

The main distinctive features of this approach as well as the key result are summarised below.

1. The approach does not postulate any certain form of the contact interaction model, but suggest its identification through a verification procedure.

2. During this identification the physical peculiarities of the dynamical process are taken into account. Particularly, the damage of the moulding due to the applied shock is considered. It is effectively represented by a non-linear viscoelastic contact layer.

3. Different verification criteria

estimating the quality of the identified model of contact interaction were offered in this work. Their performance was illustrated for a model verification problem, based on which the final recommendations for their choice were made.

4. The applicability of the approach was shown for numerical and experimental studies of a real shake-out machine. It enabled to achieve high precision in the description of its dynamics.

The approach is extendable on a broader class of vibro-impact systems and used for their analysis and synthesis.

## REFERENCES

- [1] *Vibrations in Engineering: A Handbook*. In 6 volumes. - M.: Mashinostroenie. - 1981. (In Russian)
- [2] Babitsky V.I. *The theory of vibro-impact systems: Approximate methods*. - M.: Nauka, 1978. (In Russian)
- [3] Ivanov A.P. *Dynamics of mechanical systems with collisions*. - Moscow: International Education Program, 1997. (In Russian)
- [4] Bazhenov V.A., Pogorelova O.S., Postnikova T.G., Goncharenko S.N., Comparative analysis of modeling methods for studying contact interaction in vibroimpact systems, *Strength of Materials*. N. 4, Springer New York, pp. 69 – 77, 2009.
- [5] Bazhenov V.A., Pogorelova O.S., Postnikova T.G., Luk'yanchenko O.A., Numerical investigations of the dynamic processes in vibroimpact systems in modeling impacts by a force of contact interaction, *Strength of Materials*. N. 6, Springer New York, pp. 82 – 90, 2008.
- [6] Gerega I.I. Interaction of the service load with the tool in percussive machines, *Strength of Materials*. N. 4, Springer New York, pp. 74 – 82, 1995.
- [7] Barchan E.N. Grabovskiy A.V. Improved methods of calculation and design vybivnoy transporting machines for formovachnyh lines of large casting. *Bulletin of Nat. Technical. Un-To "KhPI". Topical Issue "Of machines and CAD/CAE*. N.19 Kharkiv, NTU "KhPI", 18 – 34 pp., 2010. (In Russian)

**AT THE VERY INSTANT WHEN THE AUTHOR CAME ACROSS  
AN INEXPERIENCED BEHAVIOR**

**Yoshisuke UEDA<sup>1</sup>**  
Faculty of Science and  
Engineering, Waseda  
University, Tokyo 169-  
8555, Japan

---

**ABSTRACT**

---

The appearance of the data the author accidentally came upon during hand-made analog computer (by three years his senior Mr. M. Abe using vacuum-tubes as his research project) experiments on the 27th of November, 1961 was like a broken egg with jagged edges. The original sheet of data was now kept at Brookhaven National Laboratory in New York (BNL Photography Division Negative No. 1-380-90). The data was eventually recognized as a chaotic attractor first obtained in an actual physical system. In this presentation the author would like to reproduce the unforgettable situation before the study of chaos began.

---

**INTRODUCTION**

In this presentation, periodically forced oscillatory phenomena are leading as a whole. The subject matters of reflections were nothing but the author's subjective accounts. Accordingly, he presumed to write proper nouns, and each subject was restricted within the possible inspections by references and/or survived materials.

**2. SYNCHRONIZATION PHENOMENA**

When a periodic force is applied, or a periodic signal is injected to self-oscillatory systems, the behavior of the systems is synchronized with the external signal depending on a frequency and an amplitude of the external force. Such effects are well known as synchronization phenomena. And a region of (control) parameters (frequency and amplitude of external signal) is called synchronization regime. Self-oscillatory systems generate respective fixed oscillations whose (angular) frequencies and amplitudes are maintained constants which depend on system structures and parameter values of constituent elements.

When control parameters are given outside of synchronization regimes, asynchronous beat oscillations appear. It is well-known that the mechanism of synchronization is classified into two kinds, that is, frequency entrainment (pull-in) and (amplitude) quenching. Consequently, for intermediate values of external signals between the above mentioned two mechanisms, there may appear overlapped regime of both mechanisms in general, that is, coexisting attractors may be observed. The boundaries of different regimes are called bifurcation sets on the parameter plane.

Asynchronous beat oscillations observed in the periodically forced van der Pol's oscillator were represented by invariant simple closed curves of the mapping defined by using solutions of the equation. While among beat oscillations in general periodically forced self-oscillatory systems chaotic oscillations were subsisted. It was the author who first disclosed a chaotic oscillation in a periodically forced negative resistance oscillator. Since he met the data (like a broken egg), it rubbed him with the question "What are the possible steady states of a nonlinear system?" It seemed to give him intuitions that were shape of the attractor and movement of stroboscopic images on the attractor. In this section, Broken Egg (chaotic) Attractor and Local Bifurcation Sets are briefly explained. In both following Figures 1 and 2, items (a) were obtained in 1961, while items (b) were in 2006, truly 45 years was elapsed between these materials were obtained. The differential equation under study was

---

<sup>1</sup> Corresponding author. Email [yueda@kurenai.waseda.jp](mailto:yueda@kurenai.waseda.jp)

the second order non-autonomous system with periodic external forcing term, that is,

$$\frac{d^2x}{dt^2} - \mu(1 - \gamma x^2) \frac{dx}{dt} + x^3 = B \cos vt \quad (1)$$

It is to be remarked that the difference between periodically forced van der Pol's equation and the Eq. (1) is in the restoring term. This implies that the existence of nonlinear restoring term may be necessary condition for the existence of chaotic attractors in the second order non-autonomous periodic systems. Moreover, it is to be added that this statement is restricted to the comparatively small value of damping parameter  $\mu$  (a conjecture).

### 2.1. Broken Egg Attractor

In this section, Broken Egg Attractor is briefly explained. Figure 1 embraces many implications. The points S and D in Fig. 1 (b) are fixed points of the mapping or the transformation  $T$  of the  $(x, y)$ -plane into itself, defined by using the solutions of Eq. (1), not to mention that the variable  $y$  is the derivative of  $x$  with respect to  $t$ . The former S represents fundamental harmonic (entrained) oscillation with period  $2\pi/v$ , and is called completely le fixedstab point or simply sink. The latter D is

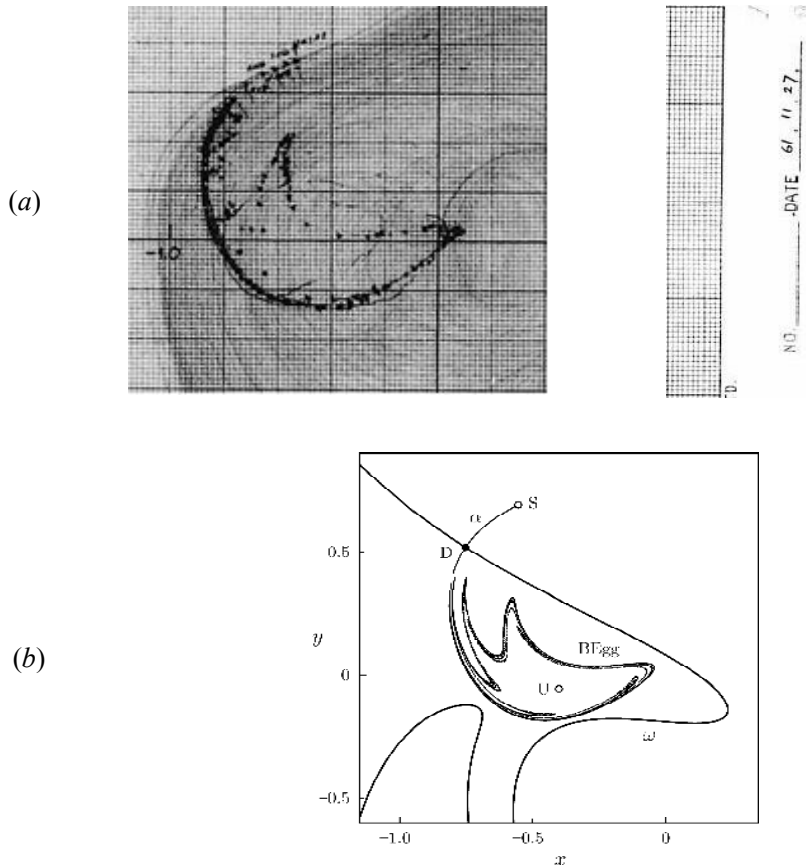


Fig. 1. (a) Partial output of an analog simulation of the equation (1) with  $\mu = 0.2$ ,  $\gamma = 8$ , and  $B = 0.35$  obtained on 27 November 1961 is shown. A continuous trajectory is drawn lightly on the  $(x, y)$ -plane and points in the stroboscopic observation at phase zero are given by heavy dots; five dots near the top are fixed points for a sequence of values at  $v = 1.01, 1.012, 1.014, 1.016$  and  $1.018$ , the remaining points are on the chaotic attractor at  $v = 1.02$  (a few points represent transient state after node-saddle bifurcation). (b) Phase portrait obtained by digital simulation. Parameters are  $v = 0.99$ , and  $B = 0.35$  (Note: In the early 1960, we had been using alphabet “ $v$ ” instead of “ $x$ ”, as a variable of the equation, however, in this report these are united to “ $x$ ”).

called directly unstable fixed point or saddle, and corresponding periodic oscillation is not easily observed due to its instability. Another attractor was called Broken Egg Attractor “BEgg” according to its appearance. The point U inside the BEgg is called completely unstable fixed point or source. It represents the capability of self-excited component of the system.

It is known that saddle type fixed (or periodic) point has  $\alpha$ -branch and  $\omega$ -branch, which are determined uniquely. In the figure,  $\omega$ -branch forms basin boundary between two attractors S and BEgg. The forcing parameters for Fig. 1(b) are given by  $\nu = 0.99$ , and  $B = 0.35$ , just inside of the boundary of frequency entrainment (see Fig. 2(b)). When  $\nu$  is increased outside the boundary of the entrainment, points S and D approach each other and coalescent on the boundary, then disappear (node-saddle or fold bifurcation). The entire  $(x, y)$ -plane becomes basin of BEgg chaotic attractor.

Figure 1(a) was obtained by analog computer experiments. This shows small numerical discrepancy between analog and digital experiments, which is inevitable. That is to say, this fact implies profound and important meaning concerning the concept of structural stability.

## 2.2. Local Bifurcation Sets

Figure 2 shows parameter regimes of external force on the  $(\nu, B)$ -plane. The reasons why we paid attention to this limited part were as follows:

- (1) In order to check appropriateness of the data obtained by applying averaging principle (only 2D autonomous systems could be attacked in those days), the aim of the author’s master thesis was to make analog simulation of the van der Pol’s equation with sinusoidal external force (non-autonomous periodic system) to confirm the validity of the data obtained from approximated averaged autonomous system. The plenty of data was almost calculated by Professor H. Shibayama.
- (2) Through this simulation study, the author acquired many valuable fundamental phenomena and concepts of non-linear dynamics. Among them, in synchronization phenomena there are differences

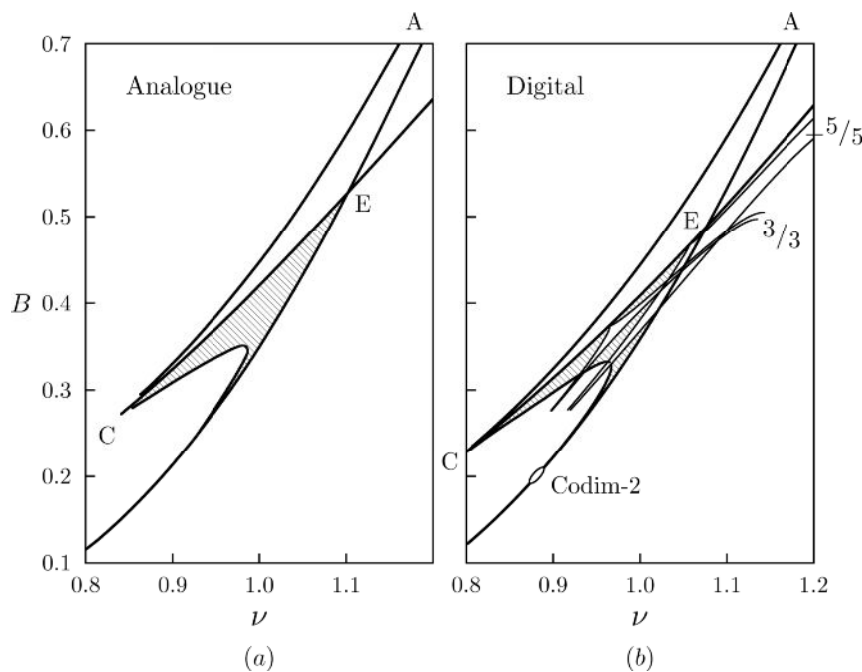


Fig. 2. (a) Partial bifurcation sets obtained by an analog simulation of the equation (1) with system parameters  $\mu = 0.2$ , and  $\gamma = 8$ . In the triangular region ACE, two point attractors coexist, and the shaded regime represents region of attractor representing beat oscillations (in addition to entrained oscillations), intrudes into the region of harmonic entrainment. (b) The same by a digital simulation.

between frequency entrainment (pull-in) and quenching mechanisms. These were well-known typical mechanisms of synchronization.

(3) As the van der Pol's equation has linear restoring term, asynchronous beat oscillations were all quasi- or almost-periodic oscillations. That is, no chaotic oscillations were observed.

(4) The author's master thesis was summarized in Fig. 12.7, p. 298 of Professor Hayashi's Book, "Nonlinear Oscillations in Physical Systems" McGraw Hill (1964).

(5) Theoretically, there are two synchronous oscillations in rather restricted regime on the  $(\nu, B)$ -plane. However, the regime was extremely small, therefore we couldn't make simulation experiments. In other words, overlapping region of entrainment and quenching is too narrow to practice simulation experiments by analog computer.

(6) Difference of phase portraits between "Entrainment" and "Quenching" occupied the author's interest in those years, hence a negative resistance oscillator was sought out, which had a wide problematic region i.e., entrainment and quenching regions overlap widely. This made analog experiment possible (see triangular regions ACE in Fig. 2(a) and 2(b)).

From the above reasons the readers can see why periodically forced negative resistance oscillator represented by Eq. (1) was taken up for study.

Small quantitative differences are observed between bifurcation sets of Figs. 2(a) and 2(b). This fact is due to the principle between analog and digital simulations. Moreover, these differences cannot be avoided anyway. It should be noted that regions indicated by 3/3 and 5/5 harmonic oscillations represent outer boundary of corresponding oscillations (i.e., hysteresis phenomena were neglected) and parallel to so-called windows. In other words, depending on the practical point of view, digital simulation results reveal impractical subtle aspects of the phenomena included in the corresponding equation (of course, this description is just the author's personal view. Appropriate concept of structural stability, or robustness should be established urgently, in order to avoid misunderstanding between virtual and real phenomena prevailing even among researchers of nonlinear dynamics).

### 3. Atmosphere at the Very Instant

When the author gives a presentation at the Conference, he will show Video Animation corresponding to Fig. 1. Unfortunately it cannot be shown here. Instead, Analog Computer Block Diagram is given in Fig. 3. Time scale was set at  $a = 2$ , this implies computer time  $2\pi/\nu$  corresponds to  $4\pi/\nu$  [sec]. System and control parameters used were given in the caption of Fig. 1. Following Fig. 4 showed some members of C. Hayashi's Laboratory in front of the analog computer.

### 4. Descendent Unsettled Problems from Experimental Studies

In this section, previous to mention unsettled problems, results concerning analog and digital simulation experiments are summarized, yet the descriptions are just author's examinations of the experimental results.

#### 4.1. Summaries of Experimental Studies

(1) When the control parameter is given inside the chaotic regimes, closure of  $\alpha$ -branch of some D or I type (saddle) periodic point represents chaotic attractor. Because in this case,  $\alpha$ -branch and  $\omega$ -branch of every saddle point (fixed or periodic) cross each other and homoclinic structure is formed. In other words, hence all  $\alpha$ -branches in the chaotic attractor seemed to be connected through heteroclinic connections, or prolongation of an  $\alpha$ -branch rises from every periodic (saddle) point inevitably crosses  $\omega$ -branch from the same saddle point or group.

(2) Let us pay attention to the totality of  $\alpha$ - and  $\omega$ -branches, almost all homoclinic and heteroclinic



the periodic solutions of the differential equation and are seemed to be distributed densely in the attractor. Infinitely many homoclinic points are also seemed to be distributed similarly.

(2) There exists no minimal set which is composed of invariant simple closed curve characterized by irrational rotation number. There seems no singular case agree with the theory of differential equations on the torus.

(3) There also exist sets of wandering points of higher orders. These are closely related to the (dis-)continuity properties of  $\alpha$ -branches composing chaotic attractors.

(4) Summarizing the above items, every point on a chaotic attractor observed in the second order non-autonomous periodic systems is classified into a fixed point, a periodic point, a homoclinic point, or a higher order wandering point. This implies that there exist no minimal set differs from  $n$ -periodic group (includes fixed point, if any).

Based on the results of simulation studies, no proof is expected to be done for the above conjectures. Regarding to the concept of structural stability of chaotic attractors, the author's ability cannot reach up to propose the concept. He strongly hopes that appropriate concept will be established in the near future.

## 6. Conclusion

This report explained how was the "Origin of Experimental Chaos Research" since early 1960 and summarized the author's conjectures about chaotic attractors observed in the second order non-autonomous periodic systems.

## References

Almost all contents of this report are stored up in the following Kyoto University Research Information Repository KURENAI (although not a little Japanese materials are included):

<http://repository.kulib.kyoto-u.ac.jp/dspace/handle/2433/68907>

<http://repository.kulib.kyoto-u.ac.jp/dspace/handle/2433/24272>

<http://repository.kulib.kyoto-u.ac.jp/dspace/handle/2433/24257>

<http://repository.kulib.kyoto-u.ac.jp/dspace/handle/2433/71101>



Fig. 4. In front of the Analog Computer from the left:

Kashimura (deceased), Nishikawa, Abe, Shibayama (deceased), Hashimoto and Ueda (Summer, 1960).

**THE BIFURCATION SET FOR A TWO-AXES VEHICLE MODEL  
WITH THE NON-LINEAR DEPENDENCE OF SLIPPING FORCES**

**Volodymyr G. Verbitskii**<sup>1</sup>,  
Donetsk Academy of Automobile Transport  
Donetsk, Ukraine.

**Valeriy G. Khrebet** ,  
Highway Engineering Institute of Donetsk  
National Technical University  
Gorlovka, Ukraine.

**Nataliya O. Velmagina**,  
Donetsk Academy of Automobile Transport  
Donetsk, Ukraine.

---

ABSTRACT

---

The approach to construct the bifurcation set of steady states for a two-axes vehicle model considering non-linear non-monotone dependences of slipping forces, is presented. Phase portraits illustrating cases of stability loss are given.

---

**1. THEORETICAL GROUNDING.**

The mathematical model of a vehicle can be presented as the dynamic system of the form:

$$\dot{x} = f(x, \theta, v). \quad (1)$$

Its steady states result from the solution of the following non-linear equations

$$f_i(x, \theta, v) = 0, \quad x \in R^n, \quad (i = 1, \dots, n). \quad (2)$$

The system has two control parameters: longitudinal motion velocity  $v$  and the turning angle  $\theta$  of the front steering wheels.

In papers [1, 2] the steady states evolution resulted from the variations of control parameters is analyzed.

Bifurcation values  $(v^*, \theta^*)$  correspond to multiple solutions  $x^*$  of the system (2).

Jacobian system is altered to zero at all points of the critical set  $x^*$ :

$$J = \left\| \frac{\partial f_i}{\partial x_j} \right\|_{x^*} = 0, \quad x^* \in M_{kp}.$$

The system (2) with the above-mentioned equation gives rise to the critical set on the basis of the steady states manifold.

At critical points of the set the steady stationary state is eliminated (these points correspond to either fold – two-fold system solutions (2), or cusp – three-fold system solutions (2)).

Any qualitative variations of stationary states for the system of control parameters result from the birth (elimination) of two singularities.

Therefore the determination of stability boundaries considering the control parameters is of interest.

Stability boundaries can be defined by constructing the bifurcation set which divides the parameters domain into a number of domains with different stationary states, determining the zones of stability or instability.

---

<sup>1</sup> Corresponding author. Email [oxsi@bigmir.net](mailto:oxsi@bigmir.net)

However, the procedure of constructing the bifurcation set in the case of dependences of sideways slipping forces with evident maximum demands a further development. Such necessity is explained by the existence of several branches of the bifurcation set.

## 2. FORMULATION OF THE PROBLEM.

### THE CONSTRUCTION OF THE BIFURCATION SET FOR A TWO-AXES VEHICLE MODEL.

Let's us analyze the system consisting of the body with a rear wheel axis firmly fixed and the front wheel module, its turning about the body is rigidly fixed (set by  $\theta$ ).

The system is subjected to the sideways reaction of the support plane – elastic wheels can move at some angle (slipping angle) to the surface of the wheel symmetry (due to elastic deformation at the point of the contact). Such situation gives rise to transverse forces resulted from the supporting plane thus interfering with sideways slipping of the wheel (slipping forces).

Let  $m$  is the vehicle mass;  $J$  is the central inertia moment of the system about the vertical axis;  $a$ ,  $b$  are distances between the centre of mass of the vehicle to the middle part of the front and rear wheel axes correspondently.

Equations of the plane-parallel motion for the velocipede two-axes scheme vehicle (vertical longitudinal plane across the middle of wheel axes is the plane of the symmetry) with the constant longitudinal constituent of the mass centre velocity are

$$\left\{ \begin{array}{l} m(\dot{u} + \omega v) = Y_1 \cos \theta + Y_2; \\ J \dot{\omega} = a Y_1 \cos \theta - Y_2 b; \\ \delta_1 = \theta - \arctg \frac{u + a\omega}{v}, \delta_2 = \arctg \frac{-u + b\omega}{v}. \end{array} \right. \quad (3)$$

where  $u$  is the transverse constituent of the vehicle's mass centre velocity;  $\omega$  is the angle velocity of the vehicle about the vertical axis;  $\delta_1$ ,  $\delta_2$  are the slipping angles for front and rear axes correspondently;  $Y_1$ ,  $Y_2$  are the sideways slipping forces as functions of slipping angles for front and rear axes correspondently.

Slipping forces are defined empirically and can be represented through different analytical dependences:

$$\begin{aligned} -\frac{v}{g}\omega + \frac{\cos(\theta)\bar{Y}_1(\delta_1)b}{l} + \frac{\bar{Y}_2(\delta_2)a}{l} &= 0, \\ \cos(\theta)\bar{Y}_1(\delta_1) - \bar{Y}_2(\delta_2) &= 0. \end{aligned} \quad (4)$$

In this case the determination of steady motion states (singularities) has the form

Where  $\bar{Y}_i(\delta_i) = Y_i(\delta_i) / N_i$  – dimensionless sideways reactions of the support plane on the axis ( $N_i$  – vertical load on the axis).

In our paper we deal with dependences of the type

$$Y_i = \frac{\gamma_i \delta_i}{\sqrt{1 + \frac{(|\delta_i| - \beta_i)^2}{(\beta_i)^2}}}, \quad (5)$$

which guarantee the nonmonotonicity of slipping forces (unlike monotone dependences at considerable slipping angle the function has descending sections).

Parameters  $\gamma_i$  and  $\beta_i$  are due to keeping geometrical characteristics of the monotone

dependences,  $Y_i = \frac{q_i \delta_i}{\sqrt{1 + \frac{(q_i \delta_i)^2}{(\varphi_i)^2}}}$ , enabling the constancy of the critical velocity for rectilinear

motion, coordination of maximum values of dimensionless slipping forces (Fig.1):

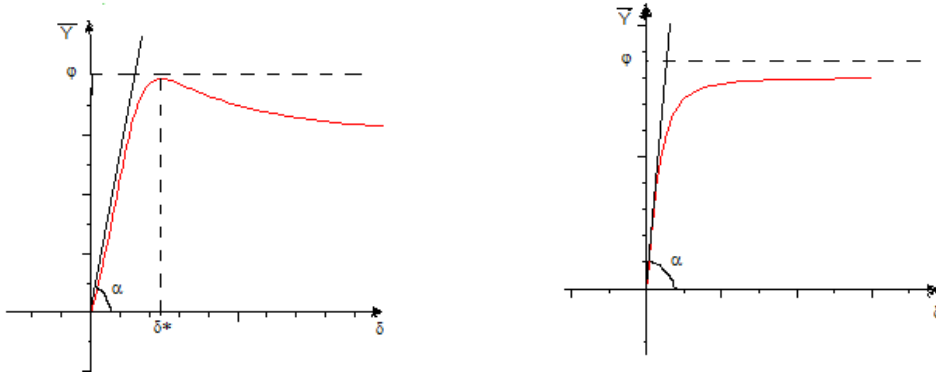


Fig.1. Non-monotone and monotone dependences of slipping angles

One analyzes the influence of the new “geometry” of slipping forces dependences on the bifurcation set.

Earlier (for monotone dependences) different types of bifurcation sets were obtained within “geometric” approach.

The original system determining the steady states has the form

$$\bar{Y}(\delta_2 - \delta_1) = \frac{v^2}{gl}(\theta + \delta_2 - \delta_1), \quad (6)$$

where the left part of the equation is a non-linear function and named “stationary curve”, the right part of the equation presents a straight line (“moving line”).

The intersection points of the “stationary curve” and “moving line” correspond to stationary states of the system (2).

Parameters  $v$  and  $\theta$  being constantly changed, the equation (6) sets the reflection of the plane with  $v$  and  $\theta$  to balanced surface.

The bifurcation set (critical set) corresponds to  $v$ ,  $\theta$  for which “the moving straight line” contacts with “the stationary curve”.

Points of the inflection of the original curve  $\bar{Y} = \bar{Y}(\delta_2 - \delta_1)$  correspond to the points of the bifurcation set cusp.

The triple solution for the balanced plane is corresponded to the cusp, double solution – to the fold.

In the case of the monotone dependences of slipping forces from slipping angles of the saturation curve, the “stationary curve” can have three points of inflection, the bifurcation set – three cuspidal points.

The symmetric “cusp” corresponds to the three-fold steady state at  $v = v_{kp}^+$ , and  $\theta = 0$  (the stability loss for rectilinear motion), where  $V_{kp} = \sqrt{\frac{glq_1q_2}{q_1 - q_2}}$ ,  $q_i = \frac{k_i}{N_i}$  are stationary dimensionless slipping coefficients [4].

In the case of descending original dependences  $\bar{Y}_i(\delta_i)$  additional points of inflection of the “moving curve”  $\bar{Y} = \bar{Y}(\delta_2 - \delta_1)$  come into being, resulting in the complication of the bifurcation set.

Let’s analyze the method of constructing the bifurcation set for definite numeric values of  $\gamma$ ,  $\beta$ :

$$Y_1 = \frac{\delta \cdot 3.300062959 \cdot \sqrt{2}}{\sqrt{1 + \frac{(|\delta| - 0.12)^2}{0.12^2}}}, \quad Y_2 = \frac{\delta \cdot 2.526513230 \cdot \sqrt{2}}{\sqrt{1 + \frac{(|\delta| - 0.15)^2}{0.15^2}}}, \quad \delta \in [-1; 1].$$

The dependence  $\bar{Y} = \bar{Y}(\delta_2 - \delta_1)$  is determined by  $\bar{Y}_1(\delta_1) = \bar{Y}(\delta_2) = \bar{Y}$ .

Critical values of  $v$ ,  $\theta$  correspond to the next equations (7)

$$\begin{aligned}\frac{v^2}{gl} &= \frac{dY}{d(\delta_2 - \delta_1)}; \\ \frac{Y}{\theta + \delta_2 - \delta_1} &= \frac{dY}{d(\delta_2 - \delta_1)},\end{aligned}\quad (7)$$

Then

$$\theta = Y \cdot Y' - (\delta_2 - \delta_1). \quad (8)$$

Therefore the system (7) gives rise to the bifurcation set having the parametric form

$$\theta = \theta(\delta_2 - \delta_1), \quad v = v(\delta_2 - \delta_1). \quad (9)$$

Sometimes  $Y$  as a parameter is more preferable than  $(\delta_2 - \delta_1)$ . The original dependences are  $Y_1 = f_1(\delta_1)$ ,  $Y_2 = f_2(\delta_2)$ . Solving them with respect to  $\delta_i$ , we can find  $\delta_1 = F_1(Y_1)$ ,  $\delta_2 = F_2(Y_2)$ . Therefore,  $G(Y) = F_2(Y_2) - F_1(Y_1)$ . In this case the final version of the equation (6) is

$$\frac{gl}{v^2} \cdot Y - \theta = G(Y). \quad (10)$$

Following the contact (Fig. 3, b) of the “stationary curve” and “moving straight line” as

$$\begin{aligned}\frac{gl}{v^2} &= \frac{dG}{d(Y)}; \\ \frac{\theta + G(Y)}{Y} &= \frac{dG}{d(Y)},\end{aligned}\quad (11)$$

we can obtain parametric equations of the bifurcation set in the form  $\theta = \theta(Y)$ ,  $v = v(Y)$

$$\begin{aligned}\theta &= Y \cdot G'(Y) - G(Y); \\ v &= \sqrt{\frac{gl}{G'(Y)}}.\end{aligned}\quad (12)$$

Then the procedure of forming function  $G(Y) = \delta_2 - \delta_1$  in the case of non-monotone dependences  $Y_i(\delta_i)$  is analyzed.

For numerical values of  $\beta, \gamma$  we define functions  $F_i(Y)$ , admitting the correlation (5) for  $\delta_i$ , we have two single-valued branches, connected at the points of turning (Fig. 2):

$$\begin{aligned}f_{11} &= \frac{0.12 \left( -|Y| + \sqrt{0.6272879344 - Y^2} \right) Y}{-Y^2 + 0.3136439672}, & f_{21} &= \frac{0.15 \left( -|Y| + \sqrt{0.5744942192 - Y^2} \right) Y}{-Y^2 + 0.2872471096}, \\ f_{12} &= \frac{0.12 \left( Y + \sqrt{0.6272879344 - Y^2} \right) Y}{Y^2 - 0.3136439672}, & f_{22} &= \frac{0.15 \left( Y + \sqrt{0.5744942192 - Y^2} \right) Y}{Y^2 - 0.2872471096}.\end{aligned}$$

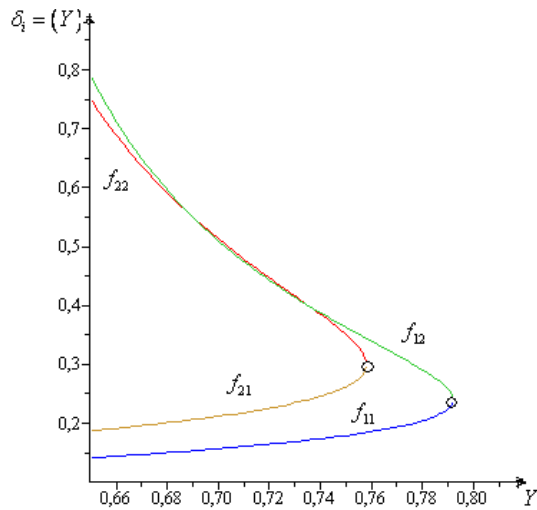


Fig. 2. Dependences of sideways slipping forces at  $\gamma_1=3.30006295, \beta_1=0.12$  and  $\gamma_2=2.52651323, \beta_2=0.15$ .

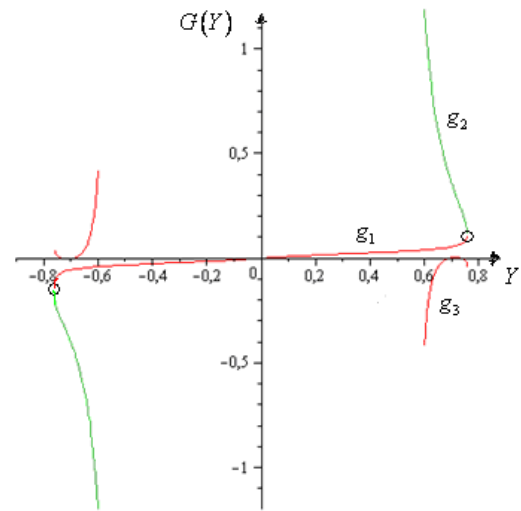


Fig. 3. Chart of stationary curve for selected  $\gamma, \beta$ .

Therefore, the function  $G(Y) = \delta_2 - \delta_1$  is determined as the difference of corresponding single-valued branches as  $f_{ij}$ , and has three branches of single-valuedness  $\{g_1, g_2, g_3\}$ ;  $g_1$  and  $g_2$  are connected at the point of turning, thus forming the “main” branch (Fig.3).

The section of the main branch up to the point of turning comes from  $G(Y) = g_1 = f_{21} - f_{11}$ , the second part of this branch has the form  $G(Y) = g_2 = f_{22} - f_{11}$ .

The additional branch of the “moving curve” is due to the descending sections of slipping forces dependences  $G(Y) = g_3 = f_{22} - f_{12}$ .

Every section of the function  $G(Y)$  in accordance with (12) has a dual curve, presenting the part of the bifurcation set (Fig.4).

The bifurcation set divides the plane of control parameters  $\theta, \nu$  into domains with different number of stationary states. It is also possible to determine the number of steady and unsteady states for each domain. The critical set of parameters being intersected, the number of stationary states is changed into two states. The number of stationary states in different domains with the control parameters plane is illustrated in Fig.4.

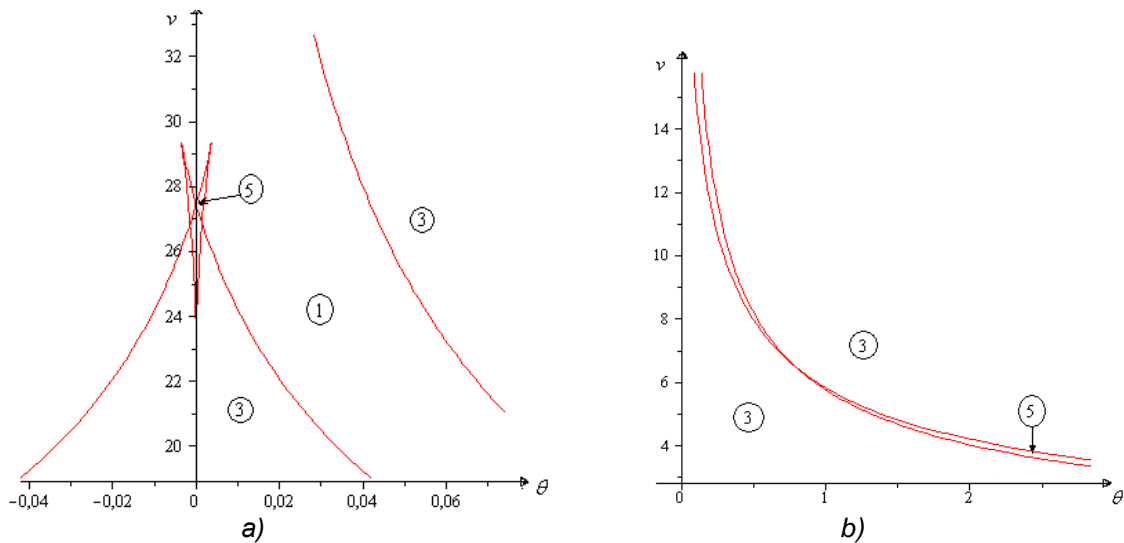


Fig. 4. The bifurcation set (non-linear dependence from a slipping angle) without “heel” moment: a) general set view, b) fragments of the set.

## CONCLUSION

Geometrical method of the stationary states determination [4] added by the algorithm of constructing the bifurcation set with Poincaré's index enables us to accomplish the preliminary analysis of the quantity of stationary states and determine the stability boundaries for the plane of control parameters in the case of the non-monotone dependences of slipping forces.

Descending sections of slipping forces lead to additional branches of the bifurcation set resulted in qualitative changes of the phase portrait and in certain cases causing new dynamic effects (because of changes within the attraction domain structure for the stable motion states).

## REFERENCES

- [1] Verbitskii V. G. Bifurcation sets and catastrophes in manifold of the steady states of pneumowheel vehicles. Prikl. Mech. Vol. 31, №3, Kiev, pp. 89-95, 1995.
- [2] Arnold V. I., Catastrophe Theory. Nauka, Moscow, 1990.
- [3] Holodniok M., Klic A., Kubicek M. and Marek M., Methods of Analysing Non-linear Dynamic Systems. Mir, Moscow, 1991.
- [4] Pevsner J.M. Theory of stability of automobile. Mashisdat, Moscow, 1947.

## GRAZING INDUCED BIFURCATIONS IN IMPACTING SYSTEMS

**M. Wiercigroch**<sup>1</sup>  
Aberdeen University  
Aberdeen, UK

---

### ABSTRACT

---

In this lecture I will discuss linear oscillators undergoing impact with secondary elastic supports, which are studied experimentally and semi-analytically for near-grazing conditions. We discovered a narrow band of chaos close to the grazing condition and this phenomenon was observed experimentally for a range of system parameters. Through numerical stability analysis, we argue that this abrupt onset to chaos is caused by a dangerous bifurcation in which two unstable period-3 orbits, created at "invisible" grazings, take part.

The experimentally observed bifurcations are explained with help from simulations based on mapping solutions between locally smooth subspaces. Smooth as well as non-smooth bifurcations are observed, and the resulting atypical bifurcations are explained, often as an interplay between them. In order to understand the observed bifurcation scenarios, a global analysis is required, due to the influence of stable and unstable orbits which are born in distant bifurcations but become important at near-grazing conditions. The good degree of correspondence between experiment and theory fully justifies the modelling approach.

---

---

<sup>1</sup> Corresponding author. Email [m.wiercigroch@abdn.ac.uk](mailto:m.wiercigroch@abdn.ac.uk)

## OSCILLATION OF SYSTEMS WHICH HAVE FORCE-DISPLACEMENT CHARACTERISTICS WITH RECTANGULAR LOOPS OF HYSTERESIS

**A. Zotov<sup>1</sup>**  
 Ufa State Petroleum  
 Technological  
 University  
 Ufa, Russia

### ABSTRACT

The article is devoted to nonlinear oscillation of passive systems which have force-displacement characteristics with rectangular loops of hysteresis resulting from the dry friction force. Under certain conditions when force-displacement characteristic has segment of zero stiffness the resonance frequencies are shifted in area of higher frequencies defined by the size of this segment.

### INTRODUCTION

The possibility of creation systems with quasi-zero-stiffness for protection of dynamic objects is now well known nowadays [1]. In the article [2] shows the possibility to creation systems with force-characteristics with rectangular hysteresis's loops resulting from the dry friction force (Fig.1). Height of hysteresis's loops is determined by the dry friction force  $R$  (where  $R = q \cdot F_*$ ,  $F_* - const$ ,  $q$  is the coefficient, which determines the height of loops,  $F_*$  is the restoring force without the friction force). If the coefficient  $q$  is more than 1 then the restoring force are absent, so  $0 \leq q \leq 1$ . Variants when  $q > 1$  are not checked.

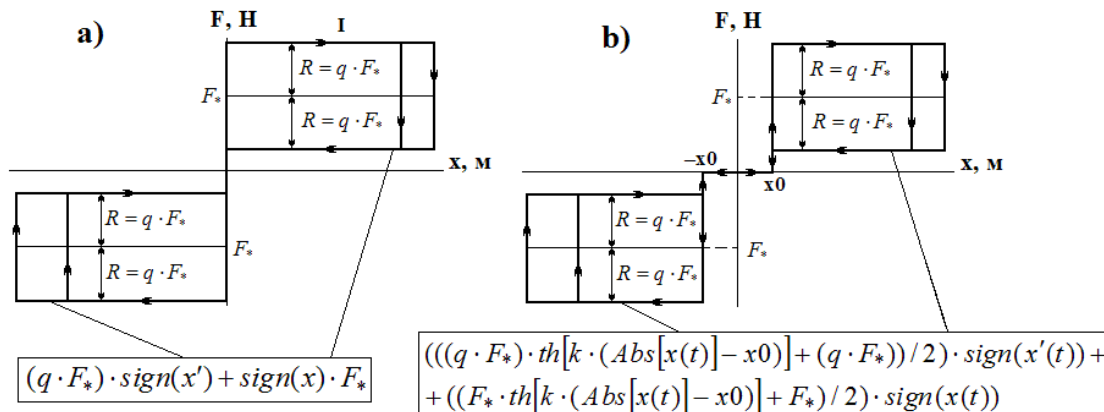


**Fig. 1 Force characteristics with loops of hysteresis**

*a – without segment of zero stiffness; b – with segment of zero stiffness ( $-x_0, x_0$ )*

Oscillation under the harmonic excitation  $F_0 \cdot \cos(p \cdot t + \varphi)$  (where  $F_0$  is the amplitude of the correction force;  $p$  is the frequency;  $\varphi$  is the initial phase) are determined both analytically and numerically. Loops of hysteresis are defined analytically by functions, shown in Fig. 1; (where  $k$  is the coefficient, which determines the inclination of loop's sides; for diagrams in the Fig. 1,  $k = 10000$ ;  $x_0$  is the value, which determines the size of segment of zero stiffness).

<sup>1</sup> Corresponding author. Email a-zot@rambler.ru

## 1. OSCILLATION OF SYSTEMS WHICH HAVE FORCE-CHARACTERISTICS WITH RECTANGULAR LOOPS OF HYSTERESIS WITHOUT SEGMENT OF ZERO STIFFNESS

Six transcendental equations are solved in order to determine analytically the oscillation of systems with force-characteristics described in Fig.1, a. Oscillations under the subject to harmonic excitation ( $F_0 \cdot \cos(p \cdot t + \varphi)$ ) are determined numerically as well. Loops of hysteresis are described by functions shown in Fig. 1, a. The differential equation of the moving object with mass  $m$  is:

$$m \cdot \ddot{x} = F_0 \cdot \cos(p \cdot t + \varphi) - \{(q \cdot F_*) \cdot \text{sign}(x') + \text{sign}(x) \cdot F_*\}, \quad (1)$$

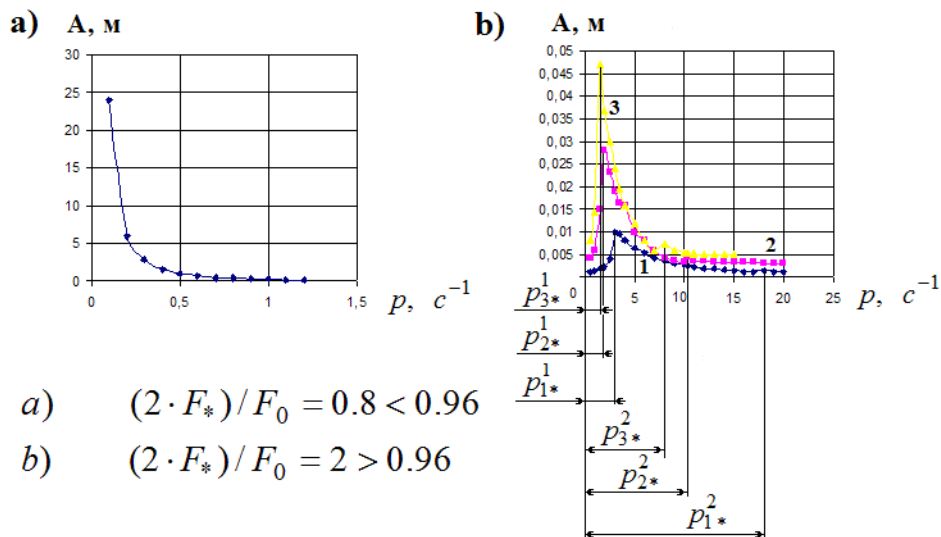
For numerical solution it is possible to determine the oscillations for different coefficients  $q$  (Fig. 1, a). For  $q=1$ , under the next relation  $(2 \cdot F_*)/F_0 \geq 0.96$ , the oscillations are vanished. The amplitude-frequency characteristics are derived for the next relation:  $2 \cdot F_*/F_0 \leq 0.96$ . The amplitude-frequency characteristic for  $2 \cdot F_*/F_0 = 0.8$  and  $F_0 = 100 \text{ H}$  is described in Fig. 2, a. The results of analytical and numerical solutions are considered coincident.

## 2. OSCILLATION OF SYSTEMS WHICH HAVE FORCE-CHARACTERISTICS WITH RECTANGULAR LOOPS OF HYSTERESIS WITH SEGMENT OF ZERO STIFFNESS

In order to determine analytically the oscillations for force characteristics shown in Fig. 1, b with segments of zero stiffness ( $x_0 \neq 0$ ) and disturbing force  $F_0 \cdot \cos(p \cdot t + \varphi)$  it is necessary to solve nine transcendental equations [2]. The oscillations are determined numerically by solving the next differential equation:

$$m \cdot x'' = F_0 \cdot \cos(p \cdot t + \varphi) - (((q \cdot F_*) \cdot \text{th}[k \cdot (\text{Abs}[x] - x_0)] - (q \cdot F_*)/2) \cdot \text{sign}(x') - ((F_* \cdot \text{th}[k \cdot (\text{Abs}[x] - x_0)] + F_*)/2) \cdot \text{sign}(x)) \quad (2)$$

To obtain the analytical solution, the nine transcendental equations are reduced to the one which is solved by the dichotomy method. Author can solve it in a specific frequency range which less than  $p^1$  (Fig. 2, b).



a)  $(2 \cdot F_*)/F_0 = 0.8 < 0.96$

b)  $(2 \cdot F_*)/F_0 = 2 > 0.96$

$$m = 500 \text{ kg}; \quad F_0 = 100 \text{ H};$$

b) 1 -  $|x_0| = 0.001 \text{ m}$ ; 2 -  $|x_0| = 0.003 \text{ m}$ ; 3 -  $|x_0| = 0.005 \text{ m}$ ;

$p_{1*}^1$ ;  $p_{2*}^1$ ;  $p_{3*}^1$  are first resonance's frequencies;  $p_{1*}^2$ ;  $p_{2*}^2$ ;  $p_{3*}^2$  are second resonance's frequencies;

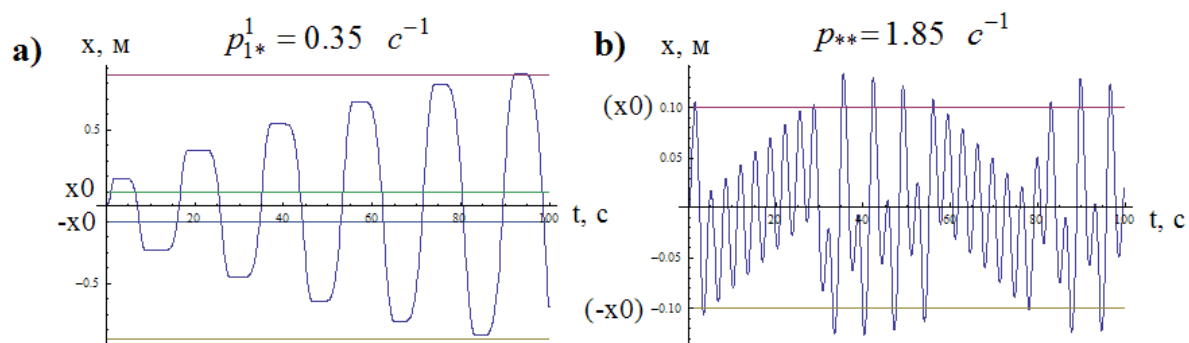
Fig. 2 Amplitude-frequency characteristics ( $q = 1$ )

The results of the analytical solution were coincided with results of the numerical one, but numerical solution of differential equation (2) was obtained for any frequencies of harmonic excitation  $p$ .

For  $x_0 = 0$  the amplitude-frequency characteristic obtained by solution of differential equation (2) is in coincident with amplitude-frequency characteristic obtained by solution of differential equation (1) (Fig. 2, a).

For  $q = 1$  and  $(2 \cdot F_*) / F_0 \geq 0.96$  for the case when  $x_0 \neq 0$  (Fig. 1, b) oscillation do not vanish as for the case when  $x_0 = 0$  (Fig. 1, a), but resonance's frequencies are shifted in area of higher frequencies. The shift depends on the area of section with zero stiffness,  $x_0$ : the more smaller is the area, the more bigger is the shift (Fig. 2, b). For the numerical solution of differential equation (2) for set-up parameters two resonance's frequencies ( $p_{1*}^1, p_{2*}^2$  - Fig. 2, b) are determined. Resonance oscillation (first resonance's frequencies) are shown in Fig. 3, a. "Oscillation stop" takes place starting from the specific frequency  $p_{**}$  (Fig. 3, b).

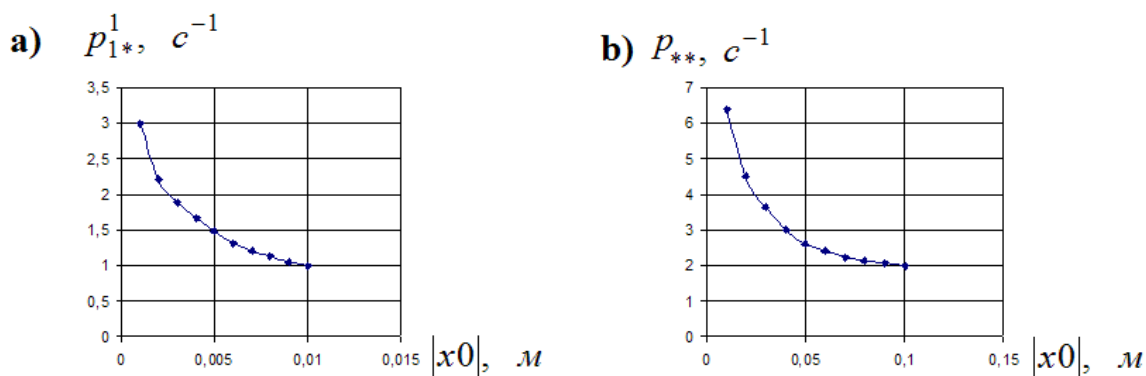
Relations between the first resonance's frequencies, "oscillation stop" frequencies and the size of segment of zero stiffness are shown in the Fig. 4.



$$m = 500 \text{ kg}; \quad F_0 = 100 \text{ H}; \quad 2 \cdot F_* / F_0 = 2; \quad |x_0| = 0.1 \text{ m}$$

a) - first resonance's frequency ( $p_{1*}^1$ ); b) "oscillation stop" ( $p_{**}$ )

Fig. 3 Oscillations



$$m = 500 \text{ kg}; \quad F_0 = 100 \text{ H}; \quad 2 \cdot F_* / F_0 = 2$$

a) first resonance's frequencies b) frequencies of "oscillation stop"

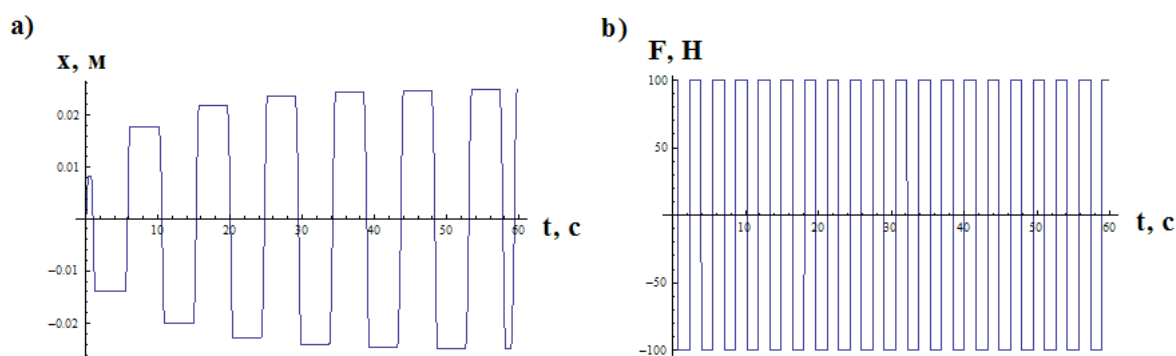
Fig. 4 Dependences of critical frequencies from size of segment of zero stiffness

Oscillation of systems, which force characteristics shown in Fig. 1, b, were determined also for excitation  $F_0 \cdot \text{sign}[\cos[p \cdot t + \varphi]]$ . The next differential equation is solved:

$$m \cdot x'' + (F_* \cdot \text{th}[k \cdot (\text{Abs}[x] + x_*)] + F_*) / 2 \cdot \text{sign}[x'] + (F_* \cdot \text{th}[k \cdot (\text{Abs}[x] + x_*)] + F_*) / 2 \cdot \text{sign}[x] = F_0 \cdot \text{sign}[\cos[p \cdot t + \varphi]] \quad (3)$$

Within specific parameters the oscillation frequency becomes in several times less than the frequency of excitation (Fig. 5). The frequency range of that effect exists is sufficiently narrow. (for

$F_0 = 100 \text{ H}$ ;  $F_* = 125 \text{ H}$ ;  $|x_0| = 0.005 \text{ m}$ ;  $\varphi = 0$ ;  $q = 1$   $p \in [1.9 - 2.4]$ ). For these parameters the relation of the oscillation frequency to the excitation frequency is little bit more than three (Fig. 5). This effect is not observed for the excitation  $F_0 \cdot \cos(p \cdot t + \varphi)$ .



$$p = 2 \text{ c}^{-1}; \quad F_0 = 100 \text{ H}; \quad F_* = 125 \text{ H}; \quad |x_0| = 0.005 \text{ m}; \quad \varphi = 0$$

a) coordinate of oscillating body; b) excitation

Fig. 5 Oscillation contraction for the excitation  $F_0 \cdot \text{sign}[\cos[p \cdot t + \varphi]]$

It should be noted that for the described cases the oscillations with stopping can be observed (dependences of the coordinates from time are rectangular, as shown in the Figs. 3, 5), that is, specific for the systems with dry friction.

## CONCLUSIONS

The considered systems of passive type with force characteristics, shown in Fig. 1, can be widely applied in scientific and technical areas, such as seismic protection, suspension brackets, impact protection and so on. The studies showed that numerical approach of the oscillations determination for described systems is more preferable than the analytical one. Some interesting effects were revealed for the numerical approach.

For the system with force characteristics shown in Fig. 1, a, the resonance frequency converges to zero. For definite ratio of the correction force to the amplitude of excitation force the oscillation vanish. If for that ratio the segment of zero stiffness appears on the characteristics (Fig. 1, b) then oscillations do not vanish but the resonance frequency is shifted into the area of high frequencies (Fig 2, b). In this paper the frequencies of "oscillation stop" were defined.

For the excitation force  $F_0 \cdot \text{sign}[\cos[p \cdot t + \varphi]]$  the multiple decreasing of oscillation frequencies was revealed in comparison to the frequency of excitation force in the small diapason of the frequencies with force characteristics shown in Fig. 1, b.

For system with force characteristics, shown in Fig.1 the frequencies with "oscillation stops" were determined, both for excitation force  $F_0 \cdot \cos(p \cdot t + \varphi)$  and  $F_0 \cdot \text{sign}[\cos[p \cdot t + \varphi]]$ .

## REFERENCES

- [1] Alabuzhev P., Gritchin A., Kim L, Migirenko G., Chon V., Stepanov P. *Vibration Protecting and Measuring Systems with Quasi-Zero Stiffness*. Hemisphere Publishing, New York, 1989.
- [2] Zotov A.N. Systems with quasi-zero-stiffness characteristic / A.N. Zotov // Proceedings. IPACS Open Access Electronic Library, OPEN LIBRARY, 6<sup>th</sup> EUROMECH Nonlinear Dynamics Conference, ENOC 2008.

## ON THE OSCILLATIONS OF NONLINEAR MAGNETOELASTIC SOLIDS

H. Altenbach<sup>1</sup>  
V.A. Eremeyev

Martin-Luther-University  
Halle-Wittenberg, Halle,  
Germany

---

### ABSTRACT

---

We investigate the nonlinear oscillations of nonlinear elastic bodies made of magnetoreological materials, i.e. so-called magnetoelastomers. For this materials the magnetic field can be significantly change the material properties, for example, the stiffness parameters. As an example the oscillations of a magnetoelastic sphere is considered. It is shown that the various regimes of oscillation exist.

---

### INTRODUCTION

Magneto-sensitive (MS) or magneto-rheological (MR) elastomers are smart materials whose mechanical properties change significantly under the influence of a magnetic field. They are widely used in the modern engineering as elements of micro-electro-mechanical systems (MEMS) is the integration of mechanical elements, sensors, actuators, and electronics on a common silicon substrate through microfabrication technology, for example, in medical devices. The behavior of MS elastomers under a time-dependent magnetic field is a complex process and up to now not investigated in all details.

MS elastomers are composed of polarizable particles, dispersed in a polymer medium, having the size of the order of few microns (typically from  $10^{-7}$  to  $10^{-5}$  m). Carrier fillers are selected based upon their electro-magnetic and thermo-mechanical properties: silicone and/or other rubber-like materials with a very small electric conductivity. The typical particle volume fraction is between 0.1 and 0.5. During the manufacturing process of MS elastomers, the isotropy condition inherent of the filler material is maintained in the final composite. Therefore, these materials are considered to be isotropic and non-conductive. However, MS elastomers become non-homogeneous due to the presence and distribution of particles in the carrier filler.

Here we formulate an initial-boundary-value problem of a MS elastomer and demonstrate the special features of the dynamic behavior of such system. As an example the nonlinear oscillations of a MS elastic sphere and ring are considered. The basic equations of MS elastomers consist of the equations of motion of the finite elasticity and the Maxwell's field equations for the vector of the magnetic induction. The constitutive equation of MS elastomers described by the strain energy function depending on 6 invariants of the left-Cauchy-Green strain tensor  $\mathbf{b}$  and the vector of magnetic induction  $\mathbf{B}$ , is presented in general. For the sake of simplicity we use the simplified version of the constitutive equation, where the elastomer is assumed to be incompressible and the dependence on the vector of magnetic induction is reduced to the dependence of its magnitude, i.e. the dependence of the strain energy on the mixed invariant is not taken into account.

As an example two one-dimensional problems are considered. The first one is the radial-symmetric deformation of a hollow sphere loaded by external pressure. Using the incompressibility equations the boundary-value problem is reduced to a nonlinear non-autonomous ordinary differential equation of second order with respect to the radial displacement. The magnetic field  $\mathbf{B}$  is assumed to be a given periodic function of time. The phase portrait of this equation is obtained. The trajectories can demonstrate the complex behavior. The influence of the material parameters on the solution

---

<sup>1</sup> Corresponding author. Email [holm.altenbach@iw.uni-halle.de](mailto:holm.altenbach@iw.uni-halle.de) (Prof. Dr.-Ing. Holm Altenbach )

behavior is analyzed in details. For one case of material parameters one can see the weak influence on the oscillations. Other values demonstrate more complex behavior for small frequency with some type of instabilities. The increase of the frequency of the magnetic field  $\mathbf{B}$  leads to the stabilization of oscillations near the solution with constant  $\mathbf{B}$ . It means that using the external magnetic field we can “control” in some sense the motion of the sphere.

## 1. BASIC EQUATIONS OF INCOMPRESSIBLE MAGNETO-ELASTOMERS

Following [1-4], let us recall the basic relations of the theory of finite magneto-elasticity. For definiteness we consider an incompressible material in the absence of external body forces. The motion of the body is described by the position-vector in the actual configuration  $\mathbf{x}$

$$\mathbf{x} = \mathbf{x}(\mathbf{X}, t) \quad (1)$$

while  $\mathbf{X}$  is the position-vector in the reference configuration. We use standard notations

$$\mathbf{F} = (\nabla_{\mathbf{x}} \mathbf{x})^T, \quad J = \det \mathbf{F}$$

where  $\mathbf{F}$  is the gradient of the position-vector  $\mathbf{x}$ ,  $\nabla_{\mathbf{x}}$  is the nabla operator with respect to  $\mathbf{x}$ . For rubber-like materials we apply the incompressibility condition

$$J = 1 \quad (2)$$

The constitutive equations of an incompressible isotropic magneto-elastic solid are given by

$$\begin{aligned} W &= W(I_1, I_2, I_4, I_5, I_6) \\ \boldsymbol{\sigma} &= -p\mathbf{I} + \mathbf{F} \cdot \frac{\partial W}{\partial \mathbf{F}} \\ \mathbf{M}_e &= -\frac{\partial W}{\partial \mathbf{B}} \end{aligned} \quad (3)$$

where  $W$  is the specific free energy given composed of the following set of invariants

$$I_1 = \text{tr} \mathbf{b}, \quad I_2 = \frac{1}{2} [(\text{tr} \mathbf{b})^2 - \text{tr} \mathbf{b}^2], \quad I_4 = B^2 \equiv |\mathbf{B}|^2, \quad I_5 = (\mathbf{b} \cdot \mathbf{B}) \cdot \mathbf{B}, \quad I_6 = (\mathbf{b}^2 \cdot \mathbf{B}) \cdot \mathbf{B}$$

where  $\mathbf{b} = \mathbf{F} \cdot \mathbf{F}^T$  is the left-Cauchy-Green strain tensor,  $\mathbf{B}$  is the vector of the magnetic induction,  $\boldsymbol{\sigma}$  is the Cauchy stress tensor,  $\mathbf{M}_e$  is the normalized vector of magnetization,  $p$  is a Lagrange multiplier associated with the constraint (2), and  $\mathbf{I}$  is the second-order identity tensor. From the physical point of view  $p$  is the hydrostatic pressure [9, 10].

The equation of motion and the field equation have the following form

$$\begin{aligned} \nabla_{\mathbf{x}} \cdot \boldsymbol{\sigma} + (\nabla_{\mathbf{x}} \mathbf{B}) \cdot \mathbf{M}_e &= \rho \dot{\mathbf{v}} \\ \nabla_{\mathbf{x}} \cdot \mathbf{B} &= 0 \end{aligned} \quad (4)$$

where  $\nabla_{\mathbf{x}}$  is the nabla operator in the actual configuration,  $\rho$  is the density,  $\mathbf{v} = \dot{\mathbf{x}}$  is the velocity,  $(\dots)$  is the material derivative with respect to the time  $t$ . Further we assume that  $\mathbf{B}$  is homogeneous and depends only on  $t$ . Then Eqs (4) reduce to the standard one

$$\nabla_{\mathbf{x}} \cdot \boldsymbol{\sigma} = \rho \dot{\mathbf{v}} \quad (5)$$

The static boundary conditions have the standard form

$$\boldsymbol{\sigma} \cdot \mathbf{n} = \mathbf{f} \quad (6)$$

where  $\mathbf{n}$  is an outer unit normal to the boundary of the body and  $\mathbf{f}$  is an external surface load.  
Let us specify the form of the energy given by

$$W = \frac{1}{2} \mu(I_4)(I_1 - 3) \quad (7)$$

with  $\mu(I_4) = \mu_0(1 + \eta I_4)$ ,  $\eta > 0$ . For small deformations  $\mu_0$  is the shear modulus in the absence of the magnetic field,  $\eta$  describes the influence of the magnetic field on the shear modulus. Equation (7) is the classical neo-Hookean model, which is widely used in the mechanics of elastomers (see, for example, [9-11]) with an elastic modulus highly depending on the magnetic field induction intensity. More general constitutive equations were considered, for instance, in [1-8]. Using (7) we obtain

$$\boldsymbol{\sigma} = -p\mathbf{I} + \mu(I_4)\mathbf{b} \quad (8)$$

Thus, the boundary-value problem (5), (6) describes the deformations of MS elastomers under action of both the external forces and the magnetic field. Let us note that Eqs (5), (6) contain  $\mathbf{B}(t)$  only as a parameter. On the other hand, the dependence  $\mathbf{B}$  on  $t$  poses one to generate and control the vibrations of MS elastomer based devices. To illustrate this idea we consider an one-dimensional problem for MS elastomers in the next section.

## 2. NONLINEAR OSCILLATIONS OF A MAGNETO-ELASTIC SPHERE

Following [12] let us consider the oscillations of a hollow magneto-elastic sphere under action of a homogenous magnetic field  $\mathbf{B} = \mathbf{B}(t) = B(t)\mathbf{e}_r$  and a inner hydrostatic pressure  $\tilde{p}$ . In the reference configuration the sphere has the inner and the outer radii  $r_0$  and  $r_1$ , respectively. In the spherically symmetric case the position-vector is given by

$$\mathbf{x} = R(r, t)\mathbf{e}_r \quad (9)$$

where  $r \in [r_0, r_1]$  is the radial component of the spherical Lagrangian coordinates and  $\mathbf{e}_r$  is the appropriate base vector (see, e.g. [9]),  $R$  is an unknown function. In the actual configuration the inner and the outer radii are  $R_0 = R(r_0, t)$  and  $R_1 = R(r_1, t)$ , respectively.

From (2) we immediately find that

$$R(r, t) = (r^3 + x(t))^{1/3} \quad (10)$$

where  $x(t)$  is a new unknown function. Thus,  $R_1 = (r_1^3 + x(t))^{1/3}$ ,  $R_0 = (r_0^3 + x(t))^{1/3}$ . Equation (10) is one of the well-known so-called universal solutions for incompressible solids (see, e.g. [9]). For magneto-elastomers the universal solutions are studied in [7]. From (10) it follows that the volume of the sphere is constant, i.e.

$$R_1^3 - R_0^3 = r_1^3 - r_0^3 \quad (11)$$

For the universal solution (10) Eq. (5) is satisfied identically by choosing of  $p = p(r, t)$ .

For spherically symmetric deformations the boundary conditions are given by

$$\sigma_{RR}(R_1, t) = 0, \quad \sigma_{RR}(R_0, t) = -\tilde{p} \quad (12)$$

where  $\sigma_{RR} = \mathbf{e}_r \cdot \boldsymbol{\sigma} \cdot \mathbf{e}_r$ . For brevity, we omitted the awkward computations, see, for details, [9], p. 348.

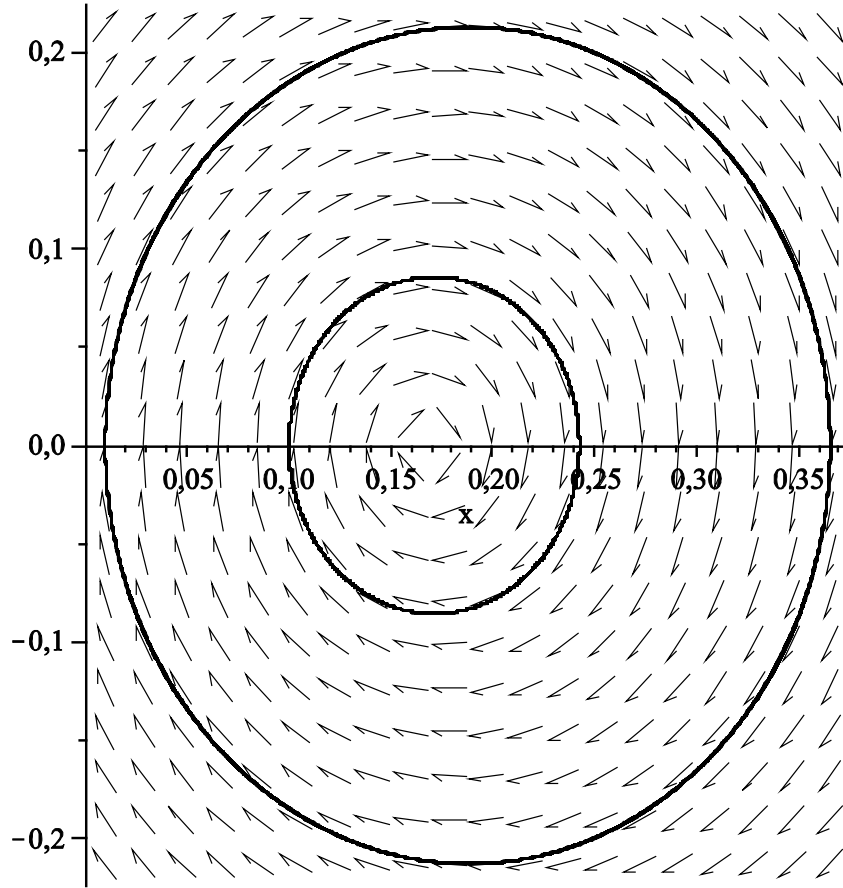


Fig. 1 Phase portrait of (14) in the absence of the magnetic field

Finally, Eqs (5), (12) can be reduced to the ordinary differential equation (ODE) with respect to  $x(t)$

$$\rho \left[ \ddot{x} \frac{R_1 - R_0}{R_1 R_0} - \frac{1}{6} \dot{x}^2 \frac{R_1^4 - R_0^4}{R_1^4 R_0^4} \right] + 12x \int_{r_0}^{r_1} \frac{R^3 + r^3}{R^7} \left( \frac{\partial W}{\partial I_1} + \frac{R^2}{r^2} \frac{\partial W}{\partial I_2} \right) dr = 3\tilde{p} \quad (13)$$

Using (7) Eq. (13) is reduced to

$$\alpha(x)\ddot{x} - \beta(x)\dot{x}^2 + \mu\gamma(x)x = \tilde{p} \quad (14)$$

where

$$\alpha(x) = \frac{1}{3} \rho \frac{R_1 - R_0}{R_1 R_0} > 0, \quad \beta(x) = \frac{1}{18} \rho \frac{R_1^4 - R_0^4}{R_1^4 R_0^4} > 0, \quad \gamma(x) = 4 \int_{r_0}^{r_1} \frac{x + 2r^3}{(x + r^3)^{7/3}} dr$$

are essentially nonlinear functions, and  $\gamma(x)$  can not be expressed in elementary functions.

Equation (14) is nonlinear non-autonomous ODE with respect to  $x(t)$  which can be solved only numerically. Let us assume a sinusoidal behavior of  $B$ :  $B(t) = B_0 \sin \omega t$ , where  $B_0$  is the magnitude, while  $\omega$  is the frequency.

Examples of numerical simulations are presented in Figs 1, 2. In Fig. 1 the phase portrait of (14) in the absence of the magnetic field ( $\mathbf{B} = 0$ ) is shown. Here the following dimensionless parameters  $\bar{r}_0 = 0.9$ ,  $\bar{r}_1 = 1$  ( $\bar{r} = r/r_1$ ),  $\bar{p} \equiv \tilde{p}/\mu = 0.01$  are used, and we keep notation  $x$  for a new dimensionless variable  $x/r_1^3$ . Two closed trajectories correspond to the initial data  $x(0) = 0.01$ ,  $\dot{x}(0) = 0$ , and  $x(0) = 0.1$ ,  $\dot{x}(0) = 0$ , respectively. In Fig. 2 two trajectories correspond to initial data

$x(0) = 0.01$  ,  $\dot{x}(0) = 0$  , and  $x(0) = 0.1$  ,  $\dot{x}(0) = 0$  , respectively. Here  $\bar{\eta} = \eta B_0^2$  and  $\bar{\omega} = \omega T$  ,  $T = \sqrt{\rho/\mu_0}$  , and the time interval is  $[0, 300T]$  . The trajectories of (14) can demonstrate complex behavior. For the case of low values of  $\bar{\eta}$  describing the dependence of the shear modulus on  $B$  one can see the weak influence on the oscillations (see top row in Fig. 2). In this case we have the behavior similar to Fig. 1. The middle and bottom rows in Fig. 2 demonstrate more complex behavior for small frequencies, one can see some type of instabilities. The increase of the frequency of  $B$  leads to the stabilization of oscillations near the solutions with constant  $\mathbf{B}$  similar to the behavior shown in Fig. 1. It means that using the external magnetic field we can “control” in some sense the motion of the sphere.

The MS cylinder demonstrates the analogous behaviour.

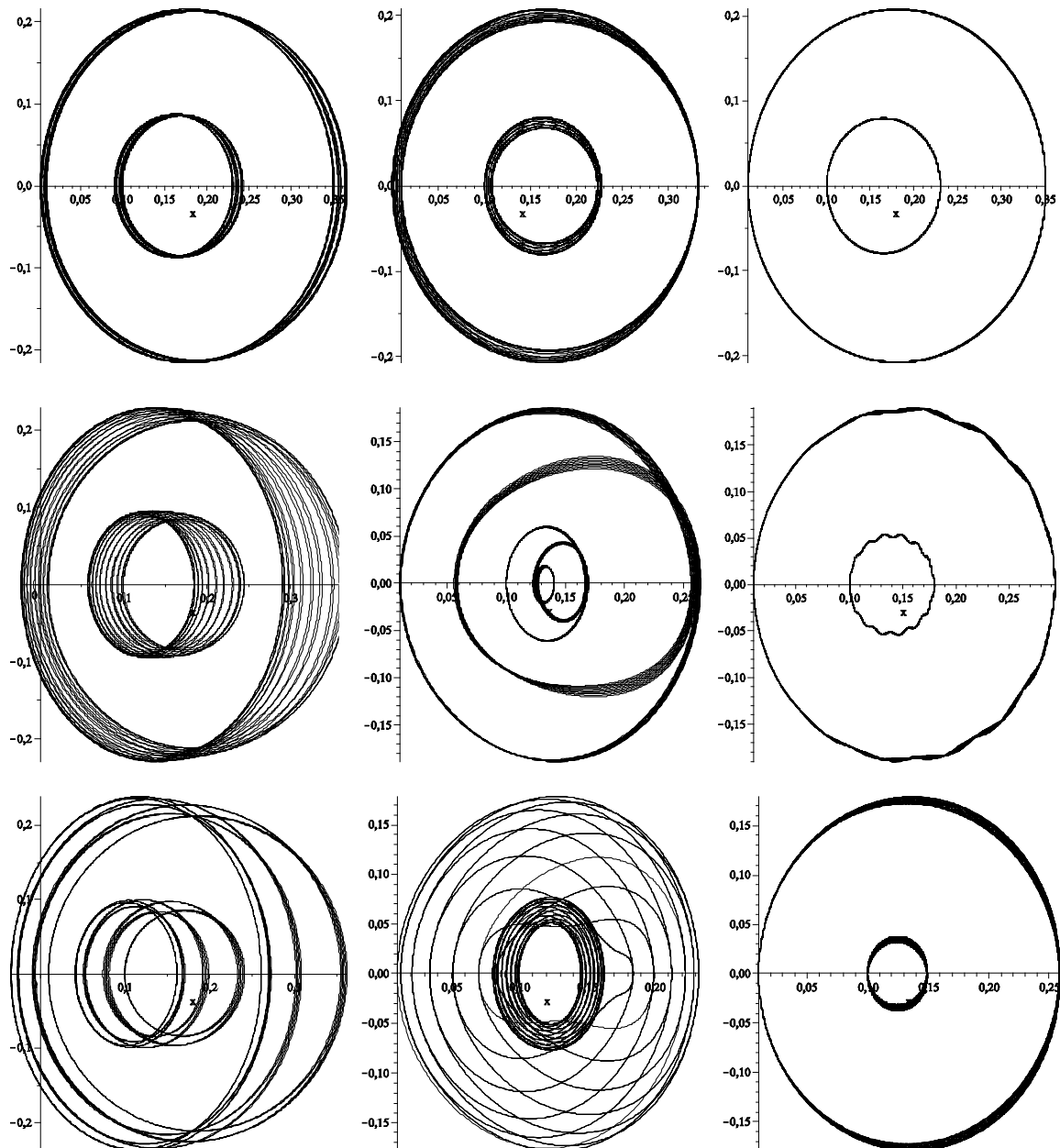


Fig. 2 Examples of trajectories of (14) for different parameters  $\bar{\eta}$  and  $\bar{\omega}$

## CONCLUSIONS

The dynamic statement of the boundary-value problems of MS elastomers under homogeneous with respect to space but time-dependent magnetic field is given. The special property of the boundary-value problem is that the coefficients of the equations of motion may depend on time. As an example, we considered the radially symmetric oscillations of a MS incompressible elastic sphere. It

was shown that using the external magnetic field one can generate and control the oscillations of the sphere. On the other hand, the considered system demonstrates complex behavior which highly depends on the type of external excitation. Such MS elastic sphere under internal pressure may be used, for example, as an actuator or working element of a microengine, based on MS elastomers.

## ACKNOWLEDGEMENTS

The research work was supported by DFG grant AL 341/33-1 and by the Russian Foundation of Basic Research under grant 09-01-00459.

## REFERENCES

- [1] Dorfmann A., Brigadnov I.A. Constitutive modelling of magneto-sensitive Cauchy-elastic solids, *Comput. Mat. Sci.*, Vol. 29, pp. 270-282, 2004.
- [2] Dorfmann A., Ogden R.W. Nonlinear magnetoelastic deformations of elastomers, *Acta Mechanica*, Vol.167, pp. 13-28, 2004.
- [3] Dorfmann A., Ogden R.W. Nonlinear magnetoelastic deformations, *Q. J. Mech. Appl. Math.*, Vol. 57, pp. 599-622, 2004.
- [4] Dorfmann A., Ogden R.W. Some problems in nonlinear magnetoelasticity, *Z. angew. Math. Phys.*, Vol. 56, pp. 718-745, 2005.
- [5] Dorfmann A., Ogden R.W. Nonlinear electroelasticity, *Acta Mechanica*, Vol. 174, pp. 167-183, 2005.
- [6] Dorfmann A., Ogden R.W., Nonlinear electroelastic deformations, *J. Elast.*, Vol. 82, pp. 99-127, 2006.
- [7] Dorfmann A., Ogden R.W., Saccomandi G. Universal relations for non-linear magnetoelastic solids, *Int. J. Non-Linear Mech.*, Vol. 39, pp. 1699-1708, 2004.
- [8] Dorfmann A., Ogden R.W., Saccomandi G. The effect of rotation on the nonlinear magnetoelastic response of a circular cylindrical tube, *Int. J. Solids Struct.*, Vol. 42, pp. 3700-3715, 2005.
- [9] Lurie A.I., *Non-linear Theory of Elasticity*, North-Holland, Amsterdam, 1990.
- [10] Lurie A.I. *Theory of Elasticity*, Springer, Berlin et al. 2005.
- [11] Treloar L.R.G. *The Physics of Rubber Elasticity*, 3<sup>rd</sup> edn, Oxford University Press, Oxford, 1975.
- [12] Altenbach H., Brigadnov I.A., Eremeyev V.A. Oscillations of a magneto-sensitive elastic sphere, *ZAMM*. 2008., Vol. 88, pp. 497 – 506, 2008.

ON THE IMPACT ON A PLATE MADE OF HYPERELASTIC FOAM

H. Altenbach<sup>1</sup>  
V. A. Eremeyev  
M. M. Ievdokymov  
Martin-Luther-University  
Halle-Wittenberg  
Halle, Germany

---

ABSTRACT

---

In the paper we present the results of the finite element modelling of an axisymmetric and non-axisymmetric impact on a circular thick plate made of hyperelastic foam. The nonlinear oscillations and the transient wave's propagation after impact are considered. The finite element analysis is performed using the ANSYS package. Large deformations are taken into account, i.e. the strains attain the level of 600%.

---

INTRODUCTION

Foams are very perspective type of composite materials applied in civil engineering, automotive and space industries [1, 2]. Polymer foams may demonstrate very large elastic strains. Hence, such foam may be considered as a non-linear hyperelastic material. Different models allowing the description of large hyperelastic strains of foams are proposed in the literature.

The existing models of foams may be classified as follows. The first type of models bases on the detailed considerations of the foam cell deformation taking into account the cell structure, the properties of cell walls and struts, the pressure change in the closed cells, etc., see [1-4] among others. The famous Kelvin model belongs to this type. On the other hand the computational efforts may be significant and there is hard to establish experimentally the real material properties of cells. The second class of models uses the description of foam as the continuum with averaged properties. Within the framework of this type models, one takes into account the structure of the foam cells, the solid material, the gas properties and other parameters in the constitutive equations at whole. The Ogden's material model is applied for the finite strains of hyperelastic foams.

Both types of models of hyperelastic foams have advantages and disadvantages. Further we apply the second approach using the Ogden's material model of hyperelastic material for moderate large strains and low level of stress field. We investigate the impact on a clamped circular plate made of hyperelastic foam using the Ogden's material model, see [2] and [5-7]. For some special choice of the material constants, Ogden's strain function  $W$  reduces to other well-known models applied in the nonlinear elasticity (neo-Hookean, Varga, Mooney-Rivlin, Blatz-Ko, etc.). By this way the behaviour of incompressible and compressible elastic materials under finite strain and, in particular, for the high compressive soft foams can be presented. The model is implemented in various finite elements packages like ANSYS, ABAQUS, MSC Marc., etc.

There are many plate-like engineering structures made of foams, for example sandwich plates with a core made of foam, laminates, etc., see [1,2] for details. The variant of the linear theory of plates made of foams summarized in [8].

The paper is organized as follows. In Sect. 1 we recall the basic equation of the three-dimensional theory of nonlinear elasticity. Further in Sect. 2 we present the numerical results. Applying the

---

<sup>1</sup> Corresponding author. Email [holm.altenbach@iw.uni-halle.de](mailto:holm.altenbach@iw.uni-halle.de) (Prof. Dr.-Ing. Holm Altenbach )

implementation in ANSYS we start the investigation with the static axisymmetric contact problem describing the indentation of a smooth rigid ball in a thick plate. The dependence of the plate deflection on the force is obtained. We also analyze the case of non-axisymmetric loading. Then we discuss the impact, i.e. the case when the ball moves with finite velocity. We consider transient waves and nonlinear oscillations of the after impact.

## 1. BASIC EQUATIONS OF 3D NON-LINEAR ELASTICITY

Following [7] in this section we present the general equations governing a finite homogeneous deformation in a compressible elastic material. The Eulerian equilibrium equations of the non-linear body are given by the relations

$$\operatorname{div} \boldsymbol{\tau} + \rho \mathbf{f} = \rho \ddot{\mathbf{r}}, \quad \boldsymbol{\tau} = J^{-1} \mathbf{F} \cdot \mathbf{S}, \quad \mathbf{S} = \frac{\partial W}{\partial \mathbf{F}}, \quad (1)$$

where  $\operatorname{div}$  is the divergence operator in the actual configuration  $\chi$ ,  $\boldsymbol{\tau}$  the Cauchy stress tensor,  $\mathbf{S}$  the 1<sup>st</sup> Piola-Kirchhoff stress tensor,  $\rho$  the material density in the actual configuration,  $\mathbf{r}$  the position vector in the actual configuration,  $\mathbf{f}$  the body force vector per unit mass,  $W$  the strain-energy function (per unit volume),  $J = \det \mathbf{F}$ , and  $\mathbf{F} = \operatorname{Grad} \mathbf{r}$  is the deformation gradient defined as in [7]. Note that here we use the notation  $\mathbf{A} \cdot \mathbf{a}$  and  $\mathbf{A} \cdot \mathbf{B}$  for the second-order tensors  $\mathbf{A}$  and  $\mathbf{B}$ , and a vector  $\mathbf{a}$  instead of the alternative way  $\mathbf{Aa}$ , and  $\mathbf{AB}$ , respectively. Further we assume the isotropic behaviour of the material, so we use the constitutive equation in the following form:

$$W = W(I_1, I_2, I_3) \quad (2)$$

where  $I_1, I_2, I_3$  are the principal invariants of the left Cauchy-Green deformation tensor  $\mathbf{b} = \mathbf{F} \cdot \mathbf{F}^T$  or the right Cauchy-Green deformation tensor  $\mathbf{c} = \mathbf{F}^T \cdot \mathbf{F}$ , defined by

$$\begin{aligned} I_1 &= \operatorname{tr} \mathbf{b} = \operatorname{tr} \mathbf{c} &= \lambda_1^2 + \lambda_2^2 + \lambda_3^2 \\ I_2 &= \frac{1}{2} [\operatorname{tr}^2 \mathbf{b} - \operatorname{tr} \mathbf{b}^2] = \frac{1}{2} [\operatorname{tr}^2 \mathbf{c} - \operatorname{tr} \mathbf{c}^2] &= \lambda_1^2 \lambda_2^2 + \lambda_2^2 \lambda_3^2 + \lambda_1^2 \lambda_3^2 \\ I_3 &= \det \mathbf{b} = \det \mathbf{c} &= \lambda_1^2 \lambda_2^2 \lambda_3^2 \end{aligned}$$

Here  $\lambda_1, \lambda_2, \lambda_3$  are the principal stretches,  $\operatorname{tr}$  denotes the trace of a second-order tensor, and  $(\dots)^T$  denotes transposed.  $\lambda_1, \lambda_2, \lambda_3$  may be also considered as the arguments of the strain function  $W$ :

$$W = W(\lambda_1, \lambda_2, \lambda_3)$$

For the isotropic material  $\mathbf{S}$  and  $\boldsymbol{\tau}$  are given by the relations

$$\begin{aligned} \mathbf{S} &= 2 \frac{\partial W}{\partial \mathbf{c}} \cdot \mathbf{F}^T = (f_0 \mathbf{c}^{-1} + f_1 \mathbf{I} + f_2 \mathbf{c}) \cdot \mathbf{F}^T \\ \boldsymbol{\tau} &= J^{-1} \mathbf{F} \cdot \mathbf{S} = f_0 \mathbf{I} + f_1 \mathbf{b} + f_2 \mathbf{b}^2 \end{aligned} \quad (3)$$

where  $\mathbf{I}$  is the unit second-order tensor,  $f_0, f_1, f_2$  are functions which may be expressed as combinations of the partial derivatives of  $W$  with respect to  $I_i$  or  $\lambda_i$ , see [7,9] for details.

For the description of the non-linear behaviour of polymeric foams the following constitutive equation is widely used [2]

$$\begin{aligned}
W &= \sum_{i=1}^N \frac{2\mu_i}{\alpha_i^2} \left[ \text{tr} \mathbf{b}^{\alpha_i/2} - 3 + \frac{1}{\beta_i} \left( \det \mathbf{F}^{-\alpha_i \beta_i} - 1 \right) \right] \\
&= \sum_{i=1}^N \frac{2\mu_i}{\alpha_i^2} \left[ \lambda_1^{\alpha_i} + \lambda_2^{\alpha_i} + \lambda_3^{\alpha_i} - 3 + \frac{1}{\beta_i} \left( J^{-\alpha_i \beta_i} - 1 \right) \right]
\end{aligned} \tag{4}$$

where  $\mu_i$ ,  $\alpha_i$ ,  $\beta_i$  are the elastic moduli ( $i = 1 \dots N$ ). Here

$$\mu = \sum_{i=1}^N \mu_i$$

denotes the initial shear modulus, while the initial bulk modulus  $k$  is given by

$$k = \sum_{i=1}^N 2\mu_i \left( \beta_i + \frac{1}{3} \right)$$

The model (4) was originally proposed by Ogden [5,6], see also [2,7] among others, where Ogden's model is used. For some special choice of the values  $\mu_i$ ,  $\alpha_i$ ,  $\beta_i$  and  $N$ , Ogden's strain function  $W$  reduces to various others models applied in the nonlinear elasticity (neo-Hookean, Varga, Mooney-Rivlin, Blatz-Ko constitutive equations, etc.).

## 2. NUMERICAL EXAMPLES

As an example we present the finite element analysis (FEA) for thick plate made of foam under the impact. The geometrical model consists of two parts – the plate and the indented rigid ball. The 20-nodes quadratic element SOLID186 is used. The FE model includes 2000 elements and 11000 nodes. Two types of loading are considered – the axisymmetric and non-axisymmetric ones. In both cases clamped boundary conditions on the lateral surface are assumed. Impact is simulated as a short-time contact with the ball. The contact problem is solved with the help the augmented Lagrange method. Free vibrations after impact are investigated numerically. For calculations the Newton-Raphson iterative method is used. During the solution 33000 equations are solved in each step. We used the following set of the Ogden's material constants:

$$\mu_1 = 1,85 \cdot 10^6 \text{ Pa}, \mu_2 = -9,2 \cdot 10^6 \text{ Pa}, \alpha_1 = 4,5, \alpha_2 = -4,5, \beta_1 = 0,92, \beta_2 = 0,92$$

The friction coefficient in the case of rubber-steel contact is assumed to be  $\zeta = 0,2$ .

The transient analyses are made for both plates with symmetrical and unsymmetrical impact cases (Fig. 1).

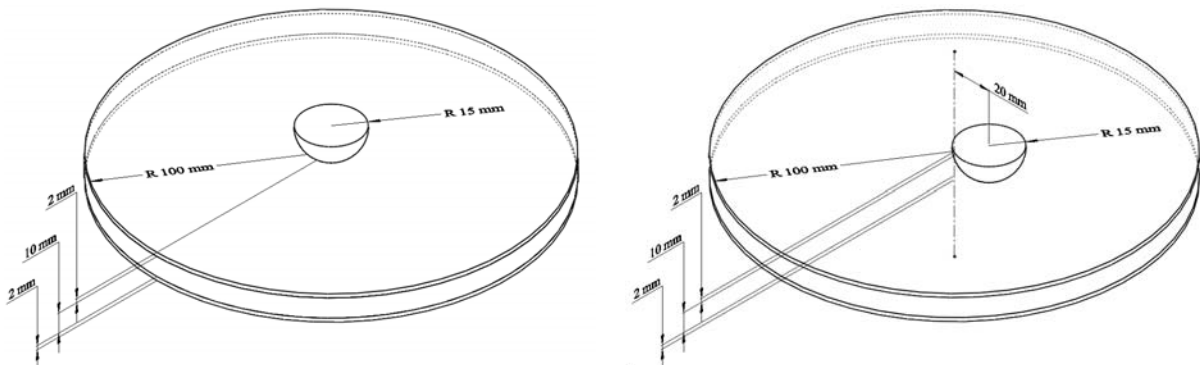
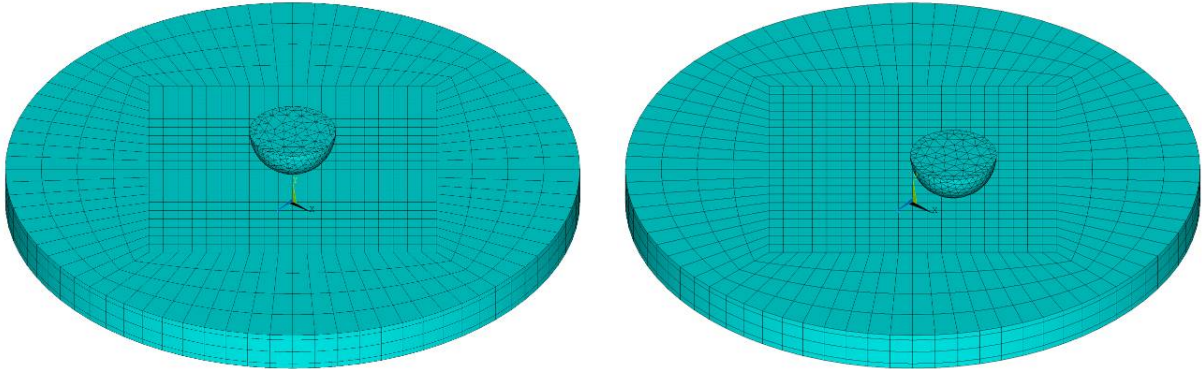


Fig. 1 Geometrical models. Axisymmetric problem (on the left) and the non-axisymmetric problem (on the right)

Numerical calculations were made with the use of program package ANSYS. The mesh of thick plates presented in Fig. 2.



*Fig. 2 Finite element mesh for layered plate for symmetrical and unsymmetrical load case*

All geometrical models include two parts – the plate and the indented rigid ball. The 20-nodes quadratic element SOLID186 is used. The FE model includes 2000 elements and 11000 nodes. Two types of loading are considered - the axisymmetric and non-axisymmetric ones. In both cases clamped boundary conditions are used. Impact is simulated as a short-time contact with the ball. The contact problem is solved with the help the augmented Lagrange method. Free vibrations after impact are investigated numerically. For calculations the Newton-Raphson iterative method is used. During the solution 33000 equations are solved in each step.

The same model, but different material constants are using for inner and outer layers. We introduce the following set of the Ogden's material constants for inner layer:

$$\mu_{in1} = 1,85 \cdot 10^6 \text{ Pa}, \mu_{in2} = -9,2 \cdot 10^6 \text{ Pa}, \alpha_{in1} = 4,5, \alpha_{in2} = -4,5, \beta_{in1} = 0,92, \beta_{in2} = 0,92$$

for outer layer:

$$\mu_{out1} = 1,85 \cdot 10^6 \text{ Pa}, \mu_{out2} = -9,2 \cdot 10^6 \text{ Pa}, \alpha_{out1} = 4,5, \alpha_{out2} = -4,5, \beta_{out1} = 0,92, \beta_{out2} = 0,92$$

The friction coefficient in the case of rubber-steel contact is assumed to be  $\zeta = 0,2$ .

The plate is fixed along lateral surface. Free vibrations of plate after impact by spherical indenter have calculated. Initial conditions applied with the using of three load intervals with different action time. 600% deflection of plate has reached during loading.

As the results displacement fields were obtained for both loading cases in dependence on time. The graph of displacement  $OY$  versus time at the central plate's point is presented in Fig. 3.

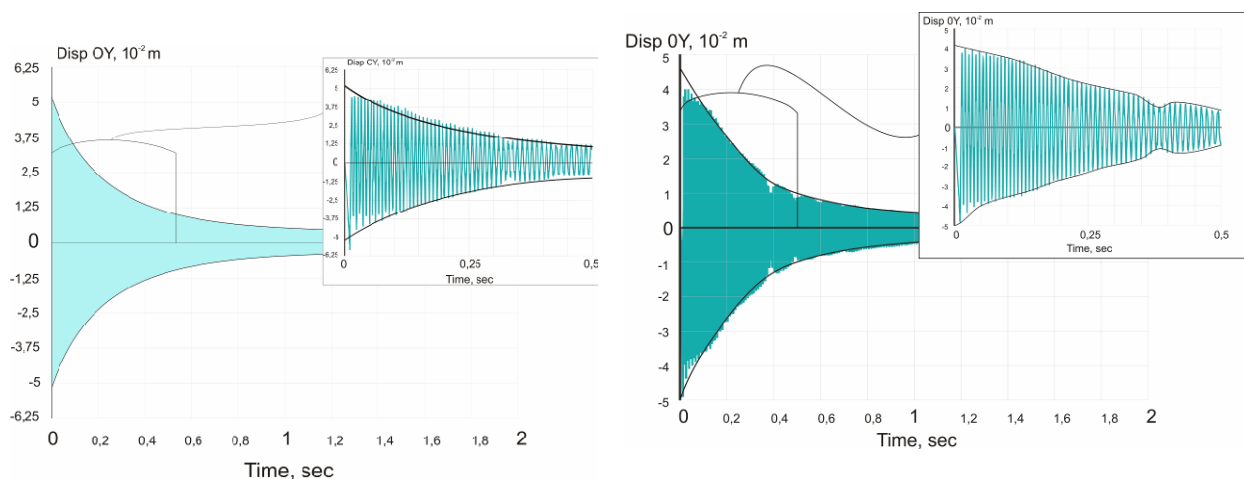


**Fig. 3 Deflections.**  
*Axisymmetric impact (on the left) and non-axisymmetric impact (on the right)*

Displacement fields have calculated for plates with symmetrical and unsymmetrical loading cases and are illustrated for different time values in fig.4.

## CONCLUSIONS

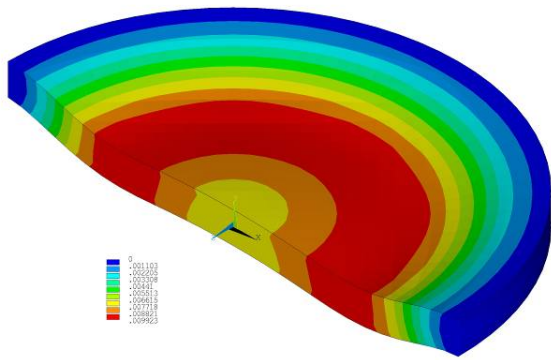
We present the results of numerical calculations of the dynamic behaviour of the thick plate made of hyperelastic foam. For numerical calculations Ogden's material model which implemented in ANSYS is used. The model can describe the large deformations of compressible materials, for example, 500-700% in the tensile tests. Two circular plates are considered. The first one made of homogeneous material while the second one has the sandwich structure. The faces are made of rubber-like material, while the core is made of foam. The impact is modelled by the short action of rigid steel ball and the nonlinear oscillations are investigated. The friction between the ball and plate is taken into account.

## ACKNOWLEDGEMENT

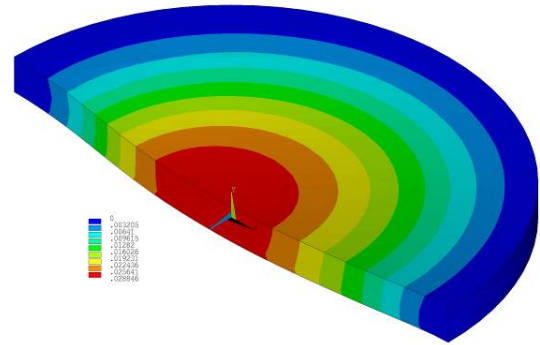
The work was supported by the DFG grant No. 341/33-1 (second author) and PhD scholarship of the state Sachsen-Anhalt (third author).

## REFERENCES

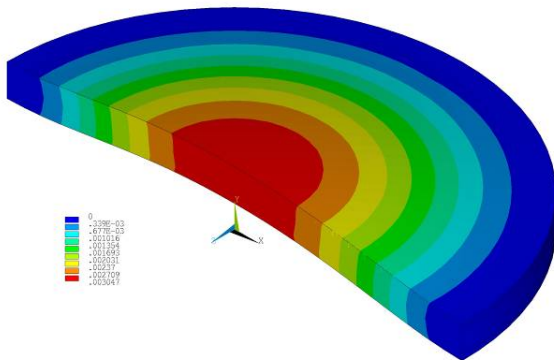
- [1] Gibson L.J., Ashby M.F. *Cellular Solids: Structure and Properties*, 2<sup>nd</sup> Edition, Cambridge Solid State Science Series, Cambridge University Press, Cambridge, 1997.
- [2] Mills N. *Polymer Foams Handbook. Engineering and Biomechanics Applications and Design Guide*, Butterworth-Heinemann, Amsterdam, 2007.
- [3] Mills N.J. The high strain mechanical response of the wet Kelvin model for open-cell foams, *International Journal of Solids and Structures*, Vol. 44, pp. 51-65, 2007.
- [4] Mills N.J., Stämpfli R., Marone F., Brühwiler P.A. Finite element micromechanics model of impact compression of closed-cell polymer foams, *International Journal of Solids and Structures*, Vol. 46, pp. 677-697, 2009.
- [5] Ogden R.W. Large deformation isotropic elasticity - on the correlation of theory and experiment for incompressible rubberlike solids, *Proc. Roy. Soc. London*, Vol. A 326, pp. 565-584, 1972.
- [6] Ogden R.W. Volume changes associated with the deformation of rubber-like solids, *Journal of the Mechanics and Physics of Solids*, Vol. 24, pp. 323-338, 1976.
- [7] Ogden R.W. *Non-Linear Elastic Deformations*, Dover Publications, New York, 1997.
- [8] Altenbach H., Eremeyev V.A. Thin-walled structures made of foams, in: H. Altenbach and A. Öchsner (Ed.), *Cellular and Porous Materials: Modeling - Testing - Application*, CISM Courses and Lecture Notes No. 521, Springer, Wien, 2010, pp. 167-242.
- [9] Lurie A.I. *Nonlinear Theory of Elasticity*, North-Holland, Amsterdam, 1990.



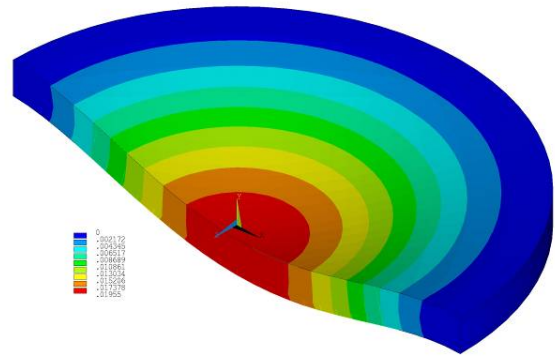
Time = 0,05 sec



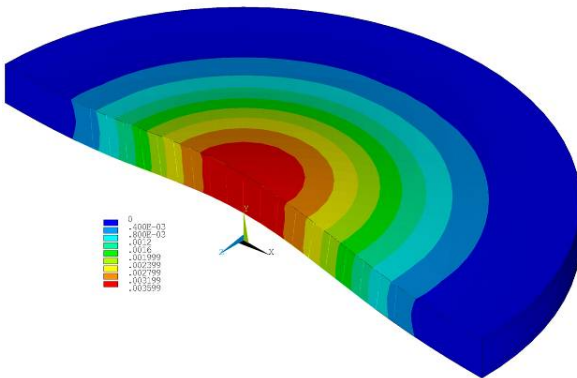
Time = 0,05 sec



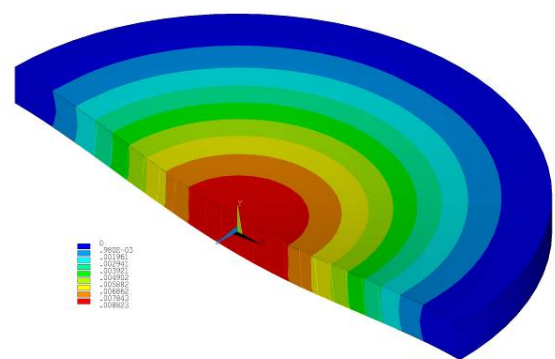
Time = 0,25 sec



Time = 0,25 sec



Time = 0,5 sec



Time = 0,5 sec

Fig. 4 Displacement magnitudes

**POLYNOMIAL VERSUS TRIGONOMETRIC EXPANSIONS FOR NONLINEAR  
VIBRATIONS OF SHELLS WITH DIFFERENT BOUNDARY CONDITIONS**

**Marco Amabili**<sup>1</sup>

Department of Mechanical  
Engineering  
McGill University  
Montreal, Quebec,  
Canada

**Yevgeniy Kurylov,  
Rinaldo Garziera**

Dipartimento di  
Ingegneria Industriale  
Università degli Studi di  
Parma  
Parma, Italy

ABSTRACT

Geometrically nonlinear forced vibrations of circular cylindrical shells with different boundary conditions are investigated. The Sanders-Koiter nonlinear shell theory, which includes in-plane inertia, is used to calculate the elastic strain energy. The shell displacements (longitudinal, circumferential and radial) are expanded by means of a double mixed series: harmonic functions for the circumferential variable and two different formulations for the longitudinal variable; these two different formulations are: (a) Chebyshev orthogonal polynomials and (b) trigonometric functions. The same formulation is applied to study different boundary conditions; results are presented for simply supported, clamped and cantilever shells. The analysis is performed in two steps: first a linear analysis is performed to identify natural modes, which are then used in the nonlinear analysis as generalized coordinates. The Lagrangian approach is applied to obtain a system of nonlinear ordinary differential equations. Different expansions involving from 14 to 40 generalized coordinates, associated with natural modes of simply supported, clamped-clamped and cantilever shells are used to study the convergence of the solution. The nonlinear equations of motion are studied by using arclength continuation method and bifurcation analysis. Numerical responses obtained in the spectral neighborhood of the lowest natural frequency are compared with results available in literature.

**INTRODUCTION**

A great number of studies on geometrically nonlinear vibrations of circular cylindrical shells is available; the literature published before 2003 has been reviewed by Amabili and Païdoussis [1]. The problem is also amply discussed by Amabili in his recent monograph [2]. Here the attention is focused on large-amplitude free and forced vibrations under harmonic excitation in radial direction. In the majority of the studies Donnell's nonlinear shallow-shell theory is applied to model the problem; see, e.g. Refs. [3-6]. However, more refined classical theories have been also used, including Donnell nonlinear shell theory retaining in-plane inertia, the Sanders-Koiter (also referred as Sanders) nonlinear shell theory, the Flügge-Lur'e-Byrne nonlinear shell theory and the Novozhilov nonlinear shell theory [7-12].

The literature review shows that several methods were developed in the past for investigating nonlinear vibrations of circular cylindrical shells with different boundary conditions. Therefore, the present study is a contribution toward developing a general framework that allows studying circular shells with different boundary conditions, comparing different expansions of mode shapes.

**1. STRAIN AND KINETIC ENERGY**

In Fig. 1, a circular cylindrical shell having radius  $R$ , length  $L$  and thickness  $h$  is represented; a cylindrical coordinate system ( $O; x, r, \theta$ ) is considered in order to take advantage of the axial symmetry of the structure; the origin is placed at the centre of one end of the shell. Three displacement fields are shown in Fig. 1: axial  $u(x, \theta, t)$ , circumferential  $v(x, \theta, t)$  and radial  $w(x, \theta, t)$

<sup>1</sup> Corresponding author. Email marco.amabili@mcgill.ca

displacement. Geometric imperfections can be considered in the theory by means of initial radial displacements  $w_0(x, \theta)$ .

The nonlinear Sanders–Koiter shell theory is used, which is a classical theory derived by using the following assumptions: (i)  $h \ll R$  and  $h \ll L$ ; (ii) the displacements are of the order of the shell thickness  $h$ ; (iii) strains are small; (iv) transverse normal stresses are negligible; (v) the normal to the undeformed middle surface remains straight and normal to the middle surface after deformation, and no thickness stretching is present (Kirchhoff–Love kinematic hypothesis); and (vi) rotary inertia is neglected.

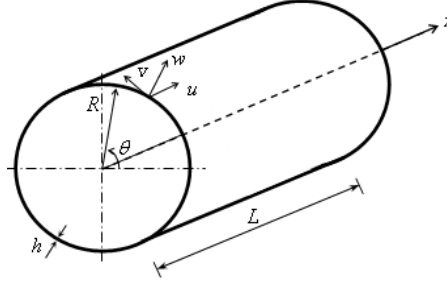


Fig. 1 Circular cylindrical shell: coordinate system and dimensions

The elastic strain energy  $U_S$  of a circular cylindrical shell is given by [2]

$$\begin{aligned}
 U_S = & \frac{1}{2} \frac{Eh}{1-\nu^2} LR \int_0^{2\pi} \int_0^L \left( \varepsilon_{x,0}^2 + \varepsilon_{x\theta,0}^2 + 2\nu \varepsilon_{x,0} \varepsilon_{x\theta,0} + \frac{1-\nu}{2} \gamma^2 \right) d\eta d\theta \\
 & + \frac{1}{2} \frac{Eh^3}{12(1-\nu^2)} LR \int_0^{2\pi} \int_0^L \left( k_x^2 + k_\theta^2 + 2\nu k_x k_\theta + \frac{1-\nu}{2} k_{x\theta}^2 \right) d\eta d\theta \\
 & + \frac{1}{2} \frac{Eh^3}{6R(1-\nu^2)} LR \int_0^{2\pi} \int_0^L \left( \varepsilon_{x,0} k_{x\theta,0} + \nu \varepsilon_{x\theta,0} k_{x,0} + \nu \varepsilon_{x\theta,0} k_{\theta,0} + k_x + \frac{1-\nu}{2} k_{x\theta} \right) d\eta d\theta + O(h^4),
 \end{aligned} \quad (1)$$

where  $O(h^4)$  is a higher-order term in  $h$  according to the Sanders–Koiter theory. The middle surface strain-displacement relationships and changes in the curvature and torsion for a circular cylindrical shell according to Sanders–Koiter nonlinear shell theory should be found in [2, 13 and 14]. The right-hand side of equation (5) can be easily interpreted: the first term is the membrane (also referred as stretching) energy and the second one is the bending energy, while the last term couples the membrane and bending energies.  $E$  is Young’s modulus and  $\nu$  is the Poisson’s ratio.

The kinetic energy  $T_S$  of a circular cylindrical shell, by neglecting rotary inertia, is given by

$$T_S = \frac{1}{2} \rho_s h LR \int_0^{2\pi} \int_0^L \left( \dot{u}^2 + \dot{v}^2 + \dot{w}^2 \right) d\eta d\theta \quad (2)$$

where  $\rho_s$  is the mass density of the shell. In equation (2) the overdot denotes time derivative.

## 2. LINEAR VIBRATIONS. MODAL ANALYSIS

In order to carry out a linear vibration analysis, in the present section, linear Sanders–Koiter theory is considered, i.e. in equation (2), only quadratic terms are retained. The best basis for expanding displacement fields is the eigenfunction basis, but only for special boundary conditions such basis can be found analytically; generally, eigenfunctions must be evaluated numerically.

Displacement fields are expanded by means of a double series: deformation in the circumferential direction is presented by harmonic functions, Chebyshev polynomials are considered in the axial direction. Let us now consider a modal vibration, i.e. a synchronous motion:

$$u(\eta, \theta, t) = U(\eta, \theta) f(t), \quad v(\eta, \theta, t) = V(\eta, \theta) f(t), \quad w(\eta, \theta, t) = W(\eta, \theta) f(t), \quad (3)$$

where  $U(\eta, \theta)$ ,  $V(\eta, \theta)$  and  $W(\eta, \theta)$  represent a modal shape. Now the modal shape is expanded in a double series in terms of Chebyshev polynomials  $T_m^*(\eta)$  and harmonic functions:

$$U(\eta, \theta) = \sum_{m=0}^{M_U} \sum_{n=0}^N \tilde{U}_{m,n} T_m^*(\eta) \cos n\theta, \quad V(\eta, \theta) = \sum_{m=0}^{M_V} \sum_{n=0}^N \tilde{V}_{m,n} T_m^*(\eta) \sin n\theta, \quad W(\eta, \theta) = \sum_{m=0}^{M_W} \sum_{n=0}^N \tilde{W}_{m,n} T_m^*(\eta) \cos n\theta, \quad (4)$$

where  $T_m^*(\eta) = T_m(2\eta - 1)$  and  $T_m(\cdot)$  is the  $m$ -th order Chebyshev polynomial.

## 2.1 Boundary conditions

Boundary conditions are considered by applying constraints to the free coefficients of expansion (4). Some of the coefficients  $\tilde{U}_{m,n}, \tilde{V}_{m,n}, \tilde{W}_{m,n}$  can be suitably chosen in order to satisfy boundary conditions.

For the simply supported shell the following boundary conditions are imposed for the mode shape:

$$w = 0, \quad v = 0, \quad M_x = 0, \quad N_x = 0 \quad \text{for } \eta = 0, 1, \quad (5)$$

Such conditions are valid for any  $\theta$  and  $n$ , therefore equations (5) are modified as follows:

$$\begin{aligned} \sum_{m=0}^{M_W} \tilde{W}_{m,n} T_m^*(\eta) = 0, \quad \sum_{m=0}^{M_V} \tilde{V}_{m,n} T_m^*(\eta) = 0, \quad \sum_{m=0}^{M_W} \tilde{W}_{m,n} T_{m,\eta\eta}^*(\eta) = 0, \quad \sum_{m=0}^{M_U} \tilde{U}_{m,n} T_{m,\eta}^*(\eta) = 0 \\ n = 0, 1, \dots \quad \text{for } \eta = 0, 1. \end{aligned} \quad (6)$$

The linear algebraic system (6) is solved in terms of the coefficients  $\tilde{U}_{1,n}, \tilde{U}_{2,n}, \tilde{V}_{0,n}, \tilde{V}_{1,n}, \tilde{W}_{0,n}, \tilde{W}_{1,n}, \tilde{W}_{2,n}, \tilde{W}_{3,n}$ ,  $n = 0, 1, \dots$ ; which can be obtained exactly in terms of remaining unknown coefficients.

For the clamped-clamped shell the following boundary conditions are imposed for the mode shape:

$$w = 0, \quad w_{,\eta\eta} = 0, \quad v = 0, \quad u = 0 \quad (7)$$

For the clamped-free shell the following boundary conditions are imposed for the mode shape:

$$w = v = u = \frac{\partial w}{\partial x} = 0 \quad \text{for } \eta = 0 \quad (8a)$$

$$N_x = N_{x\theta} + \frac{M_{x\theta}}{R} = M_x = Q_x + \frac{\partial M_{x\theta}}{R \partial \theta} = 0 \quad \text{for } \eta = 1 \quad (8b)$$

The procedure is formally the same as for simply supported boundary conditions; however, the resulting linear systems for clamped-clamped and cantilever shells are solved in terms of the following coefficients.

## 2.2 Discretization

Equations (3) and (4) are inserted into the expressions of kinetic and potential energy (for the linear system); then a set of ordinary differential equations is obtained by using Lagrange equations.

An intermediate step is the reordering of variables. A vector  $q$  containing all variables is built depending on boundary conditions [12]. For simply-supported (a), clamped-clamped (b) and clamped-free (c) shell one will have:

$$q = [\tilde{U}_{0,0}, \tilde{U}_{3,0}, \dots, \tilde{U}_{0,1}, \tilde{U}_{3,1}, \dots, \tilde{V}_{2,0}, \tilde{V}_{3,0}, \dots, \tilde{V}_{2,1}, \tilde{V}_{3,1}, \dots, \tilde{W}_{4,0}, \tilde{W}_{5,0}, \dots, \tilde{W}_{4,1}, \tilde{W}_{5,1}, \dots] f(t) \quad (9a)$$

$$q = [\tilde{U}_{2,0}, \tilde{U}_{3,0}, \dots, \tilde{U}_{2,1}, \tilde{U}_{3,1}, \dots, \tilde{V}_{2,0}, \tilde{V}_{3,0}, \dots, \tilde{V}_{2,1}, \tilde{V}_{3,1}, \dots, \tilde{W}_{4,0}, \tilde{W}_{5,0}, \dots, \tilde{W}_{4,1}, \tilde{W}_{5,1}, \dots] f(t) \quad (9b)$$

$$q = [\tilde{U}_{1,0}, \tilde{U}_{2,0}, \dots, \tilde{U}_{1,1}, \tilde{U}_{2,1}, \dots, \tilde{V}_{1,0}, \tilde{V}_{2,0}, \dots, \tilde{V}_{1,1}, \tilde{V}_{2,1}, \dots, \tilde{W}_{2,0}, \tilde{W}_{3,0}, \dots, \tilde{W}_{2,1}, \tilde{W}_{3,1}, \dots] f(t) \quad (9c)$$

Lagrange equations for free vibrations are

$$\frac{d}{dt} \left( \frac{\partial L}{\partial \dot{q}_i} \right) - \frac{\partial L}{\partial q_i} = 0, \quad i = 1, 2, \dots, N_{\max} \quad (10)$$

Using (9) and considering harmonic motion,  $f(t) = e^{j\omega t}$ , one obtains

$$(-\omega^2 M + K) q = 0 \quad (11)$$

which is the classical nonstandard eigenvalue problem that furnishes frequencies and modes of vibration.

A modal shape corresponding to the  $j$ -th mode is given by equations (4), where  $\tilde{U}_{m,n}, \tilde{V}_{m,n}, \tilde{W}_{m,n}$  are substituted with  $\tilde{U}_{m,n}^{(j)}, \tilde{V}_{m,n}^{(j)}, \tilde{W}_{m,n}^{(j)}$ , which are components of the  $j$ -th eigenvector of equation (11).

### 3. NUMERICAL RESULTS

The equations of motion have been obtained by using the *Mathematica* 6 computer software. The generic Lagrange equation  $j$  is divided by the modal mass associated with  $\ddot{q}_j$  and then is transformed in two first-order equations. The resulting  $2 \times \text{dofs}$  equations are studied by using the software AUTO 97 [15] for continuation and bifurcation analysis of nonlinear ordinary differential equations.

#### 3.1 Simply supported shell

A test case of a simply supported circular cylindrical shell is analyzed. Calculations have been performed for a shell having the following dimensions and material properties:  $L = 0.2$  m,  $R = 0.1$  m,  $h = 0.247$  mm,  $E = 71.02 \times 10^9$  Pa,  $\rho = 2796$  kg/m<sup>3</sup> and  $\nu = 0.31$ , which corresponds to a case studied by several authors [5, 10, 11].

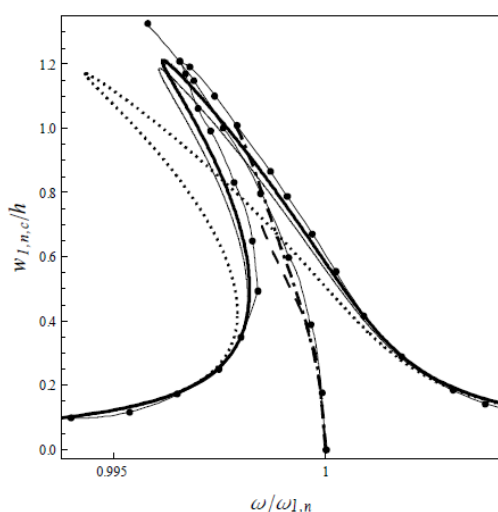


Fig. 2 Frequency response-curve for simply-supported shell. 28 dofs model (bold line) comparing with results available in literature [5, 10, 11]

Fig. 2 shows the frequency-response curve (computed by using the model with 28 dofs) of the driven mode ( $A_{m=1,n=6}(t)$ ) with companion mode participation, namely the following modes:

$$\begin{aligned} w: & (1,n), (1,2n), (1,0)-(5,0); \\ u: & (1,n), (1,2n), (1,0)-(5,0), (3,2n); \\ v: & (1,n), (1,2n), (3,2n), (1,4n), (3,4n), (1,3n). \end{aligned} \quad (12)$$

The amplitude of the external modal excitation is  $f_{1,6} = 0.0012h^2\rho\omega^2$  and the damping ratio is  $2\zeta_{1,6} = 0.001$ . The linear circular frequency of the driven and companion modes is  $\omega_{1,6} = 2\pi \times 553.33$  rad/s. Fig. 2 shows reasonably good agreement between the present results and those obtained previously.

Convergence of model (12) has also been studied, but for brevity sake it is not presented in this paper. More details one should find in [16]. Frequency-response relationship with companion mode participation (i.e. the actual response of the shell) for the model (12) should also be found there.

#### 3.2 Clamped shell

Calculations have been performed for a shell having the following dimensions and material properties:  $L = 520$  mm,  $R = 149.4$  mm,  $h = 0.519$  mm,  $E = 1.98 \times 10^{11}$  Pa,  $\rho = 7800$  kg/m<sup>3</sup> and  $\nu = 0.3$ .

The response of the circular cylindrical shell subjected to harmonic point excitation of 3 N applied in the middle of the shell in the neighbourhood of the lowest (fundamental) resonance

$\omega_{1,n} = 2\pi \times 313.7$  rad/s, corresponding to mode ( $m = 1, n = 6$ ), is given in Figure 3; only the principal (resonant) coordinates, corresponding to driven (a) and companion (b) modes, are shown for brevity. Calculations reported in this section have been performed by using an expansion involving 34 generalized coordinates (with companions), namely:

$$\begin{aligned} w: & (1,n), (1,2n), (3,2n), (1,0)-(9,0); \\ u: & (1,n), (1,2n), (3,2n), (1,0)-(9,0); \\ v: & (1,n), (1,2n), (3,n), (3,2n). \end{aligned} \quad (13)$$

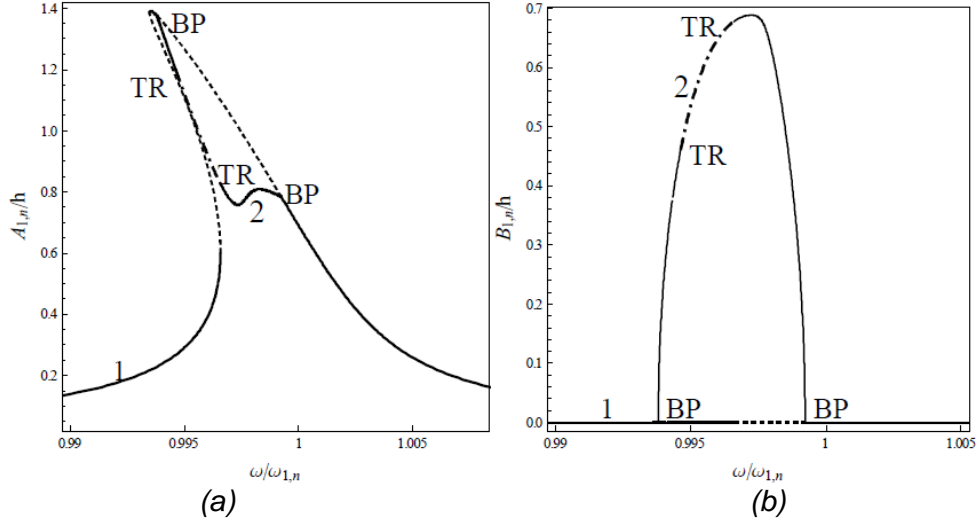


Fig. 3 Frequency-response curve for clamped shell with companion mode participation. —, Stable periodic solution; -·-, stable quasi-periodic solution; - -, unstable solutions; BP, pitchfork bifurcation; TR, Neimark-Sacker bifurcation.

Convergence of model (13) as well as comparison with results, available in literature, should be found in [16].

### 3.3 Cantilever shell

Test cases of perfect cantilever circular cylindrical shell and shell with imperfections are analyzed. Calculations have been performed for a shell having the following dimensions and material properties:  $L = 0.48$  m,  $R = 0.24$  m,  $h = 0.254$  mm,  $E = 4.65 \times 10^9$  Pa,  $\rho = 1400$  kg/m<sup>3</sup> and  $\nu = 0.38$ , which corresponds to a case studied experimentally by Chiba [17]. The mode investigated is ( $m=1, n=7$ ) which has one longitudinal half-wave and 7 circumferential waves.

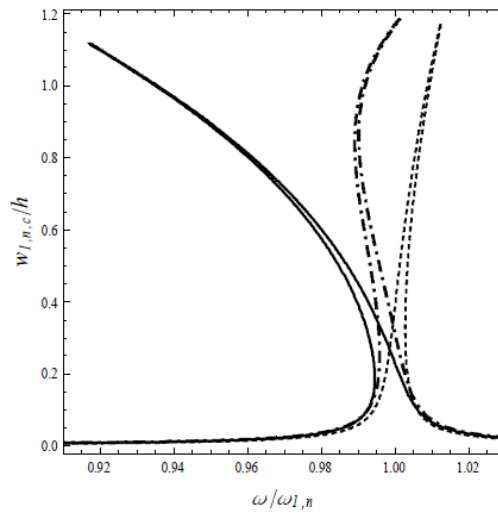


Fig. 4 Frequency-response curve for cantilever shell with imperfections having different magnitude: one thickness imperfection (dashed-dotted line), two thickness magnitude (solid line), no imperfection (dashed line).

Fig. 4 shows that presence of imperfections can significantly change the behavior of the system. Moreover, type of the system response depends also on magnitude of imperfection.

## CONCLUSIONS

The response of circular cylindrical shells with different boundary conditions has been computed by using Sanders-Koiter theory. Displacement fields were expanded by means of a double series: deformation in the circumferential direction is presented by harmonic functions, Chebyshev polynomials were considered in the axial direction.

The approach used in the present study has the advantage of being suitable to be applied to different boundary conditions, of satisfying them exactly and of being very flexible to structural modifications without complication of the solution procedure. Comparison of the present study results with results available in literature was carried out and showed good agreement.

More details of the present study should be found in [16]. Detailed report on nonlinear vibrations of cantilever shells will be published soon.

## ACKNOWLEDGEMENTS

The authors acknowledge the important help of Prof. Pellicano. The first author thanks NSERC of CANADA for his Canada Research Chair (Tier 1) and Discovery Grant, and the Canada Foundation for Innovation for the Leaders Opportunity Fund (LOF).

## REFERENCES

- [1] M. Amabili and M. P. Païdoussis, Review of studies on geometrically nonlinear vibrations and dynamics of circular cylindrical shells and panels, with and without fluid-structure interaction. *Applied Mechanics Reviews*, 56, pp. 349-381, 2003.
- [2] M. Amabili, *Nonlinear Vibrations and Stability of Shells and Plates*. New York, USA: Cambridge University Press; 2008.
- [3] D. A. Evensen, Nonlinear flexural vibrations of thin-walled circular cylinders. *NASA TN D-4090*; 1967.
- [4] E. H. Dowell and C. S. Ventres, Modal equations for the nonlinear flexural vibrations of a cylindrical shell. *International Journal of Solids and Structures*, 4, pp. 975-991, 1968.
- [5] J. C. Chen and C. D. Babcock, Nonlinear vibration of cylindrical shells. *AIAA Journal*, 13, pp. 868-876, 1975.
- [6] V. D. Kubenko, P. S. Koval'chuk and T. S. Krasnopol'skaya, Effect of initial camber on natural nonlinear vibrations of cylindrical shells. *Soviet Applied Mechanics*, 18, pp. 34-39, 1982.
- [7] M. Amabili, Nonlinear vibrations of circular cylindrical shells with different boundary conditions. *AIAA Journal*, 41, pp. 1119-1130, 2003.
- [8] M. Amabili, Theory and experiments for large-amplitude vibrations of empty and fluid-filled circular cylindrical shells with imperfections. *Journal of Sound and Vibration*, 262, pp.921-975, 2003.
- [9] P. B. Gonçalves and R. C. Batista, Non-linear vibration analysis of fluid-filled cylindrical shells. *Journal of Sound and Vibration*, 127, pp. 133-143, 1988.
- [10] M. Ganapathi and T. K. Varadan, Large amplitude vibrations of circular cylindrical shells. *Journal of Sound and Vibration*, 192, pp. 1-14, 1996.
- [11] M. Amabili, Comparison of different shell theories for large-amplitude vibrations of empty and fluid-filled circular cylindrical shells with and without imperfections: Lagrangian approach. *Journal of Sound and Vibration*, 264, pp. 1091-1125, 2003.
- [12] F. Pellicano, Vibrations of circular cylindrical shells: Theory and experiments. *Journal of Sound and Vibration*, 303, pp. 154-170, 2007.
- [13] J. L. Sanders Jr., Nonlinear theories for thin shells. *Quarterly of Applied Mathematics*, 21, pp. 21-36, 1963.
- [14] W. T. Koiter, On the nonlinear theory of thin elastic shells. I, II, III. *Proceedings Koninklijke Nederlandse Akademie van Wetenschappen*, B 69, pp. 1-54, 1966.
- [15] E. J. Doedel, A. R. Champneys, T. F. Fairgrieve, Y. A. Kuznetsov, B. Sandstede and X. Wang, *AUTO 97: Continuation and Bifurcation Software for Ordinary Differential Equations (with HomCont)*. Montreal, Canada: Concordia University; 1998.
- [16] Ye. Kurylov, M. Amabili, Polynomial versus trigonometric expansions for nonlinear vibrations of circular cylindrical shells with different boundary conditions. *Journal of Sound and Vibration*, 329, pp. 1435-1449, 2010.
- [17] M. Chiba, Non-linear hydroelastic vibration of a cantilever cylindrical tank – I. Experiment (Empty case). *International Journal of Non-Linear Mechanics* 28, pp. 591-599, 1993.

## NONLINEAR DYNAMICS OF TRAVELING WAVES OF CIRCULAR PLATES WITH CUTOUTS

**Konstantin V. Avramov**<sup>1</sup>

A.N. Podgorny Institute for  
Mechanical Engineering  
Problems  
Kharkov, Ukraine

---

### ABSTRACT

---

Geometrically nonlinear vibrations of circular plate with two cutouts are simulated by the von Karman equations with respect to displacements. R-functions are applied to obtain the vibrations modes of this plate. The nonlinear vibrations of the plate are expanded using these vibrations modes. The nonlinear dynamical system with three degree-of-freedom is derived by the Galerkin method. This system is studied by the multiple scales method.

---

The circular plate with two cutouts (Fig.1) is considered. It is assumed, that the deformations-displacements relations are nonlinear and strains-deformations relations are linear. Vibrations are treated in cylindrical coordinates  $(r, \theta, z)$ . Then the displacements of the plates material points along  $(r, \theta, z)$  are denoted by  $u_r, u_\theta, u_z$ , respectively.

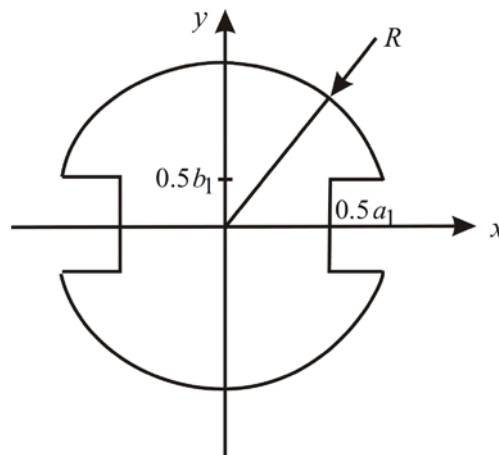


Fig.1 Circular plate with two cutouts

The Galerkin method is used to discretize the equations of plate vibrations. Then the nonlinear vibrations of plates with cutouts are expanded using eigenmodes of linear vibrations. The Rayleigh-Ritz method is used to obtain eigenmodes of vibrations. In order to satisfy the boundary conditions, the equation of the plate boundary (Fig.1) is obtained analytically. The R- function method is used to construct analytically this boundary.

The eigenmodes of circular plate with two cutouts can be presented in the following form:

$$\bar{u}_z(r, \theta) = \omega^2(r, \theta) \sum_{k=0}^m [Z_k^{(c)}(r) \cos(k\theta) + Z_k^{(s)}(r) \sin(k\theta)];$$

---

<sup>1</sup> Konstantin V. Avramov. Email [kvavr@kharkov.ua](mailto:kvavr@kharkov.ua).

$$\bar{u}_\theta(r, \theta) = \omega(r, \theta) \sum_{k=0}^m [\Theta_k^{(c)}(r) \cos(k\theta) + \Theta_k^{(s)}(r) \sin(k\theta)];$$

$$\bar{u}_r(r, \theta) = \omega(r, \theta) \sum_{k=0}^m [R_k^{(c)}(r) \cos(k\theta) + R_k^{(s)}(r) \sin(k\theta)].$$

The nonlinear dynamics of plate is described by three degree-of-freedom nonlinear dynamical system, which can be presented in the following form:

$$\ddot{q}_k + p_k^2 q_k = \sum_{i=1}^3 \sum_{l=1}^3 \sum_{\mu=1}^3 G_{il\mu}^{(k)} q_i q_l q_\mu; k = \overline{1,3}.$$

The multiple scales method is used to study this system.

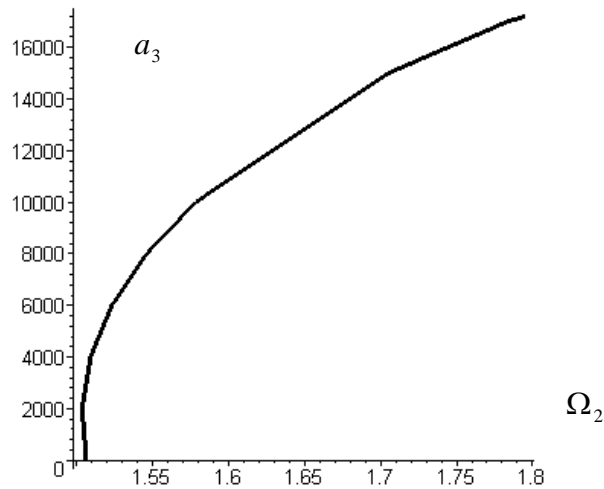


Fig.2 The backbone curves of two conjugate modes

As a result of calculations the backbone curve of traveling waves is shown on Fig.2. The complete analysis of this problem is published in the paper [1].

## REFERENCES

- [1] Avramov K.V., Tyshkovets O., Maksymenko-Sheyko K.V. Analysis of nonlinear free vibration of circular plates with cut-outs using R-function method. *ASME J. of Vibration and Acoustics*, Vol. 132 (in press).

**NONLINEAR DYNAMICS OF PLATES AND SHALLOW SHELLS INTERACTING  
WITH MOVING FLUID**

**Konstantin V. Avramov<sup>1</sup>**  
**Helena Strel'nikova**  
**Ivan Breslavsky**

A.N. Podgorny Institute for  
Mechanical Engineering  
Problems  
Kharkov, Ukraine

---

ABSTRACT

---

Self-sustained vibrations of plates at two-sided interaction with moving fluid are considered. Fluid-structure interaction is described by a hyper singular integral equation, which is solved by Galerkin method. The plate performs geometrical nonlinear vibrations, which is described by finite-degree-of-freedom nonlinear dynamical system. Nonlinear modes are developed to analyze the self-sustained vibrations.

---

**INTRODUCTION**

Interaction of thin-walled structures with moving fluid or gas takes place in marine engineering, energetic and aerospace engineering. For example, dynamic stability of ship hydrofoil and dynamics of propeller are encountered in engineering. Many efforts were made to analyze interaction of thin-walled structures with fluid and gas flow. Aero elasticity of plates, shallow and cylindrical shells is treated in the book [1]. Dowell [2] considered the dynamics of one-dimensional structure in the flow, which is described by linear piston theory. Galerkin method is used to derive finite-degree-of-freedom model. Bolotin, Grishko et. al. [3] is considered the elastic plate in the flow with supersonic speed. Many-valued steady states in the finite-degree-of-freedom model are analyzed by the direct numerical integration. Bolotin, Petrovsky et. al. [4] are studied the motions of panel in the region of divergence and flutter instabilities. It is shown [10] that six eigenmodes are enough for adequate simulation of the plate under the action of constant load in a flow. However, for some values of the system parameters, the number of modes for flutter description is equal to 30. Tang, Dowell [20] are analyzed the plate in subsonic flow. It is assumed that the flow is potential. Vortex lattice method is used to describe a fluid-structure interaction. Aero elastic instability of plate in subsonic flow is analyzed in the paper [21]. 2D, incompressible flow is considered; the pressure acting on the plate is described by linear hyper singular integral equation. The vibrations of aerodynamic surface are described by two-degree-of-freedom system in the paper [22]. The action of incompressible flow on vibrating surface is described by the lifting force and moments. Dynamics of the system is described by two nonlinear integro- differential equations.

In this paper moving fluid interacting with a plate is considered; self-sustained vibrations of the plate with geometrical nonlinearity are analyzed. The interaction of a fluid with a plate is described by the hyper singular integral equation, which is solved by Galerkin method. Self-sustained vibrations of a plate are described by finite-degree-of-freedom nonlinear dynamical system. Variant of Shaw-Pierre nonlinear modes is suggested to analyze self-sustained vibrations. Using this approach, the flutter of plate is analyzed.

**1. PROBLEM FORMULATION**

Dynamics of simply supported plate in the flow of incompressible potential fluid is considered. The flow at a distance from the plate has constant velocity  $V$  (Fig.1). The fluid dynamics is described by velocity potential  $\varphi(x, y, z, t)$ . Lateral displacements of the plate are denoted by  $w(x, y, t)$ . As normal component of the plate velocities is equal to the normal component of fluid velocities, the following relations are true:

$$\left. \frac{\partial \varphi}{\partial z} \right|_{z=w+0} = V \frac{\partial w}{\partial x} + \frac{\partial w}{\partial t}; \quad \left. \frac{\partial \varphi}{\partial z} \right|_{z=w-0} = V \frac{\partial w}{\partial x} + \frac{\partial w}{\partial t}. \quad (1)$$

---

<sup>1</sup> Konstantin V. Avramov. Email [kvavr@kharkov.ua](mailto:kvavr@kharkov.ua).

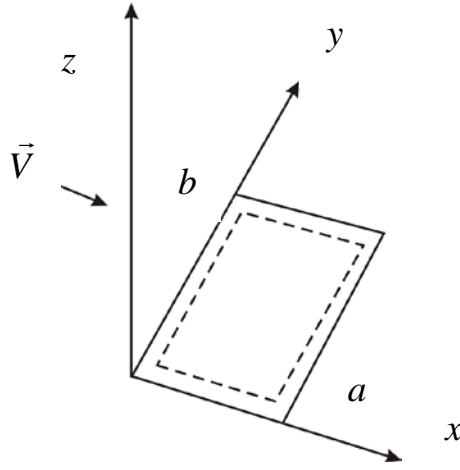


Fig. 1 Sketch of mechanical system

Using the Bernoulli's equation, the pressure acting on the plate is obtained in the following form:

$$\frac{p_+ - p_-}{\rho_w} = \frac{\partial(\varphi_- - \varphi_+)}{\partial t} + V \frac{\partial(\varphi_- - \varphi_+)}{\partial x}, \quad (2)$$

where  $p_+, p_-$  are fluid pressure acting on upper and lower sides of the plate;  $\varphi_+; \varphi_-$  are values of velocities potentials on upper and lower sides of the plate;  $\rho_w$  is fluid density. Kutta's hypothesis on the plate edges is used in the following form [18, 32]:  $p_+ \rightarrow p_-$ . The function  $\varphi(x, y, z, t)$  is presented as double-layer potential:

$$\varphi(x, y, z, t) = \frac{1}{4\pi} \int_S \gamma(\xi, t) \frac{\partial}{\partial n_\xi} \frac{1}{\sqrt{(x - \xi_1)^2 + (y - \xi_2)^2 + (z - \xi_3)^2}} dS, \quad (3)$$

where  $n_\xi$  is a unit vector of normal to the plate surface;  $\gamma(\xi, t) = \varphi_+ - \varphi_-$  is a circulation of a velocity. The equation (3) is substituted into (1); as a result the following hyper singular integral equation is obtained:

$$V \frac{\partial w}{\partial x} + \frac{\partial w}{\partial t} = \frac{1}{4\pi} \int_S \gamma(\xi, t) \frac{\partial^2}{\partial z \partial n_\xi} \left( \frac{1}{\sqrt{(x - \xi_1)^2 + (y - \xi_2)^2 + (z - \xi_3)^2}} \right) dS. \quad (4)$$

The review of the results concerning the applications of the singular integral equations to aero elasticity is presented in [36].

If flutter occurs, the plate performs geometrical nonlinear vibrations; this nonlinearity limits the vibrations amplitudes. As thin plates are considered, shear and rotational inertia are not taken into account. Therefore, the plate vibrations are described by von Karman equations:

$$\frac{h^2}{12} \nabla^4 w + \frac{(1 - \mu^2) \rho_p}{E} \ddot{w} + \frac{(1 - \mu^2) \rho_w}{Eh} (\dot{\gamma} + V \gamma'_x) = \frac{(1 - \mu^2)}{Eh} (F''_{YY} w''_{XX} - 2F''_{XY} w''_{XY} + F''_{XX} w''_{YY}); \quad (5)$$

$$\frac{1}{Eh} \nabla^4 F = (w''_{XY})^2 - w''_{XX} w''_{YY}, \quad (6)$$

where  $F$  is Airy stress function;  $h$  is plate thickness;  $\rho_p$  is a density of the plate material;  $E, \mu$  are Young's modulus and Poisson's ration.

## 2. FINITE DEGREE-OF-FREEDOM MODEL OF PLATE VIBRATIONS

The circulation of velocities is presented as a series in terms of eigenmodes of simply supported plate:

$$\gamma(\xi_1, \xi_2, t) = \sum_{l=1}^{N_1} \sum_{m=1}^{N_1} C_{lm}(t) \sin\left(\frac{l\pi \xi_1}{a}\right) \sin\left(\frac{m\pi \xi_2}{b}\right) \quad (7)$$

the lateral displacements of the plate  $w$  are the following:

$$w(x, y, t) = \sum_{r_1=1}^{N_s} \sum_{r_2=1}^{N_s} \theta_{r_1 r_2}(t) \sin\left(\frac{r_1 \pi x}{a}\right) \sin\left(\frac{r_2 \pi y}{b}\right) \quad (8)$$

The relations (7, 8) are substituted into the singular integral equation (4); the Galerkin method is used. As a result the following system of linear algebraic equations with respect to  $C_{lm}(t)$  is derived:

$$\sum_{l=1}^{N_1} \sum_{m=1}^{N_1} a_{n_1 n_2 lm} C_{lm}(t) = b_{n_1 n_2} ; n_1 = 1, \dots, N_1 ; n_2 = 1, \dots, N_1 \quad (9)$$

where

$$a_{n_1 n_2 lm} = \frac{1}{4\pi} \int_S \sin\left(\frac{n_1 \pi x}{a}\right) \sin\left(\frac{n_2 \pi y}{b}\right) dx dy \int_S \frac{\sin\left(\frac{l\pi \xi_1}{a}\right) \sin\left(\frac{m\pi \xi_2}{b}\right) d\xi_1 d\xi_2}{\left[(x-\xi_1)^2 + (y-\xi_2)^2\right]^{3/2}}$$

$$b_{n_1 n_2} = \int_S \left( V \frac{\partial w}{\partial x} + \frac{\partial w}{\partial t} \right) \sin\left(\frac{n_1 \pi x}{a}\right) \sin\left(\frac{n_2 \pi y}{b}\right) dx dy = 0.25 b V \sum_{r_1=1}^{N_s} \sum_{r_2=1}^{N_s} \theta_{r_1 r_2}(t) r_1 \delta_{r_2 n_2} \mathcal{G}_{n_1 n_2 r_1} +$$

$$+ 0.25 ab \sum_{r_1=1}^{N_s} \sum_{r_2=1}^{N_s} \dot{\theta}_{r_1 r_2}(t) \delta_{r_1 n_1} \delta_{r_2 n_2}$$

$\delta_{r_2 n_2}$  is Kronecker delta;  $\mathcal{G}_{n_1 n_2 r_1} = \frac{1 - \delta_{n_1 r_1}}{n_1 - r_1} \left[ 1 - (-1)^{n_1 - r_1} \right] + \frac{1 - (-1)^{n_1 + r_1}}{n_1 + r_1}$ . The solution of the system

(9) is presented as:

$$C_{lm} = \sum_{r_1=1}^{N_s} \sum_{r_2=1}^{N_s} C_{lm}^{(r_1 r_2)}(t) ; (l, m) = 1, \dots, N_1 \quad (10)$$

The equation (10) is substituted into (9); the systems of linear algebraic equations are derived. The solutions of these systems are the following:

$$C_{l,m}^{(r_1 r_2)} = 0.25 V b \theta_{r_1 r_2}(t) \bar{\varphi}_{l,m}^{(r_1 r_2)} + 0.25 a b \dot{\theta}_{r_1 r_2}(t) \bar{\bar{\varphi}}_{l,m}^{(r_1 r_2)} ; (l, m) = 1, \dots, N_1 ; (r_1, r_2) = 1, \dots, N_s \quad (11)$$

The parameters  $\bar{\varphi}_{l,m}^{(r_1 r_2)}$ ,  $\bar{\bar{\varphi}}_{l,m}^{(r_1 r_2)}$  are solutions of the following systems of linear algebraic equations:

$$\sum_{l=1}^{N_1} \sum_{m=1}^{N_1} a_{n_1 n_2 lm} \bar{\varphi}_{l,m}^{(r_1 r_2)} = r_1 \delta_{r_2 n_2} \mathcal{G}_{n_1 n_2 r_1} \quad (12)$$

$$\sum_{l=1}^{N_1} \sum_{m=1}^{N_1} a_{n_1 n_2 lm} \bar{\bar{\varphi}}_{l,m}^{(r_1 r_2)} = \delta_{r_1 n_1} \delta_{r_2 n_2} ; n_1, n_2 = 1, \dots, N_1 ; r_1, r_2 = 1, \dots, N_s \quad (13)$$

The finite-degree-of-freedom model of plate geometrical nonlinear vibrations is derived. The equation (8) is substituted into (6); the linear non homogeneous partial differential equation is derived. The solution of this equation can be presented as:

$$F = F_p + F_g \quad (14)$$

where  $F_p$  is partial solution of nonhomogeneous equation;  $F_g$  is general solution of homogeneous equation. Partial solution of nonhomogeneous equation has the following form:

$$0.5 F_p = \sum_{\substack{\eta_1, \eta_2, p_1, p_2=1 \\ \eta_1 \neq \eta_2}}^{N_S} \theta_{\eta_1 \eta_2} \theta_{p_1 p_2} \left[ A_{\eta_1 \eta_2 p_1 p_2}^{(1)} \cos \eta(r_2 - p_2) \cos \xi(r_1 + p_1) + A_{\eta_1 \eta_2 p_1 p_2}^{(2)} \cos \eta(r_2 + p_2) \cos \xi(r_1 - p_1) \right] + \\ + \sum_{\substack{\eta_1, \eta_2, p_1, p_2=1 \\ \eta_1 \neq \eta_2 \text{ u } p_1 \neq p_2 \\ \eta_1 \neq p_1 \text{ u } \eta_2 \neq p_2}}^{N_S} \theta_{\eta_1 \eta_2} \theta_{p_1 p_2} A_{\eta_1 \eta_2 p_1 p_2}^{(3)} \cos \eta(r_2 - p_2) \cos \xi(p_1 - r_1) + \sum_{\substack{\eta_1, \eta_2, p_1, p_2=1 \\ \eta_1 \neq \eta_2 \text{ u } p_1 \neq p_2}}^{N_S} \theta_{\eta_1 \eta_2} \theta_{p_1 p_2} A_{\eta_1 \eta_2 p_1 p_2}^{(4)} \cos \eta(r_2 + p_2) \cos \xi(p_1 + r_1). \quad (15)$$

The general solution of the homogeneous equation is equal to zero  $F_g = 0$ .

Now the solution (15) is substituted into the equation (5); the Galerkin method is applied. As a result the following dynamical system is obtained:

$$\sum_{l,m=1}^{N_S} (M_{n_1 n_2 l m} \ddot{\theta}_{lm} + D_{n_1 n_2 l m} \dot{\theta}_{lm} + K_{n_1 n_2 l m} \theta_{lm}) + R_{n_1 n_2}(\theta_{1,1}, \theta_{1,2}, \dots) = 0; \quad n_1, n_2 = 1, \dots, N_S, \quad (16)$$

where

$$R_{n_1 n_2}(\theta_{1,1}, \theta_{1,2}, \dots) = - \int_S (F_{YY}'' w_{XX}'' - 2F_{XY}'' w_{XY}'' + F_{XX}'' w_{YY}'') \sin\left(\frac{n_1 \pi x}{a}\right) \sin\left(\frac{n_2 \pi y}{b}\right) dx dy = \\ \sum_{\substack{\eta_1, \eta_2, p_1, p_2, l, m=1 \\ \eta_1 \neq \eta_2}}^{N_S} \alpha_{lm \eta_1 \eta_2 p_1 p_2}^{(n_1, n_2)} \theta_{lm} \theta_{\eta_1 \eta_2} \theta_{p_1 p_2}$$

### 3. APPLICATION OF NONLINEAR MODES FOR SELF-SUSTAINED VIBRATIONS ANALYSIS

The general approach for nonlinear modes of self-sustained vibrations analysis is suggested. In the next section these nonlinear modes are used for analysis of the plate self-sustained vibrations. The nonlinear dynamical system (16) can be presented in the following matrix form:

$$\ddot{\eta} + A \dot{\eta} + B \eta = f(\eta, \dot{\eta}) \quad f_j = \sum_{l,r,p=1}^N G_{lrp}^{(j)} \eta_l \eta_r \eta_p; \quad j = 1, \dots, N \quad (17)$$

where  $\eta = \{\eta_1, \eta_2, \dots, \eta_N\}$ ;  $f = \{f_1, \dots, f_N\}$ ;  $A = \{\alpha_{kj}\}$ ;  $B = \{\beta_{kj}\}$ . It is assumed, that the trivial equilibrium  $\eta = 0$  undergoes Hopf bifurcation and the self-sustained vibrations appear. These self-sustained vibrations are presented as the Shaw-Pierre nonlinear modes:

$$\eta_j = \bar{R}_j = a_{j1} \eta_k + a_{j2} \dot{\eta}_k + R_j(\eta_k, \dot{\eta}_k); \quad \dot{\eta}_j = \bar{F}_j = a_{N+j,1} \eta_k + a_{N+j,2} \dot{\eta}_k + F_j(\eta_k, \dot{\eta}_k) \quad (18) \\ j = 1, \dots, k-1, k+1, \dots, N$$

where  $a_{j1}; a_{j2}; a_{N+j,1}; a_{N+j,2}$  are unknown coefficients. The variables  $(\eta_k, \dot{\eta}_k)$  are chosen as master coordinates. The nonlinear functions  $R_j; F_j$  are presented in the following form:

$$R_j(\eta_k, \dot{\eta}_k) = \delta_1^{(j)} \eta_k^3 + \delta_2^{(j)} \eta_k^2 \dot{\eta}_k + \delta_3^{(j)} \eta_k \dot{\eta}_k^2 + \delta_4^{(j)} \dot{\eta}_k^3 + \dots \\ F_j(\eta_k, \dot{\eta}_k) = \varepsilon_1^{(j)} \eta_k^3 + \varepsilon_2^{(j)} \eta_k^2 \dot{\eta}_k + \varepsilon_3^{(j)} \eta_k \dot{\eta}_k^2 + \varepsilon_4^{(j)} \dot{\eta}_k^3 + \dots; \quad j = 1, \dots, k-1, k+1, \dots, N \quad (19)$$

The coefficients  $a_{j,1}; a_{j,2}; a_{N+j,1}; a_{N+j,2}$  of linear part of the nonlinear mode (18) are determined. The linear part of the system (18) is considered, which can be presented as

$$\dot{z} = \Gamma z = \begin{bmatrix} 0 & E \\ -B & -A \end{bmatrix} z, \quad (20)$$

where  $z = [z_1, \dots, z_{2N}] = [\eta, \dot{\eta}]$ . The solution of the system (20) is the following:

$$z = \sum_{j=1}^N [\Theta_{2j} W_{2j} \exp(\lambda_{2j} t) + \Theta_{2j-1} W_{2j-1} \exp(\lambda_{2j-1} t)], \quad (21)$$

where  $\lambda_i, W_i$  are eigenvalues and eigenvectors of the matrix  $\Gamma$ ;  $\lambda_{2j} = \bar{\lambda}_{2j-1}$ ;  $W_{2j} = \bar{W}_{2j-1}$ ;  $\Theta_{2j} = \bar{\Theta}_{2j-1}$  are constants of integration. If a pair of eigenvalues of the matrix  $\Gamma$  takes a form:  $\lambda_{1,2} = \pm i \chi_1$ , the self-sustained vibrations appear. The solution of the system (20) on the central manifold is presented in the following form:

$$z = \Theta_2 W_2 \exp(\lambda_2 t) + \Theta_1 W_1 \exp(\lambda_1 t) \quad (22)$$

where  $W_1 = \gamma_1 - i \delta_1$ ;  $\gamma_1 = [\gamma_1^{(1)}; \dots; \gamma_1^{(2N)}]$ ;  $\delta_1 = [\delta_1^{(1)}; \dots; \delta_1^{(2N)}]$ ;  $\Theta_1 = K_1^{(1)} - i K_1^{(2)}$ ;  $\lambda_1 = \alpha_1 - i \psi_1$ . Two elements  $\eta_k, \dot{\eta}_k$  of the vector  $z$  are presented in the following form:

$$\eta_k = \gamma_1^{(k)} \mathcal{G}_1(t) + \delta_1^{(k)} \mathcal{G}_2(t); \dot{\eta}_k = \gamma_1^{(N+k)} \mathcal{G}_1(t) + \delta_1^{(N+k)} \mathcal{G}_2(t) \quad (23)$$

where  $\mathcal{G}_1(t) = 2 \exp(\alpha_1 t) [K_1^{(1)} \cos \psi_1 t - K_1^{(2)} \sin \psi_1 t]$ ;  $\mathcal{G}_2(t) = -2 \exp(\alpha_1 t) [K_1^{(1)} \sin \psi_1 t + K_1^{(2)} \cos \psi_1 t]$ .

The rest elements of the solutions (23) are the following:

$$\eta_i = \gamma_1^{(i)} \mathcal{G}_1(t) + \delta_1^{(i)} \mathcal{G}_2(t); \dot{\eta}_i = \gamma_1^{(N+i)} \mathcal{G}_1(t) + \delta_1^{(N+i)} \mathcal{G}_2(t); i = 1, \dots, k-1, k+1, \dots, N \quad (24)$$

Solving jointly the equations (24, 23), the coefficients of linear part of the nonlinear normal mode (18) is obtained in the form:

$$a_{i1} = \frac{\gamma_1^{(i)} \delta_1^{(N+k)} - \delta_1^{(i)} \gamma_1^{(N+k)}}{\gamma_1^{(k)} \delta_1^{(N+k)} - \delta_1^{(k)} \gamma_1^{(N+k)}}; a_{i2} = \frac{\gamma_1^{(i)} \delta_1^{(k)} - \delta_1^{(i)} \gamma_1^{(k)}}{\gamma_1^{(N+k)} \delta_1^{(k)} - \delta_1^{(N+k)} \gamma_1^{(k)}} \quad (25)$$

$$i = 1, \dots, k-1, k+1, \dots, N, N+1, \dots, N+k-1, N+k+1, \dots, 2N$$

In future analysis, the ordinary procedure for nonlinear normal mode calculations [38] is used.

#### 4. NUMERICAL ANALYSIS OF VIBRATIONS

The dynamics of the plate in water flow is investigated for the following parameters:

$$E = 2 \cdot 10^{11} \text{ Pa}; \rho_p = 7.8 \cdot 10^3 \frac{\text{kg}}{\text{m}^3}; \rho_w = 1 \cdot 10^3 \frac{\text{kg}}{\text{m}^3}; \nu = 0.3; h = 0.02 \text{ m}; a = b = 0.5 \text{ m}$$

The self-sustained vibrations are studied on the basis of finite degrees-of-freedom model (23). These vibrations start-up due to Hopf bifurcation and they analyzed by the nonlinear modes. At first, nonlinear mode is determined by solution of the system of linear algebraic equations; the motions on the mode are analyzed. The calculations are performed for different Mach numbers. The results of the calculations are presented on the bifurcation diagram (Fig. 2). Stable and unstable trivial equilibrium are shown by solid and dotted lines, respectively. Limit cycle start-up at Hopf bifurcation. Behavior of such self-sustained vibrations, when the Mach number is increased, is shown by solid lines on Fig. 2.

The direct numerical integration of the system (17) is performed to check the obtained self-sustained vibrations. Points on nonlinear mode are used as initial conditions. The results of the

calculations are shown by rhombs on Fig.2. Thus, the results of the direct numerical integration are close to the data obtained by nonlinear modes.

## CONCLUSIONS

Interaction of the vibrating plate with a fluid flow is analyzed in this paper. It is assumed that a fluid is incompressible, frictionless and irrotational; the model of fluid motions is linear. Fluid-plate interaction is described by the linear hyper singular integral equation. Galerkin method is used for approximate solution of this integral equation.

For analysis of self-sustained vibrations, geometrical nonlinearity includes in the model of plate vibrations. It limits the vibrations amplitudes in the region of trivial equilibria instability.

The generalization of the Shaw-Pierre nonlinear modes for self-sustained finite degree-of-freedom system vibrations is suggested in this paper. As nonlinear modes are determined in power series, the suggested approach is valid only for moderate vibrations amplitudes.

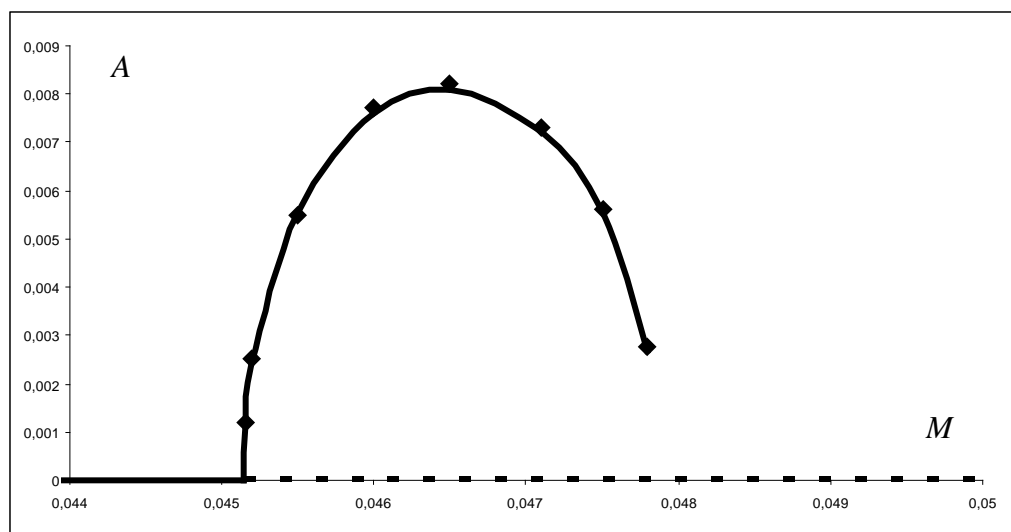


Fig.2 Bifurcation diagram of the system

## REFERENCES

- [1] Bolotin V.V. *Nonconservative problems of the theory of elastic stability*, Moscow: Fizmatgiz, 1961 (in Russian). English translation: Pergamon. Oxford. 1963.
- [2] Dowell E.H. Flutter of a buckled plate as an example of chaotic motion of a deterministic autonomous system *J. of Sound and Vibration*, Vol. 85, pp. 333-344, 1982.
- [3] Bolotin V.V., Grishko A.A., Kounadis A.N., Gantes C.J. Non-linear panel flutter in remote post-critical domains, *Int. J. of Non-Linear Mechanics*, Vol. 33, pp. 753-764, 1998.
- [4] Bolotin V.V., Petrovsky A.V., Grishko A.A. Secondary bifurcations and global instability of an aeroelastic non-linear system in the divergence domain, *J. of Sound and Vibration*, Vol. 191, pp. 431-451, 1996.
- [5] Epureanu B.I., Tang L.S., Paidoussis M.P. Coherent structures and their influence on the dynamics of aeroelastic panels, *Int. J. of Non-linear Mechanics*, Vol. 39, pp. 977-991, 2004.
- [6] Tang D., Dowell E.H. Limit cycle oscillations of two-dimensional panels in low subsonic flow, *Int. J. of Non-linear Mechanics*, Vol. 37, pp. 1199- 1209, 2002.
- [7] Kornecki A., Dowell E.H., O'Brien J. On the aeroelastic instability of two-dimensional panels in uniform incompressible flow, *J. of Sound and Vibration*, Vol. 47, pp. 163-178, 1976.
- [8] Liu L., Dowell E. The secondary bifurcation of an aeroelastic airfoil motion: effect of high harmonics, *Nonlinear dynamics*, Vol. 37, pp. 31-49, 2004.
- [9] Hess J.L. Review of integral-equation techniques for solving potential-flow problems with emphasis on the surface-source method, *Computer Methods in Applied Mechanics and Engineering*, Vol. 5, pp. 145-196, 1975.
- [10] Shaw S.W., Pierre C., Normal modes for nonlinear vibratory systems, *J. of Sound and Vibration*, Vol. 164, pp. 58-124, 1993.

**INVESTIGATION OF THE PARAMETRIC VIBRATION OF THE ORTHOTROPIC PLATES SUBJECTED TO PERIODIC IN PLANE FORCES BY MULTI-MODAL APPROXIMATION AND R-FUNCTIONS METHOD**

**Awrejcewicz J.**<sup>1</sup>

Technical University of

Lódź, Lodz, Poland

**Kurpa L.**<sup>2</sup>,

**Mazur O.**

National Technical  
University, Kharkov,  
Ukraine

ABSTRACT

The original method of studying parametric vibrations of orthotropic plate with complex shape is proposed. Suggested approach is based on combined application of variational methods and the R-functions theory. Using the proposed method and developed software the regular and chaotic regimes of T-shaped plate are analyzed.

**INTRODUCTION**

Since the elements modeled by orthotropic plates are used in different branches of industry such as aerospace, ship and transport engineering etc., the investigation of the plates nonlinear vibrations subjected to different types of load is an actual problem. The fundamental theory of studying parametrically excited vibrations plates of the rectangular form had been presented in work [4]. In recent papers [2, 3, 7] and others, new problems of parametric vibrations of the plates including their bifurcation and chaotic dynamics are studied. It should be noted that plates, which are used in applications have the different geometry. Therefore nonlinear dynamics problems of plate with complex planform have received particular interest among scientists. Generally in modern literature in the case of plate with the complex form the universal approaches via FEM (Finite Element Method) or FDM (Finite Difference Method) are used. Application of variational-structural method based on the R-functions method (RFM) [5,6] is relatively new approach for nonlinear problems. Mentioned approach has some preferences; among them first of all it is possibility to construct the system of basic functions in analytical way. The basic functions exactly satisfy the boundary conditions for plates with complex form.

In the given work the new discretization method of the nonlinear system of the differential equations with partial derivatives are proposed. The main idea of the proposed method relies on reduction of the equations governing dynamics of plates of the complex form to a system of nonlinear ordinary differential equations (ODEs) by variational methods joined with the R-functions theory. The proposed method establishes the simple connection between generated coordinates of the unknown functions and allows representation of the coefficients of the obtained ODEs in analytical form in result of solving a series of linear boundary value problems.

**1. FORMULATION**

Let us consider the nonlinear vibrations of an orthotropic plate with constant thickness  $h$  loaded by periodic in-plane force. For construction of mathematical model of task Von Karman's non-linear strain-displacement relationships are employed and the equations of motion are developed by applying the principle of virtual work. The movement equations in the mixed form have the following view [8]

$$L_1\Phi = -\frac{C_1}{2}L(w, w), \tag{1}$$

<sup>1</sup> Corresponding author. Email [awrejcew@p.lodz.pl](mailto:awrejcew@p.lodz.pl)

<sup>2</sup> Corresponding author. Email [Kurpa@kpi.kharkov.ua](mailto:Kurpa@kpi.kharkov.ua)

$$L_2 w = L(w, \Phi) - \varepsilon \frac{\partial w}{\partial t} - \frac{\partial^2 w}{\partial t^2}, \quad (2)$$

where  $w$  is deflection of the plate,  $\Phi(x, y)$  is the stress (Airy's) function being introduced by the stresses  $\sigma_x$ ,  $\sigma_y$  and  $\tau$  through the standard formulas

$$\frac{\partial^2 \Phi}{\partial y^2} = \sigma_x, \quad \frac{\partial^2 \Phi}{\partial x^2} = \sigma_y, \quad -\frac{\partial^2 \Phi}{\partial x \partial y} = \tau.$$

The linear operators  $L_1$ ,  $L_2$  in (1), (2) are defined as follows

$$L_1 = C_1 \frac{\partial}{\partial x^4} - \left( 2\mu_1 - \frac{E_1}{G} \right) \frac{\partial}{\partial x^2 \partial y^2} + \frac{\partial}{\partial y^4}, \quad (3)$$

$$L_2 = \frac{1}{12(1-\mu_1\mu_2)} \left( C_1 \frac{\partial^4}{\partial x^4} + \frac{\partial^4}{\partial y^4} + 2(C_3 + C_2) \frac{\partial^4}{\partial x^2 \partial y^2} \right), \quad (4)$$

and the expressions for nonlinear operators  $L(w, w)$ ,  $L(w, \Phi)$  are

$$L(w, w) = 2 \left( \frac{\partial^2 w}{\partial x^2} \frac{\partial^2 w}{\partial y^2} - \left( \frac{\partial^2 w}{\partial x \partial y} \right)^2 \right), \quad L(w, \Phi) = \frac{\partial^2 w}{\partial x^2} \frac{\partial^2 \Phi}{\partial y^2} + \frac{\partial^2 w}{\partial y^2} \frac{\partial^2 \Phi}{\partial x^2} - 2 \frac{\partial^2 w}{\partial x \partial y} \frac{\partial^2 \Phi}{\partial x \partial y}.$$

Note that equations (1), (2) are already presented in a non-dimensional form, and relations between dimensional and non-dimensional values are defined as

$$\bar{x} = \frac{x}{a}, \quad \bar{y} = \frac{y}{a}, \quad \bar{w} = \frac{w}{h}, \quad \bar{p} = \frac{a^2 p}{h^3 E_2}, \quad \bar{t} = \frac{h}{a^2} \sqrt{\frac{E_2}{\rho}} t, \quad \bar{\varepsilon} = \frac{a^2}{h} \sqrt{\frac{\rho}{E_2}} \varepsilon, \quad \bar{\Phi} = \frac{\Phi}{h^2 E_2}.$$

Later, bars over non-dimensional values will be omitted. The coefficients  $C_1$ ,  $C_2$  and  $C_3$  appearing in (1)-(4) are defined by the following relations

$$C_1 = \frac{E_1}{E_2}, \quad C_2 = \frac{G(1-\mu_1\mu_2)}{E_2}, \quad C_3 = \frac{G(1-\mu_1\mu_2)}{E_2} + \mu_1. \quad (5)$$

In (1)-(5)  $E_1$ ,  $E_2$  are elasticity (Young) modules,  $\mu_1$ ,  $\mu_2$  are Poisson's ratios,  $G$  is shear modulus,  $\rho$  is the plate density, and  $\varepsilon$  is a damping coefficient.

The system (1)-(2) are supplemented with initial and corresponding boundary conditions. Initial conditions for plate are taken in the form

$$w|_{t=0} = w_0, \quad w'|_{t=0} = 0,$$

The boundary conditions are introduced in various ways and they depend on plate type of support.

## 2. METHOD OF SOLUTION

Let us present the plate deflection in the following form

$$w(x, y, t) = \sum_{i=1}^n f_i(t) w_i(x, y). \quad (6)$$

Here  $w_i$  are eigenfunctions of a linear vibrations problem of the corresponded unloaded plate. Thus, the linear problem is reduced to solving the equation

$$L_2 W(x, y) = \omega_L^2 W(x, y), \quad (7)$$

where  $\omega_L$  is eigenfrequency corresponding to  $w_i$  mode of plate vibration. In what follows the problem (7) is further solved by the Ritz method combined with R-function theory.

The stress functions are sought for in the following form

$$\Phi(x, y, t) = p\Phi_0 + \sum_{i,j=1}^n f_i(t) f_j(t) \Phi_{ij}(x, y). \quad (8)$$

Here the function  $\Phi_0(x, y)$  is solution to the equation

$$L_1\Phi_0 = 0, \quad (9)$$

which satisfies conditions of the form

$$\frac{\partial^2\Phi_0}{\partial\tau^2} = -1, \quad \frac{\partial^2\Phi_0}{\partial n\partial\tau} = 0 \quad (10)$$

on loaded part of border.

The functions  $\Phi_{ij}(x, y)$  appearing in (8) are solutions to the following equations

$$L_1\Phi_{ij} = -\frac{C_1}{2}L(w_i, w_j). \quad (11)$$

The boundary conditions for functions  $\Phi_{ij}$  on unloaded part of counter are follows

$$\frac{\partial^2\Phi_{ij}}{\partial\tau^2} = 0, \quad \frac{\partial^2\Phi_{ij}}{\partial n\partial\tau} = 0 \quad (12)$$

The boundary conditions on unloaded part of the border for functions  $\Phi_0(x, y)$  and  $\Phi_{ij}(x, y)$  depend on support edge. In order to solve the problems (9), (10) and (11), (12) for plate with complex shape the matched method including the Ritz approach as well as the R-function theory is used.

Substituting expressions (6) and (8) for  $w$  and  $\Phi$  into equation (2), and applying the Bubnov-Galerkin method, we can reduce the input system of nonlinear partial differential equations (PDEs) to an appropriate system of ordinary differential equations (ODEs) of the following matrix form

$$\mathbf{f}'' + \varepsilon\mathbf{f}' + (\mathbf{C} - p\mathbf{A})\mathbf{f} + \mathbf{B}(\mathbf{f}) = 0, \quad (13)$$

where

$$\mathbf{A} = \begin{pmatrix} a_1^{(1)} & a_2^{(1)} & \dots & a_n^{(1)} \\ a_1^{(2)} & a_2^{(2)} & \dots & a_n^{(2)} \\ \dots & \dots & \dots & \dots \\ a_1^{(n)} & a_2^{(n)} & \dots & a_n^{(n)} \end{pmatrix}, \quad \mathbf{C} = \begin{pmatrix} \omega_{L,1}^2 & 0 & \dots & 0 \\ 0 & \omega_{L,2}^2 & \dots & 0 \\ 0 & 0 & \dots & 0 \\ 0 & 0 & \dots & \omega_{L,n}^2 \end{pmatrix}, \quad \mathbf{f} = \begin{pmatrix} f_1 \\ f_2 \\ \dots \\ f_n \end{pmatrix}, \quad \mathbf{f}' = \begin{pmatrix} f_1' \\ f_2' \\ \dots \\ f_n' \end{pmatrix}, \quad \mathbf{f}'' = \begin{pmatrix} f_1'' \\ f_2'' \\ \dots \\ f_n'' \end{pmatrix}, \quad \mathbf{B}(\mathbf{f}) = \begin{pmatrix} b_1 \\ b_2 \\ \dots \\ b_n \end{pmatrix},$$

where  $b_m$  is designed as  $b_m = \sum_{i,j,k=1}^n \beta_{ijk}^{(m)} f_i f_j f_k$ .

Note that the elements of the matrix  $\mathbf{A}$  and the vector  $\mathbf{B}(\mathbf{f})$  in (13) are defined through double integrals over the investigated domain by the following formulas

$$\alpha_i^{(m)} = \frac{1}{\|w_m\|^2} \iint_{\Omega} L(w_i, \Phi_0) w_m dx dy, \quad \beta_{ijk}^{(m)} = -\frac{1}{\|w_m\|^2} \iint_{\Omega} L(w_k, \Phi_{ij}) w_m dx dy.$$

### 3. NUMERICAL RESULTS

Let us consider the parametric vibrations of the orthotropic plate of complex shape shown in Figure 1.

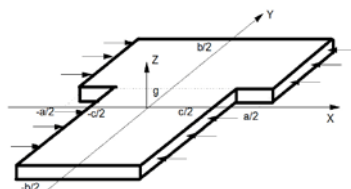


Fig. 1. A T-shaped plate

The plate is subjected to load of the form  $p = p_0 \sin \theta t$ , which is applied longitudinally along the plate edges being parallel to the axis  $OY$ . Let us deflection  $w$  satisfy the following boundary conditions

$$w = 0, \quad \frac{\partial^2 w}{\partial n^2} = 0.$$

The boundary conditions for stress function  $\Phi$  have the form

$$\frac{\partial^2 \Phi}{\partial \tau^2} = -p, \quad \frac{\partial^2 \Phi}{\partial n \partial \tau} = 0.$$

Our numerical results are obtained for material (glass-epoxy) with the following relations for the elasticity coefficients:  $E_1/E_2 = 3$ ,  $G/E_2 = 0.6$ ,  $\mu_1 = \mu_2 E_1/E_2 = 0.25$ .

It should be noted that the current plate is in a homogenous subcritical state, and the function  $\Phi_0$  can be presented in the form  $\Phi_0 = -\frac{y^2}{2}$ .

The variational formulations of the tasks (7) and (11) are reduced to finding minimum of following functionals respectively

$$I(W) = \iint_{\Omega} \left[ C_1 \left( \frac{\partial^2 W}{\partial x^2} \right)^2 + 2C_1 \mu_2 \frac{\partial^2 W}{\partial x^2} \frac{\partial^2 W}{\partial y^2} + \left( \frac{\partial^2 W}{\partial y^2} \right)^2 + 4C_2 \left( \frac{\partial^2 W}{\partial x \partial y} \right)^2 - 12(1 - \mu_1 \mu_2) \omega_L^2 W^2 \right] d\Omega,$$

$$I(\Phi_{ij}) = \iint_{\Omega} \left[ C_1 \left( \frac{\partial^2 \Phi_{ij}}{\partial x^2} \right)^2 + \frac{E_1}{G} \frac{\partial^2 \Phi_{ij}}{\partial x^2} \frac{\partial^2 \Phi_{ij}}{\partial y^2} + \left( \frac{\partial^2 \Phi_{ij}}{\partial y^2} \right)^2 - 2\mu_1 \left( \frac{\partial^2 \Phi_{ij}}{\partial x \partial y} \right)^2 + L(w_i, w_j) \Phi_{ij} \right] d\Omega.$$

The series of basic functions, which satisfy boundary conditions, is constructed by the R-function method. At first it is necessary to construct the predicate of the domain

$$\Omega = (\Omega_1 \wedge \Omega_2) \wedge (\Omega_3 \vee \Omega_4),$$

where

$$\Omega_1 = \left( f_1 = \frac{1}{a} \left( \left( \frac{a}{2} \right)^2 - x^2 \right) \geq 0 \right), \quad \Omega_2 = \left( f_2 = \frac{1}{b} \left( \left( \frac{b}{2} \right)^2 - y^2 \right) \geq 0 \right), \quad \Omega_3 = \left( f_3 = \frac{1}{c} \left( \left( \frac{c}{2} \right)^2 - x^2 \right) \geq 0 \right)$$

$$\Omega_4 = (f_4 = y - g \geq 0)$$

are sub-domains. According to RFM the equation  $\omega(x, y) = 0$ , where  $\omega(x, y) = (f_1 \wedge_0 f_2) \wedge_0 (f_3 \vee_0 f_4)$ , is the equation of the boundary domain. The symbols  $\vee_0, \wedge_0, -$  (R-disjunction, R-conjunction, R-negation) are defined as follows [5]:

$$x \vee_0 y = x + y + \sqrt{x^2 + y^2}, \quad x \wedge_0 y = x + y - \sqrt{x^2 + y^2}, \quad \bar{x} = -x.$$

For considerable boundary conditions we use the following solution structure

$$w_i = \omega \cdot P_1, \quad \Phi_{ij} = \omega^2 \cdot P_2. \quad (14)$$

The indefinite components  $P_1, P_2$  in (14) are approximated by the following power polynomials

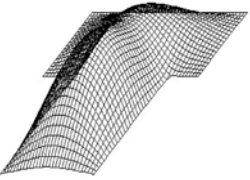
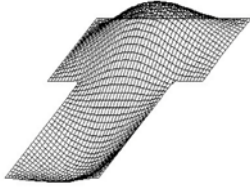
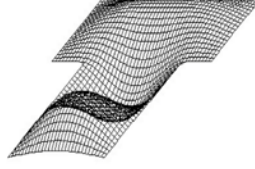
$$P_1, P_2 : 1, y, x^2, y^2, x^2 y, y^3, \dots$$

The effect of cut-out decrease on natural frequencies has been investigated. Obtained results are presented in Table 1, where  $l = g + b/2$ ,  $b/a = 1$  (see Figure 1). It should be noted that current plate is symmetric relatively to axis  $OY$  and frequencies which are corresponded to modes (1,1), (1,2), (1,3) are presented. Degeneration of plate with complex form in square plate leads to decrease of natural frequencies and approaching of their values to corresponding values for square plate.

**Table 1** Comparison of frequency parameter  $\lambda_i = a^2 / h \sqrt{\rho / E_2} \omega_{L,i}$  for various values of cutout

Geometrical parameters	$\lambda_1$	$\lambda_2$	$\lambda_3$
$c/a = 0.35, l/a = 0.2$	9.365	19.957	33.050
$c/a = 0.4, l/a = 0.1$	8.131	17.095	31.403
$c/a = 0.45, l/a = 0.05$	7.664	16.123	30.432
$c/a = 0.48, l/a = 0.02$	7.553	15.909	30.189
Square plate[1]	7.536	15.875	30.150

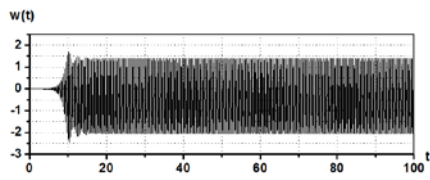
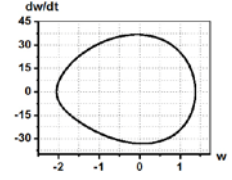
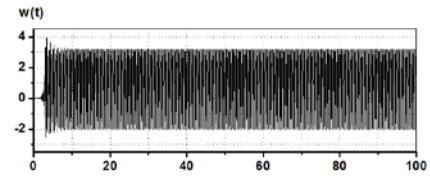
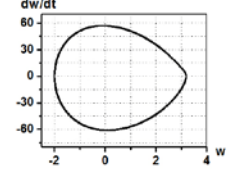
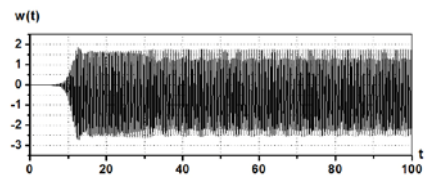
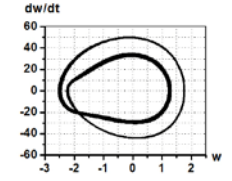
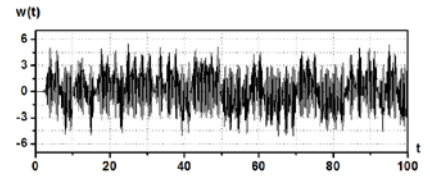
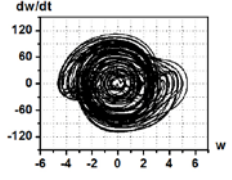
Table 2. Modes of plate vibrations

		
$\lambda_1 = 19.373$	$\lambda_2 = 22.665$	$\lambda_3 = 37.013$

Further results are obtained for  $c/a=0.6$ ,  $g/a=0.1$ ,  $b/a=1$ ,  $\varepsilon=1$ ,  $w_0=0.001$ . In Table 2 the first three modes (considering symmetry of the plate relatively to axis  $OY$ ) with the corresponding linear frequency parameters  $\lambda_i = a^2/h\sqrt{\rho/E_2}\omega_{L,i}$  are presented.

In what follows the effect of multimode approximation (three modes) on the investigated plate characteristics is further studied for a fixed value of the excited frequency  $\theta=19$  taken near the eigenfrequency and for various values of the parameter  $p_0$ . Dependencies  $w(t)$  and  $\dot{w}(w)$  are computed in the point of first mode maximum  $M(0,-0.141a)$ , and the obtained results are reported in Table 3.

Table 3. Dependences  $w(t)$ ,  $\dot{w}(w)$  obtained via third order approximation

$P_0$	One mode approximation	
12.2		
21		
$P_0$	Three modes approximation	
12.2		
21		

Analyzing of data in Table 3 one may see that results obtained with use one-mode approximation differ from results obtained applying three-mode approximation and draw a conclusion that for chaotic behavior of plate investigation one-mode approximation cannot be used.

## CONCLUSIONS

The effective numerically-analytical method of parametric regular and chaotic vibrations investigation of orthotropic plates with complex shapes and different types of boundary conditions has been proposed. The approach is based on applying a variational method and R-function theory. The numerical results are obtained for plate with complex shape using first and third order of approximations. In addition to the general theoretical results our numerical analysis has shown that

one mode approximation cannot be used in all regimes of nonlinear dynamics of the orthotropic plates, and in particular during their chaotic dynamics.

## REFERENCES

- [1]. Ambartsumian S.A., *Theory of Anisotropic Plates*. Nauka, Moscow, 1967 (in Russian).
- [2]. Awrejcewicz J., Kryszko A.V. Analysis of complex parametric vibrations of plates and shells using the Bubnov-Galerkin approach. *Applied Mechanics*, 73, pp.495- 504, 2003.
- [3]. Awrejcewicz J., Kryszko V.A., Moldenkova T., Mathematical model of dissipative parametric vibrations of flexible plates with non-homogeneous boundary conditions. *Mathematical Problems in Engineering*, pp.1-16, 2006.
- [4]. Bolotin V.V., *The Dynamic Stability of Elastic Systems*. Gos. Tech. Izdat., Moscow, 1956 (in Russian).
- [5]. Rvachev V.L. *The R-Functions theory and its Some Application*, Naukova Dumka, Kiev, 1982 (in Russian).
- [6]. Kurpa L.V., *R-functions Method for Solving Linear Problems of Bending and Vibrations of Shallow Shells*. Kharkiv NTU Press, Kharkiv, 2009 (in Russian).
- [7]. Ribeiro P., Petyt M. Non-linear free vibration of isotropic plates with internal resonance. *Int.J.of Non-Linear Mechanics*, 35, pp.263-278, 2000.
- [8]. Volmir A.S., *Nonlinear Dynamics of Plates and Shells*. Nauka, Moscow, 1972 (in Russian).

## PPF VERSUS SATURATION CONTROL FOR A STRONGLY NONLINEAR BEAM STRUCTURE

**M. Bochenski**<sup>\*1</sup>,

**J. Warminski**<sup>\*</sup>,

**W. Jarzyna**<sup>\*</sup>,

**P. Filipek**<sup>\*</sup>,

**M. Augustyniak**<sup>\*</sup>

Lublin University of  
Technology, Lublin,  
Poland, \* Department of  
Applied Mechanics,  
Faculty of Mechanical  
Engineering,

\* Department of Electrical  
Drive Systems and  
Electrical Machines,  
Faculty of Electrical  
Engineering and  
Computer Science

---

### ABSTRACT

---

This paper presents numerical results of vibration suppression of a strongly nonlinear beam structure. Coupling of a nonlinear plant with PPF and saturation controllers (NSC) is tested. Influence of variation of frequency and amplitude of excitation for the system response and controllers' effectiveness is presented. Differences between two control strategies are shown.

---

### INTRODUCTION

Coupling of two vibrating subsystems give possibilities for energy transfer from one to another. By a selection of parameters one subsystem may play a role of the vibration absorber. To get such a phenomenon, absorber's frequency must be properly tuned to excitation frequency and structural parameters of the main system. This absorption effect supports control strategies, then the absorber is used as a controller and the main structure is a plant. Depending on the tuning method few types of control strategies can be distinguished. In the Positive Position Feedback (PPF) the natural frequencies of the subsystems are tuned in one-to-one ratio [1] [1] PPF method is characterized by a linear form of coupling realized by feedback loop with displacements multiply by constant gains only. The second, Nonlinear Saturation Control strategy (NSC), is based on tuning of the subsystems' natural frequencies in two-to-one ratio and then coupling the controller and the plant by a quadratic form [3] [4] Due to the nonlinear coupling the system is more complicated and needs more attention in studies. A multiple gain and two displacement (plant and controller) are used in the NSC method .

Usually controllers are designed to reduce vibration for frequency of excitation equal to natural frequency of the main system (the plant). The plant is treated as a linear model. In this case, near the resonance zone the response of the linear system achieve the biggest value, which is to be suppressed. However, appearance of nonlinearities in the plant model leads to significant changes in shape of the plant's resonant curve and additional interaction between plant and controller may appear.

This work is focused on comparison of effectiveness of PPF and NSC control strategies taking into account a strongly nonlinear model of a plant. Influence of variation of frequency and amplitude of excitation is tested.

---

<sup>1</sup> Marcin Bochenski. Email: [m.bochenski@pollub.pl](mailto:m.bochenski@pollub.pl)

## 1. MODEL OF THE STRUCTURE

The system taken for analysis consists of a composite beam with an embedded Macro Fiber Composite (MFC) actuator, which allows execute large flexural oscillations (Fig.1). A model of the plant is based on Euler – Bernoulli beam theory with an additional nonlinear curvature component. Horizontal beam (a mechanical system) is connected by the actuator and the sensor with the controller (an electrical system). External excitation is represented by harmonic vertical motion of a beam's support (direction x in Fig.1).

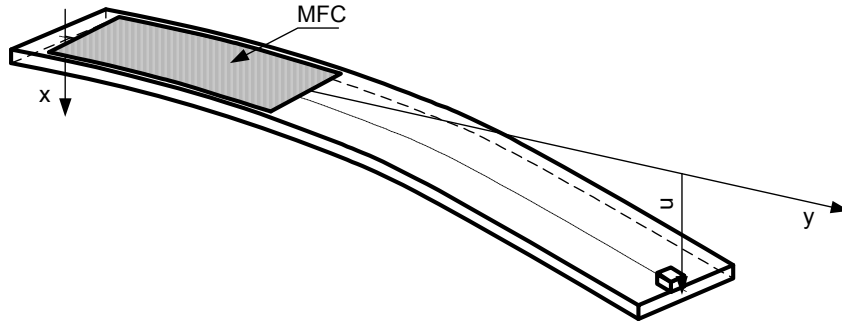


Fig. 1 Model of the system

Details of a mathematical model derivation are presented in [5]. The final equations which describe the nonlinear beam coupled with PPF (1) and NSC (2) control algorithms take form:

PPF system

$$\begin{cases} \ddot{u} + 2\mu\omega_s\dot{u} + \omega_s^2u + \beta u^3 - \delta(u\dot{u}^2 + u^2\ddot{u}) = f \cos(\Omega t) + \gamma v \\ \ddot{v} + 2\zeta\omega_c\dot{v} + \omega_c^2v = \alpha u \end{cases} \quad (1)$$

NSC system

$$\begin{cases} \ddot{u} + 2\mu\omega_s\dot{u} + \omega_s^2u + \beta u^3 - \delta(u\dot{u}^2 + u^2\ddot{u}) = f \cos(\Omega t) + \gamma v^2 \\ \ddot{v} + 2\zeta\omega_c\dot{v} + \omega_c^2v = \alpha uv \end{cases} \quad (2)$$

where  $u$  means the displacement of the beam's tip,  $v$  – denotes the controller's voltage,  $f, \Omega$  – amplitude and frequency of excitation,  $\mu, \zeta$  – damping ratio,  $\omega_s$  and  $\omega_c$  – natural frequencies of the main system (plant) and the controller, respectively. Feedback loop gains are denote  $\alpha$  and  $\gamma$ .

## 2. NUMERICAL RESULTS

Based on equations (1) and (2) numerical models of the system in Simulink software are prepared. They are tuned according to the natural frequency of the plant:  $\omega_s = 3.0631$ , then for PPF system  $\omega_c = \omega_s$ , for NSC system  $\omega_c = 0.5\omega_s$ . Simulations are performed for the excitation frequency range  $\Omega$  from 2.9 to 3.3 Hz and for two levels of amplitudes of excitation. To make interpretation of the results more convenient, analytical resonance curves for the plant response without control are additionally shown in Figs.2-4. Blue rhombus correspond to the maximal vibration amplitude of the plant with PPF control, while the red triangles with NSC control. As we can observe in Fig.2, low level of excitation ( $f = 0.03$ ) leads to almost linear plant behavior but for  $f = 0.07$  (Fig.3) influence of nonlinear terms is clearly observed. In this case maximum of the resonance curve is placed very far from the natural frequency of the beam, out of the analyzed frequency range.

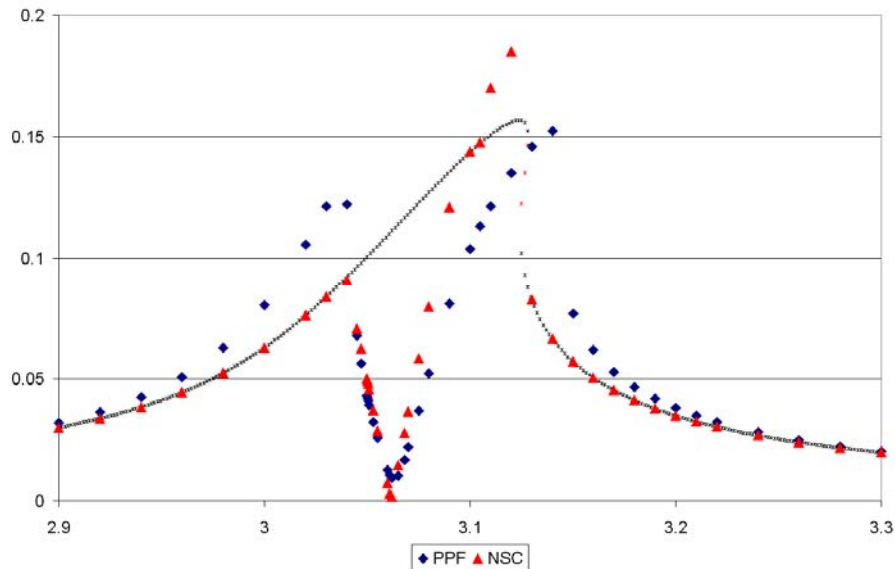


Fig. 2 The frequency response curve,  $f=0.03$

When frequency of excitation is close to the beam's natural frequency both systems show similar vibrations suppression level. However, close to the lower and upper limits of tested frequencies significant differences between analyzed controllers are observed. NSC system is not active in this area. Response of the controlled system agree to resonance curve for the no – control plant. Influence of the controller for beam's behavior is not observed. In the same area (for both amplitudes of excitation) negative effect of PPF algorithm occurs. Operation of this controller results in higher amplitude of vibration than for no – control system. For higher level of excitation ( $f = 0.07$ ) between 3.1 and 3.2 Hz significant growth of the plant response is observed (Fig.3). For both, PPF and NSC systems, beat vibrations in this region are present. However extent of this area is more wide for PPF system.

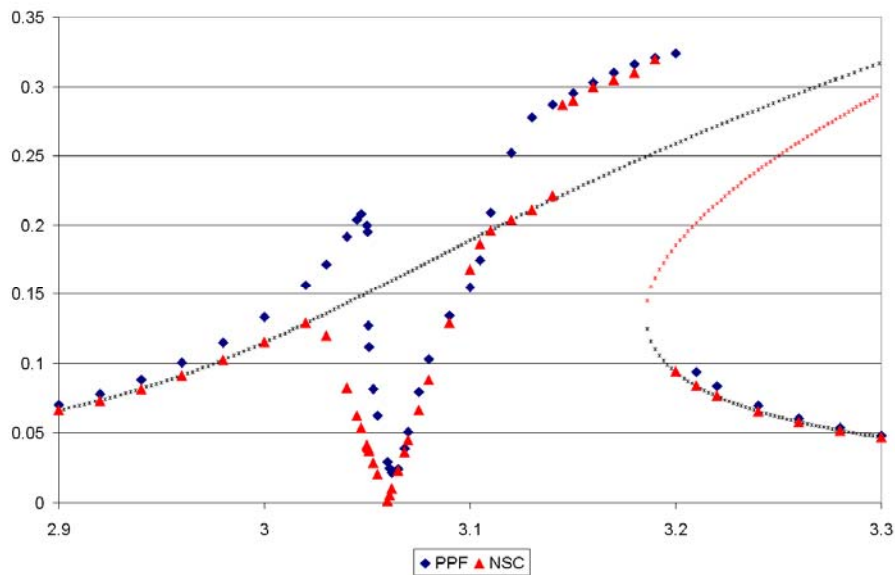


Fig. 3 The frequency response curve,  $f=0.07$

This behavior occurs also for lower amplitude of excitation ( $f = 0.03$ , Fig.2), but is not so strongly emphasized because nonlinear feature of the plant is weakly exposed. When frequency of excitation is tuned to the natural frequency of the beam both control methods work properly. The amplitude response curve takes “V” letter shape in this zone. Influence of amplitude of excitation on the resonance curve for PPF system is clearly visible in Fig.4. Beam's response for small and large amplitude of excitation there are also presented. As can be seen, comparing the resonance curves, the controller gives better vibration reduction and in a wider frequency range for low excitation level.

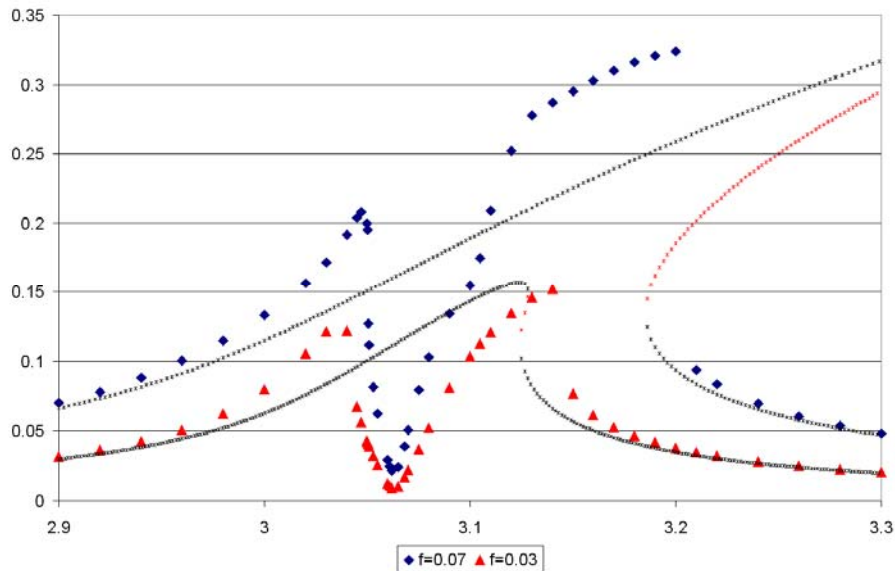


Fig. 4 The frequency response curve for PPF structure

For frequencies of excitation close to the beam's natural frequency, response of the PPF system grows along with the amplitude of excitation is increasing (Fig.4). The NSC system keeps beam's vibration on the same level despite of the change of amplitude of excitation. This feature results from occurrence of saturation phenomena [3] .

## CONCLUSIONS

On the basis of numerical simulation we may conclude that for a strongly nonlinear system NSC algorithm allows to obtain better vibration suppression than PPF controller. For both, PPF and NSC control strategies beat vibrations may occur, which lead to large amplitude plant's response. PPF system works very effectively only for weakly nonlinear plant and for frequency of excitation close to plant's natural frequency. Presented numerical results will be tested experimentally. Analysed systems will be equipped in additional module to measure current frequency related to the generated excitation.

## ACKNOWLEDGEMENT

Financial support of Structural Funds in the Operational Programme - Innovative Economy (IE OP) financed from the European Regional Development Fund - Project "Modern material technologies in aerospace industry", Nr POIG.01.01.02-00-015/08-00 is gratefully acknowledged.

## REFERENCES

- [1] Shan J., Liu H., Sun D., Slewing and vibration control of a single-link flexible manipulator by positive position feedback (PPF) *Mechatronics*, Vol. 15, pp. 487–503, 2005.
- [2] Kwak M. K., Heo S., Active vibration control of smart grid structure by multiinput and multioutput positive position feedback controller *Journal of Sound and Vibration*, Vol. 304, pp. 230–245, 2007.
- [3] Oueini S. S., Nayfeh A. H., and Pratt J. R., A Nonlinear Vibration Absorber for Flexible Structures *Nonlinear Dynamics*, Vol. 15, pp. 259–282, 1998.
- [4] Saguranrum S., Kunz D. L., Omar H. M., Numerical simulations of cantilever beam response with saturation control and full modal coupling *Computers and Structures*, Vol. 81, pp. 1499–1510, 2003.
- [5] Warminski J., Bochenski M., Jarzyna W., Filipek P., Augustyniak M., Active suppression of nonlinear composite beam vibrations by selected control algorithms. *Communications in Nonlinear Science and Numerical Simulation*, doi:10.1016/j.cnsns.2010.04.055, 2010.

## NONLINEAR OSCILLATIONS OF TURBOMACHINERY BLADES

Ivan D. Breslavsky<sup>1</sup>

ABSTRACT

Konstantin.V.  
Avramov

A.M. Podgorny Institute  
for Problems of  
Mechanical Engineering,  
Kharkov, Ukraine

The analysis of the free linear and geometrically nonlinear vibrations of the turbomachinery blades is presented in this paper. The results for the linear vibrations analysis are compared with the experimental ones. The vibrations in the case of multiple internal resonances are investigated. The analysis of nonlinear vibrations is carried out using the combination of nonlinear normal modes and the harmonic balance method.

### INTRODUCTION

The turbomachinery blades are one of the most important real applications of the shallow shells theory. Therefore, a lot of studies deal with the blade dynamics. Didkovskii [1] analyzed the parametric vibrations of turbomachinery blades in gas flow. The sufficient conditions of dynamical stability are obtained in this paper. The papers of Ross [2], Hoa [3] are devoted to linear vibration analysis of blades, which are modeled by shells. Venkatsan, Nagaraj [4] studied nonlinear vibrations of rotating blades. They came to the conclusion, that the frequency response can be hard or soft. The data of finite element analysis of turbomachinery blades are compared with experimental results in [5]. The vibrations of turbine blades under the action of longitudinal time periodic force have been considered by Chen, Peng [6]. Using geometrically nonlinear theory and the finite element method, the blade nonlinear model is obtained. Liew, Lim [7] used energetic approach to study linear vibrations of shallow shells with rectangular base and different Gaussian curvature. Mohamed Nabi and Ganesan [8] compared the beam and plate models of turbomachinery blades. They came to the conclusion that the plate models are better. The vibrations of shallow anisotropic blades are treated by Abe, Kobayashi, Yamada [9]. They used the Rayleigh-Ritz method to analyze linear vibrations. The finite-degree-of-freedom model is obtained by Bubnov-Galerkin procedure. Nonlinear vibrations of hydroturbine blades, which are modeled by pre-twisted shell with variable thickness and ring-shaped base, are treated in [10, 11]. The dependence of eigenfrequencies and eigenmodes on pre-twisted angle and thickness are investigated. Choi, Chou [12] analyze the blade vibrations taking into account the shear. The influence of shroud on vibrations is considered.

In this paper the free geometrically nonlinear oscillations of the turbomachinery blades are analyzed. The blades are considered as shallow shells of variable thickness and double curvature. Compressor blade and blade of hydroturbine are studied. The R-function method and the Rayleigh-Ritz approach are used collectively to obtain eigenmodes of linear vibrations. Nonlinear vibrations of shells are approximated by using these eigenmodes. Single-mode and multimode vibrations are studied. The backbone curves are presented and the stability of motions is analyzed.

### 1. METHOD OF ANALYSIS

The blades are modeled by shallow shells with variable thickness and double curvature. Thin blades are considered, so classical Love theory is applied. The Rayleigh-Ritz method is used to determine the eigenfrequencies and eigenmodes of linear vibrations. The potential energy of the shell can be presented as [13]:

<sup>1</sup> Corresponding author. Email [id.breslavsky@gmail.com](mailto:id.breslavsky@gmail.com)

$$\Pi = \frac{E}{2(1+\mu)} \int_{\Lambda} \left\{ \frac{1}{1-\mu} \left[ (\varepsilon_{11}^2 + 2\mu\varepsilon_{11}\varepsilon_{22} + \varepsilon_{22}^2) h(x, y) + \frac{h^3(x, y)}{12} (\chi_1^2 + 2\mu\chi_1\chi_2 + \chi_2^2) \right] + \frac{1}{2} \left[ \varepsilon_{12}^2 h(x, y) + \frac{1}{3} \tau^2 h^3(x, y) \right] \right\} AB dx dy,$$

where  $\varepsilon_1, \varepsilon_2, \gamma$  are components of membrane strains of shell middle surface;  $\chi_1, \chi_2, \tau$  are components of bending deformations of middle surface;  $A$  and  $B$  are Lamé coefficients;  $h(x, y)$  is a variable shell thickness;  $E, \mu$  are Young's modulus and Poisson's ratio. The kinetic energy of the shell has the following form:

$$T = \frac{\rho}{2} \int_{\Lambda} (\dot{w}^2 + \dot{u}^2 + \dot{v}^2) h(x, y) AB dx dy,$$

where  $u(x, y, t), v(x, y, t), w(x, y, t)$  are displacements of the middle surface points in the  $x, y, z$  directions, respectively;  $\rho$  is shell material density.

Nonlinear vibrations of the blade are approximated by eigenmodes of linear vibrations. Then the shell bending vibrations  $w(x, y, t)$  can be presented as:

$$w(x, y, t) = \sum_{i=1}^N \eta_i(t) \bar{w}_i(x, y), \quad (1)$$

where  $\bar{w}_i(x, y), i = \overline{1, N}$  are normalized eigenmodes of free linear vibrations. The displacements  $u$  and  $v$  can be presented as:

$$u(x, y, t) = \sum_{i=1}^N \eta_{i+N}(t) \bar{u}_i(x, y), \quad v(x, y, t) = \sum_{i=1}^N \eta_{i+2N}(t) \bar{v}_i(x, y), \quad (2)$$

where  $\bar{u}_i(x, y), i = \overline{1, N}$  and  $\bar{v}_i(x, y), i = \overline{1, N}$  are in-plane eigenmodes of vibrations. Using the kinetic and the potential energy, the Lagrange equations are derived. If the eigenfrequencies of longitudinal vibrations are significantly higher, than the eigenfrequencies of the bending vibrations, it is possible to neglect the in-plane inertial terms. The dependences of  $\eta_{N+1}, \dots, \eta_{3N}$  on  $\eta_1, \dots, \eta_N$  can be derived from the last  $2N$  Lagrange equations. The solution of the linear algebraic equations is substituted into the system of first  $N$  ordinary differential equations. As a result the system of  $N$  ordinary differential equations with respect to  $\eta_1, \dots, \eta_N$  is derived. After the transformation to the dimensionless modal variables  $\xi_1, \dots, \xi_N$  the system has following form:

$$\ddot{\xi}_k = f_k(\xi_1, \dots, \xi_N) = -\bar{\Omega}_k^2 \xi_k - \sum_{i=1}^N \sum_{j=1}^N l_{kij} \xi_i \xi_j - \sum_{i=1}^N \sum_{j=1}^N \sum_{g=1}^N l_{kijg} \xi_i \xi_j \xi_g, \quad k = \overline{1, N} \quad (3)$$

where  $\bar{\Omega}_k = \frac{\Omega_k}{\Omega_1}$  are dimensionless eigenfrequencies.

The Shaw-Pierre nonlinear modes [14, 15] are used to analyze the vibrations of the finite-degree-of-freedom system (30). Let us suppose, that the general coordinates  $\xi_1, \dots, \xi_M$  is active. Then the invariant manifolds of the system with internal resonances can be presented as [15]:

$$\xi_k = X_k(\xi_1, \dot{\xi}_1, \dots, \xi_M, \dot{\xi}_M); \quad \dot{\xi}_k = Y_k(\xi_1, \dot{\xi}_1, \dots, \xi_M, \dot{\xi}_M), \quad k = M+1, \dots, 2N \quad (4)$$

Nonlinear modes (4) satisfy the following partial differential equations:

$$\sum_{i=1}^M \frac{\partial X_k}{\partial \xi_i} \dot{\xi}_i + \sum_{i=1}^M \frac{\partial X_k}{\partial \dot{\xi}_i} f_i(\xi_1, \dots, \xi_M, X_{M+1}, \dots, X_{2N}) = Y_k \quad k = M+1, \dots, 2N \quad (5)$$

$$\sum_{i=1}^M \frac{\partial Y_k}{\partial \xi_i} \dot{\xi}_i + \sum_{i=1}^M \frac{\partial Y_k}{\partial \dot{\xi}_i} f_i(\xi_1, \dots, \xi_M, X_{M+1}, \dots, X_{2N}) = f_k(\xi_1, \dots, \xi_M, X_{M+1}, \dots, X_{2N})$$

The functions  $X_k, Y_k$  can be found as polynomials with respect to  $\xi_1, \dot{\xi}_1, \dots, \xi_M, \dot{\xi}_M$ . Now the equations (4) are substituted into the first  $M$  equations of the system (3). As a result, the system of  $M$  ordinary differential equations describing the motions on nonlinear mode is obtained:

$$\ddot{\xi}_k = f_k(\xi_1, \dots, \xi_M, X_{M+1}(\xi_1, \dot{\xi}_1, \dots, \xi_M, \dot{\xi}_M), \dots, X_{2N}(\xi_1, \dot{\xi}_1, \dots, \xi_M, \dot{\xi}_M)), \quad k = 1, \dots, M$$

These equations can be studied by harmonic balance method, multiple scales or other methods. The stability of motions in this work is analyzed by the Floquet-Lyapunov theory [16].

## 2. VIBRATIONS OF THE COMPRESSOR BLADE

The blade is modeled by pre-twisted shallow shell with trapezoidal base and variable thickness (Fig 1.).



Fig. 1 Sketch of blade

The boundary conditions on the clamped edge can be presented as:

$$w|_{x=0} = \frac{\partial w}{\partial n}|_{x=0} = 0, \quad u|_{x=0} = 0, \quad v|_{x=0} = 0$$

The node lines of the first eigenmodes are shown on the Figure 2. The results of the eigenmodes calculations (Fig. 2) are close to the data from [17, 18]. As follows from the calculations, the following internal resonances exist in the system:  $\bar{\Omega}_4 \approx \bar{\Omega}_5$ ;  $2\bar{\Omega}_3 \approx \bar{\Omega}_4$ ;  $2\bar{\Omega}_3 \approx \bar{\Omega}_5$ .

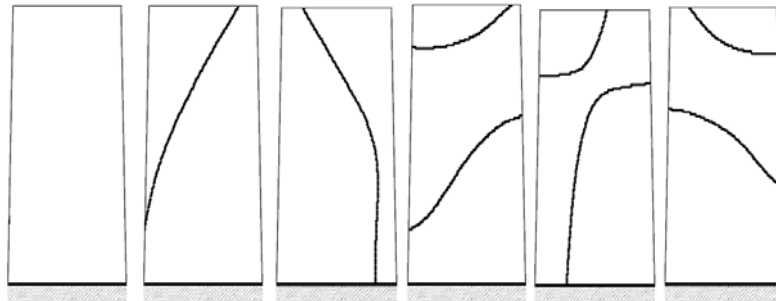


Fig. 2 Nodal lines vibrations eigenmodes

The first five eigenmodes are used in the expansions (1, 2) to obtain the finite degree-of-freedom model of the blade nonlinear vibrations. The nonlinear dynamics of this system is analyzed by nonlinear modes with  $\xi_3, \xi_4, \xi_5$  as independent variables. Figures 3-4 show the backbone curves on this invariant manifold. Unstable motions are shown by dotted lines. The multimode (Fig. 3) and single-mode motions (Fig. 4) are observed. The multimode motions can be stable (Fig. 4).

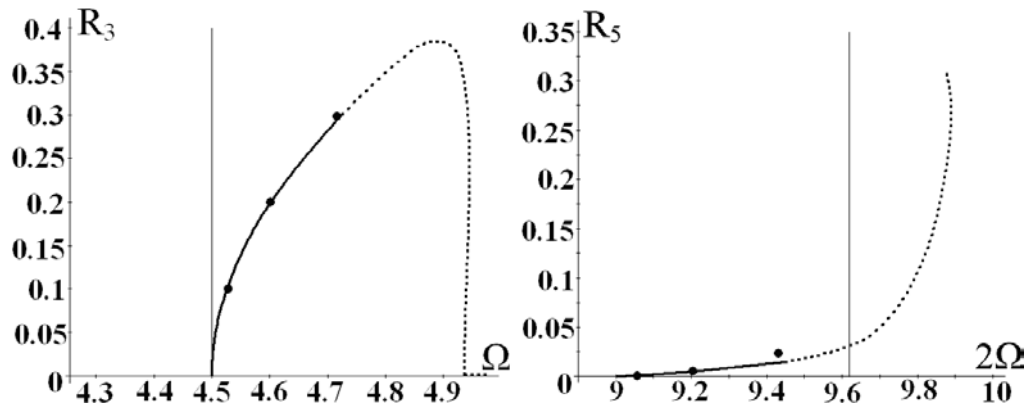


Fig. 3 The backbone curves of the vibrations with dominant general coordinate  $\xi_3$ , which excite autoparametrically the motions  $\xi_5$

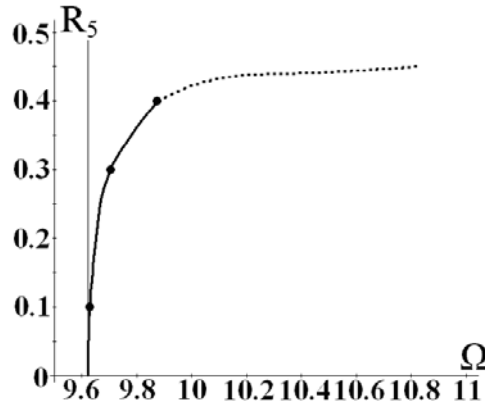


Fig. 4 The vibrations of the shell with dominant general coordinate  $\xi_5$

### 3. THE VIBRATION OF HYDROTURBINE BLADE

The blade of the axial flow turbine is described by the double-curved shallow shell with variable thickness. The shell base has a shape of ring sector, which has one rounded angle (Fig. 5). The node lines of the first eigenmodes are shown on the Figure 6, which is close to the known experimental and calculated results [19].

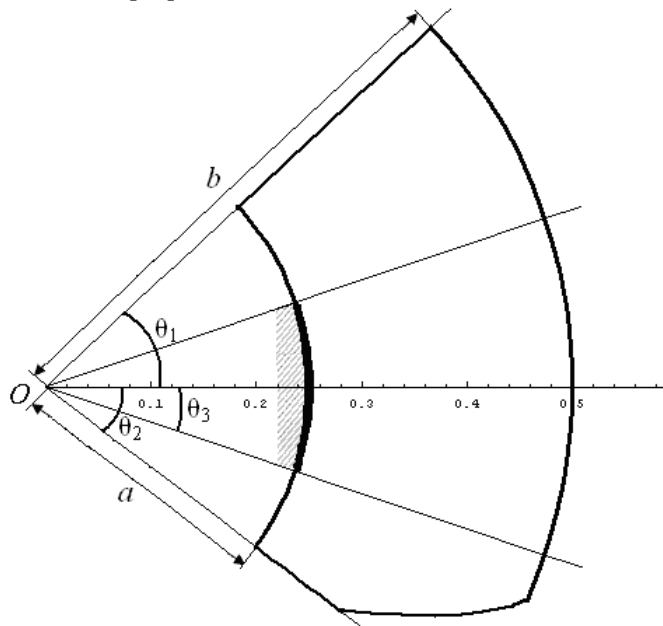


Fig. 5 Base of the shallow shell

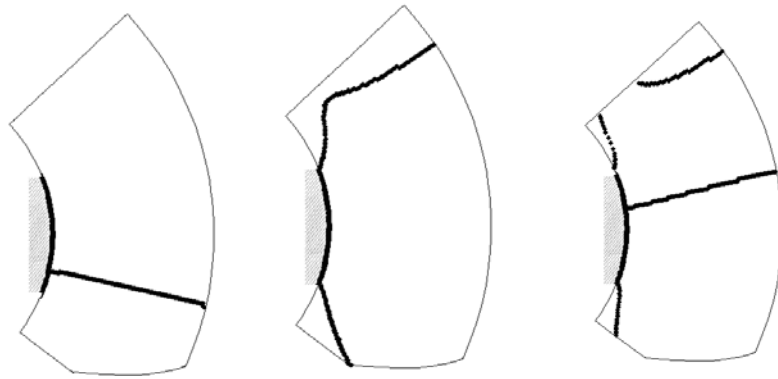


Fig. 6 Nodal lines of eigenmodes

The free nonlinear vibrations close to the first two eigenfrequencies are analyzed. In this case, three terms  $N = 3$  are enough in the expansion (1-2). Two invariant manifolds with independent variables  $\xi_1$  and  $\xi_2$  are considered. Figures 7-8 show the backbone curves.

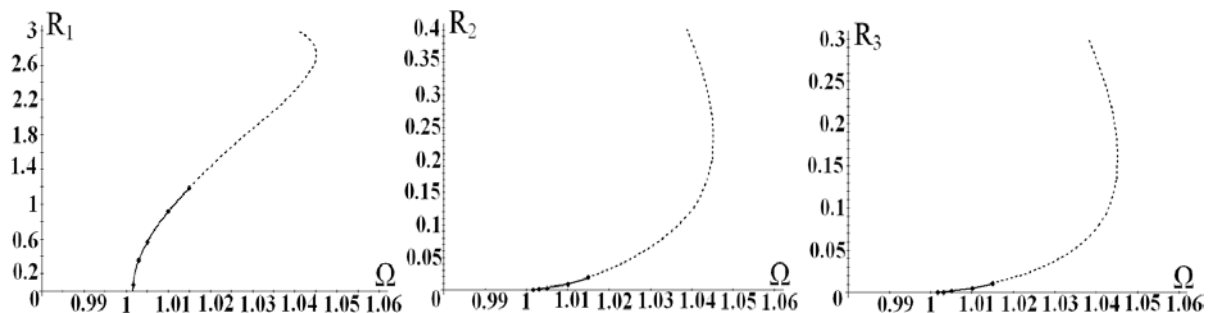


Fig. 7 The backbone curves of vibrations near the first eigenfrequency

## CONCLUSIONS

The analysis of free vibrations of turbomachinery blades are presented in this paper. The different modes of blades' nonlinear vibrations are described by hard backbone curves. It is mentioned that the amplitudes of stable vibrations of blade edges are in excess of blade thickness in this region. Therefore, nonlinear theory is required for description of blade dynamics. It is shown, that due to the presence of the internal resonances stable multimode vibrations exist in the system.

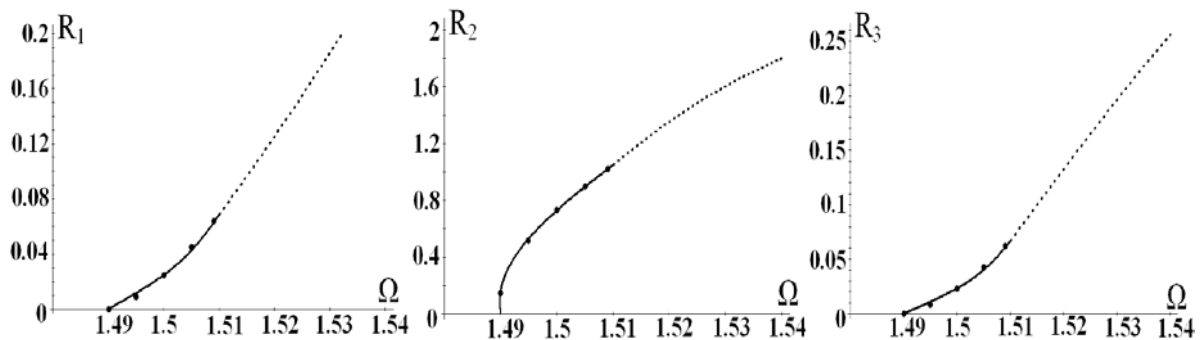


Fig. 8 The backbone curves of vibrations near the second eigenfrequency

## REFERENCES

- [1] Didkovskii, V.N. Parametric vibrations of turbomachines in a flow *Translated from Problemy Prochnosti*, 8, pp. 9-13, 1974.
- [2] Ross, C.T.F. Free vibration of thin shells *Journal of Sound and Vibration*, 39, 337-344, 1975.
- [3] Hoa, S.V. Vibration frequency of a curved blade with weighted edge *Journal of Sound and Vibration*, 79, pp. 107-119, 1981.
- [4] Venkatsan C., Nagaraj V.T. Non-linear flapping vibrations of rotating blades *Journal of Sound and Vibration*, 84, pp. 549-556, 1982.
- [5] Mindle W.L., Torvik P.J. Multiple modes in the vibration of cantilevered shells *Journal of Sound and Vibration*, 115, pp. 289-301, 1987.
- [6] Chen L.W., Peng W.K. Dynamic stability of rotating blades with geometrical non-linearity *Journal of Sound and Vibration*, 187, pp. 421-433, 1995.

- [7] Liew K.M., Lim C.W. Vibration of doubly-curved shallow shells *Acta Mechanica*, 114, pp. 95-119, 1996.
- [8] Mohamed Nabi S., Ganesan N. Comparison of beam and plate theories for free vibrations of metal matrix composite pre-twisted blades *Journal of Sound and Vibration*, 189, pp. 149-160, 1996.
- [9] Abe A., Kobayashi Y., Yamada G. Non-linear vibration characteristics of clamped laminated shallow shells *Journal of Sound and Vibration*, 234, pp. 405-426, 2000.
- [10] Hu X.X., Tsuiji T. Free vibration analysis of curved and twisted cylindrical thin panels *Journal of Sound and Vibration*, 219, pp. 63-68, 1999.
- [11] Sakiyama T., Hu X.X., Matsuda H., Morita C. Vibration of twisted and curved cylindrical panels with variable thickness *Journal of Sound and Vibration*, 254, pp. 481-502, 2002.
- [12] Choi S.-T., Chou Y.-T. Vibration analysis of elastically supported turbomachinery blades by the modified differential quadrature method *Journal of Sound and Vibration*, 240, pp. 937-953, 2001.
- [13] Grigoluk E.I., Kabanov V.V. *Stability of shells*, Nauka, Moscow, 1978. (in Russian)
- [14] Shaw S. W., Pierre C. Normal modes for nonlinear vibratory systems *Journal of Sound and Vibrations*, 164, pp. 58-124, 1993.
- [15] Jiang D., Pierre C., Shaw S.W. The construction of non-linear modes for systems with internal resonance *International Journal of Non-Linear Mechanics*, 40, pp. 729-746, 2005.
- [16] Yakubovich V.A., Starzhinskii V.M. *Linear Differential Equations with Periodic Coefficients* Wiley, New York, 1975.
- [17] Meerovich I.I. Vibrations of slightly curved and pre-twisted blades *Trudi CIAM*, 271, pp. 1-56, 1956. (in Russian)
- [18] Meerovich I.I. *Stress distribution in vibrating compressor blades*, Oborongiz, Moscow, 1961. (in Russian)
- [19] Filippov AP. *Vibrations of deformable systems*, Mashinostroenie, Moscow, 1970. (in Russian)

**NONLINEAR VIBRATIONS AND LONG-TERM STRENGTH  
OF TURBINE BLADES**

**D V. Breslavsky**<sup>1</sup>  
**O. K. Morachkovsky**  
**N. V. Shyriaieva**  
National Technical  
University "Kharkov  
Polytechnic Institute"  
Kharkov, Ukraine

---

ABSTRACT

---

The method of a durability estimation of rotating turbomachinery blades at forced flexural-flexural-torsional vibrations is offered. The method is based on the methods of Continuous Damage Mechanics and the accurate strain analysis of the pre-twisted blades at the nonlinear vibrations with moderate displacements. The method to solve the strain analysis problem and turbomachinery blades high-cycle fatigue damage estimation as a result of nonlinear vibrations is presented.

---

**INTRODUCTION**

Modernization of the existing steam turbines park is an actual problem. The decisions offered in this paper are connected with increasing the working pressure and changing the blades geometrical characteristics. In these operating conditions, the deflections of blades comparable with a thickness are possible. In this case, the new methods of an estimation of turbine' blades durability are necessary. The damage arising due to the vibrations at their geometrically nonlinear deformation were taking into account. Approaches offered earlier in [1-6] allow to estimate the deformed condition of blades at their geometrically nonlinear vibrations, and, on this basis to make the stress analysis. Following the damage theories, stated in works [7-9], it is possible to estimate the long term strength of blades.

The results of the nonlinear vibrations and the blade stress-strain analysis are considered in this paper. The estimation of blades durability by the number of cycles before failure due to high-cycle fatigue is presented. The fatigue damage of blades of steam turbine of type K-300-240 (Ukraine) was studied.

**1. THE ANALYSIS OF NONLINEAR VIBRATIONS AND STRESS-STRAIN STATE OF BLADES**

Following [1-6], the analysis of geometrically nonlinear vibrations of blades is made on the basis of pre-twisted beams with variable cross-section theory. As the beam has asymmetrical cross section, the gravity centre and the shear centre are in the different points. As the amplitudes of vibrations are commensurable with the blades thickness, the nonlinear geometric law for beam displacements and strains has to be used. In this case, strains are small and the strain-stress connection is linear. The equations of geometrically nonlinear vibrations of turbine blades were obtained in works [2-4].

The beam vibrations are considered with respect to the global coordinate system  $(\hat{x}, \hat{y}, \hat{z})$  (fig.1). It is assumed, that the beam cross sections remain planar. The coordinate system  $(\hat{\xi}, \hat{\eta}, \hat{\zeta})$  is attached to a beam cross section to predict its motions. The origin of this coordinate system is placed in the gravity centre of the cross section. Then the dynamics of the cross section is reduced to analysis of motions of the coordinate system  $(\hat{\xi}, \hat{\eta}, \hat{\zeta})$  with respect to the global system  $(\hat{x}, \hat{y}, \hat{z})$ .

---

<sup>1</sup> Corresponding author. Email [brdm@kpi.kharkov.ua](mailto:brdm@kpi.kharkov.ua)

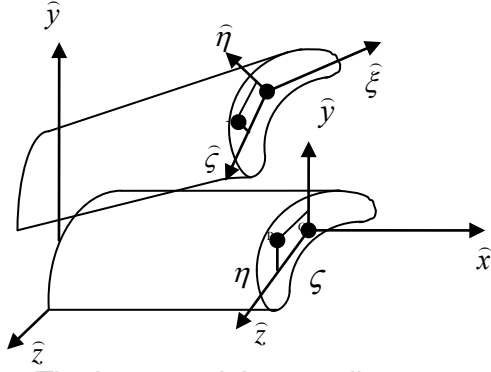


Fig. 1 The beam and the coordinates systems

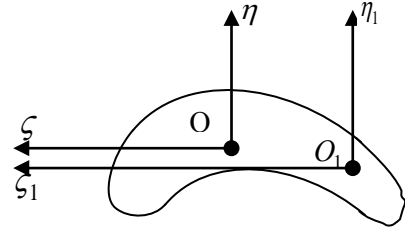


Fig. 2 The cross section of a beam

Cross section motions are described by displacements  $u, v, w$  in the directions  $\hat{x}, \hat{y}, \hat{z}$  and by three successive rotations. The angles  $\theta_z$  and  $\theta_y$  describe the beam bending vibrations in two perpendicular planes. The third rotation  $\theta_x$  takes place about the shear centre  $O_1$  and describes the torsion of a beam. The new coordinate system  $(\eta_1 O_1 \zeta_1)$  with the origin  $O_1$  in the shear centre is introduced to study this rotation (fig.2). Therefore, the cross section gravity centre  $O$  has the coordinates  $O(\eta^{(1)}, \zeta^{(1)})$  in the coordinate system  $(\eta_1 O_1 \zeta_1)$ .

The Hamilton's principle is used to derive the equations of rotating beams vibrations. Then the partial differential equations of beam nonlinear vibrations with respect to the warping have the form:

$$\begin{aligned}
 & E(w'' J_{\zeta\eta})'' + E(v'' J_{\zeta})'' - 2E(\theta_x v'' J_{\zeta\eta})'' + E[\theta_x w'' (J_{\zeta} - J_{\eta})]'' + m\ddot{v} - m\ddot{\theta}_x \zeta^{(1)} = 0; \\
 & E(w'' J_{\eta})'' + E(v'' J_{\zeta\eta})'' + E[\theta_x v'' (J_{\zeta} - J_{\eta})]'' + 2E(\theta_x w'' J_{\zeta\eta})'' + m\ddot{w} + m\ddot{\theta}_x \eta^{(1)} + P(x) \cos(\Omega t) = 0; \quad (1) \\
 & E(w'' J_{\zeta\eta} + v'' J_{\zeta}) w'' - E(w'' J_{\eta} + v'' J_{\zeta\eta}) v'' - (D_{\xi}^{(1)}(x) \theta_x') - m\ddot{v} \zeta^{(1)} + m\ddot{w} \eta^{(1)} + \ddot{\theta}_x [m(\zeta^{(1)2} + \eta^{(1)2}) + I_{\xi}] = 0; \\
 & \dot{u} = - \int_0^x \frac{\partial}{\partial t} (\theta_x v'' \zeta^{(1)} - \theta_x w'' \eta^{(1)}) dx - \int_0^x (v' \dot{v}' + w' \dot{w}') dx.
 \end{aligned}$$

where  $m$  is the weight of a beam length unit;  $E$  is the Young modulus;  $P(x) \cos(\Omega t)$  is the loading operating from gas forces;  $J_{\zeta\eta}, J_{\zeta}, J_{\eta}, D_{\xi}^{(1)}$  are the geometrical characteristics of cross-section of a blade.

The Galerkin method is used for discretization of the nonlinear partial differential equations (1). The beam vibrations are considered in the form:

$$W(x, t) = \sum_{v=1}^{N_1} q_v(t) W_v(x); \quad \theta_x(x, t) = \sum_{v=1}^{N_2} q_{v+N_1}(t) \theta_v(x); \quad V(x, t) = \sum_{v=1}^{N_3} q_{N_1+N_2+v}(t) V_v(x),$$

where  $q_1, \dots, q_{N_1+N_2+N_3}$  are the generalized coordinates of a system;  $W_v(x); \theta_v(x); V_v(x)$  are the forms of linear vibrations [3]. As the nonlinear vibrations of rotating beams close to the equilibrium position  $(q_1^{(0)}, q_8^{(0)}, q_{15}^{(0)})$ , then the change of the variables is used:

$$q_i = \theta_i + q_i^{(0)}; \quad i = \overline{1, 16}; \quad q_1^{(0)} \neq 0; \quad q_8^{(0)} \neq 0; \quad q_{15}^{(0)} \neq 0; \quad q_v^{(0)} = 0; \quad (v = \overline{2, 7, 9, 14, 16})$$

The following dynamic system is derived:

$$(M) \ddot{\theta} + (K) \theta + \Omega(G) \dot{\theta} + \Omega F(\theta, \dot{\theta}) + \Phi(\theta) = N \cos(\Omega t), \quad (2)$$

$$\theta = \begin{bmatrix} \theta_1 \\ \dots \\ \theta_{16} \end{bmatrix}; K'_{\nu\mu} = K_{\nu\mu} + \Omega^2 R_{\mu}^{(\nu)} + \tilde{K}_{\nu\mu}; (\nu = \overline{1,16}; \mu = \overline{1,16}) (K) = \begin{bmatrix} K'_{11} & \dots & K'_{1,16} \\ \dots & \dots & \dots \\ K'_{16,1} & \dots & K'_{16,16} \end{bmatrix};$$

$$f_{\nu} = \sum_{\mu=1}^2 \sum_{j=1}^{14} D_{14+\mu,j}^{(\nu)} \theta_j \dot{\theta}_{14+\mu}, (\nu = \overline{1,7}); f_l = \sum_{\nu=1}^{16} \sum_{\mu=1}^{16} D_{\nu\mu}^{(l)} \dot{\theta}_{\nu} \theta_{\mu}, (l = \overline{8,16});$$

$$\varphi_{\nu} = \sum_{\mu=1}^7 \sum_{j=1}^2 A_{\mu+7,14+j}^{(\nu)} \theta_{\mu+7} \theta_{14+j} + \sum_{\mu=1}^7 \sum_{j=1}^7 A_{\mu+7,j}^{(\nu)} \theta_{\mu+7} \theta_j; (\nu = \overline{1,7}; 15,16);$$

$$\varphi_l = \sum_{r_1=1}^7 \sum_{r_2=1}^7 A_{r_1 r_2}^{(l)} \theta_{r_1} \theta_{r_2} + \sum_{r_1=1}^2 \sum_{r_2=1}^2 A_{14+r_1,14+r_2}^{(l)} \theta_{14+r_1} \theta_{14+r_2} + \sum_{r_1=1}^2 \sum_{r_2=1}^7 A_{14+r_1,r_2}^{(l)} \theta_{14+r_1} \theta_{r_2}, l = \overline{8,14};$$

$$N = [f_1 \gamma, 0, \dots, 0]^T; f_1 = - \int_0^L W_1 W_{\nu} dx; \nu = 1, \dots, 7,$$

where  $L$  is a length of a blade.

To investigate the force vibrations in (2) the method of nonlinear normal modes in the combination with Rausher procedure was applied in works [5, 6]. On this basis, the frequency-response curves of the system and values of blades estimation parameters are derived. The further specification of the given stress peak values in a blade is carried out for 3D models by use the program complexes.

## 2. LONG-TERM FATIGUE STRENGTH ESTIMATION

Following modern approaches of the Continuous Damage Mechanics (CDM) theories, stated in works [7, 8], we will define the number of cycles before failure due to the high-cycle fatigue, using the stress analysis data at nonlinear vibrations. The fatigue damage phenomenon represents the irreversible process of accumulation of micro cracks in a material. The damaged condition is represented as initiation of a macroscopically crack (for materials of 0.1-1 mm). The fatigue damage, caused by repeating action of stresses, is defined as a function of stress cycle's number. The description of processes of the materials hidden damage in the modern mechanics is described by the concept of damage parameter [7, 8].

Consider a damage scalar parameter of  $D = D(N)$  in a point of a deformable body under the cyclic loading using hypothesis of isotropic damage. Here  $N$  is the number of loading cycles, and  $0 \leq D \leq 1$ ,  $D = 0$  for the undamaged material,  $D(N_*) = 1$  answers the material failure in a body point. Then the kinetic equation for the damage parameter is written in the following form [9]:

$$dD = f(\sigma_a / (1 - D)) dN, \quad (3)$$

where  $f(\sigma_a / (1 - D))$  is the function defined by use of stress-rupture curves under the cyclically changing stresses with peak values  $\sigma_a$ .

In the case of high cycle fatigue, the most probable limiting number of loading cycles before the failure is  $N_* > 5 \cdot 10^4 \div 5 \cdot 10^5$ . For the description of the fatigue damage accumulation the classical laws used an amplitude of variable stresses  $\sigma_a$  [7].

Then the equation (3) can be concretized, using the auto- model law [7]:

$$\frac{dD}{dN} = \frac{F \sigma_a^k}{(1 - D)^k}, \quad (4)$$

where  $F$  and  $k$  are the material's constants [11].

Processes of turbine blades loadings are characterized by static and variable loadings. For a case of joint action of static  $\sigma_0$  and cyclically changing stresses the following dependence is used

$$\sigma_a = \sigma_0 + b\sigma_m; b = \frac{\sigma_{-1}}{\sigma_a}, \quad (5)$$

where  $\sigma_m$  is an average stress of a cycle;  $\sigma_\epsilon$  is an ultimate strength;  $\sigma_{-1}$  is a fatigue limit [10]. The equation (4) is being generalized to estimate the fatigue strength. Thus, various criteria of fatigue strength are used for equivalent stress  $\sigma_\epsilon$ :

$$\frac{dD}{dN} = \frac{F\sigma_e^k}{(1-D)^k}. \quad (6)$$

Sines criterion for equivalent stress is used [7]:

$$\sigma_e = \tau_{ocm}^a = 3b\bar{\sigma}_H, \quad (7)$$

where  $\tau_{ocm}^a = \frac{\sqrt{2}}{3} \left( \frac{3}{2} \sigma_a \sigma_a \right)^{\frac{1}{2}}$  is an octahedronal stress amplitude;  $\bar{\sigma}_H = \frac{1}{3} (\sigma_{11}^m + \sigma_{22}^m + \sigma_{33}^m)$  is a hydrostatic pressure component of the cycle stress.

It is possible to define the value of limiting number of cycles till the moment of the macro crack initiation by the integration of the kinetic damage equation (6) at constant stresses

$$N_* = \frac{1}{F\sigma_e^k(k+1)}. \quad (8)$$

Thus, the durability of turbine blades can be estimated by using data of the number of cycles before failure due to high cycle fatigue (8).

### 3. DURABILITY ESTIMATIONS OF STEAM TURBINE BLADES OF TYPE K-300-240

The following data are used for calculations of steam turbine blade:  $E = 2.12 \cdot 10^5 \text{ MPa}$ ;  $G = 78 \cdot 10^5 \text{ MPa}$ ;  $\rho = 7.859 \cdot 10^3 \text{ kg/m}^3$ ;  $L = 0.342 \text{ m}$ ;  $J_\eta = 6.45 \cdot 10^{-8} \text{ m}^4$ ;  $J_\zeta = 10.91 \cdot 10^{-8} \text{ m}^4$ ;  $A = 483.391 \cdot 10^{-6} \text{ m}^2$ ;  $\zeta^{(1)} = -7.7 \cdot 10^{-3} \text{ m}$ .  $F = 3.94 \cdot 10^{-38} \left( \frac{\kappa G}{\text{mm}^2} \right)^k$ ;  $k = 16.1$ . The blade's cross-section is shown in fig. 2.

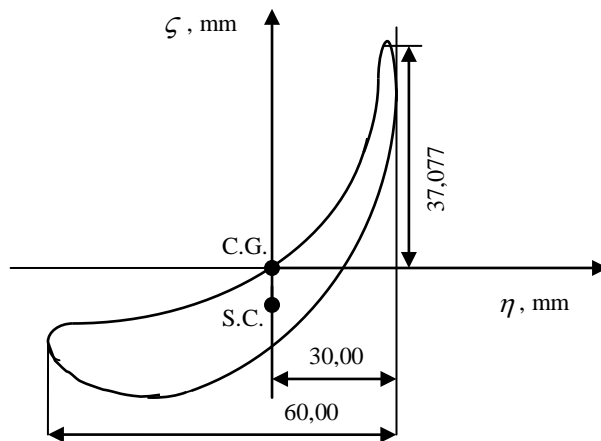


Fig. 2 The blade cross-section

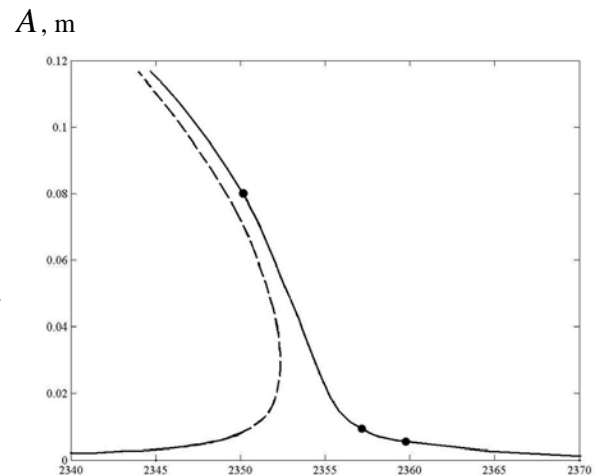


Fig. 3 The blade frequency-response curve

Applying the method of nonlinear normal modes in a combination with a Rausher procedure, the frequency-response curve of a system is presented in fig. 3. The frequency-response curve of a considered blade is soft. So the contribution of the blade rotatory inertia in the nonlinearity is bigger than the curvature of the axis displacements.

The specified analysis of the blade's 3D stress-strain state for three cases of forced vibrations amplitudes is made: 1) 0.08 m, 2) 0.006 m, 3) 0.0078 m. Calculations for the stress state in the first case have shown, that conditions of short-term durability are not satisfied ( $\sigma_{max} = 6420$  MPa,  $h_{max} = 8 \cdot 10^{-2}$ ). For a second case the von Mises equivalent peak stress distribution on a blade's surface is presented in fig.5. The distribution of the stresses in a blade, which is under the action of a static steam pressure, is presented in fig. 6.

The results of calculations are shown in tab. 2.

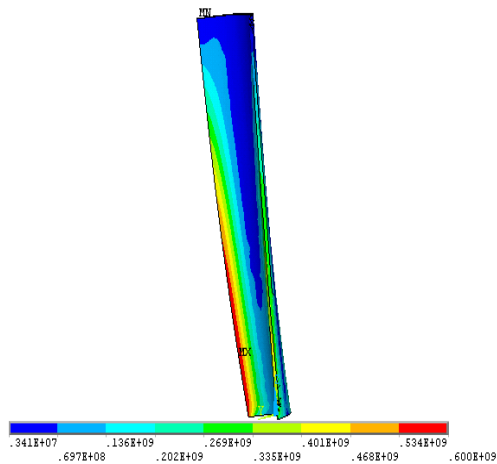


Fig. 5 The intensity values distribution of peak stresses in a blade, the maximum displacement on a free side is  $0.78 \cdot 10^{-2}$  m

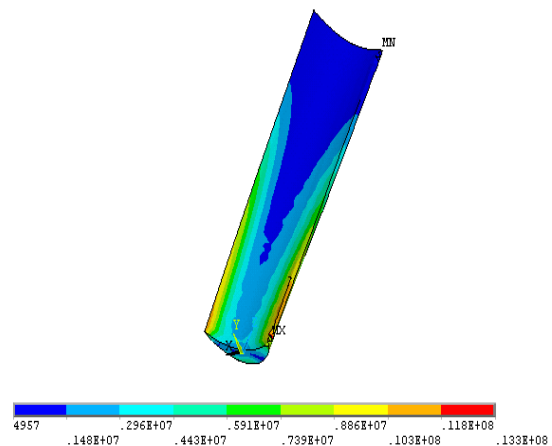


Fig. 6 Equivalent stresses in a blade under the pressure of a steam stream  $P=7$  kPa

Table 2 Characteristics of the 3-rd stage blade of the powerful steam turbine of type K-300-240

Material (steel)	T, K	Von Mises equivalent stress, MPa	Number of cycles to failure
12X13 (1X13), 403 US	423	392.7	$7.62 \cdot 10^8$
		516.2	$2.95 \cdot 10^6$
12X13 (1X13), 403 US	723	392.7	$2.42 \cdot 10^5$
		516.2	-
322 US (aged and hardened)	423	392.7	$3.32 \cdot 10^{10}$
		516.2	$4.08 \cdot 10^8$
450 US	423	392.7	$2.65 \cdot 10^9$
		516.2	$1.03 \cdot 10^7$
EI437Б	973	392.7	$1.07 \cdot 10^7$
		516.2	$4.24 \cdot 10^5$

The analysis of results shows, that only the blades made of in a special way thermo processed steel 322 (USA), and working in a mode 3 (the forced vibrations amplitude is 8 mm), are agreed with the requirements of designers. In this case, the number of cycles before failure is equal to  $4.08 \cdot 10^8$ , that is smaller than  $2 \cdot 10^7$  cycles. If requirements are softened to  $N = 1 \cdot 10^7$ , then the blades from a steel 450 (USA) also can maintain similar amplitudes. For the second mode (with amplitude of 6 mm) inadmissible are values of the operational temperatures exceeding 423 K for steel 12X13 (1X13), and for steel ЭИ437Б at  $T=973$  K a life time value should be limited by the number of cycles  $N = 1 \cdot 10^7$ .

## CONCLUSIONS

In this paper the methods of solving the nonlinear vibrations analysis problem and stress analysis problem were offered. These methods are applied to get estimations of turbine blades' low - cycle fatigue with respect to damages due to geometrically nonlinear vibrations. Using experimental curves of fatigue strength, it is possible to define the number of cycles to failure. The results are used to make conclusions on a choice of blades' materials that satisfy to the design requirements. The powerful steam turbine blades of type K-300-240 were used for investigations.

## REFERENCES

- [1] Vorobiev B.F., Shorr Yu. S. *The Theory of Pre-twisted Rods.*, Naukova Dumka, Kiev, 1983. (in Russian).
- [2] Avramov K.V., Galas O.S., Pierre C. The geometrically nonlinear flexural- flexural- torsional vibrations model of rotating beams with the account of cross-section section warping *Mechanical engineering Problems*, Vol. 2. pp. 70-76, 2007. (in Russian)
- [3] Avramov K.V., Pierre C., Shyriaieva N. Flexural- flexural- torsional nonlinear vibrations of pre-twisted rotating beams with asymmetric cross- section. *J.Vibration and Control*, Vol. 13. pp. 329–364, 2007.
- [4] Avramov K.V., Pierre C., Shyriaieva N.V. Non-linear equations of flexural-flexural-torsional oscillations of rotating beams with arbitrary cross section. *Appl.Mechanics*, Vol. 5, pp. 123–133, 2008.
- [5] Avramov K.V. The analysis of forced vibrations in mechanical systems by use of non-linear normal forms/ in 'Academician Alexander Mihajlovich Lyapunov. To the 150 anniversary from the date of birth'. Ed. L.L.Tovazhnjansky. Kharkov: NTU "KhPI", pp. 228-247, 2007. (in Russian)
- [6] Avramov K.V. Application of nonlinear normal modes to the analysis of the forced vibrations. *Appl. Mechanics*, Vol. 10, pp. 65-78, 2008. (in Russian)
- [7] Lemaitre J., Chaboche J.-L. *Mechanics of solid materials*, Cambridge University press, 1994.
- [8] Lemaitre J. *A course on damage mechanics*, Springer- Verlag, Berlin, 1996.
- [9] Gusev A.S. *Fatigue resistance and survivability of structures at random loadings*. Mechanical engineering, Moscow, 1989. (in Russian)
- [10] Troshchenko V.T., Matveev V.V., Grjaznov B.A. and other. *Load bearing ability of Gas Turbine Engine blades at vibration conditions*, Naukova dumka, Kiev, 1981. (in Russian)

## NUMERICAL AND EXPERIMENTAL INVESTIGATIONS OF FRACTURE IN THIN-WALLED STRUCTURES AT IMPACT LOADING

**D. Breslavsky<sup>1</sup>,**  
**I. Naumov,**  
**A. Onyshchenko**  
National Technical  
University "Kharkov  
Polytechnic Institute",  
Kharkov, Ukraine

---

### ABSTRACT

---

The paper contains the description of combined analytical-numerical method for solution of the problem of impact damage accumulation and fracture in thin free supported plate. The results of experimental investigations of this plate are discussed.

---

### INTRODUCTION

Mechanics of impact interaction of solids is widely developed now due to growing demands of safety in modern industrial applications. The great amount of works had been performed in the direction of impact loading of thin-walled structures [1, 2], which shows the practical necessity of these developments for automobile, rail and aircraft transport, power energetics, nuclear and chemical industry.

However, the important number of failures in thin-walled plates and shells connects with the damage accumulation in the material due to repeating impacts. Such fracture can appear in airplane and space panels, motor and turbine casings etc. Now impact damage problems are poor studied owing to deficit of experimental results in that area.

The presented paper contains the method for calculations of stress-strain state and damage distribution in thin-walled free supported rectangular plate. The method is based on the analytical solutions of boundary problem as well as on the numerical time integration schemes. The experimental results of the low-cycle impact fracture in those plates are given in the second part.

### 1. PLATE UNDER IMPACT LOADING.

Let us regard thin free supported orthotropic rectangular plate of a constant thickness. The plate is loaded by the impactor (spherical, conical or cylindrical), which at the time of the contact has the velocity  $v_0$  and mass  $m$ . Following classical approaches of W. Goldsmith [3] and A.P. Philippov [4] we'll use the combined analytical -numerical method.

The deflection in the place of contact will be considered for elasto-plastic deformation in the following form [5] :

$$\varepsilon = k \cdot P^{2/3} + \chi P^q, \quad \varepsilon = y - W \quad (1)$$

where  $P$  is a contact impact force,  $\varepsilon$  is a joint deflection of the impactor  $y$  and plate  $W$ ,  $\chi$  and  $q$  are material constants. The coefficient  $k$  is determined for regarded indentors due to relations presented in [2].

The basic unknown contact force  $P$  is determined by the following relations, which is derived from 2<sup>nd</sup> Newton law:

$$y(t) = v_0 \cdot t - \frac{1}{m} \cdot \int_0^t dt \int_0^t P(t) dt \quad (2)$$

---

<sup>1</sup> Corresponding author. Email [brdm@kpi.kharkov.ua](mailto:brdm@kpi.kharkov.ua)

Let us use the Timoshenko first order shear deformation theory for the solution of thin plate bending. Linear  $\varepsilon_x, \varepsilon_y, \varepsilon_z$  and shear  $\gamma_{xy}, \gamma_{xz}, \gamma_{yz}$  strains of the plate are connected with plate middle surface's displacements  $U_e, V_e, W$  and shear angles  $\theta_x, \theta_y$  by following relations:

$$\begin{cases} \varepsilon_x = \frac{\partial U_e}{\partial x} + \frac{\partial \theta_x}{\partial x} \cdot z; \varepsilon_y = \frac{\partial V_e}{\partial y} + \frac{\partial \theta_y}{\partial y} \cdot z; \gamma_{xy} = \frac{\partial U_e}{\partial y} + \frac{\partial V_e}{\partial x} + \left( \frac{\partial \theta_x}{\partial y} + \frac{\partial \theta_y}{\partial x} \right) \cdot z \\ \gamma_{xz} = \theta_x + \frac{\partial W}{\partial x}; \quad \gamma_{yz} = \theta_y + \frac{\partial W}{\partial y} \end{cases} \quad (3)$$

The forces and moments in the middle surface  $N = \{N_x, N_y, N_{xy}\}^T$ ,  $M = \{M_x, M_y, M_{xy}\}^T$ ,  $Q = \{Q_x, Q_y\}^T$  are connected with the displacements and curvature varyings:

$$\begin{Bmatrix} N \\ M \\ Q \end{Bmatrix} = \begin{bmatrix} A & B & 0 \\ B & D & 0 \\ 0 & 0 & \bar{A} \end{bmatrix} \begin{Bmatrix} e^0 \\ k \\ \gamma_z^0 \end{Bmatrix}, \quad (4)$$

where  $\{e^0\} = \left\{ \frac{\partial U_e}{\partial x}, \frac{\partial V_e}{\partial y}, \frac{\partial U_e}{\partial y} + \frac{\partial V_e}{\partial x} \right\}$ ,  $\{k\} = \left\{ \frac{\partial \theta_x}{\partial x}, \frac{\partial \theta_y}{\partial y}, \left( \frac{\partial \theta_x}{\partial y} + \frac{\partial \theta_y}{\partial x} \right) \right\}$ ,  $\{\gamma_z^0\} = \{\gamma_{xz}, \gamma_{yz}\}$ .

$A, B, D, \bar{A}$  are the block matrixes which are determined by the elasticity matrix coefficients for orthotropic solid:

$$\begin{Bmatrix} \sigma_x \\ \sigma_y \\ \tau_{zy} \\ \tau_{zx} \\ \tau_{xy} \end{Bmatrix} = \begin{bmatrix} C_{11} & C_{12} & 0 & 0 & 0 \\ C_{21} & C_{22} & 0 & 0 & 0 \\ 0 & 0 & C_{44} & 0 & 0 \\ 0 & 0 & 0 & C_{55} & 0 \\ 0 & 0 & 0 & 0 & C_{66} \end{bmatrix} \cdot \begin{Bmatrix} \varepsilon_x \\ \varepsilon_y \\ \gamma_{zy} \\ \gamma_{zx} \\ \gamma_{xy} \end{Bmatrix}, \quad (5)$$

$$A_{ij} = \int_{z_0}^{\bar{z}_n} C_{ij} d\bar{z}, \quad B_{ij} = \int_{z_0}^{\bar{z}_n} C_{ij} \bar{z} d\bar{z}, \quad D_{ij} = \int_{z_0}^{\bar{z}_n} C_{ij} \bar{z}^2 d\bar{z}, \quad i, j = \overline{1,3}$$

$$\bar{A}_{ij} = \int_{z_0}^{\bar{z}_n} C_{ij} d\bar{z}, \quad i, j = \overline{4,5}$$

In the case of the coordinate system which is placed in the middle surface of a plate and if it is subjected by symmetric loading, the problem of forced vibrations can be divided into two independent ones. In this case [B] is zero matrix.

$$\left\{ \begin{array}{l}
\frac{\partial Q_x}{\partial x} + \frac{\partial Q_y}{\partial y} = \rho \cdot h \cdot \frac{\partial^2 W}{\partial t^2} - q \\
\frac{\partial M_x}{\partial x} + \frac{\partial M_{xy}}{\partial y} = Q_x + \rho \cdot \frac{\left( \begin{smallmatrix} -3 & -3 \\ z_n & -z_0 \end{smallmatrix} \right)}{3} \cdot \frac{\partial^2 \theta_x}{\partial t^2} + \rho \cdot \frac{\partial^2 U_e}{\partial t^2} \cdot \frac{\left( \begin{smallmatrix} -2 & -2 \\ z_n & -z_0 \end{smallmatrix} \right)}{2} \\
\frac{\partial M_{yx}}{\partial x} + \frac{\partial M_y}{\partial y} = Q_y + \rho \cdot \frac{\left( \begin{smallmatrix} -3 & -3 \\ z_n & -z_0 \end{smallmatrix} \right)}{3} \cdot \frac{\partial^2 \theta_y}{\partial t^2} + \rho \cdot \frac{\partial^2 V_e}{\partial t^2} \cdot \frac{\left( \begin{smallmatrix} -2 & -2 \\ z_n & -z_0 \end{smallmatrix} \right)}{2} \\
\frac{\partial N_x}{\partial x} + \frac{\partial N_{xy}}{\partial y} = \rho \cdot h \cdot \frac{\partial^2 U_e}{\partial t^2} + \rho \cdot \frac{\partial^2 \theta_x}{\partial t^2} \cdot \frac{\left( \begin{smallmatrix} -2 & -2 \\ z_n & -z_0 \end{smallmatrix} \right)}{2} \\
\frac{\partial N_{xy}}{\partial x} + \frac{\partial N_y}{\partial y} = \rho \cdot h \cdot \frac{\partial^2 V_e}{\partial t^2} + \rho \cdot \frac{\partial^2 \theta_y}{\partial t^2} \cdot \frac{\left( \begin{smallmatrix} -2 & -2 \\ z_n & -z_0 \end{smallmatrix} \right)}{2}
\end{array} \right. \quad (6)$$

Here  $\bar{z}_n, \bar{z}_0$  are the coordinates of bottom and top plate's surfaces. By substituting (3) into (6), the system of equations of plate's forced oscillations, which is written on displacements, had been obtained:

$$\left\{ \begin{array}{l}
A_{11} \cdot \frac{\partial^2 U}{\partial x^2} + A_{12} \cdot \frac{\partial^2 V}{\partial x \partial y} + B_{11} \cdot \frac{\partial^2 \theta_x}{\partial x^2} + B_{12} \cdot \frac{\partial^2 \theta_y}{\partial x \partial y} + A_{33} \cdot \left( \frac{\partial^2 U}{\partial y^2} + \frac{\partial^2 V}{\partial x \partial y} \right) + \\
B_{33} \cdot \left( \frac{\partial^2 \theta_x}{\partial y^2} + \frac{\partial^2 \theta_y}{\partial x \partial y} \right) = \rho \cdot h \cdot \frac{\partial^2 U}{\partial t^2} + \rho \cdot \frac{\partial^2 \theta_x}{\partial t^2} \cdot \frac{\left( \begin{smallmatrix} -2 & -2 \\ z_n & -z_0 \end{smallmatrix} \right)}{2} \\
A_{22} \cdot \frac{\partial^2 V}{\partial y^2} + A_{12} \cdot \frac{\partial^2 U}{\partial x \partial y} + B_{22} \cdot \frac{\partial^2 \theta_y}{\partial y^2} + B_{12} \cdot \frac{\partial^2 \theta_x}{\partial x \partial y} + A_{33} \cdot \left( \frac{\partial^2 V}{\partial x^2} + \frac{\partial^2 U}{\partial x \partial y} \right) + \\
B_{33} \cdot \left( \frac{\partial^2 \theta_y}{\partial x^2} + \frac{\partial^2 \theta_x}{\partial x \partial y} \right) = \rho \cdot h \cdot \frac{\partial^2 V}{\partial t^2} + \rho \cdot \frac{\partial^2 \theta_y}{\partial t^2} \cdot \frac{\left( \begin{smallmatrix} -2 & -2 \\ z_n & -z_0 \end{smallmatrix} \right)}{2} \\
A_{55} \left( \frac{\partial \theta_x}{\partial x} + \frac{\partial^2 W}{\partial x^2} \right) + A_{44} \left( \frac{\partial \theta_y}{\partial y} + \frac{\partial^2 W}{\partial y^2} \right) = \rho \cdot h \cdot \frac{\partial^2 W}{\partial t^2} - q \\
B_{11} \cdot \frac{\partial^2 U}{\partial x^2} + B_{12} \cdot \frac{\partial^2 V}{\partial x \partial y} + D_{11} \cdot \frac{\partial^2 \theta_x}{\partial x^2} + D_{12} \cdot \frac{\partial^2 \theta_y}{\partial x \partial y} + B_{33} \cdot \left( \frac{\partial^2 U}{\partial y^2} + \frac{\partial^2 V}{\partial x \partial y} \right) + \\
D_{33} \cdot \left( \frac{\partial^2 \theta_x}{\partial y^2} + \frac{\partial^2 \theta_y}{\partial x \partial y} \right) = A_{55} \cdot \left( \theta_x + \frac{\partial W}{\partial x} \right) + \rho \cdot \frac{\left( \begin{smallmatrix} -3 & -3 \\ z_n & -z_0 \end{smallmatrix} \right)}{3} \cdot \frac{\partial^2 \theta_x}{\partial t^2} + \rho \cdot \frac{\partial^2 U_e}{\partial t^2} \cdot \frac{\left( \begin{smallmatrix} -2 & -2 \\ z_n & -z_0 \end{smallmatrix} \right)}{2} \\
B_{22} \cdot \frac{\partial^2 V}{\partial y^2} + B_{12} \cdot \frac{\partial^2 U}{\partial x \partial y} + D_{22} \cdot \frac{\partial^2 \theta_y}{\partial y^2} + D_{12} \cdot \frac{\partial^2 \theta_x}{\partial x \partial y} + B_{33} \cdot \left( \frac{\partial^2 V}{\partial x^2} + \frac{\partial^2 U}{\partial x \partial y} \right) \\
+ D_{33} \cdot \left( \frac{\partial^2 \theta_y}{\partial x^2} + \frac{\partial^2 \theta_x}{\partial x \partial y} \right) = A_{44} \cdot \left( \theta_y + \frac{\partial W}{\partial y} \right) + \rho \cdot \frac{\left( \begin{smallmatrix} -3 & -3 \\ z_n & -z_0 \end{smallmatrix} \right)}{3} \cdot \frac{\partial^2 \theta_y}{\partial t^2} + \rho \cdot \frac{\partial^2 V_e}{\partial t^2} \cdot \frac{\left( \begin{smallmatrix} -2 & -2 \\ z_n & -z_0 \end{smallmatrix} \right)}{2}
\end{array} \right. \quad (7)$$

Further the displacements, angles and loading functions are presented as an expansions on trigonometric series. Such representation of solution automatically satisfies the boundary conditions of free supported plate. After substitution of these series into system (6) we use the properties of orthogonality of trigonometric functions. As a result of the system's solution unknown functions  $P(t)$ ,  $W_{mk}(t)$ ,  $F_{mk}(t)$ ,  $H_{mk}(t)$ ,  $U_{mk}(t)$ ,  $V_{mk}(t)$  are obtained. The operational method is used.

Inverse Laplace transformation is used for transition to originals. The contact force  $P(t)$  is obtained by use the convolution theorem:

$$P(\psi) \cdot W_{mk}(\psi) \rightarrow \int_0^t P(\tau) \cdot W_{mk}(t-\tau) d\tau$$

The equations (1) and (2) are rewritten in the following form:

$$k \cdot P(t)^{\frac{2}{3}} + \chi P(t)^q = v_0 \cdot t - \frac{1}{m} \cdot \int_0^t dt \int_0^t P(t) dt - W(P(t)) \quad (8)$$

This equation is nonlinear relatively unknown contact force  $P(t)$ . For its solution let us use the numerical integration [3, 4]. The basic period of oscillation  $T_1$  is divided on  $2s$  intervals:

$\tau = \frac{T_1}{2 \cdot s} = \frac{\pi}{\omega_1 \cdot s}$ . Let us permit, that the force  $P(t)$  in each time interval is varied by linear law

$$P(t) = P_j - (P_j - P_{j-1}) \cdot \left( j - \frac{t}{\tau} \right), (j-1) \cdot \tau < t < j \cdot \tau \quad (9)$$

The equation for finding of contact force in the time moment  $t=j\tau$  is written as follows:

$$\varepsilon(j\tau) = y(j\tau) - W(j\tau) \quad (10)$$

The force value  $P(j\tau)$  is determined consequently, starting from first time interval, for which  $P_0=0$ ,  $P(\tau)=P_1$ . The calculations are organized in the following procedure. At the instant moment of impact the value of  $\varepsilon$  (for example,  $\varepsilon \approx v_0 \tau$ ) is set, further the  $P_1$  is calculated and the new precised  $\varepsilon = k \cdot (P_1)^{\frac{2}{3}} + \chi(P_1)^q$  is determined. The values of  $P_2$ ,  $P_3$  and other unknowns are calculated in similar way. The calculations perform for the time moment  $t=j\tau$ , in which  $P(j\tau)$  received the zero value, namely for the case of impactor separation from the plate. After finding of contact force another unknowns like displacements, angles  $\theta_x, \theta_y$ , moments, forces and stresses in the plate are determined.

## 2. IMPACT DAMAGE AND FRACTURE IN RECTANGULAR PLATE

Impact damage accumulation phenomenon occurs in the case of repeated impact action [6]. Its mechanism is close to low-cycle fatigue. Let us use the Rabotnov-Kachanov damage kinetic equation [7]:

$$\dot{\omega} = D \frac{(\Delta\sigma^e)^m}{(1-\omega)^m} \quad \omega(0) = 0, \quad \omega(t_*) = \omega_*, \quad (11)$$

where  $\omega$  is the damage parameter,  $\Delta\sigma^e$  is the equivalent stress calculated by stress amplitudes for each impact,  $D$  and  $m$  are the material constants in the damage law.

The calculation order in the case of the analysis of impact damage accumulation in free supported rectangular plate is following. For each case of impact loading the formulated above method is used in order to determine the maximum amplitude stress values  $\Delta\sigma_{ij}$  in each plate's point by use of determined value of impact contact force  $P$ . Further the calculated equivalent amplitude stress  $\Delta\sigma^e$  is used in (11) for calculation of the damage parameter value  $\omega$  in that points. The equivalent stress is determined by three invariants criterion [7]. Calculations are terminated if the damage parameter in one point reaches its critical value  $\omega_*$  (as a rule  $\omega_*=1$ ).

The impact damage accumulation up to fracture of considered free supported plate was studied by experimental way. The square plates with side 0.18 m and thickness 0.0015m were tested. The material of the plates is steel 12H18N10T.

Information and measuring system (IMS) had been developed in the Department of Control Systems and Processes of National Technical University 'Kharkiv Polytechnic Institute' was used for experimental analysis [8]. The appointment of system is strain registration in the processes of impact loading of thin plates. It composes from the strain gauges, signal unit sensors, unit of interface and protection, ADC board ADA-1406 and personal computer.

The IMS is the part of laboratory testing system (LTS), which additionally includes the device of plate fixation and the loading system, which works by use of electrical-mechanical pulse converter. The acceleration of the impactor is performed by use of magnetic field coil. The cylindrical impactors with diameter 0.004m were used.

Determination of the constants for damage law (11) was performed on the specimens which had been cut from same steel sheet. 6 specimens and 3 plates were tested.

The test sequence includes four groups of experiments: 1) static plate loading; 2) elastic impact of plate; 3) impact low-cycle uniaxial tests; 4) impact low-cycle plate fracture.

Experiments from first and second group were performed for calibration of the developed LTS. Static loading of the plate was used for strain gauge's calibration. The correlation between measured voltage and strains were established. After that the impact elastic loading of plates with spherical and cylindrical impactors were studied. For each strain gauge the dependencies from time were determined. Fig. 1 contains the signal plots have been obtained by the developed IMS.



Fig. 1 Strain measuring by IMS

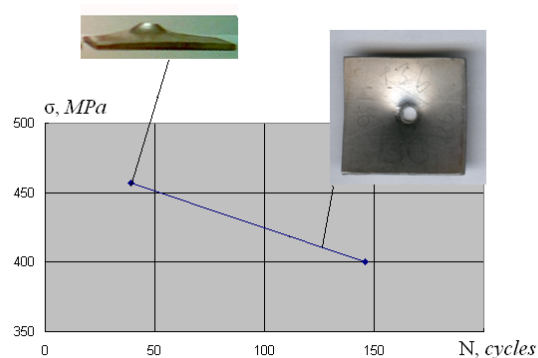


Fig.2 Impact long term data

As a result of uniaxial impact test the averaged values of the numbers of cycles to fracture were determined. For the first group with stress 400 MPa it was 146 cycles, for second, with another stress 457 MPa, it was 39 cycles. Fig. 2 contains impact low cycle long strength data, which have been obtained in these experiments, as well as the illustrations of the one destroyed specimen from each group. The fracture of specimens occurred by punching.

Material constants involve in kinetic damage equation (11) were obtained by use of experimental data. There values are:  $D=1 \cdot 10^{-29} (\text{MPa})^{-1}/\text{cycle}$ ,  $m=9.9$ .

Let us describe the experimental investigation of impact low-cycle plate fracture. The plates were placed in fixation device realizing the free support and were impacted by repeating loading up to punching. The velocity of impactor was 0.0625 m/s. The average value of the number of cycles to fracture was 79 impacts, variation of the data did not exceed 16%. Let us stress the reasonably local

character of plastic deformation of the plates, the area does not exceed of 6% of total plate's area (Fig. 3).

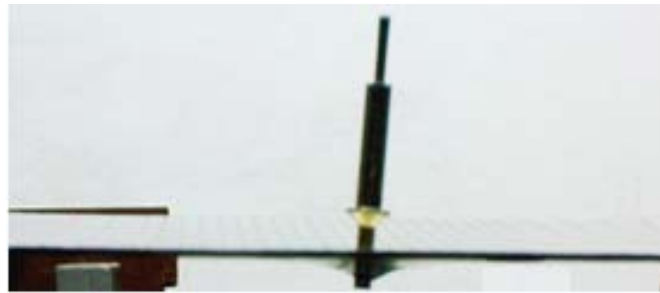


Fig.3 Impactor and plate after punching

## CONCLUSIONS

The method for solution of impact problems for thin free supported plates is given. It is based on analytical solution of boundary problem as well as on numerical for initial value one. The use of determined stress fields and kinetic damage equation for simulation of impact damage accumulation allows determine the values of lives to fracture of the plates. As usual in Nonlinear Mechanics the validation of calculational method needs the comparison between calculated and experimental data. This comparison for steel square plates will be possible after another group of experiments connected with determination of constants  $\chi$  and  $q$  in equation (1).

## AKNOWLEDGEMENT

This work was partly supported by Ukrainian Fundamental Researches State Fund, grant F25.1/042.

## REFERENCES

- [1] Ben-Dor G., Dubinsky A., Elperin T. Ballistic Impact: Recent Advances in Analytical Modeling of Plate Penetration Dynamics—a Review *Applied Mechanics Reviews*, Vol. 58, pp. 355-371, November 2005.
- [2] Field J.E. Review of experimental techniques for high rate deformation and shock studies. *Int. J. Imp. Eng.* Vol. 30, pp. 725–775, 2004.
- [3] Goldsmith W. *Impact. The Theory and Physical Behaviour of Colliding Solids*. Dover Publ. 2001.
- [4] Goloskokov E.G., Philippov A.P. *Non-stationary vibrations of deformable systems*, Naukova dumka, Kiev, 1977. (In Russian)
- [5] Ionov V.N., Ogibalov P.M. *Strength of the structural elements. Dynamics and stress value*, Vyshaja shkola, Moscow, 1980. (In Russian)
- [6] Collins J.A. *Failure of Materials in Mechanical Design: Analysis, Prediction, Prevention.-Sec*, Ed. NY: Jonn Wiley and Sons, 1993.
- [7] Lemaitre J., Chaboche J.-L. *Mechanics of solid materials*, University press, Cambridge, 1994.
- [8] Breslavsky D.V., Naumov I.V., Onyshchenko A.V. Experimental investigation of impact loading of thin plates *Visnyk NTU«KhPI»*, Vol. 38, Kharkiv, pp. 30-35, 2007. (In Russian)

**NUMERICAL MODAL ANALYSIS OF SANDWICH PLATES  
PARTIALLY DAMAGED DUE TO IMPACTS**

**Vyacheslav  
Burlayenko<sup>1</sup>**  
National Technical  
University 'KhPI'  
Kharkov, Ukraine

**Tomasz Sadowski**  
Lublin University of  
Technology  
Lublin, Poland

---

ABSTRACT

---

Dynamic responses of sandwich composite plates containing impact-induced damage are studied. A finite element formulation of the problem is developed by using the high-order sandwich plate theory. The finite element code ABAQUS is used to create a finite element model of the sandwich plate accounting for geometrical imperfections, stiffness changes and intermediate contact of detached plate parts caused by impact damage and to fulfil the free and forced vibration analyses.

---

**INTRODUCTION**

Dynamic responses of sandwich plates, which may offer the potential of 20-40 % weight saving over their metal counterparts of the same bending stiffness, are of primary importance for the design of aircrafts and spacecrafts. A good understanding of the free vibration behavior of such structural elements is essential toward a reliable prediction of their dynamic response to time-dependent external excitations, prevention of the occurrence of the resonance, and for optimal design from the vibrational point of view. Analytical, numerical and experimental studies of the dynamic response of sandwich plates have received a good deal of attention and a variety of references can be found in the free literature, e.g. [1-3]. Modal analysis being the normal issue for sandwich plates becomes a problem requiring enhanced attention when there are some imperfections within the sandwich plates such as cracks, partially damaged parts and so on. The presence of damages will affect the dynamic response of the plates and, hence, need to be studied as a single task.

One of unavoidable damages of structural components of aircrafts and spacecrafts during their in-service life is a flaw inflicted by impacts. Several works treating the dynamic flexural behavior of sandwich beams and plates have confirmed the substantial susceptibility of the sandwich structures to damage caused by the low-velocity impact of foreign objects [4]. It has been shown that the impact-induced damage greatly affects the load capacity of the structural components, causing them to fail at lower loads than expected and modifies their vibration characteristics resulting in a hazard that a construction may resonate at other working frequencies than it was initially found.

Analytical approaches for studying mechanical behaviors of sandwich structures containing the damaged core and facesheet and the imperfect core-to-facesheet interface are extremely difficult and are mostly confined by one- and two-dimensional models with through-width damaged region. A damaged beam (or plate) is being divided into separate regions, namely undamaged and damaged ones, which obey continuity conditions on their boundaries, so-called the split spanwise theory [5]. Moreover, contact-impact conditions have to be accounted for the debonded parts in the damaged region. Because of the complexity to solve this problem analytically for sandwich plates with an arbitrary form of the impacted site the finite element method (FEM) is usually utilized.

The main focus of this paper is on the study of the dynamic response of sandwich plates cored with honeycomb and polymer foams that were previously impacted. To perform the modal analysis and simulate the dynamic response, a finite element model of sandwich plates containing impact-induced damage is developed. The effects of the different sizes of the post-impact zone including local geometry perturbations and stiffness degradation on the dynamic properties are analyzed.

---

<sup>1</sup> Corresponding author. Email [burlayenko@kpi.kharkov.ua](mailto:burlayenko@kpi.kharkov.ua)

## 1. IMPACT REGION PROPERTIES

In general, low-velocity impacts with a blunt object within sandwich plates produce a permanent indentation in the facesheet accompanied with substantial core crushing damage beneath and around the impacted site and partial interface debonding (or cavity) between the facesheet and the core in the damaged area [4]. In the cases of the barely visible level of impact damage, when the facesheet remains a little damaged, the core crushing and debonding occur only. The key geometrical parameters of the representative cross-section of a sandwich specimen impacted are shown on the Fig. 1 and include the peak depth of the residual facesheet indentation  $\delta_i$ , the peak depth associated with core fracture  $\delta_c$  and planar dimension of damaged facesheet radius  $R_i$ , and planar dimension of the crushed core  $R_c$ .

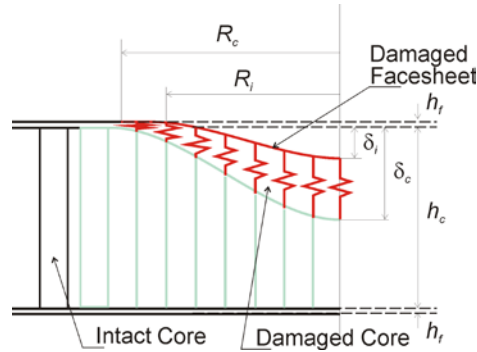


Fig. 1. Impact-damaged region.

Nevertheless, a model of the impacted sandwich plate accounting for only the impact-based geometrical perturbations are not accurate. Because the size of the area impacted depends on the properties of the core material and the relationship between the properties of the core and of those the facesheets. Thereby, the actual damage state of the supporting core, core-to-facesheet interface and impacted facesheet should be taken into account. As a consequence, to predict mechanical responses of sandwich plates subjected to impact, an accurate estimation of transverse normal and shear stresses should be a major goal of a mathematical model that is being developed.

## 2. MATHEMATICAL STATEMENT OF PROBLEM

Following the splitting theory, each of the regions split may be separately considered from each other by using the assumptions one of the sandwich theories. The finite element model developed in the Section 3 of the paper is based on the high-order sandwich theory [6] that allows the accurate modeling of interlaminar normal and shear stresses. The theory briefly is only given herein.

Let's consider a rectangular sandwich plate as a three-layer structure with a core of uniform thickness  $h_c$  and with parallel facesheets of thicknesses  $h_f$ , where subscript  $f$  has the values 1 and 2 when referring to the top and bottom facesheets, respectively. The facesheets may in general be unequal and composite laminates, and are treated as being the first-order shear (FSDT) deformable plates. The core is assumed to be a fully three-dimensional, orthotropic solid body in which warping of a cross-section and changing of core thickness can be taken into consideration. This assumption primary relates to sandwich plates with continuous solid core, like foam cores, but the adopted approach can be used in predicting the behavior of sandwich plates with discontinuous cores, like a honeycomb structure, if appropriate smeared values of the core physical properties are used. A usual cross-section of the sandwich plate in the  $x$ - $z$  plane is illustrated in Fig. 2 and shows displacements of the three layers and rotations of the facesheets in accordance with FSDT. Obviously, a similar view could be drawn related to the  $y$ - $z$  plane. Consequently, the through-thickness behavior of the displacement fields in the facesheets may be expressed in terms of 10 fundamental quantities, namely  $u_{0f}$ ,  $v_{0f}$ ,  $w_{0f}$ ,  $\varphi_{0xf}$  and  $\varphi_{0yf}$  with  $f = 1, 2$  and '0' means reference axes of the principal layers. The through-thickness behavior of the core are expressed in terms of the 10 facesheet values, on applying the interface continuity conditions and two additional fundamental quantities  $u_{0c}$  and  $v_{0c}$  that are the displacements at the core mid-plane in the  $x$ - and  $y$ -directions, respectively. Therefore, the displacements at a general point  $u$ ,  $v$ ,  $w$  in each of the layers are expressed for the facesheets  $u_f$ ,  $v_f$  and  $w_f$  with  $f = 1, 2$  and for the core  $u_c$ ,  $v_c$  and  $w_c$  as functions of the 12 fundamental quantities.

The FE formulation presents the sandwich plate as an assembly of a number of finite elements.

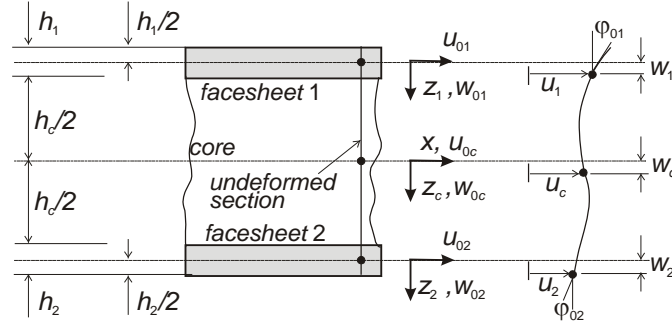


Fig. 2. Sandwich plate cross-section.

Let the approximation for displacement field vector of the each principal layer  $L$  referring to the core and the facesheets within the finite element be assumed as

$$\{u^L\} = [N^L] \{d^L\}, \quad (1)$$

where, in a contracted vector-matrix notation, that is traditional for FEM,  $[N^L]$  is the matrix of the shape functions and  $\{d^L\}$  is the nodal displacement vector of the element. Then, in the facesheets the components of the strain tensor can be obtained by using geometrically either linear or nonlinear strain-displacement equations of elasticity in conjunction with displacement fields defined early

$$\{\varepsilon^f\} = [\partial^f] \{u^f\} \text{ with } f = 1, 2, \quad (2)$$

where  $[\partial^f]$  is the matrix consisting of differential operators. In general, each of the two facesheets may be of composite laminated of arbitrary lay-up, which exhibits anisotropic mechanical properties, coupling between in-plane and out-of-plane behaviors, and through-thickness shearing. Consequently, the stress-strain relationships at a general point for the  $l$ th laminate layer are

$$\{\sigma^f\}_l = [Q]_l \{\varepsilon^f\}, \quad (3)$$

where  $Q_{rs}$  with  $r, s = 1, 2, 4, 5, 6$  are the stiffness coefficients used usually in the laminate theory [2]. Therefore, the stress resultants of the laminated composite plate can be found as

$$\{\sigma^f\} = [D^f] \{\varepsilon^f\} \quad (4)$$

The strain tensor components of the core are obtained on the basis of the 3D elasticity theory

$$\{\varepsilon^c\} = [\partial^c] \{u^c\}. \quad (5)$$

The core is assumed an orthotropic homogeneous body, then, the stress-strain relationships are

$$\{\sigma^c\} = [D^c] \{\varepsilon^c\}, \quad (6)$$

where  $D_{rs}^c$  with  $r, s = 1, \dots, 6$  are the elastic stiffness constants.

The equation of motion can be derived using Hamilton's principle

$$\delta \int_{t_1}^{t_2} (T - \Pi) dt = 0, \quad (7)$$

where  $\Pi$  denotes the potential energy that consists of the strain energy and the work done by loadings  $\{p\}$  applied to the outer surfaces and  $T$  is the kinetic energy. The strain energy is a sum of contributions of the two facesheets and the core. Consequently, we can write the variation of  $\Pi$  as

$$\delta \Pi = \sum_{i=1}^3 \int_{A^i} \int_{z_i}^{z_{i+1}} \{\delta \varepsilon^i\}^T \{\sigma^i\} dz dA - \sum_{i=1}^2 \int_{A^i} \{\delta u^i\}^T \{p\} dA \quad (8)$$

Using the discretization of the displacements (1) and substituting (2)-(6) into (8) yields

$$\delta \Pi = \sum_{i=1}^3 \int_{A^i} \int_{z_i}^{z_{i+1}} \{\delta d^i\}^T ([B]^T [D] [B]) \{d^i\} dz dA - \sum_{i=1}^2 \int_{A^i} \{\delta d^i\}^T [B]^T \{p\} dA, \quad (9)$$

where the matrices  $[B]$  and  $[D]$  consist of blocks corresponding to the matrices of the core and the facesheets, and  $[B] = [\partial][N]$  for the each principal layer.

Integrating and summarizing the terms in (9) we can finally obtain

$$\delta T = \left\{ \delta d^e \right\} \left( \left[ K^e \right] \left\{ d^e \right\} - \left\{ f^e \right\} \right), \quad (10)$$

where  $\left\{ d^e \right\}$ ,  $\left[ K^e \right]$  and  $\left\{ f^e \right\}$  are the nodal displacement vector, the stiffness matrix and the loading vector of the  $e$ th element, respectively.

In the same way the variation of the kinetic energy within the sandwich FE is given by

$$\delta T = \sum_{i=1}^3 \int_{A^i} \int_{z_i}^{z_{i+1}} \left\{ \delta u^i \right\}^T \rho^i \left\{ \ddot{u}^i \right\} dz dA, \quad (10)$$

where  $\rho^i$  is the mass density of the  $i$ th principal layer. Then,

$$\delta T = \sum_{i=1}^3 \int_{A^k} \int_{z_i}^{z_{i+1}} \left\{ \delta d^i \right\}^T \left[ N \right]^T \rho^i \left[ N \right] \left\{ \ddot{d}^i \right\} dz dA \quad (11)$$

and after the manipulations mentioned above we find

$$\delta T = \left\{ \delta d^e \right\} \left[ M^e \right] \left\{ \ddot{d}^e \right\}, \quad (12)$$

where  $\left\{ \ddot{d}^e \right\}$  and  $\left[ M^e \right]$  are the nodal acceleration vector and the mass matrix of the  $e$ th element.

The global stiffness and mass matrices are obtained by the standard assembly procedure of FEM, thus, the motion equation of the elastodynamic problem without damping is

$$\left[ M \right] \left\{ \ddot{d} \right\} + \left[ K \right] \left\{ d \right\} = \left\{ f \right\}, \quad (13)$$

where  $\left\{ d \right\}$ ,  $\left[ K \right]$ ,  $\left[ M \right]$  and  $\left\{ f \right\}$  are the corresponding global vectors and matrices.

If there is no debonding, displacements and interlaminar stresses are continuous across the interface of any of two adjacent layers. Otherwise, such continuity does not exist. One can assume that in the damaged region the debonded surfaces may longitudinally slip one with respect to the other, being in contact vertically, or can be a contact free. The stiffness and mass matrices of the damaged region do not differ from those for the undamaged one but the contact-impact conditions of detached parts plus a local damage of the core and the facesheet should be added. The contact behaviour can be accounted for through the compatibility conditions at the core–face interface, which govern the displacement and stress fields of the core as following: in the case of a contact, debonded surfaces are free of core shear stresses and have full compatibility for the displacements between the core and the facesheets; if contact does not exist, debonded surfaces are free of the core shear and normal stresses and there is a jump for displacements between the core and the facesheets. Moreover, as a result of impact both the core and the facesheet can be locally damaged. It will impair their ability to transfer stresses through the small damaged zone. Therefore, the stiffnesses in both the facesheet and the core should be reduced (or even to be zero in extremely case) throughout the damaged zone.

### 3. FINITE ELEMENT MODELLING

Dynamic characteristics such as natural frequencies and mode shapes of both intact and damaged by low velocity impact sandwich plates were calculated using the commercial FE code ABAQUS/Standard v.6.6. In accordance with the possibilities of this engineering software the free vibration analysis was performed using the linear perturbation load step, where the Lanczos or the subspace iteration methods for eigenvalues extraction were used. The direct method based on the direct solution of the steady-state dynamic equations projected onto a subspace of modes was utilized to calculate harmonic responses of the plate excited at an external harmonic concentrated force.

The 6- and 8-node general-purpose reduced integrated continuum shell elements and 6- and 8-node with incompatible mode linear solid elements were applied to discretize the facesheets and the core of sandwich plates, respectively. The general mesh was subdivided into three different zones: fine meshed impacted region, the next zone surrounding the impacted region with gradually decreased mesh density, and coarse meshed the undamaged zone. The connection between the impacted facesheet and the remained part of the sandwich plate was simulated by imposing multi-point constraints in general nodes. The shell elements selected allow to avoid the inconsistency between the displacement fields of the core and the facesheet because can correctly transfer the moment/rotation at their reference surface. The core-to-facesheet debond was modeled by removing the displacement restrictions and, thus, double nodes appear in this zone. To prevent a physically unreal penetration of the debonded parts and to simulate their contact conditions, the spring elements SPRING2 were introduced between the double nodes. This element had zero stiffness in tension and very big stiffness in compression, if the relative displacement between the nodes goes to zero. Finally, the parts of the

core and the facesheet damaged due to impact were modeled by reducing gradually the stiffness of the finite elements belonging the damaged area. For this purpose the initial stiffness coefficients of the corresponding elements were multiplied by appropriate reduction factors.

## 4. NUMERICAL RESULTS AND DISCUSSIONS

### 4.1. Test calculations

For verification of the proposed FE model test studies were firstly carried out. A simply supported foam cored sandwich beam with rectangular cross-section damaged at the middle span is used for this purpose. The numerical results of the first six natural frequencies of the damaged sandwich beam found with ABAQUS' model were compared with those analytical results given in the work of Schwartz-Givli et al. [7]. The close results were obtained and they are listed in Table 1.

Table 1. Mode frequencies of the damaged sandwich beam with foam core (Hz).

Mode No	1	2	3	4	5	6
Analysis [7]	288.98	388.32	1093.2	1146.9	1771.3	1842.2
Present FEA	293.07	433.67	1093.1	1132.0	1769.9	2080.2

### 4.2. Free vibrations of impacted sandwich plates

The influence of the total planar size of the impacted region involving the core crushing, the face sheet damage and the core-to-face sheet debonding was further studied. For this purpose, a simply supported rectangular honeycomb sandwich plate of the total area  $135 \times 180 \text{ mm}^2$  with the facesheets thickness of 1 mm and the core thickness of 5 mm, containing a circular impacted zone with planar parameter  $R_c = 30 \text{ mm}$  at the center was considered. The material properties of the plate are presented in Table 2. It is worthy to notice that the homogeneous properties of the honeycomb core were previously obtained basing on the unit cell approach by using the FEM.

Table 2. Material properties of impacted sandwich plates.

Components	Elastic constants
Honeycomb core	$E_{11} = 0.461, \text{ MPa}$ $E_{22} = 0.461, \text{ MPa}$ $E_{33} = 1494, \text{ MPa}$ $G_{12} = 0.194, \text{ MPa}$ $G_{13} = 341.7, \text{ MPa}$ $G_{23} = 192.1, \text{ MPa}$ $\rho_c = 57.17, \text{ kgm}^{-3}$
Rohacell foam	$E_c = 135, \text{ MPa}$ $G_c = 45, \text{ MPa}$ $\rho_c = 100, \text{ kgm}^{-3}$
CFRP facesheets	$E_{11} = 140, \text{ GPa}$ $E_{22} = E_{33} = 10, \text{ GPa}$ $G_{12} = G_{13} = 4.6, \text{ GPa}$ $G_{23} = 3.8, \text{ GPa}$ $\rho_f = 1650, \text{ kgm}^{-3}$
GFRP facesheets	$E_{11} = E_{33} = 16500, \text{ MPa}$ $E_{22} = 3800, \text{ MPa}$ $G_{12} = G_{23} = 1800, \text{ MPa}$ $G_{13} = 6600, \text{ MPa}$ $\rho_f = 1650, \text{ kgm}^{-3}$

Calculations showed that the natural frequencies of the impact-damaged honeycomb sandwich plate are shifted from the intact one. This effect on the higher modes is greater than the lower ones. Also, this effect does not exhibit monotonous trends when a mode number increases. Moreover, the mode shapes of the impacted plate were also changed. Purely local modes and mixed modes that are combination of local and global mode shapes often occur. Also the numerical results showed that the natural frequencies decrease with increases of the impacted region size,  $R_c$ . Besides, the frequencies change more rapidly as a mode number increases. Although this trend of the frequencies changing can be violated due to local thickening phenomenon caused by debonding which in some cases made the frequencies of the damaged plate even higher than the intact one. To show the influence of other damage characteristics produced by impact, the sandwich plate with in-plan dimensions of  $270 \times 180 \text{ mm}^2$  consisting of 2.4 mm GFRP facesheets and 50 mm Rohacell™ WF51 foam core was analyzed. The mechanical properties of the constituent materials are shown in Table 2. In analyses it was assumed that if one of the parameters of the impacted region is being varied during calculations, other ones to be constant. The influence of the cavity depth,  $\delta_c - \delta_i$ , on vibration responses of the impacted sandwich plate was firstly studied. It was found that the values of the natural frequencies of the impacted plates slightly decrease, but their mode shapes curvatures slightly increase with the cavity depth increasing. This effect of the minor changing of the lower frequencies holds for the higher ones. The same minor influence of the residual facesheet indentation depth on the natural frequencies at the cavity depth equal to 10% of the facesheet thickness was obtained. The mode shapes had more visible changes with increasing of the facesheet indentation. Finally, substantial decreasing of the natural frequencies with increasing the facesheet degradation level was found.

### 4.3. Forced vibrations of impacted sandwich plates

The forced vibration analysis of the honeycomb cantilever sandwich plate containing a post-

impact circular damage at the center, as in the previous study, was carried out. The radius of the impacted site was varied from 5 to 60 mm. The cavity depth was taken as a constant equal to half of the facesheet thickness. A harmonic concentrated load with magnitude equal to 100 N was applied in the transverse direction on the free edge of the cantilever plate with a frequency range taken from 500 to 2000 Hz as forcing frequencies. Harmonic responses of the impacted sandwich plate were calculated at the point where the force was applied for all simulated damage states. The changes in harmonic responses versus sizes of the impacted site, as the deflection-frequency curves, at the forcing frequency defined are shown in Fig 3. The dominant harmonic response is obtained at 1512.6 Hz that corresponds to the third resonance frequency of the plate damaged by impact. From the calculated results, we can conclude that the harmonic response increases when the planar size of the impacted site increases that corresponds to the stiffness degradation due to the damage presence.

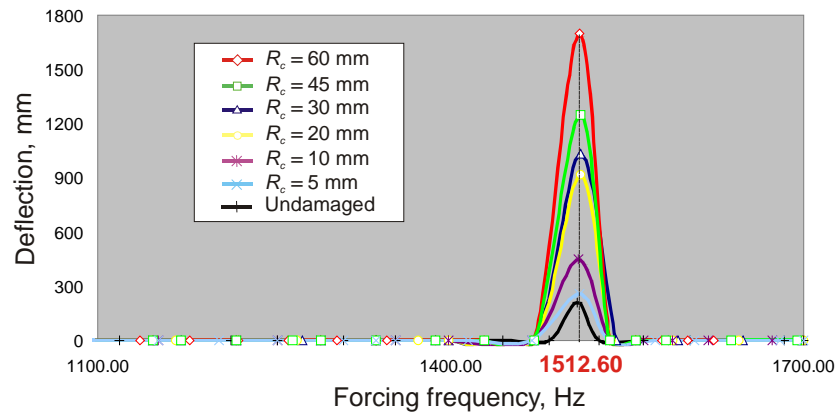


Fig. 3. Harmonic deflection responses vs radius of impacted site.

## CONCLUSIONS

In sum the following conclusions from the viewpoint of sensitivity of dynamic characteristics to the presence of impact damage can be drawn. First, both the natural frequencies and the harmonic responses of sandwich plates subjected to low velocity impact are sensitive to the presence of the impact-induced damage. In doing so, the natural frequencies usually decrease due to loss in stiffness caused by damage, while harmonic responses increase because of that. Second, the higher natural frequencies and mode shapes are more sensitive to the impact damage presence. Third, natural frequencies and associated mode shapes are the most sensitive to the planar size of the impact domain and are poorly sensitive to the damage extended through the thickness and induced in the facesheet. Fourth, the displacement harmonic responses can be primary used for detection the impact damage.

## ACKNOWLEDGEMENTS

This research was supported by the CEMCAST project funded by European Union within 7 Framework Programme, contract No 24547.

## REFERENCES

- [1] Lok T.S., Cheng Q.H. Free and forced vibration of simply supported orthotropic sandwich panel. *Computers and Structures*, 79, pp. 301-302, 2001.
- [2] Nayak A.K., Sheno R.A. Free vibration analysis of composites sandwich plates based on Reddy's high-order theory. *Composites: Part B*, 33, pp. 505-519, 2002.
- [3] Kurpa L.V., Vensel E.S. Analysis of sandwich plates of arbitrary shape. *Mechanics of Advanced Materials and Structures*, 12(1), pp. 33-43, 2005.
- [4] Scarponi C., Briotti G. and Renato B. Impact testing on composite laminates sandwich panels. *Journal of Composite Materials*, 30, pp. 1873-1911, 1996.
- [5] Ramkumar R.L., Kulkarni S.V. and Pipes R.B. Free vibration frequencies of a delaminated beam. In: *34<sup>th</sup> Annual Technical Conference, Reinforced Plastic/Composite Institute*, pp. 1-5, 1979.
- [6] Frostig Y., Baruch M. Localized load effects in high-order bending of sandwich panels. *Journal of Engineering Mechanics*, 122, pp. 1069-1076, 1996.
- [7] Schwarts-Givil H., Rabinovich O., and Frostig Y. Free vibration of delaminated unidirectional sandwich panels with a transversely flexible core and general boundary conditions – A high order approach. *Journal of Sandwich Structures and Materials*, 10, pp. 99-131, 2008.

**A HYBRID ASYMPTOTIC WKB-GALERKIN METHOD  
WITH APPLICATION TO THE CORRELATION ANALYSIS  
OF STOCHASTIC BEHAVIOUR OF NON-LINEAR SYSTEMS  
WITH TIME-DEPENDENT PARAMETERS**

**Victor Z. Gristchak<sup>1</sup>,**  
**Valentin V. Lysenko**  
Zaporizhzhia State  
University  
Zaporizhzhja, Ukraine

---

ABSTRACT

---

The method of double asymptotic expansion in aggregate with a hybrid WKB method on the base of the energy conservation law is examined in the frame of the correlation analysis of stochastic behavior of nonlinear system with time-dependent parameters under casual loading. The application of the asymptotic approaches for the analysis of forced oscillations systems with variable factor of damping on the basis of the stochastic nonlinear Duffing's equation is done. The solution is searched as a series on degrees of small parameter at nonlinear component of initial equation (external asymptotic). In this case, the initial equation can be replaced by a recurrent sequence of linear equations. The solution of the given system can be found by a method of Green's functions and WKB method (internal asymptotic). The energy conservation law is used for improving solution. Moment functions of output process are defined by average of a series. The results of visualization of deterministic solution and correlation function of output process are given.

---

## INTRODUCTION

In the paper a hybrid technique [1, 2] for obtaining of the approximate analytical solution of the second order nonlinear differential equations of type (1) with time-dependent parameters and initial conditions is applied. Generally, hybrid technique is based on using classical perturbation methods combined with some principles of definition of artificial unknown coefficients in these expansions [3], [4]. For example the Galerkin's orthogonality and variational principles, the method of least squares etc.

However, some of the above mentioned principles can be applied successfully to the solution of time-dependent problems. For example, variational principles used in the Euler's equation do not work because for time-dependent problems only the initial conditions at some moment of time are known. As well the Galerkin's orthogonality procedure does not give the reasonable results in problems for equations with variable coefficients. In this paper as the principles of definition of artificial unknown coefficients at functions of asymptotic expansions the Hamilton's principle combined with the method of the least squares are used. Approximate asymptotic solution of nonlinear equation is found with the help of the method of double asymptotic expansion [5]. Then the solution is twice specified with the help of the described hybrid technique which is based on the WKBJ-Galerkin method (internal asymptotic) [3] and the perturbation-Galerkin method (external asymptotic) [4]. On the basis of the analytical solution partial expressions for the correlation function of the output process under random loading are obtained.

## 1. DESCRIPTION OF THE HYBRID TECHNIQUE

We consider a nonlinear differential equation of the second order:

---

<sup>1</sup> Corresponding author. Email [grk@znu.edu.ua](mailto:grk@znu.edu.ua)

$$L_0 f(t) + \alpha \cdot (P(t)f^2(t) + Q(t)f^3(t)) = \gamma(t), \quad (1)$$

where  $L_0$  is a linear differential operator:

$$L_0 = \frac{\partial^2}{\partial t^2} + 2c(t) \frac{\partial}{\partial t} + \omega_0^2 \varphi(t); \quad (2)$$

$t$  is time variable;  $c(t)$ ,  $\varphi(t)$ ,  $P(t)$ ,  $Q(t)$  are some functions of time, which depend on characteristics of plate and function of the external loading;  $\gamma(t)$  is a function of the external loading;  $\omega_0$ ,  $\alpha$  are parameters of frequency of natural vibrations of the linear system and degree of non-linearity.

We will find the solution of the equation (1) in the interval of time. On the first stage of the approach we obtain the solution of equation (1) in the form of a series:

$$f(t) = f_{\text{hom}}(t) + \sum_{j=0}^{\infty} \alpha^j f_j(t), \quad (3)$$

where:  $f_{\text{hom}}(t)$ ,  $f_j(t)$  ( $j = 0, 1, \dots$ ) are unknown functions of time.

It is necessary to substitute an expression (3) and its first two derivatives into equation (1) and splitting it with powers of parameter  $\alpha$  one may obtain the recurrent system of linear differential equations as for  $f_j(t)$  ( $j = 0, 1, \dots$ )

$$L_0 f_{\text{hom}}(t) = 0 \quad (4)$$

$$L_0 f_0(t) = \gamma(t),$$

$$L_0 f_1(t) = -\left(P(t)(f_{\text{hom}}(t) + f_0(t))^2 + Q(t)(f_{\text{hom}}(t) + f_0(t))^3\right), \quad (5)$$

...

Let the operator reverse to  $L_0$  corresponds to the Volter's operator with the Green's function which is a solution of differential equation

$$L_0 h(t, \tau) = 0. \quad (6)$$

Then on the second stage it is possible to find the solution of equations of the system (5) with the help of Green's functions method [6]:

$$f_0(t) = \int_{t_0}^t h(t, \tau) \gamma(\tau) d\tau,$$

$$f_1(t) = -\int_{t_0}^t h(t, \tau) \left(P(t)(f_{\text{hom}}(t) + f_0(t))^2 + Q(t)(f_{\text{hom}}(t) + f_0(t))^3\right) d\tau, \quad (7)$$

...

On the third stage, we will find the solutions of linear homogeneous differential equations (4) and (6) with the help of the WKBJ-method in the form:

$$f_{\text{hom}}(t) = \exp\left(\int_{t_0}^t \sum_{k=0}^{\infty} \varepsilon^{k-1} \psi_k(\theta) d\theta\right), \quad h(t, \tau) = \exp\left(\int_{\tau}^t \sum_{k=0}^{\infty} \varepsilon^{k-1} \psi_k(\theta) d\theta\right) \quad (8)$$

where:  $\varepsilon = 1/\omega_0$ ;  $\psi_k(t)$  are unknown functions of time ( $k = 0, 1, \dots$ ).

Substituting expressions (8) into equations (4) and (6) and collecting coefficients at the degrees of parameter  $\varepsilon$ , we get the system of equations for functions  $\psi_k(t)$  ( $k = 0, 1, \dots$ ) and then

$$\begin{aligned}\psi_{0,1,2}(t) &= \pm i \sqrt{\varphi_c(t)}, \\ \psi_{1,1,2}(t) &= -\frac{\psi'_{0,1,2}(t)}{2\psi_{0,1,2}(t)} = -\frac{\varphi'_c(t)}{4\varphi_c(t)} = -\frac{1}{4}(\ln \varphi_c(t))', \\ &\dots\end{aligned}\tag{9}$$

where

$$\varphi_c(t) = \varphi(t) - \frac{c^2(t)}{\omega_0^2} - \frac{c'(t)}{\omega_0^2}.\tag{10}$$

On the fourth stage according to WKBJ-Galerkin method [3], the hybrid solutions of equations (4) and (6) can be represented in the form as follows

$$f_{\text{hom}_H}(t) = \exp\left(\int_{t_0}^t \sum_{k=0}^{M-1} \lambda_k \psi_k(\theta) d\theta\right), \quad h_H(t, \tau) = \exp\left(\int_{\tau}^t \sum_{k=0}^{M-1} \mu_k \psi_k(\theta) d\theta\right),\tag{11}$$

where:  $M$  is an order of approaching;  $\psi_k(t)$  ( $k = 0, \dots, M-1$ ) are functions of time, determined on the third stage,  $\lambda_k, \mu_k$  ( $k = 0, \dots, M-1$ ) are unknown coefficients which depend on the parameter  $\varepsilon$ .

Finally, if the Green's function is known, on the fifth stage by the method of perturbation-Galerkin [4], hybrid solution  $f_H(t)$  of initial differential equation (1) can be represented as [6]

$$f_H(t) = f_{\text{hom}_H}(t) + \sum_{j=0}^{N-1} \delta_j f_{j_H}(t),\tag{12}$$

where:  $N$  is an order of approaching;  $\delta_j$  ( $j = 1, \dots, N-1$ ) are unknown coefficients which depend on the parameters  $\varepsilon$  and  $\alpha$ ;

$$\begin{aligned}f_{0_H}(t) &= \int_{t_0}^t h_H(t, \tau) \gamma(\tau) d\tau \\ f_{1_H}(t) &= -\int_{t_0}^t h_H(t, \tau) \left( P(t) (f_{\text{hom}_H}(t) + f_{0_H}(t))^2 + Q(t) (f_{\text{hom}_H}(t) + f_{0_H}(t))^3 \right) d\tau, \\ &\dots\end{aligned}\tag{13}$$

We may determine unknown coefficients  $\lambda_k, \mu_k$  ( $k = 0, \dots, M-1$ ) and  $\delta_j$  ( $j = 1, \dots, N-1$ ) with help of the energy conservation law:

$$E(t) - E(t_0) = W(t),\tag{14}$$

where  $E$  is the complete energy of the system:

$$E(t) = T(t) + U(t);\tag{15}$$

$W$  is work of external and internal forces;  $U$  is potential energy;  $T$  is kinetic energy.

In our case of nonlinear vibrations of a plate we may rewrite the expression (14) in the form:

$$\int_{t_0}^t f'(\tau) \cdot (L_0 f(\tau) + \alpha \cdot (P(\tau) f^2(\tau) + Q(\tau) f^3(\tau)) - \gamma(\tau)) d\tau = 0 \quad (16)$$

In general case eq. (16) is not performed. Therefore for determination of unknown coefficients a least-squares method is applicable:

$$\int_{t_0}^T (E(t) - E(t_0) - W(t))^2 dt \rightarrow \min. \quad (17)$$

## 2. KORRELATION FUNCTIONS

The moment functions of output process (functions of bending of plate) are determined by averaging of a series (12). Let the external load  $\gamma(t)$  is a centralized random process, then the output process will be centralized too. We suppose also, that initial conditions are zero. Thus, for the second-order moment function we obtain:

$$\langle f_H(t_1) f_H(t_2) \rangle = \delta_0^2 \langle f_{0_H}(t_1) f_{0_H}(t_2) \rangle + \delta_0 \delta_1 (\langle f_{0_H}(t_1) f_{1_H}(t_2) \rangle + \langle f_{0_H}(t_2) f_{1_H}(t_1) \rangle) + \dots, \quad (18)$$

where

$$\begin{aligned} \langle f_{0_H}(t_1) f_{1_H}(t_2) \rangle &= -\delta_0 \delta_1 \int_{t_0}^{t_2} h_H(t_2, \tau) \\ &\left( P(\tau) \langle f_{0_H}(t_1) f_{0_H}^2(\tau) \rangle + Q(\tau) \langle f_{0_H}(t_1) f_{0_H}^3(\tau) \rangle \right) d\tau \end{aligned} \quad (19)$$

Here and below the angular brackets denote the mathematical expectation.

Let external load  $\gamma(t)$  is a normal random process. Then the process  $f_{0_H}(t_1)$  will be the normal random process as well. In this case the moment functions of the odd order of the zero-order approximation  $f_0(t)$  are equal to the zero. There certain relationships exist [6]:

$$\begin{aligned} \langle f_{0_H}(t_1) f_{0_H}^3(t_2) \rangle &= 3K_{f_0}(t_1, t_2) K_{f_0}(t_2, t_2), \\ \langle f_{0_H}(t_1) f_{0_H}^2(t_2) \rangle &= 0 \end{aligned}, \quad (20)$$

where  $K_{f_0}(t_1, t_2)$  is the correlation function of random process  $f_{0_H}(t)$ .

Substituting obtained results into expression (19), taking in account that both input and output processes are centralised, we get the final expression for the correlation function of the output process

$$K_f(t_1, t_2) \approx \delta_0^2 K_{f_0}(t_1, t_2) + \delta_0 \delta_1 (K_{f_0 f_1}(t_1, t_2) + K_{f_0 f_1}(t_2, t_1)) \quad (21)$$

where  $K_f(t_1, t_2)$  is the correlation function of the output process,

$$K_{f_0 f_1}(t_1, t_2) = -3 \int_{t_0}^{t_2} h_H(t_2, \tau) P(\tau) K_{f_0}(t_1, \tau) K_{f_0}(\tau, \tau) d\tau, \quad (22)$$

$K_{f_0}(t_1, t_2)$  is the correlation function of the zero-order approximation:

$$K_{f_0}(t_1, t_2) = \int_{t_0}^{t_1} \int_{t_0}^{t_2} h_H(t_1, \tau_1) h_H(t_2, \tau_2) K_\gamma(\tau_1, \tau_2) d\tau_1 d\tau_2, \quad (23)$$

$K_\gamma(t_1, t_2)$  is the correlation function of external load.

Terms of series (12) with squares and highest orders of parameter  $\alpha$ , will depend on moment functions of the processes  $f_1(t), f_2(t), \dots$ . Under normal external loading given processes will not be normal at all. Therefore, computation of next terms of expansion will cause difficulties. To overcome these difficulties we have to introduce additional hypotheses on moment functions.

### 1. NUMERICAL RESULTS

We plot asymptotic (on the basis of the WKBJ method and perturbation method at  $M = 2$  and  $N = 2$ ), hybrid (at  $M = 2$  and  $N = 2$ ), numerical and linear solutions of equation (1). Numerical realization is represented for the following parameters of equation:  $t_0 = 0, T = 40$  (i.e.  $t \in [0,40]$ ),  $\varphi = t/T + 1/10, \gamma = 1/(2T), \omega_0 = 1$ .

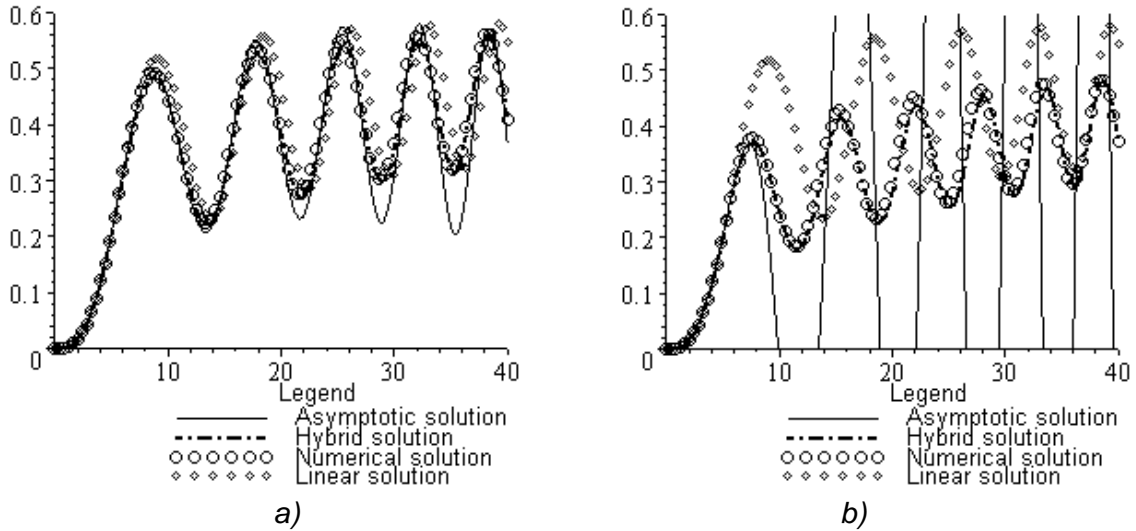


Fig. 1 Comparison of hybrid (dash-dot line) solution of the equation (1) with asymptotic (solid line), numerical (circles) and linear (diamonds) solutions;  $P = 0; Q = 1; f(0) = 0; f'(0) = 0; a) \alpha = 0,1; b) \alpha = 1$ .

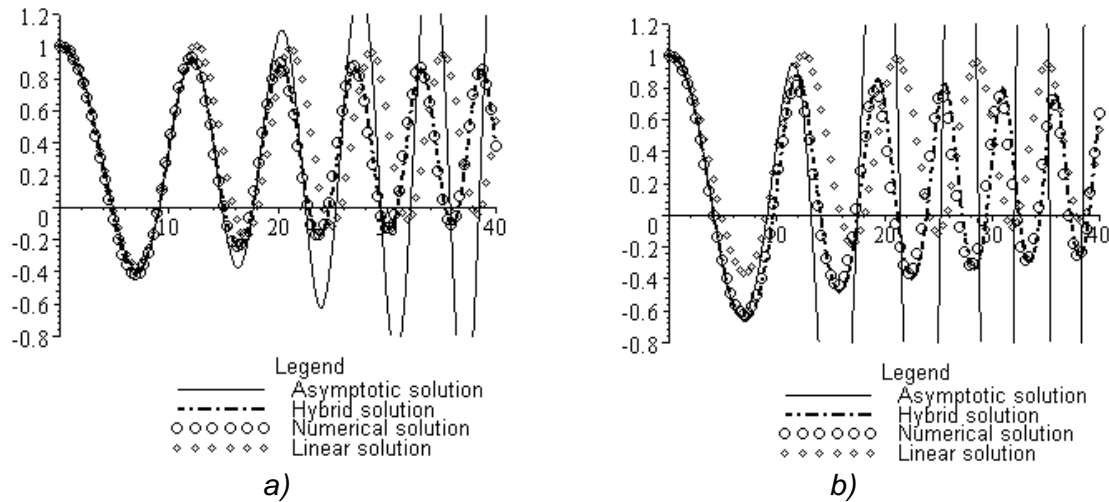


Fig. 2 Comparison of hybrid (dash-dot line) solution of the equation (1) with asymptotic (solid line), numerical (circles) and linear (diamonds) solutions;  $P = 3Q; Q = t/T; f(0) = 1; f'(0) = 0; a) \alpha = 0,1; b) \alpha = 0,5$ .

As it is shown solutions obtained by the hybrid approach compared well with numerical results on more wide ranges of change of parameter of non-linearity.

On the fig. 3-4 the results of visualization of dispersion  $D_f(t) = K_f(t, t)$  and the correlation function  $K_f(t, t)$  of output process  $f(t)$  of the nonlinear system (1) are presented. For all graphs

$t_0 = 0$ ;  $T = 3 \cdot 2\pi / \omega_0 = 3 \cdot 2\pi\varepsilon$ , where  $2\pi / \omega_0 = 2\pi\varepsilon$  – period of vibrations of a similar linear system;  $\varphi(t) = 1 - \frac{(t-t_0) w_0^2}{T-t_0} \frac{1}{10}$  (i.e. a function  $\varphi(t)$  varies linearly from one to  $1 - \omega_0^2 / 10$ ).

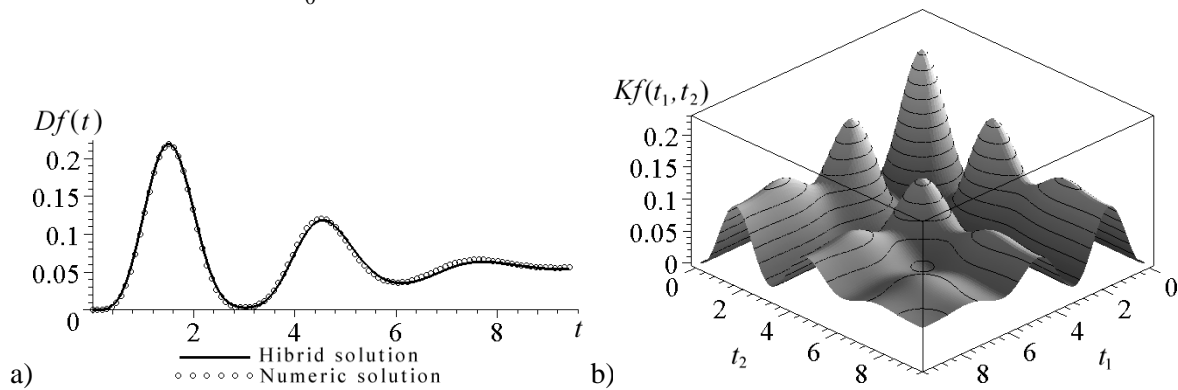


Fig. 3 The graphics of dispersion and correlation function of output process;  $\omega_0 = 2$ ;  $\alpha = 2$ ;  $K_\gamma(t_1, t_2) = 1$ ; a) dispersion; b) correlation function.

On the fig. 4 the results of visualization of dispersion  $D_f(t) = K_f(t, t)$  and correlation function  $K_f(t, t)$  of output process  $f(t)$  of the nonlinear system under loading of «white noise» type are presented.

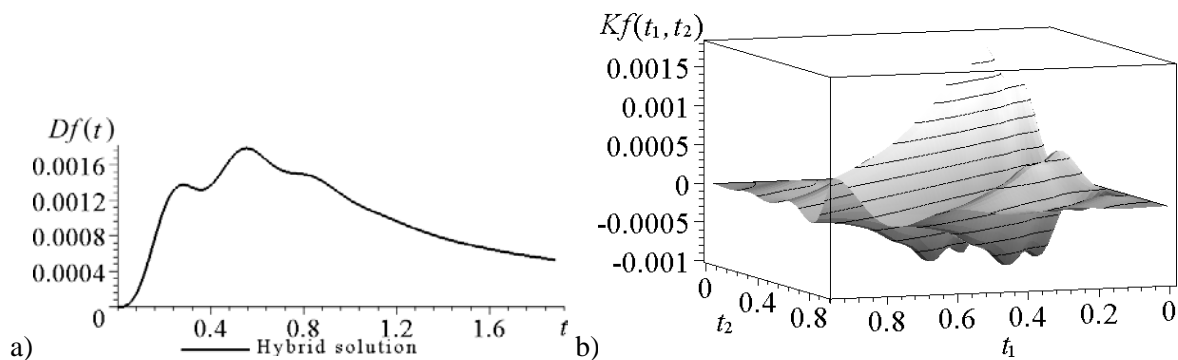


Fig. 4 The graphics of dispersion and correlation function of output process;  $\omega_0 = 10$ ;  $\alpha = 10$ ;  $K_\gamma(t_1, t_2) = \delta(t_2 - t_1)$ ; a) dispersion; b) correlation function.

## REFERENCES

- [1] Noor A.K., Peters J.M. Reduced basis technique for nonlinear analysis of structures // Proc. of the AIAA-ASME-ASCE-AHS 20<sup>th</sup> Structures, Structural Dynamics and Materials conference, St. Louis, USA, 1979. – P. 116 – 126.
- [2] Gerasimov T.S., Lysenko V.V.: A hybrid approximate solution technique and modal expansion approach with application to forced vibrations of non-homogeneous shells and plates. Proc of the 7th Conference “Shells structures, theory and applications”, Gdansk-Jurata, Poland, 2002. – P. 85-86.
- [3] Gristchak, V.Z., Dmitrijeva, Ye.M. A hybrid WKB-Galerkin method and its application // Technishe Mechanik – 1995. – №3. – P. 281-294.
- [4] Geer J.F., Andersen C.M. A hybrid perturbation-Galerkin technique for differential equations containing a parameter // Applied Mechanics Reviews. – 1989. – №42(11). – P. S69-S77.
- [5] Gristchak V.Z., Kabak V.N. Double Asymptotic Method for Nonlinear Forced Oscillations Problem of Mechanical Systems with Time Dependent Parameters // Technishe Mechanik. – 1996. – № 4. – P. 285-296.
- [6] Gristchak, V.Z., Lysenko, V.V. 2000. Method of Double Asymptotic Expansion at the Analysis of Stochastic Behavior of Nonlinear Non-stationary Systems. Euromech 413 Colloquium on “Stochastic Dynamics of Nonlinear Mechanical Systems”. Palermo, Italy, June 12-14, 2000.

THE POINCARÉ – ANDRONOV – HOPF BIFURCATIONS IN THE TORSION  
WAVE MODELS OF SUPERDEEP DRILL COLUMNS

V.I. Gulyayev<sup>1</sup>  
O.V. Glushakova  
National Transport  
University  
Kiev, Ukraine

ABSTRACT

Wave model of torsion vibrations of deep rotating drill columns is obtained. Computer simulation of the torsion auto-oscillations generations is performed. The diapason of rotation velocity values corresponding to regimes of stable periodic motions is found. It is shown that The Poincaré – Andronov – Hopf bifurcations are realized at the states limiting these diapasons. Influence of the length of the articulated drill columns on the bifurcational values of the angular velocities is analyzed. The general regularities of generation and accomplishment of the auto-oscillation processes in the articulated drill columns are established.

INTRODUCTION

In the XX century a time of easy extraction of oil and gas is finished and inasmuch as the readily accessible deposits of hydrocarbon fuels are practically depleted in the result of their intensive extraction during the last two centenaries, their drawing is out from depths of 10km holds much promise. Taking into consideration that mechanical phenomena attending these processes are very complicated and there is no producing experience of such wells drilling, it may be concluded that problems of their theoretical simulation are urgent.

At present, the vertical, inclined and horizontal bore wells are drilled in accordance with requirements of economy, demands of oil-gas industry and its technological possibilities. Great attention is paid to the questions of drilling deep wells from ground surface and sea bottom. In the drilling technology the leading position belongs to the rotor method based on the use of a drill column with a bit.

When the fuel extraction is realized from great depths, the drill efficiency is associated with the problems of revealing the emergency regimes of the DC functioning.

One of the dynamic phenomena conducing the appearance of emergency situation during drilling is a self-excitation of torsion vibrations of rotating drill columns [1,2]. Inasmuch as a drill column (DC) represents a torsion pendulum (Fig.1) with energy outflow due to dissipative interaction between the bit and broken rock at its lower part, it can transit from a stationary state to the mode of torsional auto-oscillation at violation of the energy outflow conditions.

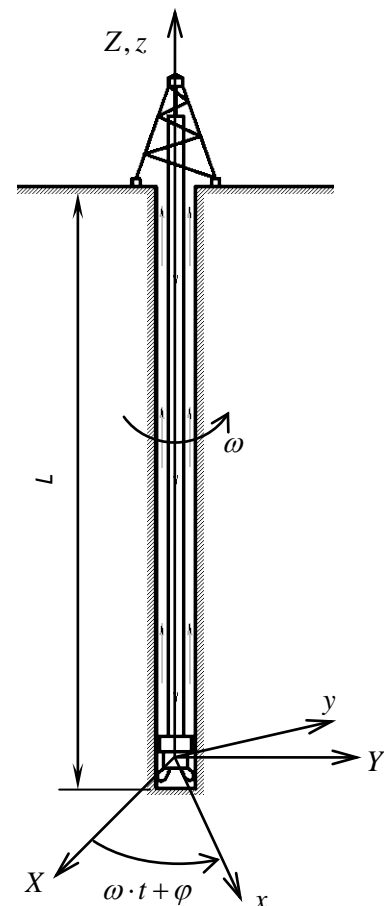


Fig. 1. Drill column scheme.

<sup>1</sup> Corresponding author. Email [valery@gulyayev.com.ua](mailto:valery@gulyayev.com.ua)

In a general case the auto-oscillations constitute non-damping periodic motions of a non-linear dissipative system which are sustained by external non-vibrational source of energy [2].

For their generating to happen, the non-linear force interaction between separate parts of the system is of importance which regulates income and expenditure of the energy and by this means gives rise to finite amplitude vibration. In drill assemblies the reason of the torsion vibration self-excitation is bifurcational disturbance of the balance between elastic force moments in the DC and the non-linear moment of the bit interaction with the well wall. By now the general regularities of these phenomena are not studied, so the problem of their theoretical simulation is urgent.

## **MATHEMATICAL AND MECHANICAL PECULIARITIES OF A TORSION WAVE PENDULUM**

In the theory of non-linear differential equations the periodical solutions are named cycles and the change of stationary solution by periodical one at transition of some distinctive parameter through a critical value is spoken of as a cycle generation or the Poincare – Andronov – Hopf bifurcation [3]. In the problems of drill column torsion dynamics the parameter exerting influence on their stationary and auto-oscillatory regimes is the angular velocity  $\omega$  of their rotation.

In the cases when an additional impact is not necessary for a mechanical system transition from an initial (stationary) state into regime of auto-vibration, the transition is designated as soft self-excitation. If the vibration begins to increase only after some initial threshold amplitude, the self-excitation is termed to be rigid.

The amplitude and frequency of the self-oscillation are determined only by the system parameters only. This is its distinction from natural vibration, whose frequency is determined by the system properties but the phase and amplitude are dictated by initial conditions, as well as from forced vibration, whose amplitude, frequency and phase are governed by an external force.

In the phase space the periodic auto-vibration corresponds to a closed trajectory attracting all the neighboring trajectories. So such a curve is generally referred to as a stable limit cycle (or attractor).

Auto-vibrational systems with several degrees of freedom and systems with distributed parameters are characterized by such phenomena as synchronization and competition of vibrations. In many cases this phenomena are responsible for initiation of well organized, complicated modes of periodic motions in dissipative unstable systems.

As applied to the phenomena accompanying drill column rotation, investigation of their auto-oscillation generating permits one to provide the answers to three important questions: 1) what values of the system parameters and manners of functioning are responsible for the torsion auto-oscillation generation; 2) what type of the oscillation self-excitation (soft or rigid) does occur; 3) what precautions should be taken to prevent the possible mode of the torsion auto-oscillation.

For the drill columns in comparatively shallow, the answers to these questions can be received with the help of simplified mathematical model constructed issuing from the consideration of an appropriate torsion pendulum with non-linear friction forces applied to its fly-wheel. In doing so the fly-wheel and the DC elements can be considered to perform torsional oscillations with the same phase and in consequence the overall elastic system can be changed by one oscillator with one DOF.

However if the DC is long, application of the torsion pendulum model for analysis of its dynamics is not justified, as vibrations of its elements cease to be synchronized. So their simulation should be performed on the basis of the wave theory.

Under real conditions this simplification is not met, as the time of the torsion wave propagation through the DC length is not multiple to the period of the lower fly-wheel vibration and for this reason its motion can attain a complicated mode. This effect can be essentially favored by the bit stick-slip dynamics inherent in the systems with dry friction. It consists in short-term stopping of the bit rotation in the time intervals, when the sum of all the moments of active and inertia forces is less than some threshold moment of friction forces which should be overcome to begin the fly-wheel slewing. During these intervals the drive device at the upper end of the DC continues to rotate with constant angular velocity  $\omega$ , the DC twists and accumulates potential energy of elastic strains. When elastic torque achieves a magnitude which is equal to the threshold value of the friction moment, the lower fly-wheel begins to rotate, the DC untwists and its potential energy begins to transform into kinetic energy of the DC and fly-wheel rotation. This rotation continues till the sum of elastic moment of the DC and inertia force moment of the fly-wheel again begins to be under the threshold value of the friction moment. As the result of this, the fly-wheel stops again and etc. Inasmuch as the functions of angular velocity and acceleration begin to be discontinuous in the described motion, the DC rotation acquires a shock character representing severe danger for the dynamic strength and stability of the

whole system. It is not rational to describe these vibrations by trigonometric functions, so numerical methods should be used.

This theory contains an important factor complicating the considered phenomenon and the problem statement. It is the effect of torsion wave action on the fly-wheel (the bit). The waves are formed as a result of elastic interaction between the fly-wheel and the DC. They achieve the DC top end, reflect and return with the delay to the lower end. Influence of this effect has not been studied yet and as shown below it reveals itself in the quantized character of the bit motion with the time quantum which is equaled the wave passage time from one end of the DC to another and reverse.

In this paper, on the basis of taking into account non-linear frictional interaction of a bit and broken rock and influence of incident wave delay effects the problem about analysis of self-excitation of wave and vibrational twisting motions in a vertical deep DC is stated and solved.

## STATEMENT OF THE PROBLEM

For an extended analysis of mechanism of the DC torsion auto-oscillation generation, assume that the system can be simulated as a wave torsional pendulum (Fig. 1). Consider the case of stationary rotation of the DC top end with constant velocity  $\omega$ . Introduce inertial coordinate system  $OXYZ$  with its origin at the bit mass center and axis  $OZ$  in line with the DC axis, as well as the coordinate system  $Oxyz$  rotating together with the DC top end.

Then the angle of the bit rotation relative to system  $OXYZ$  is  $\omega t + \varphi(0)$ , where  $\omega t$  is the angle of the DC top end rotation;  $t$  is the time;  $\varphi = \varphi(z)$  is the angle of the DC element elastic twist relative to the  $Oxyz$  system.

The equation of elastic oscillation of the torsional pendulum can be represented in the form of d'Alembert's principle

$$M^{in} + M^{fr} + M^{el} = 0 \quad (1)$$

Here  $M^{in} = M^{in}(\ddot{\varphi})$  is the moment of inertia forces acting on the bit;  $M^{fr} = M^{fr}(\omega + \dot{\varphi})$  the moment of the friction forces formed between the bit and the broken rock;  $M^{el} = M^{el}(\varphi)$  the moment of elastic forces acting on the bit at the DC twist; the dots above  $\varphi$  denote differentiation with respect to time  $t$ . Value  $M^{in}$  is calculated through the formula

$$M^{in} = -J \cdot \ddot{\varphi}, \quad (2)$$

where  $J$  is the bit inertia moment.

Moment  $M^{el}$  is determined by the equality

$$M^{el} = GI_z \frac{\partial \varphi}{\partial z}, \quad (3)$$

where  $G$  is the DC material elasticity module in shear;  $I_z$  the DC cross-section area inertia moment.

The question about the  $M^{fr}$  determining is more complicated. The models of the  $M^{fr}$  dependence on the rotary velocity  $\omega + \dot{\varphi}$  of the bit relative to the rock medium are constructed in accordance with the tribological properties of rubbing materials and their friction interaction conditions. The most commonly encountered relationships are represented by the Coulomb friction law. In its diagram the vertical segment determines the static friction moment  $M_{st}^{fr}$ , it is realized in the absence of sliding between bodies. Its limit value is equal to dynamic moment  $M_{dyn}^{fr}$ , which occurs in the bit rotation and remains constant for any value of the relative angular velocity  $\omega + \dot{\varphi}$ .

The friction force moment model with nonlinear dynamic moment is also widespread. Its feature is that the dynamic moment  $M_{dyn}^{fr}$  is less than the limit static moment  $M_{st}^{fr}$ . It should be recorded that the stick-slip effect connected with stoppings of the bit rotation relative to inertial coordinate

system  $OXYZ$  is inherent in both these models. Its mathematical explanation is associated with the presence of non-linearities in the  $M^{fr}$  expression which cannot be linearized.

If lubricating liquid is between the rubbing bodies the function  $M^{fr}(\omega + \dot{\varphi})$  can gain the form shown in Fig. 2,a. It has only segments of dynamic interaction. If conditions of dry friction are realized the  $M^{fr}$  function has also the segment of static friction (Fig. 2,b).

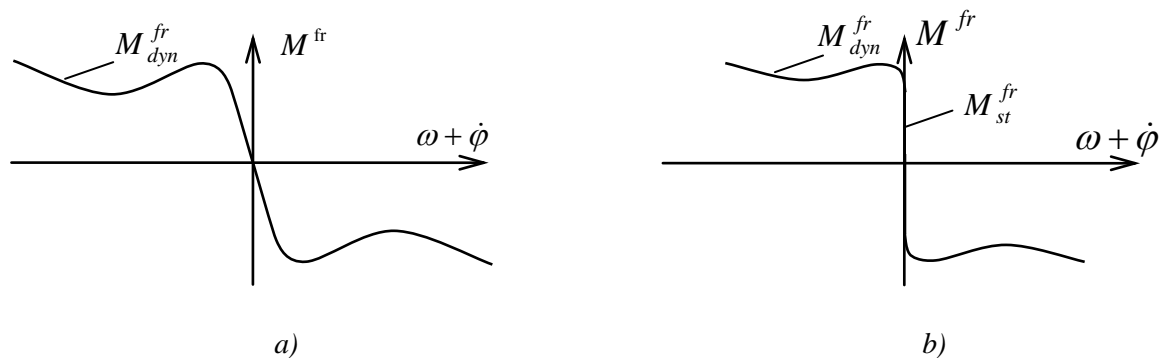


Fig. 2. Friction moment functions.

Rotary dynamics of a bit hanged at the end of a long drill column possesses specificities typical of waveguide systems. As a disturbance applied to its one end attains other end in a finite time interval, one is forced to take into consideration the disturbance delay. Indeed, if for example the DC is manufactured from steel then the velocities of longitudinal and transversal waves expressed through the elasticity moduli  $E$ ,  $G$  and density  $\rho$  are equal to  $\alpha = \sqrt{E/\rho} \approx 5100$  m/s,  $\beta = \sqrt{G/\rho} \approx 3200$  m/s, correspondingly. So if the DC length  $L = 6500$  m the torsional disturbance applied to one of its ends reaches another one and returns back in 4s only.

For this reason the DC torsion oscillation should be studied on the basis of the wave equation

$$\rho I_z \frac{\partial^2 \varphi}{\partial t^2} - G I_z \frac{\partial^2 \varphi}{\partial z^2} = 0, \quad (4)$$

where  $G$  is the DC material elasticity module in shear;  $\rho$  the material density;  $I_z$  the DC cross-section area inertia moment.

After substitution  $\beta = \sqrt{G/\rho}$  this equation is converted to the standard form

$$\frac{\partial^2 \varphi}{\partial t^2} - \beta^2 \frac{\partial^2 \varphi}{\partial z^2} = 0 \quad (5)$$

It has the d'Alembert solution

$$\varphi(z, t) = f(z - \beta t) + g(z + \beta t), \quad (6)$$

where  $f(z - \beta t)$ ,  $g(z + \beta t)$  are the arbitrary continuous functions. The first of them determines the wave propagating in the direction of the  $Oz$  axis and the reverse is true for the second one. As the waves are not dispersive they propagate without varying their profile, resulting in essential simplification of the problem solving.

Indeed, in this case the functions,  $f(z - \beta t)$ ,  $g(z + \beta t)$  are determined only by the initial conditions

$$f(z - 0) = f_0(z), \quad g(z + 0) = g_0(z), \quad (7)$$

and boundary conditions

$$\begin{aligned} F[f(0 - \beta t), g(0 + \beta t)] &= 0 \\ f(L - \beta t) + g(L + \beta t) &= 0 \end{aligned} \quad (8)$$

where  $F$  is the non-linear differential operator determining the bit motion.

Using equation (1) of the drill column bit equilibrium, one gains the constitutive differential equation of the wave pendulum vibration with delay argument

$$J \left\{ \ddot{f}(-\beta t) - \ddot{f} \left[ -\beta \left( t - \frac{2L}{\beta} \right) \right] \right\} - M^{fr} + \frac{G \cdot I_z}{\beta} \left\{ \dot{f}(-\beta t) + \dot{f} \left[ -\beta \left( t - \frac{2L}{\beta} \right) \right] \right\} = 0 \quad (9)$$

In this equation  $J$  is the bit inertia moment. Moment  $M^{fr}$  was chosen as shown in Fig.2,b.

Equation (10) is integrated numerically at a constant angular velocity  $\omega$  and prescribed initial conditions,  $q_1(0) = q_1^{(0)}$ ,  $q_2(0) = q_2^{(0)}$ . The found solutions allow determining the drill regimes accompanied by the DC torsion oscillation self-excitation, to construct their modes and to select the drill conditions excluding the system auto-oscillation.

The stated problem belongs to the case of stationary rotation, when  $\omega = const$ . But its formulation can be easily extended for non-stationary cases of the DC rotation connected with the starting and braking regimes.

## ANALYSIS OF THE RESULTS

Application of the wave torsion pendulum model for investigation of drill column vibration self-excitation permitted not only to reflect general regularities of limit cycle birth bifurcations, established on the basis of simplified 1 DOF oscillator model, but also to find radically new feature unique only to wave systems. It is associated with formation of the so-called quantized time with the resulting effect of constant angular velocity staying during time segment  $\Delta\tau$ , which is equal to the time duration of the torsion wave passing the path from the bit to the upper end and backward

$$\Delta\tau = 2L / \beta \quad (10)$$

Fig. 3,a presents  $\varphi$  as a function of  $t$  in the segment  $124 \leq t \leq 130$  s, constructed by the way of equation (9) integration with the use of the Runge-Kutta method. It can be seen that the bit vibrations have relaxational character.

Initial conditions,  $f(0) = 0$ ,  $\dot{f}(0) = 0$ , were assumed and integration step of time measured  $\Delta t = 6.474155 \cdot 10^{-6}$  s. In doing so the system parameters were chosen to be  $G = 8.077 \cdot 10^{10}$  Pa,  $I_z = 3.12 \cdot 10^{-5}$  m<sup>4</sup>,  $J = 3.1$  kg · m<sup>2</sup>; the rotation velocity  $\omega = 17$  rad / s. It should be noted, that the periodical oscillations with the period  $T \approx 1.275$  s are set very rapidly and function  $\dot{\varphi}(t)$  has the step-wise shape in the chosen scale, in spite of the function  $M^{fr}(\dot{\varphi})$  smoothness. The attempts to integrate equation (9) with other initial conditions led to the same results indicating to soft character of the oscillation self-excitation.

The outline of function  $\dot{\varphi}(t)$  in Fig. 3,b testifies that the bit oscillations proceed with jerks accompanied by large acceleration at transfer from one angular velocity level to another one.

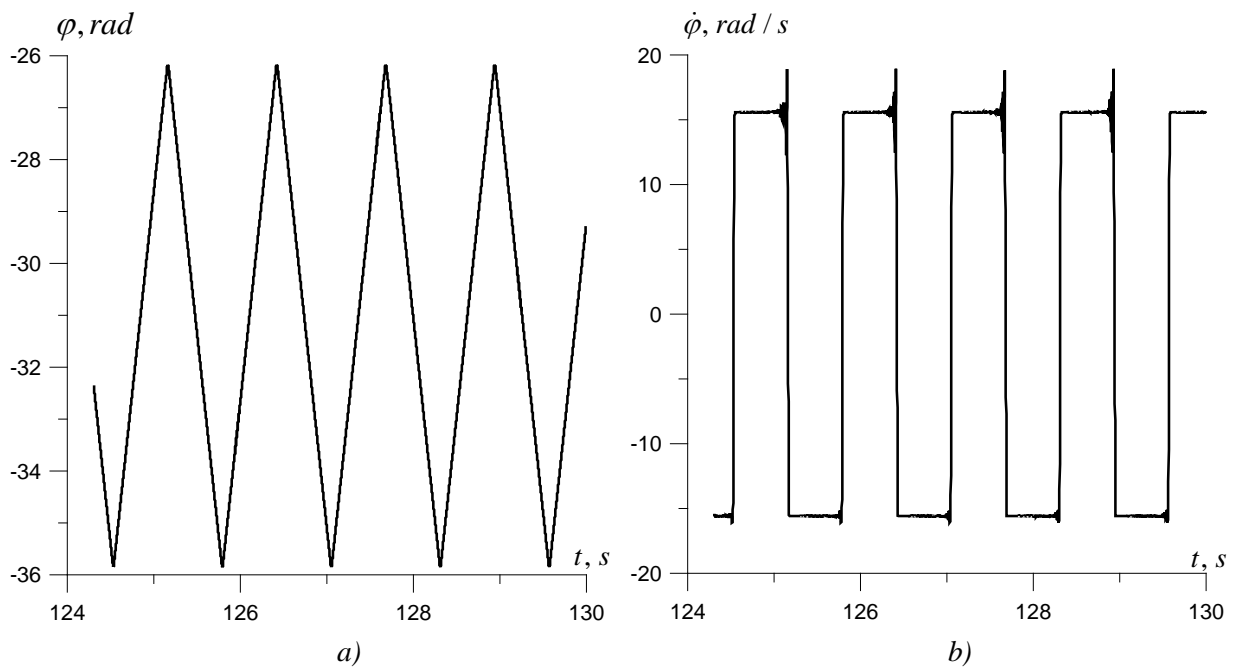


Fig. 3. Self-excitation of torsional vibrations:  
a) angle of elastic torsion;  
b) angular velocity.

## CONCLUSIONS

The problem of analysis of limit cycle birth bifurcations in the torsion wave models of superdeep drill columns is set up. The constitutive differential equation with delay argument is constructed. Analysis of its solutions permitted to establish the following features of the drill column torsion oscillation self-excitation:

1. The limit cycles of the torsion wave pendulum do not depend on initial conditions, so the self-excitation has the soft character.
2. The self-excited oscillations proceed in the manner of quantized time. The time quantum duration equals the time of the torsion wave propagation through the column doubled length.
3. The auto-oscillations prevail at low values of the DC angular velocity.

## REFERENCES

- [1] Brett J.F. The genesis of torsional drillstring vibrations. *SPE Drill. Engin.*, Vol. 7, pp.168-174, 1992.
- [2] Tucker R.W., Wang C. On the effective control of torsional vibrations in drilling systems. *J. of Sound and Vibr.*, Vol. 224, N.1, pp. 101-122, 1999.
- [3] Hassard B.D., Kazarinoff N.D., Wan Y. *Theory and Applications of Hopf Bifurcation*. Cambridge University Press. Cambridge, London, New York, New Rochelle, Melbourne, Sydney, 1981.
- [4] Gulyayev V., Hudolij S., Glushakova O. Quantized attractors in the wave torsion models of superdeep drill columns. *Int. symposium RA08 on Rare attractors and rare phenomena in nonlinear dynamics*, Riga, Latvia, p.33, 2008.
- [5] Gulyayev V.I., Glushakova, O.V., Hudolij S.N. Quantized Attractors in Wave Models of Torsion Vibrations of Deep-Hole Drill Strings. *Mechanics of Solids*, Vol. 45, N. 2, pp. 264-274, 2010.

**STOCHASTIC STABILITY OF THE DEFORMABLE FORMS AND  
VIBRATION MODES OF A PARAMETRICALLY EXCITED  
SANDWICH DOUBLE HEREDITARY BEAM SYSTEM**

---

**Katica R. (Stevanović)  
Hedrih<sup>1</sup>** ABSTRACT

Mathematical Institute  
SANU  
Belgrade, Serbia.

*Paper is dedicated to  
the honor of important  
scientist and nice  
person, **Professor  
S. T. Ariaratnam,**  
University of Waterloo,  
Canada.*

---

The coupled partial integro-differential equations of transversal stochastic vibrations of a parametrically excited sandwich double hereditary beam system were derived. The beams are graded by a hereditary material with known relaxation kernel, and it is subjected by axial stochastic external excitations. The influence of rotatory inertia of beam cross sections and transverse shear of beam cross sections under the transverse forces, and the corresponding members in the partial integro-differential equations are taken into account. Bernoulli particular integral method and Lagrange method of variation constant are used for the transformation problem of solutions. The asymptotic averaged method Krilov-Bogolyubov-Mitropolskiy is used for obtaining the first approximation of Itô stochastic differential equations and Stratonovich results. By using idea of Ariaratnam the sets of Lyapunov exponents are obtained.

---

## INTRODUCTION

The transversal vibration beam problem is classical, but in current university books on vibrations, we can find only the Euler-Bernoulli's classical partial differential equation for describing transversal beam vibrations. In monograph [20] we can find a non-linear partial differential equation for describing transversal vibrations of the beam with non-linear constitutive stress-strain relation. By using the asymptotic method of Krilov-Bogolyubov- Mitropolskiy [20, 21], many authors studied one frequency or multi-frequency non-linear oscillation regimes of deformable bodies. Specially, Hedrih [9, 9, 10, 11] studied one-single and two-frequency stationary and non-stationary regimes of non-linear transversal and forced vibration of beams. Transversal vibrations of the beam on the elastic Winckler's foundation under the action of multi-frequency forces with frequencies in the form of the first frequency resonant range of the beam was also studied by Hedrih [9], and some results of transversal vibrations of beams graded by a creep and hereditary material, were presented in References [12,13, 16].

In the university book [22] by Rašković, an extended partial differential equation of transversal ideally elastic beam vibrations was presented considering the inertia rotation of the beam's cross sections and transverse shear of the cross section. Also, in numerous papers, by using the partial differential equation of the transversal ideally elastic beam vibrations with members, by which influences of the inertia rotation of the beam's cross sections and transverse shear of the cross section by transversal forces are taken into account, and based on the monograph [19] by Nowatski as the scientific source, the complex properties of the transversal vibrations of the beam are investigated.

In paper [1] by Ariaratnam stochastic stability of visco-elastic systems under bounded noise excitation was investigated. For small damping and weak random fluctuation, asymptotic expressions are derived for the Lyapunov exponent and the rotation number using the method of stochastic averaging. From the sign of the Lyapunov exponent, the condition for asymptotic stability with probability 1 of the trivial equilibrium state is obtained. The stochastic almost-sure stability of a single degree-of-freedom linear visco-elastic system subjected to random fluctuation in the stiffness

---

<sup>1</sup> Corresponding author. Email [khedrih@eunet.rs](mailto:khedrih@eunet.rs)

parameter is investigated by Ariaratnam S. T. [2]. For small damping and weak random fluctuation, asymptotic expressions are derived for the Lyapunov exponent and the rotation number using the method of stochastic averaging. From the sign of the Lyapunov exponent, the condition for asymptotic stability with probability 1 of the trivial equilibrium state is obtained. In the paper [3] by Ariaratnam S. T. and Xie W.C. wave localization of a long continuous beam over several supports is studied. The localization factor is related to the larger of the two Lyapunov exponents associated with a product of 1-1 random wave transfer matrices. By using a theorem- due to Furstenberg- on the asymptotic properties of a product of independent and identically distributed random matrices\ the localization factors are calculated by a combination of analytical and numerical simulation methods.

In the paper [4] by Ariaratnam and Wei-Chau Xijz buckling mode localisation in large randomly disordered one-dimensional structures is studied. Furstenberg's theorem on the limiting behaviour of the product of random matrices is employed to determine the Lyapunov exponent and the localisation factor. Green's function formulation is applied to show that although the buckling loads are different for different sample structures, the buckling loads satisfy a probability distribution which depends only on the disorder parameters and is independent of the specific sample realisations for large structures. Due to the positivity of the Lyapunov exponent it is found that localised modes (bulges) may be visible for an arbitrary value of load close to the buckling loads if there exist perturbations or imperfections. In the paper [5] the dynamic stability of non-gyroscopic viscoelastic systems under multiple parametric excitations is investigated. The largest Lyapunov exponent as an indicator of the almost-sure asymptotic stability of the system is obtained by applying the stochastic averaging method together with Khasminskii's technique. The integral term arising from the viscoelastic effect is averaged by making use of Larianov's method. As an application, the flexural-torsional instability of a deep rectangular viscoelastic beam under stochastically fluctuating central load and end moments applied simultaneously is investigated. Both cases of follower and non-follower central fluctuating load are included in this analysis. Also, in paper [6] Ariaratnam and Abdelrahman presented results about stochastic stability of non-gyroscopic visco-elastic systems.

In the papers [14, 16] the influence of rotatory inertia of beam cross section and transverse shear of beam cross section under the transverse force, and the corresponding members in the partial differential equation are taken into account and by use Ariaratnam's idea [1] the expression for Lyapunov exponents are obtained and the stochastic stability of beam deformable forms and processes are investigated. Bernoulli particular integral method and Lagrange method of variation constant are used for the transformation problem of solutions. The asymptotic averaged method is used for obtaining the first approximation of Itô stochastic differential equations. The sets of Lyapunov exponents are obtained.

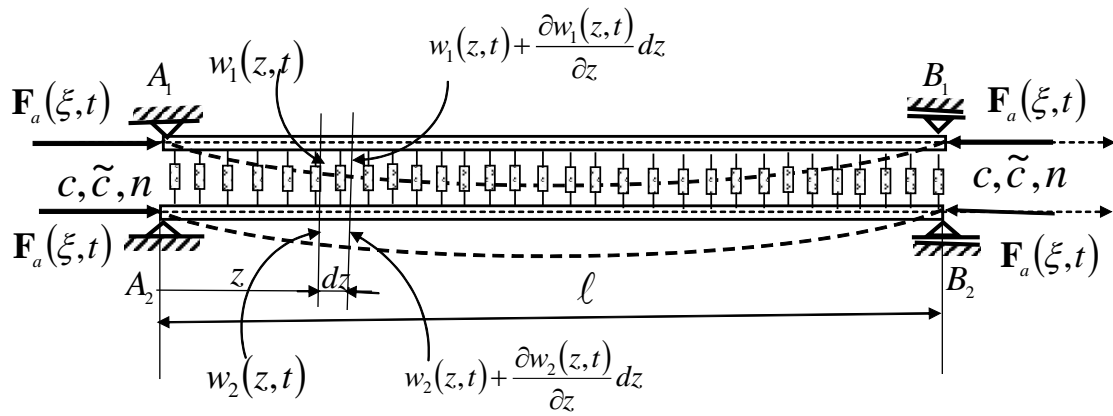
In the paper [16], the stability of a hereditary visco-elastic beam subjected to parametric random bounded excitations described by stochastic processes of small intensity is investigated. The motivation for the study of these problems is the necessity to explain the influence of rotatory inertia of beam cross sections and transverse shear of beam cross section under the transverse forces on the stability of the transversal time vibrations process of the beam, and also on the stability of the deformable beam's forms.

Paper [15] present an investigation about stochastic dynamics of hybrid systems with thermo-rheological hereditary elements. Tensor of state of the random vibrations was considered in the paper [17].

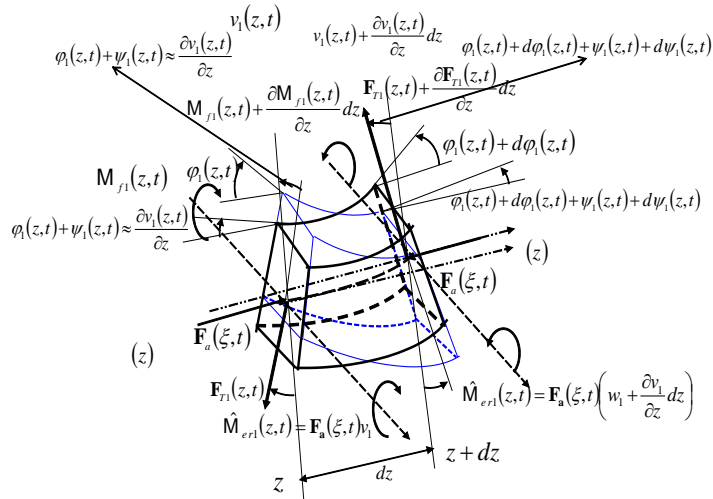
In the present paper transversal vibrations of a parametrically excited sandwich double hereditary beam system and influence of rotatory inertia and transverse shear on stochastic stability of deformable forms and processes are investigated.

## 1. CONSTITUTIVE RELATION OF THE VISCO-ELASTIC HEREDITARY BEAM

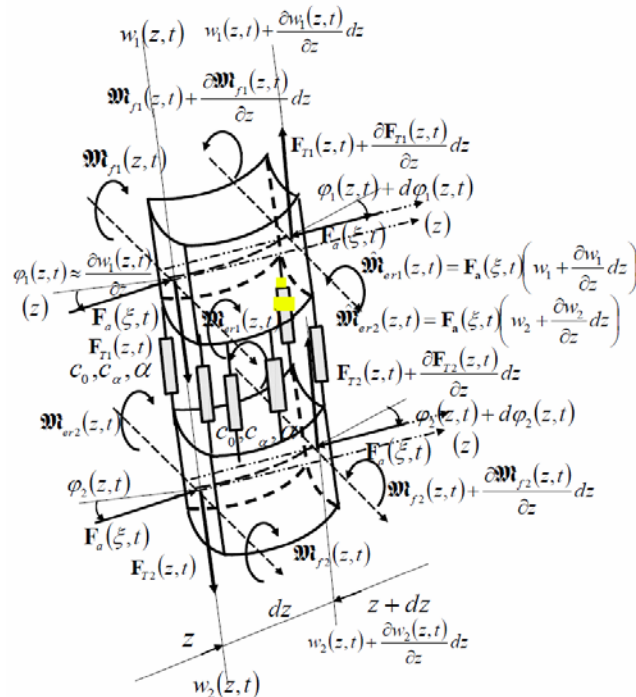
Let suppose that material of the beam is rheological with hereditary property (se Ref. [7]). Parameter of beam material are:  $n$  own material clock of the material relaxation or short relaxation time of beam material;  $E$  and  $\tilde{E}$  modulus of elasticity momentaneous behavior of material and prologueous one in long time period. In Figure 1. a\* we can see homogeneous prismatic hereditary beams with two axes symmetry of the beam cross sections with line element in deformed stressed state. For ideal visco-elastic hereditary beam and axially stressed line element at the distance  $y$  from neutral beam line, the normal stress component  $\sigma_z(z, y, t)$  for the beam cross section on the distance  $z$  from left beam end, at the moment  $t$  is:



a\*



b\*



c\*

Fig. 1. a\* Sandwich double beam hereditary system.

Cross section surface forces and moments acting on a beam element:

The influence of rotatory inertia of beam cross sections and transverse shear under the influence of transversal force in the cross section

b\*. Cross section displacement and surface forces and moments acting on a beam element - the influence of rotatory inertia of beam cross sections

c\* The sandwich double beam hereditary system elements with standard light hereditary connection

$$\sigma_z(z, y, t) = E \left[ \varepsilon_z(z, y, t) - \int_0^t \mathbf{R}(t - \tau) \varepsilon_z(z, y, \tau) d\tau \right] \quad (1)$$

where  $\varepsilon_z(z, y, t)$  is dilatation – strain of beam line element and

$$\mathbf{R}(t - \tau) = \frac{E - \tilde{E}}{nE} e^{-\frac{t-\tau}{n}} \quad (2)$$

kernel of relaxation of beam visco-elastic material with hereditary properties.

## 2. PARTIAL INTEGRO-DIFFERENTIAL EQUATIONS OF THE TRANSVERSAL VIBRATIONS OF PARAMETRICALLY EXCITED DOUBLE HEREDITARY BEAM SYSTEM

The dilatations  $\varepsilon_{zi}(z, y, t), i = 1, 2$  of corresponding beam's stressed and strained line elements at the distance  $y$  from neutral beam line and normal to the beam cross section on the distance  $z$  from left beam end, at the moment  $t$  are:

$$\varepsilon_{zi}(z, y, t) = \frac{ds_i - dz}{dz} = y \frac{\partial \varphi_i(z, t)}{\partial z}, i = 1, 2 \quad (3)$$

where  $\varphi_i(z, t), i = 1, 2$  are the component inclination angles of the tangent to the visco-elastic bended beam's line in result of pure bending beams by corresponding couple moments. With  $\psi_i(z, t), i = 1, 2$  are denoted the component inclination angle of the tangent to the visco-elastic bended beam's line in result of transverse shear as influence of the transversal forces in corresponding beam's cross section.

By introducing previous expression (3) for strain into expression of constitutive relation (1), the normal stress component  $\sigma_{zi}(z, y, t), i = 1, 2$  for the corresponding beam cross section on the distance  $z$  from left beam end, at the moment  $t$  we obtain in the following form:

$$\sigma_{zi}(z, y, t) = Ey \left[ \frac{\partial \varphi_i(z, t)}{\partial z} - \int_0^t \mathbf{R}(t - \tau) \frac{\partial \varphi_i(z, \tau)}{\partial z} d\tau \right], i = 1, 2. \quad (4)$$

In Figure 1. b\* the beam's element with length  $dz$  is presented with transversal displacements. In the results of the elimination of the component inclination angles  $\varphi_1$  and  $\varphi_2$  from the system of the four partial integro-differential equations obtained into results of Principle of dynamical equilibrium application to the double hereditary beam element, shown in Figure 1.c\*, we obtain two coupled partial integro-differential equations of the transversal vibrations of the two coupled beams of the previous sandwich double hereditary beam system in the form:

$$\begin{aligned} & \frac{\partial^2 v_1(z, t)}{\partial t^2} + c_1^2 \left[ \frac{\partial^4 v_1(z, t)}{\partial z^4} - \int_0^t \mathbf{R}(t - \tau) \left[ \frac{\partial^4 v_1(z, \tau)}{\partial z^4} \right] d\tau \right] - a_1^2 \frac{\partial^4 v_1(z, t)}{\partial t^2 \partial z^2} + b_1^2 \frac{\partial^4 v_1(z, t)}{\partial t^4} - \\ & + (a_1^2 - i_{x1}^2) \int_0^t \mathbf{R}(t - \tau) \left[ \frac{\partial^4 v_1(z, \tau)}{\partial t^2 \partial z^2} \right] d\tau + \hat{c}_1 [v_1(z, t) - v_2(z, t)] + \hat{c}_1 b_1^2 \frac{\partial^2}{\partial t^2} [v_1(z, t) - v_2(z, t)] + \\ & + \hat{c}_1 (a_1^2 - i_{x1}^2) \left[ \frac{\partial^2}{\partial z^2} [v_1(z, t) - v_2(z, t)] - \int_0^t \mathbf{R}(t - \tau) \left[ \frac{\partial^2}{\partial z^2} [v_1(z, \tau) - v_2(z, \tau)] \right] d\tau \right] - \frac{\partial}{\partial z} \left[ \hat{\mathbf{F}}_{a1}(\Xi, z, t) \frac{\partial v_1(z, t)}{\partial z} \right] = 0 \\ & \frac{\partial^2 v_2(z, t)}{\partial t^2} + c_2^2 \left[ \frac{\partial^4 v_2(z, t)}{\partial z^4} - \int_0^t \mathbf{R}(t - \tau) \left[ \frac{\partial^4 v_2(z, \tau)}{\partial z^4} \right] d\tau \right] - a_2^2 \frac{\partial^4 v_2(z, t)}{\partial t^2 \partial z^2} + b_2^2 \frac{\partial^4 v_2(z, t)}{\partial t^4} - \\ & + (a_2^2 - i_{x2}^2) \int_0^t \mathbf{R}(t - \tau) \left[ \frac{\partial^4 v_2(z, \tau)}{\partial t^2 \partial z^2} \right] d\tau - \hat{c}_2 [v_1(z, t) - v_2(z, t)] - \hat{c}_2 b_2^2 \frac{\partial^2}{\partial t^2} [v_1(z, t) - v_2(z, t)] - \\ & - \hat{c}_2 (a_2^2 - i_{x2}^2) \left[ \frac{\partial^2}{\partial z^2} [v_1(z, t) - v_2(z, t)] - \int_0^t \mathbf{R}(t - \tau) \left[ \frac{\partial^2}{\partial z^2} [v_1(z, \tau) - v_2(z, \tau)] \right] d\tau \right] - \frac{\partial}{\partial z} \left[ \hat{\mathbf{F}}_{a2}(\Xi, z, t) \frac{\partial v_2(z, t)}{\partial z} \right] = 0 \end{aligned} \quad (5)$$

where:

$$c_i^2 = i_{xi}^2 \frac{\mathbf{B}_{xi}}{(\rho \mathbf{I}_x)_i} = \frac{\mathbf{B}_{xi}}{(\rho \mathbf{A})_i} \quad a_i^2 = i_{xi}^2 \left( \frac{\kappa \mathbf{E}}{\mathbf{G}} + 1 \right) \quad a_i^2 - i_{xi}^2 = i_{xi}^2 \left( \frac{\kappa \mathbf{E}}{\mathbf{G}} \right) \quad b_i^2 = i_{xi}^2 \left( \rho \frac{\mathbf{K}}{\mathbf{G}} \right)_i$$

$$\hat{c}_i = i_{ix}^2 \frac{c}{(\rho I_x)_i} = \frac{c}{(\rho A)_i} \quad \hat{F}_{ai}(\Xi, z, t) = \frac{F_a(\Xi, z, t)}{(\rho A)_i} \quad i_{xi}^2 \left( \frac{\kappa}{GA} \right)_i c = i_{xi}^2 \left( \rho \frac{\kappa}{G} \right)_i \frac{c}{(\rho A)_i} = \hat{c}_i b_i^2$$

$$c i_{xi}^2 \frac{E_i}{\rho_i} \left( \frac{\kappa}{GA} \right)_i = i_{xi}^2 \left( \frac{\kappa E}{G} \right)_i \frac{c_i}{(\rho A)_i} = \hat{c}_i (a_i^2 - i_{xi}^2)$$

### 3. SOLUTION OF THE PARTIAL INTEGRO-DIFFERENTIAL EQUATIONS OF THE TRANSVERSAL VIBRATIONS OF PARAMETRICALLY EXCITED DOUBLE HEREDITARY BEAM SYSTEM

For the solutions of the governing system of the corresponding coupled partial integro-differential equations (5) for free double beam system oscillations, we take in the eigen amplitude function  $Z_{i(s)}(z) = Z_{(s)}(z)$ ,  $i = 1, 2$ ,  $s = 1, 2, 3, 4, \dots, \infty$  expansion with time coefficients in the form of unknown time functions  $T_{i(s)}(t)$ ,  $i = 1, 2$ ,  $s = 1, 2, 3, 4, \dots, \infty$  describing their time evolution in the form:

$$v_i(z, t) = \sum_{s=1}^{\infty} \mathbf{Z}_{(s)}(z) \mathbf{T}_{i(s)}(t), \quad i = 1, 2 \quad (6)$$

After introduce the proposed solution into partial integro-differential equations (5) and taking into account orthogonality conditions (see Refs. [13], [14] and [15]), we obtain:

$$\ddot{\mathbf{T}}_{(1)s}(t) + \frac{1}{b^2} [1 - a^2 n_s] \ddot{\mathbf{T}}_{(1)s}(t) + \frac{1}{b^2} [c^2 m_s + \hat{c} + n_s (\hat{F}_{a0} - \hat{F}_{a1} \xi(t))] \mathbf{T}_{(1)s}(t) + \frac{a^2 - i_x^2}{b^2} n_s \int_0^t \mathbf{R}(t - \tau) \ddot{\mathbf{T}}_{(1)s}(\tau) d\tau - \frac{c^2 m_s}{b^2} \int_0^t \mathbf{R}(t - \tau) \mathbf{T}_{(1)s}(\tau) d\tau - \frac{\hat{c}}{b^2} \mathbf{T}_{(2)s}(t) = 0 \quad (7)$$

$$\ddot{\mathbf{T}}_{(2)s}(t) + \frac{1}{b^2} [1 - a^2 n_s] \ddot{\mathbf{T}}_{(2)s}(t) + \frac{1}{b^2} [c^2 m_s + \hat{c} + n_s (\hat{F}_{a0} - \hat{F}_{a1} \xi(t))] \mathbf{T}_{(2)s}(t) + \frac{a^2 - i_x^2}{b^2} n_s \int_0^t \mathbf{R}(t - \tau) \ddot{\mathbf{T}}_{(2)s}(\tau) d\tau - \frac{c^2 m_s}{b^2} \int_0^t \mathbf{R}(t - \tau) \mathbf{T}_{(2)s}(\tau) d\tau - \frac{\hat{c}}{b^2} \mathbf{T}_{(1)s}(t) = 0 \quad (8)$$

where it is introduced the following notations:

$$\int_0^\ell \mathbf{Z}_s(z) \mathbf{Z}_s(z) dz = \tilde{m}_s, \quad s = r; \quad \int_0^\ell \mathbf{Z}'_s(z) \mathbf{Z}'_s(z) dz = \tilde{n}_s, \quad s \neq r$$

$$\int_0^\ell \mathbf{Z}''_s(z) \mathbf{Z}_s(z) dz = \left[ \mathbf{Z}'_s(z) \mathbf{Z}_s(z) \Big|_0^\ell - \int_0^\ell \mathbf{Z}'_s(z) \mathbf{Z}'_s(z) dz \right] = m_s \tilde{m}_s \quad (9)$$

$$\int_0^\ell \mathbf{Z}''_s(z) \mathbf{Z}_s(z) dz = -a_s \left[ \mathbf{Z}'_s(z) \mathbf{Z}_s(z) \Big|_0^\ell - \int_0^\ell \mathbf{Z}'_s(z) \mathbf{Z}'_s(z) dz \right] + b_s \int_0^\ell \mathbf{Z}_s(z) \mathbf{Z}_s(z) dz = \tilde{m}_s n_s$$

First, we concentrate our attention to the solution of the coupled ordinary differential equations (7) for the case of free own vibrations. Solution of the basic equations of the previous system (7) are proposed in the following form:

$$\mathbf{T}_{(i)s}(t) = A_{(i)s} \cos(\omega_{(s)} t + \alpha_{(s)}), \quad i = 1, 2; \quad s = 1, 2, 3, \dots \quad (10)$$

After introducing this proposed solution (10), we obtain the homogeneous system of two algebra equations with respect to the unknown amplitudes  $A_{(i)s}$ . The corresponding frequency equation is in the following form: or in the form:

$$f(\omega_{(s)}^2) = \left[ \frac{1}{b^2} (c^2 m_s + \hat{c} + n_s \hat{F}_{a0}) + \omega_{(s)}^4 - \frac{\omega_{(s)}^2}{b^2} [1 - a^2 n_s] \right]^2 - \left[ \frac{\hat{c}}{b^2} \right]^2 = 0 \quad (11)$$

Circular frequencies are roots of the previous equation and are defined by following expressions:

$$\omega_{(s)1,2}^2 = \frac{1}{2b^2} [1 - a^2 n_s] \mp \sqrt{\frac{1}{4b^4} [1 - a^2 n_s]^2 - \frac{1}{b^2} (c^2 m_s + n_s \hat{F}_{a0})} \quad (12)$$

$$\omega_{(s)3,4}^2 = \frac{1}{2b^2} [1 - a^2 n_s] \mp \sqrt{\frac{1}{4b^4} [1 - a^2 n_s]^2 - \frac{1}{b^2} (c^2 m_s + 2\hat{c} + n_s \hat{F}_{a0})} \quad (13)$$

Then, we can write the following time functions correspond to the set of the obtained own circular frequencies::

$$\begin{aligned} \mathbf{T}_{(i)s}(t) &= \sum_{r=1}^4 A_{(i)s}^{(r)} \cos(\omega_{(s)r} t + \alpha_{(s)r}), \quad i=1,2; \quad s=1,2,3,\dots \\ \mathbf{T}_{(i)s}(t) &= C_s^{1,2} \cos(\omega_{(s)1} t + \alpha_{(s)1}) + C_s^{1,2} \cos(\omega_{(s)2} t + \alpha_{(s)2}) + C_s^{3,4} \cos(\omega_{(s)3} t + \alpha_{(s)3}) + C_s^{3,4} \cos(\omega_{(s)4} t + \alpha_{(s)4}) \\ \mathbf{T}_{(2)s}(t) &= C_s^{1,2} \cos(\omega_{(s)1} t + \alpha_{(s)1}) + C_s^{1,2} \cos(\omega_{(s)2} t + \alpha_{(s)2}) - C_s^{3,4} \cos(\omega_{(s)3} t + \alpha_{(s)3}) - C_s^{3,4} \cos(\omega_{(s)4} t + \alpha_{(s)4}) \end{aligned} \quad (14)$$

These time functions are time component of the solutions for the case of the axial force acting to the sandwich double beam system when these forces are deterministic and constant intensity.

Now, following the idea presented by S.T. Ariaratnam (1995) in Reference [1], for solving the previous equations (7), we can propose that random, bonded noise axial excitation  $\xi(t)$  is taken in the following form:

$$\hat{F}_{a1}(t) = \hat{F}_{a1} \xi(t) = \hat{F}_{a1} \mu \sin[\Omega t + \sigma B(t) + \gamma] \quad (15)$$

where  $B(t)$  is the standard Wiener process, and  $\gamma$  is a random uniformly distributed variable in interval  $[0, 2\pi]$ , then  $\xi(t)$  is a stationary process having autocorrelation function and spectral density function:

$$R(\tau) = \frac{1}{2} \mu^2 e^{-\frac{\sigma^2 \tau}{2}} \cos \Omega \tau \quad (16)$$

and

$$S(\omega) = \int_{-\infty}^{+\infty} R(\tau) e^{i\omega \tau} d\tau = \frac{1}{2} \mu \sigma^2 \frac{\omega^2 + \Omega^2 + \frac{\sigma^2}{4}}{\left[ \left( \omega^2 - \Omega^2 - \frac{\sigma^2}{4} \right)^2 + \sigma^2 \omega^2 \right]} \quad (17)$$

Stochastic process  $|\xi(t)| \leq 1$  is bounded for all values of time  $t$ .

Next idea of Ariaratnam is to apply the averaging method, and for that reason we must to introduce the amplitudes  $C_s^1(t), C_s^2(t), C_s^3(t), C_s^4(t)$  and phases  $\Phi_{(s)1}(t), \Phi_{(s)2}(t), \Phi_{(s)3}(t), \Phi_{(s)4}(t)$ , which are time unknown functions, by means of the transformation relation of  $\mathbf{T}_{(i)s}(t)$ ,  $i=1,2, s=1,2,3,4,\dots,\infty$  from the case of free vibrations (14) to the case of the perturbed stochastic vibrations, in the following form:

$$\begin{aligned} \mathbf{T}_{(1)s}(t) &= C_s^1(t) \cos \Phi_{(s)1}(t) + C_s^2(t) \cos \Phi_{(s)2}(t) + C_s^3(t) \cos \Phi_{(s)3}(t) + C_s^4(t) \cos \Phi_{(s)4}(t) \\ \mathbf{T}_{(2)s}(t) &= C_s^1(t) \cos \Phi_{(s)1}(t) + C_s^2(t) \cos \Phi_{(s)2}(t) - C_s^3(t) \cos \Phi_{(s)3}(t) - C_s^4(t) \cos \Phi_{(s)4}(t) \end{aligned} \quad (18)$$

in which amplitudes  $C_s^1(t), C_s^2(t), C_s^3(t)$  and  $C_s^4(t)$  and full phases  $\Phi_{(s)1}(t), \Phi_{(s)2}(t), \Phi_{(s)3}(t)$  and  $\Phi_{(s)4}(t)$  are unknown functions of the time. It is necessary to find solutions which correspond to parametric resonant state, for which full phases  $\Phi_{(s)1}(t), \Phi_{(s)2}(t), \Phi_{(s)3}(t)$  and  $\Phi_{(s)4}(t)$  are functions of time in the proposed forms:

$$\Phi_{(s)k}(t) = \frac{\Omega}{2} t + \phi_{(s)k}(t), \quad \Delta_{(s)k} = \omega_{(s)k} - \frac{\Omega}{2}, \quad k=1,2,3,4, \quad s=1,2,3,4,\dots,\infty \quad (19)$$

We suppose that the corresponding first, second and third derivatives with respect to time of the time functions  $\mathbf{T}_{(i)s}(t)$ ,  $i=1,2, s=1,2,3,4,\dots,\infty$  are same as in case when the amplitudes  $C_s^1(t), C_s^2(t), C_s^3(t), C_s^4(t)$  and phases  $\Phi_{(s)1}(t), \Phi_{(s)2}(t), \Phi_{(s)3}(t)$  and  $\Phi_{(s)4}(t)$  are constants and correspond to the solutions of the unperturbed case. For that reason, we obtain six conditions – equations with respect to the unknown first derivatives of the unknown amplitudes  $\dot{C}_s^1(t), \dot{C}_s^2(t), \dot{C}_s^3(t), \dot{C}_s^4(t)$  and phases  $\dot{\Phi}_{(s)1}(t), \dot{\Phi}_{(s)2}(t), \dot{\Phi}_{(s)3}(t)$  and  $\dot{\Phi}_{(s)4}(t)$  with respect to the time. Substituting these time derivatives together with four derivative into system differential equations (7), we obtain system of eight equations, but in the form of homogeneous system of series of unknown expressions with sub-system determinant different them zero, then as follow we obtain

simpler system with eight equations. Now, obtained simpler system of the eight equations with unknown time functions which represent unknown amplitudes  $C_s^1(t), C_s^2(t), C_s^3(t)$  and  $C_s^4(t)$  and unknown full phases  $\Phi_{(s)1}(t), \Phi_{(s)2}(t), \Phi_{(s)3}(t)$  and  $\Phi_{(s)4}(t)$  or  $\phi_{(s)1}(t), \phi_{(s)2}(t), \phi_{(s)3}(t)$  and  $\phi_{(s)4}(t)$  which are the time functions, is not difficult to solve. By solve these equations along first time derivatives of the amplitudes  $\dot{C}_s^1(t), \dot{C}_s^2(t), \dot{C}_s^3(t)$  and  $\dot{C}_s^4(t)$  and phases  $\dot{\phi}_{(s)1}(t), \dot{\phi}_{(s)2}(t), \dot{\phi}_{(s)3}(t)$  and  $\dot{\phi}_{(s)4}(t)$ , we obtain the system of the eight, first order, integro-differential equations. We can conclude that this full system of the first order integro-differential equations contain eight coupled integro-differential equations. These integro-differential equations of the first order with respect to unknown amplitudes  $C_s^1(t), C_s^2(t), C_s^3(t)$  and  $C_s^4(t)$  and unknown phases  $\Phi_{(s)1}(t), \Phi_{(s)2}(t), \Phi_{(s)3}(t)$  and  $\Phi_{(s)4}(t)$ , or in difference of the phases  $\phi_{(s)1}(t), \phi_{(s)2}(t), \phi_{(s)3}(t)$  and  $\phi_{(s)4}(t)$ , represent example of the eight Itô stochastic integro-differential equations.

In the previous obtained system of the eight integro-differential equations,  $\xi(t)$  is the excitation of the stochastic-random process and it is taken in the form (see Ref. [1] by Ariaratnam):

$$\xi(t) = \mu \sin[\Omega t + \sigma B(t) + \gamma] = \mu \sin[\Omega t + \psi(t)] \quad (20)$$

where  $B(t)$  is the standard Wiener process and  $\gamma$  is a random variable. If  $\gamma$  is uniformly distributed in the interval  $[0, 2\pi]$ , then  $\xi(t)$  is a stationary process having autocorrelation function and spectral density. We introduce the following notations:

$$\psi(t) = \sigma B(t) + \gamma \quad \text{as well as} \quad \dot{\psi}(t) = \sigma \dot{B}(t) \quad (21)$$

Substituting the  $\xi(t)$  in obtained system equations, we obtain system of the stochastic, first order integro-differential equations, with respect to the unknown amplitudes as time functions  $C_s^1(t), C_s^2(t), C_s^3(t)$  and  $C_s^4(t)$ , and unknown phases  $\phi_{(s)1}(t), \phi_{(s)2}(t), \phi_{(s)3}(t)$  and  $\phi_{(s)4}(t)$  in the transformed form. Now, we must apply the method of averaging to the right-hand sides of obtained equations with respect to the full phases  $\Phi_{(s)1}(t), \Phi_{(s)2}(t), \Phi_{(s)3}(t)$  and  $\Phi_{(s)4}(t)$ . After averaging the right-hand sides of all other equations with respect to the full phases  $\Phi_{(s)1}(t), \Phi_{(s)2}(t), \Phi_{(s)3}(t)$  and  $\Phi_{(s)4}(t)$ , we obtain the system of averaged differential equations of the first approximation.

The averaging method for integro-differential equations developed by Krilov Bogolyubov Mitropolskiy and also Larionov (1969) is applied to obtain the so called averaged equations. Thus we assume that are:

$$\begin{aligned} \frac{1}{4(\omega_{(s)2}^2 - \omega_{(s)1}^2)\omega_{(s)1}} \frac{n_s}{b^2} \hat{F}_{a1} &= O(\varepsilon), \quad \frac{1}{4(\omega_{(s)2}^2 - \omega_{(s)1}^2)\omega_{(s)2}} \frac{n_s}{b^2} \hat{F}_{a1} = O(\varepsilon), \quad 0 < \varepsilon < 1, \\ \frac{c^2 m_s}{2b^2} \frac{1}{(\omega_{(s)2}^2 - \omega_{(s)1}^2)\omega_{(s)1}} &= O(\varepsilon), \quad \frac{c^2 m_s}{2b^2} \frac{1}{(\omega_{(s)2}^2 - \omega_{(s)1}^2)\omega_{(s)2}} = O(\varepsilon), \quad \Delta_{(s)k} = O(\varepsilon) \\ \frac{1}{4(\omega_{(s)4}^2 - \omega_{(s)3}^2)\omega_{(s)3}} \frac{n_s}{b^2} \hat{F}_{a1} &= O(\varepsilon), \quad \frac{1}{4(\omega_{(s)4}^2 - \omega_{(s)3}^2)\omega_{(s)3}} \frac{n_s}{b^2} \hat{F}_{a1} = O(\varepsilon), \quad 0 < \varepsilon < 1, \\ \frac{1}{4(\omega_{(s)4}^2 - \omega_{(s)3}^2)\omega_{(s)4}} \frac{n_s}{b^2} \hat{F}_{a1} &= O(\varepsilon), \quad \frac{1}{4(\omega_{(s)4}^2 - \omega_{(s)3}^2)\omega_{(s)4}} \frac{n_s}{b^2} \hat{F}_{a1} = O(\varepsilon) \end{aligned} \quad (22)$$

The assumption of the detuning parameter  $\Delta_{(s)k} = O(\varepsilon)$  effectively restricts, the analysis to those excitation frequencies  $\Omega$  that are in the vicinity of the frequency  $2\Omega$  of fundamental parametric resonance. After averaging the members in the right hand sides of previous stochastic Itô differential equations, we obtain the averaged differential equations in the following form:

$$\begin{aligned} \dot{C}_s^1(t) &= -\frac{1}{4(\omega_{(s)2}^2 - \omega_{(s)1}^2)\omega_{(s)1}} \frac{n_s}{b^2} \hat{F}_{a1} C_s^1(t) \cos(\psi - 2\phi_{(s)1}(t)) - \\ &\quad - \frac{a^2}{2b^2} n_s \frac{1}{(\omega_{(s)2}^2 - \omega_{(s)1}^2)\omega_{(s)1}} \left[ \omega_{(s)1}^2 \mathbf{H}_{re} \left( \frac{\Omega}{2} \right) + \omega_{(s)2}^2 \mathbf{H}_{im} \left( \frac{\Omega}{2} \right) \right] - \\ &\quad - \frac{c^2 m_s}{2b^2} \frac{1}{(\omega_{(s)2}^2 - \omega_{(s)1}^2)\omega_{(s)1}} \left[ \mathbf{H}_{re} \left( \frac{\Omega}{2} \right) + \mathbf{H}_{im} \left( \frac{\Omega}{2} \right) \right] \end{aligned}$$

$$\begin{aligned}
\dot{\phi}_{(s)1}(t) &= \Delta_{(s)1} - \frac{1}{4(\omega_{(s)2}^2 - \omega_{(s)1}^2)\omega_{(s)1}} \frac{n_s}{b^2} \hat{F}_{a1} \sin[\psi - 2\phi_{(s)1}(t)] - \\
&\quad - \frac{a^2}{2b^2} n_s \frac{1}{C_s^1(t)(\omega_{(s)2}^2 - \omega_{(s)1}^2)\omega_{(s)1}} \left[ \omega_{(s)2}^2 \mathbf{H}_{re} \left( \frac{\Omega}{2} \right) + \omega_{(s)1}^2 \mathbf{H}_{im} \left( \frac{\Omega}{2} \right) \right] + \\
&\quad - \frac{c^2 m_s}{2b^2} \frac{1}{C_s^1(t)(\omega_{(s)2}^2 - \omega_{(s)1}^2)\omega_{(s)1}} \left[ \mathbf{H}_{re} \left( \frac{\Omega}{2} \right) + \mathbf{H}_{im} \left( \frac{\Omega}{2} \right) \right] \\
\dot{C}_s^2(t) &= - \frac{1}{4(\omega_{(s)2}^2 - \omega_{(s)1}^2)\omega_{(s)2}} \frac{n_s}{b^2} \hat{F}_{a1} C_s^2(t) \cos(\psi - 2\phi_{(s)2}(t)) - \\
&\quad - \frac{a^2}{2b^2} n_s \frac{1}{(\omega_{(s)2}^2 - \omega_{(s)1}^2)\omega_{(s)2}} \left[ \omega_{(s)1}^2 \mathbf{H}_{re} \left( \frac{\Omega}{2} \right) + \omega_{(s)2}^2 \mathbf{H}_{im} \left( \frac{\Omega}{2} \right) \right] + \\
&\quad - \frac{c^2 m_s}{2b^2} \frac{1}{(\omega_{(s)2}^2 - \omega_{(s)1}^2)\omega_{(s)2}} \left[ \mathbf{H}_{re} \left( \frac{\Omega}{2} \right) + \mathbf{H}_{im} \left( \frac{\Omega}{2} \right) \right] \\
\dot{\phi}_{(s)2}(t) &= \Delta_{(s)2} - \frac{1}{4(\omega_{(s)2}^2 - \omega_{(s)1}^2)\omega_{(s)2}} \frac{n_s}{b^2} \hat{F}_{a1} \sin[\psi - 2\phi_{(s)2}(t)] - \\
&\quad - \frac{a^2}{2b^2} n_s \frac{1}{C_s^2(t)(\omega_{(s)2}^2 - \omega_{(s)1}^2)\omega_{(s)2}} \left[ \omega_{(s)2}^2 \mathbf{H}_{re} \left( \frac{\Omega}{2} \right) + \omega_{(s)1}^2 \mathbf{H}_{im} \left( \frac{\Omega}{2} \right) \right] dt + \\
&\quad - \frac{c^2 m_s}{2b^2} \frac{1}{C_s^2(t)(\omega_{(s)2}^2 - \omega_{(s)1}^2)\omega_{(s)2}} \left[ \mathbf{H}_{re} \left( \frac{\Omega}{2} \right) + \mathbf{H}_{im} \left( \frac{\Omega}{2} \right) \right] dt \\
\dot{C}_s^3(t) &= - \frac{1}{4(\omega_{(s)4}^2 - \omega_{(s)3}^2)\omega_{(s)3}} \frac{n_s}{b^2} \hat{F}_{a1} C_s^3(t) \cos(\psi - 2\phi_{(s)3}(t)) - \\
&\quad - \frac{a^2}{2b^2} n_s \frac{1}{(\omega_{(s)4}^2 - \omega_{(s)3}^2)\omega_{(s)3}} \left[ \omega_{(s)3}^2 \mathbf{H}_{re} \left( \frac{\Omega}{2} \right) + \omega_{(s)4}^2 \mathbf{H}_{im} \left( \frac{\Omega}{2} \right) \right] - \\
&\quad - \frac{c^2 m_s}{2b^2} \frac{1}{(\omega_{(s)4}^2 - \omega_{(s)3}^2)\omega_{(s)3}} \left[ \mathbf{H}_{re} \left( \frac{\Omega}{2} \right) + \mathbf{H}_{im} \left( \frac{\Omega}{2} \right) \right] \\
\dot{\phi}_{(s)3}(t) &= \Delta_{(s)3} - \frac{1}{4(\omega_{(s)4}^2 - \omega_{(s)3}^2)\omega_{(s)3}} \frac{n_s}{b^2} \hat{F}_{a1} \sin[\psi - 2\phi_{(s)3}(t)] - \\
&\quad - \frac{a^2}{2b^2} n_s \frac{1}{C_s^3(t)(\omega_{(s)4}^2 - \omega_{(s)3}^2)\omega_{(s)3}} \left[ \omega_{(s)4}^2 \mathbf{H}_{re} \left( \frac{\Omega}{2} \right) + \omega_{(s)3}^2 \mathbf{H}_{im} \left( \frac{\Omega}{2} \right) \right] + \\
&\quad - \frac{c^2 m_s}{2b^2} \frac{1}{C_s^3(t)(\omega_{(s)4}^2 - \omega_{(s)3}^2)\omega_{(s)3}} \left[ \mathbf{H}_{re} \left( \frac{\Omega}{2} \right) + \mathbf{H}_{im} \left( \frac{\Omega}{2} \right) \right] \\
\dot{C}_s^4(t) &= - \frac{1}{4(\omega_{(s)4}^2 - \omega_{(s)3}^2)\omega_{(s)4}} \frac{n_s}{b^2} \hat{F}_{a1} C_s^4(t) \cos(\psi - 2\phi_{(s)4}(t)) - \\
&\quad - \frac{a^2}{2b^2} n_s \frac{1}{(\omega_{(s)4}^2 - \omega_{(s)3}^2)\omega_{(s)4}} \left[ \omega_{(s)4}^2 \mathbf{H}_{re} \left( \frac{\Omega}{2} \right) + \omega_{(s)3}^2 \mathbf{H}_{im} \left( \frac{\Omega}{2} \right) \right] - \\
&\quad - \frac{c^2 m_s}{2b^2} \frac{1}{(\omega_{(s)4}^2 - \omega_{(s)3}^2)\omega_{(s)4}} \left[ \mathbf{H}_{re} \left( \frac{\Omega}{2} \right) + \mathbf{H}_{im} \left( \frac{\Omega}{2} \right) \right] \\
\dot{\phi}_{(s)4}(t) &= \Delta_{(s)4} - \frac{1}{4(\omega_{(s)4}^2 - \omega_{(s)3}^2)\omega_{(s)4}} \frac{n_s}{b^2} \hat{F}_{a1} \sin[\psi - 2\phi_{(s)4}(t)] - \\
&\quad - \frac{a^2}{2b^2} n_s \frac{1}{C_s^4(t)(\omega_{(s)4}^2 - \omega_{(s)3}^2)\omega_{(s)4}} \left[ \omega_{(s)3}^2 \mathbf{H}_{re} \left( \frac{\Omega}{2} \right) + \omega_{(s)4}^2 \mathbf{H}_{im} \left( \frac{\Omega}{2} \right) \right] + \\
&\quad - \frac{c^2 m_s}{2b^2} \frac{1}{C_s^4(t)(\omega_{(s)4}^2 - \omega_{(s)3}^2)\omega_{(s)4}} \left[ \mathbf{H}_{re} \left( \frac{\Omega}{2} \right) + \mathbf{H}_{im} \left( \frac{\Omega}{2} \right) \right]
\end{aligned} \tag{23}$$

where corresponding members are obtained by following expression:

$$\int_0^{+\infty} \mathbf{R}(\tau) e^{i\omega\tau} d\tau = \mathbf{H}_c(\omega) + i \mathbf{H}_s(\omega), \quad i = \sqrt{-1} \tag{24}$$

The change of variables in the following ways and in the following forms:  $\rho_s^k(t) = \ln C_s^k$ ,  $\mathcal{G}_s^k(t) = \phi_s^k(t) - \frac{1}{2}\psi$ ,  $s = 1, 2, 3, 4, \dots$ ,  $k = 1, 2, 3, 4$  where  $\psi = \sigma B(t) + \gamma$  and transforming the averaged system of differential equations into the system of averaged stochastic differential equations

with respect to the unknown amplitudes  $C_s^1(t), C_s^2(t), C_s^3(t)$  and  $C_s^4(t)$ , and unknown phases  $\phi_{(s)1}(t), \phi_{(s)2}(t), \phi_{(s)3}(t)$  and  $\phi_{(s)4}(t)$ , results in the following forms:

$$d\rho_s^k(t) = \frac{1}{C_s^k} \dot{C}_s^k dt, \quad d\vartheta_s^k(t) = \dot{\phi}_s^k(t) dt - \frac{1}{2} d\psi, \quad k = 1, 2, 3, 4 \quad (25)$$

#### 4. LYAPUNOV EXPONENTS AND STOCHASTIC STABILITY OF THE TRANSVERSAL VIBRATIONS OF PARAMETRICALLY EXCITED DOUBLE HEREDITARY BEAM SYSTEM

Let us consider the following expressions [1]:

$$\ln \left\{ [T_s^k(t)]^2 + \frac{1}{\omega_{(s)k}^2} [\dot{T}_s^k(t)]^2 \right\} = \ln \left\{ [C_s^k(t)]^2 \right\} = 2 \ln [C_s^k(t)] = 2\rho_s^k(t), \quad (26)$$

$s = 1, 2, 3, 4, \dots, \quad k = 1, 2, 3, 4$

where

$$\mathbf{T}_s(t) = \sum_{k=1}^{k=4} C_s^k(t) \cos \Phi_{(s)k}(t) = \sum_{k=1}^{k=4} T_s^k(t) \quad (27)$$

with the first derivatives in the forms

$$\dot{\mathbf{T}}_s(t) = -\sum_{k=1}^{k=4} \omega_{(s)k} C_s^k(t) \sin \Phi_{(s)k}(t) = \sum_{k=1}^{k=4} \dot{T}_s^k(t) \quad (28)$$

where we introduce the time modes as „new time component coordinates“  $T_s^k(t)$ .

The Lyapunov exponents of the system mode processes  $\lambda_s^k, \quad s = 1, 2, 3, 4, \dots, \quad k = 1, 2, 3, 4$ , [1] may be introduced by using the time modes as „new time component coordinates“  $T_s^k(t)$  and which by making use of the averaged equations becomes:

$$\lambda_s^k = \lim_{t \rightarrow \infty} \frac{1}{2t} \ln \left\{ [T_s^k(t)]^2 + \frac{1}{\omega_{(s)k}^2} [\dot{T}_s^k(t)]^2 \right\} = \lim_{t \rightarrow \infty} \frac{1}{t} \rho_s^k(t), \quad k = 1, 2, 3, 4. \quad (29)$$

Now, each separate Lyapunov exponent is a measure of the average exponential growth of the amplitudes  $C_s^1(t), C_s^2(t), C_s^3(t)$  and  $C_s^4(t)$  component processes of the corresponding „new time component coordinates“  $T_s^k(t)$  of beam transversal vibrations in the  $s$ -th form of the perturbed parametric resonance process. The Lyapunov exponents  $\lambda_s^k, \quad s = 1, 2, 3, 4, \dots, \quad k = 1, 2, 3, 4$  are the deterministic numbers with probability one (w.p.1) for the system given by averaged equations. Solutions of the averaged differential equations depend on initial values  $T_s^k(t_0)$  and  $\dot{T}_s^k(t_0)$ , and in general will be four values of the Lyapunov exponent  $\lambda_s^k, \quad s = 1, 2, 3, 4, \dots, \quad k = 1, 2, 3, 4$  in the corresponding  $s$ -th form of perturbed parametric resonance process. If both Lyapunov exponents are negative, the trivial solution in the corresponding  $s$ -th form of perturbed parametric resonance of a two-frequency process is a stable process with probability 1.

In order to calculate the expression and values for both Lyapunov exponents  $\lambda_s^k, \quad k = 1, 2, \quad s = 1, 2, 3, 4, \dots$ , we integrate both sides of two stochastic differential equations of the system (25) and we obtain the following system:

$$\begin{aligned} \rho_s^1(t) - \rho_s^1(0) &= -\frac{1}{4(\omega_{(s)2}^2 - \omega_{(s)1}^2)\omega_{(s)1}} \frac{n_s}{b^2} \hat{F}_{a1} \int_0^t \cos 2\vartheta_s^1 dt - \\ &\quad - \frac{a^2}{2b^2} n_s \frac{t}{(\omega_{(s)2}^2 - \omega_{(s)1}^2)\omega_{(s)1}} \left[ \omega_{(s)1}^2 \mathbf{H}_{re} \left( \frac{\Omega}{2} \right) + \omega_{(s)2}^2 \mathbf{H}_{im} \left( \frac{\Omega}{2} \right) \right] + \\ &\quad - \frac{c^2 m_s}{2b^2} \frac{t}{(\omega_{(s)2}^2 - \omega_{(s)1}^2)\omega_{(s)1}} \left[ \mathbf{H}_{re} \left( \frac{\Omega}{2} \right) + \mathbf{H}_{im} \left( \frac{\Omega}{2} \right) \right] \\ \rho_s^2(t) - \rho_s^2(0) &= -\frac{1}{4(\omega_{(s)2}^2 - \omega_{(s)1}^2)\omega_{(s)2}} \frac{n_s}{b^2} \hat{F}_{a1} \int_0^t \cos 2\vartheta_s^2 dt - \\ &\quad - \frac{a^2}{2b^2} n_s \frac{t}{(\omega_{(s)2}^2 - \omega_{(s)1}^2)\omega_{(s)2}} \left[ \omega_{(s)1}^2 \mathbf{H}_{re} \left( \frac{\Omega}{2} \right) + \omega_{(s)2}^2 \mathbf{H}_{im} \left( \frac{\Omega}{2} \right) \right] - \\ &\quad - \frac{c^2 m_s}{2b^2} \frac{t}{(\omega_{(s)2}^2 - \omega_{(s)1}^2)\omega_{(s)2}} \left[ \mathbf{H}_{re} \left( \frac{\Omega}{2} \right) + \mathbf{H}_{im} \left( \frac{\Omega}{2} \right) \right] \end{aligned} \quad (30)$$

$$\begin{aligned}
\rho_s^3(t) - \rho_s^3(0) &= -\frac{1}{4(\omega_{(s)4}^2 - \omega_{(s)3}^2)\omega_{(s)3}} \frac{n_s}{b^2} \hat{\mathbf{F}}_{a1} \int_0^t \cos 2\mathcal{G}_s^3 dt - \\
&\quad - \frac{a^2}{2b^2} n_s \frac{t}{(\omega_{(s)4}^2 - \omega_{(s)3}^2)\omega_{(s)3}} \left[ \omega_{(s)3}^2 \mathbf{H}_{re} \left( \frac{\Omega}{2} \right) + \omega_{(s)4}^2 \mathbf{H}_{im} \left( \frac{\Omega}{2} \right) \right] + \\
&\quad - \frac{c^2 m_s}{2b^2} \frac{t}{(\omega_{(s)4}^2 - \omega_{(s)3}^2)\omega_{(s)3}} \left[ \mathbf{H}_{re} \left( \frac{\Omega}{2} \right) + \mathbf{H}_{im} \left( \frac{\Omega}{2} \right) \right] \\
\rho_s^4(t) - \rho_s^4(0) &= -\frac{1}{4(\omega_{(s)4}^2 - \omega_{(s)3}^2)\omega_{(s)4}} \frac{n_s}{b^2} \hat{\mathbf{F}}_{a1} \int_0^t \cos 2\mathcal{G}_s^4 dt - \\
&\quad - \frac{a^2}{2b^2} n_s \frac{t}{(\omega_{(s)4}^2 - \omega_{(s)3}^2)\omega_{(s)4}} \left[ \omega_{(s)4}^2 \mathbf{H}_{re} \left( \frac{\Omega}{2} \right) + \omega_{(s)3}^2 \mathbf{H}_{im} \left( \frac{\Omega}{2} \right) \right] + \\
&\quad - \frac{c^2 m_s}{2b^2} \frac{t}{(\omega_{(s)4}^2 - \omega_{(s)3}^2)\omega_{(s)4}} \left[ \mathbf{H}_{re} \left( \frac{\Omega}{2} \right) + \mathbf{H}_{im} \left( \frac{\Omega}{2} \right) \right]
\end{aligned}$$

so that, from expressions for Lyapunov exponents  $\lambda_s^k$ ,  $s=1,2,3,4, \dots$ ,  $k=1,2,3,4$ , with previous obtained system (30), we can write the following series of the Lyapunov exponent expressions:

$$\begin{aligned}
\lambda_s^1 &= -\frac{1}{4} \mathbf{L}_s^1 \hat{\mathbf{F}}_{a1} \mathbf{F} \left( \frac{L_s^1}{\sigma^2}, \frac{4\Delta_{(s)1}}{\sigma^2} \right) - & \lambda_s^2 &= -\frac{1}{4} \mathbf{L}_s^2 \hat{\mathbf{F}}_{a1} \mathbf{F} \left( \frac{L_s^2}{\sigma^2}, \frac{4\Delta_{(s)2}}{\sigma^2} \right) - \\
&\quad - \frac{a^2}{2} \mathbf{L}_s^1 \left[ \omega_{(s)1}^2 \mathbf{H}_{re} \left( \frac{\Omega}{2} \right) + \omega_{(s)2}^2 \mathbf{H}_{im} \left( \frac{\Omega}{2} \right) \right] + & &\quad - \frac{a^2}{2} \mathbf{L}_s^2 \left[ \omega_{(s)1}^2 \mathbf{H}_{re} \left( \frac{\Omega}{2} \right) + \omega_{(s)2}^2 \mathbf{H}_{im} \left( \frac{\Omega}{2} \right) \right] - \\
&\quad - \frac{c^2 m_s}{2n_s} \mathbf{L}_s^1 \left[ \mathbf{H}_{re} \left( \frac{\Omega}{2} \right) + \mathbf{H}_{im} \left( \frac{\Omega}{2} \right) \right] & &\quad - \frac{c^2 m_s}{2n_s} \mathbf{L}_s^2 \left[ \mathbf{H}_{re} \left( \frac{\Omega}{2} \right) + \mathbf{H}_{im} \left( \frac{\Omega}{2} \right) \right]
\end{aligned}$$

with probability 1. . (37)

$$\begin{aligned}
\lambda_s^3 &= -\frac{1}{4} \mathbf{L}_s^3 \hat{\mathbf{F}}_{a1} \mathbf{F} \left( \frac{L_s^3}{\sigma^2}, \frac{4\Delta_{(s)3}}{\sigma^2} \right) - & \lambda_s^4 &= -\frac{1}{4} \mathbf{L}_s^4 \hat{\mathbf{F}}_{a1} \mathbf{F} \left( \frac{L_s^4}{\sigma^2}, \frac{4\Delta_{(s)4}}{\sigma^2} \right) - \\
&\quad - \frac{a^2}{2b^2} n_s \mathbf{L}_s^3 \left[ \omega_{(s)3}^2 \mathbf{H}_{re} \left( \frac{\Omega}{2} \right) + \omega_{(s)4}^2 \mathbf{H}_{im} \left( \frac{\Omega}{2} \right) \right] + & &\quad - \frac{a^2}{2b^2} n_s \mathbf{L}_s^4 \left[ \omega_{(s)4}^2 \mathbf{H}_{re} \left( \frac{\Omega}{2} \right) + \omega_{(s)3}^2 \mathbf{H}_{im} \left( \frac{\Omega}{2} \right) \right] + \\
&\quad - \frac{c^2 m_s}{2b^2} \mathbf{L}_s^3 \left[ \mathbf{H}_{re} \left( \frac{\Omega}{2} \right) + \mathbf{H}_{im} \left( \frac{\Omega}{2} \right) \right] & &\quad - \frac{c^2 m_s}{2b^2} \mathbf{L}_s^4 \left[ \mathbf{H}_{re} \left( \frac{\Omega}{2} \right) + \mathbf{H}_{im} \left( \frac{\Omega}{2} \right) \right]
\end{aligned}$$

with probability 1, where

$$\begin{aligned}
L_s^1(t) &= \frac{1}{(\omega_{(s)2}^2 - \omega_{(s)1}^2)\omega_{(s)1}} \frac{n_s}{b^2}, & L_s^2 &= \frac{1}{(\omega_{(s)2}^2 - \omega_{(s)1}^2)\omega_{(s)2}} \frac{n_s}{b^2} \\
L_s^3(t) &= \frac{1}{(\omega_{(s)4}^2 - \omega_{(s)3}^2)\omega_{(s)3}} \frac{n_s}{b^2}, & L_s^4 &= \frac{1}{(\omega_{(s)4}^2 - \omega_{(s)3}^2)\omega_{(s)4}} \frac{n_s}{b^2} \\
\Delta_{(s)k} &= \omega_{(s)k} - \frac{\Omega}{2} \quad s=1,2,3,4, \dots, \quad k=1,2,3,4: & & (31)
\end{aligned}$$

$$\omega_{(s)1,2}^2 = \frac{1}{2b^2} [1 - a^2 n_s] \mp \sqrt{\frac{1}{4b^4} [1 - a^2 n_s]^2 - \frac{1}{b^2} (c^2 m_s + n_s \hat{\mathbf{F}}_{ca0} + \hat{c})}$$

where the random processes  $\mathcal{G}_s^k(t)$ ,  $k=1,2,3,4$  given by previous system of the stochastic differential equations (25) can be shown to be ergodic, in which case, we can write:

$$\lim_{t \rightarrow \infty} \frac{1}{t} \int_0^t \cos 2\mathcal{G}_s^k dt = \mathbf{E}[\cos 2\mathcal{G}_s^k], \quad k=1,2,3,4, \quad \text{with probability 1.}$$

where  $\mathbf{E}[\cdot]$  denotes the expectation operator.

To this end, we set up the Fokker-Planck equation governing the invariant (or stationary) probability density functions  $p_s^k = p(\mathcal{G}_s^k)$ ,  $k=1,2,3,4$  of the processes (see [1], [25] and [26])

$\mathcal{G}_s^k(t) = \phi_s^k(t) - \psi/2$ ,  $k=1,2,3,4$  defined by the second and fourth equations from system (25) of the stochastic differential equations Itô-type:

$$\sigma^2 \frac{d^2 p(\mathcal{G}_s^k)}{d(\mathcal{G}_s^k)^2} - \frac{d}{d\mathcal{G}_s^k} \left\{ [4\Delta_{(s)k} - L_s^k \sin 2\mathcal{G}_s^k] p(\mathcal{G}_s^k) \right\} = 0, \quad k = 1, 2, 3, 4 \quad (32)$$

The solutions of the previous series of equations satisfying the periodicity conditions in the form  $p_s^k = p(\mathcal{G}_s^k) = p(\mathcal{G}_s^k + 2\pi)$ , was obtained by Stratonoviich (1967) [24]:

$$p(\mathcal{G}_s^k) = \frac{1}{C_s^k} \exp\left[ (8\Delta_{(s)k} \mathcal{G}_s^k + L_s^k \cos 2\mathcal{G}_s^k) / \sigma^2 \right] \cdot \int_{\theta_s^k}^{\pi + \theta_s^k} \exp\left[ (8\Delta_{(s)k} \tau + L_s^k \cos 2\tau) / \sigma^2 \right] d\tau, \quad (33)$$

$k = 1, 2, 3, 4$ , where normalizing constants are:

$$C_s^k = 2\pi^2 \exp\left( -\pi \frac{4\Delta_{(s)k}}{\sigma^2} \right) \left| \mathbf{I}_{iq} \left( \frac{L_s^k}{\sigma^2} \right) \right|^2, \quad k = 1, 2, 3, 4 \quad (34)$$

where  $\left| \mathbf{I}_{iq} \left( \frac{L_s^k}{\sigma^2} \right) \right|$  is the Bessel function of the imaginary argument and imaginary order and  $q = 4 \frac{\Delta_{(s)k}}{\sigma^2}$ ,  $k = 1, 2, 3, 4$ .

Using equations and results by Ariaratnam [1] and previous stochastic differential equations, the values of the mathematical expectation  $E[\cos 2\mathcal{G}_s^k]$ , for the processes  $\mathcal{G}_s^k(t) = \phi_s^k(t) - \frac{1}{2}\psi$ ,  $s = 1, 2, 3, 4, \dots$ ,  $k = 1, 2, 3, 4$  and  $\psi = \sigma B(t) + \gamma$  are found to be in the form of expressions:

$$E[\cos 2\mathcal{G}_s^k] = \mathbf{F} \left( \frac{L_s^k}{\sigma^2}, \frac{4\Delta_{(s)k}}{\sigma^2} \right), \quad k = 1, 2, 3, 4 \quad (35)$$

where

$$\mathbf{F}(z, q) = \frac{1}{2} \left[ \frac{\mathbf{I}_{1+iq}(z)}{\mathbf{I}_{iq}(z)} + \frac{\mathbf{I}_{1-iq}(z)}{\mathbf{I}_{-iq}(z)} \right] \quad (36)$$

## CONCLUSIONS

Hence, by using previous expressions for the infinite sets of the Lyapunov exponents  $\lambda_s^k$ ,  $s = 1, 2, 3, 4, \dots$ ,  $k = 1, 2, 3, 4$ , in the forms of expressions (37) with probability 1 for evaluation of the stability or instability, we must find the Lyapunov exponent with maximal values between Lyapunov exponents from defined sets, and determine kinetic parameters of the hereditary beam vibration such that this Lyapunov exponents are with negative values. This is not simple, because we need investigation of the  $\max \lambda_s^k < 0$ ,  $s = 1, 2, 3, 4, \dots$ ,  $k = 1, 2, 3, 4$ . Also, we can consider the case when only one of the  $\Delta_{(s)k} = \omega_{(s)k} - \frac{\Omega}{2}$ ,  $s = 1, 2, 3, 4, \dots$ ,  $k = 1, 2, 3, 4$ : is equal to zero, and all other different from zero; this analysis needs a large discussion.

**Acknowledgment.** *Parts of this research were supported by the Ministry of Sciences and Environmental Protection of Republic of Serbia through Mathematical Institute SANU Belgrade Grant ON144002 and Faculty of Mechanical Engineering University of Nis.*

## REFERENCES

- [1] Ariaratnam S. T. Stochastic Stability of Viscoelastic Systems under bounded Noise Excitation *IUTAM Symp. on Advances in Nonlinear Stochastic Mechanics*, Kluwer Acad. Publ. Dordrecht, pp. 11-18, 1996.
- [2] Ariaratnam S. T. Stochastic stability of linear viscoelastic systems *Probabilistic Engineering Mechanics*, Vol. 8, Issues 3-4, pp. 153-155, 1993.
- [3] Ariaratnam S. T. and Xie W.C. Wave localization in randomly disordered nearly period long continuous beams *Journal of Sound and Vibration*, 181 (1), pp. 6-11, 1995.
- [4] Ariaratnam S. T. and Wei-Chau Xijz. Buckling Mode Localisation in Randomly Disordered Continuous Beams Using a Simplified Model *Chaos, Solitons and Fractals*, Vol. 7, No. 8, pp. 1127-1144. 1996.
- [5] Ariaratnam S. T. and Abdelrahman N.M. Stochastic stability of non-gyroscopic viscoelastic systems *Int. Journal of Solids and Structures*, 41, pp. 2685-2709, 2004.
- [6] Ariaratnam S. T. and Abdelrahman N.M. Stochastic stability of non-gyroscopic viscoelastic systems *Int. Journal of Solids and Structures*, 41, pp. 2685-2709, 2004.

- [7] Goroshko O.A., Hedrih (Stevanović) K. *Analytical Dynamics of Discrete Hereditary Systems*, University of Niš, 426 p., 2001 (in Serbian).
- [8] Hedrih (Stevanović), K., One-frequency Nonlinear Forced Vibrations of Uniform Beams, *Theoretical and Applied Mechanics*, No. 4, pp. 39-50, 1978.
- [9] Hedrih (Stevanović), K. Transversal Vibration Beam on the Elastic Foundation under the Action of the Multi-Frequencies Forces with Frequencies from First Frequency Resonant Range of the Beam, *Matematicheskaya fizika*, Kiev, Vol.13, pp. 161-181, 1973 (in Russian).
- [10] Hedrih (Stevanović), K. Two-Frequencies Forced Nonstationary Vibrations of the beam, *Matematicheskaya fizika*, Kiev, Vol. 12, pp. 127-140, 1972 (in Russian).
- [11] Hedrih (Stevanović) K. Two-Frequencies Regime of the Nonlinear Transversal Free Vibrations of the Beam, in: *Analiticheskie i kachestvenniye metodi v teorii differentsialnykh uravneniy*, Ed. Yu. A. Mitropolskiy, Institut Matematiki AN USSR, Kiev, 1972, pp. 233-246 (in Russian).
- [12] Hedrih (Stevanović) K. Transversal Creep Vibrations of a Beam with Fractional Derivative Constitutive Relation Order, *Proc. of Forth International Conference on Nonlinear Mechanics (ICNM-IV)*, Edited by Wei Zang Chien et al., August 14-17, 2002, Shanghai, P.R. China, pp. 584-595, 2002.
- [13] Hedrih (Stevanović), K., Transversal Vibrations of the Hereditary Beam - Second Part: Application of S.T. Ariaratnam's Idea for Stochastic Stability Investigation of the Beam Deformable Forms Parametrically and Random Excited, Original Scientific Paper, *Tehnika, Mašinstvo*, 49 (2), pp. M1-6M, 2000 (in Serbian).
- [14] Hedrih (Stevanović) K. Transversal Vibration of a Parametrically Excited Beam: Influence of Rotatory Inertia and Transverse Shear on Stochastic Stability of Deformable Forms and Processes, *Int. Journal of Nonlinear Sciences and Numerical Simulation*, 7(1), pp.117-124, 2006.
- [15] Hedrih (Stevanović) K. Stochastic Dynamics of Hybrid Systems with Thermorheological Hereditary Elements. In book: *Modeling, Simulation and Control of Nonlinear Engineering Dynamical Systems, State-of-the-Art, Perspectives and Application*, Publisher Springer Netherlands, pp. 289-299, 2009.
- [16] Hedrih (Stevanović) K. Transversal vibration of a parametrically excited hereditary beam: Influence of rotatory inertia and transverse shear on stochastic stability of deformable forms and processes, *International IFNA-ANS Journal "Problems of nonlinear analysis in engineering systems"*, V.14, No.2(30), pp. 115-140, 2008 (in English and in Russian).  
[http://www.kcn.ru/tat\\_en/science/ans/journals/ansj\\_cnt.html](http://www.kcn.ru/tat_en/science/ans/journals/ansj_cnt.html)  
[http://www.kcn.ru/tat\\_en/science/ans/journals/ansj.html](http://www.kcn.ru/tat_en/science/ans/journals/ansj.html)
- [17] Hedrih (Stevanović) K. Tensor stanja slušajnih vibracija, (Tensor of state of the random vibrations), *Zbornik Radova Mašinskog Fakulteta Povodom 35 Godine Mašinstva, Mašinski Fakultet*, Niš University, pp. 133-136, 1995.
- [18] Janković V. S., Potić V. P. and Hedrih (Stevanović) K. *Partial differential equations and integro-differential equations with examples in engineering*, University of Niš, 347 p., 1999 (in Serbian).
- [19] Nowatski W. *Dynamics of Structured*, Arcady, 1972 (in Polish).
- [20] Mitropolyskiy, Yu. A., *Nonlinear Mechanics – Asymptotic Methods*, Institut Matematiki NAN Ukraini, Kiev, pp. 397, 1995. (in Russian)
- [21] Mitropolskiy Yu.A. and Moseenkov B.I. *Asymptotic solutions of the Partial Differential Equations*, Kiev, 1976. (in Russian)
- [22] Rašković, D., *Theory of Oscillations*, Naučna knjiga, Beograd, 503 p., 1965 (in Serbian).
- [23] Rašković D. *Steinght of Materials*, Naučna knjiga, Beograd, 426 p., 1977. (in Serbian).
- [24] Stratonovich R. I. *Topics in the Theory of Random Noise*, Vol. II, Gordon and Breach, New York, pp. 294-302, 1967.
- [25] Gikhman I. I., Dorogovtzev A. Y. On Stability of Solutions of Stochastic Differential Equation, *Ukrainian Math. Journal*, 17, No. 6, pp.3-21, 1963.
- [26] Gikhman I. I., Skorokhod A. V., *Stochastic Differential Equations*, Ergebnisse der Mathematik 72, Springer Verlag, New York, 1972.

## RESONANT JUMPS IN MULTI-FREQUENCY REGIMES OF MYLTI-CIRCULAR PLATE SYSTEM NON-LINEAR DYNAMICS

**Katica R. (Stevanović)  
Hedrih<sup>1</sup>**

Mathematical Institute  
SANU  
Belgrade, Serbia,

**Julijana Simonović**  
University of Niš,  
Niš, Serbia

ABSTRACT

By use a double circular plate system dynamics, the multi-frequency analysis of forced non-linear dynamics is pointed out. Series of the amplitude-frequency and phase-frequency graphs as well as eigenforced time functions–frequency graphs are obtained for stationary resonant states and analyzed according present singularities and triggers of coupled singularities, as well as resonant jumps.

For analyze of stationary forced resonant regimes of forced non-linear oscillations for presented model, we use the graphical presentation of the numerical experiment results over the first asymptotic approximation of the two amplitudes and two phases of the two-frequency resonant stationary regimes.

For the system of two circular plates connected with non-linear viscoelastic layer with hard or soft non-linear properties on the basis of obtained numerical and graphical results, we can conclude that non-linearity in the interconnecting distributed layer introduce in the system non-linear part of the potential energy as a energy interactions between circular plates as subsystems (deformable bodies) coupled in the hybrid system with complex component eigen forced non-linear modes, as well as mutual influence and transfer energy through all the system components of the mods. Resonant jumps, as well as „resonant forced oscillatory jumps“, trigger of coupled singularities, as well as coupled triggers of coupled singularities are reason for appearance of new questions for reasearch this non-linear forced dynamics.

### INTRODUCTION

Composing the proper mathematical model of mechanical system presents one of the most important steps in the treatment of the system. On the other way said, mathematical modeling regard on the usage of mathematical language for presents the behavior of practical systems. It plays the role of better understanding of systems features. In the more realistic description of the systems non-linearity appears both as an object's natural characteristic and the non-linearity of the systems of differential equations describing the system dynamics, which is a consequence of the choice of the coordinates of the system's description. Since, the problem is to explore and in some way control non-linearity. Theory is useful for presenting the general conclusions to the simple models while the computers are useful for obtaining the special conclusions for more complicated system dynamics.

In this paper, we will present one mechanical system, a double circular plate system with non-linear interconnecting layer, and its mathematical non-linear descriptions then treat that non-linearity in a sense of making the qualitative analysis of the system behavior.

In many engineering systems with non-linearity, single as well multi- frequency excitations are the sources of multi frequency resonant regimes appearance high as well as low frequency modes. That is visible from many experimental research results and also theoretical results (see Refs. [16] and [17]). The interaction between amplitudes and phases of the different modes in the non-linear systems with many degrees of the freedom as in the deformable body with infinite numbers frequency vibration free and forced regimes is observed theoretically in the Refs. [20] and [22] by Stevanović

<sup>1</sup> Corresponding author. Email [khedrih@eunet.rs](mailto:khedrih@eunet.rs)

K. , (1972) and (1975) by use averaging asymptotic methods Krilov-Bogoliyubov-Mitropolyskiy (see Refs. [10-15] by Mitropolyskiy, Yu. A. (1955), (1965), (1995)). This knowledge has great practical importance. In the monograph [16] by Nayfeh (2004), a coherent and unified treatment of analytical, computational, and experimental methods and concepts of modal nonlinear interactions is presented.

By using averaging and asymptotic methods Krilov-Bogolyubov- Mitropolyskiy for obtaining system of ordinary differential equations of amplitudes and phases in first approximations and expressions for energy of the excited modes depending on amplitudes, phases and frequencies of different non-linear modes are obtained by Hedrih K. in [2, 3] and by Hedrih K. and Simonović J. in [8]. By means of these asymptotic approximations, the energy analysis of mode interaction in the multi frequency free and forced vibration regimes of non-linear elastic systems (beams, plates, and shells) excited by initial conditions for free oscillation regimes was made and a series of resonant jumps as well as energy transfer features for forced regimes were identified.

Recent technological innovations have caused a considerable interest in the study of component and hybrid dynamical processes of coupled rigid and deformable bodies (plates, beams and belts) (see Refs. [2-4] and [6-8]) denoted as hybrid systems, characterized by the interaction between sub-system dynamics, governed by coupled partial differential equations with boundary and initial conditions.

In this paper, we will try to present the more realistic model with non-linearity in the connected layer and to investigate the phenomenon of passing through resonant range and appearance of one or several resonant jumps in the amplitude–frequency and phase–frequency curves of different nonlinear modes. In system with non-linearity it is noticeable the energy transfer between coupled sub-systems. For detail see Refs. [5] and [8] which contain analysis of energy transfer in double plate system dynamics.

## 1. SOLUTION IN THE FIRST ASIMPTOTIC APROXIMATION OF PDEs FOR TRANSVERSAL VIBRATIONS OF A DOUBLE PLATES SYSTEM

If we present a physical model of a double plate system, shown in the Fig. 1.a, then it is clear that the mathematical model of such a system may be expressed by the system of two coupled partial differential equations (1) [3,4] and [6,7,8] which are formulated in terms of two unknowns: the transversal displacement  $w_i(r, \varphi, t)$ ,  $i=1,2$  in direction of the axis  $z$ , of the upper plate middle surface and of the lower plate middle surface. We present the interconnecting layer as a model of one standard light visco-elastic element [1] with started spring's length  $l_0$  and nonlinearity in the elastic part of the layer as shown in Figure 1b.

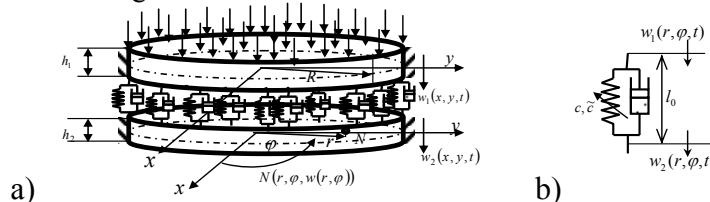


Fig. 1. a) A visco-elastically connected double circular plate system; b) model discrete element of visco-elastic non-linear interconnected layer.

The system of partial differential equations (1) is derived using Principle of dynamic equilibrium in the following forms:

$$\frac{\partial^2 w_i(r, \varphi, t)}{\partial t^2} + c_{(i)}^4 \Delta \Delta w_i(r, \varphi, t) - 2\delta_{(i)} \left[ \frac{\partial w_{i+1}(r, \varphi, t)}{\partial t} - \frac{\partial w_i(r, \varphi, t)}{\partial t} \right] - a_{(i)}^2 [w_{i+1}(r, \varphi, t) - w_i(r, \varphi, t)] = \pm \varepsilon \beta_{(i)} [w_{i+1}(r, \varphi, t) - w_i(r, \varphi, t)]^3 + \tilde{q}_{(i)}(r, \varphi, t) \quad \text{for } i=1,2 \quad (1)$$

where are :  $D_i = \frac{E h_i^3}{12(1-\nu_i^2)}$ ,  $\varepsilon \beta_{(i)} = \frac{\beta}{\rho_i h_i}$ ,  $a_{(i)}^2 = \frac{c}{\rho_i h_i}$ ,  $c_{(i)}^4 = \frac{D_i}{\rho_i h_i}$ ,  $2\delta_i = \frac{b}{\rho_i h_i}$  and the sign  $\pm$  on the right hand side

corresponds to the feathure of soft (sign +) or hard (sign -) properties of the elastic layer. We suppose that the functions of external excitation at  $nm$ -mode of oscillations are the two-frequency process in the form:  $\tilde{q}_{(i)nm}(t) = h_{01nm} \cos[\Omega_{1nm} t + \phi_{1nm}] + h_{02nm} \cos[\Omega_{2nm} t + \phi_{2nm}]$ ,  $m, n = 1, 2, \dots, \infty$ . The solution for system (1) with the visco-linear-elastic connection is taken in the form of the eigen amplitude functions  $W_{(i)nm}(r, \varphi)$ ,  $n, m = 1, 2, 3, 4, \dots, \infty$ , satisfying the same boundary conditions, expansion with time coefficients in the form of unknown time functions  $T_{(i)nm}(t)$ , that describing their time evolution (see Refs. [4] and [7]):

$$w_i(r, \varphi, t) = W_{(i)nm}(r, \varphi) T_{(i)nm}(t) = W_{(i)nm}(r, \varphi) \left[ K_{inn}^{(1)} e^{-\delta_{inn} t} R_{1nm}(t) \cos \Phi_{1nm}(t) + K_{inn}^{(2)} e^{-\delta_{inn} t} R_{2nm}(t) \cos \Phi_{2nm}(t) \right] \quad (2)$$

where are:  $K_{nm}^{(i)}$  cofactors of determinant corresponding to basic homegenous coupled system [7],  $-\hat{\delta}_{nm}$  real parts of the corresponding pair of the roots of the characteristic equation [4], and amplitudes  $R_{nm}(t)$  and phases  $\phi_{nm}(t) = \Omega_{nm}t + \phi_{nm}(t)$  unknown time functions which, we are going to obtain using the Krilov-Bogolyubov-Mitropolyskiy asymptotic method (see Refs. [10-15]). It is taken into account that defined task satisfy all necessary conditions for applying asymptotic method Krilov-Bogolyubov-Mitropolyskiy concerning small parameter and that external excitation frequencies  $\Omega_{1nm} \approx \hat{p}_{1nm}$  and  $\Omega_{2nm} \approx \hat{p}_{2nm}$  are in the resonant range intervals of the corresponding eigen frequencies of unperturbed linear system. By applying the asymptotic method, we obtain the system of the first order differential equations according unknown amplitude and phases in the first asymptotic approximation [8] as follow:

$$\begin{aligned} \dot{a}_{1nm}(t) &= -\frac{(\delta_{(1)}K_{22nm}^{(2)} + \delta_{(2)}K_{21nm}^{(2)})[K_{22nm}^{(1)} - K_{21nm}^{(1)}]}{(K_{22nm}^{(2)}K_{21nm}^{(1)} - K_{21nm}^{(2)}K_{22nm}^{(1)})}a_{1nm}(t) + \frac{K_{22nm}^{(2)}h_{01nm}}{(\Omega_{1nm} + \hat{p}_{1nm})(K_{22nm}^{(2)}K_{21nm}^{(1)} - K_{21nm}^{(2)}K_{22nm}^{(1)})} \cos \phi_{1nm} \\ \dot{\phi}_{1nm}(t) &= (\hat{p}_{1nm} - \Omega_{1nm}) - \\ &\mp \frac{\varkappa(W_{nm})\varepsilon(\beta_{(1)}K_{22}^{(2)} + \beta_{(2)}K_{21}^{(2)})}{(K_{22}^{(2)}K_{21}^{(1)} - K_{21}^{(2)}K_{22}^{(1)})} \left[ (\Omega_{1nm} + \hat{p}_{1nm}) \left[ (K_{22nm}^{(1)} - K_{21nm}^{(1)})^3 \frac{3}{8} a_{1nm}^2(t) + \frac{1}{2} (K_{22nm}^{(1)} - K_{21nm}^{(1)})(K_{22nm}^{(2)} - K_{21nm}^{(2)})^2 a_{2nm}^2(t) \right] - \right. \\ &\left. - \frac{K_{22}^{(2)}h_{01nm}}{(\Omega_{1nm} + \hat{p}_{1nm})(K_{22nm}^{(2)}K_{21nm}^{(1)} - K_{21nm}^{(2)}K_{22nm}^{(1)})} a_{1nm}(t) \right] \sin \phi_{1nm} \end{aligned} \quad (3)$$

$$\begin{aligned} \dot{a}_{2nm}(t) &= -\frac{(\delta_{(1)}K_{22nm}^{(1)} + \delta_{(2)}K_{21nm}^{(1)})[K_{22nm}^{(2)} - K_{21nm}^{(2)}]}{(K_{22nm}^{(1)}K_{21nm}^{(2)} - K_{21nm}^{(1)}K_{22nm}^{(2)})}a_{2nm}(t) + \frac{K_{22nm}^{(1)}h_{02nm}}{(\Omega_{2nm} + \hat{p}_{2nm})(K_{22nm}^{(1)}K_{21nm}^{(2)} - K_{21nm}^{(1)}K_{22nm}^{(2)})} \cos \phi_{2nm} \\ \dot{\phi}_{2nm}(t) &= (\hat{p}_{2nm} - \Omega_{2nm}) - \\ &\mp \frac{\varkappa(W_{nm})\varepsilon(\beta_{(1)}K_{22nm}^{(1)} + \beta_{(2)}K_{21nm}^{(1)})}{(\Omega_{2nm} + \hat{p}_{2nm})(K_{22nm}^{(1)}K_{21nm}^{(2)} - K_{21nm}^{(1)}K_{22nm}^{(2)})} \cdot \left[ \frac{1}{2} (K_{22nm}^{(1)} - K_{21nm}^{(1)})^2 (K_{22nm}^{(2)} - K_{21nm}^{(2)}) a_{1nm}^2(t) + (K_{22nm}^{(2)} - K_{21nm}^{(2)})^3 \frac{3}{8} a_{2nm}^2(t) \right] - \\ &\left. - \frac{K_{22nm}^{(1)}h_{02nm}}{(\Omega_{2nm} + \hat{p}_{2nm})(K_{22nm}^{(1)}K_{21nm}^{(2)} - K_{21nm}^{(1)}K_{22nm}^{(2)})} a_{2nm}(t) \right] \sin \phi_{2nm} \end{aligned} \quad (4)$$

where are:  $a_{nm}(t) = R_{nm}(t)e^{-\hat{\delta}_{nm}t}$ ,  $m, n = 1, 2, \dots, \infty$ . and  $\varkappa(W_{nm}) = \frac{\int_0^{2\pi} \int_0^{2\pi} W_{(1)nm}^4(r, \varphi) r dr d\varphi}{\int_0^{2\pi} \int_0^{2\pi} W_{(1)nm}^2(r, \varphi) r dr d\varphi}$  is coefficient of nonlinearity

influence of elastic layer. We observed the case when external distributed two-frequencies force acts at upper surfaces of upper plate with frequencies near eigen circular frequencies of coupled plate systems  $\Omega_{nm} \approx \hat{p}_{nm}$ ,  $i = 1, 2$ ,  $m, n = 1, 2, \dots, \infty$ . In this case the lower plate is free of load. This means that, we were observed the passing thought main resonant states by discrete values of the forced frequencies. Using the first asymptotic approximation of the amplitudes and phases of multi frequency particular solutions of the non-linear system dynamics (3)-(4), a numerical experiment over the non-linear modes in stationary regimes of non-linear system forced dynamics is realized.

For analyses of the stationary regime of oscillations, we equal the right hand sides of differential equations (3)-(4) for amplitudes  $R_{nm}(t)$  and difference of phases  $\phi_{nm}(t)$  with null. Eliminating the phases  $\phi_{1nm}$  and  $\phi_{2nm}$ , we obtained system of two algebraic equations by unknown amplitudes  $a_{1nm}$  and  $a_{2nm}$ , also with elimination of amplitudes  $a_{1nm}$  and  $a_{2nm}$ , we obtained the forms for phases  $\phi_{1nm}$  and  $\phi_{2nm}$  in the case of two-frequencies forced oscillations in stationary regime of one  $nm$  mode of double plate system oscillations. Solving that two systems by numerical *Newton-Kantorovic's method in computer program Mathematica*, we obtained stationary amplitudes and phases curves of two-frequencies regime of one eigen  $nm$ -shape amplitude mode oscillations in double plate system coupling with visco-elastic non-linear layer depending on frequencies of external excitation force. If we fixed the value of on external excitation frequency of two possible, we obtained amplitude-frequency curves as well as phase-frequency curves of stationary states of vibration regime in the following forms:

1\* for second external excitation frequency with constant discrete value ( $\Omega_{2nm} = const$ ) corresponding amplitude-frequency and phase-frequency curves:

$$a_{1nm} = f_1(\Omega_{1nm}), a_{2nm} = f_2(\Omega_{1nm}), \phi_{1nm} = f_3(\Omega_{1nm}) \text{ and } \phi_{2nm} = f_4(\Omega_{1nm}) \text{ and} \quad (5)$$

2\* for first external excitation frequency with constant discrete value  $\Omega_{1nm} = const$  corresponding amplitude-frequency and phase-frequency curves:

$$a_{1nm} = f_5(\Omega_{2nm}), a_{2nm} = f_6(\Omega_{2nm}), \phi_{1nm} = f_7(\Omega_{2nm}) \text{ and } \phi_{2nm} = f_8(\Omega_{2nm}). \quad (6)$$

In this extend abstract, we will present some of the amplitde-frequencies and phase-frequencies curves of stationary kinetic state in continuously exchange of fixed discrete values of one external excitation frequencies and in that sense regard system in stationary regime, and some characteristic diagrams of that amplitde-frequency and phase-frequency curves are presented on the following Figs. 2 and 3.

Let us to make a quantitative analyses of passing through discrete stationary states along resonant frequency intervals and apperance of new non-stable branches on amplitude (phase)-frequencies curves like as changes on that characteristics for the frequencies of external force in the range of eigen frequencies of coupling in one  $nm$ -eigen amplitude mode of corresponding linearized system oscillations. We take into account that system for the case when the plates are with the same boundary and material characteristics and when the upper plates has the height twice then the lower one,  $h_2 = h_1/2$ , and obtained the eigen frequencies of visco-elastic linear coupling with values:  $\hat{p}_{111} = 135.55(s^{-1})$  and  $\hat{p}_{112} = 301.14(s^{-1})$ .

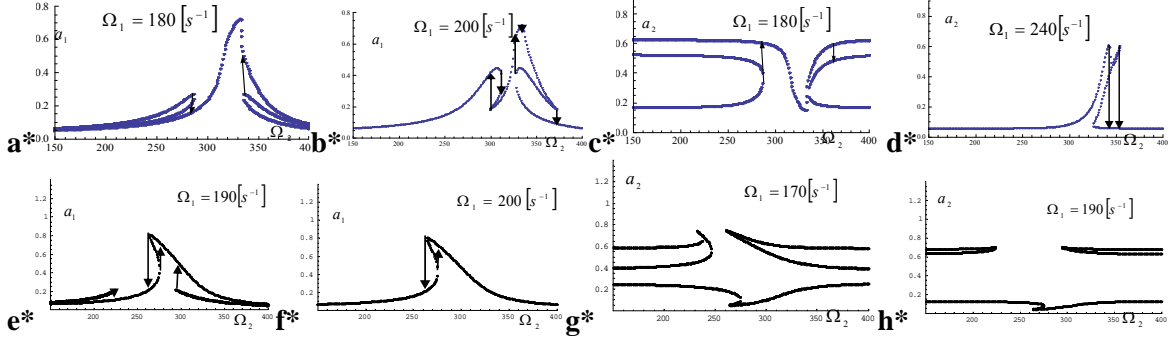


**Fig. 2.** Amplitude-frequency characteristic curves for the amplitudes of the first  $a_{1nm} = f_5(\Omega_{2nm})$  and second  $a_{2nm} = f_6(\Omega_{2nm})$  time harmonics for hard (a\*, b\*, c\*, d\*) and for soft (e\*, f\*, g\*, h\*) characteristics of interconnected layer and for the different value of excited frequency  $\Omega_{2nm}$  for discrete value of excited frequency  $\Omega_{1nm} = const$  with noted corresponding one or more resonant jumps. Arrows means directions of the resonant jumps.

The amplitude-frequency responses for two frequency like stationary vibration regimes, contain amplitudes  $a_1$  and  $a_2$  presented in Fig. 2. These shown diagrams exhibit a hardening, Figs. 2a\*, b\*, c\* and d\*, and softening, Figs. 2e\*, f\*, g\* and h\*, characteristic as a non-linear interactions between time non-linear modes of the two-frequency external excitation in the resonant interval of two external excitation frequencies close to the eigen linearized system frequencies. This is a property of hard and soft non-linearity of a visco-non-linear elastic layer and corresponding non-linear characteristic is in accordance with governing system of partial differential equations (1) for the case of the lower sign for hard non-linear characteristic, and of the upper sign for soft non-linear characteristics. That shapes are results of the modes interaction and of the particular discrete values choice of the external excitation frequencies  $\Omega_{1nm}$  used in the resonant frequency intervals belonging to corresponding eigen frequencies  $\hat{p}_{1nm}$  of the corresponding  $nm$ -th eigen amplitude shape mode of plate linear system taken in the simulations.

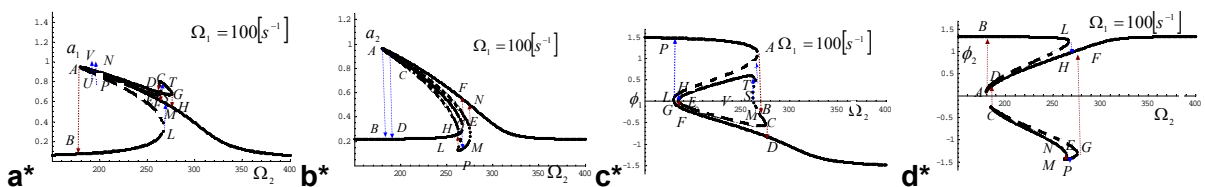


**Fig. 3.** Characteristic resonant jumps on the amplitude-frequency (a\*, b\*) curves  $a_{1nm} = f_5(\Omega_{2nm})$  and  $a_{2nm} = f_6(\Omega_{2nm})$ , and phase-frequency (c\*, d\*) curves  $\phi_{1nm} = f_7(\Omega_{2nm})$  and  $\phi_{2nm} = f_8(\Omega_{2nm})$  as a characteristic cases of the large resonant interactions between external two frequency excitation and non-linear properties of the double plate system dynamics when both frequencyes  $\Omega_{1nm}$  and  $\Omega_{2nm}$  take values from the resonant frequency intervals and casses for the apperance of the large interaction of the coupled stationary resonance regime.

Characteristic for both series of the amplitude-frequency curves for two frequency like non-linear stationary vibration regimes is that more then one pair of the resonant jumps appear, together

with more than one instability branch in the corresponding amplitude-frequency and phase-frequency curves. It is visible that in the listed Figs 3 a\*,b\*,c\* and d\*. In the listed figures branch presented in dot line correspond to unstable stationary vibration regimes.

## 2. THE TIME HARMONICS SHAPES AND THEIR MUTAL INFLUENCE

If we presents the time functions at  $nm$ -mode of oscillations of the plate systems in form of sum of two harmonics:

$$T_{(i)nm}(t) = \sum_{j=1}^2 T_{(i)nm_j}(t) = \sum_{j=1}^2 K_{inm}^{(j)} a_{jnm}(t) \cos \Phi_{jnm}(t) \quad , \quad i=1,2 \quad (7)$$

where, we use the change of amplitudes and phases by (3)-(4), and since, we have the numerical results, we are in position to present the shape of harmonics depending of frequencies of external excitations. For the chosen parameters of the system that two harmonics in the 11-mode of oscillations has the following form:

$$T_{111_1}(\Omega_1, \Omega_2) = 5.906 \cdot a_1(\Omega_1, \Omega_2) \cos[\Omega_{2(1)} \cdot t + \phi_1(\Omega_1, \Omega_2)] \quad (8a)$$

$$T_{111_2}(\Omega_1, \Omega_2) = 3.32 \cdot a_2(\Omega_1, \Omega_2) \cos[\Omega_{2(1)} \cdot t + \phi_2(\Omega_1, \Omega_2)] \quad (8b)$$

where  $\Omega_{2(1)}$  means that, we use the discrete values of the  $\Omega_2 = const$  or of the  $\Omega_1 = const$  of the external frequencies, and  $a_i(\Omega_1, \Omega_2)$  or  $\phi_i(\Omega_1, \Omega_2)$  means that, we use amplitude or phase stationary response  $a_i(\Omega_1, \Omega_2 = const)$  and  $\phi_i(\Omega_1, \Omega_2 = const)$  in one case and  $a_i(\Omega_1 = const, \Omega_2)$  and  $\phi_i(\Omega_1 = const, \Omega_2)$  in the other case.

In regard that, we considered the stationary regimes of vibrations in  $nm$ -mode of oscillations we have to use the particular moment in time so we use that the  $t = 1[s^{-1}]$ . In the Figs. 4 and 5 we present the shapes of the some time harmonics like as the shape of the time function in the 11-mod of oscillation of the plate system.

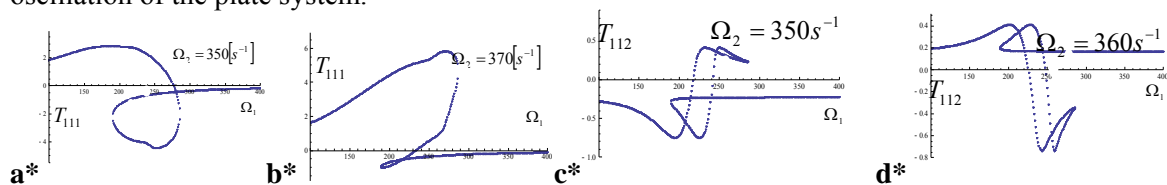


**Fig. 4.** The shapes of the first (a\*, b\*) and second (c\*, d\*) eigen forced time non-linear harmonic  $T_{111_1}(\Omega_1, \Omega_2) = 5.906 \cdot a_1(\Omega_1, \Omega_2 = const) \cos[\Omega_1 \cdot t + \phi_1(\Omega_1, \Omega_2 = const)]$  (a\*, b\*) and  $T_{111_2}(\Omega_1, \Omega_2) = 3.32 \cdot a_2(\Omega_1, \Omega_2 = const) \cos[\Omega_2 \cdot t + \phi_2(\Omega_1, \Omega_2 = const)]$  (c\*, d\*), for the different value of excited frequency  $\Omega_{1nm}$  and for discrete value of excited frequency  $\Omega_{2nm} = const$ .

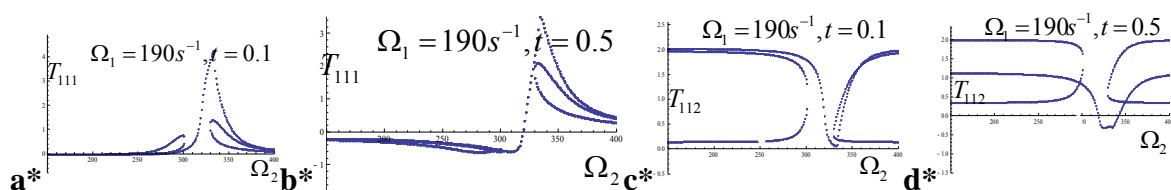


**Fig. 5.** The evolution of the shape of the first (a\*, b\*) and second (c\*, d\*) eigen forced time non-linear harmonic  $T_{111_1}(\Omega_1, \Omega_2) = 5.906 \cdot a_1(\Omega_1 = 190, \Omega_2) \cos[190 \cdot t + \phi_1(\Omega_1 = 190, \Omega_2)]$  and  $T_{111_2}(\Omega_1, \Omega_2) = 3.32 \cdot a_2(\Omega_1 = 190, \Omega_2) \cos[190 \cdot t + \phi_2(\Omega_1 = 190, \Omega_2)]$  for the different value of excited frequency  $\Omega_{2nm}$  and for discrete value of excited frequency  $\Omega_{1nm} = 190 s^{-1}$ , with  $t = 0.1[s^{-1}]$  and  $t = 0.5[s^{-1}]$

## CONCLUSIONS

For analyze of stationary regimes of non-linear oscillations for presented model, we solved system of PDE's (1) semi analytically in asymptotic first approximation. One part of solutions, were obtained numerically and presents amplitudes-frequencies and phase-frequency characteristics with identification, in the first asymptotic approximations, interaction of the non-linear component mods and non-linear resonant interactions, in the displacement of the plate middle surface points. For the case of the external excitation by two frequency force and resonant range of the frequencies, we conclude complexity in the system non-linear response, depending of initial conditions and also of other system kinetic parameters and corresponding relation between these sets of the kinetic

parameters.

**Acknowledgment.** *Parts of this research were supported by the Ministry of Sciences and Environmental Protection of Republic of Serbia through Mathematical Institute SANU Belgrade Grant ON144002 and Faculty of Mechanical Engineering University of Nis.*

## REFERENCES

- [1] Goroško O. A. and Hedrih (Stevanović) K. *Analitička dinamika (mehanika) diskretnih naslednih sistema*, (Analytical Dynamics (Mechanics) of Discrete Hereditary Systems), University of Niš, 426 p., 2001.
- [2] Hedrih (Stevanović) K. Energy analysis in the nonlinear hybrid system containing linear and nonlinear subsystem coupled by hereditary element, *Nonlinear Dynamics*, Vol. 51, No. 1, pp. 127-140, 2007.
- [3] Hedrih (Stevanović) K. Partial Fractional Order Differential Equations of Transversal Vibrations of Creep-connected Double Plate Systems, in: *Fractional Differentiation and its Applications*, Edited by Alain Le Mahaute, J. A. Tenreiro Machado, Jean Claude Trigeassou and Jocelyn Sabatier, U-Book, pp. 289-302, 2005.
- [4] Hedrih (Stevanović) K. Transversal Vibrations of Double-Plate Systems, *Acta Mechanica Sinica*, 22, pp. 487-501, 2006 (hard cover and on-line).
- [5] Katica (Stevanović) Hedrih, Energy transfer in double plate system dynamics, *Acta Mechanica Sinica*, Vol. 24, No 3, pp. 331-344, 2008.
- [6] Hedrih (Stevanović) K. and Simonović J. Transversal Vibrations of a Double Circular Plate System with Visco-elastic Layer Excited by a Random Temperature Field, *Int. Journal of Nonlinear Sciences and Numerical Simulation*, Vol. 9, No.1, pp. 47-50, 2008.
- [7] Hedrih (Stevanović) K. and Simonović J. Transversal Vibrations of a non-conservative double circular plate system, *FACTA UNIVERSITATIS Series: Mechanics, Automatic Control and Robotics*, Vol. 6, No 1, pp. 319 - 64, 2007.
- [8] Hedrih (Stevanović) K. and Simonović J. D. Non-linear dynamics of the sandwich double circular plate system, *Int. Journal of Non-Linear Mechanics*, 12, 2009.
- [9] Mitropolyskiy Yu.A. *Nestashionarniye procesi v nelinyeynih sistemah*, AN USSR, Kiev, 1955 (in Russian).
- [10] Mitropolyskiy Yu.A. Problemi asimptoticheskoy teorii nestashionarnikh kolebaniy, Nauka, Moskva, 431 p. 1964 (in Russian).
- [11] Mitropolyskiy Yu.A. and Moiseenkov B.I. *Lekciyi po primeniyeniyu metodov k recheniyu uravneniy v chastnih proizvodnih*, Inst. Math. AN USSR, Kiev, 1968 (in Russian).
- [12] Mitropolyskiy Yu.A. and Mosseenkov B.I. *Assimptoticheskiye resheniya uravneniya v chastnih proizvodnih*, Vischaya chkola, Kiev, 1976 (in Russian)
- [13] Mitropolyskiy Yu. A. *Metod usrednyeniya v nelinyeynoy mehanike*, Naukova Dumka, Kiev, 340 p., 1971.
- [14] Mitropolyskiy, Yu. A. *Nelinyeynaya mehanika-Asimptoticheskie metodi*, Institut matematiki NAN Ukraini, Kiev, 397 p., 1955.
- [15] Mitropolyskiy Yu.A., Nguyen Van Dao. *Lectures on Asymptotic Methods of Nonlinear Dynamics*, Vietnam National University Publishing House, Hanoi, 494 p., 2003.
- [16] Nayfeh A.H. and Pai, P.F. *Linear and Nonlinear Structural Mechanics*. Wiley Interscience, New York, 2004
- [17] Nayfeh A.H. Transfer of energy from high-frequency to low-frequency modes, in: *Book of abstracts. The Second International Conference "Asymptotics in Mechanics"*, St. Petersburg Marine Technical University, Russia, October 13– 16, p. 44, 1996.
- [18] Rašković, D. *Teorija oscilacija (Theory of oscillations)*. Nauna knjiga, 503 p., 1965 (in Serbian).
- [19] Simonović J. *Fenomeni dinamike mehaničkih sistema složenih struktura (Phenomen of Dynamics of Complex Structure Mechanical Systems)*, Magistar of Sciences Degree Thesis, Faculty of Mechanical Engineering in Niš, 2008 (in Serbian).
- [20] Stevanović (Hedrih) K. *Application of the Asymptotic Method for the Investigation of the Nonlinear Oscillations of Elastic Bodies - Energy Analysis of the Oscillatory Motions of Elastic Bodies*, Doctor's Degree Thesis, Niš, Yugoslavia, 1975 (in Serbian).
- [21] Stevanović (Hedrih) K. and Rašković D. Investigation of multi-frequencies vibrations in single-frequency regime in nonlinear systems with many degrees of the freedom and with slowchanging parameters, *J. Nonlin. Vibrat. Probl.*, No. 15, pp. 201–202, 1974.
- [22] Stevanović (Hedrih) K. Two-frequency nonstationary forced vibrations of the beams, *Math. Phys.*, 12, 1972.

## STABILITY OF WHIRL VIBRATIONS OF DRILL STRING BOTTOM ASSEMBLY

Sergey N. Hudoliy,  
Elena I. Borshch<sup>1</sup>  
National Transport University  
Kiev, Ukraine

### ABSTRACT

Current methods for analysis of extraordinary behavior of the drill strings, as a rule, concern their critical states related to essential change of their motion modes and contact interaction with borehole wall.

The bending vibrations of bottom hole assembly under action of a friction moment applied to the bit is considered. The analysis of vibration self-excitation mechanism is performed. It is shown that the generated moment is not conservative and it is the main reason of the system dynamic instability. The modes of bottom hole assembly whirling are constructed for different values of characteristic parameters.

### INTRODUCTION

Today, approximately 90% of all the energy consumed by mankind is accounted for by fossil hydrocarbon fuels of which oil and gas are the major ones and whose prices are skyrocketing due to their imminent depletion. Nevertheless, reconnaissance of new oil and gas reserves and progressively increasing rate of their extraction continue. As this takes place, the principal technological component of these processes is the drilling of new oil and gas bores. Even now their depths achieve several kilometers, but the problem of extraction of oil and gas from deeper tectonic levels continues to be urgent.

Rotor drilling of bore-wells realized through application of a torque  $M_z$  to the top edge of the drill string (DS) and a vertical reaction force  $R$  on the drill bit (Fig.1) can be accompanied by occurrence of some dynamic phenomena exerting essential influence on the whole working process. Among these is excitation of whirling vibrations caused by non-conservative bending of the bit shaft by contact forces.

The theoretical simulation of dynamic behavior of the DS in the drilling possess essential analytical and computational difficulties stemming from the system dependence on complicated combination of dynamic and quasi-static force factors acting on the DS in its working [1-3].

But the principal obstacle arising in attempting to analyze the dynamic bending of the DS is associated with the necessity of integrating differential equations of their vibrations in large ranges of the DS length. As the DS is equivalent to human hair by the condition of geometrical similarity, it is very flexible. For this reason equations describing its bending

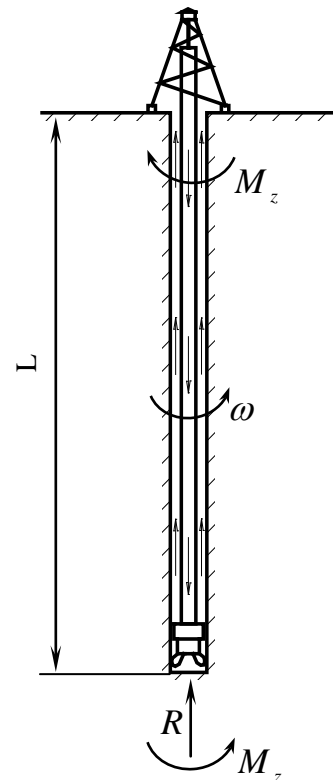


Fig. 1. Design scheme  
of a drill string

<sup>1</sup> Corresponding author. Email [borshchoi@ukr.net](mailto:borshchoi@ukr.net)

possess the so called calculation stiffness and the majority of methods of their solving are poorly convergent. So usually the problems of the DS torsion vibrations are stated, though it is accented that integrated models of the DS bending dynamics should be elaborated [4].

The first step of dynamic analysis of a complicated structure consists in study of its free vibrations. It is associated with the statement of the Sturm-Liouville boundary problem for the equations of the rotary DS dynamics. In solution of this problem, the eigen values should be calculated and eigen modes should be built for the whole length of the DS. Previously, it was not stated and solved owing to essential theoretical and calculation difficulties.

Of critical importance is also the DS rotation with the resulting generation of centrifugal and Coriolis' inertia forces. Owing to large length of the DS, frequently these forces are the main reason of instability onset and they exclude the possibility of the system vibration with one common phase, as it occurs in gyroscopic systems. These effects are completely understood in the theory of rotating shafts [5], but in the DS they are realized in more complicated forms because proceed in combination with other mechanical effects.

In service, washing liquid (mud) required to remove the crushed particles of the destructed rock moves down inside the DS. Notice, that vibrations and quasi-static stability of rectilinear and curvilinear (spiral) tubes under action of heterogeneous flows of liquids are considered in references [6].

In this paper firstly we consider a hyper long (unbounded) DS and study analytically general regularities of its natural vibrations. Then bounded DSs are studied, their first frequencies are calculated and vibration modes are built. It is shown that they have complicated spiral shapes.

## 1. STATEMENT OF THE PROBLEM

To derive equations of vibration of a rotating drill string introduce the immovable coordinate system  $OXYZ$  with its origin at the point of the DS suspension and axis  $OZ$  directed along the DS axis line. It is assumed that the DS rotates with constant angular velocity  $\omega$ . As it is assumed in the theory of rotating shaft vibration, connect the rotating coordinate system  $Oxyz$  with DS in such a way that the  $Oz$  axis coincides with the  $OZ$  axis and analyze the DS dynamics in this system. Let  $\mathbf{i}$ ,  $\mathbf{j}$ ,  $\mathbf{k}$  be the unit vectors of this system.

Small vibrations of the DS are determined with the use of the functions of elastic displacements  $u(z)$ ,  $v(z)$  in the planes  $xOz$ ,  $yOz$ , correspondingly. In the perturbed state of dynamic equilibrium these displacements are caused by action of internal longitudinal force  $T(z)$ , external torque  $M_z$ , distributed centrifugal inertia forces  $q_x^i$ ,  $q_y^i$  of rotation and distributed centrifugal inertia forces  $q_x^m$ ,  $q_y^m$  induced by motion of washing liquid (mud) inside the curved tube of the DS.

The force  $T(z)$  is accountable to distributed gravity force with intensity

$$q_z = g(\rho_t - \rho_m)F_t \quad (1)$$

and vertical reaction  $R$  of the bit contact interaction with the rock medium. It is denoted in this formula:  $g = 9.81 \text{ m/s}^2$  – the acceleration of gravity;  $\rho$  – the density of the tube material;  $\rho_m$  – the mud density;  $F_t$  – the area of the tube wall cross-section.

At the deformed state of the DS, the distributed inertia forces  $q_x^\omega$ ,  $q_y^\omega$  of the tube compound motion and the inertia forces  $q_x^m$ ,  $q_y^m$  of the moving mud act on every element of the rotating tube, so the components of total inertia forces equal

$$q_x = q_x^\omega + q_x^m, \quad q_y = q_y^\omega + q_y^m. \quad (2)$$

Vector  $\mathbf{q}^\omega = q_x^\omega \mathbf{i} + q_y^\omega \mathbf{j}$  is calculated through the equality

$$\mathbf{q}^\omega = -(\rho F + \rho_m F_m) \mathbf{a}, \quad (3)$$

where  $F_m$  is the area of the tube bore cross-section;  $\mathbf{a}$  is the absolute acceleration of the tube element.

The  $a$  value is calculated in the rotating coordinate system  $Oxyz$ , so the motion is compound and the Coriolis formula  $\mathbf{a} = \mathbf{a}^e + \mathbf{a}^r + \mathbf{a}^c$  is used for the acceleration  $a$  determination. Here  $\mathbf{a}^e$ ,  $\mathbf{a}^r$ ,  $\mathbf{a}^c$  are the bulk, the relative and the Coriolis accelerations calculated with the help of the formulas

$$\mathbf{a}^e = \boldsymbol{\omega} \times (\boldsymbol{\omega} \times \mathbf{r}), \quad \mathbf{a}^r = \frac{d^2 \mathbf{r}}{dt^2}, \quad \mathbf{a}^c = 2\boldsymbol{\omega} \times \frac{d\mathbf{r}}{dt} \quad (4)$$

Analogously the equalities for the forces acting on the internal liquid flow moving with the velocity  $V$  are deduced [6]

$$q_x^m = V^2 \rho_m F_m \frac{\partial^2 u}{\partial z^2} + 2V \rho_m F_m \frac{\partial^2 u}{\partial z \partial t}, \quad q_y^m = V^2 \rho_m F_m \frac{\partial^2 v}{\partial z^2} + 2V \rho_m F_m \frac{\partial^2 v}{\partial z \partial t}. \quad (5)$$

To formulate constitutive equations describing vibration of the DS prestressed by longitudinal force  $T$ , reaction  $R$  and torque  $M_z$ , separate its element of length  $dz$  and consider equilibrium of internal moments with respect to the axes  $Oy$ ,  $Ox$  of the rotating coordinate system  $Oxyz$

$$dM_y - Q_x dz - T du - M_z d\left(\frac{dv}{dz}\right) = 0, \quad dM_x - Q_y dz - T dv + M_z d\left(\frac{du}{dz}\right) = 0. \quad (6)$$

where  $M_y = -EI \frac{d^2 u}{dz^2}$ ,  $M_x = -EI \frac{d^2 v}{dz^2}$ ,  $Q_x$ ,  $Q_y$  are the bending moments and shear forces oriented relative to the appropriate axes.

Rearranging Eqs (1)–(6), one gains the equations determining the dynamic behavior of the rotating DS

$$\begin{aligned} & EI \frac{\partial^4 u}{\partial z^4} - \frac{\partial}{\partial z} \left( T \frac{\partial u}{\partial z} \right) - \frac{\partial^2}{\partial z^2} \left( M_z \frac{\partial v}{\partial z} \right) - (\rho F + \rho_m F_m) \omega^2 u - \\ & - 2(\rho F + \rho_m F_m) \omega \frac{\partial v}{\partial t} + V^2 \rho_m F_m \frac{\partial^2 u}{\partial z^2} + 2V \rho_m F_m \frac{\partial^2 u}{\partial z \partial t} + (\rho F + \rho_m F_m) \frac{\partial^2 u}{\partial t^2} = 0, \\ & EI \frac{\partial^4 v}{\partial z^4} - \frac{\partial}{\partial z} \left( T \frac{\partial v}{\partial z} \right) + \frac{\partial^2}{\partial z^2} \left( M_z \frac{\partial u}{\partial z} \right) - (\rho F + \rho_m F_m) \omega^2 v + \\ & + 2(\rho F + \rho_m F_m) \omega \frac{\partial u}{\partial t} + V^2 \rho_m F_m \frac{\partial^2 v}{\partial z^2} + 2V \rho_m F_m \frac{\partial^2 v}{\partial z \partial t} + (\rho F + \rho_m F_m) \frac{\partial^2 v}{\partial t^2} = 0. \end{aligned} \quad (7)$$

In application of system (7) to analysis of the DS dynamics it is usual to state the boundary value problem. However the problem about free vibration of infinite twisted rotary rod should be considered also with the aim to establish the most general regularities of the DS behavior.

## 2. THE SPIRAL STRUCTURE OF THE RUNNING BENDING WAVES

The problem of harmonic vibrations of an unbounded twisted rotary tube rod with internal flows of liquid is multiparametric and for this reason it is difficult to be analyzed. For this reason firstly consider the simplified case  $T = const$ ,  $M_z = const$  for the sake of separation of the phenomenon of free spiral wave propagation.

It can be shown that system (7) does not admit any solution in the form of stationary or running waves with nodal points, therefore we shall construct its solution in the mode of running cylindrical spiral waves

$$u(z, t) = A \cos(kz - ct), \quad v(z, t) = B \sin(kz - ct), \quad (8)$$

where  $k$  is the wave number;  $c$  the cyclic frequency.

Substituting Eqs (8) into reduced system (7) and excluding the summands containing the multiplier  $\rho_m$ , one obtains the homogeneous system of algebraic equations

$$\begin{aligned} (EIk^4 + Tk^2 - \rho F \omega^2 - \rho F c^2)A + (M_z k^3 + 2\rho F \omega c)B &= 0 \\ (M_z k^3 + 2\rho F \omega c)A + (EIk^4 + Tk^2 - \rho F \omega^2 - \rho F c^2)B &= 0 \end{aligned} \quad (9)$$

It generates the characteristic equation

$$(EIk^4 + Tk^2 - \rho F \omega^2 - \rho F c^2)^2 - (M_z k^3 + 2\rho F \omega c)^2 = 0, \quad (10)$$

connecting the wave number  $k$  and the cyclic frequency  $c$ . This equation has four roots

$$c_{1,2} = \omega \pm \frac{k}{\sqrt{\rho F}} \sqrt{EIk^2 + M_z k + T}, \quad c_{3,4} = -\omega \pm \frac{k}{\sqrt{\rho F}} \sqrt{EIk^2 - M_z k + T} \quad (11)$$

corresponding to dextral ( $A/B = 1$ ) and sinistral ( $A/B = -1$ ) spiral forms (Fig.2).

The cited reasonings permit one to make important conclusions. Firstly, only spiral bending waves can propagate in rotating twisted rods. In the second place, four different values  $c_i$  of cyclic frequency correspond to every value of the spiral pitch. Two of them conform to dextral spiral and other two are consistent with the sinistral one. The directions of their propagation and characters of their dispersive curves  $c_i = c_i(k)$  are determined by correlations between the bending stiffness  $EI$  of the rod, value  $M_z$  of the torque and value and sign of the longitudinal force  $T$ .

Phase velocities  $v_i$  of the wave propagation in the rotary coordinate system  $Oxyz$  are determined by the equalities

$$\begin{aligned} v_{1,2} &= \frac{c_{1,2}}{k} = \frac{\omega}{k} \pm \sqrt{(EIk^2 + M_z k + T) / \rho F}, \\ v_{3,4} &= \frac{c_{3,4}}{k} = -\frac{\omega}{k} \pm \sqrt{(EIk^2 - M_z k + T) / \rho F}. \end{aligned} \quad (13)$$

By the way of example the diagrams

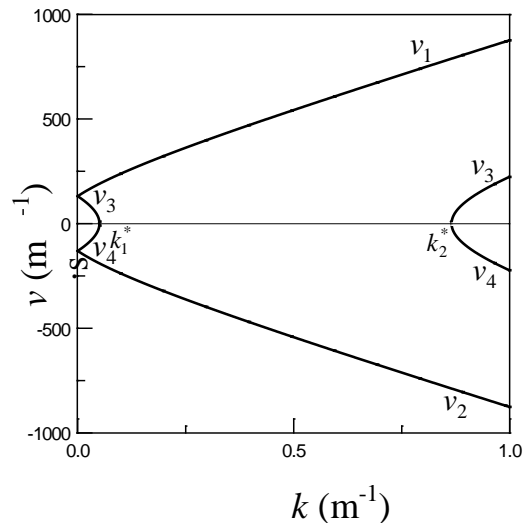


Fig. 3. Phase velocities of spiral waves at  $\omega = 0$

$v_i = v_i(k)$  ( $i = \overline{1,4}$ ) (Fig. 3) are plotted for the waves in the shapes of dextral ( $i = 1,2$ ) and sinistral ( $i = 3,4$ ) spirals, propagating in the steel tube rod of 35.5 sm in external diameter, 1.4 sm in thickness, at given values of the parameters  $EI = 4.586 \cdot 10^7 Pa \cdot m^4$ ,  $\rho F = 117 kg/m$ ,  $M_z = 4.2 \cdot 10^7 N \cdot m$ ,  $T = 2 \cdot 10^6 N$ . As the  $\omega$  value exists only as an summand in Eqs (14), (15), the calculations are performed for  $\omega = 0$ .

The gained results permit one to anticipate that the free and forced vibrations, as well as quasi-static bifurcation buckling of the DS subjected to action of torque, longitudinal force and rotary inertia forces may occur only with formation of spiral (regular or irregular) modes.

### 3. FREE BENDING VIBRATIONS OF HYPER DEEP DRILL STRINGS

System (7) can be used for analysis of free vibrations of a bounded DS. Consider that it is pinned at its ends and boundary conditions

$$u(0) = v(0) = 0, \quad u''_{zz}(0) = v''_{zz}(0) = 0, \quad u(L) = v(L) = 0, \quad u''_{zz}(L) = v''_{zz}(L) = 0 \quad (13)$$

are satisfied.

Then a periodic solution of homogeneous system (7), (13) can be constructed with the help of substitution

$$u(z, t) = U_s(z) \sin ct + U_c(z) \cos ct, \quad v(z, t) = V_s(z) \sin ct + V_c(z) \cos ct, \quad (14)$$

where  $c$  is the cyclic frequency of free vibration;  $U_s, U_c, V_s, V_c$  the unknown functions.

Substituting Eqs (14) into system (7) and separating terms containing  $\sin ct$  and  $\cos ct$ , one gains the system of four ordinary differential equations relative to the unknown variables  $U_s(z), U_c(z), V_s(z), V_c(z)$ .

To find frequencies  $c_i$  under prescribed values of  $T, M_z, \omega$ , the item-by-item analysis is used. In doing so the constitutive system of ordinary differential is represented in the vector form

$$\frac{d\mathbf{w}}{dz} = F(z)\mathbf{w} + c^2 G\mathbf{w} + cH\mathbf{w}, \quad (15)$$

$$A\mathbf{w}(0) = 0, \quad B\mathbf{w}(L) = 0. \quad (16)$$

Here  $\mathbf{w}(z)$  is the 16-dimentional unknown vector combining the variables  $U_s(z), U_c(z), V_s(z), V_c(z)$  and their derivatives;  $F(z), G, H$  are the matrices of dimension  $16 \times 16$ ; A, B are the constant matrices of dimension  $8 \times 16$  constructed from boundary conditions (18).

Solution of system (16) is represented in the Cauchy form

$$\mathbf{w}(z) = W(z) \cdot \mathbf{C}, \quad (17)$$

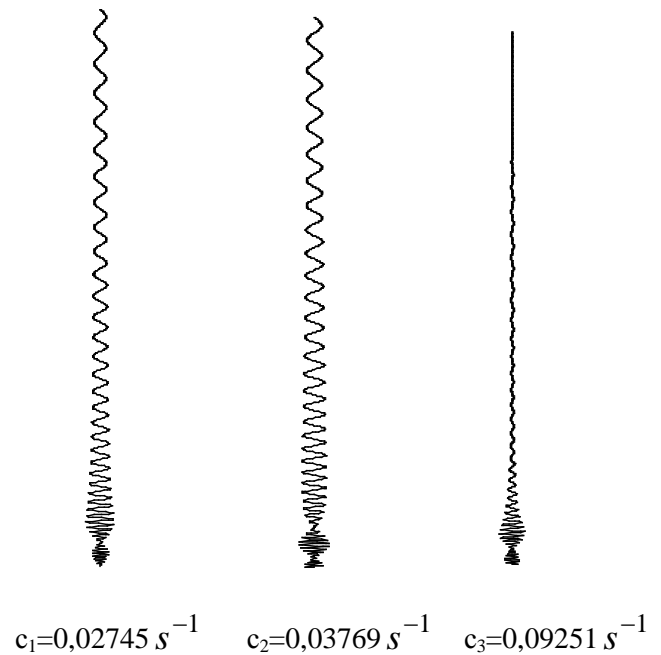


Fig 4. Modes of free vibrations of a drill string 7000 m in length

where  $W(z)$  is the Cauchy matrix of dimension  $16 \times 16$  of system (16) solutions with initial conditions  $W(0) = E$ ,  $E$  is the unit matrix,  $C$  is the required constant 16-dimensional vector.

The elaborated techniques were used for analysis of free vibrations of the DSs prestressed by torque  $M_z$  and gravity force  $T(z)$ . The DS can rest by its lower end against the bore hole bottom, so compressive reactive force  $T(L) = R = -1.6 \cdot 10^5 N$  can act on it. The influence of the internal flow of liquid was not taken into attention.

The vibration mode complication is retained also for the elongated DSs but it prevails in their lower segments, where the twisting of the harmonic curves is visible, their pitches are small and amplitudes are large (Fig.4 for the DS of 7000 m in length). With approaching to the DS middle part and further the harmonic twisting diminishes, the curves become nearly plane, their pitches enlarge and amplitudes decrease.

## CONCLUSIONS

1. The problems about free vibrations of elongated drill strings are stated with allowance made for the additional disturbing factors of longitudinal non-uniform preloading, action of torque, inertia forces of rotation and internal flow of washing liquid. The constitutive equations are deduced, methods for their solving are elaborated.
2. Relying on the constructed equations, free vibrations of unbounded elastic rods subjected to action of the mentioned factors are studied. It is shown through analysis of the appropriate dispersion equation, that free bending vibrations of these rods can be realized only in the modes of running cylindrical spiral waves. As this takes place, four different values  $c_i$  of cyclic frequency correspond to everyone value of the spiral pitch. Two of them conform to a dextral spiral and other two are consistent with a sinistral one. All these waves propagate with different phase velocities along the positive and negative directions of the longitudinal axis.

## REFERENCES

- [1] Iyoho, A.W., Meize, R.A., Millheim, K.K., and Crumine, M.J. Lessons from Integrated Analysis of GOM Drilling Performance *SPE Drilling and Completion*, March 2005, pp. 6-16, 2005.
- [2] Prassl, W.F., Peden, J.M., and Wong, K.W. A Process-Knowledge Management Approach for Assessment and Mitigation of Drilling Risks *Journal of Petroleum Science and Engineering*, Vol.49(3-4), pp. 142-161, 2005.
- [3] Christoforou, A.P., and Yigit, A.S. Dynamic Modelling of Rotating Drillstrings with Borehole Interactions *Journal of Sound and Vibration*, Vol.206(2), pp. 243-260, 1997.
- [4] Tucker, W.R., and Wang, C. An Integrated Model for Drill-String Dynamics *Journal of Sound and Vibration*, Vol.224(1), pp. 123-165, 1999.
- [5] Ziegler, H. *Principles of Structural Stability*, Blaisdell Publishing Company, Waltham-Massachusetts-Toronto-London, 1968.
- [6] Gulyaev, V.I., and Tolbatov, E.Yu. Dynamics of Spiral Tubes Containing Internal Moving Masses of Boiling Liquid *Journal of Sound and Vibration*, Vol.274(2), pp. 233-248, 2004.

## NONLINEAR PARAMETRIC VIBRATIONS OF CYLINDRICAL SHELLS

**Roman E. Kochurov**  
NTU "KhPI"  
Kharkov, Ukraine

**Konstantin V. Avramov<sup>1</sup>**  
A.N. Podgorny Institute  
for Mechanical  
Engineering Problems  
Kharkov, Ukraine

---

### ABSTRACT

---

Donnell's equations are used to predict nonlinear vibrations of cylindrical shells, which are excited by parametric dynamical load. The finite degree-of-freedom dynamical system of cylindrical shells is derived. The nonlinear modes of the shell with dissipation and without one are analyzed by harmonic balance method. These nonlinear modes correspond to the standing waves in the shell. Traveling waves are analyzed in detail.

---

### INTRODUCTION

Thin-walled structures are widely used in aerospace, nuclear, civil and mechanical engineering. Longitudinal periodic loads usually act on the shells and leads to complex dynamical behavior of the systems. Many efforts were made to study this behavior. Parametric oscillations of simply supported cylindrical shells are modeled by two interacting modes (asymmetric and axisymmetric ones) in [1]. Donnell's shallow shell equations were used to study parametric oscillations of cylindrical shells [2] and the fundamental role of axisymmetric modes in evaluating the parametric instability bounds is treated. The effect of initial imperfections on parametric oscillations of simply supported cylindrical shells was studied by Koval'chuk and Krasnopol'skaya [3]. Kubenko et al. [4] obtained theoretically and experimentally the frequency response and the region of the main parametric resonance of simply supported cylindrical shells. Pellicano et al. [5] analyzed nonlinear oscillations and dynamic instability of simply supported cylindrical shells under the action of longitudinal dynamic forces. The dynamic stability of cylindrical shells under the action of both static and periodic axial loads is treated in [6]. Analysis of nonlinear modes of cylindrical shells, which are described by three mode model, is considered in the paper [7]. Detailed reviewer of cylindrical shell dynamics is presented in [8].

Nonlinear dynamics of cylindrical shells in the case of the main parametric resonance is treated in the present paper. Cylindrical shells have dense frequency spectrum. Therefore, the case, when the three eigenfrequencies of conjugate modes are close, is considered. This case occurs frequently in shell dynamics. These three conjugate modes are taken into account in analysis of the main parametric resonance.

### 1. PROBLEM FORMULATION AND MAIN EQUATIONS

The simply supported cylindrical shell without imperfections is considered. The following time periodic distributed parametric load acts on the shell (Fig.1):

$$N_x(t) = N_1 \cos 2vt, \quad N_1 = const > 0 \quad (1)$$

where  $v$  is an excitation frequency. The vibrations of shell have moderate amplitudes. Then the strains are small and displacements are moderate and the strains- displacement relations are nonlinear. The strains and stresses satisfy the Hooke's law. In this case the following Donnell's equations describe the shell vibrations adequately [1, 5]:

---

<sup>1</sup> Konstantin V. Avramov. Email [kavramov@kharkov.ua](mailto:kavramov@kharkov.ua).

$$\frac{D}{h} \nabla^4 w + \rho \frac{\partial^2 w}{\partial t^2} = \frac{\partial^2 F}{R \partial x^2} + \left( \frac{\partial^2 w}{\partial x^2} \frac{\partial^2 F}{\partial y^2} - 2 \frac{\partial^2 w}{\partial x \partial y} \frac{\partial^2 F}{\partial x \partial y} + \frac{\partial^2 w}{\partial y^2} \frac{\partial^2 F}{\partial x^2} \right)$$

$$\frac{1}{E} \nabla^4 F = -\frac{1}{R} \frac{\partial^2 w}{\partial x^2} + \left[ \left( \frac{\partial^2 w}{\partial x \partial y} \right)^2 - \frac{\partial^2 w}{\partial x^2} \frac{\partial^2 w}{\partial y^2} \right] \quad (2)$$

where  $w$  is displacements of the middle surface points in the radial directions;  $x$ ,  $y$  are longitudinal and circumferential coordinates;  $R$ ,  $\rho$  are mean shell radius and material density;  $E$ ,  $\mu$  are Young's modulus and Poisson's ratio;  $F$  is an in-plane stress function;  $D = Eh^3 / (12(1-\mu^2))$  is a flexural rigidity.

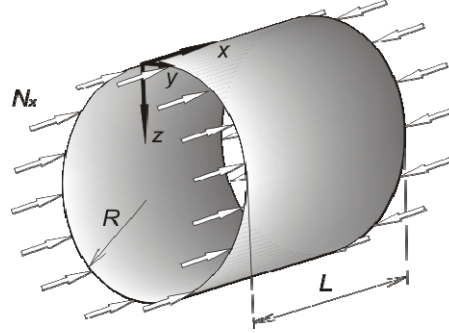


Fig. 1 Cylindrical shell

The conjugation vibrations modes  $\cos s_i y \sin r x$  and  $\sin s_i y \sin r x$  have the same frequencies of cylindrical shells vibrations. If a shell performs nonlinear vibrations, these modes can be excited jointly. As follows from the shell analysis [9], wide class of cylindrical shells has three close eigenfrequencies of conjugate modes. In future analysis the main parametric resonance is considered  $\nu \approx \omega_i; i = 1, 2, \dots, 6$ , where  $\omega_{2i-1} = \omega_{2i}; i = \overline{1, 3}$  are equal eigenfrequencies of conjugate modes. Three conjugate modes are taken into account in the expansion of the displacements in the radial directions. Then the dynamic flexure  $w$  can be presented as:

$$w = \sum_{i=1}^3 \left( f_{2i-1} \cos s_i y + f_{2i} \sin s_i y \right) \sin r x + f_7 \sin^2 r x + f_8 \quad (3)$$

where  $s_i = n_i / R$ ;  $r = m \pi / L; i = 1, 2, 3$ ;  $n_i$  is numbers of waves in circumference directions;  $m$  is a number of half-waves in  $x$  direction. The summand  $f_7 \sin^2 r x$  describes asymmetry of dynamic flexure with respect to a middle surface. The term  $f_8$  describes displacements in radial directions of shell face sections points. This term does not depend on circumference coordinate  $y$ . Therefore, the face sections can "breathe" [4].

The in-plane stress function  $F$  is determined from the second equation of the system (2), satisfying the periodicity conditions of the circumference displacements. The stress function is substituted into the first equation of the system (2) and the Galerkin method is applied to the resulted equation. Assuming that  $\dot{f}_7 = 0$ ,  $\ddot{f}_8 = 0$  [11], the finite-degree-of-freedom shell model with respect to the dimensionless variables and parameters has the following form:

$$\ddot{f}_i + \omega_i^2 f_i + f_i R_i (f_1, \dots, f_6) + G_i (f_1, \dots, f_6) + \chi_i N_x f_i = 0, \quad i = 1, 2, \dots, 6 \quad (4)$$

## 2. NONLINEAR MODES AND HARMONIC BALANCE ANALYSIS

The nonlinear dynamics of the system (4) is analyzed in this section. The equations

$$f_{2i-1} = \pm f_{2i}, \quad i = 1, 2, 3 \quad (5)$$

are exact solutions of the system (4). If the solutions (5) are substituted into (4), the following dynamical system is derived:

$$\ddot{f}_i + \omega_i^2 f_i + f_i \tilde{R}_i(f_1, f_3, f_5) + \tilde{G}_i(f_1, f_3, f_5) + \chi_i N_x f_i = 0, \quad i=1,3,5 \quad (6)$$

The solutions (5) are called nonlinear modes. These nonlinear modes are straight lines in configuration space. The dynamical system (6) describes the motions on nonlinear modes.

The harmonic balance method is used to study the motions on the nonlinear modes (6). As the nonlinear modes for the main parametric resonance are considered, the motions are presented as:

$$f_i = A_i \cos(\nu t) + B_i \sin(\nu t), \quad i=1,3,5 \quad (7)$$

Now (7) is substituted into (6) and the amplitudes of harmonics  $\cos(\nu t)$  and  $\sin(\nu t)$  are equated. As a result the following system of nonlinear algebraic equations is derived (values  $\eta_{ij}$ ,  $\chi_i$  depend on the shell parameters):

$$\begin{aligned} A_i \left( \omega_i^2 - \nu^2 + \eta_{ii} A_i^2 + \frac{1}{2} \sum_{j=1,3,5} \eta_{ij} (3A_j^2 + B_j^2) + \frac{1}{2} \chi_i N_1 \right) + G_i^{(A)}(A_1, A_3, A_5, B_1, B_3, B_5) &= 0 \\ B_i \left( \omega_i^2 - \nu^2 + \eta_{ii} B_i^2 + \frac{1}{2} \sum_{j=1,3,5} \eta_{ij} (3B_j^2 + A_j^2) - \frac{1}{2} \chi_i N_1 \right) + G_i^{(B)}(A_1, A_3, A_5, B_1, B_3, B_5) &= 0, \quad i=1,3,5 \end{aligned} \quad (8)$$

The following groups of solutions exist in the system (8):

- 1.1).  $A_1 \neq 0; A_3 = A_5 = 0; B_i = 0;$  1.2).  $B_1 \neq 0; B_3 = B_5 = 0; A_i = 0;$
- 2.1).  $A_3 \neq 0; A_1 = A_5 = 0; B_i = 0;$  2.2).  $B_3 \neq 0; B_1 = B_5 = 0; A_i = 0;$
- 3.1).  $A_5 \neq 0; A_1 = A_3 = 0; B_i = 0;$  3.2).  $B_5 \neq 0; B_1 = B_3 = 0; A_i = 0;$
- 4.1).  $A_1 \neq 0; A_5 \neq 0; A_3 = 0; B_i = 0;$  4.2).  $B_1 \neq 0; B_5 \neq 0; B_3 = 0; A_i = 0;$
- 5.1).  $A_1 \neq 0; A_3 \neq 0; A_5 \neq 0; B_i = 0;$  5.2).  $B_1 \neq 0; B_3 \neq 0; B_5 \neq 0; A_i = 0, \quad i=1,3,5 \quad (9)$

Now every group of solutions is considered separately. Fixing the value  $\nu$  with a certain step size, the solutions are determined from the system of nonlinear algebraic equations (8). The solutions (1.1 – 4.2) can be determined analytically. The solutions (5.1, 5.2) are analyzed numerically by the Newton method with respect to  $A_1, B_1, A_3, B_3, A_5, B_5$ .

Now the nonlinear vibrations of cylindrical shells are considered accounting energy dissipation. Then the linear damping is added into the system (4). The resulted system has the following form:

$$\dot{f}_i + \xi_i \dot{f}_i + \omega_i^2 f_i + f_i R_i(f_1, \dots, f_6) + G_i(f_1, \dots, f_6) + \chi_i N_x f_i = 0, \quad i=1,2,\dots,6. \quad (10)$$

Note, that the equations  $f_{2i-1} = \pm f_{2i}; i=1,2,3$  are exact solution of the system (10). These solutions correspond to nonlinear modes. Moreover, these nonlinear modes coincide with the nonlinear modes of the system without dissipation (6). The harmonic balance method is used to study these nonlinear modes and the system motions are presented in the form (7). Then the system of nonlinear algebraic equations with respect to amplitudes of harmonics (7) is derived as:

$$\begin{aligned} A_i \left( \omega_i^2 - \nu^2 + \eta_{ii} A_i^2 + \frac{1}{2} \sum_{j=1,3,5} \eta_{ij} (3A_j^2 + B_j^2) + \frac{1}{2} \chi_i N_1 \right) + B_i \xi_i \nu + G_i^{(A)}(A_1, A_3, A_5, B_1, B_3, B_5) &= 0 \\ B_i \left( \omega_i^2 - \nu^2 + \eta_{ii} B_i^2 + \frac{1}{2} \sum_{j=1,3,5} \eta_{ij} (3B_j^2 + A_j^2) - \frac{1}{2} \chi_i N_1 \right) - A_i \xi_i \nu + G_i^{(B)}(A_1, A_3, A_5, B_1, B_3, B_5) &= 0, \quad i=1,3,5 \end{aligned} \quad (11)$$

The following groups of solutions exist in the system (11):

- 1).  $A_1 \neq 0; B_1 \neq 0; A_3 = A_5 = 0; B_3 = B_5 = 0;$  2).  $A_3 \neq 0; B_3 \neq 0; A_1 = A_5 = 0; B_1 = B_5 = 0;$
- 3).  $A_5 \neq 0; B_5 \neq 0; A_1 = A_3 = 0; B_1 = B_3 = 0;$  4).  $A_1 \neq 0; A_5 \neq 0; B_1 \neq 0; B_5 \neq 0; A_3 = 0; B_3 = 0;$
- 5).  $A_1 \neq 0; A_3 \neq 0; A_5 \neq 0; B_1 \neq 0; B_3 \neq 0; B_5 \neq 0$  (12)

The solutions (12) of the system (11) are analyzed numerically. Setting the parameter  $\nu$  with a certain step, the system (11) are solved by the Newton method.

The traveling waves for the main parametric resonance, which are described by the system (10), are considered taking into account dissipation. The harmonic balance method is used to study these motions and the system vibrations are presented as:

$$f_i = A_i \cos(\nu t) + B_i \sin(\nu t), \quad f_{i+1} = A_i \sin(\nu t) + B_i \cos(\nu t), \quad i = 1, 3, 5 \quad (13)$$

Then the amplitudes of harmonics (13) are determined from the following system of nonlinear algebraic equations:

$$\begin{aligned} A_i \left( \omega_i^2 - \nu^2 + \eta_{ii} B_i^2 + \sum_{j=1,3,5} \eta_{ij} (A_j^2 + B_j^2) \pm \frac{1}{2} \chi_i N_1 \right) \pm B_i \xi_i \nu + \tilde{G}_i^{(A)}(A_1, A_3, A_5, B_1, B_3, B_5) = 0 \\ B_i \left( \omega_i^2 - \nu^2 + \eta_{ii} A_i^2 + \sum_{j=1,3,5} \eta_{ij} (A_j^2 + B_j^2) \pm \frac{1}{2} \chi_i N_1 \right) \pm A_i \xi_i \nu + \tilde{G}_i^{(B)}(A_1, A_3, A_5, B_1, B_3, B_5) = 0, \quad i = 1, 3, 5 \end{aligned} \quad (14)$$

The following groups of solutions exist in the system (14):

- 1).  $A_1 = B_1 \neq 0; A_3 = A_5 = B_3 = B_5 = 0;$  2).  $A_1 = B_1 \neq 0; A_5 = B_5 \neq 0; A_3 = B_3 = 0;$
- 3).  $A_1 = B_1 \neq 0; A_5 = B_5 \neq 0; A_3 = B_3 \neq 0$  (15)

Altering the frequency of the parametric load  $\nu$ , the system (14) is solved by the Newton method.

In order to analyze stability of periodic vibrations, the system of variational equations is derived and fundamental matrix is calculated numerically. Then the multipliers are obtained from the fundamental matrix [10].

### 3. NUMERICAL ANALYSIS OF VIBRATIONS

The shell with the parameters (16) [4] is considered. The frequencies of shell linear vibrations are also presented (rad/s) (16).

$$\begin{aligned} h = 0.002\text{m}, L = 0.4\text{m}, R = 0.2\text{m}, E = 2.1 \times 10^{11} \text{N/m}^2, \mu = 0.3, \rho = 7850 \text{kg/m}^3, N_1 = 1.5 \times 10^6 \text{N/m} \\ \omega_{3,1} = 5636.3; \omega_{4,1} = 3745.3; \omega_{5,1} = \omega_0 = 3165.0; \omega_{6,1} = 3437.2; \omega_{7,1} = 4214.3; \omega_{8,1} = 5289.5 \end{aligned} \quad (16)$$

where the first subscript indicates the wave numbers in circumference direction and the second subscript shows the number of half-waves in  $x$  directions (Fig.1). In future nonlinear analysis the modes with the following parameters are taken:  $n_1 = 4$ ;  $n_2 = 5$ ;  $n_3 = 6$ ;  $m = 1$ .

The dependence of the vibrations amplitudes  $A_1, B_1$  on the frequency  $\nu$  are presented on the frequency response (Fig.2a). The stable solutions are denoted by solid lines and the unstable solutions are shown by dashed lines. The branches of the frequency response (Fig.2a) are denoted by  $A_1^{(1)}, B_1^{(1)}$  for the cases (1.1, 1.2) of the equations (9). In this case only one pair of the conjugate modes from the expansion (3) is active. The branches  $A_1^{(2)}, B_1^{(2)}$  (Fig.2a) describe the motions with two pairs of conjugate vibrations modes. These solutions correspond to the cases (4.1) and (4.2) of the equations (9). The branches  $A_1^{(3)}, B_1^{(3)}$  of the frequency response show the vibrations with three pairs of conjugate modes, which correspond to the cases (5.1) and (5.2) of the equations (9).

The direct numerical integrations of the system (6) at different values of frequency  $\nu$  are carried out to confirm the analytical results. Using such approach, only stable solutions are derived. The data of the calculations are shown by small squares on Fig.2a. The results of the direct numerical integration are very close to the data, which are obtained by harmonic balance method.

Carrying out numerical integration on long time interval, the periodic solution is considered unstable, if the numerical trajectory escapes from the considered one to another trajectory. To study stability of the parametric vibrations the direct numerical integration of the differential equations (4) is carried out on the time interval  $t \in [0; 2000 \pi \nu^{-1}]$ . The initial conditions are determined from the equations (7, 14).

The dynamics of the system with dissipation (10) on the nonlinear modes is presented on the frequency response (Fig.2b). The numerical analysis of the traveling waves is carried out. Fig.3 shows the frequency response of the traveling waves.

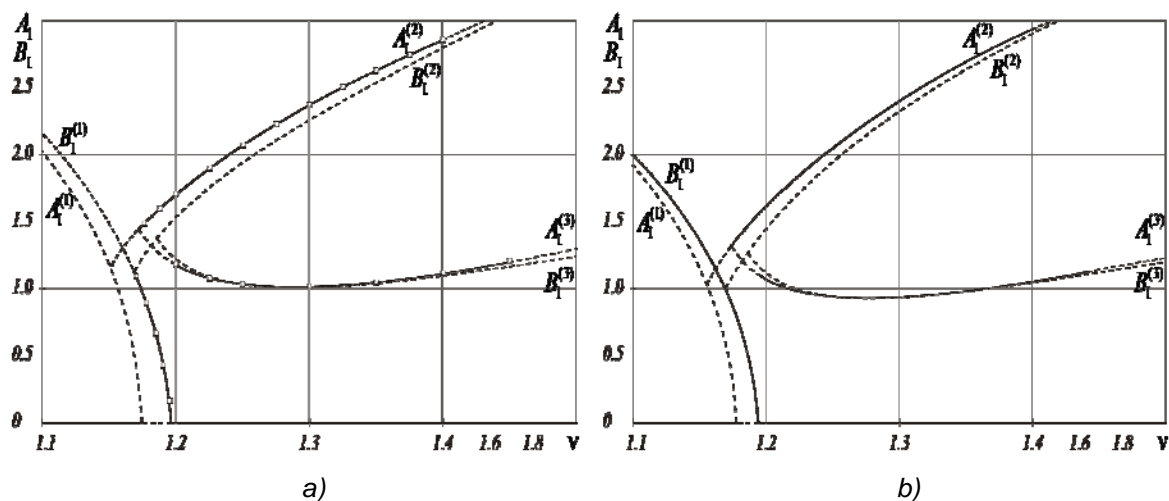


Fig. 2 Frequency response of parametric vibrations on nonlinear mode of the system a) without dissipation, b) with dissipation

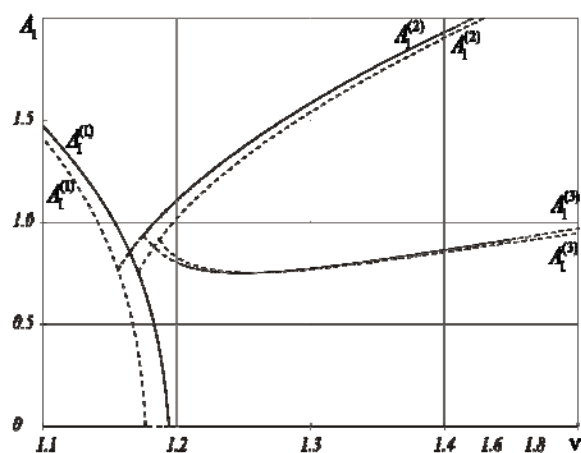


Fig. 3 Frequency response of the traveling waves of the system with dissipation

## CONCLUSIONS

One and two conjugate modes approximations of shell vibrations are not enough to predict dynamics of wide class of cylindrical shells. This is explained by closeness of the eigenfrequencies of the different conjugate modes. In this case only many modes models of shells describe the parametric vibrations adequately. The following vibrations are analyzed in this paper: a) one pair of conjugate modes is active; b) two or three pairs of conjugate modes are active.

Nonlinear modes, which are straight lines in a configuration space, are observed for many modes shells dynamics. We stress, that the same nonlinear modes exist both in the system without damping and in the system with damping. The existence of such normal modes is explained by cyclic symmetry of cylindrical shells.

Nonlinear modes and traveling waves are some solutions of the dynamical system (4). The traveling waves are described by the equations (13). As follows from the results of the analysis, the

normal modes and traveling waves exist in the frequency bands  $\nu \in [1; 1.6]$  and  $\nu \in [1.1; 1.8]$ , respectively. Thus, the frequency band  $\nu$  with two kinds of motions exists. Any one of these motions has a basin of attraction. Therefore, if the initial conditions belong to the basin of attraction of nonlinear mode or traveling waves, then nonlinear mode or traveling waves take place.

All frequency responses of nonlinear modes and traveling waves are qualitative similar. This is explained by similarity of the systems of nonlinear algebraic equations with respect to amplitudes.

## REFERENCES

- [1] Vol'mir A.S. *Nonlinear dynamics of plates and shells*, Moscow: Nauka, 1972 (in Russian).
- [2] Nagai K., Yamaki N. Dynamic stability of circular cylindrical shells under periodic compressive forces *J. Sound and Vibration*, Vol. 58, pp. 425-441, 1978.
- [3] Koval'chuk P.S., Krasnopol'skaya T.S. Resonance phenomena in nonlinear vibrations of cylindrical shells with initial imperfections *Soviet Applied. Mechanics*, Vol. 15, pp. 100-107, 1979.
- [4] Kubenko V.D., Koval'chuk P.S., Krasnopol'skaya T.S. *Nonlinear interaction of cylindrical shells*, Kiev: Naukova Dumka, 1984 [in Russian].
- [5] Pellicano F., Amabili M. Stability and vibrations of empty and fluid-filled circular cylindrical shells under static and periodic axial loads *Int. J. Solids and Structures*, Vol. 40, pp. 3229-3251, 2003.
- [6] Pellicano F. Dynamic stability and sensitivity to geometric imperfections of strongly compressed circular cylindrical shells under dynamic axial loads *Communications in Nonlinear Science and Numerical Simulations*, Vol. 14, pp. 3449-3462, 2009.
- [7] Avramov K.V., Mikhlin Yu.V., Kurilov E. Asymptotic analysis of nonlinear dynamics of simply supported cylindrical shells *Nonlinear Dynamics*, Vol. 47, pp. 331-352, 2006.
- [8] Amabili M., Païdoussis M.P. Review of studies on geometrically nonlinear vibrations and dynamics of circular cylindrical shells and panels, with and without fluid-structure interaction *Applied Mechanics Review*, Vol. 56, pp. 443-474, 2003.
- [9] Leissa A.W. *Vibrations of shells* NASA SP-288. Washington, DC: Government Printing Office, 1993.
- [10] Parker T.S., Chua L.O. *Practical numerical algorithms for chaotic systems* Springer – Verlag, New York, 1980.

## TRANSPORT AND MIXING ACROSS GULF STREAM

**Tatyana S. Krasnopolskaya**<sup>1</sup>,  
**Vladimir N. Il'chenko**  
Institute of Hydromechanics  
NASU  
Kyiv, Ukraine

**Vyacheslav V. Meleshko**,  
Kiev National Taras  
Shevchenko University  
Kyiv, Ukraine

---

### ABSTRACT

---

The new mathematical model for a stream function of a meandering jet of Gulf Stream is suggested. It is based upon a modification of the von Kármán vortex street stream function. The suggested modification allows one to approximate experimentally found main patterns in the meandering jet of Gulf Stream. This stream characterizes by the following coherent structure elements in a coordinate frame moving with a speed of the meander: 1) an eastward-propagating meandering jet; 2) regions of recirculating fluid below and above meander crests and troughs; 3) regions of westward-propagating fluid below and above the jet and recirculation regions. The inclusion of eddies above the recirculation regions and the jet enhance transport and mixing across the jet. Calculations show that more than a half of the circular area above hyperbolic points may contain warm fluid from a central area of the jet. To study mixing across the jet we examine deformation of this circular area back in time, so we can determine from which part of the jet that area is composed. Contour line tracking method conserving all topological properties in 2-D flows is used for this procedure.

---

### INTRODUCTION

Transport of warm water from the meandering jet of Gulf Stream into cold water surrounding the jet has been the focus of many recent studies. Mixing across the jet was experimentally shown in works of A. Bower [1]. Bower and Rossby [2] showed that meanders associated with Gulf Stream are responsible for much of the cross-stream motions of RAFOS floats within the jet. However, meanders alone cannot lead to the motion from one side of the jet to another. We expect that the interaction of the jet with a chain of eddies could be important in that respect. To study mixing process A. Bower [1] suggested a simple two-dimensional kinematic model. Her model describes a simple streamfunction that reproduces the kinematic features of an eastward propagating meandering jet and in this model the meander parameters affect the rate and amount of water that propagate downstream. But Bower's model does not allow for any mixing, any movement of fluid particles from one side of the jet to another. It is known that the Gulf Stream does not remain invariant in shape due to growth and diminishing of meanders. Time dependence of the meander's parameters was used by Somelson [3] to increase mixing. Another way that the Gulf Stream will change shape is by interacting with rings. The inclusion of eddies in the simple meandering jet model should enhance the mixing of fluid parcels within the jet.

The Gulf Stream frequently interacts with many rings and it can be expected that these eddies play an essential role in the distribution of tracer properties in the vicinity of the stream [4].

Our intention is to consider the enhancement of the mixing caused by the interaction of a two-dimensional jet, modelled by von Kármán vortex street [5], and Zimmerman eddies [6]. To observe the mixing that occur under interaction with eddies we examine Lagrangian particle dispersion in time.

### 1. ANALYTICAL MODEL OF THE GULF STREAM WITH EDDIES

The streamfunction in the Bower's model has the form

---

<sup>1</sup> Corresponding author. Email [t.krasnopolskaya@tue.nl](mailto:t.krasnopolskaya@tue.nl)

$$\psi(x, y, t) = \psi_0 \left\{ 1 - \tanh \left[ \frac{y - y_c}{\lambda / \cos(\alpha)} \right] \right\} \quad (1)$$

where  $\psi_0$  -- scale factor, which with  $\lambda$ , determines maximum downstream speed,  $\lambda = 40$  km, the scale width of the jet,  $y_c = A \sin[k(x - c_x t)]$  -- defines center streamline,  $A$  -- wave amplitude,  $k = 2\pi/L$  -- the wave number,  $\alpha = \tan^{-1} \{ Ak \cos[k(x - c_x t)] \}$ , direction of current. The  $\cos(\alpha)$  term is included to give the jet uniform width everywhere. It is convenient to transform the streamfunction field into a reference frame moving with the phase speed  $c_x$ , (as it was done by Bower [1]). In the moving frame, the streamfunction has the form

$$\psi'(x', y') = \psi_0 \left\{ 1 - \tanh \left[ \frac{y' - y'_c}{\lambda / \cos(\alpha')} \right] \right\} + c_x y' \quad (2)$$

where  $y'_c = A \sin(kx)$ ,  $\alpha' = \tan^{-1} [Ak \cos(kx)]$

The streamfunction in this frame is independent of time and streamlines can be interpreted as trajectories of fluid parcels relative to the moving wave.

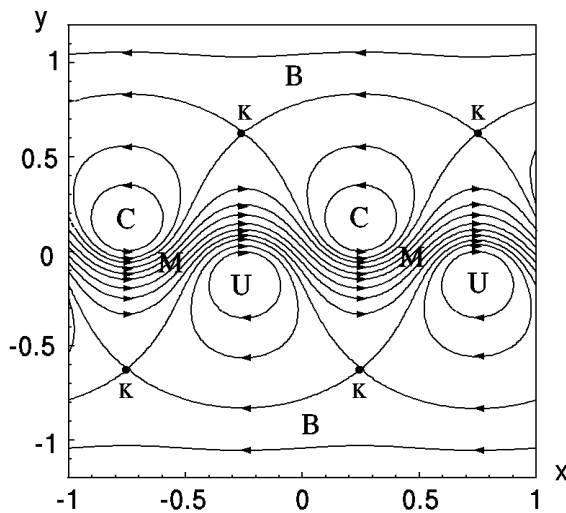


Fig.1. Coherent structure elements (the von Kármán vortex street)

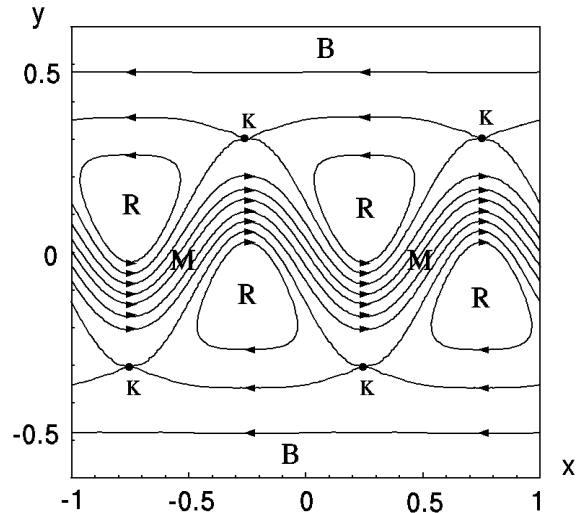


Fig.2. Coherent structure elements (the Somelson model)

The main coherent structure elements of the Gulf Stream in the moving frame are [7]: 1) an eastward-propagating meandering jet; 2) regions of fluid recirculation below and above meander crests and troughs; 3) regions of westward-propagating fluid below and above the jet and recirculation regions. We will study transport of passive particles (tracers) in such moving frame.

To study transport properties of fluid motions we suggest to use the new mathematical model for the stream function of the Gulf Stream. This new stream function is a modification of the von Kármán vortex street streamfunction. The von Kármán vortex street function describes a system of vortices behind a cylinder, which moves with a constant speed. The streamfunction of the vortex street has the same three main coherent structure elements. In the moving coordinate frame, which moves with a constant speed together with vortices, the streamfunction has the form

$$\psi(x, y) = -\frac{\Gamma}{4\pi} \ln \frac{P(x, y)}{Q(x, y)} + cy \quad (3)$$

where  $c$  is the vortex speed in the  $x$  direction;

$$P(x, y) = \cosh \frac{2\pi}{l} \left( y + \frac{h}{2} \right) + \sin \frac{2\pi x}{l}; \quad Q(x, y) = \cosh \frac{2\pi}{l} \left( y - \frac{h}{2} \right) - \sin \frac{2\pi x}{l} \quad (4)$$

or the dimensionless variables  $\tilde{x} = x/l$ ;  $\tilde{y} = y/l$  the streamfunction can be written as

$$\psi(\tilde{x}, \tilde{y}) = -\frac{1}{2k} \ln \frac{P(\tilde{x}, \tilde{y})}{Q(\tilde{x}, \tilde{y})} + \tilde{c}\tilde{y} \quad (5)$$

where  $P(\tilde{x}, \tilde{y}) = \cosh k(\tilde{y} + b) + \sin k\tilde{x}$ ;  $Q(\tilde{x}, \tilde{y}) = \cosh k(\tilde{y} - b) - \sin k\tilde{x}$

$$\tilde{\psi} = \psi/\Gamma; \quad \tilde{c} = cl/\Gamma; \quad b = h/2l; \quad k = 2\pi$$

In the Fig.1 the streamlines of the streamfunction (5) are shown. In the Fig.1 by M is shown meandering jet, by C and U the recirculation regions of cyclonic and anticyclonic rotation, by B regions of westward propagating fluid.

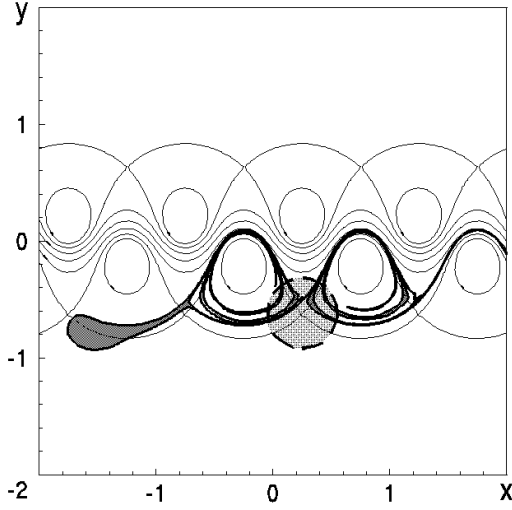


Fig.3 Chaotic advection pattern in the von Kármán model after 18 periods of tidal flow

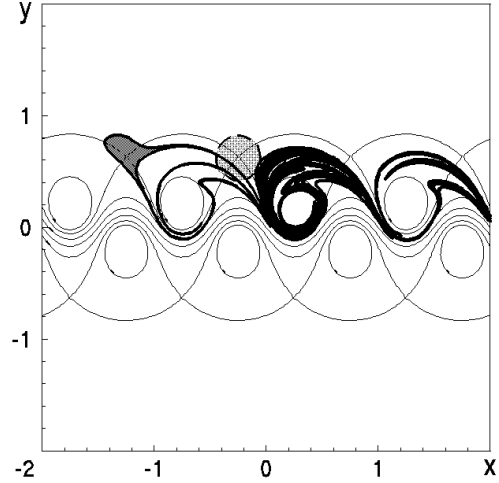


Fig.4. Mixing pattern of circular blobs in the von Kármán model with small variation after 18 periods

To compare the new model streamlines patters with the Samelson's model [3] we represent the streamlines (2) in the Fig.2 for the function (2). The flow fields in the Fig.2 and Fig.1 have hyperbolic points K .

The advection equations for passive tracers have the form

$$\dot{x} = u = -\frac{\partial \psi}{\partial y}; \quad \dot{y} = v = \frac{\partial \psi}{\partial x} \quad (6)$$

For the streamfunction (5) equations (6) could be written as

$$\begin{cases} \dot{\tilde{x}} = \frac{\cosh kb}{PQ} (\sinh kb - \sin k\tilde{x} \sinh k\tilde{y}) - c \\ \dot{\tilde{y}} = -\frac{\cosh kb}{PQ} \cos k\tilde{x} \sinh k\tilde{y} \end{cases} \quad (7)$$

To find hyperbolic points we use equations  $\dot{x} = 0$ ;  $\dot{y} = 0$  so we have, for example,

$$\tilde{x}_1 = \frac{1}{4}; \quad \tilde{x}_2 = \frac{3}{4} \quad \text{and} \quad \tilde{y}_{1,2} = \mp \frac{1}{k} \text{Arsinh} \left( \frac{1}{\tilde{c}} \cosh kb - \sinh kb \right) \quad (8)$$

Both Bower's model and von Kármán vortex street model do not allow any movement of fluid particles from one side of the jet to another or cross jet movement. Particles (passive tracers) can exhibit periodic or chaotic trajectories in the recirculation zones or along the meandering jet if we

assume that the amplitude of the streamfunction (5) has a small variation in time, say, as  $-\frac{1}{2k}(1+0.1\cos\pi t)$ .

In Fig.3, 4 chaotic advection in the von Kármán model with tidal flow velocity in the y direction (Fig.3) and in the x direction (Fig.4) are shown, when additional components are  $v_y = 0.1\cos\pi t$ ;  $v_x = 5\cos\pi t$ . Black mixing patterns of circular blobs (with dashed contour line) are shown for different initial positions of blobs. We may see as distinguished circular area (shown by grey colour) was deformed after 18 periods of variations. The whole distinguished fluid parcels will not leave the streamlines of the jet area. To introduce mixing and transport across the boundaries of the jet particles must be allowed to leave the streamlines in Fig.1 and Fig.2. For this purpose we assume that the jet interacts with a chain of topographical eddies, which locations are stationary in time. It means they move westward with constant speed  $c$  in the moving frame. For an eddy chain streamfunction we use Zimmerman [6] streamfunction, which in the rectangular non-moving coordinate system  $O'x'y'$  can be given by

$$\psi_z = \frac{1}{\pi\sqrt{2}} \sin \pi x' \sin \pi y' \quad (9)$$

It consists from square cells with vortices inside and hyperbolic points in each corner of cells. Let's put the origin of the coordinate system  $O'x'y'$  point  $O'$  (hyperbolic point of (9)) in the point (1,0) of the moving frame and turn the axis counterclockwise on an angle  $\pi/4$ . Then in the moving frame the streamfunction (9) has the form

$$\psi_z = \frac{1}{\pi\sqrt{2}} \sin \frac{\pi}{\sqrt{2}} [(x-ct) + y - 1] \sin \frac{\pi}{\sqrt{2}} [y - (x-ct) + 1] \quad (10)$$

The equations for fluid trajectories in the flow field, which is superposition of two streamfunctions (7) and (10) can be written in the form

$$\begin{cases} \dot{x} = \Gamma_1 \frac{\cosh kb}{PQ} (\sinh kb - \sin kx \sinh ky) - c - \sin \pi\sqrt{2}y \\ \dot{y} = -\Gamma_1 \frac{\cosh kb}{PQ} \cos kx \sinh ky + \sin \pi\sqrt{2}(x-ct-1) \end{cases} \quad (11)$$

where  $\Gamma_1 = 1 + \varepsilon \cos \omega t$  is an amplitude of the von Kármán vortex street function with small disturbance  $\varepsilon \cos \omega t$ , when  $\varepsilon \geq 0$  and  $\omega$  is frequency of tidal flow. In order to enhance influence only one vortex located near the hyperbolic point we choose

$$\psi_z = \frac{1}{\pi\sqrt{2}} \frac{A(t)}{B(y)} (\cos \pi\sqrt{2}y - \cos \pi\sqrt{2}(1-x+ct)) \quad (12)$$

where  $A(t) = 0.2 + \varepsilon_1 \cos \omega t$ ;  $B(y) = \exp(C_2 y)^2$ . Then, we have the following system:

$$\begin{cases} \dot{x} = \Gamma_1 \frac{\cosh kb}{PQ} (\sinh kb - \sin kx \sinh ky) - c - \frac{1}{\pi\sqrt{2}} \frac{A(t)}{B(y)} \sin \pi\sqrt{2}y + \\ \quad + \frac{C_2^2 y}{\pi\sqrt{2}} \frac{A(t)}{B(y)} (\cos \pi\sqrt{2}y - \cos \pi\sqrt{2}(1-x+ct)) \\ \dot{y} = -\Gamma_1 \frac{\cosh kb}{PQ} \cos kx \sinh ky + \sin \pi\sqrt{2}(1-x+ct) + \\ \quad + \frac{1}{\pi\sqrt{2}} \frac{A(t)}{B(y)} \sin \pi\sqrt{2}(1-x+ct) + 0.05 \cos(\omega_1 t) \end{cases} \quad (13)$$

## 2. NUMERICAL EXPERIMENT

Our study of transport and mixing across the jet is based on the description of paths of dyed blob individual particles, so we will use Lagrangian description. We will investigate of the motion of a mathematical points that move at each instant with the velocity corresponding to point instant position. Thus, the dyed particle is supposed to be inertialess, it is not subjected to diffusion. We will examine deformation of distinguished circular area back in time, so we can determine from which part of the flow that area is composed. Contour line tracking method conserving all topological properties in 2-D flows is used for this procedure. Any algorithm of contour line tracking based on the tracking of points distributed along the initial blob boundary and after this point tracking connect neighbouring points. Because of non-uniform stretching and folding of the line, two neighbouring points may appear far away from each other at some future time. The obvious way to overcome this problem is to increase the number of point. It should not be done uniformly -- but only at those parts of the initial line where considerable stretching or folding occurs. The essence of our algorithm is clear: i) if it appears that some distance  $\Delta l_k$  between two neighbouring points becomes larger than some initially prescribed value  $l_{dis}$ , insert an additional point on the initial contour in the middle between points  $k$  and  $k+1$  solve the system (13) for that one point and renumber correspondingly the initial and final arrays of points. ii) Take in any turn three points  $m-1$ ,  $m$  and  $m+1$  find the angle  $\gamma_m$ . If angle  $\gamma_m$  appears to be smaller than some prescribed value  $\gamma$  (usually  $\gamma = 120^\circ$ ), insert additional points at the initial contour line between points  $m-1$ ,  $m$  and  $m+1$  such a way that, finally, distance between all old and new points do not exceed the value  $l_{cur}$  or the angles in the polygon are larger than  $\gamma$ . An additional and important check of the proposed algorithm is the accuracy of fulfilling the area conservation condition.

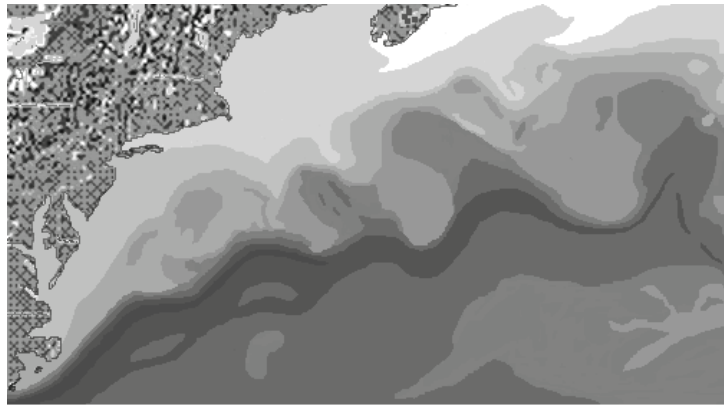


Fig.5. Satellite image of averaged sea surface temperature.

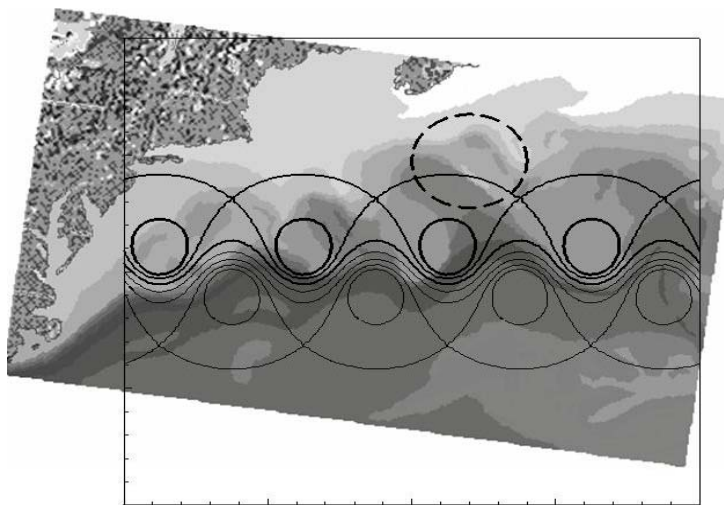


Fig.6. Satellite image of averaged sea surface temperature together with streamlines of von Kármán street.

### 3. RESULTS AND DISCUSSION

The results presented here correspond to numerical simulations of advections equations (11)-(12)  $\varepsilon = 0$ ;  $\varepsilon_1 = 0.033$ ;  $C_2 = 2$ ;  $\omega = 39.77$ ;  $\omega_1 = \omega / 120 \approx 0.33$  and different initial locations of circular blob, radius with the centre in the point (0.45, 0.95). In Fig.5 satellite image of averaged sea surface temperature is shown [8]. In the black and white graph we show only warm surface of fluid (the warmer the darker). So that meanders of Gulf Stream are shown by the darkest grey continuous color. Shore is indicated by spotted like colour.

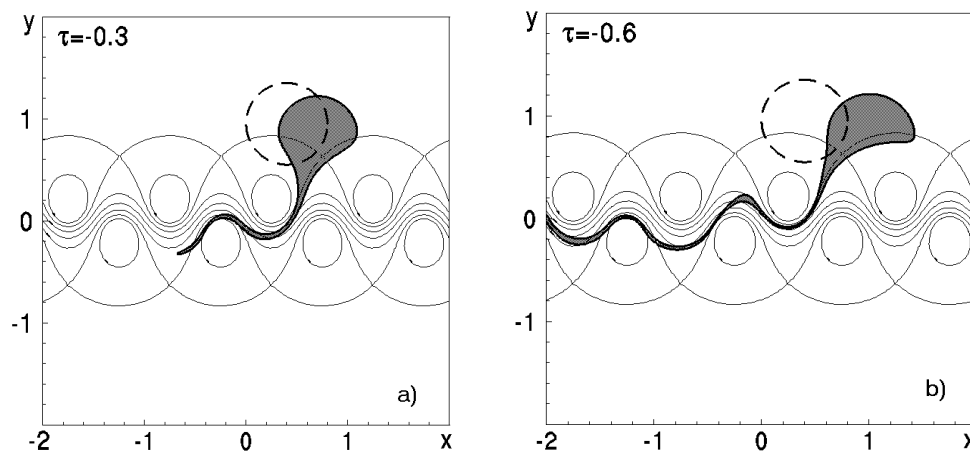


Fig.7. Deformation of circular area back in time

Above the third troughs (the third meander) a big warm fluid area is clearly seen and is shown by dark grey colour. How it was created, from which part of the jet? To answer those questions we study deformation of circular area back in time. So we study motion of particles (passive tracers) on initial contour line of the circular blob. In Fig.6,7 the locations of the circular blob are shown by dashed contour line together with streamlines of von Kármán street. In Fig.7a) the location of that blob fluid parcel at  $\tau = -0.3$  (approximately 1 days before) is shown as black area. And in Fig.7b) blob fluid parcel at  $\tau = -0.6$  (2 days before) is also shown as black area.

To estimate cross jet transport of fluid parcels we compare area of cold fluid parcel (black spot above the streamlines in the Fig.7b) and area of initial blob (with dashed contour line in the Fig.7a,b). The black area is approximately twice smaller, what means that after 2 days the circular blob will have the half of it's area warm and the half cold.

### CONCLUSION

In this study we have considered the von Kármán vortex street model of a meandering jet when it interacts with a stationary chain of eddies [4], which results in cross jet transport of fluid parcels and intensive chaotic mixing.

### REFERENCES

- [1] A. Bower, A simple kinematic mechanism for mixing fluid parcels across a meandering jet. *J. Phys. Oceanography*, Vol.21 N 1, pp.173-180, 1991.
- [2] A. Bower, H. Rossby, Evidence of cross-frontal exchange in the Gulf Stream based isopycnal RAFOS float data *J. Phys. Oceanography*, Vol.19 N 9, pp.173-180, 1989.
- [3] R. Somelson, Fluid exchange across a meandering jet *J. Phys. Oceanography*, Vol.22 N 4, pp.431-440, 1992.
- [4] H. Dijkstra, *Nonlinear Physical Oceanography*, Springer, New York, 2005.
- [5] T. Krasnopolskaya, V. Il'chenko, Kinematic model of Gulf Stream. – *Applied Hydromech.*, Vol.10 N 4, pp.41-53, 2008.
- [6] J. Zimmerman, The tidal whirlpool: a review of horizontal dispersion by tidal and residual currents *Neth. J. Sea Res.*, Vol.20 N 2/3, pp.133-154, 1986.
- [7] R. Somelson, S.Wiggins, *Lagrangian Transport in Geophysical Jets and Waves*, Springer, New York, 2005.
- [8] C. Jones, S.Winkler *Invariant manifold and Lagrangian dynamics in the ocean and atmosphere*. In: Handbook of Dynamics system (Ed.B.Fiedler), Vol.2,Elsevier Science B. V., Amsterdam, pp.55-92, 2002.

**GEOMETRICALLY NON-LINEAR VIBRATION AND MESHLESS DISCRETIZATION OF THE COMPOSITE LAMINATED SHALLOW SHELLS WITH COMPLEX SHAPE**

**L.V. Kurpa<sup>1</sup>**  
National Technical  
University «KhPI»,  
Kharkov, Ukraine

---

ABSTRACT

---

To study the geometrically non-linear vibrations of the composite laminated shallow shells with complex plan form the approach, based on meshless discretization, is proposed. Non-linear equations of motion for shallow shells based on the first order shear deformation shell theories are considered. The discretization of the motion equations is carried out by method based on expansion of the unknown functions in series for which eigenvectors of the linear vibration obtained by RFM (R-functions method) are employed as basic functions. The factors of these series are functions (generalizing coordinates) depending on time. Due to applying the basic variational principle in mechanics by Ostrogradsky-Hamilton the corresponding system of the ordinary differential equations by Euler is obtained. The non-linear ordinary differential equations are derived in terms of amplitudes of the vibration modes. The offered method is expounded for multi-modal approximation of unknown functions. Backbone curves of the spherical shallow shell with complex plan form are obtained using only the first vibration mode by the Bubnov-Galerkin method. The effects of lamination schemes on the behavior are discussed.

---

**INTRODUCTION**

Research of the geometrically non-linear vibrations of the laminated plates and open shells of different form is one of important issues of nonlinear dynamics. Due to complexity of the mathematical simulations this problem in general case may be only solved by numerical methods. Many researchers are studying this problem [1,3-5,8,9,11]. Some review of achievements in this field is presented in works [3,8,9]. The main approach which is applied to solve this problem is finite elements method (FEM) combined with method of harmonic balance, Bubnov-Galerkin, multiscales method and another. In studies [6,7] the R-functions method (RFM) has been employed and the new method of the discretization has been proposed. But this approach is effective one for laminated plates and with some accuracy can be applied to higher shallow shells. In the given paper the algorithm of meshless discretization, based on combination of the classical approaches and modern constructive means of the R-functions theory is developed. The considered approach is based on multiple-modes approximation in time of the unknown functions. It allows studying the geometrically non-linear dynamic response of the shallow shells with complex shape and different boundary conditions.

**1. FORMULATION OF THE PROBLEM**

Let us consider a laminated shallow shell of an arbitrary plan form with radii curvature  $R_x, R_y$  which consists of  $S$  layers of the constant thickness  $h_i$ . The general thickness  $h$  is defined as

$$h = \sum_{i=1}^S h_i.$$

Assume that shell under consideration has symmetric relatively of the midsurface lamination scheme and its projection in a plane is some domain  $\Omega$ . Delaminating between the layers is not. Due to shallowness the curvilinear coordinates commonly employed in shells can be directly replaced

---

<sup>1</sup> Corresponding author. Email [Kurpa@kpi.kharkov.ua](mailto:Kurpa@kpi.kharkov.ua)

by the Cartesian coordinates  $x$  and  $y$ , and the Lamé parameters are:  $A=1$ ,  $B=1$ . The displacement components at an arbitrary point of the shell are  $U$ ,  $V$ , and  $W$  in the  $x$ ,  $y$  and  $z$  directions respectively. Investigation we will carry out by first-order shear deformation theory [1,2,9].

According to the first-order shear deformation theory (FSDT) it is assumed that in-plane displacements  $U$  and  $V$  are linear functions of coordinate  $z$ , and that the transverse displacement  $W$  is constant through the thickness of the shell.

The normal to the midsurface remains straight after deformation, but not necessarily normal to the middle surface. The non-linear strain-displacement relations of the plates can be written as

$$\begin{aligned} e_x &= \varepsilon_x + z\chi_x, \quad e_y = \varepsilon_y + z\chi_y, \quad e_{xy} = \varepsilon_{xy} + z\chi_{xy}, \\ e_z &= 0, \quad e_{xz} = w_{,x} - uk_x + \psi_x, \quad e_{yz} = w_{,y} - vk_y + \psi_y \end{aligned}$$

where

$$\begin{aligned} \varepsilon_x &= u_{,x} + \frac{w}{R_x} + \frac{1}{2}w_{,x}^2, \quad \varepsilon_y = v_{,y} + \frac{w}{R_y} + \frac{1}{2}w_{,y}^2, \quad \varepsilon_{xy} = u_{,y} + v_{,x} + w_{,x}w_{,y}, \\ \varepsilon_{xz} &= w_{,x} + \psi_x, \quad \varepsilon_{yz} = w_{,y} + \psi_y, \quad \chi_x = \psi_{x,x}, \quad \chi_y = \psi_{y,y}, \quad \chi_{xy} = \psi_{x,y} + \psi_{y,x}. \end{aligned} \quad (1)$$

In these equations the subscripts following comma denote the partial differentiation and  $u$ ,  $v$  and  $w$  are the displacements at the midsurface,  $\psi_x$  and  $\psi_y$  are the rotations about the  $y$ - and  $x$ -axes respectively. Let us denote as vectors  $\{\varepsilon\} = \{\varepsilon_x; \varepsilon_y; \varepsilon_{xy}\}^T$ ,  $\{k\} = \{\psi_{x,x}; \psi_{y,y}; \psi_{x,y} + \psi_{y,x}\}^T$ , stresses  $\{N\} = \{N_x; N_y; N_{xy}\}^T$  and moments resultants  $\{M\} = \{M_x; M_y; M_{xy}\}^T$

The constitutive relations of the symmetrically laminated shell can be presented as follows

$$\begin{Bmatrix} N \\ M \end{Bmatrix} = \begin{bmatrix} C & 0 \\ 0 & D \end{bmatrix} \begin{Bmatrix} \varepsilon \\ k \end{Bmatrix}, \quad \begin{Bmatrix} Q_y \\ Q_x \end{Bmatrix} = \begin{bmatrix} C_{44} & C_{45} \\ C_{45} & C_{55} \end{bmatrix} \begin{Bmatrix} \varepsilon_{yz} \\ \varepsilon_{xz} \end{Bmatrix}, \quad (2)$$

where

$$C = \begin{bmatrix} C_{11} & C_{12} & C_{16} \\ C_{12} & C_{22} & C_{26} \\ C_{16} & C_{26} & C_{66} \end{bmatrix}, \quad D = \begin{bmatrix} D_{11} & D_{12} & D_{16} \\ D_{12} & D_{22} & D_{26} \\ D_{16} & D_{26} & D_{66} \end{bmatrix}, \quad (3)$$

Constants  $C_{ij}$  and  $D_{ij}$  (elements of matrices  $[C]$  and  $[D]$  respectively) are the stiffness coefficients of the shell, which are defined by the following expressions:

$$(C_{ij}, D_{ij}) = \sum_{m=1}^S \int_{h_m}^{h_{m+1}} B_{ij}^{(m)}(1, z^2) dz, \quad (i, j = 1, 2, 6), \quad C_{ij} = k_i^2 \sum_{m=1}^S \int_{h_m}^{h_{m+1}} B_{ij}^{(m)} dz, \quad (i, j = 4, 5)$$

Here  $B_{ij}^{(m)}$  are stiffness coefficients of the  $m$ -th layer,  $k_i$ ,  $i = \overline{4,5}$  are shear correction factors and  $h_m$  is the distance from the midsurface to the upper surface of the  $m$ -th layer. Usually the value  $k_i^2$ ,  $i = \overline{4,5}$  are taken equal to  $5/6$ . Next, we assume that  $k_4 = k_5$ , that is.  $C_{45} = C_{54}$ .

On the other part,  $\varepsilon = \varepsilon^{(L)} + \varepsilon^{(NL)}$ , where

$$\varepsilon^{(L)} = \left\{ u_{,x} + \frac{w}{R_x}; v_{,y} + \frac{w}{R_y}; u_{,y} + v_{,x} \right\}^T, \quad \varepsilon^{(NL)} = \frac{1}{2} (w_{,x}^2; w_{,y}^2; 2w_{,x}w_{,y})^T \quad (4)$$

Vector  $N = \{N_x; N_y; N_{xy}\}^T$  can also be written as follows:

$$N = N^{(L)} + N^{(NL)}, \quad N^{(L)} = C\varepsilon^{(L)}, \quad N^{(NL)} = -C\varepsilon^{(NL)} \quad (5)$$

If mass density is the same and constant for all layers and layers have the same thickness then the kinetic energy of the shell can be written as

$$T = \frac{\rho h}{2} \iint_{\Omega} \left( (u_t^2 + v_t^2 + w_t^2) + \frac{h^2}{12} (\psi_{x,t}^2 + \psi_{y,t}^2) \right) d\Omega \quad (6)$$

The strain energy of the shell is given by

$$P = \frac{1}{2} \iint_{\Omega} (N_x \varepsilon_x + N_y \varepsilon_y + N_{xy} \varepsilon_{xy} + Q_x \varepsilon_{xz} + Q_y \varepsilon_{yz} + M_x k_x + M_y k_y + M_{xy} k_{xy}) d\Omega \quad (7)$$

As shown in works [2, 8, 9] the movement equations may be obtained by Hamilton's principle

$$\int_{t_0}^{t_1} \delta(T - P) dt = 0 \quad (8)$$

Let us write the system of differential equations of the motion in operator form:

$$LU = NL + mU_{,tt}$$

where  $U, m$  are vectors  $U = \{u; v; w; \psi_x; \psi_y\}^T$ ,  $m = \{m_1, m_1, m_1, m_2, m_2\}^T$ , ( $m_1 = \rho h$ ,  $m_2 = \frac{\rho h^3}{12}$ ),

$L$  is matrix  $L = [L_{ij}]_{i,j=1,5}^{\overline{1,5}}$ . The elements  $L_{ij}$ ,  $i, j = \overline{1,5}$  of the matrix  $L$  are linear operators:

$$\begin{aligned} L_{11} &= C_1 \partial^2 - k_1^2 C_{55}, & L_{12} &= ((C_{16}, (C_{12} + C_{66}), C_{26}), \partial^2) - k_1 k_2 C_{45}, \\ L_{13} &= ((k_1(C_{11} + C_{55}) + C_{12} k_2, k_1(C_{16} + C_{45}) + C_{26} k_2), \partial), & L_{14} &= k_1 C_{55}, & L_{15} &= k_1 C_{45}, \\ L_{21} &= L_{12}, & L_{22} &= C_3 \partial^2 - k_2^2 C_{44}, & L_{23} &= ((k_1 C_{16} + k_2(C_{26} + C_{45}), k_1 C_{12} + k_2(C_{22} + C_{44})), \partial), \\ L_{24} &= k_2 C_{45}, & L_{25} &= k_2 C_{44}, & L_{31} &= -L_{13}, & L_{32} &= -L_{23}, \\ L_{33} &= ((C_{55}, C_{45}, C_{44}), \partial^2) - k_1^2 - 2k_1 k_2 - k_2^2, & L_{34} &= ((C_{55}, C_{45}), \partial), & L_{35} &= ((C_{45}, C_{44}), \partial), \\ L_{41} &= L_{14}, & L_{42} &= k_2 C_{44}, & L_{43} &= -L_{43}, & L_{44} &= D_1 \partial^2 - C_{55}, \\ L_{45} &= ((D_{16}, (D_{12} + D_{66}), D_{26}), \partial^2) - C_{44}, & L_{51} &= L_{15}, & L_{52} &= L_{25}, & L_{53} &= -L_{35}, \\ L_{54} &= ((D_{16}, (D_{12} + D_{66}), D_{26}), \partial^2) - C_{45}, & L_{55} &= D_3 \partial^2 - C_{44}, \end{aligned}$$

where  $\{C_i\}$  and  $\{D_i\}$  are  $i$ -th rows of the matrixes  $[C]$  and  $[D]$  relatively,  $\partial$  and  $\partial^2$  are differential operators which are defined as  $\partial = \{\partial_{,x}; \partial_{,y}\}^T$ ,  $\partial^2 = \{\partial_{,xx}; 2\partial_{,xy}; \partial_{,yy}\}^T$ .

The components  $NL_i$ ,  $i = \overline{1,3}$  of the vector  $NL = \{NL_1(w), NL_2(w), NL_3(u, v, w), 0, 0\}^T$  are nonlinear operators  $NL_1(w) = N_x^{(NI)},_x + N_{xy}^{(NI)},_y$ ,  $NL_2(w) = N_{xy}^{(NI)},_x + N_y^{(NI)},_x$ ,

$$NL_3(u, v, w) = (N_x w_{,x} + N_{xy} w_{,y}),_x + (N_{xy} w_{,x} + N_y w_{,y}),_y - k_1 N_x^{(NI)} - k_2 N_y^{(NI)}$$

## 2. SOLUTION PROCEDURE

Obviously that the first step is reduced to study linear problem in order to find the eigen functions  $\{U^{(c)}\} = \{u^{(c)}, v^{(c)}, w^{(c)}, \psi_x^{(c)}, \psi_y^{(c)}\}^T$  satisfying the given boundary conditions and the appropriate natural frequencies of linear vibrations shells. Note that solving linear problem we will not ignore inertia and rotation forces. Solution of linear problems has been widely discussed in works [6,7]. Let us note that in generic case this problem may be solved by RFM [10].

Let us consider in detail the solving non-linear problem. The unknown function are presented as

$$\begin{aligned} u(x, y, t) &= \sum_{k=1}^n X_k(t) u_k^{(c)}(x, y), & v(x, y, t) &= \sum_{k=1}^n Y_k(t) v_k^{(c)}(x, y), & w(x, y, t) &= \sum_{k=1}^n Z_k(t) w_k^{(c)}(x, y) \\ \psi_x(x, y, t) &= \sum_{k=1}^n R_{xk}(t) \psi_{xk}^{(c)}(x, y), & \psi_y(x, y, t) &= \sum_{k=1}^n R_{yk}(t) \psi_{yk}^{(c)}(x, y) \end{aligned} \quad (9)$$

where  $u_k^{(c)}(x, y)$ ,  $v_k^{(c)}(x, y)$ ,  $w_k^{(c)}(x, y)$ ,  $\psi_{xk}^{(c)}(x, y)$ ,  $\psi_{yk}^{(c)}(x, y)$  are  $k$ -th eigenfunctions of linear vibrations of the shell and  $X_k(t), Y_k(t), Z_k(t), R_{kx}(t), R_{ky}(t)$  are unknown functions in time. The following notation is introduced for brevity,  $q = \{X_k, Y_k, Z_k, R_{kx}, R_{ky}\}^T$ ,  $k = \overline{1, n}$ . The generic element of the time-dependent vector  $q$  is referred to as  $q_j$ . The dimension of  $q$  is  $\overline{N}$ , which is number of freedom used in the mode expansion. In order to obtain the discretized equations we will apply the main variational principle in mechanics (8) by Ostrogradsky-Hamilton. The corresponding system of equations by Euler (or Lagrange equations [2]) takes the form

$$\frac{d}{dt} \left( \frac{\partial T}{\partial \dot{q}_j} \right) - \frac{\partial T}{\partial q_j} + \frac{\partial P}{\partial q_j} = Q_j, \quad j = \overline{1, \overline{N}} \quad (10)$$

where  $T$  is kinetic energy and  $P$  is potential energy of the system,  $Q_j$  are the generalized forces obtained by differentiation of Rayleigh's dissipation function  $F$  and the virtual work  $W$  done by external forces. In the given case we assume that viscous damping is absent (e.g.  $F = 0$ ),  $\frac{\partial T}{\partial q_j} = 0$ . So the

equations (10) is simplified and taken the following form

$$\frac{d}{dt} \left( \frac{\partial T}{\partial \dot{q}_j} \right) + \frac{\partial P}{\partial q_j} = \frac{\partial W}{\partial q_j}, \quad j = \overline{1, \overline{N}} \quad (11)$$

The virtual work  $W$  done by external forces is written as

$$W = \iint_{\Omega} q_z w d\Omega$$

Let us put  $q_z = \tilde{f} \cos(\omega_e t)$ , where  $\omega_e$  is the excitation frequency,  $\tilde{f}$  is force magnitude positive in  $z$  direction. It should be noted that in nonlinear case we will ignore by inertia and rotation forces. Therefore

$$\frac{d}{dt} \left( \frac{\partial T}{\partial \dot{q}_j} \right) = \begin{cases} 0, & j = 1, 2, 3, \dots, N, \\ 0, & j = N + 1, N + 2, \dots, 2N, \\ \rho h q_{j,tt} \iint_{\Omega} w_j^2 d\Omega, & j = 2N + 1, 2N + 2, \dots, 3N, \\ 0, & j = 3N + 1, 3N + 2, \dots, 4N, \\ 0, & j = 4N + 1, 4N + 2, \dots, 5N \end{cases} \quad (12)$$

$$\frac{dw}{dq_j} = \begin{cases} 0, & j = 1, 2, 3, \dots, N, \\ 0, & j = N + 1, N + 2, \dots, 2N, \\ \tilde{f} \cos(\omega_e t) \iint_{\Omega} w_j d\Omega, & j = 2N + 1, 2N + 2, \dots, 3N, \\ 0, & j = 3N + 1, 3N + 2, \dots, 4N, \\ 0, & j = 4N + 1, 4N + 2, \dots, 5N \end{cases} \quad (13)$$

$$\frac{\partial P}{\partial q_j} = \sum_{i=1}^{\overline{N}} f_{ji} q_i + \sum_{i=1}^{\overline{N}} \sum_{k=1}^{\overline{N}} f_{jik} q_i q_k + \sum_{i=1}^{\overline{N}} \sum_{k=1}^{\overline{N}} \sum_{l=1}^{\overline{N}} f_{jikl} q_i q_k q_l \quad (14)$$

Substituting the expressions (12-14) into equations (11) we can see that equation, corresponding  $j = \overline{1, 2N}$ , and  $j = \overline{3N + 1, 5N}$  are homogeneous algebraic equations in variables  $q_j(t)$ . Therefore it is possible to find the dependence between vectors  $X(t), Y(t), R_x(t), R_y(t)$  and  $Z(t)$  in formulas (9). As result we obtain the system of  $n$  nonlinear differential equations in variables  $Z_j(t)$  of the following type:

$$Z''_j(t) + \alpha_j Z_j(t) + \sum_{i=1}^n \sum_{k=1}^n \beta_{jik} Z_i(t) Z_k(t) + \sum_{i=1}^n \sum_{k=1}^n \sum_{l=1}^n \gamma_{jikl} Z_i(t) Z_k(t) Z_l(t) = \gamma_j \tilde{f} \cos \omega_e t,$$

$$j = \overline{1, n}$$

The solving obtained system of ordinary differential equations can be performed using various approximate methods, such as the harmonic balance method (HBM), multiscale method, method of the Runge-Kutta, Bubnov-Galerkin and others.

The implementation of the proposed method will be carry out in framework POLE-RL system and MATLAB.

### 3. NUMERICAL RESULTS

The foregoing method was tested for shallow shells supported on rectangular plan form and

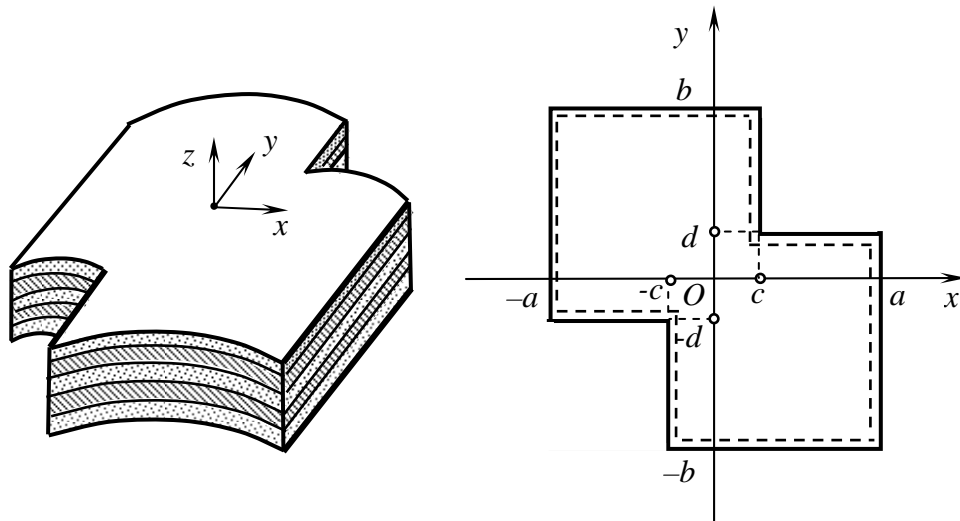


Fig. 1. The shallow shell with complex shape

obtained results have been in good agreement with available ones. Below we present the results for simply supported shells with plan form shown in Fig. 1.

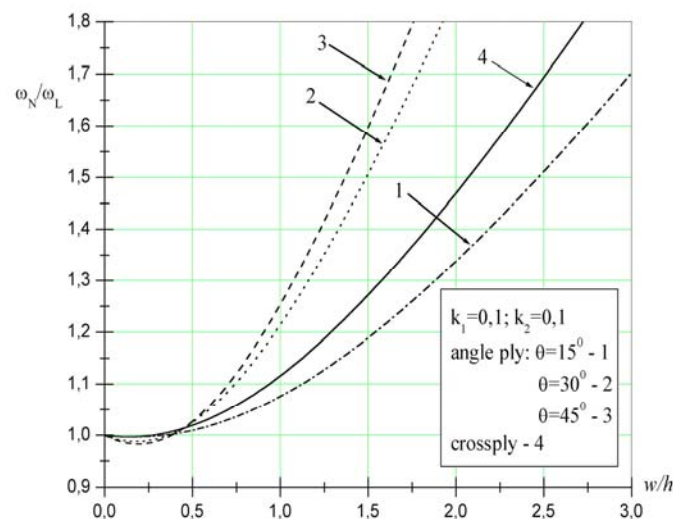


Fig.2. Backbone curves for spherical shell

It is assumed that the shell has five layers which are symmetrical relatively of middle surface. It is made of a material with the following mechanical characteristics:  $E = 25E_2$ ,  $G_{12} = G_{13} = 0.5E_2$ ,  $G_{23} = 0.2E_2$ ,  $\nu_{12} = 0.25$ . The shear factors are taken to be  $k_4^2 = k_5^2 = 5/6$ . The geometric parameters of the shell are taken as follows  $b/a = 1$ ,  $c/(2a) = d/(2a) = 0.25$ ,  $2a/R_x = 2a/R_y = 0.1$ ,  $h/(2a) = 0.1$ . The lamina scheme

is: angle-ply  $(\theta^0 / -\theta^0 / \theta^0 / -\theta^0 / \theta^0)$  and cross-ply  $(0^0 / 90^0 / 0^0 / 90^0 / 0^0)$ . For solving the procedure by Bubnov-Galerkin has been applied using only one-mode approximation.

In Fig. 2 the backbone curves for angle-ply  $\theta = 15^0, 30^0, 45^0$  and cross-ply spherical shells are presented. From analysis backbone curves it follows that the behavior of the curves has soft type for angle-ply spherical shells if  $\theta = 30^0$  and  $\theta = 45^0, 0 < w_{\max} / h < 0.4$ . For cross-ply shells and plate the corresponding backbone curves have a hard type.

## CONCLUSIONS

A numerically-analytic method is proposed to solve nonlinear vibration problems for symmetric laminated shallow shells with complex plan form. The method is worked out in frame of the refined shell theory of the first order taking shear deformation into account, and geometric nonlinear theory by von Karman-type. The created method is based on the R-functions theory and variational methods. Using multi-model approximation the initial problem has been reduced to system of the nonlinear ordinary differential equation, which may be solved by numerical approach. The method is illustrated on example of the five-layer simply supported spherical and cylindrical shallow shells which is rested on the plan of the complicated form. The layers of shell under consideration have the different lamina schemes. Effect of curvatures is studied for backbone curves.

## REFERENCES

- [1] Abe A., Kobayashi Y., Yamada G. Nonlinear dynamic behaviors of clamped laminated shallow shells with one-to-one internal resonance *Journal of Sound and Vibration*, Vol. 304, pp. 957-968, 2007.
- [2] Ambartsumian S.A. *The general theory of anisotropic shells*, Nauka, Moscow, 1974 (in Russian).
- [3] Amabili M. *Nonlinear Vibrations and Stability of Shells and Plates*, University of Parma, Italy, 2008.
- [4] Chia C.Y. Nonlinear analysis of doubly curved symmetrically laminated shallow shells with rectangular planform *Ingenieur-Archiv*, Vol. 58, pp. 252-264, 1988.
- [5] Haldar S. Free vibration of composite skewed cylindrical shell panel by finite element method *Journal of Sound and Vibration*, Vol. 311, pp.9-19, 2008.
- [6] Kurpa L.V. Nonlinear Free Vibrations of Multilayer Shallow Shells with a Symmetric Structure and with a Complicated Form of the Plan *J. Mathem. Methods and Physic. Mech. Polya*, Vol.51(2), pp.75-85, 2008 (in Russian).
- [7] Kurpa L.V., Timchenko G.N. Investigation into nonlinear vibrations of composite plates using the R-function theory *J. Strength of Materials*, Vol. 39(5), pp.529-538, 2007.
- [8] Qatu M. S. *Vibration of Laminated Shells and Plates*, Elsevier Ltd., Oxford, 2004.
- [9] Reddy J.N., Arciniega R.A. Shear Deformation Plate and Shell Theories: From Stavsky to Present *J. Mechanics of Advanced Materials and Structures*, Vol. 11, pp.535-582, 2004.
- [10] Rvachev V. L. *Theory of R-functions and some of its applications*, Naukova Dumka, Kiev, 1982 (in Russian).
- [11] Singh A.V. Linear and geometrically nonlinear vibrations of fiber reinforced laminated plates and shallow shells, *Computers and Structures*, Vol. 76, pp.277-285, 2000.

**MULTI-MODAL GEOMETRICAL NON-LINEAR FREE VIBRATIONS OF  
COMPOSITE LAMINATED PLATES WITH THE COMPLEX SHAPE**

**L.V. Kurpa<sup>1</sup>**  
**N.A. Budnikov<sup>2</sup>**  
National Technical  
University,  
Kharkov, Ukraine

---

ABSTRACT

---

Geometrically non-linear free vibrations of the composite laminated plates are investigated using new multi-modal approach to discretization of motion equations. The non-linear governing equations for laminated plates are derived by Hamilton's principle using first-order shear deformation theory. Due to proposed algorithm of the discretization all unknown functions except of transverse displacement are eliminated and governing equations are reduced to system of ordinary differential equations in time by the Bubnov-Galerkin procedure. The expansion of all unknown functions in the truncated Fourier series is performed using the eigenfunctions of the linear vibration problems and solutions of the sequence of elasticity problems. All auxiliary problems are solved by RFM (R-functions method).

---

**INTRODUCTION**

Composite materials have essential advantages with compare to isotropic materials. They possess high stiffness-to-weight ratio, high strength-to-weight ratio and another properties. So these materials are intensively used in many industrial fields. The laminated composite plates simulate many elements of modern thin-walled structures. Therefore, there have been many numbers of papers concerned with non-linear vibrations of laminated plates [1-10]. But it is impossible to say that the problem is solved, because here many unsolved questions occur. One of them is connected with geometry and boundary conditions.

In the given paper the new approach to discretization is proposed. The considered approach allows to perform multi-modal approximation in time and to analyze the geometrical non-linear free dynamic response of the plates with complex shape and different boundary conditions. This approach is based on using of the R-functions method (RFM), that is, on joined application of the variational methods and the R-functions theory. For implementation of proposed method it is needed to solve series problems: linear problem about free vibrations laminated plates and the sequence of elasticity problems.

**1. Formulation of the geometrically non-linear free vibration symmetrically laminated composite plates**

The laminated plate with an arbitrary shape, which consists of  $N$  layers of the constant thickness  $h_i$  is considered. The general thickness  $h$  is defined as  $h = \sum_{i=1}^N h_i$ . The coordinate system

$(x, y, z)$  is taken in the midsurface of the plate. The displacement components at an arbitrary point of the plate are  $U$ ,  $V$ , and  $W$  in the  $x$ ,  $y$  and  $z$  directions respectively. Assume that plate is symmetrically laminated with respect to midsurface and delamination between the layers is not. Investigation we will carry out by first-order shear deformation theory [11, 15, 16].

---

<sup>1</sup> Corresponding author. Email [Kurpa@kpi.kharkov.ua](mailto:Kurpa@kpi.kharkov.ua)

<sup>2</sup> Corresponding author. Email [Nicolas.Budnikov@gmail.com](mailto:Nicolas.Budnikov@gmail.com)

According to this theory it is assumed that in-plane displacements  $U$  and  $V$  are linear functions of coordinate  $z$ , and that the transverse displacement  $W$  is constant through the thickness of the plate. So displacements are presented as

$$U = u + z\psi_x, V = v + z\psi_y, W = w, \quad (1)$$

where  $u$ ,  $v$  and  $w$  are the displacements at the midsurface,  $\psi_x$  and  $\psi_y$  are the rotations of the midsurface about the  $y$ - and  $x$ -axes respectively.

The normal to the midsurface remains straight after deformation, but not necessarily normal to the middle surface. The non-linear strain-displacement relations of the plates can be written as

$$e_x = \varepsilon_x + z\chi_x, e_y = \varepsilon_y + z\chi_y, e_z = 0, e_{xy} = \varepsilon_{xy} + z\chi_{xy}, e_{xz} = w_{,x} + \psi_x, e_{yz} = w_{,y} + \psi_y$$

in which

$$\varepsilon_x = u_{,x} + \frac{1}{2}w_{,x}^2, \varepsilon_y = v_{,y} + \frac{1}{2}w_{,y}^2, \varepsilon_{xy} = u_{,y} + v_{,x} + w_{,x}w_{,y}, \varepsilon_{xz} = w_{,x} + \psi_x, \varepsilon_{yz} = w_{,y} + \psi_y$$

$$\chi_x = \psi_{x,x}, \chi_y = \psi_{y,y}, \chi_{xy} = \psi_{x,y} + \psi_{y,x}$$

In these equations the subscripts following comma denote the partial differentiation.

The constitutive relations of the symmetrically laminated plate can be expressed as follows

$$\begin{aligned} \{N\} &= [C] \cdot \{\varepsilon\} \\ \{M\} &= [D] \cdot \{\psi\} \end{aligned}, \quad (2)$$

$$\{Q\} = \begin{Bmatrix} Q_x \\ Q_y \end{Bmatrix} = \begin{bmatrix} C_{55} & C_{54} \\ C_{45} & C_{44} \end{bmatrix} \begin{Bmatrix} \varepsilon_{xz} \\ \varepsilon_{yz} \end{Bmatrix}$$

where

$$\{N\} = \{N_x; N_y; N_{xy}\}^T, \{M\} = \{M_x; M_y; M_{xy}\}^T, [C] = \begin{bmatrix} C_{11} & C_{12} & C_{16} \\ C_{12} & C_{22} & C_{26} \\ C_{16} & C_{26} & C_{66} \end{bmatrix}, [D] = \begin{bmatrix} D_{11} & D_{12} & D_{16} \\ D_{12} & D_{22} & D_{26} \\ D_{16} & D_{26} & D_{66} \end{bmatrix}$$

$$\{\varepsilon\} = \{\varepsilon_x; \varepsilon_y; \varepsilon_{xy}\}^T, \{\psi\} = \{\psi_{x,x}; \psi_{y,y}; \psi_{x,y} + \psi_{y,x}\}^T$$

On the other part,  $\{\varepsilon\} = \{\varepsilon^{(L)}\} + \{\varepsilon^{(NL)}\}$ , where

$$\{\varepsilon^{(L)}(u, v)\} = \{u_{,x}; v_{,y}; u_{,y} + v_{,x}\}^T, \{\varepsilon^{(NL)}(w)\} = \frac{1}{2} \{w_{,x}^2; w_{,y}^2; 2w_{,x}w_{,y}\}^T$$

Vector  $\{N\}$  can also be written as follows:

$$\{N\} = \{N^{(L)}\} + \{N^{(NL)}\}, \{N^{(L)}\} = [C] \cdot \{\varepsilon^{(L)}\}, \{N^{(NL)}\} = [C] \cdot \{\varepsilon^{(NL)}\}$$

Stiffness coefficients  $C_{ij}$  and  $D_{ij}$  (elements of matrices  $[C]$  and  $[D]$  respectively) are defined by the following expressions:

$$(C_{ij}, D_{ij}) = \sum_{m=1}^n \int_{h_m}^{h_{m+1}} B_{ij}^{(m)}(1, z^2) dz, \quad (i, j = 1, 2, 6), \quad C_{ij} = k_i^2 \sum_{m=1}^n \int_{h_m}^{h_{m+1}} B_{ij}^{(m)} dz, \quad (i, j = 4, 5)$$

Here  $B_{ij}^{(m)}$  are stiffness coefficients of the  $m$ -th layer,  $k_i$ ,  $i = \overline{4, 5}$  are shear coefficients.

Usually the value  $k_i^2$ ,  $i = \overline{4, 5}$  are taken equal to  $5/6$ . Further, we assume that  $k_4 = k_5$ , so  $C_{45} = C_{54}$ .

Coefficients  $m_i$ ,  $i = \overline{1, 2}$  are calculated by the formulas:

$$(m_1, m_2) = \sum_{m=1}^n \int_{h_m}^{h_{m+1}} \rho_m(1, z^2) dz$$

As shown in works [2, 8, 10] the movement equations may be obtained by the Hamilton's principle which is supplemented by appropriate boundary and initial conditions.

Let us write the system of differential equations of the motion in operator form:

$$[L]\{U\} = \{NL\} + \{m\}\{0, 0, w, \psi_x, \psi_y\}_{,tt}^T, \quad (4)$$

where

$$\begin{aligned} \{U\} &= \{u, v, w, \psi_x, \psi_y\}^T, \quad \{m\} = \{m_1, m_1, m_1, m_2, m_2\}^T \\ [L] &= \begin{bmatrix} L_{11} & L_{12} & 0 & 0 & 0 \\ L_{21} & L_{22} & 0 & 0 & 0 \\ 0 & 0 & L_{33} & L_{34} & L_{35} \\ 0 & 0 & L_{43} & L_{44} & L_{45} \\ 0 & 0 & L_{53} & L_{54} & L_{55} \end{bmatrix} \\ \{NL\} &= \{NL_1(w), NL_2(w), NL_3(u, v, w), 0, 0\}^T \end{aligned}$$

Here linear operators  $L_{ij}$ ,  $i, j = \overline{1,5}$  and nonlinear operators  $NL_i$ ,  $i = \overline{1,3}$  are defined as:

$$\begin{aligned} L_{11}(C) &= ((C_{11}, C_{16}, C_{66}), \nabla^2), \quad L_{12}(C) = L_{21}(C) = ((C_{16}, (C_{12} + C_{66}), C_{26}), \nabla^2), \quad L_{22}(C) = ((C_{66}, C_{26}, C_{22}), \nabla^2), \\ L_{33}(C) &= ((C_{55}, (C_{45} + C_{54}), C_{44}), \nabla^2), \quad L_{34}(C) = -L_{43}(C) = ((C_{55}, C_{45}), \nabla), \quad L_{35}(C) = -L_{53}(C) = ((C_{45}, C_{44}), \nabla), \\ L_{44}(C, D) &= L_{11}(D) - C_{55}, \quad L_{45}(C, D) = L_{54}(C, D) = L_{12}(D) - C_{45}, \quad L_{55}(C, D) = L_{22}(D) - C_{44}, \\ NL_1(w) &= -(\{L_{11}w, L_{12}w\}, \nabla w), \quad NL_2(w) = -(\{L_{12}w, L_{22}w\}, \nabla w), \quad NL_3(u, v, w) = -\{N\}^{NL} \nabla^2 w \end{aligned}$$

$$\text{where } \{\nabla\} = \left\{ \frac{\partial}{\partial x}, \frac{\partial}{\partial y} \right\}^T, \quad \{\nabla^2\} = \left\{ \frac{\partial^2}{\partial x^2}, 2 \frac{\partial^2}{\partial x \partial y}, \frac{\partial^2}{\partial y^2} \right\}^T$$

## 2. METHOD OF SOLUTION

Let us solve the linear problem of vibrations of the laminated plates. In general case the solving algorithm of this problem is developed by RFM and described in works [12–15]. Note that solving linear problem we will not ignore inertia and rotation forces.

The solution of the nonlinear problem (4) will be sought in the following form of:

$$\begin{cases} u(x, y, t) = \sum_{i=1}^n \sum_{j=1}^n y_i(t) \cdot y_j(t) \cdot u_{ij}(x, y) \\ v(x, y, t) = \sum_{i=1}^n \sum_{j=1}^n y_i(t) \cdot y_j(t) \cdot v_{ij}(x, y) \\ w(x, y, t) = \sum_{i=1}^n y_i(t) \cdot w_i^{(c)}(x, y) \\ \psi_x(x, y, t) = \sum_{i=1}^n y_i(t) \cdot \psi_{xi}^{(c)}(x, y) \\ \psi_y(x, y, t) = \sum_{i=1}^n y_i(t) \cdot \psi_{yi}^{(c)}(x, y) \end{cases} \quad (5)$$

where  $w_i^{(c)}(x, y)$ ,  $\psi_{xi}^{(c)}(x, y)$ ,  $\psi_{yi}^{(c)}(x, y)$  are eigenfunctions of linear vibrations of plate and  $u_{ij}(x, y)$ ,  $v_{ij}(x, y)$  are unknown functions.

Vector of eigenfunctions  $\{U^{(c)}\}$  and the natural frequencies of linear oscillations of the plate we can find by solving of the corresponding linear problem:

$$[L]\{U^{(c)}\} = \{m\}\{U\}_{,tt}^T, \quad (6)$$

where

$$\{U^{(c)}\} = \{u^{(c)}, v^{(c)}, w^{(c)}, \psi_x^{(c)}, \psi_y^{(c)}\}^T.$$

Solving of the linear problem we will not ignore by inertial forces. Solution of linear problems has been widely discussed [14,15], so details on this will not be dealt.

Let us substitute the relations (5) into the first two equations of the system (4). Then a system for finding the unknown functions  $u_{ij}(x, y)$  and  $v_{ij}(x, y)$  will be got as

$$\begin{bmatrix} L_{11}(C, \cdot) & L_{12}(C, \cdot) \\ L_{12}(C, \cdot) & L_{22}(C, \cdot) \end{bmatrix} \begin{Bmatrix} u_{ij} \\ v_{ij} \end{Bmatrix} = - \begin{bmatrix} L_{11}(C, w_j^{(c)}) & L_{12}(C, w_j^{(c)}) \\ L_{12}(C, w_j^{(c)}) & L_{22}(C, w_j^{(c)}) \end{bmatrix} \cdot \begin{Bmatrix} w_i^{(c)},_x \\ w_i^{(c)},_y \end{Bmatrix} \quad (7)$$

Note that the system of equations (7), supplemented by appropriate boundary conditions, coincides with the resolution of the system of equations of equilibrium for plane elasticity problem of anisotropic plate. Solving of this problem will also perform with the RFM method. Variation formulation of the problem is represented by the Lagrange functional

$$J(u_{ij}, v_{ij}) = \iint_{\Omega} \left( \{N(u_{ij}, v_{ij}, w_i^c, w_j^{(c)})\}^T \cdot \{\mathcal{E}^{(L)}(u_{ij}, v_{ij})\} \right) d\Omega, \quad (8)$$

where

$$\begin{aligned} \{N(u_{ij}, v_{ij}, w_i^{(c)}, w_j^{(c)})\} &= [C] \cdot \left( \{\mathcal{E}^{(L)}(u_{ij}, v_{ij})\} + \{\mathcal{E}^{(NL)}(w_i^{(c)}, w_j^{(c)})\} \right) \\ \{\mathcal{E}^{(L)}(u_{ij}, v_{ij})\} &= \{u_{ij,x}; v_{ij,y}; u_{ij,y} + v_{ij,x}\}^T \\ \{\mathcal{E}^{(NL)}(w_i^{(c)}, w_j^{(c)})\} &= \frac{1}{2} \left\{ (w_i^{(c)},_x w_j^{(c)},_x), (w_i^{(c)},_y w_j^{(c)},_y), (w_i^{(c)},_x w_j^{(c)},_y + w_i^{(c)},_y w_j^{(c)},_x) \right\}^T \end{aligned}$$

Substituting (5) for unknown functions  $u, v, w, \psi_x$  and  $\psi_y$  to the system (4), we can find that the last two equations are satisfied identically, while the third equation becomes as

$$\begin{aligned} m_1 \cdot \omega_L^2 \cdot \sum_{i=1}^n y_i(t) \cdot w_i^{(c)} &= m_1 \cdot \sum_{i=1}^n y_i''(t) \cdot w_i^{(c)} - \\ &- \left( \sum_{i=1}^n \sum_{j=i+1}^n \sum_{k=1}^n y_k(t) y_i(t) \cdot y_j(t) \cdot \{N(u_{ij}, v_{ij}, w_i^{(c)}, w_j^{(c)})\}^T \cdot \{\nabla^2 w_k^{(c)}\} \right). \end{aligned} \quad (9)$$

Applying the Bubnov-Galerkin's procedure to the equation (9), we can arrive at a nonlinear system of ordinary differential equations for the functions  $y_r(t)$ ,  $r = \overline{1, n}$  of the form:

$$y_r''(t) + \alpha^{(r)} y_r(t) + \sum_{i=1}^n \sum_{j=1}^n \sum_{k=1}^n \gamma_{ijk}^{(r)} y_i(t) y_j(t) y_k(t) = 0, \quad r = \overline{1, n} \quad (10)$$

The coefficients of equations (10) are determined by formulas given below:

$$\alpha^{(r)} = \frac{\omega_{Lr}^2}{\omega_{L1}^2}, \quad \gamma_{ijk}^{(r)} = - \frac{1}{m_1 \cdot \omega_{L1}^2 \cdot \|w_r^{(c)}\|^2} \iint_{\Omega} \left( \{N(u_{ij}, v_{ij}, w_i^{(c)}, w_j^{(c)})\}^T \cdot \{\nabla^2 w_k^{(c)}\} \right) \cdot w_r^{(c)} d\Omega \quad (11)$$

The solving obtained system of ordinary differential equations (10) can be performed using various approximate methods, such as the harmonic balance method (HBM), multiscale method,

method of Runge-Kutt, and other ones. If we use the single-mode approximation [16], i.e., in the expansion for the unknown functions we can preserve only the term corresponding to the fundamental frequency, then, applying the Bubnov-Galerkin method, we can obtain the explicit dependence of the ratio  $\nu(A) = \frac{\omega_N}{\omega_L}$  of nonlinear to linear frequency. This dependence is expressed by the following formula [16]:

$$\nu = \sqrt{1 + \frac{3}{4}\gamma A^2} \quad (12)$$

The implementation of the proposed method will be carry out in framework POLE-RL system and MATLAB.

## REFERENCES

- [1] Won-Hong Lee, Sung-Cheon Han Free and forced vibration analysis of laminated composite plates and shells using a 9-node assumed strain shell element, *Comput. Mech.* 39: 41–58, 2006.
- [2] Harras B., Benamar R., White R. G. Geometrically non-linear free vibration of fully clamped symmetrically laminated rectangular composite plates, *Journal of Sound and Vibration* 251(4), 579–619, 2002.
- [3] Ribeiro P., Petyt M. Non-linear free vibration of isotropic plates with internal resonance, *International Journal of Non-Linear Mechanics* 35, 263–278, 2000.
- [4] Ribeiro P., Petyt M. Multi-modal geometrical non-linear free vibration of fully clamped composite laminated plates, *Journal of Sound and Vibration* 225(1), 127–152, 1999.
- [5] Petyt M., Ribeiro P. Geometrical non-linear periodic vibration of plates, *IMECE 2000*, November 5–10, 2000.
- [6] Maloy K. Singha M. Ganapathi. Large amplitude free flexural vibrations of laminated composite skew plates, *International Journal of Non-Linear Mechanics* 39, 1709 – 1720, 2004.
- [7] Singh A.V. Linear and geometrically nonlinear vibrations of fiber reinforced laminated plates and shallow shells, *Computers and Structures* 76, 277–285, 2000.
- [8] Singha M.K., Daripa R. Nonlinear vibration of symmetrically laminated composite skew plates by finite element method, *International Journal of Non-Linear Mechanics* 42, 1144–1152, 2007.
- [9] Amabili M. *Nonlinear Vibrations and Stability of Shells and Plates*, University of Parma, Italy, 374p., 2008
- [10] Qatu M. S. *Vibration of Laminated Shells and Plates*, Elsevier Ltd., Oxford, 2004.
- [11] Ambartsumian S.A. *The general theory of anisotropic shells*. Moscow, Nauka, 1974 (in Russian)
- [12] Rvachev V. L. *Theory of R-functions and some of its applications*. Naukova Dumka, Kiev, 551 p., 1982 (in Russian).
- [13] Rvachev V. L. and Kurpa L. V., *R-functions in Problems of the Theory of Plates*, Naukova Dumka, Kiev, 176p., 1987 (in Russian).
- [14] Kurpa L. V. *R-functions method for linear bending and vibration of shallow shells problems solution*. NTU «KhPI», Kharkov, 408 p., 2009 (in Russian).
- [15] Kurpa L.V. Nonlinear Free Vibrations of Multilayer Shallow Shells with a Symmetric Structure and with a Complicated Form of the Plan. *J. Mathem. Methods and Phisic. Mech. Polya*, Vol.51, No.2, pp.75-85, 2008 (in Russian).
- [16] Volmir A.S. *Nonlinear Dynamic of the Plates and Shells*. Nauka, Moscow, 432 p. 1972.

## INVESTIGATION OF FORCED VIBRATIONS OF TURBINE BLADES IN CONSIDERATION OF ROLLING CONTACT IN THE DETACHABLE SHROUD

O. O. Larin<sup>1</sup>  
O. S. Stepchenko  
National Technical  
University "KhPI"  
Kharkov, Ukraine

---

### ABSTRACT

---

An original nonlinear discrete model of the 2 blade package which adequately describes kinematics of the dynamic contact interaction in the inter-blade detachable Z-like bandage is offered. The model via its small dimension could be efficiently used for detailed analysis of its nonlinear behavior.

---

### INTRODUCTION

An increase of the steam turbines power and demands of the magnification of their efficiency lead to the extension and complication of the turbines operating regimes on the one hand, and on the other hand lead to use new constructions of working bladings. First of all it is concerns with magnification of the length and the angle of pre-twisting of the blades of the last stages low-pressure cylinder.

The given work is devoted to the researching of the peculiarities of dynamic behaviour of the modern large length blades (Fig. 1). A shroud which has been represented as a detachable joint (Fig.1a) is used for securing the demanded strength and the technological characteristics.

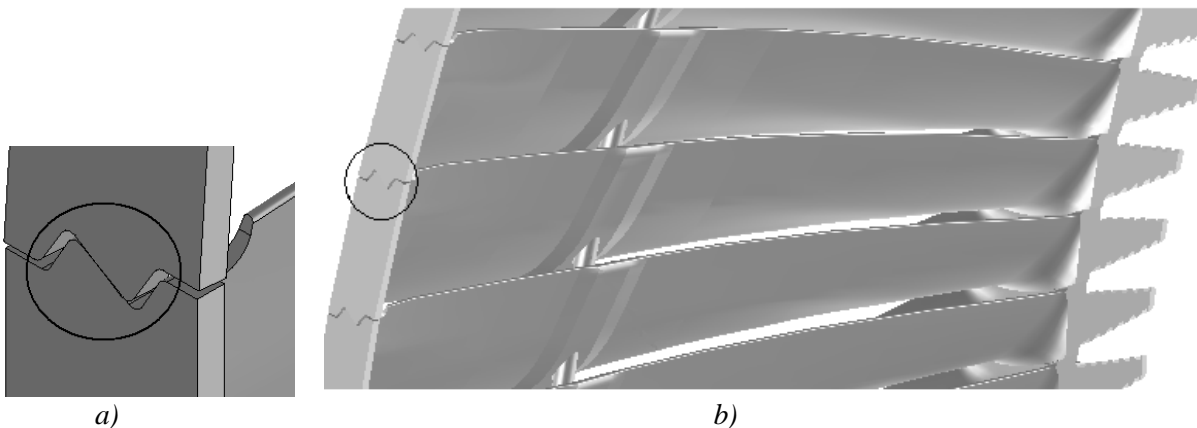


Fig. 1 Geometrical model of the blades

The initial mutual location of the contacted surfaces of the neighbour blades bandage parts has a capability of the dynamic modification due to bandage split character. This peculiarity brings into the system the structural nonlinearity which due to the smallness of studied vibrations could be also considered as the small one.

A direct numerical analysis of the nonlinear vibrations of the industrial scale bladed disk model concern with insurmountable computational difficulties. This defines a necessity of the construction an adequate small dimensional discrete model. The models of two levels are considered in the current work: detailed large dimension finite-element and small dimension discrete. Some numerical experiments have been carried out on the basis of the first model. The results are

---

<sup>1</sup> Corresponding author. Email [AlexeyA.Larin@gmail.com](mailto:AlexeyA.Larin@gmail.com)

complicated in its understanding and are not enough for making any conclusions. But they let to define a type and character of nonlinearity of inter-blade conjunction (shroud). That gives a possibility to create correct but small dimension model which could be investigated via classical methods of nonlinear dynamics.

## 1. ANALYSIS OF THE TYPE OF CONJUNCTION NONLINEARITY

The direct numerical experiments of blades vibrations for some turbine nominal operational regimes have been made on the basis of the first model [1,2]. The results of these researches have indirect confirmation at their comparison with natural experiment conducted by other authors on the similar type blades. The analysis of the blades dynamic behavior at numerical simulation has been shown, that the contact interaction has a rolling character alternately round of two positions (Fig. 2) [2].

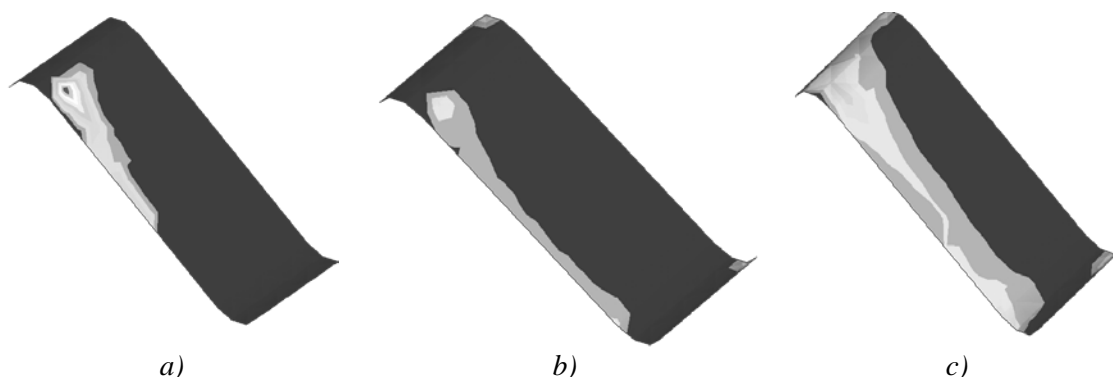


Fig. 2 The type of contact interaction in the shroud

## 2. A CONSTRUCTION OF THE DISCRETE MODEL

The second model which represents as a lumped parameters discrete model with the 8 degrees of freedom is developed for the analysis of the nonlinear dynamics of this system (Fig. 3a).

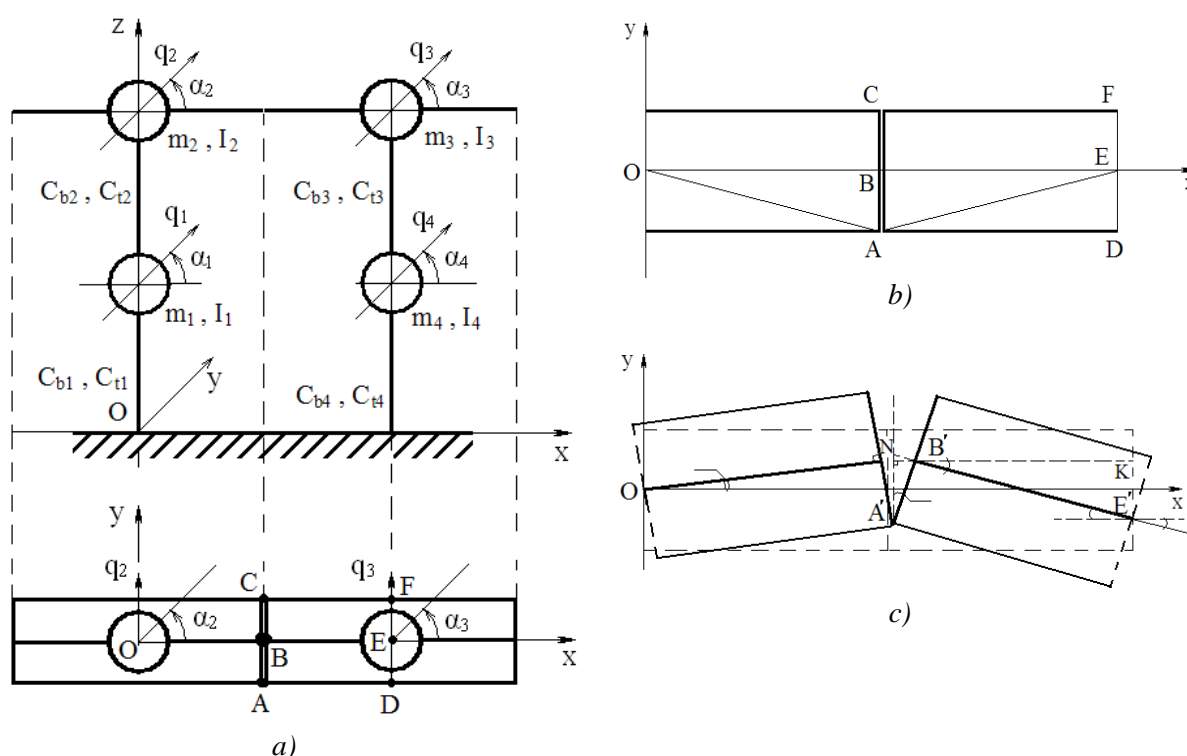


Fig. 3 Discrete model of the 2 blades

The model contains a nonlinearity, which character is keeping with kinematics of the dynamic contact, defined on the first model in the bandage joint. In the fig.3b and fig.3c the kinematic of the dynamic inter-blade interaction is shown as a scheme.

Using the geometry of state fig.3b and deformed fig.3c relationships between displacement  $q_2$ ,  $q_3$  and angles  $\alpha_2$  and  $\alpha_3$ :

$$\Delta = q_2 - q_3, \Delta = d_1 - \alpha_2 \cdot l_1 + \sqrt{l_2^2 + d_1^2 - (d_1 \cdot \alpha_2 - l_2)^2}, \quad (1)$$

$$\alpha_3 = a_1 + \sqrt{1 + a_1^2 - (1 - a_1 \cdot \alpha_2)^2}, \frac{d_1}{l_2} = a_1, \quad (2)$$

where  $d$  and  $l$  are half of bandage width and length.

Hereby the equations of motion of discrete nonlinear system consists from the two set of linear equations for 2-degrees-of-freedom banding and torsions vibrations which are got to be interrelated and nonlinear by the algebraic equations (1)-(2). So, the second model of the investigated system would be represented by the 6 coupled nonlinear equations.

Some results of the numerical solutions of this harmonically excited system are shown on the Fig.4. The results are very similar to results which were obtained in the work [3] on the base of precise FE 2-blade sector model. So, offered model could be efficiently used for detailed analysis.

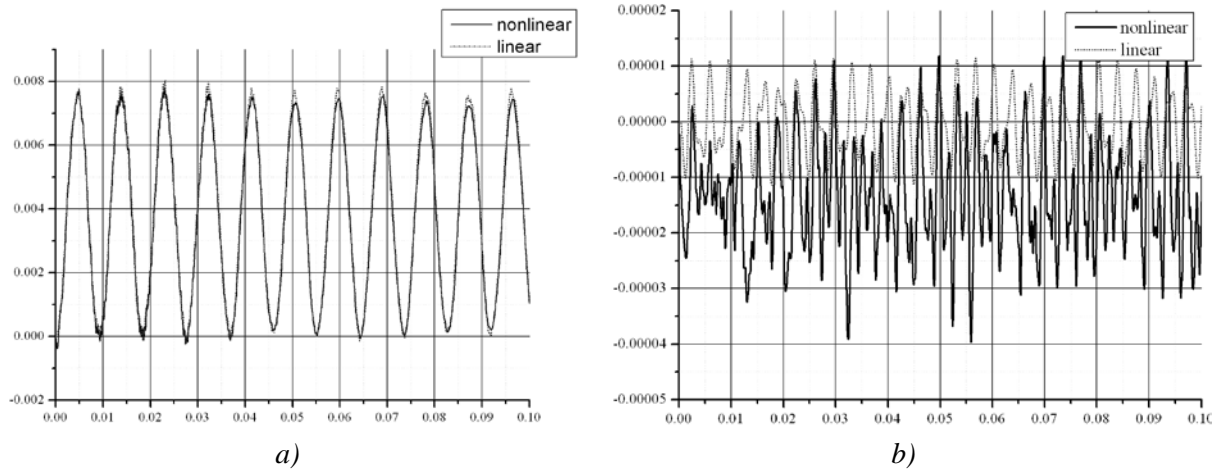


Fig. 4 Numerical calculations results

## CONCLUSIONS

In the work it is offer and approved a new nonlinear discrete model of the 2 blade package which adequately describes kinematics of the dynamic contact interaction in the inter-blade detachable Z-like bandage. The model via it small dimension could be efficiently used for detailed analysis its nonlinear behavior.

## REFERENCES

- [1] Zhovdak V.A., Larin A.A., Stepchenko A.S., Demuz Ya.D., Solyannikiva Yu.V. An investigation of dynamic contact interaction in inter-bandage conjunctions of steam turbines blades packages *The problems of the calculated mechanic and Strength of Constructions*, Dnipropetrovsk National university, Vol. 11 Dnipropetrovsk, pp. 53-62, 2007 (in Russian)
- [2] Valeriy O. Zhovdak., Oleksiy O. Larin, Oleksdandr S. Stepchenko, Yane D. Demuz, Aleksandr F. Kabanov Nonlinear vibrations of steam turbines blade packages subjected to the dynamic contact in bandage connection *Proceedings of the 2<sup>nd</sup> Intern. Conf. Nonlinear Dynamics dedicated to the 150<sup>th</sup> Anniversary of A.M. Lyapunov Sept. 25-28, 2007*, pp. 311-316, 2007. (in Russian)
- [3] V. O. Zhovdak., A.P. Zinkovskiy, O.S. Stepchenko, Ya.D. Krugliy Peculiarities of nonlinear forced vibrations of blades with detachable joints *Journal of mechanical engineering*, Kharkov, Vol. 12, N4, pp., 45-52, 2009. (in Russian)

**WEAR OF ABRADABLE COATINGS**  
Towards multi-physics analyses for the design of turbomachines

**Mathias Legrand**<sup>1</sup>  
Post-Doctoral Fellow

**Christophe Pierre**  
Dean of the Faculty of Engineering  
Structural Dynamics and Vibration  
Laboratory  
Department of Mechanical  
Engineering  
McGill University  
Montréal, Québec, Canada

---

ABSTRACT

---

Better turbomachine performances are achieved by reducing possible parasitic leakage flows through the closure of the clearance distance between blade tips and surrounding casings. Accordingly, direct contact is now considered as part of aircraft engines normal life.

In order to avoid possibly catastrophic scenarios, implementation of abrasible coatings has been widely recognized as a robust solution. Nevertheless, the process of wear undergone by abrasible coatings is not well understood. In the present work, its macroscopic behavior is numerically approximated through a piecewise linear plastic constitutive law which allows for real time access to the abrasible layer profile.

First results prove convergence in time and space of the proposed approach and show that the frequency content of the blade response is clearly affected by the presence of abrasible coatings. It seems that the opening of the clearance between the blade tip and the casing due to wear leads to large amplitudes of motion far from the usual linear conditions.

---

**INTRODUCTION**

Facing a constant need of improved performances for lower operating costs, jet engine manufacturers respond with the reduction of possible parasitic leakage flows by closing the gap between blade tips and surrounding casings. This is made possible through the implementation of abrasible coatings [1] in the compressor and turbine sections where a minimal clearance is required.

The mechanical properties of the abrasible material are of primary importance as it must preserve the incurring blade-tips from damage by being reasonably soft, but also be sufficiently hard to stand very high temperatures and high-speed gas flows with inherent solid particles. It has been detected during test runs that erosive wear of abrasible coatings may play a significant role in the rise of divergent behaviors such as propagating cracks in blade roots. Accordingly, it seems urgent to enrich the limited current knowledge of the circumstances under which they occur [2].

Modeling the erosion process in a macroscopic manner seems rather new [3] even though simple analytical derivations do exist [4]. This task is difficult because of the complex and coupled physical mechanisms involved such as dislocation, thermal gradients, large displacements and mass removal [5]. In turbomachines, where large relative displacements between contacting components together with high abrasible wear rates are observed, most of the existing theoretical statements do not seem relevant and easy to implement [6].

It is here assumed that plasticity with its inherent abilities to represent permanent deformation in a simple fashion stands as a natural first macroscopic approach in order to account for abrasible coatings erosive wear. It is thought that the behavior of the blade will be properly predicted.

---

<sup>1</sup>Corresponding author. Email: mathias.legrand@mcgill.ca

## 1 STRUCTURAL MODEL AND EQUATIONS OF MOTION

The present study deals with a single rotating blade and a surrounding casing of a low pressure compressor stage, as depicted in Fig. 1(a). Within the well-known finite element framework under the assumption of small displacements, vector  $\mathbf{u}$  stores all the displacement degrees-of-freedom of the blade and the respective mass matrix  $\mathbf{M}$ , damping matrix  $\mathbf{D}$ , stiffness matrix  $\mathbf{K}$  and contact forces  $\mathbf{F}^c$  are built accordingly. The resulting governing equations of motion take the form:

$$\mathbf{M}\ddot{\mathbf{u}} + \mathbf{D}\dot{\mathbf{u}} + \mathbf{K}\mathbf{u} + \mathbf{F}^c = \mathbf{0} \quad (1)$$

complemented with the usual contact constraints.

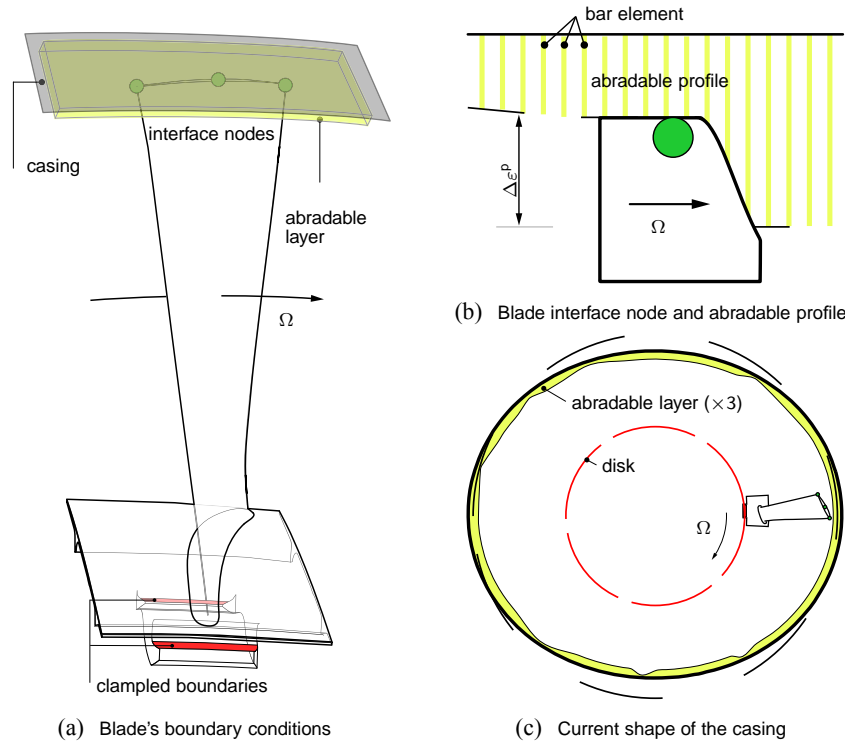


Figure 1 – Blade under investigation

The introduced finite element model of the blade is numerically too large and leads to cumbersome computation times. It is reduced through the Craig-Bampton procedure [7] where three interface nodes (leading edge, middle of the chord and trailing edge) define the contact interface with the casing, so that the contact constraints can directly be treated in the reduced space (see Fig. 1(a)). Since the chosen Craig-Bampton interface nodes of the blade, as such, do not contain any information about the *true* geometry of the blade tip, this has to be numerically included in the solution method, as illustrated in Fig. 1(b), in order to ensure space convergence of the abrasible profile.

Moreover, thorough preliminary simulations showed that the casing is insensitive to the contact interaction with the blade and is not modeled as a flexible component.

## 2 ABRADABLE CONSTITUTIVE LAW WITH PLASTICITY

As a first approach, the abrasible coating is discretized with the usual one-dimensional two-node bar elements, as displayed in Fig. 1(b), undergoing a nonlinear plastic constitutive law. By convention, strains  $\varepsilon$  and stresses  $\sigma$  are such that  $(\varepsilon, \sigma) \in \mathbb{R}^+ \times \mathbb{R}^+$ . The set of admissible stresses  $\mathbb{E}_\sigma$  is defined as follows [8]:

$$\mathbb{E}_\sigma = \{(\sigma, \alpha) \in (\mathbb{R}, \mathbb{R}) \setminus f(\sigma, \alpha) \leq 0\} \quad (2)$$

where  $\alpha : [0, T] \rightarrow \mathbb{R}$  is an internal hardening variable and  $f$ , a yield function. It is also assumed that (1) the total strain is separated in an additive way between its elastic part  $\varepsilon^e$  and plastic part  $\varepsilon^p$  such

as  $\varepsilon = \varepsilon^e + \varepsilon^p$  and (2) the relation between elastic strains and stresses is linear  $\sigma = E\varepsilon^e$ . By choice hardening is isotropic. This leads to:

$$f(\sigma, \alpha) = \sigma - (\sigma_Y + K\alpha) \quad (3)$$

where  $\sigma_Y > 0$  stands for the elastic limit and  $K \geq 0$ , for the plastic modulus of the abradable material. The second assumption yields:

$$\Delta\alpha = \Delta\varepsilon^p \quad (4)$$

and condition on the plastic flow implies the existence of a consistency parameter  $\gamma$ , such as  $\Delta\varepsilon^p = \gamma \frac{\partial f}{\partial \sigma}$ , equivalent to  $\Delta\varepsilon^p = \gamma$  because of Eq. (3). Dual variables  $\gamma$  and  $f$  obey the Kuhn-Tucker conditions, complemented by the consistency condition:

$$\gamma \geq 0; \quad f(\sigma, \alpha) \leq 0; \quad \gamma f(\sigma, \alpha) = 0; \quad \gamma \Delta f(\sigma, \alpha) = 0 \quad (5)$$

For a one-dimensional quasi-static strain formulation, the solution strategy is greatly simplified. Consider an admissible state together with an imposed increment of deformation  $\Delta\varepsilon$  within a purely elastic trial state:

$$\sigma^{\text{trial}} = E\Delta\varepsilon + \sigma; \quad \Delta\varepsilon^p = 0; \quad \Delta\alpha = 0; \quad f^{\text{trial}} = \sigma^{\text{trial}} - (\sigma_Y + K\alpha) \quad (6)$$

In order to ensure that the trial state belongs to  $\mathbb{E}_\sigma$ ,  $f^{\text{trial}}$  has to be tested:

- if  $f^{\text{trial}} \leq 0$ , trial and current states coincide;
- if  $f^{\text{trial}} > 0$ , condition (5)<sub>2</sub> is violated and the trial state has to be corrected. The commonly adopted approach, named *Return Mapping Algorithm* [9], relies on the projection of the trial state on the boundary of the yield function  $f = 0$  together with condition  $\gamma > 0$  at constant strain. Variation of Eq. (3) yields:

$$f = f^{\text{trial}} - \gamma(E + K) \quad (7)$$

Consequently,  $f = 0$  implies:

$$\gamma = \frac{f^{\text{trial}}}{E + K} \quad (8)$$

and the following update is used:

$$\sigma = \sigma^{\text{trial}} - E\gamma \quad \text{and} \quad \Delta\alpha = \Delta\varepsilon^p = \gamma \quad (9)$$

During a contact phase, the virtual work of the internal forces acting within the abradable coating for a virtual displacement  $\delta\mathbf{u}$  of the blade is equal by definition to the virtual work of the contact force for the same virtual displacement. By defining  $I = \{i \mid g(i) = 0\}$  (blue bar elements in Fig. 1(b)), equilibrium of the contact forces with the internal forces can be written as:

$$\mathbf{F}^c = \sum_{i \in I} A_i \sigma_i \quad (10)$$

where  $A_i$  stands for the cross-section area of an abradable element and depends on the density parameter.

### 3 TIME MARCHING PROCEDURE

The phenomenon under investigation is inherently transient and making use of time stepping techniques seems fairly natural. For non-smooth and non-differentiable nonlinear terms such as those mentioned above, explicit algorithms seem more relevant [10] and are adopted here.

By noting  $\mathbf{u}_{n+1}$ , the numerical approximation of the exact value  $\mathbf{u}(t_{n+1})$  at time  $t_{n+1} = t_n + h$  where  $h$  is the time-step, the classical explicit central finite difference scheme used in this work yields:

$$\ddot{\mathbf{u}}_n = \frac{\mathbf{u}_{n+1} - 2\mathbf{u}_n + \mathbf{u}_{n-1}}{h^2} \quad \text{and} \quad \dot{\mathbf{u}}_n = \frac{\mathbf{u}_{n+1} - \mathbf{u}_{n-1}}{2h} \quad (11)$$

The contact detection as well as the internal force contribution of the abradable material are handled by employing the prediction/correction technique developed in [11]. The final algorithm is then divided into four steps:

1. **prediction**, at time step  $n + 1$ , of the displacements  $\mathbf{u}$  of the blade by neglecting the abradable coating. This predicted displacement, denoted with subscript  $p$ , is expressed as:

$$\mathbf{u}_{n+1,p} = \left[ \frac{\mathbf{M}}{h^2} + \frac{\mathbf{D}}{2h} \right]^{-1} \left( \left( \frac{2\mathbf{M}}{h^2} - \mathbf{K} \right) \mathbf{u}_n + \left( \frac{\mathbf{D}}{2h} - \frac{\mathbf{M}}{h^2} \right) \mathbf{u}_{n-1} \right) \quad (12)$$

where displacements  $\mathbf{u}_n$  and  $\mathbf{u}_{n-1}$  are known.

2. **determination** of the gap function  $\mathbf{g}_{n+1,p}$  between the two contacting components. A search algorithm identifies all abradable elements  $i \in I$  being penetrated by the blade contact interface.
3. **abradable internal forces computation** through a deformation increment  $\Delta\varepsilon$  induced by the predicted penetrations between the two bodies. Subsequent strains  $\sigma_{i \in I}$ , hardening variables  $\alpha_{i \in I}$  and plastic deformations  $\varepsilon_{i \in I}^p$  are updated using the above mentioned procedure. The final vector of internal forces is calculated through Eq. (10) and the abradable profile is updated.
4. **displacement correction** consistent with the calculated contact forces [11, 12]:

$$\mathbf{u}_{n+1} = \mathbf{u}_{n+1,p} - \left[ \frac{\mathbf{M}}{h^2} + \frac{\mathbf{D}}{2h} \right]^{-1} \mathbf{F}^c \quad (13)$$

## 4 RESULTS

### 4.1 Configuration of interest

It is here assumed that a temperature gradient equivalent to a multi-harmonic two-nodal diameter load quasi-statically distorts the casing in order to absorb the initial clearances, as depicted in Fig. 1(c). The wear level is governed by the plastic law parameters  $E$ ,  $K$  and  $\sigma_Y$  illustrated in Fig. 2 and two configurations, respectively with low and high wear, are later investigated. The convergence in space

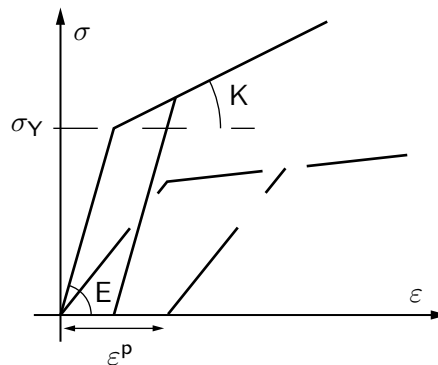


Figure 2 – Definition of the plasticity constitutive law for low (—) and high (---) wear

and time of the erosion wear law is checked. This is respectively achieved by increasing the density of abradable elements and by reducing the time-step of the numerical tool but is not displayed here for the sake of brevity.

### 4.2 Modal analysis and wear profile

Within the operating range of a low pressure compressor, only the first flexural mode is expected to be excited in a dangerous manner through direct contact. Its frequency is denoted by  $f_1$  with respect to which are normalized all the frequency results and rotational velocities  $\Omega$ .

A series of simulations has been conducted in order to understand the sensitivity of the abradable wear law and subsequent profile to the rotational velocity  $\Omega$ . Beforehand, a quick modal analysis of the blade as a linear flexible structure is required to better understand the up-coming results. Since the casing keeps a multi-harmonic two-nodal diameter shape during interaction, the first frequency of the blade will be reached for  $\Omega$  such as:

$$\Omega \text{ (Hz)} = \frac{f_1}{k} \text{ (Hz)}, \quad k = 2, 4, 6 \dots \quad (14)$$

that describes engine-order lines crossing the first frequency of resonance of the blade. In Eq. (14),  $k$  is limited to even positive integers due to the assumed shape of the casing. This condition will thus be satisfied for lower rotational velocities. In what follows, we pay attention to  $k = 4$  and  $k = 6$  since  $k = 2$  is out of the operating range in terms of  $\Omega$ .

It is well known that direct unilateral contact conditions stiffen the interacting mechanical components and modify their frequency of resonance. Accordingly, Eq. (14) could be revisited as follows:

$$\Omega \text{ (Hz)} = \frac{f_1(|\mathbf{F}^c|)}{k} \text{ (Hz)}, \quad k = 2, 4, 6 \dots \quad (15)$$

where  $|\mathbf{F}^c|$  simply refers to the amplitude of the contact forces.

Amplitude maps in Figs. 3(a) and 3(b) explicitly show the wear level in the abradable coating along the circumferential direction of the casing with respect to  $\Omega$  and implicitly indicate the number of worn lobes. For low or high rotational velocities, the shape of the casing controls the wear profile since the blade does not respond in resonance to the nonlinear contact excitation and only two lobes are worn. On the contrary, when Eq. (15) is satisfied, large amplitudes of vibration are expected: this is clearly shown for  $k = 4$  and  $k = 6$  where four lobes and six lobes are distinguishable, respectively. The contact stiffening effect is well caught by the proposed algorithm since, in Figs. 3(a) and 3(b), the worn lobe highest amplitudes should be located at  $\Omega = 0.25$  ( $k = 4$ ) and  $0.16$  ( $k = 6$ ) based on Eq. (14) but are located at  $\Omega = 0.31$  ( $k = 4$ ) and  $\Omega = 0.21$  ( $k = 6$ ) instead, see Eq. (15).

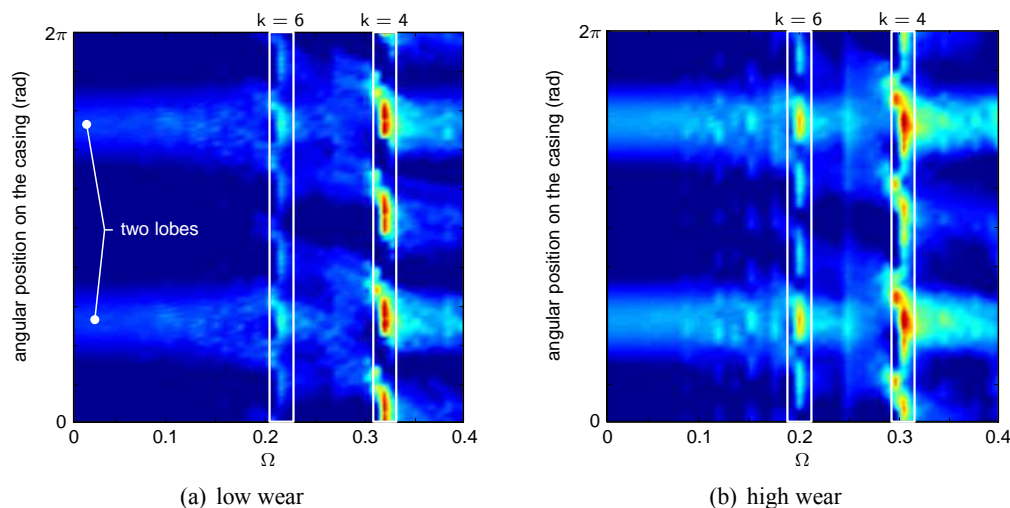


Figure 3 – Map of the final abradable profiles with respect to  $\Omega$  for interface node 1 after ten rounds of the blade

In other words, the first flexural mode of the blade is excited through intermittent contact with the casing increasing the level of erosion wear for very specific  $\Omega$ . Nevertheless, the abradable ductility, determined by mechanical parameters  $E$ ,  $K$  and  $\sigma_Y$  do modify the conditions of interaction. As can be seen in Figs. 3(a) and 3(b) again, the rotational velocities for which the blade is in resonance are slightly different, depending on the level of wear.

Obviously, all the presented results strongly depend on the adopted scenario of interaction and further investigations have to be conducted to better understand the mechanisms of wear and possible divergence. Nevertheless, they seem in good agreement with experimental observations about possible and unexpected severe vibration problems.

## CONCLUSION

The emphasis of the study has been placed on the understanding of the contact interaction occurring between a blade and a surrounding casing belonging to the low pressure compressor of an aircraft engine. The study focuses on modeling, in a realistic and macroscopic fashion, the erosion wear law of abradable coatings which are used to soften the direct contact between interacting components.

First results show that the developed model provides understandable and consistent physical results. It seems that by opening the operating clearance between the blade tip and the casing, larger motions may be expected far from the usual interaction conditions provided by the well-known Campbell diagrams.

In order to better estimate the wear parameter, comparisons with experimental results such as the ones presented in [13, 14] have to be scheduled in a near future.

## References

- [1] Yi, M., He, J., Huang, B., and Zhou, H., 1999. "Friction and wear behaviour and abrasability of abradable seal coating". *Wear*, **231**(1), pp. 47 – 53.
- [2] Jiang, J., Ahrens, J., Ulbrich, H., and Scheideler, E., 1998. "Contact model of a rotating rubbing blade". In Proceedings of the 5th International Conference on Rotor Dynamics of the IFTOMM, pp. 478 – 489.
- [3] Salles, L., Blanc, L., Thouverez, F., and Gousskov, A., 2008. "Analysis of a bladed disk with friction and fretting-wear in blade attachments". In Proceedings of GT2008 ASME Turbo Expo 2008: Power for Land, Sea and Air, no. GT2008-51112.
- [4] Rabinowicz, E., 1965. *Friction and wear of materials*. John Wiley & Sons, Inc., New-York.
- [5] Andrews, K. T., Shillor, M., Wright, S., and Klarbring, A., 1997. "A dynamic thermoviscoelastic contact problem with friction and wear". *International Journal of Engineering Science*, **35**(14), pp. 1291 – 1309.
- [6] Strömberg, N., Johansson, L., and Klarbring, A., 1996. "Derivation and analysis of a generalized standard model for contact, friction and wear". *International Journal of Solids and Structures*, **33**(13), pp. 1817 – 1836.
- [7] Craig, R., and Bampton, C., 1968. "Coupling of substructures for dynamics analyses". *AIAA Journal*, **6**(7), pp. 1313 – 1319.
- [8] Simo, J., and Hughes, T., 1998. *Computational inelasticity*. Springer.
- [9] Simo, J., and Taylor, R., 1986. "A return mapping algorithm for plane stress elastoplasticity". *International Journal for Numerical Methods in Engineering*, **22**, pp. 649 – 670.
- [10] Vola, D., Pratt, E., Raous, M., and Jean, M., 1998. "Consistent time discretization for a dynamical contact problem and complementarity techniques". *Revue Européenne des Éléments Finis*, **7**, pp. 149 – 162.
- [11] Carpenter, N., Taylor, R., and Katona, M., 1991. "Lagrange constraints for transient finite element surface contact". *International Journal for Numerical Methods in Engineering*, **32**, pp. 130 – 128.
- [12] Legrand, M., Pierre, C., Cartraud, P., and Lombard, J.-P., 2009. "Two-dimensional modeling of an aircraft engine structural bladed disk-casing modal interaction". *Journal of Sound and Vibration*, **319**(1-2), pp. 366 – 391.
- [13] Padova, C., Dunn, M., and Barton, J., 2008. "Casing treatment and blade tip configuration effects on controlled gas turbine blade tip/shroud rubs at engine conditions". In Proceedings of GT2008 ASME Turbo Expo 2008: Power for Land, Sea and Air, no. GT2008-50112.
- [14] Peyraut, F., Seichepine, J.-L., Coddet, C., and Hertter, M., 2008. "Finite element modeling of abradable materials - identification of plastic parameters and issues on minimum hardness against coating's thickness". *International Journal for Simulation and Multidisciplinary Design and Optimization*, **2**, pp. 209 – 215.

## DYNAMICS OF A TIMOSHENKO BEAM ON AN ELASTIC FOUNDATION

Arkadiy Manevich<sup>1</sup>

Dept. of Comput. Mech.  
and Strength of Structures,  
Dniepropetrovsk National  
University,  
Dniepropetrovsk, Ukraine

ABSTRACT

Free transverse waves in Timoshenko beam resting on Winkler foundation are studied. Dispersion curves are derived and analyzed in generalized dimensionless variables and parameters. Special attention is paid to clearing up the physical sense of the second spectrum of Timoshenko beam.

### INTRODUCTION

There are two main reasons for studying dynamics of Timoshenko beam (TB, Timoshenko [1, 2]). From *theoretical point of view*, the Timoshenko model has certain advantages over the classical Euler-Bernoulli (E-B) model. It is known that E-B model has non-wave character (according to E-B dynamic equation, a perturbation propagates along the beam with infinite large velocity, see, e.g., Uflyand [3]). The Timoshenko model results in an equation of wave character.

From *practical viewpoint*, Timoshenko beam model, especially in case of elastic foundation, is of great interest in view of the development of the high-velocity transport. The action of moving loads often gives rise to localized stress-strain states for which shear deformability should be taken into account.

Our interest to dynamics of Timoshenko beam was caused by the following particular problem. It is known that in the TB for each wave number there exist two natural frequencies, and so two spectra of oscillations can be separated. During last decades discussion continued about the meaning of the second spectrum (see, e. g., [4-9] and for review - Stephen [9]), and many investigators adhere to opinion that “the second spectrum predictions of TB theory should be disregarded” [9].

In this paper an analysis of free transverse waves in TB on Winkler foundation is carried out. The use of dimensionless variables and parameters (Manevich A. [10] ) make it possible to draw general relations and conclusions. One of the main goals of this paper is to show that when we consider the TB *on elastic foundation* we obtain new convincing proofs of necessity and validity of the second branch of the spectrum.

### 1. GOVERNING EQUATIONS

Equations of motion for TB on the Winkler foundation are derived using known hypotheses. Deformations of the beam are described by two independent functions – the angle of the cross section rotation  $\psi$  and the shear angle  $\gamma$  (at the neutral axis). The total slope of the bent axis is

$$\frac{\partial y}{\partial x} = \psi + \gamma \quad (1)$$

where  $y(x,t)$  is the transverse displacement. The longitudinal displacement of a point on distance  $z$  from the neutral axis and the longitudinal deformations are expressed via angle  $\psi$ :  $u = -z\psi$ ,  $\varepsilon_x = -z \partial \psi / \partial x$ .

The bending moment and the transverse shear force in the cross section are specified by known expressions:

<sup>1</sup> Corresponding author. Email [armanevich@yandex.ru](mailto:armanevich@yandex.ru)

$$M = -EJ \frac{\partial \psi}{\partial x}, \quad Q = k'A\tau = k'AG \left( \frac{\partial y}{\partial x} - \psi \right) \quad (2)$$

where  $k'$  is the coefficient which depends upon the cross section shape (see, e.g., [2]),  $A$  and  $J$  are the cross section area and the moment of inertia,  $E$  and  $G$  are moduli of elasticity in tension and shear, respectively.

Equations of the force balance for a beam loaded by a transverse load  $q_0(x,t)$  and resting on the elastic foundation with stiffness factor  $w_0$  are:

$$\frac{\partial Q}{\partial x} - \rho A \frac{\partial^2 y}{\partial t^2} + q_0(x,t) - w_0 y = 0, \quad -\rho J \frac{\partial^2 \psi}{\partial t^2} + Q - \frac{\partial M}{\partial x} = 0 \quad (3)$$

These equations with account of the above relations result in two differential equations of motion in  $y$  and  $\psi$ :

$$k'GA \frac{\partial}{\partial x} \left( \frac{\partial y}{\partial x} - \psi \right) - \rho A \frac{\partial^2 y}{\partial t^2} + q_0(x,t) - w_0 y = 0 \quad (4)$$

$$EJ \frac{\partial^3 \psi}{\partial x^3} - \rho J \frac{\partial^3 \psi}{\partial x \partial t^2} + \rho A \frac{\partial^2 y}{\partial t^2} - q_0(x,t) + w_0 y = 0 \quad (5)$$

Excluding the angle  $\psi$  we obtain the single equation with respect to the displacement  $y(x,t)$ :

$$\begin{aligned} EJ \frac{\partial^4 y}{\partial x^4} - \rho J \left( 1 + \frac{E}{k'G} \right) \frac{\partial^4 y}{\partial x^2 \partial t^2} + \frac{\rho^2 J}{k'G} \frac{\partial^4 y}{\partial t^4} + \rho A \frac{\partial^2 y}{\partial t^2} + w_0 \left[ 1 + \frac{\rho J}{k'GA} \frac{\partial^2}{\partial t^2} - \frac{EJ}{k'GA} \frac{\partial^2}{\partial x^2} \right] y = \\ = \left[ 1 + \frac{\rho J}{k'GA} \frac{\partial^2}{\partial t^2} - \frac{EJ}{k'GA} \frac{\partial^2}{\partial x^2} \right] q_0 \end{aligned} \quad (6)$$

For the free oscillation problem the right hand side in (6) is equal to zero. The boundary conditions for the set (4), (5) in variables  $y$  and  $\psi$  can be derived utilizing the Hamilton's principle.

Let us introduce dimensionless variables and parameters (Manevich A. [10]):

$$\xi = \frac{x}{r_0}, \quad Y = \frac{y}{r_0}, \quad \tau = \frac{c}{r_0} t, \quad c^2 = \frac{E}{\rho}, \quad r_0^2 = \frac{J}{A}, \quad \chi = \frac{E}{k'G}, \quad q = \frac{q_0 r_0}{EA}, \quad w = \frac{w_0 r_0^2}{EA} \quad (7)$$

Here  $c$  is the sound velocity in the beam material,  $r_0$  is the cross section radius of gyration,  $\chi$  is the shear deformability parameter,  $w$  is the foundation stiffness parameter. Note that for classical Euler-Bernoulli and Rayleigh models  $\chi = 0$ , that corresponds to infinitely large shear stiffness.

In variables (7) equations (4), (5) take the form

$$\frac{\partial}{\partial \xi} \left( \frac{\partial Y}{\partial \xi} - \psi \right) - \chi \frac{\partial^2 Y}{\partial \tau^2} + \chi q(\xi, \tau) - \chi w Y = 0 \quad (8)$$

$$\frac{\partial^3 \psi}{\partial \xi^3} - \frac{\partial^3 \psi}{\partial \xi \partial \tau^2} + \frac{\partial^2 Y}{\partial \tau^2} - q(\xi, \tau) + w Y = 0 \quad (9)$$

and equation (6) transforms into

$$\frac{\partial^4 Y}{\partial \xi^4} - (1 + \chi) \frac{\partial^4 Y}{\partial \xi^2 \partial \tau^2} + \chi \frac{\partial^4 Y}{\partial \tau^4} + \frac{\partial^2 Y}{\partial \tau^2} = \left( 1 + \chi \frac{\partial^2}{\partial \tau^2} - \chi \frac{\partial^2}{\partial \xi^2} \right) (q - w Y) \quad (10)$$

This equation includes only two generalized parameters  $\chi$  и  $w$ , characterizing the shear deformability and the foundation stiffness. From (8)-(10) one can obtain equations for particular cases of free waves and oscillations ( $q = 0$ ); for beam without elastic foundation ( $w = 0$ , this case on the base of the dimensionless equations was considered in [10]). If  $\chi = 0$  one obtains dimensionless equations for the Rayleigh model, which differs from the classical Euler-Bernoulli model (E-B) with accounting the rotatory inertia of beam (for the E-B beam on the Winkler foundation the second term in left hand side of (10) vanishes).

The obtained equations are apparently preferable in comparison with often used dimensionless equations with several parameters.

The angle  $\psi$  can be expressed via  $Y$  using equation (9). For the derivative  $\psi_\xi$  one has relationship

$$\frac{\partial^2 Y}{\partial \tau^2} + wY = \frac{\partial^2 \psi_\xi}{\partial \tau^2} - \frac{\partial^2 \psi_\xi}{\partial \xi^2} + q(\xi, \tau) \quad (11)$$

The shear angle  $\gamma = \frac{\partial y}{\partial x} - \psi = \frac{\partial Y}{\partial \xi} - \psi$  and its derivative  $\gamma_\xi$  is expressed via dimensionless variables  $Y$  and  $\psi_\xi$ :

$$\gamma_\xi \equiv \frac{\partial \gamma}{\partial \xi} = \frac{\partial^2 Y}{\partial \xi^2} - \psi_\xi \quad (12)$$

## 2. SOLUTION FOR FREE WAVES IN INFINITELY LONG BEAM

Here we consider only free waves in infinitely long beam ( $q = 0$ ), which are described by equation

$$\frac{\partial^4 Y}{\partial \xi^4} - (1 + \chi) \frac{\partial^4 Y}{\partial \xi^2 \partial \tau^2} + \chi \frac{\partial^4 Y}{\partial \tau^4} + \frac{\partial^2 Y}{\partial \tau^2} + w \left( 1 + \chi \frac{\partial^2}{\partial \tau^2} - \chi \frac{\partial^2}{\partial \xi^2} \right) Y = 0 \quad (13)$$

A solution is seeking in the form of harmonic waves

$$Y(\xi, \tau) = Y_0 e^{i(k\xi - \omega\tau)} \quad (14)$$

Substitution of (14) into (13) gives the frequency equation

$$\chi\omega^4 - \omega^2 [1 + (\chi + 1)k^2 + w\chi] + w(1 + \chi k^2) + k^4 = 0 \quad (15)$$

The roots are:

$$\omega_{1,2}^2 = \frac{1}{2\chi} [1 + (\chi + 1)k^2 + w\chi \mp \sqrt{D}] \quad (16)$$

where

$$D = (1 + (\chi + 1)k^2 + w\chi)^2 - 4\chi(w(1 + \chi k^2) + k^4) \quad (17)$$

It can be readily seen that the both roots of equation (16) are real and positive. These two eigenvalues  $\omega_1$  and  $\omega_2$  for a given wave number  $k$  determine two phase velocities for each  $k$ :  $v_{\phi,1,2} = \omega_{1,2}/k$ . The existence of two branches, or two spectra, is a principal distinction of the Timoshenko model from the E-B and Rayleigh models, which was revealed for beam without foundation in early papers ([3] and others).

Let us find relations between amplitudes of the transverse deflections  $Y$  and amplitudes of angles  $\psi_\xi$  and  $\gamma_\xi$  for each the branch. Assuming these quantities in view of (11), (12) in the form

$$Y_j(\xi, \tau) = Y_{0j} e^{i(k\xi - \omega_j \tau)}, \quad \psi_{\xi,j}(\xi, \tau) = \psi_{\xi,0j} e^{i(k\xi - \omega_j \tau)}, \quad \gamma_{\xi,j}(\xi, \tau) = \gamma_{\xi,0j} e^{i(k\xi - \omega_j \tau)} \quad (j=1,2) \quad (18)$$

and substituting into (11) with  $q = 0$  and (12), one obtains

$$\psi_{\xi,0j} = \frac{\omega_j^2 - w}{\omega_j^2 - k^2} Y_0, \quad \gamma_{\xi,0j} = \frac{k^4 - \omega_j^2 k^2 - \omega_j^2 + w}{\omega_j^2 - k^2} Y_0 \quad (j=1,2) \quad (19)$$

The following identity follows from the frequency equation (15):

$$k^4 - \omega_j^2 k^2 - \omega_j^2 + w = \chi (\omega_j^2 - k^2) (w - \omega_j^2) \quad (j=1,2)$$

Then the second relation (19) (with account of the first one) yields

$$\gamma_{\xi,0j} = -\chi (\omega_j^2 - w) Y_{0j} = -\chi (\omega_j^2 - k^2) \psi_{\xi,0j} \quad (j=1,2) \quad (20)$$

### 3. ANALYSIS OF THE SOLUTION

Consider first the simplest *limit case of long waves*  $k \rightarrow 0$ . Putting in (16)  $k = 0$ , one has

$$\omega_{1,2}^2(k=0) = \frac{1}{2\chi} [1 + w\chi \mp |1 - w\chi|] \quad (21)$$

This yields

$$\text{for } w\chi < 1: \quad \omega_1^2(k=0) = w, \quad \omega_2^2(k=0) = \frac{1}{\chi} \quad (22,a)$$

$$\text{for } w\chi > 1: \quad \omega_1^2(k=0) = \frac{1}{\chi}, \quad \omega_2^2(k=0) = w \quad (22,b)$$

At changing stiffness of the elastic foundation to the beam shear stiffness ratio the first and the second spectrum “change” with their limit points (or with analytical dependencies of these stiffness’s). The first branch in limit  $k \rightarrow 0$  is determined by the smaller of these stiffness’s, the second one – by the larger of the stiffness’s. The case  $w\chi < 1$  can be named “weak foundation”, and  $w\chi > 1$  – «strong foundation».

If  $k$  is small (but not equal to 0), then due to continuous analytical dependence (16) value of  $\omega_1^2$  is close to  $w$  for weak foundation ( $w < 1/\chi$ ), and to  $1/\chi$  for strong one ( $w > 1/\chi$ ). For  $\omega_2^2$  the picture will be opposite.

In Fig. 1 dispersion curves for frequency are presented for  $w = 0.1$  in two cases:  $\chi = 3$  (a) and  $\chi = 30$  (b). Two branches for TB are constructed (bold curves), and for comparison curves for E-B model (curves 1) and Rayleigh model (curves 2) are given. Portions of the curves for relatively small  $k$  are shown on a large scale in Fig. 2, a.

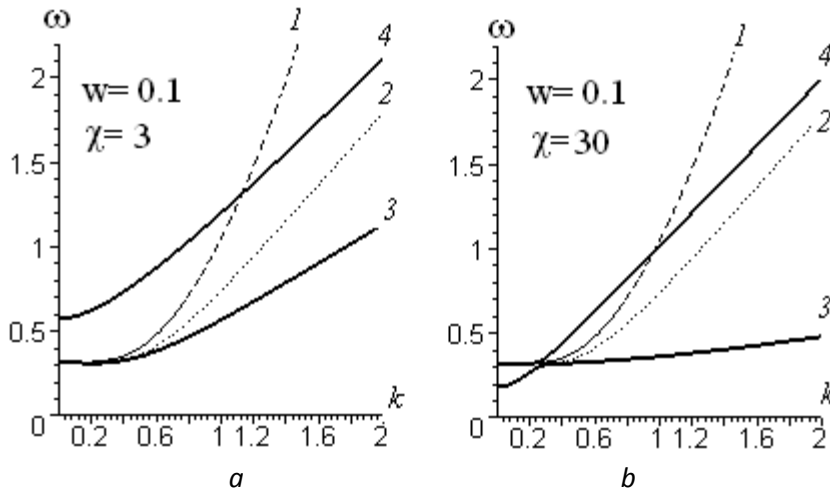


Fig. 1 Dispersion curves for frequency  $\omega-k$  for beam on elastic foundation  $w = 0,1$  in cases  $\chi = 3$  (a) and  $\chi = 30$  (b). Two branches for TB (bold curves), curves for E-B (1) and Rayleigh models (2)

In Fig. 1,a (the case of “weak” foundation) the first branch for TB (curve 3) has the same asymptotics for small  $k$ , as do the E-B and Rayleigh models (curves 1, 2), and these curves practically merge for  $k < 0.15$ . But the second branch (curve 4) at large  $k$  is close to the Rayleigh model. Note that the dispersion curves differ from those for case of beam without foundation ( $w = 0$ ) only with “shifting” their left parts (curves 1, 2, 3 originate from one of points (22,a) or (22, b), not from zero point).

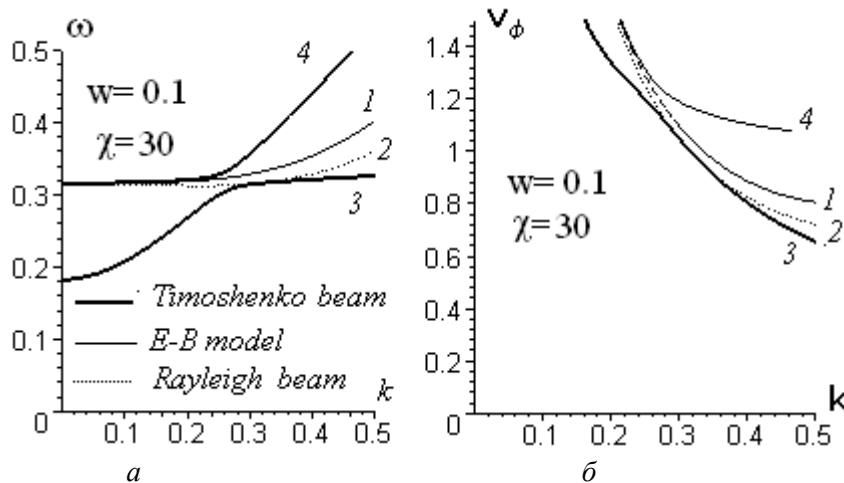


Fig. 2. Dispersion curves for frequency  $\omega-k$  (a) and phase velocity  $v_\phi-k$  (b) for beam on elastic foundation,  $w = 0,1$ ,  $\chi = 30$ , on a large scale. Two branches for TB (curves 3, 4), curves for E-B (1) and Rayleigh models (2)

But for “strong” foundation we see another picture (Fig. 1,b, Fig. 2, a). Both the branches of TB (curves 3, 4) consist of two portions. The left portion of the first branch is a continuation of the right part of the second branch, and inversely. In other words, both branches “have changed” with their portions. This peculiarity is underlined by the fact that curves for E-B and Rayleigh models (1, 2) now approach the second branch of TB model at  $k \rightarrow 0$  (not the first branch, as they do for “weak” foundation).

In Fig. 2, b, dispersion curves for phase velocity  $v_\phi-k$  are shown for moderately small  $k$  values, which demonstrate the same behavior as Fig. 2, a. We also see a twisting point on curve 3 (first branch for TB), and curves 1, 2, which were close to the curve 3, begin for small  $k$  to approach curve 4 – the second TB branch.

For elucidating the physical meaning of the second spectrum of TB let us now note that for beam without foundation one has  $\omega_1^2 - k^2 < 0$  ( $j=1$ , upper sign) and  $\omega_2^2 - k^2 > 0$ ,  $j=2$ , lower sign (it

can be proved using (16), (17)). Then it follows from (20) that for the first branch oscillations of  $\gamma_\xi$  (dimensionless curvature of the beam due to shear) occur in phase with oscillations of  $\psi_\xi$  (dimensionless curvature due to bending), and that for the second branch these oscillations occur in anti-phase.

The similar statements are also valid for the angles of shear  $\gamma$  and bending  $\psi$ . Thus, *the first spectrum of natural frequencies for beam without foundation relates to wave (oscillation) modes for which the angle of rotation of the cross section and of shear angle oscillate in phase; the second spectrum relates to waves for which these angles oscillate in anti-phase.*

It can be also proved that the similar statement is valid for the *beam on elastic foundation* in the case of “weak foundation”.

Eigenvector  $(\psi_{\xi 0}, \gamma_{\xi 0})$  (and  $(\psi_0, \gamma_0)$ ) in limit  $k \rightarrow 0$  is determined by (22). For the first branch this vector is  $(\psi_0, \gamma_0) = (1, -\chi w)$  in the case  $w < 1/\chi$ , and  $(\psi_{\xi 0}, \gamma_{\xi 0}) = (1, -1)$  in the case  $w > 1/\chi$ . For the second branch limit eigenvector is  $(\psi_0, \gamma_0) = (1, -1)$  at  $w < 1/\chi$  and  $(\psi_0, \gamma_0) = (1, -\chi w)$  at  $w > 1/\chi$ . We see again that at transition of  $w$  value through  $1/\chi$  the eigenvectors “change” occurs. This demonstrates the equivalence of two branches for the TB and refutes statement that the second spectrum of TB is “unphysical”.

## CONCLUSIONS

The presented analysis of free transverse waves in Timoshenko beam on the Winkler foundation based on dimensionless equations with two generalized parameters allows to draw principal conclusions concerning dynamics of TB. The obtained solution, in particular, brings to light the meaning of the second spectrum of TB. It is shown that both the spectra are equivalent in certain sense that refutes the view on the second branch as “unphysical” one.

## REFERENCES

- [1] Timoshenko S. On the correction for shear of the differential equation for transverse vibrations of prismatic bars, *Philosophical Magazine* (series 6) 41, 1921, pp. 744–746.
- [2] Timoshenko S. *Vibration Problems in Engineering.*, 3<sup>rd</sup> edition, D. Van Nostrand Co., Inc., 1955, 40 p.
- [3] Uflyand Ya. S. The propagation of waves in the transverse vibration of bars and plates. *Prikladnaya Matematika i Mekhanika*, 12, , 1948, pp. 287-300 (in Russian).
- [4] Anderson R. A. Flexural vibration in uniform beams according to the Timoshenko theory. *Trans. ASME, Ser. E, J. Appl. Mech.*, 20, No. 4, 1953, pp. 504-510.
- [5] Downs B. Transverse vibration of a uniform, simply supported Timoshenko beam without transverse deflection. *Trans. ASME, Ser. E, J. Appl. Mech.*, 43, No. 4, 1976, pp. 671-674.
- [6] Abbas, B. A. H., Thomas, J. The second frequency spectrum of Timoshenko beams. *J. of Sound and Vibration*, 51, No. 1, 1977, pp. 123-137.
- [7] Levinson, M. and Cooke, D. W. On the two frequency spectra of Timoshenko beams. *J. of Sound and Vibration*, 84, No. 3, 1982, pp. 319-326.
- [8] Nesterenko V. V. A theory for transverse vibrations of the Timoshenko beam. *J. Appl. Math. Mech.* 57, 1993, pp. 669-677.
- [9] Stephen, N. G. The second spectrum of Timoshenko beam theory—Further assessment. *J. of Sound and Vibration*, 292, No. 1-2, 2006, pp. 372-389.
- [10] Manevich A. Transverse waves in viscous-elastic Timoshenko beam. *Theoretical Foundations of Civil Engineering*. Warsaw, 17, 2009, pp. 217-228 (in Russian).

**GEOMETRICALLY NONLINEAR TRANSVERSAL VIBRATIONS OF  
 PLIABLE TO SHEAR AND COMPRESSION PLATES**

**M.V. Marchuk<sup>1</sup>**

*Pidstryhach Institute for  
 Applied Problems of  
 Mechanics and  
 Mathematics, NASU  
 L'viv, Ukraine*

**V.S. Pakosh**

*Pidstryhach Institute for  
 Applied Problems of  
 Mechanics and  
 Mathematics, NASU  
 L'viv, Ukraine*

---

**ABSTRACT**

---

A system of differential equations that describes nonlinear transversal vibrations and takes into account pliability to transversal shear and compression strains of composite plates is given. The parametrical analysis of dependence on fundamental frequency and amplitude of transversal vibrations of a strip-plate for hinge- fixed or hold rigidly plate is carried out.

---

**INTRODUCTION**

The laminated elements from composites are widely used in various designs and technical means under intensive cyclic loading. This loading can cause different bending proportional to the plate thickness what stipulates the geometrically non-linear character of the strain state. Therefore, to prevent the resonance phenomena the fundamental frequencies in such cases should be calculated using the geometrically nonlinear relations of the plate dynamics which take into account the pliability to transversal shear and compressive strains.

The majority of studies on nonlinear dynamics of thin-walled elements of design are based on the Karman quadratic theory being the generalization of the classical linear Kirchhoff-Lave theory for geometric nonlinearity [1]. In some works the relations of nonlinear technical theory were used, the basis of which forms the Timoshenko model [1–4]. However the theories grounding on the hypotheses of these authors do not take full account of the peculiarities of behavior of composites. Therefore this paper utilizes a mathematical model of dynamic deformation of plates, which considers the above peculiarities [5, 6]. The influence of boundary conditions on amplitude-frequency characteristics during nonlinear vibrations of composite plates has been analyzed on this basis.

**1. STATEMENT OF THE PROBLEM**

Consider a composite plate of thickness  $2h$  with effective elastic characteristics and averaged material density  $\rho$ , related to the Cartesian coordinate system  $x_i$  ( $i = 1, 2, 3$ ). Assume that one dimension of the plate exceeds considerably the other one. Then its dynamic geometrically nonlinear stress-strain state depends only on one spatial coordinate  $x_1 = x$  in its median plane. The equations of plate motion in this case may be written as [5]

$$\frac{\partial^2 u}{\partial x^2} + \frac{\partial w}{\partial x} \frac{\partial^2 w}{\partial x^2} = \frac{1}{c_1^2} \frac{\partial^2 u}{\partial t^2}, \tag{1}$$

$$\frac{\partial^2 \gamma}{\partial x^2} - \alpha_1^2 \left( \gamma + \frac{\partial w}{\partial x} \right) = \frac{1}{c_1^2} \frac{\partial^2 \gamma}{\partial t^2}, \tag{2}$$

---

<sup>1</sup> Corresponding author. Email [marchuk@iapmm.lviv.ua](mailto:marchuk@iapmm.lviv.ua)

$$\frac{\partial^2 u}{\partial x^2} \frac{\partial w}{\partial x} + \frac{\partial u}{\partial x} \frac{\partial^2 w}{\partial x^2} + \frac{3}{2} \left( \frac{\partial w}{\partial x} \right)^2 \frac{\partial^2 w}{\partial x^2} + \alpha_2^2 \frac{\partial}{\partial x} \left( \gamma + \frac{\partial w}{\partial x} \right) = \frac{1}{c_1^2} \frac{\partial^2 w}{\partial t^2}, \quad (3)$$

where  $u, w$  are relatively tangential and transversal displacements of the plate median plane,  $\gamma$  is the angle of rotation of normal element to the median plane before deformation,  $c_1 = \sqrt{\bar{B}/2\rho h}$  is the velocity of longitudinal waves propagation in the plate,  $\alpha_1^2 = A/\bar{D}$ ,  $\alpha_2^2 = \alpha_1^2 h^2/3$ ,  $\bar{B} = \frac{2Eh}{(1-\nu^2)}(1+\alpha)$ ,  $\bar{D} = \frac{h^2}{3}\bar{B}$ ,  $A = 2k'hG'$ ,  $k' = 14/15$ ,  $\alpha = \frac{(1+\nu)(\nu')^2}{1-\nu-2\nu\nu'} \frac{E}{E'}$ .

Here  $E, \nu$  are Young's modulus and Poisson's ratio in the median and equidistant to it planes;  $E', \nu'$  are the same values in the planes perpendicular to the median plane;  $G'$  – is the transversal shear modulus.

The origin of coordinate  $x$  in the middle of the plate sides perpendicular to it the sides is arranged at a distance  $2a$  one from another. Then in the case of a hinge fixing of these sides the boundary conditions are:

$$u(\pm a, t) = 0, \quad w(\pm a, t) = 0, \quad M(\pm a, t) = 0, \quad (4)$$

and for hold rigidly sides the boundary conditions are defined as

$$u(\pm a, t) = 0, \quad w(\pm a, t) = 0, \quad \gamma(\pm a, t) = 0. \quad (5)$$

The system (1)–(3) together with boundary conditions (4) or (5) forms a mathematical model of free geometrically nonlinear transversal vibrations of hinge-fixed or hold rigidly of the composite strip-plates which undergo deformations of transversal shear and compression.

The model presented describes also the forced longitudinal and shear vibrations generated by free transversal vibrations. They are also agreed with the results of investigations of quadratically nonlinear waves in elastic bodies as in Ref [7].

## 2. CONSTRUCTION OF SOLUTION

In Ref. [5] the fundamental frequency-to-amplitude of nonlinear vibrations ratio of the plate with hinge fixing of the edges  $x = \pm a$  :

$$\omega^2 = \omega_0^2 \left( 1 + \frac{3}{4} KA^2 \right), \quad (6)$$

has been analyzed, where  $\omega$  is the fundamental frequency of nonlinear natural vibrations of the plate,  $A$  is the dimensionless amplitude,  $\omega_0 = c_2 \lambda^2 / \sqrt{\alpha_1^2 + \lambda^2}$  is the fundamental frequency of linear natural vibrations of the plate,  $c_2 = \sqrt{A/2\rho h}$  is the velocity of shear wave propagation in the plate,  $\lambda = \pi/2a$ ,

$$K = K_c(1 + 4\beta), \quad \beta = \frac{\pi^2}{12} (h/a)^2 \frac{1}{k'} (E/G') \frac{1+\alpha}{1-\nu^2}. \quad (7)$$

The equality (7) has the same form as in Ref. [1] for the plate sufficiently long in one direction with hinge-fixed edges when the classical theory is applied. For motionless hinges the value of the coefficient  $K_c = 3$  was obtained in Ref. [1]. If in equality (7) passing to the limit is performed

$$\lim_{E/G' \rightarrow 0} K(E/G') = K_c = 3 \quad (8)$$

we can obtain the analogous result.

For the fundamental frequency of nonlinear transversal vibrations of the plate hold rigidly on the edges to be found, it is necessary to choose the unknown functions in (1)–(3) in such way that the boundary

conditions (5) were satisfied

$$w = W(t) \cos^2 \lambda x, \quad \gamma = Y(t) \sin 2\lambda x, \quad u = U(t) \sin 4\lambda x. \quad (9)$$

Neglecting in Eq. (2) the inertia of the element normal to the median plane [5], we obtain:

$$Y(t) = \frac{\alpha_1^2 \lambda}{\alpha_1^2 + 4\lambda^2} W(t). \quad (10)$$

To define the function  $U(t)$  from (1) we have an ordinary differential equation

$$\ddot{U}(t) + 4\omega_u^2 U(t) = \frac{1}{4} \lambda \omega_u^2 W^2(t),$$

the solution of which is written in the form

$$U(t) = C_1 \sin \omega_u t + C_2 \cos \omega_u t + \frac{1}{8} \lambda \omega_u \int_0^t W^2(\tau) \sin \omega_u(t - \tau) d\tau, \quad (11)$$

where  $\omega_u = 2\lambda c_1$  is the fundamental frequency of linear longitudinal vibrations of the plate.

From the initial condition at moment  $t = 0$  the velocity of points of the median plane along the axis is equal to zero and the median plane itself takes the form of the surface

$$w(0, x) = W(0) \cos^2 \lambda x,$$

we can define the integration constants

$$C_1 = 0, \quad C_2 = \frac{1}{16} W^2(0). \quad (12)$$

If we introduce the dimensionless values into consideration

$$\xi(t) = W(t)/2h, \quad \eta(t) = U(t)/2a \quad (13)$$

by substitution (10) and (11), with regard for (12) in (3), after application of the Bubnov-Galerkin procedure [1], we obtain the integro-differential equation for the function of dimensionless bending of the nonlinear transversal vibrations of the plate considered:

$$\begin{aligned} \ddot{\xi}(t) + (\omega_0^1)^2 \xi(t) + \frac{(\omega_0^1)^2}{2} K \xi(t) \left\{ \xi^2(t) - \left[ \xi^2(0) \cos \omega_u t + \right. \right. \\ \left. \left. + \omega_u \int_0^t \xi^2(\tau) \sin \omega_u(t - \tau) d\tau \right] \right\} = 0, \end{aligned} \quad (14)$$

where  $\omega_0^1 = \frac{4\sqrt{3}}{3} c_2 \lambda^2 / \sqrt{\alpha_1^2 + 4\lambda^2}$  is the fundamental frequency of free linear transversal vibrations of the plate hold rigidly on the edges;

$$K_1 = K_{c1}(1 + 4\beta). \quad (15)$$

The passing to the limit in (15) as the parameter pliability to transversal shear strains

$E / G'$  approaches zero

$$\lim_{E/G' \rightarrow 0} K_1(E/G') = K_{c1} = 3/4 \quad (16)$$

yields the classical result from Ref. [1].

If we integrate the equations (14) by the full period of vibrations  $T = 2\pi / \omega$  neglecting appropriate of infinitesimal values, as in Refs. [1, 5], we obtain the relation like expression (6)

$$\omega^2 = (\omega_0^1)^2 \left( 1 + \frac{3}{4} K_1 A^2 \right). \quad (17)$$

### 3. ANALYSIS OF THE RESULTS

Introduce the notations  $\mu_1$  and  $\mu_2$  for the value  $\omega$  to corresponding fundamental frequencies of natural free vibrations of the plate ratio

$$\mu_1 = \frac{\omega}{\omega_0} = \sqrt{1 + \frac{3}{4} K A^2}, \quad \mu_2 = \frac{\omega}{\omega_0} = \sqrt{1 + \frac{3}{4} K_1 A^2} \quad (18)$$

and consider the value

$$\eta = \frac{\omega_0^1}{\omega_0} = \frac{4\sqrt{3}}{3} \sqrt{\frac{1 + 4\bar{\alpha}(h/a)^2}{1 + \bar{\alpha}(h/a)^2}}, \quad \bar{\alpha} = \frac{\pi^2}{4} \frac{E}{G' k'} \frac{1}{1 - \nu^2}. \quad (19)$$

It is obvious that for  $h/a \ll 1$  and limited value of pliability to transversal shear  $E/G'$

$$\eta \approx 4\sqrt{3}/3 \approx 2,31. \quad (20)$$

In coordinates  $\mu, A$  ( $\mu = \mu_1, \mu_2$ ), we construct the backbone curves [1], illustrating the dependences between the dimensionless frequencies  $\mu_1, \mu_2$  and the dimensionless amplitude  $A$ . Moreover, for one coordinate we have the following dependence:

$$\mu_2 = \eta \mu_1. \quad (21)$$

The coefficient  $\eta$  we shall call the influence coefficient on the amplitude-frequency characteristics of hold rigidly edges which is compared with the hinge fixed. Figs. 1, 2 present the backbone curves for  $h/a = 0,1, \nu = \nu' = 0,375$  for different values  $E/G'$ :  $E/G' = 0$  shear and compression strains are absent,  $E/G' = 2(\nu + 1)$  for isotropic material,  $E/G' = 10$  and  $60$ .

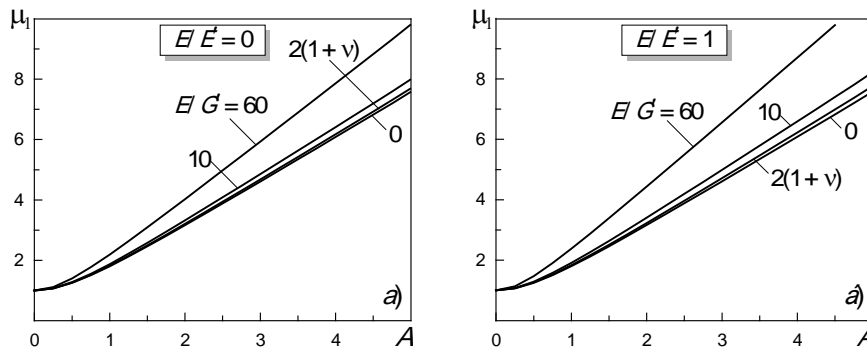


Fig.1. The dimensionless frequency  $\mu_1$  vs. the dimensionless amplitude  $A$  neglecting (a) and transversal compression for different values  $E/G'$  (b).

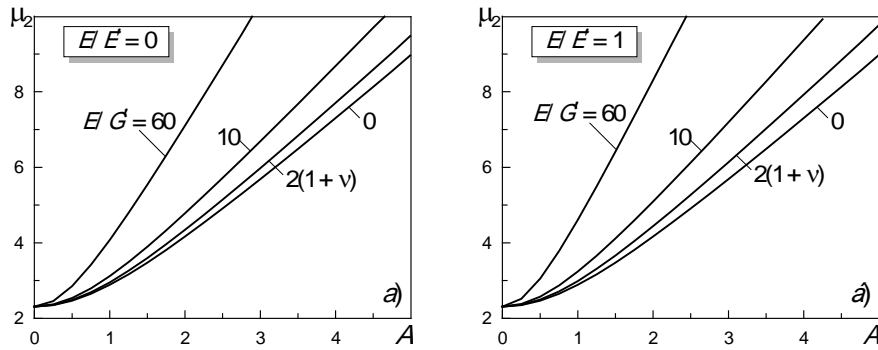


Fig.2. The dimensionless frequency  $\mu_2$  vs. the dimensionless amplitude  $A$  neglecting (a) and transversal compression for different values  $E/G'$  (b).

When parameters  $h/a$  and  $\nu$  are given we have observed a considerable influence of the edges fixing type and pliability parameter  $E/G'$  on the value  $\mu_1$  and  $\mu_2$  for  $1 \leq A \leq 5$  in comparison with classical results for  $E/G' = 0$ .

#### 4. CONCLUSION

Taking into account the pliability to transversal shear and compression strains for nonlinear vibrations of composite plates, we can increase the rigidity of the dynamic system considered. In defining the frequency of nonlinear vibrations of composite plates with amplitude close to five thicknesses, it is necessary to utilize the refined mathematical model. Provided that the edges are hold rigid the fundamental frequency increases by 2.31 times in comparison with hinge fixed edges of the plate.

#### REFERENCES

- [1] Vol'mir A.S. *Nonlinear Dynamic of Plates and Shells*. M.: Nauka, 1972.
- [2] Kurpa L. V., Timchenko G. M. Investigation into nonlinear vibrations of composite plates using the  $R$ -function theory. *Strength of Materials*, **Vol. 39**, No. 5, pp. 101–113, 2007.
- [3] Krysh'ko V.A. *Nonlinear Static and Dynamics Nonhomogeneous Shells*. Saratov: Publisher of the Saratov University, 1976.
- [4] *Mechanics of Composites: In 12v. Vol. 9: Dynamics of Construction Elements / V.D. Kubenko, A.E. Babayev, E.I. Bepalova and other*. A.S.K., Kiev, 1999.
- [5] Marchuk M.V., Pakosh V.S., Tuchapsky R.I., Khomyak M.M. Nonlinear Oscillations of Pliable to Tansversal Shear and Compressive Strains of Plates. *Mechanical Engineering*, No 11, pp. 12–15, 2001.
- [6] Marchuk M. Nonlinear Deformations and Vibrations of Pliability to Transversal Shear Strains and Compression Plates and Shells. *Mechanical Engineering*, No. 10, pp. 9–14, 2005.
- [7] Rushchitsky J.J., Tsurpal S.I. *Waves in Materials with the Microstructure*. Kyiv: Timoshenko Institute of Mechanics, National Academy of Sciences of Ukraine, 1997.

**NONLINEAR ANALYSES OF THE LAMINATED PLATES OF THE SYMMETRIC STRUCTURE SUBJECTED TO STATIC IN THE PLANE FORCES**

**Mazur O.<sup>1</sup>,  
Linnik A.,  
Tkachenko V.**  
National Technical  
University "KhPI"  
Kharkiv, Ukraine

---

ABSTRACT

---

The numerically-analytical method of nonlinear vibration research for laminated plates loaded by static in-plane force is proposed. The joint use of the R-functions and variational methods allows apply the offered approach to a plate with a complex form and different types of boundary conditions.

---

**INTRODUCTION**

The analysis of the geometrically nonlinear vibrations of composite plates and shells have received an exceptional interest in literature due to wide application of laminated plates for modeling elements in modern structures. Usually such elements have a different shape and therefore the study of dynamical behavior of these elements is a very difficult mathematical problem. In this work we propose effective approach based on using variational methods and the R-functions theory (RFM) in order to carry out the nonlinear analysis of laminated plates with an arbitrary planform and different boundary conditions, which are subjected to static load in the middle plane. Formerly this approach was successfully used for orthotropic plates [7] and for the investigation of free nonlinear vibrations of laminated plates and shells [5, 8-10]. The action of static load in the middle plane leads to the deformation of plate and affects the dynamic behavior. It should be noted that the study of plate vibrations subjected to static load is also important because it is part of the dynamic analysis of plates with periodic load, dynamic instability and parametric vibrations [2].

The proposed method is numerically implemented in the system POLE-RL and is illustrated by some examples.

**1. FORMULATION OF THE PROBLEM**

Let us consider free geometrically nonlinear vibrations of laminated plates of a symmetric structure in relation to the middle plane, which is subjected to a static load in its plane. It is assumed that the delamination of the layers is absent. The mathematical formulation of the problem is made in the framework of the classical theory based on the Kirchhoff – Love hypotheses. Let us consider the movement equations in operator form [1, 6]:

$$L_{11}(u) + L_{12}(v) = -Nl_1(w), \tag{1}$$

$$L_{21}(u) + L_{22}(v) = -Nl_2(w), \tag{2}$$

$$L_{33}(w) = -Nl_3(u, v, w) - m_1 \frac{\partial^2 w}{\partial t^2}, \tag{3}$$

where  $u, v, w$  are displacements of the plate in directions  $Ox, Oy$  and  $Oz$  respectively. In expressions (1)-(3) the differential operators  $L_{ij}, Nl_i$   $i, j = 1, 2, 3$  are defined as follows:

$$L_{11} = C_{11} \frac{\partial^2}{\partial x^2} + 2C_{16} \frac{\partial^2}{\partial x \partial y} + C_{66} \frac{\partial^2}{\partial y^2},$$

$$L_{22} = C_{66} \frac{\partial^2}{\partial x^2} + 2C_{26} \frac{\partial^2}{\partial x \partial y} + C_{22} \frac{\partial^2}{\partial y^2},$$

---

<sup>1</sup> Corresponding author. Email [Mazur.Olga@mail.ru](mailto:Mazur.Olga@mail.ru)

$$\begin{aligned}
L_{12} = L_{21} &= C_{16} \frac{\partial^2}{\partial x^2} + (C_{12} + C_{66}) \frac{\partial^2}{\partial x \partial y} + C_{26} \frac{\partial^2}{\partial y^2}, \\
L_{33} &= D_{11} \frac{\partial^4}{\partial x^4} + 2(D_{12} + 2D_{66}) \frac{\partial^4}{\partial y^2 \partial x^2} + 4D_{16} \frac{\partial^4}{\partial x^3 \partial y} + 4D_{26} \frac{\partial^4}{\partial y^3 \partial x} + D_{22} \frac{\partial^4}{\partial y^4}, \\
Nl_1 &= \frac{\partial}{\partial x} \left\{ \frac{1}{2} C_{11} \left( \frac{\partial}{\partial x} \right)^2 + \frac{1}{2} C_{12} \left( \frac{\partial}{\partial y} \right)^2 + C_{16} \frac{\partial}{\partial x} \frac{\partial}{\partial y} \right\} + \frac{\partial}{\partial y} \left\{ \frac{1}{2} C_{16} \left( \frac{\partial}{\partial x} \right)^2 + \frac{1}{2} C_{26} \left( \frac{\partial}{\partial y} \right)^2 + C_{66} \frac{\partial}{\partial x} \frac{\partial}{\partial y} \right\}, \\
Nl_2 &= \frac{\partial}{\partial x} \left\{ \frac{1}{2} C_{16} \left( \frac{\partial}{\partial x} \right)^2 + \frac{1}{2} C_{26} \left( \frac{\partial}{\partial y} \right)^2 + C_{66} \frac{\partial}{\partial x} \frac{\partial}{\partial y} \right\} + \frac{\partial}{\partial y} \left\{ \frac{1}{2} C_{12} \left( \frac{\partial}{\partial x} \right)^2 + \frac{1}{2} C_{22} \left( \frac{\partial}{\partial y} \right)^2 + C_{26} \frac{\partial}{\partial x} \frac{\partial}{\partial y} \right\}, \\
Nl_3 &= N_x \frac{\partial^2 w}{\partial x^2} + N_y \frac{\partial^2 w}{\partial y^2} + 2N_{xy} \frac{\partial^2 w}{\partial x \partial y}.
\end{aligned}$$

Here  $N_x$ ,  $N_y$ ,  $N_{xy}$  – normal and tangential forces in the middle plane, which are determined for multilayer plates by known formulas shown below in the matrix form [1]:

$$\vec{N} = (N_x, N_y, N_{xy})^T = \mathbf{C} \cdot \vec{\varepsilon}, \quad \text{where } \mathbf{C} = \begin{pmatrix} C_{11} & C_{12} & C_{16} \\ C_{12} & C_{22} & C_{26} \\ C_{16} & C_{26} & C_{66} \end{pmatrix}, \quad \vec{\varepsilon} = (\varepsilon_x, \varepsilon_y, \varepsilon_{xy})^T, \quad (4)$$

In these formulas the deformation components  $\varepsilon_x$ ,  $\varepsilon_{xy}$ ,  $\varepsilon_y$ , are defined as

$$\varepsilon_x = \frac{\partial u}{\partial x} + \frac{1}{2} \left( \frac{\partial w}{\partial x} \right)^2; \quad \varepsilon_{xy} = \frac{\partial u}{\partial y} + \frac{\partial v}{\partial x}; \quad \varepsilon_y = \frac{\partial v}{\partial y} + \frac{1}{2} \left( \frac{\partial w}{\partial y} \right)^2;$$

The values  $m_i$  and  $C_{ij}, D_{ij}$  ( $ij = 11, 22, 12, 16, 26, 66$ ), are defined as follows:

$$m_1 = \sum_{s=1}^N \int_{h_s}^{h_{s+1}} \rho_s dz, \quad (5)$$

$$(C_{ij}, D_{ij}) = \sum_{s=1}^N \int_{h_s}^{h_{s+1}} B_{ij}^{(s)}(1, z^2) dz. \quad (6)$$

In general, when the anisotropy axes do not coincide with the axes  $Ox$  and  $Oy$  elastic constants of the  $s$ -layer  $B_{ij}^{(s)}(i, j = 1, 2, 6)$  are expressed through the elastic constants of the initial system  $\tilde{B}_{ij}^{(s)}(i, j = 1, 2, 6)$  by the known formulas [1].

The system of equations is supplemented by boundary conditions, the expressions of which are determined by the way of fixing and loading of the plate boundary.

On the loaded part of the border the boundary conditions for the displacements in the plane are defined as

$$\begin{aligned}
N_n &= -p, \\
T_n &= 0.
\end{aligned} \quad (7)$$

where  $N_n, T_n$  – normal and tangential forces in the middle plane. Let us present them as follows:

$$\begin{aligned}
N_n &= N_n^{(L)} + N_n^{(D)}, \\
N_n^{(L)} &= \frac{\partial u}{\partial x} (C_{11} l^2 + C_{12} m^2 + 2C_{16} lm) + \frac{\partial v}{\partial y} (C_{12} l^2 + C_{22} m^2 + 2C_{26} lm) + \\
&\quad + \left( \frac{\partial u}{\partial y} + \frac{\partial v}{\partial x} \right) (C_{16} l^2 + C_{26} m^2 + 2C_{66} lm),
\end{aligned}$$

$$\begin{aligned}
N_n^{(D)} &= \frac{1}{2} \left( \frac{\partial w}{\partial x} \right)^2 (C_{11}l^2 + C_{12}m^2 + 2C_{16}lm) + \frac{1}{2} \left( \frac{\partial w}{\partial y} \right)^2 (C_{12}l^2 + C_{22}m^2 + 2C_{26}lm) + \\
&\quad + \frac{\partial w}{\partial y} \cdot \frac{\partial w}{\partial y} (C_{16}l^2 + C_{26}m^2 + 2C_{66}lm), \\
T_n &= T_n^{(L)} + T_n^{(D)}, \\
T_n^{(L)} &= \frac{\partial u}{\partial x} (C_{11}(l^2 - m^2) + (C_{12} - C_{11})lm) + \frac{\partial v}{\partial y} (C_{26}(l^2 - m^2) + (C_{22} - C_{12})lm) + \\
&\quad + \left( \frac{\partial u}{\partial y} + \frac{\partial v}{\partial x} \right) (C_{66}(l^2 - m^2) + (C_{26} - C_{16})lm), \\
T_n^{(D)} &= \frac{1}{2} \left( \frac{\partial w}{\partial x} \right)^2 (C_{16}(l^2 - m^2) + (C_{12} - C_{11})lm) + \frac{1}{2} \left( \frac{\partial w}{\partial y} \right)^2 (C_{26}(l^2 - m^2) + (C_{22} - C_{12})lm) + \\
&\quad + \frac{\partial w}{\partial y} \cdot \frac{\partial w}{\partial y} (C_{66}(l^2 - m^2) + (C_{26} - C_{16})lm)
\end{aligned}$$

## 2. METHOD OF SOLUTION

The proposed method consists of several stages.

**1<sup>st</sup> stage.** To determine the subcritical state of the plate it is necessary to find the functions that satisfy the following equations

$$\begin{aligned}
L_{11}u_1 + L_{12}v_1 &= 0, \\
L_{21}u_1 + L_{22}v_1 &= 0
\end{aligned} \tag{8}$$

and non-homogeneous boundary conditions

$$\begin{aligned}
N_n^{(L)}(u_1, v_1) &= -p, \\
T_n^{(L)}(u_1, v_1) &= 0.
\end{aligned}$$

It is important to note that this problem can be regarded as a plane problem of elasticity theory which variational formulation is reduced to finding the minimum of the following functional:

$$I(u_1, v_1) = \frac{1}{2} \iint_{\Omega} (N_x^{(L)} \varepsilon_x + N_y^{(L)} \varepsilon_y + N_{xy}^{(L)} \varepsilon_{xy}) d\Omega + \int_{\partial\Omega_1} N_n^{(L)} u_{1n} d\Omega_1, \tag{9}$$

where  $\partial\Omega_1$  is part of the border loaded by the external forces

$$\vec{N}_n^{(L)} = (N_x^{(L)}, N_y^{(L)}, N_{xy}^{(L)})^T = \mathbf{C} \cdot \vec{\varepsilon}^{(L)},$$

here  $\vec{\varepsilon}^{(L)} = \left( \frac{\partial u}{\partial x}, \frac{\partial v}{\partial y}, \frac{\partial u}{\partial y} + \frac{\partial v}{\partial x} \right)^T$ .

On the whole this problem may be solved by RFM.

**2<sup>nd</sup> stage.** A linear problem of the plate vibrations compressed by static load in the middle plane may be solved by Ritz method as a result of functional minimization:

$$J = \Pi_{\max} - T_{\max}, \tag{10}$$

where  $T_{\max}$  is kinetic energy of the plate and  $\Pi_{\max}$  is maximum potential energy of the plate:

$$\begin{aligned}
T_{\max} &= \frac{m_1 \omega_L^2}{2} \int_{\Omega} (u^2 + v^2 + w^2) d\Omega \\
\Pi_{\max} &= \frac{1}{2} \iint_{\Omega} [(M_x \chi_x + M_y \chi_y + M_{xy} \chi_{xy}) + \\
&\quad + p(N_x^{(L)}(u_1, v_1) \left( \frac{\partial w}{\partial x} \right)^2 + N_y^{(L)}(u_1, v_1) \left( \frac{\partial w}{\partial y} \right)^2 + N_{xy}^{(L)}(u_1, v_1) \frac{\partial w}{\partial x} \frac{\partial w}{\partial y}] dx dy.
\end{aligned}$$

where  $\omega_L$  is the natural frequency, corresponding to a given load  $p$ ,  $M_x, M_y, M_{xy}$  are bending and shear moments, which are defined for multilayer symmetric plates as follows:

$$\vec{M} = (M_x, M_y, M_{xy})^T = \mathbf{D} \cdot \vec{\chi}; \quad \text{где } \mathbf{D} = \begin{pmatrix} D_{11} & D_{12} & D_{16} \\ D_{12} & D_{22} & D_{26} \\ D_{16} & D_{26} & D_{66} \end{pmatrix}, \quad \vec{\chi} = (\chi_x, \chi_y, \chi_{xy})^T.$$

In these formulas the deformation components  $\chi_x, \chi_{xy}, \chi_y$  are defined as

$$\chi_x = -\frac{\partial^2 w}{\partial x^2}; \quad \chi_{xy} = -2\frac{\partial^2 w}{\partial x \partial y}; \quad \chi_y = -\frac{\partial^2 w}{\partial y^2},$$

Thus, the solution of the linear vibration problem is reduced to an eigenvalue problem with the appropriate boundary conditions.

**3<sup>rd</sup> stage.** Let us present unknown functions  $(u, v, w)$  in the following way:

$$\begin{aligned} w(x, y, t) &= y(t) \cdot w_1(x, y), \\ u(x, y, t) &= u_1(x, y) + y^2(t) \cdot u_2(x, y), \\ v(x, y, t) &= v_1(x, y) + y^2(t) \cdot v_2(x, y). \end{aligned} \quad (11)$$

Here  $w_1(x, y)$  is eigenfunction corresponding to the natural frequency  $\omega_L$ , and  $(u_2, v_2)$  have to satisfy the non-homogeneous linear system of the differential equations:

$$\begin{aligned} L_{11}(u_2) + L_{12}(v_2) &= -Nl_1(w_1), \\ L_{21}(u_2) + L_{22}(v_2) &= -Nl_2(w_1), \end{aligned}$$

and the following boundary conditions:

$$\begin{aligned} N_n^{(L)}(u_2, v_2) &= -N_n^{(D)}(w_1), \\ T_n^{(L)}(u_2, v_2) &= -T_n^{(D)}(w_1). \end{aligned}$$

The solution of this problem may be reduced to the variational problem of the functional minimum determination:

$$\begin{aligned} I(u_2, v_2) &= \frac{1}{2} \iint_{\Omega} (N_x \varepsilon_x + N_y \varepsilon_y + N_{xy} \varepsilon_{xy} - 2(Nl_1(w_1)u_2 + Nl_2(w_1)v_2)) d\Omega + \\ &+ \int_{\partial\Omega_1} N_n^{(D)}(u_2 l + v_2 m) + T_n^{(D)}(-u_2 m + v_2 l) d\Omega_1, \end{aligned}$$

Substituting expressions (11) into equation (3), and using the Bubnov-Galerkin method, we can obtain the following ordinary nonlinear differential equation of the Duffing's type:

$$y_1''(t) + \omega_L^2 (y(t) + \beta \cdot y^3(t)) = 0, \quad (12)$$

where  $\omega_L$  is the natural frequency of the linear plate vibration and  $\beta$  defined as follows:

$$\beta = -\frac{\int_{\Omega} Nl_3(u_2, v_2, w_1) \cdot w_1 d\Omega}{m_1 \Omega_L^2 \|w_1\|^2},$$

where  $N_x^L, N_y^L, N_{xy}^L$  are linear forces in the middle plate.

**4<sup>th</sup> stage.** The resulting differential equation (12) can be solved in different ways. We are applying the Bubnov-Galerkin method. Let us present the solution as follows

$$y(t) = A \cos \omega_N t, \quad (13)$$

where  $A$  is amplitude and  $\omega_N$  is nonlinear vibration frequency. Applying Bubnov-Galerkin method to equation (12), we obtain the relationships between the ratio of linear and nonlinear fundamental frequencies  $\nu = \omega_N / \omega_L$  and amplitude  $A$  as follows

$$\nu = \sqrt{1 + \frac{3}{4} \beta A^2}. \quad (14)$$

### 3. NUMERICAL INVESTIGATION.

Let us apply the proposed approach to the study of nonlinear vibration of the single-layer orthotropic plate (Fig. 1). Let us consider the follow boundary conditions:

$$w = 0, \frac{\partial^2 w}{\partial n^2} = 0, N_n = -p, T_n = 0, (x, y) \in \partial\Omega_1 (\Omega_1 : x = \pm \frac{a}{2}),$$

$$w = 0, \frac{\partial^2 w}{\partial n^2} = 0, N_n = 0, T_n = 0, (x, y) \in \partial\Omega_2 = \partial\Omega / \partial\Omega_1,$$

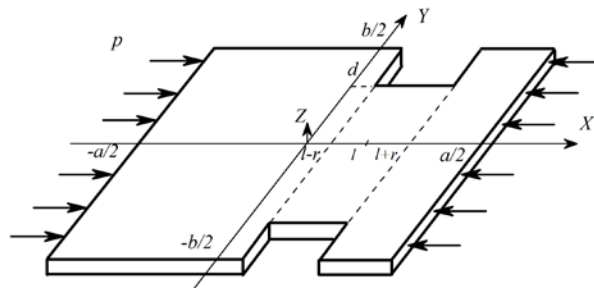


Figure 1. The single-layer orthotropic plate

For the given conditions the structure of solution [3,4] for  $u, v, w$  satisfying only the main boundary conditions takes the form of

$$u_i = P_i, v_i = P_{i+2}, i = 1, 2, w = \omega \cdot P_5, \quad (15)$$

where  $\omega(x, y) = 0$  is the equation of the whole boundary domain. The function  $\omega(x, y)$  is defined as follows

$$\omega(x, y) = f_1 \wedge_0 f_2 \wedge_0 (\bar{f}_3 \vee_0 f_4).$$

Here the functions  $f_1, f_2, f_3, f_4$  are defined as

$$f_1 = \frac{1}{a} \left( \left( \frac{a}{2} \right)^2 - x^2 \right) \geq 0, f_2 = \frac{1}{b} \left( \left( \frac{b}{2} \right)^2 - y^2 \right) \geq 0, f_3 = \frac{1}{2r} (r^2 - (x-l)^2) \geq 0, f_4 = \frac{1}{2d} (d^2 - y^2) \geq 0.$$

The symbols  $\wedge_0, \vee_0$  denote R-operations [3, 4]. In (15)  $P_i$  are indefinite components of the structure that are presented as an expansion in a series in a complete system (in this presentation power polynomials are used).

Calculations are carried out for glass – epoxy plate ( $E_1 / E_2 = 3, G / E_2 = 0.6, \nu_1 = 0.25$ ) with  $b/a = 1, pa^2 / h^3 E_2 = 1$ . The effect of a cutouts size on amplitude-frequency characteristics has been investigated for  $r/a = 0.2, 0.1, 0.05, d/a = 0.35, 0.4, 0.45, l/a = 0.1$  (Fig. 2). In Fig. 3 amplitude-frequency characteristics depending on the disposition of cutouts are presented. For such study we use various values of ratio  $l/a = 0, 0.1, 0.2, 0.3$  at fixed value of ratios  $r/a = 0.1, d/a = 0.4$ ). The analysis of the obtained results allows draw a conclusion that the size of given plate cutouts affects the characteristics considered much stronger than its disposition.

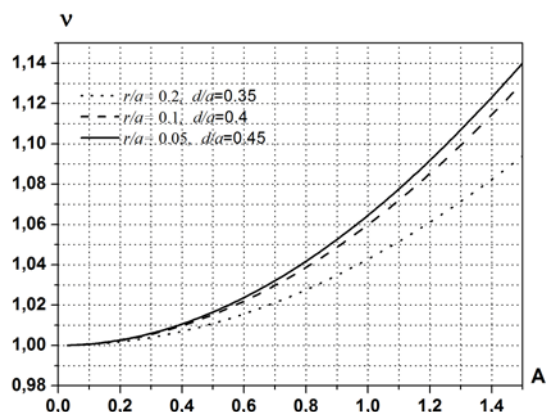


Fig. 2. Amplitude-frequency characteristics versus to cutouts size.

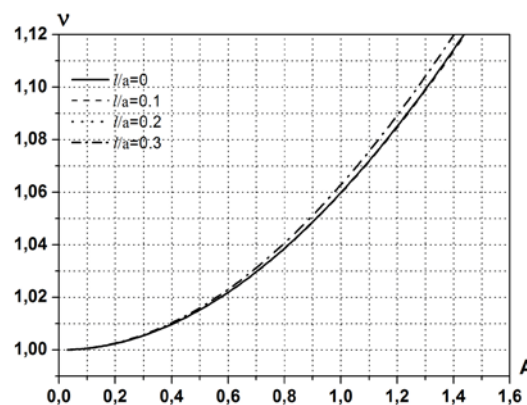


Fig. 3. Amplitude-frequency characteristics versus to cutouts disposition.

## CONCLUSIONS

The method of nonlinear vibration research of in-plane loaded laminated plates with a complex form is proposed. Due to the application of R-function theory in combination with variational methods the investigation of the movement equation is reduced to studying ordinary differential equation of the Duffing type. Using the offered method and the created software the dynamic behavior of plate with cutouts subjected by static load is studied. The effect of cutout size and cutout disposition on amplitude-frequency characteristics is analyzed.

## REFERENCES

- [1]. Ambartsumian S.A. *Theory of Anisotropic Plates*. Nauka, Moscow, 1967 (in Russian).
- [2]. Bolotin V.V. *The Dynamic Stability of Elastic Systems*. Gos. Tech. Izdat., Moscow, 1956 (in Russian).
- [3]. Rvachev V.L. *The R-Functions theory and its Some Application*, Naukova Dumka, Kiev, 1982 (in Russian).
- [4]. Kurpa L.V. *R-functions Method for Solving Linear Problems of Bending and Vibrations of Shallow Shells*. Kharkiv NTU Press, Kharkiv, 2009 (in Russian).
- [5]. Kurpa L.V., Tumchenko G.N. Free vibrations analysis of laminated plates with complex form in plane. *Applied Mechanics*, 2006, 42, №1, pp. 119-125.
- [6]. Volmir A.S., *Nonlinear Dynamics of Plates and Shells*. Nauka, Moscow, 1972 (in Russian).
- [7]. Awrejcewicz J., Kurpa L., Mazur O. Research of Stability and Nonlinear vibration of plates by R-Functions Method. In the book: *Modeling Simulation and Control of Nonlinear Engineering Dynamical Systems*. UK, Springer, 2009, pp.179-189.
- [8]. Singh A. V. Linear and geometrically nonlinear vibrations of fiber reinforced laminated plates and shallow shells. *Computers & Structures*, Vol. 76, Issues 1-3, pp. 277-285, 2000.
- [9]. Harras B., Benamar R. and White R. G. Geometrically Non-Linear Free Vibration Of Fully Clamped Symmetrically Laminated Rectangular Composite Plates. *Journal of Sound and Vibration*, Vol. 251, Issue 4, pp. 579-619, 2002.
- [10]. Zhang Y.X., Yang C.H. Recent developments in finite element analysis for laminated composite plates. *Composite Structures* 88, pp. 147–157, 2009.

**MATHEMATICAL MODELING OF DEFORMATION PROCESSES OF THE FLEXIBLE VISCOELASTIC PLATES WITH COMPLEX FORM**

**Nazirov Sh. A.**<sup>1</sup>

Uzbekistan Academy of Science,  
Tashkent, Uzbekistan

**Eshkaraeva N.G**

Uzbekistan Academy of Science,  
Karshi, Uzbekistan

ABSTRACT

The investigation method of the vibration of the flexible viscoelastic anisotropic plates is proposed. The nonlinear system of the three integro-differential equations with partial derivatives is mathematical formulation of this problem. The linearization of the problem is carried out by method of successive approximations. The obtained sequence of the linearized problems is solved by quadrature sums. The software for numerical implementation is developed.

Let us consider a mathematical model of vibrations of flexible viscoelastic plates, which is described by system of three nonlinear integro-differential equations in partial derivatives with appropriate boundary and with initial conditions.

In the derivation of the equilibrium equations Kirchhoff-Love hypotheses are used [1]

$$u_1 = u - z \frac{\partial w}{\partial x}, \quad u_2 = v - z \frac{\partial w}{\partial y}, \quad u_3 = w(x, y) \quad (1)$$

On this basis, the Cauchy relations can be written as [1]:

$$\varepsilon_{11} = \frac{\partial u}{\partial x} - z \frac{\partial^2 w}{\partial x^2} + \frac{1}{2} \left( \frac{\partial w}{\partial x} \right)^2, \quad \varepsilon_{22} = \frac{\partial v}{\partial y} - z \frac{\partial^2 w}{\partial y^2} + \frac{1}{2} \left( \frac{\partial w}{\partial y} \right)^2, \quad \varepsilon_{12} = \frac{\partial u}{\partial y} + \frac{\partial v}{\partial x} - 2z \frac{\partial^2 w}{\partial x \partial y} + \frac{\partial w}{\partial x} \frac{\partial w}{\partial y} \quad (2)$$

Kirchhoff-Love Hooke's law takes the following form [2]:

$$\sigma_{11} = B_{11}^* \varepsilon_{11} + B_{12}^* \varepsilon_{22} + B_{16}^* \varepsilon_{12}; \quad \sigma_{22} = B_{12}^* \varepsilon_{11} + B_{22}^* \varepsilon_{22} + B_{26}^* \varepsilon_{12}; \quad \sigma_{12} = B_{16}^* \varepsilon_{11} + B_{26}^* \varepsilon_{22} + B_{66}^* \varepsilon_{12} \quad (3)$$

where  $\varepsilon_{ij}$  and  $\sigma_{ij}$  ( $i = 1, 2, j = 1, 2$ ) are respectively, the components of the strain and stress vectors,

$B_{ij}^* = B_{ij} (1 - R_{ij}^*)$ ,  $R_{ij}^*[\cdot] = \int_0^t R_{ij}^*(t - \tau)[\cdot] d\tau$  is integral operator by Volterra with weak singular kernel of

heredity  $R_{ij}^*(t)$ , which can be used by Abel core, exponential or Rjanitsina-Koltunova one etc. [2-3].

Using variational principle by Ostrogradsky-Hamilton [1] and taking into account the approach by Boltzman [3, 7], the following equilibrium equations may be obtained

$$\begin{aligned} \frac{\partial N_{11}^*}{\partial x} + \frac{\partial N_{12}^*}{\partial y} + q_1 &= \rho h \frac{\partial^2 u}{\partial t^2}, \\ \frac{\partial N_{12}^*}{\partial x} + \frac{\partial N_{22}^*}{\partial y} + q_2 &= \rho h \frac{\partial^2 v}{\partial t^2}, \\ \frac{\partial^2 M_{11}^*}{\partial x^2} + 2 \frac{\partial^2 M_{12}^*}{\partial x \partial y} + \frac{\partial^2 M_{22}^*}{\partial y^2} + N_{11}^* \frac{\partial^2 w}{\partial x^2} + 2N_{12}^* \frac{\partial^2 w}{\partial x \partial y} + N_{22}^* \frac{\partial^2 w}{\partial y^2} + \left( \frac{\partial N_{11}^*}{\partial x} + \frac{\partial N_{12}^*}{\partial y} \right) \frac{\partial w}{\partial x} + \\ + \left( \frac{\partial N_{12}^*}{\partial x} + \frac{\partial N_{22}^*}{\partial y} \right) \frac{\partial w}{\partial y} + q_3 &= \rho h \frac{\partial^2 w}{\partial t^2} \end{aligned} \quad (4)$$

<sup>1</sup> Corresponding author. Email [shnazirov@mail.ru](mailto:shnazirov@mail.ru)

where  $w$  is the transverse displacement of the plate;  $u, v$  are the displacements of the plate in the mid-surface;  $q_1, q_2, q_3$  are the external loads;  $h$  is the plate thickness;  $M_{11}^*, M_{22}^*, M_{12}^*$  are the bending and twisting moments;  $N_{11}^*, N_{22}^*, N_{12}^*$  – are the normal and tangent forces;  $x, y$  are space variables;  $t$  is a time.

Let us write the expressions for stress resultants:

$$\begin{aligned} N_{11}^* &= h \left[ B_{11}^* \left( \frac{\partial u}{\partial x} + \frac{1}{2} \left( \frac{\partial w}{\partial x} \right)^2 \right) + B_{12}^* \left( \frac{\partial v}{\partial y} + \frac{1}{2} \left( \frac{\partial w}{\partial y} \right)^2 \right) + B_{16}^* \left( \frac{\partial u}{\partial y} + \frac{\partial v}{\partial x} + \frac{\partial w}{\partial x} \frac{\partial w}{\partial y} \right) \right], \\ N_{12}^* &= h \left[ B_{16}^* \left( \frac{\partial u}{\partial x} + \frac{1}{2} \left( \frac{\partial w}{\partial x} \right)^2 \right) + B_{26}^* \left( \frac{\partial v}{\partial y} + \frac{1}{2} \left( \frac{\partial w}{\partial y} \right)^2 \right) + B_{66}^* \left( \frac{\partial u}{\partial y} + \frac{\partial v}{\partial x} + \frac{\partial w}{\partial x} \frac{\partial w}{\partial y} \right) \right], \\ N_{22}^* &= h \left[ B_{12}^* \left( \frac{\partial u}{\partial x} + \frac{1}{2} \left( \frac{\partial w}{\partial x} \right)^2 \right) + B_{22}^* \left( \frac{\partial v}{\partial y} + \frac{1}{2} \left( \frac{\partial w}{\partial y} \right)^2 \right) + B_{26}^* \left( \frac{\partial u}{\partial y} + \frac{\partial v}{\partial x} + \frac{\partial w}{\partial x} \frac{\partial w}{\partial y} \right) \right], \end{aligned} \quad (5)$$

$$\begin{aligned} M_{11}^* &= - \left[ D_{11}^* \frac{\partial^2 w}{\partial x^2} + D_{12}^* \frac{\partial^2 w}{\partial y^2} + 2D_{16}^* \frac{\partial^2 w}{\partial x \partial y} \right], \\ M_{22}^* &= - \left[ D_{12}^* \frac{\partial^2 w}{\partial x^2} + D_{22}^* \frac{\partial^2 w}{\partial y^2} + 2D_{26}^* \frac{\partial^2 w}{\partial x \partial y} \right], \\ M_{12}^* &= - \left[ D_{16}^* \frac{\partial^2 w}{\partial x^2} + D_{62}^* \frac{\partial^2 w}{\partial y^2} + 2D_{66}^* \frac{\partial^2 w}{\partial x \partial y} \right] \\ D_{ij}^* &= D_{ij} (1 - R_{ij}^*), \quad D_{ij} = \frac{h^3}{12} B_{ij}, \quad (i, j = \overline{1, 6}). \end{aligned} \quad (6)$$

The equations are supplemented by boundary and initial conditions, which depend of type of fixing border of the plate.

The obtained system of nonlinear integro-differential equations are solved on the basis of the algorithm of linearization, which is based on the use of the method of successive approximations [4-5]. The initial values for displacements are put as:  $u_0 = 0$  and  $v_0 = 0$ , and the system of linear integro-differential equations is solved. Then, the obtained solution for deflection ( $w$ ) is substituted into the first two equations of the system of integro-differential equations. Further, the obtained solutions for displacements  $u, v$  are substituted into third equations of the system deflection. This process is fulfilled until satisfactory convergence for the results will be achieved. Separation of the variables is carried out by the Bubnov-Galerkin procedure [6], and R-functions by V.L. Rvachev [4]. The linearized systems of integro-differential equations with the initial condition are solved by quadrature sums method [3].

The software based on the proposed algorithm is developed. In the report, results of computational experiments for the clamped and simply supported viscoelastic flexible anisotropic plates of different shapes are discussed.

## References

- [1] Lechnitskiy S.G. *Anisotropic plates*. M.; L: Gostecheizdat, 355 p., 1947 (in Russian).
- [2] Iljushin A.A., Pobedria B.E. *Bases of Mathematical Theory of Viscoelasticity*. Nauka, Moscow, 780 p., 1970 (in Russian).
- [3] Badalov Ph.B. *Solving Methods Integral and Integro - Differential Equations of the Inherited Theory of the Viscoelasticity*. Mech.Mat., Tashkent, 247 p., 1987 (in Russian).
- [4] Rvachev V. L. and Kurpa L. V., *R-functions in Problems of the Theory of Plates*, Naukova Dumka, Kiev, 176 p., 1987 (in Russian).
- [5] Nazirov Sh.A., Eshkaraeva N.G. The Computational Algorithm of an Anisotropic Flexible Plates Calculation with the Complex Form. *Voprosi Vychislit. i Prikl. Matematiki*. Tashkent, V. 106, pp.82-8, 1999 (in Russian).
- [6] Mikhlin S.G. *Variational Methods in Mathematical Physics*. Nauka, Moscow, 512p. 1970 (in Russian).
- [7] Koltunov M.A. *Creep and Relaxation*. Higher School, Moscow, 276 p., 1976 (in Russian).

**APPLICATION OF THE R-FUNCTIONS THEORY AND SPLINE-APPROXIMATION  
TO FINDING EIGEN FUNCTIONS AS BASIC ONES FOR MESHLESS  
DISCRETIZATION OF THE LAMINATED SHALLOW SHELLS**

**A.A. Osetrov<sup>1</sup>**  
National Technical  
University, Kharkov,  
Ukraine

---

**ABSTRACT**

---

Investigation of the nonlinear dynamic behavior of composite laminated shallow shells in most cases is based on presentation of solution in a form of series by linear eigenfunctions. The proposed alternative method to extract eigenfunctions of the problem is based on the spline-approximation and the R-functions method (RFM). The first-order theory for multilayered shallow shells taking into account the shift deformations is used in a variational form.

---

Multilayered shells are widely spread in modern industry. The combination of advantageous features of composite materials and thin walled structures plays the principal role in the final designer choice. Composite materials allow create lighter constructions remaining sufficiently stiff and maintaining their strength. The choice of lamination schemes is an advanced option adding more flexibility than any isotropic material could give. On the other hand the thin walled elements maintain their stiffness and permit to decrease the used material amount. That is why the investigation of multilayered shallow shell's dynamic behavior is relevant. This relevance is proved by a number of papers published in this area [1-3]. But there are at present a lot of unsolved problems on this subject.

In the most cases when the nonlinear behavior of shells is examined the solution function is introduced in a form of series by eigenfunctions of the linear boundary problem. The correct choice of these basic functions and their number in the series allows to obtain accurate results. In the present paper an effective method of the problem eigenfunctions extraction is proposed. It is based on the R-functions theory and the spline-approximation, which allows investigate a dynamics of shallow shells with complex forms and different boundary conditions [4]. The theory used to model shallow shell's behavior is the first-order theory taking into account the shift deformations. Numerical realization of the proposed approach is based on a combined usage of mathematical package Maple and specialized algorithms programmed in C++. Nonlinear dynamics of multilayered shallow shells is to be examined further.

**REFERENCES**

- [1] Y.K. Cheung, Y.M. Fu Nonlinear static and dynamic analysis for laminated spherical caps of moderate thickness, *Nonlinear Dynamics*, No.8, pp. 251–268, 1995.
- [2] N.V.S. Naidu, P.K. Sinha Nonlinear finite element analysis of laminated composite shells in hygrothermal environments, *Composite Structures*, No.69, pp. 387–395, 2005.
- [3] L.V. Kurpa Nonlinear free vibrations of symmetrically laminated shallow shells with complex plan-form, *J. Math. Methods and Phys. Mech. Fields*, Vol.51, No.2, pp. 75-85, 2008 (in Russian).
- [4] L.V. Kurpa, A.A. Osetrov Study of free vibrations of shallow shells using the R-functions method and the spline-approximation, *J. Math. Methods and Phys. Mech. Fields*, Vol.50, No.4, pp. 83-93, 2007 (in Russian).

---

<sup>1</sup> Corresponding author. Email [andy8383@mail.ua](mailto:andy8383@mail.ua)

RESEARCH OF NATURAL OSCILLATIONS OF A PLATE  
WITH MIXED CONDITIONS OF CONTOUR FASTENING

---

**Anatoly N. Pasechnik**<sup>1</sup>

Ukrainian Academy of  
Customs  
Dnipropetrovs'k, Ukraine

**Vladimir A. Pasechnik,  
Nataly N. Novotna**

Dnipropetrovs'k National  
University  
Dnipropetrovs'k, Ukraine

---

ABSTRACT

On the basis of the method of perturbation of boundary conditions, the asymptotic method of calculation and analysis of natural oscillations of elastic rectangular plates is proposed. Mixed conditions of the plates fastening of contour, of the "pinched – hinge" type for symmetrical and asymmetrical placement of segments of the fastening, are considered.

## INTRODUCTION

In many cases the application of plates in real constructions is connected with necessity of use of different variants of fastening of certain segments of the plates contours [1]. Dynamic calculation of such constructions makes it necessary to analyze the mathematical models based on boundary value problems with such mixed boundary conditions. The development of methods for constructing solutions of these problems was the subject of the works [2–9]. Systematic work on specified issues suggests that the development of approximate analytical and numerical methods for analyze of mixed boundary value problems of the theory of plates is very topical. At present there are effective different methods of the perturbation theory to solve boundary value problems in the plates and shells theory [3, 8]. Therefore, in this paper, on the base of the method of disturbance of boundary conditions there is proposed the asymptotic method of calculation and analyze of natural oscillations of thin elastic rectangular plates with mixed conditions of the contour fastening of "pinched-hinge" type for symmetric and asymmetric placement of segments of fastening.

## 1. STATEMENT OF THE RESEARCH PROBLEM

One considers the natural oscillations of a rectangular plate with mixed conditions of contour fastening with the help of the method of disturbance of a kind of boundary conditions. The diagram of placement of segments for symmetric *a*) and asymmetric *b*) fastening of a plate is presented in the Figure 1. The appropriate dimensionless differential equations are the following [3]

$$\nabla^4 \bar{w} + \frac{\bar{m} b^4}{D} \bar{w}_{tt} = 0, \quad (1)$$

$$\nabla^4 \bar{w} = \left( \frac{\partial^2}{\partial \xi^2} + \frac{\partial^2}{\partial \eta^2} \right)^2,$$

where  $D$  is the cylindrical rigidity;  $\bar{m}$  is the reduced weight of a plate,  $a, b$  are the sizes of a plate;  $\xi, \eta$  are the dimensionless coordinates;  $\xi = x/b, \eta = y/b$ .

---

<sup>1</sup> [pasichnyk@amsu.dp.ua](mailto:pasichnyk@amsu.dp.ua)

The boundary value problem for the equation (1) is determined by the following mixed boundary conditions [8]

$$w = \eta w_{\xi\xi} = 0, \quad k \leq \xi \leq \pm 0.5, \quad (2)$$

$$w = 0, \quad w_{\eta\eta} = \bar{H}(\xi)(w_{\eta\eta} \pm w_{\eta}), \quad \eta = \pm 0.5, \quad (3)$$

where  $k = \frac{a}{b}$ ;  $\bar{H}(\xi) = H(\xi - ku) + H(-\xi - ku)$ ;  $H(\xi)$  is the Heaviside function.

## 2. THE METHOD OF CONSTRUCTION OF SOLUTION

For construction of the equation (1) solution, the method of separation of variables can be used:

$$\bar{w} = w(\xi, \eta) \cdot T(t). \quad (4)$$

After substitution of the expression (4) to the equation (1) we can receive two equations:

$$\frac{\partial^2 T}{\partial t^2} + \theta^2 T = 0, \quad (5)$$

$$\nabla^4 w - \lambda w = 0, \quad (6)$$

where  $\theta^2$  is circular frequency of natural lateral oscillations of a plate;  $\lambda = m\theta^2 b^4/D$  is the eigenvalue of the problem.

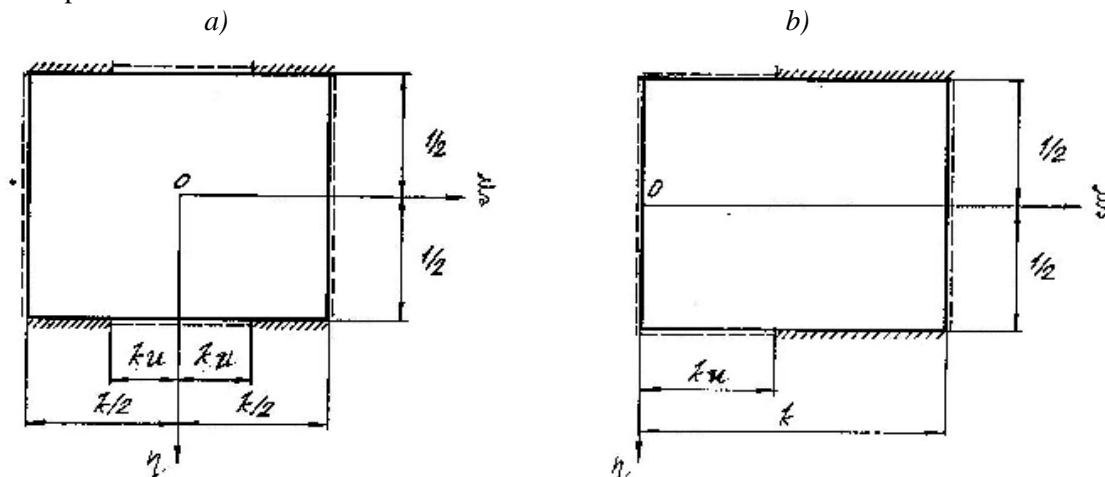


Fig. 1 The diagram of mixed conditions of fastening of a plate

According to [8] we enter the parameter  $\varepsilon$  into boundary conditions (3), under  $\varepsilon = 0$  the boundary conditions of the pin-joint type on all boundaries  $\eta = \pm 0,5$  were realized, and under  $\varepsilon = 1$  the initial mixed boundary conditions of the pinched-hinge types are realized:

$$w = 0, \quad w_{\eta\eta} = \bar{H}(\xi) \varepsilon (w_{\eta\eta} \pm w_{\eta}) \quad \text{under } \eta = \pm 0,5. \quad (7)$$

Under middle values of the parameter  $\varepsilon$  the mixed boundary conditions of elastic fastening - hinge type with the coefficient of elastic displacement  $\mu = \varepsilon/(1-\varepsilon)$  is realized.

For this purpose the small parameter method can be used for the problem natural value  $\lambda$  and the natural form  $w$ . The following power series by  $\varepsilon$  are presented:

$$w = \sum_{i=0}^{\infty} w_i \varepsilon^i; \quad \lambda = \sum_{i=0}^{\infty} \lambda_i \varepsilon^i. \quad (8)$$

Substituting series (8) to the equation (6) and boundary conditions (2), (7) and equating expressions at identical degrees of the parameter  $\varepsilon$  we are received the following recurrent sequence of the boundary value problems:

$$\varepsilon^0: \quad \nabla^4 w_0 - \lambda_0 w_0 = 0, \quad (9)$$

$$w_0 = 0, w_{0\xi\xi} = 0 \quad \text{under } \xi = \pm 0,5k, \quad w_0 = 0, w_{0\eta\eta} = 0 \quad \text{under } \eta = \pm 0,5;$$

$$\varepsilon^j : \quad \nabla^4 w_j - \lambda_0 w_j = \sum_{i=1}^j \lambda_i w_{j-1}, \quad (10)$$

$$w_j = 0, w_{j\xi\xi} = 0 \quad \text{under } \xi = \pm 0,5k, \quad w_j = 0, w_{j\eta\eta} = \pm \bar{H}(\xi) \sum_{i=0}^{j-1} w_{i\eta} \quad \text{under } \eta = \pm 0,5;$$

Let's consider the construction of solution of the problem for a case of directly symmetrical concerning axes  $\xi$  and  $\eta$  of the forms of natural oscillations.

In zero approximation one has:

$$w_0 = \xi_0 \cdot \eta_0 = \cos\left(\frac{\pi m}{k} \cdot \xi\right) \cdot \cos(\pi n \eta), \quad (11)$$

$$\lambda_0 = \pi^4 \cdot \left(n^2 + \frac{m^2}{k^2}\right)^2, \quad (n, m) = 1, 3, 5, \dots \quad (12)$$

As the first approximation we receive the following boundary value problem:

$$\nabla^4 \cdot w_1 - \lambda_0 \cdot w_1 = \lambda_1 \cdot w_0, \quad (13)$$

$$w_1 = 0, \quad w_{1\xi\xi} = 0 \quad \text{under } \xi = \pm 0,5k, \quad (14)$$

$$w_j = 0, \quad w_{j\eta\eta} = \pi n (-1)^{\frac{n-1}{2}} \bar{H}(\xi) \cos\left(\frac{\pi m}{k} \xi\right) \quad \text{under } \eta = \pm 0,5. \quad (15)$$

We can find the solution with the help of the method of decomposition:

$$w_1 = \sum_{i=1,3,\dots}^{\infty} Y_{1i} \cos\left(\frac{\pi i}{k} \xi\right). \quad (16)$$

After the substitution of the given expression to the boundary value problem (13) – (15) two boundary value problems are received:

$i = m$

$$Y_{1m}^{IV} - 2 \frac{\pi^2 m^2}{k^2} Y_{1m}^{II} - \pi^4 n^2 \left(2 \cdot \frac{m^2}{k^2} + n^2\right) Y_{1m} = \lambda_1 \cos(\pi n \eta) \quad (17)$$

$$Y_{1m} = 0 \quad Y_{1m}^{II} = \pm \pi \cdot n \cdot (-1)^{\frac{n-1}{2}} \cdot \gamma_{mm} \quad \text{under } \eta = \pm 0,5. \quad (18)$$

$i \neq m$

$$Y_{1i}^{IV} - 2 \cdot \frac{\pi^2 \cdot i^2}{k^2} \cdot Y_{1i}^{II} - \pi^4 \cdot \left(n^2 + \frac{m^2}{k^2}\right) - \frac{i^4}{k^4} \cdot Y_{1i} = 0, \quad (19)$$

$$Y_{1i}^{II} = \pm \pi \cdot n \cdot (-1)^{\frac{n-1}{2}} \cdot \gamma_{im}, \quad Y_{1i} = 0 \quad \text{under } \eta = \pm 0,5. \quad (20)$$

Here,

$$\gamma_{im} = \begin{cases} 2(0,5 - u) - \frac{1}{\pi m} \sin(2\pi mu) & \text{under } i = m, \\ \frac{4}{\pi(m^2 - i^2)} [i \sin(\pi ui) \cdot \cos(\pi um) - m \sin(\pi um) \cdot \cos(\pi ui)] & \text{under } i \neq m, \end{cases}$$

$$\bar{H}(\xi) \cos\left(\frac{\pi m}{k} \xi\right) = \sum_{i=1,3,5,\dots}^{\infty} \gamma_{im} \cos\left(\frac{\pi i}{k} \xi\right).$$

Taking into account conditions of uniform of asymptotic decomposition from the boundary value problem (17) – (18) we determine the first correction for the natural value  $\lambda_1$

$$\lambda_1 = \frac{-Y_{1m}'' Y_0' \Big|_{-0.5}^{0.5}}{\int_{-0.5}^{0.5} Y_0^2 d\eta} = 4\pi^2 n^2 \gamma_{mm}. \quad (21)$$

After determination  $\lambda_1$  we are received the following expression for  $Y_{1m}$

$$Y_{1m} = \frac{n}{\pi \alpha} \gamma_{mm} \left[ \frac{(-1)^{\frac{n-1}{2}}}{2 \operatorname{ch} \frac{\pi}{2} \beta_1} \operatorname{ch}(\pi \beta_1 \eta) - \eta s(\pi \eta) \right], \quad (22)$$

$$\alpha = n^2 + \frac{m^2}{k^2}; \quad \beta_1 = \sqrt{2 \frac{m^2}{k^2} + n^2}.$$

The solution of the problem (19) – (20) does not give corrections to the natural value, but it introduces additional items to the form of oscillations:

$$Y_{1i} = \frac{n(-1)^{\frac{n-1}{2}}}{2\pi \left( \frac{i^2}{k^2} + n^2 \right)} \gamma_{im} \left[ \frac{\operatorname{ch}(\alpha_{1i} \eta)}{\operatorname{ch} \frac{\alpha_{1i}}{2}} \frac{\left\{ \begin{array}{l} \operatorname{ch}(\varphi_{1i} \eta) \\ \operatorname{cos}(\beta_{1i} \eta) \end{array} \right\}}{\left\{ \begin{array}{l} \operatorname{ch} \frac{\varphi_{1i}}{2} \\ \operatorname{cos} \frac{\beta_{1i}}{2} \end{array} \right\}} \right], \quad \left\{ \begin{array}{l} i^2 > m^2 + n^2 k^2 \\ i^2 < m^2 + n^2 k^2 \end{array} \right\}, \quad (23)$$

$$\alpha_{1i} = \pi \sqrt{\frac{i^2 + m^2}{k^2} + n^2}; \quad \beta_{1i} = \pi \sqrt{\frac{m^2 - i^2}{k^2} + n^2}; \quad \varphi_{1i} = \pi \sqrt{\frac{i^2 - m^2}{k^2} - n^2}.$$

Summarizing the expressions (21) and (22) and taking into account the decomposition (16), we receive the first correction to the natural form  $w_1$  for directly symmetrical oscillations

$$w_1 = \frac{m}{\pi \alpha} \left\{ \gamma_{mm} \left[ \frac{(-1)^{\frac{n-1}{2}}}{2 \operatorname{ch} \frac{\pi}{2} \beta_1} \operatorname{ch}(\pi \beta_1 \eta) - \eta s(\pi \eta) \right] \left( \frac{\pi m}{k} \xi \right) + \right.$$

$$\left. + (-1)^{\frac{n-1}{2}} \sum_{i=1,3,5,\dots}^{\infty} \gamma_{im} \left[ \frac{\operatorname{ch}(\alpha_{1i} \eta)}{\operatorname{ch} \frac{\alpha_{1i}}{2}} \frac{\left\{ \begin{array}{l} \operatorname{ch}(\varphi_{1i} \eta) \\ \operatorname{cos}(\beta_{1i} \eta) \end{array} \right\}}{\left\{ \begin{array}{l} \operatorname{ch} \frac{\varphi_{1i}}{2} \\ \operatorname{cos} \frac{\beta_{1i}}{2} \end{array} \right\}} \right] \operatorname{cos} \left( \frac{\pi m}{k} \xi \right) \right\}. \quad (24)$$

Similarly we receive the expression for the second correction to the natural value  $\lambda_2$ :

$$\lambda_2 = 4\pi^2 n^2 \gamma_{mm} \left\{ 1 - \frac{\gamma_{mm}}{\pi^2 \alpha} \left[ \frac{\pi \beta_1}{2} th \frac{\pi \beta_1}{2} + \frac{n^2}{\alpha} - \frac{3}{2} \right] \right\} - \frac{2n^2}{\alpha} \sum_{i=1,3,5,\dots}^{\infty} \gamma_{im}^2 \left[ \alpha_i th \frac{\alpha_i}{2} + \left\{ \begin{array}{l} -\varphi_{1i} th \frac{\varphi_{1i}}{2} \\ \beta_{1i} tg \frac{\beta_{1i}}{2} \end{array} \right\} \right]. \quad (25)$$

Considering the central symmetrical forms of oscillations, similarly we receive the analytical expressions of the natural values and forms for any values of wave numbers by the way of sections of series of disturbance:

$$\lambda = \pi^4 \alpha^4 + 4\pi^2 \alpha^2 \gamma_{mm} \varepsilon + \left\{ 4\pi^2 n^2 \gamma_{mm} \left( 1 - \frac{\gamma_{mm}}{\pi^2 \alpha} \left[ \frac{\pi \beta_1}{2} cth^{(-1)^m} \frac{\pi \beta_1}{2} + \frac{n^2}{\alpha} - \frac{3}{2} \right] \right) - \frac{2n^4}{\alpha} \sum_{\substack{i=1,3,5,\dots \\ i=2,4,6,\dots}}^{\infty} \gamma_{im}^2 \left[ \alpha_i cth^{(-1)^j} \frac{\alpha_{1i}}{2} + \left\{ \begin{array}{l} -\varphi_{1i} cth^{(-1)^j} \frac{\varphi_{1i}}{2} \\ \beta_{1i} ctg^{(-1)^j} \frac{\beta_{1i}}{2} \end{array} \right\} \right] \right\} \varepsilon^2 + \dots, \quad (26)$$

where

$$\gamma_{im} = \begin{cases} 2(0,5 - u) + \frac{(-1)^m}{\pi m} \sin(2\pi m u) & \text{under } i = m, \\ \frac{4}{\pi(m^2 - i^2)} \left[ \begin{array}{l} i \\ m \end{array} \right] \sin(\pi u i) \cdot \cos(\pi u m) - \begin{array}{l} m \\ i \end{array} \left[ \begin{array}{l} i \\ m \end{array} \right] \sin(\pi u m) \cdot \cos(\pi u i) \end{array} & \text{under } i \neq m. \end{cases}$$

The problem of determination of natural frequencies of a plate having asymmetric segments of mixed boundary conditions (pic.1, b) can be decided the same way.

Further section of the series for the natural value must be rebuilt to the fractional rational function AP and we can calculate the the first natural value of the boundary value problem (6), (7), (2) under  $\varepsilon = 1$ .

### 3. THE ANALYSIS

Results of numerical analysis of dependence of the natural vibration frequency from the size of the segment are presented in Figure 2.

The solutions obtained on the basis of proposed approach for a plate with symmetric and asymmetric placement of the segment of substitution is represented by the curves 1, 2 and 3. The results obtained by the method of integral equations [9], 4, 5 are experimental data [9] and 6 are the results for some middle values of  $u$ , obtained by the dual series [7]. For the limiting case  $\varepsilon = 1$ , with complete pinch of the boundary of the plate  $\eta = \pm 0,5$  the first natural value problem computed on the basis of the constructed solution is equal to  $\lambda = 1,7081\pi^4$ , as obtained numerically [5, 6] –  $\lambda = 1,7050\pi^4$  (error is 0, 18%). Analysis of the data shows that in general, the discrepancy of the results obtained with certain items does not exceed 2%.

For the case of symmetrical placement of the segments of pinch the relation of the natural value to the sizes of the segment hinged pin-joint has three reference segments. On the first segment from  $u = 0,0$  up to  $u = 0,05$  with increase of parameter  $u$  the natural value decreases insignificantly. On the following segment from  $u = 0,05$  up to  $u = 0,4$  the natural values decrease almost linearly. On the third segment from  $u = 0,4$  up to  $u = 0,5$  the decreasing of the natural value also is insignificant. For the plate with asymmetrical placement of the segment of pinch these zones will place in the following limits of the parameter  $u$ : the first one,  $u = 0,0-0,2$ ; for the second one,  $u = 0,2-0,8$ ; for the third one,  $u = 0,8-1,0$ .

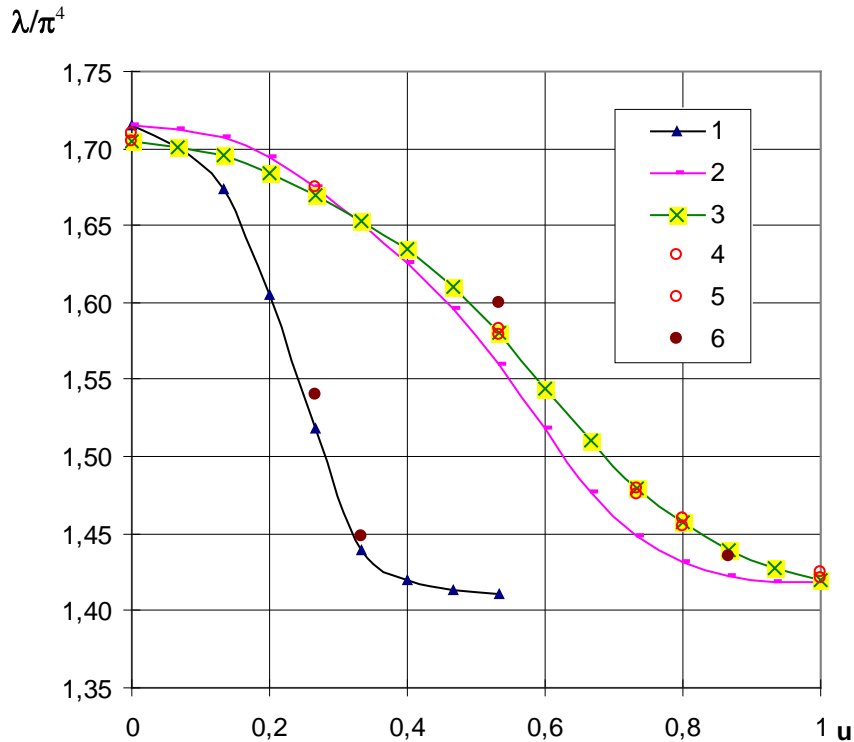


Fig. 2 The frequency of natural oscillations of pinch of the segment

## CONCLUSIONS

The given results show that small effect of the small segments of hinged pin-joint type (the first segment of the curve), and small segments of pinching (the third segment of the curve) influence a little on the natural frequency. There are also such ratios of the sizes of segments of mixed boundary conditions, at which the little change can essentially influence on the plate frequency (middle segment of the curve).

## REFERENCES

- [1] Smirnov V. A. *Calculation of Plates with Complex Contours*. Stroyizdat, M., 1978 (in Russian).
- [2] Marchenko V.A., Khruslov Ye.Ya. *Boundary Problems in Areas with Fine-grained Boundary*. Naukova Dumka, Kiev, 1974 (in Russian).
- [3] Obraztsov I.F., Nerubaylo B.V., Andrianov I.V. *Asymptotic Methods in Structural Mechanics of Heavy-wall Constructions*. Mashinostroyeniye, Moscow, 1991 (in Russian).
- [4] Volmir A.S. *Non-linear Dynamics of Plates and Membranes*. Nauka, Moscow, 1972 (in Russian).
- [5] Tymoshenko S.P. *Oscillation in Engineering*. Physmatgiz, Moscow, 1959 (in Russian).
- [6] Gontkevych V.S. *Characteristic Oscillations of Plates and Shells*. Naukova Dumka, Kiev, 1964 (in Russian).
- [7] Tseitlin A.I., Glykman B.T. Vibrations of rectangular plate with the mixed boundary conditions. *Researches of Sstructural Theory*. Vol.19, 1972, pp.185–194 (in Russian).
- [8] Andrianov I.V., Pasechnik V.A. Numerical and asymptotical method of decision of non-linear mixed boundary problems of mechanics. *Bulletin of the Dnipropetrovs'k University. Mechanics*. Issue 2, 1999, pp.5–12 (in Russian).
- [9] Ota T, Hamada M. Fundamental frequencies of simple supported but partially clamped square plates. *Bull. of Japan Soc of Mec. Eng.*, V.6, №23, pp.397–403, 1963.

## DYNAMIC INSTABILITIES OF A SEISMICALLY EXCITED SHELL WITH SHAKER-SHELL INTERACTION MODELING

**Francesco Pellicano**<sup>1</sup>  
Dept. of Mech. and Civ.  
Eng., Univ. Modena and  
Reggio E.  
Modena, Italy

---

### ABSTRACT

---

The present paper is focused on the experimental and theoretical analysis of circular cylindrical shells under seismic excitation. The shell axis is vertical, it is clamped at the base and connected to a rigid body on the top; the base provides a vertical seismic excitation. The goal is to investigate the shell response when a resonant forcing is applied: the first axisymmetric mode is excited around the resonance at relatively low frequency and low amplitude of excitation. A violent resonant phenomenon is experimentally observed as well as an interesting saturation phenomenon close to the previously mentioned resonance. A theoretical model is developed to reproduce the experimental evidence and provide an explanation of the complex dynamics observed experimentally; the model takes into account geometric shell nonlinearities, electrodynamic shaker equations and the shell shaker interaction.

---

### INTRODUCTION

Circular cylindrical shells are important elements in many Engineering fields e.g. Aerospace, Nuclear, Civil; examples of applications are: building vaults, heat exchangers, aircraft fuselages, missile and space vehicle structures, structural and non-structural car elements, tanks, pipelines. In many fields the need of more and more efficient structures in terms of strength and weight led to a strong reduction of safe factors; one of the direct consequences of weight reduction is the increasing of vibration problems.

In order to give to the reader a complete view of the research carried out in the previous decades about topics strictly related with the present work, a deep description of the literature is given in the following.

Readers interested to deepen the literature are suggested to read Refs. [1-6]: as noted by Babcock [2], the literature regarding shell modeling is perhaps too wide as thousands papers can be found on the subject. On the other hand some topics of extreme importance need further investigations: dynamic stability, post-critical behavior, sensitivity to imperfections, nonlinear vibrations and fluid structure interaction.

Kubenko and Koval'chuk [7] published an interesting review on nonlinear problems of shells, where several results were reported about parametric vibrations; in such review the limitations of reduced order models were pointed out. Babich and Khoroshun [8] presented results obtained at the S. P. Timoshenko Institute of Mechanics of the National Academy of Sciences of Ukraine over 20 years of research; the authors focused the attention on the variational-difference methods; more than 100 papers were cited. Kubenko and Koval'chuk [9] analyzed the stability and nonlinear dynamics of shells, following the historical advancements in this field, about 190 papers were deeply commented; they suggested, among the others, the effect of imperfections as an important issue to be further investigated.

Pellicano [10] presented experimental results about violent vibration phenomena appearing in a shell with seismic excitation and carrying a rigid mass on the top. In correspondence of the resonance

---

<sup>1</sup> Corresponding author. Email [Francesco.pellicano@unimore.it](mailto:Francesco.pellicano@unimore.it)

of the first axisymmetric mode, which involves mainly the translation of the top mass, a huge out of plane vibration (more than 2000g) is detected, with a relatively low excitation (about 10g).

Pellicano [11] developed a new method, based on the Nonlinear Sanders Koiter theory, suitable for handling complex boundary conditions of circular cylindrical shells and large amplitude of vibrations. The method is based on a mixed expansions considering orthogonal polynomials and harmonic functions. Among the others, the method showed good accuracy also in the case of a shell connected with a rigid body; this method is the starting point of the model developed for the present research.

In the present paper, experiments are carried out on a circular cylindrical shell, made of a polymeric material (P.E.T.) and clamped at the base by gluing its bottom to a rigid support. The axis of the cylinder is vertical and a rigid disk is connected to the shell top end. In Ref. [11] this problem was fully analyzed from a linear point of view.

Here nonlinear phenomena are investigated by exciting the shell using a shaking table and a sine excitation. Shaking the shell from the bottom induces a vertical motion of the top disk that causes axial loads due to inertia forces. Such axial loads generally give rise to axial symmetric deformations; however, in some conditions it is observed experimentally that a violent resonant phenomenon takes place, with a strong energy transfer from low to high frequencies and huge amplitude of vibration. Moreover, an interesting saturation phenomenon is observed: the response of the top disk was completely flat as the excitation frequency was changed around the first axisymmetric mode resonance.

A semi-analytical approach is proposed for reproducing experimental results and giving a deeper interpretation of the observed phenomena. The shell is modeled using the nonlinear Sanders Koiter shell; in modeling the system the effect of the top disk was accounted for applying suitable boundary conditions and considering its inertial contribution; moreover, the interaction between the shell-disk and the electro-dynamic shaking table was included in the modeling. The shell displacement fields are represented by means of a mixed series (harmonic functions and orthogonal polynomials), which are able to respect exactly geometric boundary conditions; an energy approach, based on the Lagrangian equations, is used to obtain a set of ODE that represent the original system with good accuracy.

Comparisons between experiments and numerical results show a good behavior of the model, numerical analyses furnish useful explanations about the instability observed experimentally.

## 1. THE PROBLEM: DESCRIPTION AND EXPERIMENTAL RESULTS

The system under investigation is described in Figures 1 and 2; a circular cylindrical shell, made of a polymeric material (P.E.T.), is clamped at the base by gluing its bottom to a rigid support (“fixture”); the connection is on the lateral surface of the shell, in order to increase the gluing surface, see Figure 1. A similar connection is carried out on the shell top; in this case the shell is connected to a disk made of aluminium alloy, such disk is not externally constrained; therefore, it induces a rigid body motion to the top shell end.

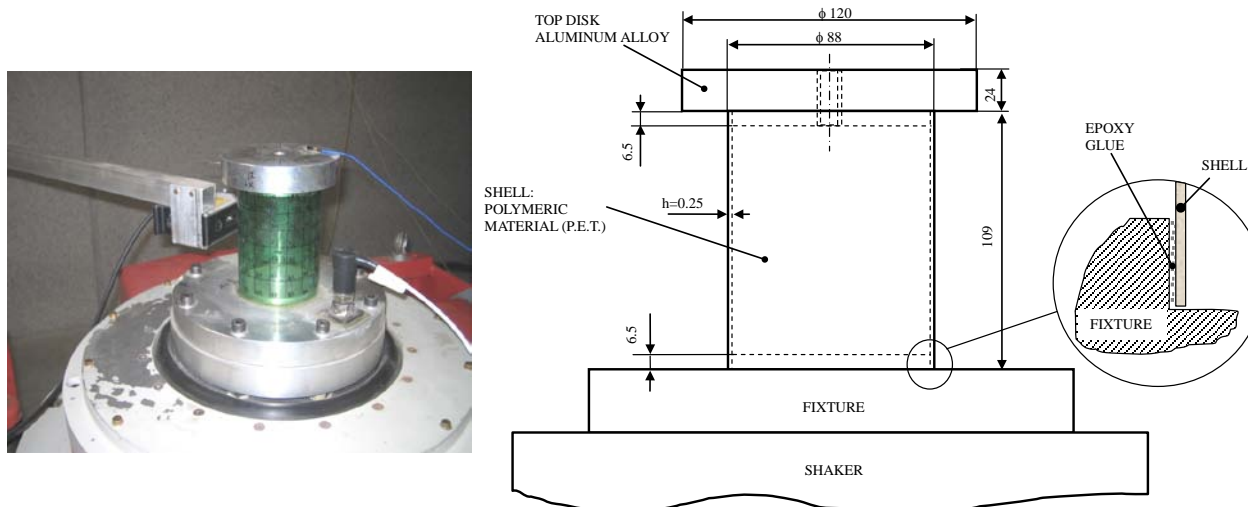
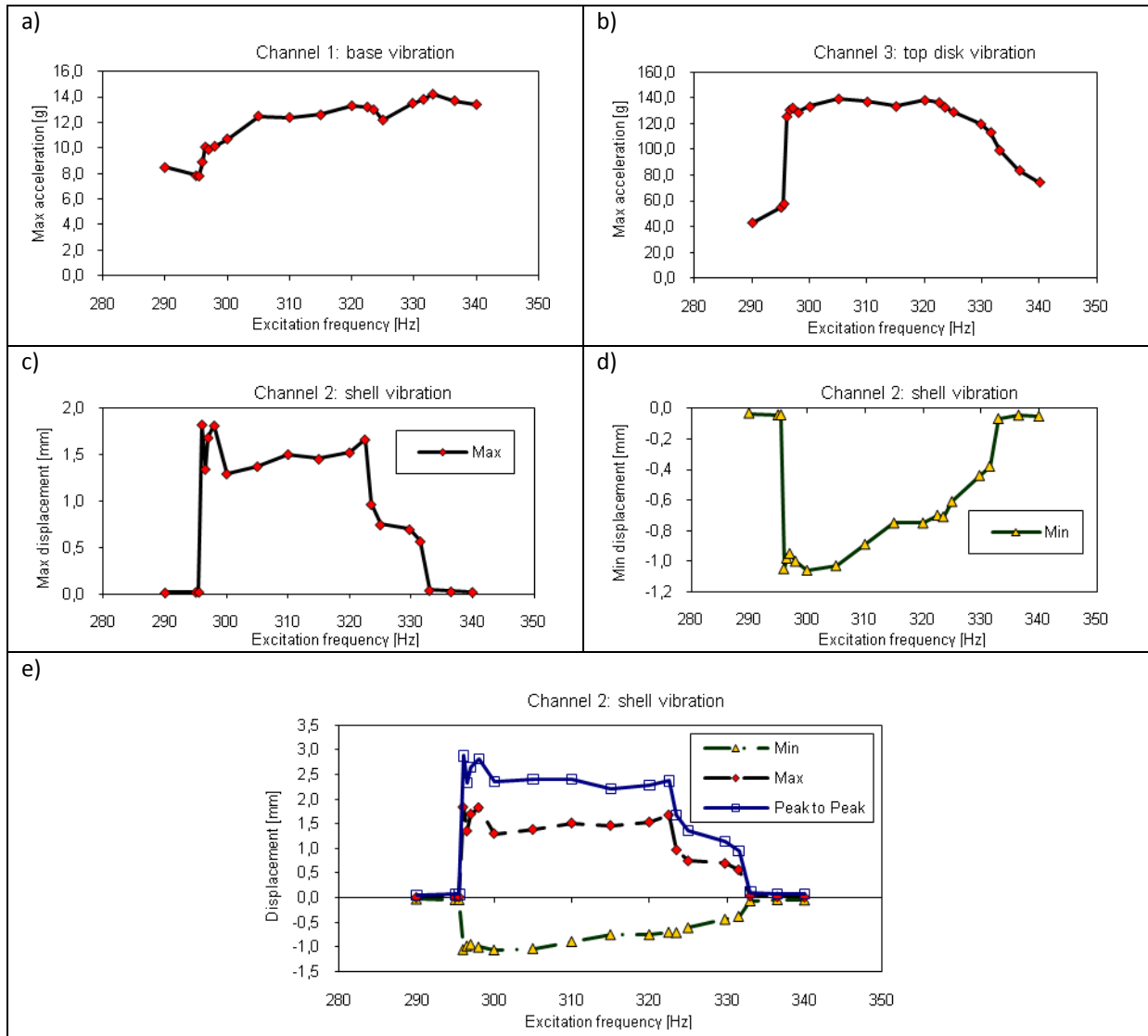


Fig. 1 Experimental setup

The fixture is bolted to a high power shaker (LDS V806, 13000N peak force, 100g maximum acceleration, 300kg payload, 1-3000Hz band frequency); such shaker is used to excite the shell from the base.

## 1.1 Experimental results

The behavior of the system is investigated when the base excitation is harmonic and close to the resonance of the first axisymmetric mode; indeed, in such conditions experiments, evidenced strong nonlinear responses.



*Fig. 2 Experimental results, harmonic excitation, amplitude of vibrations: a) base excitation amplitude (acceleration [g]), b) top disk amplitude (acceleration [g]), c) response on the shell mid-span (displacement [mm], positive inward), d) minimum response of the shell mid-span (displacement [mm], negative outward), e) maximum, minimum and peak to peak of the shell response at the mid-span.*

The goal is a deep understanding of nonlinear phenomena appearing when the first axisymmetric mode is resonant: experiments evidenced that, when the shell is excited harmonically from the base, with an excitation frequency close to the first axisymmetric mode, complex dynamic scenarios appear and the energy pumped in the system at low frequency spreads over a wide range of the spectrum.

Tests are carried out using a seismic sine excitation, close to the resonance of the first axisymmetric mode ( $m=1, n=0$ ).

The complexity and violence of vibrations due to nonlinear phenomena gave several problems to closed loop controllers of the shaking table; therefore, an open loop approach was chosen, the control is the input voltage of the shaker amplifier.

Two accelerometers and a Laser displacement sensor are used to measure the accelerations of the base, the top, and the displacement of the shell lateral surface: channel 1 (accelerometer Wilcoxon Research S 100 C) records the base acceleration (the excitation) due to the shaking table; channel 2 records the displacement of the shell in radial direction (Micro Epsilon optoNCDT 2200 Laser displacement sensor); channel 3 records the top disk acceleration (PCB M352C65 micro accelerometer); see Figure 1.

Figures 2 a-e represent the amplitudes of vibration in terms of acceleration (base and top disk vibration) or displacement (measured on the lateral surface of the shell, the vertical position is on the middle): during experiments the input voltage was sinusoidal ( $v(t)=v_0\sin(2\pi f t)$ ,  $v_0=0.07V$ ) and the frequency was moved step by step (stepped sine approach) starting from high frequency, 340Hz, and reducing up to 290Hz.

Channel 1 (Figure 2a) shows that the maximum excitation (base motion) is between 8 and 14 g; from such data one can guess that there is a strong interaction between the shaker and the shell-disk, i.e. inertia forces generated by the top disk and the shell vibration influence the shaker response; it is worthwhile to remember that the shaker control is open loop.

The top disk vibration (channel 3, figure 2b) increases as the first axisymmetric mode resonance is approached, from 340 to 333Hz the top disk response follows the usual behaviour expected by a linear resonance. However, from 333 Hz to 320 Hz the slope of the curve changes, when the excitation frequency is less than 322 Hz the top disk vibration amplitude remains flat, this happens up to 295 Hz; below such frequency the top disk response amplitude drops down suddenly and then follows a regular (linear like) behaviour.

The behaviours of base and top disk are strictly related to the dynamic phenomena appearing on the shell. Let us now follow results presented in Figure 2c, where the maximum amplitude of vibration (positive for inward shell deflection) are shown. For excitation frequencies higher than 333 Hz the shell vibration is small, about 0.04 mm (about 16% with respect to the shell thickness, 0.25mm), see Figure 2c; such small amplitude indicates that the shell deflection remains in the linear field, as nonlinearities generally arise when the deformation is of the order of the shell thickness. Reducing the excitation frequency below 333Hz, the shell vibration amplitude suddenly grow up, at 331.5 Hz the amplitude is 0.57 mm, the increment is 1325% passing from 333 Hz to 331.4 Hz (about 0.5% frequency variation); such data show that a new dynamic phenomenon appears suddenly. Another jump in the shell response is observed from 325 Hz (0.75 mm amplitude) to 320 Hz (1.53 mm), i.e. 104% increment in terms of amplitude in 5 Hz. Reducing the excitation frequency to 300 Hz does not cause a big changing in the response, which remains almost flat; from 300 Hz to 296 Hz the amplitude oscillates around 1.5 mm; then at 295 Hz the phenomenon suddenly disappears (0.022mm amplitude).

Figure 2d shows the behaviour of the minimum shell vibration (negative means outward deflection), the behaviour of the minimum vibration is similar to the maximum, but the magnitude of the minimum is smaller than the maximum. This is not surprising, it is well known that, when the amplitude of vibration is equal or larger than the shell thickness, the shell behaves nonlinearly; moreover, the shell is stiffer in outward than in inward direction.

It is to note that the dynamic phenomenon is extremely violent, it is accompanied by a strong noise (hear protections are needed), the acceleration generated on the shell are surprisingly huge. For example if the amplitude is 3 mm, and we suppose the vibration is purely harmonic at 300 Hz, an approximate estimation of the acceleration is about 1100 g! Such estimate does not consider that the shell response is no more sinusoidal, conversely it is non stationary and broad band, this means that the response spectrum contains high frequency components that can lead to a further increment of the acceleration. Some initial experiments carried out using accelerometers for the lateral shell vibration measurement, evidenced accelerations up to 2000g! See also Ref. [10]. This explains the need of a Laser Displacement sensor, such huge levels of acceleration exceed the maximum range of common accelerometers and make quite difficult the connection of the accelerometer to the shell; only micro accelerometers can be used here due to the small mass of the shell, such sensors can be connected using wax or glue, both types of connections cannot resist to huge accelerations and generally the accelerometer detaches from the shell after few seconds.

## 2. THEORETICAL RESULTS

The theoretical model of the shaker response is developed as well as the theoretical shell modeling based on the Sanders-Koiter theory. A suitable interaction between shaker and shell is considered as well as a method for solving the governing equations, which consists of a system of nonlinear partial differential equations for the shell and linear ordinary differential equations for the

shaker. Here details are not reported for the sake of brevity; see Ref. [11] for details about the shell modeling.

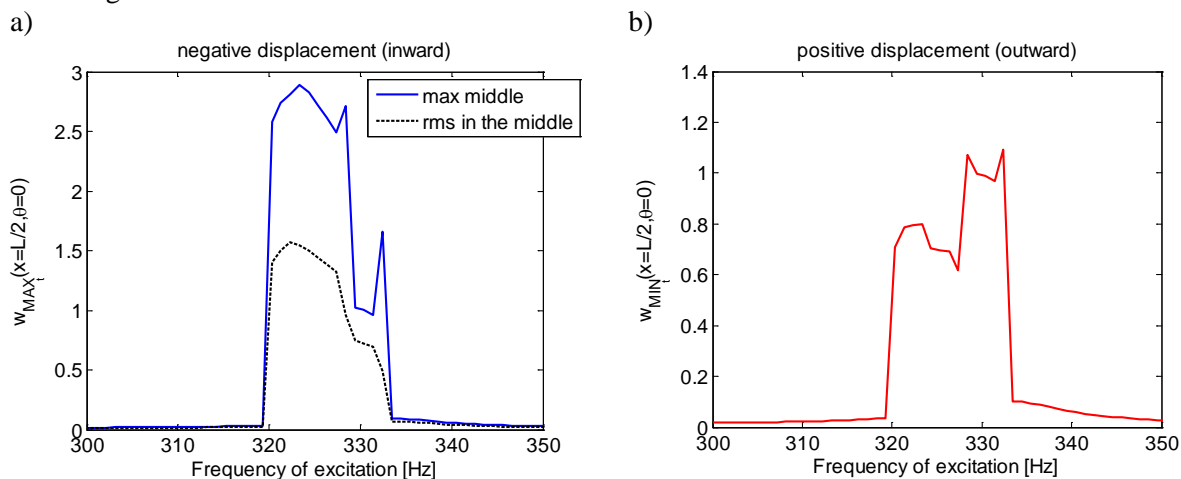


Fig. 3 Amplitude frequency diagrams, numerical simulations, backward frequency sweep, shell vibration (mm). a) inward (negative, see Fig. 15) displacement and RMS( $w$ ); b) outward (positive) displacement. Position of the simulated point measurement:  $x = \frac{L}{2}, \theta = 0$ . Excitation source: 0.09V.

Figure 3 shows results of simulations carried out considering an input voltage equal to 0.09V, this value is larger than the excitation used during the experiments (0.07V); however, below such value the numerical model did not detect any dynamic instability. Simulations are carried out by decreasing the excitation frequency. Figure 3a shows the amplitude of vibration of the shell in terms of max inward displacement and RMS, a measurement in the middle of the shell is simulated. Figure 3b shows the response in terms of max outward displacement. The simulation frequency interval is 300-350Hz; by decreasing the frequency the onset of instability is found at 333.4Hz, below such frequency the vibration amplitude is magnified, at 329.4Hz a second increment of the vibration amplitude is detected leading the maximum inward deflection to 2.7mm, a further reduction of the frequency does not cause a big amplitude variation up to 319.3Hz, where the vibration level drops down to small amplitudes. The behavior is coherent with experimental results (see Figure 2c), the numerical model overestimates the amplitude of vibration (experiments give 1.8mm max inward vibration) and underestimates the frequency range for which the instability appears (experimental instability range 295-333 Hz); this can be explained by the absence of companion modes and imperfections.

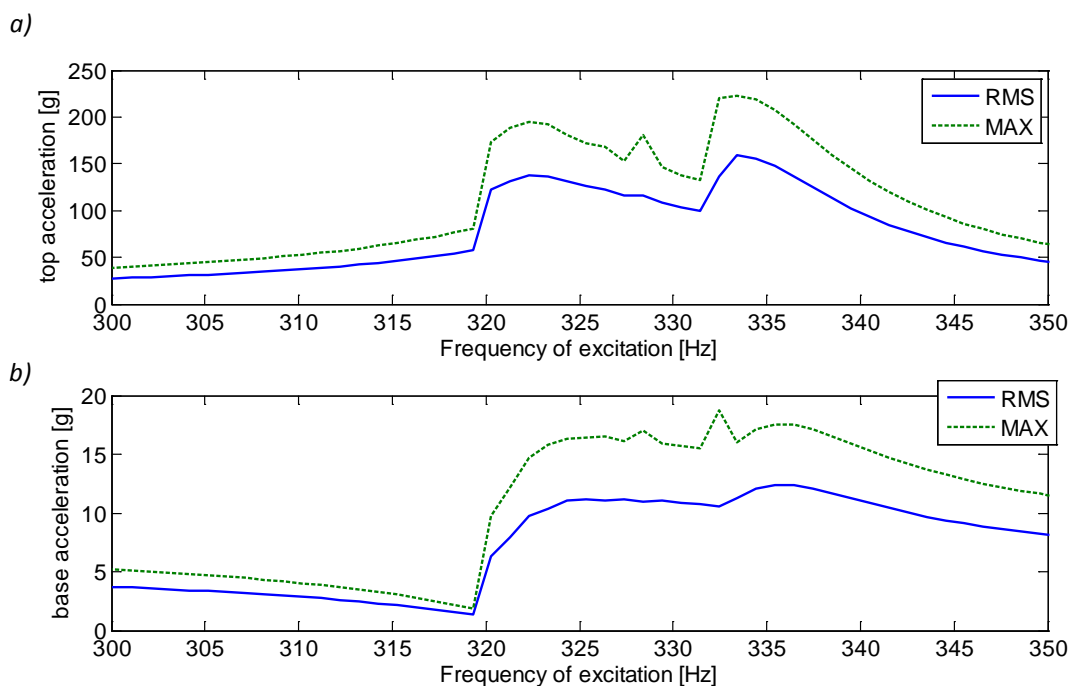


Fig. 4 Amplitude frequency diagrams, numerical simulations, excitation source 0.09V. a) top disk acceleration, b) base acceleration.

Figures 4a,b show the vibration amplitudes of top disk and base in terms of acceleration [g]; both maximum and RMS are considered. Similarly to experiments the first axisymmetric mode resonance is clearly visible outside the instability region; when the instability occurs the increment of vibration of the top disk, which is expected when the resonance condition is approached, is locked. Inside the instability region the disk acceleration remains almost flat. Figure 4b shows the base acceleration, it is never constant and is qualitatively similar to experiments. The model overestimates the top disk acceleration during the instability, which is about 90grms for experiments and fluctuates between 100 and 130grms for simulations. The simulation of the base is quantitatively quite close to experiments.

## CONCLUSIONS

In this paper an experimental investigation on the nonlinear dynamics of circular cylindrical shells excited by a seismic excitation is presented. A nonlinear model of the shell considering also the shell shaker interaction is developed.

Experiments clearly show a strong nonlinear phenomenon appearing when the first axisymmetric mode is excited: the phenomenon leads to large amplitude of vibrations in a wide range of frequencies, it appears extremely dangerous as it can lead to the collapse of the shell; moreover, it appears suddenly both increasing and decreasing the excitation frequency and is extremely violent. By observing a strong transfer of energy from low to high frequency a conjecture can be made about the nonlinear interaction among axisymmetric (directly excited) and asymmetric modes. A saturation phenomenon regarding the vibration of the top disk is observed, this is associated with the violent shell vibration; the shell behaves like an energy sink, absorbing part of the disk energy.

The theoretical model shows satisfactory agreement with experiments and clarifies the energy transfer mechanism from low frequency axisymmetric modes and high frequency asymmetric modes, confirming the conjecture arising by the experimental data analysis.

It is now clear that, in order to safely predict the response of a thin walled shell carrying a mass on the top, i.e. the typical aerospace problem for launchers, a nonlinear shell model is needed, but it is not enough: a further modeling regarding the shell mass interaction and the interaction between shell and excitation source is needed.

## REFERENCES

- [1] Leissa, A.W., 1993. *Vibration of Shells*, NASA SP-288. Washington, DC: Government Printing Office. Now available from The Acoustical Society of America.
- [2] Babcock, C.D., 1983. Shell Stability. *Journal of Applied Mechanics*, 50, 935-940.
- [3] Calladine, C.R., 1995. Understanding Imperfection-Sensitivity in the Buckling of Thin-Walled Shells. *Thin-Walled Structures*, 23, 215-235.
- [4] Teng, J.G., 1996. Buckling of thin shells: Recent advances and trends. *Applied Mechanics Reviews*, 49(4), 263-274.
- [5] Amabili, M., 2008. *Nonlinear Vibrations and Stability of Shells and Plates*, Cambridge University Press, Cambridge.
- [6] Amabili, M., Païdoussis, M.P., 2003. Review of studies on geometrically nonlinear vibrations and dynamics of circular cylindrical shells and panels, with and without fluid-structure interaction. *Applied Mechanics Reviews*, 56, 349-381.
- [7] Kubenko, V.D., Koval'chuk, P.S., 1998. Nonlinear problems of the vibration of thin shells (review). *International Applied Mechanics*. 34, 703- 728.
- [8] Babich, D. V. and Khoroshun, L. P., 2001. Stability and Natural Vibrations of Shells with Variable Geometric and Mechanical Parameters. *International Applied Mechanics*. 37(7), 837-869.
- [9] Kubenko, V. D. and Koval'chuk, P. S., 2004. Influence of Initial Geometric Imperfections on the Vibrations and Dynamic Stability of Elastic Shells. *International Applied Mechanics*, 40(8), 847-877.
- [10] Pellicano, F., 2005. Experimental analysis of seismically excited circular cylindrical shells. *Proceedings of ENOC-2005, Fifth EUROMECH Nonlinear Dynamics Conference*, Eindhoven, The Netherlands, August 7-12.
- [11] Pellicano, F., 2007. Vibrations of circular cylindrical shells: theory and experiments. *J. of Sound and Vibration*, 303, 154–170. doi:10.1016/j.jsv.2007.01.022.

**ANALYSIS OF RESONANCE NONLINEAR VIBRATIONS FOR HIGH-FIDELITY  
MODELS OF STRUCTURES WITH CONTACT INTERFACES**

**E. Petrov<sup>1</sup>**  
Imperial College, London,  
UK

---

ABSTRACT

---

A methodology for direct analysis of resonance peak amplitudes and frequencies of steady-state forced response for strongly nonlinear vibrations of structures with joints is presented. Large-scale finite element models of linear components, detailed modeling of the nonlinear contact interfaces and high-accuracy model reduction are applied in the analysis. The efficiency of the methodology is demonstrated on test cases and examples of analysis of realistic gas-turbine structures.

---

The majority of the machinery structures are assembled, jointed structures. They usually comprise several components, which interact among themselves and with other structures through contact interfaces. Forces occurring at these interfaces are essentially nonlinear due to the friction, the presence of clearances and interferences, the variation of actual contact area during vibrations, the application of devices with nonlinear properties, etc.

The gas-turbine and some other industries rely increasingly in the design practice of the critical structures with joints on the numerical analysis. This requires development of high-fidelity models and methods for effective and comprehensive analysis of nonlinear dynamics of structures with friction, gaps and other nonlinear contact interfaces.

Periodic loading, which is typical for gas-turbine and many other structures, excites mostly steady-state periodic nonlinear vibrations. Forced response levels of these vibrations at resonance peaks and values of the resonance frequencies are of particular interest since the resonance peak vibrations are usually defining integrity and longevity of a structure and, therefore, the choice of its design parameters.

In this paper effective methods are discussed which have been developed by the author for analysis of the resonance amplitude and frequencies including a direct calculation of their dependency on the variations of design parameters and excitation conditions (see details in Refs.[1]-[4]). Large-scale finite elements models, which can contain millions degrees of freedom, are used for modelling of the linear components of structures and the interactions at contact interfaces can be described in detail by a multitude of contact interface elements.

Steady-state resonance peak regimes are calculated in frequency domain using multiharmonic balance formulation for the equations of motions. All expressions for the contact interface elements including those required for calculation of resonance peaks, tracing of the solutions with parameter variation and determination of resonance peak sensitivities are derived analytically which ensures exceptionally fast and accurate calculations for all types of the advanced analysis.

High efficiency of the analysis for resonance peak forced response allows development of efficient algorithms aimed at the search contact interface parameters, which provide required resonance peak characteristics. The problem of search for the optimum parameter values is formulated and solved as the global optimization problem.

The efficiency of the methodology developed is demonstrated on a representative set of examples, which include test cases using high-fidelity finite elements models of realistic gas-turbine structures.

---

<sup>1</sup> Corresponding author. Email [y.petrov@imperial.a.uk](mailto:y.petrov@imperial.a.uk)

## REFERENCES

- [1] Petrov, E.P. and Ewins, D.J., "State-of-the-art dynamic analysis for nonlinear gas turbine structures" *J. of Aerospace Engineering, Proc. of the IMechE, Part G*, 2004, vol.218, pp.199-211
- [2] Petrov, E.P., "Method for direct parametric analysis of nonlinear forced response of bladed discs with friction contact interfaces", *Trans. ASME: J. of Turbomachinery*, 2004, Vol.126, pp.654-662
- [3] Petrov, E.P., "Direct parametric analysis of resonance regimes for nonlinear vibrations of bladed discs", *Trans. ASME: J. of Turbomachinery*, 2007, Vol.129, pp.495-502
- [4] Petrov, E.P., "Method for sensitivity analysis of resonance forced response of bladed disks with nonlinear contact interfaces", *Trans. ASME: J. of Eng. for Gas Turbines and Power*, 2009, Vol.131, pp.022510-1 - 022510-9

**EQUATION OF MOTION WITH IMPLICIT FUNCTIONS OF PHASE  
 COORDINATES VELOCITIES AND ITS APPLICATIONS FOR  
 ENGINEERING CONSTRUCTIONS RUPTURE LIFE EVALUATION**

**Yury V. Romashov<sup>1</sup>**  
 National Technical University  
 "Kharkov Polytechnic institute",  
 Kharkov, Ukraine

**ABSTRACT**

The generalized mathematical problem of image point motion is formulated for phase coordinate velocities as implicit functions which are defined by two coupled initial-boundary-value problems. Applications of this problem are presented for rupture life evaluation of engineering constructions damaged due to high temperature creep.

**INTRODUCTION**

The well-known in nonlinear dynamics state (phase) space conception has outstanding resources for generalized mathematical representation of different physical problems. Feature of problems generalized mathematical representation has especially meaning for development of software utilities necessary for this problem computer solution [1].

Engineering construction rupture life evaluation is an urgent scientific problem [2]. This problem consists in determination of the time from the beginning of operating to the limiting state occur. It is means that system has some state at the beginning time, that system state can be changed with the course of time, and that system has some limited state which can be lead over some time period. This considerations are naturally connected with state (phase) space conception in nonlinear dynamics. It is allows facilities to assume that state space conceptions could be applicable for engineering constructions rupture life evaluation. This paper objective consists in mathematical formulating of engineering constructions rupture life evaluation as problems about imaging point moving in suitable phase space.

**1. ABSTRACT MATHEMATICAL FORMULATION OF THE PROBLEM**

Structural element (body) is presented as number of points i.e. as geometric images of them material particles constituent. Set of points is consisted as geometrical area  $Y$  with boundary surface  $U$  (fig. 1). Position vector of the point of body is determined using curvilinear coordinates  $x^1, x^2, x^3$ :

$$\vec{r} = \vec{r}(x^1, x^2, x^3). \tag{1}$$

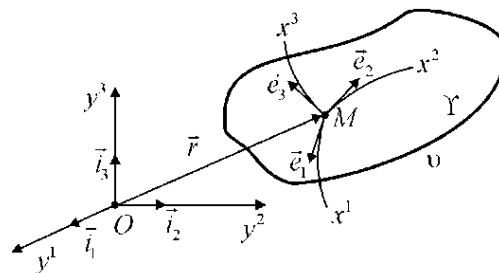


Fig. 1 Body and systems of coordinates

<sup>1</sup> Corresponding author. Email [romashev@kpi.kharkov.ua](mailto:romashev@kpi.kharkov.ua)

Let vector  $\mathbf{w} \in R^N$  (here and further  $R$  denotes real number field) is introduced as quantitative estimation of distance between state of structural element and its limited state. In analogy of damage parameter all-known in creep problems [4] components of the vector  $\mathbf{w} \in R^N$  are

$$0 \leq w^i \leq 1, i = 1, 2, \dots, N. \quad (2)$$

where  $w^i = 0, i = 1, 2, \dots, N$  values are corresponded to initial state of structural element at time  $t = 0$  and  $w^i = 1$  are corresponded to structural element limited state at the time  $t = t_*$ .

Values (2) are defined for all points of body and could be changed during time

$$w^i = w^i(t, \vec{r}), i = 1, 2, \dots, N. \quad (3)$$

Rupture life exhausting in every point of body is clearly presented by relations (3) as values (2) time depending and as geometric interpretation on phase plane in the case of  $N = 2$  (fig. 2).

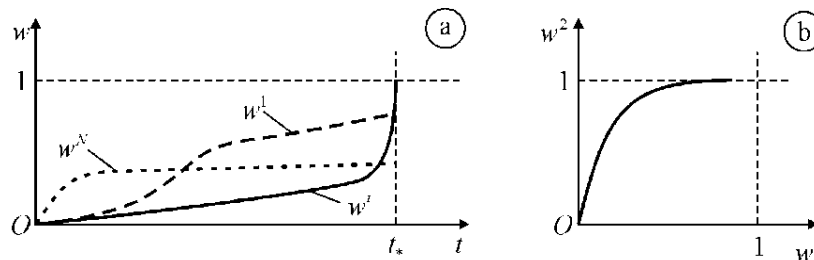


Fig. 2 Graphic presentation of structure elements rupture life exhausting as time depending (a) and as phase path (b)

It is necessary to take into account accumulation of the irreversible deformations, degradation of structures materials, micro- and macro-defects creation and progress with time for rupture life evaluation. Let these processes quantitative characteristics are denoted as  $v^1, v^2, \dots, v^S$  and are considered as components of vector  $\mathbf{v} \in R^S$ . It is necessary to take into account state structural element as deformable body for rupture life evaluation too. Let quantitative characteristics of structure element as deformable body are denoted as  $u^1, u^2, \dots, u^Q$  and are considered as components of vector  $\mathbf{u} \in R^Q$ . Components of vectors  $\mathbf{v}$  and  $\mathbf{u}$  are

$$v^i = v^i(t, \vec{r}), i = 1, 2, \dots, S. \quad (4)$$

$$u^i = u^i(t, \vec{r}), i = 1, 2, \dots, Q. \quad (5)$$

Finite set of characteristics (5) existing is based on the macroscopic definability axiom and local effect principle all-known in mechanics of deformable bodies. Finite set of characteristics (3) and (4) existing is postulated similar.

Introduced as quantitative estimations of distance between state of structural element and limited state values (2) are presented by relations (3). State in the point of body is defined by values (4) and (5). Invariance of the values (3) under time keeping, coordinate systems and choice of point reduces to relation

$$\mathbf{w} = \mathbf{w}(\tilde{\mathbf{v}}, \tilde{\mathbf{u}}). \quad (6)$$

where  $\tilde{\mathbf{v}}, \tilde{\mathbf{u}}$  - invariants of vectors  $\mathbf{v}$  and  $\mathbf{u}$ .

Mappings  $\tilde{\mathbf{v}} = \tilde{\mathbf{v}}(\mathbf{v}), \tilde{\mathbf{u}} = \tilde{\mathbf{u}}(\mathbf{u})$  define from infinite sets of vectors  $\mathbf{v}$  and  $\mathbf{u}$  invariants necessary for structural element limit state defining only and in common case are surjection's.

Relations (4)-(6) are equivalent of (3). Thus rupture life evaluation problem is reduced to vectors  $\mathbf{v}, \mathbf{u}$  and  $\mathbf{w}$  determination and phase dependence of life time exhausting analyses (fig. 2).

Differential equations for vector  $\mathbf{v}$  determination are usually based on test data such as creep and long-term strength curves, corrosion-fatigue crack velocity curves, long-term stress corrosion

cracking curves etc. Vector  $\mathbf{v}$  velocity is not explicitly dependent on time, but depended on vector  $\mathbf{v}$ , its spatial coordinates partial derivatives for given vector  $\mathbf{u}$ :

$$\begin{cases} \frac{\partial \mathbf{v}}{\partial t} = \mathbf{k}(\mathbf{v}, \mathbf{D} \cdot \mathbf{v}; \mathbf{u}), \mathbf{v}(0, \bar{r}) = \mathbf{v}_0(\bar{r}) \quad \forall \bar{r} \in Y; \\ \mathbf{B}_D \cdot \mathbf{v}(t, \bar{r}) = \mathbf{v}_B(t, \bar{r}), \mathbf{v}_B(0, \bar{r}) = \mathbf{v}_0(\bar{r}) \quad \forall \bar{r} \in \nu, \end{cases} \quad (7)$$

where  $\mathbf{k}(\mathbf{v}, \mathbf{D} \cdot \mathbf{v}; \mathbf{u})$  - given velocity of vector  $\mathbf{v}$ ;  $\mathbf{D}$  - given spatial coordinates partial derivatives included operator;  $\mathbf{v}_0(\bar{r})$  - given at initial time  $t=0$  vector  $\mathbf{v}$ ;  $\mathbf{B}_D, \mathbf{v}_B$  - given operator and vector are corresponded to boundary conditions.

Differential equations for vector  $\mathbf{u}$  determination are presented as equations of deformable body mechanics which are took into account influence of accumulation of the irreversible deformations, degradation of structures materials, micro- and macro-defects creation and progress with time on materials properties and on stress-strain state:

$$\begin{cases} \mathbf{J}(\mathbf{v}) \cdot \frac{\partial \mathbf{u}}{\partial t} + \mathbf{A}(\mathbf{v}) \cdot \mathbf{u} + \mathbf{C} \cdot \mathbf{v} = \mathbf{f}(t, \bar{r}), \mathbf{u}(0, \bar{r}) = \mathbf{u}_0(\bar{r}) \quad \forall \bar{r} \in Y; \\ \mathbf{B}_A \cdot \mathbf{u}(t, \bar{r}) = \mathbf{u}_B(t, \bar{r}), \mathbf{u}_B(0, \bar{r}) = \mathbf{u}_0(\bar{r}) \quad \forall \bar{r} \in \nu, \end{cases} \quad (8)$$

where  $\mathbf{J}(\mathbf{v}), \mathbf{A}(\mathbf{v}), \mathbf{C}$  - operators and  $\mathbf{f}$  - vector are corresponded to differential equations of deformable body mechanics which are took into account influence of accumulation of the irreversible deformations, degradation of structures materials, micro- and macro-defects creation and progress with time on materials properties and on stress-strain state;  $\mathbf{u}_0(\bar{r})$  - given at initial time  $t=0$  vector  $\mathbf{u}$ ;  $\mathbf{B}_A, \mathbf{u}_B$  - given operator and vector are corresponded to boundary conditions.

Accountable micro- and macro-defects creation and progress with time factor require to take into account corresponded changing in body's area  $Y$  and its boundary surface  $\nu$

$$Y = Y(\mathbf{v}); \nu = \nu(\mathbf{v}). \quad (9)$$

If vectors  $\mathbf{w} \in R^N$  are introduced as state (phase) space then problem (6)-(9) could be considered as problem of imaging point moving with velocity:

$$\frac{\partial \mathbf{w}}{\partial t} = \frac{\partial \mathbf{w}}{\partial \tilde{\mathbf{v}}} \frac{\partial \tilde{\mathbf{v}}}{\partial \mathbf{v}} \frac{\partial \mathbf{v}}{\partial t} + \frac{\partial \mathbf{w}}{\partial \tilde{\mathbf{u}}} \frac{\partial \tilde{\mathbf{u}}}{\partial \mathbf{u}} \frac{\partial \mathbf{u}}{\partial t}. \quad (10)$$

Right member of (10) could not been obtained explicitly and its determination consist in two coupled initial-boundary-value problems (7), (8) solving. In some elementary cases explicitly determination of velocity (10) however is possible.

## 2. SIMPLE PROBLEM ABOUT BINDERS RUPTURE LIFE EVALUATION

It is necessary to allow stress relaxation due to creep for binders (bolts, screws, studs) which are operated under higher temperatures conditions. Let equations of binder's bodies stress relaxation due to creep in simple case of homogeneous stress-strain state are presented for example as [4]:

$$\begin{cases} \frac{dc}{dt} = B\sigma^n, c(0) = 0; \\ \sigma + Ec = \sigma_0, \end{cases} \quad (11)$$

where  $c = c(t)$  - creep deformation;  $\sigma = \sigma(t)$  - stress;  $E$  - material modulus of elasticity;  $B, n$  - materials characteristics of creep;  $\sigma_0$  - gripping stress.

It is obviously that equations (11) are particular case of equations (7), (8) in sense of  $\mathbf{v} = c$ ,  $S = 1$  and  $\mathbf{u} = \sigma$ ,  $Q = 1$ . Rupture life of the high pressure vessels binder under high temperatures operated is limited by creep deformation and minimal gripping secure tightness stresses:

$$N = 2: w^1 = \frac{c}{c_*}, w^2 = \frac{\sigma - \sigma_0}{\sigma_* - \sigma_0}, \quad (12)$$

where  $c_*$  - maximal creep which is allowed for given service conditions;  $\sigma_*$  - minimal gripping stresses which secure tightness.

Relations (12) are similar on relation (6) and allow to express vectors  $\mathbf{v}$  and  $\mathbf{u}$  (values  $c$  and  $\sigma$ ) in term of vector  $\mathbf{w}$ :

$$c = c_* w^1; \sigma = \sigma_0 + (\sigma_* - \sigma_0) w^2. \quad (13)$$

Relations (13) and equations (11) reduce to:

$$\begin{cases} \frac{dw^1}{dt} = c_* B (\sigma_0 + (\sigma_* - \sigma_0) w^2)^n, w^1(0) = 0; \\ \sigma_0 + (\sigma_* - \sigma_0) w^2 + E c_* w^1 = \sigma_0. \end{cases} \quad (14)$$

High pressure and high temperature vessels binder is considered as example for [4, 5]:

$$E = 1.72 \cdot 10^5 \text{ MPa}; n = 3.736; B = 3.798 \cdot 10^{-15} \text{ MPa}^{-n} / \text{hours}; \sigma_0 = 300 \text{ MPa}; \sigma_* = 100 \text{ MPa}. \quad (15)$$

Results of equations (14) solving for input data (15) are presented in fig. 3. For taken as (15) input data rupture life of binders is near 1000 hours.

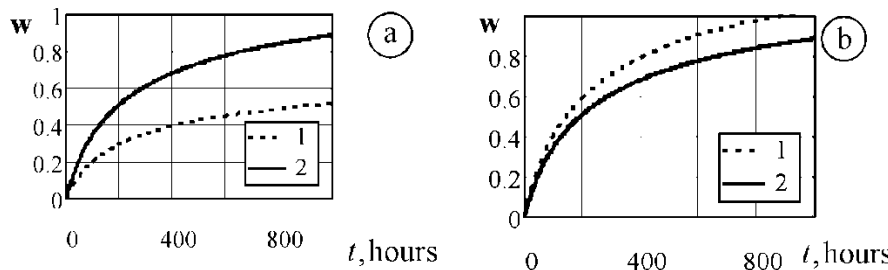


Fig. 3 Binder rupture life exhaustion  $w^1$  (1),  $w^2$  (2) for  $c_* = 0.002$  (a) and  $c_* = 0.001$  (b)

### 3. RUPTURE LIFE PROBLEMS ALGORITHMIZATION FOR STRUCTURE ELEMENTS DAMAGED DUE TO CREEP

Rupture life of structures elements in some case is assigned by creep deformations and damage parameter [3, 6]. In the case of infinitesimal deformations body's area  $\Upsilon$  and its surface  $\nu$  changing may be ignored. Equations for damaged due to creep structural elements could be presented in this case for Cartesian rectangular coordinates as

$$\begin{cases} \frac{\partial c_{ij}}{\partial t} = \frac{3}{2} \cdot \frac{B \cdot (\sigma_e^c(\sigma_{ij}))^{n-1}}{(1 - \omega^r)^m} \cdot (\sigma_{ij} - \frac{1}{3} \sigma_{kk}); c_{ij}|_{t=0} = 0; \\ \dot{\omega} = \frac{D(\sigma_e^\omega(\sigma_{ij}))^k}{(1 - \omega^r)^l}; \omega|_{t=0} = 0; \end{cases} \quad (16)$$

$$\begin{cases} -d_{ijkl} \sigma_{kl} + \frac{1}{2} \left( \frac{\partial u_i}{\partial x_j} + \frac{\partial u_j}{\partial x_i} \right) - c_{ij} = 0; \frac{\partial \sigma_{ij}}{\partial x_j} + f_i = 0; \\ (\sigma_{ij} n_j)|_{\nu_p} = p_i; u_i|_{\nu_u} = u_i^*, \end{cases} \quad (17)$$

where  $c_{ij} = c_{ij}(t, x_1, x_2, x_3)$  - creep deformations;  $\omega = \omega(t, x_1, x_2, x_3)$  - damage parameter;  $\sigma_{ij}$  - stresses;  $\sigma_e^c(\sigma_{ij})$ ,  $\sigma_e^\omega(\sigma_{ij})$  - stresses' equivalents;  $B$ ,  $D$ ,  $n$ ,  $r$ ,  $m$ ,  $k$ ,  $l$  - material creep and damage characteristics;  $d_{ijkl}$  - material elasticity characteristics;  $u_i$  - displacements;  $f_i$  - external volume forces;  $p_i$  - given on  $v_p \subset v$  surface-distributed force;  $u_i^*$  - given on  $v_u \subset v$  displacements.

Comparison between equations (16), (17) and generalized equations (7), (8) reduce that vectors  $\mathbf{v}$  and  $\mathbf{u}$  can be assigned as

$$\begin{cases} \mathbf{v} = (c_{11} & c_{22} & c_{33} & c_{12} & c_{13} & c_{23} & \omega)^T; \\ \mathbf{u} = (\sigma_{11} & \sigma_{22} & \sigma_{33} & \sigma_{12} & \sigma_{13} & \sigma_{23} & u_1 & u_2 & u_3)^T. \end{cases} \quad (18)$$

Spatial coordinate's derivatives are not entered into the equations (16) and forces of inertia are not entered into the equations (17). Thus equations (16), (17) are the particular realization of the generalized equations (7), (8):

$$\frac{\partial \mathbf{v}}{\partial t} = \mathbf{k}(\mathbf{v}; \mathbf{u}), \mathbf{v}(0, \vec{r}) = \mathbf{0} \quad \forall \vec{r} \in \Upsilon, \quad (19)$$

$$\begin{cases} \mathbf{A} \cdot \mathbf{u} + \mathbf{C} \cdot \mathbf{v} = \mathbf{f}(\vec{r}) \quad \forall \vec{r} \in \Upsilon; \\ \mathbf{B}_A \cdot \mathbf{u}(\vec{r}) = \mathbf{u}_B(\vec{r}) \quad \forall \vec{r} \in v. \end{cases} \quad (20)$$

Operator  $\mathbf{k}(\mathbf{v}; \mathbf{u})$  from equations (16) is nonlinear, but operators  $\mathbf{A}$ ,  $\mathbf{C}$ ,  $\mathbf{B}_A$  from equations (17) are linear.

Unknown solution of the problem (19), (20) is presented by approximations with given systems of spatial coordinate's trial functions and unknown coefficients as functions of time

$$\begin{cases} \mathbf{v}(t, \vec{r}) \approx \mathbf{V}_n(\vec{r}) \cdot \mathbf{v}_n(t); \mathbf{v}_n(0) = \mathbf{0}; \\ \mathbf{u}(t, \vec{r}) \approx \mathbf{u}_v(\vec{r}) + \mathbf{U}_n(\vec{r}) \cdot \mathbf{u}_n(t), \end{cases} \quad (21)$$

where  $n$  - count of trial functions;  $\mathbf{V}_n(\vec{r})$ ,  $\mathbf{U}_n(\vec{r})$  - matrices of given trial functions;  $\mathbf{u}_v(\vec{r})$  - given vector which distribute boundaries values into area;  $\mathbf{v}_n(t)$ ,  $\mathbf{u}_n(t)$  - vectors are consisted of unknown approximations coefficients.

Trial functions are chose such that all boundary conditions (20) will be identically satisfied

$$\forall \mathbf{u}_n(t): \mathbf{B}_A \cdot (\mathbf{U}_n(\vec{r}) \cdot \mathbf{u}_n(t)) = \mathbf{u}_B(\vec{r}) - \mathbf{B}_A \cdot \mathbf{u}_v(\vec{r}). \quad (22)$$

Trial functions identically satisfied conditions (22) can be constructed by R-functions methods [7] for free-form body's area and arbitrarily given boundary conditions.

Let to apply orthogonal property between trial functions and obtained for approximations (21) equations (19), (20) misalignments. Linear properties of  $\mathbf{A}$  and  $\mathbf{C}$  operators reduce to

$$\begin{cases} \mathbf{K}_n \frac{d\mathbf{v}_n}{dt} = \mathbf{k}_n(\mathbf{v}_n; \mathbf{u}_n); \\ \mathbf{A}_n \mathbf{u}_n + \mathbf{C}_n \mathbf{v}_n = \mathbf{f}_n, \end{cases} \quad (23)$$

where  $\mathbf{K}_n$ ,  $\mathbf{A}_n$  - quadratic non-singular matrices and  $\mathbf{C}_n$  - rectangular in common case matrix;  $\mathbf{f}_n$  - vector;  $\mathbf{k}_n(\mathbf{v}_n; \mathbf{u}_n)$  - nonlinear vector-function:

$$\begin{aligned} \mathbf{K}_n &= \int_{\Upsilon} \mathbf{V}_n^T \cdot \mathbf{V}_n d\Upsilon; \mathbf{k}_n(\mathbf{v}_n; \mathbf{u}_n) = \int_{\Upsilon} \mathbf{V}_n^T \cdot \mathbf{k}(\mathbf{V}_n \cdot \mathbf{v}_n; \mathbf{u}_v + \mathbf{U}_n \cdot \mathbf{u}_n) d\Upsilon; \\ \mathbf{A}_n &= \int_{\Upsilon} \mathbf{U}_n^T \cdot (\mathbf{A} \cdot \mathbf{U}_n) d\Upsilon; \mathbf{C}_n = \int_{\Upsilon} \mathbf{U}_n^T \cdot (\mathbf{C} \cdot \mathbf{V}_n) d\Upsilon = \mathbf{0}; \mathbf{f}_n = \int_{\Upsilon} \mathbf{U}_n^T \cdot (\mathbf{f} - \mathbf{A} \cdot \mathbf{u}_v) d\Upsilon. \end{aligned}$$

Vectors  $\frac{d\mathbf{v}_n}{dt}$  and  $\mathbf{u}_n$  can be solved from equations (23):

$$\begin{cases} \frac{d\mathbf{v}_n}{dt} = \mathbf{K}_n^{-1} \cdot \mathbf{k}_n(\mathbf{v}_n; \mathbf{u}_n); \\ \mathbf{u}_n = \mathbf{A}_n^{-1} \cdot (\mathbf{f}_n - \mathbf{C}_n \mathbf{v}_n). \end{cases} \quad (24)$$

Relations (24) reduce to Cauchy problem in standard form suitable for computing:

$$\begin{cases} \frac{d\mathbf{v}_n}{dt} = \mathbf{K}_n^{-1} \cdot \mathbf{k}_n(\mathbf{v}_n); \\ \mathbf{v}_n(0) = \mathbf{0}, \end{cases} \quad (25)$$

where  $\mathbf{k}_n(\mathbf{v}_n) = \mathbf{k}_n(\mathbf{v}_n; \mathbf{u}_n = \mathbf{A}_n^{-1} \cdot (\mathbf{f}_n - \mathbf{C}_n \mathbf{v}_n))$ .

Thus creep-damage problem (16), (17) is reduced to standard Cauchy problem (25) and its solution can be obtained using any all-known computational methods, Runge-Kutta for example.

## CONCLUSIONS

Engineering constructions rupture life evaluation problems are formulated as imaging point moving problems in phase space with vectors which are estimation of distance between current state of structural element and its limited state. Velocities of phase coordinates in imaging point equations of moving are implicit functions defined by two coupled initial-boundary-value problems. Applications for engineering constructions structural elements damaged due to high temperatures creep are discussed.

## REFERENCES

- [1] A.I.Kalyutik, E.F.Mosin, Yu.A.Sokovishin, E.P.Entin *Temperature Fields Computing for Solid Bodies with Moving Boundaries*, Leningrad University Publishing, Leningrad, 1987 (in Russian).
- [2] K.V.Frolov, N.A.Makhutov, G.K.Khurshudov, M.M.Gadenin Strength Resource and Engineering Safety of Technical Systems [in Russian] *Problems of Strength*, N. 5, Kiev, pp. 8-18, 2000.
- [3] J.Lemaitre, J.-L.Chaboche *Mechanics of Solid Materials*, Cambridge University Press, 1994.
- [4] I.A.Birger, G.B.Iosilevich *Thread and Flange Connections*, Mashinostroenie, Moscow, 1990 (in Russian).
- [5] S.B.Maslenkov *High-Temperature Creep-Rupture Resistant Steels and Alloys*, Metallurgiya, Moscow, 1983 (in Russian).
- [6] O.K.Morachkovskii, Yu.V. Romashov Solving Initial-Boundary-Value Creep Problems *International Applied Mechanics*, Vol. 45, N. 10, pp. 1061-1070, 2009.
- [7] L.Kurpa, V.Rvachev, E.Ventsel The R-function Method for the Free Vibration Analysis of Thin Orthotropic Plates of Arbitrary Shapes *J. Sound and Vibration*, N. 26, pp. 109-122, 2003.

## MODELING OF IMPACT DEFORMATION PROCESSES OF THE CERAMIC CONTAINER FOR RADIOACTIVE WASTE STORAGE

---

### ABSTRACT

---

**Sergey Yu. Sayenko**

National Science Centre  
"Kharkiv Institute of Physics and Technology"  
Kharkiv, Ukraine

**Oleg K. Morachkovsky<sup>1</sup>**

**Denis V. Lavinsky**  
**Vladimir N. Sobol**  
**Yuriy M. Andreev**  
National Technical  
University "Kharkiv  
Polytechnic Institute",  
Kharkiv, Ukraine

Results of researches in the field of designing containers for storage of radioactive materials are presented in the work. The purposes of researches include a development of an effective method of modeling static and dynamic deformation processes at shock impact on the ceramic container with radioactive materials at transportation. The next tasks have been solved: on the basis of the mathematical description of physic-mechanical processes of deformation of the complex design container has been chosen method of finite-element's for effective modeling of the stress-strain State of static and dynamic deformation processes in the containers made of ceramic elements; laws of deformation, estimations of durability and rigidity for designed containers have been received after calculations by means of the computer software; recommendations on perfection of a design of the container for maintenance of requirements to safety are given. Analysis Finite Element Method (FEM) has been conducted in the ANSYS system and results is presented.

---

### INTRODUCTION

One of the most probable events radiating danger at storage of a radiating active waste is connected with threats of in a regular mode of storage and/or destructions at falling at transportation, or unforeseen shock-impact on containers for the purpose of their destruction. The container is a vessel for transportation and-or storages of radioactive materials. It serves several functions: provides chemical, mechanical, thermal and radiological protection, disseminates a heat of disintegration during processing, transportations and storage. Considering quantities of radioactive materials stored in Ukraine it is possible to draw a conclusion that the damage and scales of radiating pollution in case of degradation of capacities of storage and dispersion of radioactive substances can be considerable. Therefore, in Ukraine, as well as in many other countries now there is a question of decrease in radiating danger of existing crucial objects, such as storehouses of a radioactive waste. One way is working out of new protective materials and designs on their basis for creation of containers for storage of the radioactive materials, different the raised durability, in comparison with traditional concrete. Refusal of use of packing's container from concrete it is one of variants of achievement.

Ceramic material it is crystalline solid, usually has contains silicon dioxide ( $\text{SiO}_2$ ) and other inorganic oxides, this material produce at high temperatures (800°C or above) and, usually, at elevated pressures. Among such materials most interesting materials it is the ceramic composites of system  $\text{B}_4\text{C-ZrB}_2$  received by methods of hot pressing and reactionary hot pressing of powder components on the basis of boron, carbon, carbide of boron and oxides zirconium. Told above is cause expediency of continuation the spent researches at [2] and workings out of methods of modeling of behavior of ceramic containers on the basis of  $\text{ZrO}_2$  and  $\text{B}_4\text{C}$ , and also their compositions under the influence of various dynamic loadings for rationalization design and structure of these new materials and containers.

---

<sup>1</sup> Corresponding author. Email [morachko@kpi.kharkov.ua](mailto:morachko@kpi.kharkov.ua)

## 1. PROBLEM STATEMENT

The package used to transport radioactive materials must be safe under normal and hypothetical accident conditions. These requirements for ceramic container design are verified through test or finite element (FE) analysis. Since the cost for FE analysis is less than one for test, the verification by FE analysis is mainly used. But FE analysis may show different results for the same problem due to several assumptions of models to simplify real states and modelling technique. This may have different results as FE-codes. In this paper, finite element analysis is carried out for the 5 meters free drop and the puncture condition of the hypothetical accident conditions using COSMOS and ANSYS. Energy and effective stress on each component are presented and compared between two FE codes where, the effective stress is designated the maximum von Mises stress on inner and outer walls of container. In this work, a detailed analysis of the drop problem the maximum allowable stress is performed considering several attitudes at impact in order to find which attitude results in maximum damage to the container, and which part of the container deformed severely. Once the failure mode of the hypothetical drop is defined, a full-scale drop on the container will be performed. The numerical results are compared and some analytical dimensional and physic-mechanical parameters are readjusted to obtain a better correlation between forthcoming natural test and analysis.

This paper presents the details of a simulated Programs of numerical researches conducted in support of an forthcoming natural experimental test program performed in order to prepare ceramic containers. The information regarding the waste package used in this calculation is based on the proposed designs presented by the drawings and sketches.

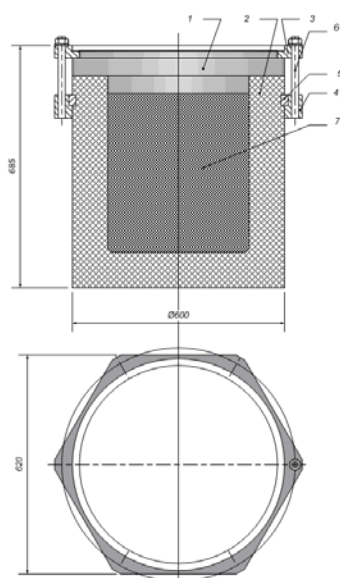


*Fig. 1 The sketches of proposed designs waste package*

The dimensions used in this calculation refer to the dimensions associated with design and the maximum dimensions. The bounding and maximum weights used.

*Table 1 – Physic-mechanical properties of materials for the ceramic container details*

Mechanical properties	Steel 30Cr13	Ceramics ZrO <sub>2</sub>
Strength at compression ( $\sigma_B$ ) <sub>c</sub> , MPa		1400
Strength at a bend ( $\sigma_B$ ) <sub>b</sub> , MPa		750
The module of elasticity $E$ , GPa	210	200
Poisson's ratio $\nu$	0.3	0.28-0.36
Impact strength $a_h$ , kg/sm <sup>2</sup>		
Density $\rho$ , g/sm <sup>3</sup>	7.8	5.8-6
Factor of friction		0.2-0.3

No	Name	m, kg
1	Cover	149.544
2	Case	626.923
3	Flange	17.0683
4	Flange	19.13
5	Ring cutting	6.45
6	Hairpin	0.337
7	Radioactive material	141.37
$\sum m$		962.5

Method of solution and numerical results are presented. A detailed conclusion and assumption are presented in publication [1,2].

## 2. METHOD OF SOLUTION

For identification of the maximum allowable stress for a pressured container made from the ceramic composites of system  $B_4C-ZrB_2$ , it is necessary to determine the stress components derived from pressure. For hermetic sealing preliminary compression of a cover by bolts is used a deformation of compression of a bolt is varied. The stress component derived from pressure contains a stress concentration factor which is dependent on pressure and hermetic sealing preliminary compression.

In this work, identification of the maximum allowable stress and stress concentration factor values is obtained by the Finite Element Method (FEM) analysis conducted in the ANSYS program is presented. A ceramic container is analyzed for a 5 m free drop to a rigid ground. The complete finite element model is built and analysis is then carried out using Program Package ANSYS. Results are again completely processed using SCA KIDIM in terms of time history plots of momentum and contact force; deformation of the container during impact; and stress/strain distribution in the container at different times.

The model assumes that all the materials are homogeneous and isotropic and that the mechanical properties are associated with an isothermal environment. The impact problem is an initial condition formulation where the velocity of the body at a time of impact is fixed at 13.2883 m/s which value is from an assumption of 5 m free-drop. The orientation of the velocity vector onto horizontal target surface defines the attitude of the body at the time of impact. The numerical analysis has been programmed to start 1msec before the time of impact, which time is required for the stabilization of initial condition.

Two distinct attitudes at impact have been considered in this study. The cases considered are: 1) Vertical impact on base assembly, 2) Oblique impact on bottom corner at angle of  $30^\circ$  from the horizontal.

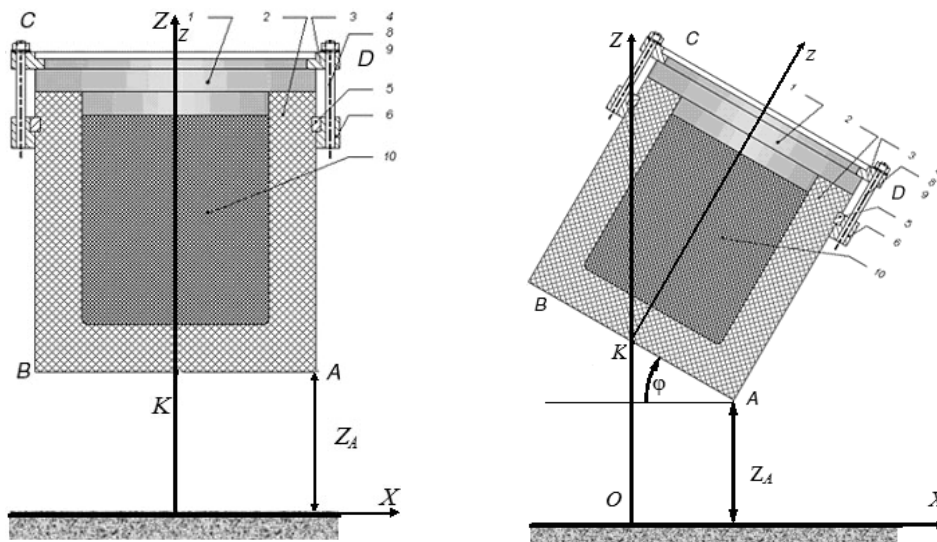


Fig. 2 The cases at impact: 1) Vertical impact on the base, 2) Oblique impact on bottom corner at angle of  $30^\circ$  from the horizontal

### 3. NUMERICAL RESULTS

For identification of the maximum allowable stress for a pressured container made from the ceramic composites of system  $B_4C-ZrB_2$ , it is necessary to determine the stress components derived from pressure. For hermetic sealing preliminary compression of a cover by bolts is used a deformation of compression of a bolt is varied. The stress component derived from pressure contains a stress concentration factor which is dependent on pressure and hermetic sealing preliminary compression.

In this work, identification of the maximum allowable stress and stress concentration factor values is obtained by the Finite Element Method (FEM) analysis conducted in the ANSYS program is presented.

FE representations of the container with radioactive materials with dimensional structure elements, weight and prepress differences are created and solved for analysis of drop events using ANSYS program. The numerical stress results are reviewed to determine the maximum response locations and magnitudes. The results of this calculation are evaluated for wall-averaged stress in tensities. The stress responses for the different FE representations are compared to each other to determine the sensitivity of the calculations to variations in the input parameters.

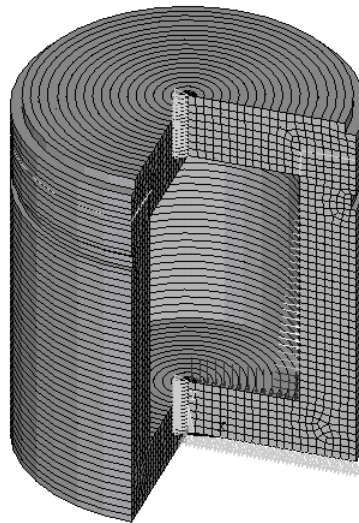


Fig. 3 Finite element model of the container

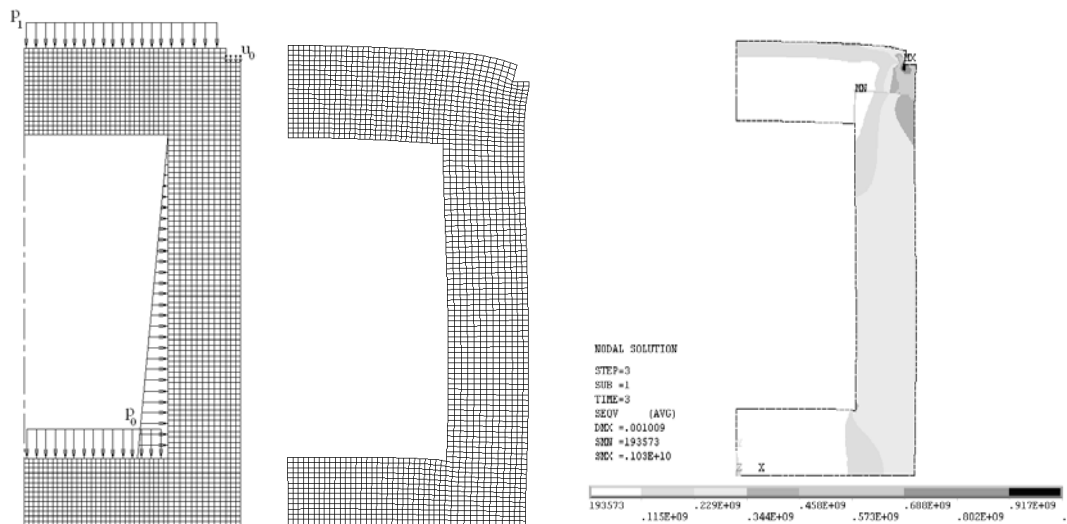


Fig. 4 Finite Element Model, Deflection Contour and Von Mises Stress at walls of container

Number of calculations for an estimation of value influence of a coupler on the strained condition and hermetic sealing preliminary compression of a cover by bolts is used. A deformation of compression of a bolt –  $U$  is varied. On Fig.5 (left figure) dependences of the maximal intensity of stress and the maximal first main stress from in a range from 0.01 mm up to 0.1 mm with step of 0.01 mm are resulted. On Fig.5 (right figure) dependences of the maximal intensity of stress and the maximal first main stress from deflection in a range from 0.1 mm up to 1 mm with step of 0.1 mm are resulted. Both in the first and in the second cases linear dependence is observed. And at size  $U=1$  mm the max-

imal value of the first main stress makes 732 MPa (stretching) that is close to limiting stress. It is found that the maximum Von Mises stress in the bottom cover is about 1000 MPa, which is significantly lower than the ultimate stress intensity of 1400 MPa. The maximum contact pressure on lines AB and AC are equal 590 MPa.

An impact analysis of a ceramic storage container using Program Package ANSYS for pre- and post-processing has been illustrated. PP/ANSYS enables the response of the container system in terms of various parameters at different stages of impact to be studied in details. The information obtained is very useful for container design.

Next example is kinetostatic problem solving by using ANSYS program software. Ceramic container has been dropped vertically from height about 0.5 m as you can see on the Fig. 2. The acceleration values are calculated at the moment of container shock and equal to  $21700 \text{ m/sec}^2$ . Such data is used as inertia loads in ANSYS software. Compression deformation of the bolt (U) was taken equal to 1mm. Solution results have been done for such case taking to account equality of geometric, mechanical and physical parameters for container to previous example. The maximal values of stress intensity by von Mises and contact pressures are less to previous solution example and equal to 856 MPa and 488 MPa respectively. Hermetic properties of the ceramic container kept safety.

It is found that damage tends to localize in the vicinity of contact with stresses and strains decreasing rapidly toward remote areas. A stainless steel ring cutting can give the impact on the container effectively. Even though the impact limiter experiences severe damage, damage on the container itself is not observed as it remains essentially elastic.

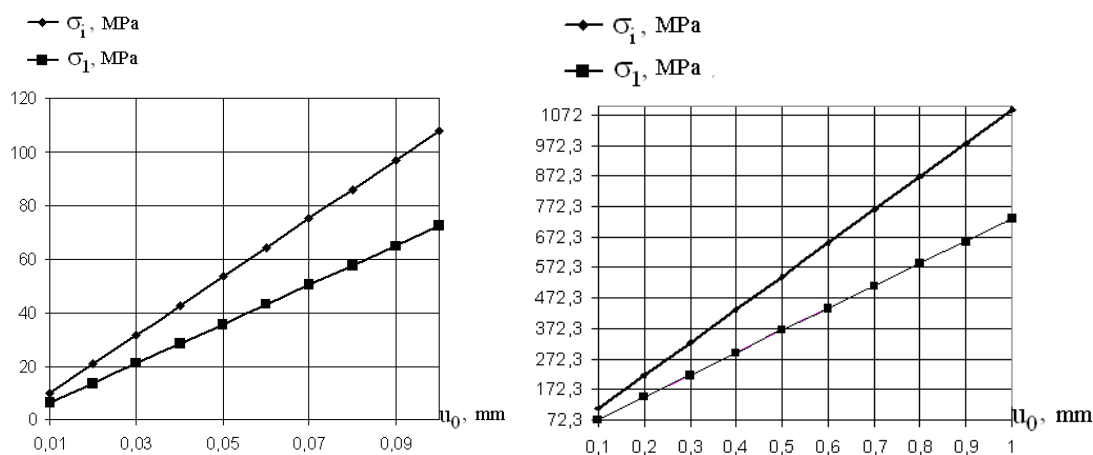


Fig. 5 Dependences of the maximal intensity and the first main stresses from U

## CONCLUSIONS

In this work, identification of the maximum allowable stress and stress concentration factor values is obtained by the Finite Element Method (FEM) analysis conducted in the ANSYS program is presented.

Results of the impact analysis described in this paper show that complex structural deformation patterns associated with the impact problem could be predicted. The time and cost for the impact testing of Type C container with complex geometries are reduced considerably. In summary, the impact simulation provides the preparer of the approval of Type C container with a convenient tool that can be used in support to licensing efforts.

## REFERENCES

- [1] Sayenko S.Yu. Technological approaches for good safety at the reference with radioactive waste, *Power, Economy, Technologies, and Ecology*, Vol. 21, N.2, pp. 27-35, 2007 (in Russian).
- [2] Nekljudov I.M., Morachkovsky O.K., Andreev Yu.M., Sayenko S.Yu., Biryukov O.V. Dynamic's Unsociable persons modeling on test for durability of containers-packing's for highly active waste of nuclear stations, *East-European Magazine of High Technologies*, Vol. 30, N.6/4, pp. 4-7, 2007 (in Russian).

## INVESTIGATION OF DYNAMICAL INSTABILITY OF VIBRATION MODES FOR LAMINATED PLATES AND SHALLOW SHELLS

**Tatyana V. Shmatko**<sup>1</sup>  
National Technical  
University «KhPI»,  
Kharkov, Ukraine

---

### ABSTRACT

---

Research method of the dynamic stability of the geometrically nonlinear vibration modes of the shallow shells with complex plan form is used. Mathematical statement of the problem is carried out in framework of reinforced theory shells of the first order. The proposed method is based on the R-functions theory, variational methods, "limited stability criterion", obtained from the definition stability by Lyapunov and method by Runge-Kutta. Numerical results for shells with complex form under transverse periodic load can be received using the realized software of designed numerically-analytical approach.

---

### INTRODUCTION

Laminated composite shallow shells are widely applied as structure components in the construction of aerospace, mechanical, ship-building and other branches. Dynamical instability analysis of composite shallow shells and plates subjected to a harmonic transverse load has received considerable attention in the literature [1, 2, 3, 4]. However the most papers consider an investigation of nonlinear vibrations of plates and shells with simple enough form. There are only few works in which laminated shallow shells or plates with a shape different from rectangular, circle or ellipse are presented. Deficiency of such papers is explained by the difficulties of construction of analytical expressions for basic functions. These functions are needed to reduce a nonlinear system of differential equations with partial derivatives to a system of the ordinary differential equations for time. One of universal approaches, which can be used for solving this problem, is founded on the application of the R-functions theory [5, 6]. This theory allows a construction of complete set of the coordinate functions for different types of boundary conditions. In this paper the R-function theory together with variational methods and the "limited criterion of stability by Lyapunov" [7] is applied as a new approach to investigate vibration modes of laminated shallow shells supported on complex plan form.

### 1. THE GOVERNING EQUATION OF THE SHALLOW SHELLS THEORY

Consider a laminated shallow shell of an arbitrary plan form constructed of a finite number  $N$  of orthotropic layers, oriented arbitrary with respect to the shell coordinates  $(x, y, z)$ . In this paper we shall only investigate symmetric laminated shallow shells. The components of the displacements at an arbitrary point of the shell in the  $x, y$  and  $z$  directions are  $u, v$  and  $w$  respectively. According to the first-order shear deformation theory, the inplane displacements  $u$  and  $v$  are linear functions of the coordinate  $z$  and the transverse displacement  $w$  is a constant throughout the thickness of the shell. Under this assumption the displacement field may be given in the following form:

$$u' = u + z\psi_x, \quad v' = v + z\psi_y, \quad w' = w$$

where  $u, v$  and  $w$  are the displacements at the middle surface,  $\psi_x$  and  $\psi_y$  are the rotations of the middle surface about the  $Oy$  and  $Ox$  axes respectively. The nonlinear strain-displacement relations of the shallow shells can be written as

$$\varepsilon'_{11} = \varepsilon_{11} + zk_x, \quad \varepsilon'_{22} = \varepsilon_{22} + zk_y, \quad \varepsilon'_{33} = 0, \quad \varepsilon'_{12} = \varepsilon_{12} + zk_{xy}, \quad \varepsilon'_{13} = w_{,x} - uk_1 + \psi_x$$

---

<sup>1</sup> Corresponding author. Email: ktv\_ua@yahoo.com

$$\varepsilon'_{23} = w_{,y} - vk_2 + \psi_y, \quad \varepsilon'_{xz} = \psi_x + w_{,x}, \quad \varepsilon'_{yz} = \psi_y + w_{,y}$$

in which

$$\varepsilon_{11} = u_{,x} + k_1 w + \frac{1}{2} w_{,x}^2, \quad \varepsilon_{22} = v_{,y} + k_2 w + \frac{1}{2} w_{,y}^2, \quad \varepsilon_{12} = u_{,x} + v_{,y} + w_{,x} w_{,y}$$

$$k_x = \psi_{x,x}, \quad k_y = \psi_{y,y}, \quad k_{xy} = \psi_{x,y} + \psi_{y,x}$$

Here  $k_1$  and  $k_2$  are two principal curvatures of shallow shells, the subscripts following a comma stand for partial differentiation. Let us present unknown functions as components of the following vector  $U = (u, v, w, \psi_x, \psi_y)^T$ , then the governing equations are derived as follows:

$$LU = -Nl(w) + m \frac{\partial^2 U}{\partial t^2} + P \quad (1)$$

where

$$L = [L_{ij}]_{i=1,5, j=1,5}, \quad Nl(w) = (Nl_1(w), Nl_2(w), Nl_3(w), 0, 0)^T$$

$$m = (m_1, m_1, m_1, m_2, m_2)^T, \quad P = (0, 0, q(x, y, t), 0, 0)^T$$

Here  $L_{ij}$  are linear differential operators, which can be expressed as follows:

$$L_{11} = C_{66} \frac{\partial^2}{\partial x^2} + 2C_{16} \frac{\partial^2}{\partial x \partial y} + C_{66} \frac{\partial^2}{\partial y^2} - k_1^2 C_{55} \cdot,$$

$$L_{22} = C_{66} \frac{\partial^2}{\partial x^2} + 2C_{26} \frac{\partial^2}{\partial x \partial y} + C_{22} \frac{\partial^2}{\partial y^2} - k_2^2 C_{44}$$

$$L_{12} = L_{21} = C_{16} \frac{\partial^2}{\partial x^2} + (C_{12} + C_{66}) \frac{\partial^2}{\partial x \partial y} + C_{26} \frac{\partial^2}{\partial y^2} - k_1 k_2 C_{45}$$

$$L_{13} = -L_{31} = \left( (k_1 C_{11} + k_2 C_{12} + k_1 C_{55}) \frac{\partial}{\partial x} + (k_1 C_{16} + k_2 C_{26} + k_1 C_{45}) \frac{\partial}{\partial y} \right)$$

$$L_{14} = L_{41} = k_1 C_{55}, \quad L_{15} = L_{51} = k_2 C_{44}$$

$$L_{23} = -L_{32} = \left( (k_1 C_{16} + k_2 C_{26} + k_2 C_{45}) \frac{\partial}{\partial x} + (k_1 C_{12} + k_2 C_{22} + k_2 C_{44}) \frac{\partial}{\partial y} \right)$$

$$L_{24} = L_{42} = k_2 C_{45}, \quad L_{25} = L_{52} = k_2 C_{44}$$

$$L_{33} = C_{55} \frac{\partial^2}{\partial x^2} + 2C_{45} \frac{\partial^2}{\partial x \partial y} + C_{44} \frac{\partial^2}{\partial y^2} - (C_{11} k_1^2 + 2C_{12} k_1 k_2 + C_{22} k_2^2)$$

$$L_{34} = L_{43} = C_{55} \frac{\partial}{\partial x} + C_{45} \frac{\partial}{\partial y}, \quad L_{35} = -L_{53} = C_{45} \frac{\partial}{\partial x} + C_{44} \frac{\partial}{\partial y}$$

$$L_{44} = D_{11} \frac{\partial^2}{\partial x^2} + 2D_{16} \frac{\partial^2}{\partial x \partial y} + D_{66} \frac{\partial^2}{\partial y^2} - C_{55}$$

$$L_{45} = L_{54} = \left( D_{16} \frac{\partial^2}{\partial x^2} + (D_{12} + D_{66}) \frac{\partial^2}{\partial x \partial y} + D_{26} \frac{\partial^2}{\partial y^2} - C_{44} \right)$$

$$L_{55} = D_{66} \frac{\partial^2}{\partial x^2} + 2D_{26} \frac{\partial^2}{\partial x \partial y} + D_{22} \frac{\partial^2}{\partial y^2} - C_{44}$$

The right part of the equation (1), that is  $Nl(w)$  is presented as follows:

$$Nl_1(w) = \frac{\partial}{\partial x} \left( \frac{1}{2} C_{11} \left( \frac{\partial w}{\partial x} \right)^2 + \frac{1}{2} C_{12} \left( \frac{\partial w}{\partial y} \right)^2 + C_{16} \frac{\partial w}{\partial x} \frac{\partial w}{\partial y} \right) +$$

$$+ \frac{\partial}{\partial y} \left( \frac{1}{2} C_{16} \left( \frac{\partial w}{\partial x} \right)^2 + \frac{1}{2} C_{26} \left( \frac{\partial w}{\partial y} \right)^2 + C_{66} \frac{\partial w}{\partial x} \frac{\partial w}{\partial y} \right),$$

$$\begin{aligned}
NL_2(w) &= \frac{\partial}{\partial x} \left( \frac{1}{2} C_{16} \left( \frac{\partial w}{\partial x} \right)^2 + \frac{1}{2} C_{26} \left( \frac{\partial w}{\partial y} \right)^2 + C_{66} \frac{\partial w}{\partial x} \cdot \frac{\partial w}{\partial y} \right) + \\
&+ \frac{\partial}{\partial y} \left( \frac{1}{2} C_{12} \left( \frac{\partial w}{\partial x} \right)^2 + \frac{1}{2} C_{22} \left( \frac{\partial w}{\partial y} \right)^2 + C_{26} \frac{\partial w}{\partial x} \cdot \frac{\partial w}{\partial y} \right), \\
NL_3(u, v, w, \psi_x, \psi_y) &= \frac{1}{2} \left( \frac{\partial w}{\partial x} \right)^2 (k_1 C_{11} + k_2 C_{12}) + \frac{1}{2} \left( \frac{\partial w}{\partial y} \right)^2 (k_1 C_{12} + k_2 C_{22}) + \\
&+ \frac{\partial w}{\partial x} \cdot \frac{\partial w}{\partial y} (k_1 C_{16} + k_2 C_{26}) + N_{11} \frac{\partial^2 w}{\partial x^2} + N_{22} \frac{\partial^2 w}{\partial y^2} + 2N_{12} \frac{\partial^2 w}{\partial x \partial y}
\end{aligned}$$

The coefficients  $C_{ij}, D_{ij}$  ( $K_{ij} = 0$ ) and  $m_j$ , ( $j = \overline{1,5}$ ) are calculated by following formulas:

$$\begin{aligned}
(C_{ij}, D_{ij}) &= \sum_{m=1}^n \int_{h_m}^{h_{m+1}} B_{ij}^{(m)}(1, z^2) dz, \quad (i, j = \overline{1,2,6}), \quad C_{ij} = k_i^2 \sum_{m=1}^n \int_{h_m}^{h_{m+1}} B_{ij}^{(m)} dz, \quad (i, j = \overline{4,5}) \\
m_j &= \sum_{m=1}^n \int_{h_m}^{h_{m+1}} \rho_m dz, \quad (j = \overline{1,2,3}), \quad m_j = \sum_{m=1}^n \int_{h_m}^{h_{m+1}} \rho_m z^2 dz, \quad (j = \overline{4,5})
\end{aligned}$$

Here  $B_{ij}^{(m)}$  are the stiffness coefficient of the  $m$ -th layer,  $k_i$  ( $i = \overline{4,5}$ ) is the shear correction factors.

## 2. SOLUTION METHOD

Let us present unknown functions with help series using the eigenfunctions  $\vec{U}_i = (u_i, v_i, w_i, \psi_{x_i}, \psi_{y_i})$  of the corresponding linear vibration problem

$$\begin{aligned}
w &= \sum_{i=1}^2 y_i(t) w_i(x, y), \quad \psi_x = \sum_{i=1}^2 y_i(t) \psi_{x_i}(x, y), \quad \psi_y = \sum_{i=1}^2 y_i(t) \psi_{y_i}(x, y) \\
u &= \sum_{i=1}^2 y_i(t) u_i(x, y) + \sum_{i=1}^2 \sum_{j=1}^2 y_i y_j u_{ij}, \quad v = \sum_{i=1}^2 y_i(t) v_i(x, y) + \sum_{i=1}^2 \sum_{j=1}^2 y_i y_j v_{ij}
\end{aligned} \quad (2)$$

The functions  $u_i, v_i, w_i, \psi_{x_i}, \psi_{y_i}$  are the components of the eigen vector  $\vec{U}_i$ , and the functions  $u_{ij}, v_{ij}$  must be solutions of the following system of the differential equations:

$$\begin{cases} L_{11} u_{ij} + L_{12} v_{ij} = -NL_1^{(2)}(w_i, w_j) \\ L_{21} u_{ij} + L_{22} v_{ij} = -NL_2^{(2)}(w_i, w_j) \end{cases} \quad (3)$$

The right parts of the system (3), denoted as operators  $NL_k^{(2)}(w_i, w_j)$ , ( $k = \overline{1,2}$ ) have the following form:

$$\begin{aligned}
NL_1^{(2)}(w_i, w_j) &= \frac{\partial w_i}{\partial x} \left( C_{11} \frac{\partial^2 w_j}{\partial x^2} + 2C_{16} \frac{\partial^2 w_j}{\partial x \partial y} + C_{66} \frac{\partial^2 w_j}{\partial y^2} \right) + \\
&+ \frac{\partial w_i}{\partial y} \left( C_{16} \frac{\partial^2 w_j}{\partial x^2} + (C_{12} + C_{66}) \frac{\partial^2 w_j}{\partial x \partial y} + C_{26} \frac{\partial^2 w_j}{\partial y^2} \right), \\
NL_2^{(2)}(w_i, w_j) &= \frac{\partial w_i}{\partial x} \left( C_{16} \frac{\partial^2 w_j}{\partial x^2} + (C_{12} + C_{66}) \frac{\partial^2 w_j}{\partial x \partial y} + C_{26} \frac{\partial^2 w_j}{\partial y^2} \right) + \\
&+ \frac{\partial w_i}{\partial y} \left( C_{66} \frac{\partial^2 w_j}{\partial x^2} + 2C_{26} \frac{\partial^2 w_j}{\partial x \partial y} + C_{22} \frac{\partial^2 w_j}{\partial y^2} \right)
\end{aligned}$$

It should be noted that the system (3), added the corresponding boundary conditions and also the natural vibration problem were carried out by RFM method [5, 6].

Substituting the expressions (2) for unknown functions  $u, v, w, \psi_x, \psi_y$  into third equations of the system (1) and applying the procedure by Bubnov-Galerkin one can obtain nonlinear system of the ordinary differential equations in  $y_1(t), y_2(t)$  of the following form:

$$\begin{aligned} y_1'' + \alpha_0^{(1)} y_1 + \alpha_{11}^{(1)} y_1^2 + \alpha_{12}^{(1)} y_1 y_2 + \alpha_{22}^{(1)} y_2^2 + \gamma_{111}^{(1)} y_1^3 + \gamma_{112}^{(1)} y_1^2 y_2 + \gamma_{122}^{(1)} y_1 y_2^2 + \gamma_{222}^{(1)} y_2^3 &= \alpha_r P(t) \\ y_2'' + \alpha_0^{(2)} y_2 + \alpha_{11}^{(2)} y_1^2 + \alpha_{12}^{(2)} y_1 y_2 + \alpha_{22}^{(2)} y_2^2 + \gamma_{111}^{(2)} y_1^3 + \gamma_{112}^{(2)} y_1^2 y_2 + \gamma_{122}^{(2)} y_1 y_2^2 + \gamma_{222}^{(2)} y_2^3 &= 0 \end{aligned} \quad (4)$$

The factors of the equations are defined by formulas:

$$\begin{aligned} \alpha_0^{(m)} &= \omega_{mL}^2 \\ \alpha_{ij}^{(m)} &= -\frac{1}{m_1 \|w_m\|^2} \iint_{\Omega} \left( k_1 N_{11p}^{(ND)}(u_{ij}, v_{ij}, w_i, w_j) + k_2 N_{22}^{(ND)}(u_{ij}, v_{ij}, w_i, w_j) + N_{11}^L(u_i, v_i, w_i) w_{i,xx} + \right. \\ &\quad \left. + N_{22}^L(u_i, v_i, w_i) w_{i,yy} + 2N_{12}^L(u_i, v_i, w_i) w_{i,xy} \right) d\Omega, \quad (m, i, j = 1, 2) \\ \gamma_{ijk}^{(m)} &= -\frac{1}{m_1 \|w\|^2} \iint_{\Omega} \left( k_1 N_{11p}^{(ND)}(u_{ij}, v_{ij}, w_i, w_j) w_{k,xx} + N_{22}^{(ND)}(u_{ij}, v_{ij}, w_i, w_j) w_{k,yy} + \right. \\ &\quad \left. + 2N_{12}^{(ND)}(u_{ij}, v_{ij}, w_i, w_j) w_{k,xy} \right) w_m d\Omega \end{aligned}$$

Let us denote the following expressions in matrix form:

$$\begin{aligned} (N_L)^T &= (N_{11}^L, N_{22}^L, N_{12}^L), \quad (N_{NL})^T = (N_{11}^{(ND)}, N_{22}^{(ND)}, N_{12}^{(ND)}) \\ C &= \begin{pmatrix} C_{11} & C_{12} & C_{16} \\ C_{12} & C_{22} & C_{26} \\ C_{16} & C_{26} & C_{66} \end{pmatrix}, \quad E_L^{sh} = \begin{pmatrix} \varepsilon_{11} \\ \varepsilon_{22} \\ \varepsilon_{12} \end{pmatrix} = \begin{pmatrix} u_{i,x} - k_1 w_1 \\ v_{i,y} - k_2 w_1 \\ v_{i,x} + u_{i,y} \end{pmatrix}, \quad E_L^{pl} = \begin{pmatrix} \varepsilon_{11} \\ \varepsilon_{22} \\ \varepsilon_{12} \end{pmatrix} = \begin{pmatrix} u_{ij,x} \\ v_{ij,y} \\ v_{ij,x} + u_{ij,y} \end{pmatrix} \\ NDW_{ij} &= \begin{pmatrix} w_{i,x} w_{j,x} \\ w_{i,y} w_{j,y} \\ w_{i,x} w_{j,y} + w_{i,y} w_{j,x} \end{pmatrix} \end{aligned}$$

Then expressions for  $N_{11p}^{(Nd)}, N_{22p}^{(Nd)}, N_{12p}^{(Nd)}, N_{11}^L, N_{22}^L, N_{12}^L$  may be defined as corresponding components of the following vectors:  $N_L = CE_L^{sh}$ ,  $N_{NL} = CE_L^{pl} + \frac{1}{2}NDW_{ij}$ .

The obtained system (4) is solved by Runge-Kutta method and special stability criterion described below.

### 3. INVESTIGATION OF STABILITY OF NONLINEAR VIBRATION MODES

Let us consider the stability of the second periodic or chaotic vibration form which is defined as  $y_2(t) = 0$ . Instability of the form  $y_2(t) = 0$  means "swap" of energy from one harmonic of the Fourier series in another one. The variables  $y_2(t), \dot{y}_2(t)$  may be considered as variations. That is why we assume that value of the variation  $y_2$  is essentially smaller than the variable  $y_1$  in zone of stability of the vibration form,  $y_2(t) = 0$ , as it is accepted in stability theory.

Limited criterion for finding instability zones of nonlinear vibration modes for considered system is applied [7]. It is assumed that initial value of the variable  $y$  is not however small variable and so the connection between constant  $\varepsilon$  and value of  $\delta$  [7] is introduced. Let the variable  $t$  be varied from 0 to  $T$ . Then the following criterion of stability/instability is taken:

*Instability of the vibration form  $y_2(t) = 0$  is fixed if the following condition*

$$|y_2(t)| \geq \rho |y_2(0)|, \quad (0 \leq t \leq T)$$

holds true. The foregoing criterion, obtained provided that value  $\delta$  can not be arbitrary small one is called as "limited criterion of stability" which is a consequence of the classical criterion of stability by Lyapunov [7,8]. Here the value  $\rho^{-1}$  is an order infinitesimal of the initial variation with respect to maximum permissible variation of  $\varepsilon$  for any  $t \geq 0$ . The increasing value  $\rho$  means that allowable initial variations are decreasing. It exists some arbitrariness while choosing  $\rho$ ; it is not by accident

because in the instability region the variations while increase  $t$  come out limits of the initial solution  $\varepsilon$ -neighborhood for any choose of parameter  $\rho$ . For definiteness this value is taken as  $\rho \leq 10$ .

For determining the finite value of parameter  $T$  experiment calculation is realized into some mesh points at chosen scale of system parameters at the fixed value of  $T$ . Increasing the value of parameter  $T$  and corresponding calculations will be continued until boundaries of instability zones are stabilized at chosen scale of variables plane.

#### 4. NUMERICAL RESULTS

Find the stability zones of the vibration forms for clamped three layers shallow spherical shells presented in Fig. 1(a) and supported on plan form shown in Fig 1(b).

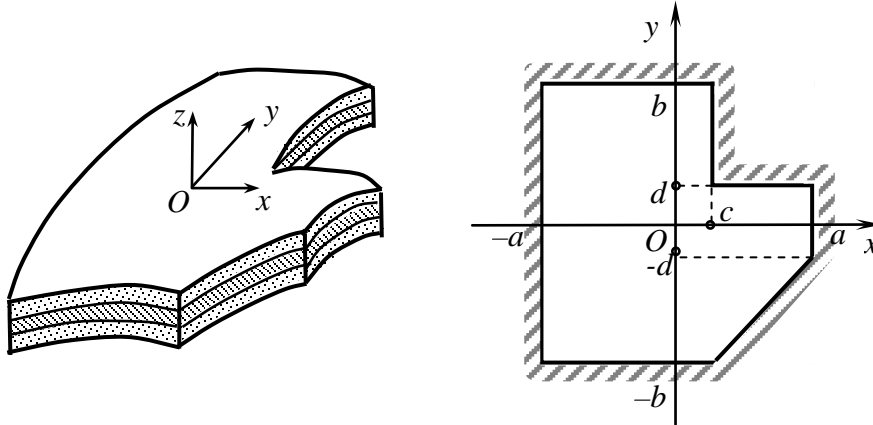


Fig.1(a,b). Plan of clamped three layers shallow shells

The shell is loaded transverse force,  $P(t) = F \cos \Omega t$ . The mechanical characteristics of the shell are:  $E = 25E_2$ ,  $G_{12} = G_{13} = 0.5E_2$ ,  $G_{23} = 0.2E_2$ ,  $\nu_{12} = 0.25$ . The shear factors are taken to be  $k_4^2 = k_5^2 = 5/6$ . The geometric parameters of the shell are taken as follows:

$$b/a = 1, \quad c/(2a) = d/(2a) = 0.25, \quad 2a/R_x = 2a/R_y = 0.1, \quad h/(2a) = 0.1$$

The boundary conditions are accepted in the following form (clamped edge):

$$w = 0, u = 0, v = 0, \psi_x = \psi_y = 0 \quad \forall (x, y) \in \partial\Omega,$$

Here  $\partial\Omega$  denotes the whole boundary of the domain, the equations of which may be constructed with help R-functions theory

$$\omega(x, y) = (f_1 \wedge_0 f_2) \wedge_0 (f_3 \vee_0 f_4) \wedge_0 f_5$$

The functions  $f_i, (i = \overline{1,5})$  are defined as follows:

$$f_1 = (b^2 - y^2)/(2b) \geq 0, \quad f_2 = (a^2 - x^2)/(2a) \geq 0, \quad f_3 = (c - x) \geq 0, \quad f_4 = (d - y) \geq 0$$

$$f_5 = ((y + b)(a - c) - (x - c)(b - d)) \geq 0$$

The expressions for R-operators  $\wedge_0, \vee_0$  are defined according to [5]. The corresponding structural formulas [5, 6] are

$$u = \omega P_1, \quad v = \omega P_2, \quad w = \omega P_3, \quad \psi_x = \omega P_4, \quad \psi_y = \omega P_5$$

Here  $P_i, (i = 1, 2, 3, 4, 5)$  are indefinite components of the constructed structures of solution, which are expanded in series in some complete system of functions. The coefficients of this expansion are sought from the stationary condition for corresponding functional.

Values of the dimensionless parameter of the natural frequency for the three layers cross-ply  $(0^0, 90^0, 0^0)$  spherical shell, panel and plate are presented in the Table 1.

Table 1. Values of the Dimensionless Frequency Parameter  $\Lambda_i = \lambda_i \frac{(2a)}{h} \sqrt{\frac{\rho}{E_2}}$

$(2a/R_x, 2a/R_y)$	$\Lambda_1$	$\Lambda_2$	$\Lambda_3$	$\Lambda_4 \dots$
(0.1, 0.1)	18.851	29.139	36.113	43.113
(0, 0.1)	18.561	29.068	36.085	43.054
(0, 0)	18.453	29.035	36.069	43.031

Instability zones are presented for cross-ply spherical shells in the Fig. 2. Term of stabilization is  $T=1000$ , that is, calculation time, at which stabilization of boundaries of instability zones are observed.

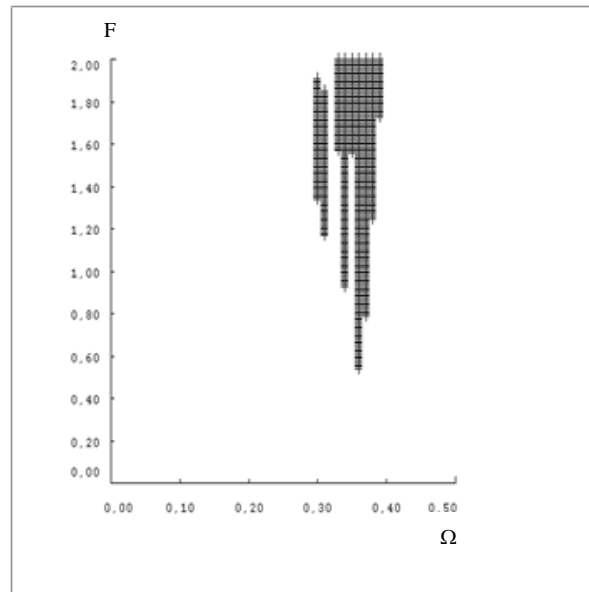


Fig.2. Instability zone for cross-ply spherical shell

Calculations were carried out in variable scale plane  $(\Omega, F)$ , where parameter  $\Omega$  was varied  $0 \leq \Omega \leq 0.5$  and parameter  $F$  was varied  $0 \leq F \leq 2$ .

Obtained results show that considered system may have instability behaviour at the parameter values starting with  $\Omega = 0.27$  and  $F = 0.42$ .

## CONCLUSION

The effective approach for investigation of stability of nonlinear vibration modes of the laminated shallow shells resting on complex plan form and having symmetric structure of layers are proposed. The method is based on R-functions theory, variational methods, special criterion of stability and method by Runge-Kutta. There is presented numerical results for clamped three layered spherical shallow shells.

## REFERENCES

- [1] Abe A., Y.Kobayashi Y., Yamada G. One-to-One Internal Resonance of Symmetric Crossply Laminated Shallow Shells, *Journal of Applied Mechanics* 68, pp. 40-649, 2001.
- [2] M.Ganapathi, T.K.Varadan, V.Balamurugan. Dynamic instability of laminated composite curved panels using finite element method, *Computers and Structures* 53, pp. 335-342, 1994.
- [3] L.W.Chen, J.Y.Yang. Dynamical instability of laminated composite plates by the finite element method, *Computers and Structures* 36, pp. 845-851, 1990.
- [4] C.W.Bert, V. Birman. Dynamic stability of shear deformable antisymmetric angle-ply plates, *Int. Journal of Solids Structure*. 24, pp. 233-238, 1987.
- [5] Rvachev V. L. *Theory of R-functions and some its applications*. Kiev, Naukova Dumka, Ukraine, 1982, 551p. (in Russian).
- [6] Rvachev V. L. and Kurpa L. V., *R-functions in Problems of the Theory of Plates*, Naukova Dumka, Kiev, 1987, 176p. (in Russian).
- [7] Mikhlin Yu.V. and Shmatko T.V. Stability of regular and chaotic modes in dynamical systems with more than one equilibrium positions, *Problems of Machine-Building*, 3-4, Vol.2, pp. 128-135, 1999.
- [8] Mikhlin Yu.V., Shmatko T.V., Manucharyan G.V. Lyapunov definition and stability of regular or chaotic vibration modes in systems with several equilibrium positions. *Computers and Structures*, 82, pp. 2733-2742, 2004.

## SURFACE WAVES IN A FLUID ANNULUS WITH A VIBRATING INNER CYLINDER

**Vyacheslav M. Spector<sup>1</sup>**

Institute of  
Hydromechanics NASU  
Kyiv, Ukraine

**Tatyana S. Krasnopol'skaya**

Institute of  
Hydromechanics NASU  
Kyiv, Ukraine

---

ABSTRACT

---

The phenomenon of excitation of fluid free-surface waves between two cylindrical shells when the inner wall vibrates is investigated. To obtain a lucid picture of energy transmission from the wavemaker motion (inner shell vibrations) to the fluid free-surface motion the method of superposition has been used. In order to do this the fluid potential  $\phi$  was presented as the sum of three harmonic functions and all eigenmodes for linear mathematical task were studied in details for any type of an excitation.

---

### INTRODUCTION

The phenomenon of deterioration of fluid free-surface waves between two cylindrical shells when the inner wall vibrates radially, is rather known [1]. The waves may be excited by harmonic axisymmetric deformations of the inner shell and depending on the vibration frequency both axisymmetric and non-symmetric wave patterns may arise. Experimental observations have revealed that waves are excited in two different resonance regimes [2]. The first type of waves corresponds to forced resonance, in which axisymmetric patterns are realized with eigenfrequencies equal to the frequency of excitation. The second kind of waves are parametric resonance waves and in this case the waves are "transverse", with their crests and troughs aligned perpendicular to the vibrating wall. These so-called cross-waves have frequencies equal to half of that of the wavemaker [3].

Garrett [4] has shown how energy is transferred from the wavemaker to the cross-wave in a mathematical model including a mean motion of the free surface. He mentioned, however, that this mean motion of the free surface is not sufficient to supply the energy to the cross-waves. Therefore, the cross-waves must derive their energy in some way directly from the wavemaker. To show direct transmission of energy from the wavemaker the method of superposition has been used and the fluid potential  $\phi$  was presented as the sum of three harmonic functions.

### 1. THEORETICAL ANALYSIS

One considers theoretically the nonlinear problem of fluid free-surface waves which are excited by inner shell vibrations in a volume between two cylinders of finite length. It is useful to relate the fluid motion to the cylindrical coordinate system  $(r, \theta, x)$ . The fluid has an average depth  $d$ ; the average position of the free surface is taken as  $x = 0$ , so that the solid tank bottom is at  $x = -d$ .

The fluid is confined between a solid outer cylinder at  $r = R_2$  and a deformable inner cylinder at average radius  $R_1 = r_1 + a_0(d)^{-1} \int_{-d}^0 \cos(\eta x) dx = r_1 + 2a_0 / \pi$ . This inner cylinder acts as the wavemaker and vibrates harmonically in such a way that the position of the wall of the inner cylinder is  $r = R_1 + \chi_1(x, t) = R_1 - (a_0 + a_1 \cos \omega t) \cos \eta x - 2a_0 / \pi$ , where  $\eta = \pi / (2d)$ . Assuming that the fluid is inviscid and incompressible, and that the induced motion is irrotational, the velocity field can be written as  $\mathbf{v} = \nabla \phi$ , with  $\phi(r, \theta, x, t)$  the velocity potential. The governing equation is

---

<sup>1</sup> Corresponding author. Email [v.m.spektor@gmail.com](mailto:v.m.spektor@gmail.com)

$$\nabla^2\phi = 0 \quad \text{on} \quad (R_1 + \chi_1 \leq r \leq R_2, 0 \leq \theta \leq 2\pi, -d \leq x \leq \zeta) \quad (1)$$

where  $\zeta(r, \theta, t)$  is free surface displacement.

The dynamic and kinematic free-surface boundary conditions are:

$$\phi_t + 1/2(\nabla\phi)^2 + g\zeta = \frac{T}{\rho}[\nabla^2\zeta - \frac{1}{2}\nabla\zeta \cdot ((\nabla\zeta)^2 \nabla\zeta)] + F(t) \quad \text{at} \quad x = \zeta(r, \theta, t) \quad (2)$$

$$\phi_x = \nabla\phi \cdot \nabla\zeta + \zeta_t \quad \text{at} \quad x = \zeta(r, \theta, t) \quad (3)$$

with  $g$  the gravitational acceleration,  $T$  the air-fluid surface tension and  $\rho$  the fluid density,  $F(t)$  is an arbitrary function of time [5]. Here and later the subscripts  $x, r, \theta, t$  signify partial differentiation.

The normal velocity vanishes at the solid flow boundaries:

$$\begin{aligned} \phi_r &= 0 & \text{at} & \quad r = R_2 \\ \phi_x &= 0 & \text{at} & \quad x = -d \end{aligned}$$

while the kinematic condition at the vibrating inner cylinder is:

$$\phi_r = \chi_t + \nabla\phi \cdot \nabla\chi_1 \quad \text{at} \quad r = R_1 + \chi_1(x, t). \quad (4)$$

Effects of the meniscus and capillarity at the contact line of the fluid's free-surface and the annular container walls were not incorporated in the formulation of the problem. We assume, that

$$\zeta_r = 0 \quad \text{at} \quad r = R_1 \quad \text{and} \quad r = R_2$$

From the experimental observations we may conclude that the pattern formation has a resonance character, every pattern having its "own" frequency.

Assuming that patterns can be described in terms of normal modes with characteristic eigenfrequencies, we expand the potential  $\phi$  and the free-surface displacement  $\zeta$  in a complete set of eigenfunctions, which are determined by linear theory. The amplitudes of these eigenfunctions are governed by the nonlinear problem (2) - (3).

The solution of the linear general non-axisymmetric boundary problem

$$\nabla^2\phi = 0 \quad \text{on} \quad (R_1 \leq r \leq R_2, 0 \leq \theta \leq 2\pi, -d \leq x \leq 0), \quad (5)$$

$$\phi_r = \chi_t \quad \text{at} \quad x = 0 \quad (a)$$

$$\phi_x = 0 \quad \text{at} \quad x = -d \quad (b)$$

$$\phi_r = 0 \quad \text{at} \quad r = R_2 \quad (c) \quad (6)$$

$$\phi_r = \chi_t \quad \text{at} \quad r = R_1 \quad (d)$$

$$\phi_\theta \Big|_{\theta=0} = \phi_\theta \Big|_{\theta=2\pi} \quad (e)$$

under arbitrary excitation of the inner cylindrical shell  $w(\theta, x, t)$  can be found in several ways. One is Grinberg's method [6]. Here the potential  $\phi$  is presented as Fourier series of the complete system of eigenfunctions in the radial and azimuthal coordinates with the coefficients as functions of the coordinate  $x$ . The inhomogeneous boundary condition at  $r = R_1$  is transformed into the right-hand side of the equation (5) due to the ordinary procedure of the Fourier series representation for the derivatives on  $r$ . The solutions of the sequence of the inhomogeneous linear differential equations in  $x$  for the expansion coefficients with inhomogeneous boundary conditions in  $x$  can be easily found by any analytical techniques. This approach yields, however, rather cumbersome expressions, in which the input of the wavemaker motion  $w(\theta, x, t)$  is not seen in a clear way. In order to obtain a more lucid picture of the transmission from the wavemaker motion to the free-surface motion it is more convenient to use another analytical method, namely, the method of superposition. The authors

are of the opinion that the application of this method is without doubt preferable for the problem in question. It provides a clear physical picture of the mechanism of energy transfer from the wavemaker to the mean level variation and every eigenmode of free-surface oscillations. The idea of the superposition method was first proposed by Lamé in his classical lectures on the theory of elasticity [7].

According to this superposition method, the potential  $\phi$  can be written as the sum of three harmonic functions:

$$\phi = \phi_0 + \phi_1 + \phi_2. \quad (7)$$

The potential  $\phi_0$  is governed by the following axisymmetric boundary problem:

$$\nabla^2 \phi_0 = 0 \quad \text{on} \quad (R_1 \leq r \leq R_2, 0 \leq \theta \leq 2\pi, -d \leq x \leq 0) \quad (8)$$

$$(\phi_0)_x = (\zeta_0)_t \quad \text{at} \quad x = 0 \quad (a)$$

$$(\phi_0)_x = 0 \quad \text{at} \quad x = -d \quad (b)$$

$$(\phi_0)_r = 0 \quad \text{at} \quad r = R_2 \quad (c) \quad (9)$$

$$(\phi_0)_r = (w_0)_t \quad \text{at} \quad r = R_1 \quad (d)$$

$$(\phi_1)_\theta |_{\theta=0} = (\phi_1)_\theta |_{\theta=2\pi} \quad (e)$$

where

$$\zeta_0(t) = \frac{1}{\pi(R_2^2 - R_1^2)} \int_0^{2\pi} \int_R^{R_2} \zeta(r, \theta, t) r dr d\theta \quad (10)$$

$$w_0(t) = \frac{1}{2\pi R_1 d} \int_0^{2\pi} \int_{-d}^0 w(\theta, x, t) R_1 dx d\theta$$

represents the mean level elevation of the fluid free surface and mean displacement of the cylindrical wavemaker, respectively. These mean values are connected by the relationship

$$(\zeta_0)_t \pi(R_2^2 - R_1^2) - 2\pi d R_1 (w_0)_t = 0 \quad (11)$$

expressing mass conservation for the incompressible fluid. Thus, for the particular case of the wavemaker excitation it is easy to derive from this relationship the mean level oscillation:

$$\zeta_{00}(t) = \frac{4R_1 d}{\pi(R_2^2 - R_1^2)} (a_1 \cos \omega t). \quad (12)$$

The potential  $\phi_1$  is governed by the following linear problem:

$$\nabla^2 \phi_1 = 0 \quad \text{on} \quad (R_1 \leq r \leq R_2, 0 \leq \theta \leq 2\pi, -d \leq x \leq 0) \quad (13)$$

$$(\phi_1)_x = (\zeta - \zeta_0)_t \quad \text{at} \quad x = 0 \quad (a)$$

$$(\phi_1)_x = 0 \quad \text{at} \quad x = -d \quad (b)$$

$$(\phi_1)_r = 0 \quad \text{at} \quad r = R_2 \quad (c) \quad (14)$$

$$(\phi_1)_r = 0 \quad \text{at} \quad r = R_1 \quad (d)$$

$$(\phi_1)_\theta |_{\theta=0} = (\phi_1)_\theta |_{\theta=2\pi} \quad (e)$$

where the conditions in the radial direction are homogeneous and in the azimuthal direction periodic. So  $\phi_1$  will be expressed as a sum of complete systems of eigenfunctions in the radial and azimuthal coordinates.

While the potential  $\phi_2$  is governed by

$$\nabla^2 \phi_2 = 0 \quad \text{on} \quad (R_1 \leq r \leq R_2, 0 \leq \theta \leq 2\pi, -d \leq x \leq 0), \quad (15)$$

$$\begin{aligned} (\phi_2)_x &= 0 & \text{at} \quad x &= 0 & (a) \\ (\phi_2)_x &= 0 & \text{at} \quad x &= -d & (b) \\ (\phi_2)_r &= 0 & \text{at} \quad r &= R_2 & (c) \\ (\phi_2)_r &= (w - w_0)_t & \text{at} \quad r &= R_1 & (d) \\ (\phi_2)_\theta \Big|_{\theta=0} &= (\phi_2)_\theta \Big|_{\theta=2\pi} & & & (e) \end{aligned} \quad (16)$$

it can be represented as a sum of eigenfunctions in the vertical (homogeneous boundary conditions (16a) and (16b)) and in the circumferential (condition of periodicity (16e)) directions. (The potential  $\phi_2$  does not cause any changes in the velocity of the displacement  $\zeta$  at the surface. However, it provides the pressure component which "supports" the free-surface motion, as can be seen from (2). This component has an excitation frequency equal to the frequency of  $w(\theta, x, t)$  in the linear approximation of the problem.)

It is worth noting that the boundary problems (8)-(9), (13)-(14) and (15)-(16) are of the Neumann type when the normal derivative of the harmonic function is prescribed. For the solutions without singularities in the corner points Green's second theorem requires that these prescribed values should satisfy the condition of zero flux across the boundary. Obviously, this property is satisfied for all three boundary problems.

The solution of the boundary problem for  $\phi_0$  can be easily found as

$$\phi_0(r, \theta, t) = -\dot{w}_0(t) \frac{R_1}{R_2^2 - R_1^2} \left( \frac{r^2}{2} - R_2^2 \ln r \right) + \dot{\zeta}_0 \frac{(d+x)^2}{2d} \quad (17)$$

(here the dot means the time derivative), which identically satisfies the Laplacian equation (8) due to the relation (11).

The solution of the linear problem (13)-(14) for  $\phi_1$  can be written in the form

$$\phi_1 = \sum_{i=0}^{\infty} \sum_{j=1}^{\infty} \phi_{ij}^{c,s}(t) \frac{\cosh k_{ij}(x+d)}{N_{ij} \cosh k_{ij}d} \psi_{ij}^{c,s}(r, \theta), \quad (18)$$

on the complete systems of azimuthal ( $\cos i\theta$ ,  $\sin i\theta$ ), and radial eigenfunctions

$$\chi_{ij}(k_{ij}r) = J_i(k_{ij}r) - \frac{J_i(k_{ij}R_1)}{Y_i(k_{ij}R_1)} Y_i(k_{ij}r)$$

with some arbitrary amplitudes  $\phi_{ij}^{c,s}(t)$ .

In the solution (18) the notations

$$\psi_{ij}^{c,s}(r, \theta) = \chi_{ij}(k_{ij}r) (\cos i\theta, \sin i\theta) \quad (19)$$

are used, where  $J_i$  and  $Y_i$  are the  $i$ -th order Bessel functions of the first and the second kind,

respectively, and  $N_{ij}$  is a normalization constant implied from the relation  $N_{ij}^2 = \int_0^{2\pi} \int_{R_1}^{R_2} (\psi_{ij}^{c,s})^2 r dr d\theta$ ,

where the index  $c$  (or  $s$ ) indicates that the eigenfunction  $\cos i\theta$  (or  $\sin i\theta$ ) is chosen as the circumferential component;  $k_{ij}$  represents the roots of the equation

$$J'_i(k_{ij}R_2) - \frac{J'_i(k_{ij}R_1)}{Y'_i(k_{ij}R_1)} Y'_i(k_{ij}R_2) = 0.$$

The system of functions  $\psi_{ij}(r, \theta)$ , with  $i = 0, 1, 2, \dots$  and  $j = 1, 2, 3, \dots$ , is a complete orthogonal system, so any function of the variables  $r$  and  $\theta$  can be represented using the usual procedure of Fourier series expansion.

Thus, the free surface displacement  $\zeta(r, \theta, t) - \zeta_0(t)$  can be written as

$$\zeta(r, \theta, t) - \zeta_0(t) = \sum_{i=0}^{\infty} \sum_{j=1}^{\infty} \zeta_{ij}^{c,s}(t) \frac{\psi_{ij}^{c,s}(r, \theta)}{N_{ij}}. \quad (20)$$

The boundary condition (14a) provides the relation between the amplitudes of the series (18) and (20) in the form:

$$\phi_{ij}^{c,s}(t) = \zeta_{ij}^{c,s}(t) (k_{ij} \tanh k_{ij} d)^{-1} \quad (21)$$

The velocity potential  $\phi_2(r, \theta, x, t)$  can be formulated in terms of an ordinary Fourier series in  $\cos \alpha_l x$  with  $\alpha_l = l\pi/d$  and in  $(\cos i\theta, \sin i\theta)$ , so that the general solution reads

$$\phi_2 = \sum_{i=0}^{\infty} \sum_{l=1}^{\infty} \Phi_{il}^{c,s}(t) \cos \alpha_l x \hat{\chi}_{il}(\alpha_l r) (\cos i\theta, \sin i\theta) \quad (22)$$

with

$$\hat{\chi}_{il}(\alpha_l r) = I_i(\alpha_l r) - \frac{I'_i(\alpha_l R_2)}{K'_i(\alpha_l R_2)} K_i(\alpha_l r)$$

where  $I_i$  and  $K_i$  the  $i$ -th order modified Bessel functions of the first and second kind, respectively.

Using the boundary condition (16d) we can explicitly define the amplitudes  $\Phi_{il}^{c,s}(t)$  as

$$\Phi_{il}^{c,s}(t) = \dot{w}_{il}^{c,s}(t) = \frac{2 - \delta_{i0}}{d\pi\alpha_l \hat{\chi}'_{il}(\alpha_l R_1)} \int_0^{2\pi} \int_{-d}^0 [\dot{w}(\theta, x, t) - \dot{w}_0(t)] \cos \alpha_l x (\cos i\theta, \sin i\theta) R_1 dx d\theta,$$

where  $\delta_{i0}$  is the Dirac function and  $\hat{\chi}'_{il}(z) = d \hat{\chi}_{il}(z) / dz$ .

To define the unknown functions  $\zeta_{ij}^{c,s}(t)$ , representing the amplitudes of directly excited free surface waves, we have to apply the linearized dynamic free-surface boundary condition (2)

$$\phi_t + g\zeta - \frac{T}{\rho} \nabla^2 \zeta = F(t) \text{ at } x = 0, \quad (23)$$

where  $\phi$  represents the total velocity potential according to (7).

Substitution of (7) into (23) leads to the functional equation on  $r$  in the interval  $(R_1, R_2)$ . Representing the radial functions  $r^2/2 - R_2^2 \ln r$  and  $\hat{\chi}_{il}(\alpha_l r)$  in the form of the expansions

$$\begin{aligned} \frac{r^2}{2} - R_2^2 \ln r &= a_{00} + \sum_{j=1}^{\infty} a_{0j} \frac{\chi_{0j}(k_{0j}r)}{N_{0j}} \\ \hat{\chi}_{il}(\alpha_l r) &= b_{i0} + \sum_{j=1}^{\infty} b_{ij} \frac{\chi_{ij}(k_{ij}r)}{N_{ij}}, \end{aligned}$$

where the coefficients  $a_{00}$ ,  $a_{0j}$ ,  $b_{i0l}$  and  $b_{lij}$  can be found by straightforward integration, we can write down the infinite sequence of ordinary differential equations for the functions  $\zeta_{ij}^{c,s}(t)$  :

$$\left\{ \begin{array}{l} \ddot{\zeta}_{0j}(t) + \omega_{0j}^2 \zeta_{0j}(t) = \ddot{w}_0(t) \frac{a_{0j} \beta_{0j} R_1}{(R_2^2 - R_1^2)} - \sum_{l=1}^{\infty} \ddot{w}_{0l}^c(t) b_{0lj} \beta_{0j}, \\ \zeta_{ij}^{c,s}(t) + \omega_{ij}^2 \zeta_{ij}(t) = - \sum_{l=1}^{\infty} \ddot{w}_{il}^{c,s}(t) b_{lij} \beta_{ij}, \end{array} \right. \quad (24)$$

where  $\beta_{ij} = k_{ij} \tanh k_{ij} d$  and  $\omega_{ij} = \left[ (gk_{ij} + \frac{T}{\rho} k_{ij}^3) \tanh k_{ij} d \right]^{1/2}$  for  $i = 0, 1, 2, \dots$  and  $j = 1, 2, 3, \dots$

The linear equations (24) represent typical equations of the forced oscillations with eigenfrequencies  $\omega_{ij}$ . Solving these linear differential equations with specified initial conditions under prescribed time dependence of the functions  $w_0(t)$  and  $w_{il}^{c,s}(t)$ , we can easily obtain the amplitudes

$\zeta_{ij}(t)$  of the fluid free-surface waves in an explicit manner.

## CONCLUSIONS

A simple mathematical model, which shows how the cross-wave can be generated directly by the wavemaker motion without having to take into account the presence of any axisymmetric waves at the free surface. This mathematical model of the excitation of the resonant cross-waves may be the easiest way to understand pattern formation on the fluid's free surface

The nonlinear problems for resonant eigenmodes could be solved in the following way. First, for finding the amplitudes of the potential  $\phi_2$  the nonlinear boundary condition (4) is applied with the expansion procedure in the series with  $\cos \alpha_l x$  and  $(\cos i\theta, \sin i\theta)$  functions. The second step is to determine the relations between the amplitudes of potential  $\phi_1$ , the functions  $\phi_{ij}(t)$  and the amplitudes  $\zeta_{ij}(t)$  of the fluid free-surface waves according to the nonlinear boundary condition (3). And finally, the dynamic condition (2) should be taken in consideration for the closure step, namely, to obtain nonlinear differential equations for resonant amplitudes under the prescribed excitation.

## REFERENCES

- [1] Becker, J.M., Miles, J.W. Standing radial cross-waves *Journal of Fluid Mechanics*, Vol. 222., pp. 471-499, 1991.
- [2] Krasnopolskaya, T.S., van Heijst, F.G.J. Wave pattern formation in a fluid annulus with a vibrating inner shell *Journal of Fluid Mechanics*, Vol. 328, pp. 229-252, 1996.
- [3] Faraday, M. On a peculiar class of acoustical figures; and on certain forms assumed by groups of particles upon vibrating elastic surface, *Philosophical Transactions of Royal Society of London A*, Vol. 121, pp. 299-340, 1831.
- [4] Garrett, C. J. R. Cross waves *Journal of Fluid Mechanics*, Vol. 41, pp. 837-849, 1970.
- [5] Lamb, H. *Hydrodynamics*, Cambridge University Press, Cambridge, 1932.
- [6] Lebedev, N. N., Skal'skaya, I. P., Uflyand, Ya. S. *Problems in Mathematical Physics*. Pergamon, Oxford, 1966.
- [7] Lamé, G. *Leçons sur la Théorie Mathématique de l'Élasticité des Corps Solides* Bachelier, Paris, 1852.

**INFLUENCE OF GAS TURBINE PARAMETERS CHANGES  
TO NONLINEAR VIBRATIONS OF ROTOR-BEARINGS SYSTEM**

**Mikhail J. Temis<sup>1</sup>**  
**Andrey M. Egorov**  
Central Institute of  
Aviation Motors  
Moscow, Russia

---

ABSTRACT

---

This paper presents results of investigation of the gas turbine rotor dynamics using beam rotor model, which includes the nonlinear stiffness and damping characteristics of oil film in journal bearings. Multidisciplinary rotor dynamic model involving shaft model, rotating disks models, support with fluid film bearing model, is developed for realization of present research. Numerical calculations are carried out for modeling the rotor amplitudes (orbits) in bearings at different operating conditions and analyzing of rotor-bearings system sensitivity on modification of its different parameters such as rotor unbalances values, rotor structural damping and oil viscosity in bearings.

---

**INTRODUCTION**

Investigation of gas turbine dynamic behavior should be carried out at different stages of its lifetime (design, assembly, operating and maintenance). At the stage of gas turbine design the engineer is interested in appropriateness of chosen technical solutions. On the other hand during gas turbine operating stage one may interested in analyzing data received from rotor dynamics monitoring system and in this data interpretation. This can be achieved by creating gas turbine rotor dynamics model taking into account gas turbine casing stiffness and damping characteristics, fluid film bearings nonlinear stiffness characteristics and rotor disks inertia characteristics. Gas turbine dynamic parameters determination concerned with rotor dynamics investigation on stationary and transient regimes, eigenvalues and eigenmodes calculation and the presence of sub- and superharmonic vibrations in the system with considerable nonlinearity, determined by fluid film. The solution of this problem is possible with the usage of modern mathematical simulation methods, models and algorithms.

In present paper within the limits of rotor dynamic model creation the gas turbine rotor beam model are created in standard FEM software and used for calculation of natural frequency value of rotor without supports. At second step nonlinear rotor model are created and tested on conformity with standard FEM software model. In further this model are used for direct integration equation of rotor-bearing system motion. The hypothesis of consecutive insertion of elastic and damping elements in unified calculation model is used for developing support model. These elements simulate elastic and damping properties of oil layer, bearing and rotor support case in gas turbine power unit. Oil flow between journal bearing surfaces is described by Reynolds equation with assumptions for parameters of oil flow in bearing taken into account. The system of equations of motion for rotor with bearing is solved by using the Newmark integration scheme, the iterative refinement of stiffness and damping matrices coefficients is performing at each time step.

---

<sup>1</sup> Corresponding author. Email [mikhail.temis@gmail.com](mailto:mikhail.temis@gmail.com)

## 1. FLUID FILM BEARING ROTOR SUPPORT MODEL

In the general case pressure distribution in a fluid film bearing defined from well-known Reynolds equation [1, 2]. Taking into account boundary conditions for the shaft rotating with angular velocity  $\omega$ , the Reynolds' equation presented in a following form:

$$\frac{\partial}{\partial s} \left( h^3 \frac{\partial p}{\partial s} \right) + \frac{\partial}{\partial z} \left( h^3 \frac{\partial p}{\partial z} \right) = 6\eta \left( \omega R \frac{dh}{ds} - 2e\omega \sin(s/R) \right), \quad (1)$$

where  $p(s, z)$  is pressure in fluid film,  $s$  is coordinate axis located on one of the sliding surfaces in the direction of relative motion;  $z$  is located on the sliding surface perpendicular to relative motion,  $h(s, z)$  is the oil film thickness;  $\eta$  is a viscosity,  $R$  is the shaft journal radius. Lateral rotor force  $Q$  acting on the bearing support is in equilibrium with bearing carrying force defined from fluid film pressure.

If the shaft axis is always parallel to the bearing axis the fluid film thickness has the form:

$$h = \delta - e \cdot \cos(s/R) + \delta_b, \quad (2)$$

where  $\delta = R_b - R$  ( $R_b$  is the bearing radius) is a radial gap in the bearing;  $e$  is the shaft journal eccentricity in the bearing,  $\delta_b(s, z)$  is gap form alteration caused by deformations of bearing and shaft journal working surfaces.

In the general case, function  $h$  depends on two coordinates,  $s$  and  $z$ , and pressure distribution. Its calculation is conducted taking into account the bearing and shaft journal reciprocal displacements counting in their motion as a rigid bodies and deformations of working surfaces. After applying the weighted residual method, considering the standard boundary conditions, applying the Finite Element Method technology and approximating the pressure and the weighting function by triangular finite elements from (1) follows the nonlinear system of FEM equations:

$$[K_f]\{p\} = \{Q_f\}, \quad (3)$$

where  $[K_f(h)]$  is a matrix of system which coefficients for bearing with compliant working surfaces are depending from pressure distribution;  $\{Q_f\}$  is the right side vector which components are depending from pressure distribution too. They both are defined by the bearing geometrical characteristics and thickness of lubrication layer.

Obtained system of equations allows find the pressure distribution in the bearing with an arbitrary law of variation of the fluid film thickness. In general  $\delta_b(s, z)$  in (2) may include displacements caused by angular shaft deformations. This enables to evaluate stiffness characteristics of the fluid film, hydrodynamic forces and moments in the bearing versus the current shaft and bearing linear and angular displacements.

The hypothesis of consecutive insertion of elastic elements in unified calculation model is used for developing support model. These elements simulate elastic properties of oil layer, bearing and rotor support case in gas turbine power unit. Thus, support reaction vector,  $\{R_{sup}^u\}$ , acting on rotor, is related with vector of shaft journal displacements  $\{U_j\}$  as follows

$$[K_{sup}]\{U_j\} = \{R_{sup}^u\}, \quad (4)$$

where  $[K_{sup}] = ([K_b]^{-1} + [K_c]^{-1})^{-1}$  is a special finite element stiffness matrix of support included in matrix  $[K_s]$ ;  $[K_b]$  is a stiffness matrix of oil layer;  $[K_c]$  is a support case stiffness matrix.

Coefficients of matrix  $[K_c]$  are determined in calculation of support case structure. Calculation of support case stiffness may be performed using finite element method. Thus the level of detailed elaboration when creating finite-element model depends on structure features. For calculation of support stiffnesses it is necessary to simulate the whole case for gas turbine power units, which cases may be represented as thin-walled structures. In order to define matrix  $[K_b]$  coefficients the problem of oil flow in gap should be solved.

## 2. ROTOR DYNAMIC MODEL

Multidisciplinary rotor dynamic model involving shaft model, rotating disks models, support model is developed for realization of present research. The beam model with distributed masses and with inertia of cross-section rotational displacement in the case of rotor bending deformation taken into consideration is used as shaft model. Disks are considered as mass points that are attached to prescribed shaft cross-sections. Their inertia characteristics include masses and inertia moments. Shaft cross-section centers of inertia offsets and disks center deviation from shaft geometrical axis are described in each shaft cross-section by the vector of initial disbalances  $\{\varepsilon_0\} = \{\varepsilon_{0x}, \varepsilon_{0y}\}$  which components define rotor inertia center coordinates in fixed coordinate system  $xyz$ . Support model is represented by special finite element which coefficients are determined in calculation process by rotor current position and rotative speed. Rotor model in fixed coordinate system constrained to unit supports is described by FEM equations in the following form

$$[M]\{\ddot{U}\} + [C(\omega)]\{\dot{U}\} + ([K_R] + [K_S])\{U\} = \{F_0\} + \omega^2[M_1]\{E_0\}, \quad (5)$$

where  $[M]$  is mass matrix of shaft and parts, attached to it;  $[C]$  is a matrix, that considers an influence of gyroscopic moments and damping in supports and seals;  $[M_1]$  is a part of matrix  $[M]$  connected with nodal linear displacements;  $\{U\}$ ,  $\{\dot{U}\}$  and  $\{\ddot{U}\}$  are the vectors of rotor nodal displacements, velocities and accelerations correspondingly;  $[K_R]$  is rotor stiffness matrix;  $[K_S]$  is the stiffness matrix that considers supports and seals influence;  $\{F_0\}$  is a vector of external forces acting on rotor;  $\{E_0\}$  is initial shaft cross-section disbalances vector, defined by vector  $\{\varepsilon_0\}$ .

Mass  $[M]$  and stiffness  $[K_R]$  matrices do not change in process of motion at established rotor rotative speed. In contrast to them, coefficients of matrices  $[K_S]$  and  $[C]$  depend not only on rotor rotative speed but also on position of curved axis of the shaft in supports. Matrix  $[K_S]$  coefficients are defined by parameters of oil flow in bearings and seals, aerodynamic forces in wheels and by the stiffness of gas turbine power unit case. Gyroscopic moments, actuating fluid flow parameters (gas or air) in sealing devices and friction in fluid film bearings have an influence on damping matrix  $[C]$  coefficients. Thus  $[K_S]$  and  $[C]$  are general form matrices, with coefficients, that nonlinearly depend on current position of the shaft axis, rotative speed and oil parameters.

The system of equations of motion (5) is solved by using the Newmark integration scheme, the iterative refinement of stiffness and damping matrices coefficients is performing at each time step.

## 3. ROTOR MOTION CALCULATION RESULTS

Investigated gas turbine rotor consist of two shafts connected by coupling. Each shaft supported in two radial hydrodynamic journal bearings. Bearing and shaft sliding surfaces are applied cylindrically shaped. Nonlinear gas turbine rotor beam model and model in standard FEM software are created. These beam models are used for further investigations of rotor dynamic behavior and are presented on Fig. 1.

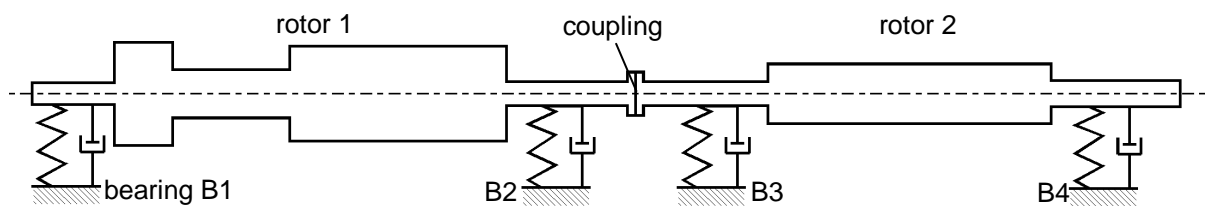


Fig. 1. Gas turbine rotor model

### 3.1 Rotor eigenfrequencies

Rotor model created in standard FEM software testing the nonlinear beam model that used below for direct integration simulation. Nonlinear rotor model verification was carried out for rigid supports and for supports with stiffness 8 MN/mm. Eigenfrequencies verification results presented in Table 1. Frequencies in both models have good conformity between each other. Rotor eigenmodes presented in Fig. 1.

Table 1. Models comparison

№	Eigenfrequencies, Hz			
	Rigid supports		Support stiffness - 8 MN/mm	
	Standard FEM software	Nonlinear beam model	Standard FEM software	Nonlinear beam model
ft1	22,10	22,12	21,68	21,70
ft2	34,35	34,51	32,23	32,35
ft3	56,31	56,77	54,86	55,29
ft4	93,32	94,34	81,81	82,72

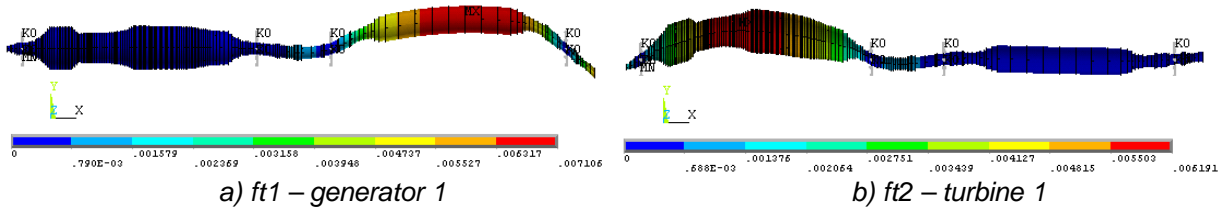


Fig. 2 Rotor eigenmodes

### 3.1 Structural damping sensitivity

The investigation of structural damping influence on rotor dynamic behavior is carried out for a structural damping  $\beta$  of 0.001, 0.002 and 0.02 of structural stiffness matrix. For current parameters calculations were carried out for rotor speeds from 0 and up to 80 Hz with step of 5 Hz. Rotor full spectrums and orbits for structural damping of 0.001, 0.002 and 0.02 presented in Fig. 3.

For  $\beta=0.001$ , in range from 20 Hz to 55 Hz the sufficient rotor vibrations on forward and backward frequencies close to ft2, double ft2 and triple ft2 exist. In contrast with 0.001 case for 0.002 case the sufficient rotor vibrations on forward and backward frequencies close to ft2, double ft2 and triple ft2 exist only in thin range near “rotor 1” first critical speed with amplitudes not exceed maximal allowable limit. For 0.02 case the sufficient rotor vibrations on forward and backward frequencies close to 1X lines exist for speeds in region near “rotor 2” second critical speed (ft3). For all other rotative frequencies not fall within range of sufficient vibrations the rotor vibrates on its rotative speed with very small amplitudes.

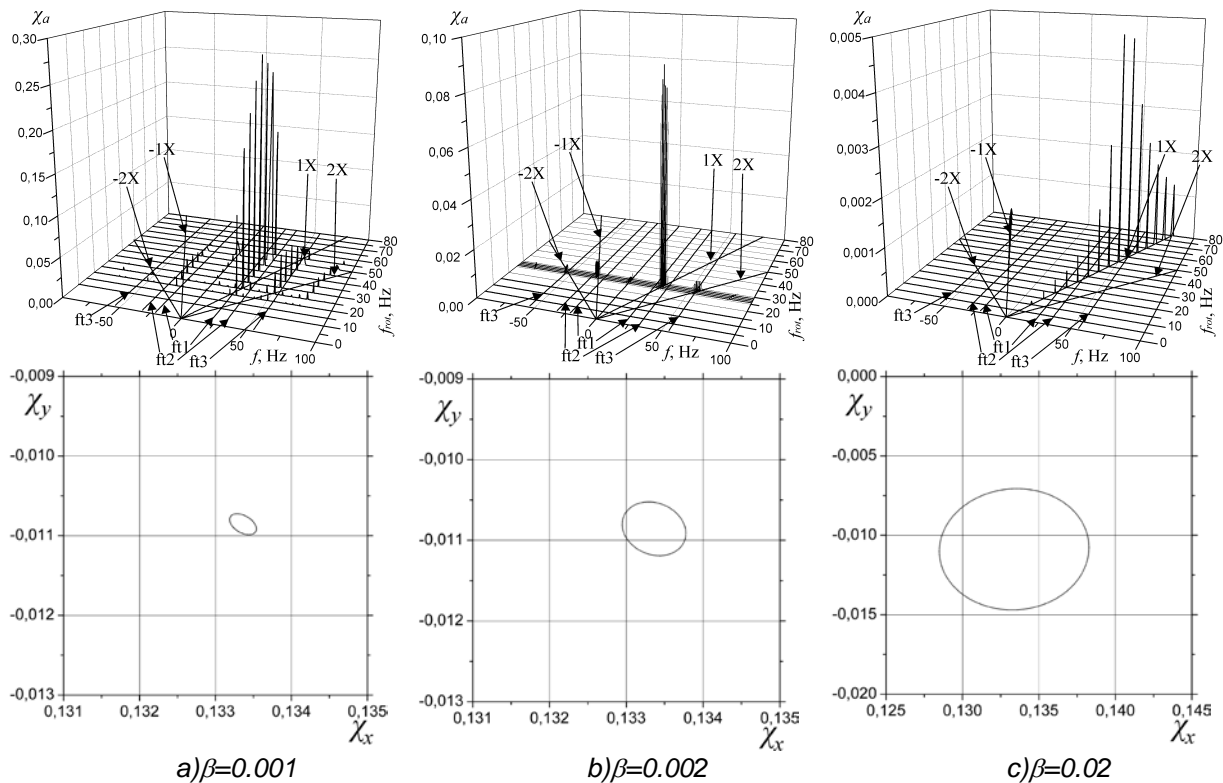


Fig 3. Rotor orbits in bearings(60Hz) and full spectra with different structural damping and lubrication viscosity 0.04 MPa·s

### 3.2 Oil viscosity sensitivity

The investigation of lubrication viscosity influence on rotor dynamic behavior were carried out for lubrication viscosity  $\eta$  of 0.02 MPa·s, 0.04 MPa·s and 0.06 MPa·s. For current parameters calculations were carried out for rotor speeds from 0 and to 80 Hz with step of 5 Hz. Rotor full spectrums and orbits for lubrication viscosity of 0.02 MPa·s, 0.04 MPa·s and 0.06 MPa·s presented in Fig. 4.

As it follows from rotor orbits and its full spectrum analysis for 0.02 MPa·s lubrication viscosity case the sufficient “rotor 1” vibrations on forward and backward frequencies close to  $ft_2$ , double  $ft_2$  and triple  $ft_2$  exist for rotor speeds in region from 30 to 65 Hz. “Rotor 2” have vibrations in this region too but with amplitudes ten times less then similar for turbine. Besides that generator have vibrations on it first critical speed ( $ft_1$ ). As it follows from rotor orbits and its full spectrum analysis for 0.04 MPa·s the sufficient vibrations on forward and backward frequencies close to  $ft_2$  and double  $ft_2$  exist for speeds in region near “rotor 1” first critical speed ( $ft_2$ ). The “rotor 2” vibrations amplitudes ten times less then similar for “rotor 1” for region began from rotor rotation frequency equal to  $ft_2$ . As it follows from rotor orbits and its full spectrum analysis for 0.06 MPa·s lubrication viscosity case its vibrates on forward and backward rotational frequencies ( $\pm 1X$ ) with small amplitudes.

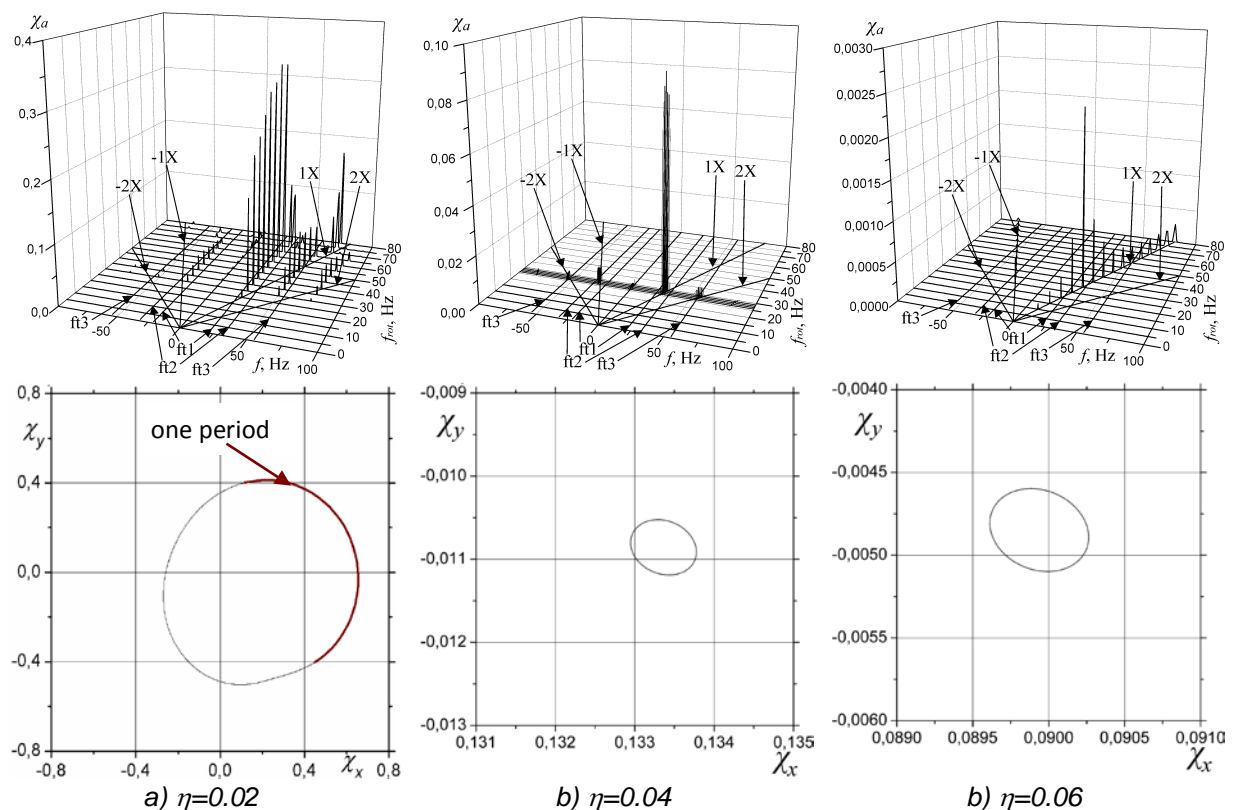


Fig 4. Rotor orbits in bearings (60Hz) and full spectra with different oil viscosity and structural damping 0.002

### 3.3 High unbalance sensitivity

The investigation of rotor orbits in bearings sensitivity were carried out for unbalance values 5 kg, 10 kg and 15 kg on radius of 1 m. For current parameters calculations were carried out for rotor speeds from 0 and up to 80 Hz with step of 5 Hz. Rotor full spectrums and orbits for unbalance values 5 kg, 10 kg and 15 kg on radius of 1 m presented in Fig. 5.

For 5 kg unbalance case the sufficient rotor vibrations on forward and backward frequencies on  $\pm 1X$  and  $\pm 2X$  lines exist in whole considered range with amplitudes of “rotor 1” vibrations amount to approximately 120  $\mu\text{m}$  and “rotor 2” vibrations amount to approximately 30  $\mu\text{m}$ . “Rotor 2” receives just frequency excitation from “rotor 1” without sufficient amplitudes growth. For 10 kg unbalance case the sufficient rotor vibrations on forward and backward frequencies on  $\pm 1X$ ,  $\pm 2X$  and  $\pm 3X$  lines exist in whole considered range with amplitudes of “rotor 1” vibrations amount to approximately 150  $\mu\text{m}$  and “rotor 2” amplitudes less then 30  $\mu\text{m}$ . For 15 kg unbalance case the sufficient rotor vibrations on forward and backward frequencies on  $\pm 1X$ ,  $\pm 2X$  and  $\pm 3X$  lines exist in whole considered range.

Besides that there are sufficient vibrations with frequency 9 Hz. In full spectrum one can see a lot of small amplitudes on different frequencies in investigated range.

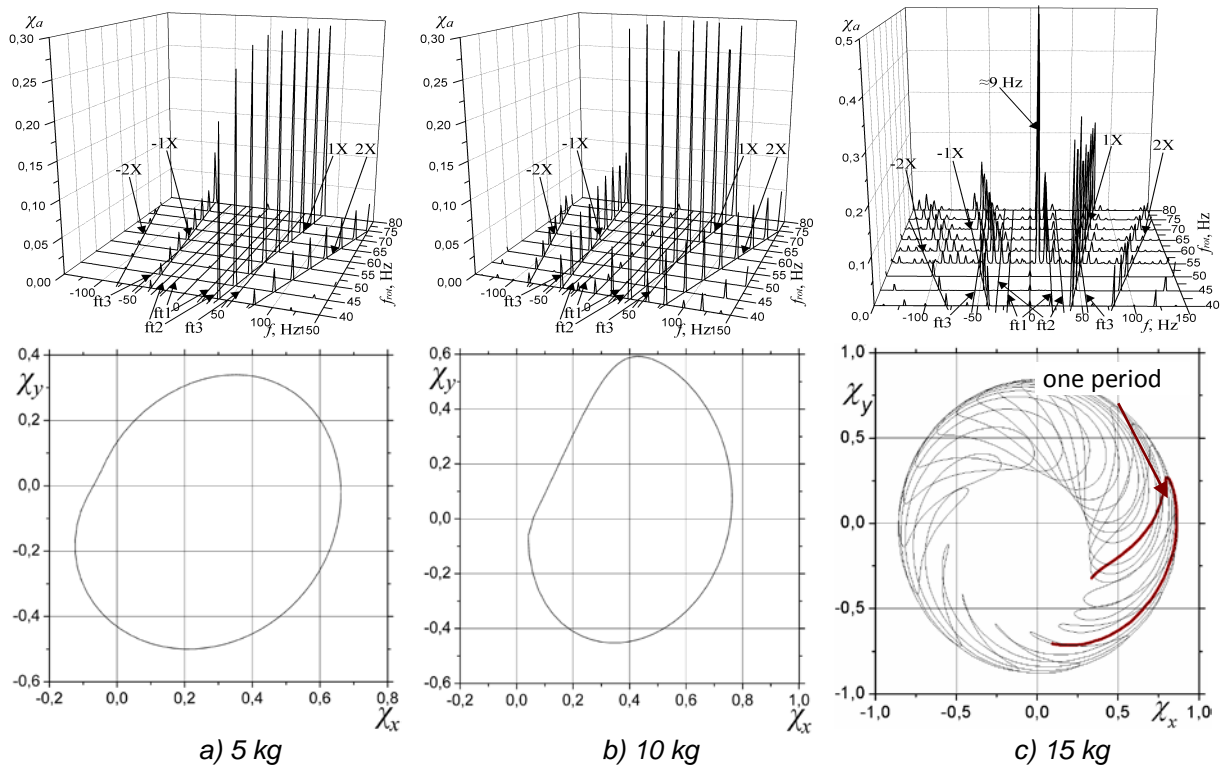


Fig 5. Rotor orbits in bearings(60Hz) and full spectra with different unbalance values

## CONCLUSIONS

The nonlinear rotor dynamics model was developed and verified using corresponding standard FEM software model. Developed model consist of beam shaft model with attached inertia elements and support with fluid film bearing model and allows calculate eigenvalues and eigenmodes, stable and unstable rotor orbits for varying model parameters. On the base of rotor dynamic model the rotor sensitivity to structural damping, oil in bearings viscosity and unbalance value varying were investigated. Influence of these system parameters on rotor orbits and vibration frequencies are shown. Borders between stable and unstable rotor operating regimes depending upon system parameters values are determined.

Presented methodology allows to change rotor system parameters such as damping, oil viscosity and unbalance values at any stage of gas turbine lifetime for decreasing rotor vibration amplitudes and improving rotor stability.

## REFERENCES

- [1] Temis J.M., Temis M.J. Influence of Elastohydrodynamic Contact Deformations in Fluid Film Bearing on High-Speed Rotor Dynamic *Proc.of the 2nd Int. Symp. on Stability Control of Rotating Machinery*, Gdansk, Poland pp. 150-159, 2003.
- [2] Temis J.M., Temis M.J. Contribution of Bearing Structure in Gas Turbine Power Unit Rotor Dynamics *Proc. of the 3rd Int. Symp. on Stability Control of Rotating Machinery*, Cleveland, Ohio, USA pp. 570-581, 2005.

## AEROELASTIC SELF-OSCILLATIONS OF PLANE CHANNEL WALL

**J.M. Temis<sup>1</sup>**  
**A.V. Selivanov**  
Central Institute of  
Aviation Motors  
Moscow, Russia

### ABSTRACT

Plane channel with wall supported by springs and damper is considered to describe seal aeroelastic oscillations. One of the channel walls has two degrees of freedom and other wall is stationary. The investigation method is based on simulation of the non-stationary gas flow in a channel to determine the aerodynamic forces, followed by the analysis of the aeroelastic stability.

Transient gas flow models are developed to obtain aerodynamic loads acting on the channel wall for two seal type (with smooth and finned channel). Corresponding rigidity and damping gas layer parameters obtained from these loads are included into the dynamic model of the seal for self-oscillations analysis.

The effect of structural parameters on the implementation of convergent oscillation and self-oscillation modes is shown; a picture of the aeroelastic stability boundary is given. A paradox of destabilization of the system with the increasing damping is observed for a certain parameter set.

### INTRODUCTION

Turbine engine performance, specific fuel consumption and service life are strongly defined by non-stationary processes, which may take place in seal ducts and channels between rotor and stator. Modern aircraft gas turbine engine have about 50-100 seals. Some of them have a smooth flowing channel (annular seals), other have a finned flowing channel (labyrinth seals).

Gas flow influence on seal/channel elements and rotor dynamic behavior is of particular interest. Possible aeroelastic vibrations, especially self-oscillations of seal walls may cause fatigue failure of seals. As a result, lifetime of structure will be reduced, and operating costs will increase.

The main subject of this paper is the simulating of seal wall aeroelastic oscillations induced by transient gas dynamic loads. Fig. 1 shows overall algorithm of the aeroelastic analysis.

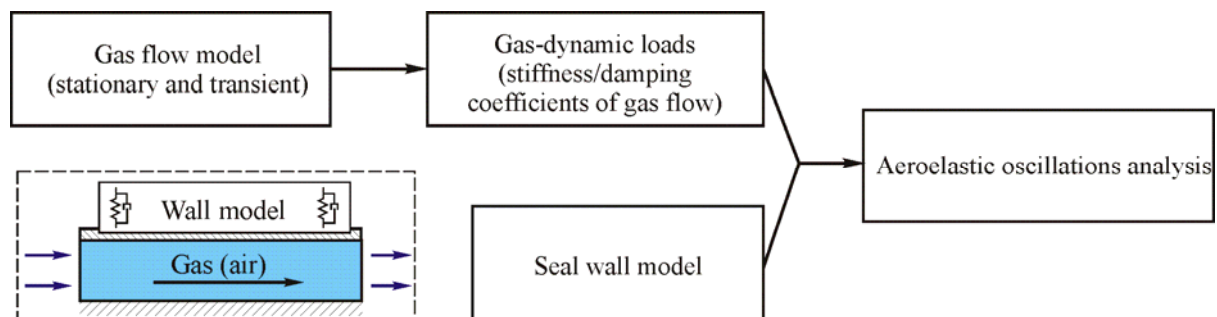


Fig. 1 The aeroelastic analysis algorithm

### AEROELASTIC SELF-OSCILLATIONS SMOOTH WALL

Plane seal models with two degrees of freedom are considered to describe aeroelastic vibrations. Channel height  $\delta$  is considered to be small in comparison with its length  $L$ . Spring dampers

<sup>1</sup>Corresponding author. Email [tejoum@ciam.ru](mailto:tejoum@ciam.ru)

with stiffness ( $k_0, k_1$ ) and damping ( $c_1$ ) coefficients imitate seal structure characteristics. External pressure  $p_e$  is constant. Moving wall is considered to be absolutely rigid.

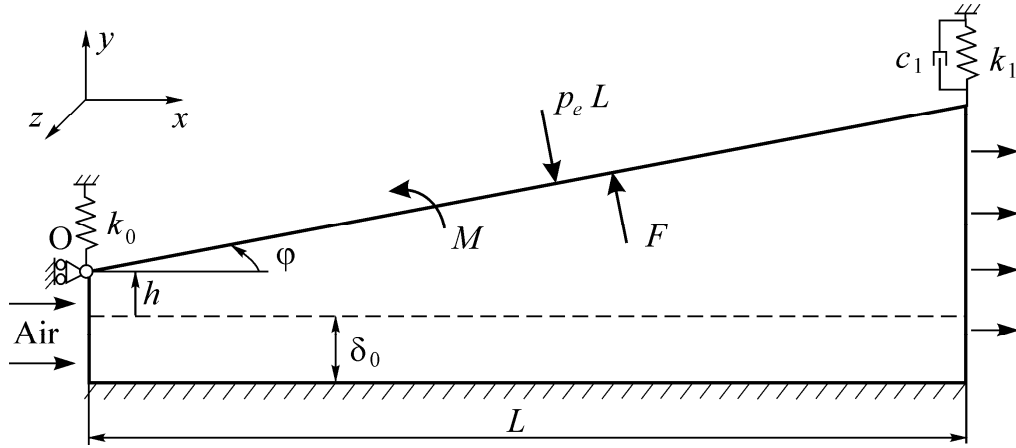


Fig. 2 Plane channel model with smooth walls

If  $\phi$  is sufficiently small, then wall oscillations are described by equations

$$\begin{cases} m\ddot{h} + \frac{mL}{2}\ddot{\phi} + c_1(\dot{h} + \dot{\phi}L) + k_0h + k_1(h + L\phi) = \Delta F \\ \frac{mL}{2}\ddot{h} + \frac{mL^2}{3}\ddot{\phi} + c_1L(\dot{h} + \dot{\phi}L) + k_1L(h + \phi L) = \Delta M \end{cases} \quad (1)$$

Here  $m$  is the wall mass;  $h$  and  $\phi$  are deviations from the static equilibrium position;  $\Delta F$  and  $\Delta M$  are the aeroelastic force and moment deviations from their values at the static equilibrium. These deviations can be represented as

$$\Delta F = \frac{\partial F}{\partial h}h + \frac{\partial F}{\partial \phi}\phi + \frac{\partial F}{\partial \dot{h}}\dot{h} + \frac{\partial F}{\partial \dot{\phi}}\dot{\phi}, \quad \Delta M = \frac{\partial M}{\partial h}h + \frac{\partial M}{\partial \phi}\phi + \frac{\partial M}{\partial \dot{h}}\dot{h} + \frac{\partial M}{\partial \dot{\phi}}\dot{\phi} \quad (2)$$

Derivatives in equations (2) are called stiffness and damping gas seal coefficients. We have

$$F(t) = \int_0^L p(x, t)dx, \quad M(t) = \int_0^L xp(x, t)dx \quad (3)$$

Transient gas flow model is developed to obtain aerodynamic loads (force  $F$  and moment  $M$ ) acting on the seal. Turbulent gas flow is generally described by a system of partial derivatives differential equations. This system consists of continuity equation, momentum equations, and energy equation. It also contains some equations, used to describe the turbulence model.

At the same time, there is a lot of experimental data that allows us to define friction coefficients, depending on Reynolds number. Thus, the problem can be simplified to one-dimensional model that reduces calculation time. For 1D gas flow model, we can write continuity equation (4), momentum equation (5), energy equation (6), and state equation  $p = \rho RT$  [3].

$$\frac{\partial(\rho S)}{\partial t} + \frac{\partial(\rho u S)}{\partial x} = 0 \quad (4)$$

$$\frac{\partial u}{\partial t} + u \frac{\partial u}{\partial x} + \frac{1}{\rho} \frac{\partial p}{\partial x} + \frac{2\tau}{\rho S} = 0 \quad (5)$$

$$\frac{\partial T^*}{\partial t} + u \frac{\partial T^*}{\partial x} - \frac{1}{\rho c_p} \frac{\partial p}{\partial t} = 0 \quad (6)$$

Here  $\rho$  is a gas density,  $u$  is a flow velocity,  $p$  is a pressure, and  $T^*$  is a stagnation temperature. Shear stress  $\tau$  is equal to  $\tau = f \rho u |u|/2$ , where wall friction factor  $f$  for a turbulent flow is equal to  $f = 0.187 \cdot \text{Re}_x^{-0.333}$ .

Deviations for  $\varphi$  and  $h$  are small, so the system can be linearized. One-dimensional modeling of transient gas flow in linear approximation is carried out using finite difference method with implicit scheme. In order to test the results, two-dimensional transient gas flow is analysed. The analysis is carried out using STAR-CD software. The difference between 1D and 2D model results (for aerodynamic force and moment) is less than 1,6%. Therefore it is valid to use one-dimensional linear approximation.

Stiffness and damping gas layer coefficients are included into the dynamic model of the seal for self-excitation vibrations analysis and boundary of aeroelastic stability evaluation.

Let us find the solution of system (1) in the following form

$$\begin{cases} h = H e^{i\omega t} \\ \varphi = \Phi e^{i\omega t} \end{cases} \quad (7)$$

where  $\omega$  is a self-oscillations frequency,  $H$  and  $\Phi$  are complex amplitudes. Combining (1), (2), (7) and writing non-trivial solution existence condition, we can determine parameters of self-excitation oscillations.

Fig. 3 represents safe operating area 1, unstable area 2, and stability threshold 3 (harmonic self-oscillations curve). It must be noted, that for some seal parameters structural linear damping  $c_1$  increase may cause oscillations increase and seal instability. This effect is similar to Mansour's anomaly and can be explained as follows: there is no direct coupling between damping coefficient increase and damping work increase for such systems [1].

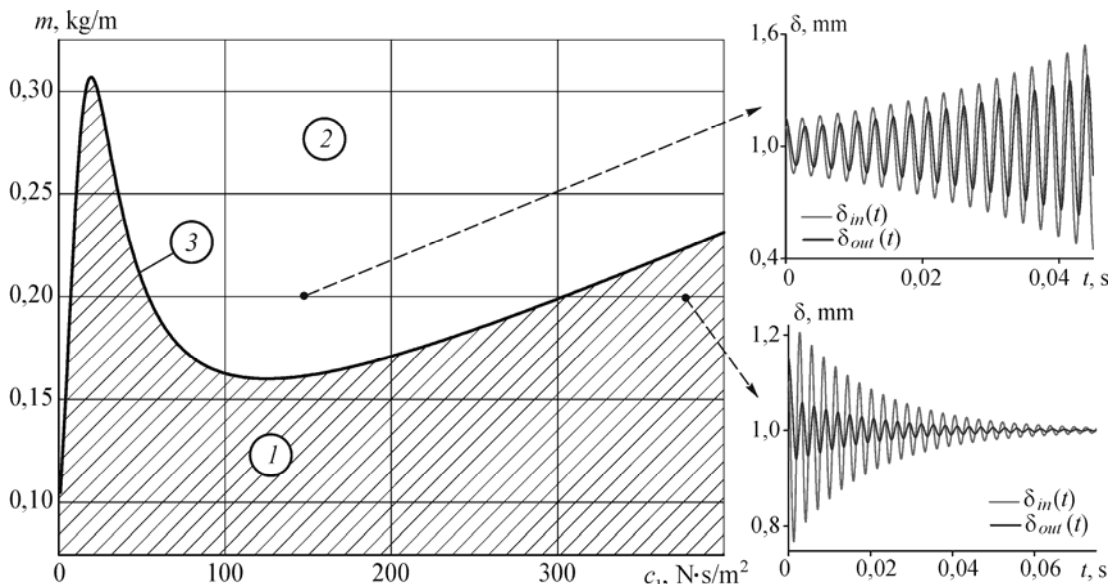
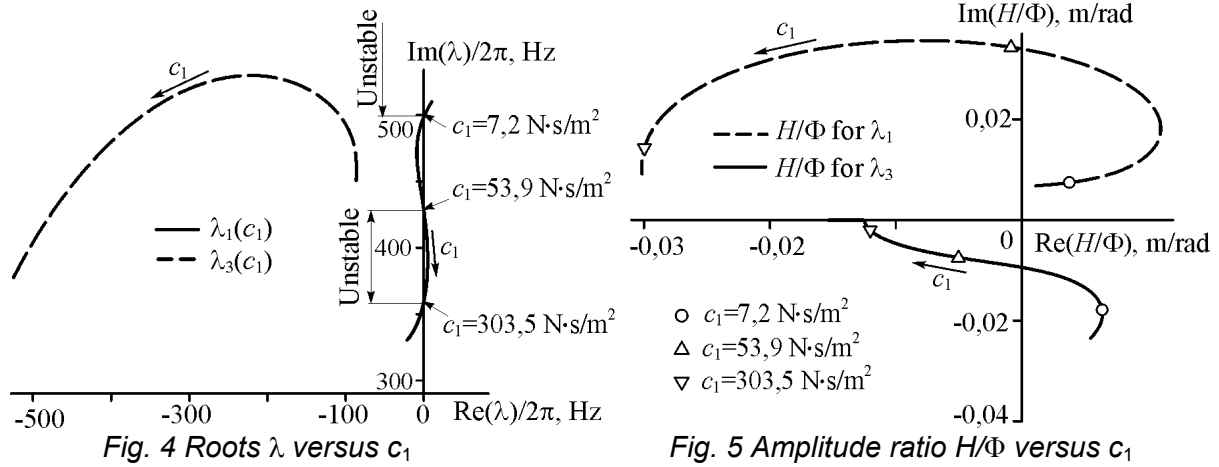


Fig. 3 Smooth seal stability region: 1 – safe operating area; 2 – unstable area; 3 – stability threshold

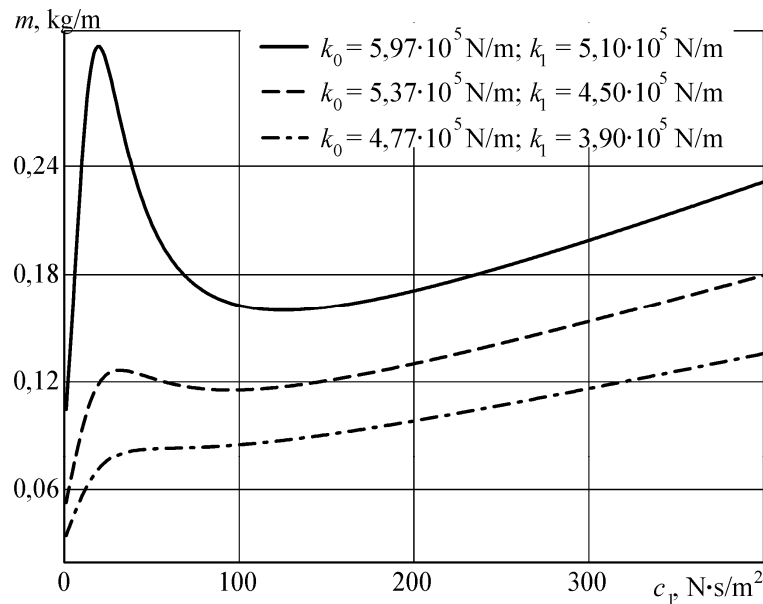
Let us consider the behavior of characteristic equation roots  $\lambda$  with damping coefficient  $c_1$  vary. As a result of characteristic equation numerical solution, two pairs of complex conjugate roots  $(\lambda_1, \lambda_2)$  and  $(\lambda_3, \lambda_4)$  are obtained.

The curves on the complex plane, represented in Fig. 4, show  $\lambda_1$  and  $\lambda_3$  versus  $c_1$  (increasing  $c_1$  is indicated by arrows). For  $\text{Re}(\lambda) < 0$  oscillations decrease exists. The intersection points of curves  $\lambda$  with ordinate axis  $\text{Re}(\lambda) = 0$  correspond to periodic self-oscillations mode and the motion is unstable in area  $\text{Re}(\lambda) > 0$ .

Fig. 5 shows complex amplitude ratio  $H/\Phi$  for  $\lambda_{1,4}$  (self-oscillations points are marked by circles or triangles).



Boundary of stability may qualitatively change, with variation of stiffness  $k_0$ ,  $k_1$ . If  $k_0$ ,  $k_1$  are “small” values, then damping increasing turns the system from oscillations increase to oscillations decrease. Nonlinear effects appear with stiffness increasing (fig. 6).



So self-oscillations may be appearing in similar gas seal structures. For more complete stability analysis and flow condition influence on the seal dynamic behavior see [2, 3].

### AEROELASTIC SELF-OSCILLATIONS FINNED WALL

This method may be applied for the determination of aerodynamic stability for different seal types, for example for labyrinth seal with finned wall (see the Fig. 7).

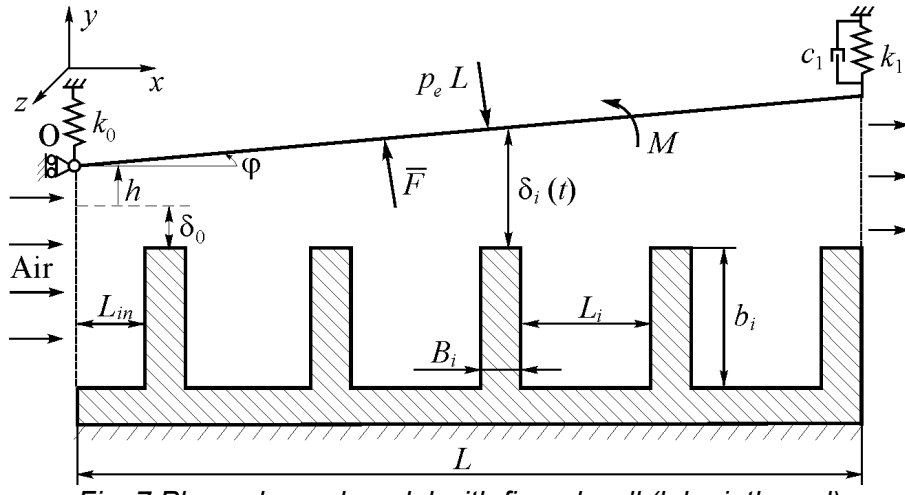


Fig. 7 Plane channel model with finned wall (labyrinth seal)

Gas flow at the labyrinth seal may be described by “one-volume” model [4]

$$\frac{\partial}{\partial t}(p_i S_i) + \mu_0 \mu_{i+1} \delta_{i+1} \sqrt{RT(p_i^2 - p_{i+1}^2)} - \mu_0 \mu_i \delta_i \sqrt{RT(p_{i-1}^2 - p_i^2)} = 0, \quad i = 1..N, \quad (8)$$

where  $N$  is number of chambers between the fins,  $S_i$  is cross-section chamber area,  $\mu_i$  is discharge coefficient

$$\mu_i = \frac{\pi}{\pi + 2 - 5\beta_i + 2\beta_i^2}, \quad \text{where } \beta_i = -1 + \left(\frac{p_{i-1}}{p_i}\right)^{(\gamma-1)/\gamma}.$$

For checking the “one-volume” model results, two-dimensional transient gas flow is analysed. As before the difference between 1D and 2D model results is less than 2%.

Fig. 8 shows stability region for finned channel. The effect of seal destabilization with increase damping coefficient isn't displayed for selected seal parameters.

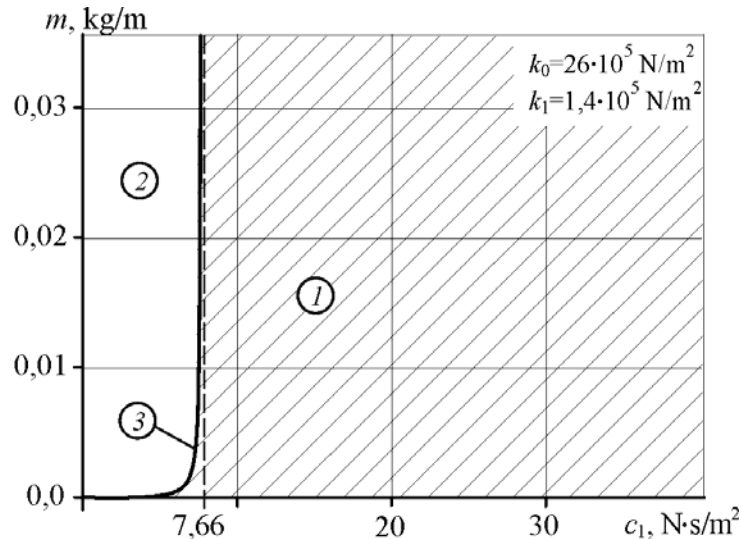


Fig. 8 Finned seal stability region: 1 – safe operating area; 2 – unstable area; 3 – stability threshold

The equations (1) and (8) can be joining to one nonlinear system, where  $\Delta F = \int_0^L p(x,t) dx - F(h_0, \varphi_0)$  and  $\Delta M = \int_0^L p(x,t) x dx - M(h_0, \varphi_0)$ .

Numerical solution of this system for different damping coefficient values is confirm stability threshold (see the Fig. 8). As example, Fig. 9 shows  $h(t)$  and  $\varphi(t)$  behavior for small damping (point from unstable area, Fig. 8).

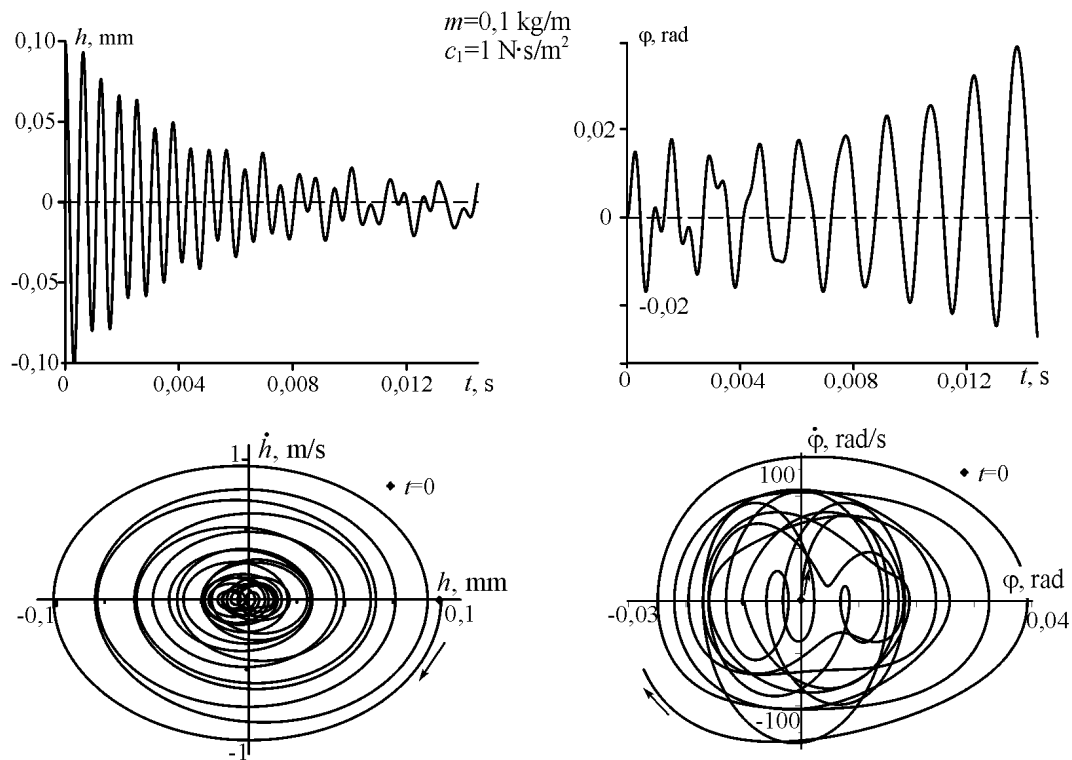


Fig. 9 Wall oscillations for different damping

## REFERENCES

- [1] Mansour W.M. Quenching of Limit Cycles of a Van der Pol Oscillator, *Journal Sound and Vibration*, Vol. 25, No. 3, pp. 395-404, 1972.
- [2] Kadaner J.S., Selivanov A.V., Temis J.M. Performance Analysis of Sealing Devices in Gas Turbine Engines *Proc. of the 3rd International Symposium on Stability Control of Rotating Machinery (ISCORMA-3)*, Cleveland, USA, 19-23 September 2005, pp. 593-604, 2005.
- [3] Temis Yu.M., Kadaner Ya.S., Selivanov A.V. Aeroelastic oscillations in a plane channel *Problems of Strength and Plasticity: High School Collection. Issue 70* Nizhni Novgorod University Press, Nizhni Novgorod. pp. 51-62, 2008 (in Russian).
- [4] Childs D.W. *Turbomachinery Rotordynamics: Phenomena, Modeling, and Analysis*. John Wiley & Sons Inc., USA, 1993, 476 p.

**RESEARCH OF THE NONLINEAR FREE VIBRATION OF THE FULLY CLAMPED COMPOSITE LAMINATED PLATES OF AN ARBITRARY PLANFORM**

**Galina N. Timchenko<sup>1</sup>,**  
**Irina O. Morachkovska,**  
**Nikolay A. Budnikov**  
 National Technical  
 University "KhPI",  
 Kharkov, Ukraine

ABSTRACT

The method of investigation of the geometrically nonlinear free vibrations of the clamped laminated plates with complex form is proposed. Method is based on using R-functions, variational method by Ritz and projection method by Bubnov-Galerkin. Mathematical formulation is fulfilled on base of the first order shear deformation theory of the plates, which is likes to the theory by Timoshenko.

**INTRODUCTION**

Nonlinear vibration problems of the laminated plates are very essential for practice because plates are common structural elements in many engineering structures. In spite of the practical importance of these problems, a survey of publications on nonlinear vibrations of plates shows that the theoretical investigations of these problems are insufficient and remains actual up to now. Due to mathematical complexity of the problem the majority of scientists take into consideration only simply supported plates with the rectangular form of the plane. In the given paper we propose the numerical-analytical approach, which can be applied to plates of the complex form.

**1. PROBLEM STATEMENT**

The mathematical statement of this problem in the framework of the first-order shear deformation theory is based on the hypothesis of a straight line, which was adopted for the whole package. The governing system is nonlinear one of the differential equations with partial derivatives written below [1, 2] in displacements,

$$L_{11}(C_{ij})u + L_{12}(C_{ij})v + Nl_1(C_{ij})w = m_1 \frac{\partial^2 u}{\partial t^2} \quad (1)$$

$$L_{21}(C_{ij})u + L_{22}(C_{ij})v + Nl_2(C_{ij})w = m_1 \frac{\partial^2 v}{\partial t^2} \quad (2)$$

$$L_{33}(C_{ij})w + L_{34}(C_{ij})w_x + L_{35}(C_{ij})w_y + Nl_3 = m_1 \frac{\partial^2 w}{\partial t^2} \quad (3)$$

$$L_{43}(C_{ij})w + L_{44}(C_{ij}, D_{ij})w_x + L_{45}(D_{ij})w_y = m_2 \frac{\partial^2 \psi_x}{\partial t^2} \quad (4)$$

$$L_{53}(C_{ij})w + L_{54}(D_{ij})w_x + L_{55}(C_{ij}, D_{ij})w_y = m_2 \frac{\partial^2 \psi_y}{\partial t^2} \quad (5)$$

The linear differential operators  $L_{ij}$ ,  $i, j = 1, 2, 3$  in the equations (1)-(5) are presented in [5, 6].

Nonlinear operators  $Nl_1, Nl_2, Nl_3$  are defined as follows:

$$Nl_1(C_{ij}) = \frac{\partial}{\partial x} \left\{ \frac{1}{2} \left( C_{11} \left( \frac{\partial}{\partial x} \right)^2 + C_{12} \left( \frac{\partial}{\partial y} \right)^2 \right) + C_{16} \frac{\partial}{\partial x} \frac{\partial}{\partial y} \right\} + \frac{\partial}{\partial y} \left\{ \frac{1}{2} \left( C_{16} \left( \frac{\partial}{\partial x} \right)^2 + \right. \right.$$

<sup>1</sup> Galina N. Timchenko. Email [gntimchenko@mail.ru](mailto:gntimchenko@mail.ru)

$$+ C_{26} \left( \frac{\partial}{\partial y} \right)^2 \Big\} + C_{66} \frac{\partial}{\partial x} \frac{\partial}{\partial y} \Big\} \quad (6)$$

$$Nl_2(C_{ij}) = \frac{\partial}{\partial x} \left\{ \frac{1}{2} \left( C_{16} \left( \frac{\partial}{\partial x} \right)^2 + C_{26} \left( \frac{\partial}{\partial y} \right)^2 \right) + C_{66} \frac{\partial}{\partial x} \frac{\partial}{\partial y} \right\} + \frac{\partial}{\partial y} \left\{ \frac{1}{2} \left( C_{12} \left( \frac{\partial}{\partial x} \right)^2 + \right. \right. \\ \left. \left. + C_{22} \left( \frac{\partial}{\partial y} \right)^2 \right) + C_{26} \frac{\partial}{\partial x} \frac{\partial}{\partial y} \right\} \quad (7)$$

$$Nl_3(C_{ij}) = \frac{\partial^2 w}{\partial x^2} \left\{ C_{11} \left( \frac{\partial u}{\partial x} + \frac{1}{2} \left( \frac{\partial w}{\partial x} \right)^2 \right) + C_{12} \left( \frac{\partial v}{\partial y} + \frac{1}{2} \left( \frac{\partial w}{\partial y} \right)^2 \right) \right\} + C_{16} \left( \frac{\partial u}{\partial y} + \frac{\partial v}{\partial x} + \frac{\partial w}{\partial x} \frac{\partial w}{\partial y} \right) \Big\} + \\ + 2 \frac{\partial^2 w}{\partial x \partial y} \left\{ C_{16} \left( \frac{\partial u}{\partial x} + \frac{1}{2} \left( \frac{\partial w}{\partial x} \right)^2 \right) + C_{26} \left( \frac{\partial v}{\partial y} + \frac{1}{2} \left( \frac{\partial w}{\partial y} \right)^2 \right) + C_{66} \left( \frac{\partial u}{\partial y} + \frac{\partial v}{\partial x} + \frac{\partial w}{\partial x} \frac{\partial w}{\partial y} \right) \right\} + \\ + \frac{\partial^2 w}{\partial y^2} \left\{ C_{12} \left( \frac{\partial u}{\partial x} + \frac{1}{2} \left( \frac{\partial w}{\partial x} \right)^2 \right) + C_{22} \left( \frac{\partial v}{\partial y} + \frac{1}{2} \left( \frac{\partial w}{\partial y} \right)^2 \right) + C_{26} \left( \frac{\partial u}{\partial y} + \frac{\partial v}{\partial x} + \frac{\partial w}{\partial x} \frac{\partial w}{\partial y} \right) \right\}, \quad (8)$$

where  $C_{ij}, D_{ij}$  are rigid characteristics [2], which are defined by the elasticity constants  $B_{jk}^i$  for every  $i$ -th layers.

In a case of the clamped edge the differential equations (1) – (5) are supplemented by the following boundary conditions:

$$u = 0, \quad v = 0, \quad \psi_x = 0, \quad \psi_y = 0, \quad w = 0. \quad (9)$$

The initial conditions are taken as follows:

$$w = w_{\max}, \quad \frac{\partial w}{\partial t} = 0. \quad (10)$$

## 2. METHOD OF SOLUTION

The first step of the proposed method is a solving of the corresponding linear problem of the laminated plates free vibration. In detail the solving algorithm of this problem has been described in [7]. The distinctive feature of the proposed method is application of the R-functions theory and variational methods. Namely, such approach allows find natural frequencies and functions in analytical form for any domain and kind of the boundary conditions, which are very important to solve the non-linear problem. The natural modes corresponding to linear vibrations of the plates have been chosen as basic functions for the representation of unknown functions.

On the next step the unknown functions  $w, \psi_x, \psi_y$  are presented in the form

$$w(x, y, t) = y_1(t) \cdot w_1(x, y), \quad \psi_x(x, y, t) = y_1(t) \cdot \psi_{x1}(x, y), \quad \psi_y(x, y, t) = y_1(t) \cdot \psi_{y1}(x, y) \quad (12)$$

here  $w_1(x, y), \psi_{x1}(x, y), \psi_{y1}(x, y)$  are the components of the eigenfunctions vector. It's obviously that equations (4) and (5) will be satisfied. In order to satisfy the equation (1) and (2) let us present the unknown functions  $u$  and  $v$  in the following form:

$$u(x, y, t) = y_1^2(t) \cdot u_2(x, y) \\ v(x, y, t) = y_1^2(t) \cdot v_2(x, y), \quad (13)$$

where  $(u_2, v_2)$  is solution of the following system of the equations

$$L_{11}(C_{ij})u_2 + L_{12}(C_{ij})v_2 = -Nl_1(C_{ij})w_1 \\ L_{21}(C_{ij})u_2 + L_{22}(C_{ij})v_2 = -Nl_2(C_{ij})w_1 \quad (14)$$

The last system coincides with the similar system for 2-dimensional elasticity problems for which the right parts play the role of mass forces. The boundary conditions are the same with (9). The RFM is applied to find these functions [3, 4]. We will ignore the inertia terms in equation (1) and (2) then it's easy to check that they be satisfied after substitution of the expressions (13).

Substituting the expressions (12), (13) for  $u(x, y, t), v(x, y, t), w(x, y, t), \psi_x(x, y, t), \psi_y(x, y, t)$  in movement equation (3) and applying the method by Bubnov-Galerkin one obtains the nonlinear ordinary differential equation in unknown functions  $y_1(t)$ :

$$y_1''(t) + \omega_L^2 y_1(t) + \beta \cdot y_1^3(t) = 0 \quad (15)$$

where coefficient  $\beta$  is defined as

$$\beta = -\frac{\int_{\Omega} (Nl_{32}(C_{ij}, u_2, v_2, w_1)) \cdot w_1 d\Omega}{\rho h \|w_1\|^2},$$

$$Nl_{32}(C_{ij}) = \frac{\partial^2 w_1}{\partial x^2} \left\{ C_{11} \frac{\partial u_2}{\partial x} + C_{12} \frac{\partial v_2}{\partial y} + \frac{1}{2} \left( C_{11} \left( \frac{\partial w_1}{\partial x} \right)^2 + C_{12} \left( \frac{\partial w_1}{\partial y} \right)^2 \right) + \right.$$

$$+ C_{16} \left( \frac{\partial u_2}{\partial y} + \frac{\partial v_2}{\partial x} + \frac{\partial w_1}{\partial x} \frac{\partial w_1}{\partial y} \right) \left. \right\} + 2 \frac{\partial^2 w_1}{\partial x \partial y} \left\{ C_{66} \left( \frac{\partial u_2}{\partial x} + \frac{\partial v_2}{\partial y} + \frac{\partial w_1}{\partial x} \frac{\partial w_1}{\partial y} \right) + \right.$$

$$+ C_{16} \left( \frac{\partial u_2}{\partial x} + \frac{1}{2} \left( \frac{\partial w_1}{\partial x} \right)^2 \right) + C_{26} \left( \frac{\partial v_2}{\partial x} + \frac{1}{2} \left( \frac{\partial w_1}{\partial y} \right)^2 \right) \left. \right\} + \frac{\partial^2 w_1}{\partial y^2} \left\{ C_{12} \left( \frac{\partial u_2}{\partial x} + \frac{1}{2} \left( \frac{\partial w_1}{\partial x} \right)^2 \right) + \right.$$

$$\left. + C_{22} \left( \frac{\partial v_2}{\partial x} + \frac{1}{2} \left( \frac{\partial w_1}{\partial y} \right)^2 \right) + C_{26} \left( \frac{\partial u_2}{\partial y} + \frac{\partial v_2}{\partial x} + \frac{\partial w_1}{\partial x} \frac{\partial w_1}{\partial y} \right) \right\}$$

Let us present the unknown function in the form:  $y(t) = A \cos \omega_N t$ . Then after application of the method by Bubnov-Galerkin to the equation (15) it is possible to get the explicit dependence  $\nu = \frac{\omega_N}{\omega_L}$ , of the ratio of the nonlinear frequency to linear one on the vibration amplitude  $A$  [1]

$$\frac{\omega_N}{\omega_L} = \sqrt{1 + \frac{3}{4} \beta \cdot A^2} \quad (16)$$

As we noted the finding of functions  $(u_2, v_2)$  is connected with solving the system (14). Obviously the system is supplemented by corresponding boundary conditions. Taking into account that we consider fully clamped plate, it is possible to prove, that this problem may be reduced to the finding point of stationary of the following functional

$$I(\bar{U}_2) = \int_{\Omega} \left\{ C_{11} \left( \frac{\partial u_2}{\partial x} \right)^2 + C_{22} \left( \frac{\partial v_2}{\partial y} \right)^2 + 2C_{12} \frac{\partial u_2}{\partial x} \frac{\partial v_2}{\partial y} + C_{66} \left( \frac{\partial u_2}{\partial y} + \frac{\partial v_2}{\partial x} \right)^2 + 2 \left( C_{16} \frac{\partial u_2}{\partial x} + \right. \right.$$

$$\left. + C_{26} \frac{\partial v_2}{\partial y} \right) \left( \frac{\partial v_2}{\partial x} + \frac{\partial u_2}{\partial y} \right) + (Nl_1(C_{ij}) w_1) u_2 + (Nl_2(C_{ij}) w_1) v_2 \left. \right\} d\Omega \quad (17)$$

where  $U_{2n} = u_2 l + v_2 m, V_{2n} = -u_2 m + v_2 l$ .

The discretization of functional (11) and (17) is fulfilled by RFM and Ritz method.

The proposed method is numerically realized in the framework of software "POLE-RL" and widely tested on many nonlinear vibration problems for plates at large amplitudes. The proposed method can be applied not only for composite plates with identical elasticity constants of layers but also for the plates of "sandwich" type.

### 3. NUMERICAL RESULTS

Let us consider the geometrically nonlinear free vibration of the laminated plates (Fig. 1) with geometric sizes:  $l = 0.75M$ ,  $a = 0.4M$ ,  $h_i = 8 \cdot 10^{-5}M$ .

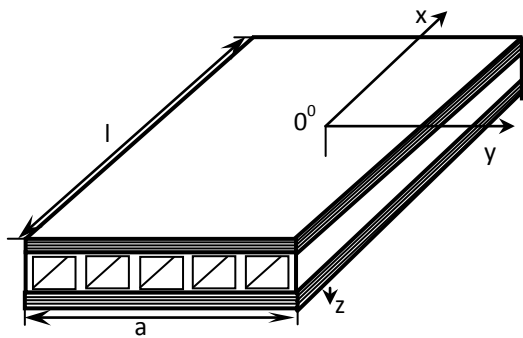


Fig. 1. The laminated plates

The shell is carried from the material with the physical characteristics:

Face layers

$$E_1 = 1.35 \cdot 10^5 \text{ MPa}, E_2 = 8 \cdot 10^3 \text{ MPa}, G_{12} = 6 \cdot 10^3 \text{ MPa}, \\ \nu_{12} = 0.286,$$

Core

$$E_1 = 0.7264 \cdot 10^5 \text{ MPa}, E_2 = 1.4528 \cdot 10^5 \text{ MPa}, \\ G_{12} = G_{23} = 1.1622 \cdot 10^5 \text{ MPa}, G_{13} = 0.5811 \cdot 10^4 \text{ MPa}, \\ \nu_{12} = 0,2552.$$

The obtained backbone curves for different lamina scheme of the layers are presented in Fig.2. Here the backbone curve  $L_1$  corresponds to lamina scheme of the layers  $[0^0/90^0]_2 \text{ core } [90^0/0^0]_2$ . Curve  $L_2$  is backbone for  $[\pm 80^0]_2 \text{ core } [\mp 80^0]_2$ , curve  $L_3$  is backbone for  $[\pm 60^0]_2 \text{ core } [\mp 60^0]_2$ , curve  $L_4$  is backbone for  $[\pm 30^0]_2 \text{ core } [\mp 30^0]_2$ . From the presented results it follows that the curve  $L_1$  is more rigid. The obtained results can be used at designing of similar elements under the transverse load.

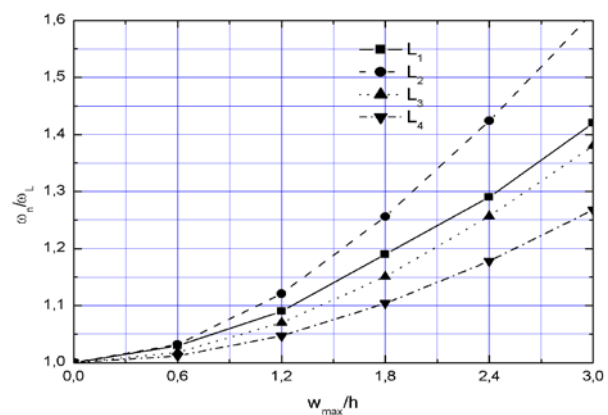


Fig. 2. Backbone curves of plate for different values of packing layers

### CONCLUSION

In this work, the method of investigation of nonlinear free vibrations of the symmetrically laminated clamped plates with an arbitrary plane form is proposed. This approach is based on R-functions theory, variational methods, and the Runge-Kutta method. The software "POLE-RL" is applied to obtain the numerical results. The investigation is carried out for the "sandwich" plate. The investigation is carried out for the "sandwich" plates. The ratio of the nonlinear frequency to linear one depending on amplitudes of vibration ( $w_{\max}/h$ ) of laminated plates pack with various face layers are received.

### REFERENCES

- [1] Vol'mir A.S. *Nonlinear Dynamics of Plates and Shells*, Nauka, Moscow, 1972 (in Russian).
- [2] Ambartsumyan S.A. *General Theory of Anisotropic Shells*, Nauka, Moscow, 1974 (in Russian).
- [3] Rvachev V.L. *The R-Functions theory and its Some Application*, Naukova Dumka, Kiev, 1982 (in Russian).
- [4] Rvachev V.L., Kurpa L.V. *The R-Functions in Problems of Plates Theory*, Naukova Dumka, Kiev, 1987 (in Russian).
- [5] L.V. Kurpa, G.N Timchenko, Investigation into nonlinear vibrations of composite plates using the R-function theory, *Strength of Materials* 39 (5), pp. 529-538, 2007.
- [6] Kurpa L.V., Timchenko G.N. Investigation geometrically nonlinear vibrations composite plates with complex form, *Dynamics and Strength of Machines* 21, pp.113 – 118, 2006 (in Russian).
- [7] Kurpa L.V., Timchenko G.N. Investigations of vibrations of laminated plates of an arbitrary form, In: *Proc. of the 8 th SSTA Conference, Jurata, Poland*, pp. 371-375, 2005.

## THE TRAJECTORIES OF SELF-REINFORCING SOLITARY WAVE IN THE GAS DISC OF GALAXIES

**Yuriy Turbal**<sup>1</sup>  
 International University of  
 Economics and  
 Humanities named after  
 academician Stepan  
 Demianchuk,  
 Rivne, Ukraine

---

### ABSTRACT

---

In this paper we consider solutions of gas dynamics equations for the galaxies in the form of solitary wave. The aim of this paper is to research the trajectories of such waves for the different cases of surface density.

---

### INTRODUCTION

Problems, related to the study of solitons and their interactions lately are of interest in many areas of fundamental and applied scientific researches. Solitons are intensively studied in hydrodynamics, fiber optics, in magnets. Solitons may occur in proteins and DNA .

Note, that the study of various processes in the disks of galaxies using hydrodynamic models are carried out by A.M. Friedman [1]. In the Research Center "Kurchatov Institute" the processes in galaxies were studied under his leadership, in particular, hydrodynamic instability in the mechanisms of spiral density waves generation .

In this paper we consider structurally stable solitary waves in a medium, which is a gas component of galaxies. The assumption of the existence of such waves follows from the equivalence of shallow water equations and equations of gas dynamics of galaxies ( see the [1]). But the existence of solitons in shallow water is a well known and experimentally verified fact. Note that in 2008, astronomers have recorded a soliton in space (the message of the European Space Agency ESA).

Solitons considered in this work are structurally stable density perturbation, localized in some small areas. Similar solitons considered in [3] as a weak asymptotic solution of equations of shallow water. In this paper such solitary waves are considered in the gas disk of galaxies. We study the trajectory of solitons.

### 1. SOLUTIONS OF GAS DYNAMICS EQUATIONS IN THE FORM OF SOLITARY WAVES

We consider the equation of gas dynamics of galaxies [2], written in polar coordinates for the case of the isentropic model and polytropic law ( $p = B\sigma^{\gamma_s}$ ) of the surface pressure and surface density:

$$\frac{\partial \sigma}{\partial t} + \sigma \left( \frac{\partial u}{\partial r} + \frac{u}{r} + \frac{\partial v}{r \partial \varphi} \right) + u \frac{\partial \sigma}{\partial r} + \frac{v \partial \sigma}{r \partial \varphi} = 0, \quad (1)$$

$$\frac{\partial u}{\partial t} + u \frac{\partial u}{\partial r} + \frac{v}{r} \frac{\partial u}{\partial \varphi} - \frac{v^2}{r} = -\frac{\partial \Phi}{\partial r} - B \gamma_s \sigma^{\gamma_s - 2} \frac{\partial \sigma}{\partial r}, \quad (2)$$

$$\frac{\partial v}{\partial t} + u \frac{\partial v}{\partial r} + \frac{v}{r} \frac{\partial v}{\partial \varphi} + \frac{uv}{r} = -\frac{1}{r} \frac{\partial \Phi}{\partial \varphi} - \sigma^{\gamma_s - 2} \frac{B \gamma_s}{r} \frac{\partial \sigma}{\partial \varphi}, \quad (3)$$

---

<sup>1</sup> Corresponding author. Email [turbaly@gmail.com](mailto:turbaly@gmail.com)

where  $u(r, \varphi, t), v(r, \varphi, t)$  are the radial and azimuthal velocity components of gas, respectively,  $\sigma(r, \varphi, t)$  is the surface density of the gas disk,  $\Phi(r, \varphi, t)$  - is the gravitational potential,  $B$  is a positive constant. Note that the system (1) - (3) is quasi-linear.

Let  $u_0(r) \equiv 0, v_0(r), \sigma_0(r), \Phi_0(r)$  are the equilibrium components of velocity, density and gravitational potential, respectively. We seek a particular solution of (1) - (3) (same as in [2]) as the sum of the equilibrium values, and some disturbances:  $\sigma(r, \varphi, t) = \sigma_0(r) + \sigma_1(r, \varphi, t), \Phi(r, \varphi, t) = \Phi_0(r) + \Phi_1(r, \varphi, t), u(r, \varphi, t) = u_1(r, \varphi, t), v(r, \varphi, t) = v_0(r) + v_1(r, \varphi, t)$ .

The area in which we consider a system (1) - (3) has the form:  $G = \{(r, \varphi) : r_0 \leq r \leq R\}$ . From (1)-(3) we get the system:

$$\begin{cases} \frac{\partial \sigma_1}{\partial t} + \frac{v_0}{r} \frac{\partial \sigma_1}{\partial \varphi} + \sigma_0 \left( \frac{\partial u_1}{\partial r} + \frac{u_1}{r} + \frac{\partial v_1}{r \partial \varphi} \right) + u_1 \frac{\partial \sigma_0}{\partial r} + \frac{1}{r} (\sigma_1 u_1 + u_1 r \frac{\partial \sigma_1}{\partial r} + \sigma_1 r \frac{\partial u_1}{\partial r} + \sigma_1 \frac{\partial v_1}{\partial \varphi} + v_1 \frac{\partial \sigma_1}{\partial \varphi}) = 0, \\ \frac{\partial u_1}{\partial t} + \frac{v_0}{r} \frac{\partial u_1}{\partial \varphi} - \frac{2v_0 v_1}{r} = - \frac{\partial \Phi_1}{\partial r} - B \gamma_s (\gamma_s - 2) \sigma_1 \sigma_0^{\gamma_s - 3} \frac{\partial \sigma_0}{\partial r} - B \gamma_s \sigma_0^{\gamma_s - 2} \frac{\partial \sigma_1}{\partial r} - \\ - B \gamma_s (\gamma_s - 2) \sigma_1 \sigma_0^{\gamma_s - 3} \frac{\partial \sigma_1}{\partial r} + \frac{v_1^2}{r} - u_1 \frac{\partial u_1}{\partial r} - \frac{v_1}{r} \frac{\partial u_1}{\partial \varphi}, \\ \frac{\partial v_1}{\partial t} + u_1 \frac{\partial v_0}{\partial r} + \frac{v_0}{r} \frac{\partial v_1}{\partial \varphi} + \frac{u_1 v_0}{r} = - \frac{1}{r} \frac{\partial \Phi_1}{\partial \varphi} - \frac{B \gamma_s}{r} \sigma_0^{\gamma_s - 2} \frac{\partial \sigma_1}{\partial \varphi} - \frac{B \gamma_s}{r} (\gamma_s - 2) \sigma_0^{\gamma_s - 3} \sigma_1 \frac{\partial \sigma_1}{\partial \varphi} - \\ - u_1 \frac{\partial v_1}{\partial r} - \frac{v_1}{r} \frac{\partial v_1}{\partial \varphi} - \frac{u_1 v_1}{r}. \end{cases} \quad (5)$$

For convenience, we introduce the vector-function perturbations

$f_1(r, \varphi, t) = (u_1(r, \varphi, t), v_1(r, \varphi, t), \sigma_1(r, \varphi, t))$ , that will be sought in the form:

$$f_1(r, \varphi, t) = \varepsilon_0 \psi_f(t) \omega(r, \varphi, t, \varepsilon). \quad (6)$$

where  $\psi_f(t) = (\psi_u(t), \psi_v(t), \psi_\sigma(t))$ ,  $\psi_u(t), \psi_v(t), \psi_\sigma(t), \tilde{r}(t), \tilde{\varphi}(t)$  are some functions,  $\tilde{r}(t) \geq 0, \psi_\sigma(t) \geq 0, \varepsilon$  is a small parameter,  $\varepsilon_0$  is some constant,

$$\omega(r, \varphi, t, \varepsilon) = \exp\left\{-\frac{g(r - \tilde{r}(t)) + g(\varphi - \tilde{\varphi}(t))}{\varepsilon}\right\}, \quad (7)$$

$g(x)$  is a nonnegative pair function, which has the properties:

1.  $g(x) \geq 0, x \in (-\infty, +\infty)$
2.  $g(0) = 0$
3.  $g(-x) = g(x)$
4. There are constants,  $\alpha_1, \tilde{\alpha}_1, \alpha_2, \tilde{\alpha}_2, c_1 > 0, c_2 > 0, 0 < \alpha_1, \tilde{\alpha}_1 < 1, 0 < \alpha_2, \tilde{\alpha}_2 < 1, \varepsilon > 0$  such that  $\tilde{c}_1 g^{\tilde{\alpha}_1}(x) \leq |g'(x)| \leq c_1 g^{\alpha_1}(x), |g''(x)| \leq c_2 g^{\alpha_2}(x)$  in the field  $\{x : g(x) \leq -\varepsilon \ln \varepsilon\}$ .

It is obvious, that such function exists (for example,  $g(x) = x^4$ ). It is evident from relation (7) that the perturbation is a solitary wave. The point of maximum of the wave moves along the trajectory, which is described in polar coordinates by the functions  $\tilde{r}(t)$  and  $\tilde{\varphi}(t)$ .

Differentiating (7), we obtain:

$$\begin{aligned} \frac{\partial f_1}{\partial r} &= -\varepsilon_0 \frac{g'(r - \tilde{r}(t))}{\varepsilon} \psi_f(t) \omega(r, \varphi, t, \varepsilon), \quad \frac{\partial f_1}{\partial \varphi} = -\varepsilon_0 \frac{g'(\varphi - \tilde{\varphi}(t))}{\varepsilon} \psi_f(t) \omega(r, \varphi, t, \varepsilon), \\ \frac{\partial f_1}{\partial t} &= \varepsilon_0 \psi_f'(t) \omega(r, \varphi, t, \varepsilon) + \frac{1}{\varepsilon} \varepsilon_0 \psi_f(t) \omega(r, \varphi, t, \varepsilon) [\tilde{\varphi}'(t) g'(\varphi - \tilde{\varphi}(t)) + \tilde{r}'(t) g'(r - \tilde{r}(t))]. \end{aligned} \quad (8)$$

The remaining arguments consist of the substitution of relations (7) - (8) into (5) and the allocation of appropriate conditions.

From the first equation (5) we obtain the following system:

$$\begin{cases} \psi_\sigma'(t) + \sigma_0 \frac{\psi_u(t)}{r} + \psi_u(t) \frac{\partial \sigma_0}{\partial r} + \frac{\psi_v(t)}{r} \frac{\partial \sigma_0}{\partial \varphi} + \frac{1}{r} \varepsilon_0 \psi_\sigma(t) \psi_u(t) \omega(r, \varphi, t, \varepsilon) = 0 \\ \tilde{\varphi}'(t) - \frac{v_0}{r} - \psi_v(t) \frac{\sigma_0}{r \psi_\sigma(t)} - \frac{2\varepsilon_0}{r} \psi_v(t) \omega(r, \varphi, t, \varepsilon) = 0 \\ \tilde{r}'(t) - \sigma_0 \psi_u(t) / \psi_\sigma(t) - 2\varepsilon_0 \psi_u(t) \omega(r, \varphi, t, \varepsilon) = 0 \end{cases} \quad (9)$$

The second and third of equations (5) can be written as:

$$\begin{aligned} \frac{\partial \Phi_1}{\partial r} = & -\varepsilon_0 \omega(r, \varphi, t, \varepsilon) (\psi_u'(t) - \frac{2v_0 \psi_v(t)}{r} - \frac{3}{2r} B D \gamma_s - 1) \sigma_0^{\gamma_s - 2} \psi_\sigma(t) + \\ & + \frac{\varepsilon_0 \psi_v^2(t) \omega(r, \varphi, t, \varepsilon)}{r} + B \gamma_s (\gamma_s - 2) \psi_\sigma(t) \sigma_0^{\gamma_s - 3} \frac{\partial \sigma_0}{\partial r} - \end{aligned} \quad (10)$$

$$\begin{aligned} & - \psi_u(t) \frac{g'(r - \tilde{r}(t))}{\varepsilon} \varepsilon_0 \omega(r, \varphi, t, \varepsilon) (\tilde{r}'(t) - B \gamma_s \sigma_0^{\gamma_s - 2} \psi_\sigma(t) / \psi_u(t) - B \gamma_s (\gamma_s - 2) \sigma_0^{\gamma_s - 3} \varepsilon_0 \psi_\sigma^2(t) / \psi_u(t) \omega(r, \varphi, t, \varepsilon) - \\ & - \varepsilon_0 \psi_u(t) \omega(r, \varphi, t, \varepsilon)) - \psi_u(t) \frac{g'(\varphi - \tilde{\varphi}(t))}{\varepsilon} \varepsilon_0 \omega(r, \varphi, t, \varepsilon) (\tilde{\varphi}'(t) - \frac{v_0}{r} - \frac{\psi_v(t)}{r} \varepsilon_0 \omega(r, \varphi, t, \varepsilon)) \\ & \frac{1}{r} \frac{\partial \Phi_1}{\partial \varphi} = -\varepsilon_0 \omega(r, \varphi, t, \varepsilon) (\psi_v'(t) + \psi_u(t) \frac{\partial v_0}{\partial r} + \frac{\psi_u(t) v_0}{r} + \frac{\psi_v(t)}{r} \frac{\partial v_0}{\partial \varphi} + \frac{\psi_u(t) \varepsilon_0 \psi_v(t) \omega(r, \varphi, t, \varepsilon)}{r} + \\ & + \frac{B \gamma_s}{r} (\gamma_s - 2) \psi_\sigma(t) \sigma_0^{\gamma_s - 3} \frac{\partial \sigma_0}{\partial \varphi} - \varepsilon_0 \omega(r, \varphi, t, \varepsilon) \frac{g'(r - \tilde{r}(t))}{\varepsilon} \psi_v(t) (\tilde{r}'(t) - \psi_u(t) \varepsilon_0 \omega(r, \varphi, t, \varepsilon)) - \\ & - \frac{g'(\varphi - \tilde{\varphi}(t))}{\varepsilon} \varepsilon_0 \omega(r, \varphi, t, \varepsilon) \psi_v(t) (\tilde{\varphi}'(t) - \frac{v_0}{r} - \frac{B \gamma_s}{r} \sigma_0^{\gamma_s - 2} \psi_\sigma(t) / \psi_v(t) - \\ & - \frac{B \gamma_s}{r} (\gamma_s - 2) \sigma_0^{\gamma_s - 3} \varepsilon_0 \psi_\sigma^2(t) / \psi_v(t) \omega(r, \varphi, t, \varepsilon) - \frac{1}{r} \varepsilon_0 \psi_v(t) \omega(r, \varphi, t, \varepsilon)) \end{aligned} \quad (11)$$

## 2 SYSTEMS OF EQUATIONS THAT DETERMINE THE TRAJECTORY OF WAVES

**Proposition 1.** Let  $\psi_u(t) = 0$ ,  $\psi_v(t) = 0$ ,  $\Phi_1(r, \varphi, t) = 0$ . Then the nonzero structure-stable perturbation of the surface density in the form (4) can be existed in the region where the surface density is constant (for the isentropic model). The trajectory of perturbations coincides with the trajectories of the gas. In the region

$G_\varepsilon^\alpha = \{(r, \varphi, t) : g(r - \tilde{r}(t)) + g(\varphi - \tilde{\varphi}(t)) < \varepsilon^{1/\alpha_1}, t \in [0, T]\}$  the relation

$$\sigma_0(\tilde{r}(t)) + (\gamma_s - 2) \varepsilon_0 \psi_\sigma(t) = O(\varepsilon^{1/\alpha_1 - 1}).$$

**Proposition 2.** Let  $\psi_v(t) \neq 0$ ,  $\psi_u(t) \neq 0$ ,  $\Phi_1(r, \varphi, t) = 0$ . Then there is a disturbance of the surface density of the form (4) for the case  $\gamma_s = 3$  and thus the following equations:

$$\sigma_0(\tilde{r}(t), \tilde{\varphi}(t), t) + \varepsilon_0 \psi_\sigma(t) \omega(\tilde{r}(t), \tilde{\varphi}(t), t, \varepsilon) = 0 \quad (12)$$

$$\begin{cases} \frac{\partial \sigma_0}{\partial t} + \frac{v_0 \partial \sigma_0}{r \partial \varphi} = 0 \\ -\frac{v_0^2}{r} = -\frac{\partial \Phi_0}{\partial r} - B \gamma_s \sigma_0 \frac{\partial \sigma_0}{\partial r} + \frac{3}{2r} D B \sigma_0^2 \\ \frac{\partial v_0}{\partial t} + \frac{v_0}{r} \frac{\partial v_0}{\partial \varphi} = -\sigma_0 \frac{3B}{r} \frac{\partial \sigma_0}{\partial \varphi} \end{cases} \quad (13)$$

$$\left\{ \begin{array}{l} \psi_u'(t) - \frac{2v_0\psi_v(t)}{\tilde{r}(t)} + \frac{3}{\tilde{r}(t)} BD\sigma^2_0(\tilde{r}(t), \tilde{\varphi}(t)) / \varepsilon_0 + \frac{\varepsilon_0\psi_v^2(t)}{\tilde{r}(t)} - 3B \frac{\partial\sigma_0}{\partial r} \sigma_0(\tilde{r}(t), \tilde{\varphi}(t)) / \varepsilon_0 = 0 \\ \psi_v'(t) + \psi_u(t) \frac{\partial v_0}{\partial r} + \frac{\psi_v(t)}{\tilde{r}(t)} \frac{\partial v_0}{\partial \varphi} + \frac{\psi_u(t)v_0}{\tilde{r}(t)} + \frac{\psi_u(t)\varepsilon_0\psi_v(t)}{\tilde{r}(t)} = 0 \\ \tilde{\varphi}'(t) - \frac{v_0}{\tilde{r}(t)} - \frac{\psi_v(t)}{\tilde{r}(t)} \varepsilon_0 = 0 \\ \tilde{r}'(t) - \psi_u(t)\varepsilon_0 = 0 \end{array} \right. \quad (14)$$

**Proposition 3.** Let  $\psi_v(t) = 0$ ,  $\psi_u(t) \neq 0$ ,  $\Phi_1(r, \phi, t) = 0$ . Then there is a disturbance of the surface density of the form (4) for the case  $\gamma_s = 3$  and thus the following equations: (12), (13),

$$\left\{ \begin{array}{l} \psi_u'(t) + \frac{3}{\tilde{r}(t)} BD\sigma^2_0(\tilde{r}(t), \tilde{\varphi}(t)) / \varepsilon_0 - 3B \frac{\partial\sigma_0}{\partial r} \sigma_0(\tilde{r}(t), \tilde{\varphi}(t)) / \varepsilon_0 = 0, \\ \frac{\partial v_0}{\partial r} + \frac{v_0}{\tilde{r}(t)} - \frac{3B}{\tilde{r}(t)\varepsilon_0} \sigma_0(\tilde{r}(t), \tilde{\varphi}(t), t) \frac{\partial\sigma_0}{\partial \varphi} = 0, \\ \tilde{\varphi}'(t) - \frac{v_0}{\tilde{r}(t)} = 0, \\ \tilde{r}'(t) - \psi_u(t)\varepsilon_0 = 0, \\ \psi_\sigma(t) = -\sigma_0(\tilde{r}(t), \tilde{\varphi}(t), t) / \varepsilon_0 \end{array} \right. \quad (15)$$

**Proposition 4.** Let  $\Phi_1 = -B\gamma_s\sigma_0^{\gamma_s-2}\varepsilon_0\psi_\sigma(t)\omega(r, \varphi, t, \varepsilon)$ ,  $\psi_v(t) \neq 0$ ,  $\psi_u(t) \neq 0$ . Then there is a disturbance of the surface density of the form (4) for the case  $\gamma_s = 2$  and thus the following equations: (12), (13),

$$\left\{ \begin{array}{l} \psi_\sigma'(t) + \sigma_0 \frac{\psi_u(t)}{r} + \psi_u(t) \frac{\partial\sigma_0}{\partial r} + \frac{1}{r} \varepsilon_0\psi_\sigma(t)\psi_u(t)\omega(r, \varphi, t, \varepsilon) = 0 \\ \psi_u'(t) - \frac{2v_0\psi_v(t)}{r} - \frac{3}{2r} BD\psi_\sigma(t) + \frac{\varepsilon_0\psi_v^2(t)\omega(r, \varphi, t, \varepsilon)}{r} = 0 \\ \psi_v'(t) + \psi_u(t) \frac{\partial v_0}{\partial r} + \frac{\psi_u(t)v_0}{r} + \frac{\psi_u(t)\varepsilon_0\psi_v(t)\omega(r, \varphi, t, \varepsilon)}{r} = 0 \\ \tilde{\varphi}'(t) - \frac{v_0}{r} - \frac{\psi_v(t)}{r} \varepsilon_0\omega(r, \varphi, t, \varepsilon) = 0 \\ \tilde{r}'(t) - \psi_u(t)\varepsilon_0\omega(r, \varphi, t, \varepsilon) = 0 \end{array} \right. \quad (16)$$

**Proposition 5.** Let  $\psi_v(t) \neq 0$ ,  $\psi_u(t) \neq 0$ ,  $\Phi_1 = (\tilde{r}'(t)\psi_u(t) - B\gamma_s\sigma_0^{\gamma_s-2}\psi_\sigma(t))\varepsilon_0\omega(r, \varphi, t, \varepsilon)$ . Then there is a disturbance of the surface density of the form (4) for the case  $1 < \gamma_s < 2$  and thus the following equations: (12), (13),

$$\begin{cases}
\psi_\sigma'(t) + \sigma_0 \frac{\psi_u(t)}{r} + \psi_u(t) \frac{\partial \sigma_0}{\partial r} + \frac{\psi_v(t)}{r} \frac{\partial \sigma_0}{\partial \varphi} + \frac{1}{r} \varepsilon_0 \psi_\sigma(t) \psi_u(t) \omega(r, \varphi, t, \varepsilon) = 0 \\
\psi_u'(t) - \frac{2v_0 \psi_v(t)}{r} - \frac{3}{2r} BD(\gamma_s - 1) \sigma_0^{\gamma_s - 2} \psi_\sigma(t) + \frac{\varepsilon_0 \psi_v^2(t) \omega(r, \varphi, t, \varepsilon)}{r} = 0 \\
\psi_v'(t) + \psi_u(t) \frac{\partial v_0}{\partial r} + \frac{\psi_u(t) v_0}{r} + \frac{\psi_v(t)}{r} \frac{\partial v_0}{\partial \varphi} + \frac{\psi_u(t) \varepsilon_0 \psi_v(t) \omega(r, \varphi, t, \varepsilon)}{r} = 0 \\
\tilde{\varphi}'(t) - \frac{v_0}{r} - \frac{\psi_v(t)}{r} \varepsilon_0 \omega(r, \varphi, t, \varepsilon) = 0 \\
\tilde{r}'(t) - \varepsilon_0 \psi_u(t) \omega(r, \varphi, t, \varepsilon) = 0 \\
B\gamma_s(\gamma_s - 2) \sigma_0^{\gamma_s - 3} \psi_\sigma^2(t) + \psi_u^2(t) = 0
\end{cases} \quad (17)$$

In the above statements obtained the general system of equations whose solutions give the trajectory of single waves. Note, that condition (12) means that the perturbation of the surface density must be negative.

### 3 THE BEHAVIOR OF WAVES IN THE REGIONS OF SURFACE DENSITY VARIATION

It is interesting to investigate the behavior of the wave as it passes through the region of increased or decreased surface density. For this study, we introduce a function  $\Delta(r, \varphi, t)$  which characterizes the density perturbation. Let  $\sigma_0(r, \varphi, t) = \tilde{\sigma}_0(r) + \Delta(r, \varphi, t)$ ,

$\frac{\partial}{\partial r} \Delta(r, \varphi, t) = \vartheta(r, \varphi, t)$ . Then  $\frac{\partial \sigma_0}{\partial r} = \frac{\partial \tilde{\sigma}_0}{\partial r} + \vartheta(r, \varphi, t)$ . By analyzing the corresponding systems (15) - (17) the conclusion can be easily obtained that the solitary wave is deflected upward surface density. In the collision of two solitary waves the effect of repulsion can be expected.

In the following figures, we see the trajectory of the maximum single disturbance of the surface density for the case where the surface density is given:

$$\sigma_0(r, \varphi, t) = e^{-\mu r} + a(e^{-(r-R)^2/H} + e^{-(r-R_1)^2/H} + e^{-(r-R_2)^2/H} + e^{-(r-R_3)^2/H})$$

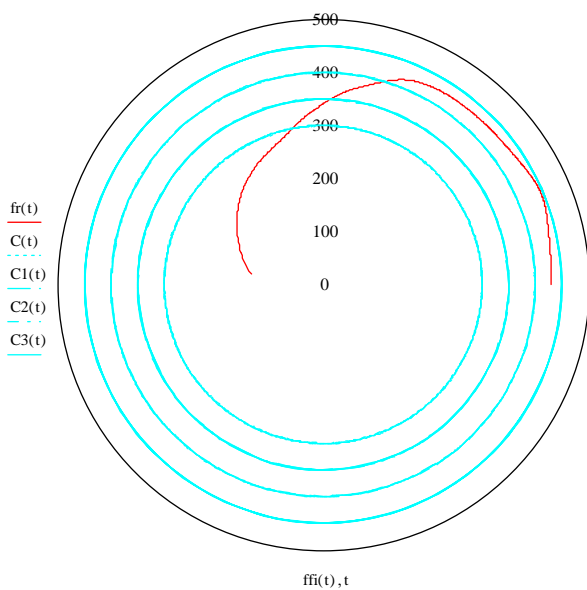


Fig. 1 The trajectory of the wave,  $a=-9, \mu = 0.01, \psi_u^0 = 4, \psi_v^0 = 150$

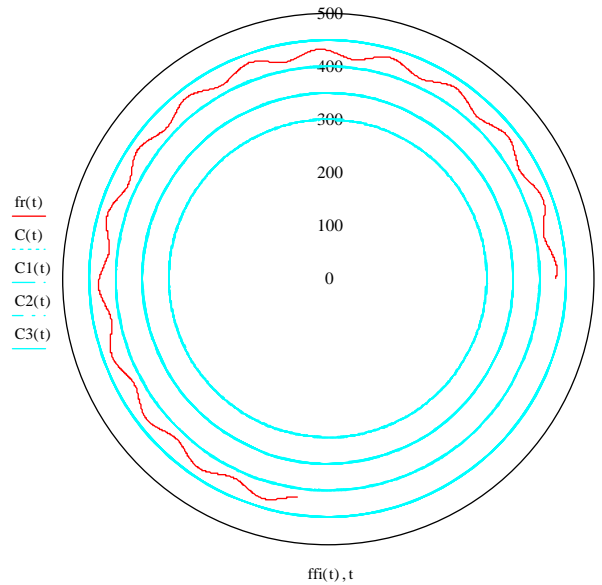


Fig. 2 The trajectory of the wave,  $a=-9, \mu = 0.01, \psi_u^0 = 44, \psi_v^0 = 150$

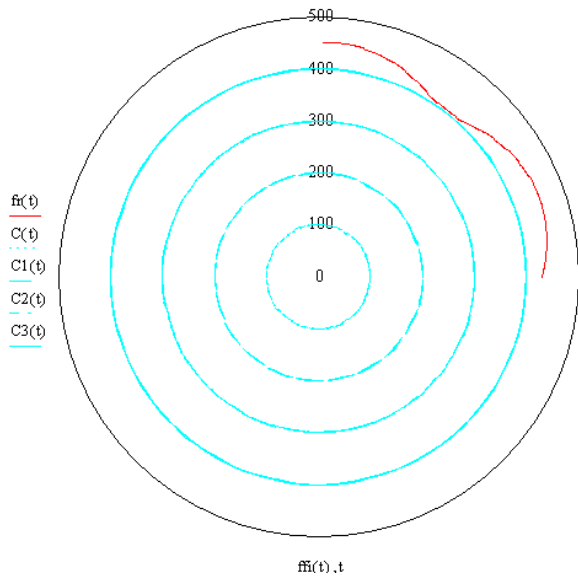


Fig. 3 The trajectory of the wave,  
 $a=-1$ ,  $\mu = 0.01$ ,  $\psi_u^0 = 44$ ,  $\psi_v^0 = 150$

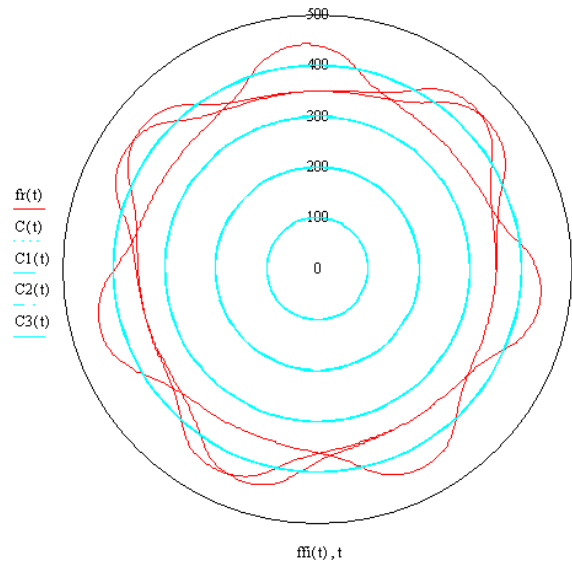


Fig. 4 The trajectory of the wave,  
 $a=4$ ,  $\mu = 0.01$ ,  $\psi_u^0 = 4$ ,  $\psi_v^0 = 70$

## CONCLUSIONS

Thus in this paper we consider the trajectory of solitary waves in a gas disk of the galaxy. Note, that the gas disk is a rotating system. The equations of gas dynamics of galaxies and shallow water equations are equivalent. This fact was considered by A.M. Friedman in [1]. We can assume that similar waves exist in shallow water, which is rotated.

## REFERENCES

- [1] Fridman A.M. Prediction and discovery of new structures in spiral galaxies *Physics-Uspeski*, N.2, pp. 121-148, 2007 .
- [2] Morozova G., Hoperskov A.V. Physics of the galaxies disk [www.astronet.ru](http://www.astronet.ru) .
- [3] Ekimov R.V. Construction of a weak asymptotic solution of the type of infinitely narrow-solitons for equations of shallow water *Proceedings of the School-Seminar*, Sudak, 2001 .
- [4] Turbal Y.V. On the partial solutions of equations of galaxies gas dynamics with oscillations like  $\delta$ -solitone. *Bulletin of the University of Kiev. Ser.: Physics and mathematics*, N.1., pp. 67-72, 2009.

**STOCHASTIC SYSTEMS UNDER PERIODIC AND WHITE NOISE EXTERNAL  
EXCITATIONS, AND THE ALTERNATIVE CLASSIFICATION FOR THE PDE  
SOLUTIONS**

**Volosov Konstantin  
Alexandrovich<sup>1</sup>,  
Sinitsyn Sergey O.,  
Volosova Alexandra K.,  
Vdovina Elena K.**  
Moscow State University of  
Railway Engineering,  
Moscow, Russia

---

ABSTRACT

---

It is shown that wide class of equations in partial derivatives (PDEs) is equivalent to a system of functional linear algebraic equations. It permits to construct exact and approximate solutions and to determine the solution character of evolution with respect to "limit attracting solution" according to eigenvalues of the matrix corresponding to the equation under consideration. K.A.Volosov proposes the alternative classification for PDE solutions on eigen values.

---

**INTRODUCTION**

The new important property of wide class PDE was found by K.A.Volosov [1-5] {see also [www.aplsmath.ru](http://www.aplsmath.ru)}. One considers now a simple case of two independent variables  $x, y$ . For an arbitrary transformation of the variables, namely,  $x = x(\xi, \delta)$ ,  $y = y(\xi, \delta)$ , it is possible to present all PDEs of the second order, or more, as  $AX = b$ , that is as a system of linear algebraic equations with respect to derivatives of the initial variables  $x(\xi, \delta), y(\xi, \delta)$  on the new variables  $\xi, \delta: x'_\xi, x'_\delta, y'_\xi, y'_\delta$ . This algebraic system has the unique solution. The same presentation is possible for a case of three and more independent variables  $x, y, t, \dots$ ,

In the present paper, we suggest this new approach to obtain closed formulae for exact solutions of the Kolmogorov-Fokker-Planck (KFP) equation. New identity is obtained which follows from conditions of the obtained algebraic system solvability. Eigenvalues are calculated in obvious form.

In this case these eigenvalues are functions of independent variables, but we use the classical terminology as in each specific point these ones are numbers. As far as there are only few exact solutions of the KFP equation (1), we refer to the analogy with quasilinear parabolic equations (7) which are well studied by many investigators who found around one hundred of exact families of solutions. We can calculate the pointed out eigenvalues for these exact solutions. Based on this comparison some important conclusion is made and it is proposed some hypothesis on the nature of the solutions evolution to so-called "attractive limits" solution of the same equation. This hypothesis by our opinion can be extended to evolution of the Cauchy problem solutions for the non-stationary KFP equation of the form (1) [6].

**1. ANALYSIS OF THE KFP EQUATION ( with Sinitsyn S.O.)**

One considers a stochastic system under periodic and white noise external excitations:  
 $x' + \alpha x = \lambda \text{Cos}(y(t)), y' = \omega + \xi_o,$   
where  $\xi_o$  is the Gaussian white noise. Then one considers the KFP equation which follows from this system

---

<sup>1</sup> Corresponding author. Email: [konstantinvolosov@yandex.ru](mailto:konstantinvolosov@yandex.ru), [volosovk@yahoo.co.uk](mailto:volosovk@yahoo.co.uk)

$$p_t' - \alpha(x p)'_x + \lambda \text{Cos}(y) p'_x + \omega p'_y - \varepsilon p''_{yy} = 0, \quad (1)$$

where  $p = p(x, y, t)$  is the density function of probability and  $\alpha, \varepsilon, \lambda, \omega$  are constants.

The proposed algorithm works in assumption that all used functions are continuously differentiable ones.

One considers for a beginning a case when in (1)  $p = p(x, y)$ . It is introduced the following arbitrary transformation of variables:

$$p(x, y) \Big|_{x=x(\xi, \delta), y=y(\xi, \delta)} = U(\xi, \delta).$$

We note that  $\det J = x'_\xi y'_\delta - x'_\delta y'_\xi \neq 0$ .

One introduces the following relation:

$$\frac{\partial p}{\partial x} \Big|_{x=x(\xi, \delta), y=y(\xi, \delta)} = Y(\xi, \delta), \quad \frac{\partial p}{\partial y} \Big|_{x=x(\xi, \delta), y=y(\xi, \delta)} = T(\xi, \delta).$$

One obtains from here the following formulas:

$$\frac{\partial U}{\partial \xi} \frac{\partial y}{\partial \delta} - \frac{\partial U}{\partial \delta} \frac{\partial y}{\partial \xi} = Y(\xi, \delta) \det J, \quad -\frac{\partial U}{\partial \xi} \frac{\partial x}{\partial \delta} + \frac{\partial U}{\partial \delta} \frac{\partial x}{\partial \xi} = T(\xi, \delta) \det J. \quad (2)$$

Equation (1) in new variables takes the form

$$\omega T + \varepsilon(x'_\delta T'_\xi - x'_\xi T'_\delta) / \det J + \lambda Y \text{Cos}(y(\xi, \delta)) - \alpha x(\xi, \delta) Y - \alpha U(\xi, \delta) = 0. \quad (3)$$

As  $p(x, y)$  is the continuously differentiable function, it must be realized a condition of equality of mixed derivatives,

$p''_{xy}(x(\xi, \delta), y(\xi, \delta)) = p''_{yx}(x(\xi, \delta), y(\xi, \delta))$ , in the variables  $\xi, \delta$ . It can write this equality in the form:

$$-\frac{\partial Y}{\partial \xi} \frac{\partial x}{\partial \delta} + \frac{\partial Y}{\partial \delta} \frac{\partial x}{\partial \xi} - \frac{\partial T}{\partial \xi} \frac{\partial y}{\partial \delta} + \frac{\partial T}{\partial \delta} \frac{\partial y}{\partial \xi} = 0 \quad (4)$$

The system of equations (2)-(4) will be analyzed by two stages.

### Theorem 1.

The implicit system of linear algebraic equations (2)-(4),  $AX = b$ , with regards to the derivatives  $X_1 = x'_\xi, X_2 = x'_\delta, X_3 = y'_\xi, X_4 = y'_\delta$  has the next unique solution:

$$x'_\xi = g_1(\xi, \delta), x'_\delta = g_2(\xi, \delta), t'_\xi = g_3(\xi, \delta), t'_\delta = g_4(\xi, \delta) \quad (5)$$

It is possible to calculate the functions  $g_i(\xi, \delta), i = 1, \dots, 4$  in obvious form, for example,

$$g_1(\xi, \delta) = [\varepsilon T T'_\xi - (\omega T - \alpha U + \lambda \text{Cos}(y(\xi, \delta))) Y - \alpha x(\xi, \delta) Y] U'_\xi / P_1(\xi, \delta).$$

Matrix  $A$  has the following form:

$$A = \begin{bmatrix} -T U'_\xi & T U'_\delta & -Y U'_\xi & Y U'_\delta \\ -T'_\xi & T'_\delta & -Y'_\xi & Y'_\delta \\ 0 & 0 & a_{33} & a_{34} \\ 0 & 0 & 0 & a_{44} \end{bmatrix}.$$

Vectors  $X, b$  have the forms:

$$X = (X_4, X_3, X_2, X_1)^\tau, \quad b = (0, 0, 0, b_4),$$

where

$$b_4 = g_1(\xi, \delta) P_1(\xi, \delta), \quad a_{33} = [\alpha U + [\alpha x(\xi, \delta) - \lambda \text{Cos}(y(\xi, \delta))] Y] U'_\xi + T(-\omega U'_\xi + \varepsilon T'_\xi),$$

$$a_{34} = [-\alpha U + [-\alpha x(\xi, \delta) - \lambda \text{Cos}(y(\xi, \delta))] Y] U'_\delta + T(\omega U'_\delta - \varepsilon T'_\delta), \quad a_{44} = P_1(\xi, \delta).$$

$$P_1(\xi, \delta) = [Y[\alpha U + [\alpha x(\xi, \delta) - \lambda \text{Cos}(y(\xi, \delta))] Y][U'_\delta T'_\xi - T'_\delta U'_\xi] + T^2 [Y'_\delta (\varepsilon T'_\xi - \omega U'_\xi) + [-\varepsilon T'_\delta + \omega U'_\delta] Y'_\xi] + T[\alpha U (Y'_\delta U'_\xi - U'_\delta Y'_\xi) + Y[[\omega T'_\delta + (\alpha x(\xi, \delta) - \lambda \text{Cos}(y(\xi, \delta))) Y'_\delta] U'_\xi - [U'_\delta (\omega T'_\xi + (\alpha x(\xi, \delta) - \lambda \text{Cos}(y(\xi, \delta))) Y'_\delta)]]].$$

The vector symbol  $\tau$  means a conjugation. The eigenvalues can be written of the form

$$\lambda_1 = a_{33}, \lambda_2 = P_1(\xi, \delta), \lambda_3 = \frac{1}{2}[M - \sqrt{D}], \lambda_4 = \frac{1}{2}[M + \sqrt{D}],$$

$$M = T'_\delta - T U'_\xi, \quad D = (T'_\delta)^2 + 2TT'_\delta U'_\xi + T[T(U'_\delta)^2 - 4U'_\delta T'_\xi]. \diamond$$

At the second stage, we consider the new first-order system (5) with respect to the functions  $x(\xi, \delta), y(\xi, \delta)$ . It is well known that the solvability of a system of this type is verified by calculating the second mixed derivatives of the functions  $x = x(\xi, \delta), y = y(\xi, \delta)$  on the arguments  $\xi$  and  $\delta$ :  $x''_{\xi\delta} = x''_{\delta\xi}, y''_{\xi\delta} = y''_{\delta\xi}$  [3, p.83], and [4, p.5].

**Example.** It is considered the more general equation KFP (1), where the second term is changed for  $\alpha(m(x)p)'_x$ , where the last function is arbitrary twice continuously differentiated function. For concrete calculations the following function is selected:  $m(x) = (\exp(\beta x) - 1)/(\exp(\beta x) + 1)$ . If the solvability condition is satisfied, we can find the exact solution for the equation (1) with  $p = p(x, y, t)$ , having the parameter  $\sigma$ . It is existed a passage to the limit by this parameter, to a stationary solution (obtained for  $p(x, y)$ ) having the some fixed value of this parameter. Corresponding formulae, which are analogical to (2)-(4) can be found in [3, p.89], [4, p.12].

### Theorem 2

Let us solution of the equation (1) is the following:

$p(x, y, t) = \exp[\alpha t + y\omega/(2\varepsilon) - t\omega^2/(4\varepsilon)]W(x, y, t)$ , which follows from the above presented condition of solvability, where the function  $W(x, y, t)$  is a solution of the equation

$$W'_t + \alpha W - \alpha(m(x)W)'_x + \lambda \text{Cos}(y) W'_x - \varepsilon W''_{yy} = 0.$$

The exact solution of this equation has the form  $\text{Cos}(y) - H(x, \exp(-t\sigma)W(x, y, t)) = 0$ , here the function  $H(x, \eta)$ ,  $\eta = \exp(-t\sigma)W(x, y, t)$ , is a solution of the equation

$$H'_x - \varepsilon H''_{\eta\eta} (H^2 - 1)/[(\alpha m(x) - \lambda H)(H'_\mu)^2] +$$

$$[\varepsilon H + \eta H'_\eta [\alpha + \sigma - \alpha m'(x)]]/(\alpha m(x) - \lambda H) = 0. \diamond \quad (6)$$

We can determine the same solution of the equation (6) in the converge power series. The function  $H(x, \eta)$  can be wrote of the form:

$$H(x, \eta) = C_0(x) + C_1(x)\eta + C_2(x)\eta^2 + C_3(x)\eta^3 + C_4(x)\eta^4 + O(\eta^5), \text{ where } \eta < 1.$$

Terms up to fourth degree are saved. Then we can use exact formulae for solutions of the algebraic equation of the fourth order. So, returning to initial variables, one has the explicit approximate solution, using the KFP equation exact solution.

Finally, note that if we put  $\sigma = \omega^2/(4\varepsilon) - \alpha$ , then the obtained solution of the non-stationary KFP equation transforms to the stationary solution of this equation with the coefficient  $p(x, y)$ . It can be wrote the ODEs system to determine coefficients  $C_i(x), i = 0, 4$ . Zero conditions at the infinity are used for this system. By using the obtained explicit approximate formulae, for  $x = 0$  we numerically construct a function having zero conditions at infinity to determine coefficients  $C_i(x)$ . Then the iteration process is formed with additional traditional non-local condition of normalization.

## 2. ON CONNECTION EIGENVALUES AND CHARACTER OF EVOLUTION OF THE SOLUTIONS OF THE NONLINEAR AND LINEAR PARABOLIC EQUATIONS

(with Volosova A.K., Vdovina E.K.)

**Remark 1.** It is not simple to construct solution of the equation (1). Problems for the equation (1) are badly studied. On the contrary, problems for the equation (7) are well studied; it investigated during a long time. Hundred families of solutions of the equation (7) and of equations similar to it can be found in papers by G.I.Barenblatt, L.D.Landau, A.N.Kolmogorov, I.G.Petrovskii, I.S.Piskunov, R.Fischer, Ya.B.Zeldovich, A.S.Kalashnikov, A.D.Polyanin, V.F.Zaitev, V.N.Denisov, E.M.Vorob'ev, V.P.Maslov and many others. References on publications by these authors can be found in [3].

K.A.Volosov made the following mathematical experiment. Using formulae for eigenvalues of the equation (7) matrix  $A$ , it is possible to calculate them on these exact solutions. As a result, we have alternative classification for the PDE solutions on the eigenvalues.

In papers [1-5] the proposed method with arbitrary transformation of variables is described for the following equation:

$$Z'_t - (K(Z)Z'_x)'_x + F(Z) = 0 \quad (7)$$

One uses the arbitrary transformation of variables of the form:  $Z(x, t)|_{x=x(\xi, \delta), t=t(\xi, \delta)} = U(\xi, \delta)$ .

We note that the determinant,  $\det J = x'_\xi t'_\delta - t'_\xi x'_\delta \neq 0$ , is nonzero. The inverse transformation of variable exists, at least locally:  $\xi = \xi(x, t)$ ,  $\delta = \delta(x, t)$ . The derivatives of the old independent variables on the new variables are determined as follows:

$$\frac{\partial x}{\partial \xi} = \det J \frac{\partial \delta}{\partial t} \frac{\partial t}{\partial \xi} = -\det J \frac{\partial \delta}{\partial x} \frac{\partial x}{\partial \delta} = -\det J \frac{\partial \xi}{\partial t} \frac{\partial t}{\partial \delta} = \det J \frac{\partial \xi}{\partial x}$$

Let us introduce the following relation:

$$K(Z) \frac{\partial Z}{\partial x} \Big|_{x=x(\xi, \delta), t=t(\xi, \delta)} = Y(\xi, \delta), \quad K(Z) \frac{\partial Z}{\partial t} \Big|_{x=x(\xi, \delta), t=t(\xi, \delta)} = T(\xi, \delta). \quad \text{We obtain the}$$

formulae:

$$\begin{aligned} K(U(\xi, \delta)) \left( \frac{\partial U}{\partial \xi} \frac{\partial t}{\partial \delta} - \frac{\partial U}{\partial \delta} \frac{\partial t}{\partial \xi} \right) &= Y(\xi, \delta) \det J, \\ K(U(\xi, \delta)) \left( -\frac{\partial U}{\partial \xi} \frac{\partial x}{\partial \delta} + \frac{\partial U}{\partial \delta} \frac{\partial x}{\partial \xi} \right) &= T(\xi, \delta) \det J \end{aligned} \quad (8)$$

The equation (7) takes the form:

$$T(\xi, \delta) - K(U) \left( \frac{\partial Y}{\partial \xi} \frac{\partial t}{\partial \delta} - \frac{\partial Y}{\partial \delta} \frac{\partial t}{\partial \xi} \right) / \det J + K(U) F(U) = 0 \quad (9)$$

Since  $Z$  is the continuously differentiable function, one has that  $\frac{\partial}{\partial t} Z'_x = \frac{\partial}{\partial x} Z'_t$  in variables  $\xi, \delta$ , or

$$-\frac{\partial x}{\partial \delta} \frac{\partial}{\partial \xi} \left[ \frac{Y}{K(U)} \right] + \frac{\partial x}{\partial \xi} \frac{\partial}{\partial \delta} \left[ \frac{Y}{K(U)} \right] - \frac{\partial t}{\partial \delta} \frac{\partial}{\partial \xi} \left[ \frac{T}{K(U)} \right] + \frac{\partial t}{\partial \xi} \frac{\partial}{\partial \delta} \left[ \frac{T}{K(U)} \right] = 0. \quad (10)$$

The system (8)-(10) will be analyzed in two stages. At the first stage, we consider the system (8)-(10) as a nonlinear algebraic equation system with respect to the derivatives  $x'_\xi, x'_\delta, t'_\xi, t'_\delta$ .

### Theorem 3.

The implicit linear algebraic equation system (8)-(10)  $AX = b$  with regards to the derivatives  $X_1 = x'_\xi, X_2 = x'_\delta, X_3 = t'_\xi, X_4 = t'_\delta$ , has the unique solution

$$x'_\xi = \Psi_1, x'_\delta = \Psi_2, t'_\xi = \Psi_3, t'_\delta = \Psi_4 \quad (11)$$

where functions  $\Psi_i, i = 1, \dots, 4$  are presented in [1-5], and the denominator in (11) is the following:

$P_1(\xi, \delta) = FK[(T Y'_\xi - Y T'_\xi) U'_\delta + (Y T'_\delta - T Y'_\delta) U'_\xi] + T Y [-U'_\delta T'_\xi + U'_\xi T'_\delta] + Y^2 [Y'_\delta T'_\xi - T'_\delta Y'_\xi] + T^2 [U'_\delta Y'_\xi - U'_\xi Y'_\delta]$ . Matrix  $A$  has the form:

$$A = \begin{bmatrix} Y U'_\delta & -Y U'_\xi & T U'_\delta & -T U'_\xi \\ a_{21} & a_{22} & a_{23} & a_{24} \\ 0 & 0 & a_{33} & a_{34} \\ 0 & 0 & 0 & a_{44} \end{bmatrix}.$$

Vectors  $X, b$  are the following:

$$X = (X_1, X_2, X_3, X_4)^T, \quad b = (0, 0, 0, b_4), \quad \text{where}$$

$$a_{21} = -K(U) Y'_\delta + Y K'(U) U'_\delta, \quad a_{22} = K(U) Y'_\xi - Y K'(U) U'_\xi,$$

$$a_{23} = -K(U) T'_\delta + T K'(U) U'_\delta, \quad b_4 = K(U) [-Y Y'_\delta + (F K(U) + T) U'_\delta] [U'_\delta Y'_\xi - Y'_\delta U'_\xi],$$

Vector symbol  $\tau$  means a conjugation. The eigenvalues have the following form:

$$\lambda_1 = a_{33}, \lambda_2 = P_1(\xi, \delta), \lambda_3 = \frac{1}{2}[M - \sqrt{D}], \lambda_4 = \frac{1}{2}[M + \sqrt{D}],$$

$$M = KY'_\xi + Y(U'_\delta - K'(U)U'_\xi), \quad D = 4YK(Y'_\delta U'_\xi - U'_\delta Y'_\xi) + [KY'_\xi + Y(U'_\delta - K'(U)U'_\xi)]^2.$$

It is proved that two conditions of solvability of the new system (11) of arbitrary functions  $U, Y, T$  always have the common multiplier [1]- [5].

K.A.Volosov with collaborators analyzed more than one hundred known, exact or approximate solutions, and calculated for them eigenvalues indicated at the Theorem 4. The astonishing regularities are obtained; see a lot of examples in [6]. It was formulated a problem of connection of the eigen values with a character of evolution and stabilization of solutions of the mixed problems for the equation (7). Analysis of calculated eigenvalues for many known solutions permits to select three cases of mixed problems [6].

The necessary conditions presented in the theorem 4 are strongly connected with an existence of the special solution  $\Omega(x, t)$  of the mixed problem (with initial and boundary conditions) formulated for the equation (7). This solution is called the “limit attracting solution”. Three cases are selected below. Note that a proof of the theorem 4 is obtained by the induction method.

**Part 1.** It exists a class of exact solutions of the mixed problems for concrete types of the equation (7) when in the presence of dissipation, and for the corresponding boundary conditions a solution of the problem tends to constant, may be to zero. It is a stabilization of the solution [7]. This result is correct as for linear equations or half-linear parabolic equations, as well for degenerate quasilinear parabolic equations of the form (7), but only in the region of the solution localization. In this case, from our point of view, the “limit attracting solution” is a constant  $\Omega(x, t) \equiv \text{constant}$ , or, may be,  $\Omega(x, t) \equiv 0$ . See papers by L.K.Martinson, A.D.Polyanin, V.N.Denisov [7], R.O.Kershner.

**Part 2.** It exists a class of the mixed problems with initial and boundary conditions. Properties of solutions of these problems are determined by properties of the function  $F(Z)$  in the equation (7). It is the famous problems by A.N.Kolmogorov, I.G.Petrovskii, I.S.Piskunov, R.Fischer and others. Solutions of such problems, as it was shown in different publications including publications by authors, tend to the “limit attracting” solutions, which are **waves** having the specific profile and velocity.

**Part 3.** If there is a stationary solution of the equation (7), that is a solution which is not depend on the independent variable  $t$ , then other solutions tend to the stationary one. In this case, from our point of view, this is the “limit attracting solution”,  $\Omega(x, t)$ . The mixed problem with initial and boundary conditions for degenerate quasilinear parabolic equations has been investigated in [8].

By results of our investigation all three cases are united.

Plan of the analysis is the following. Formulae of the Theorem 3 are applied for the next trivial transformation of variables:  $x(\xi, \delta) = \xi, t(\xi, \delta) = \delta$ , where the Jacobian is equal to unit. This transformation is isomorphism, and the equation (7) pass to itself and solutions of the equation (7) pass to itself. Then by the exact solution, obtained in papers by other authors, or by the asymptotic properties of the solution, the eigenvalues and  $Tr A$ , that is a trek of the matrix  $A$ , can be calculated directly.

In all three cases we have as a result: three eigenvalues are equal to zero, and one eigenvalue is smaller than zero in region  $\omega_1 \subset R^2$ ; or two eigenvalues smaller than zero in region  $\omega_1 \subset R^2$ .

By analogy with the dynamic systems theory we can stress that in all three cases the limit steady-states are of the knot type or of the saddle -knot type.

It is formulated the following theorem on evolution of solution of the equation in partial derivatives to the “limit attracting solution” and to propose the alternative classification for PDE solutions on the corresponding Eigen values.

**Theorem 4.** Let the conditions of the Theorem 3 are satisfied. Let unknown special solution  $\Omega(x, t)$  of the mixed problem (with initial and boundary conditions) for concrete types of the equation (7) having the special properties as the “limit attracting solution”. One assumes that in formulae of the Theorem 3 the transformation  $x(\xi, \delta) = \xi, t(\xi, \delta) = \delta$  is made.

By necessity, the determinant  $D \geq 0$ , and eigenvalues  $\lambda_2 \leq 0, \lambda_3 \leq 0$  in region  $\omega_1 \subset R^2$ ; and a sign of  $Tr A$  of the matrix  $A$  changes in a region of determination of the functions  $\lambda_i, i = 1, \dots, 4$ , then  $\Omega(x, t)$  is exist, and it is realized the limit  $Z(x, t) \rightarrow \Omega(x, t)$ , for any values of  $x$ , for  $t \rightarrow \infty$ .

**Remark 2.** We divide two following questions:

1. Which are necessary conditions of existence of the “limit attracting solution” for three problems described above?

2. How is the passage to the solution realized? In which functional spaces is it performed?

In the paper authors answer only for the first question.

In all three cases we have the difficult special steady point, namely, a saddle - knot takes place. In a region  $\omega_1 \subset R^2$  the functions  $\lambda_2(x, t), \lambda_3(x, t)$ , depend on variables and change, but the special singular point type saves. For the localized solutions the theorem 4 works only in the localization area. The proposed theory can be extended to cases of many variables and to other PDEs and to equation KFP (1) too.

## CONCLUSIONS

It is shown that wide class of equations in partial derivatives (PDEs) is equivalent to a system of functional linear algebraic equations.

## REFERENCES

- [1] Volosov K.A. in *Proc. of the Conf. "Gertsenovskie chteniya"*, April, 17-22, 2006., St. Petersburg, 2006.
- [2] Volosov K.A., Implicit Formulas for Exact Solutions of Quasilinear Partial Differential Equations. *Doklady Akademii Nauk (Notices of the RAS)*, V.418, No.1, pp.11-14, 2008.
- [3] Volosov K.A. *The Doctor Sci. Thesis*, MIEM, Moscow, <http://eqworld.ipmnet.ru>, [www.aplsmath.ru](http://www.aplsmath.ru), 2007.
- [4] Volosova, A.K. Volosov K.A. Construction of Solutions of PDE in Parametric Form. *Int. J. of Mathematics and Math.Sciences*. V.2009, Article ID, 319268, 17 p., <http://www.hindawi.com/journals/ijmms/2009/319269.html>.
- [5] Volosov K.A. Construction of solutions of quasilinear parabolic equations in parametric form. *J. of Appl. and Industrial Math.*, 2009, Vol. 3, No. 4, pp. 519-527, 2009.
- [6] Volosov K.A., Volosova A. K. , Vdovina E.K. *Construction of Solutions of PDE by an arbitrary replacement of variables*. M. MIIT, 140 p., 2010.
- [7] Denisov V.N. Stabilization of solution to the Cauchy problem for a parabolic equation with lower order coefficients and an exponentially growing initial function. *Proc. of the Steklov Institute of Mathematics*. MAIK Nauka/Interperiodica distributed exclusively by Springer Science+Business Media LLC. 0081-5438 (Print) 1531-8605 (Online). V. 261, N. 1.0.7., pp. 94-97, 2008.
- [8] Volosov K.A., Fedotov I.A. Asymptotic representations of the solution of a quasilinear parabolic equation in the vicinity of a front. *J VM IMF.*, V. 5., pp.93-101, 1983 (in Russian). English translation: *Zh.Vychisl.Mat.i Mat.Fiz.*, 23, N.5, pp. 1249-1253, 1983.

**ANALYSIS OF NONLINEAR ANHARMONIC PERTURBATIONS FOR  
AXISYMMETRIC LONGITUDINAL-SHEAR WAVES IN A CYLINDRICAL  
WAVEGUIDE**

**A.V. Yelagin**<sup>1</sup>  
Donetsk National  
University  
Ukraine, Donetsk

---

ABSTRACT

---

The numerical-analytical solution of the nonlinear generation of second harmonic axisymmetric normal elastic waves of longitudinal-shear type in a circular aluminum waveguide is obtained. Applied model of geometrically and physically nonlinear deformation is based on the Murnaghan elastic potential, a representation of finite deformations and method of decomposition of nonlinear wave movements in the rows of the small parameter.

---

**INTRODUCTION**

Investigation of nonlinear effects in the propagation of normal elastic waves in deformable waveguides of different geometric shapes has a number of important engineering applications [1,2]. It gives information about the interaction of elastic waves, which is described in the linear approximation as independent and allows describe the anharmonic effects of appearance in the waveguides waves with double frequencies. The fields of application of research of nonlinear anharmonic effects are ultrasonic wave diagnosis, seismic and acoustic electronics. Nonlinear properties of elastic waves are used in the concept of acoustoelectronic devices for integration of signals, ultrasonic convolver.

Several problems of this type are uninvestigated because of the extreme complexity of the theoretical solutions.. These include the current problem of anharmonic effects in the propagation of normal elastic waves in cylindrical three-dimensional geometry waveguides. Some aspects of the problem for the cylindrical waveguide were considered in [3,4].

**1. FORMULATION AND METHOD OF SOLUTION**

In this paper the numerical-analytical problem of definition and investigation of nonlinear second harmonics monochromatic axisymmetric normal longitudinal waves propagating along the axial direction in an isotropic circular section cylinder is presented. The waveguide in normalized cylindrical coordinates occupies the region

$$V = \{0 \leq r \leq R, 0 \leq \theta \leq 2\pi, -\infty < z < \infty\} \quad (1)$$

The lateral surface of the cylinder is rigidly fixed. Characteristics of the investigated wave field are complex functions of the wave elastic displacements  $u_\alpha(r, z, t)$  ( $\alpha = r, z$ ).

The model of nonlinear dynamic deformation of isotropic elastic media was used, taking into account the effects of geometrical and physical nonlinearity. It includes the representation of the elastic Murnaghan potential  $U$  with quadratic and cubic terms of finite deformation  $E_{\alpha\beta}$  ( $\alpha, \beta, \gamma = r, \theta, z$ )

---

<sup>1</sup> Corresponding author. Email [delyagin@inbox.ru](mailto:delyagin@inbox.ru)

$$U = \frac{\lambda + 2\mu}{2} E_1^2 - 2\mu E_2 + \frac{l + 2m}{3} E_1^3 - 2m E_1 E_2 + n E_3; \quad (2)$$

where

$$E_1 = I_1, \quad E_2 = \frac{1}{2}(I_1^2 - I_2), \quad E_3 = \frac{1}{6}(I_1^3 - 3I_1 I_2 + 2I_3);$$

$I_j$  – invariants of the strain tensor

$$I_1 = E_{rr} + E_{\theta\theta} + E_{zz}, \quad I_2 = E_{\theta\theta} E_{zz} + E_{\theta\theta} E_{rr} + E_{zz} E_{rr} - E_{rz} E_{zr}, \quad I_3 = E_{rr} E_{\theta\theta} E_{zz} - E_{rz} E_{\theta\theta} E_{zr},$$

$\lambda, \mu$  - Lamé parameters;  $l, m, n$  - elastic constants of second order for the material of the cylinder. Nonlinear representation of the tensor components of elastic deformations  $E_{\alpha\beta}$  in axisymmetrical case are given by

$$E_{rr} = \frac{\partial u}{\partial r} + \frac{1}{2} \left( \left( \frac{\partial u}{\partial r} \right)^2 + \left( \frac{\partial u}{\partial z} \right)^2 \right), \quad E_{\theta\theta} = \frac{u}{r} + \left( \frac{u}{r} \right)^2, \quad E_{zz} = \frac{\partial u}{\partial z} + \frac{1}{2} \left( \left( \frac{\partial u}{\partial r} \right)^2 + \left( \frac{\partial u}{\partial z} \right)^2 \right), \quad (3)$$

$$E_{\theta z} \equiv 0, \quad E_{rz} = \frac{1}{2} \left( \frac{\partial u}{\partial z} + \frac{\partial u}{\partial r} + \frac{\partial u}{\partial r} \frac{\partial u}{\partial z} + \frac{\partial u}{\partial r} \frac{\partial u}{\partial z} \right), \quad E_{r\theta} \equiv 0.$$

Representation of the second component of the Piola-Kirchhoff stress tensor at the base venues of the cylindrical coordinate system is consistent with this form of elastic potential and has the form

$$T_{\alpha\beta} = \frac{2\sigma}{1-2\sigma} I_1 \delta_{\alpha\beta} + 2E_{\alpha\beta} + \left[ \frac{l}{\mu} I_1^2 - \left( 2\frac{m}{\mu} - \frac{n}{\mu} \right) I_2 \right] \delta_{\alpha\beta} + \left( 2\frac{m}{\mu} - \frac{n}{\mu} \right) I_1 E_{\alpha\beta} + \frac{n}{\mu} E_{\alpha\gamma} E_{\gamma\beta} \quad (4)$$

$(\alpha, \beta, \gamma = r, \theta, z),$

where  $\delta_{\alpha\beta}$  – components of the unit tensor,  $\sigma$  - Poisson's ratio. The Lagrange stress tensor components on the main venues of the cylindrical coordinate system in axisymmetrical case, respectively, are determined by the relations

$$\begin{bmatrix} S_{rr} & S_{r\theta} & S_{rz} \\ S_{\theta r} & S_{\theta\theta} & S_{\theta z} \\ S_{zr} & S_{z\theta} & S_{zz} \end{bmatrix} = \begin{bmatrix} 1 + \frac{\partial u}{\partial r} & 0 & \frac{\partial u}{\partial z} \\ 0 & 1 + \frac{u}{r} & 0 \\ \frac{\partial u}{\partial r} & 0 & 1 + \frac{\partial u}{\partial z} \end{bmatrix} \begin{bmatrix} T_{rr} & T_{r\theta} & T_{rz} \\ T_{\theta r} & T_{\theta\theta} & T_{\theta z} \\ T_{zr} & T_{z\theta} & T_{zz} \end{bmatrix}. \quad (5)$$

In the differential form the boundary value problem, describes the investigated nonlinear wave field, involves the equation of the dynamic deformation

$$\frac{1}{r} \frac{\partial}{\partial r} (r S_{rr}) + \frac{\partial S_{rz}}{\partial z} - \frac{S_{\theta\theta}}{r} + \rho \frac{\partial^2 u_r}{\partial t^2} = 0, \quad \frac{1}{r} \frac{\partial}{\partial r} (r S_{zr}) + \frac{\partial S_{zz}}{\partial z} + \rho \frac{\partial^2 u_z}{\partial t^2} = 0 \quad (6)$$

and boundary conditions, which have the following form in the case of rigidly fixed lateral surface

$$(u_r)_{r=R} = (u_z)_{r=R} = 0;$$

In the equations (6)  $\rho$  is the density of the material of the cylinder in the undeformed state.

For the analysis of small nonlinear perturbations (anharmonic effects) in this paper it is used the search method of successive approximations, described by the first linear and second nonlinear harmonics of normal elastic waves. Analysis of nonlinear effects in the propagation of normal axisymmetric longitudinal waves for a cylinder with a rigidly clamped lateral surface in the first linear approximation reduces to the next homogeneous spectral boundary value problem for the functions of the wave elastic displacements  $u_r^{(l)}, u_z^{(l)}$  :

$$\rho \frac{\partial^2 u_r^{(l)}}{\partial t^2} + \frac{1}{r} \frac{\partial}{\partial r} (r S_{rr}^{(l)}(u_r^{(l)}, u_z^{(l)})) + \frac{\partial S_{rz}^{(l)}(u_r^{(l)}, u_z^{(l)})}{\partial z} - \frac{S_{\theta\theta}^{(l)}(u_r^{(l)}, u_z^{(l)})}{r} = 0; \quad (7)$$

$$\rho \frac{\partial^2 u_z^{(l)}}{\partial t^2} + \frac{1}{r} \frac{\partial}{\partial r} (r S_{zr}^{(l)}(u_r^{(l)}, u_z^{(l)})) + \frac{\partial S_{zz}^{(l)}(u_r^{(l)}, u_z^{(l)})}{\partial z} = 0,$$

with the following boundary conditions

$$(u_r^{(l)})_{r=R} = 0, (u_z^{(l)})_{r=R} = 0; \quad (8)$$

We have inhomogeneous boundary value problem for determining the complex functions of the wave elastic displacements  $u_r^{(n)}, u_z^{(n)}$  of the second nonlinear harmonics normal axisymmetric waves of torsion. It includes an inhomogeneous system of differential equations:

$$\rho \frac{\partial^2 u_r^{(n)}}{\partial t^2} + \frac{1}{r} \frac{\partial}{\partial r} (r S_{rr}^{(l)}(u_r^{(n)}, u_z^{(n)})) + \frac{\partial S_{rz}^{(l)}(u_r^{(n)}, u_z^{(n)})}{\partial z} - \frac{S_{\theta\theta}^{(l)}(u_r^{(n)}, u_z^{(n)})}{r} =$$

$$= -\frac{1}{r} \frac{\partial}{\partial r} (r S_{rr}^{(n)}(u_r^{(l)}, u_z^{(l)})) - \frac{\partial S_{rz}^{(n)}(u_r^{(l)}, u_z^{(l)})}{\partial z} + \frac{S_{\theta\theta}^{(n)}(u_r^{(l)}, u_z^{(l)})}{r}; \quad (9)$$

$$\rho \frac{\partial^2 u_z^{(n)}}{\partial t^2} + \frac{1}{r} \frac{\partial}{\partial r} (r S_{zr}^{(l)}(u_r^{(n)}, u_z^{(n)})) + \frac{\partial S_{zz}^{(l)}(u_r^{(n)}, u_z^{(n)})}{\partial z} =$$

$$= -\frac{1}{r} \frac{\partial}{\partial r} (r S_{zr}^{(n)}(u_r^{(l)}, u_z^{(l)})) - \frac{\partial S_{zz}^{(n)}(u_r^{(l)}, u_z^{(l)})}{\partial z};$$

with boundary conditions of the form

$$(u_r^{(n)})_{r=R} = 0, (u_z^{(n)})_{r=R} = 0. \quad (10)$$

Solutions of wave equations of linear boundary value problems (7), (8), which describe the axisymmetric longitudinal-shear normal waves in cylinder, can be represented as

$$u_r^{(l)} = -A_1 \tilde{\alpha} J_1(\tilde{\alpha} r) + A_2 i k J_1(\tilde{\beta} r); \quad (11)$$

$$u_z^{(l)} = A_1 i k J_0(\tilde{\alpha} r) - A_2 \tilde{\beta} J_0(\tilde{\beta} r),$$

where  $u_r^{(l)}, u_z^{(l)}$  – are complex functions of dynamic displacement in a normal wave with angular frequency  $\omega$ , wave number  $k$  and phase velocity  $v$ ;  $v_s = (\mu/\rho)^{1/2}$  – the phase velocity of linear shear waves;  $J_n(\gamma r)$  – cylindrical Bessel function;  $A$  – an arbitrary amplitude factor. From the boundary

conditions of spectral problems (10) and (11) in this case, the dispersion relations was obtained, which define the full spectrum of linear axisymmetrical normal longitudinal-shear waves in the cylinder. These relations have the form

$$k^2 J_0\left(\sqrt{-k^2 + \frac{\Omega^2}{\zeta}} r\right) J_1\left(\sqrt{-k^2 + \Omega^2} r\right) + \sqrt{-k^2 + \Omega^2} \sqrt{-k^2 + \frac{\Omega^2}{\zeta}} J_0\left(\sqrt{-k^2 + \Omega^2} r\right) J_1\left(\sqrt{-k^2 + \frac{\Omega^2}{\zeta}} r\right) = 0$$

where  $\Omega$  is the dimensionless normalized frequency parameter  $\Omega = \omega R/v_s$ ,  $\tilde{k} = kR$  – dimensionless normalized wave number;  $\tilde{\alpha}^2 = \Omega^2/\zeta^2 - k^2$ ;  $\tilde{\beta}^2 = \Omega^2 - k^2$ ;  $\zeta^2 = 2(1-\nu)/(1-2\nu)$ .

The solution of the inhomogeneous boundary value problem (9), (10) on the basis of the algorithm developed analytical transformations was obtained in the form:

$$u_r^{(n)} = -2B_1 \tilde{\alpha} J_1(2\tilde{\alpha}r) + B_2 ik J_1(2\tilde{\beta}r) + F_1(r); \quad (12)$$

$$u_z^{(n)} = B_1 ik J_0(2\tilde{\alpha}r) - 2B_2 \tilde{\beta} J_0(2\tilde{\beta}r) + F_2(r),$$

$$\text{where } F_1(r) = \sum_{p=1}^{\infty} a_p r^p; \quad F_2(r) = \sum_{p=1}^{\infty} b_p r^p; \quad B_1 = (\chi_{12} F_2(R) - \chi_{22} F_1(R)) / (\chi_{11} \chi_{22} - \chi_{21} \chi_{12});$$

$$B_2 = (\chi_{11} F_2(R) - \chi_{21} F_1(R)) / (\chi_{12} \chi_{21} - \chi_{11} \chi_{22}); \quad \chi_{11} = -2\tilde{\alpha} J_1(2\tilde{\alpha}r); \quad \chi_{12} = ik J_1(2\tilde{\beta}r); \quad \chi_{21} = ik J_0(2\tilde{\alpha}r);$$

$$\chi_{22} = -2\tilde{\beta} J_0(2\tilde{\beta}r).$$

Here  $a_p$ ,  $b_p$  - coefficients of the power series, which was obtained as a partial solution of inhomogeneous equations (9). To calculate these coefficients, the following recurrence formulas were received:

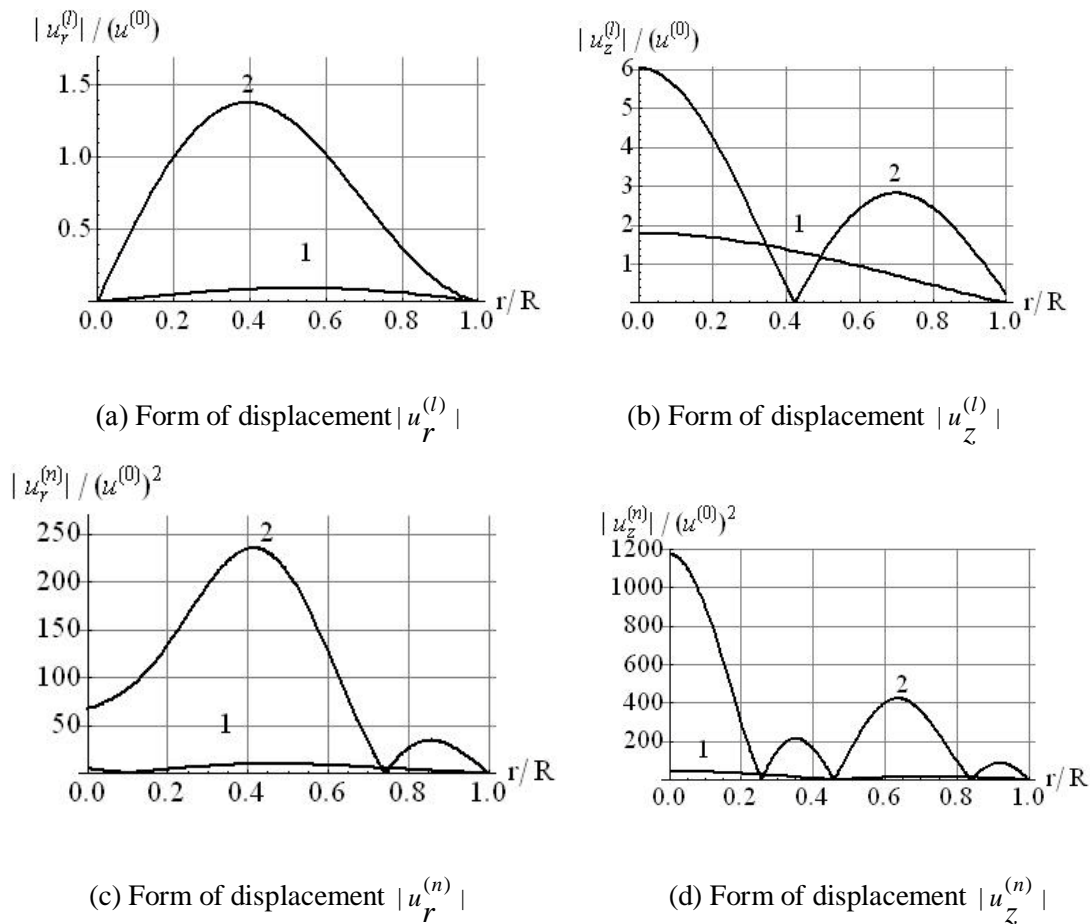
$$a_1 = \alpha_1 / \Delta_{13}^{(1)}; \quad b_1 = \beta_1 / \Delta_{23}^{(1)}; \quad a_2 = \frac{\alpha_2 - b_1 \Delta_{14}^{(1)}}{\Delta_{12}^{(1)} + 2\Delta_{13}^{(1)} + 2\Delta_{15}^{(1)}}; \quad b_2 = \frac{\beta_2 - a_1 (\Delta_{22}^{(1)} - \Delta_{24}^{(1)})}{2\Delta_{23}^{(1)} + 2\Delta_{25}^{(1)}};$$

$$a_{p+2} = \frac{\alpha_{p+2} - \Delta_{11}^{(1)} a_p - \Delta_{14}^{(1)} (p+1) b_{p+1}}{\Delta_{12}^{(1)} + \Delta_{13}^{(1)} (p+2) + \Delta_{15}^{(1)} (p+2)(p+1)}; \quad b_{p+2} = \frac{\beta_{p+2} - \Delta_{21}^{(1)} b_p - \Delta_{22}^{(1)} a_{p+1} - \Delta_{24}^{(1)} (p+1) a_{p+1}}{\Delta_{23}^{(1)} (p+2) + \Delta_{25}^{(1)} (p+2)(p+1)}.$$

## 2. NUMERICAL RESULTS

Numerical research of nonlinear anharmonic effects was realized for the waveguide of duralumin with following physical and mechanical constants  $\rho = 2.79 \cdot 10^3 \text{ kg/m}^3$ ;  $\sigma = 0.31$ ;  $\mu = 2.6 \cdot 10^{10} \text{ Pa}$ ;  $\lambda = 2\sigma\mu/(1-2\sigma) = 4.2 \cdot 10^{10} \text{ Pa}$ ;  $l = -26.46 \cdot 10^{10} \text{ Pa}$ ;  $m = 38.22 \cdot 10^{10} \text{ Pa}$ ;  $n = 36.26 \cdot 10^{10} \text{ Pa}$ .

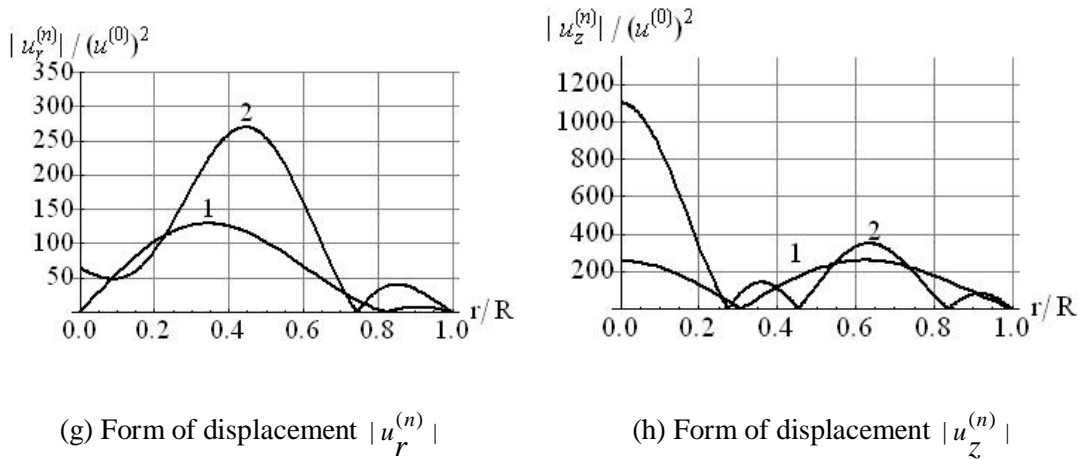
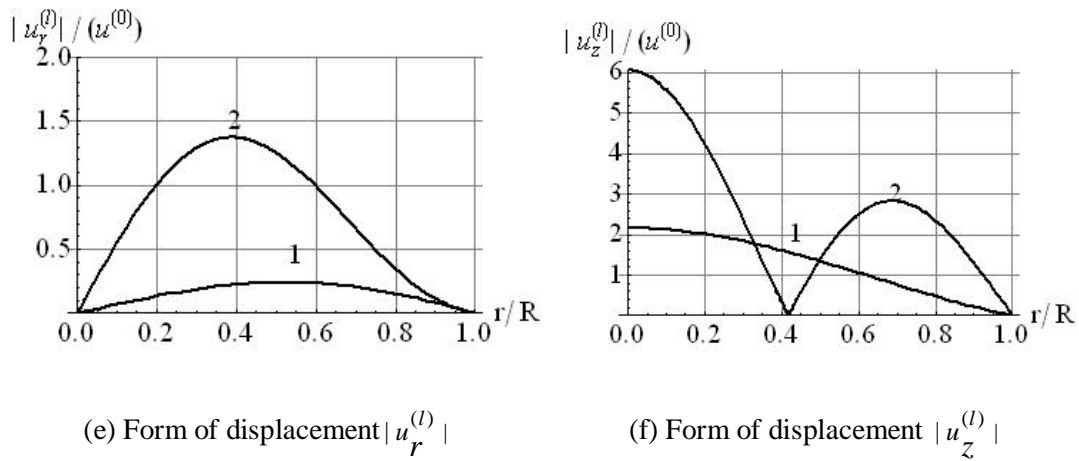
On the base of obtained solutions the radial distribution of dimensionless normalized amplitudes for the wave displacements in the travelling normal longitudinal-shear waves with a relative length and  $\lambda = 5R$  from first and second modes of the dispersion spectrum, and for displacements of their non-linear second harmonics were calculated.



1- the first mode, 2- the second mode

*Fig.1 – Amplitude forms of displacement in first linear and second nonlinear harmonics for the longitudinal-shear waves with  $\lambda = 10R$  in a cylinder with fixed boundary.*

Analysis of the Figures 1-2 allows in particular to make a conclusion about the considerable influence of the parameter of the relative length of the normal waves on the distributions of forms wave displacements along the radial coordinate in the waveguide cross section for nonlinear second harmonic compared to the amplitude of vibrational displacements in the forms of linear normal modes.



1- the first mode, 2- the second mode

Fig.2 – Amplitude forms of displacement in first linear and second nonlinear harmonics for the longitudinal-shear waves with  $\lambda = 5R$  in a cylinder with fixed boundary.

### CONCLUSIONS

In the article the analytical representations for the second harmonics of the normal longitudinal-shear waves in an isotropic cylinder are obtained for the first time. Some estimates of the amplitudes of nonlinear perturbations for waves of torsion of different relative lengths are presented.

### REFERENCES

[1] Kurenaya K. I. Analysis of nonlinear ultraacoustic wave properties in germanium monocrystal layer, *Journal of Computational and Applied Mechanics*. Vol. 6, No. 1, pp. 67-82, 2005.

[2] Lemanov V. V. Nonlinear effects in the propagation of high frequency elastic waves in crystals. Vol. 20, pp. 259–267, 1974.

[3] Sugimoto N. Nonlinear mode coupling of elastic waves, *Acoustical Society of America*. Vol. 62, N 1, pp. 23-32, 1977.

[4] Yelagin A.V. Nonlinear second harmonics axisymmetric waves of torsion in a cylindrical waveguide with a clamped surface, *Problems of Computational Mechanics and Strength of Structures*. Vol. 14, pp. 347–354, 2010.

**MODELING CREEP RATCHETING OF AN ALUMINUM-SILICON  
EUTECTIC ALLOY**

**H. Altenbach**<sup>1</sup>

Martin-Luther-University  
Halle-Wittenberg  
Halle, Germany

**S. Kozhar**

Otto-von-Guericke-  
University Magdeburg  
Magdeburg, Germany

**K. Naumenko**

Martin-Luther-University  
Halle-Wittenberg  
Halle, Germany

ABSTRACT

Eutectic AlSi12CuNiMg cast alloy combines excellent mechanical properties with good castability and is commonly used for piston applications. Creep responses of this alloy under constant and cyclic force at elevated temperatures of 250°C and 300°C are presented. In addition, the alloy is studied in both P-refined and Sr-modified conditions at temperature of 300°C. The T6 heat treatment is used to affect the microstructure and hardness. Based on experimental data correlations between the microstructure and the force-controlled low-cycle fatigue are found. The fracture surfaces of the specimens are investigated with the help of the optical and scanning electron microscopy.

For the description of the material behavior a unified model of viscoplasticity is suggested. The primary and secondary stages of experimental curves are modeled with the help of a non-linear kinematic hardening rule and the classical creep functions of stress. To describe the final part of the tertiary creep stage, the damage variable has to be applied.

**INTRODUCTION**

The eutectic aluminium alloy AlSi12CuNiMg investigated in the present work is widely used for load-bearing structural components in the automotive industry. The most important areas of application for the alloy are pistons for combustion engines, gears, pump parts, wear-resistant and heat-resistant parts of all kinds owing to its high strength at elevated temperatures and low thermal expansion coefficient. Nevertheless, to apply these alloys successfully in highly loaded components, it is essential to understand their strength properties under various loading conditions [1, 2].

The goal of the present study is to:

- describe the alloy behavior under applied static and cyclic loading at an elevated temperature in P-refined condition;
- examine the effect of the microstructure on the low cycle fatigue strength at 300°C in both P-refined and Sr-modified condition.

*Table 1 Chemical composition of the studied alloys (wt.%)*

Alloy code	Si	Cu	Ni	Mg	Mn	Fe	Ti	P	Sr	other	Al
M-F	12.65	1.11	0.81	0.99	0.20	0.28	0.05	<0.001	0.025	<0.01	rem.
R-T6	12.72	1.07	0.95	1.12	0.16	0.41	0.05	0.005	<0.0005	<0.01	rem.
M-T6	12.44	1.14	0.88	0.99	0.19	0.24	0.04	<0.001	0.027	<0.01	rem.

<sup>1</sup> Corresponding author. Email [holm.altenbach@iw.uni-halle.de](mailto:holm.altenbach@iw.uni-halle.de) (Prof. Dr.-Ing. Holm Altenbach)

## 1. EXPERIMENTAL PROCEDURE

The cast aluminum alloy AlSi12CuNiMg was used in three conditions: P-refined and heat-treated (hereafter termed alloy R-T6), Sr-modified in the as-cast state (M-F), and Sr-modified after T6 heat treatment (M-T6). The chemical composition of the alloys is shown in Table 1. P-refined and Sr-modified samples were heat-treated under T6 conditions, i.e. solution treated at 510°C for 6 h in an air circulate furnace, water quenched at 50°C, naturally aged at room temperature for 24 h, and then artificially aged at 165°C for 8 h. Microstructural changes were examined using optical and scanning electron microscopy.

Tensile testing of specimens was carried out at room temperature and at 300°C in a Zwick Z250 testing machine in accordance with the DIN EN 10002 procedure. Three tensile tests were carried out for each alloy and temperature value. The test specimens were held during 15 min at 300°C before mechanical testing. The hardness of the as-cast and heat-treated specimens was measured at room temperature with a Brinell hardness tester with a load of 62.5 kg and a ball diameter of 2.5 mm.

Specimens for creep and cyclic testing with a diameter of 5 mm, length of 120 mm and gauge length of 50 mm were machined from the ingots. The surfaces of the specimens were polished. Tests were performed on a servohydraulic fatigue testing machine MTS-810 with 250 kN maximum load. To measure the strain, an extensometer with a gauge length of 12.5 mm was applied. The specimens were heated with a 5 kW induction heater. The thermal strain was subtracted from the total strain.

Force-controlled fatigue tests were conducted at an elevated temperature in laboratory air under low cycle fatigue conditions. The minimum to maximum stress ratio was kept at 0. This means that the cycling was fulfilled in the pure tensile state without a stress reversal, i.e. cyclic creep or ratcheting condition. Later on some of the broken specimens were observed with the help of light microscopy and scanning electron microscopy to determine the damage mechanisms.

The loading conditions for given alloys are summarized in Table 2.

*Table 2 Fulfilled experiments*

Alloy code	Tensile test	Creep test	Cyclic test ( $R_\sigma = 0$ )
M-F	T = 20, 300°C	—	T = 300°C      f = 0.1 Hz
R-T6	T = 20, 250, 300°C	T = 250, 300°C	T = 250, 300°C      f = 0.1, 1 Hz
M-T6	T = 20, 300°C	—	T = 300°C      f = 0.1 Hz

## 2. EXPERIMENTAL RESULTS

The microstructure of the investigated alloys is presented in Fig. 1. For both M-F and M-T6 alloys the addition of strontium causes a complete elimination of primary silicon crystals. However, the specimens with the modified structures contain spherical pores that can be explained by contamination with hydrogen during the addition of strontium. The porosity value obtained for strontium modified alloys M-F and M-T6 is 2.6%. In contrast to that the porosity value for alloy R-T6 is only 0.5%. The modified eutectic silicon fibers, regions of dendritic aluminum and intermetallics can be seen in the microstructure of the modified alloy M-F in the as-cast condition (Fig. 1a). Addition of phosphorus has led to the refinement of the primary silicon crystals in the alloy R-T6. The aluminum matrix of this alloy R-T6 contains primary silicon as well as eutectic acicular silicon and numerous intermetallics (Fig. 1b).

The effect of T6 heat-treatment for both the refined R-T6 and modified M-T6 alloys leads to essential changes in their structures and properties. After tempering of the refined R-T6 alloy, the primary silicon crystals and eutectic silicon needles show only some spheroidizing. The modified and heat-treated alloy M-T6 shows distinctly more uniform and refined structures due to the combined effects of modification and T6 heat treatment (Fig. 2), i.e., the eutectic silicon is rounded and creates a partially broken eutectic network.

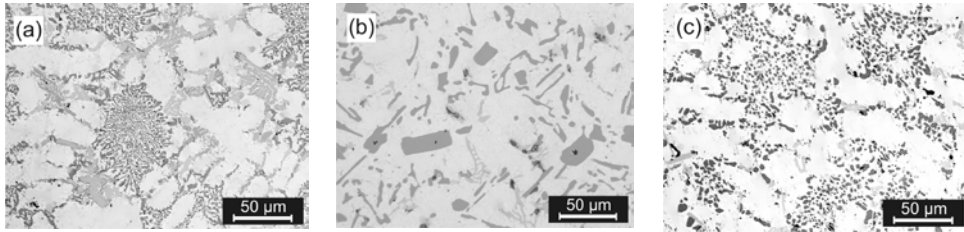


Fig. 1 Microstructure of M-F alloy (a), R-T6 alloy (b) and M-T6 alloy (c). Light microscope observation with magnification of 500

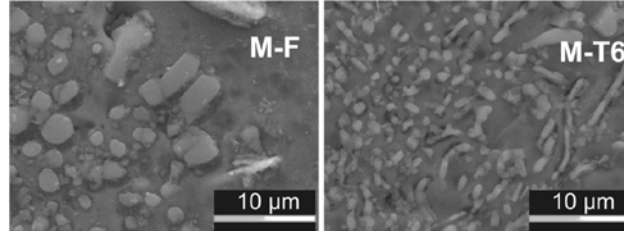


Fig. 2 SEM micrographs of the Sr-modified M-F and M-T6 alloys

Table 3 presents the average tensile properties of investigated alloys at 20°C and 300°C. It is apparent that the heat treatment can be highly beneficial for alloys performance. The highest ductility is found in the modified alloy in the as-cast condition, M-F. The Brinell hardness for the M-F alloy at 20°C is determined as HB 90. Both heat-treated alloys R-T6 and M-T6 show the same hardness value of HB 143.

Table 3 Ultimate tensile strength (UTS), yield strength (YS), and ultimate elongation (UE) for investigated alloys

Alloy code	at 20°C			at 300°C		
	YS, MPa	UTS, MPa	UE, %	YS, MPa	UTS, MPa	UE, %
M-F	132	208	1.0	99	110	5.6
R-T6	350	358	0.3	136	149	2.9
M-T6	341	363	0.8	138	143	4.8

The results of fulfilled tests for P-refined alloy are shown in Fig. 3. In spite of the fact that specimens tested at the higher loading frequency had a higher number of cycles to failure, values of time to rupture were found to be close, especially for the case of 300°C.

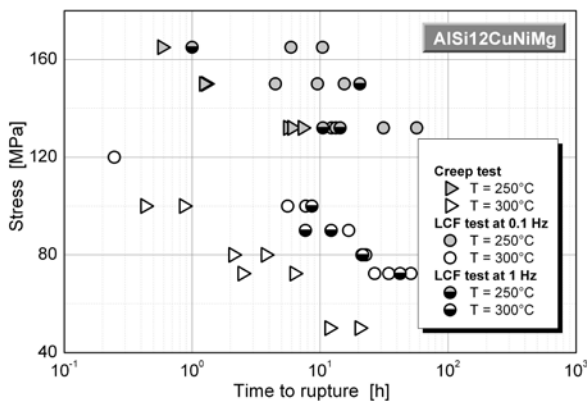


Fig. 3 Dependence of time to rupture vs. applied maximum stress for R-T6-alloy

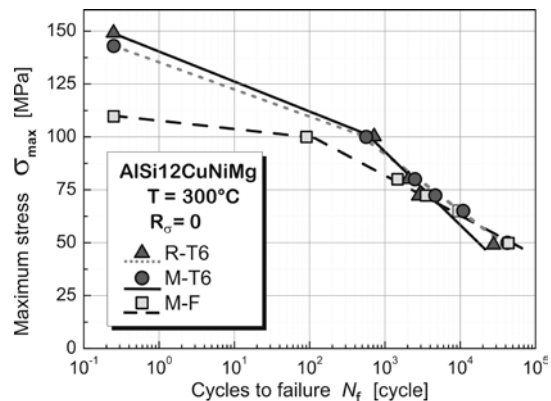


Fig. 4 Relationship between applied maximum stress and fatigue life of cycles to failure for investigated alloy conditions at 300°C

The averages of fatigue lives obtained for each maximum stress value in cyclic loading test at frequency of 0.1Hz are straight line fitted in Fig. 4. The experimental points on the far left correspond to creep strength values.

### 3. DISCUSSION

All investigated alloys show cyclic creep deformation response during low cycle fatigue tests under applied stresses. The comparison of ratcheting rate values shows that the M-F alloy accumulates permanent deformation during cyclic loading more rapidly than the heat-treated alloys. As a result, the Sr-modified alloy M-F has the lowest strength at low cycle fatigue loading at applied maximum stress higher than 65 MPa. This result is consistent with the observation [3] that Al-Si alloys with higher matrix hardness show better thermal fatigue resistance when compared to the Al-Si alloys without heat treatment. Under applied maximum stress lower than 65 MPa, similar values of fatigue lives for modified M-F and M-T6 alloys are expected. This can be explained by deterioration of mechanical properties in the M-T6 alloy due to overageing.

To establish the fracture mode, several ruptured specimens are observed with the help of optical and scanning electron microscopy. Primary silicon particles in the refined alloy R-T6 have a detrimental influence on fatigue behaviour. Cracking was often observed, particularly in large particles with a higher aspect ratio. The silicon particles appear to be sites for crack nucleation and propagation during loading. The decohesion and cracking of silicon particles at the fracture surface (see Fig. 5) reveal that these particles contribute to increasing the propagation rate of fatigue cracks and to shortening the fatigue life. The fracture process also includes the coalescence of voids and dimples in the matrix around those broken hard particles. For all R-T6 specimens, the fracture morphology consists of cleavage fracture of brittle-phase precipitates and cellular ductile fracture of the aluminum matrix with a high density of microdimples.

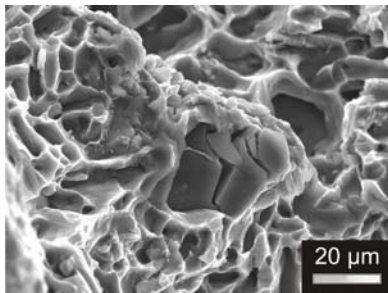


Fig. 5 SEM image of cracked silicon on a fracture surface of the specimen, R-T6

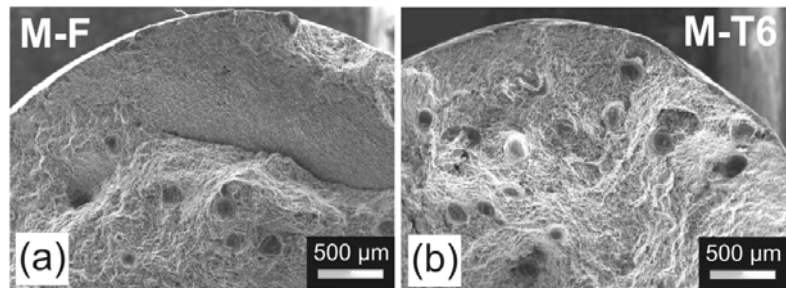


Fig. 6 SEM image of fracture surfaces after LCF testing with a maximum stress of 72 MPa: (a) M-F alloy and (b) M-T6 alloy

The observation of fracture surfaces of Sr-modified specimens in as-cast condition M-F and after heat treatment M-T6 leads to the conclusion that the porosity is the key factor affecting the fatigue strength in these alloys. No significant differences of fracture surfaces of modified alloy specimens between as-cast state M-F and the heat-treated state M-T6 are found (Fig.6). After observation of the fracture profile of M-T6 alloy specimens it is found that the main fracture path crosses the boundary zone eutectic/dendrites boundary of the alloy and the regions with pores.

Our results show that the Sr-modified and heat-treated alloy M-T6 displays slightly longer fatigue life compared to the refined alloy after T6 tempering R-T6 for applied maximum stress higher than 65 MPa in spite of the fact that the tested specimens of alloy M-T6 have casting imperfection of the gas porosity type. One may assume that the coarse and irregular morphology of silicon in the refined structure provides convenient paths for the crack to debond or cut through relatively easily, while the perfect spheroidizing of the eutectic silicon exerts more resistance to crack nucleation and crack growth.

### 4. MODELLING

It is known that deformation of metals at elevated temperature is rate-dependent process. In this case the unified theory of viscoplasticity may be applied [4]. We can start from a simple constitutive equation in the form of  $\dot{\epsilon}_{in} = f_{\sigma}(\sigma_{eq})f_T(T)$ .

Three functions of stress are applied to characterize minimum creep rate of R-T6 alloy [5]

$$\dot{\epsilon}_{\min} = A\sigma^n, \quad (1)$$

$$\dot{\epsilon}_{\min} = A \sinh(B\sigma), \quad (2)$$

$$\dot{\epsilon}_{\min} = A \frac{\sigma}{B} \left[ 1 + \left( \frac{\sigma}{B} \right)^{n-1} \right] \quad (3)$$

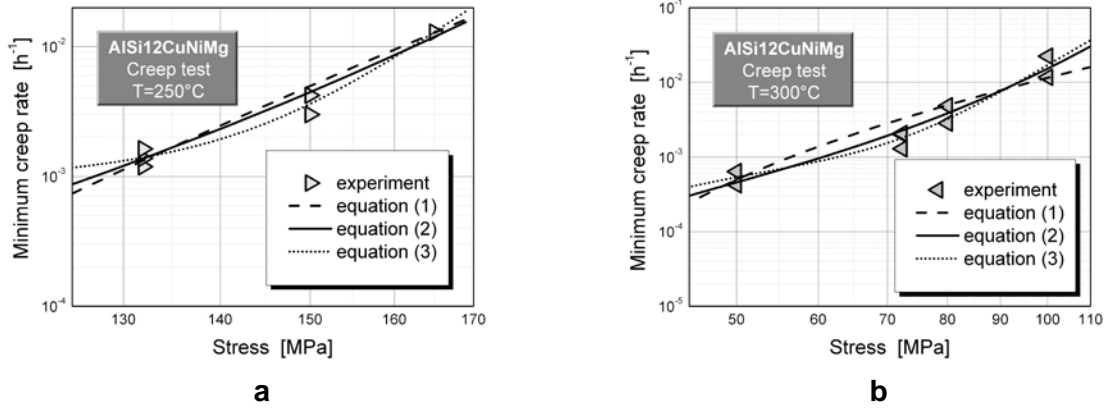


Fig. 7 Minimum creep rate vs. stress for R-T6 alloy at 250°C(a) and 300°C(b)

Figure 7 show that the hyperbolic sine law (2) describes the creep test results quite well. Introducing the function of stress (2) to be hyperbolic sine law, we can rewrite for uniaxial case

$$\dot{\epsilon}_{in} = A \sinh[B(\sigma - X)] \operatorname{sgn}(\sigma - X), \quad (4)$$

where X is the back stress, A and B are constants.

Evolution law of the back stress can be defined as non-linear kinematic hardening law

$$\dot{X} = C\dot{\epsilon}_{in} - D|\dot{\epsilon}_{in}|X \quad (5)$$

Equations (4) and (5) give possibility to simulate the primary and stationary stages of creep, as well as the strain ratcheting during cyclic loading with nonzero mean stress. The material constants were determined from results of tensile and creep tests. The verification of the model was done by comparison the calculated minimum ratcheting rate with values determined from tensile peak strain versus time experimental plots of R-T6 alloy (fig. 8).

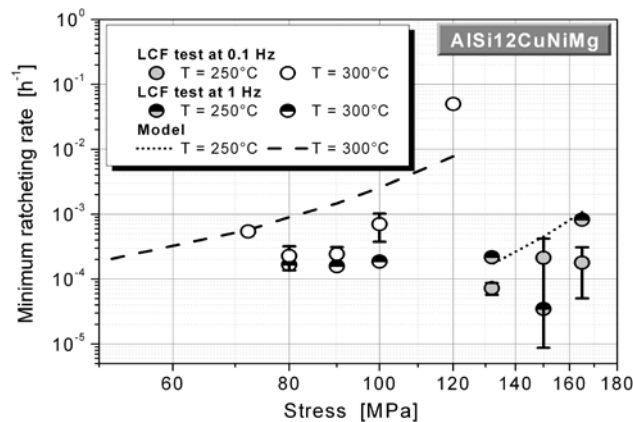


Fig. 8 Minimum ratcheting rate vs. stress for R-T6 alloy tested at temperature of 300°C.

The proposed model predicts the minimum ratcheting rate values good. To take into account tertiary creep, damage variables and damage evolution equations have to be included into proposed unified model.

## CONCLUSION

Based on results from this study, we may conclude as follows:

1. Brittle fracture and decohesion of primary silicon particles together with the void growth and coalescence in the matrix are found to be the major factors affecting failure behavior of P-refined AlSi12CuNiMg alloy in the T6 condition.
2. Gas porosity is the main factor affecting the low cycle fatigue life of Sr-modified AlSi12CuNiMg alloy at elevated temperature.
3. The LCF behavior of P-refined and Sr-modified AlSi12CuNiMg alloys can be significantly improved by T6 heat treatment.
4. Under applied maximum stress lower than 65 MPa the number of cycles to failure for Sr-modified AlSi12CuNiMg alloy in both the as-cast and the T6 conditions is nearly similar due to deleterious effect of overageing of the heat-treated alloy during fatigue testing at temperature of 300°C.
5. The proposed simple unified model can well predict the material response under applied static and cyclic loading. To simulate the tertiary creep, damage variable will be introduced.

## REFERENCES

- [1] Moreira M.F., Fuoco R. Characteristics of Fatigue Fractures in Al-Si Cast Components *AFS Trans.* Paper 06-122, pp. 1-15, 2006.
- [2] Silva F.S. Fatigue on engine pistons – A compendium of case studies *Eng. Failure Anal.*, Vol. 13, pp. 480-492, 2006.
- [3] Firouzdar V., Rajabi M., Nejati E., Khomamizadeh F. Effect of microstructural constituents on the thermal fatigue life of A319 aluminum alloy, *Mater. Sci. Eng.*, Vol. A 454-455, pp. 528-535, 2007.
- [4] Chaboche J.L. A review of some plasticity and viscoplasticity constitutive theories *Int. J. Plasticity*, Vol. 24, pp. 1642–1693, 2008.
- [5] Naumenko K., Altenbach H. *Modeling of creep for structural analysis*, Springer, 2007.

## RATCHETING SIMULATION OF STRUCTURAL STEEL UNDER LOW-CYCLE ASYMMETRIC LOADING

**Borodii M.V.**<sup>1</sup>

**Adamchuk M.P.**

G.S. Pisarenko Institute  
for Problems of Strength,  
National Academy of  
Sciences of Ukraine, Kyiv,  
Ukraine

ABSTRACT

Dependence of the cyclic creep rate in stainless steels 1020 and 1026 on the amplitude and mean value of a loading cycle in the space of stresses is investigated. To simulate the process, constitutive equations of the endochronic theory of plasticity with the improved hereditary kernel were employed. It is shown that the model proposed allows describing with a sufficient accuracy the kinetics of the stress-strain state of specimens under low-cycle asymmetric loading based on the smallest number of basic experiments.

### INTRODUCTION

It is known that the operation of actual thin-walled structures, such as pipes and pressure vessels, under cyclic loading with high nominal stresses can be accompanied by the phenomenon of accumulation of oriented deformations whose intensity and nature are responsible for the rate of attaining the limiting state and service life of structure. This effect is called “cyclic creep” or “ratcheting”. It is experimentally observed under stress-controlled loading higher the yield stress of cyclically-anisotropic materials or unsymmetrical loading of cyclically-isotropic materials. The main peculiarity of this effect is that the hysteresis loops induced are never closed and, as a result, the recorded strain gradually creeps in the direction of the mean stress. In the region of low-cycle fatigue this factor influences appreciably the lifetime of the structural materials. The phenomenon of cyclic creep of the material is not necessary caused by time effects as is case of classical creep. To the large extent, it is determined by the anisotropy of the material, both initial and acquired in the process of loading. The intensity of the processes of cyclic creep depends on the properties of the material (isotropic, anisotropic, hardening, softening), the loading mode (stress ratio, nonproportionality of the path of loading cycles, loading frequency), the plasticity margin, temperature, etc.

At present, a significant amount of research [1-4] is devoted to problems of investigations and simulation of cyclic loading. This is explained by both practical needs and by the necessity of having constitution relations capable of describing the inelastic behavior of materials. In the last decades, considerable progress in this field has been attained due to the appearance of numerous experimental and theoretical works [5-7] devoted to the improvement of the applicability of various version of the theory of plasticity to the case of cyclic asymmetrical loading.

The aim of this work is to develop a constitutive model of cyclic plasticity for the prediction of complex processes of loading, both strain- and stress-controlled, for uniaxial and biaxial low-cycle loading.

### 1. BASIC EQUATIONS OF THE MODEL

We shall restrict our consideration to the mechanical behavior of incompressible plastic materials in the case of low strains. Assuming that the material is initially isotropic we shall use constitutive equations of the endochronic theory of plasticity [9] which are the modification of

<sup>1</sup> Corresponding author. Email bor@ipp.kiev.ua

Valanis's endochronic theory [8]. Then in the deviatoric Il'yushin's vector space, the basic equations of this theory are

$$\mathbf{s} = s_y \frac{d\mathbf{e}^p}{dz} + \int_0^z J(z-z') \frac{d\mathbf{e}^p}{dz'} dz', \quad (1)$$

$$d\xi = F(z, \Delta\varepsilon^p, l^p, \Phi), \quad (2)$$

$$d\xi^2 = q(d\mathbf{e}^p \cdot d\mathbf{e}^p), \quad (3)$$

where  $s_y$  is the yield stress,  $F$  is the hardening function and  $J(z)$  is the kernel of the integral equation (heredity function). The total strain vector is presented as the sum of elastic and plastic components

$$d\mathbf{e} = d\mathbf{e}^p + \frac{d\mathbf{s}}{2\mu}. \quad (4)$$

In the case of the simple tension-compression loading Eq. (1) can be written as follows:

$$\sigma = \sigma_y \frac{d\varepsilon^p}{dz} + \int_0^z E(z-z') \frac{d\varepsilon^p}{dz'} dz' \quad (5)$$

where  $\sigma_y = \frac{2}{3}s_y$ ,  $E(z) = 3J(z)$ ,  $q = \frac{2}{3}$ ,  $d\xi = d\varepsilon^p$ .

For the cyclically stabilizing materials it is most convenient to use the hardening function

$$F(z) = C - (C-1)e^{-\beta z} \quad (6)$$

and regular heredity function

$$E(z) = E_1 e^{-\alpha z} + E_2 \quad (7)$$

where  $E_1$ ,  $E_2$ ,  $\alpha$  are material characteristics.

To construct a simple model for describing the anisotropy of materials under unsymmetrical loading we assume that the hardening function  $F(z)$  is isotropic. Then the anisotropic behavior arises during nonelastic loading only, and it is characterized by the difference of the kinematic hardening for tension and compression semicycles. Since the strain hardening under unsymmetrical cyclic loading depends on the mode of loading, mean and amplitude stresses of the cycle, one can suggest the dependence of this hardening on both the measure of the deformation process and the stress level attained in the previous semicycle. To take into consideration the latter factor, it is convenient to use the parameter  $\delta$ , proposed by Dafalias and Popov [10]. This parameter is the "distance" in the stress space between the maximum stress state for the given semicycle and the bounding surface. The bounding surface is centered at the origin, grows isotropically each time its stress level is exceeded and represents the highest level of the stress state attained in the loading history. In the uniaxial case the bounding surface is represented by the two lines  $\sigma_B$ , as shown in Fig. 1. Based on the aforesaid, one can write the heredity function as follows:

$$E(z, \delta) = E_1 e^{-\alpha z} + E_2(\delta), \quad (8)$$

which implies the different values  $E_2$  for tension and compression semicycles under unsymmetrical loading.

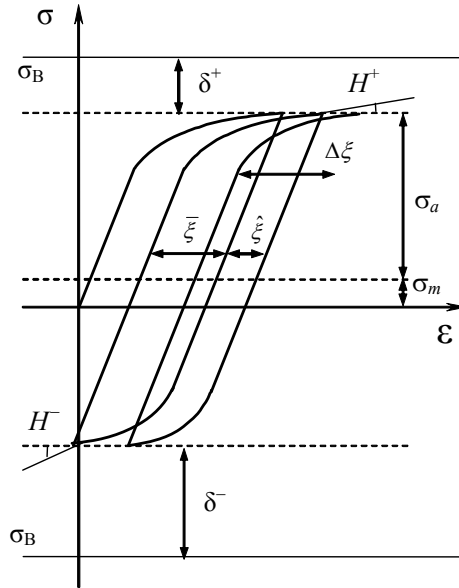


Fig. 1 Block loading scheme and designations

The relationship between the stresses and the internal time (5) under arbitrary uniaxial cyclic loading for  $k$ -th semicycle can be written in the form

$$\sigma = (-1)^k \left[ \sigma_y F(z) + \int_{z_k}^z E(z-z') F(z') dz' \right] + \sum_{i=0}^{z_i} (-1)^i \int_{z_{i-1}}^{z_i} E(z-z') F(z') dz' . \quad (9)$$

We define the current modulus of plasticity as

$$H = \frac{d\sigma}{d\varepsilon^p} = \frac{d\sigma}{dz} \cdot \frac{dz}{d\varepsilon^p} = \left| \frac{d\sigma}{dz} \cdot \frac{1}{F(z)} \right| = \frac{1}{F(z)} \left[ \sigma_y \dot{F}(z) + \int_0^z \dot{E}(z-z') F(z') dz' \right] + E(0) \quad (10)$$

where the overdot denotes the operation of differentiation with respect to  $z$ .

## 2. MODELING OF UNIAXIAL RATCHETING

Let us use the above equations to describe the deformation of specimens fabricated from the AISI 1020 cyclic softening carbon steel and AISI 1026 cyclic stable carbon steel under block loading [3]. The first block was the strain symmetric cycling in the range of 2%. Then the specimens were unloaded to approximately zero stress, after which the control cyclic loading followed with different values of mean and amplitude stresses of the cycle. Numerical modeling of the such loading involved a step-by-step procedure for the control of the deformation process. The baseline experiments and the calculation and experimental techniques for specifying the basic unknown functions and the material constants are described in detail elsewhere [9].

The main peculiarity of the given model is to set the correct functional dependence of parameter  $E_2$  of the heredity function on the  $\delta$  [11, 12] of the preceding semicycle. For initially isotropic materials such dependence can be built on the basis of a single basic experiment performed by complex program. First the strain symmetric loading is performed until the steady state is attained. Then follows the stress unsymmetrical cycling at lower stresses also until the steady state and finally monotone loading to the stress level of the first stage is effected. During the first block we determine the parameter  $E_2$  for  $\delta = 0$ . From the second loading block we can determine the  $E_2$  for the tension and compression semicycles.

We use Eq. (10) to get the plastic modulus under unsymmetrical loading in the steady state case. Then for the arbitrary point  $B$  of the tension semicycle if we use the designation which is accepted in Fig. 1 we can write the equation

$$H^+ = E_1 (1 - U^+) + E_2 (\delta^-), \quad (11)$$

where

$$U^+ = 1 - 2e^{-\alpha\Delta z} \left( 1 - \frac{e^{-\alpha(2\bar{z}+\hat{z})} - e^{-\alpha\bar{z}}}{e^{-\alpha(2\bar{z}+\hat{z})} - 1} \right). \quad (12)$$

The intrinsic time intervals  $\Delta z, \bar{z}, \hat{z}$  correspond the measures  $\Delta\xi, \bar{\xi}, \hat{\xi}$  which connected by the expression  $dz = d\xi/C$ . Now we can readily get the  $E_2(\delta^-)$  value if the modulus  $H^+$  is determined from the experiment. Another  $E_2$  value at the  $\delta^+$  can be found from the equality

$$E_2(\delta^+)_{\bar{\xi}} = E_2(\delta^-)_{(\bar{\xi} + \hat{\xi})} \quad (13)$$

obtained from the theoretical analysis of the steady hysteresis loops at ratcheting with the constant rate.

The shape of the  $E_2(\delta)$  function can be determined after the approximation of the obtained values by the appropriate function. In our case we use dependence in a following form

$$E_2(\delta) = E_2(0) + a\delta^b \cdot D^n \quad (14)$$

where  $a, b$  and  $n$  - parameters of model.

The first summand Eq. (14) is the limiting value that corresponds to  $E_2(\delta)$  on the memory surface, and is determined from experimental date. In the second summand expression (14) first factor  $a\delta^b$  take into account influence on  $E_2(\delta)$  mean stress and second factor -  $D^n$  take into account influence stress amplitude. Parameter  $D$  defined as follows:

$$D = \frac{\sigma_a - \sigma_s}{\sigma_a^{bas} - \sigma_s} \quad (15)$$

where  $\sigma_a$  - amplitude stress,  $\sigma_a^{bas}$  - is the amplitude stress of the basic experiment,  $\sigma_s$  - radius of surface plasticity in the stabilized condition, defined as

$$\sigma_s = \sigma_y F(z \rightarrow \infty) = \sigma_y C \quad (16)$$

### 3. MODEL VERIFICATION

The equations presented above are now used for description of uniaxial block loading of specimens made of cyclically softening CS 1020 and cyclically stable CS 1026 steels. We use the experimental data presented in [3]. In all cases, the first loading block was realized as straining with symmetric cycles and a range of total strains of 2%. In the second block, we applied stress-controlled asymmetric loading with different values of the mean and amplitude stresses.

For numerical analysis, we created a special computational program. It was used to perform all necessary calculation. Parameters of the model for the two studied materials used in calculation contained in the Table 1.

*Table 1 Parameters of the model cyclic plasticity*

Steel	$E$ , ksi	$\sigma_{T1}$ , ksi	$E_1$ , ksi	$E_2(0)$ , ksi	$\alpha$	$C$	$\beta_1$	$\beta_2$
CS1020	25125	40	25298,5	1721	965	0,78	12,4	30
CS1026	26320	20	19600,0	650	1051	0,95	20	20

According to (11) was specified functional dependence  $E_2(\delta)$  on value of  $\delta$  in case of asymmetric cyclic loading studied materials, namely:

$$E_2(\delta) = E_2(0) - 6,3 \cdot 10^{-7} \cdot \delta^6 \cdot D^8 \quad \text{for CS1020}$$

$$E_2(\delta) = E_2(0) - 0,51 \cdot \delta^2 \cdot D^4 \quad \text{for CS1026}$$

The results of numerical calculation are presented in Figs. 2 and 3. In figure 2, we present the results of computation (solid lines), experimental date (doted lines) and results of computation by Hassan and Kyriakides [3] (dashed lines) for CS 1020 steel subjected to asymmetric loading in the form of the dependence of the maximum strain in a cycle on the number of loading cycles for various values of the mean stress (Fig. 2a) and different amplitudes of stress cycles (Fig. 2b). In Fig. 3 results for steel 1026 are accordingly presented.

The comparison of the numerical results with the experimental data shows the efficiency of the proposed model for the description of cyclic creep both in the first loading cycles and in stationary mode. It is worth noting that more precise results were obtained in the case where asymmetric loading is simulated varying the amplitude stress for a constant value of the mean stress. At the same time, all these theoretical predictions are completely covered by spread in the experimental data. For more exact predictions, one may either use other functional dependences for the approximation of the quantities  $E_2$  and  $\delta$  or perform at least two basic tests.

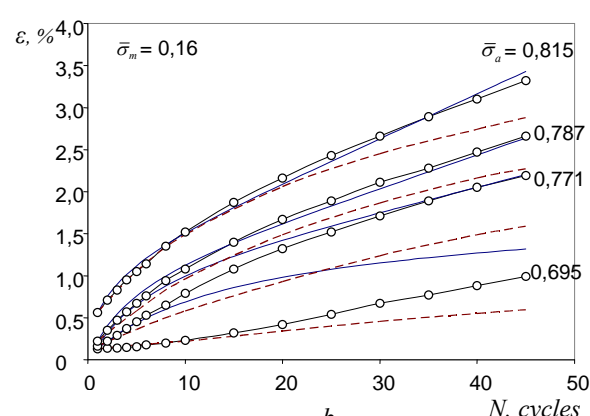
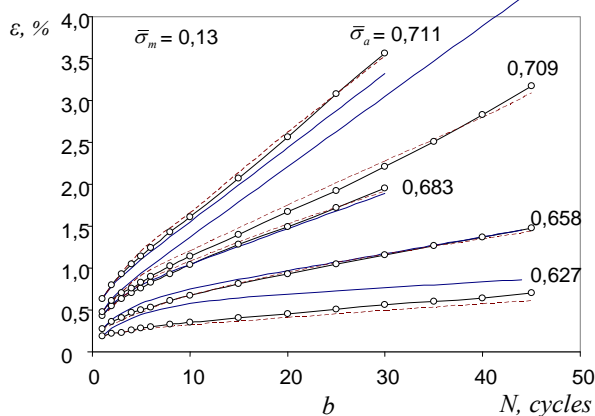
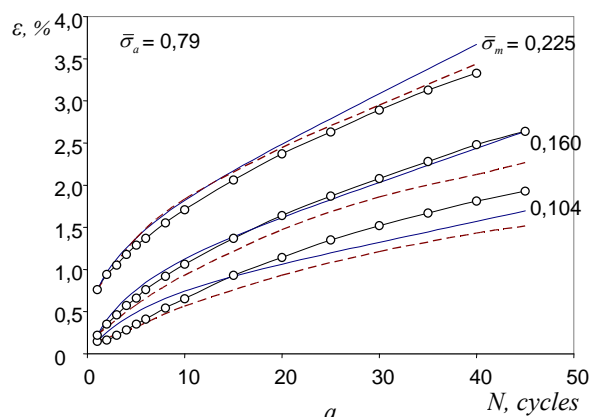
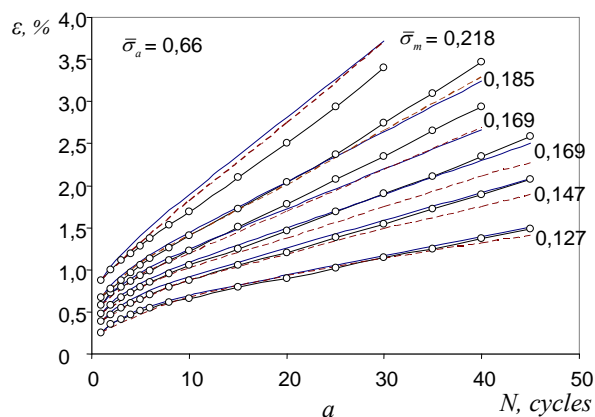


Fig. 2 Dependence of the maximum strain in a cycle on the number of loading cycles for CS 1020 steel

Fig. 3 Dependence of the maximum strain in a cycle on the number of loading cycles for CS 1026 steel

## CONCLUSIONS

Constitutive equations of the endochronic theory of plasticity for describing of the unsymmetrical stress-controlled loading are presented. New rule of the kinematic hardening is introduced for characterizing an induced anisotropy under such loading. A discrete scale of the intrinsic time and the evolutionary equation of the hardening function suggested in the work make it possible to obtain simple constitutive equation for modeling the complex histories of cyclic loading.

Analysis of the modeling results of uniaxial ratcheting testifies we have obtained a satisfactory description of the stress-strain kinetics under unsymmetrical stress cycling.

## REFERENCES

- [1] Coffin L.F. The stability of metals under cyclic plastic strain *Trans ASME D.*, Vol. 82, N. 3. pp. 671-682, 1960.
- [2] Ruggles M.B. Krempl E. The influence of the test temperature on the ratchetting behavior of type 304 stainless steel *ASME J. Engng. Mat. and Techn.*, Vol. 111, p. 318, 1989.
- [3] Hassan T., Kyriakides S. Ratcheting in cyclic plasticity, part I: uniaxial behaviour *Int. J. Plasticity*. Vol. 8, pp. 91–116, 1992.
- [4] McDowell D.L. Stress state dependence of cyclic ratchetting behavior of two rail steels *Int. J. Plasticity*, Vol. 11, p. 397, 1995.
- [5] Chaboche J.L. On some modifications of kinematic hardening to improve the description of ratcheting effects *Int. J. Plasticity*, Vol. 7, pp. 661–678, 1991.
- [6] Ohno N., Wang J.D. Kinematic hardening rules for simulation of ratcheting behaviour. *Eur. J. Mech.*, Vol. 13. p. 519, 1994.
- [7] Tanaka E. A non-proportionality parameter and a viscoplastic constitutive model taking into account amplitude dependences and memory effects of isotropic hardening, *Eur. J. Mech., A/Solids*, Vol. 13, p. 155, 1994
- [8] Valanis K.C. Fundamental consequences of a new intrinsic time measure plasticity as a limit of the endochronic theory, *Arch. Mech.*, Vol. 32, pp. 171-191, 1980.
- [9] Kucher N.K., Borodii M.V. A version of endochronic theory of plasticity for describing non-proportional cyclic deformation, *Int. J. Non-Linear Mech.*, Vol. 28, pp. 267-278, 1993.
- [10] Dafalias Y.F., Popov E.P. Plastic internal variables formalism of cyclic plasticity, *ASME J. Appl. Mech.*, Vol. 43, pp. 645, 1976.
- [11] Borodii M.V. Model of plasticity aimed at the prediction of cyclic creep, *Strength of Materials*, Vol. 30, N. 6. pp. 611-615. 1998.
- [12] Borodii M.V. Modelling of the asymmetric low-cycle loading in the space of stresses, *Strength of Materials*, Vol. 30, N. 5. pp. 472-480. 1998.

## CREEP-DAMAGE BEHAVIOUR OF THIN SHELLS SUBJECTED TO CYCLIC LOADING

**D.Breslavsky**

National Technical  
University 'KhPI', Kharkov,  
Ukraine

**A.Chuprynin,**

Kharkov National  
Academy of Municipal  
Economy, Ukraine

**O.Tatarinova**

National Technical  
University 'KhPI', Kharkov,  
Ukraine

---

### ABSTRACT

---

The paper presents the method of solution for cyclic creep problems of thin shell structures. The non-symmetrical loading and geometry are considered. The method of solution is based on the combination of asymptotic methods and averaging on the period of cyclic loading. The variational problem statement had been done and the FEM home-made code was used for numerical simulation of thin shell structures. The long-term strength in cyclic creep conditions of the flue pipe of jet engine was studied numerically and the distributions of displacements, forces and damage parameter were obtained.

---

### INTRODUCTION

Structural thin shell elements are common in modern high-temperature technique. Operation of gas turbine engines, pipes, blocks of power machines and chambers of engines, heat exchangers, reactor equipment etc under the joint action of the quasi-static and cyclic loading is accompanied by development of irreversible creep strains and damage accumulation. Creep of materials under cyclic loading is attributed to cyclic creep, but depending on the frequency and level of loading the different types of creep and damage accumulation are observed. Thus, under cyclic loading with a frequency  $f \geq 1 \dots 3$  Hz the rate of creep does not depend on the frequency of cyclic processes, and the fracture occurs due to creep mechanisms. Such creep phenomenon by the classification of S.Taira and R. Oh-tani [1] is called the dynamic creep. The number of cycles to failure in this case, as a rule, exceeds  $N = 10^5$  cycles. In conditions of low-cycle creep, when  $N < 10^5$ , stress periods are a lot more (seconds or hours).

In connection with the special requirements for durability and reliability of structures, the significant results in creep-damage calculations are currently obtained [2-4]. However, the description of the stress-strain state of structures subjected to cyclic loading with the joint action of loads with different periods, remain poorly understood. The methods for estimation of an influence of mono- and polyharmonic loading with frequencies  $\approx 1 \dots 3$  Hz on creep -damage processes in plates and shells were discussed in [2-4]. This paper contains the problem statement and methods for solving problems of creep and damage accumulation in thin shells under combined cyclic loading with very different periods.

### 1. CREEP AND DAMAGE IN THE CASE OF COMBINED CYCLIC LOADING

Let us consider the combined cyclic loading  $\sigma = \sigma_0 + \sigma_1 + \sigma_2$  with simultaneous action of a constant stress  $\sigma_0$ , slowly changing stress  $\sigma_1$  with the cyclic frequency  $f_1$  of the cycle period  $T$  and stress  $\sigma_2$  which is rapidly changing with the frequency  $f_2$  (exceeding 1 Hz).

In general, stress  $\sigma_1$  is determined by the parameters of the operating cycle (e.g. flight cycle for aircraft engine) with the slowly increasing and decreasing amplitude. Within such a cycle the stress in structural elements are usually accompanied by rapidly changing cyclical stress (e.g., caused by vibrations) which leads to the development of dynamic creep. This paper discusses the combined loading, which activates the creep-damage mechanisms are corresponding to the combined action of the dynamic and low-cycle creep.

Thus, the stress law for the combined cyclic loading can be written in the following form:

$$\sigma = \sigma^0 + \sigma^1 + \sigma^2 = \sigma^0 \left( 1 + \sum_{k=1}^{\infty} M_k \sin\left(\frac{2\pi k}{T}t + \beta_k\right) + A \sin\left(\frac{2\pi}{T_2}t\right) \right) \quad (1)$$

where  $A = \frac{\sigma^a}{\sigma^0}$ ;  $M_k = \frac{\sigma^{ak}}{\sigma^0}$  - are the amplitude coefficients in dynamic and cyclic creep processes correspondently,  $\sigma^0 \neq 0$

Let us regard the Bailey-Norton flow rule and Kachanov-Rabotnov damage equation for single stress state:

$$\dot{c} = B \frac{(\sigma)^n}{(1-\omega)^k}; \dot{\omega} = D \frac{(\sigma)^r}{(1-\omega)^l}, \quad \omega(0) = 0, \quad \omega(t_*) = \omega_*, \quad (2)$$

where  $c(t)$ ,  $\omega(t)$  are irreversible creep strain and damage parameter;  $\omega_*$  is the damage parameter's value in the moment of the finishing of hidden damage accumulation process  $t_*$ .

To describe the processes of creep and damage accumulation for the combined loading the technique of asymptotic expansions and averaging on the period proposed in [2] was applied.

Asymptotic expansions on the small parameter  $\mu = T/t$  allow to present the processes in two time scales, the 'slow'  $t$  and the 'fast'  $\xi$ ,  $\xi = \tau/T$ ,  $\tau = t/\mu$ , in the following form :

$$c \cong c^0(t) + \mu c^1(\xi), \quad \omega \cong \omega^0(t) + \mu \omega^1(\xi), \quad (3)$$

where  $c^0(t)$ ,  $\omega^0(t)$  are the functions which correspond to basic 'slow' creep and damage process as well as we have for 'fast' periodic processes the functions  $c^1(\xi)$ ,  $\omega^1(t, \xi)$ . Considering that the creep and damage due to creep depend only on the slow time, after averaging over the period we have:  $\langle c^1(\xi) \rangle \cong 0$ ,  $\langle \omega^1(\xi) \rangle \cong 0$ , and we can escape from 'fast' time'  $\xi$  in the expansions (3).

In this case of cyclic combined loading the creep-damage equations are accepted as follows:

$$\dot{c}_{ij} = B g_n K_n \frac{3(\sigma_i^0)^{n-1}}{2(1-\omega)^k} S_{ij}^0, \quad \dot{\omega} = D g_r K_r \frac{(\sigma_e^{\omega 0})^r}{(1-\omega)^l}, \quad \omega(0) = 0, \quad \omega(t_*) = 1, \quad (4)$$

where

$$g_n = \int_0^1 \left( 1 + \sum_{k=1}^{\infty} M_k \sin(2\pi k \xi + \beta_k) \right)^n d\xi, \quad K_n = \int_0^1 (1 + A_n \sin(2\pi \xi))^n d\xi, \quad A_n = \frac{A}{g_n^{1/n}};$$

$$g_r = \int_0^1 \left( 1 + \sum_{k=1}^{\infty} M_k \sin(2\pi k \xi + \beta_k) \right)^r d\xi, \quad K_r = \int_0^1 (1 + A_r \sin(2\pi \xi))^r d\xi, \quad A_r = \frac{A}{g_r^{1/r}};$$

are the functions of the stress cycle asymmetry coefficients:  $A = \frac{\sigma_e^a}{\sigma_e^0}$ ,  $M_k = \frac{\sigma_e^{ak}}{\sigma_e^0}$ ;  $B$ ,  $D$ ,  $n$ ,  $r$ ,  $k$ ,  $l$  are the constants in creep-damage laws, determined for fixed temperature  $T^0$  by creep and long term strength curves;  $S_{ij}^0$  are the components of stress tensor  $\sigma_{ij}^0$ .

## 2. PROBLEM STATEMENT FOR CREEP OF CYCLICALLY LOADED THIN SHELLS

Let us formulate the problem by use of described in [2-4] approach, under which the original problem is reduced to solving two related initial-boundary problems. The first of them corresponds to the problem of forced vibrations of elastic shells under harmonic loading. The second one, which describes the creep under a static component of the load jointly with the state equations (4). These problems are connected by calculated amplitude stress cycle asymmetry coefficients.

Let us consider a shell of revolution with arbitrary generatrix in non-axisymmetric stress-strain state in creep conditions. Due to using of FEM, let us cover the surface of the shell by the set of conical surfaces, using piecewise linear approximation of the generatrix.

For common used designations of displacements  $\mathbf{u}$  ( $u, v, w$ ), curvature variations  $\chi$ , strains  $\boldsymbol{\varepsilon}$  etc the geometrical relations can be written:

$$\begin{aligned} \varepsilon_{11} &= \varepsilon_{11}^m + z\chi_{11}; \quad \varepsilon_{22} = \varepsilon_{22}^m + z\chi_{22}; \quad \varepsilon_{12} = \varepsilon_{12}^m + 2z\chi_{12}; \\ \varepsilon_{11}^m &= \frac{\partial u}{\partial s}; \quad \varepsilon_{22}^m = \frac{\partial v}{r\partial s} + \frac{u}{r}\cos\alpha + \frac{w}{r}\sin\alpha; \quad \varepsilon_{12}^m = \frac{\partial u}{r\partial\varphi} + \frac{\partial v}{\partial s} - \frac{v}{r}\cos\alpha; \\ \chi_{11} &= \frac{\partial^2 w}{\partial s^2}, \quad \chi_{22} = \frac{\partial^2 w}{r^2\partial\varphi^2} + \frac{\cos\alpha}{r}\frac{\partial w}{\partial s} - \frac{\sin\alpha}{r^2}\frac{\partial v}{\partial\varphi}; \quad \chi_{12} = 2\frac{\partial^2 w}{r\partial s\partial\varphi} - \frac{\partial w}{r^2\partial\varphi}\cos\alpha + \frac{v}{r^2}\sin\alpha\cos\alpha - \frac{\partial v}{\partial s}\frac{\sin\alpha}{r}, \end{aligned} \quad (5)$$

where  $\alpha$  is an angle between the axis of revolution and the generatrix;  $r$  is a distance from axis of revolution to shell middle surface.

In a creep conditions the total strain at the shell point consists of elastic and irreversible parts:  $\varepsilon_{ij} = e_{ij} + c_{ij}$ ,  $i, j = 1, 2$ . So, let us write the physical law in the following form:

$$\sigma_{11} = \frac{E}{1-\nu^2}(\varepsilon_{11} + \nu\varepsilon_{22}) - \frac{E}{1-\nu^2}(c_{11} + \nu c_{22}); \quad \sigma_{22} = \frac{E}{1-\nu^2}(\varepsilon_{22} + \nu\varepsilon_{11}) - \frac{E}{1-\nu^2}(c_{22} + \nu c_{11}); \quad \sigma_{12} = G\varepsilon_{12} - Gc_{12}, \quad (6)$$

where  $E, G$  are the Young and shear modulus correspondently,  $\nu$  is the Poisson ratio.

Substituting the expression (5) into (6), let us connect the membrane forces  $N_{ij}$ , bending and torsional moments  $M_{ij}$  with the geometrical unknowns:

$$\begin{aligned} N_{11} &= \frac{Eh}{1-\nu^2}(\varepsilon_{11}^m + \nu\varepsilon_{22}^m) - N_{11}^c; \quad N_{22} = \frac{Eh}{1-\nu^2}(\varepsilon_{22}^m + \nu\varepsilon_{11}^m) - N_{22}^c; \quad S = Gh\varepsilon_{12}^m - S^c; \\ M_{11} &= D(\chi_{11}^m + \nu\chi_{22}^m) - M_{11}^c; \quad M_{22} = D(\chi_{22}^m + \nu\chi_{11}^m) - M_{22}^c; \quad H = D(1-\nu)\chi_{12}^m - H^c. \end{aligned} \quad (7)$$

$$\begin{aligned} \text{Here } N_{11}^c &= \frac{E}{1-\nu^2} \int_{-h/2}^{h/2} (c_{11} + \nu c_{22}) dz; \quad N_{22}^c = \frac{E}{1-\nu^2} \int_{-h/2}^{h/2} (c_{22} + \nu c_{11}) dz; \quad S^c = \frac{E}{2(1+\nu)} \int_{-h/2}^{h/2} c_{12} dz; \\ M_{11}^c &= \frac{E}{1-\nu^2} \int_{-h/2}^{h/2} (c_{11} + \nu c_{22}) z dz; \quad M_{22}^c = \frac{E}{1-\nu^2} \int_{-h/2}^{h/2} (c_{22} + \nu c_{11}) z dz; \quad H^c = \frac{E}{2(1+\nu)} \int_{-h/2}^{h/2} c_{12} z dz \end{aligned}$$

are the additional power factors, caused by irreversible creep strains of metal.

By use the Lagrange variational principle and equations (5) and (7), the variational equality is obtained:

$$\int_S (b_{ijkl} \varepsilon_{ij}^m \delta \varepsilon_{ij}^m - d_{ijkl} \chi_{kl} \delta \chi_{ij}) dS - \int_S p \delta w dS - \int_S N_{ij}^c \delta \varepsilon_{ij}^m dS + \int_S M_{ij}^c \delta \chi_{ij} dS = 0, \quad (8)$$

here  $\delta \varepsilon_{ij}^m$  and  $\delta \chi_{ij}$  are the variations of the total strain components as well as curvature variation in the shell;  $p$  is the vector of loading;  $\delta w$  is the variation of normal displacements.

$$b_{ijkl} = \frac{Eh}{1-\nu^2} \left( \delta_{ik} \delta_{jl} \frac{1-\nu}{2} + \nu \delta_{ij} \delta_{kl} \right); \quad d_{ijkl} = \frac{Eh^3}{12(1-\nu^2)} \left( \delta_{ik} \delta_{jl} \frac{1-\nu}{2} + \nu \delta_{ij} \delta_{kl} \right).$$

Let us use for this problem solution the FEM approach with 4-nodal finite element of conical shell [5]. The shape functions of third order are used. Using vector-matrix representation of relations (5-8), we finally obtain the variational equation in the following form :

$$\frac{1}{2} \left( \int_S \delta \boldsymbol{\varepsilon}^T [E] \boldsymbol{\varepsilon} dS \right) - \int_S \left( \left( N_1 \frac{\partial w}{\partial s} \right)_{,1} + \frac{1}{r} \left( S \frac{\partial w}{\partial \varphi} \right)_{,1} + \frac{1}{r} \left( S \frac{\partial w}{\partial s} \right)_{,2} + \frac{1}{r^2} \left( N_2 \frac{\partial w}{\partial \varphi} \right)_{,2} \right) \delta w dS - \int_S \delta \{u\}^T \{p\} dS = 0, \quad (9)$$

where  $[E]$  is the matrix of elasticity.

Equilibrium condition in a node leads to the summation of the components of internal and external forces on all elements containing this node. Hence, substituting in equation (9) the integration over the shell by a sum of integrals over finite elements, we obtain:

$$\sum_e \frac{1}{2} \int_{S^e} (\delta\{q\}^T [D]^T [E] [D] \delta\{q\}) dS - \sum_e \int_{S^e} (\delta\{q\}^T [D]^T [P_m] \{c_m\}) dS - \sum_e \int_S (\delta\{q\}^T [B]^T \{p^p\}) dS - \sum_e \int_S (\delta\{q\}^T [B]^T \{p\}) dS = 0, \quad (10)$$

where  $\{q\}$  is a vector of nodal displacements in the element  $e$ .

Thus, the use of FEM allows reduce the variational equality (10) to a system of linear algebraic equations

$$[K]\{\Delta\} = \{P^v\} + \{P^c\} + \{P^p\} + \{P^n\}, \quad (11)$$

where  $[K]$  is a global stiffness matrix;  $\{P^v\}$  is a vector of external nodal forces,  $\{P^v\} = \sum_e \int_{S^e} [\Phi]^T \{p\} dS$ ;  $\{P^c\}$  is a vector of nodal forces, caused by creep strains,

$\{P^c\} = \sum_e \int_{S^e} [B]^T [R] \{c\} dS$ ,  $\{P^p\}$  is a vector of nodal forces caused by projection of generalized forces

on the shell's normal,  $\{P^p\} = \sum_e \int_{S^e} [\Phi]^T \{p^p\} dS$ ;  $\{P^n\}$  is a vector of nodal forces caused by non-linear

components of elastic strains,  $\{P^n\} = \sum_e \int_{S^e} [B]^T [R] \{\varepsilon_n\} dS$ .

To describe the processes of high temperature creep and the associated damage, which take place in shells, let us use the constitutive equations (4). As was shown, in order to use them we need to obtain the distributions of amplitude stresses. So, the problem of forced oscillations has to be solved.

In these problems it is necessary to determine the mass matrix of the system:  $[M] = \sum_e \int_V [B]^T \rho [B] dS$ .

Then the basic equation has to be following:

$$([K] - \Omega^2 [M])\{q_a^k\} = \{P_a^k\}, \quad (12)$$

where  $([K] - \Omega^2 [M])$  is a matrix of 'dynamic stiffness' of the system;  $\{q_a^k\}$  is a vector of amplitude values of nodal displacements. The components of the vector  $\{P_a^k\}$  are determined by amplitude values of load's harmonic part:  $p(t) = p_0 + p_a \sin(2\pi f_2 t)$ .

The system (12) is solved relatively  $\{q_a^k\}$  by the frontal method, and further the amplitude von Mises equivalent stresses are determined. The system of algebraic equations (12) is solved by Cholesky method.

The presented method for cyclic creep-damage simulation in thin shell structures is realized as application package for IBM-type computers.

### 3. ESTIMATION OF LONG-TERM STRENGTH OF AVIATION GAS TURBINE CORPS

Let us consider the results of numerical studies in the cyclic creep and damage in the flue pipe of gas turbine engine AI-20. By use of the developed software let us simulate it by the combination of cylindrical and conical shells. FE model consists of 650 elements is presented on the Fig. 1.

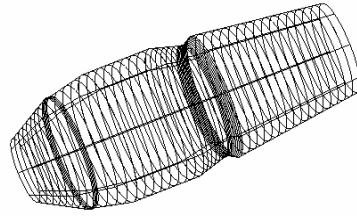


Fig. 1 FE model of flue pipe of gas turbine engine AI-20

The working temperatures of flue pipes are 700-900°C [6]. Therefore, for the their manufacturing the high-temperature steels EI435 and EI437B are used. The flue pipe made from EI437B steel was studied. The material constants for constitutive equations (4), which were obtained after the processing of test data, are:  $B=1.31 \times 10^{-6} \text{MPa}^{-n}/\text{h}$ ,  $n=k=4.12$ ,  $D=2.08 \times 10^{-5} \text{MPa}^{-r}/\text{h}$ ,  $r=l=4.5$ . Simulation was performed for following values: length is 2 m, initial diameter of burning zone is 0.4 m, the nozzle angle is 37°, diameter of cylindrical part of primary zone is 0.8 m; exit diameter of secondary part is 0.7 m with nozzle angle 7°. The height of walls is 0.001 m.

Two types of loading were considered. First one is connected with high frequency oscillations caused by fuel burning. The second type of loading is connected with plane evolution and acceleration.

Distribution of pressure in the combustion chamber of modern aircraft matches the form of the cycle, which is shown in Fig.2 [7].

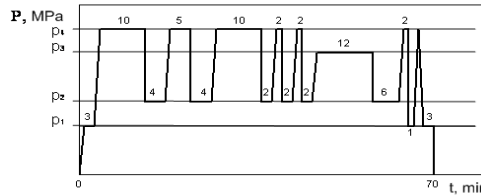


Fig. 2 Typical flying cycle

So, to calculate the stress-strain state of GTE and its long term strength in creep conditions let us consider the joint action of static load  $p_0$ , cyclic load component similar to shown in Fig. 2 and harmonic loading with amplitude value  $p_a$ , which is caused by wall vibration in primary-combustion zone:

$$p(t) = p_0 + \sum_{k=1}^{\infty} \frac{2}{\pi k} \sin\left(\frac{2\pi k}{T} t\right) \left( p_1 (1 - \cos(\pi k)) + (p_1 - p_2) \left( \cos\left(\frac{33\pi k}{35}\right) - \cos\left(\frac{3\pi k}{70}\right) \right) + \right. \\ \left. (p_3 - p_4) \left( \cos\left(\frac{11\pi k}{35}\right) + \cos\left(\frac{18\pi k}{35}\right) + \cos\left(\frac{13\pi k}{70}\right) - \cos\left(\frac{13\pi k}{35}\right) - \cos\left(\frac{32\pi k}{35}\right) + \cos\left(\frac{22\pi k}{35}\right) - \cos\left(\frac{3\pi k}{5}\right) - \right. \right. \\ \left. \left. - \cos\left(\frac{17\pi k}{70}\right) + \cos\left(\frac{4\pi k}{7}\right) - \cos\left(\frac{19\pi k}{35}\right) + (p_4 - p_3) \left( \cos\left(\frac{23\pi k}{35}\right) - \cos\left(\frac{29\pi k}{35}\right) \right) \right) \right) + p_a \sin(2\pi f_2 t). \quad (13)$$

The influence of the vibrations for secondary zone is negligible, so for it the last summand in (13) can be omitted.

The numerical simulation of long term strength of the considered flue pipe had been performed, the determined time to fracture is equal to 660 h. The results are presented on Figs.3 – 6. Curve 1 had been built for the initial time moment as well as curve 2 corresponds to the time 660 h, when the process of hidden damage accumulation was finished. Fig.3 and 4 contain the distribution of normal and axial displacements along the flue pipe. Fig 5 and 6 contain the distribution of axial and circumferential forces.

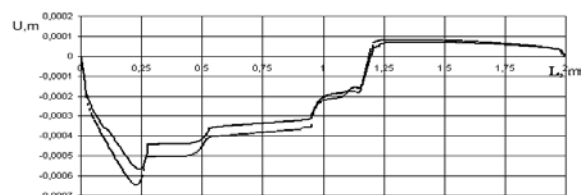
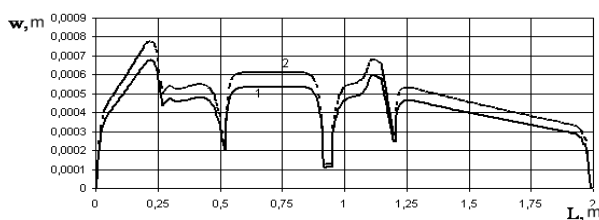


Fig. 4 Axial displacement along the flue

Fig. 3 Normal deflection along the flue pipe

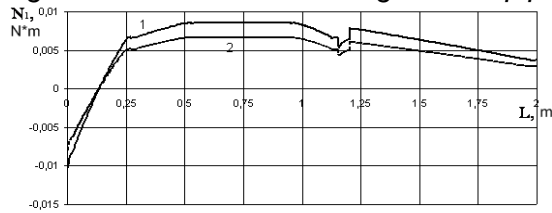


Fig. 5 Axial force distribution

The damage parameter's distribution on outer surface of flue pipe is presented in Fig. 7. Here the Fig 7,a contains the data for first 10 hours of damage accumulation, Fig. 7,b corresponds to  $t=660 h$ .

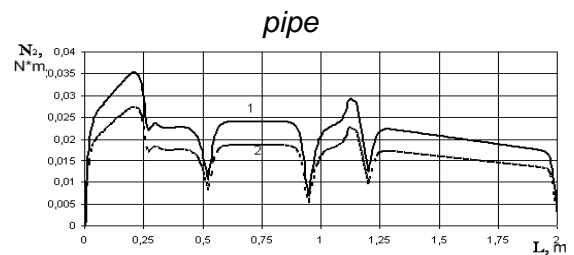


Fig. 6 Circumferential force distribution



a – 10 hours; b – fracture moment,  $t=660$  hours

Fig. 7 Damage distribution on the outer surface of flue pipe

Deformation feature of the considered flue pipe is the fact, that irreversible normal and axial displacements are very small (0.1mm) that visually in operation cannot be noticed. However, the damage accumulation proceeds just due to creep mechanisms.

Thus, the result of numerical simulation of the cyclic creep in flue pipe of gas turbine engine is the place, where fracture occurs. This one corresponds to the burning zone. Analysis of the distribution of damage parameter shows that in the shell presents another area with its very large values - the region of transition between primary and secondary zones ( $\omega = 0.58 - 0.68$ ). When some design parameters and values that characterize the load will be changed, it is very likely macro-crack occurrence and in this place.

## REFERENCES

- [1] Taira S., Ohtani R. *Theory of high-temperature strength of materials*, Metallurgia Publ., Moscow, 1986. (In Russian)
- [2] Morachkovsky O.K. About non-linear problems of creep under the action of fast oscillating field *Appl.Mech*, Vol. 28, No 8, pp. 17-23, 1992. (In Russian)
- [3] Altenbach H., Breslavsky D., Morachkovsky O., Naumenko K. Cyclic Creep-Damage in Thin-Walled Structures *Journal of Strain Analysis for Engineering Design*, Vol.35, No 1, pp. 1-11, 2000.
- [4] Breslavsky D.V., Morachkovsky O.K., Tatarinova O.A. High-temperature creep and long-term strength of structural elements under cyclic loading *Strength of Materials*, Vol. 40, pp. 531-537, 2008.
- [5] Usyukin V.I. *Structural mechanics of spacecrafts*. - Moscow.: Mashinostroenie, 1988. (In Russian)
- [6] Hyde T.H., Xia L., Becker A.A.. Prediction of creep failure in aeroengine materials under multi-axial stress states *Int. j. Mech. Sci*, Vol. 38, No 4, pp. 385-403, 1996.
- [7] Collins J.A. *Failure of Materials in Mechanical Design: Analysis, Prediction, Prevention*, Sec. Ed. NY: Jonn Wiley and Sons, 1993.

**HIGH TEMPERATURE CREEP AND DAMAGE ACCUMULATION IN  
CYCLICALLY LOADED AXISYMMETRICAL BODIES OF REVOLUTION**

**D.Breslavsky**

**Yu.Korytko**

**O.Morachkovsky**

National Technical  
University 'KhPI', Kharkov,  
Ukraine

---

**ABSTRACT**

---

The paper presents the constitutive equations as well as the data of numerical simulation of creep-damage problems of cyclically loaded and heated axisymmetrical structural members. The procedure of constitutive equations deriving is discussed. The experimental and numerical data have been obtained for cyclically heated specimens made from high-quality steel were compared in order to verify the flow rule and damage parameter equation. The problem of creep and damage accumulation in the nipples of the regenerator for catalytic cracking of petroleum was analyzed with consideration of different temperature cycle parameters.

---

**INTRODUCTION**

The study of high-temperature long term behaviour of structural members, which calculation schemes correspond to bodies of revolution, needs significant efforts due to necessity of their safety ensuring. One of the important cases of such behaviour includes the joint action of static and cyclic stress and temperature fields. The creep-damage processes in materials and structures, which are working under similar conditions, are often the reason of lifetime limitation.

The creep-damage studies of materials are working under cyclic loading, have been started in 1970<sup>th</sup> for general type of the cycle, characterizing by introduction of elastic, plastic and creep strain [1]. A great amount of investigations has been done in this direction [1, 2].

From the other hand, the design procedure of major types of structural members demands the absence of plastic strains in initial moments of their work. This fact allows to essentially simplify the general procedure of cyclic creep-damage analysis.

The papers [3, 4] contains the mathematical problem statements and methods of solution for different cases of joint action of static and cyclic stresses, where the assumption of non-varying temperature distribution has been used. The real working conditions of structures which are used in nuclear, power and chemical industry are characterized by temperature variation through their operational cycle.

The aim of presented paper is to discuss the method for creep-damage simulation of bodies of revolution, subjected to cyclic stress loading and cyclic heating. The constitutive equations, which are using for calculations, were obtained by use of asymptotic expansions method and verified by numerous experimental investigations, foremost of S.Taira [5] and G.Guarnieri [6]. The numerical simulation of high-temperature creep-damage in nipple of petroleum cracking's regenerator will be considered as an example.

**1. CREEP-DAMAGE ASSESSMENT METHOD. CONSTITUTIVE EQUATIONS**

For creep and damage calculations under complex stress state the cyclic creep constitutive equations were suggested in [3]. Combined cyclic loading with constant and cyclically varied stress components were considered and obtained results were experimentally verified.

Creep of metal specimen will be regarded by use of general kinetic structural parameters theory, developed by Yu.N.Rabotnov [7]. Bailey-Norton and Rabotnov-Kachanov equations were

accepted for uniaxial creep-damage law. Widely spread exponential form of temperature dependence was used [1, 7]:

$$\dot{c} = B \frac{(\sigma)^n}{(1-\omega)^k} \exp\left(\frac{-H}{R\varphi}\right); \quad \dot{\omega} = D \frac{(\sigma)^r}{(1-\omega)^l} \exp\left(\frac{-H}{R\varphi}\right); \quad \omega(0) = \omega_0, \quad \omega(t_*) = \omega_*. \quad (1)$$

Here  $c(t)$  is irreversible creep strain;  $\omega(t)$  is damage parameter;  $B, D, n, r, k, l$  are material constants identified by experimental creep and long-term strength material curves;  $H$  is the activation energy of creep processes in material;  $R$  is the universal gas constant;  $\omega_*$  is the value of damage parameter in the end of hidden failure at time moment  $t_*$ .

Constitutive equations included creep strain rate and damage accumulation dependence from cyclically varied stress were obtained in [3] on the base of two time scale method and asymptotic expansions with averaging on the period in the following form:

$$\dot{c} = B g_n \frac{(\sigma^0)^n}{(1-\omega)^k}, \quad g_n = \int_0^1 \left(1 + \sum_{k=1}^{\infty} M_k \sin(2\pi k \xi)\right)^n d\xi, \quad (2)$$

$$\dot{\omega} = D g_r \frac{(\sigma^0)^r}{(1-\omega)^l}, \quad \omega(0) = \omega_0, \quad \omega(t_*) = \omega_*, \quad g_r = \int_0^1 \left(1 + \sum_{k=1}^{\infty} M_k \sin(2\pi k \xi)\right)^r d\xi. \quad (3)$$

Here  $g_n, g_r$  are the coefficient functions of cyclic loading amplitudes.

Let us use the similar approach for obtaining the flow rule for creep strain and kinetic damage law for the case of cyclically varying temperature.

Combined cyclic temperature  $\varphi = \varphi^0 + \varphi^1$  will be considered, where  $\varphi^0$  is a constant temperature and  $\varphi^1$  is a cyclically varying one. Temperature  $\varphi^1$  can be presented as a Fourier periodical series, than law for cyclic temperature will have a next form:

$$\varphi = \varphi^0 + \varphi^1 = \varphi^0 \left(1 + \sum_{l=1}^{\infty} M_l^T \sin\left(\frac{2\pi l}{T} t + \beta_l^T\right)\right). \quad (4)$$

The  $M_l^T = \frac{\varphi^{al}}{\varphi^0}$  denotes the asymmetry parameter of temperature cycle. It corresponds to the ratio of amplitude temperature to static temperature value, which takes place through the period of cycle.

Incompatibility of main and cyclic periods of combined temperature action allowed to use the methods of asymptotic expansions and averaging on the period of temperature cycle for simulation of cyclic creep and damage accumulation.

Firstly the deformation under constant stress will be considered. Let us use the assumption about the essential exceeding of the general duration of creep process  $t_*$  comparing with period value  $T$  of temperature  $\varphi$  cyclic component. So why small parameter  $\mu = \frac{T}{t_*} \ll 1$  and two time scales were put into consideration. First one will be denoted by  $t$  and corresponds to main creep process, second time  $\xi = \frac{t}{T}$  will be the time of the temperature cycle,  $0 \leq \xi \leq 1$ .

Asymptotic solutions can be written in the form of small parameter expansions:

$$c \cong c^0(t) + \mu c^1(\xi), \quad (5)$$

$$\omega \cong \omega^0(t) + \mu \omega^1(\xi), \quad (6)$$

where  $c^0(t)$ ,  $\omega^0(t)$ ,  $c^1(\xi)$ ,  $\omega^1(\xi)$  are functions of main creep-damage process in ‘slow’ time scale and periodically process in ‘fast’ time scale  $\xi$ .

Taking into account, that creep strain and creep damage parameter depend only on ‘slow’ time and their averaged on the period  $T_\phi$  of ‘fast’ time  $\xi$  values are equal to zero:

$$\langle c^1(\xi) \rangle = \int_0^1 c^1(\xi) d\xi \cong 0, \quad \langle \omega^1(\xi) \rangle = \int_0^1 \omega^1(\xi) d\xi \cong 0, \quad (7)$$

only ‘slow’ time remains in expansions (5), (6).

Thus, for cyclic temperature varying, by use of asymptotic expansions technique [5] for equations (1) after averaging on the cycle period  $T$ , the following expressions were obtained:

$$\dot{c} = B g_n^T \frac{(\sigma^0)^n}{(1-\omega)^k}, \quad g_n^T = \int_0^1 \exp \left( \frac{-Q}{\varphi^0 \left( 1 + \sum_{l=1}^{\infty} M_l^T \sin(2\pi l \xi) \right)} \right) d\xi, \quad (8)$$

$$\dot{\omega} = D g_r^T \frac{(\sigma^0)^r}{(1-\omega)^l}, \quad \omega(0) = \omega_0, \quad \omega(t_*) = \omega_*, \quad g_r^T = \int_0^1 \exp \left( \frac{-\bar{Q}}{\varphi^0 \left( 1 + \sum_{l=1}^{\infty} M_l^T \sin(2\pi l \xi) \right)} \right) d\xi, \quad (9)$$

Here  $g_n^T$ ,  $g_r^T$  are the coefficient functions of cyclic heating.

For more complex processes of combined action of cyclic stress and temperature varying the new cyclic thermal creep constitutive equations were obtained:

$$\dot{c} = B g_n g_n^T \frac{(\sigma^0)^n}{(1-\omega)^k}; \quad \dot{\omega} = D g_r g_r^T \frac{(\sigma^0)^r}{(1-\omega)^l}, \quad \omega(0) = \omega_0, \quad \omega(t_*) = \omega_*. \quad (10)$$

Equations (10) were generalized to the case of complex stress state:

$$\dot{c}_{ij} = \frac{3}{2} B \frac{(\sigma_i^0)^{n-1} g_n g_n^T}{(1-\omega)^k} s_{ij}^0, \quad \dot{\omega} = D g_r g_r^T \frac{(\sigma_e^0)^r}{(1-\omega)^l}, \quad \omega(0) = \omega_0, \quad \omega(t_*) = \omega_*. \quad (11)$$

Here  $c_{ij}$  denotes the components of creep strain tensor,  $s_{ij}^0$  are the stress deviator components;  $\sigma_e^0$  and  $\sigma_i^0$  are equivalent stress defined from definite strength criterion and von Mises equivalent stress respectively.

Obtained constitutive equations allow to perform the mathematical definition of non-linear material straining under joint cyclic loading and heating.

## 2. VERIFICATION OF CONSTITUTIVE EQUATIONS

Numerical cyclic creep and damage curves, were obtained by use of constitutive equations (10) were verified by use of different experimental data [5, 6]. Cyclic creep-damage behavior of steels, titanium and nickel-based alloys were analyzed. Some comparisons of creep and damage curves were obtained under cyclic heating had been analyzed in [3].

Here let us present only one example of creep and long-term strength curves of the 1H18N9T steel (which is similar to USA S 321 steel), had been obtained numerically in this paper and experimentally by authors of [8].

After experimental curves processing for temperature range 913–1013 K, the values of material constants for constitutive equations (10) were found:  $B=1.94 \times 10^7$  MPa<sup>n</sup>/min,  $Q=3.56 \times 10^4$  K,  $D=0.118$  MPa<sup>m</sup>/min,  $\bar{Q}=3.4 \times 10^4$  K,  $n=2.35$ ,  $m=5.86$ ,  $k=l=1.12$ .

Temperature was varied by triangular law [8] with cycle parameters  $\varphi_0 = 913$  K;  $\varphi_a = 20 - 100$  K. Minimum cycle temperature were 913K for all cycles, maximum cycle temperature were 1013K for cycle 1, 993K for cycle 2, as well as 973K, 953K and 933 K for 3<sup>rd</sup>, 4<sup>h</sup> and 5<sup>th</sup> cycles respectively.

Let us analyze the cyclic creep data. For cycles 3, 4 and 5 the creep strain curves were obtained by use equations (10) and compared with experimental data from [8] (scattered in fig. 1). Here curve 1 means to maximum cycle temperature 973K (cycle 3), curve 2 and 3 corresponds to 4th and 5th cycles

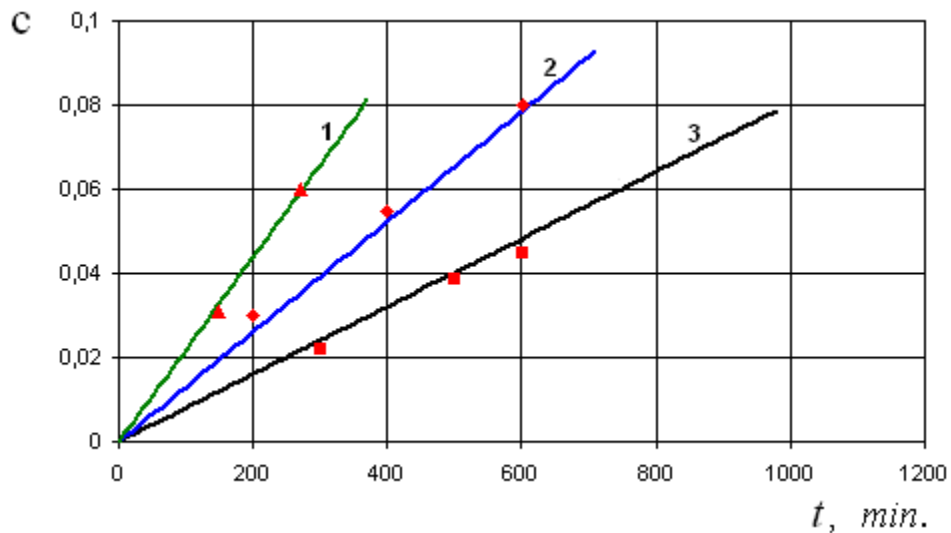


Fig. 1 Cyclic creep curves for steel 1H8N9T

Fig. 2 contains the long-term strength curves for all temperature cycles 1-5. Experimental data are scatter presented.

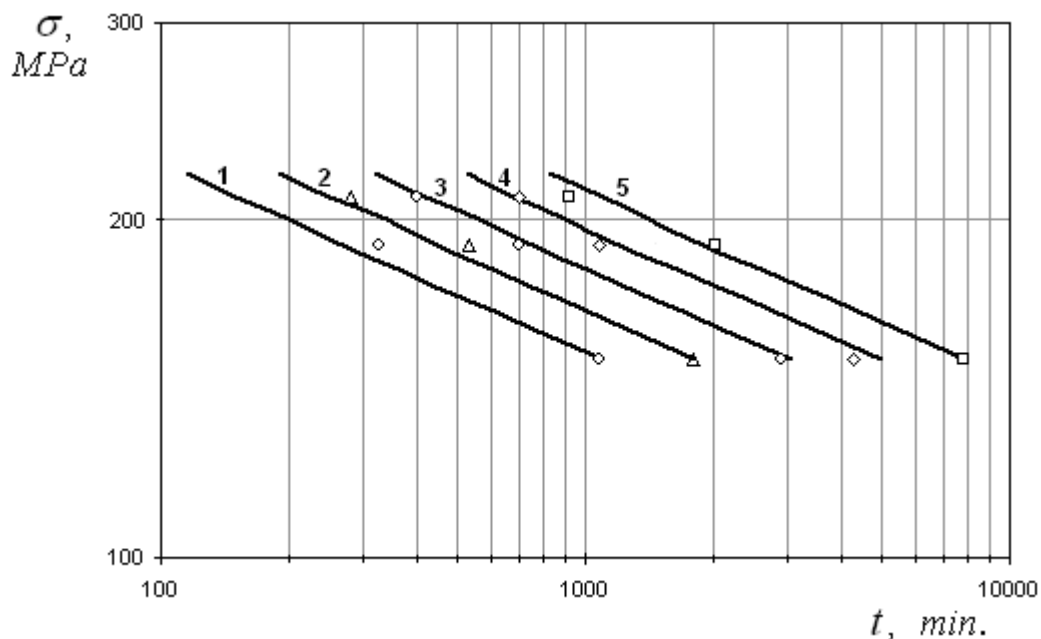


Fig. 2 Long-term strength curves for steel 1H8N9T

Analysis of calculated and experimental data shows that their difference doesn't exceed 8%, what can be regarded as satisfactory result for engineering creep calculations.

### 3. CYCLIC CREEP DAMAGE IN NIPPLES OF REGENERATOR FOR CATALYTIC CRACKING OF PETROLEUM

Numerical simulation of creep and damage accumulation processes in cyclically loaded and heated structural members were performed by use of combination of FEM and multi-step predictor – corrector time integration scheme. The finite elements with triangular cross-section and linear shape functions were used. The components of strain rate tensors and damage parameter's values are determined by constitutive equations (11).

Below let us consider the practical example of similar numerical simulation were made by use of home-made code, have been designed for 2d creep problems [9].

Cyclic creep and damage accumulation problem were studied for nipples of regenerator of catalytic cracking of petroleum. The calculation scheme of axisymmetrical bodies of revolution was used.

Air diffuser pipe bends, used in petroleum refining industry, equipped with two lines of nipples oriented to opposite sides and directed down with angle 45° to the vertical [10]. Nipple is a branch pipe with a variable section through canal. Expanded canal exit zone allows to reach air flow total widening and its overflow rate lowering. These effects should to prevent catalyst in-flow to the stream periphery, nipple erosion deterioration and should minimize catalyst abrasion (fig. 3).

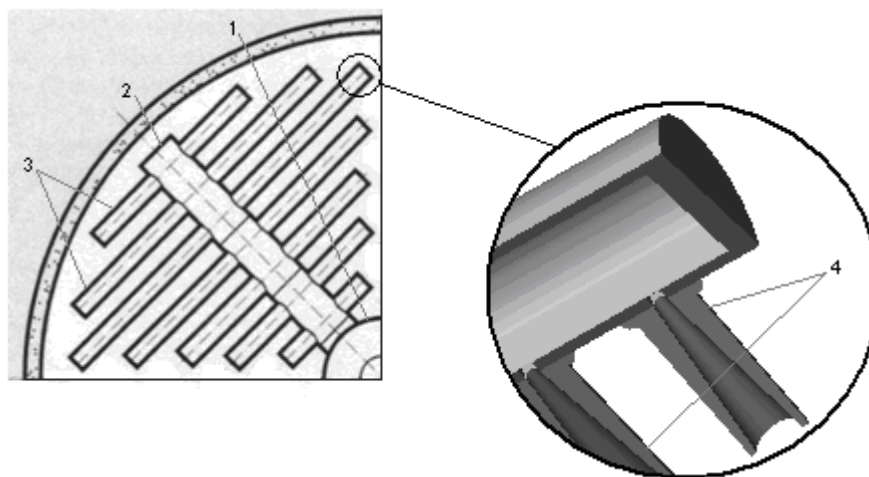


Fig. 3 ¼ part of regenerator air diffuser  
1 – central collector; 2 – distribution pipe; 3 – air diffuser pipe bend; 4 - nipple

Table 1 Time of the finishing of hidden damage process in nipples from different temperature zones

		Temperature on the internal nipple surface		
		823K	833K	843K
Temperature varying on the external nipple surface	903K – 943K	143 200 minutes = 3.3 months		
	898K – 948K	121 800 minutes = 2.82 months	228 300 minutes = 5.28 months	
	893K – 953K		184 200 minutes = 4.26 months	
	888K – 958K		148 900 minutes = 3.45 months	280 000 minutes = 6.48 months
	883K – 963K			220 000 minutes = 5.09 months
Results without accounting temperature cyclic character on the external nipple surface, constant temperature T= 923K				
		206 900 minutes = 4.78 months	460 000 minutes = 10.65 months	1.065e <sup>6</sup> minutes = 24.65 months

Nipples are made from chromium-nickel steel 1H18N9T, which creep cyclic behavior was analyzed in previous section. Air pressure inside the nipple is 0.294 MPa, catalyst pressure inside the regenerator is 0.25 MPa. Nipple is operated in extreme temperature conditions, induced by considerable difference between temperatures on external and internal surfaces of the nipple.

Temperature singularities of air diffuser device operation were analyzed. Temperature conditions of nipples operation are different and vary depending on distance to the central collector. Complex numerical investigations allowed to define the time of the hidden damage accumulation, which was considered in the paper as a failure of nipples from different temperature zones (table 1).

It was established, that nipples failure happened as a result only of high-temperature cyclic creep-damage mechanisms, which were developed in quite short time of their functioning (often not more than half a year). Finishing of hidden damage process and appearance of macroscopic defects has been occurred on the internal nipple surface in the place of its mounting to the air diffuser pipe bend.

Also, maximal rate values of air stream are typical for pointed places. Macroscopic defects (cracks, splits), which were occurred there owing to cyclic creep, could cause the appearance of the areas of maximal stream turbulence and erosion processes would be significantly intensified.

## CONCLUSIONS

New constitutive equations are suitable for numerical calculation of 2d creep-damage problems at the case of joint action of cyclic loading and heating are presented. These equations are involved in numerical method, which is founded on the special asymptotic procedure and the approach of averaging on the period. The method allows to essentially simplify the calculation procedure by way of transition from integration through each cycle to simulation of averaged process of cyclic loading and heating. The procedure of verification and validation involves the comparison between numerical and experimental data for single and complex stress state as well as the numerical and analytical data for problems, which have exact solutions. The cases of different temperature ranges and types of cycles were analyzed. The problem of long-term strength at the conditions of creep and damage accumulation at the cyclically heated nipple of regenerator for catalytic cracking of petroleum is discussed. Analysis of the data of numerical simulation allows to determine the place of macro-crack initiation as well as the fracture time of the nipple. The set of creep-damage problems for nipples are operating in zones with different temperature cycles, were analyzed after numerical simulation. The zones with minimum long-term strength values were found.

## REFERENCES

- [1] Lemaitre J., Chaboche J.-L. *Mechanics of solid materials*, University press, Cambridge, 1994.
- [2] Penny R.K., Marriott D.L. *Design for creep*, Chapman and Hall, London, 1995.
- [3] Breslavsky D.V., Morachkovsky O.K., Tatarinova O.A. High-temperature creep and long-term strength of structural elements under cyclic loading *Strength of Materials*, Vol. 40, pp 531-537, 2008.
- [4] Breslavsky D. Simulation of Creep and Damage Effects in Structural Members under Fast Cyclic Load *Zeitschrift fuer Angewandte Mathematik und Mechanik, ZAMM, Applied Mathematics and Mechanics*, Vol. 78, pp. S301-S302, 1998.
- [5] Taira S., Ohtani R. *Theory of high-temperature strength of materials*, Metallurgia Publ., Moscow, 1986. (In Russian)
- [6] Guarnieri G. Characteristics of long-term strength of sheet materials under cyclic loading and temperatures *High-temperature alloys at varying temperatures and stresses*, Gosenergoizdat Publ., Leningrad, pp 65-111, 1960. (In Russian)
- [7] Rabotnov Yu.N. *Creep problems in structural members*, North Holland, Amsterdam, 1969.
- [8] Pysarenko G.S., Mozharovsky N.S., Antipov E.A. *Plasticity and strength of materials under non-stationary loading*, Naukova dumka, Kyiv, 1984. (In Russian).
- [9] Breslavsky D.V., Korytko Yu.N., Lysak P.N. Software for Finite Element simulation of two-dimensional problems of creep theory *Visnyk NTU«KhPI»*, Vol. 38, Kharkiv, pp. 24-29, 2007. (In Russian)
- [10] Solyar B.Z., Glazov L.Sh., Klimtseva E.A. and others Reconstruction of the reactor block for catalytic cracking on the Г-43-107M/1 equipment. First stage. *Chemistry and technology of fuel and motor oil*, Vol. 6, pp.8-13, 2002. (In Russian)

## ON ACCOUNTING FOR DEFORMATION BY TWINNING IN THE THEORY OF MICROSTRAINS

**Yuri A. Chernyakov**  
Dnepropetrovsk National  
University,  
Dnepropetrovsk, Ukraine

**Alexander S.  
Polishchuk<sup>1</sup>**  
Dnepropetrovsk National  
University,  
Dnepropetrovsk, Ukraine

---

### ABSTRACT

---

In a variety of known plasticity models it is assumed that inelastic deformation occurs by plastic slip in crystals with different orientations which is true for many common polycrystalline metals. However, another mechanism of inelastic deformation, known as mechanical twinning, is dominant for a wide range of magnesium, aluminum, titanium, nickel, copper and other alloys. For modeling materials which exhibit twinning the generalized variant of the theory of microstrains is developed. Heterogeneity of a representative volume element is modeled by introducing a domain of micro particles with different yield limits and orientations. At the scale of micro particles both twinning and slip deformation laws, which account for particle interaction, are introduced. Connection between mechanical behavior of particles and entire representative volume element is accomplished by introducing averaging rule and Kroner-type relation. Proposed variant of the theory can be used for predicting material's response to complex unproportional and cyclic loading.

---

### INTRODUCTION

Modern industry demands the development of new experimentally verified constitutive models. The simplicity of the created theories was the demand of last few decades, but it is not true anymore. Accurate description of material's response in the most complex situations is a first priority now. Such direction is supported by modern experimental and computational equipment. Irreversible deformation in real polycrystalline and multiphase materials develops on multiple size scales simultaneously [1].

One of the microstructural models, which gives good results for a wide range of polycrystalline materials is the theory of plasticity which accounts the microstrains [2]. This theory does not emphasize individual microscopic features, but approximately reproduces material's micro structure, grain interaction laws, response of a single crystal and tends to capture only statistical laws of inelastic deformation. To account of the heterogeneity of plastic deformation which presents the consequence of grained structure and various lattice defects, a representative volume element (RVE) is used as the domain of micro particles of an arbitrary nature. Plastic strain of the RVE is formed by local plastic strains of all micro particles. So the core assumption of the theory is that overall statistical response of anisotropic crystals can be approximated by isotropic particles with different orientations and yield limits.

Experimental verification showed that the proposed approach allowed the modeling of material's response to non-proportional loading with good accuracy. It was also shown that the theory can handle nontrivial unsymmetrical cyclic behavior.

However in the theory of microstrains and in many other well-known plasticity models it is assumed that inelastic deformation occurs only by plastic slip. This assumption is true for many commonly used metals. However, recent researches showed that another mechanism of inelastic deformation, known as mechanical twinning, plays a dominant role in a wide range of metallic alloys, which are used in modern branches of industry due to their special and even unusual mechanical properties [1, 3]. Twinning plays the important role in the inelastic deformation of some magnesium,

---

<sup>1</sup>Corresponding author. Email [tensorsigma@gmail.com](mailto:tensorsigma@gmail.com)

aluminum, titanium, nickel, copper and other metallic alloys. Furthermore, inelastic deformation of metals known as shape memory alloys is connected with so-called martensitic transformation, which is a special case of twinning [4, 5].

In the present work, for the purpose of modeling the response of materials which deform by both twinning and plastic slip, the generalized variant of the theory of microstrains is developed.

## 1. GOVERNING EQUATIONS

In the theory of microstrains a RVE is modelled as a domain of micro particles with distinct initial yield limits  $\tau$  and orientations  $\hat{\mu}_0$ . Except direct physical meaning, these values serve as a particle's labels. We assume that yield limits are distributed with certain density  $\Phi(\tau)$ . The domain of all initial orientations we denote as  $\Omega$  and define it as follows [6]:

$$\Omega = \left\{ \hat{\mu}_0 = \sin \varphi \hat{e} / \sqrt{3} + \cos \varphi \hat{\alpha}, \text{tr} \hat{\alpha}_0 = 0, \hat{\alpha} : \hat{\alpha} = w(\xi_\alpha) \right\},$$

where "tr" stands for trace, ":" denotes double contraction of tensors,  $\hat{e}$  is the second order identity tensor,  $\varphi$  and  $w(\xi)$  are material constant and function which govern the influence of hydrostatic pressure and stress state type on the inelastic response,  $\xi_\alpha$  is the Lode angle for  $\hat{\alpha}$  tensor and it is defined by the following equation:

$$\xi_\alpha = \frac{1}{3} \arctan \frac{(9 / 2 \text{tr}(\text{dev} \hat{\alpha})^3)^{1/3}}{\sqrt{3 / 2 \text{dev} \hat{\alpha} : \text{dev} \hat{\alpha}}},$$

where "dev" is the tensor's deviator.

The constant  $\varphi$  and function  $w(\xi)$  allow accounting for the influence of stress state type on the inelastic deformation. It was shown that simple choice  $w(\xi) = \delta(\xi - \xi_0)$ , where  $\xi_0 \in [0, \pi / 3]$  is material constant, leads to a wide 2-parametric family of initial yield surfaces which allow accounting for strength differential effect:

$$-\sqrt{3} \sin \varphi p + \sqrt{2 / 3} \cos \varphi \cos(\xi_0 - \theta) q - \tau_{min} = 0,$$

where  $p$  is hydrostatic pressure,  $q$  is von Mises equivalent stress,  $\theta$  is Lode angle and  $\tau_{min}$  is the minimum yield limit of all particles.

Also by assuming  $w = 1$  and  $\varphi = 0$  we can obtain the original variant of the theory [2] which leads to von Misses initial yield condition.

Orientation of a micro particle may change from original in the course of inelastic deformation, so we denote current orientation as  $\hat{\mu}$ . The current orientation defines the direction for development of inelastic deformation. Generally both plastic and twinning deformation can occur in a micro particle:

$$\dot{\hat{\varepsilon}}_p(\hat{\mu}_0, \tau) = \dot{\lambda}(\hat{\mu}_0, \tau) \hat{\mu}, \quad \dot{\hat{\varepsilon}}_{tw}(\hat{\mu}_0, \tau) = \dot{\eta}(\hat{\mu}_0, \tau) \hat{\mu},$$

where  $\hat{\varepsilon}_p$  and  $\hat{\varepsilon}_{tw}$  are plastic and twinning strain tensors,  $\dot{\lambda}$  and  $\dot{\eta}$  are plasticity and twinning parameters.

Like in a classical flow theories, the plasticity parameter  $\dot{\lambda}$  is required to be positive during the process of active plastic straining:  $\dot{\lambda}(\hat{\mu}_0, \tau) > 0$ . The twinning parameter  $\dot{\eta}$  is positive if the active twinning process takes place. However, unlike the plasticity parameter, it may also be negative during the detwinning. So, one of the following equations holds, depending on the direction of the process:  $\dot{\eta}(\hat{\mu}_0, \tau) > 0$  or  $\dot{\eta}(\hat{\mu}_0, \tau) < 0$ . Another important feature of the twinning process is the boundedness of twinning strains. Therefore we assume that  $0 \leq \eta(\hat{\mu}_0, \tau) \leq \eta_{max}$ , where  $\eta_{max}$  is the maximum possible twinning strain, which is a material constant, and generally can vary from one particle to another. If the twinning parameter reaches one of the critical values, the twinning process stops and the particles can exhibit purely elastic or elastoplastic behaviour. Although a reverse process is possible in this case.

Microscopic inelastic deformation starts when the local yield or twinning condition is satisfied:  $F(\hat{\tau}) = 0$ , where  $\hat{\tau}$  is defined separately for twinning, detwinning and plasticity:

$$\hat{\tau}(\hat{\mu}_0, \tau) = \begin{cases} \hat{\sigma}(\hat{\mu}_0, \tau) - \hat{\rho}_1(\hat{\mu}_0, \tau) & \text{for plasticity,} \\ \hat{\sigma}(\hat{\mu}_0, \tau) - \hat{\rho}_2(\hat{\mu}_0, \tau) & \text{for twinning,} \\ \hat{\sigma}(\hat{\mu}_0, \tau) - \hat{\rho}_3(\hat{\mu}_0, \tau) & \text{for detwinning.} \end{cases}$$

In the last equation tensors  $\hat{\rho}_i, i=1,2,3$  define internal stresses which appear in a micro particle due to interaction with other particles as a result of inelastic straining. Initial fields of internal stresses and their evolution laws are specified:

$$\begin{aligned} \hat{\rho}_i(\hat{\mu}_0, \tau) \Big|_{t=0} &= \hat{\rho}_{i0}(\hat{\mu}_0, \tau), \quad i=1,2,3, \\ \dot{\hat{\rho}}_i(\hat{\mu}_0, \tau) &= \sum_{j=1}^3 \int_0^{\infty} \Phi(\tau') d\tau' \int_{\Omega} \tilde{R}_{ij}(\hat{\mu}_0, \tau, \hat{\mu}'_0, \tau') : \hat{\varepsilon}_j(\hat{\mu}'_0, \tau') d\Omega', \end{aligned}$$

where  $\tilde{R}_{ij}(\hat{\mu}, \tau, \hat{\mu}', \tau')$  are the fourth rank tensor kernels which govern interaction between particles with different orientations and yield limits,  $\hat{\varepsilon}_j, j=1,2,3$  are plastic, twinning and detwinning strains correspondingly.

Let us examine the interaction law. Of course an interaction kernel of any complexity can be introduced however there are no experiments to verify such kernel directly and therefore it is reasonable [1,7] to use simple expressions accounting only for major macroscopic laws of deformation:

$$\tilde{R}(\hat{\mu}, \tau, \hat{\mu}', \tau') = \begin{cases} R_1^* \delta_{\mu\mu'} \hat{\mu} \hat{\mu}' + R_2^* \tilde{\mathcal{I}} + R_3^* \hat{\mu} \hat{\mu}', & (\hat{\mu}, \tau) \in \Omega^*, \\ R_4^* \delta_{\mu\mu'} \hat{\mu} \hat{\mu}' + R_2^* \tilde{\mathcal{I}} + R_3^* \hat{\mu} \hat{\mu}', & (-\hat{\mu}, \tau) \in \Omega^*, \\ R_2^* \tilde{\mathcal{I}} + R_3^* \hat{\mu} \hat{\mu}', & \text{otherwise,} \end{cases}$$

where  $\delta_{\mu\mu'}$  is the Dirac's delta function which is nonzero if  $\hat{\mu} = \hat{\mu}'$ ,  $\tilde{\mathcal{I}}$  is the fourth rank isotropic identity tensor and  $R_k^*$  are scalar material functions, which are defined as follows:

$$\begin{aligned} R_k^* &= \frac{R_k(\tau, \xi)}{w^2(\xi_{\mu})}, \quad k=1,3,4, \\ R_2^* &= G(\xi) \left( R_2(\tau, \xi) + R_{2\rho}(\tau, \xi) \sqrt{\hat{\rho} : \hat{\rho}} \right). \end{aligned}$$

In the last expression the term with  $R_1^*$  describes the hardening which occurs in the actively deforming particles due to their own inelastic deformation and the  $R_1(\tau, \xi_{\mu})$  is the corresponding hardening modulus which may be different for particles with different yield limits and Lode angles. However good results can be often achieved by assuming all  $R_k = const$ . The term with  $R_2^*$  describes the hardening of all particles in the direction of macroscopic inelastic strain rate which is equivalent to well-known kinematic hardening mechanism,  $R_2(\tau, \xi_{\mu})$  is the kinematic hardening modulus and  $R_{2\rho}(\tau, \xi_{\mu})$  governs the relaxation of internal stresses which is important for modelling materials exhibiting ratcheting. The term with  $R_3^*$  as it can be easily observed is responsible for isotropic hardening. And the last term which contains  $R_4^*$  governs the behaviour of particles with directions opposite to the actively deforming particles which is important for modelling cyclically unstable materials.

The expression for the local yield function is defined as follows

$$F_{(\hat{\mu}_0, \tau)}(\hat{\tau}) = \cos(\kappa) \hat{\mu}_0 : \hat{\tau} + \sin(\kappa) f \sqrt{\text{dev } \hat{\tau} : \text{dev } \hat{\tau}} = 0,$$

where  $\kappa$  is the material constant which defines degree of a particle's anisotropy.

Particle's current orientation  $\hat{\mu}$  is defined as the gradient of local yield function  $F(\hat{\tau})$ :

$$\hat{\mu} = \frac{\partial F(\hat{\tau})}{\partial \hat{\tau}}.$$

The macroscopic strain rate is decomposed into sum of elastic, plastic and twinning strains:

$$\langle \hat{\varepsilon} \rangle = \langle \hat{\varepsilon}_e \rangle + \langle \hat{\varepsilon}_p \rangle + \langle \hat{\varepsilon}_{tw} \rangle.$$

Elastic part of the strains is governed by the linear Hooke's law, and elastic constants are assumed to be independent of inelastic strains:

$$\langle \hat{\sigma} \rangle = \tilde{C}^e : \langle \hat{\varepsilon} \rangle, \tilde{C}^e = \frac{1}{E} \left( (1 + \nu) \tilde{I} - \frac{\nu}{3} \tilde{e} \tilde{e} \right),$$

where  $E$  and  $\nu$  are Young modulus and Poisson's ratio.

Macroscopic plastic and twinning strain rates are defined as the integrals over the corresponding domains of active particles:

$$\langle \hat{\varepsilon}_p \rangle = \int_{\Omega_p^*} \hat{\varepsilon}_p G_p(\xi_\mu) d\tau d\Omega, \langle \hat{\varepsilon}_{tw} \rangle = \int_{\Omega_{tw}^*} \hat{\varepsilon}_{tw} G_{tw}(\xi_\mu) d\tau d\Omega.$$

where  $\xi_\mu$  is the Lode angle for  $\hat{\mu}$ ,  $G_p(\xi_\mu)$  and  $G_{tw}(\xi_\mu)$  are the weight functions,  $\Omega^*$  denotes the domain of actively deforming particles.

Additional expression which establishes connection between micro and macro variables is introduced in the form of Kroner's relation:

$$\langle \hat{\sigma} \rangle - \hat{\sigma}(\hat{\mu}, \tau) = m \left( \hat{\varepsilon}_p(\hat{\mu}, \tau) + \hat{\varepsilon}_{tw}(\hat{\mu}, \tau) - \langle \hat{\varepsilon}_p \rangle - \langle \hat{\varepsilon}_{tw} \rangle \right).$$

where  $m$  is a material constant which defines the deviation of microscopic stresses and strains from corresponding macroscopic values.

Aforementioned equations form the basic set of the governing equations. Providing all material functions and constants are specified directly, these equations can be used to obtain a relation between stress and strain rates.

## CONCLUSIONS

Nowadays available computational potential doesn't limit engineers and even very complex models can be used to simulate mechanical response of real structures. So the microstructural approach in constitutive modeling becomes even more important. This is especially actual for materials which exhibit twinning as they often have a variety of nontrivial physical and mechanical features like strength differential, strong temperature dependence, complex cyclic response, superelasticity and shape memory effect. The variant of the theory of microstrains which accounts for both twinning and plasticity is discussed in the paper. This theory accounts for the heterogeneity of the plastic deformation in a RVE by introducing a domain of interacting micro particles. Such approach allows obtaining well-known hardening mechanisms: isotropic, kinematic and vertex point thus allowing to simulate material's response to non-proportional loading. Also theory gives good possibilities for modeling plastic strain accumulation in the non-ideal superelasticity, ratcheting and other mechanical effects which appear in complex cyclic processes.

## REFERENCES

[1] Poluchin P.I., Gorelik S.S., Vorontsov V.K. *Physical Grounds of Plastic Deformation*, Metallurgy, Moscow, 1982. (in Russian)

- [2] Novozhilov V.V., Kadashevich Yu.I., Chernyakov Yu.A. Theory of Plasticity Taking Account Micro Strains, *Journal of Engineering Materials and Technology*, Vol. 284, pp. 821-823, 1985. (in Russian)
- [3] Lou X.Y., Li M., Boger R.K., Agnew S.R., Wagoner R.H. Hardening Evolution of AZ31B Mg Sheet, *International Journal of Plasticity*, Vol. 23, pp. 44 – 86, 2007.
- [4] Lichachev V.A., Kuzmin S.L., Kamentceva Z.P. *Shape Memory Effect*, LGU, Leningrad, 1987. (in Russian)
- [5] Grabea C., Bruhns O.T. Path Dependence and Multiaxial Behavior of a Polycrystalline NiTi Alloy Within the Pseudoelastic and Pseudoplastic Temperature Regimes, *International Journal of Plasticity*, Vol. 25, pp. 513 – 545, 2009.
- [6] Chernyakov Yu.A., Polishchuk A.S. Generalized Variant of the Theory of Micro Strains, *Theoretical and applied mechanics*, Vol. 44, pp. 158 – 163, 2008. (in Russian)
- [7] Chernyakov Yu.A., Shneider V.P. Modeling Complex Cyclic Loading With the Theory of Plasticity which Accounts for Micro Strains, *Reports of the National Academy of Sciences of Ukraine*, Vol. 6, pp. 56 – 59, 2006. (in Russian)

**TOWARDS COUPLED FINITE ELEMENT MODELING  
OF GRAIN GROWTH WITH PLASTICITY**

**Slawa Gladkov<sup>1</sup>**  
ICAMS, Ruhr-University,  
Bochum, Germany

**Bob Svendsen**  
Institute of Mechanics,  
TU Dortmund, Germany

---

ABSTRACT

---

The purpose of this work is the finite element formulation of diffuse interface (continuum) model for the grain growth. Strategies for spatial (staggered/monolithic) and time (implicit/explicit) discretizations will be discussed and numerical results will be presented.

---

**INTRODUCTION**

During industrial hot forming processes such as e.g. extrusion, hot rolling, or hot forging, materials undergo both mechanical deformation and recrystallization. Usually both phenomena influence each other in a complicated way, and it is exactly this influence of recrystallization on a material's ductility and strength that effects the appeal of a hot forming method.

The purpose of this work is (i) the formulation and application of a continuum field approach to the phenomenological modeling of the behavior of technological alloys undergoing recrystallization (grain growth-coarsening) and attendant plastic deformation and (ii) development of reliable numerical schemes for solution of arising coupled mechanical-grain growth models using finite element techniques [1]. At the current stage only the results for the grain growth are presented.

The interface between two phases on the atomic scale is a “mushy” one. Usual approach to model interfaces on the meso scale is to use a sharp interface model. This kind of the problem statement might be numerically quite complicated because one must impose boundary conditions on the moving interface. Contrary to this, here a relaxed (or diffused over a finite width) interface is employed (Fig. 1).

With the help of so called phase field[2,3], a field defined on the whole domain of the simulation and serving as a relaxed characteristic function and volume fraction for each phase, one can distinguish between different phases. It should be mentioned that the term “phase” here might be treated not only as a physical phase, but also in any other context. Particularly for the application in grain growth phase fields are used to describe grain orientations and consequently grain boundaries.

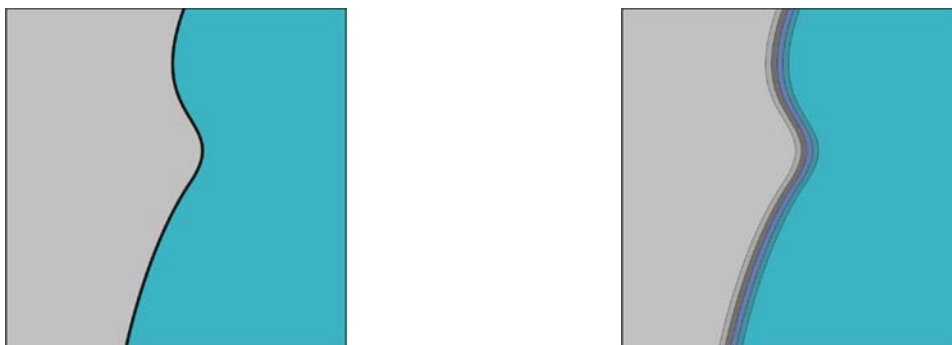


*Fig. 1 Sharp (left) vs diffuse (right) interface*

---

<sup>1</sup> Corresponding author. Email [svyatoslav.gladkov@udo.edu](mailto:svyatoslav.gladkov@udo.edu)

## 1. MODEL FORMULATION

In this work a grain growth model developed in [4] is employed. This model utilize diffuse interface approach where each grain orientation is described by a separate relaxed characteristic function – a phase field, which is a function of space and time. Then Cahn-Allen type partial differential equations are derived for the evolution of phase fields:

$$\dot{\phi}_i = -L_i \left( -\alpha\phi_i + \beta\phi_i^3 + 2\gamma\phi_i \sum_{j \neq i}^p \phi_j^2 - \kappa_i \nabla \cdot \nabla \phi_i \right), \quad i = 1, 2, \dots, p, \quad (1)$$

where  $\phi_i$  is a phase field indicating the  $i^{th}$  grain orientation,  $p$  is a total number of grain orientations under considerations,  $L_i$  are relaxation coefficients,  $\kappa_i$  are gradient energy coefficients and  $\alpha, \beta, \gamma$  are positive constants. Following[4]  $\alpha = \beta = \gamma = L_i = 1$ ,  $\kappa_i = 2$  and simplified model equations are:

$$\dot{\phi}_i = 2\nabla \cdot \nabla \phi_i + \phi_i \left( 1 + \phi_i^2 - 2 \sum_j^p \phi_j^2 \right), \quad i = 1, 2, \dots, p. \quad (2)$$

Problem formulation must be competed with the initial and boundary conditions. Initial conditions are set to random values in range  $(-0.001; 0.001)$  for all  $\phi_i$  to emulate initially “liquid” phase. Then crystallization takes place and grain microstructure is formed. Boundary conditions are set to homogeneous Neumann, i.e.  $\nabla \phi_i \cdot \mathbf{n} = 0 \forall i$ .

## 2. NUMERICAL TREATMENT

Numerically the above stated problem (2) is solved using tri-linear finite elements in space and semi-implicit first order scheme in time. All calculations are performed in open source finite element library `deal.II` [5] and post-processed in `ParaView`. Details are presented in the following subsections.

### 2.1 Spatial discretization

In space the problem is discretized using Bubnov-Galerkin approach and its weak form is:

$$\int_{\Omega} \phi^* \dot{\phi}_i dx = - \int_{\Omega} 2\nabla \phi^* \cdot \nabla \phi_i - \phi^* \phi_i \left( 1 + \phi_i^2 - 2 \sum_j^p \phi_j^2 \right) dx, \quad i = 1, 2, \dots, p, \quad (3)$$

where  $\Omega$  is domain under consideration and  $\phi^*$  is a test function.

There are two possibilities to discretize this problem in space: monolithic and staggered. Monolithic approach leads to definition in each finite element node  $p$  degrees of freedom (DOFs), what in the final end leads to enormous system matrix size and makes problem numerically non-treatable. Staggered scheme leads to definition of only  $p$  scalar finite element fields and sequential update of them. This scheme is employed here and actually written in the equation (3).

### 2.2 Time discretization

Explicit time discretization for a problem (3) leads to very small time steps. On the other hand fully implicit scheme leads to very long computation times due to re-assembly of the system matrix on each step and Newton-Raphson procedure. In this work semi-implicit scheme is used. In this case only linear part (mass matrix and discrete Laplacian) are sought in the new time step and the local nonlinear part is taken from the previous time step. This formulation allows firstly to build up system matrix only once and use it for all time steps and secondly to avoid Newton-Raphson iterations:

$$\int_{\Omega} \frac{1}{\Delta t} \phi^* \phi_i^{t+1} + 2\nabla \phi^* \cdot \nabla \phi_i^{t+1} dx = \int_{\Omega} \phi^* \phi_i \left( \frac{1}{\Delta t} + 1 + \phi_i^2 - 2 \sum_j^p \phi_j^2 \right) dx, \quad i = 1, 2, \dots, p, \quad (4)$$

where  $\phi_i^{t+1}$  is unknown solution on the new time step,  $\phi_i$  is solution from the previous time step and  $\Delta t$  is time step.

## 2.3 Numerical results

For numerical simulations following parameters were taken:  $\Omega = [0, 200]^3$ ,  $N_{elements} = 100^3$ ,  $\Delta t = 0.5$ ,  $t_{final} = 200\Delta t$ ,  $p = 30$  (all dimensionless). On Fig. 2 two snapshots of the numerical solution are shown.

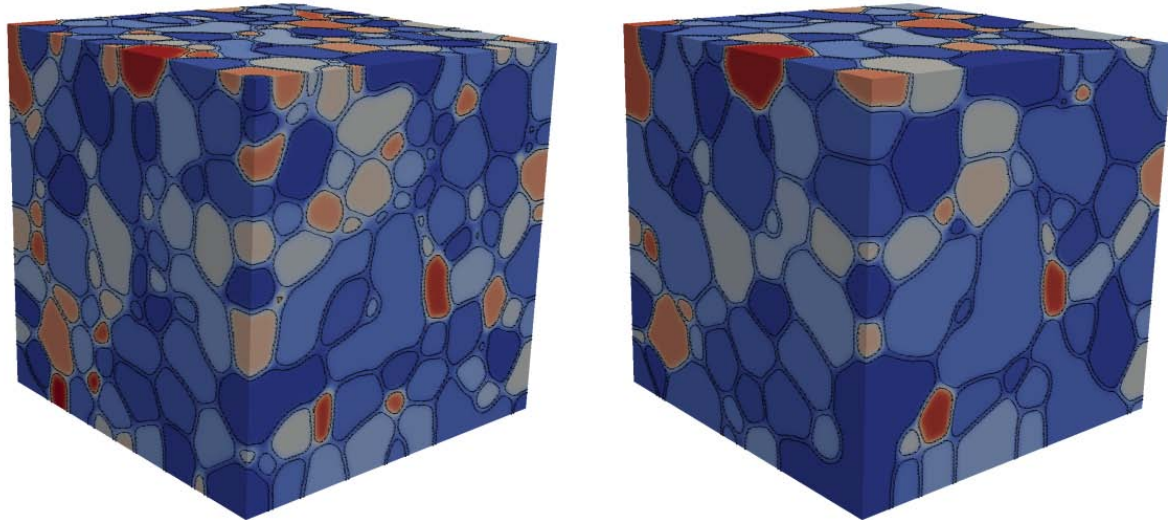


Fig. 2 Snapshots of the grain structure for  $t = 50$  (left) and  $t = t_{final} = 100$  (right)

## CONCLUSIONS AND OUTLOOK

Model formulation and numerical results for a grain growth were presented. Results show appropriate qualitative behavior for a normal grain growth/evolution. Next step is a coupling of the multi phase field (MPF) grain growth model of [6] with large strain plastic behavior based on the continuum mixture theory[7] and development of numerical methods for solutions of such problems. Several attempts in this direction were already reported mainly limiting to the case of small-strain plasticity. But to develop models for a case of large strain inelasticity we would like to describe the mechanical structure in the framework of a thermodynamic, internal-variable-based formulation in which the deformation and temperature are in general coupled[8]. Coupling between the mechanical fields, phase-fields and the temperature field arises via the mechanical dissipation during the deformation process as well as by the spatial distribution of the areas of different phases being modeled by the order parameter.

## REFERENCES

- [1] Stiemer M. et al. Efficient and reliable finite element techniques for phase field models, *International Journal of Materials Research*, Vol. 101, pp. 498-502, 2010.
- [2] Chen L.-Q. Phase-field models for microstructure evolution, *Annual Review of Materials Research*, Vol. 32, pp. 113-140, 2002.
- [3] Steinbach I. Phase-field models in materials science, *Modelling and Simulation in Materials Science and Engineering*, Vol. 17, pp. 1-31, 2009.
- [4] Fan D., Chen L.-Q. Computer simulation of grain growth using a continuum field model, *Acta Materialia*, Vol. 45, pp. 611-622, 1997.
- [5] Bangerth W., Hartmann R., Kanschat G., deal.II - a general-purpose object-oriented finite element library, *ACM Trans. on Mathematical Software*, Vol. 33, pp. 24/1-24/27, 2007.
- [6] Steinbach I., Apel M. Multi phase field model for solid state transformation with elastic strain, *Physica D*, Vol. 217, pp. 153-160, 2006.
- [7] Svendsen B. On the Constituent Structure of a Classical Mixture, *Meccanica*, Vol. 32, pp. 13-32, 1997.
- [8] Garcia E. R., Bishop C. M., Carter W. C. Thermodynamically consistent variational principles with applications to electrically and magnetically active systems, *Acta Materialia*, Vol. 52, pp. 11-21, 2004.

## AN INFLUENCE OF LONG-TERM EXPLOITATION ON MATERIAL BEHAVIOUR UNDER CONSTANT AND MONOTONICALLY INCREASING LOADING

**Z.L. Kowalewski**<sup>1</sup>

**S. Mackiewicz**

**J. Szelażek**

Institute of Fundamental  
Technological Research  
Warsaw, Poland

**T. Szymczak**

Motor Transport Institute  
Warsaw, Poland

**B. Augustyniak**

Gdańsk University of  
Technology  
Gdańsk, Poland

---

ABSTRACT

---

The paper is devoted to an analysis of creep damage at elevated temperatures and structural degradation due to plastic deformation at room temperature of selected steels commonly applied in power plants (40HNMA, 13HMF). The materials were tested in the as-received state, however, in the case of the 13HMF steel also after different periods of exploitation (76000h and 144000h at elevated temperature (813K) under internal pressure (14 bars)). Destructive and non-destructive testing methods were applied to assess a material degradation. As destructive methods the standard tension tests were carried out after every kind of prestraining. Subsequently, an evolution of the selected tension parameters was taken into account for damage identification. In order to assess a damage development during the creep and plastic deformation the tests for both steels were interrupted for a range of the selected strain magnitudes. The ultrasonic and magnetic techniques were used as the non-destructive methods for damage evaluation. The last step of the experimental programme contained microscopic observations. A good correlation of mechanical and selected non-destructive parameters identifying damage was achieved for the tested steels. It gives very promising tool for degradation assessments appearing in pipelines at power stations.

---

### INTRODUCTION

All kinds of materials subjected to exploitation loadings suffer variations of their mechanical properties. Depending on the working conditions the variations of some selected parameters of these materials may attain such magnitudes that their further exploitation is risky due to possible failures. Such situations are dangerous for the devices posing a major threat to environment and human security. Power plants are the typical examples. Figure 1 presents the results showing a drastic reduction of creep lifetime of the 13HMF steel used for pipeline subjected to the long time exploitation at elevated temperature (813K) under internal pressure (14 bars). To avoid an unpredictable catastrophic accidents due to such effect as that shown in Fig.1 a systematic monitoring must be carrying out.

There are many testing techniques commonly used for damage assessments. Among them we can generally distinguish destructive, and non-destructive methods. Having the parameters of destructive and non-destructive methods for damage development evaluation it is worth to analyze their variation in order to find possible correlations.

The ultrasonic and magnetic techniques were selected as the non-destructive methods for damage development evaluation. In the case of ultrasonic method the acoustic birefringence coefficient was used to identify damage development in the tested steels. In the case of magnetic technique the classical Barkhausen effect (HBE) and magnetoacoustic emission (MAE) were measured. It is shown that both magnetic parameters are sensitive on the level of material damage.

(a)

(b)

(c)

---

<sup>1</sup> E-mail: [zkowalew@ippt.gov.pl](mailto:zkowalew@ippt.gov.pl)

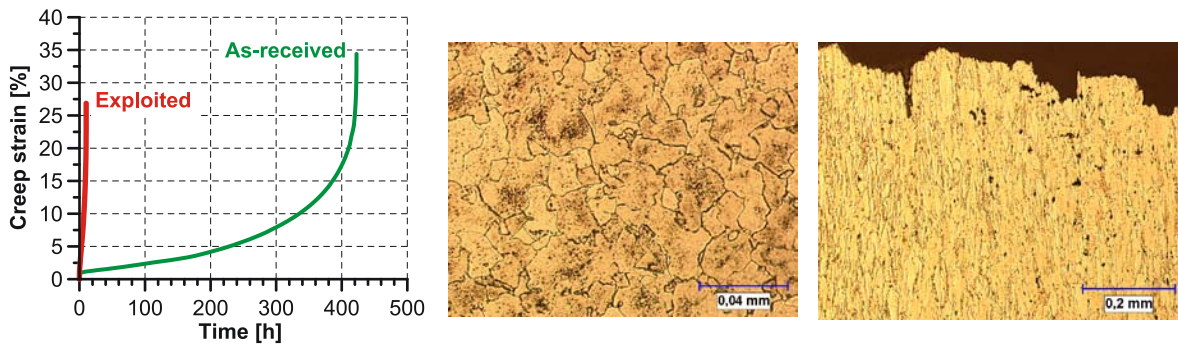


Fig. 1 Comparison of tensile creep curves ( $\sigma=230$  MPa,  $T=773$ K) for the 13HMF steel in the as-received state and after exploitation by a period of 144000 h (a), and its metallographic structures for the initial state (b) and after 144000 h of work (c)

## 1. DETAILS OF EXPERIMENTAL TECHNIQUE

Uniaxial tension creep tests were carried out using plane specimens for two kinds of steel, i.e. 40HNMA and 13HMF. All tests were conducted in the same conditions for each steel, i.e. the stress level was equal to 250 MPa, and temperature - 773 K. In order to assess a damage development during the process of creep the tests were interrupted for a range of the selected time periods, which correspond to the increasing amounts of creep strain. Some selected magnitudes of deformation were also applied to prestrain specimens by means of plastic flow at room temperature.

After prestraining the ultrasonic and magnetic investigations were carried out to identify a damage development in the tested steels. In the next step of the experimental procedure, the same specimens were mounted on a hydraulic servo-controlled MTS testing machine and then stretched until failure was achieved. The results of standard tensile tests were used to evaluate variation of typical mechanical parameters, i.e. Young's modulus, yield point, ultimate tensile stress. The last step of the experimental programme contained microscopic observation using optical and scanning microscopes.

In order to assess damage development during creep the tests for the 40HNMA steel were interrupted after 100h, 241h, 360h, 452h, 550h, 792h, 929h and 988h, which correspond to increasing amounts of creep strain from 0.34% up to 6.5%. In the case of 13HMF the tests were interrupted after 149h, 300h, 360h, 407h, 441h, 587h, 664h, 796h and 1720h (strain range 5.92% - 34.1%).

## 2. EXPERIMENTAL RESULTS OF THE DESTRUCTIVE TESTS

In order to assess damage development of the steels prestrained due to creep or plastic flow the standard tensile tests were carried out. The tensile characteristics for the tested materials after prestraining are presented in Fig. 2a for the 40HNMA steel and in Fig. 2b for the 13HMF steel. In all of these diagrams the characteristics for the prestrained steel are compared with the tensile curve of the steels in the as-received state.

On the basis of these tensile characteristics, Fig. 2, variations of the basic mechanical parameters of both steels, due to deformation achieved by prior creep or plastic flow were determined. It was observed for both materials, that the Young's modulus is almost insensitive to the magnitude of creep and plastic deformations. Contrary to the Young's modulus the other considered tension test parameters, especially the yield point and the ultimate tensile stress, Figs 3 and 4, exhibit clear dependence on the level of prestraining.

Taking into account the results presented for the 40HNMA steel in Figs 2a and 3 it is easy to note that this material exhibits a significant softening effect due to the creep prestraining, expressed by a large decrease of the yield point and ultimate tensile stress. An opposite effect can be observed for this material prestrained due to plastic deformation at room temperature. In this case the prior deformation leads to a hardening effect.

More details of investigations on the 40HNMA steel are described in [1, 2].

On the basis of tensile characteristics for the 13HMF steel after creep prestraining, Fig. 2b, it is easy to notice that the results are different than those for the 40HNMA obtained. The material exhibits a significant hardening effect for both types of prestraining, expressed by an increase of the yield point, Fig. 4a, and ultimate tensile stress, Fig. 4b. The effect is slightly weaker for the prior deformation due to creep. Such results achieved for the 13HMF steel do not allow to distinguish a type of an initial loading history in the same way as it is possible for the 40HMNA steel.

(a)

(b)

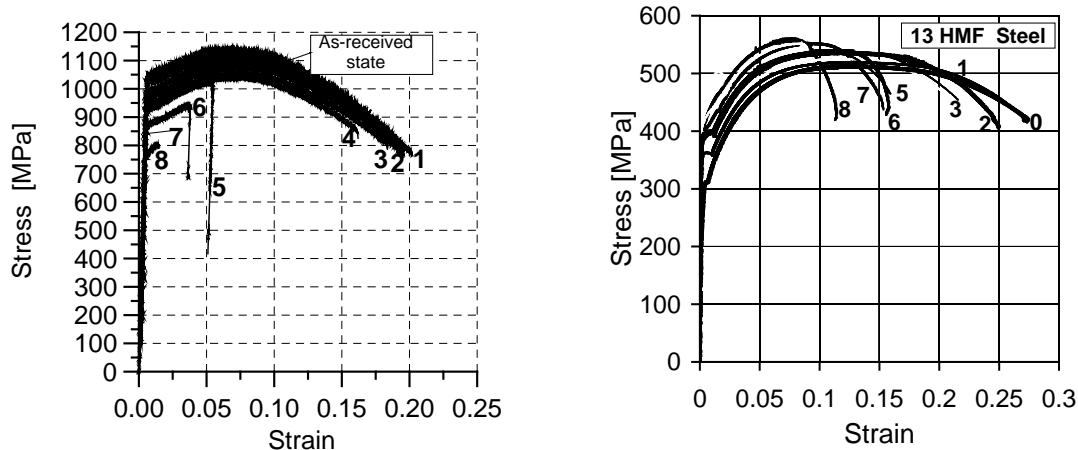


Fig. 2 Tension characteristics of: (a) the 40HNMA steel after creep for 100h (1), 241h (2), 360h (3), 452h (4), 550h (5), 792h (6), 929h (7) and 988h (8), and (b) the 13HMF steel after creep for 149h (1), 300h (2), 360h (3), 407h (4), 441h (5), 587h (6), 664h (7), 796h (8) and 1720h (9)

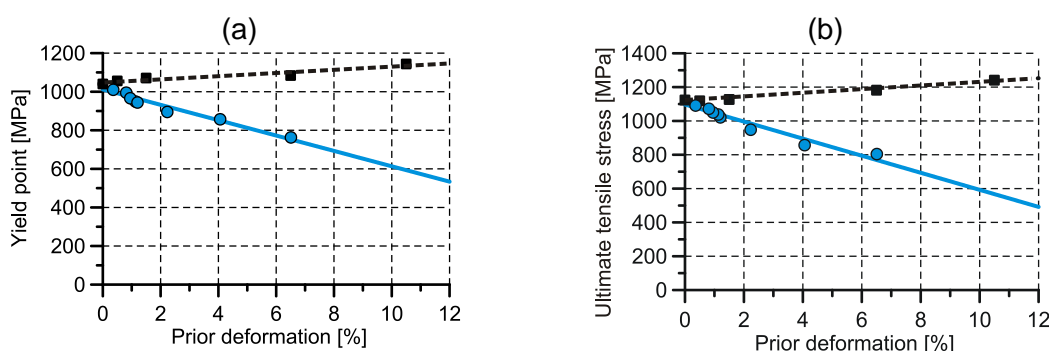


Fig. 3 Variation of the tensile parameters for the 40HNMA steel due to creep (solid lines) and plastic (broken lines) deformations: (a) yield point; (b) ultimate tensile stress

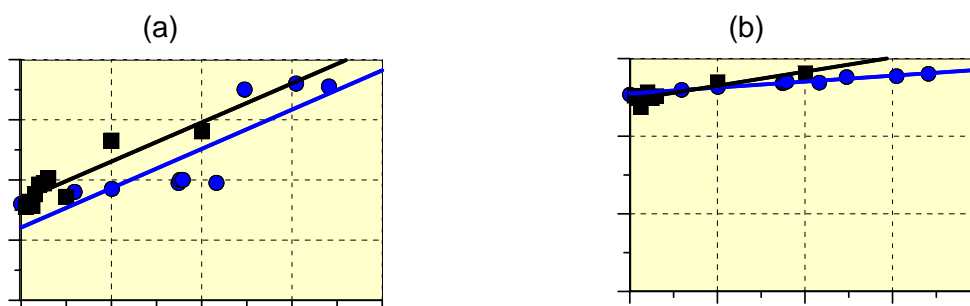


Fig. 4 Variation of tensile parameters of the 13HMF steel due to creep (solid lines) and plastic (broken lines) deformations: (a) yield point; (b) ultimate tensile stress

### 3. EXPERIMENTAL RESULTS OF THE NON-DESTRUCTIVE TESTS

#### 3.1 Evaluation of damage development using ultrasonic techniques

Figure 5 presents mean values of the acoustic birefringence measured in specimens after creep or plastic deformation. The birefringence was measured in the fixtures, where the texture of the material was assumed to be unchanged during creep testing, and in the working part of the specimen. Values of birefringence measured in the fixture exhibit some scatter around zero, Fig.5a. This scatter is a picture of birefringence evaluation accuracy and the initial acoustic homogeneity of the specimen. In the deformed part of specimen the birefringence depends on the amount of deformation. It can be noticed that birefringence variations due to creep are significantly higher than birefringence scatter for the non-deformed material. The acoustic birefringence was measured at several points along the working part of each specimen, thus enabling its maximum to be found. For the maximum creep prestrained specimen, where the necking was visible, the birefringence maximum was measured in the specimen neck. For less deformed specimens, in which necking was not observed, one can expect that

the birefringence maximum indicates the region of maximum micro defect concentration. These regions can be treated as the sources of future macro defects leading finally to failure. The plots presented in Fig. 5 indicate that the acoustic birefringence is sensitive to the amount of prior deformation. Another advantage of this parameter is also well represented in Fig. 5a. Namely, it is very sensitive to the form of prior deformation. This feature is especially well revealed in the case of the birefringence determined for the 40HNMA steel, Fig. 5a. For specimens prestrained due to creep the increase of this parameter is observed with the increase of prior deformation. An opposite effect was achieved for specimens prestrained due to the plastic deformation at room temperature, i.e. with the increase of prior deformation a decrease of the birefringence was obtained. The effects obtained for the 40HNMA steel were not confirmed by the ultrasonic tests carried out on the 13HMF steel. In this case the same tendency may be observed independently on a type of prior deformation, i.e. decrease of the acoustic birefringence with an increase of deformation level. It has to be emphasized however, that such effect corresponds in some way to that which can be observed on basis of the results of destructive tests presented in the previous section. More details concerning the results and testing technique are available in [3-5].

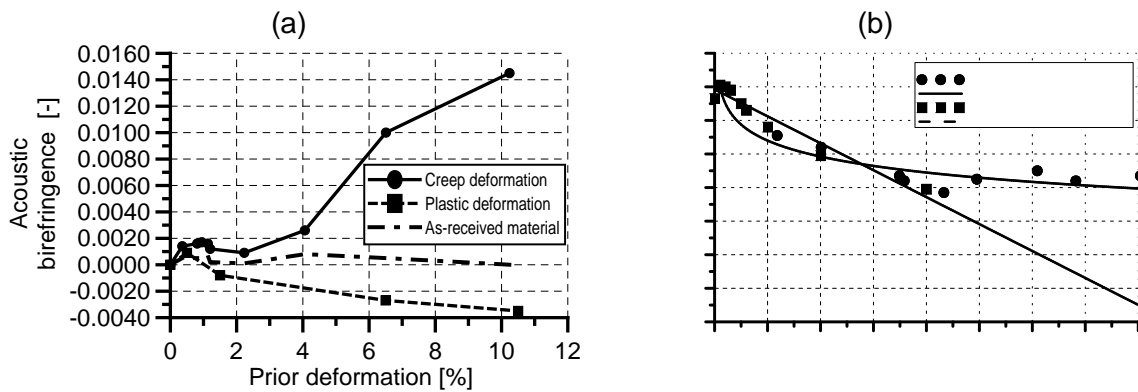


Fig. 5 Acoustic birefringence  $B$  variations due to prior deformation for: (a) 40HNMA steel; (b) 13HMF steel

### 3.2 Evaluation of damage development using magnetic techniques

Two magnetic techniques for non-destructive testing were applied, i.e. measurement of Barkhausen effect (HBE) and magneto-acoustic emission (MAE) [6-8]. Both effects are due to abrupt movement of magnetic domain walls depicted from microstructural defects when sample is magnetised. The samples at laboratory tests were magnetised by the solenoid and a magnetic flux generated in the sample was closed by C-core like shaped yoke. Magnetizing current (delivered by current source) had a triangular like waveform and frequency of order 0.1 Hz. Its intensity was proportional to the voltage  $Ug$ . Two sensors were used: (a) the pickup coil (PC), and (b) the acoustic emission transducer (AET). Voltage signal induced at PC was used for magnetic hysteresis loop  $B(H)$  evaluation (low frequency component) as well as for HBE analysis (high frequency component). Intensity of HBE is given by rms (root mean square) voltage  $Ub$  envelopes. In this case the maximum ( $Ub_{pp}$ ) of  $Ub$  for one period of magnetisation is compared. Analogue analysis is performed for MAE voltage signal from the AET. The magnetic coercivity  $Hc$ , evaluated from the  $B(H)$  hysteresis loop plots, is also compared. An influence of plastic flow and creep damage on the basic magnetic properties can be analysed using  $B(H)$  hysteresis loops. The representative results showing variations of the  $B(H)$  hysteresis loops are presented in Figs 6 and 7 for the 13HMF steel. The curves obtained for an undamaged specimen ( $\epsilon = 0\%$ ) and for all the damaged ones are compared. The quantity  $Ug$  denotes the voltage proportional to the driving current intensity, and hence – magnetic field strength  $H$ . The as described features of the HBE intensity are well presented by means of plots showing a dependence between the amplitudes of  $Ub$  envelopes and magnitudes of prior deformation - peak to peak values  $Ub_{pp}$  in Fig. 8. Thus, one can say that the HBE intensity as a function of the resulting prestrain peaks firstly and then decreases monotonically when amplitudes of the  $Ub$  envelopes are compared. The curves in Fig. 8 reveal also that creep damage leads to a smaller ‘decrease’ of the HBE intensity than that observed for specimens after plastic flow. Comparing two plots in the figure it can be seen that the  $Ub$  signal properties such as the amplitude for the highest strain after creep damage are roughly the same as for the analogous signals for the last stage of plastic flow.

A synthetic description of the MAE properties as a function of prior deformation is given by plots shown in Fig. 9 (amplitudes of the MAE envelopes). Amplitudes of the MAE intensity decrease for both cases but the dynamics of their change is different.

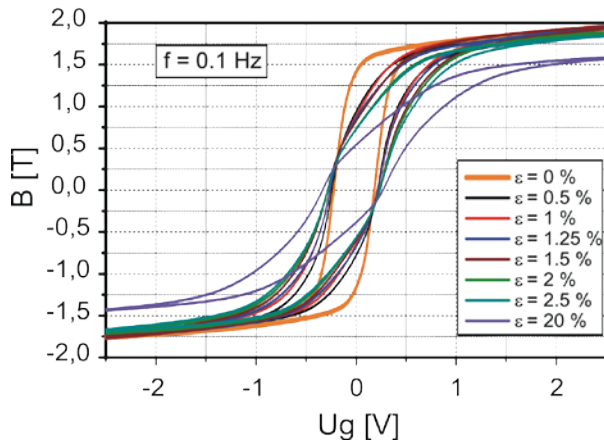


Fig. 6 Magnetic hysteresis loops of undamaged and damaged specimens due to plastic flow of the 13HMF steel

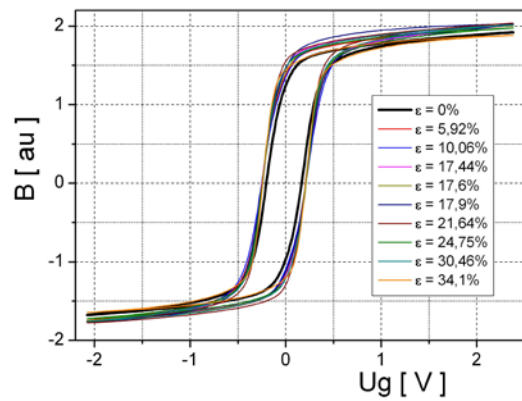


Fig. 7 Magnetic hysteresis loops of undamaged and damaged specimens due to creep of the 13HMF steel

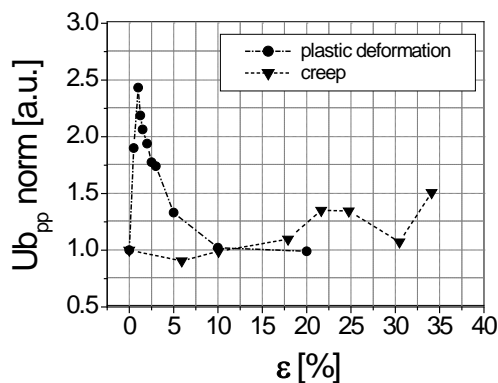


Fig. 8 Relation between the amplitudes of  $U_b$  envelopes and prior deformation due to plastic flow (circles) and creep (triangles)

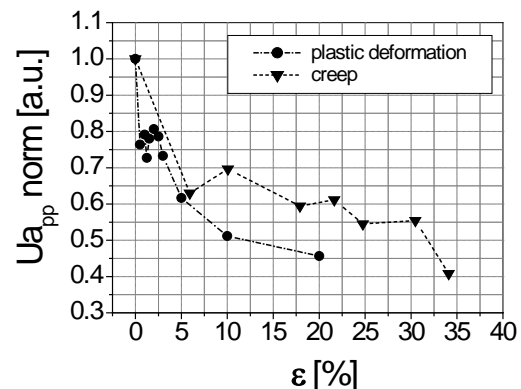


Fig. 9 Relation between amplitudes of  $U_a$  envelopes and prior deformation due to plastic flow (circles) and creep (triangles)

#### 4. IDENTIFICATION OF DAMAGE USING METALLOGRAPHIC OBSERVATIONS

In the final step of the experimental programme microscopic observations were carried out. The metallographic assessments were performed by means of optical microscope (Olympus PMG3 - in macro- and micro- ranges) as well as by means of scanning electron microscopy (SEM - JEOL 6360 LA) techniques [9]. All observations were done in non-etched and etched state. The effect of voids formation was observed along the longitudinal metallographic sections prepared from specimens after completion of the mechanical tests. Then, the selected geometrical parameters of existing voids were determined by means of the image analysis in the optical microscopy range. The following parameters were determined: depth of void [mm], mean area fraction of voids ( $A_A$  [%]) related to the unit area of metallographic sample ( $1 \text{ mm}^2$ ) and mean quantity of voids -  $N_A$  [ $1/\text{mm}^2$ ], Fig. 10b.

The comparison of microstructural effects in the 40HNMA steel and determined geometrical parameters show the greatest damage at test 8 (Fig. 2), Fig. 10. It is characteristic that the voids dimensions are bigger in the perpendicular direction with respect to the specimen axis than those observed parallel one. For lower magnitudes of prior creep deformation the damage was connected rather with the nonmetallic inclusions. In all these cases the fragmentations of existing nonmetallic inclusions, and subsequently, voids formation were observed. The microstructure for all specimens was the same, i.e. sorbite with remaining the needle martensite configuration.

(a)

(b)

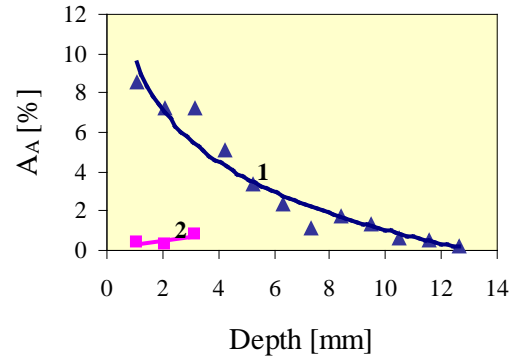
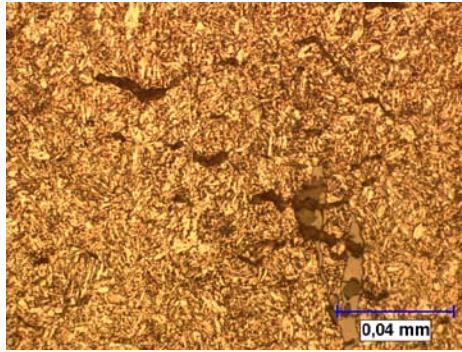


Fig. 10 Microstructural observations of the 40HNMA: (a) strong damage close to fracture surface, magnification 500x; (b) changes of the void area fractions ( $A_A$  [%]) as a function of distance from the fracture surface for 40HNMA steel deformed due to: (1) creep up to 6.5%; (2) plastic flow up to fracture (19%)

## CONCLUSIONS

The results show that ultrasonic and magnetic parameters can be good indicators of material degradation and can help to find the regions where material properties are changed due to prestraining.

In order to evaluate damage progress in specimens made of the 40HNMA and 13HMF steels, instead of velocity and attenuation measurement typically used in ultrasonic investigations, the acoustic birefringence  $B$  measurements were successfully applied.

In the case of magnetic investigations for damage identification the measurements of the Barkhausen effect (HBE) and the magneto-acoustic emission (MAE) were applied. Both effects show that the magnetic properties are highly influenced by prior deformation, and moreover, they are sensitive not only to the magnitude of prior deformation, but also to the way it is introduced.

## ACKNOWLEDGEMENT

The support from the National Centre for Research and Development (Poland) under grant NR 15-0049-04/2008 is greatly appreciated.

## REFERENCES

- [1] Kowalewski Z.L., Szelążek J., Mackiewicz S., Pietrzak K., Augustyniak B. *International Journal of Modern Physics Letter B*, Vol. 22, No 31/32, p. 5533, 2008.
- [2] Kowalewski Z.L., Szelążek J., Mackiewicz S., Pietrzak K., Augustyniak B. *Journal of Multiscale Modeling*, Vol. 1, No 3&4, p. 479, 2009.
- [3] Kowalewski Z.L., Mackiewicz S., Szelążek J., Deputat J. *Proc. of XXI Symp. on Experimental Mechanics of Solid Body*, ed. J. Stupnicki, Warsaw University of Technology, 2004.
- [4] Mackiewicz S., Kowalewski Z.L., Szelążek J., Deputat J. *Mechanical Review*, Vol. 7/8, p. 15, 2005.
- [5] Szelążek J., Mackiewicz S., Kowalewski Z.L. *NDT and E International*, Vol. 42, p. 150, 2009.
- [6] Sablik M.J., Augustyniak B. *Wiley Encyclopedia of Electrical and Electronics Engineering*, ed. J.G. Webster, J. Wiley&Sons, New York, 1999.
- [7] Augustyniak B., Chmielewski M., Sablik M.J. *IEEE- Trans. on Magnetics*, Vol. 36, No. 5, p. 3624, 2000.
- [8] Augustyniak B., Chmielewski M., Piotrowski L., Kowalewski Z. *IEEE Transactions on Magnetics*, Vol. 4, No. 11, p. 3273, 2008.
- [9] Pietrzak K., Kowalewski Z.L., Rudnik D., Wojciechowski A. *Proc. of the XIV International Symposium on Plasticity and Its Current Applications*, ed. A. Khan, NEC Press, Baltimore, 2008.

## PROBLEM STATEMENT OF DYNAMIC CREEP FOR ISOTROPIC AND ORTHOTROPIC BODIES

**Oleg K.  
 Morachkovsky<sup>1</sup>  
 Vladimir N. Sobol**  
 National Technical  
 University "Kharkiv  
 Polytechnic Institute",  
 Kharkiv, Ukraine

---

### ABSTRACT

---

Mathematical problem statement of dynamic creep for isotropic and orthotropic bodies is presented in the paper. The cyclic creep-damage theory of Breslavsky-Morachkovsky is used. Numerical methods for the solution of such creep problems is considered, where the mixed variational functional and RFM (Rvachov's Functions method), or finite element method (FEM), are applied. Numerical results of the creep problem analysis for plate with centered hole under tension are given.

---

### INTRODUCTION

It is necessary to take into account the creep phenomena in long-term strength analysis of structural elements with exploitation at elevated temperatures. This process leads to evaluation of creep irreversible strains and damage parameter and finally to predict the fracture. The most of structural members in aviation and space-rocket techniques have such exploitation conditions and are made from materials with anisotropic creep properties. A lot of such elements are used under action of quasi-static loadings and non-stationary physical and mechanical rapidly oscillating fields (aero-hydrodynamic streams with pulsations, etc.). In the paper a problem statement of dynamic creep for isotropic and orthotropic bodies is considered. Solution methods and numerical results are presented.

### 1. PROBLEM STATEMENT

Let us consider the main statement of dynamic creep-damage problem for solids. In Cartesian coordinate system,  $x_i$ ,  $i=1,2,3$ , one considers a space body with volume  $V$ , and surface  $S$ :  $S = S_t \cup S_u$ , where  $S_t$ ,  $S_u$  are surface parts of the body, under acting external distributed forces and boundary conditions.

In standard form the complete system of the initial-boundary-value problem of creep for bodies subjected to action of volume forces, surface forces and oscillating harmonic loading can be written in tensor form (1) as

$$\begin{aligned} \sigma_{ij,j} + f_i &= \rho \dot{v}_i, \quad \varepsilon_{ij} = 1/2(u_{j,i} + u_{i,j}), \quad \varepsilon_{ij} = d_{ijkl} \sigma_{kl} + c_{ij}, \quad x_i \in V \\ \sigma_{ij} n_j &= p_i^0 + \Phi_i(t) - x_i \in S_t, \quad u_i - u_i^* = 0 - x_i \in S_u \\ u_i(x, 0) &= v_i(x, 0) = c_{ij}(x, 0) = 0 \end{aligned} \quad (1)$$

The system (1) includes equilibrium, physical, and geometric equations.

It can be taken into account that complete strain tensor consists of a sum of reversible elastic strain and irreversible creep strain tensors. Creep strain tensor can be determined by using creep state equations.

Oscillating fields of external forces can be described as the following singly-periodic and harmonic function:

---

<sup>1</sup> Corresponding author. Email [morachko@kpi.kharkov.ua](mailto:morachko@kpi.kharkov.ua)

$$\Phi_i(t) = p_i \cdot \sin\left(\frac{2\pi}{T}t\right) \quad (2)$$

where  $p_i$  are amplitude values of corresponding surface loads.

Functions  $\Phi_i(t)$  are singly-periodic and harmonic functions with cycle  $T$ , that  $T/t_* \ll 1$ ,  $t_*$  is a rupture time during the creep process.

By using the method of asymptotic expansions by the small parameter  $\mu = T/t_*$ , and the averaging procedure along the period, we reduce the original initial-boundary-value problem of creep of bodies subjected to the action of harmonic loading, to two correlated initial-boundary-value problems in two time scales (slow  $t$  and fast  $\xi$ ) [1].

Equations of the first problem can be written as the following:

$$\begin{aligned} \sigma_{ij,j}^0 + f_i &= \rho \dot{v}_i, \quad \varepsilon_{ij}^0 = d_{ijkl} \sigma_{kl}^0 + c_{ij}^0, \quad x_i \in V \\ \sigma_{ij}^0 n_j &= p_i^0 - x_i \in S_t, \quad u_i^0 - u_i^* = 0 - x_i \in S_u \\ u_i^0(0) &= v_i^0(0) = 0, \quad c_{ij}^0(0) = 0 \end{aligned} \quad (3)$$

where all functions are slowly varying ones in the macroscopic time scale  $t$ .

Equations of the second problem is written in the form:

$$\begin{aligned} \sigma_{ij}^1 &= \frac{1}{\mu^2} \rho u_{,\xi\xi}^1, \quad \varepsilon_{ij}^1 = d_{ijkl} \sigma_{kl}^1, \quad x_i \in V \\ \sigma_{ij}^1 n_j &= \Phi_i(\xi), \quad x_i \in S_t; \\ u_i^1(0) &= v_i^1(0) = 0, \quad c_{ij}^1 = 0, \quad 0 \leq \xi \leq 1 \end{aligned} \quad (4)$$

where all functions are fast varying ones in the microscopic time scale  $\xi$ .

Equations of the systems (3, 4) must be expanded by state equation of dynamic creep. From the creep state equation we can determine irreversible creep strains and damage parameter.

In early works for isotropic materials it has been used the Rabotnov-Kachanov theory with a scalar damage or continuity parameters [5]. However such theory can't be used to describe the anisotropic creep. Vector and tensor models for a presentation of the damage parameter for anisotropic creep are suggested by many famous scientists (Rabotnov Yu.M., Kachanov L.M., Shesterikov S.A., Murakami S., Betten J. and others). Physical interpretation of the damage parameter in vector or tensor form is the density in microvolume of different defects in the form of voids, microcracks, vacancies, dislocation processes etc. Defects in material accumulate at elevated temperature due to the creep process. This fact is proved by experimental data in metallurgical science.

State equations of dynamic creep for isotropic material have been written [1-3] as

$$\begin{aligned} \dot{c}_{ij} &= \frac{3}{2} \cdot \frac{B \sigma_i^{n-1} (1 + H(A))}{(1 - \omega^r)^l} \cdot s_{ij}, \quad \dot{\omega} = \frac{B \sigma_e^m (1 + K(A))}{(1 - \omega^r)^k}, \quad \omega(0) = 0, \quad \omega(t_*) = 1 \\ H(A) &= \frac{n(n-1)}{4} A^2 \left( 1 + \frac{(n-2)(n-3)}{16} A^2 \right) \\ K(A) &= \frac{m(m-1)}{4} A^2 \left( 1 + \frac{(m-2)(m-3)}{16} A^2 \right), \quad A = \frac{\sigma_i^a}{\sigma_i} \end{aligned} \quad (5)$$

State equations of dynamic creep for orthotropic materials can be presented

$$\dot{\underline{c}} = b_{1111}^{(N+1)/2} \frac{\bar{\sigma}_2^{N-1} (1+H(A))}{(1-\omega)^N} [B] \underline{\sigma}, \quad \dot{\omega} = d_{1111}^{k/2} \frac{\sigma_{*2}^k (1+G(A))}{(1-\omega)^{k+S}}, \quad \omega(0)=0, \quad \omega(t_*)=1 \quad (6)$$

$$\dot{\underline{\omega}} = d_{1111}^{k/2} \frac{\sigma_{*2}^{k-2} (1+G(A))}{(1-\omega)^{k+S-1}} [D] \underline{\sigma} \quad (7)$$

Where

$\dot{\underline{c}} = (\dot{c}_{11}, \dot{c}_{22}, 2\dot{c}_{12})^T$ ,  $\underline{\sigma} = (\sigma_{11}, \sigma_{22}, \sigma_{12})^T$ ,  $\dot{\underline{\omega}} = (\dot{\omega}_{11}, \dot{\omega}_{22}, 2\dot{\omega}_{12})^T$  - are respectively vectors of the creep strain rate, stresses and damage parameter;

$\bar{\sigma}_2^2 = \underline{\sigma}^T [B] \underline{\sigma}$ ,  $\sigma_{*2}^2 = \underline{\sigma}^T [D] \underline{\sigma}$  - are the invariants of stress tensors;

$A = \frac{\sigma_i^a}{\bar{\sigma}_2}$  - is the asymmetry parameter of stress;

$\sigma_i^a$  - is the intensity of the amplitude of stress;

$\dot{\omega} = \underline{\sigma}^T \dot{\underline{\omega}}$  - is the specific power dissipation due to damages.

Particularly, for transversally-isotropic materials matrixes of material properties are

$$[B] = \begin{pmatrix} 1 & \beta_{12} & 0 \\ \beta_{21} & \beta_{22} & 0 \\ 0 & 0 & 4\beta \end{pmatrix}, \quad [D] = \begin{pmatrix} 1 & \delta_{12} & 0 \\ \delta_{21} & \delta_{22} & 0 \\ 0 & 0 & 4\delta \end{pmatrix}$$

$$\beta_{12} = -\frac{1}{2}, \beta_{22} = \frac{b_{2222}}{b_{1111}}, 4\beta = \frac{b_{1212}}{b_{1111}}, \delta_{12} = -\frac{1}{2}, \delta_{22} = \frac{d_{2222}}{d_{1111}}, 4\delta = \frac{d_{1212}}{d_{1111}}$$

A detailed conclusion and assumption of the state equations for anisotropic creep taking into account the damage parameter are presented in [1,7,8].

## 2. METHOD OF SOLUTION

The complete system of initial-boundary-value problem of dynamic creep for bodies (3, 4, 6, 7) can be solved by using two methods.

The first one is based on the variational statement by using variational-structural method of the R – functions theory [4]. The second one is FEM [2].

The variation principle for the mixed functional is given. It is formulated on independently varied functions of strains and stress for known creep strains at arbitrary time moment.

To solve the boundary-initial value creep problem (3) the mixed variational functional can be written as the following:

$$R_{u\sigma} = \iiint_V \left[ \frac{1}{2} \sigma_{ij} (u_{i,j} + u_{j,i}) - \sigma_{ij} C_{ij} - \Lambda(\sigma_{ij}) - (f_i - \rho \dot{v}_i) u_i \right] dV -$$

$$- \iint_{S_i} p_i^0 u_i dS - \iint_{S_u} n_i \sigma_{ij} (u_j - u_j^*) dS \quad (8)$$

The first variation of the functional (8) can be presented as

$$\delta R_{u\sigma} = \iiint_V \left[ \delta \sigma_{ij} \left\{ \frac{1}{2} (u_{j,i} + u_{i,j}) - d_{ijkl} \sigma_{kl} - c_{ij} \right\} - \delta u_i (\sigma_{ij} + f_i - \rho \dot{v}_i) \right] dV$$

$$- \iint_{S_u} n_i \delta \sigma_{ij} (u_j - u_j^*) dS - \iint_{S_i} (\sigma_{ij} n_i - p_j^0) \delta u_j dS \quad (9)$$

Numerical method for a solution of the boundary – initial value creep problems (3) is used, the Runge–Kutta–Merson and RFM methods are applied [4].

By using the variational-structural theory of R – functions or FEM we have complete resolving

system of equations in a standard form:

$$[K]\{u\} = \{F\} + \{F^{cr}\} \quad (10)$$

The second problem is considered on the "fast" scale and corresponds to forced oscillations of an elastic body under the action of harmonic loading. For determining of amplitude values of stresses in such case we must to solve the next system of equations:

$$([K] - \Omega^2 [M])\{q_*^1\} = \{p_*^1\} \quad (11)$$

where  $\{q_*^1\}$  is the amplitude values vector of nodal displacement (FEM) or free components in structures (variational-structural method) under action of forced harmonic oscillation of a body with eigen frequency  $\Omega$ ;  $[K]$ ,  $[M]$  are stiffness and mass matrixes of a body;  $\{p_*^1\}$  is the amplitude values vector of loads. Methods for solution of the equations in the form (11) are well known [1-4].

### 3. NUMERICAL RESULTS

Let us consider a thin-walled rectangular plate with centered hole (Fig. 1) under tension along the axis OX. The plate is made from materials with transversally-isotropic properties during creep process.

Creep problem for the rectangular plate under tension of axial force  $S = 30$  MPa, is presented (Fig. 1). Geometric parameters of the plate are a side  $2b=0.2$  m, and the centered hole equal to  $0.02$  m.

In a case when the oscillation component of loading is absent ( $A = 0$ ), the relations (6,7) turn into ordinary relations of the anisotropic creep theory  $H(A) = G(A) = 0$ .

Numerical results are given in ANSYS software and were compared with known results at initial time [6]. Type of finite elements PLANE 183 has been taken, number of elements is equal 461 FE. Plate material is the aluminium alloy D16AT at  $275^{\circ}\text{C}$  with the following mechanical properties: elasticity module  $E = 65$  GPa, Poisson's ratio  $\nu = 0.42$ . The numerical values of material constants of state equations and damage (6, 7) are obtained by materials creep curves processing for D16AT at  $275^{\circ}$  and have been given in the paper [7].

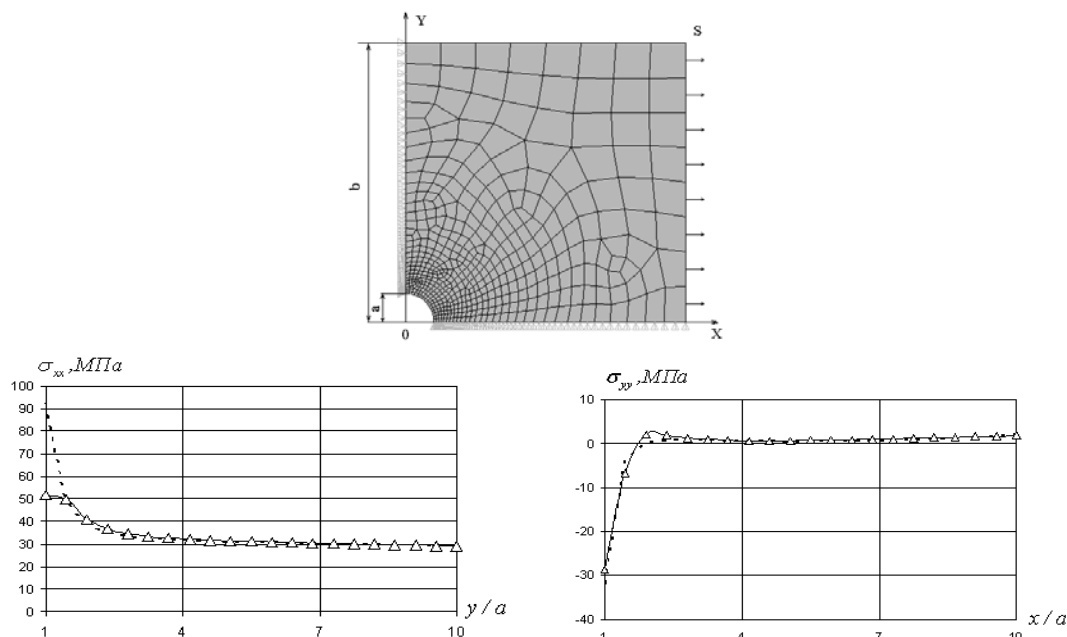


Fig. 1 Axial stresses curves (dash line -  $t=0$  h, solid line and markers -  $t=15$  h)

As an example of calculation, we consider the anisotropic creep of rectangular plate depending on the angle orientation of main axes of anisotropic material properties ( $\theta^\circ$ ) to axis OX during the creep process.

At the beginning the calculation have been done for the case of  $\theta^\circ = 0$ . In the Fig. 1 we can see a distribution of axes stresses and its change in time.

In the table 1 comparisons of maximum values of stress intensity and creep strains from anisotropy axes orientations are given.

*Table 1 Maximum values of stress intensity and creep strains*

<b>Anisotropy axes orientation, <math>\theta^\circ</math></b>	<b>Maximum value of stress intensity <math>\sigma_i</math>, MPa</b>	<b>Maximum value of creep strain intensity <math>\varepsilon_i</math>, %</b>
0	56.283	0.9754
30	64.53	0.64
45	66.3	0.51
90	55.987	1.2

## CONCLUSIONS

The general statement of boundary-initial problems of dynamic anisotropic creep for bodies is given in the paper. The state equations in incremental form of dynamic anisotropic creep for isotropic and transversally-isotropic materials with damage parameter have been shown. Methods of analysis to solve these problems are presented on the basis of RFM – variational-structure and FEM methods. FEM solutions of anisotropic creep for plates with centered hole under tension load have been done. It is established that if a plate is made from transversally-isotropic materials, then in a case of coincidence of anisotropic properties axis with tension axis one has the maximum long-term durability, intensity of stresses redistribution near the plate hole and an increasing level of creep strains. For the angle of main anisotropic axis orientation  $\theta^\circ = 30^0, 45^0$  we can see in the plate a less intensity of stress redistribution and accumulating of creep strains.

## REFERENCES

- [1] Breslavsky D., Morachkovsky O. Nonlinear creep and rupture of plane bodies under the action of rapidly oscillating loads, *Prikl. Mehan.*, Vol. 34, N. 3, Kyiv, pp. 97-103, 1998. (In Russian)
- [2] Anishchenko G., Breslavskii D., Morachkovskii O. Creep and long-term strength of herringbone lock joints of gas-turbine engines under the combined action of static and cyclic loads, *Strength of Materials*, Vol. 30, N. 1, pp. 25-30, 1998.
- [3] Breslavsky D., Morachkovsky O., Tatarinova O. High-temperature creep and long-term strength of structural elements under cyclic loading. *Strength of Materials*, Vol. 40, N. 5, pp. 531-537, 2008.
- [4] Morachkovsky O., Sobol V., Zamula A. The methods for solution of static and dynamic creep problems for bodies of revolution, *International conference "Nonlinear Dynamics"*, Kharkov, pp. 133-136, 2004.
- [5] Rabotnov Yu.N. *Creep of structural members*, Nauka, Moscow, 1966. (In Russian)
- [6] Demidov V. *Theory of elasticity*, Vyshcha shkola, Moscow, 1978. (In Russian)
- [7] Morachkovsky O., Pasynok M. The creep damage model of transversally-isotropic metals, *6th International Symposium on Creep and Coupled Processes*, Białowieża, pp. 367-375, 1998.
- [8] Morachkovsky O., Konkin V. Creep and long-term strength of light alloys with anisotropic properties, *Problemy prochnosti*, N. 5, pp. 38-42, 1987. (In Russian)

**A DIRECT METHOD FOR THE CYCLIC ELASTOPLASTIC ANALYSIS OF  
SIMPLE STRUCTURES**

**K.V.Spiliopoulos<sup>1</sup>**  
**K.D.Panagiotou**

Institute of Structural  
Analysis and Antiseismic  
Research,  
National Technical  
University of Athens,  
Athens, Greece

---

ABSTRACT

---

A direct method for the cyclic elastoplastic analysis of structures is presented. The method is based on the decomposition of the steady cyclic state residual stress distribution into Fourier series. The coefficients of the series are evaluated in an iterative way by satisfying equilibrium and compatibility at some preselected time points inside the cycle. The procedure is under development and in the present work is applied to a simple one-dimensional three bar structure. Three different load cases are shown to lead, using the approach, to either adaptation, alternating plasticity or incremental collapse.

---

**INTRODUCTION**

There are structures such as nuclear reactors, aircraft gas turbine propulsion engines, etc. that operate in high levels of loads and temperature. High levels of loading exist also in civil engineering structures like heavy traffic on bridges and pavements, earthquake loading etc.

The complete response of a structure, which is subjected to a given mechanical loading and exhibits inelastic time independent plastic strains is quite complex. The reason for the complexity is the need to perform calculations over the lifetime history of the structure. The computation of the whole loading history, however, leads to lengthy and expensive incremental calculations, especially for structures with large number of degrees of freedom. Therefore, it is very useful to develop computational approaches for straightforward calculations of the possible stabilized state under repeated thermomechanical loading.

Direct cyclic methods offer this alternative. The ingredient of these methods is the existence of a steady state at the end of the loading procedure for structures made of ductile material.

The advantage that direct methods offer with respect to time-stepping ones has been exploited by many researchers. A state-of-the art may be found in Weichert and Ponter (eds.) [1].

A direct method has been proposed by Spiliopoulos [2] in the context of the cyclic loading analysis of creeping structures. The irreversibility of the nonlinear material dictates the existence of residual stresses together with the elastic stresses. It is the distribution of the residual stresses that is sought at the cyclic stress state. The method is based first on decomposing the unknown residual stress in Fourier series and then trying to find the coefficients of this series.

In the present work a direct method is investigated, that has the same foundations with [2] and may be applied to structures made of elastic perfectly plastic material. The plastic behaviour of the material is approximated using the well known Ramberg-Osgood formula [4].

Preliminary results are reported herein for a three-bar truss subjected to various types and values of loading that may lead to either elastic shakedown or alternating plasticity or incremental collapse. Results for more complex structures are expected to be available during the Conference.

---

<sup>1</sup>Corresponding author. Email [kvspilio@central.ntua.gr](mailto:kvspilio@central.ntua.gr)

## 1. THE STEADY CYCLIC STRESS STATE

According to the theorem of Frederick and Armstrong [3], the stress distribution  $\sigma$  of a structure subjected to cyclic loading of period  $T$  becomes also cyclic with time having the same period as the applied loading, when the cyclic stationary state has been reached. In this steady state the stress  $\sigma$  may be decomposed into two parts: Assuming a purely elastic material behaviour, the first part is a cyclic elastic stress  $\sigma^{el}(t)$  that equilibrates the cyclic loading that is applied, and the second part is a self-equilibrating stress  $\rho(t)$  which is due to inelasticity. Thus one can write:

$$\sigma(t) = \sigma^{el}(t) + \rho(t) \quad (1)$$

### 1.1 Fourier Decomposition of Residual Stresses

In order to calculate, therefore, this cyclic stress distribution, it is sufficient to compute the residual stress distribution of the cyclic stress state  $\rho(t)$ . Since this stress also becomes periodic, it may be decomposed in its Fourier series over the period of loading, as this can be done for any periodic function:

$$\rho(t) = \frac{a_0}{2} + \sum_{k=1}^{\infty} \left( a_k \cos \frac{2k\pi t}{T} + b_k \sin \frac{2k\pi t}{T} \right) \quad (2)$$

where the coefficients  $a_0$ ,  $a_k$  and  $b_k$ ,  $k = 1, 2, \dots$  are called the Fourier coefficients of the Fourier series. Thus the problem is converted to a problem of evaluating the Fourier coefficients of the various terms of the series. These coefficients may be calculated in an iterative way, using the time derivatives of the residual stresses to which these coefficients are shown to be directly connected [2].

### 1.2 Formulation for 1-D problem

An iterative form to establish the Fourier coefficients is given in [2]:

$$a_k^{(\mu+1)} = -\frac{1}{k\pi} \int_0^T [\dot{\rho}_i^{(\mu)}(t)] \sin \frac{2k\pi t}{T} dt \quad (3)$$

$$b_k^{(\mu+1)} = \frac{1}{k\pi} \int_0^T [\dot{\rho}_i^{(\mu)}(t)] \cos \frac{2k\pi t}{T} dt \quad (4)$$

$$\frac{a_0^{(\mu+1)}}{2} = -\sum_{k=1}^{\infty} a_k^{(\mu+1)} + \frac{a_0^{(\mu)}}{2} + \sum_{k=1}^{\infty} a_k^{(\mu)} + \int_0^T [\dot{\rho}_i^{(\mu)}(t)] dt \quad (5)$$

where  $(\mu)$  and  $(\mu+1)$  denote two consecutive iterations.

Iterations stop when there is virtually no difference in the values of the coefficients between two iterations.

## 2. EXAMPLES OF APPLICATION

An example of application of the method presented above is the three-bar structure which is shown in Fig. 1. The structure is subjected to cyclic loads  $V(t)$ ,  $H(t)$ , which are applied at node 4. All the members of the truss have equal cross section  $A$  and are made of the same material. This is a one dimensional stress problem and the plastic behaviour is simulated by the well-known Ramberg – Osgood relationship [4]:

$$\dot{\epsilon}_i^{pl} = \frac{3}{7} \frac{\sigma_y}{E} \left[ \frac{\sigma_i}{\sigma_y} \right]^n \quad (6)$$

where  $\sigma_y$  is the yield stress of the material,  $E$  is the Young's modulus,  $\sigma_i = \sigma_i^{el} + \rho_i$  is the current stress for each bar  $i = 1, 2, 3$  and  $n$  is a constant that depends on the material. In order to simulate the elastic-rigid plastic behavior, commonly used values for  $n$  are  $\sim 10$  or greater.

The stress states, in the two inclined bars, are identical, due to symmetry. If at an instant of time, inside the cycle, one satisfies the condition of compatibility together with equation (1), we may obtain an expression for the time derivatives of the residual stresses in the three bars in terms of the plastic strains that develop:

$$\dot{\epsilon}_1^{pl} + \dot{\epsilon}_3^{pl} - \frac{1}{2}\dot{\epsilon}_2^{pl} = \frac{1}{E} \left[ \frac{1}{2}\dot{\rho}_1 - \dot{\rho}_2 - \dot{\rho}_3 \right] \quad (7)$$

whereas from equilibrium considerations the residual stress rate in the vertical bar 2 is given by:

$$\dot{\rho}_2 = -\dot{\rho}_1 = -\dot{\rho}_3 \quad (8)$$

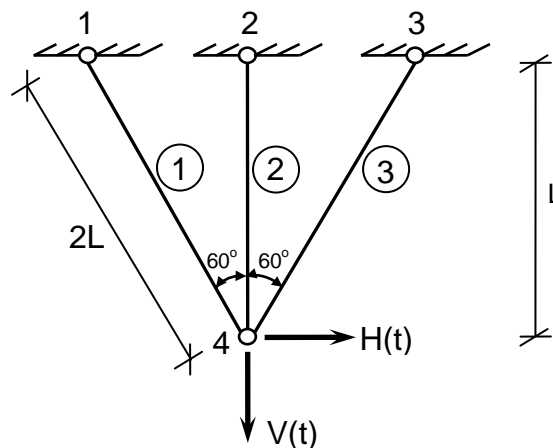


Fig. 1 Three bar truss example

The structure was assumed to be made of steel. The following geometrical and material data were used:  $L = 300\text{cm}$ , Young's modulus  $E = .21 \times 10^5 \text{ kN/cm}^2$  and yield stress  $\sigma_y = 400\text{kN/cm}^2$ . All the elements of the truss have an equal cross-sectional area of  $A = 5\text{cm}^2$ . In order to have a good approximation to the rigid-plastic behaviour we impose the constant  $n$  in the Ramberg – Osgood relationship equal to 50.

Three cases of loading have been considered to test the aforementioned methodology. Each of these cases leads to different cyclic behaviour. The time variation of each load case over four cycles can be seen in Fig. 2a, 3a, 4a. The results for the elements 1, 3 are equal to the ones of element 2, but with opposite sign.

a) The first cyclic loading case has the following variation with time:

$$V(t) = 300 \sin^2(\pi t), H(t) = 0 \quad (9)$$

The analysis shows that bar 2 initially yields in tension and bars 1, 3 remain in the elastic region. The final steady cyclic state residual stress distribution for the elements 1, 3 inside the cycle, that was computed, may be seen in Fig. 2b. It may be observed that this load case leads to elastic shakedown.

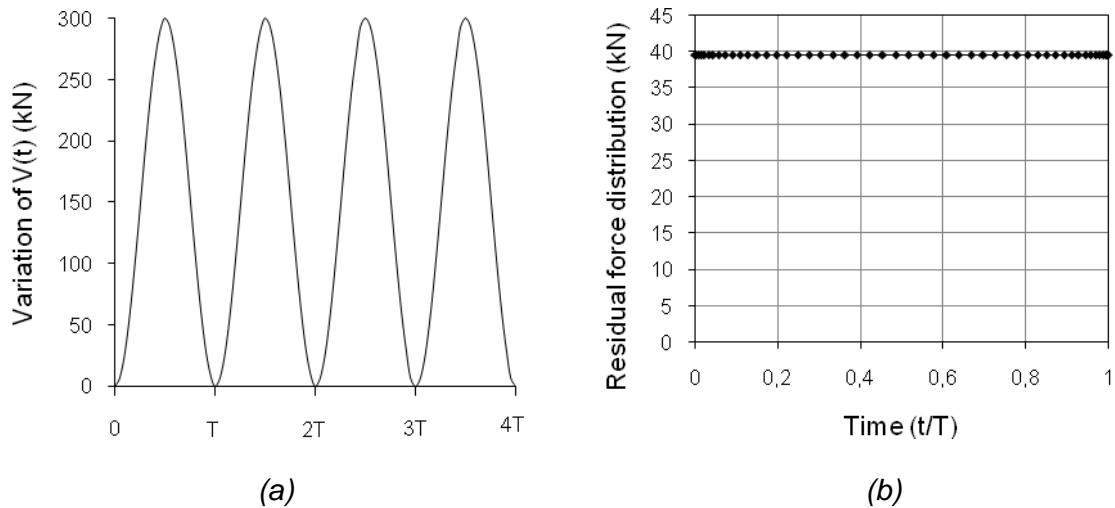


Fig. 2 (a) Load variation with time over four periods for load case a, (b) Steady cyclic state residual force distribution inside a cycle for load case a (elements 1,3)

b) The second cyclic loading case has the following variation with time:

$$V(t) = 300 \sin(2\pi t), H(t) = 0 \quad (10)$$

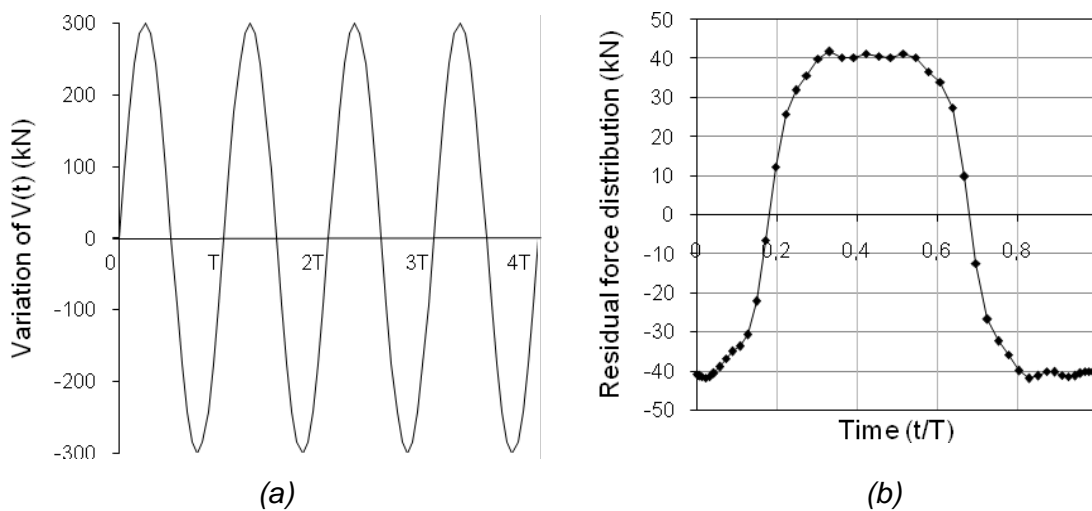


Fig. 3 (a) Load variation with time over four periods for load case b, (b) Steady cyclic state residual force distribution inside a cycle for load case b (elements 1,3)

The analysis shows that during the first half of the cycle bar 2 yields in tension and during the second half, bar 2 yields in compression. We also see that the plastic strain rates for the bar 2 change sign inside the cycle. Therefore this load case leads the structure to alternating plasticity. The steady cyclic state residual stress distribution for the elements 1, 3 inside the cycle, that was computed, may be seen in Fig. 3b.

c) The third cyclic loading case includes a variation with time of both the vertical and the horizontal load:

$$V(t) = 350 \sin^2(\pi t), H(t) = 200 \sin(2\pi t) \quad (11)$$

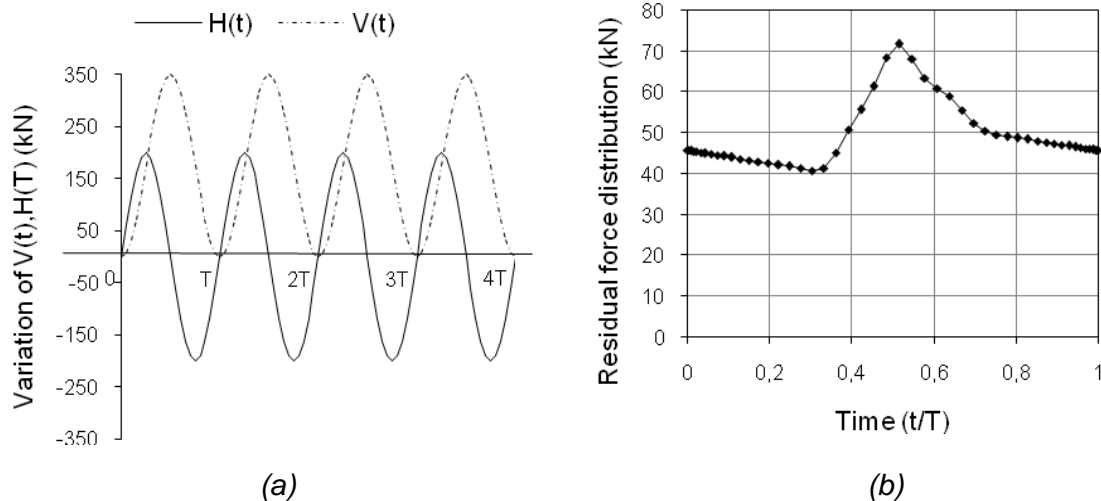


Fig. 4 (a) Load variation with time over four periods for load case c, (b) Steady cyclic state residual force distribution inside a cycle for load case c (elements 1,3)

The results obtained by the analysis show that during the first half of the cycle bar 2 yields in tension and during the second half bar 3 yields also in tension. We also see that the total change in the plastic strains over the cycle is non zero, therefore this load case leads the structure to incremental collapse. The steady cyclic state residual stress distribution inside a cycle for the elements 1, 3 that was computed, may be seen in Fig. 4b.

Due to the high value of  $n$  in order for convergence to take place, an indirect update of the Fourier coefficients was used, like the one suggested in [2], which is based on a special acceleration procedure for nonlinear systems of equations (Isaacson and Keller [5]). A very few number of terms of the Fourier series generally proved sufficient. A limited number of time points inside the cycle are needed, mainly to properly describe the time variation of the load.

All the three cases were tested using a time-stepping finite element program FEAP 8.2 [6] and the results were found in good agreement.

## CONCLUSIONS

In the present work a method is proposed that may be used for the elastoplastic analysis of simple structures under cyclic loading. The method makes possible to estimate the steady cyclic state of stress without following time stepping calculations. It is based on the decomposition of the residual stress distribution into Fourier series whose coefficients are calculated by iterations. The method which is herein applied to a simple 3-bar truss is capable to establish whether the structure adapts itself or not, according to the loading prescribed.

## REFERENCES

- [1] Weichert D., Ponter A. (eds). *Limit states of materials and structures*, Springer, 2009.
- [2] Spiliopoulos K.V. A simplified method to predict the steady cyclic stress state of creeping structures, *ASME Jnl. Appl. Mech.*, Vol. 69, pp. 148-153, 2002.
- [3] Frederick C.O., Armstrong P.J. Convergent internal stresses and steady cyclic states of stress *Jnl. Strain Anal.*, Vol. 1, pp. 154-169, 1966.
- [4] Ramberg W., Osgood W.R. Description of stress-strain curves by three parameters, *Technical Note No. 902, National Advisory Committee For Aeronautics*, Washington DC, 1943.
- [5] Isaacson E., Keller H.B. *Analysis of Numerical Methods*, J. Wiley and Sons, New York, 1966.
- [6] FEAP 8.2. *A Finite Element Analysis Program*, Taylor RL, Berkeley, California, 2008.

## A CONTACT-STABILIZED NEWMARK METHOD FOR COUPLED DYNAMICAL THERMO-ELASTIC PBLEM

**Anton Tkachuk<sup>1</sup>**

Institute für Baustatik und  
 Baudynamik, University  
 Stuttgart, Germany

ABSTRACT

A Lagrange multipliers formulation for dynamical frictionless thermo-elastic contact problem is considered. Thermal deformations and dependency of contact thermal resistance on contact pressure are assumed to be the only two coupling effects. Application of standard Newmark method to the problem may lead to spurious numerical oscillations of contact pressures and heat fluxes, inaccurate or divergent solutions. A modification of the Newmark method is proposed where contact contributions are integrated non-monolithically with backward Euler. Elimination of spurious numerical oscillations is shown in a numerical example.

### INTRODUCTION

Dynamical contact problems arise in many practical applications such as turbines, combustion engines and manufacturing. In many cases both mechanical and thermal loads play important role. If contact area and pressure change during the process, then contact heat fluxes vary strongly. The contact heat fluxes influence the temperature distribution and, consequently, thermal deformations, which may cause the change of contact area. Thus, such thermo-mechanical contact problem is intrinsically coupled and non-linear.

One may formulate these contact conditions in a weak form using Lagrange multipliers. Then independent fields of contact pressure and heat fluxes are introduced on the contact interface. Contact pressures play role of Lagrange multipliers for impenetration condition. Heat fluxes satisfy energy balance equations (for details see [1,2]). Spatial discretization of the weak form with FE reduces problem to a system of differential-algebraic equations as follows

$$\begin{cases} \mathbf{M}_{uu} \ddot{\mathbf{d}} + \mathbf{f}_{int}(\mathbf{d}, \dot{\mathbf{d}}, \mathbf{T}) + \mathbf{f}_c(\boldsymbol{\lambda}, \mathbf{d}) = \mathbf{f}_{ext}(t) \\ \mathbf{M}_{TT} \dot{\mathbf{T}} + \mathbf{r}_{int}(\dot{\mathbf{d}}, \mathbf{T}) + \mathbf{r}_c(\boldsymbol{\lambda}, \mathbf{d}, \mathbf{T}) = \mathbf{r}_{ext}(t) \\ \mathbf{g}(\mathbf{d}) \geq \mathbf{0}, \boldsymbol{\lambda} \leq \mathbf{0}, \mathbf{g}(\mathbf{d})\boldsymbol{\lambda} = \mathbf{0} \\ \mathbf{r}_c(\boldsymbol{\lambda}, \mathbf{d}, \mathbf{T})\mathbf{g}(\mathbf{d}) = \mathbf{0} \end{cases} \quad (1)$$

with  $\mathbf{M}_{uu}$  and  $\mathbf{M}_{TT}$  are matrices of mass and heat capacities;  $\mathbf{f}_{int}$  and  $\mathbf{r}_{int}$  are internal force and heat source vectors; vectors  $\mathbf{f}_{ext}$  and  $\mathbf{r}_{ext}$  are external loads; vectors  $\boldsymbol{\lambda}, \mathbf{d}, \mathbf{T}$  are unknown contact pressures, displacements and temperatures and  $\mathbf{f}_c, \mathbf{r}_c$  and  $\mathbf{g}$  are contact forces, heat fluxes and constraints.

Initial conditions are specified for displacements, velocities and temperatures. Moreover, initial conditions should not violate contact conditions and be consistent with active constraints, which also imply additional constraints on initial velocities. Initial Lagrange multipliers are recovered from equilibrium [1,3]. Altogether they read as follows

<sup>1</sup> Corresponding author. Email tkachuk@ibb.uni-stuttgart.de

$$\left\{ \begin{array}{l} \mathbf{d} = \mathbf{d}_0, \dot{\mathbf{d}} = \dot{\mathbf{d}}_0, \mathbf{T} = \mathbf{T}_0 \\ \mathbf{g}(\mathbf{d}_0) \geq \mathbf{0}, \mathbf{r}_c(\lambda_0, \mathbf{d}_0, \mathbf{T}_0) \mathbf{g}(\mathbf{d}_0) = \mathbf{0} \\ \mathbf{g}(\mathbf{d}_0) \frac{d}{d\mathbf{d}} \mathbf{g} \dot{\mathbf{d}}_0 = \mathbf{0} \\ \mathbf{g}(\mathbf{d}_0) \left( \dot{\mathbf{d}}_0 \frac{d^2}{d\mathbf{d}^2} \mathbf{g} \dot{\mathbf{d}}_0 + \frac{d}{d\mathbf{d}} \mathbf{g} \mathbf{M}_{uu}^{-1} [\mathbf{f}_{ext}(t_0) - \mathbf{f}_{int}(\mathbf{d}_0, \dot{\mathbf{d}}_0, \mathbf{T}_0) - \mathbf{f}_c(\lambda_0, \mathbf{d}_0)] \right) = \mathbf{0} \end{array} \right. \quad (2)$$

In case of thermo-hyperelastic material, velocities  $\dot{\mathbf{d}}$  do not explicitly enter  $\mathbf{f}_{int}$  term. Thus system finally reduces to

$$\left\{ \begin{array}{l} \mathbf{M}_{uu} \ddot{\mathbf{d}} + \mathbf{f}_{int}(\mathbf{d}, \mathbf{T}) + \mathbf{f}_c(\lambda, \mathbf{d}) = \mathbf{f}_{ext}(t) \\ \mathbf{M}_{TT} \ddot{\mathbf{T}} + \mathbf{r}_{int}(\dot{\mathbf{d}}, \mathbf{T}) + \mathbf{r}_c(\lambda, \mathbf{d}, \mathbf{T}) = \mathbf{r}_{ext}(t) \\ \mathbf{g}(\mathbf{d}) \geq \mathbf{0}, \lambda \leq \mathbf{0}, \mathbf{g}(\mathbf{d})\lambda = \mathbf{0} \\ \mathbf{r}_c(\lambda, \mathbf{d}, \mathbf{T})\mathbf{g}(\mathbf{d}) = \mathbf{0} \end{array} \right. \quad (3)$$

Note, the equations (1.3-5) are nothing else but Karush-Kuhn-Tucker conditions and equation (1.6) means heat insulation in case of positive gap, i.e. contact heat conductance  $1/h_c = \Delta T/q_c$  vanishes [4]. Actually, the main challenge arises from non-smooth subsidiary conditions that are illustrated of Fig.1.

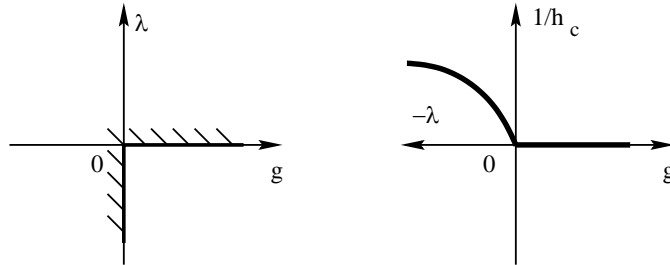


Fig. 1 Pressure/gap and contact conductance/gap relations

Rigorous analysis of the systems shows that it is a DAE with differential index 3, i.e. 3 additional differentiations are necessary to transform it into an explicit first-order system (for details see [3]). Such systems are known for number instabilities and numerical problems.

Improper time integration of the system might lead to artificial numerical oscillations of Lagrange multipliers [1-5]. This increases numerical cost and spoils accuracy. In some pathological cases divergent results may be obtained [6].

The most efficient way to repair such defect is to modify an existing time integration scheme with special treatment of the constraints. On the one hand ordinary users are familiar with such methods. On the other hand only few coding is necessary to get valuable results. Newmark method gives such opportunity. As backward methods are generally known for their stability, one can modify predictor to treat contact constraints using backward Euler (due to ideas of Lane et. al. [7]). The other idea is to include an additional projector on the predictor step. Standard Newmark predictor leads to strong violation of the constraints, which means expensive correction phase [5]. Both methods are reported to be successful in elimination of artificial oscillations for mechanical problems. However, they introduce artificial damping and generally are not energy preserving [5,7].

Here we present modification of the predictor step with backward Euler integration of the contact contributions that is extended for thermo-elastic problem. A numerical example illustrates efficiency of the proposed approach.

## 1. Standard Newmark scheme for thermo-elastic contact problem

As a starting point we use standard Newmark method (see [2,5,7]). It assumes following integration rule for the variables, predictor and corrector

$$\begin{cases} \mathbf{d}_{n+1} = \mathbf{d}_n + \Delta t \dot{\mathbf{d}}_n + \frac{\Delta t^2}{2} ((1-2\beta)\ddot{\mathbf{d}}_n + 2\beta\ddot{\mathbf{d}}_{n+1}) \\ \dot{\mathbf{d}}_{n+1} = \dot{\mathbf{d}}_n + \Delta t ((1-\gamma)\ddot{\mathbf{d}}_n + \gamma\ddot{\mathbf{d}}_{n+1}) \\ \mathbf{T}_{n+1} = \mathbf{T}_n + \Delta t ((1-\gamma)\dot{\mathbf{T}}_n + \gamma\dot{\mathbf{T}}_{n+1}) \end{cases} \quad (4)$$

$$\begin{cases} \tilde{\mathbf{d}}_{n+1} = \mathbf{d}_n + \Delta t \dot{\mathbf{d}}_n + \frac{\Delta t^2}{2} (1-2\beta)\mathbf{M}_{uu}^{-1}(\mathbf{f}_{ext,n} - \mathbf{f}_{int,n} - \mathbf{f}_{c,n}) \\ \tilde{\mathbf{T}}_{n+1} = \mathbf{T}_n + \Delta t(1-\gamma)\mathbf{M}_{TT}^{-1}(\mathbf{r}_{ext,n} - \mathbf{r}_{int,n} - \mathbf{r}_{c,n}) \end{cases} \quad (5)$$

$$\begin{cases} \mathbf{d}_{n+1} = \tilde{\mathbf{d}}_{n+1} + \beta\Delta t^2\mathbf{M}_{uu}^{-1}(\mathbf{f}_{ext,n+1} - \mathbf{f}_{int,n+1} - \mathbf{f}_{c,n+1}) \\ \mathbf{T}_{n+1} = \tilde{\mathbf{T}}_{n+1} + \Delta t\gamma\mathbf{M}_{TT}^{-1}(\mathbf{r}_{ext,n+1} - \mathbf{r}_{int,n+1} - \mathbf{r}_{c,n+1}) \\ \mathbf{g}(\mathbf{d}_{n+1}) \geq \mathbf{0}, \lambda_{n+1} \leq \mathbf{0}, \mathbf{g}(\mathbf{d}_{n+1})\lambda_{n+1} = \mathbf{0} \\ \mathbf{r}_c(\lambda_{n+1}, \mathbf{d}_{n+1}, \mathbf{T}_{n+1})\mathbf{g}(\mathbf{d}_{n+1}) = \mathbf{0} \end{cases} \quad (6)$$

The corrector system of equations (6) is implicit, i.e.  $\mathbf{d}_{n+1}$ ,  $\mathbf{T}_{n+1}$  and  $\lambda_{n+1}$  enters both left and right hand side of equation. It is also a non-linear system, which means it should be solved iteratively, i.e. with Newton-Raphson method. A consistent with (6) tangent reads as follows

$$\mathbf{A} = \begin{bmatrix} \frac{1}{\beta\Delta t^2}\mathbf{M}_{uu} + \mathbf{K}_{uu} + \lambda\mathbf{H} & \mathbf{K}_{uT} & \mathbf{G}^T \\ \mathbf{D}_{Tu} + \mathbf{K}_{Tu}^c & \frac{1}{\gamma\Delta t}\mathbf{M}_{TT} + \mathbf{K}_{TT} + \mathbf{K}_{TT}^c & \mathbf{K}_{T\lambda} \\ \mathbf{G} & \mathbf{0} & \mathbf{0} \end{bmatrix} \quad (7)$$

with  $\mathbf{G} = \frac{d\mathbf{g}}{d\mathbf{d}}$  and  $\mathbf{H} = \frac{d^2\mathbf{g}}{d\mathbf{d}^2}$  – gradient and Hessian of constraints;  $\mathbf{K}_{uu} = \frac{d\mathbf{f}_{int}}{d\mathbf{d}}$  and  $\mathbf{K}_{uT} = \frac{d\mathbf{f}_{int}}{d\mathbf{T}}$  – tangent stiffness and thermoelastic stiffness;  $\mathbf{K}_{TT} = \frac{d\mathbf{r}_{int}}{d\mathbf{T}}$ ,  $\mathbf{K}_{Tu}^c = \frac{d\mathbf{r}_c}{d\mathbf{d}}$ ,  $\mathbf{K}_{T\lambda} = \frac{d\mathbf{r}_c}{d\lambda}$  and  $\mathbf{K}_{TT}^c = \frac{d\mathbf{r}_c}{d\mathbf{T}}$  – conductivity matrices;  $\mathbf{D}_{Tu}$  – thermoelastic damping matrix.

## 2. Modified predictor for thermo-elastic contact problem

Instead of applying monolithic integration rule for external, internal, inertial and contact forces, it is suggested to integrate  $\mathbf{f}_c$  and  $\mathbf{r}_c$  non-monolithically with backward Euler. It doesn't change update rule (4), because contact terms do not explicitly enter it. The standard predictor (5) uses contact contributions on the previous step  $\mathbf{f}_{c,n}$  and  $\mathbf{r}_{c,n}$ . Now we exclude them from the predictor.

Contribution of new values  $\mathbf{f}_{c,n+1}$  and  $\mathbf{r}_{c,n+1}$  in corrector is calculated as  $\Delta t^2\mathbf{M}_{uu}^{-1}\mathbf{f}_{c,n+1}$  and  $\Delta t\mathbf{M}_{TT}^{-1}\mathbf{r}_{c,n+1}$ . Thus consistent expressions for predictor, corrector and algorithmic tangent read

$$\begin{cases} \tilde{\mathbf{d}}_{n+1} = \mathbf{d}_n + \Delta t \dot{\mathbf{d}}_n + \frac{\Delta t^2}{2} (1 - 2\beta) \mathbf{M}_{uu}^{-1} (\mathbf{f}_{ext,n} - \mathbf{f}_{int,n}) \\ \tilde{\mathbf{T}}_{n+1} = \mathbf{T}_n + \Delta t (1 - \gamma) \mathbf{M}_{TT}^{-1} (\mathbf{r}_{ext,n} - \mathbf{r}_{int,n}) \end{cases} \quad (8)$$

$$\begin{cases} \mathbf{d}_{n+1} = \tilde{\mathbf{d}}_{n+1} + \beta \Delta t^2 \mathbf{M}_{uu}^{-1} (\mathbf{f}_{ext,n+1} - \mathbf{f}_{int,n+1} - \mathbf{f}_{c,n+1} / \beta) \\ \mathbf{T}_{n+1} = \tilde{\mathbf{T}}_{n+1} + \Delta t \gamma \mathbf{M}_{TT}^{-1} (\mathbf{r}_{ext,n+1} - \mathbf{r}_{int,n+1} - \mathbf{r}_{c,n+1} / \gamma) \\ \mathbf{g}(\mathbf{d}_{n+1}) \geq \mathbf{0}, \lambda_{n+1} \leq \mathbf{0}, \mathbf{g}(\mathbf{d}_{n+1}) \lambda_{n+1} = \mathbf{0} \\ \mathbf{r}_c(\lambda_{n+1}, \mathbf{d}_{n+1}, \mathbf{T}_{n+1}) \mathbf{g}(\mathbf{d}_{n+1}) = \mathbf{0} \end{cases} \quad (9)$$

$$\mathbf{A} = \begin{bmatrix} \frac{1}{\beta \Delta t^2} \mathbf{M}_{uu} + \mathbf{K}_{uu} + \lambda \mathbf{H} / \beta & \mathbf{K}_{uT} & \mathbf{G}^T / \beta \\ \mathbf{D}_{Tu} + \mathbf{K}_{Tu}^c / \gamma & \frac{1}{\gamma \Delta t} \mathbf{M}_{TT} + \mathbf{K}_{TT} + \mathbf{K}_{TT}^c / \gamma & \mathbf{K}_{T\lambda} / \gamma \\ \mathbf{G} & \mathbf{0} & \mathbf{0} \end{bmatrix} \quad (10)$$

The advantages of the proposed modification are straightforward implementation and consistent coupled time integration. The disadvantages are two additional matrix inversions in predictor step, zeroes on diagonal of algorithmic tangent and lack of its symmetry. If we use lumped matrixes the overhead of matrix inversions is neglectable [5]. Usage of dual Lagrange multipliers allows us to eliminate zeroes on diagonal [1]. But, unfortunately, symmetric algorithmic tangent cannot be achieved within proposed approach.

### 3. Numerical example

Proposed algorithm was initially implemented and tested in computer algebra system Maple. As a numerical example we chose a problem of dynamical snap-through of a shallow arch. Despite simplicity of the example, it shows spurious oscillation of contact resultants, large sliding contact with high degree of nonlinearity and sufficient coupling between fields.

Two thermo-hyperelastic truss elements are used (St. Venant-Kirchhoff material [1]). Abrupt force  $F$  is applied in vertical direction. In addition the middle node is constrained to slide along rigid circle as shown on Fig.2. The temperature of the obstacle was defined as function of vertical displacement  $T_c = (372 - 100 d_y) \text{ K}$ , which makes term  $\mathbf{K}_{Tu}^c \neq \mathbf{0}$ .

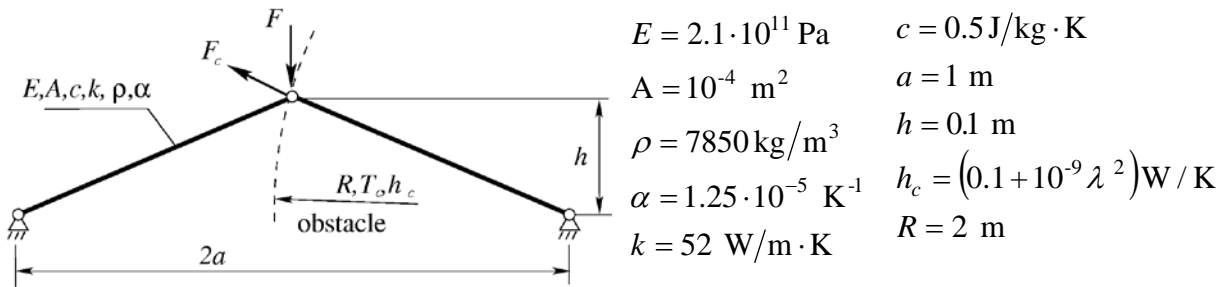


Fig.2 Setup of numerical example

Both standard and modified schemes were tested with default parameters for Newmark  $\beta = 0.25$ ,  $\gamma = 0.5$ , and constant time step  $\Delta t = 0.0005 \text{ s}$ . Lagrange multipliers over time are shown on Fig.3.

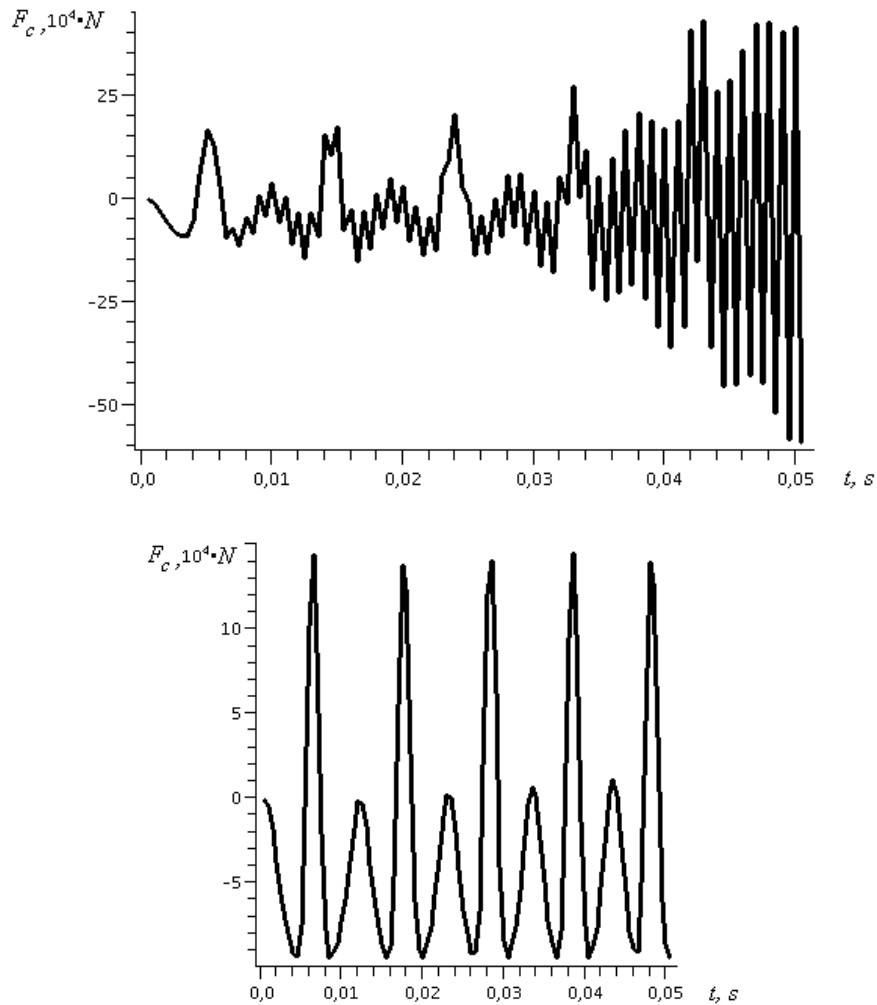


Fig.3. Lagrange multipliers from standard (upper) vs. modified (below) scheme

More pronounced difference shows up in temperature at middle node. Overestimation of contact force leads to overestimation of contact heat conductance and contact heat fluxes. Therefore the standard Newmark scheme fails to predict correctly temperatures (Fig.4) and should not be used for this problem together with Lagrange multipliers formulation (however, we did not study behavior of standard scheme together with penalty formulation).

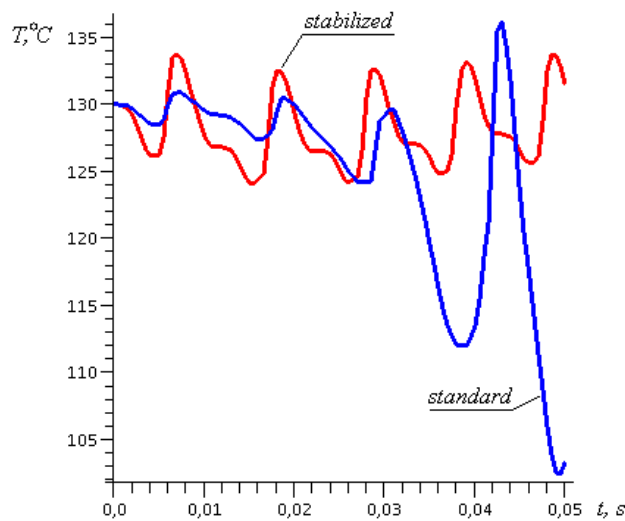


Fig.4. Temperature at middle node ( $^{\circ}C$ ) over time

## CONCLUSIONS

Standard Newmark scheme may fail for dynamical thermo-elastic contact problem. Modification of predictor/corrector of Newmark method is proposed. It is shown that this modification eliminates oscillation of Lagrange multipliers. In the future we plan to implement the method to two-body frictional contact in 3D, study the question whether it is necessary to do an additional projection to admissible set during predictor step.

## ACKNOWLEDGMENTS

This work couldn't be done without continuous discussions and encouragement from my colleagues Thomas Cichosz and Manfred Bischoff from Institute für Baustatik und Baudynamik, Stuttgart University, Germany.

## REFERENCES

- [1] S. Hieber, B. Wohlmuth Thermo-mechanical contact problems on non-matching meshes, *Comput. Methods Appl. Mech. Engrg.*, Vol. 198, 1338-1350, 2009.
- [2] T.A. Laursen *Computational Contact and Impact Mechanics*, Springer, 2002.
- [3] U. M. Ascher, L.R. Petzold *Computer Methods for Ordinary Differential Equations and Differential-Algebraic Equations*, SIAM, Philadelphia, 1998.
- [4] D.Pantuso, K.-J. Bathe, P. A. Bouzinov A finite element procedure for the analysis of thermo-mechanical solids in contact *Computer and Structures*, Vol.75, pp 551-573, 2000.
- [5] P. Deufflhard, R. Krause, S. Ertel A contact-stabilized Newmark method for dynamical contact problems *International Journal for Numerical Methods in Engineering*, Vol. 73, pp. 1274-1290, 2008.
- [6] S. Hartmann *Kontaktanalyse dünnwandiger Strukturen bei großen Deformationen*, Ph.D. thesis, Bericht Nr. 49 (2007), Institut für Baustatik und Baudynamik der Universität Stuttgart, 2007.
- [7] C. Kane, E.A. Repetto, M. Ortiz, J.E. Marsden Finite element analysis of nonsmooth contact, *Comput. Methods Appl. Mech. Engrg.*, Vol. 180, 1-26, 1999.

## TWO-MECHANISM MODELS AND MODELLING OF CREEP

**Michael Wolff**<sup>1</sup>  
University of Bremen  
Bremen, Germany

**Michael Böhm**  
University of Bremen  
Bremen, Germany

---

### ABSTRACT

---

Two-mechanism models (or, generally, multi-mechanism models) are a useful tool for modelling of complex material behaviour, in particular for modelling of interaction of creep and plasticity. As we will demonstrate, pure creep can also be modelled by two-mechanism models.

---

### INTRODUCTION

1) Two-mechanism (or, generally, multi-mechanism) models have been studied and applied for the last twenty years. Their characteristic trait is the additive decomposition of the inelastic (i.e., plastic or visco-plastic, e.g.) strain into two (or multi) parts (sometimes called “mechanisms”) in the case of small deformations. In comparison with rheological models (cf. [1], e.g.), there is an interaction between these mechanisms (see Figure 1). This interaction allows to describe important observable effects, but, it requires additional efforts in modelling and simulation. Each inelastic strain part may exhibit plastic, creep or general inelastic behaviour. The (thermo-)elastic strain is not regarded as an own mechanism. Each mechanism has its own internal variables with corresponding evolution equations. Moreover, each mechanism may have an own yield criterion, or, there may be common yield criteria for several mechanisms. Thus, in the case of two mechanisms, there are possible models of the type 2M1C and 2M2C. That means two mechanisms with one or two yield criteria. A mechanism without yield criterion like creep can be formally treated as a mechanism with its own criterion with zero yield stress.

If the inelastic strain is seen as one mechanism (as it was historically first), one refers to a “unified model” (or “Chaboche” model) (cf. the survey [2] and the references cited therein). (That means plastic and viscous components are considered together in the same variable.) As explained in [3] and [4], there are experimentally observable effects (inverse strain-rate sensibility, e.g.) which can be qualitatively correctly described by the two-mechanism approach.

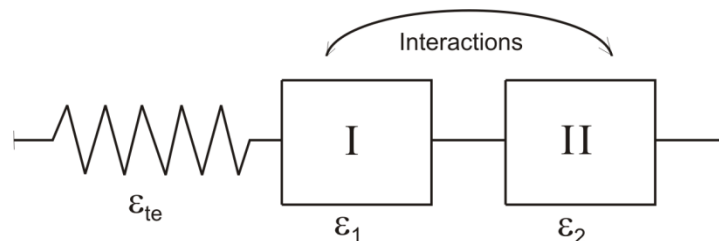


*Fig. 1 Scheme of a two-mechanism model. The two inelastic mechanisms 1 and 2 have their own evolution equations. But, they are not independent from each other. The thermoelastic strain  $\varepsilon_{te}$  is usually not regarded as a mechanism*

2) For modelling and applications of multi-mechanism models we refer to [3], [4], [5], [6], [2], [7], [8], [9], [10] and the references therein.

---

<sup>1</sup> Corresponding author: mwolff@math.uni-bremen.de

3) Two-mechanism models have been applied in modelling of cyclic plasticity (cf. [7], [8],[10], e.g.) and of steel behaviour (cf. [11] and the references therein). Moreover, there is a large variety of papers dealing with complex material behavior of metals, soils, composites, biological tissues etc. in which the inelastic strain is decomposed into several parts. But, as a rule, multi-mechanism models are not directly addressed. In [9], some references can be found.

4) Creep is a complex phenomenon of material behaviour. Thus, there are several approaches of modelling (cf. [12]). To our knowledge, creep (alone) is not modelled in the framework of 2M models. In this note, we propose first steps for doing so.

## 1. SOME CLASSES OF TWO-MECHANISM MODELS

In short we provide important basic relations for 2M models. Due to the limitation of this extended abstract, we only deal with 2M2C models. Besides, these models can well describe possible interactions of plasticity and creep as well as creep alone.

### 1.1 General assertions

In the framework of small deformations, the balance equation of momentum and energy as well as the Clausius-Duhem inequality are given by

$$\rho \ddot{\mathbf{u}} - \operatorname{div} \boldsymbol{\sigma} = \mathbf{f}, \quad \rho \dot{e} + \operatorname{div} \mathbf{q} = \boldsymbol{\sigma} : \dot{\boldsymbol{\varepsilon}} + r \quad (1)$$

$$-\rho \dot{\psi} - \rho \eta \dot{\theta} + \boldsymbol{\sigma} : \dot{\boldsymbol{\varepsilon}} - \frac{1}{\theta} \cdot \nabla \theta \geq 0 \quad (2)$$

The relations (1) and (2) have to be fulfilled in the space-time domain  $\Omega \times ]0, T[$ . The notation is standard:  $\rho$  - density in the reference configuration, that means for  $t = 0$ ,  $\mathbf{u}$  - displacement vector,  $\boldsymbol{\varepsilon}$  - linearized Green strain tensor,  $\theta$  - absolute temperature,  $\boldsymbol{\sigma}$  - Cauchy stress tensor,  $\mathbf{f}$  - volume density of external forces,  $e$  - mass density of the internal energy,  $\mathbf{q}$  - heat-flux density vector,  $r$  - volume density of heat supply,  $\psi$  - mass density of free (or Helmholtz) energy,  $\eta$  - mass density of entropy. The time derivative is denoted by a dot.  $\boldsymbol{\alpha} : \boldsymbol{\beta}$  is the scalar product of the tensors  $\boldsymbol{\alpha}$  and  $\boldsymbol{\beta}$ ,  $\mathbf{q} \cdot \mathbf{p}$  is the scalar product of the vectors  $\mathbf{p}$  and  $\mathbf{q}$ . We note the well-known relations

$$\boldsymbol{\varepsilon} = \boldsymbol{\varepsilon}(\mathbf{u}) := \frac{1}{2} (\nabla \mathbf{u} + \nabla \mathbf{u}^T), \quad \psi = e - \theta \eta \quad (3)$$

In the general case of inelastic material behaviour, the full strain  $\boldsymbol{\varepsilon}$  is split up via

$$\boldsymbol{\varepsilon} = \boldsymbol{\varepsilon}_{te} + \boldsymbol{\varepsilon}_{in} \quad (4)$$

( $\boldsymbol{\varepsilon}_{te}$  - thermoelastic strain,  $\boldsymbol{\varepsilon}_{in}$  - inelastic strain). Usually, the inelastic strain is assumed to be traceless, i.e.

$$\operatorname{tr}(\boldsymbol{\varepsilon}_{in}) = 0 \quad (5)$$

The accumulated inelastic strain is defined by

$$s_{in}(x, t) := \int_0^t \left( \frac{2}{3} \dot{\boldsymbol{\varepsilon}}_{in}(x, \tau) : \dot{\boldsymbol{\varepsilon}}_{in}(x, \tau) \right)^{\frac{1}{2}} d\tau \quad (6)$$

We propose for the free energy  $\psi$  the split

$$\psi = \psi_{te} + \psi_{in} \quad (7)$$

The thermoelastic part  $\psi_{te}$  is standard (cf. [9] for details) and leads to the usual material law connecting stress and thermoelastic strain:

$$\boldsymbol{\sigma} = 2\mu \boldsymbol{\varepsilon}_{te}^* + K \operatorname{tr}(\boldsymbol{\varepsilon}_{te}) \mathbf{I} - 3K\alpha(\theta - \theta_0) \mathbf{I} \quad (8)$$

$\mu > 0$  - shear modulus,  $K > 0$  - compression modulus,  $\alpha$  - linear heat-dilatation coefficient,  $\theta_0$  - initial temperature, i.e.  $t = 0$ ,  $\mathbf{I}$  - unity tensor,  $\boldsymbol{\varepsilon}_{te}^*$  - deviator of  $\boldsymbol{\varepsilon}_{te}$ , defined (in 3d case) by

$$\boldsymbol{\varepsilon}_{te}^e = \boldsymbol{\varepsilon}_{te} - \frac{1}{3} \text{tr}(\boldsymbol{\varepsilon}_{te}) \mathbf{1} \quad (9)$$

We assume that the inelastic part  $\psi_{in}$  of  $\psi$  has the general form

$$\psi_{in} = \psi_{in}(\boldsymbol{\xi}, \theta) \quad (10)$$

$\boldsymbol{\xi} = (\xi_1, \dots, \xi_m)$  ( $\xi$  - scalars or tensors) represent the internal variables. Further on, these variables will be chosen in accordance with concrete models under consideration. In the case of damage, the thermoelastic part  $\psi_{te}$  of the free energy may depend on internal variables too (cf. [12], e.g.). Internal variables have to fulfil evolution equations which are usually ordinary differential equations (ODE) with respect to the time  $t$ . As a rule, one poses zero initial conditions, i.e.

$$\xi_j(0) = 0 \quad \text{for } j = 1, \dots, m \quad (11)$$

Using standard arguments of thermodynamics (cf. [12], [13], e.g.) and assuming Fourier's heat-conduction law, from (2) one obtains the remaining dissipation inequality:

$$\boldsymbol{\sigma} : \dot{\boldsymbol{\varepsilon}} - \rho \sum_{j=1}^m \frac{\partial \psi_{in}}{\partial \xi_j} : \dot{\xi}_j \geq 0 \quad (12)$$

If (12) is fulfilled for arbitrarily chosen sets of variables, then the model under consideration is thermodynamically consistent.

Until now, the relations developed above are addressed to one-mechanism models ("Chaboche" models) as well as to two-mechanism models.

In the theory of 2M models the following decomposition is crucial:

$$\boldsymbol{\varepsilon}_{in} = A_1 \boldsymbol{\varepsilon}_1 + A_2 \boldsymbol{\varepsilon}_2 \quad (13)$$

$A_1, A_2$  are positive real numbers. As usual, the inelastic strains are trace-less:

$$\text{tr}(\boldsymbol{\varepsilon}_1) = \text{tr}(\boldsymbol{\varepsilon}_2) = 0 \quad (14)$$

Remark 1. (i) The parameters  $A_1$  and  $A_2$  open opportunities for further extensions and special applications. We refer to [5]. In many applications,  $A_1$  and  $A_2$  are equal to 1, but, they can depend on further quantities. For instance, they can constitute phase fraction in complex materials (steel, shape memory alloys, e.g.). In this sense, here is a bridge from the macro to the meso (or micro) level of modelling.

(ii) In case of  $n$  mechanisms, instead of (13), one has the split

$$\boldsymbol{\varepsilon}_{in} = \sum_{j=1}^m A_j \boldsymbol{\varepsilon}_j \quad (15)$$

with  $A_j > 0$ . In this note, we preferably deal with 2M models.

For both  $\boldsymbol{\varepsilon}_j$  we introduce *separate* accumulations

$$s_j(\boldsymbol{x}, t) := \int_0^t \left( \frac{2}{3} \dot{\boldsymbol{\varepsilon}}_j(\boldsymbol{x}, \tau) : \dot{\boldsymbol{\varepsilon}}_j(\boldsymbol{x}, \tau) \right)^{\frac{1}{2}} d\tau, \quad j = 1, 2 \quad (16)$$

Note, that  $s_{in}$  (as defined in (6)) is *not* the sum of  $s_1$  and  $s_2$ .

We introduce the local stresses  $\boldsymbol{\sigma}_1, \boldsymbol{\sigma}_2$  via

$$\boldsymbol{\sigma}_j = A_j \boldsymbol{\sigma} \quad (17)$$

To develop further the theory, 2M1C and 2M2C models are separately considered. As mentioned above, here, we only deal with 2M2C models.

## 1.2 Two-mechanism models with two yield criteria

To focus, here, we do not consider isotropic hardening in the case of (visco-)plastic mechanisms. Thus, the forthcoming explanations will become shorter. However, the main idea of the two-mechanism approach (mutual coupling of mechanisms) can be made clear. We refer to [9] and [10] for detailed descriptions.

The ansatz for the inelastic part of the free energy in (10) will be specialised in the following way: Assuming the internal variables to be given  $\xi = (\alpha_1, \alpha_2)$ , we suppose

$$\psi_{in} = \psi_{in}(\theta, \alpha_1, \alpha_2) := \frac{1}{3\rho} (c_{11}(\theta) \alpha_1 : \alpha_1 + 2c_{12}(\theta) \alpha_1 : \alpha_2 + c_{22}(\theta) \alpha_2 : \alpha_2) \quad (18)$$

The tensorial symmetric internal variables of strain type  $\alpha_1$  and  $\alpha_2$  are related to kinematic hardening and associated with the mechanisms  $\epsilon_1$  and  $\epsilon_2$ , respectively.

Remark 2. For “frozen” temperature, the inelastic free energy  $\psi_{in}$  in (18) is a convex function with respect to  $\alpha_1$  and  $\alpha_2$ , if there hold (for all admissible  $\theta$ ) the conditions

$$c_{11}(\theta) \geq 0, \quad c_{12}^2(\theta) \leq c_{11}(\theta)c_{22}(\theta) \quad (19)$$

Clearly, the quadratic form in (18) is also positive semi-definite.

The definition of the backstresses  $\mathbf{X}_1$  and  $\mathbf{X}_2$  associated with the mechanisms  $\epsilon_1$  and  $\epsilon_2$ , respectively, and (18) give

$$\mathbf{X}_1 := \rho \frac{\partial \psi_{in}}{\partial \alpha_1} = \frac{2}{3} c_{11} \alpha_1 + \frac{2}{3} c_{12} \alpha_2, \quad \mathbf{X}_2 := \rho \frac{\partial \psi_{in}}{\partial \alpha_2} = \frac{2}{3} c_{12} \alpha_1 + \frac{2}{3} c_{22} \alpha_2 \quad (20)$$

The relations (12), (13), (17) and (18) imply the following remaining inequality

$$(\sigma_1 - \mathbf{X}_1) : \dot{\epsilon}_1 + (\sigma_2 - \mathbf{X}_2) : \dot{\epsilon}_2 + \mathbf{X}_1 : (\dot{\epsilon}_1 - \dot{\alpha}_1) + \mathbf{X}_2 : (\dot{\epsilon}_2 - \dot{\alpha}_2) \geq 0 \quad (21)$$

Based on the von Mises stress, we define the quantities

$$J_j := \sigma_{vM}(\sigma_j - \mathbf{X}_j) := \left( \frac{3}{2} (\sigma_j^* - \mathbf{X}_j^*) : (\sigma_j^* - \mathbf{X}_j^*) \right)^{\frac{1}{2}} \quad j = 1, 2 \quad (22)$$

( $\sigma_{vM}(\sigma)$  - von Mises equivalent stress of  $\sigma$ ) and the *two* yield functions

$$f_j(\sigma_1, \sigma_2, \mathbf{X}_1, \mathbf{X}_2, R_{0j}) := J_j - R_{0j} \quad j = 1, 2 \quad (23)$$

( $R_{0j}$  is the yield stress of the  $j^{\text{th}}$  mechanism in case of plasticity. To focus, we do not consider isotropic hardening.) and finally,

$$\mathbf{n}_j := -\frac{\partial f_j}{\partial \mathbf{X}_j} = \frac{3}{2} \frac{\sigma_j^* - \mathbf{X}_j^*}{J_j} \quad j = 1, 2 \quad (24)$$

We assume evolution laws for the inelastic mechanisms  $\epsilon_1$  and  $\epsilon_2$  in a *common* form for all inelastic mechanisms:

$$\dot{\epsilon}_j = \lambda_j \mathbf{n}_j \quad j = 1, 2 \quad (25)$$

The relations (16), (22), (24) and (25) yield

$$\lambda_j = \dot{s}_j \quad j = 1, 2 \quad (26)$$

To distinguish between plastic and creep behaviour, we define the inelastic multipliers  $\lambda_j$  in a suitable way. Clearly, both mechanisms can be of the same kind, but, they can differ, too.

Plastic mechanism: If the  $j^{\text{th}}$  mechanism is plastic, the (plastic) multiplier  $\lambda_j \geq 0$  has to fulfil

$$\lambda_j = 0, \quad \text{if } f_j(\sigma_1, \sigma_2, \mathbf{X}_1, \mathbf{X}_2, R_{0j}) < 0 \quad (27)$$

$$\lambda_j \geq 0, \quad \text{if} \quad f_j(\boldsymbol{\sigma}_1, \boldsymbol{\sigma}_2, \mathbf{X}_1, \mathbf{X}_2, R_{0j}) = 0 \quad (28)$$

As usual in plasticity,  $\lambda_j$  can be expressed via loading conditions (cf. [13], e.g.). In numerical schemes, approximations of  $\lambda_j$  will be determined simultaneously with other quantities.

Creep mechanism: If the  $j^{\text{th}}$  mechanism models creep, the multiplier  $\lambda_j$  can be defined by

$$\lambda_j := \alpha_j \left( \frac{\sigma_{VM}(\boldsymbol{\sigma}_j - \mathbf{X}_j)}{D_j} \right)^{m_j} s_j^{k_j} \quad j = 1, 2 \quad (29)$$

$\alpha_j > 0$ ,  $m_j > 0$ ,  $k_j$  generally depend on temperature  $\theta$ ,  $s_j$  is the accumulation in accordance with (16). The drag stress  $D_j > 0$  may be constant, or it may have an own evolution (cf. [2], e.g.). Via the exponent  $k_j$  the stadia of creep can be distinguished:

- $k_j < 0$  - primary creep,
- $k_j = 0$  - secondary creep,
- $k_j > 0$  - tertiary one.

Clearly, in the case of creep there is no yield stress. Formally, one can use a yield function as in (23) without  $R_{0j}$ .

Note that viscoplastic mechanisms can be dealt with analogously. There remain the evolution equations for the internal variables  $\boldsymbol{\alpha}_j$ . We make a common proposal for plastic and creep behaviour:

$$\dot{\boldsymbol{\alpha}}_j = \dot{\boldsymbol{\epsilon}}_j - \frac{3}{2} \sum_{i=1}^2 b_{ji} \mathbf{X}_i \lambda_i \quad j = 1, 2 \quad (30)$$

This proposal extends the wide-spread approach which is covered by  $b_{12} = b_{21} = 0$  (cf. [2], e.g.). To save thermodynamic consistency, we require that the (generally temperature dependent) matrix  $\mathbf{b}$  is positive semi-definite. However, the matrix  $\mathbf{b}$  is not necessarily symmetric. This gives more possibilities for modelling. We demonstrate this in short. For *constant*  $c_{ij}$ , (20) and (30) imply the following generalised Armstrong-Frederick relations (cf. [2], e.g.):

$$\dot{\mathbf{X}}_1 = \frac{2}{3} c_{11} \dot{\boldsymbol{\epsilon}}_1 - c_{11} (b_{11} \mathbf{X}_1 + b_{12} \mathbf{X}_2) \lambda_1 + \frac{2}{3} c_{12} \dot{\boldsymbol{\epsilon}}_2 - c_{12} (b_{21} \mathbf{X}_1 + b_{22} \mathbf{X}_2) \lambda_2 \quad (31)$$

$$\dot{\mathbf{X}}_2 = \frac{2}{3} c_{12} \dot{\boldsymbol{\epsilon}}_1 - c_{12} (b_{11} \mathbf{X}_1 + b_{12} \mathbf{X}_2) \lambda_1 + \frac{2}{3} c_{22} \dot{\boldsymbol{\epsilon}}_2 - c_{22} (b_{21} \mathbf{X}_1 + b_{22} \mathbf{X}_2) \lambda_2 \quad (32)$$

If  $c_{12} = 0$ ,  $b_{12} = 0$ ,  $b_{11} > 0$ , and  $b_{22} > 0$ , the backstress  $\mathbf{X}_1$  has an influence on the evolution of  $\mathbf{X}_2$ , but not vice versa. Under the assumption “matrix  $\mathbf{b}$  positive semi-definit”, the above model is thermodynamically consistent for plastic and creep mechanisms (cf. (21)).

## CONCLUSIONS

In this extended abstract, only some basic items of 2M models could be sketched. In our conference contribution, we intend to deal with:

- further approaches for evolution equations,
- thermodynamic consistency in non-standard cases,
- 3M models,
- problems of parameter optimisation,
- formulation of arising mathematical problems.

## ACKNOWLEDGEMENT

This work has partially been supported by the Deutsche Forschungsgemeinschaft (DFG) via the Collaborative Research Centre SFB 570 “Distortion Engineering” at the University of Bremen as well as via the research project BO1144/4-1 “Mehr-Mechanismen-Modelle”.

## REFERENCES

- [1] Palmov V.A. *Vibrations of elasto-plastic bodies*, Springer-Verlag, Berlin, 1998.
- [2] Chaboche J. L. A review of some plasticity and viscoplasticity theories, *Int. J. of Plast.*, Vol. 24, pp. 1642-1693, 2008.
- [3] Contesti E., Cailletaud G. Description of creep-plasticity interaction with non-unified constitutive equations: application to an austenitic steel, *Nucl. Eng. Des.*, Vol. 116, pp. 265-280, 1989.

- [4] Cailletaud G., Sai K. Study of plastic/viscoplastic models with various inelastic mechanisms, *Int. J. of Plast.*, Vol. 11, pp. 991-1005, 1995.
- [5] Sai K., Cailletaud G. Multi-mechanism models for the description of ratcheting: Effect of the scale transition rule and of the coupling between hardening variables, *Int. J. of Plast.*, Vol. 23, pp. 1589-1617, 2007.
- [6] Wolff M., Taleb L. Consistency for two multi-mechanism models in isothermal plasticity, *Int. J. of Plast.*, Vol. 24, pp. 2059-2083, 2008.
- [7] Hassan T., Taleb L., Krishna S. Influence of non-proportional loading on ratcheting responses and simulations by two recent cyclic plasticity models, *Int. J. of Plast.*, Vol. 24, pp. 1863-1889, 2008.
- [8] Taleb L., Cailletaud G. An updated version of the multi-mechanism model for cyclic plasticity, *Int. J. of Plast.*, Vol. 26, pp. 859-874, 2010.
- [9] Wolff M., Böhm M., Taleb L. Two-mechanism models with plastic mechanisms - modelling in continuum-mechanical framework, *Berichte aus der Technomathematik*, 10-05, Universität Bremen, Germany, 2010.
- [10] Sai K Multi-mechanism models: Present state and future trends, in press *Int. J. of Plast.*, 2010.
- [11] Wolff M., Böhm M., Helm D. Material behaviour of steel – modelling of complex phenomena and thermodynamic consistency, *Int. J. of Plast.*, Vol. 24, pp. 746-774, 2008.
- [12] Naumenko K., Altenbach H. *Modeling Of Creep For Structural Analysis*, Springer-Verlag, Berlin, 2007.
- [13] Besson J., Cailletaud G., Chaboche J.-L., Forest S. *Mécanique non linéaire des matériaux*, Hermes Science Europe Ltd, Paris, 2001.
- [14] Haupt P. *Continuum Mechanics and Theory of Materials*, Springer-Verlag, Berlin, 2002.

**NUMERICAL SIMULATION OF CRACK TIP OPENING AT STATIC AND  
DYNAMIC CREEP**

**P. Yasniy**

**V. Hlado**

**S. Fedak**

**I. Shulhan**

Ternopil Ivan Pul'uj State  
Technical University,  
Ternopil, Ukraine

---

**ABSTRACT**

---

The paper presents the finite element model for studying of brittle inclusions influence in the material on opening in the crack tip in the conditions of static and dynamic creep, when the parameters of structural heterogeneousness are taken into consideration. Using this model, there have been studied the influence of shape ratio and specific part of inclusions of heterogeneous material on the crack tip opening and material damage at static and dynamic creep.

---

**INTRODUCTION**

During monotonously increasing loading of elasto-plastic body with a sharp crack, there occurs opening of its tip to the particular point  $\delta_k$ , on reaching which the crack begins to spread. In conditions of creep of cracked body the gradual increase of its opening takes place as a results of creep processes. In the proximity of crack front, because of large stress in the material, the cavities, gaps, submicrocracks, etc. are formed which is denoted by the trajectory of its growth during further expansion.

The crack tip opening's rate during creep depends much on loading applied. In particular, the cyclic component of loading noticeably influences on both deformation of the materials and microstructural changes [1]. During dynamic creep repeated change of loading from minimum to maximum point takes place, and is followed by the increase of plastic deformation [2]. Plastic deformation storage at creep conditions depends on loading regime while cyclic component noticeably decreases durability in comparison with static loading [2,3].

At the creep conditions in components (inclusion or matrix) of heterogeneous alloy the ultimate state can be reached, and as the reason of this, the local parts of the components will be fractured. This causes strain redistribution in the material. Finite element method (FEM) simulation of inclusion's influence on the crack growth trajectory in composite with aluminum matrix was presented in [4,5].

Modeling of inclusions clustering influences aluminum alloy damage, void and microcracks formation had been done in [6]. It was shown that the failure stress of composites increases with increasing the average nearest-neighbor distance between the particles in the composite, and with decreasing the degree of clustering of particles.

The modeling of the influence of size and mechanical property features of inclusion on crack growth had been presented [7-9]. Numerical results for an edge-cracked, graded specimen show that the particle shape and orientation for the same phase volume fractions have negligible effects on fracture reliability, even for graded materials with a high modular ratio [8].

The influence of the specific part and inclusions shape ratio on crack tip opening at the creep and dynamic creep conditions is not studied well.

In this article the FEM modeling of brittle inclusions fracture in the heterogeneous material on crack tip opening in the conditions of creep and dynamic creep is made, when the parameters of specific part and inclusions shape ratio is taken into consideration.

## 1. METHODS OF INVESTIGATION

For studying of influence of brittle inclusions fracture in the material on opening in the crack tip at the conditions of static creep and dynamic creep, the FEM model was developed (Fig.1). In the crack tip the structurally non-homogenous elements are regarded. The model consists of three components: plastic matrix, brittle inclusion, that are placed in matrix according to two-dimension normal law of distribution and material itself, which is modeled (Fig.1). The inclusions are oriented in the direction of loading application.

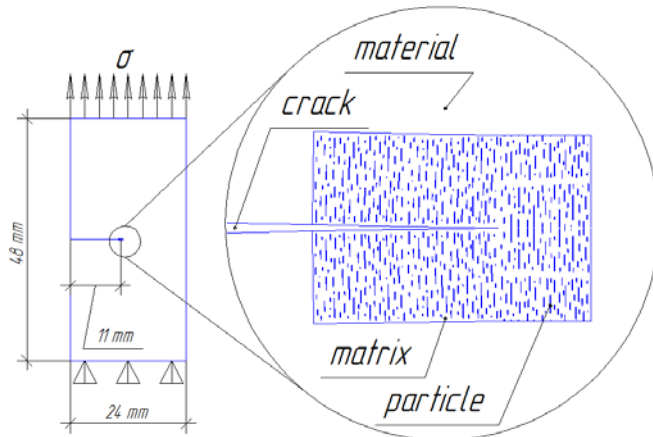


Fig. 1 Calculation model with crack with structurally heterogeneous block in the crack tip

its vertical motion was limited (Fig.1). Finite element net for the models was created by means of two-dimensional element Plane 82 [11]. The element has the qualities of quadratic displacements representation and is used for modeling with irregular net of finite elements. It has eight nodes, with two degrees of freedom in each node. The element has the features of plasticity, hyperelasticity, creep, hardness, increase at existence of loading, noticeable displacements and strains. The element can take quadrangular and triangular shape. The modelling was made in the plane strain conditions. For calculations the option of matrix and inclusions fracture was activated in the model. Fracture was made by method, described in [12], when unsteadiness of tension fields and deformations in the crack tip was taken into account.

Creep was modelled at constant stress intensity factor (SIF)  $K_s$  (curve 1, Fig. 3). Dynamic creep was modelled with implementation of high-frequency ( $f = 25$  Hz) and low-amplitude ( $K_a = \pm 1,1 \text{ MPa} \sqrt{m}$ ) component (curve 2) on constant loading. The meaning of maximum SIF at dynamic creep conditions  $K_{\max}$  was ensured, when  $K_s = K_{\max} = 31,1 \text{ MPa} \sqrt{m}$ .

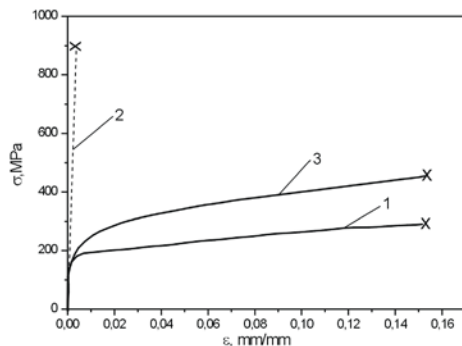


Fig. 2 Diagrams of deformation for matrix (1), inclusions (2) and total diagram for strain of the material (3)

It was admitted that inclusions deform only elastically and elasticity module of the 1-st kind is bigger than that of the matrix (Fig.2). Complete mechanical characteristics of matrix (curve 1) and inclusions (curve 2) interaction correspond the diagram of material deformation (curve 3). Mechanical characteristics of models structural components were equal to analogical characteristics of Al6Mg alloy [10].

The calculations were made in elastoplastic aspect. The effort was applied to the upper horizontal line of the model, the lower line was fixed, and

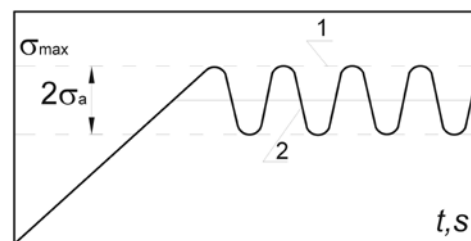
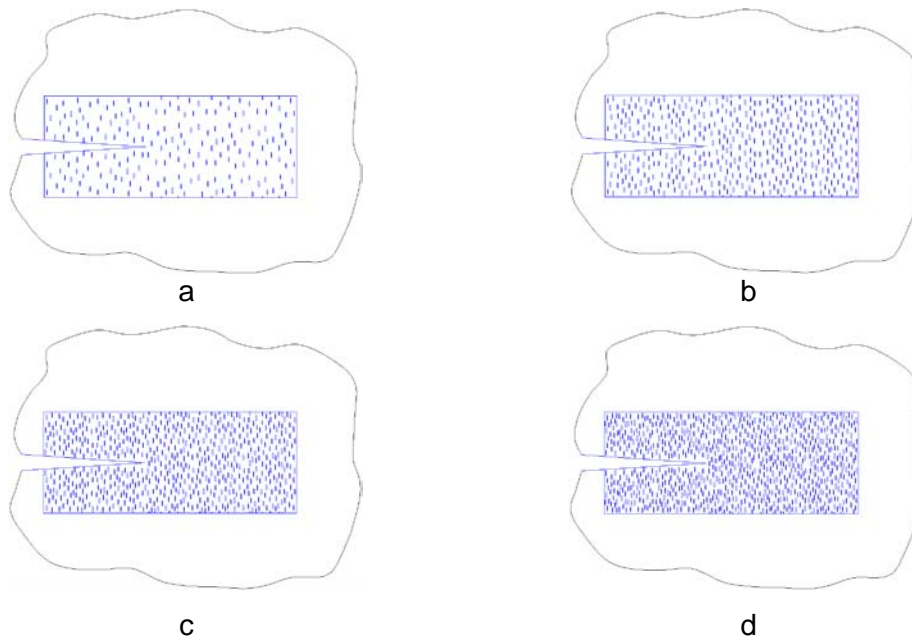


Fig. 3 Scheme of loading during testing: 1 – static creep; 2 – dynamic creep

For studying of influence of structural unhomogeneous parameters (specific part (S) and shape ratio ( $\alpha$ ) of inclusions) on crack tip opening and strength at creep and dynamic creep conditions, in software complex ANSYS two groups of finite element models were developed.

The first group of models (Fig.4) was used for studying the influence of specific part of inclusions S on crack tip opening. In all four models of this group the inclusions size was not changed: inclusion diameter  $d = 0,1 \mu\text{m}$ , inclusion length  $l = 0,8 \mu\text{m}$ .



*Fig. 4 Calculation models for studying of specific part influence on crack tip opening: a – S=3%; b – S=6%; c – S=9%; d – S=12%*

The influence of inclusion shape ratio on crack tip opening was studied on the second model group. In all models the specific part ( $S=6\%$ ) and the diameter of inclusion ( $d = 0,1 \mu\text{m}$ ) remained unchanged.

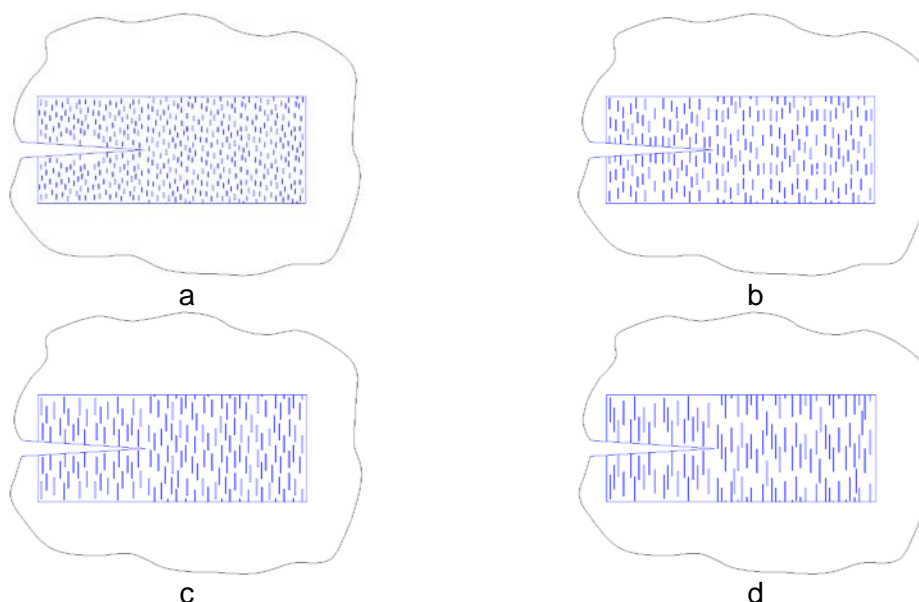


*Fig. 5 Calculation models for studying of influence of inclusion shape ratio on crack tip opening: a –  $\alpha = 8$ ; b –  $\alpha = 16$ ; c –  $\alpha = 25$ ; d –  $\alpha = 36$*

The model loading has grown iteratively ranging from 0 to  $31,1 \text{ MPa}\sqrt{m}$  with the iteration step  $0,1 \text{ MPa}\sqrt{m}$ . On every loading step, the condition of inclusions and matrix fracture was checked

and elements, which satisfied that conditions (limit stress of matrix fracture  $\sigma_f^{matrix} = 825MPa$ , as well as for inclusions fracture  $\sigma_f^{particles} = 1100MPa$  [12]) were deactivated.

For crack tip opening calculation, specially created post-processor macroses were used on every iterational step of loading. Application of these macroses gives the possibility to automate receiving the calculation results and their working out. During calculations the damage of the simulated material in the vicinity of the crack tip in the models of the first and second group at static and dynamic loading, has been studied. For this purpose in the area of critical strain of inclusion fracture (Fig. 6), the area of all voids, which appeared as a result of structural component fracture, was found.

The relation of these voids size to the area analyzed denotes damage of the material ( $\omega$ ). The size of structurally unhomogenous block in the crack tip was defined by the area on which normal strains are equal to those of inclusions fracture.

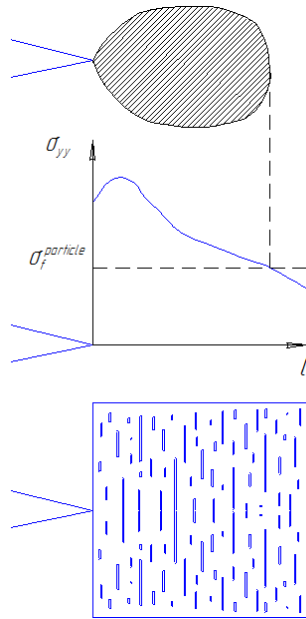


Fig. 6 Area of material damage measurement

To calculate the crack tip opening the known EMP method [13] with taking into consideration the real strain, was used. It is based on supposition that material deformation in the crack creep tip can be modeled by the smooth specimen creep with a length  $L_{ref}$  at uniaxial test with stress  $\sigma_{ref}$ :

$$\sigma_{ref} = \frac{P \cdot \sigma_{0,2}}{P_{0,2}}, \quad (1)$$

where  $\sigma_{0,2}$  is the yield stress;  $P_{0,2}$  is the strength at the strain 0,2%.

The length of the conventional smooth specimen was taken as proportional to the width of remaining undestroyed part of a cracked specimen:

$$L_{ref} = \gamma (b - l), \quad (2)$$

where  $\gamma$  – ratio;  $b$  – specimen width;  $l$  – crack length.

The  $\gamma$  ratio was defined from the terms that length increase  $\Delta L_{ref}$  of conventional specimen was equal to smooth specimen crack tip opening increase because of creep:

$$\Delta L_{ref} = \Delta \delta. \quad (3)$$

Creep strain increase of the smooth specimen  $\Delta L_{ref}/L_{ref} = p$  is satisfactorily described by relation of creep strain on time, when shape ratio change and specific part of inclusions are taken into consideration [14]:

$$p = \left( \frac{\sigma_{ref}}{1 - \omega} \right)^{C_1} t^{C_2} \alpha^{C_3} (C_4 + C_5 S), \quad (4)$$

where  $C_1, C_2, C_3, C_4, C_5$  are the constants.

On the basis of equation (4) the increasing of the opening  $\Delta \delta$  in the creep conditions is described as follows:

$$\Delta \delta = \left( \frac{\sigma_{ref}}{1 - \omega} \right)^{C_1} t^{C_2} \alpha^{C_3} (C_4 + C_5 S) \cdot L_{ref}. \quad (5)$$

## 2. RESULTS OF CALCULATIONS AND DISCUSSION

On Fig. 7 the fragments of models in the creep (a) and dynamic creep (b) conditions at equal material damage (total area of voids that appeared) are shown. The quantity and voids size considerably depends on type of loading applied to the calculation model. At creep, big voids are formed but their number is not large (Fig.7a). Vice versa, at dynamic creep small sized voids appear, but their quantity is larger (Fig.7b).

During simulation of creep and dynamic creep processes, damage of material model was considered and on every iterational step in the time of loading opening in the crack tip has been measured. The dependence between the crack tip opening and loading time in the conditions of creep and dynamic creep at different specific part of inclusions and shape ratio is presented on Fig. 8. Cyclic

component of the loading causes bigger crack tip opening in comparison with static loading at constant SIF  $K_{\max}$ . When the specific part of inclusions increases (Fig.8a) strength of the material grows and plasticity in around the crack is getting less. It causes crack tip opening decrease at equal loading time. Inclusions shape ratio growth at constant diameter causes the inclusions length growth and material armation, as a results, the crack tip opening is getting less at the same time of loading application. Eq. (5) was used to describe the crack tip opening increase in time  $\Delta\delta$  at creep and dynamic creep. When  $\gamma=0,18$  [15], stated for every model (S,  $\alpha$  - const),  $L_{ref}$  and  $\sigma_{ref}$  are found. Damage ( $\omega$ ) was defined in the equal time (5 min) according to the methods described. On Fig.8 the results, received by FEM and re-calculation by formula (5) with material damage taken into consideration, are shown. Accuracy between the calculation data by formula (5) and results received by FEM is not bigger than 12,5%.

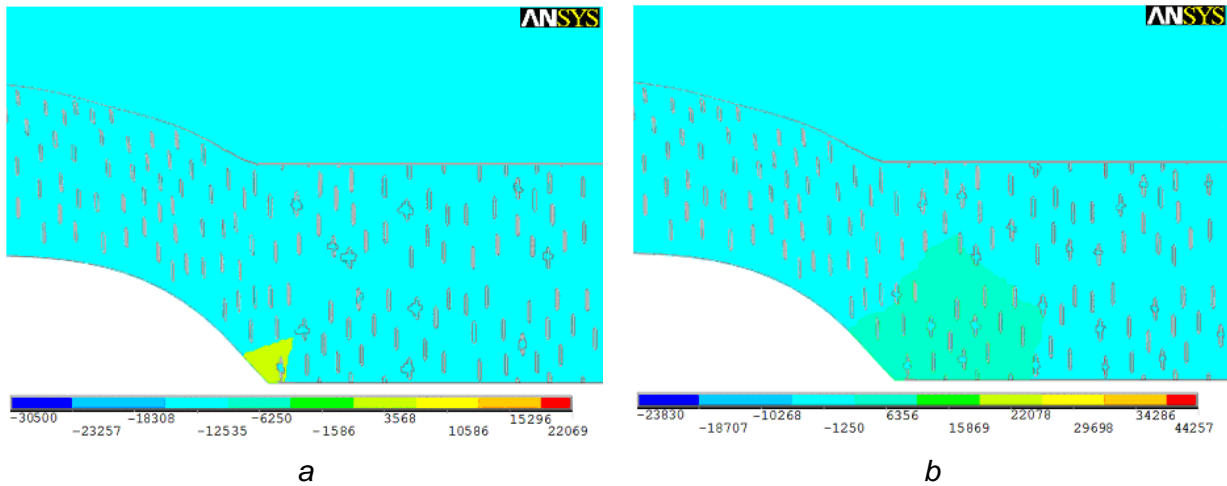


Fig. 7 Material damage in the crack tip at: a – creep; b – dynamic creep

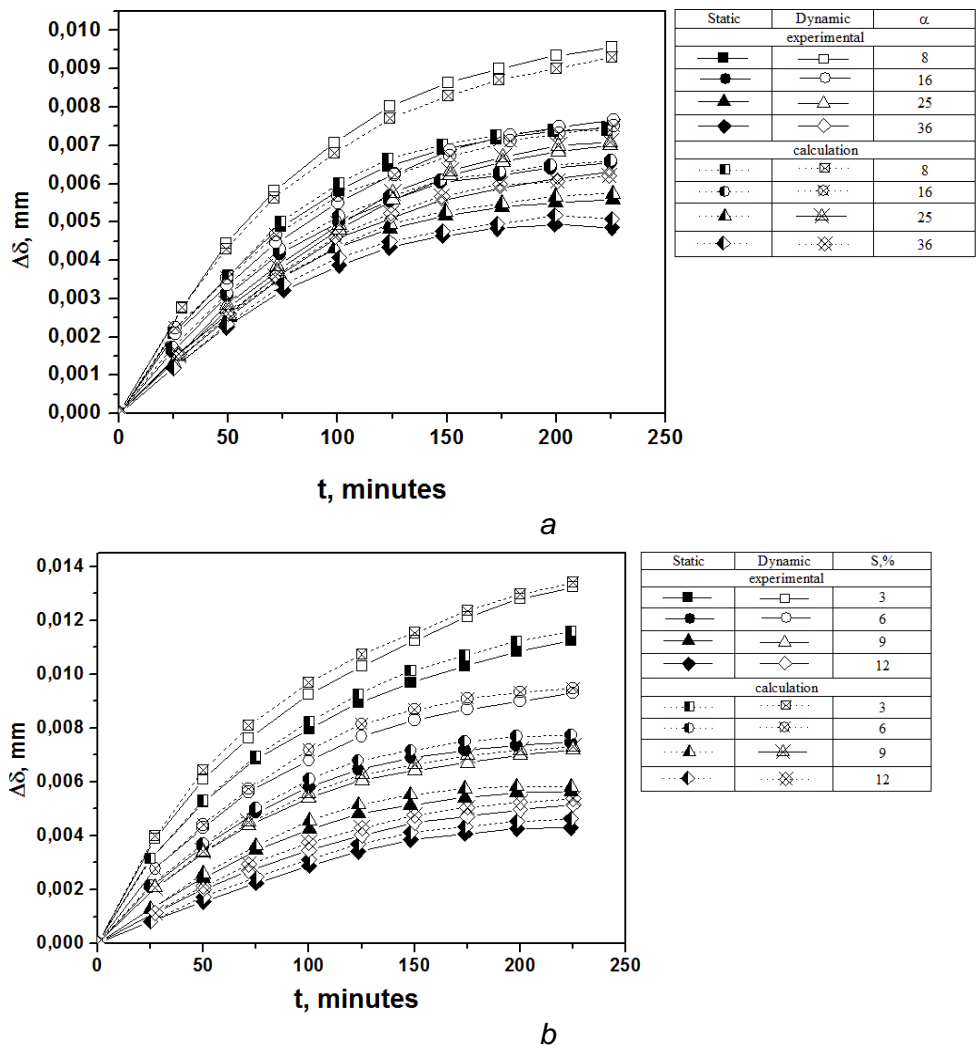


Fig. 8 Relation crack tip opening  $\Delta\delta$  to loading time  $t$  at creep and dynamic creep: a – at different inclusions shape ratio; b – at different specific part of inclusions

## CONCLUSIONS

The finite element model for studying of influence of brittle inclusions in the material on opening in the crack tip in the conditions of static and dynamic creep is made, when the parameters of structural heterogeneity is taken into consideration. Using this model the influence of shape ratio and specific part of inclusions of heterogeneous material on the crack tip opening increase and material damage at static and dynamic creep was studied.

It is stated that within the increase of the specific part and inclusions shape ratio of crack tip opening in the conditions of static and dynamic creep is decreased. It should be noted that dynamic creep is followed by larger crack tip opening than at static one.

It was found that at the same damage of heterogeneous material in the crack tip at static creep small amount of voids with larger geometric parameters is formed, and at dynamic creep bigger amount of small sized voids is observed.

The methods of crack tip opening increase calculation on the basis of EMP method is proposed with taking into consideration the damage of the material in the conditions of static and dynamic creep which includes shape ratio and specific part of inclusions of heterogeneous material. The results, received by EMP method and the proposed finite element model, have been compared.

## REFERENCES

- [1] Troshchenko V.T., Lebedev A.A., Stryzhalo V.A. et. al. *Mechanical behavior of materials at different loading types*, Kyiv, 2000. (in Russian)
- [2] Stryzhalo V.A. *Cyclic durability and creep of metals at low-cyclic loading in the condition of low and high temperatures*, Kyiv, 1978. (in Russian)

- [3] Pysarenko G.S., Mozharovskyi N.S. *Equations and limit tasks of theory of elasticity and creep: Reference book*, Kyiv, 1981. (in Russian).
- [4] Grabowski G., Pedzich Z. Residual stresses in particulate composites with alumina and zirconia matrices *Journal of the European Ceramic Society*, Vol. 27, pp. 1287–1292, 2007.
- [5] Moon R.J., Hoffman M., Rodel J., Tochino S., Pezzotti G. Evaluation of crack-tip stress fields on microstructural-scale fracture in Al–Al<sub>2</sub>O<sub>3</sub> interpenetrating network composites *Acta Materialia*, Vol. 57, pp. 570–581, 2009.
- [6] Mishnaevsky L.Jr., Derrien K., Baptiste D. Effect of microstructure of particle reinforced composites on the damage evolution: probabilistic and numerical analysis *Composites Science and Technology*, Vol. 64, pp. 1805–1818, 2004.
- [7] Mishnaevsky L.Jr., Weber U., Schmauder S. Numerical analysis of the effect of microstructures of particle-reinforced metallic materials on the crack growth and fracture resistance *International Journal of Fracture*, Vol. 125, pp. 33–50, 2004.
- [8] Chakraborty A., Rahman S. A parametric study on probabilistic fracture of functionally graded composites by a concurrent multiscale method *Probabilistic Engineering Mechanics*, Vol. 24, pp. 438–451, 2009.
- [9] Ayyar A., Chawla N. Microstructure-based modeling of the influence of particle spatial distribution and fracture on crack growth in particle-reinforced composites *Acta Materialia*, Vol. 55, pp. 6064–6073, 2007.
- [10] Yasniy P.V., Pyndus Y.I., Hlado V.B., Shulhan I.V. Methods of modelling of brittle inclusions fracture in the material using the method of finite elements *Actual problems of dynamics and strength of composites and constructions: models, methods, solutions*. Materials of International scientific technical conference (June 1-3, 2007, Samara), Orel, 2007. (in Russian)
- [11] Yasniy P.V., Shulhan I.V., Hlado V.B., Pyndus Y.I. Considering of materials structural heterogenousness of materials while modelling by means of Finite Element Method *The 7-th Ukrainian-Polish symposium 'Actual tasks of heterogenous composites mechanics'*, Lviv, pp. 43–44, 2007. (in Ukrainian)
- [12] Yasniy P.V., Pyndus Yu.I., Hlado V.B., Shulhan I.V. Computer modeling of the jump-like deformation of AMg6 alloy *Materials Science*, Vol. 44, N. 1, pp. 43–48, 2008.
- [13] Bensussan P., Piques R., Pineau A. *Nonlinear Fracture Mechanics*, Vol.1: Time-Dependent Fracture. - ASTM STP 995, Philadelphia, pp.27–54, 1989.
- [14] Yasniy P., Hlado V., Fedak S., Shulhan I. Influence of form's coefficient and density of particles on Al-alloy creep *Mechanical engineering*, Vol. 11, pp. 7–11, 2008. (in Ukrainian).
- [15] Yasniy P., Galushchak M., Fedak S. Estimation of Al-Mg6 alloy crack opening at dynamic creep *Mechanical engineering*, Vol. 6, pp.10–12, 2001. (in Ukrainian)

## ALPHABETICAL INDEX

<b>A</b>		Grabovsky A.V.	207
Adamchuk M.P.	455	Grechnev A.G.	67
Akulenko L.	9	Gristchak V.Z.	290
Altenbach H.	230,236, 449	Gulyayev V.I.	296
Amabili M.	242	<b>H</b>	
Andrianov I.V.	15	Harutyunyan E. Zh.	73
Andreev Yu.M.	398	Hedrih K.R.	78,84,302, 314
Augustyniak B.	481	Hlado V.	509
Augustyniak M.	96,262	Hudoliy S.N.	320
Avramov K.V.	21,248,250, 266,326	<b>I</b>	
Awrejcewicz J.	27,256	Ievdokymov M.M.	236
<b>B</b>		Il'chenko V.N.	332
Batkhin A.B.	33	Ivanov I.	90
Bezuglova G.	56	<b>J</b>	
Blekhman I.I.	39	Jarzyna W.	96,262
Bochenski M.	96,262	Jevstignejev V.Y.	177
Borodii M.V.	455	Jović S.	84
Borshch E.I.	320	<b>K</b>	
Borysiuk O.V.	21	Khrebet V.G.	219
Böhm M.	503	Kireenkov A.A.	102
Breslavsky D.V.	272,278, 461, 467	Kivshar Yu.	108
Breslavsky I.D.	250,266	Klimenko A.A.	146
Budnikov N.A.	344,427	Kochurov R.E.	326
Bula I.	45	Kondrashov R.E.	62
Burlayenko V.	284	Korytko Yu.	467
Bychkov A.	50	Kosevich Yu. A.	109
<b>C</b>		Kovalev A.S.	67
Chechin G.	56	Kowalewski Z.L.	481
Chernyakov Yu.A.	473	Kozhar S.	449
Chuprynin A.	461	Krasnopolskaya T.S.	164,332, 409
<b>D</b>		Krot P.V.	115
Dragunov T.N.	62	Kulyabko V.V.	121
Dzyubak L.P.	27	Kurpa L.V.	256,338, 344
<b>E</b>		Kurylov Y.	242
Egorov A.M.	415	Kyselova O.G.	125
Eremeyev V.A.	230,236	<b>L</b>	
Eshkaraeva N.G.	375	Larin O.O.	349
<b>F</b>		Lavinsky D.V.	398
Fedak S.	509	Legrand M.	352
Filipek P.	262	Leshchenko D.	9
<b>G</b>		Linnik A.	369
Garziera R.	242	Lykah V.A.	129
Gladkov S.	478	Lysenko V.V.	290
Glushakova O.V.	296	<b>M</b>	
Goncharov P.	56	Mackiewicz S.	481
		Manevich A.	358

Manevich L.I.	109,200	Simonović J.	314
Marchuk M.V.	364	Sinitsyn S.O.	437
Martynenko G.	135	Sirenko V.A.	189
Mazur O.	256,369	Smirnov V.V.	200
Meleshko V.V.	332	Sobol V.N.	398,487
Merkuryev M.	141	Sokolova S.V.	177
Mikhlin Yu.V.	146,152, 170	Spector V.M.	409
Morachkovska I.O.	427	Spiliopoulos K.V.	492
Morachkovsky O.K.	272,398, 467,487	Stepchenko O.S.	349
Morozov A.D.	62	Strel'nikova H.	250
Mukherjee I.	158	Svendsen B.	478
<b>N</b>		Syrkin E.S.	129
Nastenka I.A.	125	Szelązek J.	481
Naumenko K.	449	Szymczak T.	481
Naumov I.	278	<b>T</b>	
Nazirov Sh.A.	375	Tatarinova O.	461
Novotna N.N.	378	Temis J.M.	421
<b>O</b>		Temis M.J.	415
Olevs'kyi V.I.	15	Timchenko G.N.	427
Onyshchenko A.	278	Tkachenko V.	369
Osetrov A.A.	377	Tkachuk A.	497
<b>P</b>		Tkachuk M.A.	207
Pakosh V.S.	364	Tkachuk M.M.	207
Panagiotou K.D.	492	Turbal Yu.	431
Pankratova M.L.	67	<b>U</b>	
Pasechnik A.N.	378	Ueda Y.	213
Pasechnik V.A.	378	<b>V</b>	
Pechernyi V.A.	183	Vdovina E.K.	437
Pechuk E.D.	164	Veljović L.	78
Pellicano F.	384	Velmagina N.O.	219
Perepelkin N.V.	170	Verbitskii V.G.	219
Petrov E.	390	Volosov K.A.	437
Pierre C.	352	Volosova A.K.	437
Pilipchuk V.N.	176	<b>W</b>	
Polishchuk A.S.	473	Warمیński J.	96,262
Polukoshko S.N.	177	Wiercigroch M.	225
<b>R</b>		Wolff M.	503
Rachinskaya A.	9	<b>Y</b>	
Raičević V.	84	Yaroshevich N.P.	39
Romashov Yu.V.	392	Yasniy P.	509
Rudnyeva G.V.	152	Yelagin A.V.	443
<b>S</b>		<b>Z</b>	
Sadowski T.	284	Zinkevich Y.	9
Sayenko S.Yu.	398	Zotov A.	226
Selivanov A.V.	421	.	.
Shmatko T.V.	403		
Shulhan I.	509		
Shvets A.Yu.	183,189		
Shyriaieva N.V.	272		
Sidorenko V.V.	195		

# MEMORY SHEET

## НАУКОВЕ ВИДАННЯ

The Third International Conference “Nonlinear Dynamics – 2010”  
Dedicated to the 125<sup>th</sup> Anniversary of the National Technical University  
“Kharkov Polytechnic Institute”.  
Proceedings.

Упорядники: Ю.В.Міхлін, М.В. Перепелкін.

Відповідальний секретар: Р.Є. Кочуров.

Оформлювання оригінал-макету: М.В. Перепелкін, Г.В. Руднева.

Дизайн обкладинки Г.В. Руднева.

Матеріали збірника публікуються в авторському варіанті без редагування.